

**TWELFT INTERNATIONAL CONFERENCE ON  
ELECTRICAL MACHINES, DRIVES AND POWER SYSTEMS**

Supported by  **IEEE** Bulgaria Section  
**VDE**



**PROCEEDINGS**

**VOLUME 1**

**16-18 October 2008  
Sofia, BULGARIA**

TWELFT INTERNATIONAL CONFERENCE ON  
ELECTRICAL MACHINES, DRIVES AND POWER SYSTEMS

# ELMA 2008

16 – 18 October 2008, Sofia, BULGARIA

## PROCEEDINGS

Supported by:  **IEEE** Bulgaria Section  
**VDE**

Organised by:

Union of electronics, electrical engineering  
and telecommunications (CEEC) – EUREL Member  
Technical University of Sofia  
Technical University of Varna  
Technical University of Gabrovo  
University of Rousse

ELMA 2008 – XII International Conference on  
Electrical Machines, Drives and Power Systems  
16 – 18 October 2008, Sofia, BULGARIA

## Proceedings

Editorial board: Gancho Bojilov, Dimitar Sotirov, George Todorov,  
Zahari Zarkov

Printed by AVANGARD, Sofia, Bulgaria

Number of copies: 150

Printing of this edition has been financially supported by  
The Technical University of Sofia

**ISSN 1313-4965**

These Proceedings are reviewed by members of The Program Committee.

**Disclaimer:** The authors are fully responsible for respecting the authors' rights, industrial and patent properties.

## **ELMA 2008 is supported also by:**

- ELPROM TRAF0 CH Kyustendil
- SPARKY ELTOS Lovech
- ELPROM – ZEM Sofia
- ELDOMINVEST Varna
- DENIMA Sofia
- ABB-Avangard Sevlievo
- HYUNDAY Heavy Industries
- ELMOT Veliko Tarnovo
- DIT-M Sofia
- MMOTORS Etropole
- CERB Sofia
- Prof. Gancho Bojilov and Yassen Bojilov
- PRIOR Sofia
- ZAVN Dobrich
- ELECTROINVENT Sofia
- ELPROM – IEP
- ELPROM – ILEP
- TROYAN MOTOR
- INOVATICS Sofia
- DENI-EN-K Sofia
- ELISOT Sofia
- DNT Varna, Plovdiv, Bourgas, Rouse



---

## STEERING COMMITTEE

---

---

### CONFERENCE CHAIRMEN

---

<b>Gancho BOJILOV</b>	CEEC
<b>Dimitar SOTIROV</b>	Technical University of Sofia

---

---

### ORGANIZING COMMITTEE

---

**Chairman:**

**Vladimir LAZAROV**                      Technical University of Sofia, Bulgaria

**Secretariat:**

<b>Ivan VASSILEV</b>	CEEC, Bulgaria
<b>George TODOROV</b>	Technical University of Sofia, Bulgaria
<b>Zahari ZARKOV</b>	Technical University of Sofia, Bulgaria
<b>Yuli STAFUNSKI</b>	Technical University of Varna, Bulgaria

---

---

### INTERNATIONAL PROGRAM COMMITTEE

---

**Viktor BESPALOV** – Technical University – Moscow, Russia  
**Stanislaw BOLKOWSKY** – SEP, Warsaw, Poland  
**Gerard-Andre CAPOLINO** – Université de Picardie, France, Chair of ICEM  
**Milan CHUNDEV** – University “ Sts. Cyril & Methodius”, Skopie , Macedonia  
**Manuel Perez DONSION** – Vigo University, Spain  
**Gerhard DREGER** – VDE – Frankfurt, Germany  
**Pancho DUNDAROV** – CEEC, Bulgaria  
**Masato ENOKIZONO** – Oita University, Japan  
**Bulent ERTAN** – Middle East Technical University, Ankara, Turkey  
**Ionescu FLORIN** – UPB Bucharest , Romania  
**Bruno FRANCOIS** – Ecole Centrale – Lille, France  
**Antonios KLADAS** – NTUA , Greece  
**Afef LEBouc** – LEG – INPG, France  
**Jiri LETTL** – CVUT – Prague, Czech Republic  
**Gerard MEUNIER** – LEG – INPG, France  
**Emil MITEV** – Polytechnic Radom, Poland  
**Gilles NOTTON** – Université de Corse, France  
**Lidija PETKOVSKA** – University “ Sts. Cyril & Methodius”, Skopie , Macedonia  
**Viktor PETROUSHIN** – Odessa Polytechnic Institute, Ukraine  
**Michel POLOUJADOFF** – Université Pierre et Marie Curie, Paris, France  
**Ioan POPA** – University of Craiova, Romania  
**Viktor POPOV** – Technical University of St. Petersburg , Russia  
**Mircea RADULESKU** – Technical University of Cluj-Napoca, Romania  
**Saifur RAHMAN** – Virginia Tech, USA  
**Christian SCHAEFFER** – LEG – INPG, France  
**Wolfgang SCHROPPEL** – Technical University of Chemnitz, Germany  
**Sergey SHIRINSKY** – Technical University – Moscow, Russia  
**Emil SOKOLOV** – Technical University, Sofia, Bulgaria  
**John TEGOPOULOS** – NTUA, Greece  
**Christian VASSEUR** – Université de Lille, France

---

**NATIONAL PROGRAM COMMITTEE**

---

**Alexander ALEXANDROV** - Technical University of Sofia  
**Rumen ATANASOV** – BCEE  
**Lyubomir BALGARANOV** - Technical University of Sofia  
**Ivelin BUROV** - BDS  
**Dimitar DIMITROV** - Technical University of Varna  
**Peter DINEFF** - Technical University of Sofia  
**Nikolai DJAGAROV** - Technical University of Varna  
**Valentin FILIPOV** – ZEM Sofia  
**Vasil GOSPODINOV** - Technical University of Sofia  
**Nikola GRADINAROV** - Technical University of Sofia  
**Stefcho GUNINSKI** - Technical University of Sofia  
**Marin HRISTOV** - Technical University of Sofia  
**Kostadin ILIEV** - Technical University of Sofia, branch Plovdiv  
**Todor IONKOV** - Technical University of Sofia  
**Dimitar JETCHEV** - Technical University of Sofia  
**Anatoli IVANOV** – SPARKY Eltos  
**Nikola KALOYANOV** - Technical University of Sofia  
**Maria KANEVA** - Technical University of Sofia  
**Yordan KOLEV** – IEEE Bulgaria section  
**Sava KONTROV** - Technical University of Varna  
**Anastasia KRASTEVA** - Technical University of Sofia  
**Iliana MARINOVA** - Technical University of Sofia  
**Maria MARINOVA** - Technical University of Varna  
**Deshka MARKOVA** - Technical University of Gabrovo  
**Alexandar MAVRODIEV** – CERB Sofia  
**Nikolai MICHAILOV** – Rousse University  
**Miho MIHOV** - Technical University of Sofia  
**Mincho MINCHEV** - Technical University of Sofia  
**Petar NAKOV** - Technical University of Sofia  
**Petko NOTOV** - Technical University of Sofia  
**Ivaylo PANAYOTOV** – Elprom Trafo SN Kyustendil  
**Angel PACHAMANOV** - Technical University of Sofia  
**Lazar PETKANICHIN** - Technical University of Sofia  
**Petar PETROV** – INOVATIX  
**Encho POPOV** – DENI-EN Ltd  
**Emil RATZ** - Technical University of Sofia  
**Plamen RIZOV** - Technical University of Sofia

**Georgi SAVOV** - ELPROM Harmanli

**Stanimira SHISHKOVA** - Technical University of Sofia, branch Plovdiv

**Nikola SHOYLEV** – UCTM Sofia

**Yordan SHOPOV** - Technical University of Sofia

**Rumiana STANCHEVA** - Technical University of Sofia

**Stefan TABAKOV** – Technical University of Sofia

**Ivan TZANKOV** – ELMOT Veliko Tarnovo

**Slavka TZANOVA** – Technical University of Sofia

**Raina TZENEVA** - Technical University of Sofia

**Angel TZOLOV** – Technical University of Sofia

**Hristo VASSILEV** - Technical University of Sofia

**Petko VITANOV** - Bulgarian Academy of Sciences

**Pencho VLADIMIROV** - Technical University of Gabrovo

**Ivan YATCHEV** - Technical University of Sofia

**Kiril ZAHARINOV** - Technical University of Sofia

# TABLE OF CONTENTS

## INVITED PAPERS

<b>PL.1 Long Range Power Generation R&amp;D Planning Chalanges.....</b>	<b>1</b>
István Krómer and Zoltan Bessenyei <i>Institute for Electric Power Research, Budapest, Hungary</i>	
<b>PL.2 BDS Relationships with European Organizations for Standardization CEN, CENELEC, ETSI.....</b>	<b>7</b>
Ivelin Burov <i>Chairman of the BDS managing board, Bulgaria</i>	

## ELECTRICAL MACHINES and DRIVES

<b>EM.1 Finite Element Analysis of Electromagnetic Phenomena in a Small Three-Phase Transformer.....</b>	<b>14</b>
Mihail Digalovski and Lidija Petkovska <i>Ss. Cyril and Methodius University, Skopje, Macedonia</i>	
<b>EM.2 Iron loss characterization and prediction in electrical machines.....</b>	<b>20</b>
Afef Kedous-Lebouc <i>Grenoble Electrical Engineering Laboratory G2Elab, Grenoble-INP, France</i>	
<b>EM.3 Simulink implementation of three phase double fed induction motor model.....</b>	<b>24</b>
Sameer Khader <i>Palestine Polytechnic University, Hebron- West Bank</i>	
<b>EM.4 Using Reactive Power which is Generated in the Induction Motor for Estimation of Time Constant for the Rotor.....</b>	<b>31</b>
Dragan Vidanovski, Mirka Radevska and Blagoja Arapinoski <i>Faculty of Technical Sciences, Bitola, Macedonia</i>	
<b>EM.5 FEM Computation of ANORAD Synchronous Brushless Linear Motor.....</b>	<b>35</b>
Blagoja Arapinoski, Mirka Radevska and Dragan Vidanovski <i>Faculty of Technical Sciences, Bitola, Macedonia</i>	
<b>EM.6 Variable Speed AC Drives.....</b>	<b>39</b>
Emil Sokolov <i>Technical University of Sofia, Bulgaria</i>	
<b>EM.7 Performance characteristics of induction motor under V/f speed control.....</b>	<b>44</b>
Dimitar Jetchev and George Todorov <i>Technical University of Sofia, Bulgaria</i>	
<b>EM.8 Start-up process of induction motor fed by frequency cinverter.....</b>	<b>48</b>
George Todorov and Dimitar Jetchev <i>Technical University of Sofia, Bulgaria</i>	
<b>EM.9 Study of a synchronous excitation generator with rotating rectifier.....</b>	<b>51</b>
Dimitar Sotirov, Plamen Rizov, Ivailo Panayotov, Dimitar Bozhov, Boyan Krachev and Vladimir Doychev <i>Technical University of Sofia, Bulgaria</i>	
<b>EM.10 Problems in joint work of a synchronous generator with an uncontrolled rectifier.....</b>	<b>56</b>
Dimitar Sotirov, Ivailo Panayotov, Dimitar Bozhov, Boyan Krachev and Vladimir Doychev <i>Technical University of Sofia, Bulgaria</i>	
<b>EM.11 Experimental Detection of Faults of Induction Motor Electric Drives.....</b>	<b>61</b>
Olympiada A. Syggeridou and Maria G. Ioannides <i>National Technical University of Athens, Greece</i>	

## POWER SYSTEMS I

<b>PS.1 Review of Some Technical and Economic Features of Energy Storage Technologies for Distribution System Integration.....</b>	<b>67</b>
Gauthier Delille and Bruno François <i>Ecole Centrale de Lille, France</i>	

<b>PS.2 On the Methodology and Normative Regulations of Efficient Electrical Consumption.....</b>	<b>73</b>
Kondyu Andonov, Anka Krasteva, Ognyan Dinolov, Liudmil Mihailov, Valentin Kirchev*, Tasko Ermenkov**	
<i>Technical University of Russe, Bulgaria</i>	
<i>*State Energy and Water Regulatory Commission, Bulgaria</i>	
<i>**Energy Efficiency Agency, Sofia, Bulgaria</i>	
<b>PS.3 Applications for Short-Term Optimal Power Planning in Liberalized Power Markets.....</b>	<b>78</b>
Dimo Stoilov, Penko Gyurov, Danail Ignatovski	
<i>Technical University of Sofia, Bulgaria</i>	
<b>PS.4 Market Share Increasing In a Retail Electricity Market Using Reinforcement Learning.....</b>	<b>84</b>
Babak Behbahani, Seyed Hossein Hosseinian	
<i>Amirkabir University, Tehran, Iran</i>	
<b>PS.5 The experience of using high-voltage controllable magnetic reactors in electrical network 110-500 kV.....</b>	<b>89</b>
Aleksandr Bryantsev, Viktor Bespalov, Svetlana Dyagileva	
<i>Moscow Power Engineering Institute, Russia</i>	
<b>PS.6 Electromagnetic compatibility and resources of terminators overstressings in networks 0,4 - 10 kV.....</b>	<b>93</b>
Igor Kosorlukov, Valery Polyakov, Vyacheslav Prikhodchenko, Oleg Solyakov*, Lev Shpitz	
<i>Technical University of Samara, Russia</i>	
<i>**“MRSK Volgy” – “Samarskye RS” Samara, Russia</i>	
<b>PS.7 Electromagnetic Field Analysis in Vicinity of Power Lines.....</b>	<b>97</b>
Mirjana Perić, Saša S. Ilić and Slavoljub Aleksić	
<i>University of Niš, Serbia</i>	

<b>RENEWABLE ENERGY SOURCES</b>
---------------------------------

<b>RES.1 Variability of solar and wind energy outputs in relation with the weather and climate conditions in Bulgaria.....</b>	<b>103</b>
Peter Ivanov	
<i>Department of Meteorology of NIMH at BAS, Sofia, Bulgaria</i>	
<b>RES.2 Distributed Generation and Renewable Energy Sources in Republic of Macedonia.....</b>	<b>109</b>
Frantisek Janicek, Dragan Minovski, Anton Cusevski*, Emil Krondiak	
<i>Slovak University of Technology, Bratislava, Slovak Republic</i>	
<i>*Ss. Cyril and Methodius University, Skopje, Macedonia</i>	
<b>RES.3 Diagnoses of wind energy.....</b>	<b>113</b>
Oudie Bennouna, Nicolas Heraud, Mohamed Ainan Kahyen and Ahmed Youssouf	
<i>University of Corsica, France</i>	
<b>RES.4 Seasonal variation of PV efficiency for various technologies and module inclinations.....</b>	<b>118</b>
Gilles Notton, Vladimir Lazarov*, Ludmil Stoyanov*, Said Diaf and Nicolas Heraud	
<i>University of Corsica, France</i>	
<i>*Technical University of Sofia, Bulgaria</i>	
<b>RES.5 First approach of a Matlab/Simulink simulation for a PV/T solar collector behavior.....</b>	<b>124</b>
Gilles Notton, Nicolas Heraud, Christian Cristofari, Ahmed Youssouf and Mohamed Ainan Kahyen	
<i>University of Corsica, France</i>	
<b>RES.6 Current state of research and industrial application of biogas technologies in Bulgaria.....</b>	<b>130</b>
Ivan Simeonov, Ludmil Nikolov, Danka Galabova, Elena Chorukova	
<i>Institute of Microbiology, Bulgarian Academy of Sciences, Sofia</i>	
<b>RES.7 Comparison of Energy Conversion Systems for Variable Speed Wind Turbine Application.....</b>	<b>136</b>
Daniel Roye, Vladimir Lazarov*, Dimitar Spirov*, Ludmil Stoyanov*	
<i>Grenoble Institute of Technology, France</i>	
<i>*Technical University of Sofia, Bulgaria</i>	
<b>RES.8 Productivity of Medium Wind Turbines According to Wind Weibull Distribution: Application to Various Bulgarian Sites.....</b>	<b>142</b>
Gilles Notton, Vladimir Lazarov*, Ludmil Stoyanov*	
<i>University of Corsica, France</i>	
<i>*Technical University of Sofia, Bulgaria</i>	
<b>RES.9 Modeling of the Wind Energy Conversion System Components.....</b>	<b>147</b>
Teofana Puleva	
<i>Technical University of Sofia, Bulgaria</i>	

## POWER SYSTEMS II

<b>PS.8 Development of Diagnostic Algorithm Based on Fault Gas Average Concentrations.....</b>	<b>153</b>
<i>Janis Dirba and Sandra Vitolina Riga Technical University, Latvia</i>	
<b>PS.9 Simulation of an electrical power system of compressor station of the main gas pipeline with electricity generating plant of own needs.....</b>	<b>157</b>
<i>Valery Goldshtein, Pavel Grachev, Youri Koubarkov Technical University of Samara, Russia</i>	
<b>PS.10 Applying of an informational - analytical complex for the solution of technological and computational problems in electrical power systems of gas mains with high-voltage electric motors.....</b>	<b>160</b>
<i>Valery Goldshtein, Pavel Grachev, Youri Koubarkov Technical University of Samara, Russia</i>	
<b>PS.11 Probabilistic approach for thermal and electrodynamic stresses distribution functions.....</b>	<b>164</b>
<i>Ciprian Nemes, Florin Munteanu Technical University of Iasi, Romania</i>	
<b>PS.12 Optimal Operation Planning of Mosul Hydro Power Complex Part I: Mathematical Models.....</b>	<b>169</b>
<i>Dimo Stoilov, Maria Kaneva, Fawaz Syltan* Technical University of Sofia, Bulgaria * Technical College – Mosul, Iraq</i>	
<b>PS.13 Optimal Operation Planning of Mosul Hydro Power Complex. Part II: Simulation Results and Analysis.....</b>	<b>175</b>
<i>Fawaz Syltan*, Dimo Stoilov Technical University of Sofia, Bulgaria * Technical College – Mosul, Iraq</i>	
<b>PS.14 Electric Energy Quality in Low Voltage Electricity Supply System.....</b>	<b>182</b>
<i>Svetlana Tzvetkova, Vania Tzvetkova* Technical University of Sofia, Bulgaria *Vocational Secondary School of Railway Transport, Gorna Oriahovitza, Bulgaria</i>	

## ENERGY EFFICIENCY and POWER QUALITY

<b>EPQ.1 LabVIEW Software Processing of the Power Quality Parameter Measuring Results.....</b>	<b>186</b>
<i>Milan M. Simić, Dragan S. Kovačević* and Božidar R. Dimitrijević University of Niš, Serbia * Electrical Engineering Institute Nikola Tesla, Belgrade, Serbia</i>	
<b>EPQ.2 Energy Efficiency in Vector Controlled Variable Speed Drives VSD.....</b>	<b>191</b>
<i>Goran Rafajlovski and Krste Najdenkoski Ss. Cyril and Methodius University, Skopje, Macedonia</i>	
<b>EPQ.3 General Methods for Energy-Efficiency Investigation and Evaluation of Induction Motor Drives.....</b>	<b>197</b>
<i>Ognyan Dinolov Technical University of Russe, Bulgaria</i>	
<b>EPQ.4 Technical and Economic Efficiency of Power Transformers On-line Diagnostic System Utilization.....</b>	<b>202</b>
<i>Lyubomir V. Dimitrov Technical University of Varna, Bulgaria</i>	
<b>EPQ.5 Minimizing lighting flux of luminaries for street lighting systems designed by Small Target Visibility Criteria.....</b>	<b>206</b>
<i>Hristo Vasilev, Stanimir Stefanov and Krassimir Velinov Technical University of Sofia, Bulgaria</i>	
<b>EPQ.6 Optimization of LED's Lighting Distribution in Road Lighting Luminaire.....</b>	<b>211</b>
<i>Valchan Gueorgiev, Hristo Vasilev Technical University of Sofia, Bulgaria</i>	
<b>EPQ.7 Improving the Efficiency of Lighting in Public Alleys by Accounting for Diffuse-Reflected Luminous Flux.....</b>	<b>217</b>
<i>Angel Pachamanov, Konstantin Hristov, Vessela Daskalova Technical University of Sofia, Bulgaria</i>	

## GENERAL PROBLEMS IN ELECTRICAL ENGINEERING

<b>EE.1 European Trends in Interdisciplinary Postgraduate Education.....</b>	<b>222</b>
Maria G. Ioannides, Rossie Betcheva* and Fotini Ioannidou	
<i>National Technical University of Athens, Greece</i>	
<i>* University of Chemical Technology and Metallurgy, Sofia, Bulgaria</i>	
<b>EE.2 Magnetic field calculus for block permanent magnet system.....</b>	<b>228</b>
Ana Mladenović and Slavoljub Aleksić	
<i>University of Niš, Serbia</i>	
<b>EE.3 Nonlinear Grounding Design: Sphere Grounding Electrode.....</b>	<b>232</b>
Bojana Petković, Zlata Cvetković and Slavoljub Aleksić	
<i>University of Niš, Serbia</i>	
<b>EE.4 Linear Electric Circuit Analysis based on the Graph Theory obtaining all Possible Paths in the Graph Model.....</b>	<b>237</b>
Simona Filipova-Petrakieva, Valeri Mladenov	
<i>Technical University of Sofia, Bulgaria</i>	
<b>EE.5 Reconstruction of Current Density Vectors by Locally Measured Magnetic Field Data.....</b>	<b>242</b>
Iliana Marinova and Valentin Mateev	
<i>Technical University of Sofia, Bulgaria</i>	
<b>EE.6 Magnetic Field Visualization by Array Sensor Systems.....</b>	<b>246</b>
Valentin Mateev and Iliana Marinova	
<i>Technical University of Sofia, Bulgaria</i>	
<b>EE.7 The Switching Analysis of the Three-Phase Bridge Rectifier.....</b>	<b>251</b>
Mitică Iustinian Neacă	
<i>University of Craiova, Romania</i>	
<b>EE.8 The Influence of the Output's Deforming Regime of a Commanded Rectifier over its Input Functioning Regime.....</b>	<b>255</b>
Mitică Iustinian Neacă, Andreea Maria Neacă	
<i>University of Craiova, Romania</i>	
<b>EE.9 PSPICE Investigation of Transients in the Multiphase Bridge Transistor DC-DC Converters with Charge Mode Control.....</b>	<b>260</b>
Georgi Kunov, Elissaveta Gadjeva and Marian Popov	
<i>Technical University of Sofia, Bulgaria</i>	

## TECHNOLOGIES

<b>T.1 Equipment for Infrared Cleaning of Oil Contaminations .....</b>	<b>265</b>
Peter Dineff, Nikola Shojlev*, Tamara Pencheva**, Petko Mashkov** and Berkant Gyoch**	
<i>Technical University of Sofia, Bulgaria</i>	
<i>*University of Chemical Technology and Metallurgy, Sofia, Bulgaria</i>	
<i>**Technical University of Russe, Bulgaria</i>	
<b>T.2 Infrared Oil Contamination Cleaning Technology for Polymer Surfaces.....</b>	<b>270</b>
Peter Dineff, Nikola Shojlev*, Tamara Pencheva**, Petko Mashkov** and Berkant Gyoch**	
<i>Technical University of Sofia, Bulgaria</i>	
<i>* University of Chemical Technology and Metallurgy, Sofia, Bulgaria</i>	
<i>**Technical University of Russe, Bulgaria</i>	
<b>T.3 Modeling of processes at polyamide parts' IR welding.....</b>	<b>275</b>
Angel Valchev, Petko Mashkov, Tamara Pencheva, Berkant Gyoch	
<i>Technical University of Russe, Bulgaria</i>	
<b>T.4 Modeling of heat transfer during soldering process by control of operation of heaters.....</b>	<b>281</b>
Sava Kontrov, Maria Marinova, Angel Valchev*, Tamara Pencheva*, Borislav Dimitrov	
<i>Technical University of Varna, Bulgaria</i>	
<i>* Technical University of Russe, Bulgaria</i>	

<b>T.5 Spontaneous Filamentary Pattern Formation in One-Dimensional Dielectric-Barrier Discharge at Atmospheric Pressure in Air.....</b>	<b>286</b>
Peter Dineff and Dilyana Gospodinova <i>Technical University of Sofia, Bulgaria</i>	
<b>T.6 Methods for Test and Analysis of Electrical Machines and Transformers Insulation.....</b>	<b>292</b>
Lyubomir Dimitrov and Stefka Kanturska* <i>Technical University of Varna, Bulgaria</i> <i>*Free University of Varna, Bulgaria</i>	
<b>T.7 Equipment for infrared welding of large area plastic details.....</b>	<b>297</b>
Petko Mashkov, Tamara Pencheva, Berkant Gyoch, Angel Valchev <i>Technical University of Russe, Bulgaria</i>	
<b>T.8 Analysis of Thermal Field of LED Heat Sinks for Road Luminaires.....</b>	<b>302</b>
Valchan Gueorgiev, Ivan Yatchev, Krastio Hinov <i>Technical University of Sofia, Bulgaria</i>	

## POSTERS

<b>PO.1 Modelling of Electric Field Treatment of Granular Materials.....</b>	<b>307</b>
Gantcho Bojilov, Ilona Seikova and Ivan Yatchev <i>Technical University of Sofia, Bulgaria</i>	
<b>PO.2 Determination of Induction Machine Parameters in Case of Dynamic and Steady-State Operating Modes.....</b>	<b>313</b>
Dimitar Spirov, Pencho Vladimirov <i>Technical University of Gabrovo, Bulgaria</i>	
<b>PO.3 Computer System for Analysis of the Size of Vibrations at Frequency Control of Induction Motors.....</b>	<b>317</b>
Totyo Iliev, Plamen Danailov <i>Technical University of Gabrovo, Bulgaria</i>	
<b>PO.4 Electromagnetic Parameters of a Non-Salient-Pole Vortex Machine Taking into Account the Influence of the Working Chamber.....</b>	<b>320</b>
Konstantin Kostov <i>University of Mining and Geology "St. I. Rilski", Sofia, Bulgaria</i>	
<b>PO.5 Simplified Method of Defining the Torque, the Shaft Load Moment and the Moment of Inertia for Power Tools.....</b>	<b>323</b>
Milko Dochev <i>Technical College, Lovetch, Bulgaria</i>	
<b>PO.6 Electro drive system with single-tree phase quasyresonance cycloconverter.....</b>	<b>325</b>
Tsvetozar Petkov and Lubomir Genchev <i>Technical University of Gabrovo, Bulgaria</i>	
<b>PO.7 Global Irradiance throughout the Day in Gabrovo.....</b>	<b>329</b>
Milka Konsulova <i>Technical University of Gabrovo, Bulgaria</i>	
<b>PO.8 Analysis of the Daily and Monthly Solar Radiation for the Region of Ruse.....</b>	<b>332</b>
Ivaylo Stoyanov and Nicolay Mihailov <i>Technical University of Russe, Bulgaria</i>	
<b>PO.9 Determination of the Electrical Energy, Obtained From Direct Transformation of Solar Energy from a PV Generator.....</b>	<b>336</b>
Ivaylo Stoyanov <i>Technical University of Russe, Bulgaria</i>	
<b>PO.10 Current Hour Consumption Forecast.....</b>	<b>341</b>
Rositsa Angelova, Todor Gichev and Galina Cherneva <i>Higher School of Transport, Sofia, Bulgaria</i>	
<b>PO.11 Voltage phase angles determination by distributed intelligence.....</b>	<b>344</b>
Lazar Petkanchin <i>Technical University of Sofia, Bulgaria</i>	



<b>PO.12 Asset Optimization in EPS.....</b>	<b>347</b>
Maria Kaneva <i>Technical University of Sofia, Bulgaria</i>	
<b>PO.13 Sensor Button 2 / The next generation Sensor Button / .....</b>	<b>351</b>
Dimitar Nurkov <i>Technical University of Sofia, Bulgaria</i> <i>* University of Corsica, Corte, France</i>	
<b>PO.14 Investigation of High Power Bolted Busbar Connectors with Longitudinal Slots.....</b>	<b>354</b>
Raina Tzeneva <i>Technical University of Sofia, Bulgaria</i>	
<b>PO.15 Theoretical Analysis on Implementing Electric Filters in a Poultry Farm.....</b>	<b>359</b>
Dimcho Kiriakov <i>Technical University of Russe, Bulgaria</i>	
<b>PO.16 Algorithm for Determining the Layout of Electric Filters while Implementing Them in Poultry Farms.....</b>	<b>362</b>
Dimcho Kiriakov and Nikolay Mihailov <i>Technical University of Russe, Bulgaria</i>	
<b>PO.17 A method of synthesis of proton exchange membrane fuel cell.....</b>	<b>365</b>
Ruslan Ivanov <i>Technical University of Sofia, Bulgaria</i>	
<b>PO.18 Measuring Electrical and Thermal Characteristic Using a Digital Multimeter and LabVIEW.....</b>	<b>369</b>
Stoill Stannev <i>Hyundai Heavy Industries Co. Bulgaria</i>	
<b>PO.19 Impact of Wall Luminance on Surface Luminance in Road Tunnels.....</b>	<b>373</b>
Angel Pachamanov, Dessislava Pachamanova*, Kirilka Ivanova <i>Technical University of Sofia, Bulgaria</i> <i>*Mathematics and Sciences Division of Babson College, USA</i>	
<b>PO.20 Impact of Diffuse-Reflected Luminous Flux on Wall Luminance in Road Tunnels.....</b>	<b>378</b>
Angel Pachamanov, Stoyan Petrov, Vesselina Rahneva <i>Technical University of Sofia, Bulgaria</i>	
<b>PO.21 Start-up process of high-pressure sodium lamps.....</b>	<b>383</b>
Galia Georgieva-Taskova <i>Technical University of Sofia, Bulgaria</i>	

# Long range power generation R&D planning challenges

Prof. Dr. I. Krómer, dr. Z. Bessenyei

**Abstract:** *The purpose of long-term power generation R&D is to develop technology options that will provide a hedge against future scenarios in which current technologies will no longer be capable of providing the security of supply, competitiveness and sustainability.*

*Evaluation of the long term energy forecasts made in the past frequently concludes that a large number of them and associated policy recommendations turned out to be inaccurate or even mistaken. Moreover, forecasts of energy technology innovation and commercialization have often been highly inaccurate and overly optimistic. In the context of energy planning, the problem of uncertainty recently receives a lot of attention.*

*The paper presents an uncertainty matrix in order to capture uncertainties in energy future planning in a broader way, including multiple aspects in an explicit and systematic way. The paper outlines a number of elements of past forecasts that were correct and may well persist into the future and facilitates the long-term technology forecast. Important R&D areas come to light when examining the key issues including uncertainties that affect the future power generation mix. Only a diverse portfolio of power generation technologies including fossil, renewable, nuclear based generation and dispersed energy resources will meet the world's energy needs.*

## Introduction

During the last decades the investments in energy research and development (R&D) have declined in most of the industrial countries. To a great extent this reduction in commitments to energy R&D efforts reflected the perception that energy had become a matter of lesser urgency, relative to other social priorities. The ideological shift forward the deregulation of key infrastructure industries, such as electricity and gas utilities, has placed pressure on R&D investments too.

With the introduction of market competition in the electricity industry, R&D investments have grown smaller. While public and private sector energy R&D investments have declined, major new energy related challenges have appeared on the horizon that demand significant and sustained commitments to the development of new energy technologies. These challenges are made greater still by projections that the global energy use expected to grow dramatically and a large part of the new demand will be met by fossil fuels.

To help to address the many challenges facing the electric power industry in the next decades broad-range planning of technology R&D priorities is needed.

In this report we consider the long-term R&D planning process as illustrated in Fig.1.

The methodology provides the following information for the planning.

- Long-term energy needs that a technology concept does address.
- Key technical performance factors that favour the technology.
- Critical technical problems that must be resolved for the technology to become viable.
- Merits of alternative development approaches.

In order to better understand possible developments in the future, it is necessary to consider why the future looks so uncertain from where we stand today. This is explained by reference to the historical and current trends, which are analysed within the framework of the industry changes in the last decades.

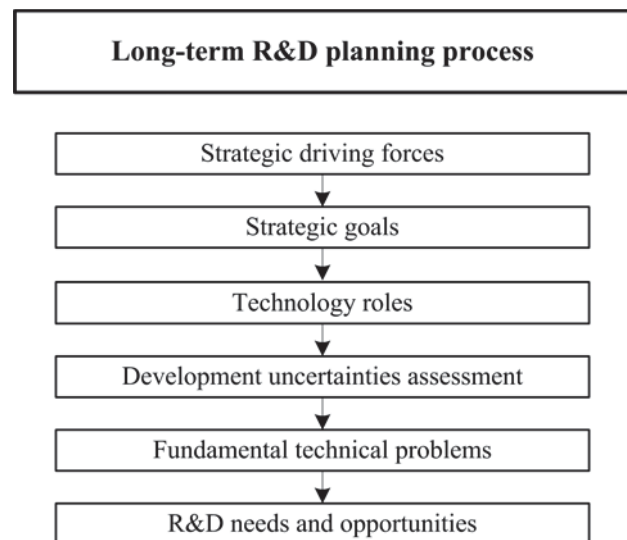


Fig.1. R&D planning process

## 1. Uncertainty assessment

The identification of the real options of a long-term energy strategy should be driven by the identification of the uncertainties towards which reactions will be possible.

In the twentieth century the electric power industry had gone through a long and stable development period, being regulated, centrally planned and operated by vertically integrated utilities. While in today's fragmented organizational structures of the power system, the use of regulatory endorsement alone cannot assure its health, but the pure market system presents a tendency toward a boom and bust investment cycle.

Traditional integrated planning of generation and transmission systems, conducted by vertically integrated

utilities under state regulatory oversight, has been replaced in recent years by planning conducted by multiple and competitive players. Furthermore, variables such as load forecasts, location and amount of new generation and type and timing of new facilities are more uncertain than in the formerly regulated system.

An uncertainty matrix was developed in order to allow for capturing uncertainties in energy forecasting in a broader and systematic way.

The matrix provides a categorization of uncertainties by the type of knowledge relationship and the objective of uncertainty. It distinguishes between three types of knowledge relationships that are assumed to be established among an actor and an object. Those are unpredictability, incomplete knowledge and multiple knowledge frames.

Each of the three knowledge relationships can refer to different objects of uncertainty within the natural, technical and social systems.

The use of uncertainty matrix (Table 1) offers a new and more structured way of approaching the issue of uncertainty [1].

**Table 1**

*Uncertainty matrix*

Object \ Source of uncertainty	Incomplete knowledge	Unpredictable behaviour	Conflicting knowledge frame
Natural system (e.g. -climate change -ecosystem -resources)	e.g. about climate change	e.g. carbon sequestration	e.g. about the climate change consequences
Technical system (e.g. -infrastructure -technologies)	e.g. about emerging sustainable technologies	e.g. cost perspective of emerging technologies	e.g. about the industry adaptation to climate change
Social system (e.g. -stakeholders -economic aspects -political aspects -legal aspects)	e.g. about the future regulatory framework	e.g. power and fuel markets	e.g. about the social value of energy externalities

## 2. Projections of future energy demand and supply

Over the past decades, long-range energy forecasting has been extremely difficult and a large portion of the forecasts, predictions and associated policy

recommendations turned to be inaccurate and mistaken. For example, the price of oil is one of the most important commodity prices in the world. Nevertheless, for decades, oil prices have refused to behave as predicted. Similarly, forecasts of energy technology innovation and commercialization have often been inaccurate and overly optimistic [2].

However, a number of elements of past forecasts were correct and may well persist into the future, they include the following:

- The gradual electrification of the economy will continue and the economy will become more electricity intensive.
- Natural gas will continue to increase its share in primary fuel-mix, although it is uncertain how long this trend will last.
- Environmental protection will remain a high priority and global warming will remain a major concern.
- Energy technologies, technology requirements and technology development will be more influenced by environmental concerns.
- The shape and form of the energy industries will likely change, but precisely how remains uncertain.
- World population will continue to increase primarily in the developing countries. They will account for an increasing share of world energy consumption. Therefore future energy and environmental technology development will be increasingly dictated by developing nations' needs.
- Increased world carbon emissions are likely inevitable under any realistic scenario.
- Renewables will continue to increase in importance and account for a larger share of energy mix, however, their overall contribution will remain modest.

The quick responses to the rapidly changing political and economical realities frequently results in new energy priorities and shifting in R&D spending. The changing priorities lead to different fuel/technology mix scenarios. A recent national study [3] describes four different future fuel-mix scenarios (Fig.2 – Fig.5.). The uncertainty of the future fuel-mix suggests a wide range of power generation R&D needs.

## 3. Central power generation R&D needs

A forward looking and balanced approach to meeting future energy needs require the continued development of traditional energy sources and aggressive efforts to improve their energy efficiency and promote alternative energy sources.

Energy use patterns change slowly and the majority of the energy needs continue to be satisfied from fossil fuels. New central electric power generation will come from a variety of sources including coal, wind and possible nuclear.

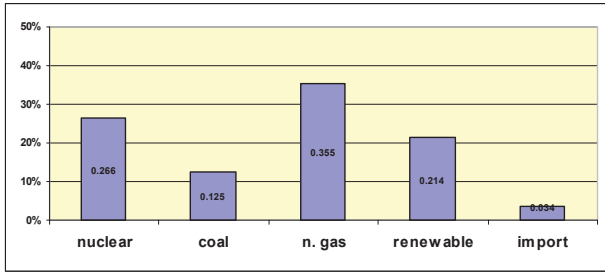


Fig.2. "Renewable focused" scenario 2020

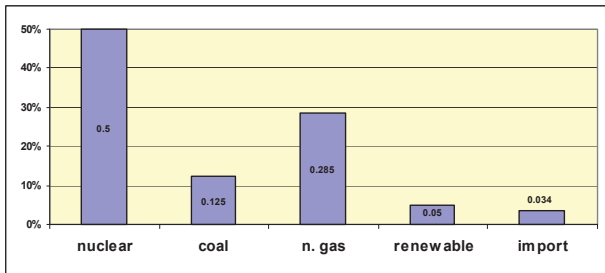


Fig.3. "Nuclear oriented" scenario 2020

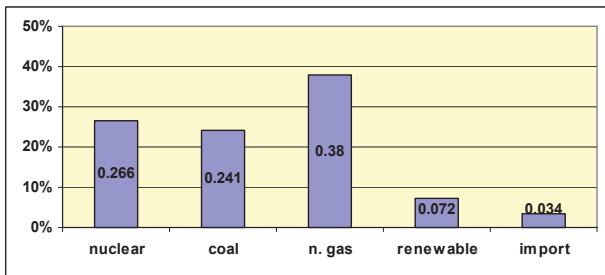


Fig.4. "Coal use" scenario 2020

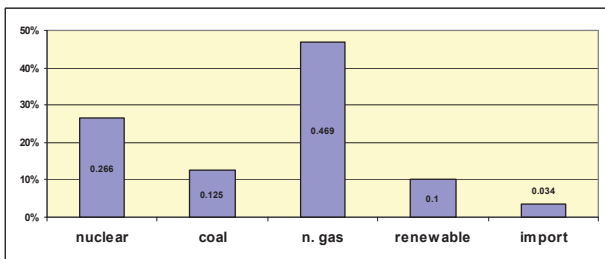


Fig.5. "Natural gas based" scenario 2020

The overall objectives of the power plants R&D can be stated as:

- produce electricity at competitive costs
- minimize environmental impact associated with fossil fuels
- attain high efficiency

In the central power generation area the following technology development fields have to be addressed in details:

- existing plants,
- future nuclear plants,
- natural gas fired generation technologies,
- coal power generation technologies,
- renewable resources,

Continued high performance of the existing central plants will be maintained by combining design

improvements to critical equipment, innovative solutions for inspection, condition assessment, remaining life prediction and risk-based maintenance and replacement strategies. The R&D goals include equipment reliability programs, development of technology to provide nuclear fuel that meets future performance requirements, analysis of reactor vessel and other internal issues, demonstration of the adequacy of steam generators, a proven license renewal procedure and improved technologies for radioactive waste management. It can be stated that because the continued safe, reliable operation of the aging existing fleet of NPP-s is such a critical part of the electricity system in any case, the related R&D needs are less sensitive to the future scenarios than those of other power generation categories.

Nuclear power provides significant portion of electricity generation. The nuclear power industry has demonstrated that electricity can be reliably produced without contributing to global climate change. In Hungary almost 40% of the total electricity consumption supplied from NPP.

Nuclear energy seems to enter a renaissance. There is a strong interest for new plant construction. The critical R&D needs in the area of future nuclear power capabilities can be summarized in the following items:

- demonstrate reliability, reduce capital and operating cost and construction time,
- develop advanced nuclear generation options including production of hydrogen,
- develop a closed nuclear fuel cycle.

The power plant average conversion efficiency of fossil fuels into electricity is as low as about 30% today. That is practically the same efficiency we had several decades ago. An increase of efficiency by one percent point improves not only the power plant's profitability, but also avoids the emission of up to 15.000 tons CO<sub>2</sub> per year at a 200MW power plant.

In the 1990s natural gas fired combustion turbines and combined cycles became the preferred technology choice for power production due to the availability of natural gas at relatively low cost. However, increasing natural gas prices can provide a disincentive to increase further reliance on combustion turbine based power plants. Obviously, the R&D needs for combustion turbines include increasing efficiency up to 60-75%, enabling fuel flexibility (with syngas and liquefied natural gas), enabling turn down and enhancing durability [4,5].

Coal is abundant with the potential to provide hundreds of years of power. Its price is relatively low, stable and less sensitive to international oil/gas price fluctuation. Boosting power plant efficiency to high levels yields environmental benefits. Direct benefits include reduced energy consumption and environmental impacts from coal mining and transportation and at the power plant itself, reduced water consumption, less waste heat, fewer solid combustion products and reduced air

emissions. Integrated Gasification Combined Cycle Technology (IGCC) systems can combine the high efficiency (55-60%), low emissions with the ability to run on syngas which is coal derived. Today, efficiency of commercially offered IGCC plant has climbed to 40 percent. Technology R&D needs have been identified that can significantly increase the efficiency and reduce the cost of IGCC plants with CO<sub>2</sub> capture.

Advanced coal combustion technologies include pulverized coal units with high steam temperatures increasing efficiency. Successfully raising the steam temperature is primarily a matter of developing materials that can withstand the relevant temperature.

As fossil fuel prices rise and CO<sub>2</sub> restrictions increase, power producers will benefit from adding renewable energy sources to the generation mix. R&D is needed to improve the performance, availability and cost effectiveness of new and existing renewable capacity. Grid integration issues to reduce losses and minimize operating issues must be addressed as well.

Because renewable energy is relatively new, planners and operators of bulk-power systems have limited experience to make changes that may be needed to integrate large-scale renewable power into the existing power grid. R&D is needed to address the technical and associated cost issues related to the impacts of intermittency, ramping, fluctuating outputs, lack of control, system dispatch, load following and load balancing. Solutions for energy storage, integrating wind and hydroelectric energy, and reducing the costs of biomass fuel collection and transportation will boost efficiency, increasing the contribution of renewable energy sources to total power generation.

#### 4. Dispersed generation R&D needs

The dispersed generation and its related issues are considered as a possible tool which may be used for mitigating some problems of energy production and consumption.

In our readings the dispersed generation means:

- Power and heat (if applicable) generating unit based on any kind of energy conversion techniques;
- Unit is fuelled by any kind of resources available locally;
- Depending on the way of operation and local needs the unit is equipped with – over the basic instrumentation and control equipment – storage capacity (electricity and/or heat), communication and metering tools.

To have the future R&D needs of dispersed generation been understood its present status should be clarified first. The future R&D must be focused on the weakness of the DG technologies available nowadays. Table 2 collects information on the capital and operational costs, emission and efficiency of DG technologies [6]. Some notes:

- Only the main groups of DG technologies are listed;
- CCGT is used as reference centralised technology;

- Both absolute and both specific costs vary in wide range, that is why specific values were compared and relative indicators are presented;
- Efficiency is calculated for electricity produced and for heat and power if CHP option is available.

**Table 2**

*Comparison of features*

Technologies	Costs				Emission	Efficiency	
	Capital	Operational	Maintenance	Fuel		Electricity [%]	Total [%]
CCGT	+	++	++	++	++	51	90
WIND	+	+	+	-	-	25	NA
PV	+++	+	+	-	-	13	NA
RECG	++	++	++	++	++	40	85
RECD	++	++	++	++	++	40	85
STIR	+++	++	++	+	+	25	92
MT	+++	++	++	++	++	35	80
FC	+++	+++	+++	+++	+	45	85
ORC	+++	++	++	+	+	30	80

Keys to the tables:

- -: none, +: low, ++: medium, +++: high;
- NA: not applicable
- CCGT: combined cycle gas turbine;
- WIND: wind turbine;
- PV: photovoltaic panel;
- RECG: natural or biogas fuelled reciprocating engine;
- RECD: diesel or bio-diesel oil fuelled reciprocating engine;
- STIR: Stirling engine;
- MT: micro-turbine;
- FC: fuel cell;
- ORC: organic Rankine cycle (low temperature) system.

The dispersed generation in some sense is reincarnation of electricity supply solutions existed before the development of country or continent level electricity grids and at the same time DG represents and needs very high-tech solutions both as generators both as new entities on the grid formed to the needs of centralised power plants. Evaluating the performance reports of DG one can recognise that the price of these technologies is very high and there are technical and administrative barriers in front of their application. The dispersed generation related R&D requirements may be grouped around five focuses:

- Technological development;
- Fuel issues;
- Operation related development;
- Transmission and distribution network related development;



- Management and regulatory issues.

From point of view of technological development we should distinguish between matured and emerging DG technologies. Wind turbine and reciprocating engine classes are considered as matured. Several types in wide power range are available at moderate price. Revolutionary changes of their features are not expected. Slow and moderate efficiency increasing and a moderate extension of the operating wind speed range are expected in case of wind turbines. In case of reciprocating engines we have faced to similar situation. Here the R&D needs are focused on the fuel. Success of second generation biogas production development efforts is expected within a few years. With respect to the increasing food prices the importance of the oilseed based bio-diesel will probably decreasing.

The other technologies that are considered as emerging from technological and market point of view are available on the market, but their price is extremely high – comparing to traditional heat and power production possibilities. The levelised price of technology groups of Table 1. are compared to estimated average production price (EUAVPR) of EU27 and shown in Fig.6.

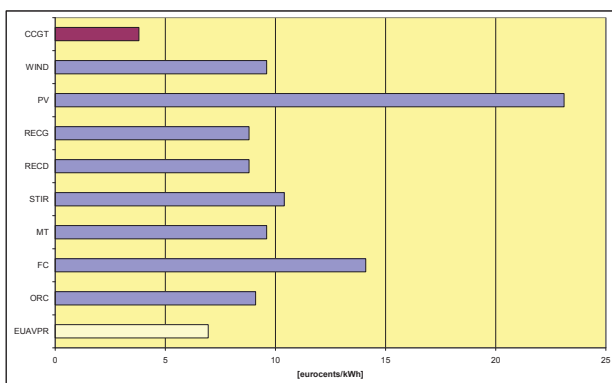


Fig.6. Levelised cost of DG technologies and reference cases

As absolutely renewable based technology, the photovoltaic systems are very popular in countries – in Germany first of all – where direct subsidies and tax refunds help the installation and the operation is also profitable, being the distribution system operators are obliged to takeover the electricity produced by PV systems. Different kinds of fuel cells have been promising for a long time, but the short lifetime and high maintenance needs are disadvantages just like ten years ago. The future research needs related to these technologies are targeting materials science and chemistry. PV based generation needs cheaper photovoltaic materials with higher efficiency. The newest results using nanotechnology (nanotubes and fullerenes in combination) are exciting. The fuel cell applications need better materials for membrane and breakthrough in hydrogen generation. Nowadays in fuel cell systems a reformer is needed to convert the natural gas or other hydrocarbon source. This method reduces the efficiency,

and pushes back the fuel cell system to hydrocarbon based technology.

Small scale PV and wind systems usually are equipped with storage facility. Battery or flywheel type storages have rapidly developed in the last decade, but we are far away from cheap, reliable, maintenance-free, high power storage facilities.

It is very difficult to estimate the time horizon of the R&D needs. Micro turbines are expected to be “plug and play” equipment for 2010. “Plug and play” means that the old boiler can be simply changed to micro turbine – or similar DG unit – without extra architectural and piping work increasing the installation costs. This feature is very important at small scale residential and/or commercial applications. Nowadays the footprint, the maintenance needs and the necessary knowledge to operation all are higher than necessary to traditional heating boilers. The newest predictions say 2015 – 2020 are the years when fuel cells and micro turbines will become mass product. Similar expectations are for small ORC systems operated at low temperature and powered by low quality fuel or low temperature waste heat.

Features and applicability of all DG technologies except wind and PV depends on quality and availability of fuel. The question of fuel was partly discussed in the previous section of centralised power plants. Natural gas and other gases and biomass can also be used at DG installations. Emphasizing the “using locally available fuel” feature of DGs we should deal with low quality biomass, biogas and combustible waste. Application of these fuels needs strong combustion engineering research and development. R&D targets:

- Development of fuel preparation, cleaning, chopping;
- Furnace development for low quality fuels, with respect to the low fire heat, optimal firing, cleaning of flue gas (cleaning and/or capturing known and new pollutants).

The combustion engineers are ready to solve these tasks, but the price of the resulted clean technology is not acceptable now. The energy price increase will help this development but the use of the low quality fuels without hi-tech furnace producing extra pollution is a real danger in poorer countries.

The DGs may be operated

- in islanded mode;
- in grid connected mode, when the electricity used locally, i.e. the amount of the power bought from the grid is reduced by the power produced by the DG and there is not any export to the grid;
- in grid connected mode, when the connection allows the bidirectional flow of power i.e. the superfluous power exported;
- in grid connected mode when all the electricity produced is sold (typical solution for PV systems without storage facility but with high takeover price).

In islanded mode the future R&D needs are basically technology related. The grid-tied operation offer further possibilities and generate further R&D needs. An individual DG installation can be optimised by power quality and energy price. More DG can be co-operated under supervision of an aggregator. Aggregator is a new entity between distribution system operator and costumers having DG facility. The aggregated DGs can offer different services: production, balancing, reactive power and ancillary services. From point of view of system operator all services can be important. The operation of aggregated DGs can be optimised along different requirements: income maximising, RES use maximising, cost minimising and so on. The possibilities for optimising are based on flexibility of production using DG and on flexibility of electricity consumption. To perform the optimal operation

- ability of real-time remote control of DGs;
- ability of metering;
- and ability of communication

are needed.

There are remotely readable meters, controllers and communication (GSM or Internet based) facilities, but these are not manufactured according to widely accepted standards and are not mass products, so they make the aggregated DGs very expensive and load the installation process with extra effort interfacing the units. Further R&D efforts are needed to produce cheap, standardised metering, communication and control units in mass production.

The efficiency is the key factor. Moreover the efficiency of all the technologies except the wind and PV changes with partial load, namely decreasing. The efficiency of production of electricity is under 50%. The efficiency of combined heat and power (CHP) generation is higher, in some case is over 95%. From point of view of individual and society level benefits the scaling of a DG is very important. The produced heat and cool can be used locally, dumping causes local thermal load on the environment. The proper management of individual or aggregated DGs needs detailed knowledge on energy costuming features of the users (load profile), on their demand flexibility and on availability of the fuel. DG players are mainly expected from commercial and residential sector, where these issues have not been discussed in details but necessary within a few years.

If dispersed generators are allocated at costumers and connected to distribution network the protection structure of the grid should be modified. The basic issues and solutions are known but technical and economical effects of these modifications are not analysed yet.

Thought the question of services was mentioned earlier it touches management and regulatory issues too. The regulatory body supported by technical organisations should determine the set of services which are useful in a power system of a country and should determine how these services can be used optimally from point of view social benefits.

## Conclusion

The unprecedented challenges facing the electric utility industry include envisioning how future uncertainties will affect technology R&D strategies. New central power generation will come from a variety of sources including fossil, nuclear and renewable resources. The uncertainty of the future fuel-mix suggests a wide range of power generation R&D needs.

Analyses show that investment in efficiency improvements to conventional power plant technologies may be more valuable than investment in immature technologies for the next first generation portfolio. The relative importance of the R&D options for the future portfolios will depend on the outcomes of the first generation.

DG could have a significant impact on the future of electricity delivery systems, including better asset utilization and less expensive system upgrades to meet new demands. Because distributed generation devices are almost exclusively fuelled with natural gas, natural gas price has a dramatic effect on the cost-effectiveness of DG projects. Much R&D remains to be performed to reduce the costs of DG technologies and improve equipment efficiency for end-users, while facilitating applications in concert with the needs of grid.

## References

- [1] Bruguach, M. et al.: Towards a relational concept of uncertainty. MOPAN Conference 2007. Leuven, Belgium
- [2] Bezdek, R. H.; Wendling, R. M.: A Half Century of Long-Range Energy Forecasts, Journal of Fusion Energy, Vol.21. No. 3/4 December 2002. p. 155-172.
- [3] Stróbl, A.: Hungarian Power Plant Survey, [www.enpol2000.hu](http://www.enpol2000.hu)
- [4] Mityusin, V. Sz., Moiseeva, L. N., Petrenya Ju. K.: Development of Russia's Power Engineering in the Long Term and New Challenges faced by the Industry of Constructing Power Machinery and Equipment. Thermal Engineering (Russian) 2008. No. 1., p. 4-6.
- [5] Rao, A. D. et al.: Power Plant System Configurations for the 21<sup>st</sup> Century, ASME, 2002. Amsterdam
- [6] Krómer, I., Bessenyei, Z.: DG technologies; Part 1; technical details: features, status & future comparison; EU-DEEP internal report, 2007.

# BDS Relationships with European Organizations for Standardization

## CEN, CENELEC, ETSI

Ivelin Burov  
Chairman of the BDS managing board



Standardization began at national level in the late nineteenth Century. In a number of different countries, industry associations came together to rationalise dimensions, specifications, test methods, safety requirements and terminologies for their mutual benefit and for the general public good. These bodies were generally non-governmental, non-profit-distributing, private associations. Because these standards bodies were generally established through industry initiatives, their work was market-lead and market-responsive.

In the electrotechnical field it was realised from the earliest days that national standards were of limited value and that international cooperation between national standards bodies was crucial for their effectiveness. IEC was established in 1906 as an association of national electrotechnical committees.

In other fields of standardization, the International Standards Association was set up in the Nineteen Twenties and with the economic liberalisation of the post-War era, and the increasing globalization of production and markets, this led to the establishment of ISO in 1947.

With the increasing integration of countries and economies within Europe there was a need for similar cooperation at a regional level and CEN and CENELEC were established in their current forms in 1961 and 1973, respectively.

The fundamental values and principles of standardization are mandated by the statutes and rules of association of the national, regional and international bodies, and are elaborated in their codes of ethics and detailed operational rules and procedures. There is a high

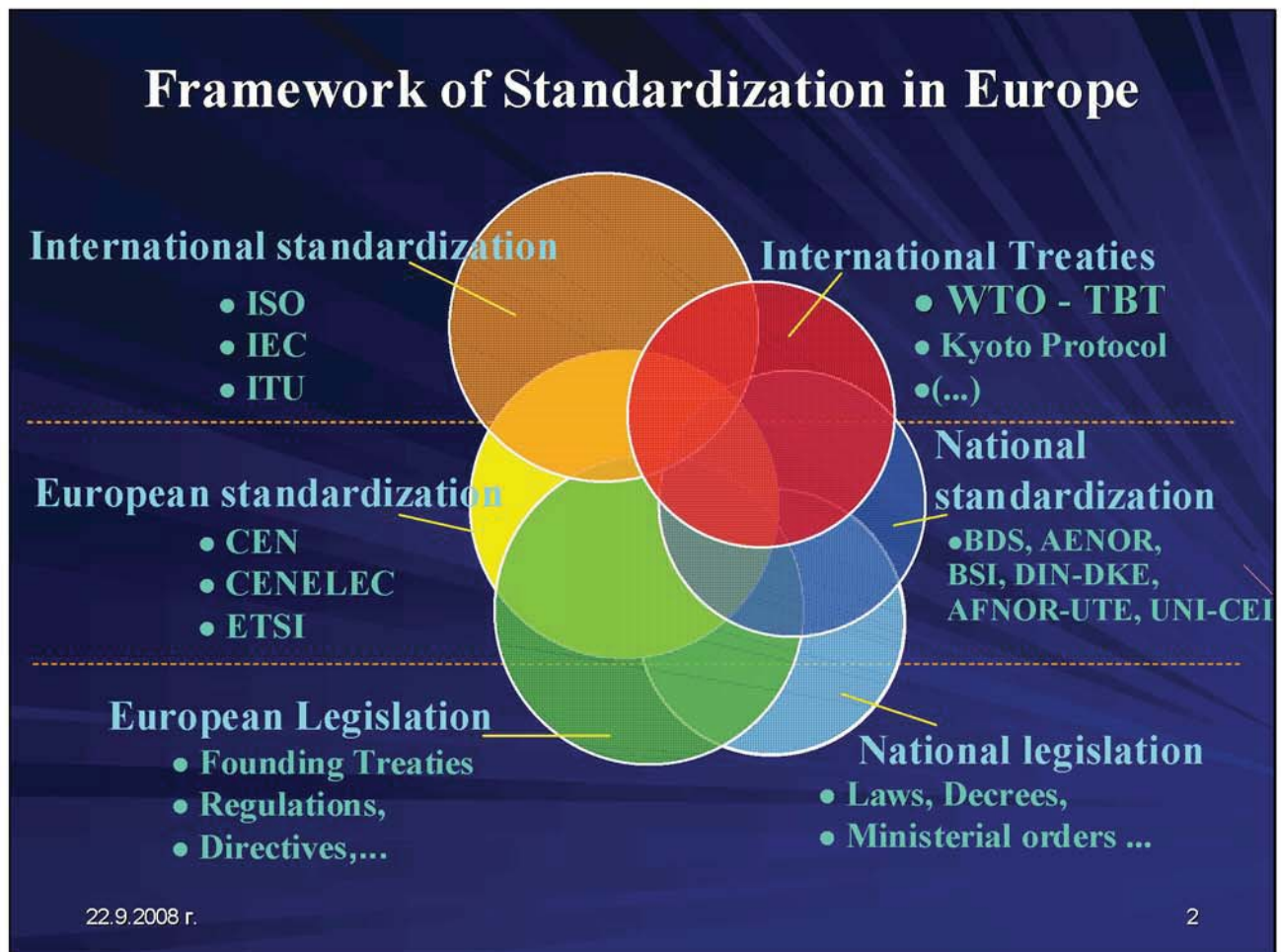


degree of commonality in these rules, despite the different legal structures of the various national standards bodies.

The trend of standardization has increasingly been from the national to the international arena. At the European level, European Standards are rapidly replacing national standards and, wherever appropriate, European Standards are derived from, or developed in parallel with, International Standards under the accords established between CEN and ISO (the Vienna Agreement) and CENELEC and IEC (the Dresden

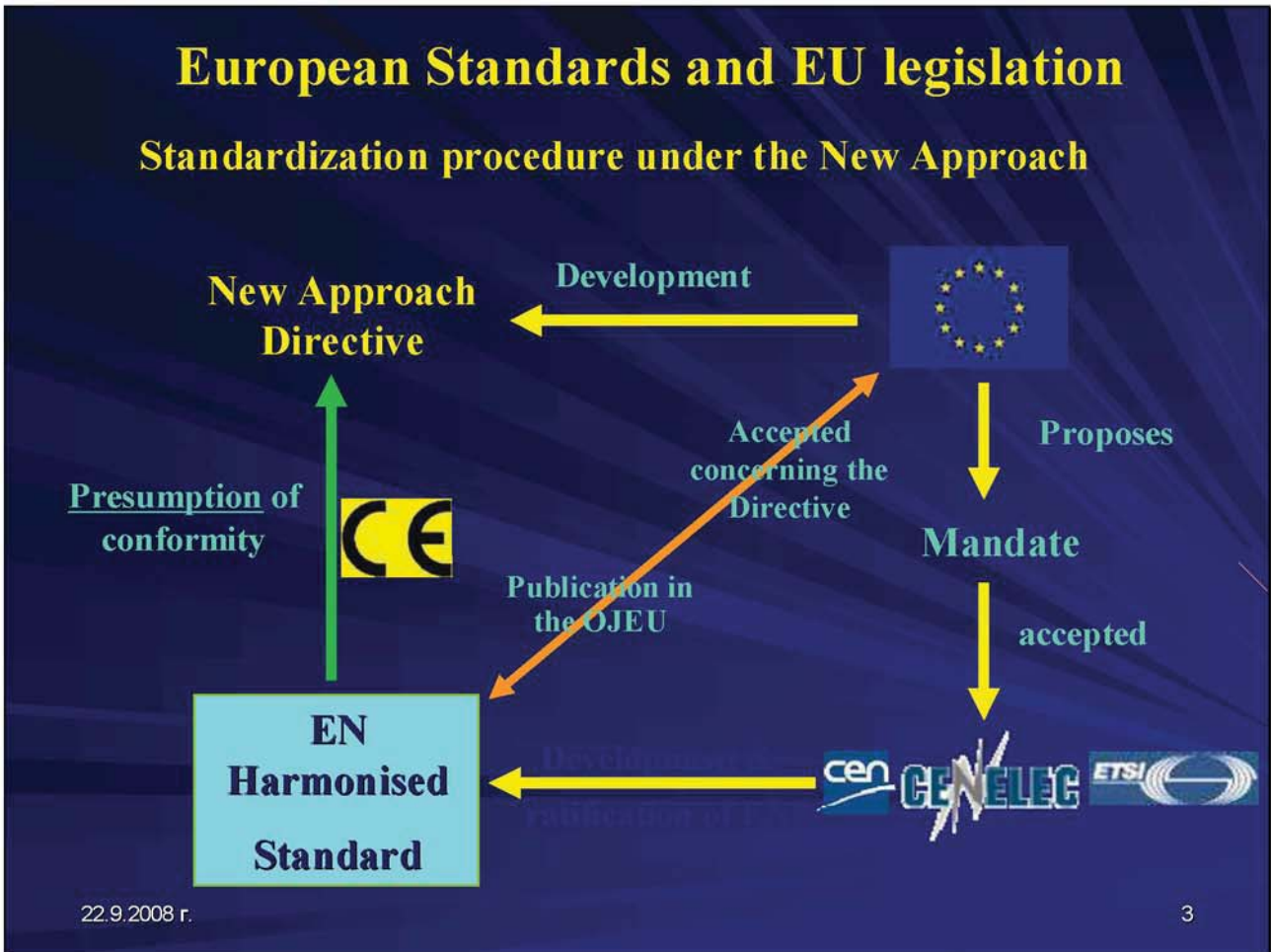
Agreement). This trend is anticipated to continue and intensify.

Standards have also been identified by the WTO as a key element in promoting competition and opening up world markets, by reducing and ultimately eliminating technical barriers to trade. This requirement has also been incorporated into the rules and statutes of standards bodies at all levels and they are all signatories to the Code of Good Practice for standardising bodies, annexed to the WTO TBT Agreement.



Harmonized standards are European standards (EN), produced under mandate from the European Commission (EC) or from the European Free Trade Association (EFTA) for supporting the essential requirements of "New Approach" Directives. Compliance with Harmonized standards is voluntary. Nevertheless it remains the most efficient way to demonstrate compliance of products with the corresponding essential requirements of the EC directives. Annex Z of each standard, developed under mandate provides information for which essential requirements of directives shall be applied the respective harmonized standard.

In order to become harmonized standards the Member States have the task to translate the titles of standards into their national language and send them via CEN/CENELEC to the EC and EFTA Secretariat for publication of the reference in the Official Journal of EU. Thus the European standards, developed by CEN or CENELEC, following a mandate issued by the EC become harmonized standards and since their date of publication they can be applied for providing presumption of conformity of products to the corresponding EC directives.



CEN, the European Committee for Standardization, was founded in 1961 by the national standards bodies in the European Economic Community and EFTA countries.

Now CEN is contributing to the objectives of the European Union and European Economic Area with voluntary technical standards which promote free trade, the safety of workers and consumers, interoperability of networks, environmental protection, exploitation of research and development programmes, and public procurement.

CEN is a non-profit making technical organization set up under Belgian law.

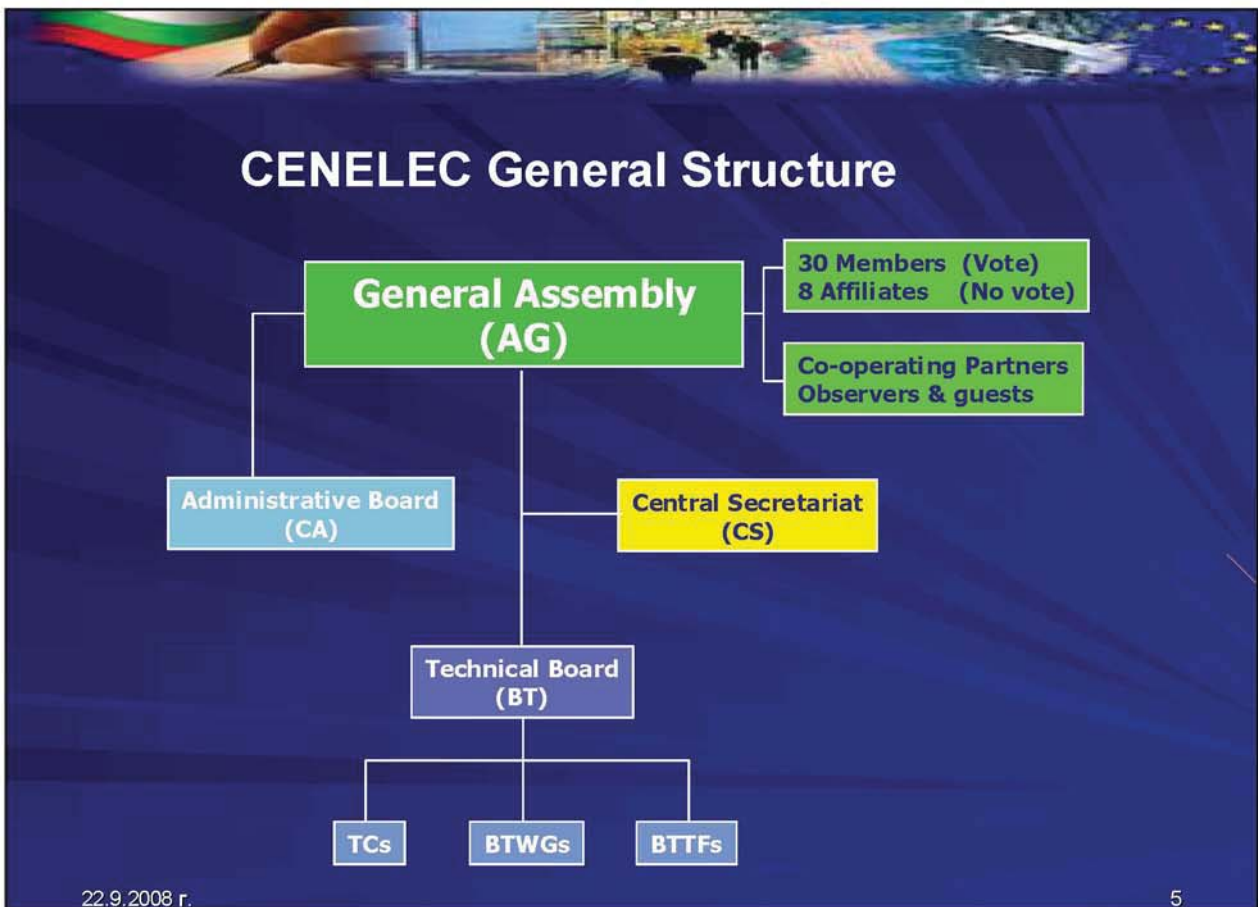
CENELEC, the **European Committee for Electrotechnical Standardization**, was created in 1973 as a result of the merger of two previous European organizations: CENELCOM and CENEL. Nowadays, CENELEC is a non-profit technical organization set up under Belgian law and composed of the National Electrotechnical Committees of 30 European countries.

In addition, 8 National Committees from neighbouring countries are participating in CENELEC work with an Affiliate status.

CENELEC members have been working together in the interests of European harmonization since the 1950s, creating both standards requested by the market and harmonized standards in support of European legislation and which have helped to shape the European Internal Market. CENELEC works with 15,000 technical experts from 30 European countries. Its work directly increases market potential, encourages technological development and guarantees the safety and health of consumers and workers.

CENELEC's mission is to prepare voluntary electrotechnical standards that help develop the Single European Market/European Economic Area for electrical and electronic goods and services removing barriers to trade, creating new markets and cutting compliance costs.



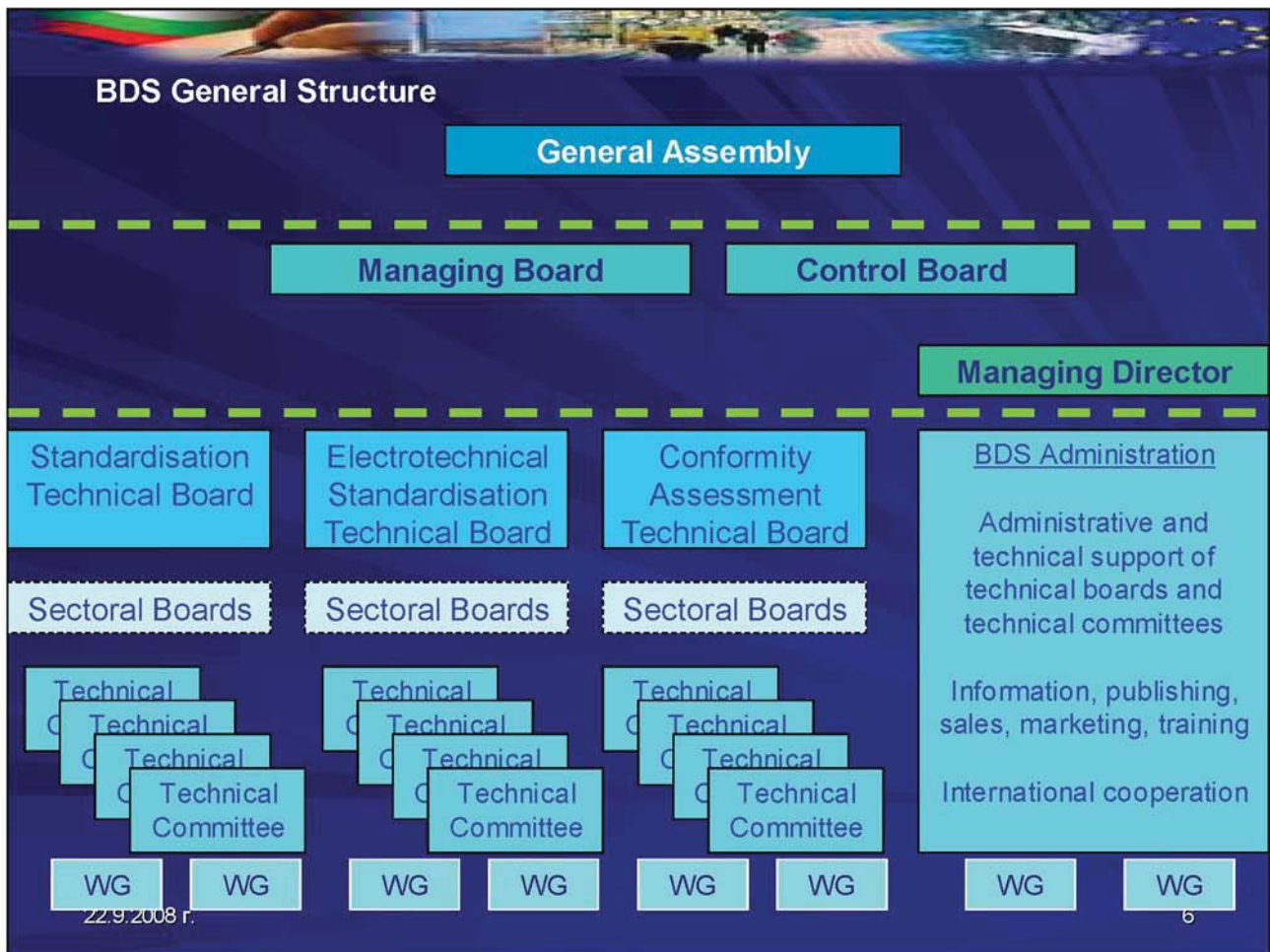


The Bulgarian Institute for Standardization (BDS) is the National Standards Body in the Republic of Bulgaria. BDS has been created according to the Law on National Standardization, published in 2005 (State Gazette, issue 88 of 4 November 2005). The Bulgarian Institute for Standardization is an independent non-governmental organization whose members are all interested in standardization activities parties. Superior governing body is the General Assembly, electing the members of the Managing Board among the representatives of the organizations-members of BDS. As a non-profit organization BDS operates for the public benefit of society.

BDS activities are concentrated not only on the

continuous improvement of national standardization system and on the attraction of new participants in the national standardization activities, but also on the better functioning and organization of BDS work.

Taking into account the principles of standardization – equal footing, transparency and consensus, BDS makes efforts to balance the interests of all stakeholders both in private and public sectors which means clearly established balanced participation in the national standardization process of producers, traders, suppliers, consumers, research and academic establishments, conformity assessment bodies, state bodies and other public organizations.





CENELEC has granted Membership status with full rights and obligations, from 6 January 2007 onwards, to BDS - The Bulgarian Institute for Standardization.



BDS, becomes the 30th National Member of the European Committee for Standardization (CEN) from 15 January 2007



22.9.2008 г.

7

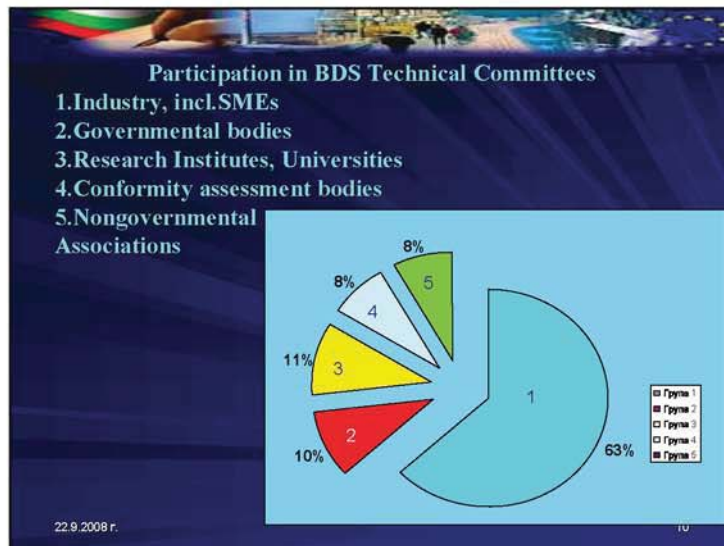
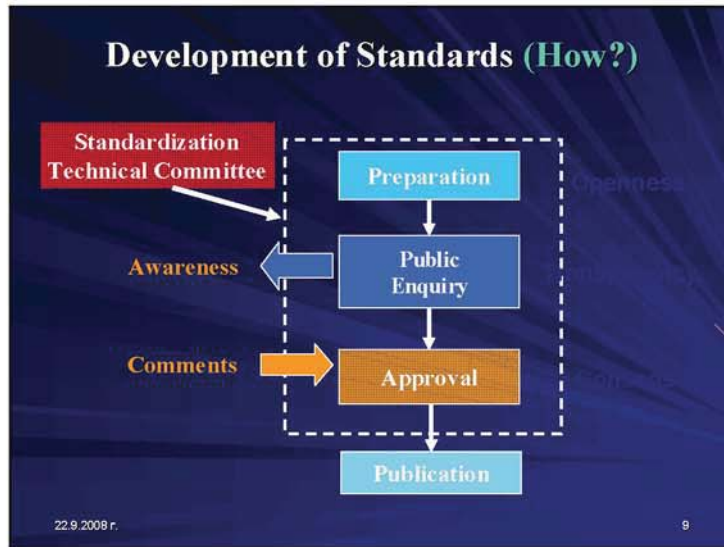
**BDS IS NOT A MEMBER OF ETSI**



**BUT:**  
**BDS/TC 47 and**  
**BDS/TC 57**  
**are working in the area of ETSI**

22.9.2008 г.

8



**WWW.BDS-BG.ORG**

**INFORMATION CENTER**  
**TEL: 02 8174 523**  
**FAX: 02 873 55 97**  
**INFO @ BDS-BG.ORG**  
**THANKS FOR YOUR ATTENTION!**

22.9.2008 r. 11

# Finite Element Analysis of Electromagnetic Phenomena in a Small Three-Phase Transformer

Mihail Digalovski and Lidija Petkovska

**Abstract:** In the paper is presented the Finite Element Analysis (FEA) of electromagnetic phenomena in a small three phase transformer under various operating conditions: no-load, rated load and short circuit. For these regimes, a series of finite element simulations are performed and magnetic field distribution of the transformer is obtained. The magnetic flux density is calculated numerically and presented on charts. The special emphasize is put on calculation the magnetizing and leakage inductance of the transformer.

**Keywords:** three-phase transformer, finite element method, magnetic field, flux density, inductances.

## Introduction

In the analysis of electromagnetic devices and, in particular the open-core transformers, the electromagnetic phenomena are always non-linear, due to the presence of ferromagnetic materials in their topology. In order to get better understanding of the electromagnetic behavior of an investigated electromagnetic device, it is essential to predict as accurate as possible the magnetic field distribution in its interior. The calculation of magnetic field in an electromagnetic device, with classical approach by using analytical circuit theory, is practically impossible. In this sense, when using traditional methods for field problem analysis of a small three phase transformer, the magnetic field is known only approximately; the determination of characteristics is based on a rough idea of the field distribution in different parts of the transformer magnetic core. Consequently, this methodology appears to be improper. Recently, the Finite Element Method (FEM) has been widely proved to be efficient when dealing with complicated geometries and in particular, with nonlinear field problems.

The magnetic field is described by well known system of Maxwell's equations; because of the nonlinearity of the core materials in the transformer structure, equations have to be solved iteratively and simultaneously. The computational results presented in the paper are obtained by using the Finite Element Method (FEM).

## Object of Study

The object of study is a small three phase laboratory core-type transformer in an open geometry design; there is a possibility to connect both primary and secondary windings either in star (wye) or in delta connection. In the paper, the investigated transformer is with wye-wye connections; the rated data for this case are:  $S_n=500\text{ VA}$ ;  $U_1/U_2=380/42\text{ V}$ ;  $I_1/I_2=0.78/6.9\text{ A}$ ;  $f_n=50\text{ Hz}$ ;  $Yy0$ . The front view of the transformer is presented in Fig.1.



Fig.1. Front view of the transformer

## FEM Model of the Transformer

The FEM calculations are carried out by using the 2D FEMM software [1]. In fact, the problem is more 3D than 2D, but the three-dimensional effects of the transformer topology are taken into consideration when developing the FEM model of the transformer. The 2D field planar problem is the most suitable to the transformer geometry. The time-harmonic FEM approach, at rated frequency  $f_n=50\text{ Hz}$ , is employed.

First, the FEM model of the transformer is derived. Due to the open geometry of the studied transformer, the domain boundary is defined away from the core and windings. All material properties are written in the corresponding input databases. Windings are defined with number of turns and wire diameter; for magnetic core the exact magnetizing characteristic is included. Boundary conditions are of the Dirichlet type (1 order); they are set on the outer lines of the domain. Three-phase currents being displaced in time for  $2\pi/3$  are assigned in a way that the mid core winding is carrying the referential (rated) current; FEM model is presented in Fig.2.

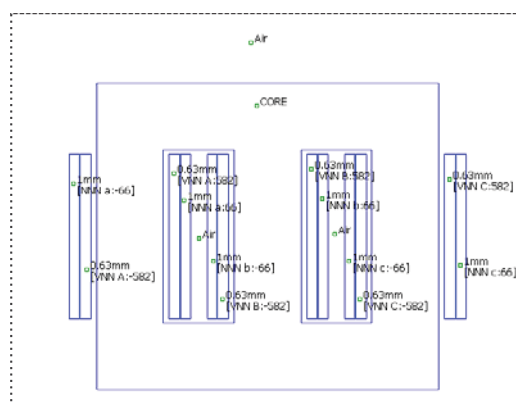


Fig.2. FEM model of the transformer



In order to improve the FEM model of the transformer and to assure getting more accurate computational results, the transformer was thoroughly tested in the laboratory. All relevant operating regimes were investigated and the windings' current at no-load, rated load and short-circuit were recorded. Also, there was determined the number of windings' turns. The results obtained from testing are used as input data in the more reliable FEM model of the transformer. The magnetizing characteristic of the core was measured, too; it is presented in Fig.3.

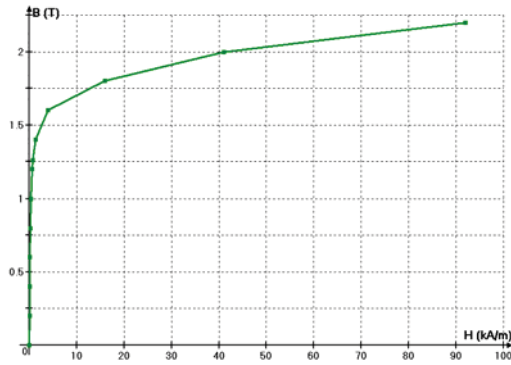


Fig.3. Magnetizing characteristic of the transformer core

By running the pre-processor in the FEMM software, the finite element mesh is generated. The mesh presented in Fig.4 is spread in the whole investigated domain; it is consisted of  $N=14,266$  nodes and  $E=28,249$  elements.

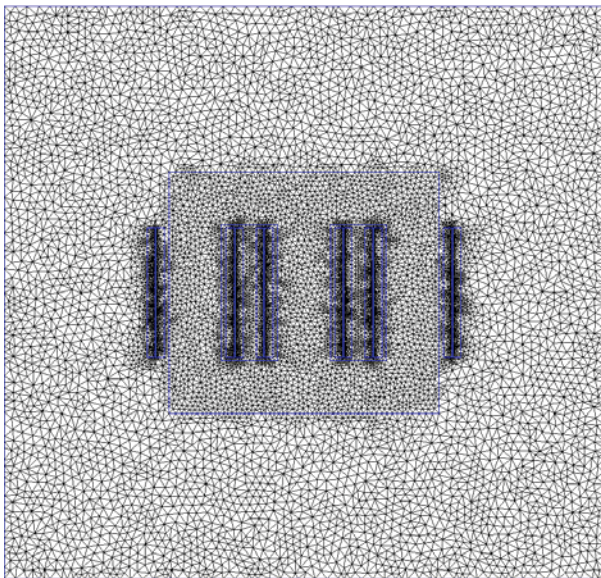


Fig.4. Finite element mesh in the whole domain

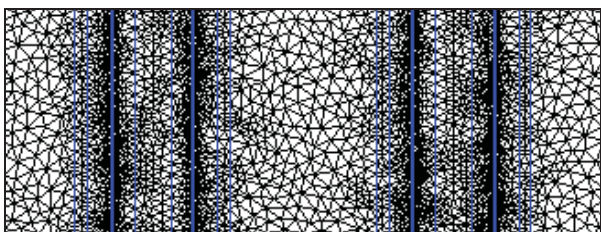


Fig.5. Part of the mesh in the domains of interest

When dealing with calculation of the winding leakage inductances, the domains of interest are located in the winding gaps. In order to provide correct numerical computational results, the mesh in these regions should be dense enough; the case is presented in Fig.5.

### FEM Results

The knowledge of electromagnetic phenomena in the transformer could serve as an excellent guide not only for carrying out the analysis of steady-state operating modes, but especially for transient regimes, where the exact knowledge of the transformer parameters is very important issue. Consequently, the computational results of the magnetic field solution will be employed for numerical determination of the transformer parameters.

For these purposes, the series of FEM simulations are performed [2]. Different steady-state operating regimes are analyzed. The presentation of the most interesting results is given in continuation.

First, the conditions in the investigated transformer at no-load operating regime are analyzed. The current is flowing in the primary winding only, while the secondary is open-circuited. The exact value of the input current in the transformer FEM model is determined from testing. The magnetic field seen through flux density distribution and flux-lines in the transformer is presented in Fig.6.

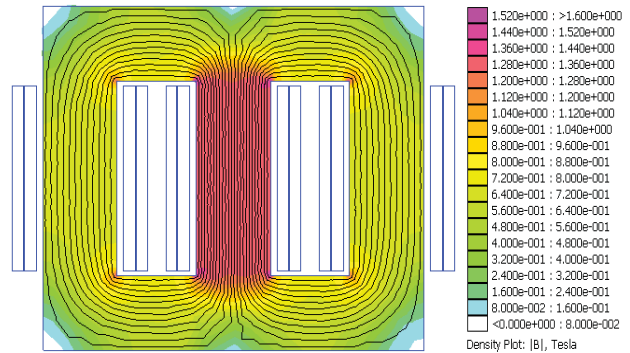


Fig.6. Magnetic field distribution at no-load operation

In the analyzed regime, the current of phase B (in the middle core leg) is adopted to be with maximum value, while in the side legs (phase A and phase C) the currents are with an opposite sign, having the half value of the ampere-turns. Consequently, as seen in Fig.6, the middle leg of the magnetic core will be the most saturated.

When the transformer is operating at rated load, the distribution of the winding currents, compared to the previous regime, is quite different. In this case, the both windings, primary and secondary, are energized with the corresponding values of rated currents. The influence of the magnetizing current is taken into consideration; thus, the angular displacement between winding currents of the same phase is not equal to  $180^\circ$ . The magnetic field in the transformer core is presented in Fig.7; obviously, it is almost the same as at no-load regime. The explanation can be found in the fact that the same magnetizing current is exciting the magnetic field in the transformer core.



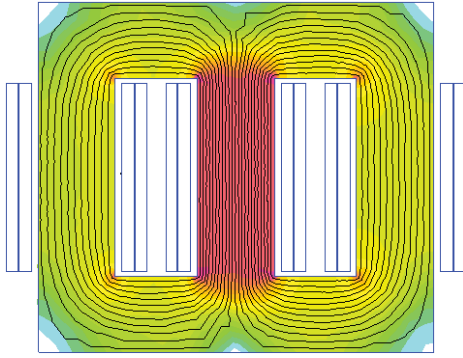
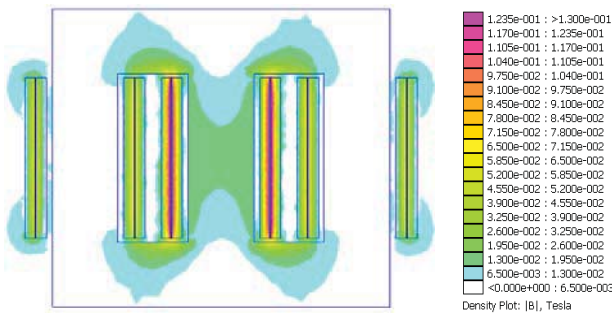


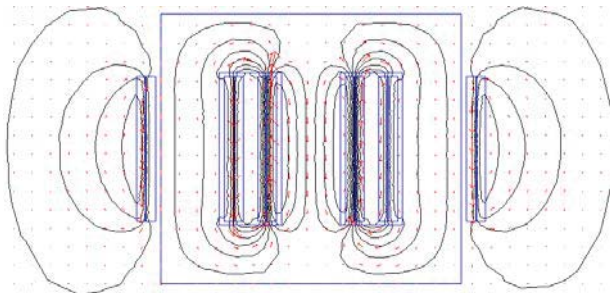
Fig.7. Magnetic field distribution at rated load

The bolted short circuit at the transformer terminals while it is supplied by rated voltage, due to the currents significantly exceeding the limited values, is completely damaging the device; on the other hand, this regime is good to be employed for determination of the windings' leakage inductances. In fact, for the same purpose one can use the laboratory testing results at reduced voltage, but this case is not quite corresponding to the real occurrences and the results are not reliable.

One of the main advantages of the FEM simulations is the possibility to calculate the leakage inductance of the transformer windings as they appear in the reality; we are going to use the simulation of the bolted short circuit operating regime. The magnetic flux distribution in two different ways is presented in Fig.8 (a) and (b).



(a) Flux density in the domain



(b) Flux lines and flux density vector

Fig.8. Magnetic field distribution at bolted short-circuit

In this operating regime the transformer core is completely demagnetized, what can be easily noticed from the legend attached to the figure (a); while in the previous two figures the maximum value of the flux density is 1.6 (T), here above it is only 0.13 (T).

The flux lines, as well as the vector of the flux density for the same simulation are presented in figure (b); it is evident that the main part of the equipotential lines ( $A=\text{const.}$ ) is gathered in the windings gaps, thus defining the leakage field of the transformer and the corresponding winding leakage inductances.

### FEM Analysis

By running the postprocessor in *FEMM* software it is possible to calculate numerically a diversity of integrals: along a line, on a surface and in a volume. The skilled and experienced user certainly can easily compute a diversity of characteristics and parameters: leakage flux, flux linkages, flux density, magnetic field energy and coenergy, forces, inductances etc [3].

The FEMM software is enabling in the simplest way to determine the most important characteristics and parameters of the investigated transformer.

### No-load Flux Characteristic

To obtain the no-load characteristic of the transformer we calculate the flux along the mid-line  $\ell$  of the mid-leg of the core, as marked with blue arrows in Fig.9.

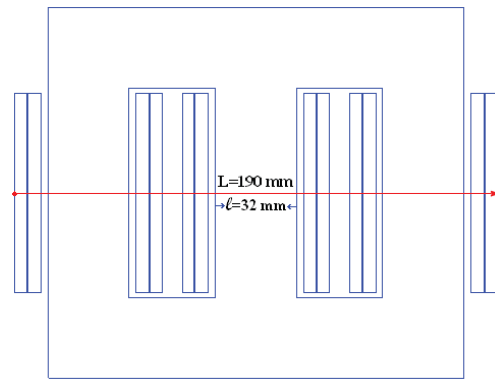


Fig.9. Lines defining mid-core flux and flux density distribution

The values of magnetic vector potential in each point of the investigated domain obtained from FEM solver are used in the FEM post-processor for calculation of the flux in the middle core leg. From the magnetic field theory for closed and bounded systems, the flux is computed by numerical integration of the following equation:

$$(1) \quad \Phi_g = \int_{\Sigma} \text{rot} \mathbf{A} \cdot d\mathbf{S} = \oint_C \mathbf{A} \cdot d\mathbf{r} = \int_{\Sigma} \mathbf{B} \cdot d\mathbf{S} .$$

The integration path is the width of the mid-leg  $\ell$  as indicated in Fig.9. The results of numerical calculations are given in Table 1, while the characteristic is presented in Fig.10. The flux  $\Phi$  is presented in dependence of the variation of primary current, while the secondary winding is kept opened.

Table 1

No-load characteristic

$I_0$ (A)	0.02	0.06	0.12	0.18	0.24
$\Phi$ (mVs)	0.205	1.145	1.653	1.803	1.881

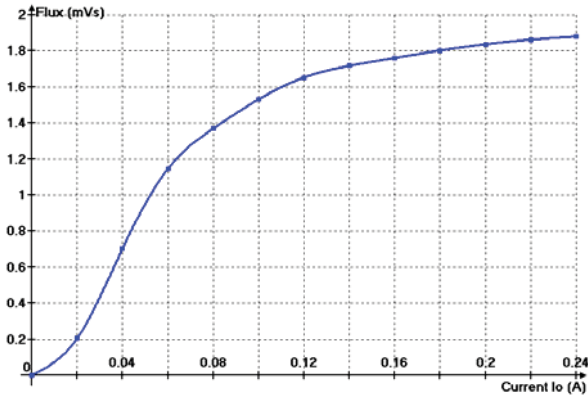


Fig.10. No-load flux characteristic of the transformer

### Flux Density Distribution

For numerical computation of the flux density  $\mathbf{B}$  it is used the basic relation introduced in the definition of the magnetic vector potential  $\mathbf{A}$ , i.e.:

$$(2) \quad \nabla \times \mathbf{A} = \mathbf{B}$$

The FEMM software package enables comprehensive presentation of the spatial distribution of magnetic flux density along an arbitrary selected line. In the next figures the distribution along the mid-core line, marked in red in Fig.9, is presented. At the same operating regimes of the transformer, as previously defined no-load, rated load and bolted short-circuit, the characteristics are presented in Fig.11, Fig.12 and Fig.13, respectively.

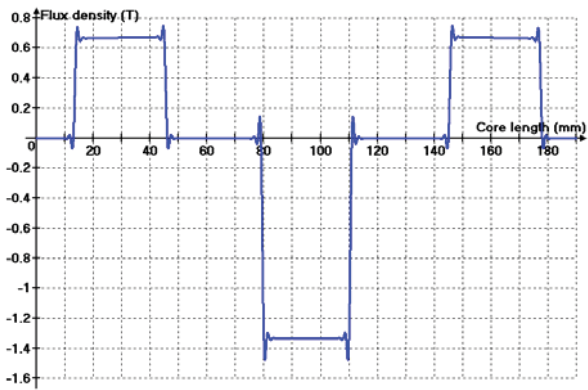


Fig.11. Spatial distribution of magnetic flux density at no-load

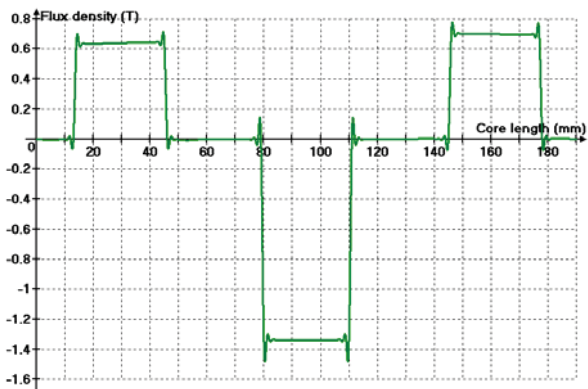


Fig.12. Distribution of magnetic flux density at rated load

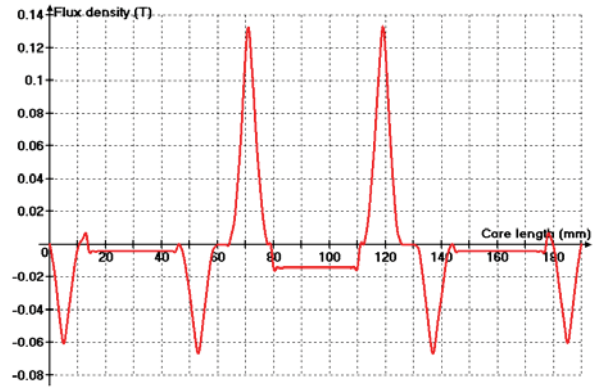


Fig.13. Distribution of magnetic flux density at short circuit

The above presented diagrams are used for carrying out the profound analysis of magnetic field properties of the transformer, regarding both intensity and shape.

### Computation of Inductances

When nonlinear materials are involved in an analyzed geometry and the core is saturated, the computation of inductances gets somewhat more complicated and is quite dependent on the particular case.

There exist a number of well established numerical methods of finding inductances and, generally speaking, all work very well. The values of inductance determined from FEM computational results usually agree well with measured results. Results of inductance calculation converge quickly with decreasing mesh size, what means with increasing the mesh density. Consequently, when analyzing the open transformer by FEM, a particular attention is paid on the windings regions, where the main change of the magnetic occurrences takes place; the case has been shown in Fig.5.

### Magnetizing inductance

Depending of the analyzed problem, one can compute either apparent or differential magnetizing inductance, which is due to the nonlinear characteristic of the core materials a function of the currents  $i$  flowing at *no-load* operating regime through the transformer windings.

The magnetizing inductance of the transformer can be calculated in several ways, by using different numerical approaches based on the FEM results [5-8].

First, the inductance  $L_m$  will be computed numerically from the magnetic energy in the domain of transformer core. Once the postprocessor of the software FEMM has been run, the magnetizing inductance can be derived from the *magnetic energy equation* in a form:

$$(3) \quad W_m = \frac{1}{2} L_m I^2$$

The FEM approach to obtain *stored magnetic energy* in the non-linear domains is via the integral:

$$(4) \quad W_m = \frac{1}{2} \int_V \mathbf{B} \cdot \mathbf{H} \, dV$$

The integral has to be taken over the *entire* problem domain and is directly computed from energy integration in FEMM post-processor. The magnetizing inductance is calculated from the expression derived from equations (3) and (4) in a form:

$$(5) \quad L_m = \frac{2 \cdot W_m}{I^2} = \frac{\int_V B \cdot H \, dV}{I^2}$$

The magnetizing inductance  $L_m$  is calculated for the middle leg of the transformer core, where is placed the phase winding  $B$ ; due to the symmetry, the result will be obviously valid for the other two phases, as well.

At no-load, when the magnetizing current in the windings is  $I_0$ , the magnetic energy accumulated in the mid-leg is  $W = 0.05996$  (J), thus determining the value of magnetizing inductance  $L_m = 3.58$  (H); consequently, the magnetizing reactance, calculated at the rated value of the frequency  $f_n = 50\text{Hz}$ , will be  $X_m = 1124.12$  ( $\Omega$ ).

### Computation of leakage inductances

When computing the leakage inductance of windings, in order to take into account electromagnetic phenomena in the whole studied domain of the transformer, due to its open geometry in the surrounding area, it is requested to determine not only leakage fluxes in the coils windows in X-Y cross-section, but also the extra flux components which are passing on the surface Z-Y orthogonal to it.

The computational procedure for calculation leakage inductance  $L_\sigma$  of the transformer windings is developed in continuation. In this case, one uses the magnetic energy stored in the regions carrying out excitation currents, i.e. the windings domain. Another way of expressing the total magnetic field energy in the magnetic problems is via the following integral:

$$(6) \quad W_m = \frac{1}{2} \int_V \mathbf{A} \cdot \mathbf{J} \, dV$$

Setting the last expression for magnetic energy and equation (3), written in terms of  $L_\sigma$ , equal to one another and solving them yields:

$$(7) \quad L_\sigma = \frac{\int_V \mathbf{A} \cdot \mathbf{J} \, dV}{I^2}$$

For the example problem,  $J$  is nonzero only inside the coils, so the  $\mathbf{A} \cdot \mathbf{J}$  integral need only be taken over the coils. But, it should be pointed out that FEMM software [1] is the 2D program, so when dealing with leakage fields we strongly suggest taking into consideration the two projection planes of the transformer: first one is the X-Y and the second is Z-Y plane. Doing calculations in this way, the two components of the leakage inductance are determined: the component  $L_{\sigma X-Y}$  and  $L_{\sigma Z-Y}$ . At the end, these two components are added to each other and the more accurate value of the leakage inductance is computed. In Fig.14 (a) and (b) are indicated in green the domains where the calculations of  $L_\sigma$  are performed.

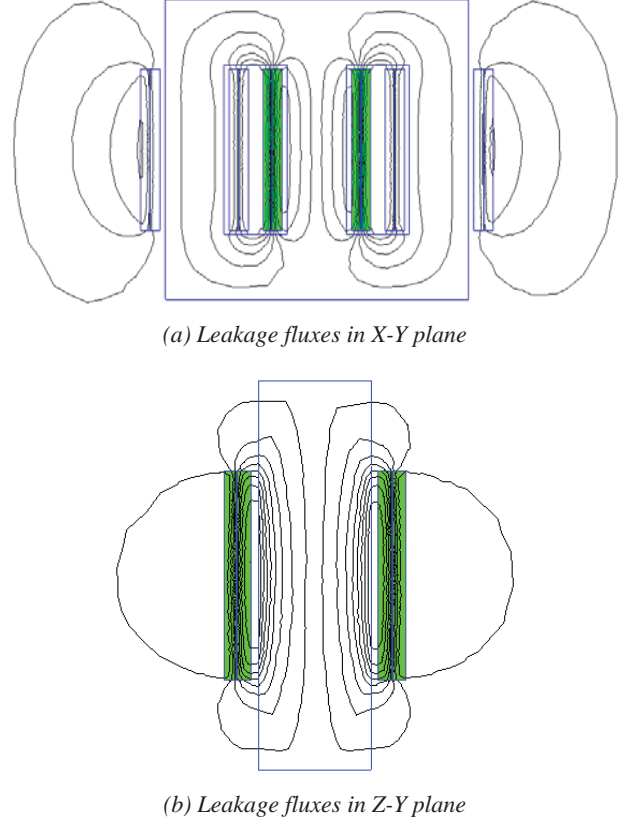


Fig.14. FEM models for leakage inductance calculation

The leakage fields in a transformer are the most evident at bolted short circuit regime, when the magnetic field is distributed just in the windings gaps, as it can be noticed in Fig.14 (a) and (b) for the both analyzed planes.

In these figures, one can find the justification of the authors' suggestion to consider the both planes where the leakage fields take place. Namely, although for 2D planar field problems it is accepted the plane X-Y to be usually the main, the magnetic vector potential at short circuit current  $I_{Ik} = 14.65$  A is with value  $A_{max} = 0.515$  mVs/m; on the other hand, at the same operating regime the value of the leakage magnetic field in the Z-Y plane is  $A_{max} = 0.637$  mVs/m, what means higher field intensity of 23.7%.

Similarly as previous, in the case of calculating the magnetizing inductance, we are using the central leg of the transformer core and the currents flowing in the windings of the phase B. The currents are set to values corresponding to the bolted short circuit regime of the analyzed transformer.

Obtaining directly from the FEMM post-processor in the current carrying domains the values of the integral  $\int_V \mathbf{A} \cdot \mathbf{J} \cdot dV$ , for the leakage fields displayed in X-Y and Z-Y plane separately, the leakage inductance per phase is calculated by using equation (7); the computational results are given in continuation.

$$L_{\sigma X-Y} = 1.663 \text{ (mH)}$$

$$L_{\sigma Z-Y} = 2.414 \text{ (mH)}$$



The final result of the performed calculations yields to the value for the total winding leakage inductance:

$$L_{\sigma} = L_{\sigma X-Y} + L_{\sigma Z-Y} = 4.077 \text{ (mH)},$$

while the leakage reactance becomes:

$$X_{\sigma} = \omega L_{\sigma} = 2\pi f_n L_{\sigma} = 1.281 \text{ (\Omega)}.$$

### Comparative Analysis

The paper is focused on electromagnetic field analysis of the transformer through the magnetic field properties and parameters. The studied transformer at the beginning was recalculated in accordance with the rated data and known parameters; in this way, by an analytical approach all relevant parameters and characteristics for transformer performance evaluation have been determined.

Afterwards, the transformer has been thoroughly tested in the laboratory and the operating regimes used in the FEM simulations were experimentally verified; the same calculated parameters and characteristics have been measured. The output results obtained from the FEM simulations are numerically calculated; they are excellent basis for carrying out the comparative analysis of the studied transformer.

The magnetizing reactance as well as the winding leakage reactance per phase, calculated by the three mentioned above approaches are presented comparatively in Table 2

Table 2  
*Comparison of the results*

Method Parameter	FEMM	Analytical calculation	Measured
$X_m$ (Ω)	1124.12	1209.2	1201.63
$X_{\sigma}$ (Ω)	1.281	2.78	1.64

The results of magnetizing reactance obtained by the three methods are showing excellent agreement. Despite this fact, calculation of a leakage reactance is erroneous; the explanation can be found in the fact that analytical methods are not quite precise, while the FEM calculations when dealing with planar field problems do not take into account the cylindrical shape of the windings.

### Conclusion

In the paper the 2D FEM simulation procedures of a small three-phase transformer is presented. Three typical steady-state operating regimes are analysed. The most important parameters and characteristics are determined and full electromagnetic field analysis is accomplished.

The FEM has been proved as powerful tool for electromagnetic field analysis. The future task is foreseen to be the transient performance analysis of the studied transformer. This work, and in particular the presented results, will be used as good basis and relevant guide.

### References

- [1] D. Meeker, Finite Element Method Magnetics-FEMM, User's Manual, Vers. 4.2, 2007; <http://femm.foster-miller.net>.
- [2] L. Petkovska, G. Cvetkovski, V. Sarac. Different Aspects of Magnetic Field Computation in Electrical Machines, Book of Abstracts of 10th International Symposium IGTE'2002, p.p. 73; on CD pp. 1-6, Graz, Austria, 2002.
- [3] L. Petkovska, G. Cvetkovski: Different Approaches to Inductance Calculation of E-I Gapped Iron Core Inductor, Journal Przeglad Elektrotechniczny, PE Vol. 82, No. 5, pp. 36-40, Warsaw, Poland, May 2006.
- [4] F. Mlakar, I. Kloar. Small Transformers and Inductors, Manual for Electrical Engineers, Vol. 8, Published by Elektrotehniski Vestnik, Ljubljana, Slovenia, 1970.
- [5] N. Bianchi. Electrical Machine Analysis Using Finite Elements", Book, pp. 141—165, CRC Press, Taylor & Francis Group, Boca Raton, FL, USA 2005.
- [6] Z. Kolondzovski, L. Petkovska. Identification of a Synchronous Generator Parameters Via Finite Element Analysis, in the Book of Abstracts of the 11<sup>th</sup> International Symposium on Numerical Field Calculation in Electrical Engineering – IGTE'2004, p.p. 96; full manuscript published on CD p.p. 1-6, Seggauberg (Graz), Austria, 2004.
- [7] L. Petkovska, G. Cvetkovski: "Different Approaches to Inductance Calculation of E-I Gapped Iron Core Inductor", Journal Przeglad Elektrotechniczny, Vol. 82, No. 5, pp. 36-40, Warsaw, Poland, May 2006.

### Biographies



**Mihail Digalovski** was born on September 16, 1980 in Skopje, Republic of Macedonia. He studied the curriculum of Industrial Power Engineering and Automation at the Faculty of Electrical Engineering from the Ss. Cyril & Methodius University in Skopje. He graduated in 2004 and received the BSc EE degree. At the moment he is a PhD student of the course of Electrical Machines and Transformers at the Faculty of Electrical Engineering & IT.

His field of interest includes transformers, electrical machines and drives, electric power measurements and diagnostic.

Mihail Digalovski is with the Faculty of Electrical Engineering and Information Technologies, Ss. Cyril and Methodius University, Karpos II b.b., 1000 Skopje, Macedonia (e-mail: [mdigi2006@yahoo.com](mailto:mdigi2006@yahoo.com)).



**Lidija Petkovska**, has received the BSc EE in 1967 from Faculty of Electrical Engineering, University of Belgrade (Yugoslavia), while the MSc EE in 1980 and Doctoral degree in 1991 from the Faculty of Electrical Engineering at Ss. Cyril & Methodius University in Skopje. Today she is a full professor at the Department of Electrical Machines, Transformers and Apparatus and a Head of the Laboratory of Electrical Machines.

Her field of interest covers wide area of problems including transformers and electrical machines, and in particular design, testing, simulations and FEM calculations. She has published more than 220 papers in scientific journals and conference proceedings.

Lidija Petkovska is with the Faculty of Electrical Engineering and Information Technologies, Ss. Cyril and Methodius University, Karpos II b.b., 1000 Skopje, Macedonia (e-mail: [lidijap@feit.ukim.edu.mk](mailto:lidijap@feit.ukim.edu.mk)).

# Iron loss characterization and prediction in electrical machines

Afef Kedous-Lebouc

**Abstract:** This paper presents an overview of iron loss modeling in electrical machines and the experience of the G2Elab in the field during this last decade. The iron loss estimation method developed uses Flux2D™ finite element simulation and a dynamic hysteresis model called Loss Surface model (LS model). The method is applied to several machines working at load or no load operations. In most cases, the iron loss predictions are better than 20 %. The result obtained for a high speed machine is developed in more details in this paper.

**Keywords:** Electrical machines, dynamic Hysteresis model, iron loss, finite element simulation.

## Introduction

Nowadays, a precise determination of iron loss in electrical machines is a significant sizing factor to improve and to develop new, original and high efficiency structures. This determination can be achieved by computation and requires both a better understanding of magnetic material operating in machines and reliable and robust methods for iron loss estimation. This paper presents an overview of iron loss modeling in electrical machines and the experience of the G2Elab in the field during this last decade.

## Working conditions in Electrical machines and non conventional magnetic material behavior

In electrical machine, the magnetic circuit is submitted to hard working conditions: saturation, non sinusoidal waveform and high frequency harmonics, unidirectional or multidirectional excitation, mechanical stress, etc. This systematically leads to additional iron losses which can not be correctly predicted with classical material characteristics because of the high dependence of soft magnetic materials to excitation conditions [1,4]. Figures 1 and 2 show examples of the waveforms observed in an electrical machines and how the magnetic material behaves. This highlights its sensitivity to the working conditions.

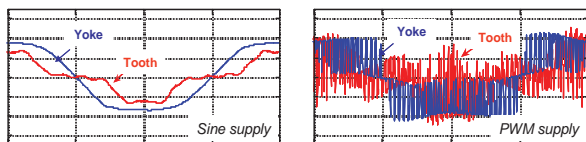


Figure 1: Induced emf measured around a tooth and a yoke of an induction motor supplied by a sine and PWM voltage

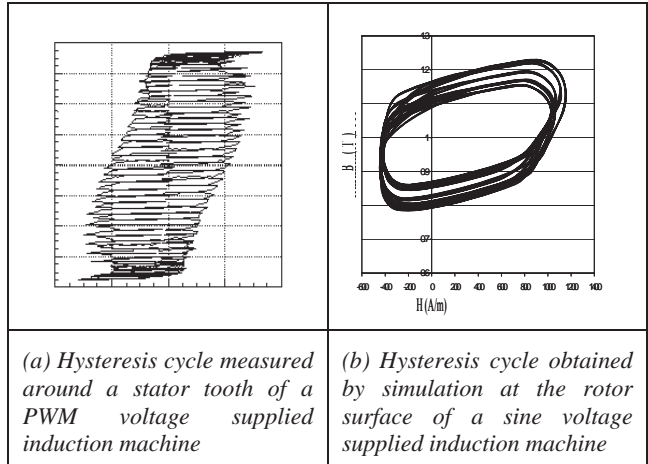


Figure 2: Magnetic behaviors of electrical steels inside an induction machine

## Iron loss modeling in electrical machines

Several approaches have been developed during this last decade in order to evaluate the iron loss in electrical machines [2,3],[5,8]. They are based on analytical or numerical magnetic loss or hysteresis models. For magnetic loss model, we can mention the well-known Bertotti model [9,10]. This model is based on the decomposition into three terms: hysteresis loss, classical eddy current loss and excess loss and to a statistical theory of magnetic domains. It was established first for alternative sinusoidal waveforms. Then, it has been extended by Fiorillo to non sinusoidal and also rotational excitations [11].

At G2Elab, the method investigated is called LS (Loss Surface) and combines a finite element simulation of the magnetic structure under investigation and a dynamic hysteresis model (LS model) [5,6]. LS model can predict the H(B) loop as a function of frequency and induction time evolution

In this approach, Flux2D finite element simulation is first used to evaluate the time evolution of the induction in every point of the structure and then the model is applied to post process the local and total iron loss (Fig.3 and Fig.4).

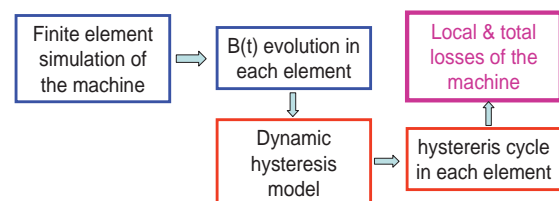


Figure 3: Iron loss calculation approach

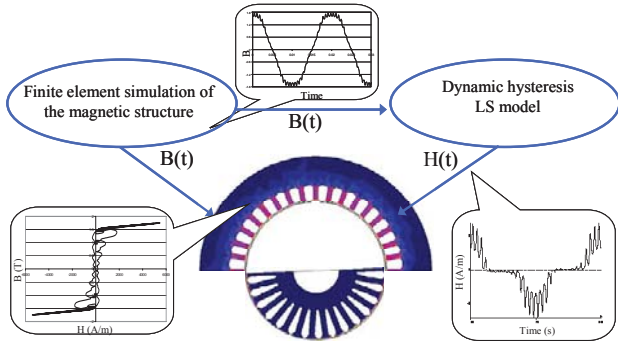


Figure 4: Iron loss distribution in an induction motor obtained thanks to the LS approach

### Description of the LS hysteresis model

The LS [hysteresis](#) model is a scalar model which links the external applied field  $H$  to the average induction  $B$  considered in the cross section of the sheet. It is a global model which takes into account all the dynamic effects in the material [12].

The model is based on  $dB/dt$  parameter and considers that the magnetic field is completely defined knowing at each time  $B(t)$  and  $dB/dt$ . It is identified experimentally thanks to a characteristic surface  $H(B, dB/dt)$ . This surface is determined experimentally under a controlled triangular induction  $B(t)$  and variable frequency (Fig. 5).

In the model, the field  $H(B, dB/dt)$  is decomposed into a static  $H_{static}(B, History)$  and dynamic  $H_{dynamic}(B, dB/dt)$  contributions for which analytical formulation are found :

- $H_{static}(B, History)$  depends on  $B$  level and its history. It is [described](#) by a simple static hysteresis model which is a sum of an anhysteretic field and a friction field. It is identified by a major and two intermediate static hysteresis loops.
- $H_{dynamic}(B, dB/dt)$  is calculated from the experimental dynamic surface thanks to an analytical interpolation considering polynomial functions.

This model has been tested for several materials grades and under variable frequency and waveform excitations. In almost cases the model reproduces the material behavior within 10% (Fig. 6).

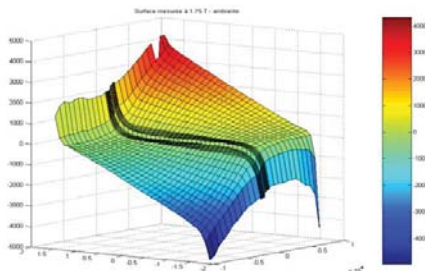


Figure 5:  $H(B, dB/dt)$  surface measured at 1.75T, M700-65P

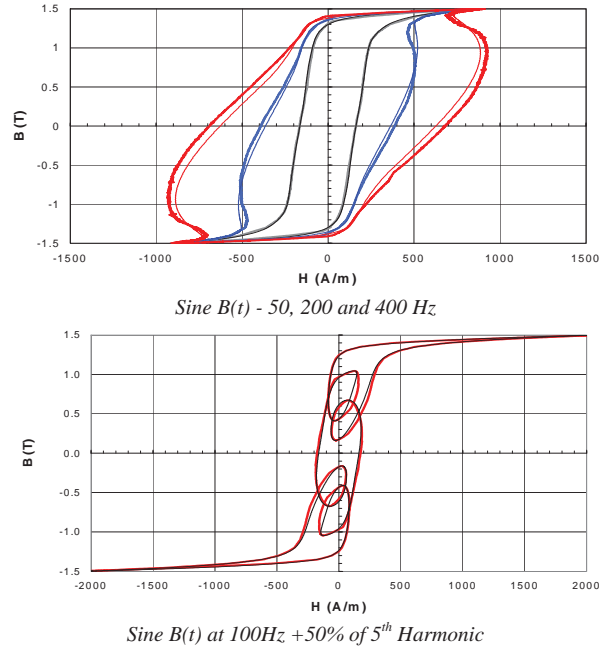


Figure 6: Comparison between measured and predicted hysteresis loops, M400-50A

### Application to electrical machine iron loss calculation

The iron prediction LS model is now implemented in the Flux2D™ software as a post-processing module with a database of 9 non oriented electrical steel sheets. It has been applied on three squirrel cage induction motors and two permanent magnets synchronous machines [13,16].

Validations have been performed at a local level and then at a global one following these two main investigations:

- Simulations of the machines have been performed considering a precise description of the geometry of the machine and most of electrical and mechanical phenomena: rotor motion, voltage supply, machine end effects, eddy current losses in the cage or in the permanent magnets, etc. In all cases, the soft magnetic materials are supposed to be isotropic, non conductor and without hysteresis.
- The iron losses of the machine have been determined using loss separation method. Suitable benches have been developed. Some machines are especially instrumented magnetically [and](#) / or thermally in order to control the local temperature and induction waveform of the material [17]. Several machine operating conditions have been tested: no load, loaded and variable speed.

In almost cases, discrepancies between estimations and experiments were better than 20%.

## Study of a high speed electrical machine

The studied machine is a 40 kVA machine dedicated to electric vehicle. It is a permanent magnets synchronous motor running up to 8000 rpm. This speed corresponds to a material working frequency of 800Hz. The stator is made of M330-35A electrical steels and has 72 slots. The rotor is also made of M330-35A grades steel. It includes 48 NdFeB magnets stick at the surface and retained by a glass fiber ring. The all parts are press fitted in a water cooled aluminum housing.

The LS model has been characterized and tested for the M330-35A grade material used in this machine. It allows the magnetic losses to be predicted with better than 15% as it is shown in Table 1.

Table 1: Comparisons between calculated and measured magnetic losses

B(t)	f (Hz)	$(P_{model} - P_{exp})/P_{exp}$ (%)		
		1.0 T	1.3T	1.5 T
sine	50	-14	-13	-6
	400	-2	-5	2
	1000	4	-4	-3
	2000	12	-3	-5
	2500	14	-5	-4
		1.0T	1.5T	1.7T
sine + 50% harm.5, 180°phase	50	6	-4	0
	100	8	-2	1
sine + 50%harm.11, 180°phase	50	0	-9	-7
	100	4	3	-2

Simulations and experiments have been performed for 2000, 5000, and 8000 rpm speeds and for unload and load operations. In simulations, the electrical circuit which is associated to the geometry of the machine includes two parts as it is shown in Fig. 7: the first one represents the electrical supply and the second is used for eddy current in the magnets.

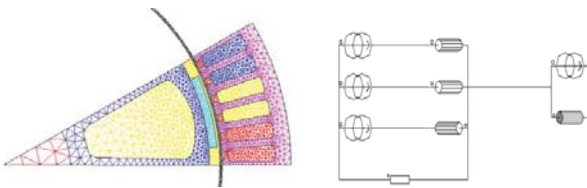


Figure 7: Geometry, meshing and associated electrical circuit

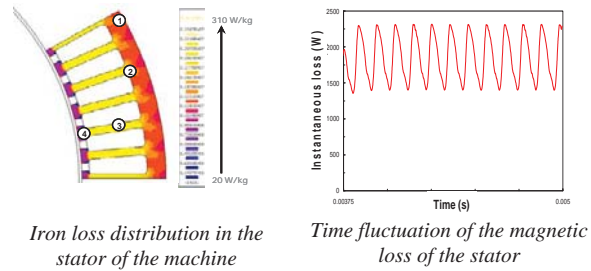
Figure 8 gives some results as the iron loss distribution in the machine stator and the local hysteresis loops obtained in the teeth and the yoke of the stator.

To achieve this study, two main problems have been overcome:

- The first one concerned the mechanical losses determination. These losses are due to the ventilation system and the bearings. They are very

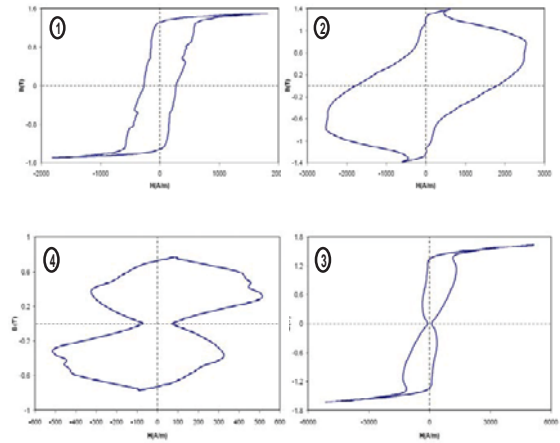
difficult to evaluate because of the remanent flux induced by the magnets. Indeed, the traditional method, used for synchronous machines, which extrapolates at zero the characteristic curve of losses as a function of the square voltage, is no more valid. So an equivalent rotor without permanent magnets was built and used for the tests. The measured mechanical losses have been about 10% of the machine iron ones.

- The second problem was "how to consider the effects of the stator punching?". In fact, the teeth of this machine were very thin of 2.8 mm width. Therefore a degradation of the material properties can be suspected. So, the simultaneous effects of punching and frequency on B(H) curves and losses have been evaluated thanks to a suitable Grid structure [18]. Then they have been introduced in the 2D FEM simulation. The additional losses induced by this phenomenon have been 15 to 30 % of the stator losses.



Iron loss distribution in the stator of the machine

Time fluctuation of the magnetic loss of the stator



Local hysteresis loops obtained at different points of the stator

Fig. 8. Some results obtained by simulation on the studied machine, no load conditions, 2000 rpm

Table 2 summaries the main results obtained for this machine and compares prediction and experiment. The proposed LS model and its associate method allow the iron loss of this high speed machine to be predicted within 20%.



Table 2: Measured and predicted iron loss of the machine

	Speed (frequency)	Iron loss (W)		Difference
		experiment	estimation	
No load	2000 rpm (200 Hz)	324	268	17%
	5000 rpm (500 Hz)	1283	994	23%
	8000 rpm (800 Hz)	2733	2197	20%
Load	2000 rpm (200 Hz)	332	335	0%
	5000 rpm (500 Hz)	1409	1143	19%
	8000 rpm (800 Hz)	3029	2461	19%

## Conclusion

This paper presents results of large investigations carried out at G2Elab in the field of characterization and modeling of iron loss in electrical machines. The LS approach developed enables to estimate correctly iron losses in any electromagnetic device and to localize them in the magnetic circuit. This should help designers to improve motor efficiency.

## Acknowledgements

This work has been carried in the frame of strong collaborations with LEROY SOMER and the GIRTOM "Groupement des Industriels et Centres de Recherche dans le domaine des Tôles Magnétiques" managed by the GIMELEC, and composed by the companies LEROY SOMER, EDF, THALES, DGA). It is the results of several PhD Theses: Christophe Cester, Thierry Chevalier, Alban Marino and Thierry Gautreau. The author would like to thank all of them for their contributions and financial supports.

## References

- [1] Moses A.J. and Radley G. S., "Experimental simulation of magnetic flux and power loss distribution in the stator core of a large rotating machine", *JMMM19*, 1980, pp 60-62.
- [2] Shunji Takada et al, "Magnetic losses of electrical iron sheet in squirrel-cage induction motor driven by PWM inverter", *IEEE Trans.on Magn.*, Vol. 33, N° 5, 1997, pp 3760-3762
- [3] Cester C. et al, "Iron loss under practical working conditions of a PWM powered induction motor", *IEEE Trans. on Magn.*, Vol. 33, No. 5, 1997, pp 3766-3768.
- [4] Spornic S., Kedous-Lebouc A., Cornut B., Waveform dependence of magnetic properties under rotating field", 5<sup>th</sup> Int. 2DM Problem Workshop, 1997, France, EDP Sciences, ISBN 2-86883-347-0, pp 79-86.
- [5] Chevalier T., Kedous-Lebouc A., Cornut B. and Cester C. Estimation of magnetic loss in an induction motor fed with sinusoidal supply using a finite element software and a new approach to dynamic hysteresis, *IEEE Trans. Mag.*, vol. 35, N°5, 1999, pp. 3400-3402
- [6] Marino A., Kedous-Lebouc A., Cornut B., Manfè Ph. Iron loss prediction in an induction motor, Int. Conf. SMM16, Germany, 2003[]
- [7] De Wulf M. Aciers électriques non orientés pour machines électriques et autres applications : Progrès récents dans les techniques de caractérisation, les nouvelles qualités de matériaux et les outils de modélisation, Chapitre 2 du chapitre

2 du volume "Matériaux magnétiques en Génie Electrique 1" sous la direction de A. Kedous-Lebouc, Editions Hermès – Lavoisier, 2006, ISBN 2-7462-1165-3

- [9] Bertotti G., Physical interpretation of eddy current losses in ferromagnetic materials. I. Theoretical considerations, *J. Appl. Phys.* 57 (6), 1985, pp. 2110-2117
- [10] Bertotti G. and Pasquale M., Physical interpretation of induction and frequency dependence of power loss in soft magnetic materials, *IEEE Trans. on Magn.*, Vol. 28, No 5, 1992, pp 2787-2789
- [11] Fiorillo F. and Novikov A., An improved approach to power losses in magnetic laminations under non sinusoidal induction waveform, *IEEE Trans. on Magn.*, Vol. 26, No. 5, 1990, pp 2904-2910.
- [12] Chevalier T., Kedous-Lebouc A., Cornut B., A new dynamic hysteresis model for electrical steel sheet, *Physica B: Physics of Condensed Matter*, Vol. 275/1-3, 2000, pp. 197-201
- [13] Cester C., Etude des pertes magnétiques d'une machine asynchrone à vitesse variable alimentée par convertisseurs statiques, PhD Thesis, INPG, France, 1996
- [14] Chevalier T., Modélisation et mesure des pertes fer dans les machines électriques, application à la machine asynchrone, PhD Thesis, INPG, France, 1999
- [15] Marino A., Caractérisation et modélisation des pertes fer dans les machines électriques fonctionnant en charge, PhD Thesis, INPG, France, 2003
- [16] Gautreau T., Estimation des pertes fer dans les machines électriques. Modèle d'Hystérésis Loss Surface et application aux machines synchrones à aimants, PhD Thesis, INPG, France, 2005
- [17] Marino A., Kedous-Lebouc A., Cornut B., Manfè Ph., Trigeol J. F., Induction machine magnetic and thermal behaviour, Int. Conf. SMM16, Germany, 2003
- [18] Kedous-Lebouc A., Gautreau T. and Chevalier T., Effects of the stator punching on the iron loss of a high speed synchronous machine, 9<sup>th</sup> Int. workshop on 1 & 2 DM measurements and testing Workshop, Poland, 2006.



**Afef Kedous-Lebouc** was born in Hammam-Lif, Tunisia, on December 1. 1957. She has received her Electrical Engineer and PhD degrees from the "Institut National Polytechnique de Grenoble" in 1982 and 1985.

She is a Senior CNRS Researcher at G2Elab (Grenoble Electrical Engineering Laboratory - former LEG).

Her main activity interests are soft magnetic materials and their integration in electrical engineering applications: non conventional characterization, magnetic behavior modeling and use in electromagnetic devices. Since 2002, she is also involved in a new research theme on "New giant magnetocaloric effect materials and applications in magnetic refrigeration around room temperature

Afef Kedous Lebouc is with Grenoble Electrical Engineering Laboratory G2Elab, Grenoble-INP - UJF - CNRS UMR 5269, Bat. ENSE3, BP 46 38402 Saint Martin d'Hères Cedex, France (afef.lebouc@g2elab.inpg.fr)



# Simulink Implementation of Three-Phase Double Fed Induction Motor Model

Sameer Khader

**Abstract:** In this paper, a modular Simulink implementation of a double fed induction motor (DFIM) model is described through a step-by-step approach. With the modular system, each block solves one of the model equation; therefore, unlike black box models, all of the machine parameters are accessible for control verification purposes.

After the implementation of motor model, example is given with the model that used proposed approach. At the same time studying the influence of system parameters on the motor torque-speed performances and circuit current is realized with purpose to obtain optimized motor operation mode with respect to minimized ripples, increasing efficiency, and reliable operation.

**Keywords:** Computer Simulation, Synchronous Motors, Induction Motor, Vector Control, and PWM.

## Introduction

Under normal conditions, with fixed supply voltage and frequency, the speed of an induction motor is almost constant, though it varies slightly with the load. With the development of power electronics technologies over the past decades [1,2,3] the motor speed varies efficiently by using so called variable voltage variable frequency supply converter(VVVF). If the converter is connected to the stator of the machine, it must be rated for the full motor power and is correspondingly expensive with up to 4 times the motor cost. If the converter is connected to the rotor of the machine, through brushes and slip rings, it may be rated for less than the full motor power depending on the required speed range .

This machine is called Double Fed Induction Machine(DFIM). The earlier method for speed control was the so-called cascade connection of two machines sharing a common shaft and load. Where variation the speed being made by resistors or autotransformers connected to the stator of second machine. This cascade double fed machine is called the Doubly Fed Twin Stator Induction Machine (DFTSIM) [4,5].

In general the rotors of these machines are wound rotors with identical construction. Aiming at reducing the motor cost, eliminating the brushes of the rotor, limiting the rotor losses; and increasing the system efficiency wound rotors are replaced by squirrel cage rotors with various cage slots configuration, as well shown on

figure1, where two identical three phase balanced windings are used.

Where the first one is called primary (main) denoted by subscript "p" which is the power winding of the system, and another winding called control machine denoted by subscript "c". The control machine together with the converter circuit acts as bi-directional slip energy converter.

The DFTSIM can operate in the synchronous mode, in which there is a single frequency of current in the rotor, and the rotor speed is a simple function of the stator supply frequency of pole pairs. For the sake of step-by-step observation of the motor behaviors, a Matlab/ Simulink approach should be described hereinafter.

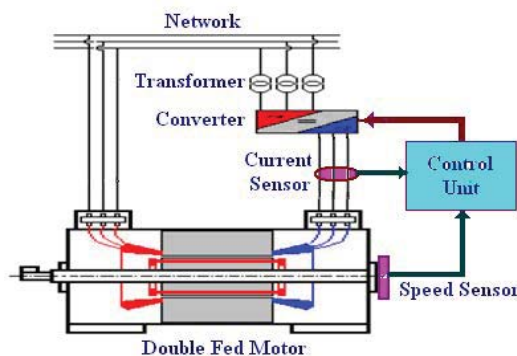


Fig.1. Double Fed Twin Stator Induction Motor.

When an electrical machine is simulated in circuit simulators like PSpice, its steady state model is used. But, for electrical drive studies, the transient behavior is also important. One advantage of Simulink over circuit simulator[6,7] is the ease in modeling, the transient of electrical machines and drives, and the ability to include drive controls in the simulation.

As long as the equations are known, any drive and control algorithms can be modeled in Simulink. However, the equations by themselves are not always enough; some experiences with differential equation solving is required.

Simulink induction machines models are available in several publications, but they appear to be black-boxes with no initial details. Some of available publications recommend using S-functions, which are software source codes for Simulink blocks, but using this approach needs programming knowledge required to access to the model variables.

In this paper, a modular, easy to understand Simulink Double Fed Induction Motor model is described, starting with motor classification, mathematical modeling of the motor electromagnetic behaviors, building up the Simulink models and subsystems, then connecting all the model together and running up the simulation[8,9].

### Mathematical Modeling

In order to simplify the system analysis, the following assumption were made:

- Symmetrical three-phase windings for both stators are distributed in such way to produce sinusoidal space vector of magnetic flux in the active air gap.
- The saturation effect of magnetic circuit is negligible.
- The core and mechanical losses are negligible.

Two circuit approaches are to be investigated:

#### Double Fed Induction Motor

In this motor the stator windings are connected to the system network, with fixed voltage and frequency, while the rotor is wound type and connect via slip rings to a VVVF supply. Fig.2 illustrated per phase equivalent circuit, where the following equations can be expressed:

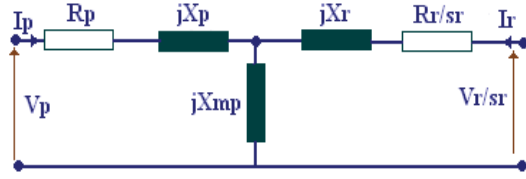


Fig.2. Per phase equivalent circuit of DFIM.

$$(1) \quad [I] = [Y] \cdot [V]$$

Where:

$$[I] = [I_p \ I_r]^T, \quad [V] = [V_p \ V_r]^T$$

$$[Y] = \begin{bmatrix} R_p + jX_p & jX_{m_p} \\ jX_{m_p} & R_r/s_r \end{bmatrix}^{-1}$$

$$\text{and } X_p = \omega_e L_p, \quad X_r = \omega_e L_r; \\ X_{m_p} = \omega_e L_{m_p}, \quad s_r = \omega_r / \omega_p; \\ V_p = V_p e^{j\theta_p}, \quad V_r = V_r e^{j\theta_r}, \quad \omega_p = \omega_e / P_p.$$

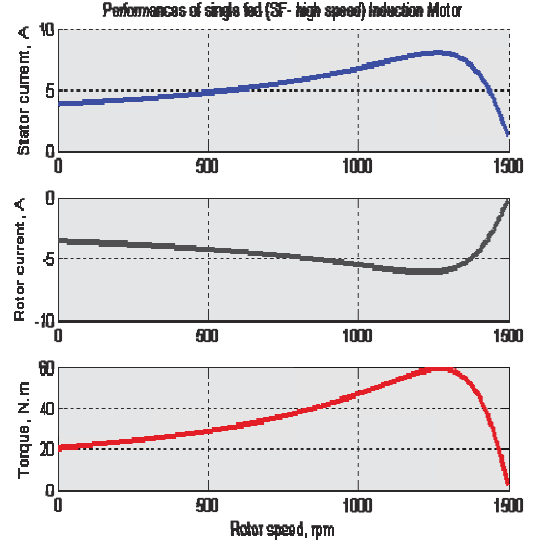
The electromagnetic torque of DFIM taking into account the equivalent circuit of fig.2 is :

$$(2) \quad T_{em} = 3 P_p \cdot L_{m_p} \cdot \Im(I_p \cdot I_r^*)$$

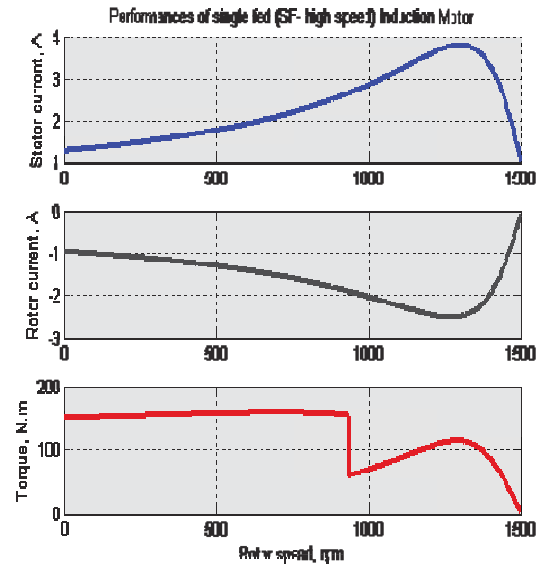
The control variable in case of DFIM is the rotor voltage characterized with variable both magnitude and phase . The torque eq.(2) can be written in terms of rotor voltage as follows:

$$(3) \quad T_{em} = 3 P_p \cdot L_{m_p} \cdot \Im((Y_{11} \cdot V_p + Y_{12} \cdot V_r)(Y_{21}^* \cdot V_p^* + Y_{22}^* \cdot V_r^*))$$

The motor currents and electromagnetic torque obtained throughout Matlab simulation are shown on fig.3. In this figure, the rotor voltage is varied while the stator voltage is fixed at given primary voltage and frequency. It's worthy to mention that when the rotor voltage is adjusted to zero, it can be described as squirrel cage rotor with shorted end terminals.



a) Zero rotor voltage



b) Rotor voltage > 0

Fig.3. Motor currents, and torque at DFIM with variable rotor voltage.

#### Double Fed Twin Stator Induction Motor

As shown in fig.1, DF-TSIM has two independent stators located at the same place and energized throughout two independent voltage sources. First source is called main source (primary) and characterized with fixed voltage and frequency, while the second (control)

source permits voltage and frequency regulation throughout driving circuits called converter. DFTSIM can be mathematically described in terms of voltage controlled mode or current controlled mode. Hereinafter a voltage controlled mode should be described[10]:

### Voltage controlled Mode:

The motor equivalent circuit of DFTSIM is shown on figure4, where the motor is energized by two sources while the rotor of both stators forms closed secondary circuit, with counter action of electromagnetic processes.

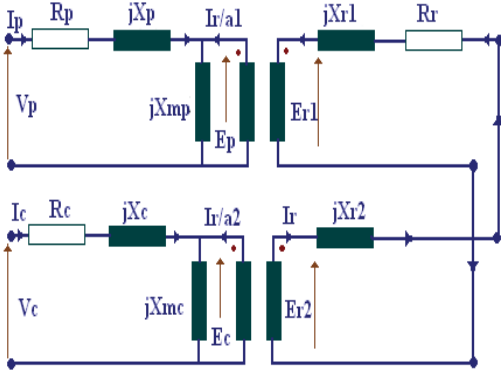


Fig.4. Equivalent circuit of DFTSIM per phase.

For the purpose of simplification in description of the mathematical modeling an approximated circuit referred to the primary winding is proposed and illustrated on figure 5.

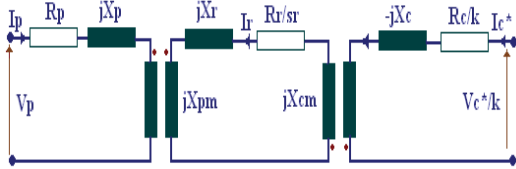


Fig.5. Equivalent circuit of DFTSIM referred to the power winding.

### Mathematical Modeling

Way out from the approximated equivalent circuit referred to the primary winding and by applying the second Kirchhoff's law, the following equations in matrix form at steady state operation can be derived:

$$(4) \quad [V_{mod}] = [Z_{mod}] \cdot [I_{mod}]$$

Where

$$[V_{mod}] = \left[ V_p \quad \frac{V_c^*}{k} \quad 0 \right]^T$$

$$[I_{mod}] = [I_p \quad I_c^* \quad I_r]^T$$

and

$$(5) \quad [Z_{mod}] = \begin{bmatrix} R_p + jX_p & 0 & jX_{pm} \\ 0 & R_c - jX_c & -jX_{cm} \\ jX_{pm} & jX_{cm} & \left( \frac{R'_r}{sr} + jX'_r \right) \end{bmatrix}$$

where

$k = \omega_p / \omega_c$  is the speed ratio between angular velocities of primary and secondary windings respectively;  
 $\omega_p = 2\pi f_p / P_p$ ;  $\omega_c = 2\pi f_c / P_c$ ; angular velocity of both main and control windings respectively;

$P_p, P_c$  are the main and control windings poles respectively, and  $sr$  – critical slip;

$X_{pm}, X_{cm}$ , magnetizing reactance of main and control windings respectively;

$R_p, X_p$ , main winding resistance and reactance respectively;

$R_c, X_c$ , control winding resistance and reactance respectively;

$R_r, X_r$ , rotor resistance and reactance respectively;

$I_p, I_c, I_r$ , main, control and rotor current respectively;

The produced electromagnetic torque due to interaction between yield magnetic fluxes of both windings and rotor circuit in rms phasors can be expressed as follow:

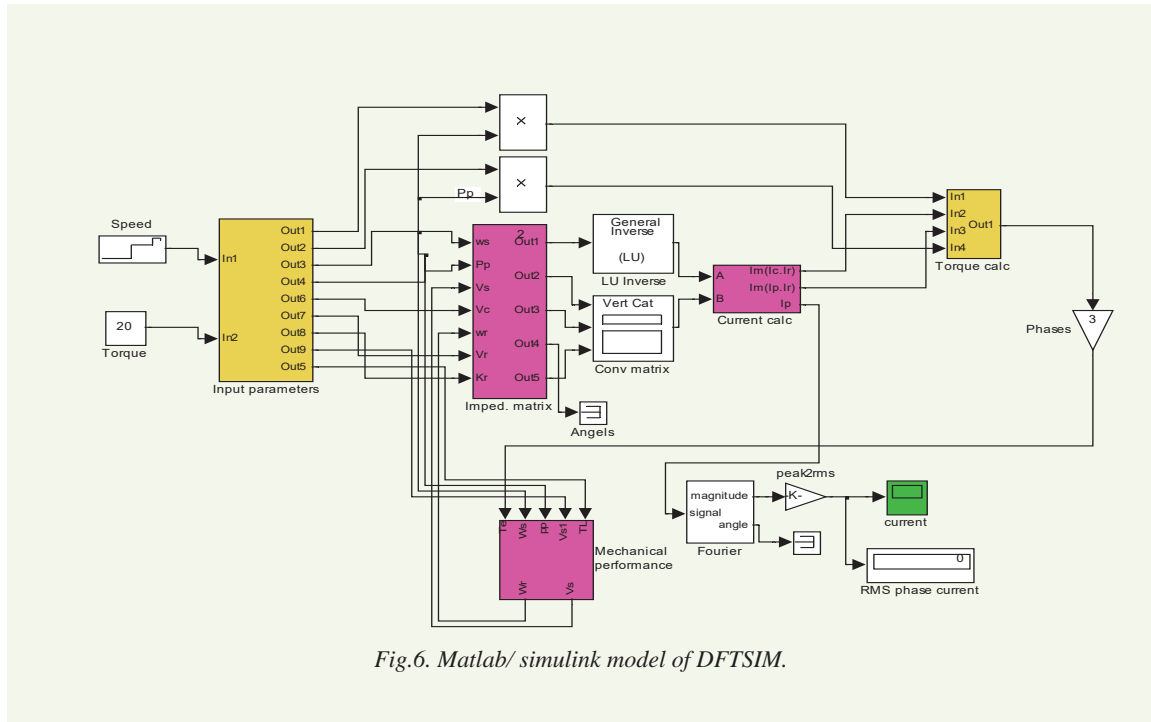
$$(6) \quad T_{em} = T_{main} + T_{cont} \\ = 3P_p \cdot L_{mp} \cdot \Im(I_p \cdot I_r^*) + P_c \cdot L_{mc} \cdot \Im(I_c \cdot I_r)$$

Where:  $L_{mp}, L_{mc}$  are magnetizing inductances of main and control windings respectively.

The motor speed due to the obtained torque and control action of both magnetic field can be expressed:

$$(7) \quad n = 120 \cdot (f_p + f_c) / (P_p + P_c)$$

Where  $f_p, f_c$  are the frequency of both main and control sources, respectively.

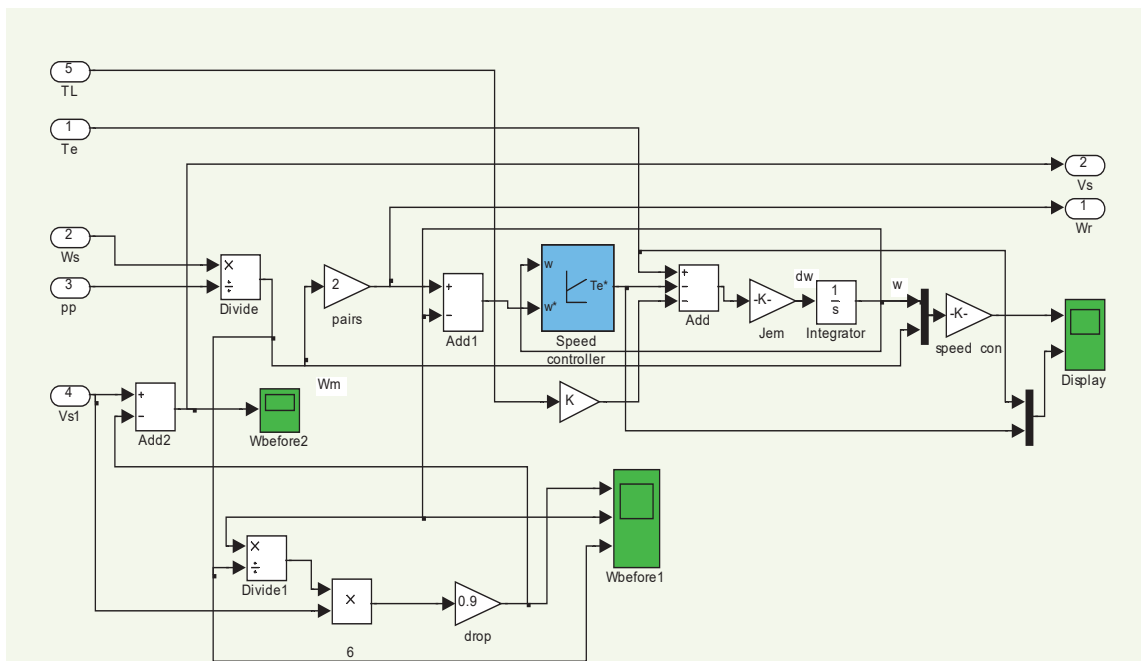


### Matlab/ Simulink Model

Matlab/ Simulink model (approach) is applied in order to observe the dynamic behaviors of motor speed, electromagnetic torque, and currents .

Fig.6 illustrates the major circuit of Matlab/ Simulink approach, where both main and control voltage, and circuit parameters can be controlled consequently.

The electromechanical performances of DFTSIM are calculated throughout running of Simulink subsystem as well shown on figure7, where speed-torque regulation unit consisting of speed controller taking into account rotor equation, and back emf estimator.



## Simulation Study

### 1. Machine Parameters

The machine parameters used in the simulations process are of a prototype motor with data of: 4 poles, 7.5kW, 50N.m, 380V,  $\Delta/Y$  connected, 50Hz, 15A. The parameters of the machines, estimated off line, on a per-phase, with all quantities referred to the primary, and reactance calculated at 50Hz, are given in table 1.

Motor parameters

Table 1.

$R_p=3.63\Omega$	$R_c=3.63\Omega$	$R_r=1.26\Omega$
$X_p=27.4\Omega$	$X_c=27.4\Omega$	$X_r=27.4\Omega$
$X_{pm}=36.6\Omega$	$X_{cm}=36.6\Omega$	$P_c=2P_p$

### 2. Simulation Results:

Taking into account the motor data and applied

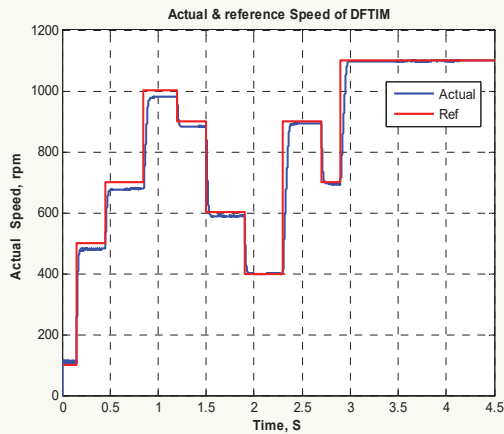


Fig.8. Motor speed at constant loading.

modular approach, some of simulation results are displayed as follows:

☒ The motor speed at various levels is illustrated on fig.8, where the actual speed follows the reference one, and the motor draws current corresponds to the required

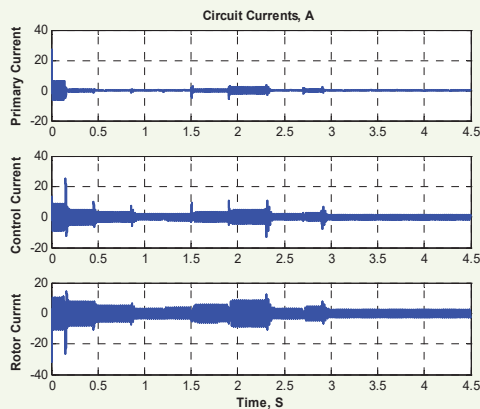


Fig.9. Instantaneous circuit currents at variable speed and constant loading.

speed and given loading torque.

☒ The circuit currents : as the motor speed varies at fixed loading, the circuit currents varies consequently, as well shown on fig.9. The control winding draws relatively high current at low speed, while the main windings current was kept at relatively small acceptable values in the rating limits.

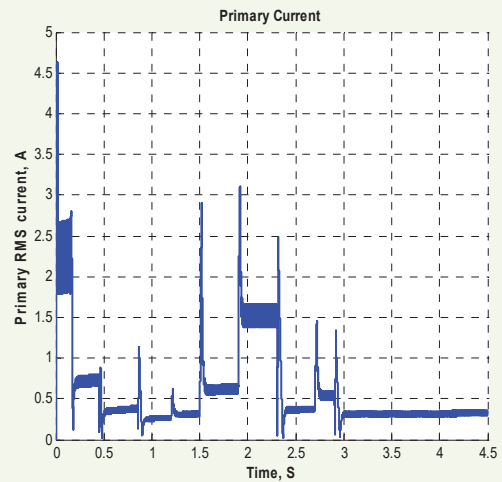


Fig.10. Main winding rms current at various speed.

☒ The rms phasor of main winding current at various speed and constant loading is shown on fig.10.

☒ The produced electromagnetic torque of DFTSIM consists of two components, the interaction of rotor current with both main winding and control winding currents respectively ( $T_{main}$  &  $T_{cont}$ ). Fig.11 illustrates the change of both torque components as the motor speed varies.

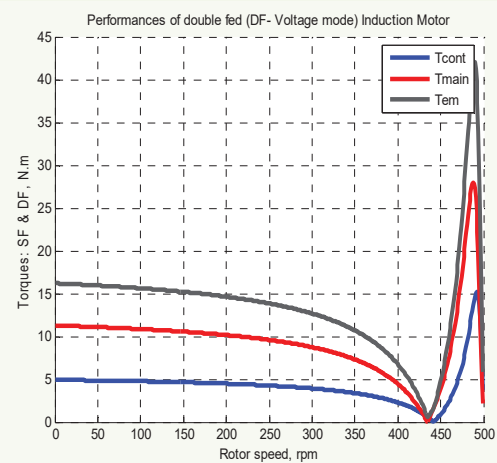


Fig.11. Torque components at DFTSIM voltage control mode.

### Comparison Analysis

Depending on the motor operation mode DFIM (single fed mode SF) and DFTSIM ( double fed mode DF), the following relation can be discussed and compared with each other as follows:

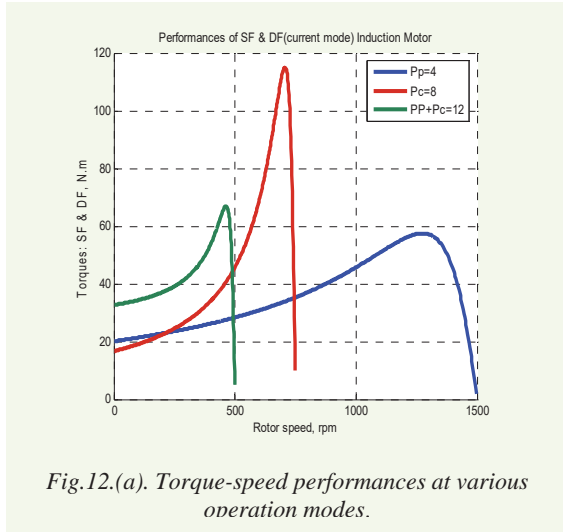


Fig.12.(a). Torque-speed performances at various operation modes.

- ✓ Electromagnetic torque, and current, varies consequently as well shown on fig.12 (a), and (b). respectively.

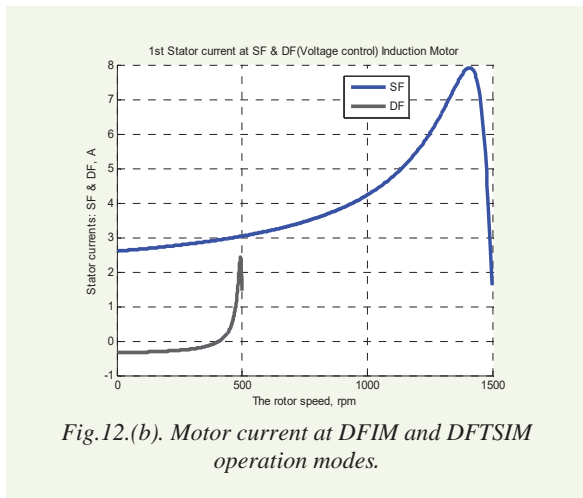


Fig.12.(b). Motor current at DFIM and DFTSIM operation modes.

- ✓ Comparison analysis of motor torque with respect to voltage control and current control mode are applied. As well shown from fig.12(c), voltage control mode permits regeneration of energy back to the source at given speed, while current control mode holds constant operation mode.
- ✓ Comparison analysis with respect to motor speed at different values of control voltage  $V_c$ . Raising  $V_c$  from 0V to 120V leads to proportional increasing of motor speed as well shown on fig.13, where the effect of  $V_c$  is observable at low speeds of the motor.

- ✓ Comparison analysis with respect to the main stator rms current at variable control voltage  $V_c$ .

As well shown on fig.14, where at low speed injecting control voltage  $V_c$  reduces the circuit current, therefore the copper losses reduces significantly.

- ✓ Comparison analysis with respect to motor electromagnetic torque at variable control voltage.

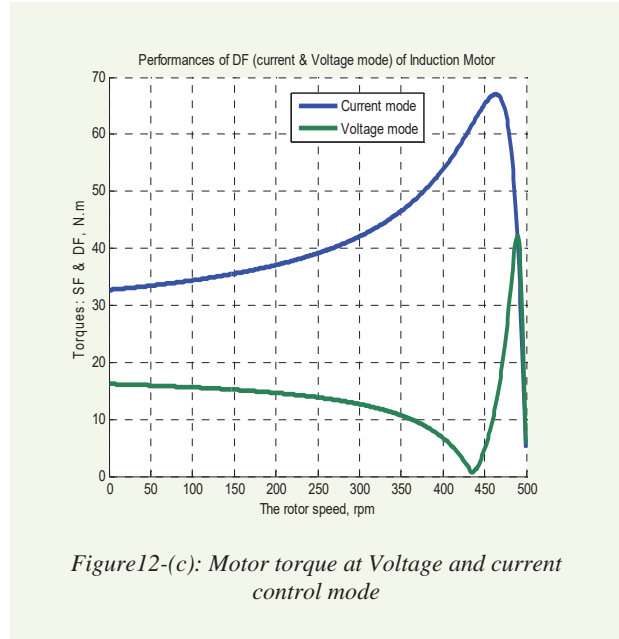


Figure12-(c): Motor torque at Voltage and current control mode

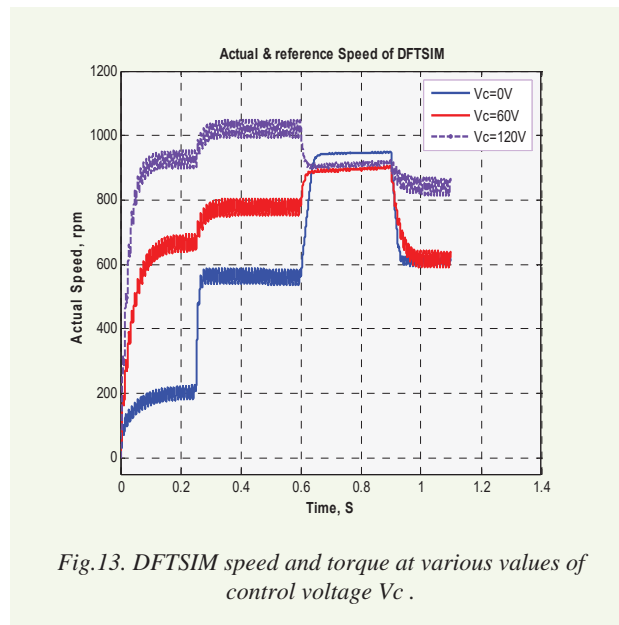


Fig.13. DFTSIM speed and torque at various values of control voltage  $V_c$ .

### Conclusion

The proposed mathematical model described the relationship between the electromagnetic torque and the control variables of DFTSIM. The analytical solution of circuit equations have been developed and implemented



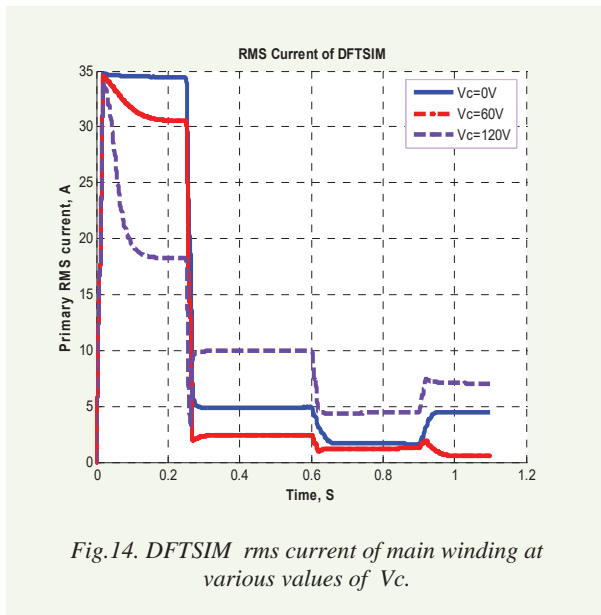


Fig.14. DFTSIM rms current of main winding at various values of  $V_c$ .

in Matlab/ simulink environment. Unlike most other induction machine model implementations. With introducing this model, user can access to all the internal machines variables for getting an insight into the machine operation. Furthermore, the ease of implementing controls with this model is also demonstrated with examples.

As well observed from the simulation results energizing the control winding with appropriate alternating voltage acts directly on motor speed, torque, and system currents. Applying control voltage also is efficient at low motor speed, while at high speed this change is unobservable.

The effect of rotor configuration and circuit by applying Simulink approach should be discussed in another paper.

## References

- [1] Ozpineci, B. Tolbert, L., " Simulink Implementation of Induction Machine Model- A Modular Approach, IAS- IEEE,2003, Vol.1, pp.728-734.
- [2] Dumitrescu, A. Fodor, D., Jokinen, T., Rosu, M., Bucurencio,S., " Modeling and Simulation of electric drive systems using Matlab/Simulink environments", International conference on Electric Machines and Drives(IEMD), 1999, pp.451-453.
- [3] Bimal K. Bose, Modern Power Electronics and AC drives, Prentice Hall 2002.
- [4] Roberts, P., McMahan,R., Tavner, P., Maciejowski,J., Flack, J., Wang, X., " Performance of rotors for the brushless doubly fed induction machine," proc. 16th ICEM conference, September 2004, pp.450-455, Poland.
- [5] Boardman, G., Zhu, J, Ha, Q., ' Dynamic and Steady State modeling of Brushless Doubly Fed Induction machines", ICEM,2001, China, August2001, pp.412-415.
- [6] Boardman, G., Zhu, J, Ha, Q.,' general reference Frame Modeling of DFIM Using Space Vectors," Proc. Of the Australian Power Eng. Conf. AUPEC'2002, Australia, 2002.
- [7] Poddar, G., Ranganathan,V., " Sensorless field-oriented control for double inverter-fed wound-rotor induction motor drive", IEEE trans. On Ind. Electronics, Vol.51, Issue 5, 2004, pp.1089-1096.
- [8] Liao, Y., " Design of BDFIM for adjustable speed drive applications, " Proc. IEEE IAS Annual Mtg, 6-10 October, 1996, pp.850-855.
- [9] Roberts, P., " A Study of Brushless Doubly-Fed Induction Machine", Ph.D. Dissertation, Univ. of Cambridge, 2005
- [10] Boardman, G., Zhu, J., Ha, Q.," Analysis of the Steady State Performances of Doubly Fed Induction Machines", Faculty of Eng., University of Technology, Sydney, Australia, 2004.

## Biography



**Sameer Hanna Khader** was born in Jenien-Palestine 1962. He received a Master's degree in Electrical Engineering from the Institute of Electrical & Mechanical Engineering, Sofia-Bulgaria in 1988. And Ph.D. degree from TU-Sofia in 1993.

Since 1995 he worked in the college of Engineering and technology at Palestine Polytechnic University (PPU) as a Lecturer and researcher in the Field of Electrical Machines and Power Electronics 1999-2001: Chairman of department of Electrical & Computer Engineering at College of Engineering & technology, PPU. 2001-2004 Dean of College of Applied Professions, PPU. 2004- till now Vice president for Academic Affairs at PPU. He has various works in the field of Brushless dc machines, and several projects with local industry.

In 2008, he was awarded by the USAID-AMIDEAST for University Teaching Excellence in Palestine.

### The Author Address:

College of Engineering and Technology  
Palestine Polytechnic University  
Hebron- West Bank, P.O.Box 198,  
Phone: +972 2 2230068; Fax: +972 2 2224977;  
E-mail: sameer@ppu.edu.  
PALESTINE

# Using Reactive Power which is Generated in the Induction Motor for Estimation of Time Constant for the Rotor

Dragan Vidanovski, Mirka Radevska and Blagoja Arapinoski

**Abstract:** very important element in exploitation and control of induction motor is knowledge of real thermal conditions inside the motor. This paper gives new method for calculation of Rotor Time Constant when the motor is regulated with any kind of inverter.

**Keywords:** Estimate Rotor Time Constant, Estimate Reactive Power, and Estimate Rotor Resistance

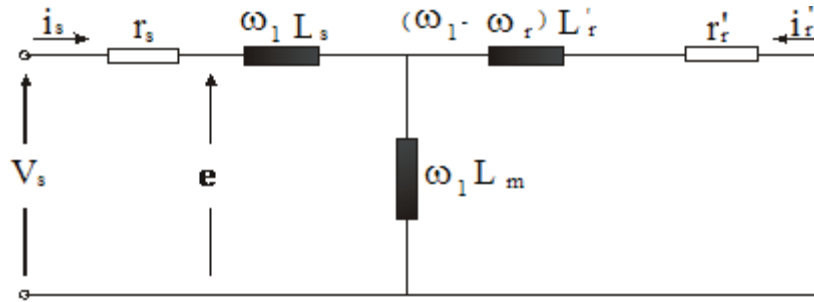
## Introduction

The purpose of this paper is to present how to solve the problem of changing rotor resistance when motor works. Usually the change of rotor resistance is 50% of rotor resistance in the ambient temperature (because the rotor is totally closed, the temperature is rise up to

130°C from the ambient). Rotor resistance is input in parameter list in the “image” of the motor in the inverter. When inverter doesn’t know the real rotor resistance, estimation of slip angular velocity  $\omega_s$  is not correct, and inverter is losing control for angle, from rotor flux and magneto motor force. This cause variation of torque, and oscillation of motor drive (this oscillations have 2 to 5 Hz period and they might cause damage for the drive).

## Estimation of d and q axis component of stator voltage

For estimation of stator voltage we will start with T equivalent scheme of induction motor.



$$(1) \quad \vec{v}_s = r_s \vec{i}_s + \vec{e}$$

Where  $e = -\frac{d\psi_s}{dt}$

Flux linkages of the stator is

$$(2) \quad \psi_s = N_s \cdot \Phi_{POL} \cdot \cos \omega_1 t$$

$$\frac{d\psi_s}{dt} = N_s \frac{d\Phi_{POL}}{dt} \cos \omega_1 t - \omega_1 N_s \Phi_{POL} \sin \omega_1 t$$

$$(3) \quad \frac{d\vec{\psi}_s}{dt} = \frac{d\vec{\psi}_s}{dt} - j\omega_1 \vec{\psi}_s$$

where  $\omega_1 N_s \Phi_{POL} \sin \omega_1 t$  is orthogonal from  $N_s \Phi_{POL} \cos \omega_1 t$ .

$$(4) \quad \vec{v}_s = r_s \vec{i}_s - \frac{d\vec{\psi}_s}{dt} + j\omega_1 \vec{\psi}_s$$

$$(5) \quad \begin{aligned} \vec{\psi}_s &= x_1 \vec{i}_s + x_m \vec{i}_r' \\ x_1 &= \omega_1 (L_s + L_m); \\ x_m &= (\omega_1 - \omega_r) L_m \end{aligned}$$

$$(6) \quad \psi_s = \omega_1 (L_s + L_m) \vec{i}_s + (\omega_1 - \omega_r) L_m \vec{i}_r'$$

If the referent  $qd0$  system is connected with stator, than angular velocity of stator is  $\omega_1 = 0$ ,

$$\vec{v}_s = r_s \vec{i}_s - \frac{d}{dt} [\omega_1 (L_s + L_m) \vec{i}_s + (\omega_1 - \omega_r) L_m \vec{i}_r']$$

Where  $\omega_r$  is rotor angular velocity, and  $s\omega_1 = \omega_1 - \omega_r$  is slip angular velocity,



$s = \frac{\omega_1 - \omega_r}{\omega_1}$  is slip coefficient

$$(7) \quad \vec{v}_s = r_s \vec{i}_s + \frac{d(\omega_r L_m \vec{i}_r)}{dt} \frac{L_r'}{L_r}$$

$$(8) \quad \vec{v}_s = r_s \vec{i}_s + \frac{L_m}{L_r} \omega_r L_r' \frac{d\vec{i}_r'}{dt}$$

$\omega_r L_r' \frac{d\vec{i}_r'}{dt} = \frac{d\psi_r'}{dt}$  is changes in rotor flux,

the voltage in stationary regime is:

$$\vec{v}_s = r_s \vec{i}_s + \frac{L_m}{L_r} \frac{d\psi_r'}{dt}$$

The induction motor can be represented by the following differential equations in  $qd0$  axes fixed in the stator ( $\omega_1 = 0$ ),

$$v_s^{qd0} = \omega_1 \begin{bmatrix} 0 & 1 & 0 \\ -1 & 0 & 0 \\ 0 & 0 & 0 \end{bmatrix} \psi_s^{qd0} + p_p \psi_s^{qd0} + r_s i_s^{qd0}$$

$$(9) \quad v_{qs} = \underbrace{\omega_1}_{0} \cdot \psi_{ds} + p_p \psi_{qs} + r_s i_{qs}$$

$$v_{ds} = -\underbrace{\omega_1}_{0} \cdot \psi_{qs} + p_p \psi_{ds} + r_s i_{ds}$$

$$(10) \quad v_{ds} = r_s i_{ds} + p_p \psi_{ds}$$

$$v_{qs} = r_s i_{qs} + p_p \psi_{qs}$$

$$(11) \quad \begin{cases} \psi_{ds} = L_m i_{dr}' + L_s i_{ds} \\ \psi_{qs} = L_s i_{qs} + L_m i_{qr}' \end{cases}$$

$$(12) \quad \begin{cases} \psi_{dr}' = L_m i_{ds} + L_r' i_{dr}' \\ \psi_{qr}' = L_m i_{qs} + L_r' i_{qr}' \end{cases}$$

$$(13) \quad v_{ds} = r_s i_{ds} + p_p (L_m i_{dr}' + L_s i_{ds})$$

$$(14) \quad i_{dr}' = \frac{\psi_{dr}' - L_m i_{ds}}{L_r'}$$

$$v_{ds} = r_s i_{ds} + p_p \left( \frac{L_m}{L_r'} \psi_{dr}' - \frac{L_m^2}{L_r'} i_{ds} + L_s i_{ds} \right)$$

$$v_{ds} = r_s i_{ds} + \frac{L_m}{L_r'} p_p \psi_{dr}' + \frac{(L_s L_r' - L_m^2)}{L_r'} p_p i_{ds}$$

Where  $L_s' = \frac{L_s L_r' - L_m^2}{L_r'}$  is transient leakage inductance, and

$\sigma = \frac{L_s'}{L_s} = \frac{L_s L_r' - L_m^2}{L_s L_r'}$  is total coefficient of leakage inductance.

$$(15) \quad v_{ds} = r_s i_{ds} + \frac{L_m}{L_r'} p_p \psi_{dr}' + \sigma L_s p_p i_{ds}$$

In the same equations we can solve  $v_{qs}$

### Estimation of d and q axis component of rotor voltage

If the referent  $qd0$  system is connected with stator, than angular velocity of stator is  $\omega_1 = 0$  from T equivalent scheme of induction motor, we can estimate rotor voltage

$$v_r^{qd0} = (\omega_1 - \omega_r) \begin{bmatrix} 0 & 1 & 0 \\ -1 & 0 & 0 \\ 0 & 0 & 0 \end{bmatrix} \psi_r^{qd0} + p_p \psi_r^{qd0} + r_r' i_r^{qd0}$$

for  $d$  we can find

$$(16) \quad v_{dr}' = 0 = r_r' i_{dr}' + p_p \psi_{dr}' - (\omega_1 - \omega_r) \psi_{qr}'$$

Because the rotor flux is constant, the flux  $(\omega_1 - \omega_r) \psi_{qr}'$  is orthogonal than  $\psi_{dr}'$ , we can write:

$$(17) \quad (\omega_1 - \omega_r) \psi_{qr}' = j(\omega_1 - \omega_r) \psi_{dr}'$$

$$(18) \quad 0 = r_r' i_{dr}' + p_p \psi_{dr}' - \omega_1 \psi_{qr}'$$

$$(19) \quad i_{dr}' = \frac{\psi_{dr}' - L_m i_{ds}}{L_r'}$$

$$(20) \quad p_p \psi_{dr}' + \frac{r_r'}{L_r'} (\psi_{dr}' - L_m i_{ds}) - \omega_1 \psi_{qr}' = 0$$

$$(21) \quad p_p \psi_{dr}' + \frac{1}{\frac{L_r'}{r_r'}} (\psi_{dr}' - L_m i_{ds}) - j \omega_1 \psi_{dr}' = 0$$

$$(22) \quad p_p \psi_{dr}' + \frac{1}{\tau_r} \psi_{dr}' - \frac{L_m}{\tau_r} i_{ds} - j \omega_1 \psi_{dr}' = 0$$

$$(23) -\frac{L_m}{\tau_r} i_{ds} + p_p \psi'_{dr} + \frac{1}{\tau_r} \psi'_{dr} - j\omega_1 \psi'_{dr} = 0$$

$\omega_1 = \frac{P}{2} \omega_r$  where  $P$  is number of pairs of poles,  $\omega_1$  is angular velocity of stator field.

$$(24) -\frac{L_m}{\tau_r} i_{ds} + p_p \psi'_{dr} + \frac{1}{\tau_r} \psi'_{dr} - j\frac{P}{2} \omega_r \psi'_{dr} = 0$$

### Estimation of reactive power which is generated in the induction motor

If we take equations from previous we can make these matrixes for stator and rotor voltages

$$(25) \begin{bmatrix} \vec{v}_s \\ 0 \end{bmatrix} = \begin{bmatrix} r_s & p_p \frac{L_m}{L_r} \\ -\frac{L_m}{\tau_r} & p_p + \frac{1}{\tau_r} - j\frac{P}{2} \omega_r \end{bmatrix} \begin{bmatrix} \vec{i}_s \\ \vec{\psi}'_r \end{bmatrix}$$

From second equation we can find for flux of the rotor

$$(26) \vec{\psi}'_r = \frac{L_m}{\tau_r} \frac{\vec{i}_s}{\left( p_p + \frac{1}{\tau_r} - j\frac{P}{2} \omega_r \right)}$$

The equation for reactive power lose for magnetization of the rotor is

$$(27) q_m = \text{Im} \left[ p_p \vec{\psi}'_r \vec{i}_s^c \right]$$

Where  $\vec{i}_s^c$  is conjugate complex stator current

$$(28) q_m = \text{Im} \left[ p_p \frac{L_m \cdot \vec{i}_s \cdot \vec{i}_s^c}{1 + \left( p_p - j\frac{P}{2} \omega_r \right) \tau_r} \right]$$

In the stationary regime is  $p_p = j\omega_1$ , then reactive power is:

$$(29) q_m = \text{Im} \left[ \frac{j\omega_1 L_m i_s^2}{1 + \left( j\omega_1 - j\frac{P}{2} \omega_r \right) \tau_r} \right]$$

The effective value of reactive power is

$$(30) q_m = \frac{\omega_1 L_m i_s^2}{1 + \left( \omega_1 - \frac{P}{2} \omega_r \right)^2 \tau_r^2}$$

From other side the reactive power can be estimated from

$$(31) q_m = \text{Im} \left[ \vec{v}_s \vec{i}_s^c \right]$$

From these equations we can measure reactive power with instruments. From the equation (15)

$$(32) \vec{v}_s = r_s \vec{i}_s + \frac{L_m}{L_r} p_p \vec{\psi}'_r + \sigma L_s p_p \vec{i}_s$$

$$(33) \hat{q}_m = \text{Im} \left[ \left( r_s \vec{i}_s + \frac{L_m}{L_r} p_p \vec{\psi}'_r + \sigma L_s p_p \vec{i}_s \right) \vec{i}_s^c \right]$$

$$(34) \hat{q}_m = \text{Im} \left[ r_s i_s^2 + \left( \sigma L_s p_p \vec{i}_s + \frac{L_m}{L_r} p_p \vec{\psi}'_r \right) \vec{i}_s^c \right]$$

The part of equation  $r_s i_s^2$  is always real and measured reactive power is

$$(35) \hat{q}_m = \text{Im} \left[ \left( \sigma L_s p_p \vec{i}_s + \frac{L_m}{L_r} p_p \vec{\psi}'_r \right) \vec{i}_s^c \right]$$

With knowledge of measured reactive power, we can estimate the rotor time constant

$$(36) \tau_r = \frac{\omega_1 L_m i_s^2 - \hat{q}_m}{\sqrt{\left( \omega_1 - \frac{P}{2} \omega_r \right)^2 \hat{q}_m}}$$

With measurement of reactive power  $q_m$  from equation (31) and estimated value from equation (35)  $\hat{q}_m$ , we can calculate changes of reactive power

$$(37) \Delta q = q_m - \hat{q}_m$$

Now it is possible to estimate rotor time constant  $\tau_r$  and from that calculation we can calculate flux of the rotor

$$(38) \quad \psi_r' = \frac{L_m}{\tau_r} \frac{\vec{i}_s}{\left( p_p + \frac{1}{\tau_r} - j \frac{p}{2} \omega_r \right)}$$

The condition for vector regulation in stationary regime is

$$(39) \quad \omega - \omega_r = \frac{r_r' i_{qs}^s}{L_r' i_{ds}^s} = \frac{1}{\tau_r} \frac{i_{qs}^s}{i_{ds}^s}$$

## Conclusion

With this paper, we present method for estimation of rotor time constant with knowledge of reactive power for magnetization of the rotor core. We presented that from equation (37) we can calculate rotor flux. In the modern types of inverters, equipped with DSP we can easily calculated rotor flux in very short time.

## References

- [1] Beguenane R., Benbouzid M.E.H. Induction Motor Thermal Monitoring by Means of Rotor Resistance Identification. IEEE Transactions on Energy Conversions, vol. 14, No 3, September 1999.
- [2] Boldea I., Nasar S.A. Electric Drives. CRC press 1999.
- [3] Krause P., Wasynczuk O., Sudhoff S. Analysis of Electric Machinery. IEEE 1995
- [4] Mircevski S. Motor Drives and Applications. ETF Skopje.
- [5] Vidanovski D. Vector Control Analysis of Drive with Asynchronous Square Cage Motors during the Heavy Load. Master thesis, ETF Skopje 2004.
- [6] Vidanovski D., Mircevski S., Andonov Z. Induction Motors Thermal Monitoring with Combined Method. 11<sup>th</sup> International Symposium on Power Electronics – Ee 2001, Novi Sad, November 2001.

## Biographies



Dragan Vidanovski was born in Bitola, od May 18, 1961. **Education:** 2004, M. Sc. Faculty of Electrical Engineering, University "St. Cyril and Methodius", Skopje, Macedonia. <http://www.ukim.edu.mk/> Thesis title: "Vectors control analysis of drive with asynchronous square cage motors during the heavy load".

Area: Using of electrical drive systems

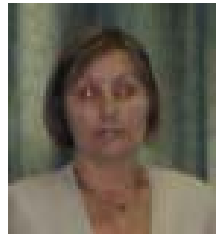
and regulation.

**Employment record:** 2005 – present Assistant Professor Faculty of Technical Sciences, University of St. "Clement of Ohrid" at Bitola, Macedonia. <http://www.uklo.edu.mk/>

1986 – present: Principal Electrical Engineer

Mining and Energy Combine (REK) Bitola (three units of 225 MW)

E-mail: [vidan.d@gmail.com](mailto:vidan.d@gmail.com)



**Mirka Radevska** was born in Bitola, Macedonia on July 3 1952. She studied at the Technical University of Skopje Macedonia and received Dr. degree from the same university in 1996

Since 1978 she worked in the Faculty of Technical Sciences of the University of Bitola as a Lecturer and researcher in the field of electrical machines and electrical drives.

Mirka Popnikolova Radevska is with the Faculty of Technical Sciences, I.L.Ribar bb, 7000 Bitola, Macedonia,

E-mail: [mirka.radevska@uklo.edu.mk](mailto:mirka.radevska@uklo.edu.mk)



**Blagoja Arapinoski** was born in Prilep, Macedonia on November 10, 1982. He graduated in the Technical University - Bitola and now is in the process of second Master degree, second year from the same university.

His field of interest includes electrical machines, electrical drives, electrical networks and renewable energy sources (electrical aspects).

Blagoja Arapinoski is with the Faculty of Technical Sciences, I.L.Ribar bb, 7000 Bitola, Macedonia, E-mail: [blagojarp@mt.net.mk](mailto:blagojarp@mt.net.mk)

# FEM Computation of ANORAD Synchronous Brushless linear motor

Blagoja Arapinoski, Mirka Radevska and Dragan Vidanovski

**Abstract:** In this paper will be presented an approach to improved nonlinear magnetic field analyses of the ANORAD Linear brushless synchronous motor(ASBSM), on the basis of Finite Elements Method (FEM) By using the iterative procedure, FEM it will be calculated the distribution of magnetic field in the cross-section of the ASBLM. The electromagnetic field on the basis of the fluxes and flux densities will be defined and the electromagnetic continuous force will be calculated.

**Keywords:** Finite Elements Method, Anorad Linear Brushless Synchronous motor, Electromagnetic field, ANORAD.

## Introduction

For complex regions as those in electromagnetic devices an attractive and powerful numerical method for solution of electromagnetic field problems is the Finite Element Method (FEM). By the application of this method in the three dimensional domains (3D), an important contribution to the magnetic field is done. This program package FEM-3D for application of the Finite Element Method for calculation of the magnetic distribution have been developed and applied in different kinds of electromagnetic devices.

In this case the rated data of the ANORAD Linear Synchronous motor that will be analyzed in this paper are:  $I_n = 3.4A$ ,  $U_n = 220V$ .

The Linear Synchronous motor (ASBLM) analyzed in this paper is product of ANORAD Corporation, and all begin data and dimensions were taken of Brushless Linear motor type LEB-S-2-S (ANORAD) with no cooling system. Type and dimensions of (ASBLM) will be analyzed is presented on Fig. 1. and Fig. 2. respectively.



Fig.1. ANORAD SBLM LEB-S-2-S

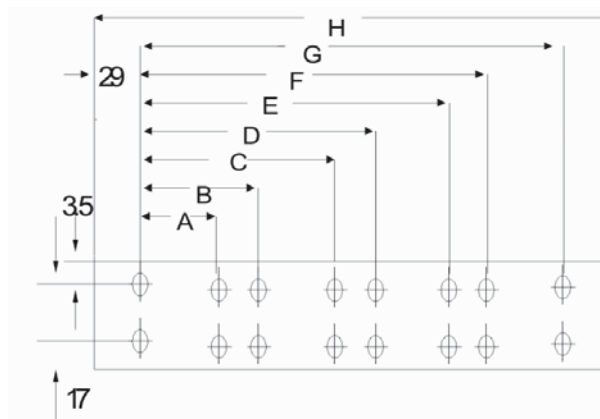


Fig.2. Dimension of ANORAD LSM LEB S-2-S

Table 1

Dimension of analyzed motor

Dimension of LEB S-2-S										
leght	A	B	C	D	E	F	G	H	J	K
[mm]	80	/	/	/	/	/	/	140	40	123

Dimensions: Magnet assembly 75x34mm, magnet pitch 15mm, coil assembly 140x66x80mm, depth 30mm and coil pitch 20mm.

## Magnetic Field Analysis

To perform the analysis, a three dimensional numerical calculation of the magnetic vector potential and flux density in the domain of ASBLM is required. FEM has possibility to solve magnetic vector potential and consequent magnetic flux density by solving relevant set of Maxwell equations for magneto static case as well as for time harmonic case (case with low frequency). In magneto static case field intensity  $H$ , and flux density  $B$ , must obey:

$$(1) \quad \text{rot}H = J$$

$$(2) \quad \text{div}B = 0$$

Where  $H$ -is magnetic field,  $J$ -is the current density. The magnetic flux density  $B$  was computed using the relationship:

$$(3) \quad B = \mu \cdot H$$

FEM goes about finding a field that satisfies Eq. 1 - Eq. 3 via a magnetic vector potential. Flux density is written in terms of the vector potential  $A$ , as:

$$(4) \quad B = \text{rot}A$$

When definition of B satisfies Eq. 2, then Eq. 1, have form:

$$(5) \quad \text{rot}\left(\frac{1}{\mu(B)} \text{div}A\right) = J$$

In a first step in program pre-processing part, input is the geometry and material properties for all domains of ASBLM. This includes current density and conductivity for windings and magnetic properties for parallel steel plates with NdFeB permanent magnets mounted on the internal surface. In order to be able to solve the problem with FEM, boundary conditions on the outer electromagnets geometry must be defined. For analyzed linear synchronous motor Dirichlet boundary conditions are used. On Fig. 3 mesh of finite elements is presented which is derived fully automatically and it is consisted of 976 nodes and 1724 finite elements.

On Fig. 3, mesh of finite elements is presented which is derived fully automatically.

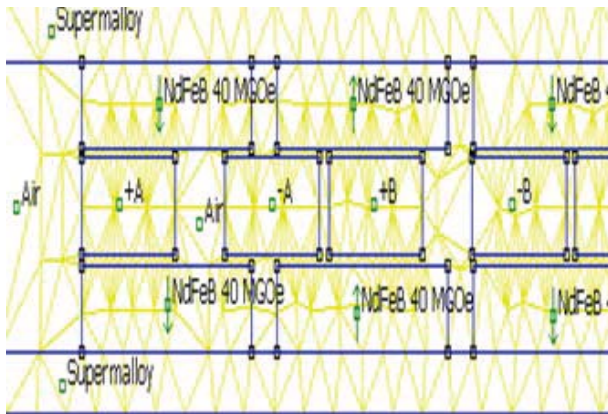


Fig.3 Part of finite elements mesh in cross section of ASBLM.

When a more accurate calculation of the magnetic vector potential is needed, then mesh density should be increased especially on interface between two different materials. In that case contour of integration passes at least two elements away from any interface or boundaries. Greater mesh density increases the computation time. So, the good way to find mesh which is “dense enough” in order necessary accuracy to be achieved and still computation time to be reasonably small is comparison of results from different mesh densities can be picked smallest mesh which gives convergence to the desired digit of accuracy.

Selected results of the finite element analysis are presented in Fig. 4. to Fig. 6. As can be seen from the Figures all results are very regular for a motor with those characteristics.

At Figure 6 is presented magnetic flux density distribution in the air gap and is very regular, sinusoidal. The magnitude is around 0.6T which is responsible result for this type of motor, (motor with coreless stator).

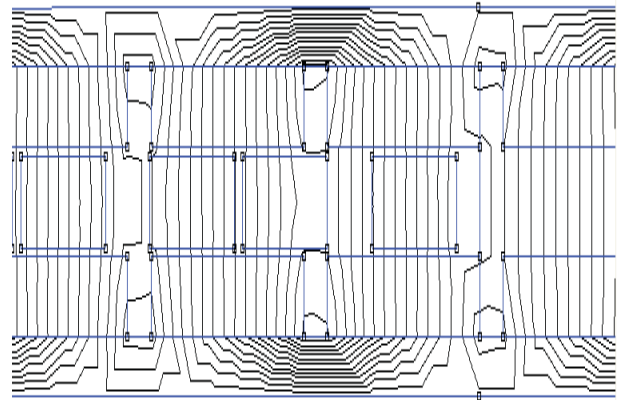


Fig. 4. Distribution of magnetic flux in ASBLM.

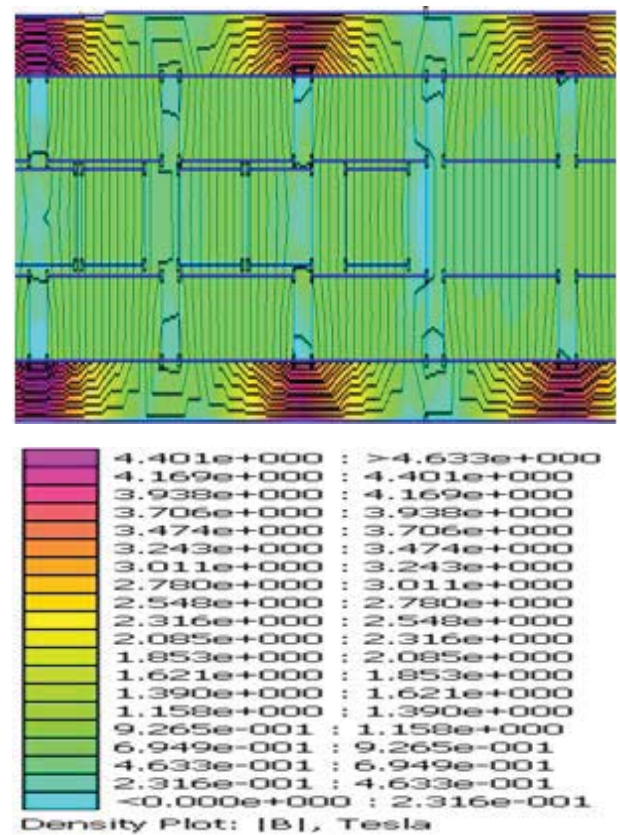


Fig. 5. Magnetic field density on ASBLM

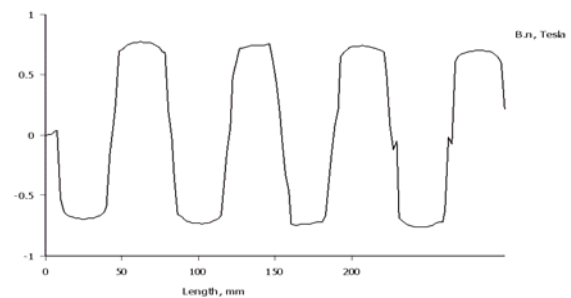


Fig. 6. Magnetic flux density calculated in the middle of the air gap between two PM assemblies.



## Calculation of electromagnetic force

The knowledge of electromagnetic forces characteristics is very important matter for analysis of ASBLM. In this paper numerical calculation of electromechanical forces that are calculated on the base of Maxwell's Stress Tensor and Weighted Stress Tensor are applied on the ASBLM.

Maxwell's Stress Tensor prescribes a force per unit area by magnetic field on a surface. The net force on an object is obtained by creating surface totally enclosing the object of interest and integrating the magnetic stress over that surface.

The differential force produced is:

$$(6) \quad dF = \frac{1}{2} (H(B \cdot n) + B(H \cdot n) - (H \cdot B)n)$$

where  $n$  denotes the direction normal to the surface at the point of interest.

Weighted Stress Tensor Integral greatly simplifies the computation of forces, as compared to evaluating forces via the stress tensor line integral of differentiation of co-energy. Merely select the blocks upon which force is to be computed and evaluate the integral. No particular "art" is required in getting good force results (as opposed to the Stress tensor line integral), although results tend to be more accurate with finer meshing around the region upon which the force is to be computed. One limitation of the Weighted Stress Tensor integral is that the regions upon which the force is being computed must be entirely surrounded by air/or abutting a boundary. In cases in which the desired region abuts a non-air region, force results may be deduced from differentiation of co-energy.

On Fig. 7. and Fig. 8. are presented two different types for calculated force.

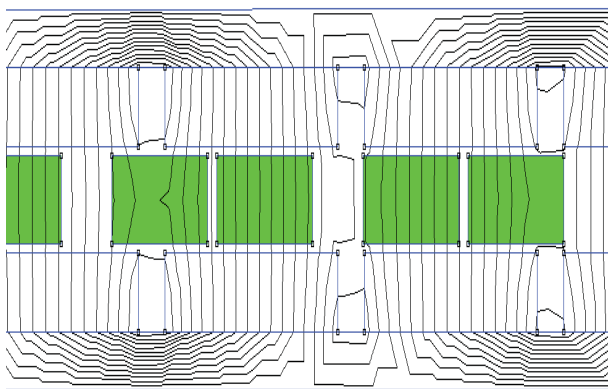


Fig. 7. Calculation of force with weighted stress tensor.

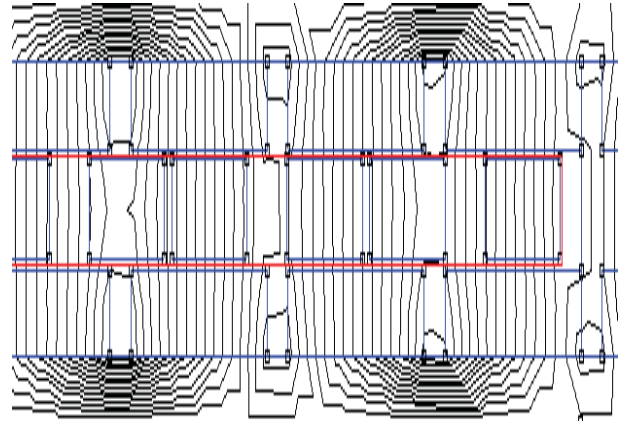


Fig. 8. Calculation of force with Maxwell stress tensor.

The calculations were done for current rated (3.4A), and results were: force with weighted stress tensor has been 85N, and with Maxwell stress tensor 105N.

## Conclusion

Linear synchronous motor with permanent magnet has been presented. The nonlinear magnetic field analyses and computation of electromagnetic and electromechanical characteristics are presented. For this purpose as the most suitable, Finite Element Method is applied. Additionally electromagnetic forces are calculated for rated current. Also in this paper forces is computed via Maxwell's Stress Tensor and Weighted Stress Tensor. Concludes of this investigation is that weighted stress tensor is much practical and give better results for calculated force.

## References

- [1] M. R. Popnikolova, M. Cundev, L.Petkovska. Nonlinear Electromagnetic Field Calculation in Solid Salient Poles synchronous Motor. Proc. of EPNC 96, Poznan, Poland, 1996.
- [2] M. Popnikolova Radevska. Calculation of Electromechanical Characteristics on Overband Magnetic Separator with Finite Elements. ICEST 2006, p.p. 367-370, Sofia, Bulgaria 2006.
- [3] ELECTROMAGNETIC DEVICES. John Wiley & Sons, New York-London-Sydney.
- [4] Young, M. The Technical Writer's Handbook. Mill Valley. CA, University Science, 1989.
- [5] M. Hippner, Z. Piech. RIPPLE FREE LINEAR SYNCHRONOUS MOTOR. ICEM 1998, pp. 845-850, Instambul – Turkey.
- [6] Hanselmann, D.C Brushless Peramanent-magnet motor design. Mc Graw – Hill, 1994.

## Biographies

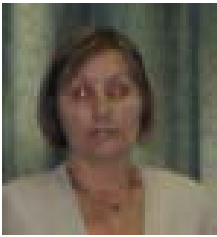


**Blagoja Arapinoski** was born in Prilep, Macedonia on November 10, 1982. He graduated from the Faculty of Technical Sciences, University of “St. Clement of Ohrid” at Bitola, Macedonia. <http://www.uklo.edu.mk/> and now is in the process of second Master degree, second year from the same university.

His field of interest includes electrical machines, electrical drives, electrical

networks and renewable energy sources (electrical aspects).

Blagoja Arapinoski is with the Faculty of Technical Sciences, I.L.Ribar bb, 7000 Bitola, Macedonia, E-mail: [blagojarp@mt.net.mk](mailto:blagojarp@mt.net.mk)



**Mirka Popnikolova Radevska** was born in Bitola, Macedonia on July 3 1952. He studied at the Technical University of Skopje Macedonia and received Dr. degree from the same university in 1996

Since 1978 he worked in the Faculty of Technical Sciences of the University of Bitola as a Lecturer and researcher in the field of electrical machines and electrical drives.

Mirka Popnikolova Radevska is with the Faculty of Technical Sciences, I.L.Ribar bb, 7000 Bitola, Macedonia, E-mail: [mirka.radevska@uklo.edu.mk](mailto:mirka.radevska@uklo.edu.mk)



**Dragan Vidanovski** was born in Bitola, od May 18, 1961. **Education:**

2004, M. Sc. Faculty of Electrical Engineering, University "St. Cyril and Methodius", Skopje, Macedonia.

<http://www.ukim.edu.mk/> Thesis title: “Vectors control analysis of drive with asynchronous square cage motors during the heavy load”

Area: Using of elctrical drive systems and regulation.

**Employment record:** 2005 – present Assistant Professor Faculty of Technical Sciences, University of St. “Clement of Ohrid” at Bitola, Macedonia. <http://www.uklo.edu.mk/>

1986 – present: Principal Electrical Engineer

Mining and Energy Combine (REK) Bitola (three units of 225 MW)

E-mail: [vidan.d@gmail.com](mailto:vidan.d@gmail.com)

# Variable Speed AC Drives

Emil Sokolov

**Abstract:** *The paper presents main features and property improvements of the advanced variable speed AC drives. The steady-state characteristics, components of losses and efficiency of induction motor and permanent magnet synchronous motor at vector control are compared. The operation of both motors in two regions of regulation and by different degree of loading is analyzed. The influence of number of poles is also considered. The obtained numerical results may be useful for development of high-efficiency drives.*

**Keywords:** *loss components, efficiency*

## Introduction and classifying

The most modern production and transport technologies demand employment of high-performance variable frequency AC drives. The extensive field of application involves two main groups: general-purpose industrial drives and special variable speed drives.

Numerous industrial drives operated normally with standard three-phase squirrel-cage induction motors (IM) and in fewer cases with conventional synchronous motors (SM). The motors are fed by inverters with open-loop voltage-frequency control for variable torque loads or constant torque loads. Sensorless vector control is also utilized. According to the supply voltage they are for low voltage 380/460 V, medium voltage 6/6,6 kV and high voltage up to 13,8 kV. The power range of motors is from 1 kW to about 15 MW. Working machines of all kinds in industry are driven, for instance: pumps, fans, compressors, mills, cranes, electric hoists, lifts, excavators, mixers, extruders, centrifuges, conveyors, textile, paper and printing machines etc.

The energy saving is a very important property of the variable speed drives. An example is the flow regulation of a blower (pump) by the speed instead by throttling. Inverter control can reduce the power consumption of IM up to 60 % as compared with conventional control, when the air flow (water flow) is about 60 % from rated value. So energy effectiveness of new or existing drives could be improved. The huge number of AC drives hold large potential for energy saving.

The sine wave PWM is a certain method for digital control of inverter voltage. High-performance requirements include limited harmonics contain in output side of the inverter as well as in source line side without filtering. Preference features are also control quality, low maintenance, high efficiency, power factor and reliability.

The general-purpose industrial drives are regulated upwards until rated speed of the motors. At continuous operations in the lower speed range the load torque

should be decreased due to reduced cooling of the self-ventilation.

In the special variable speed drives operated special AC motors, which are completely incorporated with the drive mechanism and control system. The induction motors are suitable for many applications that call for high overload capability and smooth running, especially at low speeds. A considerable power density is achieved by means of external fan cooling or liquid cooling. The motors are equipped with feedback sensor for closed loop vector control. The main motor parameters, identified by test, are introduced in adaptive models to perform precise control. A constant output range of 1:3 relative to rated speed is possible. The motor speed may vary across 1:1000 range with speed accuracy up to  $\pm 0,01$  %. The starting torque can be 200 % or more.

The permanent magnet synchronous motors (PMSM) have seen a significant increase in use not only for servo drives. The use of rare-earth magnets offers high torque to weight ratio, compact sizes and quick dynamic response. The motors are integrated with encoder for speed and position control.

From speed zero up to rated speed the PMSM deliver practically constant torque, specified for continuous or intermittent duty. The peak torques can be reached until 6 times rated value. The high stator currents generate them must be permissible for a short-term overload without risk of demagnetization or inverter failure. The maximum torque together with the low rotor inertia ensures fast acceleration and deceleration at transients.

Running with high cycle rates and frequent peak loads, small torque ripple at low speeds and high precision of positioning are essential features of the PM servomotors.

The special variable speed AC drives have a wide area of application: traction drive of electric locomotives, vehicles for urban traffic (trams, rapid transit, underground railway), ship screw and steering drives, autonomous vehicles (electric and hybrid cars, electric trucks, mine battery locomotives), machine tools, spindle drives, robots, manipulators, automation technologies, household goods (washing machines, refrigerators, air conditioning), drives of auxiliary automobile devices etc. Many special drives are realized without gearboxes.

Drive systems of large compressors, pumps, blowers and test stands are made by high-speed IM with magnetic bearings for maximum speed up to 15000 rpm. Special SM with exciting winding operated in some powerful high-speed gearless drives, for example boiler feed pumps, natural gas and air compressors.

The short review shows how manifold are the conditions, requirements and types of variable speed AC

drives. Also different methods of vector control are developed, such as field-oriented control, direct torque control etc. Despite the great diversity in more cases a modern drive should be provides optimum electromagnetic condition of the motor during steady-state and transient operation.

Most available papers generally treated dynamic behavior of AC drives. However, the steady-state operating characteristics and efficiency are very important for drives with continuous or moderate duty. The loss reduction leads to economical service and limit heating of the motor.

A comparative analysis of some problems of the vector controlled AC motors is presented below..

### Operation of IM and PMSM in two regions

The operation in two regions (constant torque and constant power output) is typical for many industrial and traction drives. Here the computed steady-state characteristics of two four-pole motors (IM and PMSM) are compared.

Both motors have identical ratings: 15 kW, 1500 rpm, 95,5 N.m. The stator stacks and stator windings are identical. The main dimensions of stator core are: outer diameter 244 mm, internal diameter 160 mm and length 180 mm.

The IM has resistances  $R_s = 0,13 \Omega$ ,  $R_r = 0,125 \Omega$ , leakage inductances  $l_s = l_r = 0,64$  mH and a given function of mutual inductance  $L_m$  versus magnetizing current. Thus, the saturation produced by main flux is included in the analysis.

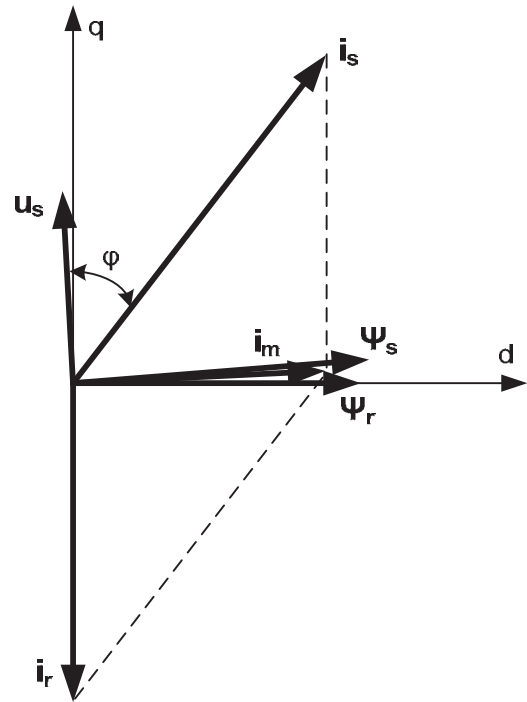
The PMSM has surface-mounted permanent magnets ( $L_d = L_q$ ). The rotor flux linkage  $\Psi_f = 0,63$  Wb is constant.

Two modes of each motor with equal terminal voltage and field-oriented control in d-q reference frame are considered. Figure 1a shows space vector diagram of the IM for rated speed and load. In figure 1b the space vector diagram at rated output with maximum speed (3 times rated value) for the same IM is shown. Figure 2 illustrates space vector diagrams of the PMSM for rated speed (Fig. 2a) and for maximum speed (Fig. 2b), both at rated output. All quantities of the figures are in one and the same scale.

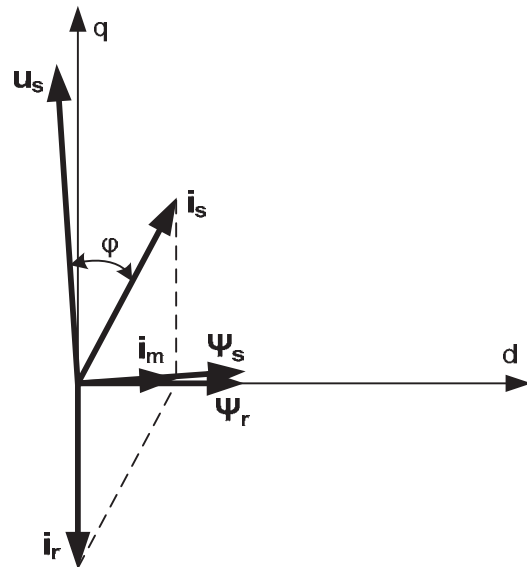
An ideal vector control has excellent performance if the torque-producing current component  $i_{rq}$  (respectively  $i_q$  for PMSM) is oriented on quadrature axis, while the spatial position of rotor flux linkage  $\Psi_r$  (respectively  $\Psi_f$  for PMSM) coincide with direct axis (see the figures).

The magnitude of stator voltage  $u_s$  depends major from the stator flux linkage  $\Psi_s$  and frequency  $f_s$ . It set to be close that the DC bus voltage limited the absolute value of stator voltage for maximum speed and full-load of the motors in field-weakening domain (Figures 1b and 2b). As well a sufficient voltage reserve for dynamic processes is available at rated speed.

As indicated Figure 2b, field weakening of PMSM may be achieved by a counter current component  $i_d$ , which generates opposite flux relative to the rotor flux.



a



b

Fig.1

Then the motor is overexcited – current  $i_s$  leading (Fig. 2b), in contrast to rated speed where PMSM operates as underexcited motor – current  $i_s$  lagging (Fig. 2a).

A comparison of main data, loss components and efficiency of the IM and PMSM for three working points is given in Table 1.

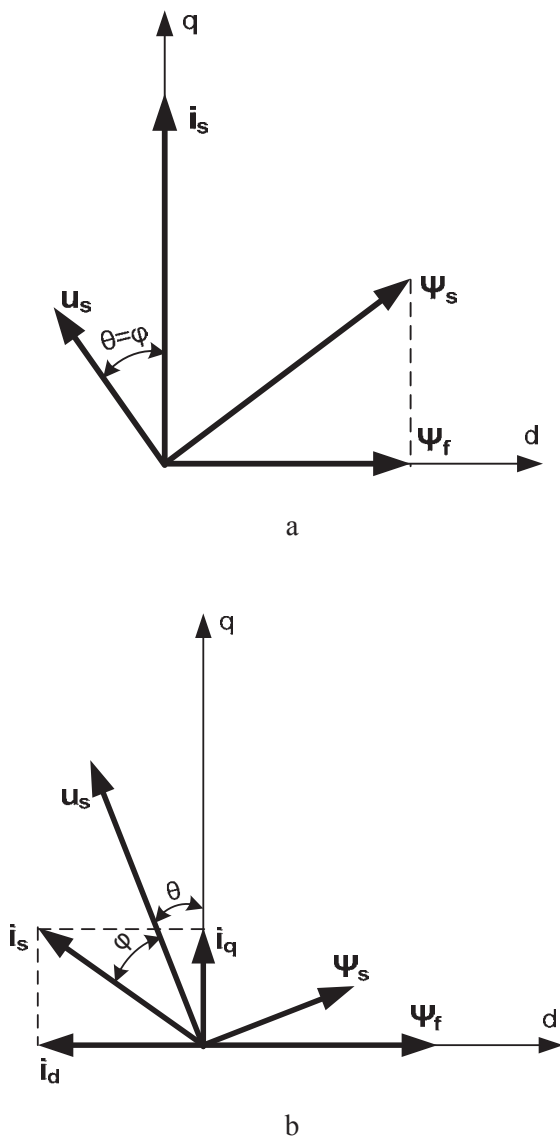


Fig.2

The flux of IM is produced from magnetizing current  $i_m$ . Therefore, the stator current  $i_s$  and stator winding losses  $p_s$  of the IM are greater than these of PMSM. However, since in field-weakening zone a current component  $i_d$  is applied, the reactive power and stator current of PMSM have been increase in this mode.

Other problem of IM is the rotor winding losses  $p_r$  and rotor heating. The PMSM has not this disadvantage and that is favorable for totally enclosed constructions.

The iron losses  $p_{Fe}$  are associated with stator flux linkage and frequency. They are approximate even in both motors. Although the speeds in each separate mode are equal, the IM operates with slip frequency  $\omega_{sl}$  and with a little higher stator frequency. For the three modes in Table 1  $\omega_{sl}$  is constant, but the slip  $s$  vary by hyperbola versus the speed.

Table 1

	Half rated speed		Rated speed		Field-weakening	
	IM	PMSM	IM	PMSM	IM	PMSM
n, rpm	750	750	1500	1500	4500	4500
T, N.m	95,5	95,5	95,5	95,5	31,83	31,83
P, kW	7,5	7,5	15	15	15	15
$f_s$ , Hz	26,11	25	51,11	50	151,1	150
$\omega_{sl}$ , $s^{-1}$	7	-	7	-	7	-
s, %	4,25	-	2,17	-	0,734	-
$ i_s $ , A	54,7	50,5	54,7	50,5	27,9	28,5
$ u_s $ , V	132	132	256	256	425	425
$\Psi_s$ , Wb	0,779	0,807	0,779	0,807	0,445	0,443
$p_s$ , W	584	498	584	498	152	159
$p_r$ , W	334	-	334	-	111	-
$p_{Fe}$ , W	209	212	500	522	668	656
$p_m$ , W	24	24	50	50	180	180
$p_{add}$ , W	75	86	75	86	75	86
$\Sigma p$ , W	1226	820	1543	1156	1186	1081
$\eta$ , %	86,0	90,1	90,7	92,8	92,7	93,3

The friction and windage losses are designated as  $p_m$ .

The additional losses  $p_{add}$  in the rotor of PMSM somewhat increases due to relatively good conductivity of the rare-earth magnets and the eddy currents in them, producing by stator high harmonics.

Finally, the PMSM has lower total losses and quite higher efficiency, particularly in the constant torque range of control.

### IM and PMSM under different load

The AC motors do not work only on rated load. More motors are commonly operated at 70 to 80 percent of full load, sometimes at fairly less load. The results of calculating parameters, losses and efficiency of IM and PMSM in dependence from load torque are presented in this part. The motors are the same as these in the previous section. The operating characteristics at constant speed 1500 rpm are given in Table 2 (for IM) and in Table 3 (for PMSM). The first columns of the tables concern data for rated load.

Table 2

T, N.m	95,5	75,0	47,8	20,0	10,0
$\omega_{sl}$ , $s^{-1}$	7,0	6,28	5,15	3,58	2,64
$f_s$ , Hz	51,11	51,0	50,82	50,57	50,42
$\Psi_{rd}$ , Wb	0,755	0,706	0,622	0,482	0,398
$i_{rq}$ , A	42,2	35,4	25,6	13,8	8,4
$i_m$ , A	33,28	27,17	20,74	14,39	11,37
$L_m$ , mH	22,7	26,0	30,0	33,5	35,0
$i_s$ , A	54,7	45,3	33,4	20,15	14,23
$u_s$ , V	256	237	207	158	130
$\Psi_s$ , Wb	0,779	0,725	0,636	0,492	0,405
$p_s$ , W	584	400	217,5	79	39,5
$p_r$ , W	334	235	123	36	13
$p_{Fe}$ , W	500	436	339	203	139
$p_{add}$ , W	75	51	28	10	5
$\Sigma p$ , W	1543	1172	757,5	378	246,5
$\eta$ , %	90,7	91,0	90,8	89,3	86,4



Because of the vector control of IM, the stator voltage decreases considerable when load torque decreases. That causes reduction of the stator flux and magnetizing current. Hence, the windings and core losses also decreases. Therefore, the efficiency of the IM is relative high and constant up to least load.

**Table 3**

T, N.m	95,5	75,0	47,8	20,0	10,0
$i_s=i_q, A$	50,53	39,68	25,29	10,58	5,29
$f_s, Hz$	50	50	50	50	50
$\Psi_s, Wb$	0,807	0,745	0,679	0,639	0,632
$u_s, V$	256	238	216	202	199
$p_s, W$	498	307	125	22	5,5
$p_{Fe}, W$	522	445	370	327	320
$p_m, W$	50	50	50	50	50
$p_{add}, W$	86	53	21,5	4	1
$\Sigma p, W$	1156	855	566,5	403	376,5
$\eta, \%$	92,8	93,2	93,0	88,6	80,7

The torque developed from PMSM is directly proportional to the quadrature axis component of stator current, if the reluctance torque is zero. From the tables can be seen that PMSM has higher efficiency as compared to IM up to about half rated output. But the stator flux linkage and stator voltage of PMSM decreases in a lesser extent as the loading decreases. This effect is due to the constant value of the rotor flux linkage and leads to a weaker change of the core losses. As a result the efficiency of the motor cut down at lower loads.

### Different number of poles

At design of a special variable speed drive has been place the following question: what number of poles and frequency are appropriate for rated speed of the motor. The answer is not evident always because several variants are possible.

Two variants of an induction motor performed as 4-pole and 8-pole are compared here for rated speed and load. The ratings of the motor are: 18 kW, 1200 rpm, 143,24 N.m, 285 V, delta connection.

As shows Table 4 the outer diameter, core length and air gap length are the same. In the two variants are identical also: number of slots, number of parallel circuits and wires, stator-slots fill factor. In addition, very near are the values of air gap flux density, stator current density and the flux densities of teeth and yoke.

The number of turns in series per phase, winding factors and internal diameters are determined in accordance with the relationship:

$$(wk_w D_i)_{2p=4} = (wk_w D_i)_{2p=8}$$

By implement of above condition becomes equalization of the product between stator flux linkage and frequency in the two variants.

**Table 4**

	2p = 4	2p = 8		2p = 4	2p = 8
$D_a, mm$	270	270	$f_s, Hz$	41,3	81,6
$D_i, mm$	164	190	$I_s, A$	43,0	49,2
$l, mm$	230	230	$I_m, A$	12,5	24,4
$\delta, mm$	0,5	0,5	$B_\delta, T$	0,697	0,705
$Z_s$	48	48	$J_s, A/mm^2$	4,7	4,8
$Z_r$	44	44	$J_r, A/mm^2$	3,1	2,4
$a$	2	2	$R_s, \Omega$	0,296	0,190
$n_e$	3	3	$R_r, \Omega$	0,289	0,176
$k_f$	0,656	0,655	$p_s, W$	679	570
$q$	4	2	$p_r, W$	592	365
$\beta$	0,833	0,833	$p_{Fe}, W$	242	440
$w$	112	96	$p_m, W$	49	57
$k_w$	0,926	0,934	$p_{add}, W$	90	90
$G_{Cu}, kg$	12,7	10,1	$\Sigma p, W$	1652	1522
$G_{Al}, kg$	4,2	4,5	$\eta, \%$	91,6	92,2

The magnetizing current  $I_m$  of 8-pole motor is higher. But the stator winding resistance is smaller due to shorter end connections and less turns. By this reason the 8-pole motor has lower stator winding loss than 4-pole although its stator current  $I_s$  is higher. Both rotor currents, referred to the stator, are equal. The higher rotor winding loss of 4-pole motor results from increased rotor resistance. Inverse is the relation between the core losses in the two variants because of the different frequencies.

It is obvious that the total losses and efficiency depends from the balance between windings and core losses. In the considered case the 8-pole motor has advantage. Moreover, its stator winding has less weight. The data from comparison of the number of poles for PMSM are similar.

An important advantage of the AC motors with large number of poles is the lower inductance due to smaller number of turns and more pole pairs. In considered variants the ratio between the electrical time constants of four-pole and eight-pole IM is 2,5 what influence on the fast dynamic response. The PMSM have lower electrical time constant than IM.

Besides, should be emphasized that the eight-pole motor is more suitable for optimization of lamination geometry. Such optimizing procedure may be carried out by means of finite element method. The main dimensions and winding data, including the number of poles, must be treated as independent variables. The parameters at maximum speed of the drive should be also taken into account for final solution.

### Conclusion

By way of comparison the steady-state characteristics of IM and PMSM are analyzed. On the basis of concrete data of the motors and assuming an ideal vector control comparable condition are defined, as far as is possible. Numerical results for the parameters, components of losses and efficiency at operation in two regions of

regulation are obtained. In addition, the efficiency has been in focus on the research of vector controlled IM and PMSM at different degree of loading. The influence of number of poles is also evaluated. Cost estimate of the motors remain outside this study.

The determination of actual losses and theirs reduction is important for development of high-efficiency variable speed AC drives. In this respect the vector control contribute to an economical energy conversion.

### References

- [1] Vas P. Vector control of AC machines. Oxford Clarendon Pres, 1990.
- [2] Sokolov E., D. Dimitrov. Comparison between computed and test results of vector controlled induction motor, International Conference on Electrical Drives and Power Electronics, Kosice, 1992.
- [3] Sokolov E., M. Minchev, S. Bratkov. Traction drive of electric truck with induction motor. Ninth International Conference on Electrical Machines, Drives and Technologies ELMA'99, Varna, 1999.
- [4] Sokolov E., A. Mushmov. Direct vector control of induction motor. Ninth International Conference on Electrical Machines, Drives and Technologies ELMA'99, Varna, 1999.
- [5] Leonard W. Control of electrical drive. Springer Verlag, 2001.
- [6] Product information of GE, ABB, Schneider, Siemens, Alstom, Ansaldo, Allen-Bradley, Mitsubishi, Bosch, AMK.



**Emil Sokolov** – Professor, D. Sc., Department of Electrical Machines, Faculty of Electrical Engineering, Technical University of Sofia, 8 Kl. Ohridski str., 1000 Sofia, BULGARIA.

e-mail: [erso@tu-sofia.bg](mailto:erso@tu-sofia.bg)

# Performance characteristics of induction motor under V/f speed control

Dimitar Jetchev and George Todorov

**Abstract:** An analysis of steady-state operation and performance characteristics of an induction motor with volt per hertz speed control is presented in this paper. Machine model and algorithm have been developed for calculation the motor's characteristics at variation of the voltage-frequency reference and the load. The variation of electric and magnetic quantities and the characteristics with V/f control without and with IR compensation are analyzed and discussed.

**Keywords:** induction motor, scalar speed control.

## Introduction

In industrialized countries approximately 50% of the electrical power consumption accounts to electric motors. Although the energy conversion in electric machines is with high efficiency, their more efficient use is quite reasonable tendency and can lead to significant energy savings. This makes the industry to use drives with variable speed motors everywhere speed control of the mechanisms is necessary. Years ago the speed control was exclusive domain of DC motors and they were used to drive adjustable speed mechanisms such as conveyors, lifts, extruders, mills, pumps, textile, paper and printing machines etc. In the recent years the improvement in semiconductor technology and control techniques gives an opportunity to improve the performance characteristics of the drives with induction motors and increase their efficiency also. Nowadays the induction motors are widely used in variable speed drives, increasingly replacing the DC machines in various industrial applications.

Two basic methods for AC motor speed control have been developed – volt per hertz or scalar control and vector control. The scalar control method is derived from the steady state machine model. The inverter is relatively simple and cheap. The method does not require observation of the motor speed and currents during operation. This makes the speed to vary at different loads, significantly at low voltage-frequency reference. Despite this the method is satisfactory for industrial and domestic low performance applications where the speed accuracy is not required.

The vector control methods are developed on the bases of dynamic machine model and are aimed to permanent control of the magnetic flux linkage in chosen frame reference. This has been achieved by decomposing the stator current into two components – flux-producing current and torque-producing current. The independent control of these components gives the induction machine an opportunity to operate in four-quadrant regulation just

like separately excited DC machine. The vector control methods provide better dynamic performance, speed control accuracy and energy efficiency of the AC drives than these with scalar control. The main disadvantages are the necessity of feedback (position, speed, current), complicated computational transformations, more complicated and expensive controller.

Subject of the present paper is the operation of induction motor with scalar frequency control. A steady state mathematical model of the motor and algorithm for calculation of the performance characteristics are developed. The variation of electric and magnetic quantities and the characteristics of a four-pole 4 kW induction motor are analyzed at variation of the load for different voltage-frequency reference.

## Mathematical model of induction motor for scalar speed control

The mathematical model of induction motor for scalar speed control is derived from well known equivalent T circuit. In order to describe the processes more accurate, it don't use the assumptions that have usually been made from many authors for analyses of frequency controlled induction motors. The non-linear dependence between the electromotive force and magnetizing current, the influence of slot leakage flux and skin effect have been taken into account and included in the model. The core losses and their change with speed regulation have been taken into account also. At referred voltage and frequency, recalculation of the equivalent circuit equations is made for each load level, to obtain the correct values of the emf, motor flux and magnetic flux density for each particular sector of the magnetic circuit. The magnetic core losses are calculated with these specified values of the magnetic flux density and are used in the model.

Under the scalar speed control the range of frequency regulation is usually divided in two regions – below and over the base frequency. The relationship between the input voltage and frequency is linear within the first region. In practical frequency converters with scalar control two cases for this region are realized – proportionality between voltage and frequency

$$(1) \quad \frac{U}{f} = K = const$$

or

$$(2) \quad U = U_0 + K \cdot f .$$

The offset voltage  $U_0$  (initial voltage at 0 Hz) is used for IR compensation – to overcome the voltage drop

created by the stator current in the stator winding resistance.

In the region over the base frequency the input voltage remains constant with the increase of frequency – Fig.1.

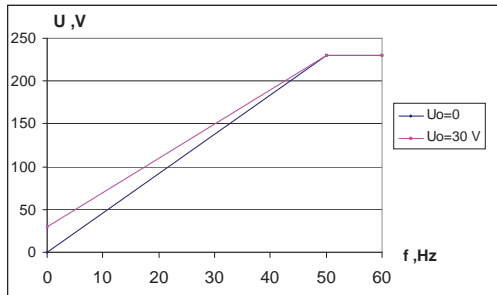


Fig. 1. Input voltage - frequency

In the discussed model base frequency is 50 Hz and base voltage is equal to the rated – 230 V line-to-neutral for “star” connected stator windings or 400 V line-to-line for “delta” connected windings. The offset voltage  $U_0$  can be adjusted between 0 и 30 V.

### Maximum torque

The volt-per-hertz control principle is based on the aim to maintain the motor magnetic flux and the maximum torque produced by the motor uniform through the full range of speed control. Theoretically it is assumed that the maximum torque is approximately quadratic function of the ratio of input voltage and frequency and consequently the maximum torque is proportional to the magnetic flux. This assumption is correct only when the influence of stator winding resistance is negligible. In practice this resistance is negligible in high power motors but for the most of general purpose motors (low and middle power motors) it influences on the motor operation and could not be neglected.

Calculations of electric and magnetic quantities and performance characteristics have been made for 4 kW four-pole induction motor with the proposed model. The characteristics have been analyzed for both cases –

without IR compensation -  $\frac{U}{f} = const$  ( $U_0 = 0$ ) and with

compensation (adjustment of  $U_0 > 0$ ).

The calculated characteristics of the torque, when the motor is fed by the converter without IR compensation, are shown in Fig.2 for several values of voltage-frequency reference. The same characteristics with offset voltage  $U_0 = 15$  V are shown in Fig.3. It is clearly seen that contrary to the theoretical assumption the maximum torque shows significant reduction with reduction of referred frequency for both cases. It was found that the magnetic flux density at maximum torque decreases with reduction of the

frequency at  $\frac{U}{f} = const$  speed control case – Fig.4.

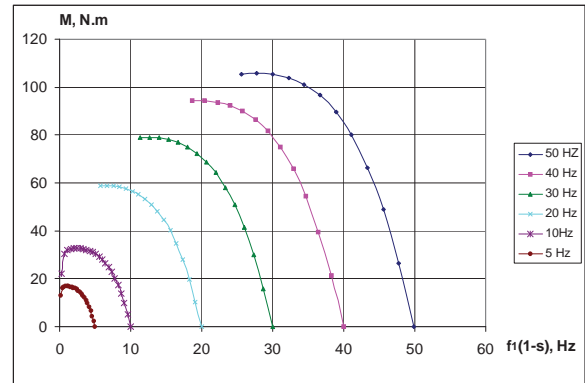


Fig. 2. Torque of the motor fed with  $\frac{U}{f} = const$

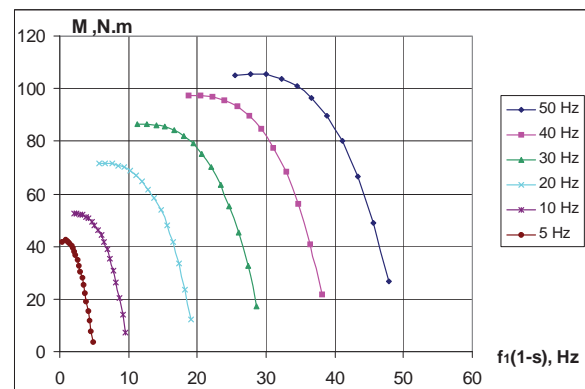


Fig. 3. Torque of the motor fed with IR compensation –  $U_0=15$  V

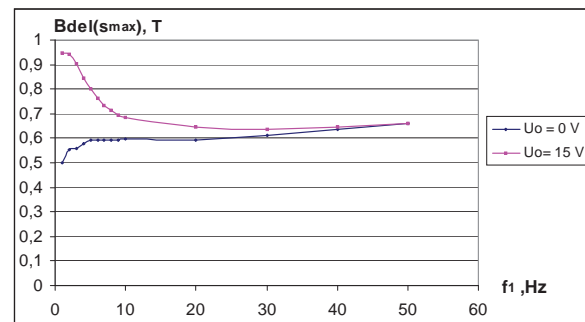


Fig. 4. Magnetic flux density at maximum torque

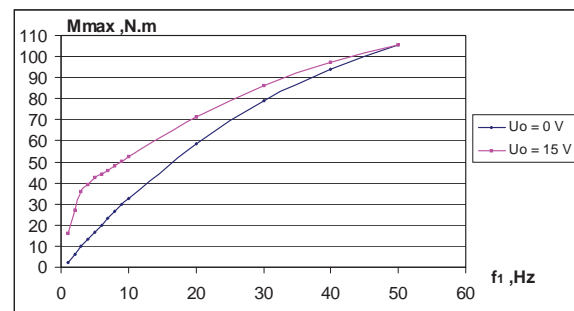


Fig. 5. Maximum torque vs. frequency reference

The voltage offset leads to increase of the magnetic flux density and the maximum torque for low frequencies. Although the increase in flux density is significant, the increase in the motor torque is small – Fig.5. This result demonstrates the influence of the stator resistance and allows concluding that the scalar control does not provide operation with uniform maximum torque for wide speed range.

### Electric and magnetic quantities

The variation of stator current and air gap magnetic flux density with the load are analyzed for different voltage-frequency reference. The characteristics for  $U/f = const$  are shown in Fig. 6 and Fig.7.

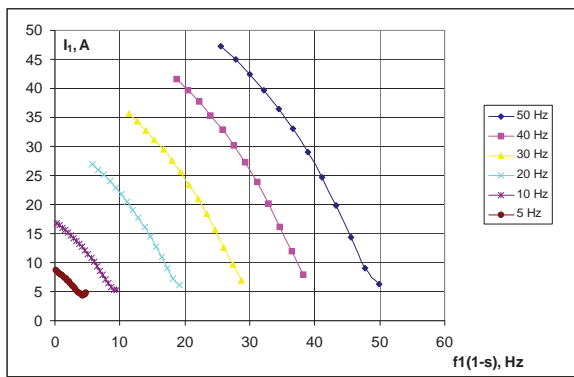


Fig. 6. Stator current for the motor fed with  $U/f = const$

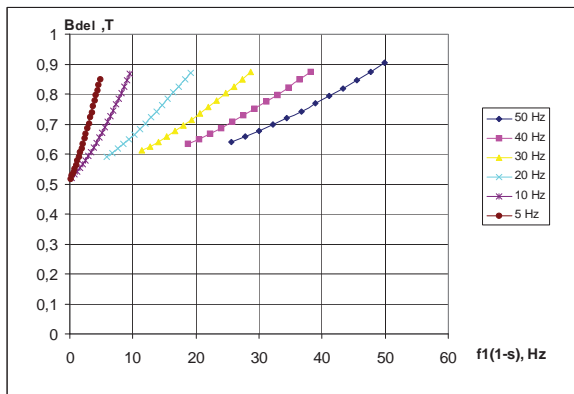


Fig. 7. Air gap flux density for the motor fed with  $U/f = const$

It stands to reason that with the load increase the motor current increases and the flux density decreases. Whereas the slope of current characteristics is uniform for all referred frequencies, the slope of magnetic flux density characteristics increases with the reduction of frequency reference. The reason for this increased slope is the influence of the voltage drop created by the stator current on the stator resistance, which causes reduction in the electromotive force. The voltage offset can not overcome it although the air gap magnetic flux density at low frequencies reaches values over 1 T – Fig.8. On the other hand these high values of the flux density lead to

increased saturation of the motor magnetic core, increase in the magnetizing current and the stator current of the motor – Fig.9.

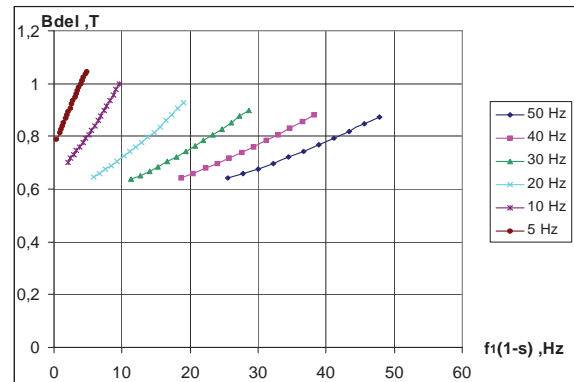


Fig. 8. Air gap flux density for the motor fed with voltage offset  $U_0 = 15 V$

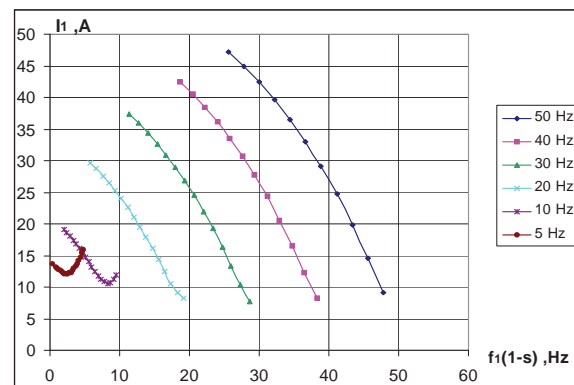


Fig. 9. Stator current for the motor fed with voltage offset  $U_0 = 15 V$

Consider the motor operate laded with rated torque and speed control in the range below the based frequency is applied. The stator current remains approximately equal to the rated motor current for rotor speeds down to  $300 \text{ min}^{-1}$  and then increases – Fig.10. In combination with worsen cooling conditions this may cause windings' overheating. Hence, if the motor is intended for continuous operation with low speed, its design should include independent cooling system.

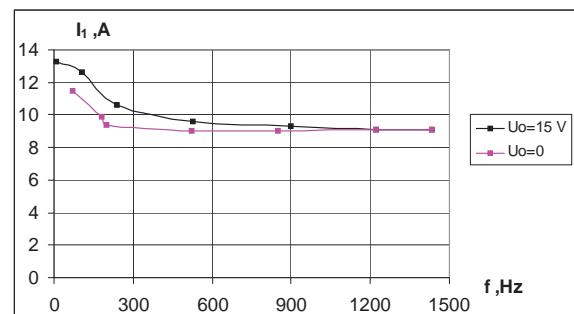


Fig.10. Stator current at  $M=Mr=const$



## Energy saving

It stands to reason that the possibility to control the motor speed gives significant energy saving and it is one of the reasons for increased implementation of the variable speed drives. Although the U/f scalar control is less effective compared to vector control methods, it provides the drive reduced power consumption.

When the motor operates with constant load and variable speed, its energy consumption goes down approximately proportional to the speed reduction. The input power of 4 kW motor for different reference frequencies is shown in Fig.11. The motor operates in the full range with constant load torque of 26.6 N.m, which is its rated torque. The power consumption is 4800 W at 400 V/50 Hz and 1215 W at 80 V/10 Hz.

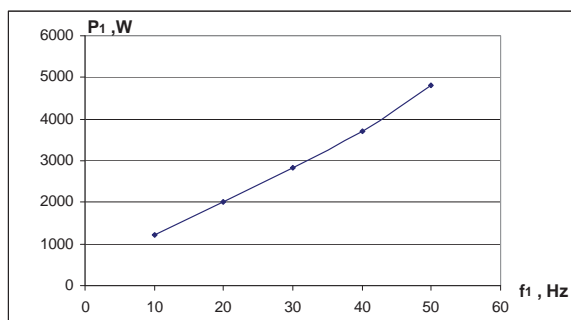


Fig.11. Power input vs. frequency reference

## Conclusion

The mathematical model and algorithm for analyses the operation and performance characteristics of induction motor fed by frequency inverter with volt-per-hertz control is presented. The calculated values for electric and magnetic quantities, performance characteristics and maximum torque for different voltage-frequency references can be obtained with the aid of the algorithm.

The results from the analyses performed for several motors with different power demonstrate that scalar control method can not provide operation with uniform maximum torque, even when IR compensation with voltage offset at low frequencies is applied. Nevertheless, the proposed algorithm gives an opportunity to predict and analyze the characteristics of the motor and obtain optimum voltage offset according to expected load conditions.

## References

- [1] Жечев, Д. Методи, алгоритми и програмни продукти за електромагнитни изчисления на променливотокови машини и електрозадвигвания с асинхронни двигатели при честотно регулиране. Дисертация, ТУ-София, 1999.
- [2] Bose, B.K. Power electronics and AC drives. Prentice Hall, 1986.
- [3] Delaleau, B., J. Louis, R. Ortega. Modeling and control of induction motors. Int. Journal Appl.Math.Comput.Sci., Vol.11, No.1, 2001, pp.105-129.

[4] Munoz-Garcia, A., T.A Lipo, D. Novotny. A new induction motor V/f control method capable of high-performance regulation at low speeds. IEEE Trans. On Industry Applications Vol.34, No.4, July/August 1998.

[5] Murphy, J.M.D., F.G. Turnbull. Power electronic control of AC motors. Pergamon Press, 1989.

## Biographies



**Dimitar Jetchev** was born in Plovdiv, Bulgaria, on September 18, 1940. He studied at the Technical University of Sofia and received Ph.D. degree from the same university in 1999.

He worked in the Faculty of Electrical Engineering as an Associate Professor in the field of electrical machines, frequency control, electromagnetic calculations.

Dimitar Jetchev is with the Faculty of Electrical Engineering, Technical University of Sofia, 8, Kl. Ohridski Blvd., 1000 Sofia, Bulgaria (e-mail: jetch@tu-sofia.bg).



**George Todorov** was born in Sofia, Bulgaria, on December 16, 1954. He graduated at the Technical University of Sofia in 1980 and received Ph.D. degree from the same university in 1994.

Since 1998 is Associate Professor at the Dept. of Electrical Machines.

His field of interest includes electrical machines, design optimization, electro-mechanical devices.

George Todorov is with the Faculty of Electrical Engineering, Technical University of Sofia, 8, Kl. Ohridski Blvd., 1000 Sofia, Bulgaria (e-mail: gtto@tu-sofia.bg).

# Start-up process of induction motor fed by frequency converter

George Todorov and Dimitar Jetchev

**Abstract:** The start-up process of asynchronous motor fed from frequency converter with  $U/f$  control has been discussed. The starting current and frequency when the motor accelerates with different static load torque are analyzed to obtain optimum starting conditions. Comparison with the start-up at full voltage is made and it suggests that modification in the design of motors intended for variable-frequency speed control, gives an opportunity to achieve higher maximum torque without exceeding the starting current limits.

**Keywords:** induction motor; starting current, torque and frequency.

## Introduction

Some induction motors operate electrical drives where the starting conditions are not severe, such as fans, blowers and pumps. These motors are not required to produce high starting torque and their design usually has a low-resistance single cage rotor. Other class of motors is designed to drive cranes, lifts, conveyers, mills etc., where higher starting torque and low starting current are required. With suitable shapes and arrangements for rotor bars, squirrel-cage rotors are designed to use the inductive effect of the slot-leakage flux on the current distribution, resulting in an increase in the resistance and decrease in the leakage inductance of the bar. This design uses deep-bar or double-cage rotor and provides good starting characteristics at the expense of lower maximum torque and running efficiency.

The most common dynamic problem for conventional motors is that the across-the-line starting at full voltage is always associated with heavy inrush current. The maximum of the current occurs at standstill and a limit for this value is used as a constraint at the motor design. The contemporary industry drives use mainly variable speed motors to achieve more flexibility, better performance and energy savings. The motors are fed from frequency converters with scalar or vector control and their start-up process differs from the full voltage start. The converter provides the motor power supply of increased voltage and frequency with various steps for smooth rotor acceleration. This nature of the starting process gives new interpretation of the starting current and starting torque and suggests opportunities for some changes in the motor design. The present paper discusses the start-up processes of induction motors under scalar speed control which are used in electric drives with low dynamic performance applications. The processes are analyzed based on steady-state theory and use steady state speed-current and speed-torque characteristics. Such an analysis neglects the effects of electric transients

which occur and subside much faster than electromechanical dynamics of interest.

## Stator current of induction motor fed by frequency converter

Like for across-the-line start-up at full voltage/full frequency, the current at standstill is called starting current. The difference is in the fact that frequency converter start-up turns the rotor into rotation at the lowest frequency and voltage. During the starting process they raise and bring the motor to the referred speed. This leads to change in the magnitude of the starting current and in the current-speed characteristic. The current-speed curves for a 4 kW, four-pole induction motor are shown in Fig.1 – the dashed line is for full voltage start, the solid line – for frequency converter start. In order to calculate the current at frequency converter start, it is necessary to assign the torque required to turn the load (static load torque). The characteristic in Fig.1 is calculated with rated load torque and frequency converter performing  $U/f = const$  speed control.

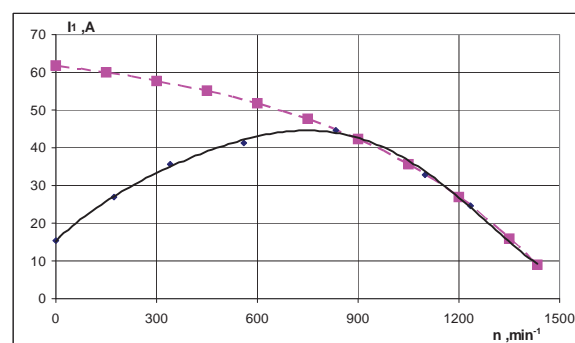


Fig. 1. Current-speed characteristics for 4 kW four-pole induction motor

Significant difference occurs in the starting current and between the curves for the speed range from standstill to speed, corresponding to the motor breakdown torque. The starting current for across-the-line start-up at full voltage 400 V/50 Hz is 61,9 A and decreases as the rotor speeds up. At frequency converter start-up the rotor turns into rotation with 41,4 V / 9 Hz and starting current of only 15,3 A. By raising the voltage and frequency the rotor accelerates, the motor current increases, reaching its maximum value for speed corresponding to the breakdown torque and then decreases to the full load current. With the increase of the static load the starting current raises (Fig.2), but it was found out that even if the torque required to turn the load is 2,5 times the rated

torque, the starting current is lower than those at across-the-line start-up at full voltage and than the current corresponding to speed at which maximum torque occurs.

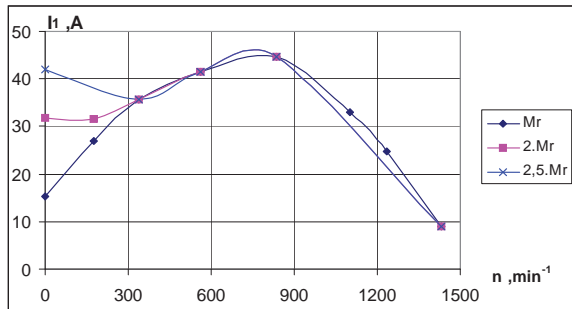


Fig.2. Current for acceleration with different static torque

Consequently the maximum value of the stator current during acceleration process of the induction motor fed by frequency converter is associated with the speed corresponding to the breakdown torque. Furthermore, this value is lower than the starting current at full voltage/full frequency start-up.

### Starting frequency

The starting process of the frequency converter fed motors is smoother when the rotor turns into rotation with reduced starting current and lowest starting frequency. A simple solution for lowering the starting frequency and current is to adjust the frequency converter with a fitting offset voltage. This opportunity is illustrated in fig.3.

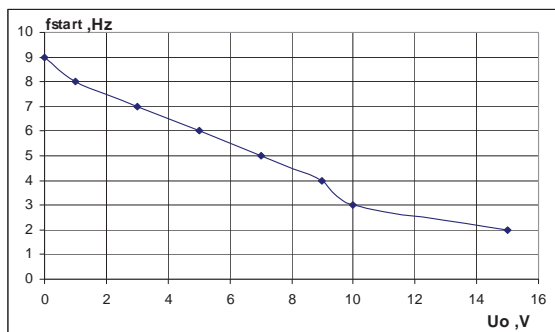


Fig.3. Reduction of the starting frequency with variation of  $U_0$

For the example under consideration the motor will turn the rated static load with starting current 15,3 A and starting frequency 9 Hz without voltage offset (Fig.3 and Fig.4). Raising the offset voltage the starting frequency and current reduce and with  $U_0=10$  V starting frequency is 3 Hz and starting current – 9,5 A.

Thus it was found out that IR compensation besides increase in the motor torque at low frequency reference, leads to reduction of the starting frequency and the starting current. This gives an opportunity to find the favourable starting conditions depending on the torque required to turn the load by choosing appropriate voltage offset  $U_0$ . This is illustrated in Fig.5 for several values of the static load torque.

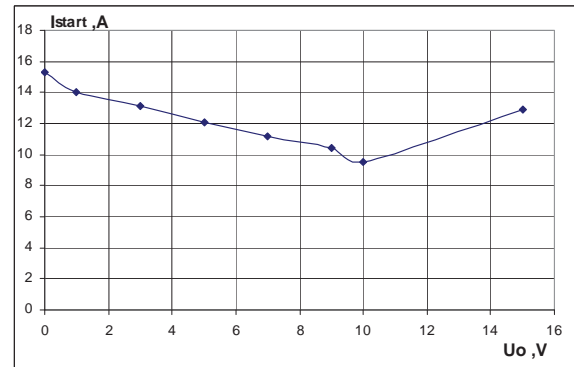


Fig. 4. Starting current with variation of  $U_0$

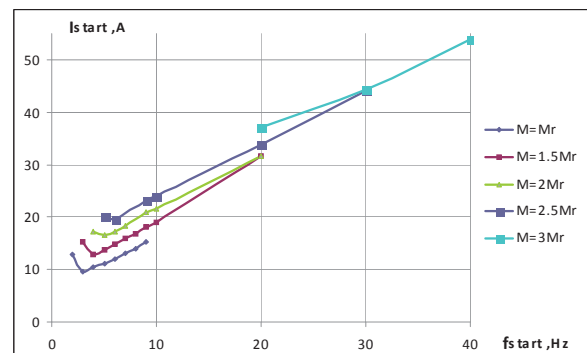


Fig.5. Starting current and starting frequency for different static load torque

### Design of induction motor for variable speed drives

It is well known that the conventional induction motors design uses the inductive effect of the slot-leakage flux on the current distribution in the rotor bars to achieve good starting characteristics. It uses deep-bar or double-squirrel cage rotors, in which the effective rotor resistance and leakage inductance change with the slip. The result is higher starting torque with low starting current but at the expense of somewhat lower running performance – internal maximum torque and efficiency.

As it was shown in previous sections, the maximum value of the stator current of the induction motor fed by frequency converter is not the starting current, but the current associated with the speed at which the maximum torque occurs. The starting current is lower than those at across-the-line start-up at full voltage, even if high torque is required to turn the load. In this case the use of inductive effect of the slot-leakage flux is not necessary and this provides an opportunity for some changes in the induction motor design. One simple option to achieve higher internal maximum torque and efficiency is to change the rotor bars geometry so that lower their resistance and leakage inductance. Reduction of the leakage inductance has bigger effect on the magnitude of the maximum torque. At the same time it leads to increase in the motor current at standstill and in the current for all speeds also. It was found that during acceleration the motor current reaches its maximum at speed at which maximum torque occurs. Hence the

following constraint in the motor design may be used: the maximum current during acceleration should not exceed the starting current of the conventional motor at full voltage start-up.

As an example a modification in the design of a four-pole 11 kW induction motor with rated current 21,4 A is given for illustration of a compromise between running requirements and those of start-up. The initial motor is standard general purpose and uses double-cage rotor with 28 slots. The slots depth is 28 mm and the slots area is 101 mm<sup>2</sup>. The rotor resistance, referred to the stator is 0,271 Ω at 20 °C, leakage inductance at 50 Hz – 1,792 Ω. Some of characteristics are given in Table 1.

**Table 1**

*Initial design - double-cage rotor*

$\eta, \%$	$M_{st}^*$	$I_{st}^*$	$I_{st}, A$	$M_{max}^*$	$I_1, A$ at $M_{max}$
89.18	3.14	6.74	144	3.2	104.5

The modified design uses single cage rotor. The number of slots is unchanged, slots area is approximately same (101 mm<sup>2</sup>) but the depth is reduced to 21,2 mm. Now rotor resistance at 20 °C is 0,238 Ω, leakage inductance at 50 Hz – 0,811 Ω. The rated current decreases with 0,5 A and the efficiency increases with 1%. The reduced values of the rotor resistance and inductance cause significant raise of the starting current at across-the-line start-up at full voltage. Some of its characteristics at 400 V / 50 Hz are shown in Table2.

**Table 2**

*Modified design - single-cage rotor*

$\eta, \%$	$M_{st}^*$	$I_{st}^*$	$I_{st}, A$	$M_{max}^*$	$I_1, A$ at $M_{max}$
90,24	4.09	10.27	215.9	5.09	144.25

Adjusting an appropriate offset voltage, the frequency converter provides the motor smooth starting process with lowest frequency and current. The current during the acceleration does not exceed the starting current of the initial motor even when the torque required to turn the load is several times greater than the rated torque. An important advantage of the modified design is the increase of 59% in the maximum torque and 1% in the motor efficiency.

The result of an analysis shows that the motor will start at 17,8 V/2 Hz and starting current 31,5 A when the torque required to turn the load is 1,5 times the rated torque. With the required torque 3 times the rated torque the motor will start at 31,7 V/3 Hz and starting current 56,6 A. The curves of the motor current during acceleration for these two cases are shown in Fig.6 compared to the current of the initial motor.

## Conclusion

The starting process of an induction motor, fed by frequency converter is associated with current which

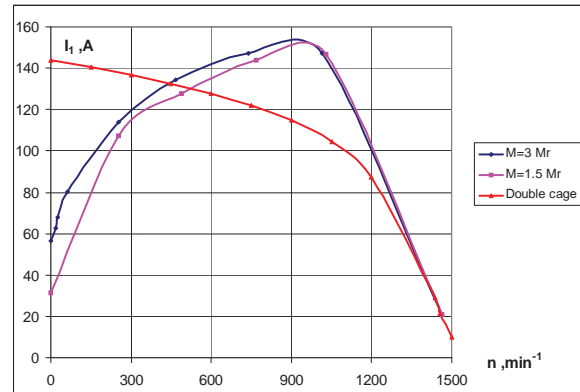


*Fig. 6. Current-speed curves for initial and modified 11 kW induction motor*

values during acceleration are lower than the starting current at across-the-line full voltage start-up, even when the torque required to turn the load is several times the rated torque. The starting is smooth, with low frequency and starting current.

Modification in the rotor design which aims to reduce the rotor leakage inductance makes a compromise between running requirements and those of start-up and allows significant increase in the maximum torque of the motor.

## References

- [1] Murphy, J.M.D., F.G. Turnbull. Power electronic control of AC motors. Pergamon Press, 1989.
- [2] B. Bose, Power Electronics and Variable Frequency Drives. New York: IEEE Press, 1996.
- [3] Slaets, B P., Van Roy, R. Belmans, K. Hameyer. Energy Efficiency of Induction Machines. Katholieke Universiteit Leuven, Belgium, 2003.

## Biographies



**George Todorov** was born in Sofia, Bulgaria, on December 16, 1954. He graduated at the Technical University of Sofia in 1980 and received Ph.D. degree from the same university in 1994.

Since 1998 is Associate Professor at the Dept. of Electrical Machines.

His field of interest includes electrical machines, design optimization, electro-mechanical devices.

George Todorov is with the Faculty of Electrical Engineering, Technical University of Sofia, 8, Kl. Ohridski Blvd., 1000 Sofia, Bulgaria (e-mail: gtto@tu-sofia.bg).



**Dimitar Jetchev** was born in Plovdiv, Bulgaria, on September 18, 1940. He studied at the Technical University of Sofia and received Ph.D. degree from the same university in 1999.

He worked in the Faculty of Electrical Engineering as an Associate Professor in the field of electrical machines, frequency control, electromagnetic calculations.

Dimitar Jetchev is with the Faculty of Electrical Engineering, Technical University of Sofia, 8, Kl. Ohridski Blvd., 1000 Sofia, Bulgaria (e-mail: jetch@tu-sofia.bg).



# Study of a synchronous excitation generator with rotating rectifier

Dimitar Sotirov, Plamen Rizov, Ivailo Panayotov, Dimitar Bozhov,  
Boyan Krachev and Vladimir Doychev

**Abstract:** *The development of today's synchronous machines is tightly connected with use of brushless excitation systems. They have advantages like high exploitation reliability, long-term operation, low power for control and they don't need any special maintenance during exploitation. Leading hydro generators and other synchronous machines manufacturers like ALSTOM, GENERAL ELECTRIC, ABB, ELECTROSILA and others use such excitation generators in a wide range of power which reaches 1000 MW for turbogenerators. In our country these excitation generators are manufactured for relatively low synchronous generator's power of the order of a few hundreds kW. Attempting to use them at higher powers, leads to some problems such as overheating the exciter's inductor steel. The analyzing of these problems, particularly the excitation generator's magnetic field study, as well as their elimination is the subject of the present project.*

## Study method

Analytical model of an exciter with rotating rectifier is developed using finite-element method (FEM), by means of which the influence of the armature reaction over the magnetic induction distribution curve in the air gap under the inductor's pole.

The simulation model for this study consists of the following stages:

1. Choosing the method for solving the electromagnetic problem:

Taking in mind the nature of the electromagnetic processes that lead to pulsations in the magnetic flux in the solid parts of the inductor, a numerical method for solving the electromagnetic problem is chosen, based on FEM.

2. Choosing a geometry area of the exciter with rotating rectifier to implement the FEM analysis.

Taking in mind the symmetry in the geometry area of the exciter with rotating rectifier in radial direction, the area limits to six rotor poles. For this purpose a radial direction section of the poles is examined which is situated perpendicular to the poles' axis. Thus the model is defined as planar, while when calculating the magnetic flux, the actual stator length in axial direction is taken.

3. Magnetic circuit of the simulation model

It consists of the stator (inductor) magnetic cores, the rotor and the air gap. The magnetic induction in the air gap is excited from the interaction of the stator poles' excitation winding, which the excitation current flows through and the armature winding, through which flows the current to the rotating rectifier. The steel is modeled with the relevant magnetization curves. Thus the

magnetic cores saturation is read, which value is very close to the actual.

4. Choosing the control area in the magnetic circuit

Controlling the magnetic induction and magnetic flux values is made in the air gap in the middle of the pole. The air gap is even, with some difference in the area facing an armature tooth or a slot.

5. Choosing the mathematical algorithm for simulating electric field in a synchronous exciter with rotating rectifier.

The mathematical algorithm is based on the first law of Maxwell for the electromagnetic field.

6. Choosing the mathematical apparatus of the finite-element method.

The basic principle of finite-element method is in breaking the studied area into large number of elementary regions with finite dimensions. In each of these regions (so called finite elements) the unknown function is approximated with a first, second or third power polynomial. Spline functions are used as approximating functions. These are functions that are interconnected on the border between adjacent finite elements. By the spline functions, a continuity of the unknown function is provided. Also with the higher range splines, continuity of its provided derivatives. The approximation with spline functions is connected with different finite elements geometric forms; in the simulation model first range triangles are used. They cover the entire examined area and form a finite elements mesh. With the first range triangles there are three knots and the spline functions are linear. Interconnection for the unknown function only is provided. The triangle points are common and represent the mesh support knots, which covers the studied area of the synchronous exciter.

## Calculation results and finite-elements analysis of the exciter's magnetic field.

The calculations and the analysis are made for the initial (uncorrected) construction of the exciter of the HPP Retizhe 3 hydro generator, manufactured by Elprom ZEM, with the following data:

- Nominal rectified voltage  $U_n = 58$  V;
- Nominal rectified current  $I_n = 425$  A;
- Nominal angular velocity  $n_n = 750$  min<sup>-1</sup>;
- Number of poles  $2p = 16$ ;
- Number of rotor slots  $Z_r = 48$ .

One interval of the current flowing through phase A and B is analyzed for the exciter's nominal operation, without taking into consideration the phase current lag from the



electromotive force (emf). Since the exciter's load is a hydro generator's excitation winding, which characterizes by a long time constant (the order of 0.5 to 1 second), it can be assumed that in steady state, within the interval of conducting of two phases, their current is constant. The calculations are made for six rotor positions, situated evenly in relation to the rotor boundary positions within the interval in which the current flows in phase A and B. A stationary problem is solved, without taking into account the damper effect of the currents in the magnetic core's solid parts. The picture in fig. 1 shows the machine's field in the initial state of the conducting phase A and B interval. In fig. 1a is shown a picture of the field while nominal excitation and armature current is flowing. In fig. 1b respectively a picture of the field while only nominal armature current flows. Fig. 1c shows the magnetic induction distribution curve in the air gap under the inductor pole for the both cases. Respectively in fig.

2, 3, 4, 5 and 6 are shown pictures of the field and the magnetic induction distribution curve in the air gap under the inductor pole for the rotor rotated respectively at 12°, 24°, 36°, 48° and 60° (electrical) in relation to the initial position in fig. 1. The strong influence of the quadrature armature reaction over the magnetic induction distribution curve is apparent, due to the non-saturated magnetic circuit, small number slots for a pole and phase ( $q=1$ ) and the specific load nature, as for this case the latter is three-phase bridge rectifier. From the air gap magnetic induction distribution curve, for the examined rotor positions, the average induction  $B_{av}$  is calculated.  $B_{av}$  varies from 0.587T in the initial rotor position to 0.536T in the end position, i.e. within one interval of the diode conducting direct pulsation of the field is 9%. This result corresponds to the experimental study of the exciter, the results of which are given in [7].

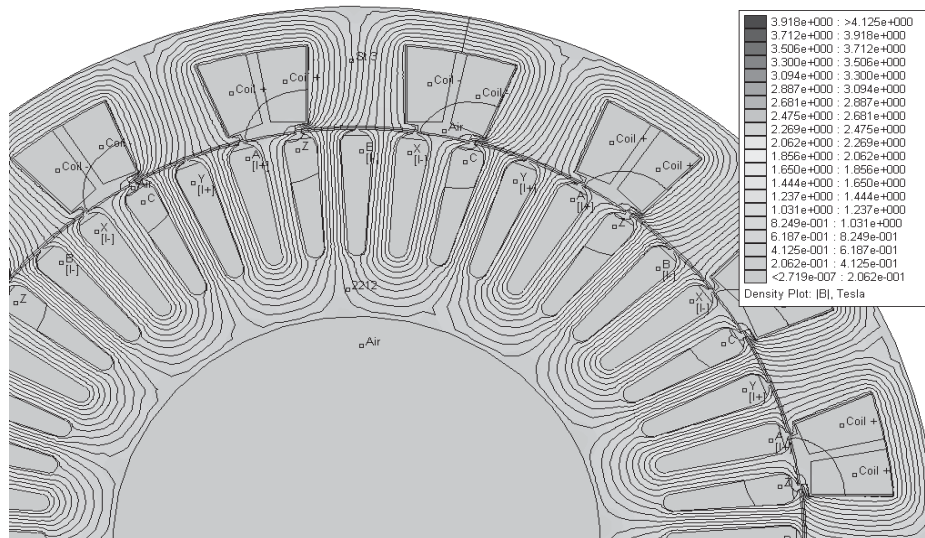


Fig.1a. Picture of the field while nominal excitation and armature current is flowing in the initial state of the conducting phase A and B interval.

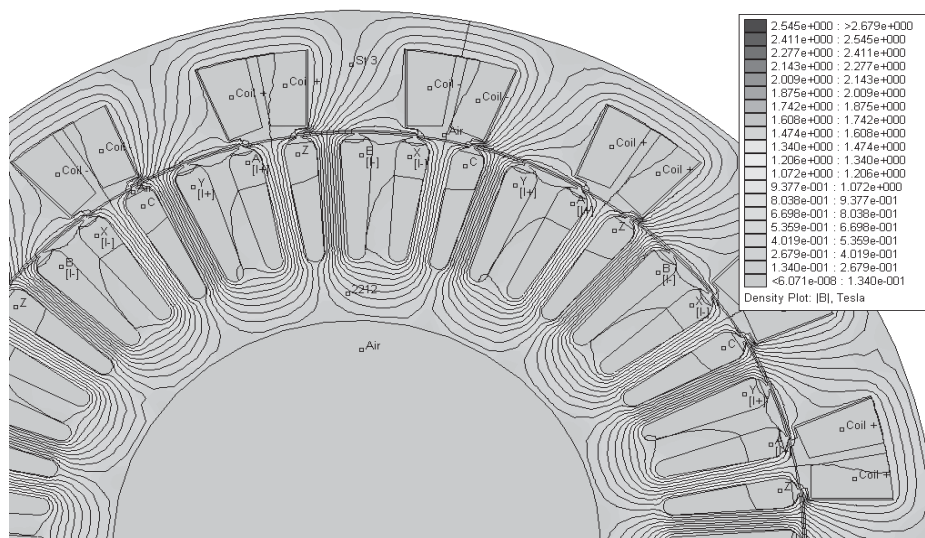


Fig.1b. Picture of the field while nominal excitation and armature current is flowing in the initial state of the conducting phase A and B interval.

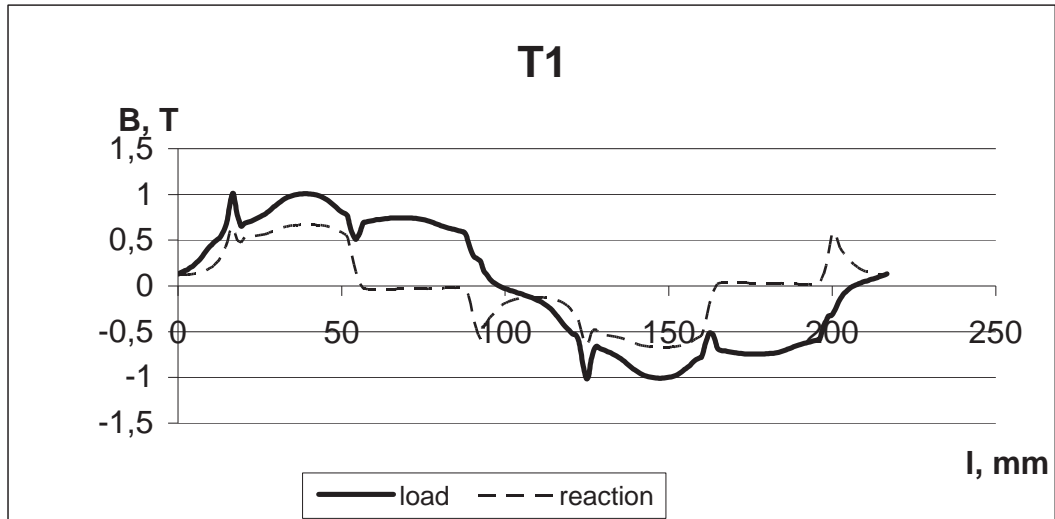


Fig.1c. The magnetic induction distribution curve in the air gap under the inductor pole for the both cases.

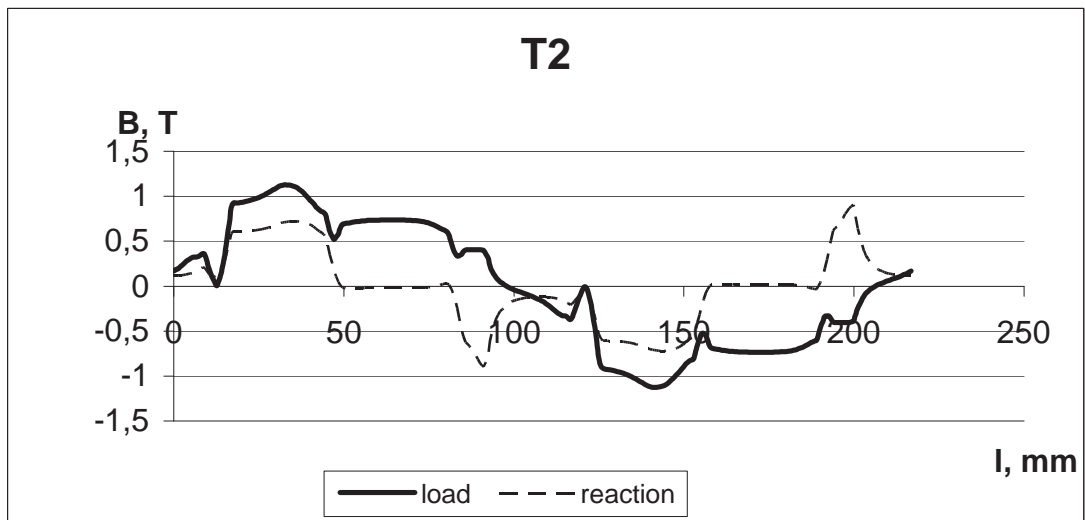


Fig.2. The magnetic induction distribution curve in the air gap under the inductor pole for the both cases for 12° electrical.

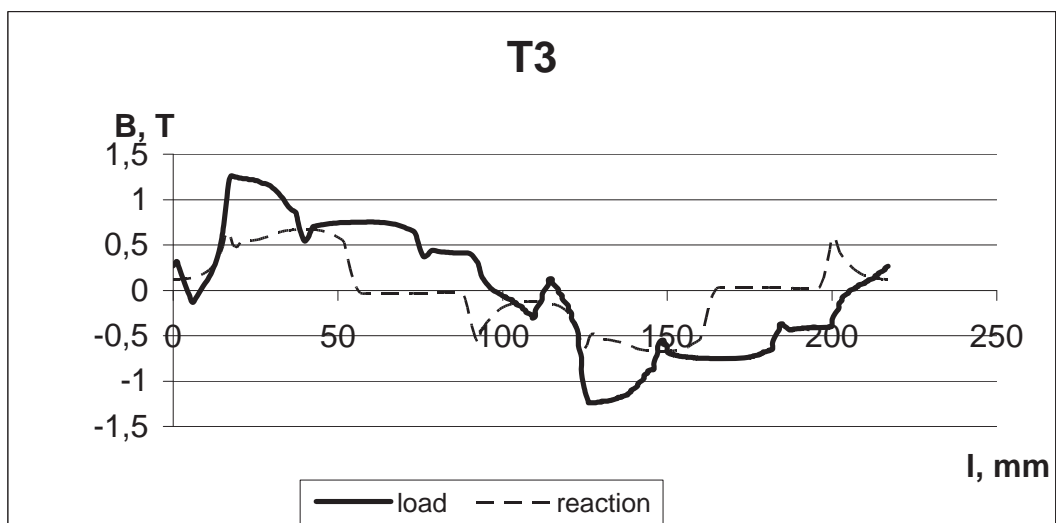


Fig.3. The magnetic induction distribution curve in the air gap under the inductor pole for the both cases for 24° electrical.

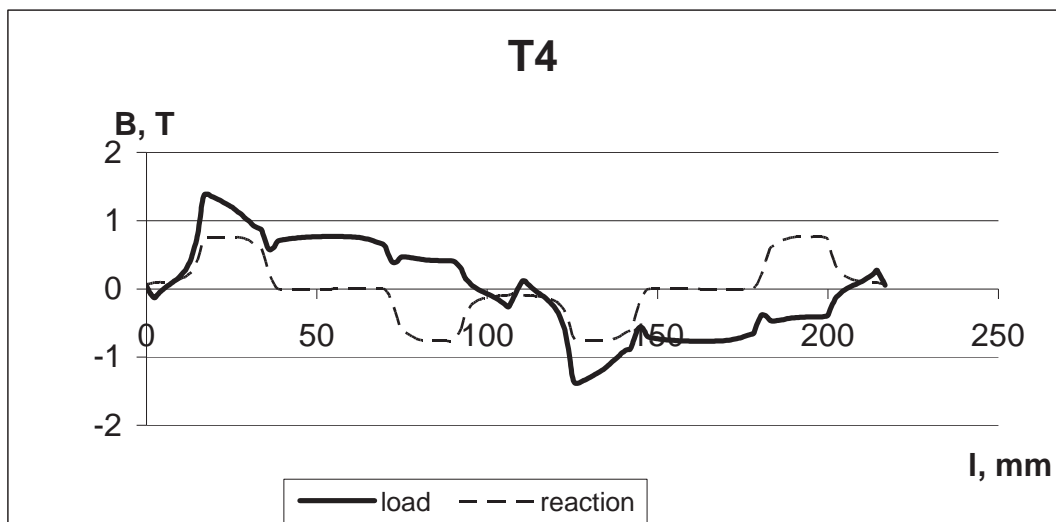


Fig.4. The magnetic induction distribution curve in the air gap under the inductor pole for the both cases for 36° electrical.

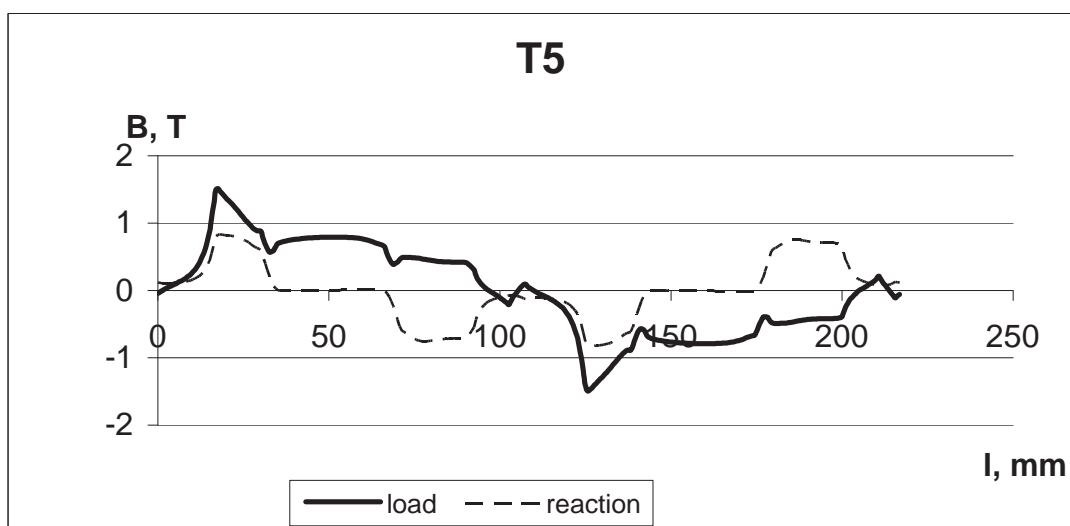


Fig.5. The magnetic induction distribution curve in the air gap under the inductor pole for the both cases for 48° electrical.

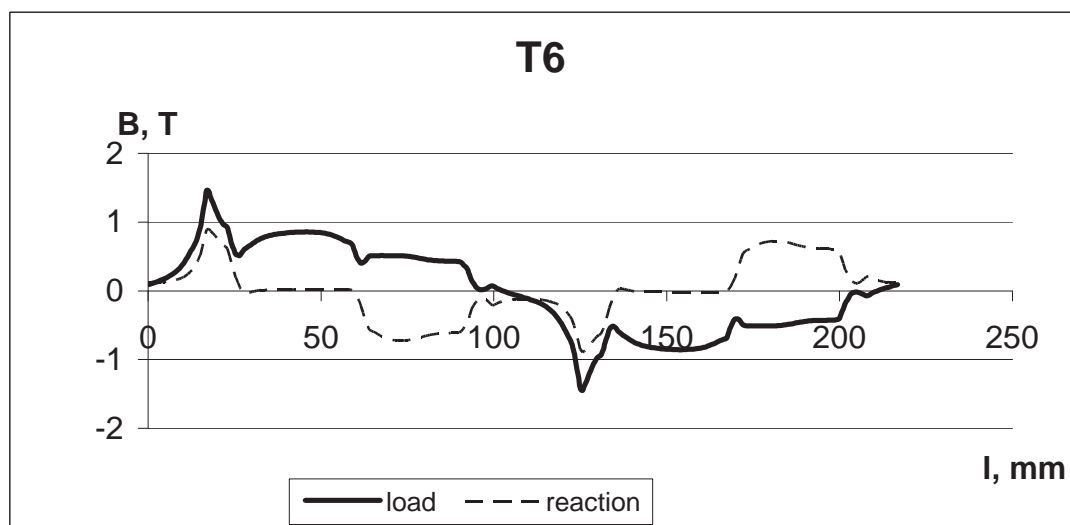


Fig.6. The magnetic induction distribution curve in the air gap under the inductor pole for the both cases for 60° electrical.

## Conclusion

1. From the air gap magnetic induction spatial distribution curve under load (fig. 1c, 2c, 3c, 4c, 5c and 6c), can be seen that in the pole's output end, the armature reaction is magnetizing and the magnetic induction is increasing, in relation to idle running state, from 50% at the beginning of the conduction of two phases interval up to 100%. The area with the increasing induction decreases with the rotation of the rotor due to shifting of the rotor teeth in relation to the stator poles. In the input pole end at the beginning of the conduction of two phases interval a slight field reduction occurs, due to the armature reaction.
2. With the rotation of the rotor, from the initial moment of conducting the two phases, the zone of increasing the field strength in the output pole end shrinks, while in the input pole end zone an increased interval can be seen, with magnetic induction close to zero. This leads to decreasing the magnetic induction average value and the equivalent armature reaction demagnetizing influence, which in this case reaches up to 9%.
3. The air gap magnetic induction spatial distribution curve under load is non-sinusoidal and varies in a wide range with the rotation of the rotor. This forms a salient non-sinusoidal shape of the phase emf and alters the rotor position so that a current would flow through the two examined phases.
4. From the obtained results can be seen that with the rotation of the rotor significant by amplitude direct and quadrature magnetic induction pulsations in the air gap and respectively in the exciter poles. In solid steel implemented stator poles and yoke, these magnetic induction pulsations lead to eddy currents and hysteresis losses and could cause malfunctions. For this purpose the inductor should be made from lamellated steel, although the magnetic flux is constant.

## References

- [1] Ангелов А.М., Д.А. Димитров. Электрически машини, I и II част. Техника, София, 1976, 1988.
- [2] Абрамов А.И., А.В. Иванов-Смоленский. Проектирование гидрогенераторов и синхронных компенсаторов. Высшая школа, Москва, 2001.
- [3] Копылов И. П. Электрические машины. Высшая школа, Москва, 2000.
- [4] Шуйский В. П. Расчет электрических машин. Энергия, Ленинград, 1968.
- [5] Силвесстер П, Шумилов Ю. Метод конечных элементов. Мир, Москва, 1969.
- [6] Guerin Chr. Modelisation de regions minces et prise en compte de la saturation des materiaux magnetiques en regme harmonique. These de l'INPG, Laboratoire d'Electrotechnique de Grenoble, 1994.
- [7] Sotirov D. K., I. Panayotov, D. Bozhov, B. Krachev, V. Doychev. Problems in joint work of a synchronous generator with an uncontrolled rectifier. ELMA 2008, Sofia, 2008.

## Biographies



**Dimitar Sotirov** was born in Velingrad, Bulgaria, on Mart 1, 1946. He graduated the Technical University of Sofia and acquired Dr degree from the same university in 1983.

Since 1969 he worked in the Faculty of Electrical Engineering of the Technical University of Sofia as a Lecturer, Associate Professor, 1986 and Head of Department of Electrical Machines, 2000.

Dimitar Sotirov is with the Faculty of Electrical Engineering, Technical University of Sofia, 8, Kl. Ohridski Blvd., 1000 Sofia, Bulgaria, e-mail: dkso@tu-sofia.bg.



**Plamen Rizov** was born in Berkovitsa, Bulgaria, on December 23, 1960. He graduated the Technical University of Sofia and acquired Dr degree from the same university in 1998.

Since 1991 he worked in the Faculty of Electrical Engineering of the Technical University of Sofia as a Lecturer and Associate Professor, 2002.

Plamen Rizov is with the Faculty of Electrical Engineering, Technical University of Sofia, 8, Kl. Ohridski Blvd., 1000 Sofia, Bulgaria, e-mail: pmri@tu-sofia.bg.



**Dimitar BOZHOV** was born in Varna, Bulgaria on October 6, 1978. He graduated the Technical University of Sofia and acquired Master degree in Electrical Engineering in 2005. He has been a PhD student in the Department of Electrical Engineering of the Technical University of Sofia since 2005.

His field of interests is electrical networks, electrical machines and 3D digital prototyping. e-mail: bojov@tu-sofia.bg



**Ivaylo PANAYOTOV** was born in Tervel, Bulgaria, on January 28, 1980. He studied at the Technical University of Sofia-Bulgaria and received Eng. degree from the same university in 2004.

Since 2002 he worked in the Electrical Machines Industry now is director APPE of "Elprom trafo CH"AD Kustendil, Dondukov 63, email: i.panayotov@elpromch.com



**Boyan KRACHEV** was born in Yambol, Bulgaria on November 22, 1981. He graduated the Technical University of Sofia and acquired Master degree in Electrical Engineering in 2007. He has been a PhD student in the Department of Electrical Engineering of the Technical University of Sofia since 2007.

His field of interests is electrical networks, electrical machines and 3D digital prototyping. e-mail: krachev@abv.bg



**Vladimir DOYCHEV** was born in Stara Zagora, Bulgaria on July 19, 1975. He graduated the Technical University of Sofia and acquired Master degree in Electrical Engineering in 2001. He has been a PhD student in the Department of Electrical Engineering of the Technical University of Sofia since 2006.

His field of interests is electrical networks, electrical machines and 3D digital prototyping. e-mail: vl\_doychev@abv.bg

# Problems in joint work of a synchronous generator with an uncontrolled rectifier

Dimitar Sotirov, Ivailo Panayotov, Dimitar Bozhov,  
Boyan Krachev and Vladimir Doychev

**Abstract:** Development of the modern synchronous machines is inextricably bound up with using of brushless systems for excitation. They have significant advantages as high exploitation reliability, life, require low power for control, and do not need a special maintenance in exploitation. Leading manufacturers of hydro generators and other synchronous machines as ALSTOM, GENERAL ELECTRIC, ABB, Electrosila and other are using such exciters for a wide range of powers, and with the turbo generators they reach up to 1000 MW. In Bulgaria such exciters are produced for relatively small powers of the synchronous generator by few hundred kW. The experiment to use them at high powers leads to problems related to heating over the permissible limits of the exciter's inductor steel. The analysis of these problems and their removal is an object of this study.

**Keywords:** hydro generator, exciter, armature reaction.

## Characteristics of the co-work of a synchronous generator with a self-operating diode rectifier

In fig.1 is shown the general configuration of an exciter with the rotating rectifier (RR) and the excitation winding of the hydro generator (EW of HG).

The excitation winding of the hydro generator is powered by a control block which includes controllable thyristor rectifier and a circuitry for its control. The armature winding of the exciter is connected with a rotating three-phase bridge rectifier to which output is connected the exciter winding of the hydro generator.

During rotation of the armature in its winding a symmetrical system of voltages inducts which are applied to the rotating rectifier. In every moment of time a pair of diodes omits one from the anode group D1, D3 and D5, and one from the cathode group D2, D4 and D6. Omits this group of diodes to which passes the biggest in the

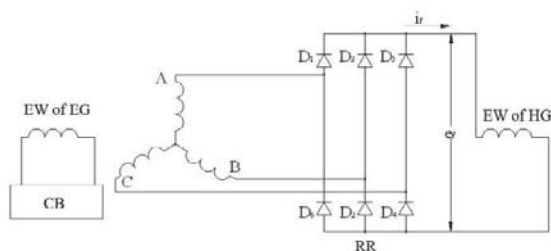


Fig. 1

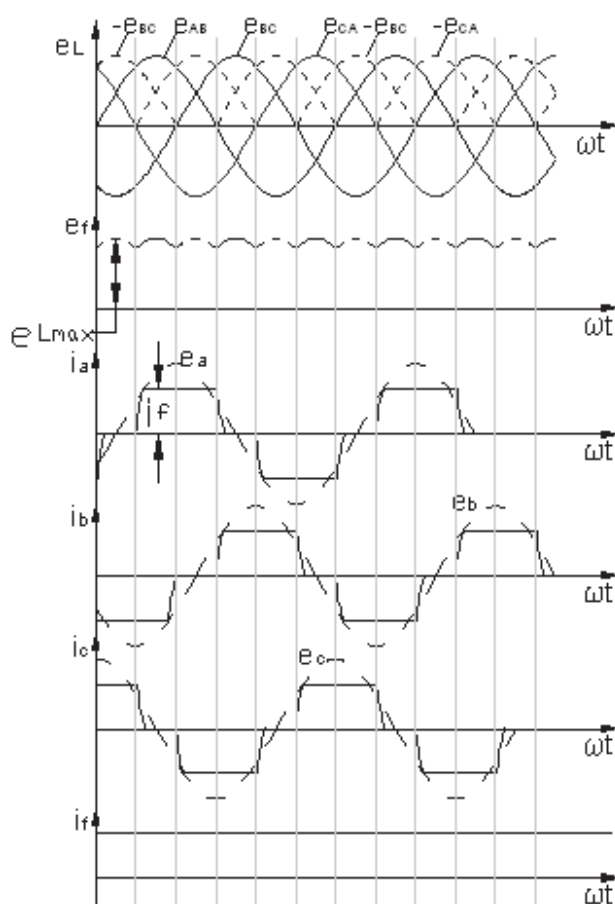


Fig. 2

moment linear voltage as it is shown at fig. 2 for case of sinusoidal linear voltages. It is evident that for interval of  $\omega t$  equal to  $60^\circ$  electrical, current is flowing through these two phases whose linear voltage is maximal. The current of each phase is with a form close to rectangular, and there is rotation of an interval of flowing of positive current with duration  $120^\circ$  electrical, a pause without current of  $60^\circ$  electrical, and interval of flowing of negative current with duration  $120^\circ$  electrical and etc. it follows from this that the space vector of the armature reaction  $F_a$  for what interval of conducting of two phases will be immovable compared to the armature and will be moving compared to the poles of the inductor. In case of transfer of the current from one phase to another (commutation of the current) the process does not run immediately due to the inductivity of diffusion of the phase winding. For the account of the reserved



electromagnetic energy of a known interval will be flowing the three phases and the current in the chain after the rectifier will be constant, the current in the switching off phase fade away lightly, and in the switching on phase will increase lightly, as it is evident from fig. 2. The duration of this interval is as longer as the inductivity of diffusion of the phase is bigger and respectively the reserved energy  $LI^2/2$  is bigger.

At fig. 3 is shown the space vector diagram of the first harmonic of the magnetomotive forces of the armature and the inductor at omitting of diodes D1 and D2 (fig. 2).

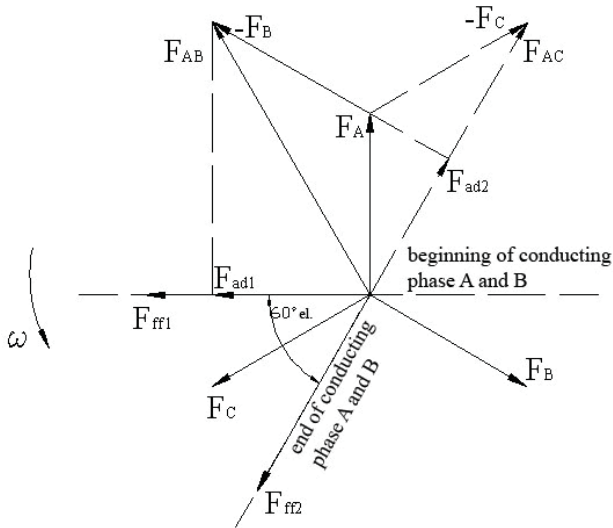


Fig. 3

It is evident that in the beginning of the examined interval the direct component of the armature reaction  $F_{ad1}$  is with the same direction with the vector of mmf of the inductor  $F_{ff1}$ , i.e. is magnetizing, and at its end armature reaction  $F_{ad2}$  is with opposite direction of  $F_{ff2}$  – i.e. is demagnetizing. Moreover the average values of the direct component of armature reaction for one interval of conducting of two phases is practically equal to zero, i.e. there is no resulting demagnetizing and magnetizing action, and its maximum value equals to  $\pm 0.5F_a$ . This leads to significant direct pulsations of the magnetic flux, which are inducing big currents in the solid parts of the stator (the inductor). The quadrature component of armature reaction in an analogical way lead to significant cross pulsations of the magnetic flux, which also leads to inducing of significant by magnitude currents in the solid poles. The space diagrams of armature reaction and mmf of the poles for the beginning and the end of the interval of conducting of phases A and B with the real non-sinusoidal curve is shown at fig. 4.

In case of significant by magnitude channel diffusion there is getting a big inductive resistance of diffusion, which leads to significant lag of the current from emf of the phase and the mean value of the pulsating direct component of armature reaction is getting demagnetizing.

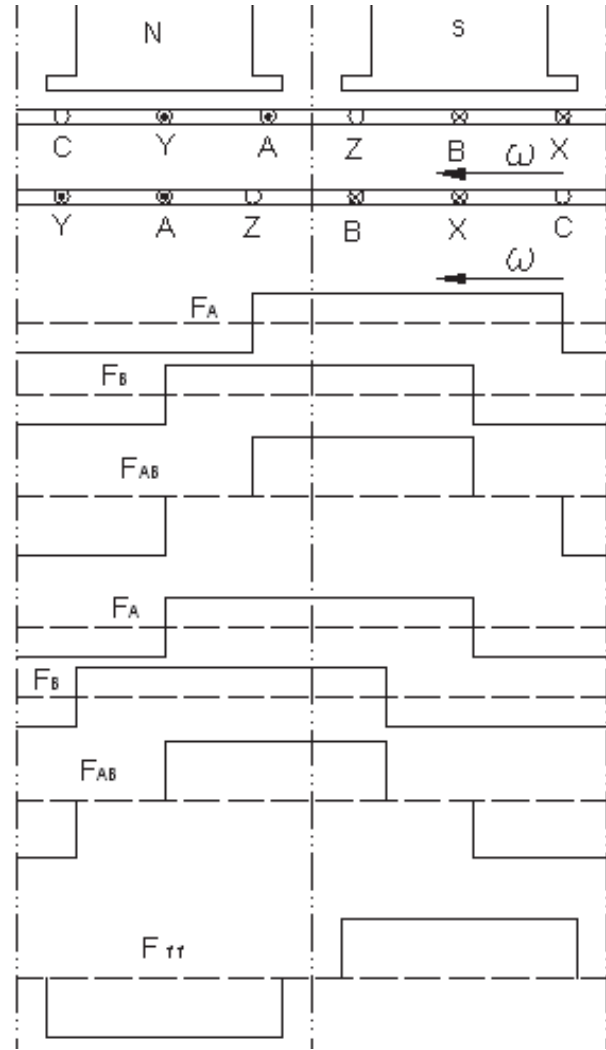


Fig. 4

## Experimental studies

For realization of experimental studies there a synchronous exciter generator is used with rotating rectifier for hydro generator produced by Elprom ZEM, working MBES Retizhe 1. The exciter has the following nominal data:

- Nominal rectified voltage  $U_n = 52,5$  V;
- Nominal rectified current  $I_n = 270$  A;
- Nominal angular velocity  $n = 600$  min<sup>-1</sup>;
- Number of poles  $2p = 16$ ;
- Number of rotor slots  $Z_r = 48$ .
- Winding with diametrical step and number of slots for a pole and phase  $q = 1$ ;
- Magnetic conductor of the stator (the inductor) – made from solid steel.

Due to the specific of the construction of the hydro generator and the exciter there is no access to the armature winding of the exciter, and the voltage and the current of the armature cannot be measured. In order to be received an information for the direct pulsations of the magnetic flux of the inductor a measuring coil is used

with number of windings  $w = 10$ , wound around the pole terminal in such a way that comprise the magnetic flux of the pole toward the aerial interspace. Moreover around the yoke between two poles a second measuring coil is wound with number of windings  $w = 10$  for the purposes of the experiment. The oscillograms of the voltages, inducted in the measuring coils are made with a digital two channel oscilloscope Hewlett Packard HP54601B with a probe, with scope 10:1. On the other channel of the oscilloscope through a differential voltage probe and a voltage measuring transformer 10/0.1kV there is passing the phase voltage of the hydro generator in such a way that simultaneously are making the oscillograms of emf from the measuring coils and the phase voltage of the HG. In order to evaluate the losses in the steel of the stator magnetic conductor with a mercury thermometer the temperature of the steel of the inductor is measured. The thermometer is placed in an opening, pierced in the inductor against a pole placed at the highest point of the yoke.

There are experiments made during work of the hydro generator in parallel with the network by entering different states of work of the hydro generator, respectively different values of the excitation current and loading of the exciter. There are made experiments with two values of the load for active load and with inductive and capacitive factor of the power  $\cos\phi$ . There is measuring also the temperature of the yoke of the inductor, and because of danger of non permissible heating the temperature is reporting before reaching of determined value. The ambient temperature during the measuring is  $10^{\circ}\text{C}$ .

The data for the regimes of work are given in Table 1.

**Table 1**

State of work of the HG		1	2	3	4	5	6
U	kV	3.8	3.9	4.0	4.05	4.2	3.85
$I_1$	A	184	164	176	240	260	268
$I_2$	A	180	160	176	236	260	264
$I_3$	A	212	192	212	284	316	312
$P_{HG}$	kW	1095	1095	1095	1650	1650	1650
$\cos\phi$	-	0.91	1.0	0.909	0.994	0.897	0.906
$U_{ff}$	V	71.5	91	118	121	158	82
$I_{ff}$	A	4.1	5.2	6.75	6.7	8.6	4.4
$T_{yoke}$	$^{\circ}\text{C}$	-	-	-	-	56	60.6

For the time of conducting of the experiment temperature of the yoke  $t_{corpus} = 67.5^{\circ}$  is reached and gradient of increase  $1.2^{\circ}$  on 2 minutes from  $64.4^{\circ}$  to  $66.8^{\circ}$ , and decreasing up to  $0.8^{\circ}$  for 4 minutes – measured with load 6 -  $I_{ff} = 4.4$  A.

For each state of loading there are made oscillograms of emf of the phase and emf, inducted in the two measuring coils. At fig. 7 there are shown the oscillograms of emf of the measuring coil, situated over the pole Ecoilpole, of emf of the measuring coil, situated over the yoke Ecoilyoke and the phase voltage of the hydro generator UphHG with state of loading 4.

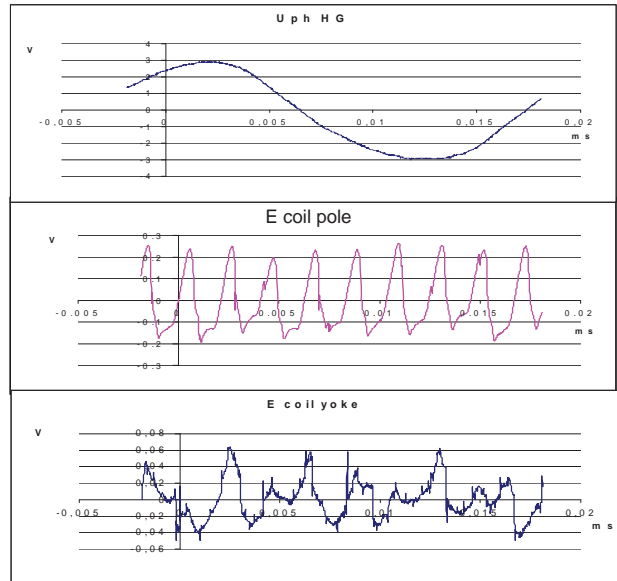


*Fig. 6*

The pulsations of emf are due to pulsations of the direct component of armature reaction, which have a frequency determined from the frequency of the current in the armature winding of the exciter and the frequency of the commutations of the diodes of the rectifier. For one period of emf of the exciter there are getting 6 pulsations of the armature reaction, respectively of the flux. Taking into consideration besides that the exciter is with number of poles  $2p_E = 16$ , and the HG is with number of poles  $2p_{HG} = 10$ , the period of the pulsations of emf of the measuring coil  $T_{mc}$ , given through the period of the pulsations of emf of HG is getting as follow

$$T_{mc} = \left( \frac{T_{HG} p_{HG}}{6 p_E} \right) = \frac{T_{HG}}{9.6}$$

To this period of the pulsations corresponds frequency  $f = 50 * 9.6 = 480\text{Hz}$ .

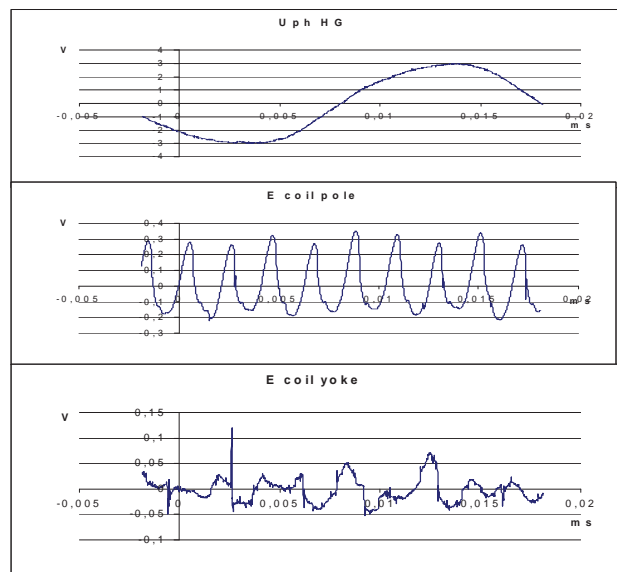


*Fig. 7*

From the oscillograms it is evident that this proportion is exactly observed, i.e. in one period of emf of the generator there are 9.6 periods of emf of the measuring coil. As it was shown with every commutation of the diodes the current is transferring to new two phases as the one phase remains the same, so that the direct component armature reaction which at the end of the previous interval has reached maximum demagnetizing value becomes with minimum demagnetizing value. The interval for which is making this change corresponds to the interval for which the current from the switching off phase is transferring to the switching on phase. After that for interval of  $60^\circ$  electrical with turning of the armature, the direct component of armature reaction lightly is changing from maximum demagnetizing value to minimum demagnetizing value. This cycle of change of the direct component of armature reaction lead to respectively change of the magnetic flux and inducing of emf in the measuring coil.

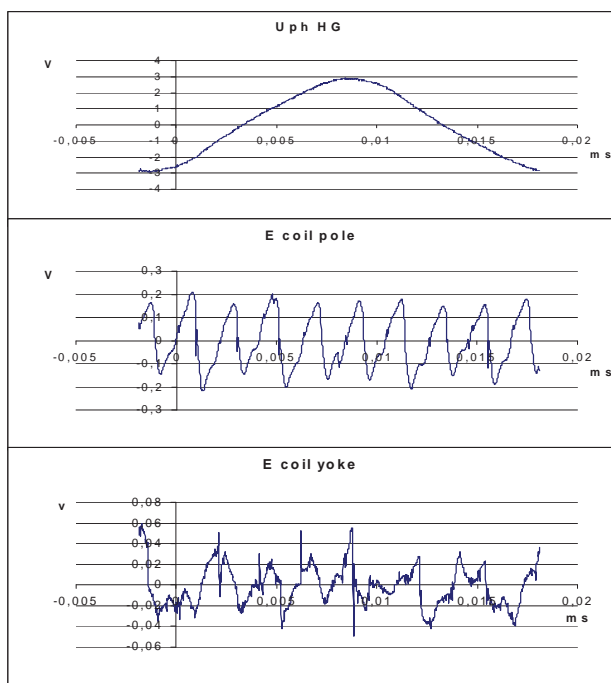


Fig. 8

Due to the damp action of the currents induced in the solid poles, the size of the pulsation of the current is small, but the currents in the poles lead to big losses and warming up of the magnetic conductor of the inductor. The oscillograms received exactly correspond to the characteristics of joint work of a synchronous generator with diode rectifier. From the oscillograms of emf of the measuring coil, situated over the yoke it is evident that the pulsations of emf and the flux in the yoke are not so exactly expressed, as in the previous oscillograms since there are laying of pulsations from the flux from different neighbour poles, but show that there are pulsations also on the flux in the yoke, and their amplitude is several times lesser than that in the pole.

At fig. 7 and 8 there are shown analogical oscillograms respectively with regimes of loading 5 and 6. From the oscillograms in these states of loading it is evident that the amplitude of the pulsations of the flux is proportional to the size of the excitation current of the exciter  $I_{BB}$ . This is because the armature current of the exciter, respectively the direct component of armature reaction are proportional to  $I_{BB}$  in unsaturated magnetic chain. The deviations from the exact proportional dependency are due from one side to the non linearity of the chain which can not be reported in first approximation and due to the fact that during the conduction of the experiment it was not possible the machines to be warmed up to the determined temperature and during the work their resistances, participating in the circuit of excitation are not changing. Independently of these inexactnesses the received results categorically confirm the conclusions made.

#### Conclusions

From the conducted experimental studies there the following conclusions can be made:

The studied machines are made with a synchronous generator working with load three-phase bridge diode rectifier with a possibility for adjustment of the armature current in wide limits through change of the excitation current, with unsaturated magnetic chain, with sheet armature winding with diametrical step and  $q=1$ , yoke and poles of the inductor from solid steel. Due to the characteristics of the regimes of work of such generator significant pulsations of the magnetic flux are occurring with frequency 480Hz for the studied exciter as a result of the specific character of the armature reaction. These pulsations of the current are raising losses in the solid parts of the magnetic conductor which in nominal state by roughly calculations are reaching 7-8 kW and more. The experience from the exploitation of the exciter shows that as a result of these losses the solid parts of the magnetic conductor of the inductor are warming up inadmissible and practically the machine can not work for long time in nominal state. In order to restrict the over heating of the solid sections of the magnetic conductor of the inductor the exciter must work at outgoing power around 2.5 times less than the nominal.

The analysis shows that besides the objectively conditioned by the principle of action of the machine reasons there are also reasons connected with the parameters of the machine. Firstly this is the incorrect choice of type of channels of the armature which are too deep. This leads to high value of the inductive resistance of diffusion of the armature winding and too high value of the inductive voltage drop  $E\sigma = \chi\sigma I\phi_H = 128.4V$  with nominal phase voltage  $U_{H\phi} = 26.4V$ , respectively to leaving of the current from emf of the phase to an angle close to  $\pi/2$  and reaction of the current of the phase almost entirely direct demagnetizing. In order to get the necessary phase voltage the designers of the exciter were forced to increase the number of the windings in the armature winding, and in this way the direct demagnetizing components of the reaction of the current

of the armature increased and in order to overcome it were necessary to increase the magnetomotive force of the excitation winding through more than double increase of the number of the windings of the excitation winding. At the end through significant increase of the expenditures for active material there are reached the necessary voltage and current of the output of the exciter. It is indicative for the case that emf on idle running and with load of the exciter of HG in Retije 1 are  $E_0 = 330V$  and  $E_\delta = 134V$  at  $\psi = 82^\circ$  for nominal phase voltage  $U_{H\phi} = 26.4 V$ . It is analogical the situation for an exciter with the same construction, but with other winding and nominal data, installed in MVES Retije 3, respectively  $E_0 = 268V$  and  $E_\delta = 104V$  at  $\psi = 80^\circ$  and nominal phase voltage  $U_{H\phi} = 28.9 V$ . It is evident that the proportion  $E_0/U_{H\phi}$  for Retije 1 and 3 is respectively 12.5 and 9.3, which is inadmissible high and confirms the above said. The problem is that the excessively increase of the armature reaction leads to proportionally increase of the amplitude of the pulsations of the direct and demagnetizing component, and thus also of the direct and cross pulsations of the magnetic flux of the inductor which is with solid magnetic conductor. The eddy currents occurring in the magnetic conductor are with high amplitude and lead to losses which in nominal state cause heating of the surface of the yoke by  $150 - 160^\circ C$  and after there are taken special measures for possible maximum increase of the cooling of the machines.

The experience of the leading companies – producers of such type of machines point out that for resolving such problems constructive solutions are used, differing from the one used in the described machines. The analysis made shows that with appropriate design of the machine even in decrease of the expenditures of active materials (the conductor material can be decreased up to two times), exciters can work in nominal state without inadmissible overheating.

## References

- [1] Ангелов А.М., Д.А. Димитров. Электрические машины, I и II част. Техника, София, 1976, 1988.
- [2] Абрамов А. И., А. В. Иванов-Смоленский. Проектирование гидрогенераторов и синхронных компенсаторов. Высшая школа, Москва, 2001.
- [3] Копылов И. П. Электрические машины. Высшая школа, Москва, 2000.
- [4] Шуйский В. П. Расчет электрических машин. Энергия, Ленинград, 1968.
- [5] Лютер Р. А. Расчет синхронных машин. Энергия, Ленинград, 1979.

## Biographies



Bulgaria, e-mail: dkso@tu-sofia.bg.

**Dimitar Sotirov** was born in Velingrad, Bulgaria, on Mart 1, 1946. He graduated the Technical University of Sofia and acquired Dr degree from the same university in 1983.

Since 1969 he worked in the Faculty of Electrical Engineering of the Technical University of Sofia as a Lecturer, Associate Professor, 1986 and Head of Department of Electrical Machines, 2000.

Dimitar Sotirov is with the Faculty of Electrical Engineering, Technical University of Sofia, 8, Kl. Ohridski Blvd., 1000 Sofia,



**Dimitar BOZHOF** was born in Varna, Bulgaria on October 6, 1978. He graduated the Technical University of Sofia and acquired Master degree in Electrical Engineering in 2005. He has been a PhD student in the Department of Electrical Engineering of the Technical University of Sofia since 2005.

His field of interests is electrical networks, electrical machines and 3D digital prototyping. e-mail: bojov@tu-sofia.bg



**Ivaylo PANAYOTOV** was born in Tervel, Bulgaria, on January 28, 1980. He studied at the Technical University of Sofia-Bulgaria and received Eng. degree from the same university in 2004.

Since 2002 he worked in the Electrical Machines Industry now is director APPE of "Elprom trafo CH"AD Kustendil, Dondukov 63, email: i.panayotov@elpromch.com



**Boyan KRACHEV** was born in Yambol, Bulgaria on November 22, 1981. He graduated the Technical University of Sofia and acquired Master degree in Electrical Engineering in 2007. He has been a PhD student in the Department of Electrical Engineering of the Technical University of Sofia since 2007.

His field of interests is electrical networks, electrical machines and 3D digital prototyping. e-mail: krachev@abv.bg



prototyping. e-mail: vl\_doychev@abv.bg

**Vladimir DOYCHEV** was born in Stara Zagora, Bulgaria on July 19, 1975. He graduated the Technical University of Sofia and acquired Master degree in Electrical Engineering in 2001. He has been a PhD student in the Department of Electrical Engineering of the Technical University of Sofia since 2006.

His field of interests is electrical networks, electrical machines and 3D digital



# Experimental Detection of Faults of Induction Motor Electric Drives

Olympiada A. Syggeridou and Maria G. Ioannides

**Abstract:** The study of the diagnosis and detection methods of faults in electric drives was undertaken by the authors, by a thorough examination of faults and the existent techniques referred in worldwide literature.

The software for their organization in a database and for their retrieving was developed first. Last, their experimental study was carried out for some particular selected laboratory cases.

This experimental investigation deals with the problem of diagnosis and detection of induction motor faults produced by three phase voltage unbalanced supply. The paper presents the experimental set-up, the measurements technique and the results that confirm the procedure of detection of voltage unbalance.

**Keywords:** Fault Detection, Faults diagnosis, induction motors, electric drives

## Introduction

The study of the diagnosis and detection of faults in electric drives was undertaken by the authors.

A thorough examination of faults was carried out and the existent techniques referred in worldwide literature were studied and reported in [1]-[2]. For their organization in a database and their retrieving and handling, the software was developed as reported in [3]-[7]. Experimental study was carried out for some particular operating cases and is continuing in the Electric Drives Laboratory of the National Technical University of Athens. Their reporting is the purpose of this paper.

This experimental investigation deals with the problem of diagnosis and detection of some induction motor faults, such as produced by voltage unbalance asymmetrical supply.

## Experimental Setup

For the investigation of operation of induction motor drives in conditions of stator voltage unbalance, the experimental setup shown in Figure 1 was implemented.

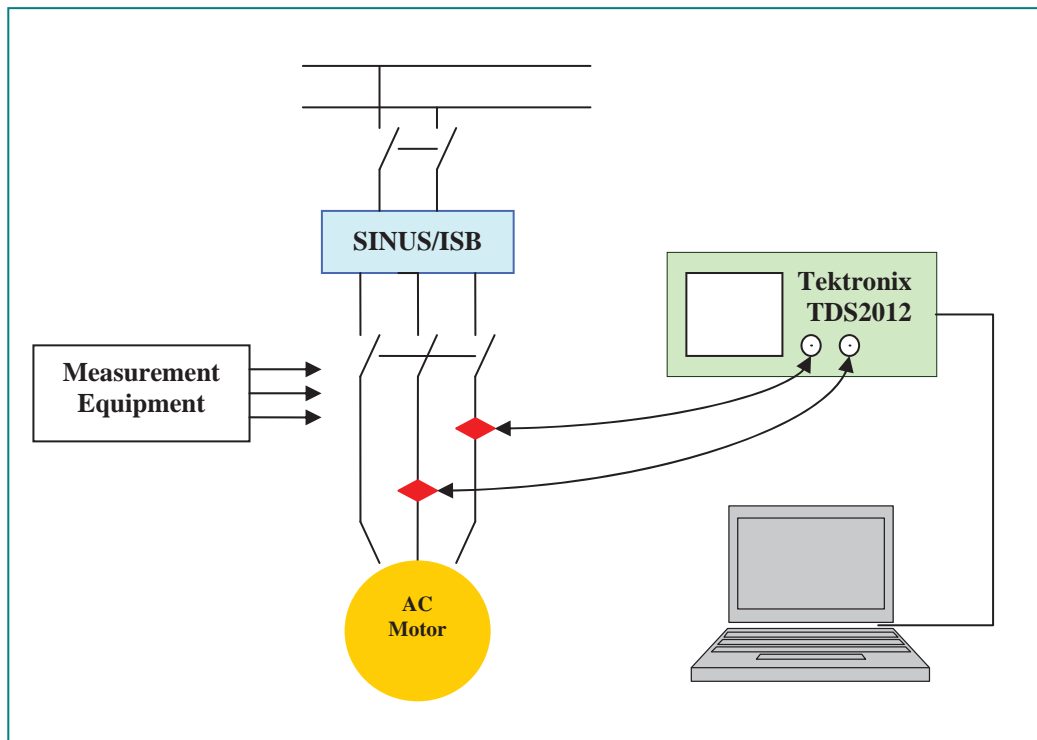


Fig.1. The experimental setup



It involves an induction motor with rated data of 1 kW, 50 Hz, 220/380 V, 4.6/2.6 A, 1400 rpm, 4 poles. It is Y/Y connected and supplied from a digital-controlled inverter (series SINUS/ISB). The inverter is used for controlling the speed of the motor. The motor is connected to a digital storage oscilloscope (Tektronix TDS2012 equipped with the TDS2CMA module) by using current sensors (Tektronix A622 100 Amp AC/DC current probes). The measurement equipment is interfaced to a computer. All measured data are transmitted and saved to the hard disk and processed by using Matlab software.

The stator current is sampled at 500 Hz sampling rate and analysed by using the Fast Fourier Transform (FFT) spectrum that contains 1024 points for each measurement. All experiments were done at no load and reduced supply line voltage 220 Vac.

### Experimental Method and Results

The induction motor is tested in two different situations:

- In symmetrical supply conditions, in order to determine the current of the motor without faults that will be considered as reference;
- Supplied with unbalanced stator voltage, at different values of voltage magnitude; The unbalanced situation is simulated by adding ohmic resistance  $R$  in series to one phase. The magnitude of  $R$  can be varied in order to obtain different degrees of voltage unbalance.

The stator current FFT spectra visualized with the digital oscilloscope for

- symmetrical supply condition is shown in Figure 2 and,
- for two cases of stator voltage unbalance produced by  $R=34 \Omega$  and  $R=101 \Omega$  are shown in Figures 3 and 4, respectively.

The sampled data are transmitted to the computer and plotted in Matlab environment. Their graphical representations are shown in Figures 5, 6 and 7, respectively.

The filtered FFT spectra of the stator current for different degrees of stator voltage unbalance ( $R>0$  such as  $R=34 \Omega$  and  $R=101 \Omega$ ) are compared to their respective in case of symmetrical operation ( $R=0$ ). Other cases of voltage unbalance were also studied for  $R=3\Omega$ ,  $R=72\Omega$ ,  $R=130\Omega$ . The results of this study are shown in Figure 8, and the comparison and discussion issues in Figures 9 and 10.

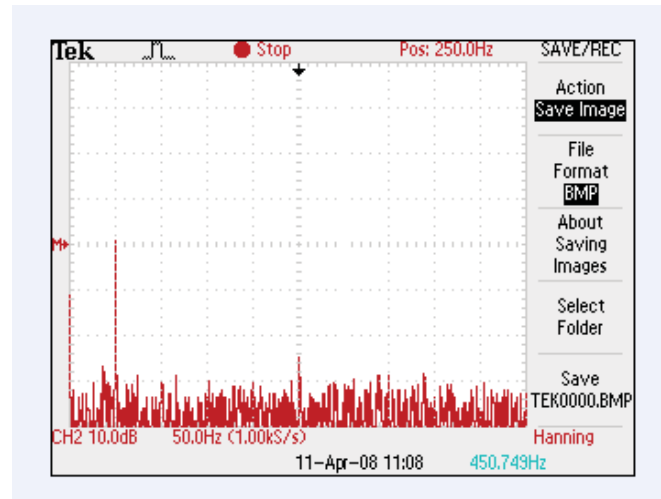


Fig. 2. Stator current: the FFT spectrum for symmetrical supply condition ( $R=0$ ). Screen.

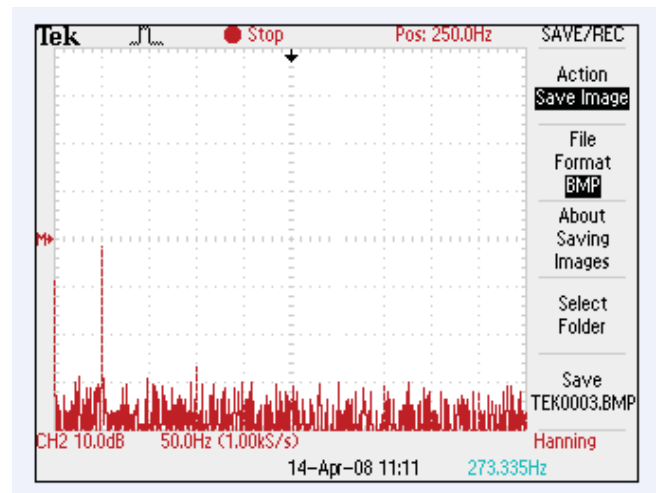


Fig. 3. Stator current: the FFT spectrum for voltage unbalance ( $R=34 \Omega$ ). Screen.

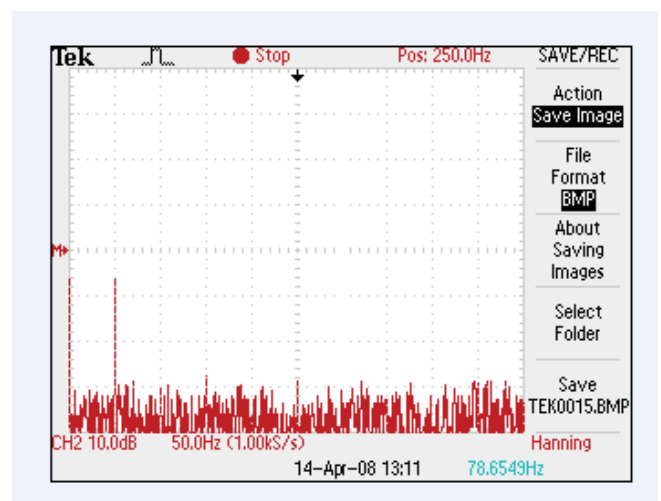


Fig. 4. Stator current: the FFT spectrum for voltage unbalance ( $R=101 \Omega$ ). Screen.

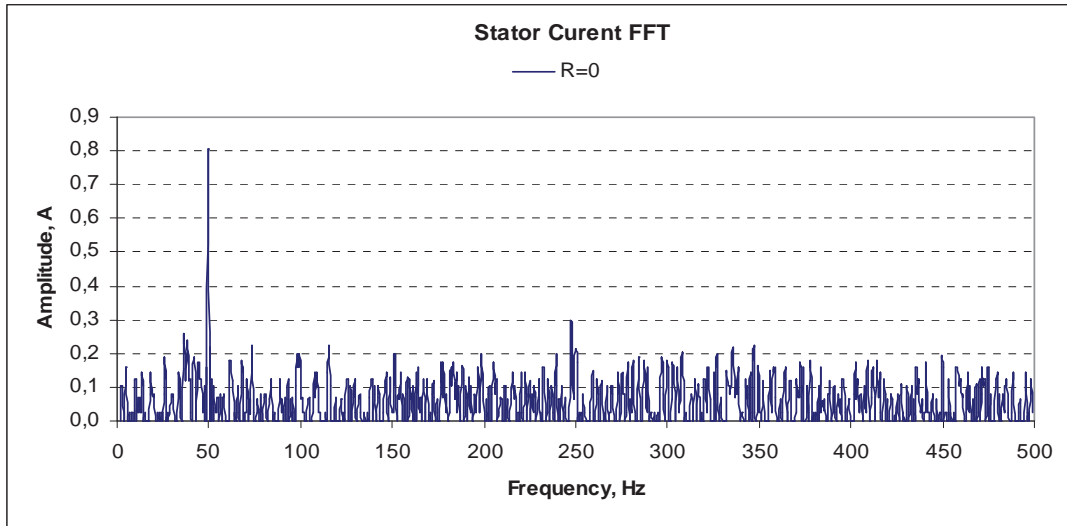


Fig. 5. Stator current: the FFT spectrum for symmetrical supply condition ( $R=0$ ).

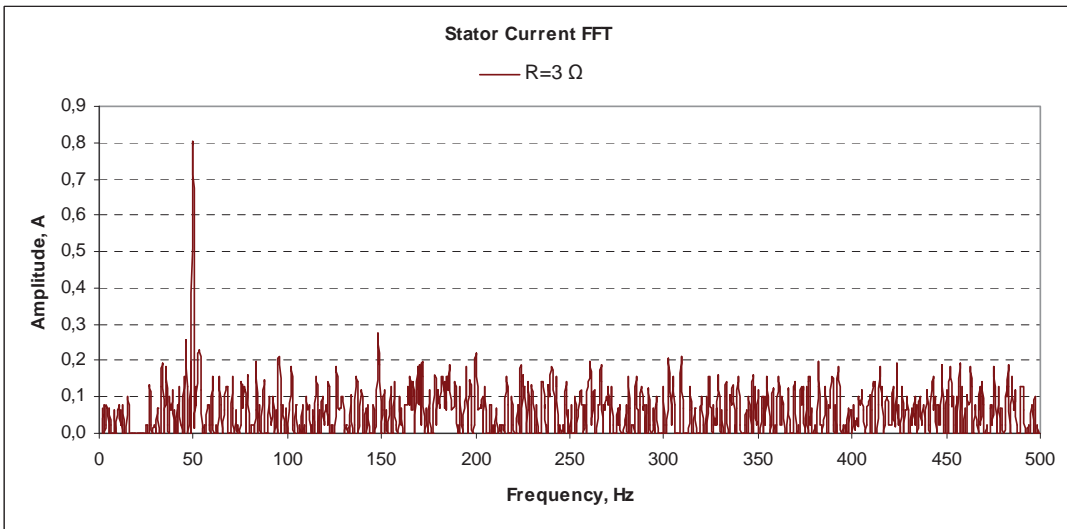


Fig. 6. Stator current: the FFT spectrum for voltage unbalance ( $R=3 \Omega$ ).

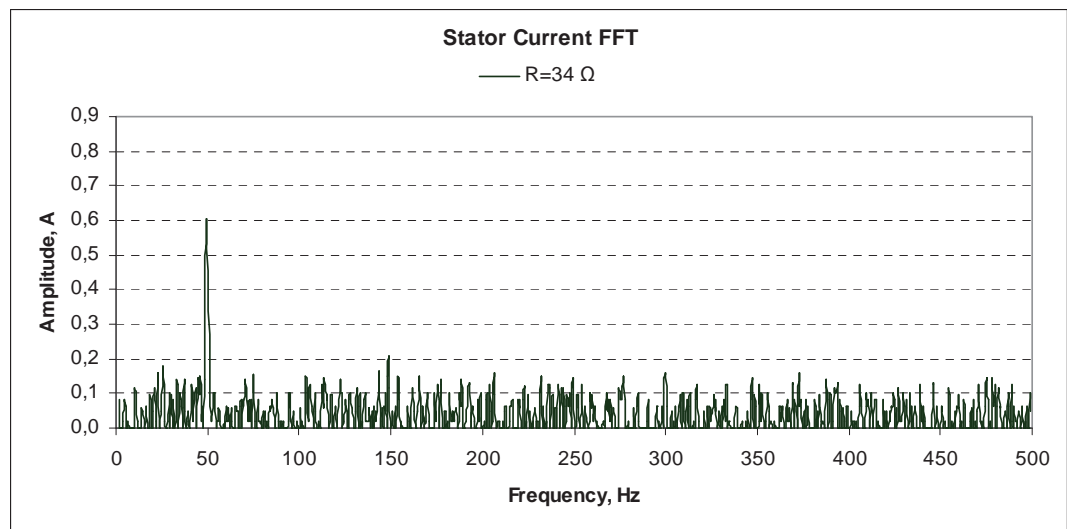


Fig. 7. Stator current: the FFT spectrum for voltage unbalance ( $R=34 \Omega$ ).

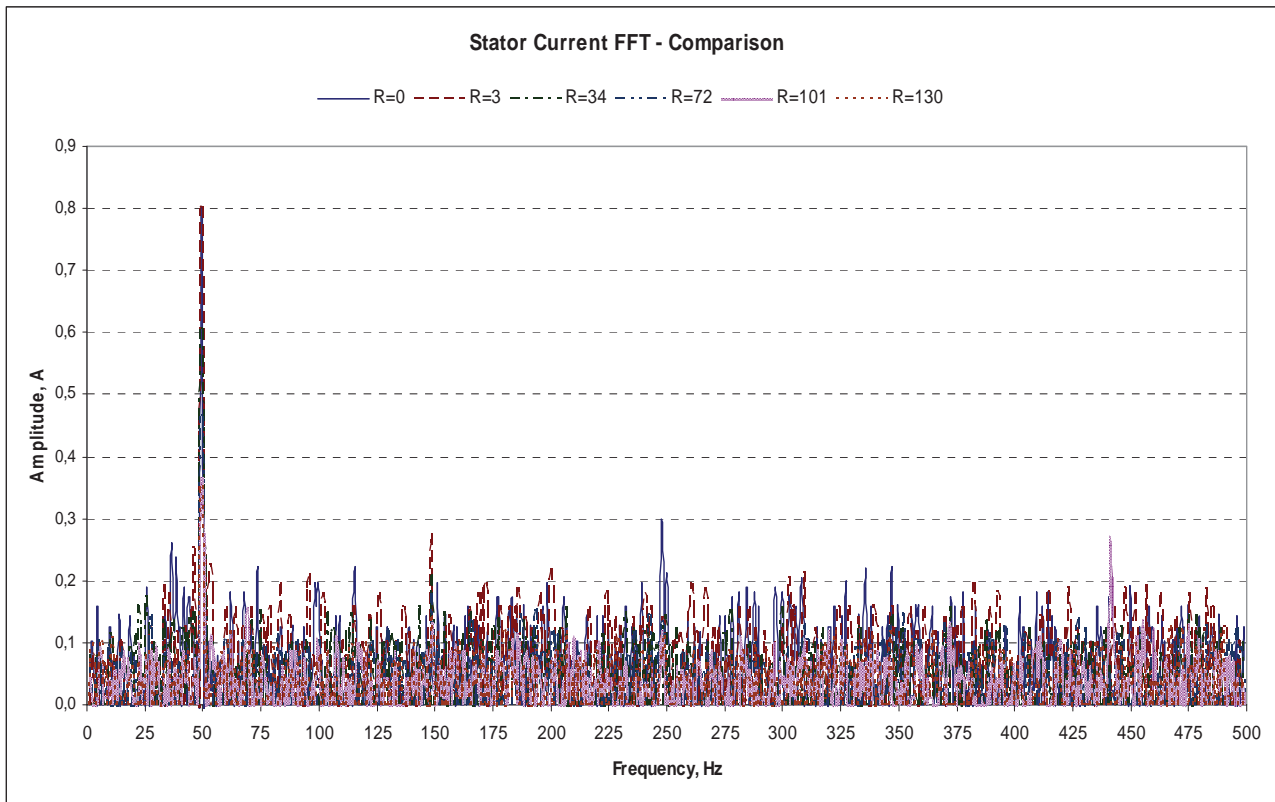


Fig. 8. Stator current harmonics: the FFT spectrum for different degrees of unbalance

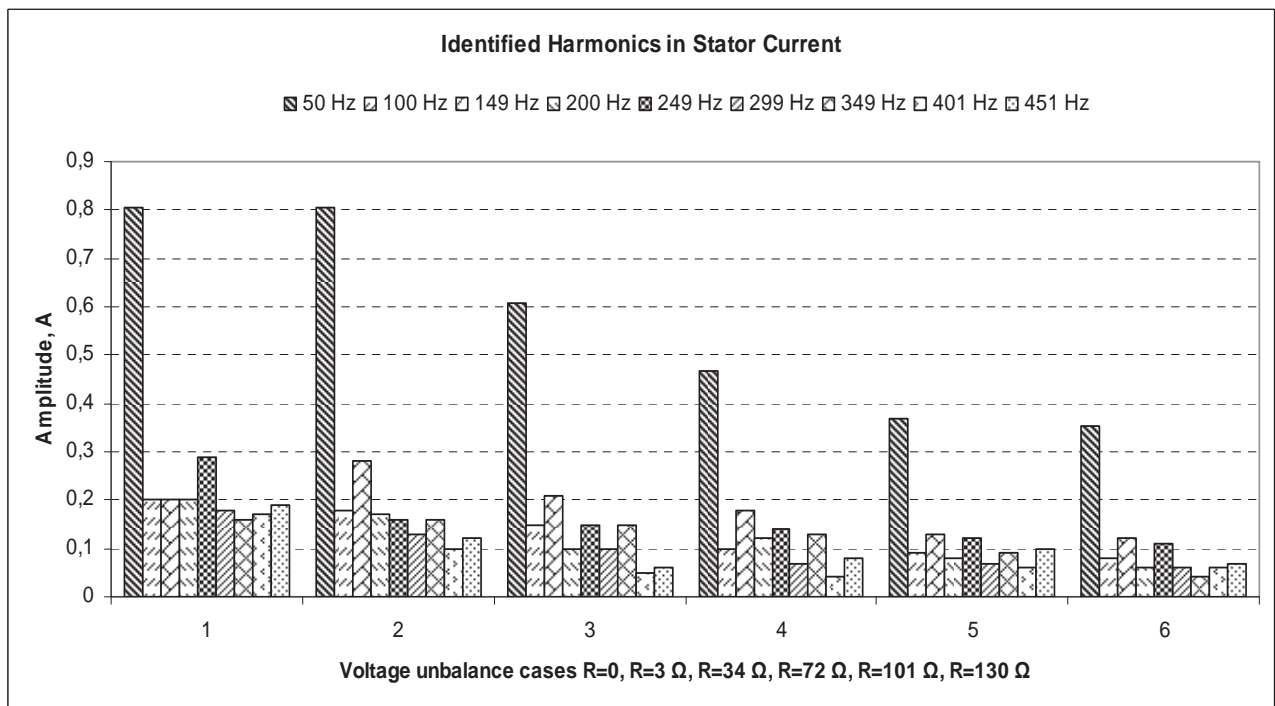


Fig. 9. Variation of first nine current harmonics for symmetrical ( $R=0$ ) and five different cases of voltage unbalance ( $R=3$ ,  $R=34$ ,  $R=72$ ,  $R=101$ ,  $R=130\Omega$ )

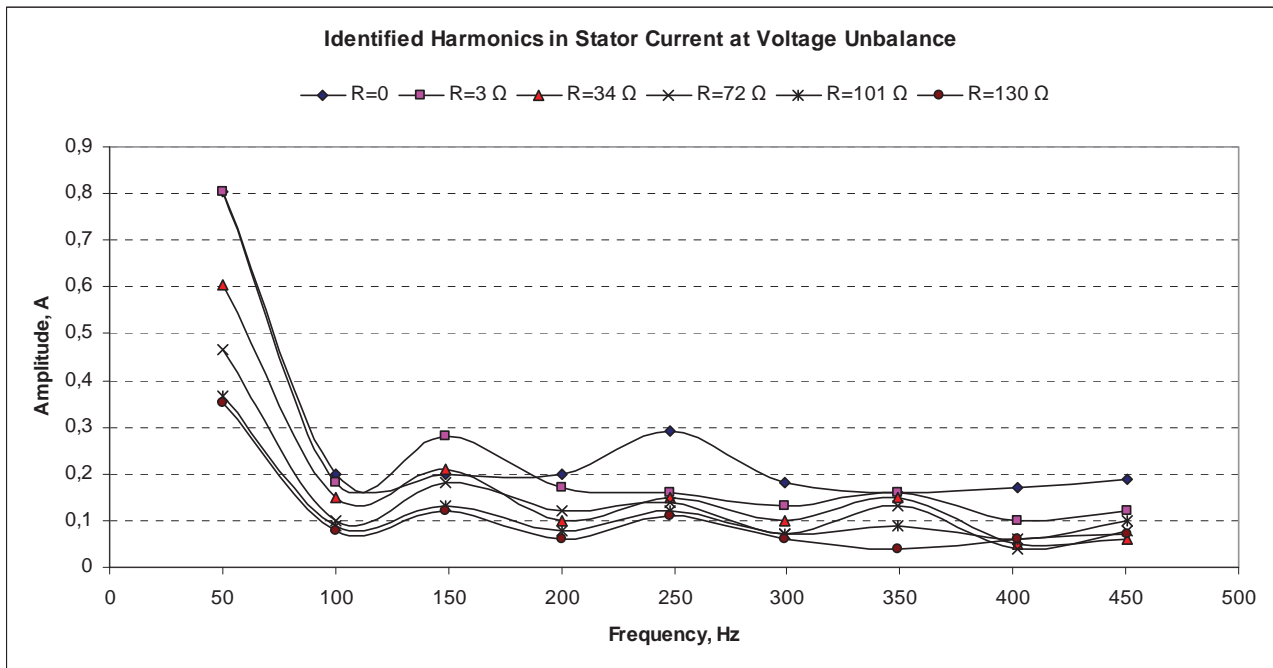


Fig. 10. Variation of first nine harmonics of stator current for each case of unbalanced voltage supply

We identified the major spectral components of the stator current:

- in case of symmetrical operation, the first harmonic of supply frequency were identified at 50 Hz and the fifth at 249 Hz, that corresponds to 250Hz;
- in case of unbalanced stator voltage, the first harmonic were identified at 50 Hz, the third harmonic and 149 Hz and the fifth at 249 Hz.

In unbalanced situations, from the comparison to the case of balanced voltage supply, we observe:

- the diminish of amplitude of fundamental and of fifth, seventh and ninth harmonic component, and,
- at the same time, the increase of amplitude of the third harmonic of stator current.

All other amplitudes of harmonics decrease when the degree of stator voltage unbalance increased.

## Conclusions

In this paper was presented the experimental investigation by using the methodology of stator current monitoring for diagnostic purposes in cases of voltage unbalanced supply of induction motor drives.

In the case of stator voltage unbalance, the amplitude of the fundamental frequency component of the stator current decreases, the third harmonic component increases and the fifth, the seventh and the ninth decreases, as compared to the respective amplitudes in symmetrical operation.

One of the spectral components influenced by the asymmetry of supply of induction motor is the third harmonic of supply frequency, whose amplitude increases.

Other spectral components, such as the even harmonics of the supply frequency are of the interest to the fault diagnosis of induction motor electric drives. They are currently the subject of further study. Also, under study are the operation and diagnosis of faults at full load, overload and overvoltages.

## References

- [1] O. A. Syggeridou and M. G. Ioannides. Diagnostic Methods for AC Electric Motors. Part 1: Mechanical, Chemical and Thermal Monitoring. Proceedings of the 4<sup>th</sup> International Conference Power and Energy Systems EURO-PES 2004, ISBN: 0-88986-395-04, ISSN: 1284-7891, June 28-30, 2004, Rhodes, Greece, pp. 605-607.
- [2] O. A. Syggeridou and M. G. Ioannides, Diagnostic Methods for AC Electric Motors. Part 2: Electromechanical Monitoring. Proceedings of the 4<sup>th</sup>

International Conference Power and Energy Systems EURO-PES 2004, ISBN: 0-88986-395-04, ISSN: 1284-7891, June 28-30, 2004, Rhodes, Greece, pp. 608-613.

- [3] O. A. Syggeridou and M. G. Ioannides, A Computer-Based Tool for the Fault Detection of AC Electric Motors. International Scientific Conference "*Internet-Education-Science-2004*", October 5-9, 2004, Vinnytsia, Ukraina, pp. 132-133.
- [4] O. A. Syggeridou and M. G. Ioannides, Development of a Computer Program for Failures and Diagnostics of AC Electric Motors. Proceedings of the 3rd International Conference on Systems, Signals, Devices SSD'05, March 21-24, 2005, Soussa, Tunisia, pp. 1-5.
- [5] O. A. Syggeridou, M. G. Ioannides, Induction Motors' Faults Detection and Diagnosis by Using Dedicated Software. Book of Digests of the 4th Japanese-Mediterranean Workshop on Applied Electromagnetic Engineering for Magnetic, Superconducting and Nano-Materials JAPMED'4, Cairo, Egypt, September 17-20, 2005, pp. 113-114.
- [6] O. A. Syggeridou and M. G. Ioannides, An Information System for Faults Detection and Diagnosis of Electric Machines. Proceedings of the XII International Symposium on Electromagnetic Fields in Mechatronics, Electrical and Electronic Engineering – ISEF'2005 September 15-17, 2005, Baiona, Spain, pp. 1-6.
- [7] O. A. Syggeridou, M. G. Ioannides, Induction Motors' Faults Detection and Diagnosis by Using Dedicated Software. Journal of Materials Processing Technology, Elsevier, Volume 181, Issues 1-3, 1 January 2007, pp. 313-317.

## Biographies



**Olympiada A. Syggeridou** is Research Assistant in the Faculty of Electrical & Computer Engineering of the National Technical University of Athens, Greece and Laboratory Teaching Staff in the Technological Educational Institute of Piraeus. Her research area covers diagnosis and detection of faults in electric drives and electrical machines.

She participated in research projects funded by the Greek government and European Community. Is author of approx. 15 journal and conference proceedings papers. She participated to many international conferences and workshops. Is Member of Technical Chamber of Greece TCG.

**Address for correspondence: National Technical University of Athens, Faculty of Electrical and Computer Engineering, Heroon Polytechniou 9, 15773, Athens, Greece, [osygger@central.ntua.gr](mailto:osygger@central.ntua.gr)**



**Maria G. Ioannides** is Professor in the School of Electrical & Computer Engineering of the National Technical University of Athens, Greece. Her research area covers control of electric drives, small and special electric motors, renewable energy sources, biocomputing, education methods curriculum development, women in sciences. Participated as scientific responsible or principal investigator in more than 30 research projects of the Greek government, European Community and U.S.A.

Dr. Ioannides is the author of more than 200 journal papers, conference proceedings papers, technical books and technical reports. Is member and reviewer in many Scientific Committees of International Conferences and International Journals and participated to more than 70 international conferences and workshops.

Dr. Ioannides is Senior Member of IEEE, Member of Electric Machinery Committee of IEEE, IASTED, Technical Chamber of Greece, Electromechanical Energy Conversion Committee of TCG.

**Address for correspondence: National Technical University of Athens, Faculty of Electrical and Computer Engineering, Heroon Polytechniou 9, 15773 Athens, Greece, [mioannid@ece.ntua.gr](mailto:mioannid@ece.ntua.gr); [www.ntua.gr](http://www.ntua.gr)**



# A Review of Some Technical and Economic Features of Energy Storage Technologies for Distribution System Integration

Gauthier Delille and Bruno François

**Abstract:** *This paper deals with the results of a study aiming to assess the suitability of various energy storage technologies for medium-term (2015) integration into distribution systems. Based on a review of many scientific and industrial materials, and by taking into account a few hypotheses, a shortlist of some properties to consider was first identified and defined. More than twenty storage techniques were then studied and nine of them were found to be particularly suited. An up-to-date overview of their performances is given at the end of the article.*

**Keywords:** *energy storage technologies, distribution grids, distributed energy resources, smartgrids.*

## Introduction

In the future, distribution grids and power systems will carry on facing many challenges. On the one hand, increasing peak loads and the appearance of plug-in electric or hybrid vehicles will result in the need for grid reinforcements, which will probably come up against a growing public opposition. On the other hand, the continued development of renewable generation will bring variability that will have to be addressed when significant penetration levels are reached.

Besides, oil prices have fetched unprecedented levels lately and the International Energy Agency anticipates continued market tightness to 2013 [1]. Raw materials are now quite expensive too, as well as new grid equipment.

Such a context calls standard practices into question and might bring new market opportunities for technical options that were previously unable to compete with conventional solutions for utility distribution systems. That is a reason why Distributed Energy Storage Systems (DESS) have received considerable attention over the past few years. New products have recently found their way to the market and some stationary applications have been successfully demonstrated (e.g. peak shaving for capital deferral), while others are still under investigation (as output fluctuation mitigation of wind farms).

This paper deals with Energy Storage Technologies (EST) and their medium-term (around 2015) integration into distribution grids. With this aim in view, it handles the characterization of EST and provides an up-to-date overview of the properties of selected storage techniques.

## Preliminary considerations

The present review of EST is an intermediate step to an ongoing analysis of the potential of DESS to contribute to the advanced management of distribution grids, allowing for example a better integration of renewable energy sources, asset utilization improvements

or power quality and reliability enhancements. In France, distribution systems are radial and consist of medium-voltage (MV, mainly 20kV) and low-voltage (LV, exclusively 400V) underground and overhead lines. They are operated either by ERDF, the national distribution network subsidiary of EDF or by non state-owned, local electric distribution utilities.

## Methodology

An extensive literature review on EST was first conducted, including both very broad studies (such as [2]-[10]) and technology-specific resources ([11]-[20]). Specification sheets of various existing energy storage products were also collected and, whenever necessary, manufacturers were contacted for further information.

It soon appeared that there are multiple ways of characterizing EST: depending on the application requirements, some pieces of information can be more or less critical, leading to potentially different approaches of the problem. For example, among the technical features of EST, peak power density (W/kg) and specific energy (Wh/kg) are often considered to be key parameters for vehicle applications whereas they appear to be relatively secondary for stationary systems. That is why an analysis of the characteristics to prioritize from a system-level perspective was conducted in order to maximize the pertinence of the review. The main result of this preliminary study was a characterization table adapted to the specific needs of this project.

The data gathered from the literature and manufacturers was then crosschecked to complete the characterization table of some fifteen EST. This comprehensive analysis was used to draw conclusions about the potential of each considered technology for medium-term distribution grid integration.

## What is a DESS?

Based on the definition of distributed generation provided by [21], DESS might be seen as energy storage within distribution grids or on the customer side of the network. Fig.1 shows the generic structure of an ESS.

The first remarkable part is, of course, the **Energy Storage Device** (ESD) itself, i.e. the component in which the energy is stored to be released later, after deduction of some losses. Electricity is a physical phenomenon realizing an instantaneous energy transfer and therefore cannot be stored as it is. Another form of energy is thus used as intermediary storage medium, such as chemical potential energy for batteries, gravitational potential energy for pumped hydro or kinetic energy for flywheels.

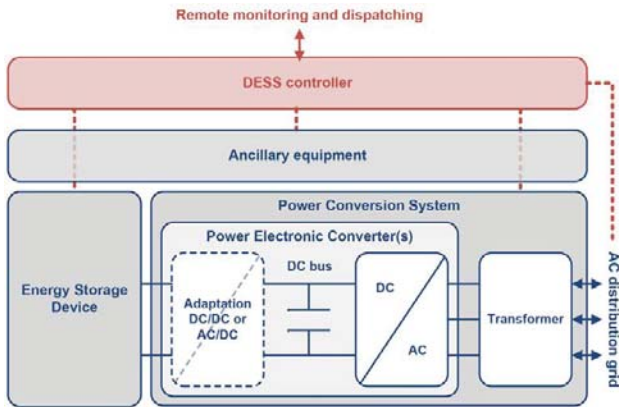


Fig.1. Typical layout of (battery) energy storage systems

With the exception of CAES and pumped hydro, all the EST addressed herein have DC power output or variable-frequency AC output (flywheels). A **Power Conversion System (PCS)** is thus used to interface the ESD to the 50-Hz or 60-Hz AC voltage of the grid. It usually includes a power electronic bidirectional inverter, monitoring/control systems, protective devices, a step-up transformer and harmonic filters [2][12]. Additional converter(s) are sometimes required to match the output voltage level and/or waveform of the ESD to the DC bus, or to control power flows in parallel multi-string or multi-storage configurations.

Finally, some **ancillary equipment** is often needed to perform functions such as ESD and PCS cooling/heating or environmental control (e.g. ventilation).

### Some parameters for EST characterization

#### Storage capacity and power range

The energy storage capacity is the amount of charge or energy that can be delivered by an ESD during a single discharge. For electrochemical devices, it depends on various factors, such as the final limiting voltage, the condition of the battery, its age, the temperature and the discharge rate. The influence of the latter is particularly substantial and appears clearly on a Ragone chart, which plots specific energy versus specific power. It is a widespread tool that can be helpful for sizing purposes, but which is also extensively used to compare the performances of EST (an example is given in [9]).

Fig.2 shows the Ragone chart of a commercial nickel-cadmium battery. The rated capacity is the energy recovered during a 5-hour discharge ( $C_5$ ). At higher rate, increasing losses and the diffusion processes of reactants reduce the actual amount of energy retrieved during a single discharge or vice versa at lower rate. Therefore, it is customary to distinguish the rated capacity  $W_{rd}$  and the retrievable capacity under specific conditions  $W_{ut}$  [8].

The charge/discharge power an ESS can exchange with the grid depends on the power rating of its electromechanical or power electronic converter ( $P_{max}$ ). This one can be sized allowing for pulse discharges, provided their impacts on the lifetime, energy efficiency and retrievable capacity of the ESD are suitably taken

into account. From the point of view of the grid operator, two properties seem quite useful to assess the adequacy of EST for distribution system applications:

- The medium-term **feasible system power range**. The lower bound is linked to the smallest single ESD (module) of the considered technology whereas the maximum can derive from various factors such as technical limits, complexity or costs.
- The **discharge duration at rated power** ( $T_C$ ).

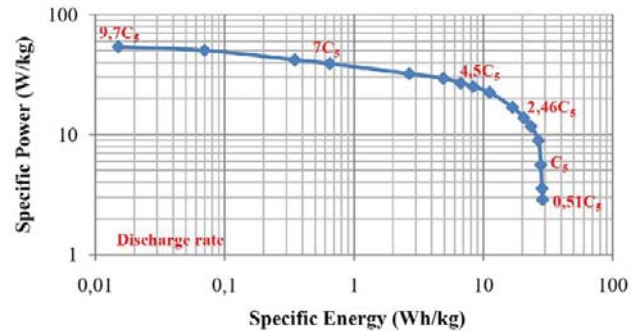


Fig.2. Ragone chart of a commercial nickel-cadmium battery

#### Lifetime

At some point, ESD cease working or their performances have decreased an extent that they cannot fulfil their object, or be economically justified anymore. For example, an electrochemical device is usually considered failing when its capacity reaches a given fraction (typically 60% or 80% [2][7]) of its initial value. At least two ways to assess the expected lifetime of EST are commonly defined [2][5][8]:

- The first is the so-called intrinsic or calendar lifetime. It is the statistical **maximum service life** ( $D_T$ , in years) of a given EST independently of its use, no matter whether it is appealed to or not.
- The second integrates the progressive defacement of the device due to its utilization. **This expected cycle life** ( $N_{max}$ , in cycles) is usually quoted under certain hypotheses: Depth of Discharge (DoD), mean State of Charge (SoC), charge/discharge rates, etc. Knowing the duty cycles and the frequency of use of an ESS allows deducing from  $N_{max}$  the order of magnitude of its cycle life in years.

The actual service life can therefore be much lower than  $D_T$  as the working conditions of an ESS harden.

#### Energy efficiency

The energy efficiency of EST can be defined different ways, depending on the storage technique, the subsystems of the DESS taken into account to make the computation and the time horizon. For example, various instantaneous, round-trip or long-term efficiencies are more or less frequently encountered.

The literature of ESS usually quotes round-trip efficiencies based on one or more realistic cycles for a given application. Since the energy efficiency depends strongly on the duty cycle, these figures should be

regarded as indications. Within the context of the present study, it was chosen to focus on:

- The **DC round-trip efficiency** of the EST ( $\eta_{DC}$ ). This is the ratio between the released energy and the stored energy, quoted for the ESD alone or including a possible adaptation converter (e.g. a rectifier for flywheels). The AC round-trip efficiency ( $\eta_{AC}$ ) is obtained by multiplying  $\eta_{DC}$  by a factor between 0.8 and 0.9 to allow for PCS losses.
- The **self-discharge rate** of the device, expressed in percent of the stored energy lost per day or month. It is a key parameter to assess the potential of EST for applications requiring long-term charge retention. It is noteworthy that the self-discharge usually depends very much on the temperature. The energy consumption of ancillary equipment, when significant, is sometimes considered as additional self-discharge by the literature of EST.

### Specific energy and footprint

The dimensions of EST are much less critical for stationary than for vehicle applications. Within the framework of the present project, the **output specific energy** ( $E_M$  in Wh/kg) and **output energy density** ( $E_V$  in Wh/m<sup>3</sup>) or **footprint** ( $E_S$  in m<sup>2</sup>/MWh) were recorded. They may notably be useful for niche applications with space constraints, like underground power substations.

### Costs

Following the example of energy efficiency, the cost of ESD must be considered vigilantly. The profitability of a DESS and comparisons should be based on a life cycle cost analysis including the initial, O&M and disposal cost of ESD, PCS and ancillary equipment, as well as balance of plant (engineering, construction management, land, etc.) [2][8]. Some data about PCS economics and the O&M costs of ESS is provided by [2] but these cost scales were very difficult to crosscheck with other sources, as they are seldom mentioned.

**Initial capital cost** of ESD, on which we focus herein, can be integrally expressed per kW ( $C_P$ ) or per kWh ( $C_E$ ), depending on the sizing factor: power or energy. For some EST, these two dimensions are relatively independent and can therefore be included separately using partial costs per kW ( $C_{PP}$ ) and per kWh ( $C_{PE}$ ). In that case, the capital cost of the considered ESD can be computed using the equation (1) [8].

$$(1) \quad \text{Capital Cost} = C_{PP}P_{\max} + C_{PE}W_{ut}.$$

### Some other useful characteristics

To assess EST adequacy for various applications, the system **response time** is also a critical piece of information.

Finally, three qualitative criteria have been taken into consideration: the **industrial maturity** of EST (technical/commercial), the **environmental impact and public acceptability** (including various factors such as toxicity of materials, safety, recyclability, etc.) and the

**operating constraints** (maximal DoD, charge/discharge powers, operational conditions, etc.). For comparison purposes, a grading system ranging from 1 (worst case) to 5 (best case) was used for these parameters.

## Scope and results of the study

Various storage techniques have been used so far for stationary applications and many others are still at a pre-commercial stage or undergoing research with an eye for the future. Among them, about twenty EST were considered within the framework of the present analysis. History and operational principles are not tackled herein, but are described in detail by [2], [3] and [8]. Table 1 shows the EST that were investigated.

**Table 1**

*A list of the reviewed EST*

General Classification		Technology	Notation
Chemical	"Standard"	Lead-acid	PbA
		Nickel-cadmium	NiCd
		Nickel-metal hydride	NiMH
		Nickel-zinc	NiZn
		Lithium(-ion)	Li
		Metal-air	Metal-air
	High-temperature	Sodium-sulphur	NAS
		Sodium-nickel-chloride	ZEBRA
	Redox-flow	Polysulfide bromide (Regenesys)	PSB
		Vanadium-vanadium	VRB
		Zinc-bromine	ZnBr
		Cerium-zinc	CeZn
	-	Hydrogen/fuel cell	H <sub>2</sub> /PAC
	Mechanical	Pumped hydro	PH
Compressed-air energy storage		CAES	
Small-Scale (Subsurface) CAES		SS-CAES	
Advanced-adiabatic CAES		AA-CAES	
Hydro-pneumatic		HyP	
Flywheel energy storage		FES	
Magnetic	Superconducting magnetic ES	SMES	
Electrostatic	Ultracapacitors	UC	
Thermal	Thermal energy storage	TES	

### Confronting EST to some requirements

In the light of the literature review, it became obvious that some EST does not meet all the minimum requirements for a short to medium-term integration into distribution grids.

The most discriminating criterion was indisputably maturity. Indeed, the hypothesis of an industrial deployment in 2015 requires that a stabilized product range already exists for stationary applications and is currently being tested in the field, or very close to be. CeZn, SS-CAES, AA-CAES, HyP and TES (all at the R&D stage) were thus ruled out, as well as NiZn (developed so far for cordless products and vehicle applications) and H<sub>2</sub>/PAC (still evolving, in conjunction with technical and economic competitiveness issues).

Two more EST should be turned down because of technical considerations, even if commercial products have been available for years. On the one hand, in spite of their impressive features (high specific energy of 150 to more than 300Wh/kg, environmental friendliness and



moderated costs), metal-air batteries have a very difficult and inefficient electrical recharging ( $\eta_{DC}=40\text{-}50\%$ ). On the other hand, SMES systems need cryogenic cooling that requires energy-intensive equipment and specific O&M know-how [2], thus limiting their competitiveness and commercial expansion.

Then, since a licence on its intellectual property was sold by RWE in 2004, the development activities of the PSB redox-flow technology have come to a standstill and the two large-scale (12MW/10h) demonstration plants under construction at the time were never completed, with subsequent financial consequences (e.g. \$20m net project loss for Tennessee Valley Authority [22]). Even if a new effort was made to drive it to the market, it would probably take years to regain investors' confidence.

Although NiCd technology has been successfully demonstrated in the 27MW/15min ESS in Fairbanks, Alaska, NiCd is uncertain because of the current regulatory banishment of cadmium within the European Union, which is now effective for portable batteries [23].

Finally, PH and CAES, in addition to be site-specific, are to be left-out because their power range (usually more than 100MW per unit) does not fit at the distribution level. For example, in France, current regulations set the maximum rated power of generating units at 250kVA and 17MW for connection at LV and MV respectively [24].

### *What technologies for near-future DESS?*

In the end, nine technologies became distinguishable by their apparent better adequacy and relative readiness for integration into distribution grids. They are briefly introduced in the following paragraphs and an overview of their characteristics is provided in Table 2, as well as those of PH and CAES for information.

**PbA** is widespread, indisputably mature and has a quite long history of use for grid-connected stationary applications from the middle 1980s, as shown in [3]. Its main advantages are its low cost, pretty good efficiency and very high availability in various application-specific products [2]. However, it has quite low specific energy, moderate lifetime, includes toxic materials and is temperature-sensitive and globally outperformed by newer techniques [2][5]. It can be considered as a very good reference for comparison purposes.

**NiMH** batteries made their way to the market in the early 90s and were developed very quickly for electronic devices such as mobile phones and laptops. Their specific energy is about twice as high as PbA, with a competitive lifetime, low maintenance and lower temperature sensitivity, but quite high self-discharge (about 20% a month) [5][11]. Vehicle applications are now offering them good perspectives, with expected price reductions.

**Li** batteries started challenging NiMH for portable applications in the 1990s and are now emerging on the vehicle market segment. They are known for their high power and energy densities as well as for their good efficiency and lifetime, but are still expensive and subject to safety concerns for large-scale systems [5][10].

**NAS** batteries were first demonstrated for stationary applications in the 1990s and found their way to the market in 2002 (50kW/7.2h modules). Thanks to their high efficiency, above-average energy density and good lifetime, they have been strongly developed for MW-scale, grid-connected applications, such as peak shaving (see [12]), power quality and fluctuation mitigation in wind farms. Their main drawback is the need for thermal management to keep the internal temperature of the module at about 300°C during non-use time, thus reducing the overall efficiency of NAS systems (~20% of  $W_{rd}$  is thus lost each day during standstill) [2][7].

**ZEBRA** batteries are also high-temperature devices presenting more or less the same features as NAS, excepted their lifetime, which appears to be lower (1000-1500 cycles at 80% DoD as against 5000). They were originally designed for vehicle applications and their potential for stationary ESS was demonstrated later through a few experiments. Their industrial development is still relatively limited at the moment [7][13].

**VRB** is a redox-flow technology that has been commercialised over the past few years for stationary systems ranging from a few kW to bespoke installations of several MW. Its main advantages are its modularity, the independence of power and discharge time, environmentally friendliness of the materials and good lifetime. Nevertheless, VRB devices need energy-consuming ancillary equipment for electrolyte circulation and have quite low specific energy. Demonstrations for a few grid-connected applications are in progress [2][7].

**ZnBr**, redox-flow batteries as well, have quite similar advantages/drawbacks as VRB apart from a lower lifetime and a fixed discharge time at maximal power of about 2h-2h30 for intrinsic, technical reasons. Moreover, a zinc deposit on the anode of the battery should be removed all the 5-10 cycles, requiring a complete discharge (stripping) [2]. Modules (50kWh) and complete units are commercially available at present and a list of recent demonstration projects is provided by [3].

**FES** products are currently available under various constructions, ranging from conventional steel rotors to advanced composite structures, which are still being developed. The large majority of flywheels are designed for power applications, presenting a very high cycle-life and outstanding efficiency. Their self-discharge is however quite high, usually leading to the loss of full capacity in no more than a few hours [2]. FES is currently being demonstrated for frequency regulation.

**UC** is another technology for high power applications available since the early 2000s and showing very good cycle life and efficiency, at the cost of low energy density and environmental concerns for some products comprising acetonitrile. Current applications of UC include notably electric vehicles and regenerative braking for urban transportation.

### **Discussion**

The characterisation of various EST using such a common set of properties raised some difficulties in

**Table 2**

*Some characteristics of EST for DESS, compared with two mature bulk-storage techniques ([2]-[20])*

Technology	Medium-term, feasible system power range	Typical discharge duration at rated power	Shortest feasible response time	DC round-trip efficiency (%)	Self-discharge rate (% per unit of time)	Specific energy (Wh/kg)	Energy density (Wh/liter) and/or footprint (m <sup>2</sup> /MWh)	Maximum service (calendar) lifetime (years)	Expected cycle-life at 80% DoD (number of cycles)	Cost per kW of the ESD alone (€/kW)	Cost per kWh of the ESD alone (€/kWh)	Medium-term maturity for stationary applications (/5)	Operating constraints (/5)	Environmental impact and acceptability (/5)
PbA	f.kW-f.10MW	2-8h	f.1ms	70-85	1-5% month	25-35	60-130	3-12	200-1500	Not relevant	25-250	5	2	3
NiMH	f.kW-f.MW	f.10min-f.hours	f.1ms	65-75	15-25% month	50-100	80-300	10-15	1500-2000	Not relevant	400-2000*	3	4	4
Li	f.kW-1MW	f.hours	f.1ms	85-90	2-10% month	60-180	150-400	10-15	f.1000	Not relevant	300-1500*	2	4	3
NAS	50kW-f.10MW	7-9h	f.1ms <sup>a</sup>	85-90	Low <sup>b</sup> 14-24%	100-120	120-150	15	~5000	1000-2500	115-350	4	4	3-4
ZEBRA	5kW-500kW	2-10h	f.1ms <sup>a</sup>	85-90	Low <sup>b</sup> 7-17%	95-120	130-190	11	1000-1500	200-400*	500	2	3	3-4
VRB	f.kW-10MW <sup>3</sup>	f.hours <sup>c</sup>	f.1ms <sup>a</sup>	80-85	Low <sup>b</sup> f%	12-15 <sup>d</sup>	11-17 <sup>d</sup> 20-120	10-15	~10000	C <sub>pp</sub> =~3500*	C <sub>pe</sub> =~400*	3	4	3-4
ZnBr	25kW-f.MW	2h30	f.1ms <sup>a</sup>	75-80	1% hour	30-40	10-15 ~30	~10	1000-2000*	700	300	3	3	3-4
FES	f.kW-f.10MW	10s-f.hours <sup>e</sup>	f.1ms	85-95	20-10 <sup>3</sup> % hour	1-10	5-20	20	10000-10 <sup>7</sup>	150-3000	Not available	3	3-4	3-4
UC	f.kW-f.MW	1s-f.10s	f.1ms	85-98	f.%-50% day	2-15	3-10	~10	10000-1000000	100-500	5.10 <sup>4</sup> -1.5.10 <sup>5</sup>	3	3-4	3
PH	100MW-f.GW	20-40h	Minutes	65-80 AC/AC	Very low	2 (water, 1000m)	2 (water, 1000m)	40-60	50000-200000*	C <sub>pp</sub> =500 -1500	C <sub>pe</sub> =5-30	5	1	1-2
CAES	100MW-f.GW	4-30h	Minutes	40-55 AC/AC	Very low	Not available	1-18 (air only)	30-40	10000-25000*	C <sub>pp</sub> =450 -550	C <sub>pe</sub> =5-30	4-5	1	1-2

f.-a few, <sup>a</sup>-under conditions: for example, NAS and ZEBRA must be kept at operating temperature, <sup>b</sup>-the energy consumption of ancillary equipment (given in percent of the nominal capacity per day) must be taken into account during non-use time, <sup>c</sup>-Discharge time and power are independent in VRB systems, <sup>d</sup>-electrolyte only, <sup>e</sup>-just a very few products have T<sub>c</sub>>f.minutes, \*-insufficient data for crosschecking, confirmation required.

terms of compatibility and comparability of the data. A significant dispersal in the collected information was noticed. It can be explained, on the one hand, by the fact that many application-specific constructions are usually available for a same EST (for example high-power and high-energy batteries) and, on the other hand, because DESS are highly non-linear devices: the performances of a given ESD vary in accordance with its duty cycle.

Moreover, the definitions of the characteristics quoted by the literature of EST usually may change from one source to another, making crosschecking quite arduous.

That is why the proposed figures should be considered as guidelines. An analysis throughout a complete life cycle is indispensable for comparing DESS to other solutions within a decision making process, both on the economical and environmental levels. Such a characterisation could also be prepared for a given application as an intermediate step: by selecting only dedicated products for some EST, the dispersal would presumably be much lower.

Besides, the suggested set of properties could be generously completed with additional factors such as transportability, cell voltage, maintenance frequency, etc.

**Conclusion**

This article deals with the suitability of EST for medium-term (2015) integration into distribution systems. More than twenty EST were characterised within the framework of the present review and nine of

them rose through the ranks: seven “standard”, high-temperature or redox-flow batteries (PbA, NiMH, Li, NAS, ZEBRA, VRB, ZnBr), plus FES and UC.

Planned further work includes the study of the current opportunities of multi-service DESS in liberalized power systems and the modelling of the more promising.

**Acknowledgements**

This work was funded by EDF and ADEME (French Agency for the Environment and Energy Management).

The authors kindly acknowledge Stéphane BISCAGLIA (ADEME), Eric PEIRANO (ADEME), Gilles MALARANGE (EDF R&D) and Mehana CHAMI (EDF R&D) for their involvement in the management of the present PhD research project. Besides, a considerable technical support was received from Régine CLAVREUL, Alain COMTE, Lionel JAMY and Stéphane LASCAUD from EDF R&D.

**References**

[1] IEA press release (08)14, *Despite Slowing Oil Demand, IEA Sees Continued Market Tightness Over the Medium Term*, 2008, available: <http://www.iea.org>.  
 [2] *EPRI-DOE Handbook of Energy Storage for Transmission and Distribution Applications*, EPRI, Palo Alto, CA, and the US Department of Energy, Washington, DC: 2003. 1001834.  
 [3] EA Technology for the British Department of Trade and Industry, *Review of Electrical Energy Storage Technologies and*



*Systems and their Potential for the UK*, contract n°DG/DTI/00050/00/00, URN n°04/1876, 2004, available: <http://www.berr.gov.uk/files/file15185.pdf>.

[4] British Department of Trade and Industry, *Regenesys Utility Scale Energy Storage – Overview report of combined energy storage and renewable generation*, contract n°K/EL/00246/00/00, URN n°04/1047, 2004, available: <http://www.berr.gov.uk/files/file15180.pdf>.

[5] INVESTIRE Network, *Final Publishable Technical Report (and nine other reports on various energy storage technologies)*, contract n°ENK5-CT-200-20336, 5th Framework Programme, 2004, available: <http://ired.iset.uni-kassel.de/investire/index.html>.

[6] The Australian Greenhouse Office, Department of the Environment and Heritage, *advanced electricity storage technology programme – Energy Storage Technologies: a review paper*, ISBN 1 921120 37 1, 2005.

[7] KONSTANTINOS E., DESPOINA D., *1.5a – Report on Use of Energy Storage Units*, DISPOWER, in D1.5 deliverable, del\_2005\_0058, 2005.

[8] IBRAHIM H. et al., *Energy storage systems – Characteristics and comparisons*, Renewable and Sustainable Energy Reviews, doi:10.1016/j.rser.2007.01.023, 2007.

[9] VAN DEN BOSSCHE P., VERGELS F., VAN MIERLO J., MATHEYS J., VAN AUTENBOER W., *SUBAT: An assessment of sustainable battery technology*, Journal of Power Sources, Volume 162, Issue 2, 2006, pages 913-919.

[10] MARIYAPPAN J., BLACK M., STRBAC G., HEMMI K., *Cost and Technical Opportunities for Electricity Storage Technologies*, GreenNet, Work Package 3, 2004.

[11] KOPERA J., *Considerations for the utilization of NiMH battery technology in stationary applications*, The Battcon 2005 Proceedings, Florida, 2005, available: <http://www.battcon.com>.

[12] NOURAI A., *Installation of the First Distributed Energy Storage System (DESS) at American Electric Power (AEP) – A Study for the DOE Energy Storage Program*, Sandia National Laboratories, SAND2007-3580, 2007, available: <http://www.osti.gov/bridge/>.

[13] DUSTMANN C., *Advances in ZEBRA batteries*, Journal of Power Sources 127, pp. 85-92, 2004.

[14] British Department of Trade and Industry, *Regenesys Utility Scale Energy Storage – Project summary*, contract n°K/EL/00246/00/00, URN n°04/1048, 2004, available: <http://www.berr.gov.uk/files/file16056.pdf>.

[15] JONSHAGEN B., *The zinc bromine battery for Renewable Energy Storage*, presentation, Proceedings of the first International Renewable Energy Storage Conference (IRES-I), Gelsenkirchen (Germany), October 30-31 2006.

[16] JOSSEN A., UWE SAUER D., *Advances in Redox-Flow batteries*, presentation, Proceedings of the first International Renewable Energy Storage Conference (IRES-I), Gelsenkirchen (Germany), October 30-31 2006.

[17] ENSMP/CENERG, 1.5b – *Fuel cell/Electrolyser combinations for long-term storage*, NNES-2001-00075, DISPOWER, in D1.5 deliverable, del\_2005\_0058, 2005.

[18] LEMOFOUET S., *Investigation and optimization of hybrid electricity storage systems based on compressed air and supercapacitors*, thesis EPFL n°3628, defended on 10/20/2006, available: <http://library.epfl.ch/theses/?nr=3628>.

[19] RIZOUG N., *Modélisation électrique et énergétique des supercondensateurs et méthodes de caractérisation :*

*Application au cyclage d'un module de supercondensateurs basse tension en grande puissance*, thesis Ecole Centrale de Lille n°20, defended in Lille on 02/28/2006, available: [http://hal.archives-ouvertes.fr/docs/00/06/65/36/PDF/These\\_Nassim\\_RIZOUG\\_L2EP\\_LILLE.pdf](http://hal.archives-ouvertes.fr/docs/00/06/65/36/PDF/These_Nassim_RIZOUG_L2EP_LILLE.pdf).

[20] SARRE G., *Advanced PV Energy Storage System with Lithium-Ion Batteries*, Proceedings of the first International Renewable Energy Storage Conference (IRES-I), Gelsenkirchen (Germany), October 30-31 2006.

[21] ACKERMANN T., ANDERSSON G., SODER L., *Distributed generation: a definition*, Electric Power Systems Research n°57, 2001, pp. 195-204.

[22] Tennessee Valley Authority, *2004 Information Statement*, available: [http://www.tva.gov/finance/reports/pdf/tva2004info\\_statement.pdf](http://www.tva.gov/finance/reports/pdf/tva2004info_statement.pdf).

[23] Directive 2006/66/EC of the European Parliament and of the Council of 6 September 2006, *on batteries and accumulators and [...] repealing Directive 91/157/EEC*, available: <http://eur-lex.europa.eu>.

[24] Departmental order NOR: DEVE0808815A of 23 April 2008 issued by the French Ministry of energy, *technical requirements for distribution grid connection of generation units*. Available: <http://www.legifrance.gouv.fr>.

## Biographies



**Gauthier Delille** was born in Lens, France, on March 23, 1984. He graduated in multi-disciplinary engineering from Ecole Centrale de Lille (France) and received a second Master's degree in "Electrical Energy and Sustainable Development" from the University of Lille in 2007.

His field of interest includes power systems, distribution grids and distributed energy resources. At present, he is a PhD student, working closely together with EDF R&D and the French Agency for the Environment and Energy Management (ADEME).

Gauthier Delille is a member of the Laboratory of Electrical Engineering (L2EP) in Lille. He is with Ecole Centrale de Lille, Cité Scientifique, BP 48, 59651 Villeneuve d'Ascq Cedex, France (email : [gauthier.delille@centraliens-lille.org](mailto:gauthier.delille@centraliens-lille.org)).



**Bruno François** was born in Saint-Amand-les-Eaux, France, on January 19, 1969. He received the PhD degree from the University of Lille, France, in 1996.

His field of interest includes power electronics, renewable energy sources and power systems. He is currently working on renewable energy based active generators and on the design of advanced energy management systems.

Bruno François is a member of the Laboratory of Electrical Engineering (L2EP) in Lille. He is an Associate Professor at the department of Electrical Engineering of Ecole Centrale de Lille, Cité Scientifique, BP 48, 59651 Villeneuve d'Ascq Cedex, France (e-mail: [bruno.francois@ec-lille.fr](mailto:bruno.francois@ec-lille.fr)).

# On the Methodology and Normative Regulations of Efficient Electrical Consumption

Kondyu Andonov, Anka Krasteva, Ognyan Dinolov, Liudmil Mihailov,  
Valentin Kirchev and Tasko Ermenkov

**Abstract:** It is suggested the electric consumers classifications to be fulfilled not by branches but by physical forms of electric energy conversion, and by mutual connection of electrical consumers. The levels for efficient electric energy use are defined according to the classifications. General dependences for determination of electric consumption levels are drawn.

**Keywords:** normative regulations, energy efficiency, methods of investigation

## Introduction

The investigation and estimation of effective electric energy use is obligatory processes that derive from the accepted regulations for power characteristics of objects and energy efficiency (EE) investigation [6, 9, 12, 14]. As uniform methods and rules are developed and approved for buildings [12, 13], there are no such detailed methods and regulations regarding electric-supplied machines, units and power systems. EE investigation of electrical consumers should be reduced to uniform methods, classification indications and criteria. Similar approach is not approved until now as EE usages are various according to specificity of processes, machines and power systems [7]. Similarly, the opinion that the investigation should be conducted by branches exists [10]. Generally, the electric consumption analysis shows that there are opportunities the complex of rules, methods and means (instruments) for EE investigation in electrical consumers to be reduced to integrated methodological basis.

The **research purpose** is to give proof of uniform methodological basis as a first stage of creating the instruments for EE investigation and estimation in electrical consumers.

## Normative Regulations in Bulgaria and Ways of Energy-Efficiency Assessment in Electrical Consumers

Power engineering is one of the branches in that a state policy exists and the normative regulations for solving the EE problems are ensured in principle. With developing of these laws and rules, a number of considerations exist that should be considered in further policy on effective use of electrical energy:

- initiating of the exergy beginning for quantitative and qualitative criteria estimation of the technologies for electric power generation and consumption;

- developing and strengthening of uniform normative base and criteria for EE estimation and prices formation in electrical energy generation, transportation, distribution and consumption;
- classifying of electric consumers not by branches and by the physical method applied for energy conversion;
- creating of uniform methods and instruments for automated investigations of objects for efficient electrical energy usage.

In short, efforts are needed in order to place the problem, named *Energy Efficiency in Electric Power Engineering* on a scientific fundamental. The problem can be solved if the physical laws for electrical consumption assessment and the conditions for optimum (in technical standpoint) consumers operation are set as an initial principle.

## Initial Conditions for Creating of Methodological Model for Energy-Efficiency Estimation

### *Consumers Classification by Organization Indications of Electrical Consumers*

It is the custom, electrical consumers to be classified by branches (industry, agriculture, domestic sector etc.). Each of the branches, sub-branches and objects have there specificity and it is important an account to be given of it. If the classification is realized on this basis, an indefinite multitude of indices will exists and most of them will be doubled. Another classification scheme is rational – by technological indications. Two basic groups of electric consumers can be separated – the first of technologically unattached, and second of technologically attached consumers.

**Group 1. Technologically unattached** (“free consumers”). The group covers the domestic sector, tourism, administration centers: all domestic consumers, electrothermic appliances, microwave ovens, washing machines, electronic audio and video technics, lighting etc.

**Group 2. Technologically attached.** The group covers consumers of production activities and fields. Two types of production systems are characteristic:

*Discrete electric-supplied systems* [4]. Electric power consumption of particular machines, units, systems, workshops etc. is described with the discrete production theory.

*Flow electric-supplied systems* [1, 2, 5]. The efficient electric consumption conditions of particular machines, installations and systems derive from the flow production theory. Consumers: CHP power plants, systems, installations; chemical, food, wine and tobacco industries, agriculture, transport systems etc.

### **Consumers Classification by Physical Forms of Electrical Energy Conversion**

Each process or activity is described with a theoretically requisite (minimum) consumption for running the process or the necessary quantity of work to be done. This level is fixed from the corresponding physical laws and processes. This means that every consumer has one basic level that is its physical foundation. Therefore, the consumers classification by the physical forms of electrical energy conversion is of primary importance. The power consumed that derives from the physically-determined level should be accepted for *absolutely effective (standard, efficient and unavoidable) consumption*. The physical forms of electrical energy conversion (consumption) are three: conversion into mechanical, thermal and radiant energy (Table 1). Irrespective of their locations, technologically unattached and attached consumers redistribute towards each of the forms.

**Table 1**

*Consumers Classification by the Form in which Electrical Energy Converts*

Conversion forms	Consumers
1. Mechanical	Electric powered machines and units in all fields of national economy.
2. Thermal	Induction and electric resistance heating in industry and domestic sector.
3. Radiant	Lamps and sources of radiant energy – irradiation and lighting systems.

According to the electric consumers classification in technological aspect (attached and unattached) and by the physical forms of electric energy conversion (Table 1), the following assessment levels of efficient electric energy use are defined.

### **Levels for efficiency assessment of electrical consumption**

#### **1. Physical (Basic) Level**

**In case of conversion of electrical energy into mechanical.** The level is referred to consumers with that electrical energy converts into mechanical energy (Table 1). It covers the groups of technologically unattached and attached consumers. That are processes related to electric powered machines and units where a counteraction to drag torques in cutting, drilling,

fragmentation, grinding, mixing exists (machine-building, electric powered domestic appliances, electric transport, housing construction etc.).

**Machines and units drive.** The consumed power level will be determined through angular  $\omega(t)$  or line  $v(t)$  speed in case of technological operations doing and rising of drag torques  $M_s(t)$  and forces  $F_s(t)$  in working mechanisms.

**Using of electrical energy for gravity forces counteraction.** Those are processes related to transportation of fluids and loads of small solids. Physically requisite energy for ensuring of the process of transportation is determined by the mass density  $\rho$ , acceleration of gravity  $g$ , quantity flow of load transported  $Q(t)$  and the altitude  $H=h_2-h_1$  of load transportation [1, 2, 3, 5].

**In case of conversion of electrical energy into thermal.** That are processes related to heat treatment of materials and foods – direct and indirect (inductive; dielectric) heating of materials and fluids. The energy absorbed in processed materials is effective. It can be determined by the thermal capacity  $C_T$ , the mass of materials  $m$  and the desired temperature of heating  $t$ .

**In case of conversion of electrical energy into radiant.** Here, a basic quantity is the radiant energy absorbed  $W_a$  with given spectral sensitivity of receiver  $\alpha(\lambda, t)$ . The effective part of  $W_a$  is  $W_e$ . This energy converts into desired for the particular technological process form of energy – electrical or chemical energy and other.

Basic level of electric energy consumed can be obtained previously in conformity with production processes ensured. Power balances should be drawn up through it and measures for economy of energy have to be organized towards it.

#### **2. Level of Optimum Electrical Energy Consumption**

Optimum consumption level can be reached only in case of such organizing of production activities, such machines and units adjustment so that each of it works with a minimum relative electric consumption (reciprocal efficiency value) [2, 4]. Conditions for reducing to the optimum level of electric consumption of particular equipment or technological processes are general and determined by the dependences given in Table 2 [4, 8].

#### **Symbols:**

$W_f$  is the basic electric energy consumption, kWh;

$W_{pol}$ ,  $W_{pol,opt}$  are the effective electric energy consumptions in cases of no optimum and optimum consumers operation, respectively, kWh;

$W_{Z,OL}$ ,  $W_{Z,OPT}$  – electric energy losses in consumers under no optimum and optimum operation, kWh;

$W_Z$ ,  $W_{Z,OPT}$  – technical losses of electrical energy under no optimum and optimum operation of a consumer or a group of consumers involved into investigated technological process or object, kWh;

$W_{ph}$ ,  $W_{ph,opt}$  - no-load electric energy consumption of objects under no optimum and optimum consumers operation, kWh;

**Table 2**  
Generalized dependences for consumption levels determination in electrical consumers

<b>No optimum operation</b>	
(1)	$W_{ph} = \sum_1^n P_{ph_i} \cdot \tau_i$
(2)	$W_{pol} = W_f + W_{Z,OL}$
(3)	$W_{ph} = W_{ph,opt} + \Delta W_{ph}$
(4)	$W_Z = W_{ph} + W_{Z,OL}$
(5)	$W_L = W_f + W_{Z,OL} + W_{ph} = W_{pol} + W_{ph}$
(6)	$E = \frac{W_{pol}}{W_L}$
(7)	$\Delta\tau_i = \tau_i - \tau_{i,opt}$
<b>Optimum operation</b>	
(8)	$W_{ph,opt} = \sum_{i=1}^{i=n} P_{ph_i} \cdot \tau_{i,opt}$
(9)	$W_{pol,opt} = W_f + W_{Z,opt}$
(10)	$W_{Z,opt} = W_{ph,opt} + W_{Z,OL}$
(11)	$W_{opt} = W_f + W_{Z,opt} + W_{ph,opt}$
(12)	$E_{opt} = \frac{W_{pol,opt}}{W_{opt}}$
(13)	$\alpha = \frac{W_L}{W_{opt}}; \beta = \frac{W_{ph}}{W_{ph,opt}} = \frac{\tau_i}{\tau_{i,opt}}$

$\Delta W_{ph}$  – extra losses due to no-load operation of objects with no optimum conditions, kWh;

$\Delta W_{opt}$  – extra electrical energy losses due to increased load of object in optimum operation, kWh;

$W_L, W_{L,opt}$  – electrical energy consumption in no optimum and optimum operation of objects, kWh;

$W_Z$  – net losses of electrical energy, kWh;

$W_{tech}, W_{tech,opt}$  – technical electrical energy losses in optimum and no optimum operation of consumers, kWh;

$W_{INK}$  – encashed quantity of electrical energy, kWh;

$W_{IZT}$  – electrical energy supplied by source, kWh;

$E, E_{opt}$  – relative electrical energy consumption in no optimum and optimum operation of consumers;

$\tau_{i,opt}$  – time spent with optimum operation of consumers, h;

$\Delta\tau_i$  – working time savings, h;

$\alpha$  – coefficient of over-consumption of total quantity of electrical energy;

$\beta$  – coefficient of over-expenditure of electrical energy losses.

### 3. Level of actual electric-energy consumption, $W$

This is the actual consumed electric energy in case of real operation and with concrete parameters of investigated technological process, consumer or consumers group. In optimum operation it is  $W_{opt}$ , and in no optimum operation -  $W_L$ .

### 4. Level of encashed electrical energy, $W_{INK}$

It is important using this level in order to ascertain and control eventual thefts, dead lines of electric energy encashing and paying, and costs to be planned, accounted and distributed.

### 5. Level of electric-energy total losses, $W_Z$

Electric-energy total losses can be separated to technical and trade losses [10]. For given time period, electric-energy total losses are a difference between electric energy supplied by source  $W_{IZT}$  and encashed for that period electrical energy  $W_{INK}$ .

### 6. Level of technical electric-energy losses

These losses can be determined in case of optimum and no optimum consumers operation by the expressions (14) и (15).

With optimum operation:

$$(14) \quad \begin{aligned} W_{mexh,opt} &= W_{ph,opt} + W_{Z,opt} = \\ &= W_{ph,opt} + W_{Z,OL} + \Delta W_{opt} \end{aligned}$$

With no optimum operation:

$$(15) \quad \begin{aligned} W_{mexh,opt} &= W_{ph,opt} + W_{Z,opt} = \\ &= W_{ph,opt} + W_{Z,OL} + \Delta W_{opt} \end{aligned}$$

### 7. Level of trade electric-energy losses, $W_{targ}$

The quantity of these losses is determined as a difference between net and technical losses of electric energy:

$$(16) \quad W_{mьpз} = W_Z - W_{mexh}$$

### 8. Level of electrical energy supplied by source, $W_{IZT}$

It is determined through the formula:

$$(17) \quad W_{IZT} = W_f + W_Z$$

Measuring of electrical energy consumed for distribution enterprises subscribers can be conducted at low or average voltage sides (LV and AV). The measuring location is the joining location of subscriber to LV electric distribution power network and the measuring is organized at AV side in case of subscribers with their own step-down power transformer AV/0.4 kV [11]

## Conclusions

1. The theses presented show that there is objective indispensability and potential for reducing the normative regulations of efficient electrical power consumption to a uniform methodical basis.

2. According to the synthesis, in case of energy-efficiency investigations, three groups of consumers divided by the physical forms of electric energy conversion are differentiated: group 1 – conversion of electric energy into mechanical; group 2 – conversion of electric energy into thermal energy; group 3 – conversion into radiating flux and light.

3. The realized synthesis shows that the electric consumers, in case of their energy-efficiency research,



should be classified not by branches and production groups but by the factors that determine the physically-necessary electrical consumption  $W_f$ .

4. The offered dependences for determination of the physical consumption level  $W_f$  are the tool for electric consumption modeling according to the consumers groups. The physical level should be a standard for electric demand controlling in a particular process, object or company. Measures for energy-efficiency increase in electrical consumers without change in equipment and production technologies might only lead to a decrease in current consumption level. Otherwise, they can decrease the basic and actual consumption level.

5. The optimal electric consumption level  $W_{opt}$  also has a model character. This is the theoretically attainable level with given equipment and production technologies. It can be found with the aid of technical data for machines and equipment and it should be an integral part of the firms and objects energy balance. The estimation on the effects from offered electric energy saving measures should be conducted towards to the optimum level and according to the methods developed as well as the synthesized criteria  $\alpha$  and  $\beta$ .

6. The investigation results are a precondition for a uniform methodological setting in energy-efficiency investigations of electric consumers and electric consumption control in every object, firm or company, irrespective of their processes and activities features.

## References

- [1] Andonov K., O. Dinolov, V. Kirchev, G. Nedev. Energy-Efficiency Investigation of a Complex System for Coal Preparation. *Energetica*, №5, 2008.
- [2] Andonov K., O. Dinolov, V. Kirchev, G. Nedev. Energy-Efficiency Investigation of a Coal-Feeding System. *Energetica*, №8, 2007, pp. 26 – 33.
- [3] Dinolov O. Specificity and Factors with Energy-Efficiency Evaluation of Coal Preparation Systems in Heat-Electric Generating Plants. - Proceedings of *Angel Kanchev* University of Ruse, Vol. 46, Series 3.1, 2007, pp. 23 – 27.
- [4] Dinolov O. Generalized Model for Energy Efficiency Estimation of Induction-Motor Drives. *Energetica*, 2007, № 5, pp. 37 – 43.
- [5] Dinolov O., G. Nedev, V. Kirchev, K. Andonov. Energy-Efficiency Investigation of a Dust Preparing System with Intermediate Bunker. Proceedings of *Angel Kanchev* University of Ruse, Vol. 46, Series 3.1, 2007, pp. 16 – 22.
- [6] Energy Strategy of the Republic of Bulgaria, 2004.
- [7] Kirchev V., O. Dinolov. A Comparative Study of Possibilities for Energy-Efficiency Increasing in Induction-Motor Drives. *Energetica*, 2008, №1, pp. 35 – 43.
- [8] Krasteva A., K. Andonov, Kr. Enimanev, G. Popov. Research of Influence of Pump Systems Control Regime on Effective Electrical Energy Use. *Selskostopanska Technica*, №4, 2004.
- [9] Law of Energy Efficiency – DV, №18/ 19 February, 2004.
- [10] Law of Power Engineering – DV, №107 / 7 December, 2003, modified №18/ 2004 and №18/2005.
- [11] Norms for Electric Power Measuring, Decision of DKEVR № A-1 / 10 April, 2007.
- [12] Regulation №18 / 12 November, 2004 for Power Characteristics of Objects.
- [13] Regulation №19 / 12 November, 2004 of Building Certificating for Energy Efficiency.
- [14] Regulation №21 / 12 November, 2004 for Energy Efficiency Investigation – DV, №112, 2004.

## Biography



**Kondyu Andonov** was born in Gavrailovo, Bulgaria on March 01, 1945. He studied at VIMMESS, Ruse, Bulgaria and received a Dr. Sc. degree at the same university in 2005.

Since 1995 he has worked in the Faculty of Electrical Engineering, Electronics & Automation of the Ruse University as a Lecturer and researcher in the fields of energy efficiency, renewable energy sources, electrical apparatuses, short circuits, modeling and

investigation in electric power engineering, optimization of processes and power systems and others.

Since 2007 he is the Head of the Specialized Science Council on Agriculatural and Forest Engineering at VAC, Bulgaria.

Kondyu Andonov is the leader of the Department of Electric Supply & Equipment, University of Ruse, 8 Studentska Str., 7017 Ruse, Bulgaria (e-mail: kandonov@ru.acad.bg).



**Anka Krasteva** was born in Tsar Kaloyan, Bulgaria, on December 2, 1968. She studied at the Technical University of Ruse, Bulgaria and received a Dr. degree from the same university in 2003.

Since 1996 she has worked in the Silistra Branch of Ruse University as a Lecturer and researcher in the field of investigation of electric energy consumption in industrial objects.

Anka Krasteva is the leader of the Department of Engineering and Natural Sciences in Silistra Branch of Ruse University, 1 Albena Str., 7500 Silistra, Bulgaria (e-mail: pkj@abv.bg).



**Ognyan Dinolov** was born in Svishtov, Bulgaria, on May 15, 1981. He studied at the *Angel Kanchev* University of Ruse, Bulgaria and received a Master degree from the same university in 2005.

His field of interest includes energy efficiency, renewable energy sources and high-efficiency motors. Today he is a PhD student in the Department of Electric Supply & Equipment at the *Angel Kanchev* University of Ruse, Bulgaria.

Ognyan Dinolov is with the Department of Electric Supply & Equipment, University of Ruse, 8 Studentska Str., 7017 Ruse, Bulgaria (e-mail: dinolov@googlemail.com).



**Liudmil Mihailov** was born in Golyamo Vranovo, Bulgaria on February 6, 1957. He studied at VTU *Angel Kanchev* - Bulgaria and received a Dr. degree from the same university in 1990.

Since 1995 he has worked in the Faculty of Electrical Engineering, Electronics and Automation of the Ruse University as a Lecturer and researcher in the fields of relay protection, electric substations, energy efficiency and

short-circuit currents.



Liudmil Mihailov is with the Department of Electric Supply and Equipment, University of Ruse, 8 Studentska Str., 7017 Ruse, Bulgaria (e-mail: lmihaylov@ru.acad.bg).



**Valentin Kirchev** has studied at Technical University in Russe, Bulgaria and received a Master degree from the same university with distinction. He made a PhD thesis in electricity networks and systems, Professor at Plovdiv Technical University.

He held various administrative positions in scientific field. He is a member of the Specialized Scientific Council on Electrical Engineering of the Supreme Academic Committee. He is an author of a number of student books and publications in the field of electric power engineering. He has a long-standing experience as a manager in the energy sector in Bulgaria.

Since December, 2006 he is the Deputy Chairman of the State Energy and Water Regulatory Commission (SEWRC). Currently he is responsible for the activities in energy sector of the SEWRC, including the sector monitoring.

Valentin Kirchev is with the State Energy and Water Regulatory Commission, 8-10 Dondukov Str., 1000 Sofia, Bulgaria (e-mail: vkirchev@dker.bg).



**Tasko Ermenkov** was born in Sofia, Bulgaria on October 4, 1955. He studied at the Moscow International Relations Institute, Moscow, USSR, specialty - *International Economic Relations*.

He has done a qualification course on Investment and Financial Analysis of Infrastructural Projects in Institute for Public-Private Partnership, Washington, USA. He worked in Ministry of Labour and Social Policy – Director of the Project Management Unit

*Reform for increasing the Welfare of the Bulgarian Children* in its part, funded by a World Bank Loan, as well as he is a member of the Steering Committee of the whole project, funded also by EU donation. Tasko Ermenkov has been a coordinator of a Project for Capacity Increasing of the Social Support System in Bulgaria, funded by the Institutional Development Fund (IDF) of the World Bank.

Since June, 2003 Tasko Ermenkov is the Executive Director of the Energy Efficiency Agency, 37 Ekzarh Josif Str., 1000 Sofia, Bulgaria (e-mail: Ermenkov@seea.government.bg).

# Applications for Short-Term Optimal Power Planning in Liberalized Power Markets

Dimo Stoilov, Penko Gyurov, Danail Ignatovski

**Abstract:** *The liberalization of the power markets creates changes in the planning and operation of the electric power systems. The roles and functions of the market players, as well the system operators, modify. The set of information and calculation tools used to solve the player's tasks undergo changes. In this article we present the essence of a research on applications for short-term optimal power planning requisite for the Bulgarian system operator at the liberalized market conditions.*

**Keywords:** *System Operator (SO), Power Planning, Applications (tools)*

## Introduction

In parallel with the technical progress, all countries, except Switzerland, opted for liberalization of their electricity markets as means to increase the public welfare through the so called deregulation of the natural monopolies. The classical vertically integrated companies have been reorganized in order to commercially unbundle the activities on generation, transmission, distribution, electricity supply and consumption.

The objective of each newly emerged market structure (producer, service provider, transmitter, distributor, supplier, trader and consumer of electricity) is not any more the previous common objective: sustainable balance between the generation and the consumption at the minimum possible total costs, and the specific purpose: participation for maximum profit. The assumption is that the free commercial participation of the producers at each of the regulated markets enables achieving the most profitable prices for them, and through their competition in the direct contracting with consumers – optimal costs for the society.

The deeper the liberalization has gone into a given electric power system, the more the main dispatch tasks undergo certain changes as number, order of implementation and nature. Some of them are assumed by other market players (roles), others are modified, and new ones are added. A main precondition for the viability of the electricity market remains the task of the system operator for on-going balancing between generation and consumption, as well as the task for the reliable functioning of the electric power system.

Not only in Bulgaria are the liberalization and the market structure at such an incomplete uncertain stage of successive changes. Such is the case also in other countries. In normal countries progress is achieved thanks to the negative experience acquired so far, as well as orientation to better solutions.

The overall information regarding liberalization also undergoes dynamic changes. During the recent 8 – 10 years more than 1000 serious research materials dedicated directly to the issue of the electricity market have been published in the leading western magazines, the Internet and the other sources available to us. The majority of them discuss, among other issues, the EPS active power optimization. It could be summarized that in these publications still there is no prevailing opinion on the selection of the market structures and of the active power optimization tools for them.

For the purposes of [1] the authors have studied 133 articles from magazines and the materials of four companies (ADICA, AREVA, PSR and SIEMENS). It is not possible to present their list therefore the bibliography refers only to the main sources that summarize the essence of numerous publications. In [2] the market models at liberalized electricity market are presented. In [3] the development of the optimization problems, solved by the system operators in the planning and management of the active capacities, is presented, and in [4] – the market participant's problems are explained. In [1] these models and problems are further developed and grouped in a volume of 112 pages, in order to analyze and assess the impact of the development of the markets models and rules in Bulgaria on the tool sets used in the CDU, as well as to forecast the modernization of these same tool sets.

Tool sets are identified on the basis of the system roles performed by the market players. This article focuses on the sets for system operation planning and dispatch control. The sets for the market functions of the SO and the market administrator (MA) are mentioned only if necessary either to complete the presentation or to point out the functional or information dependencies between the two types of applications.

## Factors determining the tasks of the System Operator

The market model selected by political decision is a major factor that determines the functional duties and the tasks of the System Operator. Most often the outline of this model is stipulated by an act and the relevant secondary legislation, i.e. by the regulatory framework.

The second major factor is the specific character of the electricity generation, transmission and distribution. It requires to trade with electricity diversified by sources, specified for each single market period (most often hour), as well as with the so called ancillary services (all types of reserves; regulation of frequency, and exchanges and transmission capacities etc.) via so called system services

(dispatch planning and control). In fact, one and the same source sells several goods during the same market period, which has to be strictly allocated, provided and settled for the terms before, during and after the delivery accordingly. The trade with electricity, ancillary services or transmission capacity may be performed simultaneously or successively (initially the ancillary services, and then – the electricity). Both scenarios have their own market and technological advantages and drawbacks.

Due to the specific character of electricity an absolutely free market may not exist. Organized balancing of the electricity generation with the electricity consumption is necessary. Two balance mechanisms are applied. The first one performs the balancing through balancing groups established in advance with a coordinator who is financially responsible for imbalances of his group. The second one uses balancing market where balancing electricity is traded. Usually each market player is obliged to supply for each dispatch interval proposals for the balance energy that it may supply or may obtain for the price offered.

The necessity of preliminary dispatch planning and operational control of the electricity balance between the generation and the consumption imposes the establishing of a system of successive markets or one electricity market extended in time. In both cases the EPS is operated in the long term (annually and more), weekly, day-and-night and hourly market and market in real time, i. e. balancing market.

Most often the electricity and the reserves are traded at unbundled markets. The optimal solution would be simultaneous dispatch planning and management of the electricity and the reserves. Integrated preliminary markets are designed, at which the electricity, reserves and the transmission capacities are offered simultaneously. The following objective functions are possible: 1. minimization of the producer's costs; 2. minimization of the consumer's payments; 3. maximization of the public welfare.

The rules of market functioning and the requirements to the players in the electricity markets, including the system operator, are changing constantly. This imposes the elaboration and implementation of more and more new applications for planning, management and control. Therefore the functions assigned to these applications are numerous and various. Part of them has optimization nature – overall or partial. A representative is the function for preliminary trade (from years to hours ahead). It comprises analysis of the possible market transactions, their statistics, risk assessment and comparison to the purchases and sales at the spot market (most often power exchange). Preliminary trade with electricity, ancillary and transmission services takes place and the loads, transmission restrictions, the ancillary services needs, etc. are forecasted.

Other similar factors influencing the applications are the functions related to determination of the Market Clearing Price (MCP) for each trade interval, as well as

determination of the traded volumes of demand and supply.

As before, under market conditions the unit commitment (UC) for each dispatch interval is a significant planning function. After the liberalization the UC is performed by the system operator in more rare cases. For Bulgarian fragmented producers the unit commitment problem is almost meaningless due to the limited total number of the available units.

The liberalization of the electricity markets and the retreat from the vertically integrated system structures pushes forward in the dispatch planning and management the so called business problems. Often here the models used are optimization ones as well. The optimal planning and management of the combined pool-bilateral markets also brings difficulties. It is necessary to determine the most profitable ratio between the energy sold under bilateral contracts and the energy from the relevant auctions, which is a dynamic optimization problem without a clear solution.

It is undisputable that the classic optimization procedures that may be used also in the liberalized markets of electricity and system services fall in “conflict of interest” with the market traditions. The conflict between the procedures “auction” and “optimal power flow” is the strongest because the object “public welfare” and “minimum costs” cannot be equalized. It shall be assumed that the centrally organized schedule of the energy system, using the Optimal Power Flow (OPF), is balanced regarding generation and consumption, but it does not bring the maximum possible profit to each of the producers, which they would obtain in case the establishing of the schedule is their duty. The auction procedure (i. e. the Market Clearing Price) with objective function public welfare maximization provides also for unit commitment for each considered hour. There are also practices for solving the conflict between two most often used procedures. It is admissible to compare the results between these two contrasting procedures. The result may be directly compared for the same hour. It was found that the auction procedure deteriorates the economic efficiency for the relevant hour, by resulting in comparative loss in finance and cross subsidizing compared to the complex optimization. This shall be born in mind for Bulgarian market practice as well.

### **Considerations for tools selection**

There are two points of view to the changes that shall be introduced in the EPS operation planning and dispatch control with the liberalization of the electricity markets. According to the first one everything remains the same, only new operational organization is necessary. According to the second one – everything is totally changed, clear separation of the functions of all newly assigned roles is also necessary, including the power exchange or individual traders and the market administrator as an organizational unit of the System Operator. The truth is somewhere in the middle and is determined by the traditions in the relevant country.

For example it is obvious that for the purposes of the long-term and middle-term operation planning the available models, algorithms and programmes of the type resources forecast and assessment, hydrothermal coordination, unit commitment, economic dispatch, import and export of electricity assessment, etc. may be used without significant changes. The transition to weekly and daily planning requires above all new organization in the use of the programme products and systems, which may remain, more or less, without significant changes.

The difference between the two types of markets (the availability or the lack of preliminary power exchange market), predetermines a number of instants directly related to the weekly and daily operation planning:

- the lack of preliminary market eliminates the use of “Market Clearing Price” as an optimization procedure but provides opportunities for applying the group of models, algorithms and programmes for complex optimization (hydrothermal coordination, unit commitment, economic dispatch, OPF);
- the existence of a preliminary market allows the “Market Clearing Price” procedure but does not allow overall complex optimization, which imposes the use of heuristics for the provision of rational rule for disconnection of units and sufficient reserves.

In both types of markets it is possible to use: the power flow and OPF models and programmes, check for admissibility of the supply schedules (bottlenecks); the models and programmes for hydrothermal coordination („insertion” of the available water quantities in the load diagram).

As regards the unit commitment and economic dispatch procedures the following considerations are valid:

- their centralized use in short-term operation planning is the write decision that, properly included in the liberalized market structure, provides for the necessary reserve and the lowest price of electricity from the point of view of the consumers;
- if such use is not provided in the legislation in force, for example with the necessity to ensure the reserves in advance, it will probably be contested by some independent producers as discrimination and repealed to the advantage of own unit scheduling.

All such considerations are analyzed in detail in [1] pursuant the Bulgarian Energy Act and the Rules for the EPS Operation.

The act provides for the independent behavior of the system operator in performing his functions because as a daughter company of NEK an opportunity presents itself for market competition limitation. For example between the property on the Power System Operator (PSO) and the independence of his management decisions, between the responsibilities of NEK as a Public Supplier and his

ownership of the big HPPs and Pump Storage HPPs, which are managed by the SO; between the ownership on the transmission grid and the access to the grid etc.

Interest provokes the wording of Art. 109, Par. 3, namely: „PSO establishes a coordinated schedule of the planned outages of the generating capacities and the transmission grid elements according to the criterion for maximum reliability.” Perhaps this text could be interpret in the meaning that PSO establishes a centralized schedule of the planned outages according to the criterion maximum reliability. However this may be contested by some producers as deprivation of their independence or equal treatment. Obviously the legislator has foreseen that not all of the market participants will participate in the optimization by their own decision. Therefore the legal option has been created for the PSO to oblige the producers with the determined periods of outages. Vice versa, restricting the role of the system operator to a mere coordination of the outages has had a fatal outcome with the example of the Californian liberalization.

Due to the significant influence of HPPs on the amount of the total operation costs, often the main problem for optimal distribution of production in mixed systems is called problem for hydrothermal coordination (coordination between the HPPs and TPPs in covering the daily and weekly load diagrams). It comprises the economic dispatch (ED) problem of the TPP units as well. Thus is formulated the problem for weekly and daily active power optimization of the PS operation, while considering the impact of the electricity grid and the possible integral restrictions related to the planned daily and weekly consumption of energy resources for the individual power plants.

One of the important new market problems is the introduction of a simultaneous optimal market for energy and ancillary services. It is based on the local marginal prices of energy and of the regional marginal prices of the ancillary services for regulation up, down, spinning and cold reserve. These are the following day and following hour markets, based on auctions for energy and ancillary services. An optimal power flow programme is used, which ensures reserve capacity from the already committed units with the power exchanges participation. It distributes the loads while satisfying the power flow equations, the ancillary services requirements and the transmission restrictions. The possible congestions may be controlled through repeated power flow calculation.

The concept for the market as a game that offers solutions through achieving of economically competitive balance is more than 150 years old. On the other hand the common market modeling methodology may be defined as controlled iterative change of each player own market behavior by the moment when neither of them may unilaterally increase his profit without decreasing the profits of others. In view of the difficulties in organizing these iterations and their control it is suggested after performing certain transformations, the model game to become a three levels decision making procedure in the following forward and reverse order: system operator –



independent producer – power unit. There are indications that the utilization of this new procedure may turn out to be very successful.

In conclusion to this section, it is important to underline that if the transmission network users do not duly present to the system operator the bilaterally contracted by them schedules, allocated by consumption buses and accordingly supply nodes (units), the system operator will not be able to perform his duties.

### Tool Sets Structure

The necessary active power planning tools are created or purchased on the basis of the role performed by the different market players in the information exchange among them.

The sets of tools for the different users of the power transmission grid, accordingly power distribution networks are directly dependent on the national market rules and the set of tools implemented by the Power System Operator (PSO).

The Power System Operator performs a lot of roles. Its necessary tools for all the roles vary depending on the characteristics of the different national markets. Fig. 1 illustrates one such set of tools. It has been taken from the description of the information and computing system of SIEMENS: "SINAUT Spectrum" [5]. The module principle of such a system is symbolized by honey-comb cells.

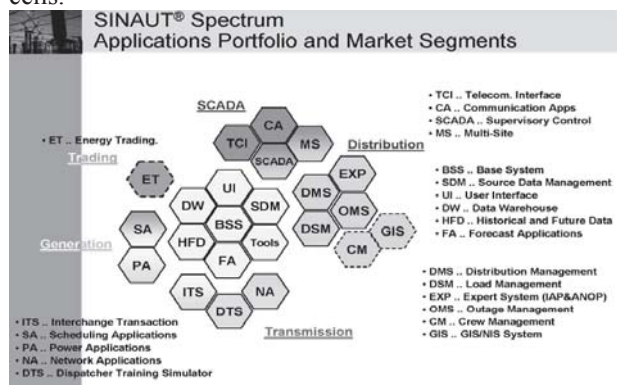


Fig.1. The Exemplary Set of Applications for a System Operator which exercise also the distribution functions

In the middle of the “bee nest” is the basic subsystem that manages the sources of data, interface the users, the different data bases and the forecasting applications. This is the so called “integrating infrastructure” that enables the use of common data and common results as well in varying order of switching of the different programmes in the operation of the different subsystems. Around the basic subsystem are grouped the SCADA subsystem, the distribution subsystem, the transmission subsystem, the generation subsystem and the trade subsystem. Each such subsystem unites the different tools on information and functional basis.

The SCADA subsystem unites the tools for interface of the telecommunication facilities, supervisory control and data acquisition and the multifunctional devices. It is

a highly developed conventional subsystem related above all to the real time control.

The distribution subsystem serves the operator of the distribution network to manage the distribution, the consumption, the outages of grid elements etc.

The transmission subsystem comprises a set of applications for control of the transmission grid (for defining and control of the available transmission capacities, for management of existing or newly emerged congestions, for creation, approval, check, implementation and revision of the interchange and internal power schedules). The system interface provides the necessary environment for connection with all the market players and with the external environment. It enables all users of the power transmission system to communicate with the PSO and to supply the necessary data in advance compared to the moment of real transmission and supply of electricity. Some specialized tools in this subsystem have functions for coordination of the outages of generation units and main transmission grid elements; for determining the system needs of different types of ancillary services and their management. Other specialized applications serve the functions of transmission reliability. For example a module similar to the traditional EMS comprises: real time network analysis (topology, state estimation, power flow, accident analysis, optimal power flow); load forecasting – for the whole system and by nodes, steady state and dynamic stability tests; voltage stability, etc. Another module (group of functions for network planning) comprises functions on long-term transmission plan; assessment of transmission service requests; stable congestion management; construction of transmission equipment.

Depending on the market model and the specific rules modules could be added for functions related to trade, including real time imbalances, settlement and bills determination function, archiving of data function, etc. They are usually considered as a part of the tool sets for the market administration (see below).

The generation subsystem comprises the instruments for active powers planning and control. It directly depends on the market rules and undergoes evolution according to the degree of liberalization, the type and organization of the markets.

Last but not least in importance is the trade subsystem, which is the one most frequently changing and completing because it is most dependent on the changes of the trading rules in the respective country. It may comprise the following functions:

- Preliminary trade (ranging from a given period/ periods during the coming years to hours during the following day). This is a main block in the tool sets for market administration because the long term trade is used as a means to protect from the risk in purchase and sale of electricity on the spot market. The traded goods include: energy, ancillary services and transmission capacities. Forecasts are made of



the prices, loads, constraints and necessities, bids and offers are accepted for the different goods;

- Real time market runs. This is a block of tools that regulates the trade in goods that are sold in real time (by the last possible time before the moment of supply). Most often it comprises applicable software for determining the functions of demand and supply and for determining the Market Clearing Price (MCP);
- Management of the market for imbalances: i) balancing energy – until the moment of supply and ii) imbalance – after the moment of supply. Obviously this market is the most specific and various, which predetermines the variety in composition of the tool sets for its service;
- Unit commitment. In some markets the UC is performed by the generation companies and is called unit commitment according to the prices, and in other markets – by the system operator and is called reliability concerned unit commitment. The tools are selected according to the local rules;
- Creation and control of all schedules subject to the market;
- Determining the mutual obligations that have arisen among the market players – quantitative and financial settlement;
- market monitoring, including automated block for acquisition and recording of various data for compliance with the market rules, as well as with the rules for Electric Power System management (the regulatory provisions), including market power execution;
- Market simulations that are directly related to the previous functions to a large degree;
- Archiving the data and the market results.

To illustrate this, Fig. 2 shows the information and computing system of the united electric power system of the Middle West in the USA [6]. There the subsystems of the day-ahead and real time markets are presented as simple blocks in an overall information system of an independent regional market operator, which, it has to be noted, differs from that of a national market operator.

The individual tools number (programme packages) in the sets of one national dispatch centre for the short-term cycle planning (week, day and real time) is at least about 20. Only the traditional EMS related mainly to the real time, comprise five programming packages. The well known economic dispatch problem within a day horizon includes in its tools suit at least 6-7 main and preparatory problems. After the liberalization this number will comprise also one additional set of tools that serves the management of the material and financial assets; control and management of the financial risk; participation in the different markets; motivation of the commercial decisions; assessment of the competitive environment; regulation of the market relations, market accountancy.

The set of applications for EPS operation planning and control in market conditions processes a large

volume of information that may not be processed in a different manner except the one provided in the commercial and functional rules. For each single market period the market players send to the system operator approximately the following type of data: energy block, available capacity, ancillary services; quantities, price, time intervals, no-load running costs, start-up costs, operation constraints – operation range, load change rate and restrictions in time; bilaterally contracted schedules etc. The data are sent in strictly defined market-specific formats and periods of time. The system operator or its units also process and send to the users of the grid a variety of data, part of which are confirmed and another part rejected or awarded offers and requests etc. Significant volume of free-access information is also sent, such as clearing prices and traded quantities. For example a market player in the North-West states sends to the ISO/RTO about 50 000 components (of the data) daily. All this predetermines very high functional requirements to the tool sets for planning and management of the EPS in the specific market liberalization. On the other hand even upon introduction of a possible “standard” (USA) or “harmonized” (Europe) market structure, the necessary communications and tools in one market will differ significantly from these in other markets. This assessment gives rise to serious worry that it is hardly possible to borrow a set of applications from one market in order to implement this same set in another market. In such cases it will be necessary to introduce changes and amendments, and requires a lot of work to create the technological models to be used by the relevant programme packages and modules.

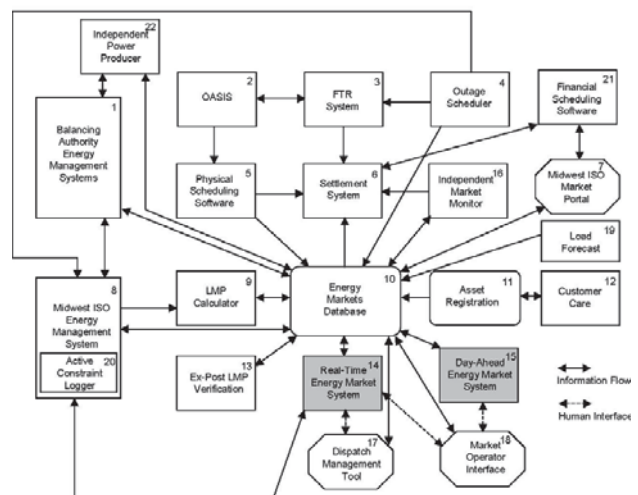


Fig.2. The information and computing system of the Middle West United Electric Power System in the USA

## Conclusion

The above-stated illustrates the necessity of detailed analysis and assessment of the delivered and implemented in our (Bulgarian) dispatch centers hardware-software tools and especially the software related to the optimal EPS operation planning, the real

time control and organization and management of the liberalized electricity market. Here are some more important conclusions from the carried out in [1] analysis, updated by the present period:

- The available since the beginning of 2000 optimization programmes for hydrothermal coordination (HTC), unit commitment (UC) and economic dispatch (ED) are not sufficiently integrated to the overall interface of all the remaining modules and have to be updated, according to the expected new market model.
- The available since 2002 but not yet implemented programme subsystems and system technological modules (Siemens platform) for balancing market and functional solutions (clearing and settlement) shall be assessed compared to the future market model in our country.
- The introduced in 1999 in the Central Dispatch (CD) and in 2005 in the Territorial Dispatch Centers (RDC) new management system SINAUT Spectrum of Siemens is an open module and distributed management system. It comprises all the necessary functions and together with the so called extension or additional modules of SCADA – SINAUT Spectrum is probably one of the best in Europe because it provides the following functions through the relevant subsystem basic modules: 1. Basic system services (BSS); 2. Management of data from different sources (SDM); 3. User interface (UI); 4. Tele-control interface (TCI). 5. SCADA applications; 6. Chronologic information system (HIS); 7. Communication applications (CA); 8. Use of multiple work places in dispatch centers (MS); 9. Power applications (PA); 10. Network applications (NA); 11. Dispatcher training simulator (DTS); 12. Data warehouse (DWH).
- The supplied in 2007 by Siemens platform for organization and management of the liberalized electricity market in Bulgaria is directly related to the introduced in the National and Territorial Dispatch Centers basic and extended system SINAUT Spectrum. It should be implemented in compliance with the development of the market rules and the remaining information subsystems.

Finally we emphasize on the necessity to consider the perspectives for development of the regional (Balkan) electric power and balancing markets when schedule the projects for modernization of the tool sets for the Bulgarian National Dispatch Centre.

## References

- [1] Parametric Analyses of Available and Modern Tools for Optimal Short-Term Active Power Planning in Liberalized Markets, Final Research Report, BSREC, Sofia, April, 2007.
- [2] Stoilov, D., Ianev K. Active Power Optimization in Liberalized Market Conditions: Part I – Market Models. Energetika Journal, 2006, No. 1, pp. 27-32, No. 2-3, pp. 36-44, ISSN 0324-1521.

[3] Stoilov, D., Ianev K., Active Power Optimization in Liberalized Market Conditions: Part II – System Operator Problems. Energetika Journal, 2006, No. 4, pp. 31-40, ISSN 0324-1521.

[4] Stoilov, D., Ianev K., Active Power Optimization in Liberalized Market Conditions: Part III – Market Participants Problems. Energetika Journal, 2006, No. 6, pp. 15-18, ISSN 0324-1521.

[5] SINAUT®Spectrum, Modules for Generation Control Systems, K.Weingast, Presentation, 13.10.2006;

[6] The Midwest Independent System Operator (ISO) Business Practices Manual (BPM) for Energy Markets, v.7, December 18, 2007.

## Biographies



**Dr. Dimo Stoilov** was born in Plovdiv, Bulgaria in 1969. In 1995 he graduated from the Electric Power Engineering Department of the Technical University (TU) – Sofia as M.Sc. in electrical engineering. He holds a M.Sc. in Applied Mathematics (TU-Sofia, 1998) and a Ph.D. (TU-Sofia, 2003) in Electric Power Grids and Systems. In the period 1997-2005 he worked as expert in the National Dispatch Center of the NEK-EAD.

In 2005 he joined the Electrical Engineering Faculty of TU-Sofia, where in 2008 he was awarded the position of associate professor in Power Grids and Systems. His major interests are in the fields of power systems operation planning and control.

Dr. Dimo Stoilov is with the Faculty of Electrical Engineering, Technical University of Sofia, 8, Kl. Ohridski Blvd., 1000 Sofia, Bulgaria (e-mail: dstoilov@tu-sofia.bg).



**Dr. Penko Gjurov** graduated from the Electric Power Engineering Department of the Technical University (TU) – Sofia as M.Sc. in electrical engineering in 1958. In the period 1958-1983 he worked in the National Dispatch Center of the Bulgarian power system. He was awarded a Ph.D. degree in Electric Power Grids and Systems (1986) and became senior research fellow and head of the “Energo kibernetika” Institute under the Ministry of Energy.

Currently he is engaged in numerous consultancy activities. His major research interests are in the fields of power systems operation planning and control, and power systems security.



**Danail Ignatovski** graduated from the Electric Engineering Department of the Technical University (TU) – Sofia as M.Sc. in electrical engineering in 1960. In the period 1960-1998 he worked as a research fellow in the Energy Scientific Research Institute (Energo projekt). In 1977 he carried out a training course in the research department of EdF.

Since 1998 is engaged in consultancy with Natsionalna Elektricheska Kompania–EAD, State Energy and Water Regulatory Commission, etc. His major research interests are in the fields of power systems development and security of transmission and distribution networks.

# Market Share Increasing in a Retail Electricity Market Using Reinforcement Learning

Babak Behbahani, Seyed Hossein Hosseinian

**Abstract:** In many countries, the focus of electricity restructuring has moved on from creating competition in generation to creating competitive electricity market for consumers. Opening electricity market in consumer side, need competitive electricity markets names Retailers. Electricity retailers set up contracts with generation companies (GENCOs) and with end users to meet their load requirements at agreed upon tariff. Considering the uncertainties in the power market, the problem faced by retailer is designing contracts, both at the supply and end-user levels. The question is what price must each retailer sale to costumers, to maximize its profit. This paper presents a Q-learning Based model for retailers to choose best pricing strategy in a restructured power market.

**Keywords:** Power System restructuring, Reinforcement Learning, Retail Electricity Market

## Introduction

One result of restructuring in electricity market is the emergence of third-party entities known as retailers .Retail contracts with suppliers and consumers, range from a simple fixed-price, fixed-quantity contract for a fixed time period —where the retailer takes all the risk-or to a more collaborative arrangement where the supplier and the retailer work on a profit and risk-sharing arrangement [1]. Consequently, the typical retailer faces the problem of setting up contracts on both the supplier and end-users side, in order to protect himself from settlement risk. If the price from the supplier is higher than prices in contracts with end-users, then the retailer will lose money and be forced out of business. Therefore, it is essential that the retailer have the right strategy and processes to price electricity to end-users. [2, 3]

In this paper, we describe behavior of retailers and consumers within a framework of retail competition and use Q-learning technique as a reinforcement learning method for retailer decision. This framework allows capturing the idea that, if this model has time to learn, act rationally in the market.

The paper organized as follow, section 2 describe Q-learning basis. Section 3 describes models for market participants and section 4 illustrates simulated market structure and present results.

## Reinforcement learning basis

Reinforcement learning is a computational approach to understanding and automating goal-directed learning

and decision-making [4]. It is distinguished from other computational approaches by its emphasis on learning by the individual from direct interaction with its environment as shown in Figure 1.

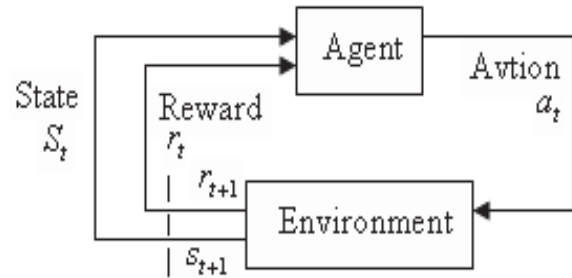


Fig. 1: The agent environment interaction in reinforcement learning

An agent in each State (S), chooses a current action (a), and performs it. The environment responds by giving the agent a reward  $r_{t+1} = r(s_t, a_t)$  and by producing the succeeding state  $s_{t+1} = \delta(s_t, a_t)$

Here the functions  $\delta$  and  $r$  are the part of the environment and are not necessarily known to the agent. An optimal policy is a policy that can maximize the possible reward from a state, called value,  $V^{\pi(s)}$  for all states. (1) is a typical definition of this:

$$(1) \quad \begin{aligned} V^{\pi}(S_t) &= r_{t+1} + \gamma r_{t+2} + \gamma^2 r_{t+3} + \dots \\ &= \sum_{k=0}^{\infty} \gamma^k r_{t+k+1} \end{aligned}$$

Here  $\gamma(0 < \gamma < 1)$  is a constant that determines the relative value of delayed versus immediate rewards

## Q-learning

Q-learning is one of the most popular techniques in reinforcement learning methods, because of simplicity and good responsibility. This technique contains a table known as Q-table. After having identified the current state, each agent looks at what his experience suggests to be the best action in this scenario. More technically, he selects the action with maximum Q-value corresponding to current state. To balance the exploration (to explore possible better strategies) and exploitation (to exploit the best strategies found by past experience), soft-max (strategy select randomly based on T parameter instead of

selecting the best strategies in order to explore possible better strategies) is used in the proposed action selection. That is, during the action selection process, an agent selects most of the time an action with maximum Q-value in the state  $s$ . with a probability given from Boltzman distribution.

$$p(x) = \frac{\exp(x/T)}{\sum_{i=1}^n \exp(\frac{x_i}{T})}$$

$p(x)$ : Probability of choosing  $x$

$T$ : Parameter known as temperature

At the end of each stage, agents have learnt something more on their choice. Thus, Q-values are updated, using (1)-(2).

## Market and participants Models

### Genco's

We proposed that market operation is Pay as Bid. When all consumer loads and Genco's prices distinct for each hour, ISO solve SCUC problem to assign market clearing price (MCP). The SCUC is formulated as an optimization problem which minimizes power system operating costs. The equation solve in the SCUC are shown here:

$$(2) \quad \min \sum_{j \in J} \sum_{k \in K} \lambda_j(k) g_j(k) + b_j y_j(k)$$

In order to solve this problem, ISO should apply power system and market constraints described in appendix 1

### Costumers

Demand for a consumer at each time is related to difference parameters. Generally we can propose the consumer load as a function of some parameters such this:

$$E = f(\text{Weather, time, } \rho, \text{Economic, } P_r)$$

Influence of each parameter on various loads is dissimilar and is relevant to the property of load, time and many other conditions. In this paper we model the consumers' behavior as a function we can find in [5].

$$E(t) = E_0(t) \left\{ 1 + \frac{B(t) [\rho(t) - \rho_0(t)]}{\rho_0(t)} \right\}$$

$E_0$  Is consumed load for a customer when price= $\rho_0$  and contain the parameters such as weather, economic and so on.  $E_0$  define for 24 hours in day.  $\beta$  is the load elasticity, mean the impress of price variation on

load deviation. ( $E = \frac{\Delta E / E}{\Delta \rho / \rho}$ ).

Load elasticity ( $\beta$ ) is a number between 0 and -1, greater  $\beta$  means greater elasticity.

Another important dynamic trait we assumed for costumer is costumer decision curve. This trait is our tool to specify the costumer right for change his retailer. Figure 3 shows a typical costumer decision curve.

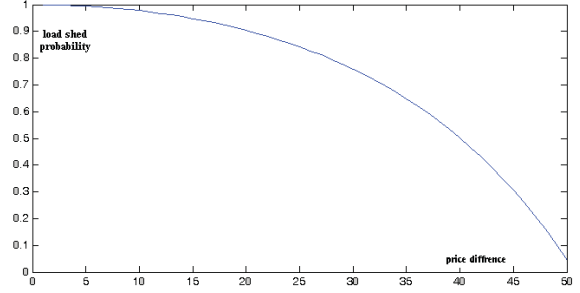


Fig.3 Typical customer decision curve

This curve show the probability of changing retailer by costumer base on the difference between retailer price and other offered price. We choose this curve because costumers have inertia to change his retailer, after that with retailer price increase, costumer desertion will grow. We use this concept as function  $P_{ac}$ . In order to model consumers in this paper, we set a base load profile for each consumer. Figure 4 show base load for bus2 as a sample of these profiles.

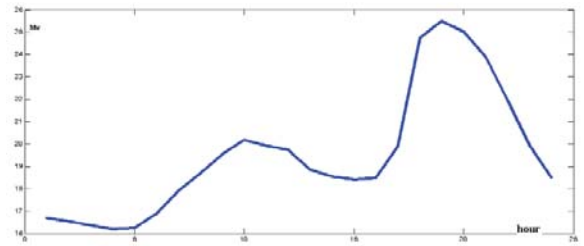


Fig.4. Load profile for group of consumers in bus2

### Retailers

In this section we introduce an objective function for retailers in a liberated power market. This model consist the main revenues and costs for retailer. We use this function as reward function in our model.

The objective function represents expected net profit to maximize. This objective function is broken up into the following pieces:

#### 1) Expected end-user revenues

The element of the profit function corresponds to the income is obtained by multiplying the kWh selling price applied to each customer, during each period

A main limitation for retailer to offer high price, is consumer ability to change his electricity provider easily. Mathematically, retailer income in consumer side is:



$$P_r \times L_r \times P_{AC}$$

2) Expected supply costs;

Each electricity provider has a contract with supplier to procurement enough electricity for consumers in consumers' contract period.

The electric energy purchase cost is

$$C_{tot} = L_p \times P_c$$

3) Expected spot market settlement revenues/costs;

Retailer should sale/buy excess/shortage electricity base on predicted load and actual load of consumers. ISO, base on total loads and total production in each hour, set regulatory price to buy and sale electricity. We suppose that ISO buy/sale electricity in  $reg\_price=1.1 \times mcp$  when market has more production than consumption and  $reg\_price=0.9 \times mcp$  vise versa.

Mathematically, we display this part of retailer cost/income:

$$(L_r - L_s) \times P_{reg-price}$$

4) Network Access Tariffs (Access Costs).

Network access tariff in market is containing two elements; electric power contracted with distribution/transmission system and transmitted power during contract period.

$$\sum \sigma_1 \times L_r + \sum \sigma_2 \times L_p$$

As above-mentioned, the objective function to be Maximized includes incoming element related to the sales, and other elements of electric energy purchase and access costs. The obtained profit can be expressed by the following expression

$$\text{Revenue} = [P_r \times L_r \times P_{AC}]$$

$$-[L_{S_i} \times mcp + \sum_i P_{ci} L_{Si}]$$

$$+[(L_r - L_s) \times P_{reg-price}]$$

$$- \sum \sigma_1 \times L_r + \sum \sigma_2 \times L_p$$

## Simulation and results

As a system for simulation and market participant operation modeling we choose 30-bus and 41-line standard IEEE network (Fig.5). We have 5 Genco in this structure. We can find basic data for these Genco's in appendix 2.

Consumers, Gencos modeled as we described in section 3. ISO solve SCUC to find MCP.

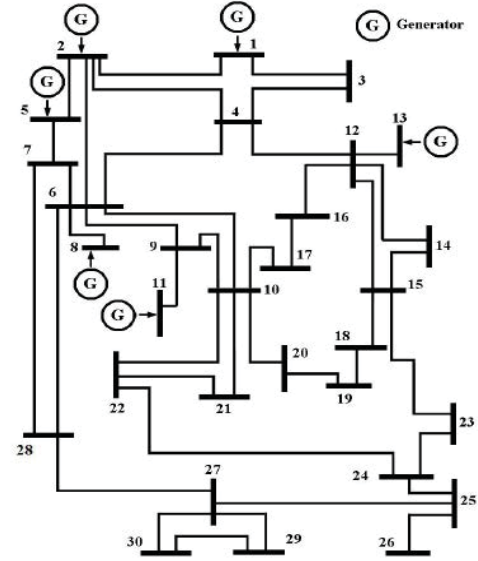


Fig.5. Studied network- 30 bus IEEE standard power system

To specify environment state at each stage we use two parameters, MCP and retail contract load. Agent select best price according to its strategy. We examine three pricing strategy, flat rate price, Time of Use pricing (TOU) and Real Time Pricing (RTP). In each strategy, at each state, agent selects an action between  $30 \times 10$  actions. We define each action as a percent of MCP. At the end of each stage, agents have learnt something more on their optimal choice. Thus, Q-values are updated, using (1)-(2). We supposed that the reward that retailer (agent) gets from the market (environment) is his revenue at each time period (base on the strategy selection) which formulated in section 3.

We propose that retailer has a contract with costumers in bus2. Then simulate market for 120 day, using SBB/CONOPT under GAMS software (<http://www.gams.com>), we can see MCP in last two week in Fig 6. We examine three different price strategies for retailer; fix pricing, Peak/off peak pricing and real time pricing. For simplify showing result we propose that clearing time for retail market set to 1 day.

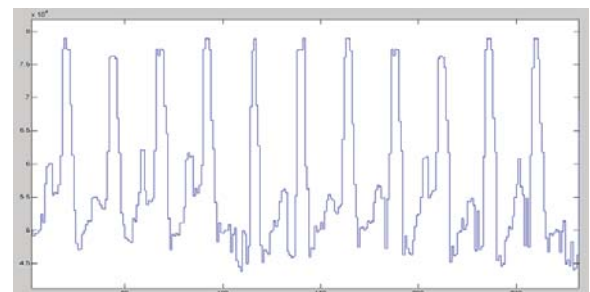


Fig.6. Market clearing price for last two weeks

From simulation result, we found that Q-learning model for retailer requires two month enough exploration



to find best price. Figure 7 shows the final revenue for retailer in two months.

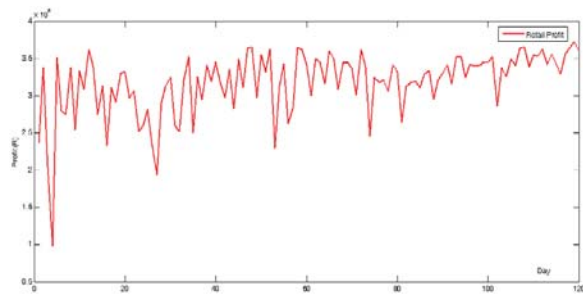


Fig.7. Retailer profit through learning process for 120 days

For more details we focus on last two weeks. On these days, we set T low, so that retailer exploitation is much more than exploration.

In Figure 8 we can find suggested flat rate price.

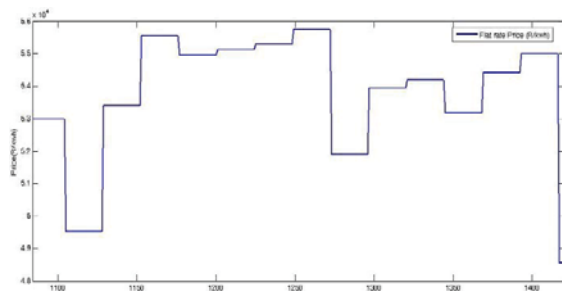


Fig.8. Retailer suggested price for last two weeks

Now consider the case retailer wants to increase its market share. We name this strategy attractive strategy. In this strategy, retailer suggests a price lower than normal price and tolerate a short term losses for long term benefits. In Figure 9 we can see retailer income in comparison with normal strategy.

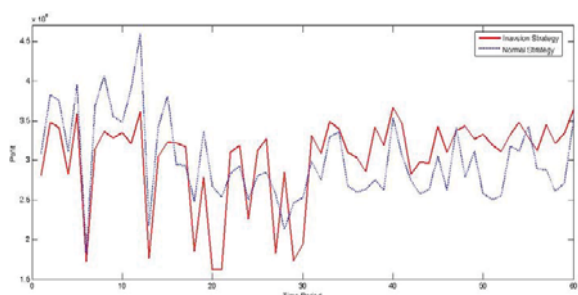


Fig.9. Retailer incomes in two strategy

We can see that in first days we have a loss and Market share is shown in Figure 10. Increasing of load is shown in this figure.

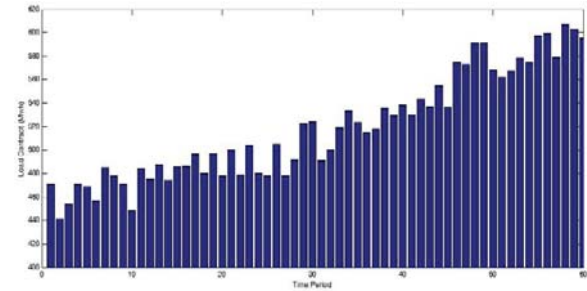


Fig.10. Retailer contracts loads

## Conclusion

In this paper we present a Reinforcement learning model for a retail electricity market to select best price for consumers due to his strategy. We use Q-learning to optimize profit function we introduce in paper. We found that with a two month exploration, retail can select best strategy. We can see this model help the retailer to increase its market share optimally.

## References

- [1] Gabriel, S.A., et al. Optimal Price and Quantity Determination for Retail electric Power Contracts. IEEE TRANSACTIONS ON POWER SYSTEMS, VOL. 21, NO. 1, FEBRUARY 2006.
- [2] Gabriel, S.A., M.F. Genc, and S. Balakrishnan. A simulation approach to balancing annual risk and reward in retail electrical power markets. IEEE Trans. Power Syst., vol. 17, no. 4, pp. 1050–1057, Nov. 2002.
- [3] Karandikar, R.G., S.A. Khaparde, S.V. Kulkarni., Quantifying price risk of electricity retailer based on CAPM and RAROC methodology. Electrical Power and Energy Systems 29 (2007) 803–809.
- [4] Sutton, R.S., and A.G. Barto. Reinforcement Learning: An Introduction. Cambridge, Massachusetts: MIT Press, 1998.
- [5] Yusta, J.M., et al. Optimal electricity price calculation model for retailers in a deregulated market. Electrical Power and Energy Systems, 27, (2005), pp. 437–447.
- [6] Hopper, N., et al. Customer response to day-ahead market hourly pricing: Choices and performance. Utilities Policy 14 (2006) 126e134

## Symbols

- $a$  : action
- $T$  : Temperature parameter
- $\gamma$  : Discount factor
- $S$  : state
- $E$  : consumer load
- $\rho$  : price
- $E_0$  : consumer load  
at a base price( $\rho_0$ )
- $t$  : Time

$\beta$ : elasticity

$P_r$ : retailer price

$L_r$ : Retailer actual load

$P_{ac}$ : probability of changing

retailer with consumer

$C$ : cost

$L_p$ : predicted load

$P_c$ : contract price

$L_s$ : bought load from supplier

Reg – price: regulatory price

## Appendix 2

Genco's parameter used in this paper.

GEN CO	Generator or Buses	A For Genco [S]	$P_{max}$ For Genco [MW]	For $P_{min}$ Genco [MW]	d For Genco [R/MW]	b For Genco [R]	UT For Genco	DT For Genco
G1	1	142/7	100	20	10/7	200	5	3
G2	2	218/3	80	10	18/1	100	4	2
G5	5	81/1	50	10	13/3	80	3	2
G8	8	81/3	50	10	13/4	80	3	2
G11	11	118/8	20	5	37/9	30	1	1
G13	13	287/1	70	10	19/3	95	4	2

## Appendices

### Appendix 1

The constraints of the optimization problem are:

- (2)  $\sum_{l \in T(s)} f_l(k) = load_s(k) - g_s(k)$
- (3)  $|f_l(k)| \leq f_{l,max} \quad \forall l \in L, k \in K$   
 $\forall j \in J, k \in K:$
- (4)  $v_j(k) p_{j,min} \leq g_j(k) \leq v_j(k) p_{j,max}$
- (5)  $[x_j(k-1) - UT_j][v_j(k-1) - v_j(k)] \geq 0$
- (6)  $y_j(k) - z_j(k-1) = v_j(k) - v_j(k-1)$
- (7)  $[x_j(k-1) + DT_j][v_j(k) - v_j(k-1)] \leq 0$
- (8)  $y_j(k) + z_j(k) \leq 1$
- (9)  $v_j(k), y_j(k), z_j(k) \in \{0,1\}$

Equation (2) guarantees that the load of each bus (and as a result, the overall load of the system) is provided at any time.

Equation (3) defines the upper limitation of the possible power flow, through the transmission lines. In this equation, the value of  $g_s(k)$  equals  $g_j(k)$  if the bus includes the generator (with the index of  $l$ ), and otherwise  $g_s(k)$  equals zero. Also the polarity of  $f_l$  is defined by assuming the polarity of the power entering the bus as positive. Equation (4) illustrates the power generator limitations and (5) and (6) show the minimum on-time and off-time limitations, respectively.

# The experience of using high-voltage controllable magnetic reactors in electrical network 110-500 kV

Aleksandr Bryantsev, Viktor Bepalov, Svetlana Dyagileva

***Abstract** Capital constraints, regulatory pressure and increased economy transfer between companies have prompted increased loading of the interconnected transmission and distribution systems. The goal of a reactive management program is to improve the utilization of the interconnected transmission and distribution system, and provide reliable and low cost service to customers. This paper has described a reactive management program that Tomsk and Tumen Powers has developed and implemented on its systems.*

**Keyword:** reactive power, sources of reactive power, controllable magnetic reactors, reactive power compensation.

## Introduction

The analysis of the large failures which what happened recently, has shown that one of the main reasons of their occurrence is reactive power imbalance. Increase of reactive power flows lead to decrease in stability in high-voltage networks 110-500 kV. In this connection, the question of reactive power compensation became the main question maintainability of power systems of the Russian Federation.

Deficiency of reactive power can lead to the following:

- Greater loading of reactive power of generators of power stations leads to current overload of generators;
- Reactive power loads the system reducing the distribution of active power and thus the overall economy of electricity generation;
- Lack of reactive power the system to caused a voltage reduction in the units of electricity networks and in point of consumption.

In elements of electricity network flows of reactive power appears which counter to direction of flows of active power that leads to increase of pressure in units and to increase in losses of power, under surplus of reactive power. The given mode is characteristic for the period of the light loads in a network.

Generating reactive power at the point of consumption helps energy production and thus saves energy. It frees power plant capacity for the production of active power and reduces losses in transmission and distribution systems. At the same time, there is a higher capacity available for the transmission of active power.

To generate reactive power at the power plant is uneconomical, producing losses in the electricity

network. This leads to increased use of primary energy. In transmission and distribution systems, reactive power requires as much capacity as active power.

Reactive power compensation - one of the most effective means of rational use of the electric power.

Traditional methods of compensation reactive power:

- Synchronous generators;
- Synchronous equalisers;
- The synchronous engines working in a mode of overexcitation;
- Statics thyristors compensators;

In the majority of system problems and the more so for systems of electrosupply of the industrial enterprises should will be applied Sources of Reactive Power (SRP), capable to generate reactive power. To such SRP synchronous machines and condenser batteries concern. However the synchronous machines possessing ability smoothly to adjust reactive power possess greater inertia. The main lack of traditional sources of indemnification of reactive power is that all of them are calculated on a pressure up to 35 kV. Condenser batteries possess high speed (10-20 ms) at step regulation of reactive power. But in a number of problems step regulation is unacceptable. Therefore apply combined high-voltage SRP which are capable to adjust smoothly at high speed reactive power. Such SRP consist of adjustable in steps capacitor banks and smoothly adjustable reactor, included in parallel.

During recent years the controllable magnetic reactors (CMR) are intensely developed and utilized in high-voltage network 110-500 kV for the compensation of power load. Currently, dozens of controllable magnetic reactors with power 25, 32, 63, 100, 180 MVar for all voltage classes are already installed or going to be installed soon. The controllable magnetic reactors guarantee the decrease in power losses, stabilization of voltage, and increase in capacity and reliability of high-voltage electrical networks. The experience of utilization demonstrated their exceptional reliability. Because of that, main direction of technical policy FSK RAO UES (Federal company of electrical networks in Russia) includes utilization of controllable magnetic reactors as one of the most perspective modernization method for electrical networks of Russian Federation.

The success of the controllable magnetic reactors is obvious because their cost is significantly less, and functionally they can completely replace the thyristor-reactor group of static compensator (STC) together

with increasing transformer. Also, the controllable reactor's construction is not different from regular 2- or 3- winding transformer's construction. Together with a battery of static condensers, the controllable magnetic reactor is able to perform the functions of synchronous or static compensator, using the same amount of voltage. For several years, RAO UES of Russia has been successfully utilizing four such complexes (the controllable reactor together with a battery of static condensers). Their high efficiency and exceptional reliability made a foundation for design of new high-voltage (110 kV and more) reversible complexes with transverse compensation, based on the controllable magnetic reactors. This work was done at Moscow Institute of Energy together with the company OAO "Electrical Controllable Reactors" because FSK (Russian Federal Company of networks) launched the program of creation and utilization of complexes FACTS.

### The device and principle of action system of automatic control

Basic scheme SRP is shown in figure 1. Where 1 - controllable magnetic reactor (CMR), 2 - the capacitor bank, 3 - control system (CS), 4 - switch, VT - voltage transformer, CT - current transformer.

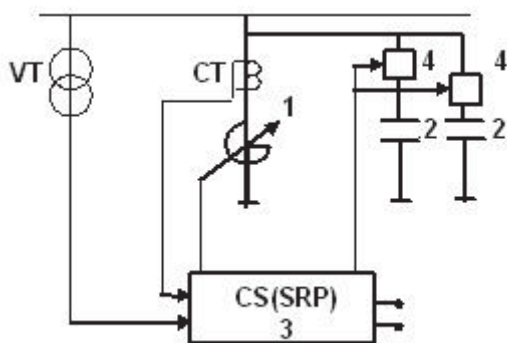


Fig.1 Basic scheme SRP

Control of SRP is carried out as follows: In a control system 3 establish the pressure of a network set for regulation (stabilization), the minimal current of a reactor, the maximal current of a reactor and a delay of time  $\Delta t$  between next switching section condenser batteries (inclusions or switching-off of switches 4 and 5). Usually interval of time  $\Delta t$  makes 1-10 minutes depending on parameters SRP and a network. Then controllable magnetic reactors 1 connect to a network.

In a network surplus of reactive power because of capacitor currents of the distributed capacity of a high-voltage network on the ground takes place at small loading of a network or its absence (at night). As a result the pressure in a network increases above the set pressure that is fixed by transformers of pressure VT and control system 3 which develops a command on increase in a current magnetic a reactor 1. As a result the current of a reactor 1 increases (down to the

maximal current), SRP passes in a mode of consumption of automatically adjustable reactive power and automatic stabilization of a pressure in a network. Thus control system 3 traces change of a pressure because of fluctuations of loading in a network, increasing or reducing a current magnetic a reactor 1.

At the further increase in loading in a network there is a lack of reactive power, control system 3, reacting on a voltage reduction, and checking a condition of a current of a reactor 1 less minimal, gives a command on inclusion of the switch 4 - on connection to a network of one section of the condenser battery 2, translating SRP in a mode of development of reactive power.

At the maximal loading of a network again there are conditions, at which pressure of a network less than the set pressure and a current of a reactor 1 less minimal. Control system 3 gives a command on inclusion of the switch 5, connecting to a network the second section of the condenser battery 2, and translates SRP in a mode of development of jet capacity down to maximal (at the minimal current of a reactor).

At decrease in loading (to transition at night) in a network there is a surplus of reactive power and increase of a pressure. From SRP transition from a mode of delivery of reactive power to a mode of consumption of reactive power is required. Therefore control system 3 develops commands on increase in a current of a reactor and at switching-off unit the condenser battery.

### Experience of application of compensating devices

*Substation 110kV "Igolskaya" and "Dvurechenskay" for electrosupply of oil deposits JSC "Tomskneft" (October 2004-March 2005)*

By an outcome of 2003 on oil deposits Southern Vasygan JSC "Tomskneft" there was a crisis situation. Throughput of an electricity transmission 110 kV «Parabel-Lugieckay-Igolskay-Krapivinskay» has been settled, and levels of a pressure on Substation-110 "Krapivinskay" did not exceed 85% nominal. And only in August-October, 2004 after input on Substation-110 "Igolskay" capacitor bank 23 MVAR, an controllable magnetic reactors (CMR) 25 MVAR and Substation-110 kV "Dvurechenskay" with capacitor bank 23 and CMR-25 the situation has changed radically in the best party. Throughput has grown on 30-50%, levels of a pressure have reached 105-110% nominal and can be adjusted in a wide range depending on modes.

Even the short period of operation of reactors RTU-25000/110-Y1 allows to note, that reactors together with batteries of static condensers:

1. Provide optimum streams of reactive power allowing to finish transferred capacity up to



maximum permissible on section of wires. On a condition of loadings for March 2005 100 % mutual reservation of electric loadings of an electricity transmission "Parabel-Dvurechenskay-Chapaevka" are provided. Necessity of translation of region on a pressure 220 kV has lost the urgency.

2. Reduce losses of active capacity in wires Substation -110 kV. At loading 72 MW losses make 7,5 MW against 11,9 MW, including in networks of JSC "Energotomskneft" 1.8 MW against 2.9 MW.
3. Provide smooth automatic stabilization of the set levels of a pressure in the established modes, at reduction of number switching capacitors banks and control under load in tens times.

#### ***Results of installation SRP on substations "Tauricheskay", "Vandmtor", "Novogodnya"***

In 2007 have been carried out researches on 256 substations of the Tyumen region, on parameters  $\tan\phi$ ,  $K$ ,  $U_{110}$ ,  $I_k$ . Results have shown, that installation SRP is necessary more than on 1/3 all substations. In this connection 2008 in electric networks JSC "Tyumenenergo" on substations "Tauricheskay", "Vandmtor" and "Novogodnya", compensating devices by the general capacity 225 MVar (on 75 MVar on everyone substations) have been entered into work. On each of substations have been established capacitors banks capacity 2x25 MVar and controllable magnetic reactor capacity 1x25 MVar. It has enabled to increase throughput of transmission lines and has allowed to reduce probability of switching-off of consumers at failures of a pressure.

#### ***Results of an initial stage of operation SRP 110/50/25 on substation "Tauricheskay"***

The analysis of results of measurements shows, that after implementation SRP -110/50/25 on substation "Tauricheskay" the pressure on trunks 110 kV this substation has increased on 3÷4,4 %, and fluctuations of a pressure are lowered more than in 5 times. Owing to increase of a pressure on trunks 110 kV substation "Tauricheskay" positions control under load of transformers on the substations receiving from it a feed have changed also.

Besides after implementation SRP -110/50/25 on substation "Tauricheskay" loading by reactive power of feeding lines and autotransformers has changed.

#### ***Results of an initial stage of operation SRP-110/50/25 on substation "Novogodnya"***

Substation "Novogodnya" it is involved in electrosupply of oil extracting of JSC "Gaspromneft-NNG". This substation is removed from the large feeding centers (from substations 220 kV "Vingapur" on 52 kilometers, from substation 220 kV "Young-Yaha" on 161 kilometers) owing to what, the given unit had low static stability and a low level of a pressure in

repair and after emergency operations. Changes of parameters of a mode of a network after implementation SRP -110/50/25 on substation "Novogodnya" the following:

1. On substation "Novogodnya" and adjoining unit the pressure is increased by 1,5 % and are lowered fluctuations of a pressure of 2 times.
2. Loading by reactive power of feeding lines and autotransformers on substation "Vingapur" on a full current on 3,8 %, on reactive power on 2 % has changed.

Owing to change of streams of reactive power after commissioning SRP-110/50/25 losses of capacity in networks of branch JSC "Tyumenenergo" have decreased on 1,8 %.

#### ***Results of an initial stage of operation SRP 110/50/25 on substations "Vandmtor"***

Changes of parameters of a mode of a network before implementation SRP-110/50/25 on substations "Vandmtor" the following:

1. On substations "Vandmtor" and adjoining unit the pressure is increased by 2,5 % and are lowered fluctuations of a pressure of 3,5-5 times.
2. Loading by reactive power of feeding lines and autotransformers has changed

Owing to change of streams of reactive power on 1,1 MW losses of capacity in a network of branch of JSC "Tyumenenergo" "Energocomplex". As a result loading of a network have decreased has decreased with 253,3 MW up to 252,2 MW.

#### **Conclusion**

1. Installation SRP has allowed to increase pressure in the centers of a feed of substations from 1,3 up to 4 % and as to automate process of stabilization of a pressure in units of loading in normal modes and at emergency indignations (technology FACTS), and to unload transformers on reactive power.
2. All the actions spent within the limits of these projects, are directed on increase of reliability of electrosupply of consumers. In particular, owing to unloading of an electric network from overflows of reactive power, throughput of a network has raised at simultaneous decrease in losses.
3. One of the main economic substantiations of connection high-voltage operated Sources of Reactive Power (SRP = controllable magnetic reactor + capacitors banks) 110-500 kV is the opportunity of additional connection of consumers, and also performance of emergency and scheduled repairs without restriction of consumption of capacity.

A well designed reactive power compensation program allows better use of the installed capability of transmission and distribution facilities.



## Biographies



**Aleksandr Bryantsev** was born in Kondopoga, Russia, June 13, 1951. He studied at the Kazakh Politechnical Institute of Alma-Ata, Kazakhstan and received degree Candidate of Technical Scinces in 1978 the same university.

In 1992 he received Dr. degree from Moscow Power Engineering Institute. His basic industrial results a theory of controllible ferromagnetic devices ultimate saturation of magnetic circuits was developed and on its base magnetization controlled reactors of 6-500 kV were offered. He is today worked in Faculty of Electrical Networks of the Moscow Power Engineering Institute.

Aleksandr Bryantsev is with the Faculty of Electrical Networks Moscow Power Engineering Institute, Krasnokazarmennaya, 14, Moscow 111250 Russia (e-mail: [bma@mail.ru](mailto:bma@mail.ru)).



**Viktor Bepalov** was born in Vladivostok, Russia, March 13, 1937. He studied at the Moscow Power Engineering Institute and received Dr. degree the same university. He is today worked professor in Faculty Electric Machines, Moscow Power Engineering Institute.

His field of interest includes electrical machines, transformers, reactors and electrical generator.

Viktor Bepalov is with the Faculty of Electric Machines, Moscow Power Engineering Institute, Krasnokazarmennaya, 14, Moscow 111250 Russia (e-mail: [BepalovVY@mpei.ru](mailto:BepalovVY@mpei.ru) )



**Svetlana Dyagileva** was born in Reutov, Russia, on November 04, 1984. She studied at the Moscow Power Engineering Institute (MPEI) and received Master degree from the same institute in 2007.

Her field of interest includes electrical machines, electrical networks and controllible magnetic reactors. She is today studies postgraduate MPEI and worked in field electrical networks.

Svetlana Dyagileva is with the Faculty of Electric Machines, Moscow Power Engineering Institute, Krasnokazarmennaya, 14, Moscow 111250 Russia (e-mail: [svetix@inbox.ru](mailto:svetix@inbox.ru) ).

# Electromagnetic compatibility and resources of terminators overstressings in networks 0,4 - 10 kV

Igor Kosorlukov, Valery Polyakov, Vyacheslav Prikhodchenko, Oleg Solyakov, Lev Shpitz

**Abstract** Under consideration are the questions of defining the technological resources of nonlinear overvoltage limiters 0.4-10 kV, factors, which influence the running consumption of the named resources, resulting wearing out of the overvoltage limiters and taking these factors into account, when designing and operating electrical networks.

**Keywords:** technological resources, nonlinear overvoltage limiters information, electrical networks, electrical power system, mathematical model,.

Nonlinear overvoltage suppressors (NOS) are one of the most effective means of protection of an electric equipment from overvoltage and maintenance electromagnetic compatibilities (EMS) [1-5]. Result of their work, that is restriction overvoltage on protected electro-installations, should be the remaining voltage which are not exceeding levels, regulated by directive documents and standards [1].

One of the basic conditions thus is the requirement of effective work NOS as the protective device at all stages of its life cycle as, as well as any electroinstallation, NOS it is subject to ageing and the deterioration of technical characteristics connected to it.

It demands strict performance of rules of a choice, installation and operation NOS [3,5], and also the control of the named characteristics and forecasting of negative consequences of their change as NOS should not reduce reliability of a protected electric equipment inadequate work and, especially, the damages [5,6].

While in service in electric networks NOS are exposed to numerous electromagnetic and other physical influences. To them concern, first of all, the working voltage constantly influencing isolation and basic elements NOS - varistors, short-term atmospheric both internal an overvoltage and currents accompanying them, and also the long stationary increases of the working voltage arising in various established and unsteady operating modes of electric networks.

Besides on a physical condition of zinc-oxide varistors, as basic elements NOS, significant negative influence render increase of humidity and temperatures.

These influences as it has been told above, worsen working technical characteristics NOS, and these deterioration collect, having, basically, cumulative character. It

results in a result in irreversible changes and, as consequence, to NOS failure. Otherwise it is possible to tell, that the named various influences develop physical opportunities NOS to overcome their consequences that it is possible to determine concept of technological resource  $P$  and its charge  $\Delta P$ . It is necessary, on the one hand, for delimitation of life cycle NOS, and, on the other hand, for forecasting change of performance data NOS up to such condition when its further operation becomes in part or completely not productive or - under abnormal condition dangerous.

Told allows to determine obvious connection of the passport resource  $P_n$  determined by corresponding normative documents NOS prior to the beginning of operation, current resource  $P_m$  and its charge  $\Delta P$  as  $P_m = P_n - \Delta P$  above.

Passport resource  $P_n$  NOS is defined for lives of the device which is guaranteed by the factory - manufacturer on the basis of procedural technical tests and operating experience at observance of rules and the normative requirements stated in the passport documentation.

While in service development of a resource can be supervised on size of a current of the conductivity having the characteristic tendency to increase eventually of operation of the protective device. For example, on the data [6] received in conditions of experiment, it is marked sharp (in 10-100 times) increase in this current in the last of 20 % of time of life NOS. At what, up to this border growth of a current occurs approximately in regular intervals. Experience shows, that, for example, for columns of varistors in diameter of 28 mm, at the current of conductivity exceeding 0.4 mA, operation NOS should be stopped.

Term of a life of varistors  $t_{\text{жс}}$ , now in use in various designs NOS approximately is described by exponential dependence  $t_{\text{жс}} = K_1 \cdot \exp [(K_2 \cdot K_3 \cdot U) / T]$ , where  $K_1, K_2, K_3$  - constant factors which are determined experimentally,  $U$  - relative value of an influencing voltage of industrial frequency in shares from a remaining voltage at a basic current,  $T$  - temperature of varistors OPN in ° K.

Told allows to classify normal above is long enclosed working voltage  $U_{\text{паб}}$  as one of the most essential factors of ageing NOS, and its intensity, alongside with size  $U_{\text{паб}}$ , it is determined by internal structure and temperature of varistors [6].

The specific factor of development of resource NOS are temporary quasi-stationary increases of a voltage. They arise, as on industrial and close to it, and also on the

maximum and lowest harmonious frequencies. The reasons of their occurrence are, for example, short circuits on the ground, breakages of wires both others emergency and operational switching. Here it is possible to relate resonant and ferrosesonant processes. It is possible to name prominent feature of these electromagnetic influences small attenuation or its practical absence.

In networks 0.4-35 kV on the data [4,5] temporary stationary overvoltage on separate electroinstallations at duration up to 1, 20 and 60 s with frequency rates  $K_{nepU}$ , accordingly, 1.47, 1.31 and 1.15 relative units. Arise up to 30 and more times one year.

These of an overvoltage exceed the greatest allowable for concrete NOS. Their values are standardize in the form of the "allowable voltage – time" dependance, having a linear falling kind with average values of frequency rates (from  $U_{pa\bar{a}}$ ) in a range (1.5 - 1.1) in half-logarithmic scale on time from 0.1 up to 100000 s is normalized by manufacturers of [3] devices as dependences ". The development of parameters (U, t) of the given kind of overvoltage for limits of the named dependence regulated by the manufacturer assumes excess of a resource and rather probable destruction NOS. Otherwise there is a partial development of a resource. The question on it cumulativeness demands additional separate research.

Appreciably the charge of technological resource of NOS is defined with internal overvoltage and, first of all, by amplitudes of switching currents through NOS which depend on a place and conditions of their installation and from characteristics of a network, in particular, values of the preincluded resistance of substation. Thus the currents arising at commutation in symmetric and asymmetrical modes have the greatest value, and also at successful and unsuccessful three-phase repeated inclusions.

Comparison of actual and maintained overvoltage levels [3-5], influencing on isolation of an electric equipment of electric networks 0.4-10 kV, allows to draw a conclusion on necessity of restriction of overvoltage size with application of protective devices, devices of relay protection and network automatics.

The analysis shows, that the technological resource and, accordingly, expected service life of NOS is defined by their arrangement in a network, constructive performance of devices, probabilistic characteristics of their reliability, change of resource NOS during the set interval of time, and also probabilistic characteristics of frequency rates overvoltages.

For definition of the charge of resource NOS at influences of internal overvoltages and, finally, its service life it is necessary to estimate amount of these influences and first of all switching currents through the protective device. In conformity with the data [3-5] on the basis of the statistical information received under operating conditions, natural experiments and tests, and also mathematical modelling, the reason of occurrence and the maximal values of frequency rates of internal overvoltages in net-

works 0.4-10 kV can be formulated and appreciated as follows.

- Inclusion and switching-off of air and cable lines (accordingly, 3.5 and 4,0-4,3).
- Switching-off of the non-loaded transformers (5,0-6,0).
- Switching-off double short-circuit (SC) on the ground (3.3).
- Switching-off biphas SC (2.0-3.0).
- Non-simultaneous inclusion of phases at start-up of electric motors (3.0-3.4).
- Inclusion of electric motors at automatic transfer switch or automatic recloser (4.2)
- Switching-off of electric motors (4.0-6.0).
- Switching of loading by vacuum switches (2.6-7.0).
- Arc short circuits on the ground (2.3-3.2).
- Resonant increases of a voltage (2.0).

As follows from results of an estimation of the greatest values internal overvoltage in networks 0.4-10 kV, their maximum levels take place at switching loading

by vacuum switches (up to  $7.0 \cdot U_{\phi}$ ), and also at switching-off of electric motors and the non-loaded transformers (up to  $6.0 \cdot U_{\phi}$ ). The average values of switching pulse voltage at their duration 1000-5000 mks for rated voltage of a network 0.4, 6 and 10 kV have, accordingly, values 3.5, 27 and 43 kV [3-5].

Approximately switching currents through NOS can be determined on expression [5] as  $I_K = (K_{max} - K_{ocm}) \cdot U_{\phi M} \cdot A / Z_{\phi}$ , kA, where  $K_{max}$  - the maximal frequency rates unlimited overvoltage,  $K_{ocm}$  - frequency rates remaining overvoltages,  $U_{\phi M}$  - the maximal working phase voltage, kV,  $A$  - the correction factors dependent on installation site NOS,  $Z_{\phi}$  - wave resistance of one phase of a line, the Ohm.

Now, using the statistical data of operation on amount of possible internal overvoltages, listed above, and also by analogy to [6] functions of distribution of a spent resource, it is possible to estimate approximately  $p_i = f(I_K, \gamma)$  - a population mean of a spent resource for  $i$  the reasons of occurrence internal overvoltages and a corresponding current, and then its total size for a year  $P_{\Sigma 200} = \sum f(I_{ki}, \gamma)$ . In expression for  $p_i$  in conformity about [6] empirical factor  $\gamma$ , approximately taking into account manufacture of a resource from current influences, it is accepted equal  $\gamma \approx 3.6$ , that further will demand additional researches and specification.

Now  $t_{cn.NOS}$  at influences internal overvoltages and, in particular, switching currents, it is possible to determine service life NOS, comparing size of the annual charge of resource  $P_{\Sigma 200}$  with initial, determined on the basis of nameplate data of the manufacturer. According to these data NOS should maintain  $N_u=20$  switching test current pulses of the rectangular form with duration not less than 2000 mks with set amplitude  $I_{2000}$  in A. Togda service life NOS it will be determined as  $t_{cn.NOS} = N_u \cdot I_{2000} / P_{\Sigma 200}$ , years.

For definition of the charge of resource NOS at influences storm overvoltages and its service life it is necessary to estimate amount of these influences and first of all storm currents through the protective device.

Pulse currents were investigated through NOS 6-10 kV, established on substations. Currents have been fixed on a course of settlement plotting dangerous waves (PDW). We shall consider a technique of research of pulse currents, for example, for NOS, established for protection of the power transformer.

Construction PDW is made by consecutive increase in amplitude  $A$  (kV), coming on substation from a transmission line of the idealized oblique-angled storm wave (at the fixed duration of its front  $t_{\phi}$ ). It results in increase pulse overvoltages on isolation of the transformer. Values  $A$  and  $t_{\phi}$  will determine current point PDW when the amplitude named pulse overvoltages will touch the level of allowable pulse influences determined as

$U_{oon} = I \cdot I \cdot (U_{ns} - U_{nom}/2)$ , where  $U_{ns}$  - a full pulse test wave which is accepted in accordance with GOST 1516-76, and  $U_{nom}$  - the rated voltage of the transformer which is taking into account its excitation at arrival of storm waves. Thus the current through NOS is fixed. Thus, together with construction PDW as dependences  $A = A(t_{\phi})$  in all an interesting range  $t_{\phi}$ , are determined pulse currents through NOS.

The analysis has shown, that these currents for NOS 6-10 kV do not surpass size 1.2 kA and are, basically, in an interval 0.3-0.5 kA. Despite of it, the settlement pulse current further is accepted equal 1.2 kA. Similarly, but the simplified estimation for NOS 0.4 kV receives a current 0.6 kA.

NOS, as well as other protective devices included in units of the circuit, in settlement procedures represent the mathematical models constructed on a basis of current-voltage (CVC) and volt-sec (VSC) characteristics.

The voltage on NOS by its principle of action (on other protective devices after operation) can be determined by interpolator method on the following equation:  $U = U(i) + i \cdot Z_{\phi} = f(i)$ , where  $U$  - value of a voltage of the equivalent wave coming on NOS,  $U(i)$  - a voltage on it, calculated on CVC,  $i$  - a current through the device,  $Z_{\phi}$  - wave resistance of release to the device.

The table of values of function  $f(i)$  can be calculated preliminary for characteristic NOS CVC points. After that for definition of a voltage on NOS it is enough to make two operations:

a) Return interpolation is made for the calculated value of voltage  $U$  under the table  $f(i)$ , that is there is a value of a current through NOS;

b) According to the calculated value of a current  $i$  direct interpolation determines a voltage on NOS under the table, corresponding CVC NOS.

CVC NOS is modelled approximately. It is set by coordinates of the several points, for example to five, that corresponds to approximation by its four pieces of straight lines. Thus CVC is recommended to have three average points near to an excess. For each piece of ap-

proximation the equation of straight line  $U_{omn} = E + i \cdot s$ , where  $E$  - ordinate of a point of crossing of continuation of the given piece with an axis of ordinates,  $s$  - inclination of a straight line of the current piece of approximation CVC enters the name. This equation is solved together with equation  $U_{omn} = U - i \cdot Z_{\phi}$  power failures on wave resistance of a bus arrangement part leading to NOS. From the decisions received for pieces of approximation, the least value will be closest to value on valid nonlinear CVC NOS.

After transformations the algorithm of calculation of a voltage on NOS looks like [5]  $U_{omn} = A \cdot U + B = 2 \cdot s \cdot U / (Z_{\phi} + s) + E \cdot Z_{\phi} / (Z_{\phi} + s)$ ,

Where  $A = 2 \cdot s / (Z_{\phi} + s)$ ,  $B = E \cdot Z_{\phi} / (Z_{\phi} + s)$  - factors which are calculated prior to the beginning of calculation of wave process at a stage of processing of the initial information about NOS and allow to determine a voltage on NOS only two arithmetic actions. Further, for a finding of the voltage closest to the valid value on NOS from all  $U_{omn}$ , calculated for each piece of approximation CVC, it is necessary, as it was already spoken above, to choose from them the least [5]. After that on any of the above mentioned equations for  $U_{omn}$  it is possible to find necessary current values of a current through NOS from which further or on a course of calculation of transient the greatest peak value  $I_z$  is determined.

At definition of service life at storm influences on NOS it is necessary to estimate their annual probable number by techniques of definition of lightning guard reliability substations and, in particular, separate electro-installations, for example, transformers [2,3,5].

Using the positions similar to definition of the charge of resource NOS for switching currents, it is possible to estimate approximately  $P_i = f(I_z, \gamma)$  - a population mean of a spent resource for  $i$  the reasons of occurrence of storm influences and a corresponding current, and then its total size for one year  $P \sum_{\text{год}} = \sum f(I_{zi}, \gamma)$ . In expression for  $P_i$  empirical factor  $\gamma$ , approximately taking into account development of a resource from current influences the same as earlier, it is accepted equal  $\gamma \approx 3.6$  that will similarly demand additional researches and specification.

Now  $t_{ca, NOS}$  at influences storm overvoltage and, in particular, storm pulse currents, it is possible to determine service life NOS, comparing the same as and for the switching currents, the corresponding size of the annual charge of a resource with initial, determined on the basis of nameplate data of the manufacturer. According to these data NOS should maintain  $N_u = 20$  storm test current pulses of the normalized form 8/20 mks with amplitude  $I_{8/20}$  set in passport NOS in A. Then NOS service life it will be determined as  $t_{ca, NOS} = N_u \cdot I_{8/20} / P \sum_{\text{год}}$ , years.

The specified definition of full resource NOS should be made in view of all factors influencing its development as the charge of a resource in life cycle occurs in common and cumulatively on all named directions, and also even at temperature influences, humidity and other reasons of deterioration of physical and electric characteristics of devices.



Doubtless objective integrated estimation of the current condition of the device is the control of a current of the conductivity, discussed above to which theoretically and results of all physical influences on NOS are technologically connected.

The calculations executed in conformity with stated positions for terminators 0.4, 6 and 10 kV, show, that resources of modern zinc-oxide NOS with switching currents 100-500 A lie within the limits of 20-50 years.

## Conclusions

Questions of definition of technological resources of nonlinear overvoltage suppressors 0.4, 10 kV are considered. The factors influencing the current charge of these resources, connected to them ageing of overvoltage protection devices and the account of the named positions in designing and operation of electric networks are estimated.

## References

- [1] GOST P 50397-92. Compatibility of electromagnetic means.
- [2] Kostenko M.V., Efimov B.V., Zarhi I.M., Gumerova N.I. analysis of lightning guard reliability of substations. L.: the Science, 1981.
- [3] Lyskov J.N., Demina O.J., Kuzmicheva K.I., etc. Methodical instructions on application of terminators in electric networks 6-35 kV. - M., 2001.
- [4] Abramovich B.N., Polischuk V.V. Electromagnetic compatibility of an electric equipment of electric networks 6-35 kV. Power in oil-and-gas production. M.; 2002. № 1. p. 5-9.
- [5] Albokrinov V.S., Goldshtejn V.G., Halilov F.H. Overvoltage and protection against them in electroinstallations of a petroleum industry. Samara: Publishing house " Samara university ", 1997.
- [6] Kolichev A.V. Research of influence of change of characteristics of protective devices on a parameter of reliability of protection of substations 35-500 kV from overvoltage. Thesis of Cand.Tech.Sci., SPbGTU, 2002.

## Biographies



**Igor Kosorlukov** was born in Samara, Russia, on July 17, 1987. He is a 5<sup>th</sup> year student of Technical University of Samara-Russia of the Faculty of Electrical Engineering. His field of interest includes areas of engineering of high tensions and electromagnetic compatibility. (e-mail:kosorlukov@hotmail.ru, tel. 8-846-334-09-73)



**Vyacheslav Prihodchenko** was born in Aktyubinsk, Kazakhstan, on December 8, 1938. He studied at the Technical University of Samara-Russia, and has defended a thesis and has received a degree of the candidate of engineering science in 1974 in Technical University of Samara. Since 1966 he worked in the Faculty of Electrical Engineering of the Technical University of Samara as a Lecturer and researcher in the field of application of liquid metals in electrical contacts and current-carrying parts of high-current devices. Vyacheslav Prihodchenko is with the Faculty of Electrical Engineering, Technical University of Samara, 224, Pervomaiskaya st., 443010 Samara, Russia



**Oleg Solyakov** was born in Samara, Russia, on May 16, 1969. He studied at the Technical University of Samara-Russia, and has defended a thesis and has received a degree of the candidate of engineering science in 2007 in Technical University of Samara. His field of interest includes overvoltages in circuits and ways of their protection. Oleg Solyakov is with the "MRSK Volgy" – "Samarskye RS" department, 106, k.204, Novosadovaya st., Samara, Russia.



**Valery Polyakov** was born in Amurskaya obl., on January 15, 1939. He studied at the Technical University of S-Peterburg-Russia, and has defended a thesis and has received a degree of the candidate of engineering science in 1989 in Technical University of S-Peterburg. His field of interest includes maintenance and diagnostics of isolation and overvoltages protection devices. Valery Polyakov is with "United Diagnostics Center, St. Petersburg, Russia.



**Lev Shpitz** was born in Samara, Russia, on July 3, 1985. He studied at the Nayanova University of Samara-Russia. His field of interest include software engineering for operational modes of electrical power systems.

# Electromagnetic Field Analysis in Vicinity of Power Lines

Mirjana Perić, Saša S. Ilić and Slavoljub Aleksić

**Abstract:** In this paper an electromagnetic field distribution in vicinity of power lines is considered. An analytical method will be applied. The obtained results will be compared with the finite element method results. A procedure for the electromagnetic field reduction under the power line will be presented. Also, an optimal conductors combination for obtaining satisfied results for electromagnetic field distribution under the power line will be determined.

**Keywords:** electromagnetic field, power lines, analytical method, finite element method.

## Introduction

A complete human population is exposed to magnetic and electric field influences of natural Earth field and fields from artificial sources at work and at free time. There is difference in exposure dose which varieties during the day and season [1]. Exposure during certain work tasks is larger than what people normally experience. Such tasks can be, for example, working at energised substations or near power lines.

Over the years, scientists have attempted to prove the extremely low frequencies (ELF) interaction theories on living beings. Magnetic and electric fields can induce currents and electric fields inside human bodies [2]. However, scientist cannot say with certainty that such exposure is safe for us. Some scientific studies show that those fields may cause the DNA damage, which initiate the cancer. On the other side, other studies have not found such association [3]. The electro-equipment manufactures persistently deny this effects existence, although the statistics show opposite results. Therefore it is understandable why the National and International agencies have difficulties to form standards for the maximal human ELF field exposure [4].

Some scientific studies show that the magnetic field components produced by power lines have more relevant influence to possible health effects than the electric field components [5]. The main reason for that is because the magnetic fields are difficult to shield and they can penetrate surrounding buildings and into human bodies compared to electric fields.

In this paper will be considered two types of high voltage, three-phase power lines, which configurations are shown in Figs. 1 and 2. Those power lines are commonly used in Serbian electric power system [6-8].

An analytical method and the finite element method (FEM) [9] will be applied for electromagnetic fields calculation in vicinity of these power lines. All results will be shown in the power line plane. Especially it will be considered the height of 1.7m above the ground level that

corresponds to an average human height. In order to reduce the electromagnetic field levels in the vicinity of power lines, different combinations of the power line conductors will be considered.



Fig.1. 2x400 kV three-phase power line.



Fig.2. 2x110 kV three-phase power line.

## Analytical approach

The power line emits electric and magnetic fields. In this paper the power lines will be analysed using sinusoidal steady-state field theory in two dimensions. The two-dimension simplification over three dimensions assumes that the lines are straight and go for a sufficient distance toward infinity to make two-dimensional analysis valid [10]. High-voltage lines are generally well balanced and sinusoidal. This usually can lead to close correspondence between calculated and measured fields.

Where more complicated configurations are encountered, such as in distribution systems, three-dimensional

computations can be used, but are limited by undesired unbalance, unknown magnitude, and undesired unknown current return paths.

In Fig. 3, a cross section of power line with  $N$  conductors placed above the ground is shown. The earth is considered as a semi-conducting paramagnetic area with conductivity  $\sigma$ , relative permittivity  $\epsilon_r$  and relative permeability  $\mu_r \approx 1$ .

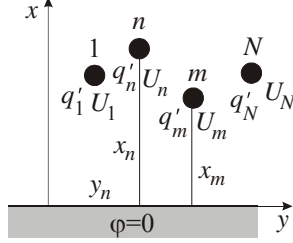


Fig.3. Power line cross-section.

The electromagnetic field components can be determined using the superposition principle and the image theorem in conducting mirror. Namely, the electric field components can be calculated when power line is open-circuit and magnetic field components can be determined when the power line conductors are short-circuited. In [6] the electromagnetic field components are determined as:

$$(1) \quad E_x = \sum_{n=1}^N \frac{q'_n}{2\pi\epsilon_0} \left[ \frac{x-x_n}{R_{1n}^2} - \frac{\underline{\epsilon}-\epsilon_0}{\underline{\epsilon}+\epsilon_0} \frac{x+x_n}{R_{2n}^2} \right],$$

$$(2) \quad E_y = \sum_{n=1}^N \frac{q'_n}{2\pi\epsilon_0} \left[ \frac{y-y_n}{R_{1n}^2} - \frac{\underline{\epsilon}-\epsilon_0}{\underline{\epsilon}+\epsilon_0} \frac{y-y_n}{R_{2n}^2} \right],$$

$$(3) \quad E_z = \frac{j\omega\mu_0}{2\pi} \sum_{n=1}^N I_n \left[ \ln R_{1n} + \frac{\mu-\mu_0}{\mu+\mu_0} \ln R_{2n} \right],$$

$$(4) \quad H_x = -\sum_{n=1}^N \frac{I_n}{2\pi} \left[ \frac{y-y_n}{R_{1n}^2} + \frac{\mu-\mu_0}{\mu+\mu_0} \frac{y-y_n}{R_{2n}^2} \right],$$

$$(5) \quad H_y = \sum_{n=1}^N \frac{I_n}{2\pi} \left[ \frac{x-x_n}{R_{1n}^2} + \frac{\mu-\mu_0}{\mu+\mu_0} \frac{x+x_n}{R_{2n}^2} \right],$$

$$(6) \quad H_z = \frac{j\omega}{2\pi} \sum_{n=1}^N q'_n \left[ \arctan\left(\frac{y-y_n}{x-x_n}\right) - \frac{\underline{\epsilon}-\epsilon_0}{\underline{\epsilon}+\epsilon_0} \arctan\left(\frac{y-y_n}{x-x_n}\right) \right],$$

where  $\underline{\epsilon} = \epsilon - j\sigma/\omega$ ,  $q'_n$  is the charge per unit length of  $n$ th conductor and  $I_n$  is the current intensity of  $n$ th conductor of power line.

With

$$(7) \quad R_{1n} = \sqrt{(x-x_n)^2 + (y-y_n)^2} \text{ and}$$

$$(8) \quad R_{2n} = \sqrt{(x+x_n)^2 + (y-y_n)^2},$$

the distances between the  $n$ th conductor of the power line and its image in the plane mirror from the point  $M(x,y)$  are denoted, Fig. 4.

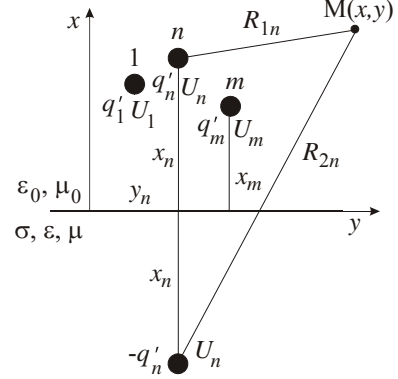


Fig.4. Image theorem.

The voltages between the power line conductors and the ground, so called phase voltages,  $U_n$ ,  $n=1, 2, \dots, N$ , can be expressed as

$$(9) \quad U_n = \sum_{m=1}^N a_{nm} q'_m, \quad n=1, 2, \dots, N,$$

where

$$(10) \quad a_{nm} = \frac{1}{4\pi\epsilon_0} \ln \frac{(x_n+x_m)^2 + (y_n-y_m)^2}{(x_n-x_m)^2 + (y_n-y_m)^2 + a_n^2 \delta_{nm}}$$

are potential coefficients, and  $a_n$  is radius of  $n$ th power line conductor. With  $\delta_{nm}$  Kronecker symbol is denoted.

The electric and magnetic field components can be also determined using following expressions

$$(11) \quad E_x = -\partial\phi/\partial x, \quad E_y = -\partial\phi/\partial y,$$

$$(12) \quad B_x = \partial A/\partial y, \quad B_y = -\partial A/\partial x,$$

where

$$(13) \quad \phi = -\frac{1}{2\pi\epsilon_0} \sum_{n=1}^N q'_n \left( \ln R_{1n} - \frac{\underline{\epsilon}-\epsilon_0}{\underline{\epsilon}+\epsilon_0} \ln R_{2n} \right)$$

is the electric scalar potential, and

$$(14) \quad \mathbf{A} = A\hat{z},$$

$$A = -\frac{\mu_0}{2\pi} \sum_{n=1}^N I_n \left( \ln R_{1n} + \frac{\mu-\mu_0}{\mu+\mu_0} \ln R_{2n} \right)$$

is the magnetic vector potential.

Expressions (13) and (14) can be simplified using that  $\mu \approx \mu_0$ ,  $3 \leq \epsilon_r \leq 11$  and  $10^{-3} \text{ S/m} \leq \sigma \leq 10^{-5} \text{ S/m}$ .

Thus,

$$(15) \quad \phi = -\frac{1}{2\pi\epsilon_0} \sum_{n=1}^N q'_n \ln \frac{R_{1n}}{R_{2n}} \text{ and}$$

$$(16) \quad A = A\hat{z}, \quad A = -\frac{\mu_0}{2\pi} \sum_{n=1}^N I_n \ln R_{1n}.$$

Using expressions (1)-(6) or (11)-(14) it is possible to calculate the electric and magnetic fields in power line surroundings

$$(17) \quad E_e = \sqrt{E_x E_x^* + E_y E_y^* + E_z E_z^*} \quad \text{and}$$

$$(18) \quad H_e = \sqrt{H_x H_x^* + H_y H_y^* + H_z H_z^*}.$$

## Examples

### 2x400 kV power line

In this paper a 400kV three-phase power line with two subconductors per phase and two grounding lines is considered, Fig. 5 [6-8, 11].

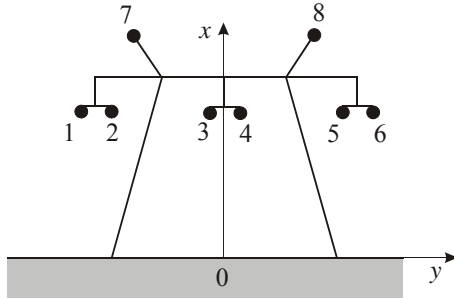


Fig.5. Double circuit 400kV three-phase power line.

In Table 1 the power line parameters are shown [6]. The radius of the power line conductors is 15mm.

Using the expressions (12), (16) or (4-6) and expression (18) it is possible to calculate the magnetic flux density distribution in vicinity of the 400kV power line. That result is shown in Fig. 6. For our research is important to determine the magnetic flux distribution at height 1.70m. That height corresponds to an average human height.

So, the magnetic flux density distribution at height 1.70m above the ground level in the 400kV power line surroundings is presented in Fig. 7. In the same figure, the obtained result is compared with FEM result obtained using software package [9].

Using the expressions (9), (11), (13) and (17), the electric field distribution can be also calculated. From (13) is evident that it must be taken into consideration the pha-

se angle between the voltage and currents in different systems. That will be done using the complex values of the charge per unit length and voltage of  $n$ th conductor in the system of linear equations given by (9).

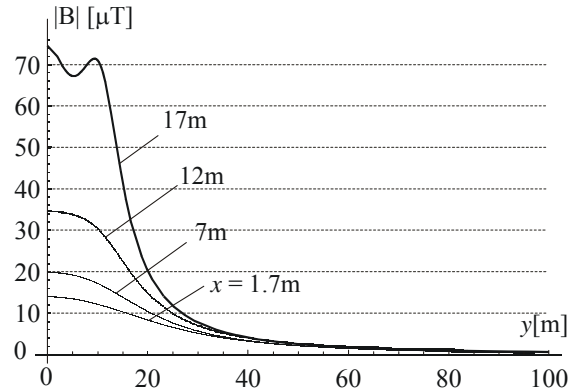


Fig.6. Magnetic flux density distribution in vicinity of 400kV three-phase power line for different heights above the ground level.

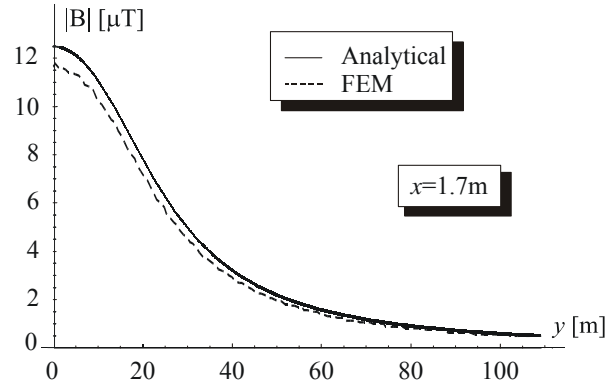


Fig.7. Magnetic flux density distribution in vicinity of 400kV three-phase power line – Results comparison.

In Fig. 8 the electric field distribution in vicinity of power line from Fig. 5 is shown. The distribution is given for different heights above the ground level.

Unfortunately, the electric field distribution can't be compared with FEM result. The reason is in non-possibility to use the complex values of voltages and line charges as input values in femm simulation.

The obtained results for electromagnetic field distribution show that these field components rapidly decrease from the power line.

Table 1

Power line parameters used for electromagnetic field determination for  $U_f = 400 / \sqrt{3}$  [kV],  $I_1 = 800$  [A] and  $s = 2\pi / 3$ .

$n$	Phase I		Phase II		Phase III		Grounding wires	
	1	2	3	4	5	6	7	8
$x_n$ [m]	21.5	21.5	21.5	21.5	21.5	21.5	26	26
$y_n$ [m]	-11.2	-10.8	-0.2	0.2	10.8	11.2	-7	7
$I_n$	$I_1 e^{j0}$	$I_1 e^{j0}$	$I_1 e^{js}$	$I_1 e^{js}$	$I_1 e^{-js}$	$I_1 e^{-js}$	0	0
$U_n$	$U_f e^{j0}$	$U_f e^{j0}$	$U_f e^{js}$	$U_f e^{js}$	$U_f e^{-js}$	$U_f e^{-js}$	0	0



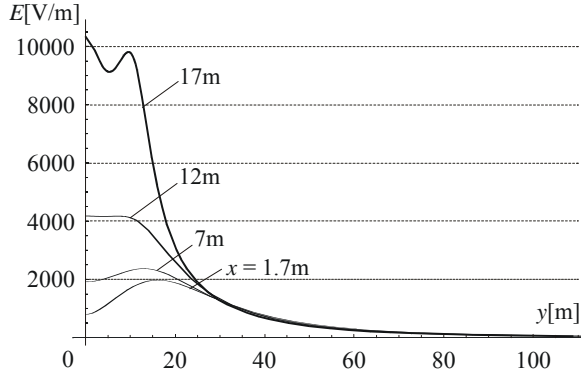


Fig. 8. Electric field distribution in vicinity of 400kV three-phase power line for different heights above the ground level.

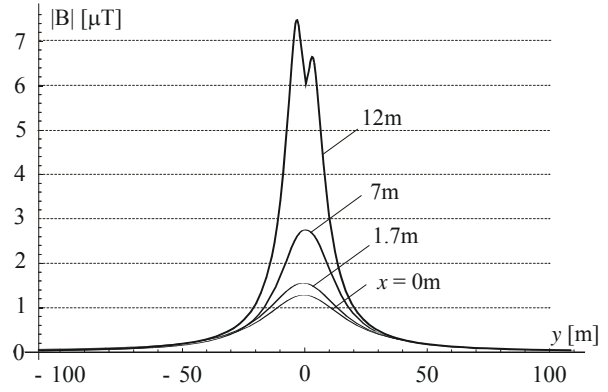


Fig. 10. Magnetic flux density distribution in vicinity of 2x110kV three-phase power line for different heights above the ground level.

### 2x110 kV power line

As an asymmetrical case, a 2x110kV power line is considered, Fig. 9 [7]. The used parameters are shown in Table 2. In Fig. 10 the magnetic flux density distribution for different heights above the ground level is shown.

The result obtained using the analytical method is compared with FEM result [9] in Fig. 11. Those results are shown for height 1.7m above the ground level. From this figure excellent results agreement can be noticed.

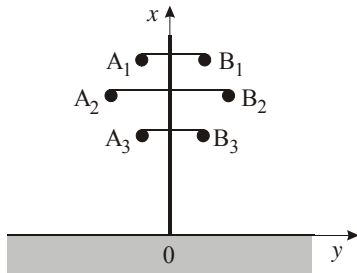


Fig. 9. 2x110kV three-phase power line.

In Fig. 12, the electric field distribution in vicinity of power line presented in Fig. 9 is shown. That distribution is given for different heights above the ground level.

### Electromagnetic field reduction

Thirty-five years ago, the electric field influence was the major subject when possible health effects of power lines were discussed.

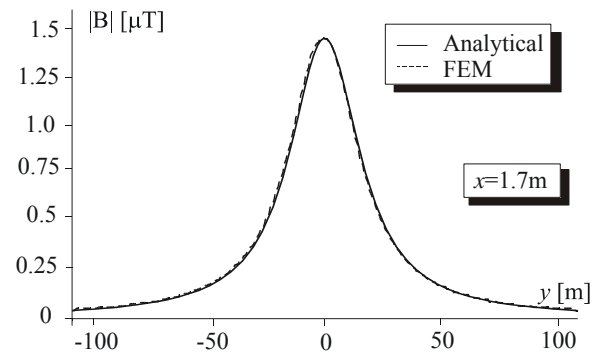


Fig. 11. Magnetic flux density distribution in vicinity of 2x110kV three-phase power line – Results comparison.

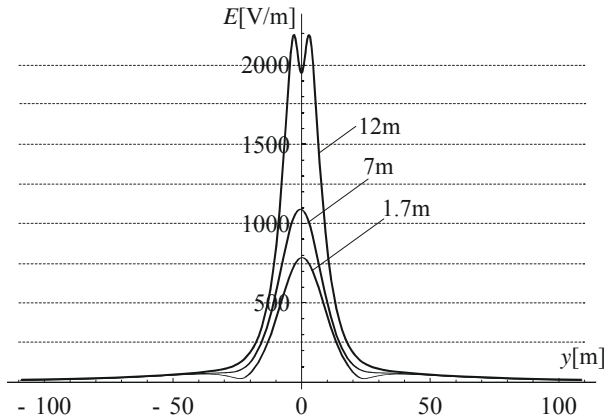


Fig. 12. Electric field distribution in vicinity of 2x110kV three-phase power line for different heights above the ground level.

Table 2

Power line parameters used for electromagnetic field determination for  $U_f = 110/\sqrt{3}$  [kV],  $I_1 = 200$  [A],

$I_2 = 160$  [A] and  $s = 2\pi/3$ .

	Phase I		Phase II		Phase III	
$n$	A1	B1	A2	B2	A3	B3
$x_n$ [m]	23.30	23.30	19.55	19.55	15.8	15.8
$y_n$ [m]	-2.6	2.6	-4.3	4.3	-2.7	2.7
$I_n$	$I_1 e^{j0}$	$I_2 e^{j0}$	$I_1 e^{js}$	$I_2 e^{js}$	$I_1 e^{-js}$	$I_2 e^{-js}$
$U_n$	$U_f e^{j0}$	$U_f e^{j0}$	$U_f e^{js}$	$U_f e^{js}$	$U_f e^{-js}$	$U_f e^{-js}$

This was because calculations of the electric current induced in a human under typical transmission lines showed that the electric field was the dominant contributor. Since 1979, with the publication of a landmark epidemiological study, the concern has been gradually shifting to magnetic fields [12].

In that study, a surrogate for the magnetic field (rather than the magnetic field itself) was found to have a weak but statistically significant effect on childhood leukaemia.

The other epidemiological studies have failed to either establish or reject an association between magnetic fields and health outcomes. So, scientists continue with interest and research in this area. It is interesting to note that no study has found a statistically significant association between the electric field and any health outcome.

A number of countries established limits on the magnitude of the power-frequency electromagnetic fields. In [10, 13-15] the limited field values along the transmission right-of way (ROW) are given. So, it can be found that the maximal value of electric and magnetic field in vicinity of power lines should be less than 5 kV/m and 0.2-10  $\mu\text{T}$ , respectively.

From obtained results in previous analysis it is evident that the magnetic field levels in the power line surroundings are high. There are a variety of techniques used to redesign power lines to result in reduced fields.

These include reducing the spacing of wires to changing the configuration of the wires in space [16]. Some studies show that many power lines designed for reducing magnetic fields have larger electric fields at the conductor surface [12]. Also, magnetic fields can be reduced using different arrangement of power line phase conductors.

The commonly used circuit configurations are: horizontal, vertical and equilateral (Delta) arrangement [5, 17].

In [7] several combinations of 2x110 kV power line conductors placed in Delta arrangement are considered, Fig. 13. The obtained results for some combinations are shown in Fig. 14.

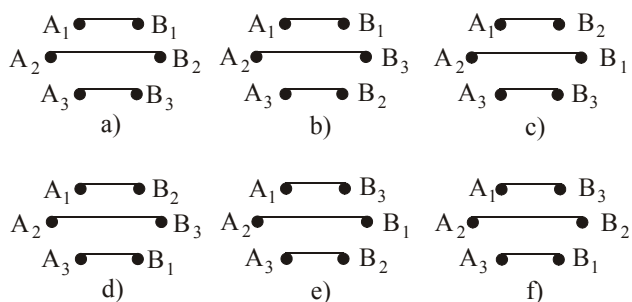


Fig.13. Different combinations of power line conductors.

In order to determine an optimal conductors combination a computer program is developed. The obtained results are shown in Table 3.

From this table is evident that the combination no. 6 (Fig. 13f) gives the minimal value of magnetic flux density under the power line.

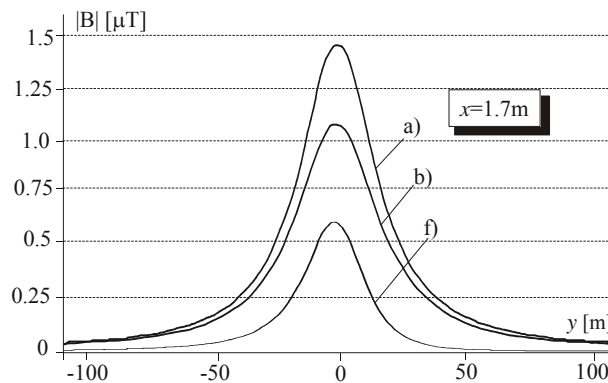


Fig.14. Magnetic flux density distribution for combinations of power line conductors from Fig.13.

**Table 3**  
Magnetic flux density under the 2x110 kV power line for different conductors combinations.

Combinations from Fig. 13		Magnetic flux density ( $\mu\text{T}$ ) in point (1.7m, 0m)
1.	a	1.451520
2.	b	1.090460
3.	c	1.450510
4.	d	0.872618
5.	e	0.872618
6.	f	0.580292

### Conclusion

In recent years, ELF fields of 50/60Hz are a subject of most health effects researches and regulatory activities. Because of that in this paper is analysed the electromagnetic field distribution in the vicinity of two types of commonly used power lines.

An analytical method and the finite element method are applied for these calculations. A very good agreement between analytical and numerical results is obtained. The magnetic level decreases rapidly from the power line to the edge of the right-of way. But, for the people, which work in the vicinity of the power lines, these high levels can have influences on their health. At higher distances from the ground level the electromagnetic fields have bigger values. Different combinations of power line conductors are considered with an aim to reduce the magnetic field intensity under the power line. Satisfying results are obtained.

Further work should include the measurement on the considered high-voltage power lines [18]. Those measured values will be compared with femm simulation results and calculated values. Also, a human body model [19, 20] will be placed in vicinity of power line in order to calculate penetrated values of the power-frequency electromagnetic field.

### References

[1] Langsjo, T. et al. Occupational exposure to 50 Hz electric fields at substation. 16<sup>th</sup> World Congress on Ergonomics – IEA 2006, Maastricht, The Netherlands, 2006.

[2] Habaash, R. W. Y. Electromagnetic fields and radiation – human bioeffects and safety. Marcel Dekker, Inc., New York, 1996.

[3] Repacholi, M., B. Greenebaum. Interaction of static and extremely low frequency electric and magnetic fields with living systems: health effects and research needs. *Bioelectromagnetics* 20:133-160, 1999.

[4] EMF in your environment. United States Environmental Protection Agency, Office of Radiation and Indoor Air (6603J), 1992.

[5] El-Fouly, T. H. M. et al. Power transmission lines generated electric and magnetic field calculations. Proc. of the COSMOL Multiphysics User's Conference, Boston, USA, 2005.

[6] Veličković, D. M. Protection from non-ionising radiation (in Serbian). Engineering and Technical Conference, Belgrade, pp. 1-21, 1997.

[7] Perić, M., S. Ilić, S. Aleksić, D. Stojanović. Magnetic field distribution in power line surroundings. 8<sup>th</sup> International Conference on Applied Electromagnetics – IIEC 2007, Niš, Serbia, CD-proceedings, Session O1-9, Sept. 2007.

[8] Milutinov, M., A. Juhas, M. Prša. Electric field strength and polarization of multi three-phase power line. 8<sup>th</sup> International Conference on Applied Electromagnetics – IIEC 2007, Niš, Serbia, CD-proceedings, Session O1-8, Sept. 2007.

[9] femm 4.0 software, <http://femm.berlios.de>.

[10] Carpenter, D. and S. Ayrapetyan (Editors). Biological Effects of Electric and Magnetic Fields – Sources and Mechanisms. Volume 1, Academic Press.

[11] Ferlič, R., M. Trlep. Analysis of electric and magnetic fields in the vicinity of 400 kV high-voltage power lines (in Slovenian). *Elektrotehniški vestnik* 74(1-2): 1-6, 2007.

[12] Olsen, R. Power-transmission electromagnetics. *IEEE Antennas and Propagation Magazine*, Vol. 36, No. 6, pp. 7-16, Dec. 1994.

[13] Radiation Protection Standard – Exposure limits for electric and magnetic fields – 0 Hz to 3 kHz. Australian Radiation Protection and Nuclear Safety Agency, 2006.

[14] Guidelines for limiting exposure to time-varying electric, magnetic, and electromagnetic fields (Up to 300 GHz), ICNIRP.

[15] IEEE (Institute of Electrical and Electronics Engineers) standard. 2003. National electrical safety code, 2003 ed. New York: Institute of Electrical and Electronics Engineers, Inc.

[16] Olsen, R. Electromagnetic fields from power lines. *IEEE International Symposium on EMC*, pp.138-143, 1993.

[17] King, R., S. Sandler. Electric field and currents induced in organs of the human body when exposed to ELF and VLF electromagnetic fields. *Radio Science*, Vol. 31, No. 5, pp. 1153-1167, Sept.-Oct. 1996.

[18] Abreu Silveira, C. de, R. Soares. Electromagnetic environment measurement under steady-state conditions in utility substations. 2006 IEEE PES Transmission and Distribution Conference and Exposition Latin America, Venezuela.

[19] Gonzales, M. C. et al. Boundary element modeling of the realistic human body exposed to extremely-low frequency (ELF) electric fields: computational and geometrical aspects. *IEEE Trans. on Electromagnetic Compatibility*, Vol. 49, No.1, February 2007.

[20] Yamazaki, K. et al. Investigation of ELF magnetically induced currents inside the human body: development of estimation tools and effect of organ conductivity. *Electrical Engineering in Japan*, Vol. 134, No. 2, 2001.

## Biographies



**Mirjana Perić** was born in Niš, Serbia, in 1976. She received Dipl. Ing. and M. Sc. degree from the Faculty of Electronic Engineering (FEE), University of Niš, Serbia, in 2000 and 2006, respectively.

Since 2001 she has been working as a teaching and researching assistant at the Department of Theoretical Electrical Engineering at the FEE in Niš. She is currently a PhD student at the FEE, also.

Her researching areas are: EM field theory, numerical methods in electromagnetics, bioeffects of EM field and program packages application in electromagnetics.

Mirjana Perić is with the Faculty of Electronic Engineering, University of Niš, Aleksandra Medvedeva 14, 18000 Niš, Serbia (e-mail: [mirjana.peric@elfak.ni.ac.yu](mailto:mirjana.peric@elfak.ni.ac.yu)).



**Saša S. Ilić** was born in Niš, Serbia, on July 24, 1970. In 1990 he enrolled at the Faculty of Electronic Engineering, University of Niš, Serbia. He chose the electronics and telecommunications major and he received Dipl. Ing. degree in 1995 from the FEE of the University of Niš. From January 1998 up to now, he has engaged to the Department of Theoretical Electrical Engineering, at the FEE of the University of Niš.

In 2001 he received M. Sc. degree at the FEE. His researching areas are: lightning protection systems, low-frequency EM fields penetrated into human body and microstrip transmission lines with isotropic, anisotropic and bianisotropic media.

Saša S. Ilić is with the Faculty of Electronic Engineering, University of Niš, Aleksandra Medvedeva 14, 18000 Niš, Serbia (e-mail: [sasa.ilic@elfak.ni.ac.yu](mailto:sasa.ilic@elfak.ni.ac.yu)).



**Slavoljub Aleksić** was born in Berčinac, Serbia, in 1951. He enrolled in the Faculty of Electronic Engineering (FEE), University of Niš in 1970. He received Dipl. Ing., M. Sc. and Ph. D. degree at the FEE in 1975, 1979 and 1997, respectively.

He elected for an assistant, associate and full professor at the same Department in 1980, 1997 and 2008, respectively.

Now, he is a chief of Department of Theoretical Electrical Engineering. He is giving one part of lectures for subject Electrical Engineering from 1996. He is also giving the lectures for subject Electromagnetics.

Slavoljub Aleksić is with the Faculty of Electronic Engineering, University of Niš, Aleksandra Medvedeva 14, 18000 Niš, Serbia (e-mail: [slavoljub.aleksic@elfak.ni.ac.yu](mailto:slavoljub.aleksic@elfak.ni.ac.yu)).

# Variability of Solar and Wind Energy Outputs in Relation with the Weather and Climate Conditions in Bulgaria

Peter Ivanov

**Abstract.** The summary results of different national and international project are done in the paper. The influence of weather and climate conditions on heat and electricity generation by different technologies utilizing solar and wind energy is discussed in the paper. The daily and seasonal course of solar radiation and wind speed are shown in the work. The daily and seasonal course of generated solar and wind energy are discussed based on different examples. The possible climatic scenario in Europe toward the year 2050 and 2089 are shown and how future climate will influence on the renewable energy technologies.

**Keywords:** solar radiation, solar energy, wind speed, wind energy, energy density flow

## 1. Introduction

Electricity and heat generation in Bulgaria is based on fossil fuels, nuclear energy and hydro potential. Classical energy resources in the country are insignificant. Renewable energy sources (RES) represent an alternative for development of an inexhaustible, ecologically clean energy.

Classical energy sources (oil, gas and coal) are deposited in the Earth dept for ancient years and they do not depend on weather and climate conditions like it is valid for renewables, especially solar and wind energy.

The electric system is designed to handle unexpected swings in energy supply and demand, such as significant changes in consumer demand or even the failure of a large power plant or transmission line. There are several areas in Europe, including Spain, Germany, and Denmark, where wind power already supplies over 20 percent of the electricity with no adverse effects on the reliability of the system. Several important renewable energy sources, such as geothermal, bioenergy, and landfill gas systems can operate around the clock. Renewable energy can increase the reliability of the overall system, by diversifying our resource base and using supplies that are not vulnerable to periodic shortages or other supply interruptions.

From the meteorological point of view two are the main problems that solar and wind energy affect on the distributed energy system:

The first one is related with the variability of weather conditions and variable outputs of energy by different technologies. For example wind generations start for operation at 3-5 m/s wind speed, operate in nominal

power at 11-15 m/s and stopped at 25 m/s, to avoid possible damages or crash of the system.

The electricity and heat generation by solar and wind have hourly, daily, seasonal and multi-annual variation based on the variability of a given source.

The second problem is related with the forecast of solar radiation and wind speed. Basically this is valid for wind speed especially hourly or minutes wind speed course and wind energy outputs, as well as so called “energy” calms when the wind turbines do not operate due to the lack of necessary conditions for working process.

It is very important issues when the maximal energy needs coincide with the “energy” calms in daily and seasonal course, when the national electric system operator has to use additional electricity generated capacity to cover electricity needs.

## 2. Thermal conversion of solar radiation

### 2.1. Sun shine duration

The summary results of DEMO SOLAR EAST-WEST EU INCO-Copernicus Project No 4051/1998-2002 during two consecutive years (2001-2002) are presented below. This includes weather conditions and received, converted and consumed solar energy by both solar installations-with selective and non-selective collector's fields mounted in the main NIMH's building in 2000. Fig.1 represents sun shine duration during two consecutive project's years 2001 and 2002 in comparison with the climate norm (1961-90), in Sofia.

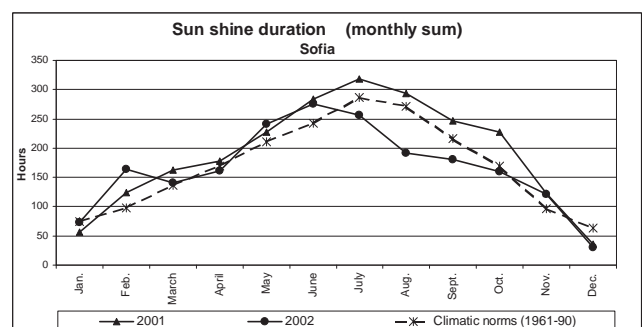


Fig.1. Yearly course of sunshine duration during 2001 and 2002

Apart from February (Fig.1), the year 2002 was less sunny than 2001 especially after June when, monthly hours of sunshine duration were less than 250 hours per month. The annual sums of sunshine duration were as



follows: 2276 hours for 2001, 1993 hours for 2002 and 2035 for the norm (1961-90).

### 2.2. Ambient temperature

Excluding February, June, November and December the monthly average air temperature in 2002 was lower one than during 2001, with differences of 3-4 °C, and it was close to the norm during the remaining months of the year. The annual average values were as follows: 10.8 °C for 2001, 10.8 °C for 2002 and 10 °C for the norm (1961-90).

Summarizing the weather conditions in Sofia during the years 2001 and 2002, it should be noted that the two consecutive years 2001 and 2002 had absolutely different weather conditions - the year 2001 was hot and dry, while the year 2002 – cold and wet. These conditions influenced on the operational performance of the solar installations.

### 2.3. Hourly variation of solar radiation and energy outputs

Fig.2 represents 15 minutes observations of TSR received on collector's field and hot water temperature in different points of the boiler during a sunny spring's day. As it states from the observations the installation starts at 10.30 o'clock in the morning, when the dT is 3°C and stops at 07 o'clock p.m., after sunset. The hot water temperature is increasing in the storage tank during this spring sunny day following the course of solar radiation.

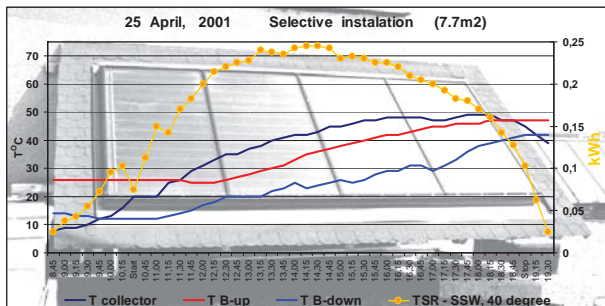


Fig.2. 15 min. observations results of selective solar installation

Solar installation is working without any additional auxiliary heating even during winter season when it can produce hot water up to 40 °C(Fig.3). Hot water temperature in typical summer's day can reach and exceeds 80 °C (Fig.4). Average hot water temperature in typical summer's day is 66 °C .

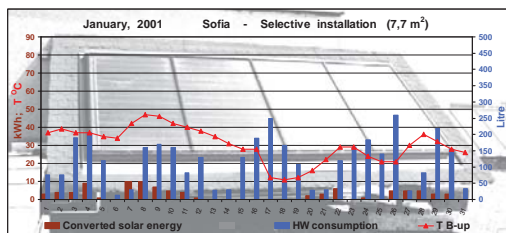


Fig.3 . Hot water output by selective solar installation during typical winter's day

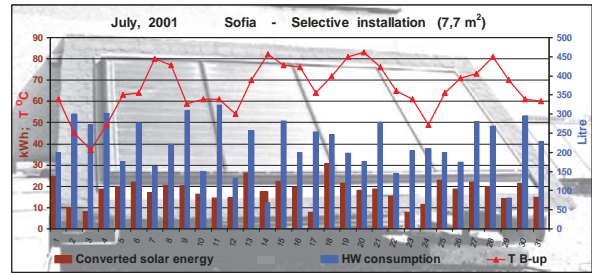


Fig.4 . Hot water output by selective solar installation during typical summer's day

### 2.4. Monthly variation of received solar energy on inclined collector's field

Following the weather conditions, TSR received on the collector's field (Fig.5) during the year 2001 was in average 10.2 % higher in comparison with the year 2002. Absolute values exceeded 1200 kWh during June and July 2001 and respectively 1000-1100 kWh in the same months of 2002.

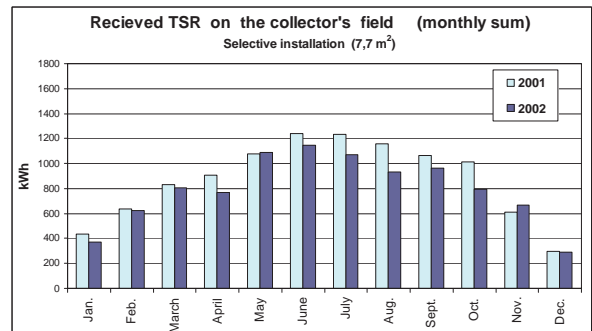


Fig.5. Monthly sum of received total solar radiation on collector's field of selective type of solar installation during 2001 and 2002

The converted per m<sup>2</sup> energy (Fig.6) has higher values in half of the months of 2002 - in January'02, February'02, reaching a maximum value of 82.4 kWh/m<sup>2</sup> per month during July'02. This resulted from higher values of HW consumption. For the remaining months, the 2001 values predominated. In average, the converted per m<sup>2</sup> energy was 3.7 % higher in the cloudy 2002 (605.3 kWh/m<sup>2</sup> per month) in comparison with the sunny 2001 (583.5 kWh/m<sup>2</sup> per month). Such result may be explained by consumption disturbances in 2001.

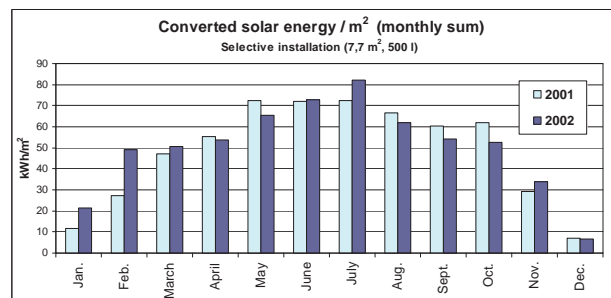


Fig.6. Monthly sum of TSR and converted solar energy per m<sup>2</sup> by selective solar installations during the 2001

The annual value of received (per  $m^2$ ) solar energy on tilted ( $40^\circ$ ) SSW surface during the year 2001 was  $1363.8 \text{ kWh}/m^2$ , with monthly values ranging from  $28 \text{ kWh}/m^2$  in December to  $161.1 \text{ kWh}/m^2$  in June-Fig.7. In average, a share of 42.8 % ( $4491.7 \text{ kWh}$ ) from total solar energy received on selective collector's field ( $10501 \text{ kWh}$ ) was converted and 26.7 % ( $3972.2 \text{ kWh}$ )-respectively by the non-selective collector installation (with total amount of received solar energy  $14865 \text{ kWh}$ ). This means that the selective collector installation transforms solar energy more efficiently than the non-selective collector installation.

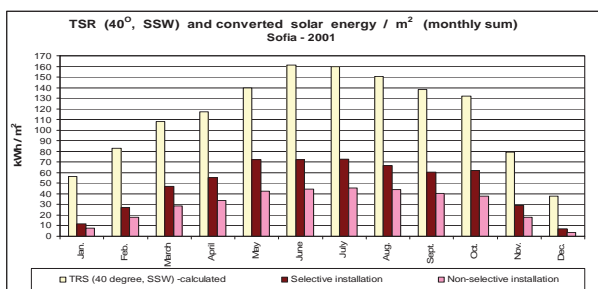


Fig.7. Monthly sum of converted solar radiation per  $m^2$  by selective type of solar installation during 2001 and 2002

More detailed information, concerning hot water temperature in the boilers, is presented in Fig.8, where it is indicated what was the solar contribution in hot water production, provided by the different installations and different seasons.

The average hot water temperature during the period from the mid-November till the first ten-day period of February was below  $40^\circ\text{C}$ .

During the rest of the year, the hot water temperature was higher than  $40^\circ\text{C}$ . From the last ten-day period of April till the last ten-day period of October, the average HW temperature was higher than  $50^\circ\text{C}$ .

From the first ten-day period of June till the first ten-day period of October, the HW temperature was higher than  $60^\circ\text{C}$ . As it is seen in the graph, supplementary hot water heating was needed during the period from mid-November till the first ten days of February.

These results are valid for the available technical equipment, operated at the NIMH and described in the beginning of this report, and correspond to the weather conditions during the year 2001, to the actual hot water consumption and also to other factors. It should be noted that the solar installations were operated without any auxiliary heating, so the produced heat energy resulted from solar energy profit only.

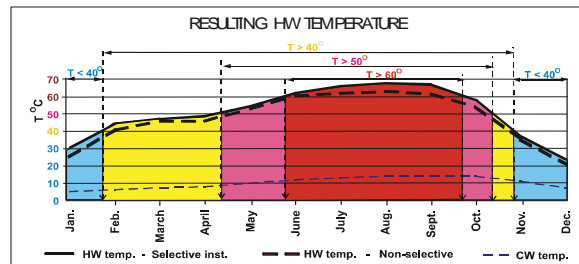


Fig.8. Resulting hot water temperature by both installations expressed as a solar fraction

### 3. Electricity conversion of solar radiation through PV generators

There are done in Fig.9 monthly and daily sums of total solar radiation (TSR) received in the Sevlievo region on optimal surface with orientation azimuth equal to  $-3$  degree and inclination angle of  $33$  degree. As it can be seen annual average TSR has  $3.9 \text{ kWh}/m^2/\text{day}$  value and it is changing from  $2,0 \text{ kWh}/m^2/\text{day}$ , in December, till  $5,7 \text{ kWh}/m^2/\text{day}$ , in July.

Accordingly having annual average values of  $119,7 \text{ kWh}/m^2/\text{month}$  TSR is changing from  $62 \text{ kWh}/m^2/\text{month}$ , in December, till  $176 \text{ kWh}/m^2/\text{month}$ , in July.

The total annual sum of TSR received on optimal inclinational surface is  $1434 \text{ kWh}/m^2/\text{year}$ .

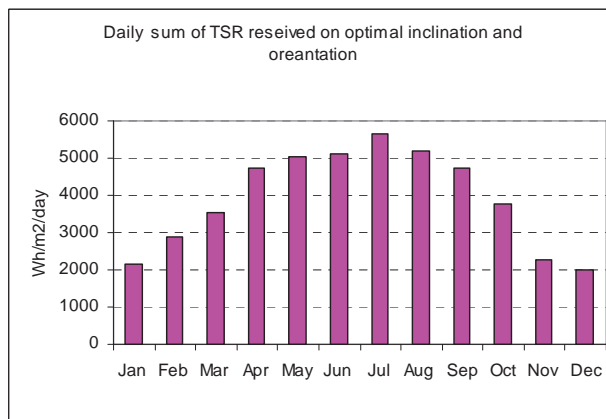


Fig.9. Daily sum of TSR received on optimal inclination surface near Sevlievo

There are presented in Fig.10 and Fig.11 monthly and daily average electricity generation by one  $\text{kWp}$  PV stationary and two axis trace systems (in  $\text{kWh}/\text{month}$  and  $\text{kWh}/\text{day}$ ) installed near Sevlievo.

As it states from the figures 15% of the annual PV electricity may be generated during winter season (January, February and March), 28 % during spring season ( March, April, May), 33 % during summer season (June, July, August) and 38 % during autumn season (September, October, November). So, 62 % of the annual

PV electricity generation can be expected during warm half year period, when it is observed maximum electricity needs for air condition, and the rest 38%, during the cold part of the year. Two axis tracing system gives annually 1% more energy than stationary one.

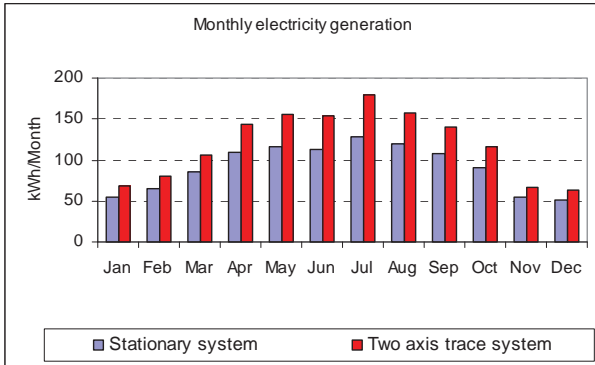


Fig.10. Monthly average electricity generation by one kWp PV stationary and two axis trace systems (in kWh/month) installed near Sevlievo

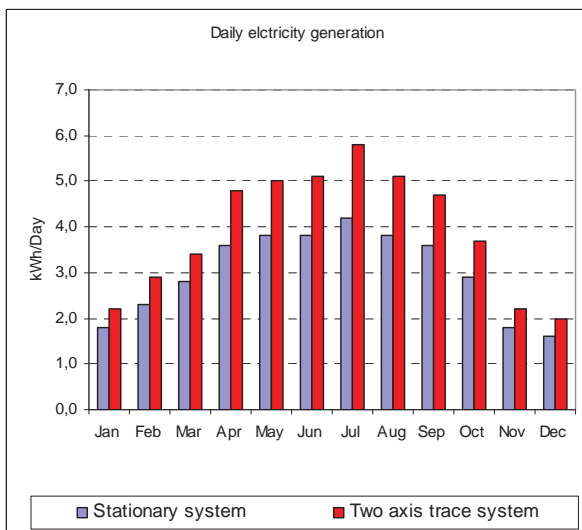


Fig.11. Daily average electricity generation by one kWp PV stationary and two axis trace systems (in kWh/day) installed near Sevlievo

## 4. Wind energy

### 4.1. Daily and seasonal variation of wind speed

One of the main wind characteristics is wind speed, determining its energy valuables. Due to different reasons (sun activity, atmosphere turbulence, heat changes and others) wind speed has accidental character. As a result it is very difficult to make prognoses of the power that a given wind generator can outputs for a short time period. For a long time period (minimum 10 years) the total

electricity generation can be calculated hopefully as well the wind speed and frequency occurrence of different wind speeds is changing from one to another year, but the power forecasting is possible.

There are presented in Fig.12, 13 and 14 wind speed changes for different time series intervals (10 minutes, hour, month, year, 10 years).

Fig.12 represents hourly average 10 min. course of wind speed (m/s) during January'05 near Kavarna for elevation of 50 m.a.g.l.



Fig.12. Hourly average 10 min. course of wind speed (m/s) during January'05 near Kavarna, h=50 m.a.g.l.

Fig.13 represents yearly average wind speed variation during the period from 1981 till 1990 in Murgash peak for elevation of 10 m.a.g.l. The annual average wind speed is oscillating around 8 m/s with a weak trend decreasing toward the year 1990.

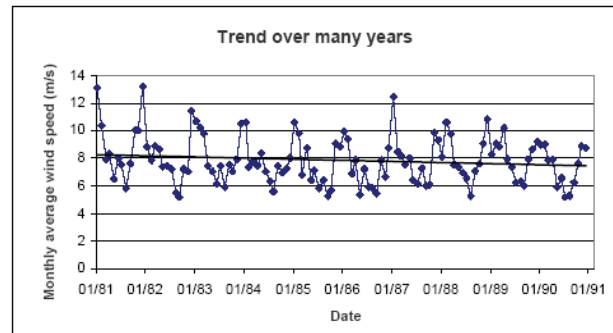


Fig.13. Yearly average wind speed variation during the period from 1981 till 1990 in Murgash peak, h=10 m.a.g.l.

The next Fig.14 gives monthly values of wind speed for every one of the investigated 10 years period. It is seen that the maximal values are observed during the cold half year period and minimal values- during the worm half year period, that is typically for our middle latitude region of the Northern hemisphere.

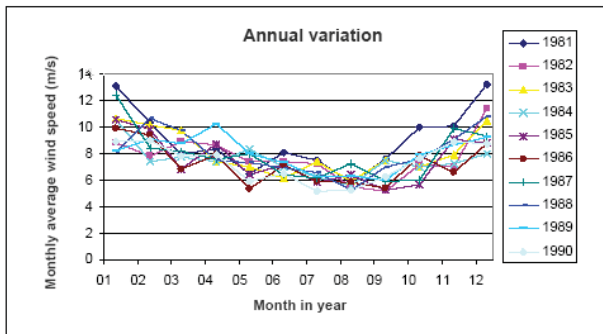


Fig.14. Monthly average wind speed variation during 10 years period (1981-1990) in Murgash peak,  $h=10$  m.a.g.l.

Fig.15 gives monthly average, maximal and minimal 10 min. values of wind speed (m/s) in the region of Kavaranana for elevation of 25 m.a.g.l.

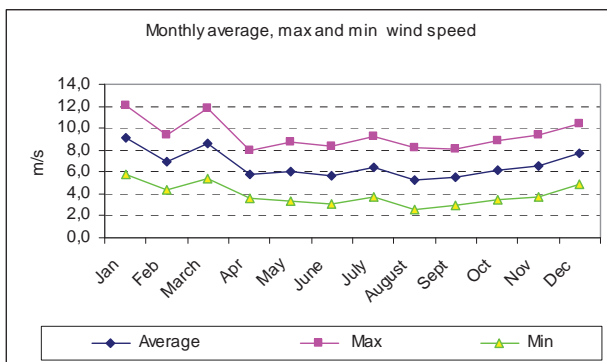


Fig.15. Monthly average, maximal and minimal 10 min. values of wind speed (m/s) in the region of Kavaranana,  $h=25$  m.a.g.l.

Fig.16 gives monthly average, maximal and minimal 10 min. values of wind energy density flow (Wat/m<sup>2</sup>) in the region of Kavaranana for elevation of 25 m.a.g.l. It is visible the largest variation of energy density flow in comparison with the wind speed due to the functional dependence of wind power from wind speed and air density according to the equation:  $q=1/2\rho V^3$ .

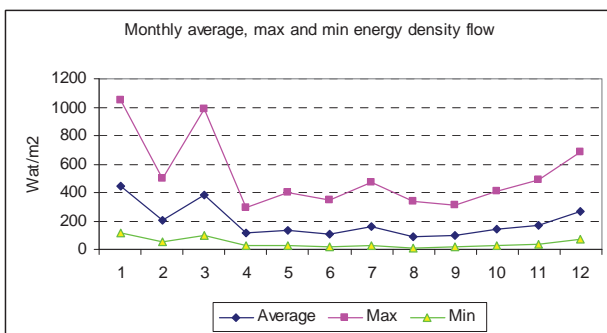


Fig.16. Monthly average, maximal and minimal values of 10 min. wind energy density flow (Wat/m<sup>2</sup>) in Kavaranana region  $h=25$  m.a.g.l.

The daily and yearly course of wind speed and wind energy density flow are very important characteristics for integrating a given wind park into the distributed energy grid. Electricity needs are maximal during middle part of day time and evening and minimal- during morning time. In one year period electricity consumption is maximal during cold half year period and minimal during the warm year period.

As it can be seen from Fig.17, 31.6 % of the annual electricity may be generated during winter season (January, February and March), 20.4 % during spring season (March, April, May), 21.1 % during summer season (June, July, August) and 27.0 % during autumn season (September, October, November) in Kavarna region. So, 51.9 % of the annual electricity generation can be expected during cold half year period, when it is observed maximum electricity consumption in the country, and the rest 48.1 %, during the worm part of the year that is coincided with the electricity consumption in the country.

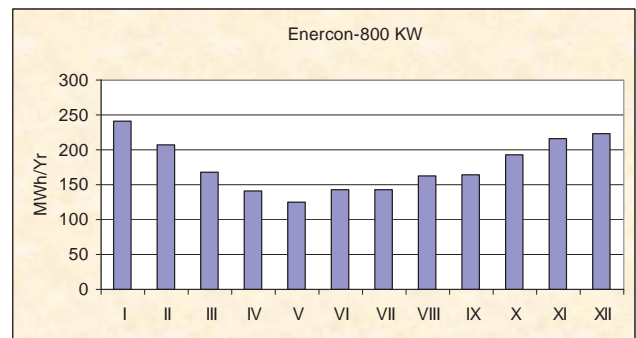


Fig.17. Yearly course of electricity generation by WT "Enercon"- 0.8 MW in the region of v.Rakovski, Kavarna region

## 5. Climate change and renewable energy development

Global climate change influence significantly on the development of different renewable energy technologies including usage of solar and wind.

According to IPCC investigations the air temperature in Europe was increased with 0.8-1.0 °C to the end of the XX century. The sun shine duration is increase during winter time, while during the rest of the seasons it is not observed any changes.

Recent investigations do not show any changes of the global atmosphere circulation hence there are not observed any changes in wind speed and wind directions.

Climate changes are expected in the field of air temperature and they are calculated to be higher with 4-6 °C toward the end of XXI century, according to the investigations made by V.Alexandrov for Bulgaria.



Decreasing of precipitation is expected to be 10-20 % less than the norm (1961-90) toward the end of XXI century according to the same investigation.

Expected increasing of air temperature and decreasing of precipitations will influenced to the development of some renewable technologies, basically utilization of water current for electricity generation. In this case some technologies, like thermal heat and PV solar electricity conversion, will increase significantly coinciding with the heat and electricity consumption during summer and autumn seasons.

## 6. Basic conclusions

Two are the main problems that solar and wind energy affect on the distributed energy system:

- The first one is related with the variability of weather conditions and variable outputs of energy by different technologies.
- The second problem is related with the forecast of solar radiation and wind speed.
- Solar radiation and wind are renewable energy sources that are strongly depended by weather and climate conditions. They have daily, yearly and multi-annual course that determine electricity and heat production.
- The vast amount of solar heat and electricity can be generated by different technologies during summer and autumn seasons and it coincides with the air condition period of the year.
- The majority of wind energy can be generated during the cold half year period when it is observed maximal wind speed that coincide with maximal electricity consumption in the country.

## Acknowledgements

The author would like to thank the Bulgarian National Research Fund for the financial support (contract EE106/07).

## References

- [1] Alexandrov V. Climate Fluctuation and Change and its Influence on the Ecosystems South-East and Central Parts of Europe, as well as SE part of the USA. Doctors thesis. Sankt Petersburg, Russia. p. , (in Russian).
- [2] Ivanov P., L. Trifonova. Practical use of solar radiation for hot water production. Part one. J."Bulgarian Journal of Meteorology and Hydrology", v. 13,No:3-4, pp.76-85, Sofia, 2002,
- [3] Ivanov P., L. Trifonova. Summary results of DEMO SOLAR EAST-WEST project during two consecutive years ( 2001-2002). Part two. J."Bulgarian Journal of Meteorology and Hydrology", v.14, No:1-2, Sofia, 2003 .
- [4] Ivanov P. Practical usage of solar energy in Bulgaria for hot water production, Sofia, J..Energy, vol.4, 2007, pp.28-37, (in Bulgarian).

- [5] Ivanov P. Practical usage of wind in Bulgaria for electricity generation.(monograph), Publ.house: "Investpres". P.145, Sofia, 2007, (in Bulgarian).



**Peter Ivanov** was born in v.Rakita, Pleven region, Bulgaria, on January 20, 1944. He graduated in Odessa State Institute of Meteorology and Hydrology - Odessa, former USSR and received Dr. degree in the same institutive.

His field of interest includes meteorology, climatology, solar and wind energy investigations and technology application. He has realized five international projects in the

field of renewables.

Peter Ivanov is head of Climatology section at the Department of Meteorology of NIMH at BAS, Tzarigradsko shousee 66 blvd., 1784 Sofia, Bulgaria (e-mail: [Peter.ivanov@meteo.bg](mailto:Peter.ivanov@meteo.bg)). He is Chief Executive of the Bulgarian Wind Power Association.

# Distributed Generation and Renewable Energy Sources in Republic of Macedonia

Frantisek Janicek, Dragan Minovski, Anton Cusevski and Emil Krondiak

**Abstract:** Renewable energy sources become very important and attractive in the last few years. Power generation from renewable sources is growing from year to year and will continue to grow during the coming years. Republic of Macedonia is trying to attend this process and make big efforts to increase production of electricity from renewable energy sources. In this article will be present state and perspectives of using of renewable energy sources (small hydro, wind, photovoltaic (PV) and biomass) and distributed generation in Republic of Macedonia, main problem and tools for promoting their development and utilization.

**Keywords:** energy, electric power, Renewable energy sources, wind, hydroenergy, biomass, sunenergy

## Introduction

The Republic of Macedonia is a landlocked, mountainous country, with area of 25713 km<sup>3</sup> and population of 2,1 million. Total consumption of energy in the Republic of Macedonia is around 120,000 TJ annually. In primary energy consumption, oil accounts for 30%, coal for about 52%, natural gas 2-3%, and the remaining around 15% are hydro energy, wood and geothermal energy. Domestic energy production covers about 60% of demand and 40% are provided from imports.

## Electric power system of Macedonia

The total installed capacity for electricity production is 1 581,365 MW. Installed capacity from thermal power plants are 1 005 MW and installed capacity from hydro power plants are 576,365 MW. There 3 thermal power plants: TPP Bitola (3x225MW), TPP Oslomej (1x120MW) and TPP Negotino (1x210MW). Also there are 7 bigger hydro power plants HPP Vrutok – 172 MW, HPP Tikves – 116 MW, HPP Spilje – 84 MW, HPP Kozjak – 80 MW, HPP Globocica – 42 MW, HPP Raven – 21,6 MW, HPP Vrben – 12,8 MW and 23 small hydro power plants with total installed power of 47, 965 MW.

Electric power needs in Macedonia continually grow, and that is why in the last years domestic producing capacities from the thermal and hydro power plants work with maximum of their power, unfortunately, this is not enough for the electric power needs in Macedonia. Around 70% from the total consumption, are from the domestic resources, and the rest 30% are from import.

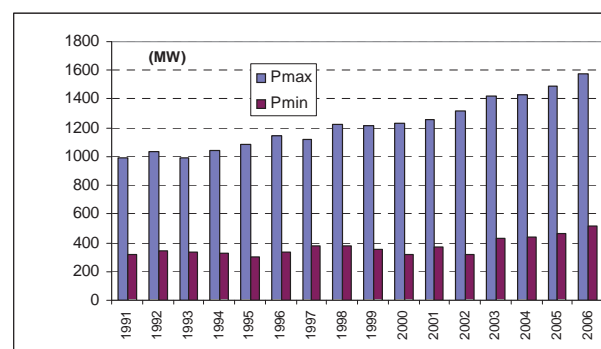
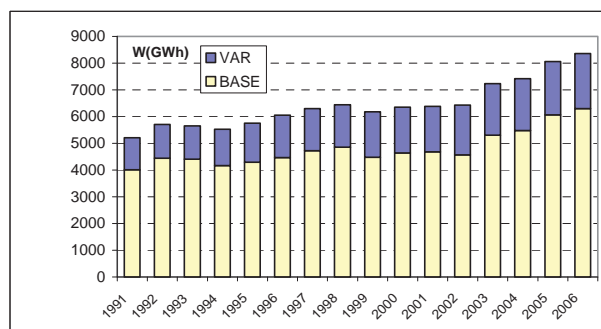


Fig.1. Electric consumption in Macedonia from 1991 to 2006 and maximum and minimum power in the years

Total distribution consumption in 2006 was 4774 GWh. In each town separately is presented in the next table:

**Table 1**  
Review of the distributive consumption of the electric power in Macedonia in each town separately

Distribution	Consumption (GWh)	Distribution	Consumption (GWh)
Skopje	1711	Resen	50
Tetovo	359	Kavadarci	95
Ohrid	202	Negotino	69
Bitola	319	Valandovo	22
Prilep	224	Gevgelija	121
Veles	172	Radovis	44
Kumanovo	275	Kocani	91
Stip	134	Berovo	31
Strumica	182	Delcevo	41
Gostivar	209	Vinica	39
Debar	44	Probistip	25
Kicevo	83	Kratovo	15
Struga	127	Kr. Palanka	34
Mak. Brod	12	Sv. Nikole	46

## Renewable energy sources in Macedonia and its potential

### Hydro energy

The consumption of the renewable energy sources in Macedonia is mainly from the hydroenergetic objects. Depending on the hydrological conditions during the year, from 15 % to 18% from the annual production of the electric power in Macedonia, is acquired from hydroenergy. But the consumption of the hydroenergy potential in the country, is very low and is around 27%. According to exact analyses and studies, the total theoretical hydroenergy potential is 8 863 GWh, the technical potential is 5524,2 GWh, while the consumed potential is around 1500GWh. According to the river basin it is presented in the following table:

Table 2

Hydroenergy potential in Macedonia

River basin	Theoretical potential	Technical potential	Used potential
	GWh	GWh	GWh
Vardar	6660	4559,3	1150
Crn Drim	2203	964,9	339
TOTAL	8863	5524,2	1489

There exist a lot of projects for bigger consumption hydroenergy potential. In the the period to come, hydropower plant Matka 2 with installed power of 36,6 MGW, will be put in operation. At the moment the tender procedure is going on for 3 hydropower plants: Cebren, Galiste and Boskov Most. Also, down the river Vardar, are predicted 12 cascaded hydropower plants with total installed power of.....MW. The potential for building micro and small hydropower plants in Macedonia is very big. According to the studies from 1980 that potential is 1 087,53 GWh, while the total number of power plants is around 400. That potential is given on the following map.

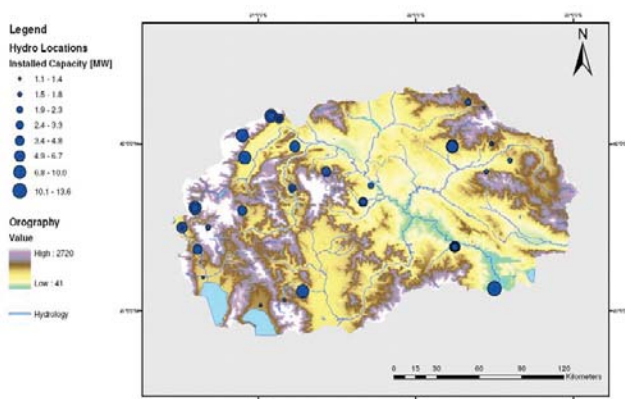


Fig.2. Map of hydro location in Republic of Macedonia

The privileged tariff for selling the electric power produced in small hydropower plants, is given in the following table:

Table 3

Price for electric power produced from SHPP

Level	Monthly produced electric power energy (MWh)	Price (€/MWh)
1	1 – 85 000	120.00
2	85 001 – 170 000	80.00
3	170 001 – 350 000	60.00
4	350 001 – 700 000	50.00
5	More then 700 001	45.00

### Solar energy

The big potential in Macedonia is for using the solar energy. The area of Macedonia is between 41 and 43 latitude, where the intensity of the solar energy, according to the recent measurements, is very advantageous and it is with the approximate 2200 solar hours per year. From the recent calculations from the measurements, come up the following values of the intensity of the solar energy in Macedonia:

Table 4

Intensity of the solar energy in Macedonia

Place	Wh/m2 day
Berovo	4150
Bitola	4250
Ohrid	4350
Prilep	4200
Skopje	4000
Lazaropole	4050

### Geothermal energy

Republic of Macedonia abounds in low -middle – entalping geothermal resources. The temperature of these geothermal resources do not allow their exploitation for production of electric power, but allow production heat for different application. There is a traditional use of this energy for heating orangeries, public objects and drying agricultural products. At the moment the quantity of these geothermal resources (approximately 210GWh- annually) in the total energy consumption is very low (approximately 0,5%).

### Biomass

The potential of the biomass in the Republic of Macedonia, like other renewable energy potentials, is not yet detail analysed. But, according to some of the studies, Macedonia as a country in which the agricultural and stockbreeding are developed, biomass potential is relatively big. According to the energy balance, biomass takes part with 7,6 % with brute energy supply in the Republic of Macedonia. In general, it is the tree for

heating in householders. According to the data, from Studies in Macedonia, the total installed production capacity from biomass can be from 117 to 167 MW. The privileged tariff for selling the electric power produced in power plants in biogas, is given in the following table:

**Table 4**

*Price for electric power produced from biomass*

Group	Installed power	Privileged tariff (Eurocents/kWh)
1	≤ 500 kW	13, 00
2	> 500 kW	11, 00

### **Wind energy**

The Vardar river basin from Kumanovo to Gevgelija is considered to be the most favourable area for wind energy applications. Other areas of possible importance are the Pelagonia region, Kriva Palanka, Ohrid and other mountain areas.

The privileged tariff for selling the electric power from wind power plants is 8,9 EUR cents/ kWh. In the following picture it is given a map of winds in the Republic of Macedonia, made with satellite shots.

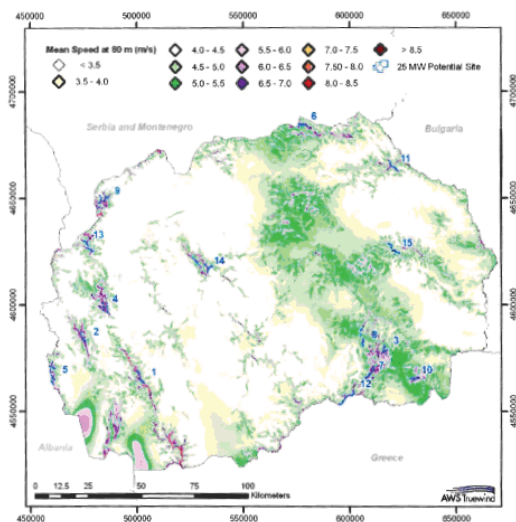


**Fig.3** Map of winds in the Republic of Macedonia, made with satellite shots

### **Legislation regulatory related for renewable energy sources in Macedonia**

The procedure for building objects for electric power production from renewable energy sources is regulated regarding to:

- Energy Law
- Space and urban planning law
- Building law
- Law for building area
- Law for environment
- Ordination for specifying projects and criteria according to which the need for applying the

procedure for estimating the impacts on the environment would be affirmed

- Book of regulations for the circumstances, manner and the procedure for issuing, changing and taking away license for doing energy activities
- Grid code for transmission
- Grid code for distribution of electric power

For building and working on objects for electric power producing from renewable energy sources, the subjects interested in this, would have to provide the following documents:

- Authority for building new production objects for production of electric power (according to the energy law)
- Solving the property legal relations ( according to the law for building area)
- Conditions for planning the space for making an urban project
- Permission for building ( according to building law)
  - Solution for the circumstances for location (according to Space and urban planning law)
  - Estimation of the impact on the environment (according to law for environment and Ordination for specifying projects and criteria according to which the need for applying the procedure for estimating the impacts on the environment would be affirmed)
  - Permission for building (according to building law)
- License for doing energy activities production of electric power (according to Energy Law and Book of regulations for the circumstances, manner and the procedure for issuing, changing and taking away license for doing energy activities )
- Permission for usage (according to the building law)
- Connecting to the electric power system (according to Grid Codes for transmission and distribution of electric power)
- Getting with attributes of privileged producer and guaranty for origin of the electric power form the renewable energy sources.

### **Impact of renewable energy sources on electric power system**

The impact of the renewable energy sources of the stability of the energetic system will be significant. Renewable energy sources have either technical or economic impact on the electric power system working. Because of its unpredictability, wind power plants have the biggest impact on the stable working of the power system. Other sources like the biomass, geothermal energy and water and Sun, do not have this problem in a wide range, but have relatively good predictability. Some quantities of biomass and biogas may be accumulated and



the quantities of produced electric power may be known in advance with precise exactness. If the hydropower plants are with accumulations deepening on the size of the accumulation, may be accumulated some of quantities of the electric power and the production to be assumed to a precise exactness. If they are run of rivers, production may be predicted with smaller exactness. The intensity of the solar rays is changing within a year, depending on the season in a period of 24h (if the movable panels are not installed) and in a one day period depends on the moving of the clouds. Because of this predictability is very small. Because of the wind unpredictability, at the moment of installing, big power plants, there appear a line of requests. As one of the most important requests is keeping bigger reserve of energy from ancillary services during the working of the power plants. This reserved energy as well as the energy from the renewable energy sources, is much higher than the basic energy price, and that will have a huge impact on the last price of electric power for the last users. This must be taken in consideration in developing the renewable energy projects in Macedonia in the next period.

### Conclusion

As can be seen from above and the statistics, we can say that the potential for using the renewable energy sources in Macedonia are very big. The Republic of Macedonia is not yet member state of European Union but is doing a great progress towards the use of renewable energy. The price for electric power energy produced from them are in the range like in other European countries. But the investments in this sector are very small. The biggest problem for development the renewable energy projects is very difficult legislation process. Republic of Macedonia must do some advancement for liberalization the building of renewable energy projects.

### Acknowledgements

This work was supported in part by the Ministry of Education of Slovak Republic Grant AV-120-Jan-Sk1.

### References

- [1] Energy policy in Republic of Macedonia, Ministry of economy of the Republic of Macedonia [www.economy.gov.mk](http://www.economy.gov.mk).
- [2] Annual report for 2006 of Energy Regulatory Commission of R. Macedonia [www.erc.gov.mk](http://www.erc.gov.mk)
- [3] Energy Statistics of R. Macedonia 1991-2006
- [4] Bernard, M., Ptáček, J., Modlitba, P.: Dopad rozvoje vetrných elektráren na provoz ES ČR. Zborník z konferencie Elektroenergetika 2004, Brno, 2004
- [5] Janiček, F., et al. Obnoviteľné zdroje energie 1: Technológie pre udržateľnú budúcnosť FEI STU, Bratislava : Renesans, 2007, 176s, ISBN 978-80-969777-0-3 (Janiček: OZE1)
- [6] Ministry of economy – Republic of Macedonia "Study for possible SHPP in Republic of Macedonia"

### Biographies

**Frantisek Janicek** is from Slovakia .He studied at the Faculty of Electrical engineering and information technology - Slovak University of Technology in Bratislava

His field of interest includes electrical networks, electrical machines and renewable energy sources.

Frantisek Janicek is with the Faculty of Electrical engineering and information technology - Slovak University of Technology in Bratislava, Ilkovicova 3, 812 19 Bratislava 1, Slovak Republic (e-mail: [franisek.janicek@stuba.sk](mailto:franisek.janicek@stuba.sk))



**Dragan Minovski** was born in Skopje, Republic of Macedonia, on February 4, 1980. He studied at the Ss. Cyril and Methodius University in Skopje and received Ing. degree from the same university in 2004.

Since 2005 he worked in the Ministry of economy in Macedonia in department of energy. At the moment he is at the Slovak University of Technology in Bratislava – Faculty of Electrical engineering and

information technology.

Minovski Dragan is with the Faculty of Electrical engineering and information technology - Slovak University of Technology in Bratislava, Ilkovicova 3, 812 19 Bratislava 1, Slovak Republic (e-mail: [dragan.minovski@stuba.sk](mailto:dragan.minovski@stuba.sk))

**Anton Causevski** was born in Skopje, Republic of Macedonia, on 31 March 1967.He studied at the Ss. Cyril and Methodius University in Skopje and received PhD. degree from the same university.

His field of interest includes nuclear energy, electrical machines, electrical networks and renewable energy sources.

Anton Causevski is with the Faculty of Electrical engineering and information technology, Ss. Cyril and Methodius University in Skopje, Karpos 2 bb, P. fax 574 Skopje, Republic of Macedonia,(e-mail - [caus@feit.ukim.edu.mk](mailto:caus@feit.ukim.edu.mk))

**Emil Krondiak** is from Slovakia .He studied at the Faculty of Electrical engineering and information technology - Slovak University of Technology in Bratislava

Emil Krondiak is with the Faculty of Electrical engineering and information technology - Slovak University of Technology in Bratislava, Ilkovicova 3, 812 19 Bratislava 1, Slovak Republic (e-mail: [emil.krondiak@seps.sk](mailto:emil.krondiak@seps.sk))

# Diagnosis on Wind Energy

Ouadie Bennouna, Nicolas Héraud, Mohamed Ainan Kahyeh and Ahmed Youssouf

**Abstract:** Using a polynomial approximation, this paper presents a procedure to deduce unmeasured variables for linear dynamic systems. The technique can be extended also to identify and estimate gross errors. Finally, this method is applied to the Doubly Fed Induction Generator (D.F.I.G) of a wind turbine.

**Keywords:** Data validation, dynamic case, gross error detection, polynomial approximation, unmeasured variables.

## Introduction

Imprecision on instruments used to obtain experimental data, can lead to poor decisions that will affect many parts of the process. The procedure of data reconciliation can reduce the impact caused by measurements errors on the performance of the process using redundant measured variables. The problem of data reconciliation in dynamic processes received attention only recently, although it was first tackled using an extended Kalman filter by Stanley and Mah [1]; Darouach and Zasadzinski [2] proposed a recursive technique to solve the constrained least squares optimization problem. Kao, Tamhane and Mah [3] studied the effect of serially correlated data on gross error detection; Rollins and Devanathan [4] improved on the estimation accuracy using a maximum likelihood function. Other methods have been presented for dynamic data reconciliation: Ramamurthi, Sistu and Bequette [5] proposed a technique based on a successively linearized horizon; Karjala and Himmelblau [6] rely on neural networks and Albuquerque and Biegler [7] on a discretization of the system using Runge Kutta methods. Bagajewicz and Jiang [8] proposed an integral method for dynamic data reconciliation based on a polynomial representation.

The method presented in a previous papers [9,10], is extended to allow data validation in the unmeasured variables case. The application is chosen in an interesting domain: the development of renewable energy.

## Polynomial approximation

Consider the following classic model of dynamic linear systems:

$$(1) \quad \frac{dx'}{dt} = A'x' + B'u'$$

Because of some variables are unmeasured, they have to be eliminated from the previous equation. Using simple linear combination, the system can be rewritten in the following way:

$$(2) \quad C \frac{dx}{dt} = Ax + Bu$$

where  $x, u$  are all measured.

Consider now the following  $s$ -order polynomial representation of  $x$  and  $u$  :

$$(3) \quad x = \sum_{k=0}^s \alpha_k t^k$$

$$(4) \quad u = \sum_{k=0}^s \beta_k t^k$$

thus (2) is equivalent to writing

$$(5) \quad C \left( \sum_{k=0}^{s-1} (k+1) \alpha_{k+1} t^k \right) = A \left( \sum_{k=0}^s \alpha_k t^k \right) + B \left( \sum_{k=0}^s \beta_k t^k \right)$$

since this equation is valid for all  $t$ , then

$$(6) \quad Ck\alpha_k = A\alpha_{(k-1)} + B\beta_{(k-1)} \text{ for } k=1, \dots, s$$

$$A\alpha_s + B\beta_s = 0$$

now consider the case on  $n+1$  measurements and assume that measurement's errors are normally distributed around a mean value. The maximum of the likelihood is obtained by solving:

$$(7) \quad \text{Min} \sum_{i=0}^n \{ (u_i - u_i^+)^T S_U^{-1} (u_i - u_i^+) + (x_i - x_i^+)^T S_X^{-1} (x_i - x_i^+) \}$$

where

$S_X$ : variance matrix of  $x$ .

$S_U$ : variance matrix of  $u$ .

Or, in terms of the polynomial coefficients,

$$(8) \quad \text{Min} \{ (T_\beta \beta - u^+)^T R_U^{-1} (T_\beta \beta - u^+) + (T_\alpha \alpha - x^+)^T R_X^{-1} (T_\alpha \alpha - x^+) \}$$

under the constraint  $R_m \alpha = D_m \beta$

where

$$\alpha = \begin{bmatrix} \alpha_0 \\ \cdot \\ \cdot \\ \cdot \\ \alpha_s \end{bmatrix}, \beta = \begin{bmatrix} \beta_0 \\ \cdot \\ \cdot \\ \cdot \\ \beta_s \end{bmatrix}$$

Measurements are:

$$u^+ = \begin{bmatrix} u_0^+ \\ \vdots \\ u_n^+ \end{bmatrix}, x^+ = \begin{bmatrix} x_0^+ \\ \vdots \\ x_n^+ \end{bmatrix}$$

All matrices are given by:

$$D_m = \begin{bmatrix} B & 0 & \dots & \dots & 0 \\ 0 & B & 0 & \dots & 0 \\ \vdots & \vdots & \vdots & \vdots & \vdots \\ \vdots & \vdots & \vdots & \vdots & \vdots \\ 0 & 0 & \dots & \dots & B \end{bmatrix}$$

$$R_m = \begin{bmatrix} -A & C & 0 & \dots & \dots & 0 \\ 0 & -A & 2C & 0 & \dots & 0 \\ \vdots & \vdots & \vdots & \vdots & \vdots & \vdots \\ \vdots & \vdots & \vdots & \vdots & \vdots & \vdots \\ \vdots & \vdots & \vdots & -A & sC & \vdots \\ 0 & 0 & \dots & \dots & \dots & -A \end{bmatrix}$$

$$R_U^{-1} = \begin{bmatrix} S_U^{-1} & 0 & \dots & \dots & 0 \\ 0 & S_U^{-1} & \dots & \dots & 0 \\ \vdots & \vdots & \vdots & \vdots & \vdots \\ \vdots & \vdots & \vdots & \vdots & \vdots \\ 0 & 0 & \dots & \dots & S_U^{-1} \end{bmatrix}$$

$$R_X^{-1} = \begin{bmatrix} S_X^{-1} & 0 & \dots & \dots & 0 \\ 0 & S_X^{-1} & \dots & \dots & 0 \\ \vdots & \vdots & \vdots & \vdots & \vdots \\ \vdots & \vdots & \vdots & \vdots & \vdots \\ 0 & 0 & \dots & \dots & S_X^{-1} \end{bmatrix}$$

$$T_\alpha = \begin{bmatrix} I & 0 & \dots & \dots & 0 \\ I & t_1 I & \dots & \dots & t_1^s I \\ \vdots & \vdots & \vdots & \vdots & \vdots \\ \vdots & \vdots & \vdots & \vdots & \vdots \\ I & t_n I & \dots & \dots & t_n^s I \end{bmatrix}$$

$$T_\beta = \begin{bmatrix} I & 0 & \dots & \dots & 0 \\ I & t_1 I & \dots & \dots & t_1^s I \\ \vdots & \vdots & \vdots & \vdots & \vdots \\ \vdots & \vdots & \vdots & \vdots & \vdots \\ I & t_n I & \dots & \dots & t_n^s I \end{bmatrix}$$

$T_\alpha$  and  $T_\beta$  don't have necessarily the same order.

Assume that the measurements are taken at equal intervals  $h$ . Then:

$$T_{\alpha,\beta} = \begin{bmatrix} I & 0 & \dots & \dots & 0 \\ I & hI & \dots & \dots & h^s I \\ \vdots & \vdots & \vdots & \vdots & \vdots \\ \vdots & \vdots & \vdots & \vdots & \vdots \\ I & nhI & \dots & \dots & n^s h^s I \end{bmatrix}$$

The problem can be rewritten as follows:

$$(9) \quad \text{Min}(z^T Q^{-1} z + w^T z)$$

under the constraint  $Mz = 0$

where,

$$z = \begin{pmatrix} \beta \\ \alpha \end{pmatrix}, w = -2 \begin{pmatrix} (R_U^{-1} T_\beta)^T u^+ \\ (R_X^{-1} T_\alpha)^T x^+ \end{pmatrix}$$

$$Q^{-1} = \begin{pmatrix} (T_\beta^T R_U^{-1} T_\beta) & 0 \\ 0 & (T_\alpha^T R_X^{-1} T_\alpha) \end{pmatrix}, M = \begin{pmatrix} -D_m & R_m \end{pmatrix}$$

The solution to this problem is:

$$(10) \quad z = [I - QM^T (MQM^T)^{-1} M] (-\frac{1}{2} Qw)$$

From the vector  $z$ , both vectors  $x$  and  $u$  can be reconstituted.

Finally, the estimation of the unmeasured variables can be done using equation (1).

## Application

The procedure seen previously is applied to the Doubly Fed Induction Generator (D.F.I.G) of a wind turbine. It concerns the validation of measurements taken from sensors. Other publications have been appeared to detect parameter faults of the electrical machines [11,12]. The model of this generator is:

$$(11) \quad \frac{d}{dt} \begin{pmatrix} i_{as} \\ i_{\beta s} \\ i_{ar} \\ i_{\beta r} \end{pmatrix} = \frac{1}{(L_s L_r - L_h^2)} \begin{pmatrix} -R_s L_r & \omega_m L_h^2 & L_h R_r & \omega_m L_r L_h \\ -\omega_m L_h^2 & -R_s L_r & -\omega_m L_r L_h & L_h R_r \\ L_h R_s & -\omega_m L_s L_h & -R_s L_r & -\omega_m L_s L_r \\ \omega_m L_s L_h & L_h R_s & \omega_m L_s L_r & -R_s L_r \end{pmatrix} \begin{pmatrix} i_{as} \\ i_{\beta s} \\ i_{ar} \\ i_{\beta r} \end{pmatrix} + \frac{1}{(L_s L_r - L_h^2)} \begin{pmatrix} L_r & 0 & -L_h & 0 \\ 0 & L_r & 0 & -L_h \\ -L_h & 0 & L_s & 0 \\ 0 & -L_h & 0 & L_s \end{pmatrix} \begin{pmatrix} u_{as} \\ u_{\beta s} \\ u_{ar} \\ u_{\beta r} \end{pmatrix}$$

where:

$i_{\alpha s, \beta s}$  are alpha and beta axis stator currents.

$i_{\alpha r, \beta r}$  are alpha and beta axis rotor currents.

$u_{\alpha s, \beta s}$  are alpha and beta axis stator voltages.

$u_{\alpha r, \beta r}$  are alpha and beta axis rotor voltages.

$\omega_m$  is the generator rotor speed.

$L_s$  is the stator inductance.

$L_r$  is the rotor inductance.

$L_h$  is the mutual inductance.

$R_s$  is the stator resistance

$R_r$  is the rotor inductance.

The model of the Doubly Fed Induction Generator (D.F.I.G) can be rewritten as equation (1), where:

$$x' = \begin{pmatrix} i_{\alpha s} \\ i_{\beta s} \\ i_{\alpha r} \\ i_{\beta r} \end{pmatrix}, u' = \begin{pmatrix} u_{\alpha s} \\ u_{\beta s} \\ u_{\alpha r} \\ u_{\beta r} \end{pmatrix}$$

$$A' = \frac{1}{(L_s L_r - L_h^2)} \begin{pmatrix} -R_s L_r & \omega_m L_h^2 & L_h R_r & \omega_m L_r L_h \\ -\omega_m L_h^2 & -R_s L_r & -\omega_m L_r L_h & L_h R_r \\ L_h R_s & -\omega_m L_s L_h & -R_s L_r & -\omega_m L_s L_r \\ \omega_m L_s L_h & L_h R_s & \omega_m L_s L_r & -R_s L_r \end{pmatrix}$$

$$B' = \frac{1}{(L_s L_r - L_h^2)} \begin{pmatrix} L_r & 0 & -L_h & 0 \\ 0 & L_r & 0 & -L_h \\ -L_h & 0 & L_s & 0 \\ 0 & -L_h & 0 & L_s \end{pmatrix}$$

If  $i_{\alpha s}$  is unmeasured, using linear combination, the problem can be rewritten as equation (2) where:

$$x = \begin{pmatrix} i_{\beta s} \\ i_{\alpha r} \\ i_{\beta r} \end{pmatrix}, u = \begin{pmatrix} u_{\alpha s} \\ u_{\beta s} \\ u_{\alpha r} \\ u_{\beta r} \end{pmatrix}$$

$$C = \begin{pmatrix} R_s & \omega_m L_h & 0 \\ 0 & \omega_m L_s & -R_s \end{pmatrix}$$

$$A = \begin{pmatrix} -(R_s^2 L_r + \omega_m^2 L_s L_h^2) & -\omega_m L_h (L_r R_s + R_r L_s) & L_h (R_r R_s - \omega_m^2 L_s L_r) \\ -L_h (\omega_m^2 L_s^2 + R_s^2) & -\omega_m L_h (L_s R_r + R_r L_s) & L_s (-\omega_m^2 L_r L_s + R_s R_r) \end{pmatrix}$$

$$B = \begin{pmatrix} -\omega_m L_h^2 & R_s L_r & \omega_m L_h L_s & -R_s L_h \\ -\omega_m L_h L_s & R_s L_h & \omega_m L_s^2 & -R_s L_s \end{pmatrix}$$

Using a numeric simulator (Matlab/Simulink), figures 1 to 7 show the results of a test at 1300tr / min .

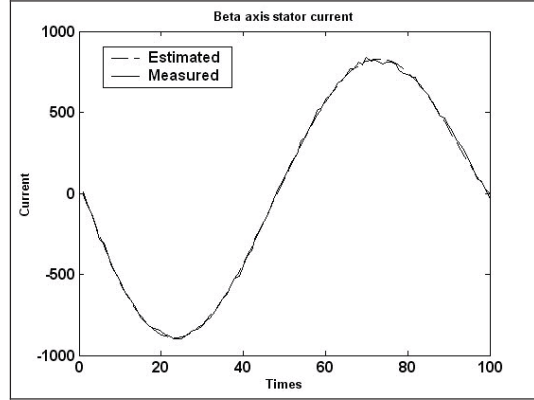


Fig. 1. Beta axis stator current

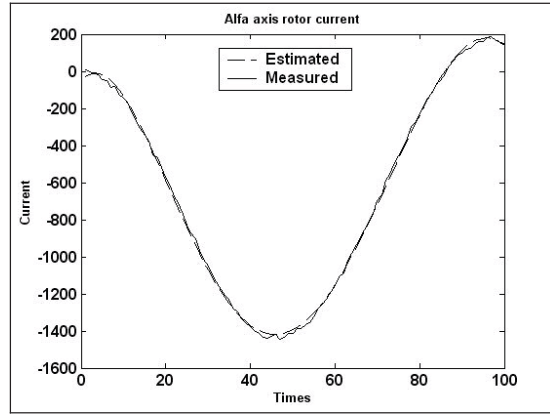


Fig. 2. Alfa axis rotor current

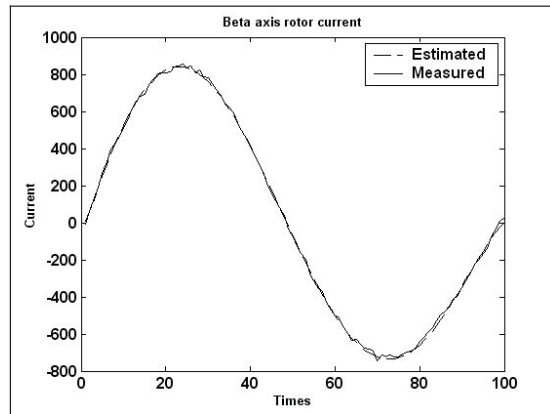


Fig. 3. Beta axis rotor current



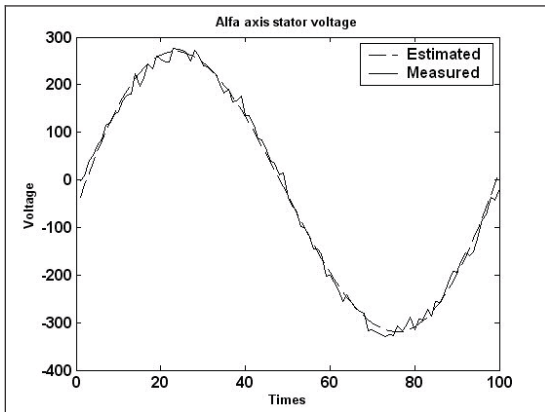


Fig. 4. Alfa axis stator voltage

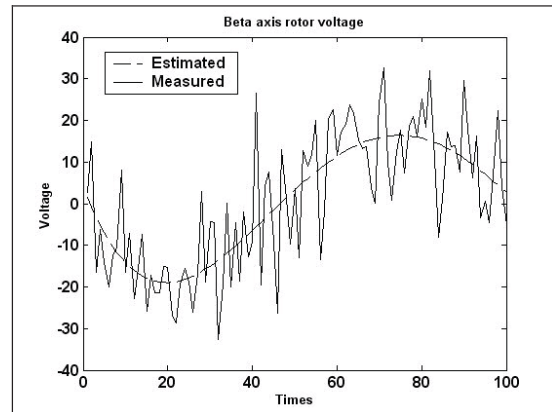


Fig. 7. Beta axis rotor voltage

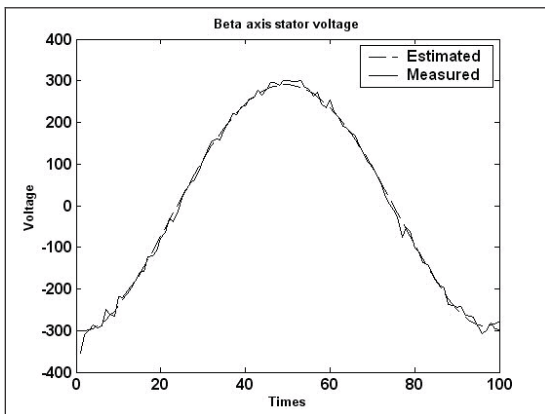


Fig. 5. Beta axis stator voltage

Now that estimation of measured variables is done, figure 8 shows the estimation of  $i_{\alpha s}$ , which is unmeasured:

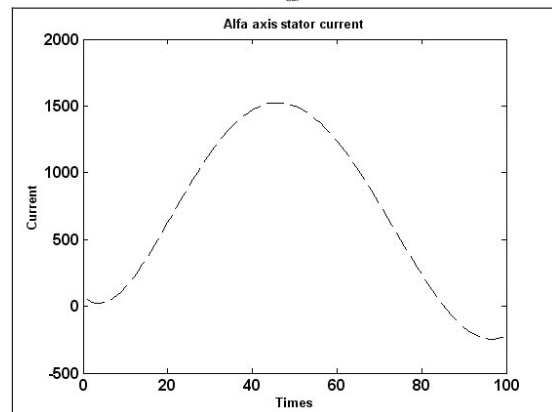


Fig. 8. Alfa axis stator current

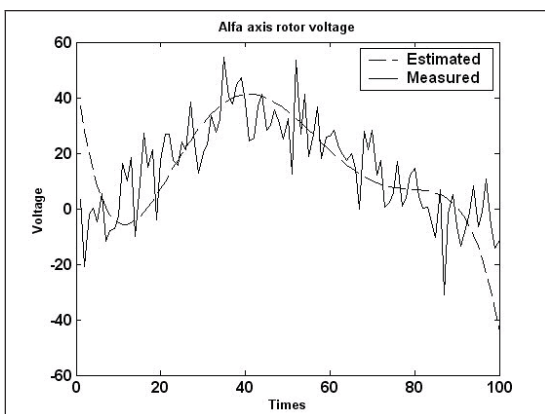


Fig. 6. Alfa axis rotor voltage

## Conclusion

This method allows the validation of measurements of the system and the deduction of the unmeasured variables. It can be extended to detect, identify and estimate gross errors on the system: this is the subject of our futur work. It has already been shown that good results can be obtain when all variables are measured.

## Acknowledgements

The work presented in this paper was carried out with financial support from the Collectivité Territoriale de la Corse (CTC). Authors want to acknowledge and thank also people who have contributed to the preparation of the paper.

## References

- [1] Stanley G.M., R.S.H. Mah. Estimation of flows and temperatures in process networks. *AIChE Journal*, vol. 23, 1977, pp. 642-650.
- [2] Darouach M., M. Zasadzinski. Data reconciliation in generalized linear dynamic systems. *American Institute of Chemical Engineering Journal*, vol. 37, 1991, p. 193.
- [3] Kao C. S., A. C. Tamhane, R. S. H. Mah. Gross error detection in serially correlated process data. 2. Dynamic systems. *Industrial Engineering & Chemical Research*, vol. 31, 1992, p. 254.
- [4] Rollins D. K., S. Devanathan. Unbiased estimation in dynamic data reconciliation. *American Institute of Chemical Engineering Journal*, vol. 39, 1993, p. 1330.
- [5] Ramamurthi Y., P. B. Sistu, B.W. Bequette. Control-relevant dynamic data reconciliation and parameter estimation. *Computers & Chemical Engineering*, vol. 17, 1993, p. 41.
- [6] Karjala T. W., D. M. Himmelblau. Dynamic reconciliation of data via recurrent neural nets and the extended kalman filter. *American Institute of Chemical Engineering Journal*, vol. 42, 1996, p. 2225.
- [7] Albuquerque J. S., L. T. Biegler. Data reconciliation and gross-error detection for dynamic systems. *American Institute of Chemical Engineering Journal*, vol. 42, 1996, p. 2841.
- [8] Bagajewicz M. J., Q. Jiang. Integral approach to plant linear dynamic reconciliation. *AIChE Journal*, vol. 43, 1997, pp. 2546-2558.
- [9] Bennouna O., N. Héraud, M. Rodriguez, H. Camblong. Data reconciliation & gross error detection applied to wind power. *ImechE vol. 221 Part I, Systems and Control Engineering*, 2007.
- [10] Bennouna O., N. Héraud, H. Camblong, M. Rodriguez. Diagnosis of the doubly-fed induction generator of a wind turbine. *Wind Engineering*, vol. 29, no. 5, 2005, pp. 431-448.
- [11] Khatounian F., E. Monmasson, F. Berthreau, E. Delaleau, J. P. Louis. Control of a doubly fed induction generator for aircraft application. *IEEE- IECON, Roanoke, Etats-Unis*, 2003.
- [12] N. Patin. Filtrage actif appliqué à une machine asynchrone à double alimentation sur réseau autonome. *JCGE 2005, Montpellier, France*, 2005.

## Biographies



ouadie.benouna@esigelec.fr).

**Ouadie Bennouna** received the Ph. D. degree from the University of Corsica, France, in 2006, and the Dipl. Ing. degree in mechanical engineering from the ENSAM (Ecole Nationale Supérieure d'Arts & Métiers), Morocco, in 2003. He joined the IRSEEM (Institut de Recherche en Systèmes Electroniques Embraqués) in February 2008. His research interests include diagnosis and error detection, signal processing, and neural networks (email:



**Nicolas Héraud** was born in France on september 15, 1962. He received his Ph.D. degree in Automatic and Electrical Engineering from Institut National Polytechnique de Lorraine in 1991. Since 1992, he teaches at the University of Corse as professor and he is at the CNRS (UMR 6134). His field of interest includes data reconciliation and process diagnosis on

renewable energy systems (email: heraud@univ-corse.fr)



**Mohamed Ainan Kahyeh** was born in Djibouti on January 15, 1971, he's actually *PhD Student in Automatic Control and Renewable energy* in sandwich model between *Università di Corsica* and *University of Djibouti* after several years of works in industrial field. Since 1999, he's *the head of the maintenance department* in Boulaos Power Plant (Djibouti) and part-time teacher at the Institute of Technology in Djibouti (University of Djibouti). He was graduated in 1996 in *Electrical Engineering* in the *Ecole Nationale d'Ingénieurs de Sfax* (TUNISIA). He also obtained a *Master degree of Business Administration* in 2004 in the *University of Poitiers* (France).



panels connected to the network. (email: ahmed\_houssein\_youssouf@univ.edu.dj, houssein@univ-corse.fr).

**Ahmed Houssein** was born in Djibouti, holder of Master of Research in Electronics, is currently PhD student in applied automatics for renewable energies (SOLAR). He he teaches at the Djibouti University in alternation between the Djibouti University and the Corsica University UMR 6134 CNRS. His main objective is to analyze impacts of decentralized productions on the distribution networks, fault detection of PV

# SEASONAL VARIATION OF PV EFFICIENCY FOR VARIOUS TECHNOLOGIES AND MODULE INCLINATIONS

Gilles Notton, Vladimir Lazarov, Ludmil Stoyanov, Said Diaf and Nicolas Heraud

**Abstract:** We estimate the efficiency of 4 technologies of PV modules under various meteorological conditions. The production is estimated in optimal conditions because in the case of a grid connected PV system, the inverter integrates always a MPPT. The seasonal variation is studied and the influence of the PV module inclination is taken into account.

**Keywords:** photovoltaic system; optimization; PV technologies;

## Introduction

The purpose of this work is to estimate the productivity of PV modules under a wide variety of weather conditions (13 studied locations in Bulgaria and Corsica). The kWh produced by a PV array will be calculated as the sum of hourly production all over the year. This hourly production depends on many parameters as:

- actual  $P_{\text{rated}}$  of the PV array
- solar irradiation on the PV module plane;
- the PV module temperature  $T_{\text{PV}}$
- electrical losses



Fig. 1. Position of the studied locations.

Thus, in a first part, we will show the various models for the PV efficiency (for several PV technologies) depending on various meteorological data and electrical characteristics of PV modules. Then, in a second part, after a presentation of the solar radiation model, the monthly PV efficiency is computed for each technology for various PV modules inclinations.

## Some models of PV efficiency and PV power

The ambient temperature and the solar irradiance have high effects on the PV efficiency and must be taken into account in any model. The most known model is:

$$(1) \quad \eta_{\text{PV}} = \eta_{\text{ref}} \left[ 1 - \beta(\theta_{\text{cell}} - \theta_{\text{cell,ref}}) + \gamma \log \frac{\phi}{\phi_{\text{ref}}} \right]$$

with  $\eta_{\text{ref}}$  the reference module efficiency at PV cell temperature  $\theta_{\text{cell,ref}}$  of 25°C and at a solar irradiance  $\phi$  equal to 1000 W.m<sup>-2</sup>.  $\gamma$  and  $\beta$  are the solar irradiance and temperature coefficients for the PV module.  $\theta_{\text{cell}}$  is the PV cell temperature which depends on the environmental conditions. Generally, these parameters ( $\theta_{\text{cell,ref}}$ ,  $\eta_{\text{ref}}$ ,  $\beta$ ,  $\gamma$ ) are given by the PV manufacturer, but  $\gamma$  and  $\beta$  depend on the material used for the PV module. Evans [1] suggested to use for the silicon  $\beta=0.0048^\circ\text{C}^{-1}$  and  $\gamma=0.12$  and for a CIS module  $\beta=0.006^\circ\text{C}^{-1}$ . Most often equation (1) is seen with  $\gamma=0$  [2-4].

In Eq (1), the PV cell temperature appears and must be calculated from meteorological data and PV modules characteristics. The most common manner to determine the cell temperature  $\theta_{\text{cell}}$  consists in using the NOCT (Normal Operating Cell Temperature). The value of this parameter is given by the PV module manufacturer.  $\theta_{\text{cell}}$  depends on the ambient temperature  $\theta_a$  and on the solar irradiance  $\phi$  according to Eq.(2) :

$$(2) \quad \theta_{\text{cell}} = \theta_a + (\text{NOCT} - 20^\circ\text{C}) \frac{\phi}{800}$$

Another formulation for the Si solar cells efficiency is given by Paatero and Lund [5]:

$$(3) \quad \eta_{\text{PV}} = \eta_r \left[ 1 - \alpha \left( \frac{\phi}{18} + \theta_a - 20 \right) \right]$$

with  $\alpha=0.0042$  the temperature correction factor.

We plotted in Fig. 2. the relative Si PV module efficiency calculated from the Eq. (1) with  $\gamma=0$  and  $\gamma=0.12$  and by Eq. (3). We note that the influence of the temperature on the efficiency is 0.48%/°C for Eq. (1) with  $\gamma=0$  and 0.42%/°C using Eq. (3) what is in accordance with manufacturers data and with the literature. Using Eq (1) with  $\gamma=0.12$ , for a constant cell temperature, the PV efficiency increases with an increase of the solar irradiance, but for a given ambient temperature, the efficiency begins to increase then decreases because for high solar irradiance the cell temperature is high and the influence of the temperature counterbalances the solar irradiance effect.

The form of the curve, for a given ambient temperature, is different according to the model used. In

Eq. (1) with  $\gamma=0.12$  we note a decrease of the PV efficiency for low solar irradiance, this observation is confirmed in experimental studies by various authors [6-9] and explained by Bucher [10]. For many commercial modules, we note a severe reduction of module efficiency at low light levels. The efficiency can drop with 55-90% of its value at STC below 200 W/m<sup>2</sup>. As these low irradiation levels can carry no-negligible amounts of energy, they are especially important for the design of photovoltaic systems.

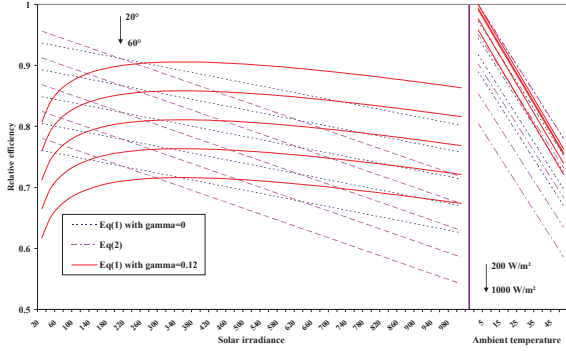


Fig. 2. Influence of temperature and solar irradiance on PV module efficiency.

These models are not usable for aSi, CdTe or CIS technology for which the influence of the temperature and the solar irradiance are different. The crystalline silicon modules performances are better in winter than summer (about 10% better for p-Si) while the reverse is true for amorphous silicon because crystalline modules have larger negative temperature coefficients. The amorphous modules have over 20% improvements in efficiency in the summertime. These different performances of PV modules according to the time period and the environmental conditions are due to thermal and spectral effects varying according to the PV technology.

It is interesting to take into account the PV technology and consequently to use various formulations or parameter values depending on the PV module type. Durisch *et al* [11] developed a new method for the calculation of the energy yield of photovoltaic modules at selected sites. They used a semi-empirical efficiency formulation taking into account three parameters: cell temperature  $\theta_{cell}$ , solar irradiance  $\phi$  and relative air mass AM. The general model representing all module types is:

$$(4) \quad \eta = p \left[ q \frac{\phi}{\phi_0} + \left( \frac{\phi}{\phi_0} \right)^m \right] \times \left[ 1 + r \frac{\theta_{cell}}{\theta_{cell,0}} + s \frac{AM}{AM_0} + \left( \frac{AM}{AM_0} \right)^u \right]$$

with  $\phi_0=1000\text{W/m}^2$ ,  $\theta_{cell,0}=25^\circ\text{C}$  and  $AM_0=1.5$ . AM is calculated according to Kasten and Young [12]:

$$(5) \quad AM = 1 / \left[ \cos \theta_z + 0.50572(96,07995 - \theta_z)^{-1.6364} \right]$$

The parameters p, q, m, r, s and u are determined for [13]: m-Si (BP 585F); p-Si (Kyocera LA361K51S), a-Si (UniSolar UPM US-30); CIS (Siemens ST40). The various coefficients are available in reference [11]. To calculate  $\theta_{cell}$ , we used the Ross formula [12]:

$$(6) \quad \theta_{cell} = \theta_a + h\phi$$

h is the Ross coefficient [11].

The maximum power generated by the PV plant can be calculated using directly an expression giving  $P_{max}$  or using the separated expressions of  $V_{mp}$  (max power voltage) and  $I_{mp}$  (max power current) and determining  $P_{max}$  (maximum power) by

$$(7) \quad P_{max} = I_{mp} \times V_{mp}$$

Two models have been tested to calculate  $P_{max}$ . The first one developed by Borowy and Salameh [14] uses manufacturer data: the formulas for calculating the optimum operating point current and voltage under arbitrary conditions have the following forms:

$$(8) \quad I_{mp} = I_{sc,ref} \left\{ 1 - C_1 \left[ \exp \left( \frac{V_{mp,ref}}{C_2 V_{oc,ref}} \right) - 1 \right] \right\} + \Delta I$$

$$(9) \quad V_{mp} = V_{mp,ref} \left[ 1 + 0.0539 \log_{10} \left( \frac{\phi}{\phi_{ref}} \right) \right] + \beta_0 \Delta \theta$$

$$(10) \quad C_1 = \left( 1 - \frac{I_{mp,ref}}{I_{sc,ref}} \right) \exp \left[ - \frac{V_{mp,ref}}{C_2 V_{oc,ref}} \right] \quad \text{and} \quad C_2 = \frac{\frac{V_{mp,ref}}{V_{oc,ref}} - 1}{\ln \left( 1 - \frac{I_{mp,ref}}{I_{sc,ref}} \right)}$$

$$(11) \quad \Delta I = \alpha_0 \left( \frac{\phi}{\phi_{ref}} \right) \Delta T + \left( \frac{\phi}{\phi_{ref}} - 1 \right) I_{sc,ref}$$

$$(12) \quad \Delta \theta = \theta_{cell} - \theta_{cell,ref}$$

with  $\alpha_0$  and  $\beta_0$  respectively the module current and voltage temperature coefficient. Another model used by Labbé [15] and based on an empirical formula is :

$$(13) \quad P_{max} = \frac{\phi}{\phi_{ref}} \left[ P_{mp,ref} + \gamma_0 (\theta_{cell} - \theta_{cell,ref}) \right]$$

with  $\gamma_0$  the module power temperature coefficient.

All these formulations allow to calculate  $P_{max}$  for a PV module; but to determine  $P_{max}$  for the total PV array, we must introduce a loss factor.

### Experimental Verification

We have a PV system connected to the electrical grid with a nine 85 Wp mSi BP585F modules array and a 700 W Sunny Boy 1000 SMA inverter which automatically adjusts PV array load to provide maximum efficiency of solar panels by a MPPT means (Fig. 3).



Fig. 3. The grid connected PV system.



We plotted in Fig. 4. the experimental PV array efficiency versus the solar irradiance on the PV module for various cell temperatures. We observe a decreasing of the efficiency for low irradiances (below about 200 W/m<sup>2</sup>) and for high ones as predicted by the literature.

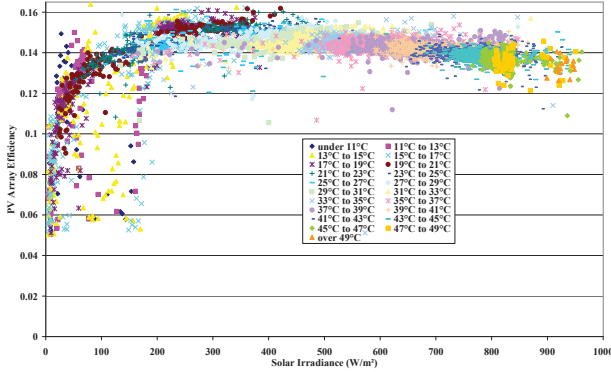


Fig. 4. BP 585F m-Si PV array efficiency.

In Fig. 5, we see the PV array power versus the solar irradiance for various cell temperatures. To illustrate the temperature influence, linear interpolations have been plotted for three cell temperatures intervals.

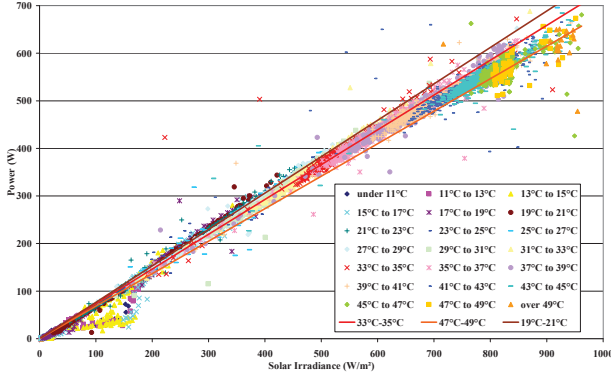


Fig. 5. BP 585F m-Si PV array power

We calculated the experimental power and compared it with maximum power estimated by the 5 equations with  $\theta_{cell}$  calculated from ambient temperature using the NOCT formulation. We introduced an electrical loss factor equal to 0.95. We present in Fig. 6. the results for a clear and cloudy sky day. The absolute and relative values of the mean bias (MBE) and root mean square (RMSE) errors are in Table 1.

Table 1

Statistical parameters RMSE and MBE.

Model	MBE		RMSE		Place
	%	W	%	W	
Evans	0.12	0.43	8.65	29.74	2
Paatero	4.60	15.81	10.03	34.47	4
Durisch	0.63	2.18	8.62	29.63	1
Borowy	-6.38	-1.93	11.13	38.25	5
Labbé	1.11	3.83	9.14	31.40	3

The Durish model and the Evans model give similar results from a RMSE point of view but the first model has for advantage to model all types of technologies in changing only the values of the parameters. All the

models overestimated the reality excepted for the Borowy model.

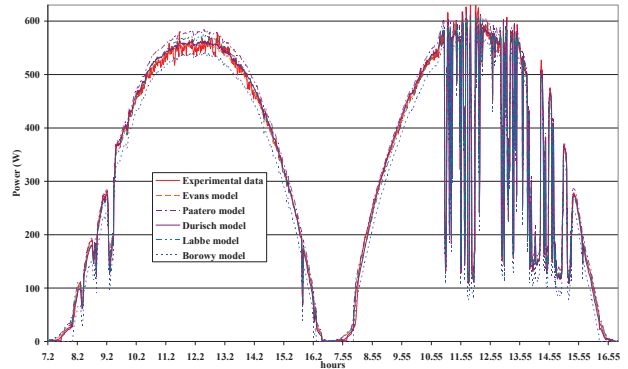


Fig. 6. Experimental verification

The application of the Durish model allows us to draw in Fig. 7. the efficiency behaviour in relative variation for the 4 PV module technologies versus air temperature and solar irradiance

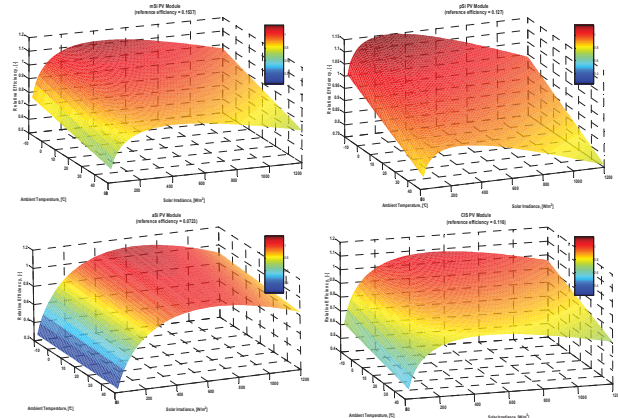


Fig. 7. Variation of the PV efficiency for each technology.

We note, as previously said, that a-Si PV module is less sensitive to an increase of ambient temperature. If the temperature influence is so important it is because it is the ambient temperature and not the cell temperature which is considered in this Fig. 7; thus, the solar irradiance influences two times: a first one in the cell temperature formula and secondly in the efficiency formula.

As said by Bucher [10], all PV devices are spectrally sensitive, and the sun spectrum changes with the distance the light has to travel through the atmosphere (relative air mass AM). c-Si and CIS have a broad spectral responsivity (300-1120 nm for Si), leading to a large spectral absorption. Amorphous silicon shows a smaller spectral band (350 800 nm), absorb less photons but show higher voltages. Now, if the sun spectrum changes during a day, a part of the incident spectrum may not be converted for solar cells with a small spectral band. The AM reaches 5 for a zenith angle near 80° i.e. when the sun rises or set thus rarely AM will be higher than 5. We looked for the air mass influence on the PV module efficiency for the four technologies (AM varied from 1 to 10) taking a constant cell temperature equal to 25°C. Te



influence is not very important excepted for high AM (>5) but this case occurs only at sunset and sunrise and when hourly values of environmental parameters will be used in a production study these values of AM will be not reached.

### Estimation of hourly tilted solar irradiation

The solar module is placed at any slope angle, then the horizontal solar radiation data must be converted into tilted solar global radiation. In this context, two studies have been performed [16-17] to quantify the accuracy of various well-known models of the literature: several combinations of models have been tested and allow to calculate these data with a relative root means square error (RRMSE) around 10 %, reaching 8.2 % for the best combination. We chose a combination of two models: CLIMED2 model [18] to calculate the horizontal diffuse component from global one and the Klucher model [19] to compute the tilted global radiation from horizontal diffuse and global radiation. The hourly total radiation received on a tilted surface  $I_\beta$  may be expressed by:

$$(14) \quad I_\beta = I_{b,\beta} + I_{r,\beta} + I_{d,\beta}$$

with  $I_{b,\beta}$ ,  $I_{r,\beta}$ , and  $I_{d,\beta}$  the hourly beam, reflected and sky diffuse radiation on the tilted surface. These components are calculated from hourly global  $I$  and diffuse radiation  $I_d$  on a horizontal plane. At first, the horizontal diffuse solar radiation  $I_d$  must be estimated then the three components are calculated  $I_{b,\beta}$  and  $I_{r,\beta}$  by common expressions [20] and  $I_{d,\beta}$  by the Klucher model [19].

In [18], the authors developed a model called CLIMED2 on the basis of the data collected in various Mediterranean sites:

$$(15) \quad \begin{cases} f = 0.995 - 0.081 M_T & \text{for } M_T \leq 0.21 \\ f = 0.724 + 2.738 M_T - 8.32 M_T^2 + 4.967 M_T^3 & \text{for } 0.21 < M_T \leq 0.76 \\ f = 0.180 & \text{for } M_T > 0.76 \end{cases}$$

where  $f$  is the diffuse fraction defined by  $f=I_d/I$  and  $M_T$  is the hourly clearness index. This model has been tested on meteorological data of Ajaccio and the relative root mean square error (RRMSE) is 36.52% what is not very good but, between all the tested models, there is not a model largely better than another one.

Klucher [19] developed the following model using a factor  $F=1-(I_d/I)^2$ :

$$(16) \quad I_{d,\beta} = I_d \left[ 0.5 \left( 1 + \cos\left(\frac{\beta}{2}\right) \right) \right] \left[ 1 + F \sin^3\left(\frac{\beta}{2}\right) \right] \left[ 1 + F \cos^2(\theta) \sin^3(\theta_z) \right]$$

This model has been tested on Ajaccio and the RRMSE is 7.05%. Finally using eq. (14), the hourly global radiation on titled plane can be determined with a RRMSE equal to about 10%. For two particular days, the various components calculated by our method are shown Fig. 8.

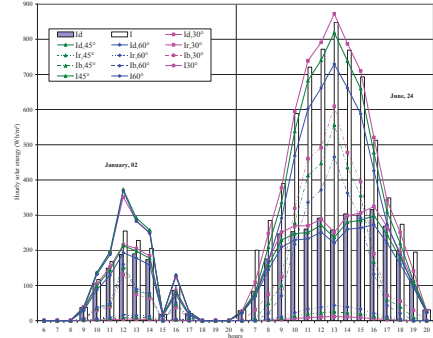


Fig. 8. Determination of hourly components of solar radiation on a tilted plane from hourly horizontal solar irradiation

### Monthly variation of the PV efficiency

We calculated the monthly mean value of the PV efficiency according to the used technology for the 13 studied locations. In Figs. 9.a and 9.b, the results are shown for Ajaccio and Sofia.

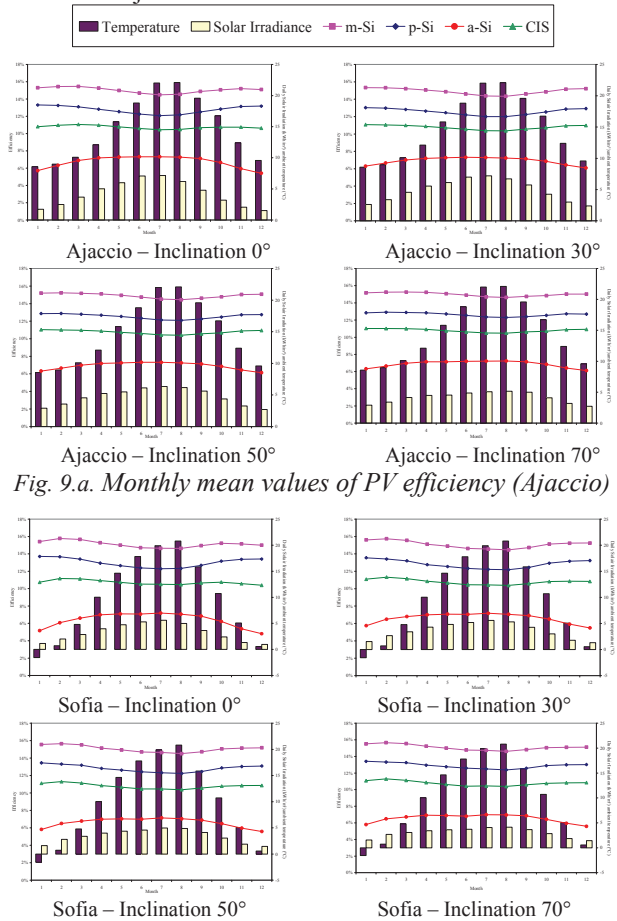


Fig. 9.a. Monthly mean values of PV efficiency (Ajaccio)

Fig. 9.b. Monthly mean values of PV efficiency (Sofia)

We note that for m-Si and p-Si the variation is quite similar according to the month, the maximum is reached during winter (low temperature) and the minimum during summer due to the negative impact of the temperature on the PV efficiency. For CIS the monthly variation is less sensitive. Concerning the a-Si technology, the monthly variation is different - the maximum efficiency is obtained during summer and the lowest one during

winter. For a-Si, the variation of the PV efficiency versus the month is more important (difference of 26% between the lowest and highest monthly efficiency value) than for other PV technologies (mSi : 6.3%, pSi 9.2% and CIS : 5.54%). Our results are confirmed by Williams *et al* [21] on experimental data collected in Loughborough in UK. In these experimental data, the p-Si efficiency is improved by 10% during winter and our calculation gives an increase of about 11%. The variation of the a-Si efficiency is about 30% between winter and summer, result confirmed by Williams [31]. In the two previous examples (Ajaccio and Sofia) we note some differences particularly about the efficiency value: the PV efficiencies are higher in Sofia than in Ajaccio because the lower temperatures in Bulgaria than in Corsica particularly during winter. The coldest site in our study is Botev situated at 2389m high and consequently the PV efficiencies reach higher values (see Fig. 10)

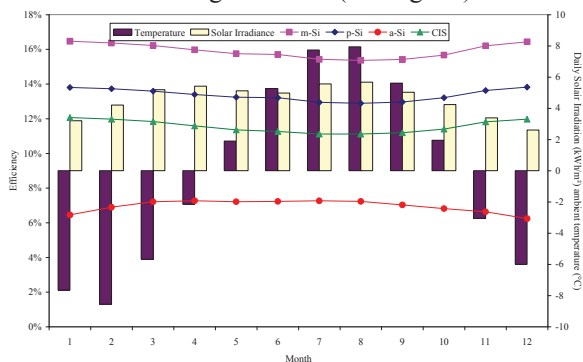


Fig. 10. Monthly mean values of PV efficiency (Botev)

Compared with Sofia, the efficiency is increased in absolute value of about 0.72 % for m-Si, 0.25% for p-Si, 0.73 % for CIS and 0.09% for a-Si. The influence of the site is more important for CIS, p-Si and m-Si technology than for a-Si one. In fact, we note that the a-Si efficiency does not vary very much according to the site.

In Figs 9.a and 9.b, we noted that the PV efficiency variation is less important for tilted PV modules than for horizontal PV module. We plotted in Fig. 11 for each PV technology the influence of the inclination (for Ajaccio).

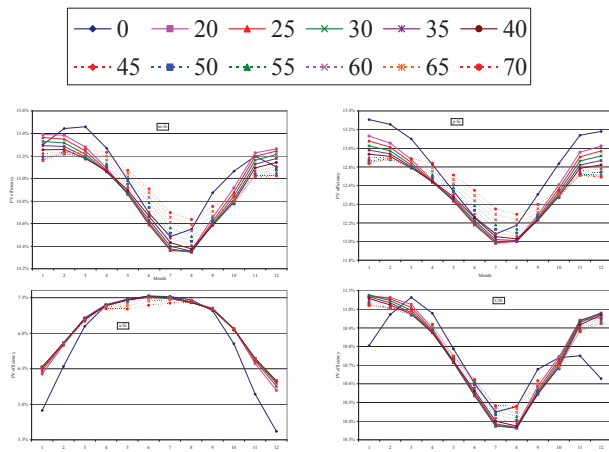


Fig. 11. Influence of the inclination on the PV efficiency

For m-Si, p-Si and CIS, we note that:

- the efficiency is higher in winter for low inclination;
- the efficiency is higher in summer for high inclination.

In fact, the PV efficiency is negatively influenced by the PV module temperature depending on the ambient temperature (the same for all inclinations) and by the solar irradiance; this solar irradiance and consequently the PV cell temperature is upper during winter for high inclination and during summer for low inclination; the PV efficiency will be smaller (higher) during winter (during summer) for high inclination.

But, we must keep in mind that, as solar irradiation is higher in winter for high inclinations, the productivity of the PV module, despite the decrease in its efficiency, will be more important for high inclinations; it is the same thing for low inclinations during summer.

The sensitivity of a-Si module to the temperature being reversed (positive influence) and lower, we see that the inclination influence is inversed and smaller.

### Conclusion

The meteorological conditions have not the same influence on the PV modules efficiency according to the technology used. If for m-Si, p-Si and CIS the efficiency varies in the same way, the amorphous silicium gives better results during winter in term of efficiency. In a next study, we will connect to these various PV modules types a grid-connected inverter and we will look if the optimal sizing of global connected PV system varies according to the PV technology and/or the inverter type and according to the PV array inclination.

### Acknowledgements

The authors would like to thank the University Agency of French-speaking communities (AUF), the French Agency for Environment Energy Management (ADEME) and the French Ministry of Foreign Affairs (via Eco-Net program) for their financial supports.

### References

- [1] Evans, D.L. Simplified method for predicting photovoltaic array output. *Solar Energy* 1981;27(6):555-560.
- [2] Evans, D.L., Florschuetz, L.W. Cost studies on terrestrial photovoltaic power systems with sunlight concentration. *Solar Energy* 1977;19:255.
- [3] Hegazy, A.A. Comparative study of the performances of four photovoltaic/thermal solar air collectors. *En. Conv. Mgt* 2000;41:861-881.
- [4] Bergene, T, Lovik, O. Model calculations on a flat-plate solar heat collector with integrated solar cells. *Solar Energy* 1995;55(6):453-462.
- [5] Paatero, J.V., Lund, P.D. Effects of large-scale photovoltaic power integration on electricity distribution networks, *Renewable Energy* 2007; 32:216-234.
- [6] Moring, H.D., Stellbogen, D., Schaffler, R., Oelting, S., Gegenwart, R. Outdoor performance of polycrystalline thin film PV modules in different European climates. 19<sup>th</sup> EPSEC 2004, Paris, France.

[7] Armani, M., Sparber, W., Parretta, A., Antonini, A., Butturi, M., Stefancich, M. Performance monitoring of different PV systems installed in Northern Italy. 22<sup>nd</sup> EPEC 2007, Milano, Italy.

[8] Smiley, E.W., Stamenic, L., Jones, J.D., Stojanovic, M. Performance modelling of building integrated photovoltaic systems. 16th EPSEC 2000, Glasgow, UK.

[9] Ramsome, S. A summary of outdoor testing and modelling of PV systems. PVSAT3 Congress 2007, Durham.

[10] Bucher, K. Site dependence of the energy collection of PV modules. Solar En. Mat. and Solar Cells 1997;47:85-94.

[11] Durisch, W., Bitnar, B., Mayor, J.C., Kiess, H., Lam, K.H., Close, J. Efficiency model for photovoltaic modules and demonstration of its application to energy yield estimation. Sol. En. Mat. Sol. cells 2007;91:79-84.

[12] Kasten, F., Young, A.T. Revised optical air mass tables and approximation formula. Appl. Optics 1989;28:4735-4738.

[13] Ross, R.G. Interface design considerations for terrestrial solar cell modules. 12<sup>th</sup> IEEE PSEC 1976, Baton Rouge, 801-806.

[14] Borowy, B.S., Salameh, Z.M. Methodology for optimally sizing the combination of a battery bank and PV array in a Wind/PV hybrid system. IEEE Transactions on energy conversion 1996;11(2):367-375.

[15] Labbé, J. L'hydrogène électrolytique comme moyen de stockage d'énergie électrique pour systèmes PV isolés. Ph-D thesis, Ecole des Mines de Paris, CEP, Sophia-Antipolis, December 2006.

[16] Notton, G, Cristofari, C, Muselli, M, Poggi, P. Calculation on an hourly basis of solar diffuse irradiations from global data for horizontal surfaces in Ajaccio. Energy Conversion and Management 2004; 45:2849-2866.

[17] Notton, G, Poggi, P, Cristofari, C. Predicting hourly solar irradiations on inclined surfaces based on the horizontal measurements: Performances of the association of well-known mathematical models. Energy Conversion and Management 2006; 47.13-14:1816-1829.

[18] De Miguel, A, Bilbao, J, Aguiar, R, Kambezidis, H, Negro E. Diffuse solar irradiation model evaluation in the North Mediterranean belt area. Solar Energy 2001; 70(2):143-153.

[19] Klucher, TM. Evaluation of models to predict insolation on tilted surfaces. Solar Energy 1979; 23(2):111-114.

[20] Iqbal, M. An introduction to solar radiation. Academic Press, Canada, ISBN:0-12-373752-4, 1983.

[21] Williams, S.R., Gottschalg, R., Infield, D.G. PV modules real operating performance in the UK, a temperate maritime climate. 19<sup>th</sup> EPSEC, 7-11 June 2004, Paris, France.

## Biographies



**Gilles Notton** was born in Saint Avold, France, on January 23, 1964. He studied at the University of Corsica and received Dr. degree in 1992 and Research Agreement in 2002 from the same university His field of interest includes renewable energy systems and renewable sources. He is today assistant professor and responsible of the French Research ADEME network between France and Oriental and Central European Countries. Gilles Notton is with the

Research Centre of Vignola, University of Corsica, UMR CNRS 6134,

route des Sanguinaires, F20000 Ajaccio, France (e-mail: [gilles.notton@univ-corse.fr](mailto:gilles.notton@univ-corse.fr))



**Vladimir Lazarov** was born in Sofia, Bulgaria. He graduated from the Technical University - Sofia, and there received his PhD. His field of interest includes electrical machines with electronic commutation, small electrical machines, renewable energy sources (electrical aspects). He is today with the Faculty of Electrical Engineering of the Technical University – Sofia and is responsible for the “Laboratory on Renewable Energy Sources” (email:

[vl\\_lazarov@tu-sofia.bg](mailto:vl_lazarov@tu-sofia.bg)).



**Ludmil Stoyanov** was born in Sofia, Bulgaria, on June 13, 1981. He graduated from the Technical University - Sofia, and received second Master degree from ENSIEG-INPG, France.

His field of interest includes electrical machines, electrical networks and renewable energy sources (electrical aspects). He is today a PhD student in the Faculty of Electrical Engineering of the Technical

University – Sofia. Ludmil Stoyanov is with the Faculty of Electrical Engineering, Technical University of Sofia, 8, Kl. Ohridski Blvd., 1000 Sofia, Bulgaria (e-mail: [stoyanov\\_ludmil@abv.bg](mailto:stoyanov_ludmil@abv.bg))



**Said Diaf** was born in Annaba, Algeria, on July 24, 1964. He received his Electrical Engineering Diploma from Annaba University and his Magister diploma from Boumerdes University, Algeria. In 1993, Said Diaf joined the Development Center of Renewable Energy, at Algiers as researcher in solar energy division. Actually, he prepares his PhD diploma. His areas of interest are photovoltaic and wind energy conversion systems.



**Nicolas Heraud** was born in France on september 15, 1962. He received his Ph.D. degree in Automatic and Electrical Engineering from Institut National Polytechnique de Lorraine in 1991. Since 1992, he teaches at the University of Corse as professor and he is at the CNRS (UMR 6134). His field of interest includes data reconciliation and process diagnosis on renewable energy systems.

# First Approach of a Matlab/Simulink® Simulation For a PV/T Solar Collector Behaviour

Gilles Notton, Nicolas Héraud, Christian Cristofari, Ahmed Youssouf and Mohamed Ainan Kahyeh

**Abstract:** Researchers develop hybrid PV/thermal collectors (PV/T) generating both electric power and hot water or hot air. In this work, the thermal behaviour of a PV/T solar collector is dynamically modelled with matlab/simulink® for various system configurations in order to establish a comprehensible description of the thermal exchanges.

**Keywords:** Hybrid, Modelling, Performance

## Introduction

A part of the absorbed solar radiation by a photovoltaic panel is not converted into electricity and contributes to increase the module temperature, then reducing the electrical efficiency. This fact leads to develop hybrid PV/thermal collectors (PV/T) which generate electric power and hot water or hot air. The photovoltaic cells are in thermal contact with a solar heat absorber and the excess heat generated by the photovoltaic cells serves as an input for the thermal system. During the operation, a heat carrier fluid removes heat from the absorber and PV cells. These cooled cells operate at a low and stable temperature increasing their efficiency is decreasing with temperature. The collected heat can be used as preheated water (Fig.1).

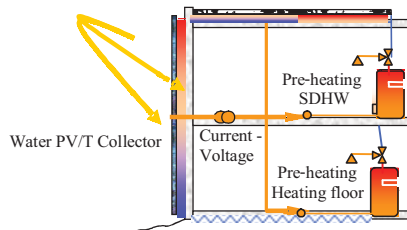


Fig. 1: Utilization of a PV/T solar collector .

The main advantages of such a solar collectors are [1,2]:

- at first, of economical order compared to a combination of separate thermal and photovoltaic panels;
- the area covered with a PV/T collector produces more electrical and thermal energy than a corresponding area covered half with standard PV panels and half with conventional thermal collector. This is particularly useful because the space on a roof of a house is often reduced. The average temperature of operation for the PV/T collector being generally lower than for a standard PV module, its electrical production will be increased. A PV/T collector provide architectural uniformity on a roof compared with an association of two separate ones.

We present a model of the thermal behaviour of various PV/T solar collectors in a matlab/simulink® software environment. Simulink® is a platform for multidomain simulation and Model-Based Design of dynamic systems. It provides an interactive graphical environment and a customizable set of block libraries that let you accurately design, simulate, implement, and test control, signal processing, communications, and other time-varying systems. Thus, this software is well adapted to our problematic because each autonomous working block can represent an essential PV/T Collector component and their physical and thermal properties can be easily modified. Within these blocks, the properties are modelled using both physical and thermodynamical equations. This software has often been used by numerous researchers in dynamical modelling of thermal system [3-4] and other renewable energy systems [5-6].

## The studied PV/T solar collector

The studied PV/T collector is composed of a pSi module pasted to an absorber-exchanger which transforms the solar radiation to heat. This “absorber-exchanger” has back and side insulations (expanded polyurethane), inserted in the body of the collector which allows a good mechanical behavior of the collector structure (Fig. 2). The fluid is distributed uniformly under the absorber surface. The water flows are parallel. A header pipe supplies each pipe and another one collects the warm fluid. The absorber-exchanger in copolymer material must satisfy the following constraints: UV protected, high thermal conductivity, water-resistant and glycol-resistant, good thermal range of utilization (-10/+150°C), a good mechanical strength and a chemical stability. We selected an anti-UV treated polycarbonate which is the cheapest polymer and satisfying all the constraints. We chose for this study a PV/T solar collector without a cover glass (i.e. without green house effect).

The use of a polymer absorber has been studied by Van Nierkerk *et al.* [7] to evaluate the performances of parallel tubes collectors in south of Africa. The variation of geometrical variables such as tube diameter, tube spacing and pitch was studied for optimising the collector performances. The best configuration is obtained for an inter tube spacing equal to zero. It appears that the configuration of the flat plate collector is the most important parameter which affects collector performance.



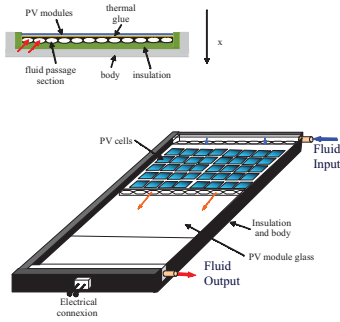


Fig. 2: The photovoltaic/thermal solar collector.

### The PV module

We considered the m-Si Photowatt PWX 500 module (thickness of 0.2 mm). The encapsulation of cells is made between two sheets of tempered glass with high transmittance. The peak power at a junction temperature equal to 25°C is 49 W at  $\pm 10\%$ .

For the PV module properties, Notton *et al* [8] obtained from the manufacturer the following data :

- For the glass : normal transmittance :  $\tau_{\text{glass}}=0.95$ ; normal absorptivity :  $\alpha_{\text{glass}}=0.05$ ; emissivity  $\epsilon_{\text{glass}}=0.85$ ; thermal conductivity :  $\lambda_{\text{glass}}=1.8 \text{ W.m}^{-1}.\text{K}^{-1}$ ; density :  $\rho_{\text{glass}}=2700 \text{ kg.m}^{-3}$ ; specific heat capacity  $C_{\text{glass}}=750 \text{ J.kg}^{-1}.\text{K}^{-1}$ ; thickness:  $e_{\text{glass}}=3.2 \text{ mm}$ .
- For the EVA (ethylene vinyl acetate) : thermal conductivity :  $\lambda_{\text{EVA}}=0.35 \text{ W.m}^{-1}.\text{K}^{-1}$  [18]; thickness:  $e_{\text{EVA}}=0.22 \text{ mm}$ .
- For PV cells: normal absorptivity :  $\tau_{\text{PV}}=0.9$ ; thermal conductivity :  $\lambda_{\text{PV}}=130 \text{ W.m}^{-1}.\text{K}^{-1}$ ; density :  $\rho_{\text{PV}}=2330 \text{ kg.m}^{-3}$ ; specific heat capacity  $C_{\text{PV}}=836 \text{ J.kg}^{-1}.\text{K}^{-1}$ ; thickness:  $e_{\text{PV}}=0.22 \text{ mm}$ .

### The thermal adhesive.

The PV modules are pasted on the absorber and the thermal adhesive is an important component of the PV/T collector because it must provide a good thermal contact between the electrical part and the thermal part. Rossel *et al* [9] showed the importance of this component; his theoretical analysis confirmed that thermal conduction of the paste is a critical parameter essentially in the manufacturing process. Using his mathematical method, he shows that the variation of the adhesive conductivity affects substantially the overall performance; thus, an adhesive with a thermal conductivity 100% better would increase efficiency around 13.5%. We chose to use the same adhesive that Zondag *et al* [10] i.e. a highly conductive glue with a thermal conductivity  $\lambda_{\text{glue}}=0.85 \text{ W.m}^{-1}.\text{K}^{-1}$  in a layer of 50  $\mu\text{m}$  thickness.

### The absorber

The “absorber-exchanger” of the PV/T collector has back and side insulations (expanded polyurethane), which is inserted in the body of the collector which allows a good mechanical behaviour of the collector structure. The thermal properties are : thermal conductivity :  $\lambda_{\text{abs}}=0.775 \text{ W.m}^{-1}.\text{K}^{-1}$ ; density :  $\rho_{\text{abs}}=1,18 \text{ kg.m}^{-3}$ ; specific heat

capacity  $C_{\text{abs}}=1200 \text{ J.kg}^{-1}.\text{K}^{-1}$ . The absorber is shown on Fig. 3.



Fig. 3: Polycarbonate absorber sizing.

The fluid layer thickness (height of the fluid passage section) has been optimized in a previous work [11] and the optimal value has been found equal to 1 cm.

### The insulation

This ‘absorber-exchanger’ has back and side insulation (in expanded polyurethane,  $\rho_{\text{ins}}=80 \text{ kg.m}^{-3}$ ,  $\lambda_{\text{ins}}=0.022 \text{ W.m}^{-1}.\text{K}^{-1}$ ,  $C_{\text{abs}}=1120 \text{ J.kg}^{-1}.\text{K}^{-1}$ ) inserted in the body of the collector which allows a good mechanical behaviour of the collector structure.

As for the water layer thickness, an optimization of the insulation was implemented [11] and showed that the optimal insulation thickness is 20 mm.

### Mathematical model

Zondag *et al* [1] studied 4 numerical models, a 3D dynamic model and three steady state models that are 3D, 2D and 1D. These models are based on energy balances between various components of the PV/T collector. Zondag *et al* [10] applied the same 1D stationary model to 9 various configurations. Based on the control-volume finite difference approach, Chow [12] developed an explicit dynamical model for a single-glazed flat-plate PV/T collector. A transport delay fluid flow was incorporated.

### Dynamical model.

The operation of a PV/T collector is inherently dynamic. A steady-state model is not suitable for predicting working temperatures of the PV module and the heat-removal fluids during periods of fluctuating irradiance or intermittent fluid flow. Several authors, as Rossel *et al* [9], Ji *et al* [13] and Coventry *et al* [14] developed a 1D dynamical model. We chose to use a dynamical model for reasons previously described and a 1D model for two main reasons:

- firstly, the heat exchanges into the PV/T collector occur mainly between the various components of this solar collector i.e. mainly in only one direction, the thickness of the collector noted  $x$  on Fig. 2. This fact is shown by Zondag *et al* [1] comparing the results computed from a 1D, 2D and 3D model;
- secondly, the calculation time is reduced but the results computed by this type of model are satisfying.

### Thermal hypotheses.

Our simulation uses the following hypotheses:

- All material properties are presumed to be independent of temperature and equal on both sides;
- The part of solar radiation which is not converted into electrical energy is absorbed by the PV cells as thermal energy [1,8,10,12-14];

- The absorbed solar irradiance is calculated using a method based on the ASHRAE convention [15].
  - The linearized radiative conductances are used because the temperatures are sufficiently low;
  - We neglect the radiative thermal exchanges between the components of the solar collector [1-2;8,10;9-13];
  - The thermal exchange between the absorber and the water are conductive and convective [11];
  - For the back side of the insulation, we neglect radiative exchanges and used only convective ones [11-12];
  - The water flow rate is supposed identical into all fluid passage section [11];
  - The ambient temperature is equal on all module sides;
  - The input water temperature is considered as constant;
- We consider that our PV/T collector runs in open circuit i.e. the water only pass one time in the absorber.

### Equations

For each node, a thermal energy balance taking into account radiative, convective and conductive exchanges between the nodes and with the environment is applied. The energy accumulated by unity of time by the element is given by the first term of the balance equations. The simulation is done by dividing the PV/T collector into seven isothermal regions:

- the front glass cover (fg) (sheet of tempered glass with high transmittance),
- the PV cells (pv) onto EVA and glass fibre
- the back glass cover (bg), the top of the absorber (ta)
- the fluid (f)
- the bottom of the absorber (ba)
- the insulation and the body (ins)

A detailed description of these regions and the topologic diagram are shown in Fig. 4. To simplify the equations, we used conductances  $G$  to replace resistances  $R$  with  $G=1/R$ . For the front glass:

$$(1) \quad \rho_{fg} A_{fg} e_{fg} C_{fg} \frac{dT_{fg}}{dt} = \Phi_1 A_{PV} + G_{conv,fg,a} (T_a - T_{fg}) +$$

$$G_{r,fg,sky} (T_{sky} - T_{fg}) + G_{r,fg,gro} (T_{gro} - T_{fg}) + G_{cd,fg,pv} (T_{pv} - T_{fg})$$

In equation (1), the terms of the second member are respectively the thermal power exchanged by convection (conv) between the front glass (fg) and the air, by radiation (r) between respectively the glass and the sky on the one hand and between the glass and the ground on the other hand, the thermal power exchanged by conduction (cd) between the glass and the photovoltaic cells (pv) and the thermal power absorbed by the glass. For the photovoltaic cells:

$$(2) \quad \rho_{PV} A_{PV} e_{PV} C_{PV} \frac{dT_{PV}}{dt} = G_{cd,pv,fg} (T_{fg} - T_{PV}) + G_{cd,pv,bg} (T_{bg} - T_{PV}) + \Phi_2 A_{PV}$$

In Eq. (2), the two first terms of the second member are respectively the heat power exchanged by conduction between the cells and the front and back glasses. The third term is the flux received per unit area by the PV cells. For the back glass:

(3)

$$\rho_{bg} A_{bg} e_{bg} C_{bg} \frac{dT_{bg}}{dt} = G_{cd,bg,ta} (T_{ta} - T_{bg}) + G_{cd,bg,pv} (T_{pv} - T_{bg})$$

The terms of the second member are the thermal power exchanged by conduction between the back glass (bg) and the top of the absorber on the one hand and between the back glass and the PV cells. For the half-top of the absorber:

(4)

$$\rho_{ta} A_{ta} e_{ta} C_{ta} \frac{dT_{ta}}{dt} = G_{cd,bg,ta} (T_{bg} - T_{ta}) + G_{cd,ba,ta} (T_{ba} - T_{ta}) + G_{cd,f,ta} (T_f - T_{ta})$$

For the fluid:

(5)

$$\rho_f A_f e_f C_f \frac{dT_f}{dt} = G_{conv,ta,f} (T_{ta} - T_f) + G_{conv,ba,f} (T_{ba} - T_f) + G_{r,fg,gro} (T_{gro} - T_{fg}) + \Phi_3 A$$

For the half-bottom of the absorber:

(6)

$$\rho_{ba} A_{ba} e_{ba} C_{ba} \frac{dT_{ba}}{dt} = G_{cd,ta,ba} (T_{ta} - T_{ba}) + G_{cd,ins,ba} (T_{ins} - T_{ba}) + G_{conv,f,ta} (T_f - T_{ba})$$

For the insulation:

(7)

$$\rho_{ins} A_{ins} e_{ta} C_{ins} \frac{dT_{ins}}{dt} = G_{cd,ba,ins} (T_{ta} - T_{ins}) + G_{conv,ins,a} (T_{ins} - T_a)$$

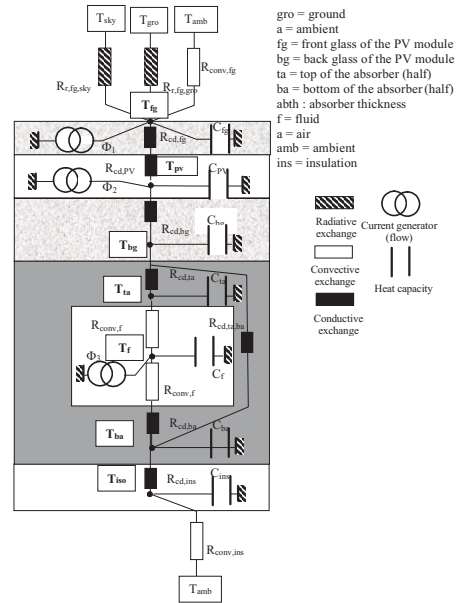


Fig. 4. Topologic diagram of the PV/T Solar collector.

### Expression of the various thermal coefficients

#### The thermal exchanges

The conductive conductance has the expression:

$$(8) \quad G_{cond} = \frac{\lambda A}{e}$$

The convective conductance is:

$$(9) \quad G_{conv} = hA$$

Notton *et al* [8] compared various expressions for the convective conductance in the frame of the modeling of the double-glass polycrystalline PV module. From this study, the convective conductance chosen for the thermal exchange between the front glass and the environment is the Cole and Sturrock formula [16].

For the convective exchange between the absorber and the fluid in the one part and between the insulation and the environment in the other part, we used as suggested by Cristofari *et al* [11] the formula developed by L ev eque [17] and by Schott [18].

The linearized radiative conductances between a surface *i* and the sky or the ground ( $G_{r,i,sky}$  or  $G_{r,i,gro}$ ) is expressed by :

$$(10) \quad G_{r,i,gro} = \varepsilon_{fg} F_{i,gro} \sigma A \left( T_i + T_{gro} \right) \left( T_i^2 + T_{gro}^2 \right)$$

$$(11) \quad G_{r,i,sky} = \varepsilon_{fg} F_{i,sky} \sigma A \left( T_i + T_{sky} \right) \left( T_i^2 + T_{sky}^2 \right)$$

The configuration factors between the front or back cover and the sky or the ground for the PV module are :

$$(12), (13) \quad F_{fg,sky} = \frac{1}{2}(1 + \cos \beta) \quad F_{fg,gro} = \frac{1}{2}(1 - \cos \beta)$$

Several expressions allows us to calculate the sky temperature. We chose to use the expression given by Swinbank [19] :

$$(14) \quad T_{sky} = 0.0552 \times T_a^{1.5} \text{ with } T_a \text{ in K}$$

For the ground temperature we consider that it is equal to the ambient temperature.

### The Energy flux

Two incoming fluxes per unit area take place in the thermal balance equations  $\phi_1$  and  $\phi_2$ . The energy flux  $\phi_1$  which occurs on the front glass is the part of the solar radiation that is absorbed by the glass. It is expressed by :

$$(15) \quad \phi_1 = \alpha_{fg} \times \phi_{solar}$$

with  $\alpha_{fg}$  the absorption coefficient of the front glass.

The energy flux  $\phi_2$  on the PV cells is divided into two terms : the first one is the solar radiation absorbed by the cells after being passed through the glass and the second one is the PV power produced by square meter of the PV module area. It can be written as:

$$(16) \quad \phi_2 = \frac{\alpha_{pv} \times \tau_{fg} \times \phi_{solar} \times A - P_{pv}}{A} = \alpha_{pv} \times \tau_{fg} \times \phi_{solar} - \frac{P_{pv}}{A}$$

with  $\alpha_{pv}$  the absorption coefficient of the PV cells and  $\tau_{fg}$  the transmittance of the glass.

In practice, the absorptivity and the transmittance of the glass are not constant because they are dependent on sun position, with a 20-30% reduction at small values of incident radiation (sunset and sunrise) [18]. In our study, we used a method often applied in the solar collector modelling. This method doesn't allow one to determine  $\tau_{fg}$

and  $\tau_{fg} \times \alpha_{pv}$  but to calculate the expressions  $\alpha_{fg} \times \phi_{solar}$  and  $\alpha_{pv} \times \tau_{fg} \times \phi_{solar}$  [2].

The output energy flux corresponds to the electrical power produced by the PV cells. To model such a PV electrical power, we used an energy model using the PV cells efficiency by :

$$(17) \quad P_{pv} = \eta \phi_{solar} A$$

For the efficiency calculation, we used :

$$(18) \quad \eta = \eta_{ref} \left[ 1 - \beta_0 (T_{pv} - T_{ref}) + \gamma \text{Log} \phi_{solar} \right]$$

where  $\eta_{ref}$  is the reference module efficiency at a PV cell temperature  $T_{ref}$  of 25°C and at a solar irradiance  $\phi_{solar}$  equal to 1000 W.m<sup>-2</sup>.  $\gamma$  and  $\beta_0$  are respectively the solar irradiance and temperature coefficients for the PV module.  $T_{pv}$  is the PV cell temperature which depends on the environmental conditions. These parameters ( $T_{ref}, \eta_{ref}, \beta_0, \gamma$ ) are given by the PV manufacturer, but  $\gamma$  and  $\beta_0$  depend on the material used for the PV module. Several authors suggest to use for the Si  $\beta_0 = 0.0048^\circ\text{C}^{-1}$ . Most often this equation is seen with  $\gamma = 0$ . This equation has been validated in a previous work [8]. According to Photowatt, the reference efficiency of the PV modules used in this study is 13%.

### Method of solution.

All the energy balances can be written in the guise of a differential matrix equation :

$$(19) \quad [C] \frac{d\vec{T}(t)}{dt} = [M] \vec{T}(t) + [S] \vec{E}(t)$$

$\vec{T}(t)$  is a vector containing system temperatures at the 7 nodes of the mesh, [C] is a diagonal matrix (dimension: 7) with all the values of the thermal capacities of the material, [M] is a squared matrix (dimension: 7x7) with all the heat exchange coefficients between the elements of the mesh, [S] is a matrix (dimension: 7x5) which joins together the 5 input physical parameters (or excitations) expressed by the vector  $\vec{E}(t)$  ( $\phi_{solar}, I_b, T_{gro}, T_a, T_{sky}$ ) and 7 elements of the mesh. By solving the equations of this analogical model, we get directly the expression of the temperature for each node of the model in function at the input parameters. This equation system is solved by the Dormand-Prince method corresponding to a Runge Kutta Merson's method (order 4).

### Matlab/Simulink<sup>®</sup> Simulation

MATLAB and Simulink form the core environment for a Model-Based Design to create accurate mathematical models of physical system behavior. To effectively design a system and accurately predict its performance, designers must understand the behavior of the entire system. The graphical, block-diagram paradigm of the MathWorks environment lets us drag-and-drop predefined modeling elements, connect them together, and create models of dynamic systems. These dynamic systems can be

continuous-time, multi-rate discrete-time, or virtually any combination of the three. We can create custom model elements or reuse legacy code-based models by incorporating C, Fortran, or Ada code directly into the modeling environment.

On Fig.5, we see the bloc diagram structure of the PV/T collector model. Each bloc is a special function:

- 1 and 2 : meteorological data
- 3 and 4 : fluid parameter (input temperature, flow rate)
- 5 is the vector  $\vec{E}(t)$  (Eq. 19.) by coupling the blocs 1 and 2
- 6 is the matrix [C];
- 7 and 8 are respectively the matrix [M] and [S].

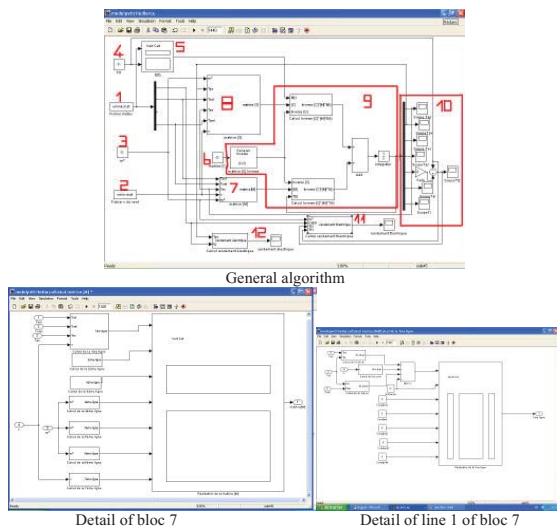


Fig. 5. Bloc diagrams Structure of the PV/T solar collector with Matlab/Simulink®.

## Results

Measured meteorological data have been used and have been introduced in Bloc Diagram 1 and 2; these data (wind speed and direction, direct and global solar radiations, ambient temperature) are collected with a time step equal to 1 minute but this time step can be modified.

The objective of this paper is to show the adaptability of Matlab/Simulink to our modelling and not to show the performance of our PV/T collector; it will be a future work that he is in progress and will be published later.

We chose a flow rate equal to  $5.10^{-3}$  kg/s according to a previous work [20] and the solar collector is in opened-loop. This configuration is not very realistic but it is the first stage of a complete study of the performance of the PV/T solar collector. The input water temperature has been taken constant depending on the month. As an example, for April, the input water temperature  $T_{fl}$  is 14°C. The global solar irradiance and ambient temperature of the April, 26 2005 in Ajaccio is shown on Fig. 6 as these data appear on the screen of the computer

From these data, the results of the calculation of the various temperatures have been computed using Matlab/Simulink, the temperatures of the seven various

part of the PV/T solar collector shown on Fig. 4 are calculated (upper glass of the PV module, p-Si cells, Lower glass, absorber, water fluid, insulation and body). An illustration is shown on Fig. 7 for the April, 26.

In the same conditions, it is possible to calculate the performances of the system in calculating the electrical or thermal efficiency. As an example, we plotted on Fig. 8 the evolution of the electrical efficiency during the same day.

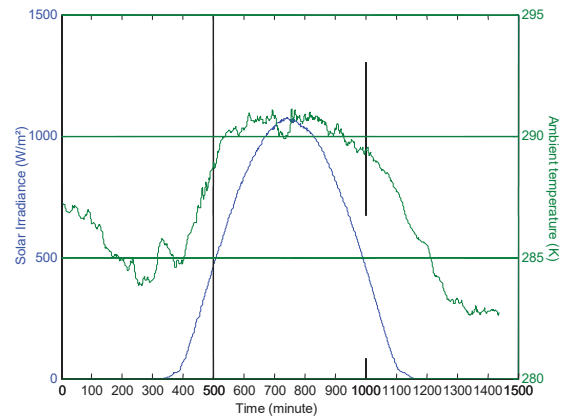


Fig. 6. Meteorological conditions (total solar irradiance and ambient temperature) for the April, 21.

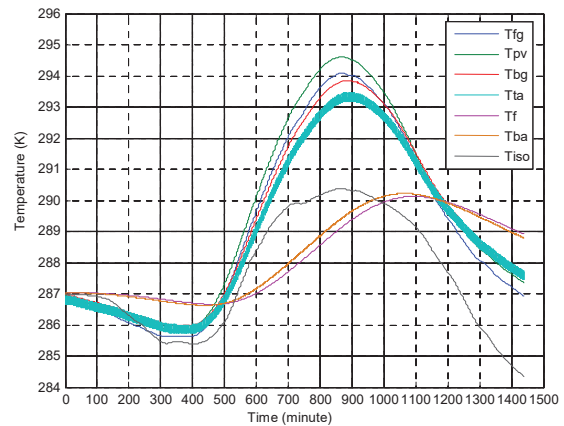


Fig. 7. Evolution of the seven temperatures of the PV/T solar collector.

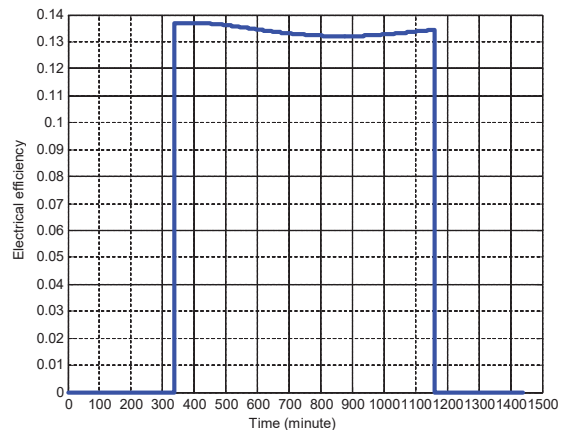


Fig. 8. Evolution of the electrical efficiency.



This solar collector has not a cover and consequently there is no green effect but adding a cover is easily realizable because it is only necessary to add a node in our modelization. But, if you want to change the characteristics, the software used is very well adapted; as an example, we changed the material of the absorber, replacing the polycarbonate by copper. The results are quite similar but the thermal conductivity is higher and the difference of temperatures between the two part of the absorber is very low reducing also the temperature of the PV cell and improving its efficiency.

## Conclusion

The Matlab/Simulink<sup>®</sup> is very practical software for the simulation elaborated in our work and to estimate the performance of the system. This technique can be transposable to other PV/T solar collector configurations. We can easily determine the best configuration and material for each part of the solar collector and thus improve its performances.

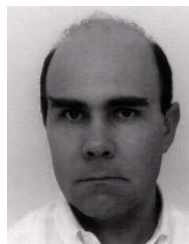
## References

- [1] Zondag H.A., D.W. De Vrie, W.G.J. Van Helden, R.J.C Van Zolingen, A.A. Van Steenhoven. *Solar Energy* 72-2, 2002, p.113.
- [2] Sandnes B., J. Rekestad., *Solar Energy* 72-1 (2002) 63.
- [3] C. Graf , A. Vath, N.Nicoloso. *J. Power Sources*, 155, 2006, p. 52.
- [4] Skrijanc I., B. Zupan, B. Furlan, A. Krainer. *Building and Environment* 36, 2001, p. 1023.
- [5] Hedström L., C. Wallmark, P. Alvfors, M. Rissanen, B. Stridh, J. Ekman. *J.Power Sources* 131, 2004, p.340.
- [6] Maclay J.D., J. Brouwer, G. Scott Samuelsen. *Int. J. Hydrogen Energy* 31, 2006, p. 994.
- [7] Van Niekerk W.M.K., C.G. du Toit, T.B. Scheffler. *Solar Energy* 58, 1996, p.39.
- [8] Notton G., C. Cristofari, M. Mattei., P. Poggi.. *Applied Thermal Engineering* 25, 2005, 2854.
- [9] Rosell J.L., X. Vallverdú, M.A. Lechón, M. Ibáñez. *Energy Convers.Manag.* 46, 2005, p. 3034.
- [10] Zondag H.A., D.W. De Vrie, W.G.J. Van Helden, R.J.C. Van Zolingen. *Solar Energy* 74, 2003, p.253.
- [11] Cristofari C., G. Notton, P. Poggi, A. Louche, *Solar Energy* 72-2, 2002, p. 99.
- [12] Chow T.T.. *Solar Energy* 75, 2003, p. 143.
- [13] Jie J., T.T. Chow, H. Wei. *Build. and Envir.* 38, 2003, p.1327.
- [14] Coventry J.S.. *Proceeding of Solar 2002. Australian and New Zealand Solar Energy Society*, 2002.
- [15] Tsilingiris P.T.. *Solar Energy* 60-5, 1997, p. 245.
- [16] Cole R.J., N.S. Sturrock. *Build. and Envir.* 12, 1977, p. 207.
- [17] Lévêque M.A.. *Les lois de transmission de chaleur par convection. Annal. Mines Mem.* 13, 1982, p. 201.
- [18] Schott T.. 6th PVSEC Conference, 1985, p. 392.
- [19] Swinbank W.C.. *Quarterly Journal of the Royal Meteorological Society* 89, 1963, p. 339.
- [20] Cristofari C., G. Notton, P. Poggi, A. Louche. *Int. J. Thermal Sciences* 42-5, 2003, p. 455.

## Biographies



**Gilles Notton** was born in Saint Avold, France, on January 23, 1964. He studied at the University of Corsica and received Dr. degree in 1992 and Research Agreement in 2002 from the same university His field of interest includes renewable energy systems and renewable sources. He is today assistant professor and responsible of the French Research ADEME network between France and Oriental and Central European Countries. Gilles Notton is with the Research Centre of Vignola, University of Corsica, UMR CNRS 6134, route des Sanguinaires, F20000 Ajaccio, France (e-mail: gilles.notton@univ-corse.fr).



**Nicolas Héraud** was born in France on september 15, 1962. He received his Ph.D. degree in Automatic and Electrical Engineering from Institut National Polytechnique de Lorraine in 1991. Since 1992, he teaches at the University of Corse as professor and he is at the CNRS (UMR 6134). His field of interest includes data reconciliation and process diagnosis on renewable energy systems. (email: heraud@univ-corse.fr)



**Christian Cristofari** was born in Ajaccio on July 19, 1966. His field of interest includes solar radiation, renewable hybrid systems and thermal solar systems. He is today assistant professor and is director of the Technology University Institute of Corsica. He was Engineer (1994-1998), Director of Technology incubator (1998-2002). (email :Christian.cristofari@iut.univ-corse.fr)



**Ahmed Houssein** was born in Djibouti, holder of Master of Research in Electronics, is currently PhD student in applied automatics for renewable energies. He teaches at the Djibouti University in alternation between the Djibouti University and the Corsica University UMR 6134 CNRS.(email:, houssein@univ-corse.fr).



**Mohamed Ainan Kahyeh** was born in Djibouti on January 15, 1971, he's actually PhD Student in Automatic Control and Renewable energy in sandwich model between Università di Corsica and University of Djibouti after several years of works in industrial field. Since 1999, he's the head of the maintenance department in Boulaos Power Plant (Djibouti) and part-time teacher at the Institute of Technology in Djibouti (University of Djibouti). He was graduated in 1996 in Electrical Engineering in the Ecole Nationale d'Ingénieurs de Sfax (Tunisia).He obtained a Master degree of Business Administration in 2004 in the University of Poitiers (France).

# Current State of Research and Industrial Application of Biogas Technologies in Bulgaria

Ivan Simeonov, Ludmil Nikolov, Danka Galabova and Elena Chorukova

**Abstract:** In this paper the Bulgarian experience in the field of biogas production from organic wastes is presented. The industrial experience consists mainly of two biogas plants worked in the late 80<sup>th</sup> of the 20<sup>th</sup> century.

In the paper the attention is pointed out on the scientific results in this field of a multidisciplinary team of the Stephan Angeloff Institute of microbiology of the Bulgarian Academy of Sciences. These results are summarized from a lot of published paper. Some new achievements are presented as well.

**Keywords:** organic wastes, anaerobic digestion, biogas, methane, energy

## I. Introduction

Anaerobic digestion (AD) is an effective biotechnological process for treatment of different agricultural, municipal and industrial wastes [1,2]. It combines environmental depollution (ecological aspect) with production of renewable energy – biogas, which main component is methane (energetical aspect).

The paper has the goal to:

1. Summarize Bulgarian industrial-scale experience in the field of biogas and biogas technologies and the current state concerning the total number of animals, quantity of manure and potential amount of biogas production in Bulgaria.

2. Represent the long-year scientific research of a multidisciplinary team of the Institute of Microbiology of the Bulgarian Academy of Sciences over the process of AD of organic wastes (single and mixtures) by studying the influence of some appropriate stimulating substances and surfactants at different stages of the AD, as well as developing new models and algorithms in order to optimize and control it.

## II. Industrial experience

### 2.1. Podgumer biogas plant

Due to the high pollution of the river Iskar area by big cattle farms, an experimental industrial-scale biogas plant construction in the village of Podgumer (near Sofia) started by government decision in 1982 with the following parameters: treating dung from 5 000 heads of cattle; two methane tanks of 1 500 m<sup>3</sup>; two gas holders of 500 m<sup>3</sup>; two boilers heating 650 dm<sup>3</sup> water /hour; incoming organic waste per day - 141 m<sup>3</sup>; dry matter content - 9-13%; hydrolytic retention time - 22 days; mesophilic process; daily biogas production – 2 000 m<sup>3</sup>; biogas utilization for thermal energy production (hay drying in summer); producing manure for 400 hectares. The period of

operation of this biogas plant was 1986 - 1990 (in 1991 the farm was closed down).

### 2.2. Biala Rada biogas plant

This biogas plant started operation in August 1989 near a big swine farm. Biogas from a 1 500 m<sup>3</sup> methane tank was used for hot water. The period of operation of this biogas plant was only 1 year (in 1991 the farm was closed down).

In our days there are no biogas plants in operation in Bulgaria.

### 2.3. Biogas from sewage treatment plants

Nowadays 38 plants with possibility for anaerobic treatment of the activated sludge (only 2 ones with operating methane tanks) are in operation in Bulgaria and about 32 plants are under construction.

## III. Scientific research

### 3.1. Laboratory equipment at the Institute of Microbiology

Five “pseudohomogeneous” anaerobic continuously stirred tank bioreactors (CSTBR) were used in the run of the investigation with full volumes: one of 20 dm<sup>3</sup>, two of 3 dm<sup>3</sup> and two of 2 dm<sup>3</sup>. A new anaerobic biofilm bioreactor (working volume of 1.4 dm<sup>3</sup>) has been developed. All reactors are equipped with automatic control systems to maintain mesophilic conditions (temperature 34±0.5°C) and shielded against light. To measure the volume of the obtained biogas, every bioreactor was provided with a water-displacement gasholder.

### 3.2. Materials

For the purpose of the study, the following materials were used as substrates (separately and in mixtures): activated sludge (AS) from the Sofia Municipal Wastewater Treatment Plant; cattle dung; pig's dung, poultry litter, milk whey.

**Surfactants.** The surfactants used in this study were the biosurfactant produced by *Pseudomonas* sp. S-17 and chemical surfactant Triton X-100 (scintillation grade) purchased from Kochlight Laboratories Ltd.

**Chemicals.** All chemicals for the analyses were analytical grade and were obtained from commercial sources.

### 3.3. Methods

**pH** was measured by Seibold pH-meter Type G 104 equipped with Ingold 465 combined pH-electrode.

CH<sub>4</sub> and CO<sub>2</sub> in the biogas have been measured with Drager X-am 7000 (DragerSensor Smart IR Ex-68 10 460).

Chemical oxygen demand (COD) was determined by means of the Open Reflux Method according to the APHA Standard Methods of Examination of Water and Wastewater.

Biological oxygen demand (BOD<sub>5</sub>) was determined by standard method and specialized device for oxygen concentration measurement.

The volatile fatty acids (VFA) and the ratio VFA/bicarbonate alkalinity were determined according to the Ripley method.

### 3.4. Results and discussion

#### 3.4.1. AD of a single substrate

##### 3.4.1.1. AD of cattle dung [3]

Laboratory experiments in “pseudohomogeneous” CSTBR with cattle dung (working volume of 2 dm<sup>3</sup>) have been made with step-wise changes of the input action  $D_1$  as shown on Table 1. The biogas production  $Q$  is shown on Fig. 1.

**Table 1**

Input step-wise changes for the biogas production shown on Fig. 1

Day	$D_1$ [day <sup>-1</sup> ]
1 - 18	0.05
19 - 56	0.025
57 - 75	0.075
76 - 90	0.1
91 - 120	0.125
121 - 132	0.025

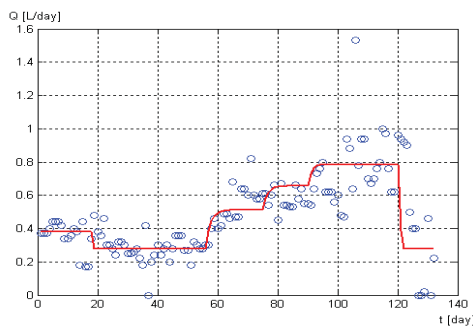


Fig.1. Biogas production  $Q$  in laboratory “pseudohomogeneous” CSTBR with cattle dung for step-wise changes of the input action  $D_1$  from Table 1

On Fig. 2 the start-up of the anaerobic biofilm bioreactor with cattle dung (working volume of 1.4 dm<sup>3</sup>) is presented, where  $Q$  is the produced biogas flow rate and  $F$  is the volume of the influent/effluent flow of liquid.

It is evident that the specific biogas production in the second case is greater than in the first.

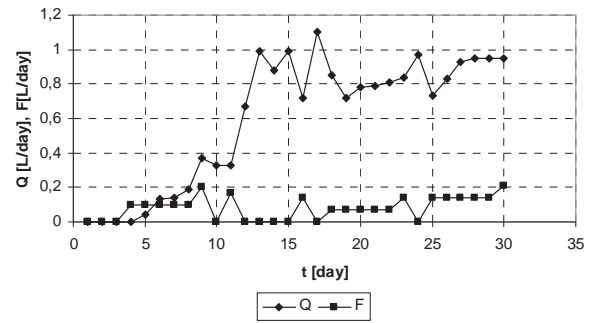


Fig. 2. Start-up of anaerobic biofilm bioreactor with cattle dung

##### 3.4.1.2. AD of swine dung

Laboratory experiments in “pseudohomogeneous” CSTBR with swine dung (working volume of 2 dm<sup>3</sup>) have been made. The start-up of the bioreactor in this case is shown on Fig. 3, where  $Q$  is the production rate of biogas with the indicated methane (CH<sub>4</sub>) and carbon dioxide (CO<sub>2</sub>) content.

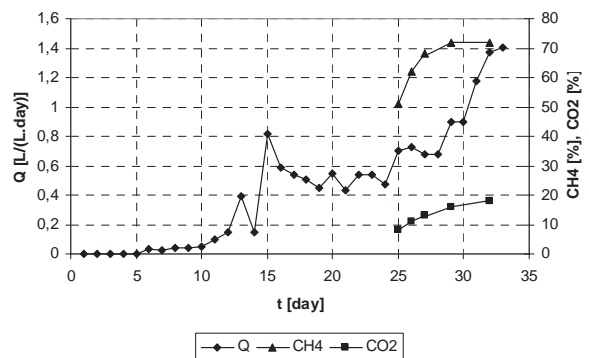


Fig. 3. Start-up of CSTBR with swine dung.

##### 3.4.1.3. AD of poultry litter [4]

Laboratory experiments in “pseudohomogeneous” CSTBR with poultry litter (working volume of 1 dm<sup>3</sup>) have been made for step-wise changes of the input action  $D_1$  (Fig. 4).

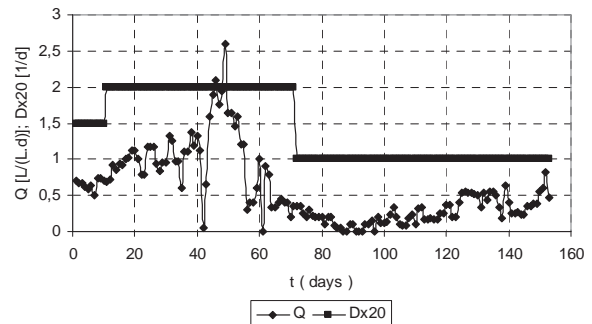


Fig. 4. Anaerobic bioreactor with poultry litter

In the case of AD of poultry litter some instability occurs.

### 3.4.1.3. AD of activated sludge in a cascade of two bioreactors

Laboratory experiments are carried out in a cascade of two anaerobic bioreactors (Fig. 5) with step-wise changes of the input action  $D$  [5] and of the dry weight concentration of the influent activated sludge for the BR 1 (Fig. 6 and 7).

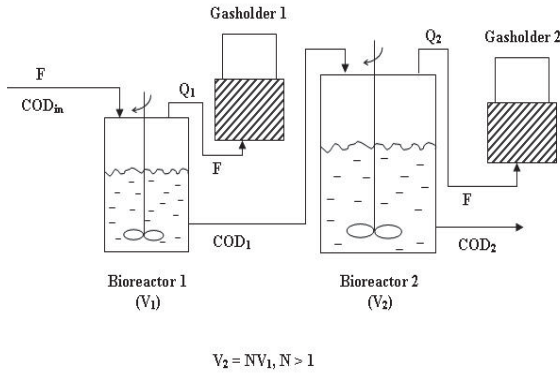


Fig. 5. Principle scheme of a cascade of two anaerobic bioreactors

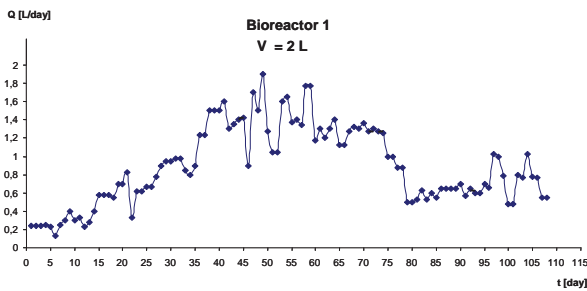


Fig. 6. Biogas yield from BR 1 (with working volume of  $2 \text{ dm}^3$ ) in the case of step-wise changes of  $D$  (from 0.025 to 0.075 in  $5^{\text{th}}$  day) and of the dry weight concentration (see Table 2) of influent activated sludge

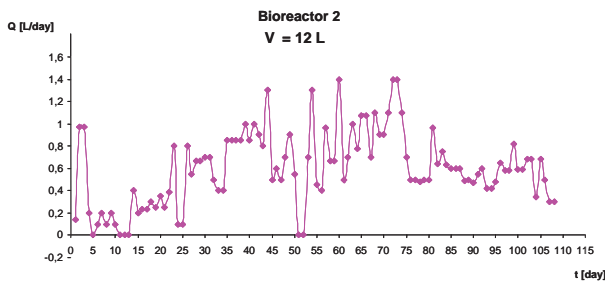


Fig. 7. Biogas yield from BR 2 (with working volume of  $14 \text{ dm}^3$ ) in the case of variations of  $D$  (from 0.00357 to 0.0107 in  $5^{\text{th}}$  day) and of the dry weight concentration of the influent activated sludge for the BR 1

The overall biogas production in this case is greater than in the case of a single bioreactor.

The contents of  $\text{CH}_4$  (maximal) and  $\text{CO}_2$  in the biogas obtained from single substrates are shown in Table 3.

Table 2  
Dry weight concentration of influent activated sludge

Days	Dry weight
6-15	7.3 %
16-39	10 %
40-55	8 %
6-73	7.5 %
74-83	4 %
84-112	4.1 %

Table 3  
Contents of  $\text{CH}_4$  and  $\text{CO}_2$  in the biogas

Substrate	$\text{CH}_4$ [%]	$\text{CO}_2$ [%]
Cattle dung	82	16
Swine dung	68	1,8
Poultry litter	71	18
Activated sludge	68	15

On the basis of the obtained maximal content of  $\text{CH}_4$  in the biogas produced from different wastes (Table 3) the equivalent production of electrical (E) or thermal (Q) energy from  $1 \text{ m}^3$  of biogas are calculated [6] (see Table 4).

Table 4  
Production of electrical or thermal energy

Waste	E, kWh/ $\text{m}^3$ $\eta_{\text{en}}=0,36$	Q, MJ/ $\text{m}^3$ $\eta_{\text{ron}}=0,9$
Cattle dung	2,738	24,264
Swine dung	2,269	20,421
Poultry litter	2,369	21,321
Activated sludge	2,269	20,421

### 3.4.2. AD of a mixture of two substrates [7]

AD of mixtures of different substrates is a new trend in biogas production. It gives the possibilities to stimulate the AD of some not so easy susceptible to this process materials by mixing them with others which are easier degradable. On Fig. 8 some results of AD of a mixture of cattle dung and milk whey in different ratios are shown. The increase in the content of whey up to 75% in the mixture leads to an increase of the biogas yield, and content of 75% - 90% leads to a dramatic drop in the daily biogas production  $Q$ . The tendency to stimulation of the process with up to 75% whey in the mixture and the inhibition with up to 90% is observable in the changes of COD as well. It is obvious that there is a correlation between the higher jump in the whey content, the peak in the VFA and the drop in the biogas yield between days 80 and 160. After reverting to previous lower whey content (50%), a recover in the process is observable.

On Fig. 9 some results of the process of anaerobic digestion of a mixture of waste from industrial alcohol production and cattle dung are shown. The addition of waste of 20 % causes unstable increase in the biogas yield. A higher increase in  $Q$  is observable at waste content of 40% in the mixture. At this value of the ratio waste/cattle dung the biogas yield is more stable as well.



Above this content of waste, the biogas yield decreases and the process becomes more unstable.

A static map for the biogas production from mixtures of two substrates is shown on Fig. 10.

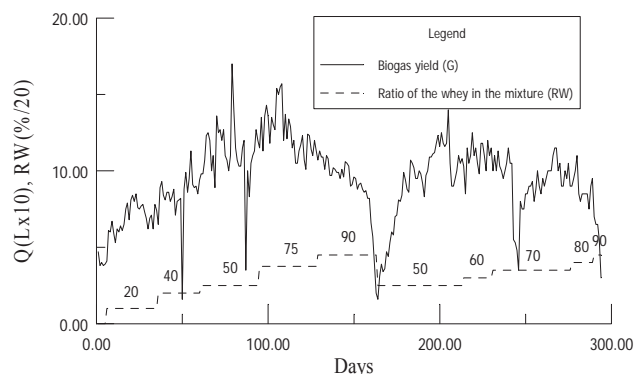


Fig. 8. AD of a mixture of cattle dung and milk whey in different ratios

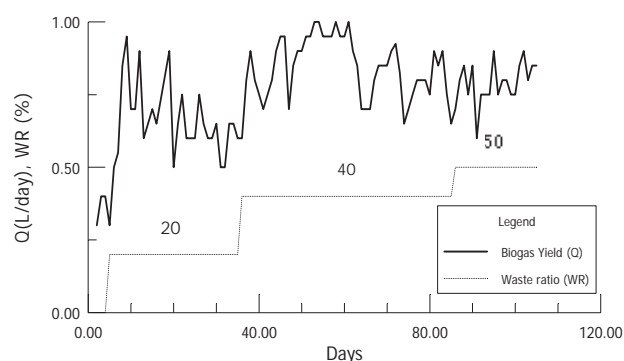


Fig. 9. AD of a mixture of waste from industrial alcohol production and cattle dung

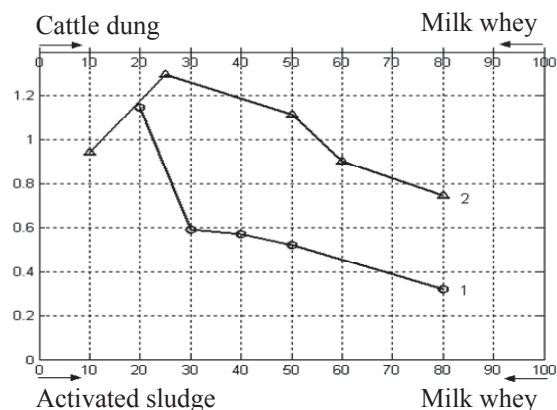


Fig. 10. Biogas production with two-component mixtures (1 – mixture “activated sludge – milk whey”, 2 – mixture “cattle dung – milk whey”)

Table 5

Biogas production and COD for a cascade of two bioreactors

$D_1$ (day <sup>-1</sup> )	$Q_1$ (L/day)	COD <sub>1</sub> (gO/L)	$D_2$ (day <sup>-1</sup> )	$Q_2$ (L/day)	COD <sub>2</sub> (gO/L)
0.025	0.46	2.2	0.004	0.2	0.8
0.05	1.0	2.76	0.008	0.25	0.92

Laboratory experiments are carried out in a cascade of two anaerobic bioreactors with mixture of sludge (70 %) and milk whey (30 %) with COD = 10.2 (gO/L) at mesophilic temperature of 34 °C. As an example some results are shown in Table 5 [8].

### 3.4.4. AD of a mixture of three substrates [7]

A static map for the biogas production from mixtures of three substrates is shown on Fig. 11. A clear maximum for the biogas production exists for an appropriate ratio of the different substrates.

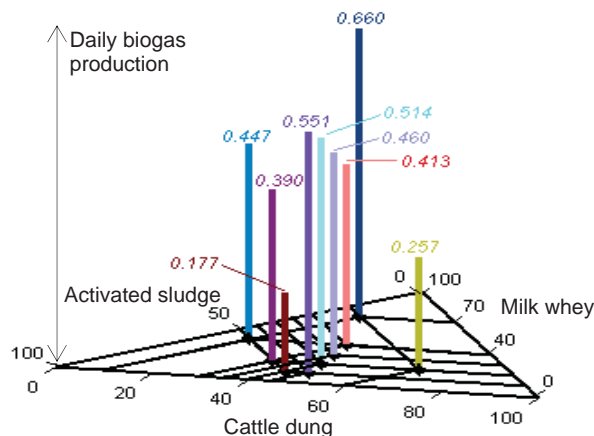


Fig. 11. Daily biogas production  $Q$  [ $\text{dm}^3 \cdot \text{day}^{-1}$ ] for a mixture of three substrates ( $D = 0.0025 \text{ day}^{-1}$ )

### 3.4.5. The effect of some surfactants on the process

The effects of a biosurfactant from *Pseudomonas sp.* and the chemical surfactant Triton X-100 on the growth and cell surface permeability of aerobic and anaerobic bacteria isolated from a laboratory bioreactor (1 dm<sup>3</sup> working volume,  $t=34$  °C, pH=6.8, fed once daily) digesting cattle dung with 16 g COD/L were studied. Microbial growth (followed by changes in OD570 of the cultures) and the cell surface permeability (according to the amount of the extracellular protein) were determined in the absence and presence of the two surfactants: biosurfactant (0.06 %) and Triton X-100 (0.05%).

The obtained results showed that the action of both surfactants on the aerobic and on the anaerobic isolates was different. They stimulated the growth of the anaerobes and the extracellular metabolite transport of the aerobes. These effects could be explained with the fact that the surfactants promoted cell surface changes leading to intensifying the effect of two surfactants with different origin, biosurfactant-rhamnolipid from intracellular and extracellular membrane transport of biologically active compounds.

### 3.4.6. Modelling and optimization of the AD

Deterministic and ANN models have been developed on the basis of these laboratory experimental data [8, 10-13].

Static input-output characteristics  $Q = f(D)$  present a clear maximum for the biogas production  $Q$  for appropriate value of the dilution rate  $D$  for all AD mathematical models, as shown on Fig. 12 [9, 12]. Different control and optimization algorithms based on mathematical models of the AD have been developed [8, 14].

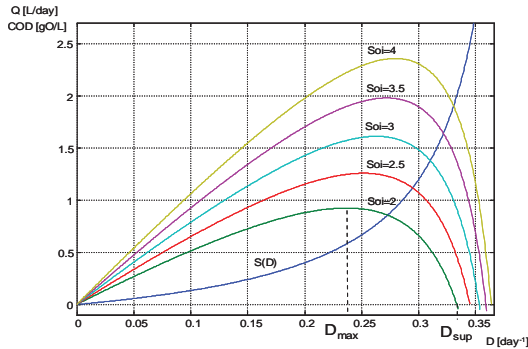


Fig. 12. Static input-output characteristics for all AD mathematical models

Some results from training of an ANN model [10] with input  $D_1$  and output  $Q$  are shown on Fig.1, where real experimental data for the reaction of the output ( $Q_{exp}$ ) on the input action from Table 1 are presented with circles and the predictive neural model output ( $Q_m$ ) for the same input action - with continuous line.

The neural model  $D_1$ - $Q$  possesses as good approximating properties as the appropriate deterministic model of [16], however its design is much easier.

An ANN model for the cascade of two anaerobic bioreactors working with mixture of sludge (70 %) and milk whey (30 %) has been developed [11]. Validation of the neural model has been made with real experimental data. The results are shown on Fig. 13 for BR1 and on Fig. 14 for BR2. The described neural model could be used as one-step-ahead predictor of the biogas flow rates in both bioreactors for different dilution rates.

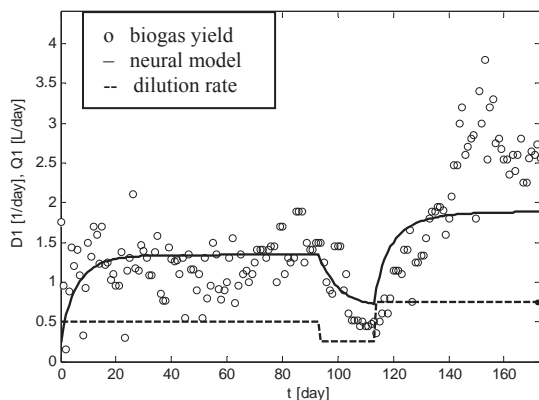


Fig. 13. Real data  $Q_{1exp}$ , neural model output  $Q_1$  and input action  $D_1$  for BR 1

#### IV. Current state

Some information concerning the total number of animals, total quantity of manure and potential amount of

biogas production in Bulgaria are shown in Table 6 and Table 7.

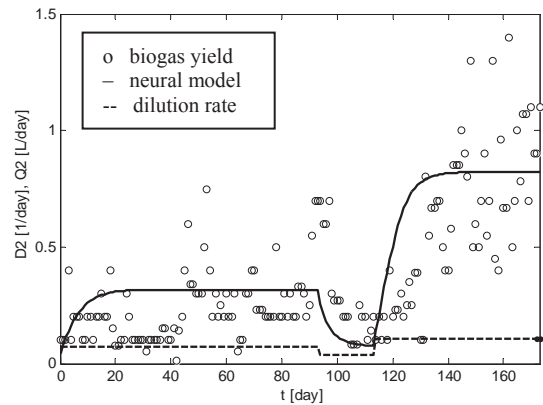


Fig. 14. Real data  $Q_{2exp}$ , neural model output  $Q_2$  and input action  $D_2$  for BR 2

Table 6

Total number of animals

Type of animals	Total number for the country (in thousands)	Note
Total livestock	633,2	Towards 01.05.2006
Total swine	956,2	Towards 01.05.2006
Total poultry	17 204,5	Towards 31.12.2006
Total buffalo cows	8	Towards 01.05.2006

Table 7

Total quantity of manure production

Manure's producer	Production (ton/year)	Potential biogas production (million m <sup>3</sup> )
Cattle	10 063 671	161
Swine	1 354 132	25,7
Poultry	1 314 684,5	30,2
<b>Total</b>	<b>12 732 487</b>	<b>219,9</b>

Analysing the above presented tables, one may conclude that the AD technologies are in a good position for resolving some ecological and energy problems for Bulgaria.

#### V. Conclusion

Summarizing our scientific results the main conclusion is that the anaerobic co-digestion of different organic wastes (in optimal ratio) presents a very promising way for sensible increasing of the efficiency of the AD. For high amount of biogas production and process stabilization industrial automatic control and real time optimization systems will be very useful.

Very promising perspectives for biogas production exist in Bulgaria in the context of the EU policy in the

field of renewable energy sources. However national strategy and support from governmental authorities are necessary. The former industrial experience and the scientific results described above are a good basis for the elaboration of a Bulgarian National program "Biogas and biogas technologies".

### Acknowledgements

This work was supported by contract No D 01-376/06 of the Bulgarian National Science Fund.

### References

- [1] Price E. C., P. N. Cheremisinoff, Biogas production and utilisation, Ann Arbor Science Publishers, Michigan, 1981.
- [2] Dubrovskis V., V.Viesturs, Anaerobic digestion of agricultural wastes, Zinatne, Riga, 1988 (in Russian).
- [3] Simeonov I., S. Mihajlova, A. Mirkov, I. Petkov, E. Chorukova, Biogas production from organic wastes in laboratory pseudohomogeneous bioreactors, Ecological Engineering and Environment Protection, 2, 2007, 23-32 (in Bulgarian).
- [4] Simeonov I., Y. Petkov, B. Baykov, S. Mihajlova, A.Mirkov, Laboratory studies upon biogaz production from poultry litter, Ecological Engineering and Environment Protection, 3-4, 2006, 88-97 (in Bulgarian).
- [5] Simeonov I., D. Galabova, S. Mihajlova, A. Mirkov, B. Kalchev, Anaerobic digestion of organic wastes in a cascade of bioreactors, Ecological Engineering and Environment Protection, 3-4, 2007, 56-64 (in Bulgarian).
- [6] Bonev B. I., T. I. Totev, Burning of energetical fuels, IK „Kota”, Sofia, 2002 (in Bulgarian).
- [7] Nikolov L., I. Simeonov, D. Karakashev, E. Chorukova, D. Galabova, Anaerobic digestion of complex mixture of organic wastes, Engineering and Environment Protection, 3, 2004, 42-52 (in Bulgarian).
- [8] Simeonov H., S. Stoyanov, Modelling and extremum seeking control of a cascade of two anaerobic bioreactors, Proc. of the 16<sup>th</sup> Int. Conf. on Control Systems and Computer Science, Bucharest, 22-25 May 2007, on CD.
- [9] Simeonov I., S. Yordanov, Analysis of nonlinear dynamical models of the anaerobic degradation of organic wastes, Journal of the technical University of Gabrovo, Vol. 35, 2007, 51-56.
- [10] Simeonov I., E. Chorukova, Anaerobic digestion modelling with artificial neural networks, C.R. de BAS, Tome 61, No 4, 2008, pp.505-512
- [11] Chorukova E., I. Simeonov, Neural model of the anaerobic digestion process in a cascade of two bioreactors, Proc. of the Int. Conf. "Automatics and Informatics'07", Sofia, 03-06.10.2007, Vol. II, III-43-46.
- [12] Simeonov I., Mathematical modeling and parameters estimation of anaerobic fermentation process, Bioprocess Engineering, Vol. 21, No 4, 1999, 377-381.
- [13] Simeonov I., D.Galabova and I.Queinnec, Investigations and mathematical modelling of the anaerobic digestion of organic wastes with addition of electron acceptors, Proc. 9th Word Congress "Anaerobic Digestion 2001", Antwerpen, Sept. 2-5, 2001, 381-383.
- [14] Simeonov I, N. Noykova, S. Stoyanov (2004). Modelling and extremum seeking control of the anaerobic digestion,

IFAC workshop DECOM-TT, Bansko (Bulgaria) Oct. 3-5, 2004, 289-294.



**Ivan Simeonov** was born in Dermantzi, Bulgaria, on January 28, 1948. He studied at the Technical University of Sofia-Bulgaria and received PhD degree from the same university in 1981.

Since 1981 he worked in the Bulgarian Academy of Sciences as a researcher and senior research associate (since 1886) in the field of Bioautomatics and Biotechnologies. He was Assoc. Prof. in the Technical University of Sofia, the Technical University

of Gabrovo and the New Bulgarian University

At present **Ivan Simeonov** is the Head of the research group "Mathematical Modeling and Computer Science" of the "St. Angeloff", Institute of Microbiology Bulgarian Academy of Sciences, Acad.G. Bonchev St., Block 26, Sofia 1113, Bulgaria (E-mail: [ISSIM@microbio.bas.bg](mailto:ISSIM@microbio.bas.bg)).



Elena **Chorukova** was born in Kostenetz, Bulgaria, on April 19, 1971. She received the MSc degree in Bioengineering from the Technical University of Sofia, Bulgaria, in 1994. Since 2000 she has been a Research Associate at the Bulgarian Academy of Sciences, in the research group "Mathematical Modeling and Computer Science" of the "Stephan Angeloff" Institute of Microbiology, Acad.G. Bonchev St., Block 26, Sofia 1113, Bulgaria (E-mail: [elena@microbio.bas.bg](mailto:elena@microbio.bas.bg)).



**Danka Galabova**, Associate Professor in Institute of Microbiology, BAS. **Education:** M.Sc., Chemistry, University of Sofia, Sofia; Ph.D. in Biology, Bulgarian Academy of Sciences. Postdoctoral positions in the Department of Chemistry and Applied Chemistry of University of Salford, England, and in the Department of Biology, University of South Carolina, USA.

**Professional Experience:** Head of the Department of Microbial Biochemistry, Institute of Microbiology - BAS. Coordinator of projects supported by National Science Foundation, Ministry of Education and Sciences. National Co-ordinator of INCO-COPERNICUS Project (Contract No ICOP-DEMO 2023). Over 80 refereed scientific papers in the fields of physiology and biochemistry of bacteria and yeasts, microbial enzymes, bioremediation of oil- and metal- contaminated sites, surface-active compounds, biochemistry and microbiology of anaerobic digestion. (e-mail: [dgal@microbio.bas.bg](mailto:dgal@microbio.bas.bg))



**Ludmil Nikolov**, Associate Professor in Sofia University. **Education:** Dipl. Eng. (1968) and Ph.D (1971), Chemical Engineering, St. Petersburg Technological Institute, Russia.

**Professional experience:** Head of the Laboratory of Bioprocess Systems of Biological Faculty of Sofia University. Visiting professor in Lyonnaise des Eaux, France; Department of Chemical Engineering and Bioprocess Engineering, University of Amsterdam; International Center of Biotechnology, Osaka University, Japan. Chief Expert of Biotechnology, National Association of Biotechnology and Chemistry of Bulgaria; Deputy Director of the National Research Centre of Biotechnology under the State Committee for Science and Technical Progress and Bulgarian Academy of Science. National co-ordinator of international projects DP/BUL/004/ and DP/BUL/007/ under the aegis of United Nations Development Program (UNDP). Over 90 refereed scientific papers, patents and contracts with industry in the fields of Chemical Process Modelling, Environmental Protection and Bioreactor Systems Modelling.

# Comparison of Energy Conversion Systems for Variable Speed Wind Turbine Application

Daniel Roye, Vladimir Lazarov, Dimitar Spirov, Ludmil Stoyanov

**Abstract:** This paper proposes a study and comparison of two different concepts for variable speed wind turbine generation systems. The first concept consists of synchronous generator and back-to-back voltage source converter (VSC), while the second concept comprises a synchronous generator, a diode rectifier, a DC chopper and an inverter. Dynamic models and control schemes of each element are performed. To verify the models presented and to analyze the dynamic behavior simulations with MATLAB/Simulink software have been conducted. Simulations results prove the validity of the models and control schemes.

**Keywords:** wind energy system, synchronous generator, voltage source converter, diode rectifier, DC chopper, modeling, and simulation.

## Introduction

In recent years, there has been an important development of wind energy conversion systems (WECS). In fact, at present, wind energy is the most promising alternative to the traditional energy sources and competitive energy source. With its inexhaustible potential and without any significant negative environmental impacts, wind generation is an appropriate and accessible technology for sustainable economic growth and development. Thus, the investigation of whole wind energy conversion chains, e.g. wind power extraction, mechanical conversion, electrical production and transformation, grid integration, is an important in order to understand and improve the quality of the wind turbine generation system.

There are two principal concepts of wind conversion, namely fixed-speed wind generation and variable speed wind generation. These two concepts have determined the emergence of a number of different configurations of WECS which are in use today. These could be categorized according to their mechanical and electrical components. As regards to the electrical part, the wind power plants are separated by the type of electrical generators and converters. The most widespread electrical generators in the wind power industry are the synchronous generators (SGs), the permanent magnet synchronous generators (PMSGs), the doubly-fed induction generators (DFIGs) and the squirrel cage induction generators (SCIGs) [1]. Only the SCIG can not be used in the variable speed wind generation concept. Two types of converter configuration are most widespread: configuration with diode rectifier, DC chopper and inverter, and configuration with two back-to-back VSCs. These two configurations are indispensable for

variable speed operation, when the generator is fully decoupled from the grid.

Appropriate simulations are required to provide adequate comparison. Although the modeling of each element is comparatively easy to perform, the study and control of the whole conversion system, comprising subsystems with different dynamics, is quite complex. This is why an accurate model of WECS is needed for dynamic simulations. This paper attempts to analyze and compare the complete model of variable speed wind turbine with a permanent magnet synchronous generator and two different converter configurations. The wind turbine model is developed in the Matlab/SIMULINK® software environment and can be used for different type of simulations. A different approach can be used for the modeling of the permanent magnet synchronous generator. This approach is based on either stator voltages or flux as state variables [2]. The power converters are also programmed in the Matlab/SIMULINK® environment

## Energy Conversion System Configurations

### Configuration With Back-to-Back Converter

A configuration of variable speed wind turbine based on a permanent magnet synchronous generator is depicted in fig. 1. This configuration can also be used with synchronous generator with wound rotor, which is separately excited. For the purposes of this study, we have chosen a permanent magnet synchronous generator because of its high flux density, small size and smaller weight, as well as its flexible design structure. The PMSG is convenient for gearless operation of the wind turbine. The generator is connected with two 3-phase PWM voltage source converters in a back-to-back scheme [3]. In this case, the power can flow in two directions.

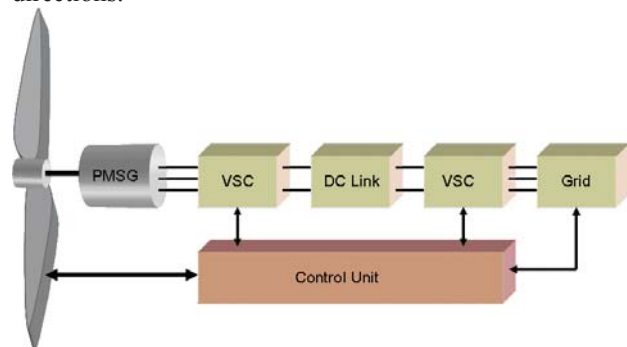


Fig. 1. Back-to-back voltage source converter.



## Wind Turbine Configuration With Full Size AC-DC-AC Converter

In this configuration the AC power from the PMSG is converted into DC power through a diode rectifier circuit and is then boosted by a step-up boost DC chopper. The chopper maintains the DC voltage constant during variable speed operation of the turbine. Thus, the DC link large capacitor is not needed and the control and operation of the PWM voltage source is facilitated. This leads to a comparatively simpler structure. The proposed scheme is shown in fig. 2.

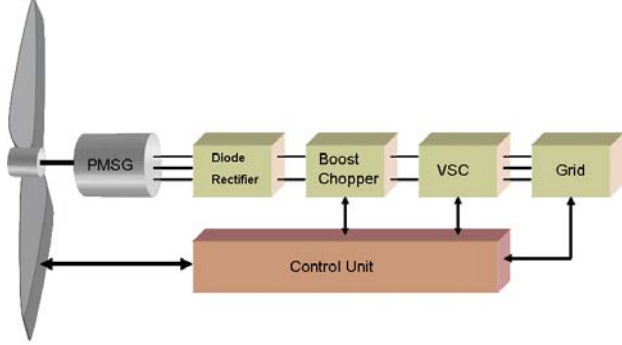


Fig. 2. Configuration with Diode rectifier, DC Boost converter and Inverter.

## System Modeling

In order to investigate the different modes of operations of the WECS, it is necessary to model every element of the conversion system and to perform some simulations. The conversion chain consists of a wind turbine, a permanent magnet synchronous generator and power converters. The models are developed in the Matlab/SIMULINK® software environment.

### Wind Turbine Model

The wind turbine extracts power from wind and converts it into mechanical power. The model of the wind turbine is based on well known aerodynamic and mechanical equations, which can be found in [4], [5].

### Permanent Magnet Synchronous Generator Model

The equations describing the dynamic of permanent magnet synchronous generator are Park equations in rotor reference frame [6], [7]:

$$u_d = -R_s i_d + \frac{d\lambda_d}{dt} - \omega \lambda_q \quad (1)$$

$$u_q = -R_s i_q + \frac{d\lambda_q}{dt} + \omega \lambda_d$$

$$\lambda_d = -L_{ls} i_d + L_{md} (i_m' - i_d) \quad (2)$$

$$\lambda_q = -L_{ls} i_q + L_{mq} i_q$$

where  $u_{dq}$ ,  $i_{dq}$ ,  $\lambda_{dq}$  are dq axis voltages, currents and flux linkages,  $L_{ls}$  is stator leakage inductance,  $R_s$  is stator winding resistance,  $L_{md}$  and  $L_{mq}$  are d and q axes magnetizing inductances,  $i_m'$  is magnetizing current of the permanent magnets,  $\omega$  is the electrical frequency. The electromagnetic torque can be calculated from:

$$\tau_G = \frac{3}{2} p i_q (\lambda_m + (L_d - L_q) i_d) \quad (3)$$

Where  $\lambda_m$  is the permanent magnetic flux,  $p$  is the number of pole pairs. If the inductances of d and q axis are equal, the electromagnetic torque can be regulated by q-axis current.

### Back-to-Back Converter

Three-phase voltage source converters are suitable for high power industrial application, providing almost sinusoidal currents. The two VSCs in Back-to-Back converter are modeled (assuming that the semiconductor switches are ideal - without voltage drop and losses) in the same way (in respect of the positive/negative sign of the voltages and currents in the rectifier and the inverter) using (4)-(6). The state variables are AC currents and DC voltage. This converter allows bidirectional power flow. The equivalent circuit is shown in fig. 3 and the equations for SIMULINK implementation are given below [8]:

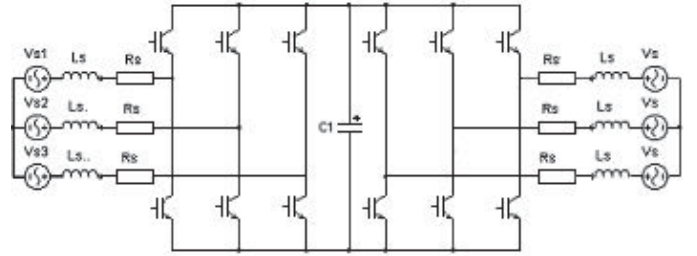


Fig. 3. Equivalent circuit Back-to-back converter.

$$I_{s1} = \frac{1}{L_s} \int (V_{s1} - V_{s1n} - R_s I_{s1}) dt$$

$$I_{s2} = \frac{1}{L_s} \int (V_{s2} - V_{s2n} - R_s I_{s2}) dt \quad (4)$$

$$I_{s3} = \frac{1}{L_s} \int (V_{s3} - V_{s3n} - R_s I_{s3}) dt$$

$$V_{s1n} = \frac{2}{3} V_{dc} \gamma - \frac{1}{3} V_{dc} \gamma - \frac{1}{3} V_{dc} \gamma \quad (5)$$

$$V_{s2n} = -\frac{1}{3} V_{dc} \gamma + \frac{2}{3} V_{dc} \gamma - \frac{1}{3} V_{dc} \gamma$$

$$V_{s3n} = -\frac{1}{3}V_{dc}\gamma - \frac{1}{3}V_{dc}\gamma + \frac{2}{3}V_{dc}\gamma$$

The load current is:

$$(6) \quad I_0 = I_{s1}\gamma + I_{s2}\gamma + I_{s3}\gamma$$

In (5) and (6),  $\gamma$  stand for the binary variable, which determines the condition of each switch. The control is trying to form, via PWM methods, such  $\gamma$  that satisfies normal operation of the converter at near unity power factor, hence:

$\gamma=1$ , if S1, S4 are driven ON and S2, S3 are driven OFF  
 $\gamma=-1$ , if S2, S3 are driven ON and S1, S4 are driven OFF

### Diode Rectifier and DC Boost Chopper

The mathematical model of the diode rectifier is relatively simple [9]. It is assumed that generator power is converted in DC power, hence:

$$(7) \quad 3V_g I_g = V_{dc} I_{dc}$$

The three-phase diode rectifier circuit has the characteristics in which the phase of largest line-to-line generator voltage is conducted. Thus, the mean value of the DC voltage is shown as:

$$(8) \quad V_{dc} = \frac{3}{\pi} \int_{-\frac{\pi}{6}}^{\frac{\pi}{6}} V_{LL} \cos \theta d\theta = \frac{3\sqrt{2}}{\pi} V_{LL} = \frac{3\sqrt{6}}{\pi} V_s$$

The boost converter allows for the adaptation of the rectifier DC voltage and the DC bus voltage. The advantages of using a step-up boost converter are: relatively simple control implementation, insurance of constant DC voltage for the inverter, which improve the inverter operation and cost efficient filtering of the voltage and current signals. The DC chopper scheme is shown in fig. 4 and the model is performed using (9):

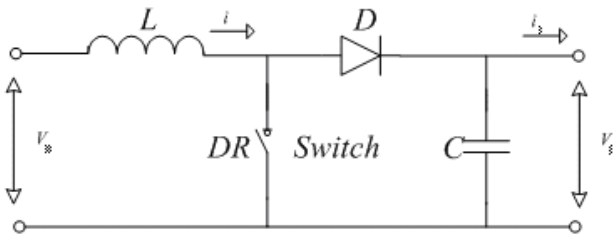


Fig.4. Equivalent circuit Boost converter.

$$(9) \quad L \frac{di}{dt} = V_{dc} - V_0 \cdot (1 - \alpha)$$

$$C \frac{dV_0}{dt} = i \cdot (1 - \alpha) - \frac{V_0}{r} - i_0$$

Where  $\alpha$  is the duty ratio. The state variables are the current through the inductance  $L$  and the DC voltage  $V_0$ . The control manipulates the duty ratio in way to boost the

rectifier DC voltage, while keeping a constant unity power ratio.

### Control Strategy

There are two principal control strategies for WECS, which contribute to maximum power extraction at various wind speed: pitch angle control and generator torque control. The pitch angle is directly related to power coefficient  $C_p$ . This control is used thoroughly to limit the aerodynamic power in above-rated wind speed in order to keep turbine in rated design power. In low wind speeds, the pitch control is rarely use and the angle is fixed at some optimal point. Possible scheme of pitch controller is shown on fig. 5 [11]

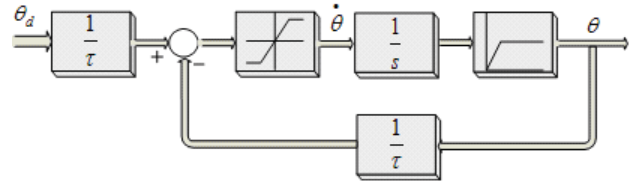


Fig. 5. Pitch angle regulator.

The generator torque control is used to limit the rotor speed in certain boundaries. As the wind speed change, the rotor will accelerate and decelerate continuously in order to maintain the constant tip-speed ratio that gives the maximum power coefficient.

For the configuration of fig. 1, the voltage source rectifier and the voltage source inverter are controlled via current control methods. Thereby, the generator-side converter regulates the generator current in such way that maximum power point is tracking correctly. The three-phase hysteresis current control is one of the simplest methods to control the line currents [12], [13]. The hysteresis current control is based on feedback loops with hysteresis comparators. When the error between reference and actual value exceed a predetermined tolerance band, the control produces directly switching signals for the power devices. The current reference template is generated through a maximum power point tracking (MPPT) look-up table. The control scheme is shown on fig. 6. The advantage is the simple and robust structure, as so the excellent dynamic performance. The main disadvantages are the variable switching frequency and wide line current spectrum [14].

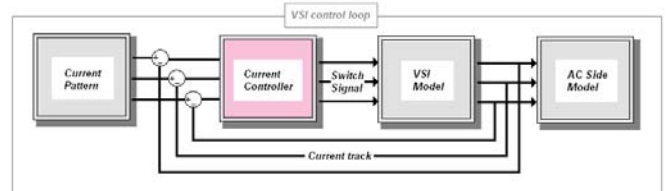


Fig. 6. Hysteresis current control scheme

For the configuration of fig. 2, as the diode rectifier cannot regulate current nor voltage, the speed control is achieved through predetermined maximum output torque look-up table in accordance with generator speed. The

generator speed can be obtained by filtering the DC output voltage from the diode rectifier, since the excitation is constant and the rotor speed is proportional to the peak output voltage. The reference DC current then is calculated from the look-up table. Thus, using the sliding mode control [14], the boost chopper is enforced to control the current in the input inductor, in order to maintain the desired generator speed and to insure constant DC voltage to the voltage source inverter. The proposed scheme is shown on fig. 7. The control goal  $I_{dc} = I_{dc\_ref}^*$  is performed by the sliding surface  $S(I_{dc}, t)$  defined as:

$$(10) \quad S(I_{dc}, t) = (I_{dc\_ref} - I_{dc}) = 0$$

Thus, the switching function is defined as:

$$(11) \quad \gamma = \begin{cases} 1, & \text{if } k(I_{dc\_ref} - I_{dc}) \leq -\Delta I \\ 0, & \text{if } k(I_{dc\_ref} - I_{dc}) \geq \Delta I \end{cases}$$

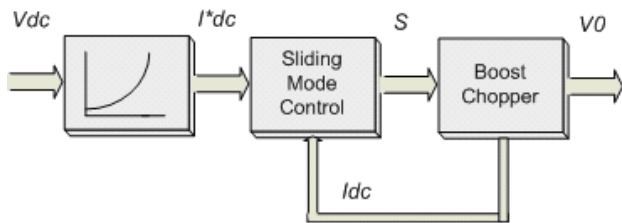


Fig. 7. Boost chopper control algorithm

The approach is similar to current mode control, but PWM modulator is not needed. The switch of the chopper is driven ON and OFF just when needed at the variable switching frequency. The main advantage in comparison with the classical control method is its robust structure and good dynamic response [14]. The Sliding mode controller is comparatively easy for implementation. However, there is a limitation is that the sliding mode control requires sensing the input current.

### Simulation Studies

The model system performance is tested under steady state conditions and transient realistic wind conditions. Thus, the proposed models of WECS have been implemented in MATLAB/SIMULINK. The steady state operating points are chosen to verify the consistency of both models. The dynamic simulation provides information for comparison between the models and control schemes. The simulations have been performed with parameters shown in Tables I-III. The simulation results are given in fig 8-fig. 17.

Table 1  
Generator parameters

Model	P	V <sub>LL</sub>	R <sub>s</sub>	L <sub>d</sub>	L <sub>q</sub>
PMSG	80	400V	0.031Ω	0.1mH	0.05mH

Table 2

Boost chopper parameters

Model	C	L
Boost Chopper	0.5mF	2mH

Table 3

DC Link capacitance

Model	C
Back-to-Back converter	10mF

### Dynamic simulation:

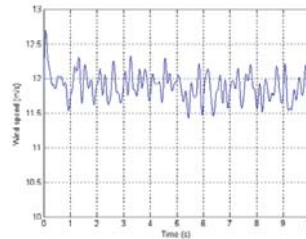


Fig. 8 Wind speed

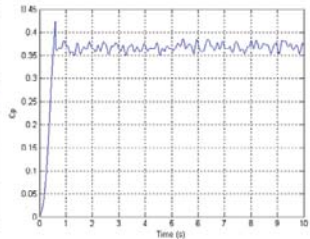


Fig. 9 Power coefficient Cp

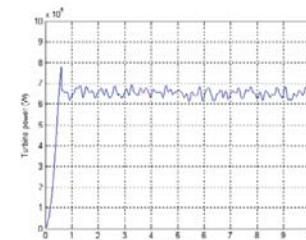


Fig. 10 Turbine power

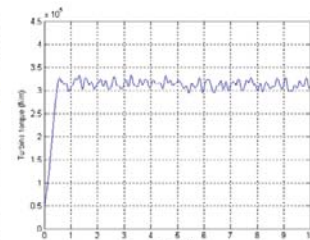


Fig. 11 Turbine torque

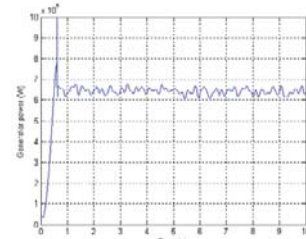


Fig. 12 Generator power

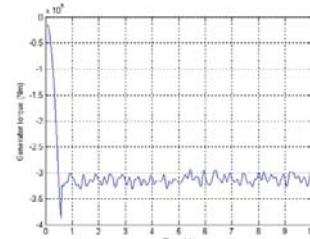


Fig. 13 Generator torque

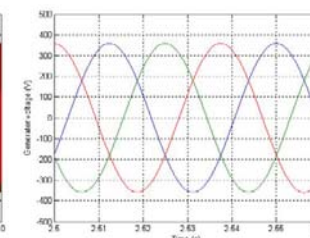
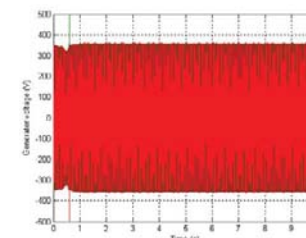


Fig. 14 Generator voltages



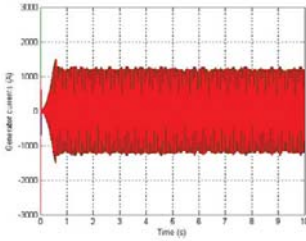


Fig.15. Generator currents Back-to-back configuration

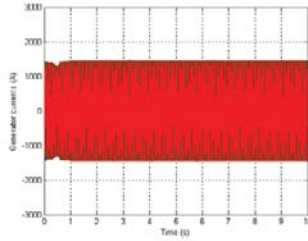


Fig.16. Generator currents Diode rectifier-Boost chopper-VSC configuration

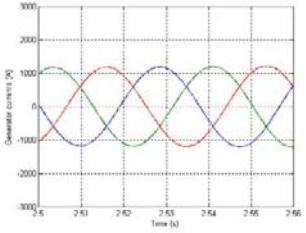


Fig.17. Generator currents Back-to-back configuration

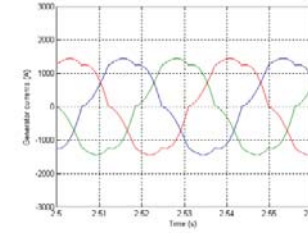


Fig.18. Generator currents Diode-rectifier-Boost chopper-VSC configuration

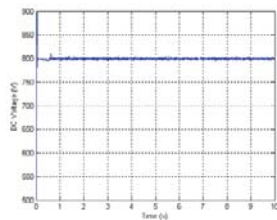


Fig.19. DC voltage Back-to-back configuration

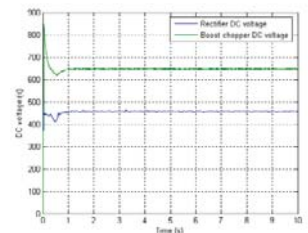


Fig.20. DC voltages Diode rectifier-Boost chopper-VSC configuration

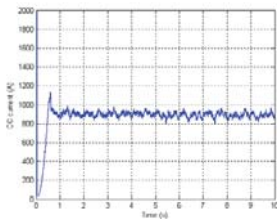


Fig.21. DC current Back-to-back configuration

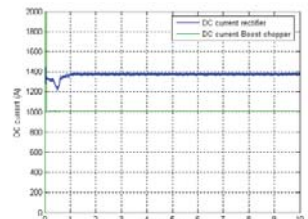


Fig.22. DC currents Diode rectifier-Boost chopper-VSC configuration

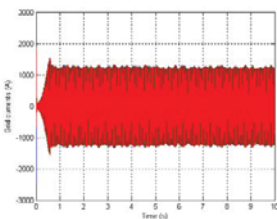
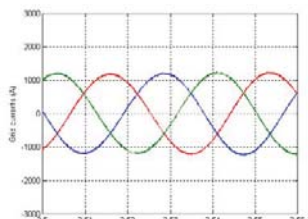


Fig. 23. Grid currents



The simulation shows that both types of converters have similar performance. Nevertheless, the generator currents differ, as it is shown on fig. 17 and fig.18. In the case of the configuration of fig. 2, the currents have almost sinusoidal form, which is not the case with the currents from diode rectifier.

Fig. 19 shows that the DC voltage in the configuration with back-to-back converter is greater than the diode rectifier DC voltage. His amplitude is almost the same, but oscillates slightly. In the simulation, the DC link capacitor in the configuration of fig. 2 is larger than that one in the other configuration, which may raise the implementation and maintain cost. The form and amplitude of the grid currents are similar.

## Conclusion

The performed simulations have shown no significant difference between the two proposed configurations. Although, there are some specific distinctions: the generator currents, DC link voltages and different aspect of transient processes.

The non sinusoidal currents lead to generator losses and to a power drop at the stator terminals. However, the losses in the diode rectifier are less than in the voltage source rectifier. The force commutated rectifier produces almost sinusoidal currents and can control both generator voltages and currents, so the MPPT control is full-proof. But, in view of the important losses in the rectifier and the high price of the device, this configuration remains expensive for implementation. The diode rectifier has the advantage of low cost and low losses. For implementation of MPPT strategy, a DC-DC converter is mandatory.

The behavior of both inverters is similar, while the DC link voltage is in the appropriate range. For normal operation of the inverter, the DC chopper voltage appears to be more appropriate. In the back-to-back converter, the DC voltage level is higher and large capacitor is needed. Nevertheless, with controlled VSCs the reactive power can be limited or controlled.

## Acknowledgement

The authors would like to thank the French Government for the PhD grant, and ADEME and ECO-net program for the financial support.

The authors also would like to thank the Bulgarian National Research Fund for the financial support (contract EE 106/07) and the Technical University-Sofia for the co-financing (contract 08451c1)

## References

- [1] L.H. Hansen, L. Helle, F. Blaabjerg, E. Ritchie, S. Munk-Nielsen, H. Bindner, P. Sørensen, B.Bak-Jensen, "Conceptual survey of Generators and Power Electronics for Wind Turbines", Risø National Laboratory, December 2001, 106 p., ISBN 87-550-2745-8.
- [2] P. Krause, O. Wasynczuk, S. Sudhoff *Analysis of Electric Machinery and Drive Systems*, 2<sup>nd</sup> Edition, Wiley-IEEE Press, 2002.



- [3] A. Carlsson, "The back-to-back converter: control and design", PhD Thesis, Lund Institute of Technology, Sweden 1998.
- [4] M. O. L. Hansen *Aerodynamics of Wind Turbines*, 2<sup>nd</sup> Edition, Earthscan, London, 2008.
- [5] E. Muljadi, C.P. Butterfield, "Pitch-controlled variable-speed wind turbine generation" *Conference Record of 1999 IEEE Industry Applications Conf.*, pp. 323 – 330, vol.1.
- [6] P. Kundur *Power System Stability and Control*, McGraw-Hill, 1994.
- [7] A. B. Dehkordi, A. M. Gole, T. L. Maguire, "Permanent Magnet Synchronous Machine Model for Real-Time Simulation", *Presented at 2005 International Conference on Power Systems Transients, Montreal, Canada [Online]*. Available: [http://www.ipst.org/TechPapers/2005/IPST05\\_Paper159.pdf](http://www.ipst.org/TechPapers/2005/IPST05_Paper159.pdf)
- [8] V.F Pires, J.F.A. Silva, "Teaching nonlinear modeling, simulation, and control of electronic power converters using MATLAB/SIMULINK", *IEEE Trans. On Education*, Vol. 45, pp.253 – 261, Aug. 2002.
- [9] Marques, G.D., "A simple and accurate system simulation of three-phase diode rectifiers" *Proc. of the IEEE 24th Annual Conference IECON Vol. 1*, pp:416 – 42, 1998
- [10] F. D. Bianchi, H. DeBattista, R. J. Mantz *Wind Turbine Control Systems, Principles, Modelling and Gain Scheduling Design*, Springer, London, 2007.
- [11] D. M. Brod, D. W. Novotny, "Current Control of VSI-PWM Inverters", *IEEE Trans. Industry Application*, Vol. 21, No. 4, pp. 562-570.
- [12] B. K. Bose, "An Adaptive Hysteresis-Band Current Control Technique of a Voltage-Fed PWM Inverter for Machine Drive System", *IEEE Trans. Industrial Electronics*, Vol. 37, No. 5, pp. 402-408.
- [13] R. Pöllänen, "Converter-Flux Based Current Control of Voltage Source PWM Rectifiers-Analysis and Implementation", PhD Thesis, Lappeenranta University of Technology, Finland 2003.
- [14] H. Sira-Ramirez, G. Escobar, R. Ortega, "On Passivity-Based Sliding Mode Control of Switched DC-DC Power Converters", *Proc. 1996 IEEE Conf. on Decision and Control*, pp. 2525 - 2526 vol.3.

## Biographies



**Daniel Roye**, born in France in 1946, received his Engineer from Institut National Polytechnique de Grenoble (France) in 1969. He joined this Institute for teaching and research in Electrical Engineering and he received his PHD and HDR respectively in 1974 and 1983. He has been first involved in various electrical machines studies. Then his activities have been oriented toward drives controls, mainly Field Oriented Control and Direct Torque Control of induction machines. He is currently co-manager of the Power System Group of G2ELab, in Grenoble Institute of Technology and Professor at that Institute. His main field of interest is Renewable Energy Control and Integration and building energy optimization.



**Vladimir Lazarov** was born in Sofia, Bulgaria. He graduated from the Technical University - Sofia, and there received his PhD. His field of interest includes electrical machines with electronic commutation, small electrical machines, renewable energy sources (electrical aspects). Vladimir Lazarov is with the Faculty of Electrical Engineering, Technical University of Sofia, and he is responsible for the "Laboratory on Renewable Energy Sources".

(e-mail: vl\_lazarov@tu-sofia.bg)



**Dimitar Spirov** was born in Sliven, Bulgaria, on May 13, 1981. He received the M.S. degree in electrical engineering from the Technical University – Sofia in 2004. Now he is pursuing Ph. D. degree at the Faculty of Electrical Engineering, Technical University –Sofia and G2ELab, Grenoble Institute of Technology. His field of interest includes wind power, power converters, electrical machines and renewable energy sources. (e-mail: d\_spirov@tu-sofia.bg)



**Ludmil Stoyanov** was born in Sofia, Bulgaria, on June 13, 1981. He graduated from the Technical University - Sofia, and received second Master degree from ENSIEG-INPG, France. His field of interest includes electrical machines, electrical networks and renewable energy sources (electrical aspects). He is today PhD student in the Faculty of Electrical Engineering of the Technical University – Sofia. (e-mail: ludiss@tu-sofia.bg)

# Productivity of Medium Wind Turbines According to Wind Weibull Distribution: Application to Various Bulgarian Sites

Gilles Notton, Vladimir Lazarov, Ludmil Stoyanov

**Abstract:** This paper estimates the wind distribution characteristics impact on the production of small-scale wind turbines (WT) with various power curves profiles. After an inventory of small WT available in the market, 8 power curves have been chosen and the influence of meteorological conditions on their production is studied. At last, the comparison of small wind energy conversion systems (WECS) performances on eight sites in Bulgaria shows that the production can vary largely for the same site according to the WECS type.

**Keywords:** Weibull wind distribution, small wind turbine, Bulgaria, wind potential

## Introduction

The estimation of energy output for small-scale wind power generators is the subject of this article. In a first part, we perform a general study on the influence of the wind speed distribution on the energy production of small wind turbine characterized by various different power curves. 8 types of power curves have been chosen after an inventory of small wind turbines available in the market and are used for the production estimation.

Then, in a second part, the wind energy potential of 8 sites in Bulgaria is analyzed based on one year of recorded wind data. Using the Weibull model, time series data are analyzed and distributional parameters are estimated for probability distributions on an annual basis. From the technical data provided by small turbine manufacturers, the capacity factor of 59 wind turbines are calculated for the sites and the machines performance according to the site characteristics are estimated and compared.

The wind turbine production can be obtained as combination of her power profile and the site wind distribution, as shown in Fig.1.

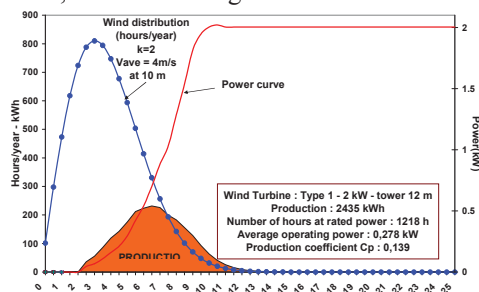


Fig.1. Methodology for production estimation

## Weibull distribution approach

The WECS energy output can be obtained using the wind speed probability distribution and the turbine power

curve. The Weibull probability density functions are commonly used and widely adopted [1-6]. This function is a special case of a generalized two parameters gamma distribution and can be characterized by its probability density function  $f(V)$  and cumulative distribution function  $F(V)$  with the following formulas:

$$(1) \quad f(V) = \left(\frac{k}{A}\right) \left(\frac{V}{A}\right)^{(k-1)} \exp\left[-\left(\frac{V}{A}\right)^k\right]$$

$$(2) \quad F(V) = 1 - \exp\left[-\left(\frac{V}{A}\right)^k\right]$$

where  $A$  is the scale parameter in m/s,  $k$  is the unitless shape parameter and  $V$  the wind speed.

With the probability function knowledge, we can define the average wind speed and the standard deviation are defined by:

$$(3) \quad \bar{V} = \int_0^{\infty} V \cdot f(V) dV$$

$$(4) \quad \sigma = \left[ \int_0^{\infty} (V - \bar{V})^2 f(V) dV \right]^{\frac{1}{2}}$$

or also

$$(5) \quad \bar{V} = A \Gamma\left(1 + \frac{1}{k}\right)$$

$$(6) \quad \sigma^2 = A^2 \Gamma\left(1 + \frac{2}{k}\right) - \bar{V}^2$$

where  $\Gamma(x)$  is the well-known Gamma function defined by:

$$(7) \quad \Gamma(x) = \int_0^{+\infty} t^{x-1} \exp(-t) dt$$

The most commonly method to calculate the Weibull distribution parameters consists in using the equation (2) and to take, two times, the logarithm of the equality two terms and to employ a least-squares fit method to the observed distribution (see Fig.2).

Others interesting wind speeds are computed:

- the most probable wind speed  $V_{mp}$  which represents the most frequent wind speed expressed by [5,7]:

$$(8) \quad V_{mp} = A \left(\frac{k-1}{k}\right)^{\frac{1}{k}}$$

- the wind speed carrying the maximum energy  $V_{max,E}$  expressed by :

$$(9) \quad V_{\max,E} = A \left( \frac{k+2}{k} \right)^{1/k}$$

- the median wind speed  $V_{med}$  which is the speed dividing in two equal parts the wind speed distribution:

$$(10) \quad V_{med} = A \ln(2)^{1/k}$$

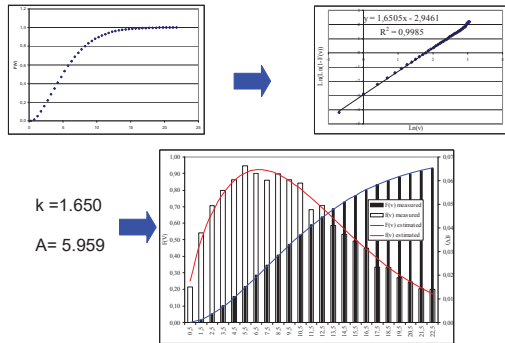


Fig.2. Methodology used to determine the Weibull distribution parameters

### Influence of Weibull distribution parameters

We plotted in Fig.3 some wind distributions for various annual average wind speeds and various values of the parameter k.

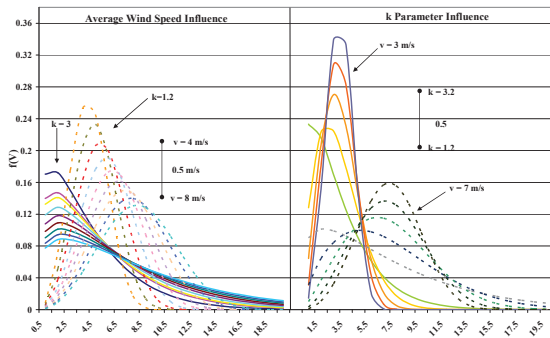


Fig.3. Influence of the Weibull parameters on the wind speed distribution

More k increases, more the distribution curve is pointed. Increasing the parameter k increases the frequency of apparition of a wind speed class without influencing the scale of wind speeds. When the average wind speed increases, the scale of wind speed is more important, the high wind speeds appear, there are more wind speed classes but the frequency of each wind speed class decreases.

In Fig.4, we present the annual average wind speed and k influence on the parameter A, the median, the most probable and the maximum energy wind speeds.

We note that:

- for a given k, an increase of the average wind speed induces an increase of the other speeds for obvious reasons ;

- the influence of k on the parameter A is low and on the median wind speed not very significant;

- the most energetic wind speed decreases when k increases.

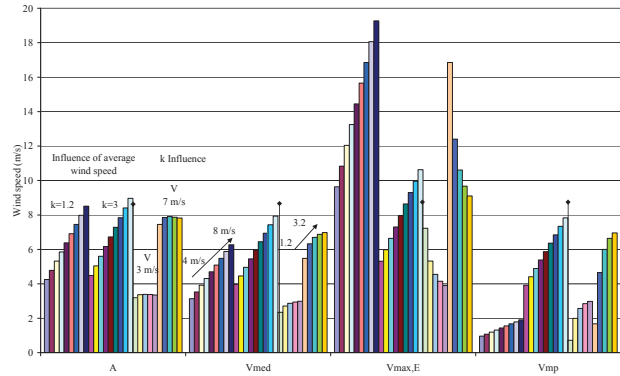


Fig.4. Influence of the Weibull parameters on characteristic wind speeds

### Small wind turbines power profiles

It is well known that the wind power varies as the wind speed cube, but the WECS output power is a more complicated function of the wind speed. Some characteristics wind speeds are used for its definition:  $V_c$ ,  $V_r$ ,  $V_{off}$  and  $P_r$ , respectively cut-in speed, rated wind speed, cut-off wind speed and rated output power of the turbine.

If the power curves of large wind turbines are often similar, for small and medium WECS the power curves vary. We realized an inventory (not exhaustive) of small and medium size WECS (from 0.2 to 20 kW) available on the market. To do it, we used the wind turbine manufacturers list in Europe and out of Europe given by the SWIIS Consortium [8] (Small Wind Industry Implementation Strategy) which promotes the small wind turbines in Europe. We made a list of technical characteristics of 77 WECS with 59 power curves.

To make this study independent of the rated power of the WECS, we divide the electrical power P by the rated power  $P_r$ , defining the parameter p by:

$$(11) \quad p = \frac{P}{P_r}$$

8 types of power profiles have been chosen after our inventory and are plotted in Fig.5.

These profiles are distinguished:

- mainly, by the form of the function between  $V_c$  and  $V_r$ . These varied forms will influence on the WECS productivity at low wind speeds i.e. for low annual average wind speed but also for a low value of the Weibull distribution shape parameter;

- by the form of the part between  $V_r$  and  $V_{off}$ ; this part is often constant, sometimes inferior or superior to the nominal power and for the type 3 with a cut-off wind speed less than 25 m/s. For the types 6, 7 and 8, this part of the curve is not constant. This modification will have a consequence for the production at high wind speeds on windy site or in site with a high value of the Weibull distribution shape parameter.

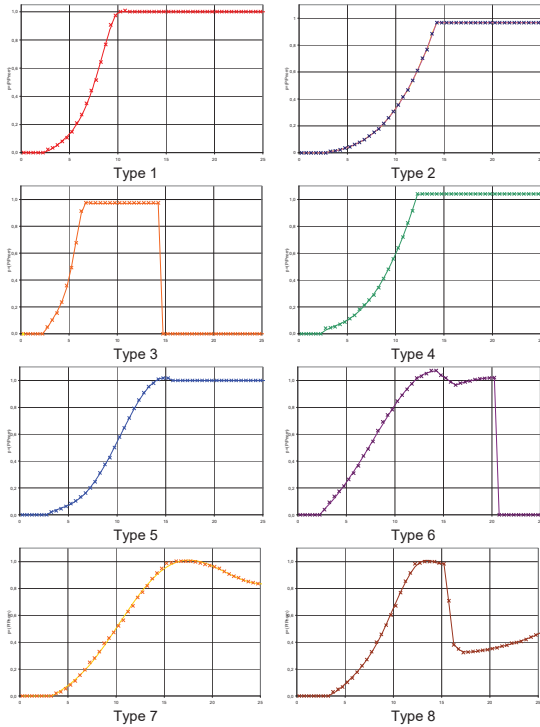


Fig.5. 8 types of power profiles deduced from our inventory and used in this study

### WECS Productivity

We studied the productivity of various wind turbines (characterized by their power curve profile) under various wind conditions (characterized by the annual mean wind speed and the shape factor  $k$  of the Weibull distribution). We calculated the production per kW (equivalent to a time) for every 8 WECS profiles presented above.

The hub height has been taken at 12 m and the wind speed data have been measured at a height equal to 10 m. We calculated the wind speed at the hub height from the measured wind speed using Justus' formula [9] and taken the wind shear exponent equal to 0.150. We plotted in Fig.6. the production per kW of the 8 types of WECS versus the  $k$  value and the annual average wind speed. For the left figures, the annual wind speed varies between 2 and 10 m/s and for the right one, the annual wind speed reaches 20 m/s. Generally, the annual average wind speed of a given site rarely exceeds 10 m/s but we wanted to see how the production curve behaves for higher wind speeds even if the annual wind speed variation domain is not realistic. We observe that the form of the 3D-curves is different according to the WECS type and that the top of the 3D-curve reaches variable values. For the left curves, we note that:

- the highest values of the top are reached for the types 1, 3 and 6 because the small rated wind speed and the high production at low wind speed;
- the worst production is obtained for the Type 2 machine because the exponential form of the power curve for  $V < V_r$  does not allow a high production; for the types

2, 4, 5, 7 and 8 the form of the curve for  $V < 10$  m/s is approximately the same.

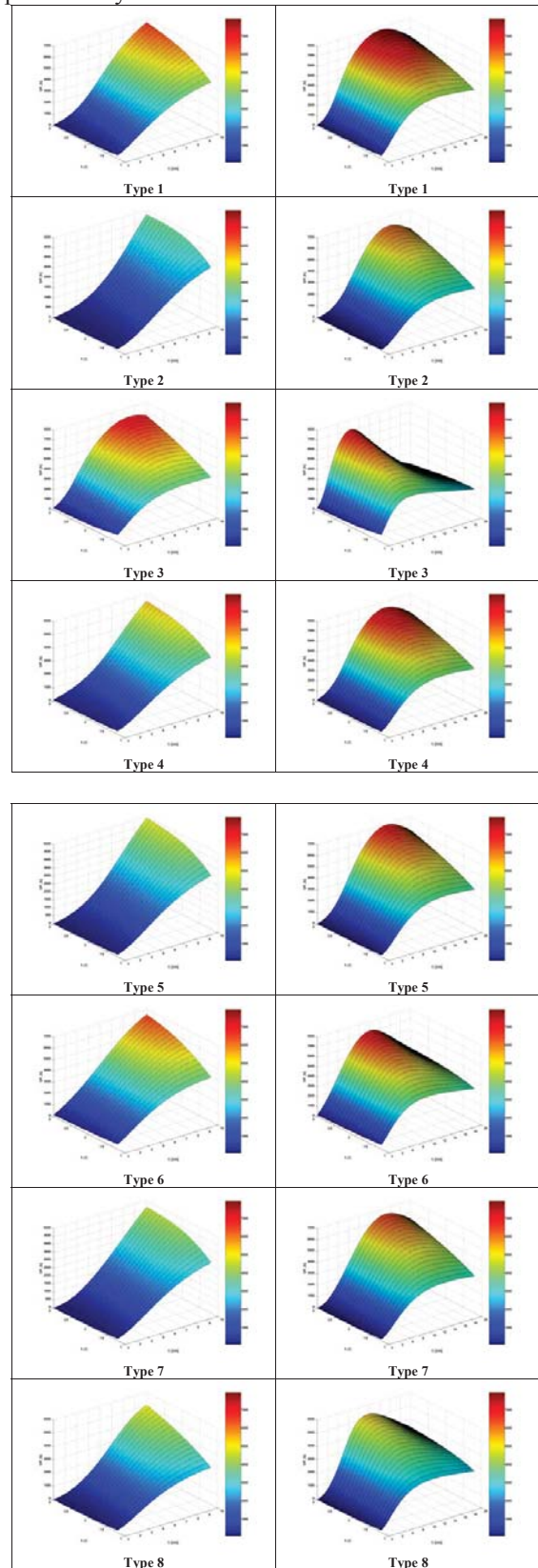


Fig.6. Productivity of WECS according to Weibull distribution



- all the WECS types give the same form to the 3D-curve excepted for the type 3 for which the rated power is reached for a lower wind speed value.

For the right curves, we note a decrease of the production after a given value of wind speed due to the presence of the cut-off wind speed after which the produced power becomes null or very low. The types 3 and 8 WECS differ from the other ones by the value of their cut-off wind speeds (less than 25 m/s) and consequently their production curves begin to decrease for lower wind speeds.

### Wind potential of some sites in Bulgaria

We applied this methodology to 8 Bulgarian sites which situation is shown in Fig.7 and the geographical coordinates of each site is reported in Table 1.



Fig.7. Situation of the studied areas

Table 1

Geographical coordinates of studied sites

City	Longitude	Latitude	Altitude
Botev	24°50' E	42°40' N	2389m
Chirpan	25°20' E	42°12' N	175 m
Kaliakra	28°28' E	43°22' N	64 m
Kurdjali	25°22' E	41°39' N	240 m
Plevan	24°34' E	43°27' N	131 m
Sandanski	23°16' E	41°31' N	206 m
Sofia	23°20' E	42°41' N	588 m
Varna	27°55' E	43°12' N	14 m

The wind turbine annual production estimation, for a given site, needs the knowledge of his wind distribution. For the studied sites this distribution is given in Fig.8.

We calculated the productivity of the each WECS type in these 8 Bulgarian sites and we noted that this production is very different for a same wind turbine peak power and the same site according to the power profile of this WT (Fig.9.). Between the best type (type 3) and the worst one (type 2), the variation of the production per kW can reach 665% in relative value (Varna) and 3500 kWh/kW in absolute value (Kaliakra). The importance of the variation in relative value does not only depend on the annual wind speed of the site. In absolute value, more the site is windy more the difference of production between two WECS is high.

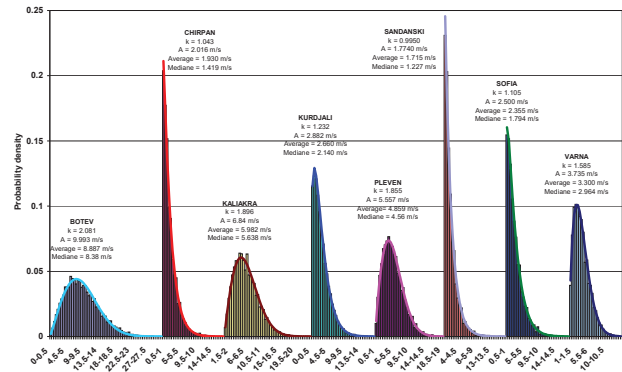


Fig.8. Weibull distribution for the studied sites in Bulgaria

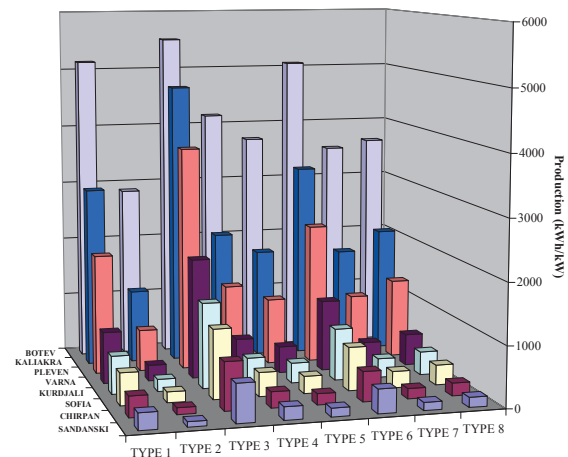


Fig.9. Production versus the WT type

As said above we made an inventory of small and medium scale wind turbines in the market. 59 WECS power profiles have been inventoried and used in this work. The productivity per kW of each WECS has been computed for each studied site and the results are shown in Fig.10.

We note a high variability of the WECS electrical production according to the small and medium scale WECS. The production variation shows that it is impossible from only the knowledge of the WT peak power to estimate its productivity because it depends strongly to the power curve.

### Conclusion

We studied the wind speed Weibull distribution influence on small and medium scale wind turbines productivity. The influence of the two parameters of the Weibull distribution (annual average wind speed and shape parameter k) has been estimated.

A case study has been realized on various sites located in Bulgaria. The wind potential of each site has been estimated.

From an inventory of small and medium scale WECS, 8 power curve profiles have been chosen and have been used to estimate the annual production per unit of power on each site.

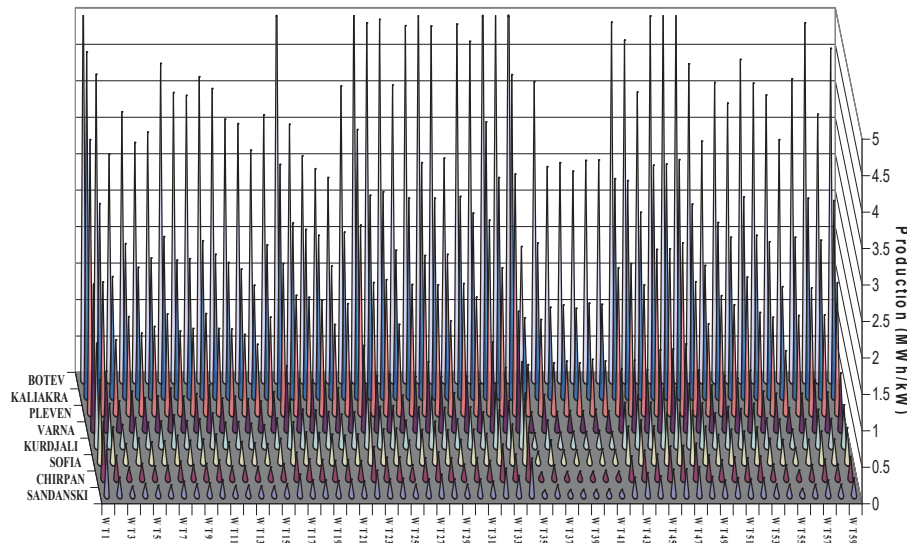


Fig.10. Production for all WT

### Acknowledgements

The authors would like to thank the University Agency of French-speaking communities (AUF), the French Agency for Environment Energy Management (ADEME) and the French Ministry of Foreign Affairs (via Eco-Net program) for their financial supports.

### References

- [1] Elamouri M, Ben Amar F. Wind energy potential in Tunisia. *Renewable Energy* 2008;33:758-768.
- [2] Kaldellis JK. The wind potential on the maximum wind energy penetration in autonomous electrical grids. *Renewable Energy* 2008 (in press).
- [3] Chang TJ, Tu YL. Evaluation of monthly capacity factor of WECS using chronological and probabilistic wind speed data: a case study of Taiwan. *Renewable Energy* 2007;32:1999-2010.
- [4] Ngala GM, Alkali B, Aji MA. Viability of wind energy as a power generation source in Maiduguri, Borno state, Nigeria. *Renewable Energy* 2007;32:2242-2246.
- [5] Bagiorgas HS, Assimakopoulos MN, Theoharopoulos D, Matthopoulos D, Mihalakakou GK. Electricity generation using wind energy conversion systems in the area of Western Greece. *Energy Convers Manage* 2007;48:1640-1655.
- [6] Celik AN. Energy output estimation for small-scale wind power generators using Weibull-representative wind data. *Journal of Wind Engineering and Industrial Aerodynamics* 2003;91:693-707.
- [7] Akpinar EK, Akpinar S. An assessment on seasonal analysis of wind energy characteristics and wind turbine characteristics. *Energy Convers Manage* 2005;46:1848-67.
- [8] SWIIS (Small Wind Industry Implementation Strategy). List of Wind Turbines manufacturers, 2008; <<http://www.smallwindindustry.org>>.
- [9] Justus CG. Winds and system performances. Philadelphia; Franklin Institute Press, 1978.

### Biographies



**Gilles Notton** was born in Saint Avold, France, on January 23, 1964. He studied at the University of Corsica and received Dr. degree in 1992 and Research Agreement in 2002 from the same university His field of interest includes renewable energy systems and renewable sources. He is today assistant professor and responsible of the French Research ADEME network between France and Oriental and Central European Countries. Gilles Notton is with the

Research Centre of Vignola, University o Corsica, UMR CNRS 6134, route des Sanguinaires, F20000 Ajaccio, France (e-mail: [gilles.notton@univ-corse.fr](mailto:gilles.notton@univ-corse.fr))



**Vladimir Lazarov** was born in Sofia, Bulgaria. He graduated from the Technical University - Sofia, and there received his PhD. His field of interest includes electrical machines with electronic commutation, small electrical machines, renewable energy sources (electrical aspects). He is today with the Faculty of Electrical Engineering of the Technical University of Sofia, 8, Kl. Ohridski Blvd., 1000 Sofia, Bulgaria and is responsible for the "Laboratory on

Renewable Energy Sources" (email: [vl\\_lazarov@tu-sofia.bg](mailto:vl_lazarov@tu-sofia.bg)).



**Ludmil Stoyanov** was born in Sofia, Bulgaria, on June 13, 1981. He graduated from the Technical University - Sofia, and received second Master degree from ENSIEG-INPG, France.

His field of interest includes electrical machines, electrical networks and renewable energy sources (electrical aspects). He is today a PhD student in the Faculty of Electrical Engineering of the Technical University – Sofia. Ludmil Stoyanov is with the Faculty of Electrical Engineering, Technical University of Sofia, 8, Kl. Ohridski Blvd., 1000 Sofia, Bulgaria (e-mail: [stoyanov\\_ludmil@abv.bg](mailto:stoyanov_ludmil@abv.bg))

# Modelling of the Wind Energy Conversion System Components

Teofana Puleva

**Abstract:** The dynamic behaviour of the wind energy conversion system (WECS) is studied. The wind turbine model is separated into several subsystems: models for the aerodynamics, pitch actuator and drive train. The mathematical description of wind statistics is given. An approach for computation of stochastic process with a given spectral density function is explored. The proposed procedure is especially effective for a non rational shaping filter transfer function.

**Keywords:** wind turbine, modelling, spectral density function

## Introduction

The wind energy is by far the fastest-growing renewable energy resource. The wind turbine capacity installed in Europe increased during the last years at an average annual growth rate superior to 30% [1]. The cost of electricity provided by wind power facilities has been dropping since the 1980s. These cost reduction are due to new technologies and more reliable turbine.

Control plays a very important role in modern WECS. The wind turbine control enables a better use of the turbine capacity. Wind turbines are complex mechanical systems comprising flexible bodies installed in the three-dimensional wind speed field. The aerodynamic forces induced by the wind passing through the rotor are highly nonlinear. These nonlinearities lead to the significant variations in the dynamic behaviour of the system over its operating range. Therefore their modelling is a nontrivial task. In order to design effective control laws more precise WECS component models are required. The identification procedure used in the modelling process is especially effective if assumptions regarding the dynamics of the system components are made. It finds the order and parameters of the model that best meets the WECS dynamics at each operating condition. Since the operating points are determined by the wind speed, which is a non-controllable input variable, it is necessary to take measurement during long periods. The data collected during intervals of stationary wind speed are therefore

used to identify a linear model valid for that wind condition. Thus, a family of linear models is obtained [2]. The identification procedure is especially effective if it is supported by the theoretical description of the system components dynamics based on the basic physical principles and laws. In the next section the mathematical description of the WECS components is considered. The modelling is the first stage in WECS analysis and design.

## The Wind and Wind Turbine Modelling

In the modelling of the wind turbine generating system (WTGS) operation in the electric power system it is necessary to make a decomposition of the model into sub-models. The block-diagram of the WECS is presented in Fig.1. The model consists of the following components: *wind power block*, computing the power in the stream; *wind wheel power block*, computing the power extracted by the wind wheel from the air on the basis of the rotor power coefficient; *blades transition block*; describing the blade pitching system, *mechanical eigenswings block*, and *drive train block*.

## Wind Dynamics Modelling

The wind velocity usually varies considerably and has a stochastic character. Therefore in general the wind should be modelled as a stochastic process. By definition, turbulence includes all wind speed fluctuations with frequencies above the spectral gap. Therefore it contains all components in the range from seconds to minutes. Wind turbulence at given point in space is stochastically described by means of its power spectrum. Two widely accepted models are the von Karman spectrum [3, 9]

$$(1) \quad S(\omega) = \frac{K_v}{[1 + (\omega T_v)^2]^{5/6}},$$

and the Kaimal spectrum [9]

$$(2) \quad S(\omega) = \frac{K_v}{[1 + \omega T_v]^{5/3}}.$$

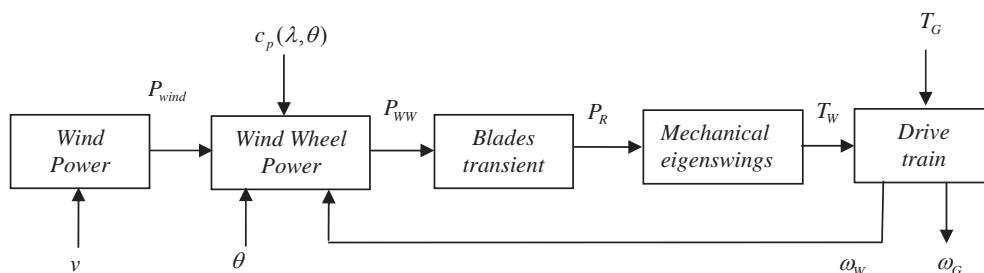


Fig.1. Structure of the wind turbine model

The constant  $T_V$  determines the frequency bandwidth of the turbulence whereas  $K_V$  is associated to the turbulence power. In the time domain  $T_V$  is also a measure of the correlation time of the turbulence. Both parameters depend on the mean wind speed as well as on the topography of the terrain. For instance, in the case of the *Karman* spectrum, these coefficients are approximated by

$$(3) \quad K_V = 0.475\sigma_v^2 \frac{L_v}{V_m(z)},$$

$$(4) \quad T_V = \frac{L_v}{V_m(z)},$$

where  $L_v$  is the correlation length of the turbulence and  $\sigma_v$  is the turbulence intensity defined as the ratio of turbulence power to mean wind speed, i.e.

$$(5) \quad \sigma_v = \frac{\sigma_v}{V_m(z)} \approx \frac{1}{\ln(z/z_0)},$$

where the parameter  $z$  is the height above ground level, and the parameter  $z_0$  is the roughness length. Typical values for  $z_0$  are given in [4]. Both  $L_v$  and  $\sigma_v$  are specific to the terrain and can be experimentally obtained from wind speed measures. The correlation length  $L_v$  generally takes values ranging from 100 to 330 m, whereas the turbulence intensity  $\sigma_v$  takes values between 0.1 and 0.2. Equation (5) says that turbulence intensity decreases with height.

In order to generate the stochastic process with *Karman* spectrum the following computational procedure can be used. The shaping filter transfer function is

$$(6) \quad W_f(p) = \frac{\sqrt{k_v}}{(1 + j\omega T_V)^{5/6}}.$$

This transfer function is non rational, therefore the standard approach for random number generator design with desired spectral density function can not be used. The proposed approach is based on the relationship between the real frequency response  $P(\omega)$  and the system step response

$$(7) \quad h(t) = \frac{2}{\pi} \int_0^\infty \frac{P(\omega)}{\omega} \sin \omega t d\omega.$$

Using the impulse response  $w(t)$  and Duhamel's integral the system output can be computed

$$y(t) = \int_0^\infty w(\theta)u(t-\theta)d\theta.$$

If an input signal  $u(t)$  is a white noise with intensity  $V_u$ , and the real frequency response corresponds to the

shaping filter (6), the resulting output  $y(t)$  will have a desired spectral density function described by (1). The computation procedure can be realized in the following sequence

*Step1.* Real frequency response computation using (6);

*Step 2.* Step response computation for each time  $t_i$  using the discrete realization of (7)

$$(8) \quad h(t_i) = \frac{2}{\pi} \sum_{\omega_k=0}^{\omega_{k \max}} \frac{P(\omega_k)}{\omega_k} \sin(\omega_k t_i) \Delta\omega,$$

where the frequency  $\omega_{k \max}$  satisfies  $P(\omega_{k \max}) \leq 0.05P_{\max}$ .

*Step3.* Impulse response computation

$$(9) \quad w(t_i) = h(t_i) - h(t_{i-1}).$$

*Step4.* Output signal computation

$$(10) \quad y(t_i) = \sum_{t_k=0}^{t_i} w(t_k)u(t_i - t_k).$$

The described approach allows exact computation of stochastic process with a given spectral density function. The proposed procedure is especially effective for non rational shaping filter transfer function.

In many tasks of WECS analysis and application the wind variation is modelled as a sum of harmonics with frequencies in range 0.1 – 10 Hz. Wind gusts are usually also included in the wind model [8]

$$(11) \quad v(t) = v_0 \left[ 1 + \sum_k A_k \sin \omega_k t \right] + v_g(t),$$

where  $v_0$  is the mean value of the wind velocity;  $A_k$  - amplitude of the  $k$ th harmonic;  $\omega_k$  - frequency of the  $k$ th harmonic;  $v_g(t)$  - wind gust.

Wind gusts can be modelled by the following function

$$(12) \quad v_g(t) = \frac{2v_{g \max}}{1 + e^{-4[\sin(\omega_g t) - 1]}}$$

where  $v_{g \max}$  is the gust amplitude and  $\omega_g$  is the gust frequency ( $\omega_g = 2\pi/T_g$ ). The gust amplitude varies up to 10 m/s and the gust period can be in the range  $T_g = [10, 50] s$ . The block diagram of this simplified model is presented in Fig.2.

### Wind Stream Power

The kinetic energy in air of an object of mass  $m$  moving with speed  $v$  is equal to

$$(13) \quad E = \frac{1}{2}mv^2.$$

The power in the moving air (assuming constant wind velocity) is equal to



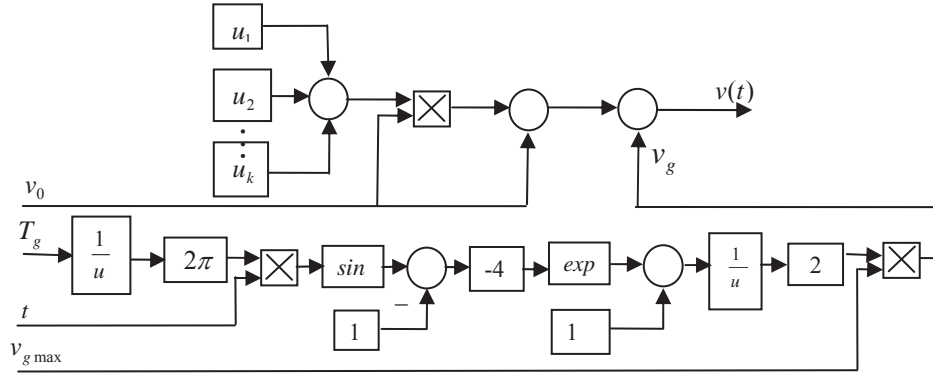


Fig. 2. Wind dynamics model block diagram

$$(14) \quad P_{wind} = \frac{dE}{dt} = \frac{1}{2} \dot{m} v^2,$$

where  $\dot{m}$  is the mass flow rate per seconds. When the air passes across an area  $A$  (the area swept by the rotor blades) the power in the air can be computed as

$$(15) \quad P_{wind} = \frac{1}{2} \rho A v^3,$$

where  $\rho$  is the air density.

### Mechanical Power Extracted from the Wind

The air energy described by (13) can not be transferred into another type of energy (e.g. mechanical) with a hundred percent conversion efficiency by any energy converter. The mechanical power extracted from the air stream by the energy converter is equal to

$$(16) \quad P_{ww} = \frac{1}{4} \rho A (v_1^2 - v_2^2) (v_1 + v_2),$$

where  $v_1$  and  $v_2$  are the air velocity before and after the converter respectively. Equation (16) is usually used in the following form

$$(17) \quad P_{ww} = c_p P_{wind} = \frac{1}{2} c_p \rho A v_1^3,$$

where the power coefficient (*Betz's factor*)  $c_p < 1$ . It is the ratio of the mechanical power extracted by the converter to the power in the air stream. The power factor reaches a maximum value equal to  $c_p = 0.593$  when the speed ratio is equal to  $v_2/v_1 = 1/3$ . The power coefficient of real converter  $c_p$  achieves lower values than that computed above because of various aerodynamic losses that depend on the rotor construction (number and shape of blades, weight, stiffness, etc.). The rotor power coefficient is usually given as a function of two parameters: the tip-speed ratio  $\lambda$  and the blade pitch angle  $\theta$ . The tip-speed ratio is

$$(18) \quad \lambda = \frac{u}{v_1} = \frac{\omega R}{v_1},$$

where  $u$  is the tangential velocity of the blade tip;  $\omega$  - angular velocity of the rotor;  $R$  - rotor radius (blade length).

The blade pitch angle is defined as the angle between the plane of rotation and the blade cross-section chord.

The mechanical power  $P_{ww}$  extracted from the wind converter and the torque  $T_{ww}$  for the given rotor (described by  $c_p$ ,  $c_T$  coefficients and the rotor radius  $R$ ) and for the given wind velocity  $v_1$ , rotor angular velocity  $\omega$  and blade pitch angle  $\theta$  can be computed as

$$(19) \quad P_{ww} = c_p(\lambda, \theta) P_{wind} = 0.5 c_p(\lambda, \theta) \rho A v_1^3,$$

$$(20) \quad T_{ww} = \frac{P_{ww}}{\omega} = 0.5 c_T(\lambda, \theta) \rho A v_1^2 R.$$

The rotor power and torque coefficient in these models can be utilized in the form of look-up tables or in the form of a function. The second approach is presented below, where the general function defining the rotor power coefficient  $c_p$  as a function of the tip-speed ratio and the blade pitch angle is defined as follows [8]:

$$(21) \quad c_p(\lambda, \theta) = c_1 \left( c_2 \frac{1}{\Lambda} - c_3 \theta - c_4 \theta^x - c_5 \right) e^{-c_6 \frac{1}{\Lambda}}.$$

Because the function depends on the WTGS rotor type, the coefficients  $c_1 - c_6$  and  $x$  can be different for various turbines. Additionally, the parameter  $\Lambda$  is also defined in various ways. For example, the parameter  $1/\Lambda$  can be defined as [8]

$$(22) \quad \frac{1}{\Lambda} = \frac{1}{\lambda + 0.08\theta} - \frac{0.035}{1 + \theta^3},$$

while the coefficients  $c_1 - c_6$  are proposed as equal to  $c_1 = 0.5$ ,  $c_2 = 116$ ,  $c_3 = 0.4$ ,  $c_4 = 0$ ,  $c_5 = 5$ ,  $c_6 = 21$  ( $x$  is not used here because of  $c_4 = 0$ ).

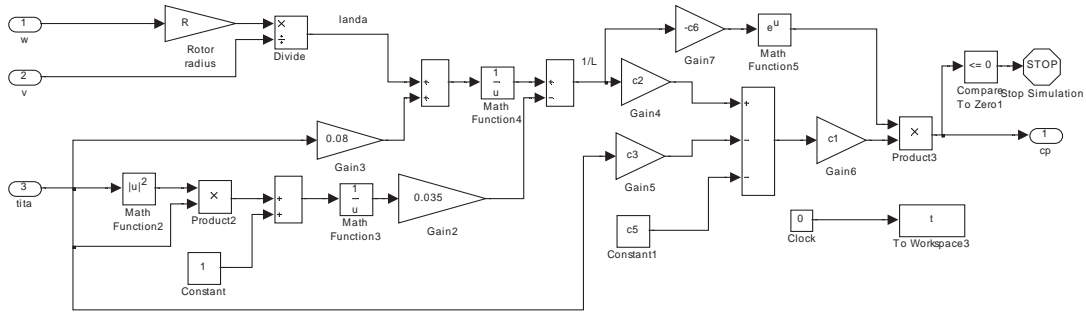


Fig.3. Power coefficient modelling block diagram

In Fig.3 the power coefficient block diagram is shown. An example of the  $c_p(\lambda, \theta)$  characteristics computed taking into account (21) and (22) for  $\lambda \in [2, 16]$  and various blade pitch angles  $\theta$  is presented in two-dimensional graph in Fig.4.

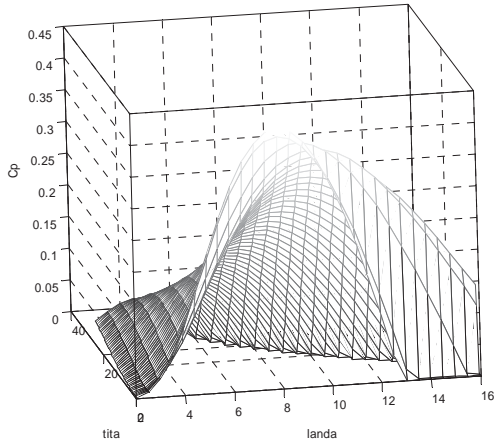


Fig.4. Analytical approximation of  $c_p(\lambda, \theta)$  characteristics

### Blade Pitching System

Although passive stall regulation is a simpler alternative for power limitation, the pitch control is usually preferred in medium to large wind turbine. The pitch actuator is a nonlinear servo that generally rotates all the blades (or part of them) in unison. In closed loop the pitch actuator can be modelled as a first-order dynamic system with saturation in the amplitude and derivative of the output signal [5, 6]. In Fig. 5 a block diagram of the first-order actuator model is shown. The dynamic behaviour of the pitch actuator operating in its linear region is described by the differential equation

$$(23) \quad \dot{\theta} = -\frac{1}{T} \theta + \frac{1}{T} \theta_{ref},$$

where  $\theta$  and  $\theta_{ref}$  are the actual and desired pitch angles, respectively.

Typically  $\theta$  ranges from  $-2^\circ$  to  $30^\circ$  and varies at a maximum rate of  $\pm 10^\circ/s$  [9].

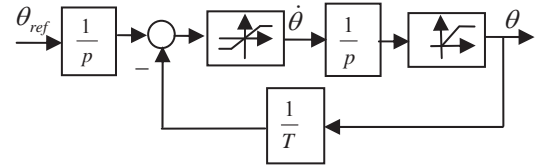


Fig.5. Model of the pitch angle actuator

Power regulation may demand fast and large correction of pitch angle. Therefore, the bounds on the rate of change and amplitude of the pitch angle have appreciable effects on the power regulation features.

### Wind Wheel Dynamics

The process of energy conversion from wind to mechanical energy has a dynamic nature. This is because of the air features and the wind wheel mechanical characteristics. Some authors propose modelling the process of the energy conversion by the wind wheel as a first-order differential equation described by the lead-lag transfer function. The function parameters  $k_w$ ,  $T_{w1} > T_{w2}$  vary and depend on the rotor speed and the blade configuration and type [8]

$$(24) \quad W(p) = \frac{P_R(p)}{P_{ww}(p)} = k_w \frac{T_{w1} p + 1}{T_{w2} p + 1}.$$

For medium-size WTGS with asynchronous generator and stall type power control system, the parameters can be estimated as  $k_w = 1$ ,  $T_{w1} = 3.3 s$ ,  $T_{w2} = 0.9 s$ .

### Mechanical Eigenswings Modelling

When analyzing the WTGS operation in the power system and its influence on the power system and power quality, it is necessary to take into consideration the effects that act on the rotor as torsion oscillations. These oscillations (mechanical eigenswings) go through the shaft and generator on to the electric part of the WTGS and appear as harmonics in the electric power supplied to the grid. The main mechanical eigenswings that appear in the electric power are related to the following effects:

- Asymmetry in the wind turbine;
- Vortex tower interaction;
- Blade eigenswings (depend on the construction).

The research and experiments in [7, 8] show that the above-mentioned eigenswings are the only possible eigenswings in three-blade wind wheel. The mechanical eigenswings can be modelled as a set of harmonic signals added to the power  $P_R$  extracted from the wind. Therefore the power passed through the drive train can be modelled by the following equations [8]

$$(25) \quad P_W = P_R + P_R \sum_{k=1}^3 A_k \left( \sum_{m=1}^2 a_{km} g_{km}(t) \right) h_k(t),$$

$$(26) \quad g_{km}(t) = \sin \left( \int_0^t m \omega_k(\tau) d\tau + \varphi_{km} \right),$$

where the index  $k$  refer to the  $k$ th kind of eigenswings, index  $m$  refer to the  $m$ th harmonics, and  $A_k$  is the magnitude;  $\omega_k$  - frequency;  $h_k(t)$  - modulation;  $g_{km}$  - distribution;  $a_{km}$  - normalized magnitude of  $g_{km}$ ;  $\varphi_{km}$  - phase. Typical values of the parameters describing the mechanical eigenswings are presented in Tabl. 1.

**Table 1**

Typical values of the mechanical eigenswings parameters

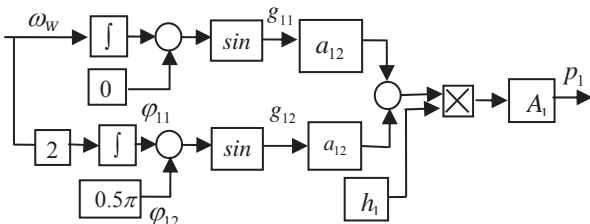
$k$	Source of eigenswings	$A_k$	$\omega_k$ [rad/s]	$h_k(t)$
1	Asymmetry	0.01	$\omega_W$	1
2	Vortex tower interaction	0.08	$3\omega_W$	1
3	Blades	0.15	$2\pi \cdot 4.5$	$0.5(g_{11}(t) + g_{21}(t))$

$k$	Source of eigenswings	$m$	$a_{km}$	$\varphi_{km}$ [rad]
1	Asymmetry	1	0.8	0
		2	0.2	$\pi/2$
2	Vortex tower interaction	1	0.5	0
		2	0.5	$\pi/2$
3	Blades	1	1.0	0

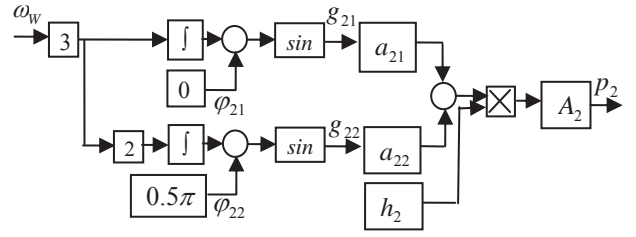
In Fig. 6 the main steps in modelling of (25) - (26) are presented. The resulting output power is

$$(27) \quad P_W = P_R + P_R (p_1 + p_2 + p_3),$$

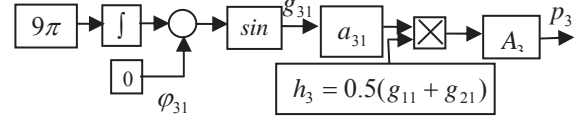
where the  $p_i$  components are the local power fluctuations generated from the  $i$ th source of eigenswings.



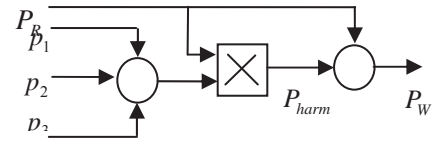
a. Mechanical eigenswings component  $k=1$



b. Mechanical eigenswings component  $k=2$



c. Mechanical eigenswings component  $k=3$



d. Resulting output power

Fig.6. Mechanical eigenswings modelling

### Drive Train Model

The drive train of a wind turbine generator system consists of a blade – pitching mechanism, a hub with blades, a rotor shaft and a gearbox with breaker and generator. The moment of inertia of the wind wheel is about 90% of the drive train total moment, while the generator rotor moment of inertia is equal to about 6-8%. The remaining parts of the drive train comprise the rest (2-4%) of the total moment of inertia. At the same time the generator represents the biggest torsion stiffness. The stiffness of the rotor shaft is about a hundred times less and the stiffness of the hub with blades is about fifty times less than the generator stiffness. Therefore the torsion vibrations of the drive train elements can highly influence the WTGS performance.

The acceptable and common way to model the WTGS rotor is to treat the rotor as a number of discrete masses connected by springs defined by damping and stiffness coefficients. The minimal realization of the drive train as an element of the WTGS model in the power system operation analysis is based on the assumption of two lumped masses only: the generator (with gearbox) mass and the hub with blades (wind wheel) mass.

We consider the two-mass model, but with an explicit defined gearbox transmission ratio  $\nu$ . The graphical form of the model is presented in Fig. 7.

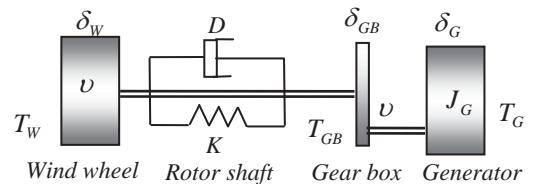


Fig. 7. Two-mass drive train model with gearbox

In this model the superscript ( $W$ ) denotes the wind wheel, and the superscript ( $G$ ) denotes the generator side of the gearbox. The rotor shaft model is defined here by the damping and the stiffness coefficients  $D$  and  $K$ . The influence of the generator shaft is neglected here because the generator shaft is usually shorter than the rotor shaft and at the same time the torque acting on the generator shaft is  $\nu$  times lower than the torque acting on the rotor shaft, result of the gearbox operation. The drive train presented in Fig. 7 can be described by the following set of equations:

$$(28) \quad J_W \frac{d^2 \delta_W}{dt^2} = T_W - T_{GB},$$

$$(29) \quad J_G \frac{d^2 \delta_G}{dt^2} = T_W - \frac{T_{GB}}{\nu},$$

$$(30) \quad T_{GB} = K(\delta_W - \delta_{GB}) + D \left( \frac{d\delta_W}{dt} - \frac{d\delta_{GB}}{dt} \right),$$

where  $\omega_G = \nu \omega_{GB}$ ,  $\delta_G = \nu \delta_{GB}$ .

The block diagram of two-mass drive train model with gearbox in accordance with the equations (28)-(30) is presented in Fig. 8.

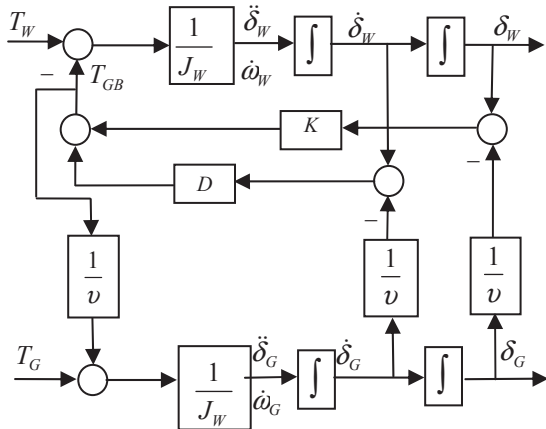


Fig. 8. Block diagram of two-mass drive train model with gearbox

The derived sub-models are combined into a complete model of WECS, shown in Fig. 9.

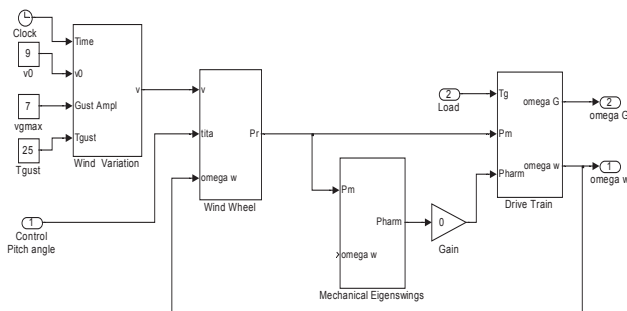


Fig. 9. Block diagram of WECS

## Conclusion

In this paper the mathematical descriptions of the main WECS components are explored. The block diagrams of the sub-system models are presented. On their base the complete WECS model is created. These models are a part of the complete WTGS model. The stochastic behaviour of the wind dynamics model is studied. An approach that allows exact computation of stochastic process with a given spectral density function is proposed. This procedure is especially effective for a non rational shaping filter transfer function. On the base of plant model different control systems and strategies can be designed and explored.

## Acknowledgement

The author would like to thank the Bulgarian National Research Fund for the financial support (contract EE 106/07) and the Technical University-Sofia for the co-financing (contract 08451c1).

## References

- [1] EWEA (2004) *Wind industry factsheets*. Technical reports. European Wind Association (EWEA). <http://www.ewea.org>
- [2] van Baars, G. and Bongers, P. (1994). Closed loop system identification of an industrial wind turbine system: experiment design and first validation results. Proceedings of the 33th Conference on Decision and Control, pp.625-630. Lake Buena Vista, USA.
- [3] Leithead, W., de la Salle, S., and Reardon, D. (1991). Role and objectives of control for wind turbines. *IEE Proceedings-C*, 135-148.
- [4] Burton, T., Sharpe D., Jenkins N., and Bossanyi E. (2001). *Wind Energy handbook*, JohnWiley&Sons.
- [5] Leithead, W., and Connor, B. (2000). Control of variable speed wind turbine: dynamic models. *International Journal of Control*, 1173-1189.
- [6] Thiringer, T. and Peterson, A. (2005). Control of variable – speed pitch regulated wind turbine. Technical report, Chalmers University of Technology, Göteborg, Sweden.
- [7] Akhmatow, V., Knudsen, H., Nielsen, A. (2000). Advanced simulation of windmills in the electric power supply, *J Electrical Power & Energy System*, pp.421-434.
- [8] Lubosny, Z. (2003) *Wind Turbine Operation in Electric Power System*, Springer.
- [9] Bianchi, F., H. De Batista, R. Mantz (2007). *Wind Turbine Control System*, Springer.



**Teofana Puleva** was born in Haskovo, Bulgaria, in 1957. She graduated the Technical University of Sofia as an engineer on automatic control. From 1981 to 1989 she worked at the Research Institute for Power Engineering – hydro power engineering control group. She received Ph.D. degree in 2006 from the Technical University of Sofia. Her scientific interests are in the field of modelling, linear and optimal control systems, adaptive control and application of these methodologies to renewable power plants control. Teofana Puleva is with the Faculty of Automatics, Technical University of Sofia, 8, Kl. Ohridski Blvd., 1000 Sofia, Bulgaria (e-mail: tpuleva@tu-sofia.bg)



# Development of Diagnostic Algorithm Based on Fault Gas Average Concentrations

Janis Dirba and Sandra Vitolina

**Abstract:** The paper gives a short insight into the structure of Latvian high voltage transmission network. The situation in the field of power transformers' diagnostics is analyzed, focusing mainly on the specific features of their maintenance in Latvia. Classification of the most commonly used dissolved gas analysis (DGA) data interpretation methods is given in this paper as well as causes for developing new methods are analyzed. Comparative diagnostic criterion is proposed which is based on typical gas concentration typical level.

**Keywords:** diagnostics, dissolved gas analysis (DGA), power transformers, reliability

## Introduction - Description of High Voltage Transmission Network in Latvia

Electrical network with the voltage 330 kV provides energy to the internal load centers as well as performs energy transmission between southern and northern parts of integrated energy system of the Baltic States. Electrical network with the voltage 110 kV serves for energy supply to the biggest load points. The scheme of the high voltage transmission network in Latvia is shown in Fig.1.

Electrical lines and substations with the voltage 330 kV and 110 kV are the base of the transmission network in Latvia. Current high voltage transmission network developed intensively in the time period from the 1950's to 1990's. Currently, as shown in Table 1, it is composed of 130 substations with 256 power transformers set up with installed capacity 6943 MVA [1].

Table 1

Transformers in the transmission network in Latvia

The highest voltage (kV)	The number of substations	The number of transformers	The installed capacity (MVA)
330	14	19	2825
110	116	237	4118
Total:	130	256	6943

The majority of transformers are put into operation in time period since 1971 till 1990. There are 97 (nearly 40%) power transformers with working life above 30 years, and the number of failures in the high voltage equipment is with tendency to increase. Accordingly the issues of power transformers' diagnostics and prolonging unit's rated working life are topical.

In the late years specific features of transformers' maintenance in Latvia are related to relatively low load. Current high voltage transmission network can provide the transmission of electric energy up to 13 TWh in a year. Today at an average the loading of transmission network and substations reach 60 %, because in the time period from 1991 to 1993 there was sudden decrease of electrical energy consumption. Since 1993 electrical energy consumption became stable and starts to grow slowly in the past few years [2, 3].

On the one hand relatively low load promotes better preservation of transformers' isolation; on the other hand it makes unit's technical condition assessment difficult because the low loading hides possible problems involving heated unit's elements as a result of dissipation flow as well as reduced efficiency of cooling system. The fact has to be considered that at lower temperatures absorption of ageing products in surface of cellulose notably intensifies, thus dissembling actual unit's technical condition. This consideration must be taken in account when the results of dissolved gases analysis (DGA) in oil are interpreted.

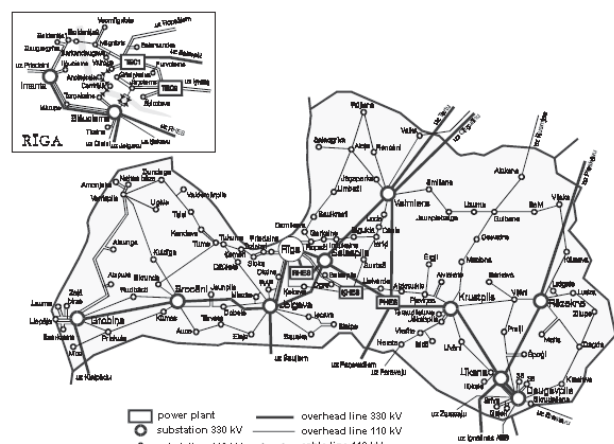


Fig.1. High voltage transmission network in Latvia.

## Problematic Character of Interpretation DGA Results Interpretation

Detection of the faults in their early stage provides high coefficient of readiness of electrical equipment, including power transformers, as it makes possible to perform necessary precautionary measures in time. Variety of different diagnostic methods and assessment criteria can be applied in practice, however dissolved in oil key gas (hydrogen H<sub>2</sub>, methane CH<sub>4</sub>, ethane C<sub>2</sub>H<sub>6</sub>,

ethylene C<sub>2</sub>H<sub>4</sub>, acetylene C<sub>2</sub>H<sub>2</sub>, carbon monoxide CO, carbon dioxide CO<sub>2</sub>) analysis (DGA) is rated as the most important and the most informative method for transformer's technical condition assessment [4].

There are numerous different DGA interpretation methods, which generally can be divided into 3 groups as shown in Table 2.

**Table 2**  
*Classification of DGA interpretation methods*

Group	The gained results	Example of a method
Methods based on key gas concentration limits	Mainly prescribe comparison of current DGA data sample with definite gas concentration limits, thus gaining initial unit's technical condition assessment, mostly the information about the existence of the defect	Total dissolved combustible gas TDCG method (standard IEEE C57-104) [5], key gas method [6], Experience based methods worked out by companies [e.g. 7, 8] etc.
Key gas ratio methods	Prescribe analysis of various key gas ratios (such as CH <sub>4</sub> /H <sub>2</sub> , C <sub>2</sub> H <sub>2</sub> /C <sub>2</sub> H <sub>4</sub> , CO <sub>2</sub> /CO, C <sub>2</sub> H <sub>2</sub> /H <sub>2</sub> etc.) to determine the type and progressing rapidity of the possible defect in power transformer	Dornenburg method [9], Rogers Ratio method [10], Duval Triangle method [11], logarithmic nomograph method [12], standard's IEC599 method [13] etc.
Artificial intelligence methods	Automatic DGA data processing, consideration of unit's specific features, maintenance history, working conditions etc., thus increasing accuracy of unit's technical condition assessment.	Expert systems, interpretation methods based on fuzzy logic or artificial neural networks [e.g. 14, 15].

Expected lifetime and possible defects of power transformers varies widely depending on the manufacturer's design, quality of assembly, materials used, operating history, current operating conditions and current unit's age, maintenance history, and other factors. Thus not a single one-interpretation method can be used for all-purpose application.

Dissolved in oil key gas concentration limits given in the international standards (IEC, IEEE etc.) are tentative and recommendable values. There are numerous researches that show necessity of modifying and differentiate gas concentration levels.

More than a half of power transformers in Latvia have operated above their rated working life thereby power transformer's technical condition assessment considering unit's actual working life parameter is topical issue. It is generally known fact that transformer's isolation parameters changes in the course of time and thus indications of the DGA measurements may differ. Thus it is substantially to open up an opportunity to gain the dissimilar technical condition assessments and different types of possible defects for power transformers with identical DGA data sample but with different current age.

There are various possible versions how to consider current age of power transformers during interpretation of the DGA results such as, for example:

- To estimate and to apply coefficients for separate groups of power transformers with varied age;
- To use key gas concentration average or typical level for separate groups of power transformers with varied age.

The second option of calculating average key gas concentration for varied transformer age groups is analysed on the basis of a case study in this paper. This indicator can be used as a comparative diagnostic criterion.

If key gas concentration of a particular transformer increases above average level of accordant group, the possibility of having a fault also increases, and even if a real fault in particular unit isn't established, the risk factor is still heightened. Thus the use of estimated key gas average levels allows marking out transformers with possible defects that requires additional diagnostic actions, for example, more frequent oil sampling or additional diagnostic testing.

It has to be mentioned that another important aspect that requires readjustment of gas concentration limits given in the international standards is relatively low loading of power transformer's in Latvia [16]. There are 4 basic variations of DGA data interpretation, as shown in Table 3.

**Table 3**  
*Basic condition of DGA data interpretation*

Condition	Key gas concentration limits exceeded	Presence of defect in unit
S <sub>1</sub>	No	No
S <sub>2</sub>	Yes	No
S <sub>3</sub>	No	Yes
S <sub>4</sub>	Yes	Yes

All these conditions can be observed in practice, though condition S<sub>3</sub>, when key gas concentration limits based on standards or other diagnostic methods are not

exceeded but at the same time there is a defect in the unit, is the most undesirable condition. Primary cause of the condition S<sub>3</sub> is long-drawn, low compared to rated, load of a particular power transformer [17]. In accordance with above mentioned higher possibility of defect in a unit even if key gas concentration values don't exceed definite levels, additional caution should be applied at interpretation process of DGA data from power transformers whose loading are low.

### Application of mathematical statistic elements in processing the DGA results

The probability of having a defect in power transformer is related to gas concentration levels. Below certain concentration levels, the probability of having a failure is lower, thus significant primary assessment information can be obtained by calculating individual key gas concentration limits as diagnostic criterion. The probability of having a failure may increase at values much above these limits, and for even though it may never occur; the risk of having one is high. Accordingly for the purpose of monitoring transformer technical condition preferable to mark out units with probable defects, that requires more often DGA sampling. The less are these gas concentration limits the larger amount of power transformers will be marked out for intensified control, and vice versa.

The probability of the appearance frequency of all seven key (H<sub>2</sub>, CH<sub>4</sub>, C<sub>2</sub>H<sub>6</sub>, C<sub>2</sub>H<sub>4</sub>, C<sub>2</sub>H<sub>2</sub>, CO, CO<sub>2</sub>) gases has to be calculated. The size of interval *c* can be determined by formula (1)

$$(1) \quad c = \frac{x_{\max} - x_{\min}}{1 + 3,32 \cdot \lg n}$$

The probability *P<sub>n</sub>*, which characterizes the appearance frequency of particular gas concentration, can be found by formula (2)

$$(2) \quad P_n = \frac{p_i}{T}$$

where T – total amount of transformers;

$p_i = \frac{n_i}{n}$ , *n<sub>i</sub>* – appearance frequency of particular gas concentration; *n* – selection size.

Individual key gas concentration limits are calculated as integral function (3)

$$(3) \quad F_{ni} = \sum_{i=1}^k P_{ni}$$

where *k* ≤ *n*.

The concentration limit for the particular gas is determined at *F<sub>ni</sub>* = 0,9.

### Case Study

For the purpose of this research 224 110 kV power transformers in Latvian transmission network were subdivided into following 5 age groups as shown in Table 4. Such classification was chosen since it gives possibility to analyze the DGA data separately for:

- New and comparatively new transformers – groups № I and № II,
- Units' whose rated working life draws to an end (that in accordance with [18] is 25 years) – group № III, and transformers' that slightly exceed rated working life – group IV,
- Unit's that exceed rated working life for more than 5 years – group № V.

**Table 4**

*Grouping of transformers according to working life*

Group №	Current age	Proportion of units in the group
I	0 – 9 years	4%
II	10 – 19 years	8%
III	20 – 25 years	23%
IV	26 – 30 years	25%
V	> 30 years	40%

Calculation of average or typical gas concentration levels of 7 key gases – H<sub>2</sub>, CH<sub>4</sub>, C<sub>2</sub>H<sub>6</sub>, C<sub>2</sub>H<sub>4</sub>, C<sub>2</sub>H<sub>2</sub>, CO, CO<sub>2</sub> – for original DGA data sample and each representative DGA sample (classified according to unit's current age) was estimated in accordance with methodology described above. It prescribes determination of the length and number of calculation subintervals, estimation of the probability which characterizes the appearance frequency of particular gas concentration, and finally average individual key gas concentration limits are calculated as integral function.

It has to be mentioned that key gas concentration level of power transformers in Latvian transmission network is relatively low; most calculated typical values *μ<sub>i</sub>* are less than 50% of limit concentration values *A<sub>i</sub>* prescribed in IEC standards. Heightened concentration level over 50% of accordant limit concentration is observed for carbon monoxide CO ( $\frac{\mu_i}{A_i} = 68.2\%$ ) and concentration over 100% of accordant limit concentration is observed for acetylene C<sub>2</sub>H<sub>2</sub> ( $\frac{\mu_i}{A_i} = 113\%$ ) in transformers with the voltage level 110 kV.

Key fault gas typical concentration levels for representative DGA data samples of power transformers classified to unit's current age is given in Table 5.

As shown in Fig. 2. typical key gas concentration level for group I is higher than for group II, which could be attributable to the factor that change of obsolete transformers to the new units basically is performed in the most responsible and the most difficult in the aspect of maintenance locations of the transmission network. As of the group II typical gas concentration values increase for almost all key gases (with the exception of C<sub>2</sub>H<sub>4</sub>). Particularly evident augment can be observed for hydrogen H<sub>2</sub> (from  $\frac{\mu_i}{A_i} = 5.7\%$  for group II up to

$$\frac{\mu_i}{A_i} = 35.3\% \text{ for group V}).$$

**Table 5**

Key fault gas typical concentration levels for transformers with voltage level 110 kV classified according to unit's current age

Key gas	Typical value $\mu$ , ppm				
	I	II	III	IV	V
H <sub>2</sub>	19.4	5.7	7.3	11.9	35.3
CH <sub>4</sub>	7.8	3.6	4.7	8.3	8.3
C <sub>2</sub> H <sub>6</sub>	4.2	1.5	3.6	4.0	5.1
C <sub>2</sub> H <sub>4</sub>	27.5	5.9	34.2	61	8.5
C <sub>2</sub> H <sub>2</sub>	9.6	4.1	13.1	24.6	18.7
CO	363.1	190.3	247.7	325.2	355.1
CO <sub>2</sub>	2786.8	1267.7	1725.6	2067.1	2635.4
<sup>1)</sup>	10	19	51	56	88
<sup>2)</sup>	65	186	507	658	912

<sup>1)</sup> The number of transformers in the representative sample

<sup>2)</sup> Data samples for each key gas

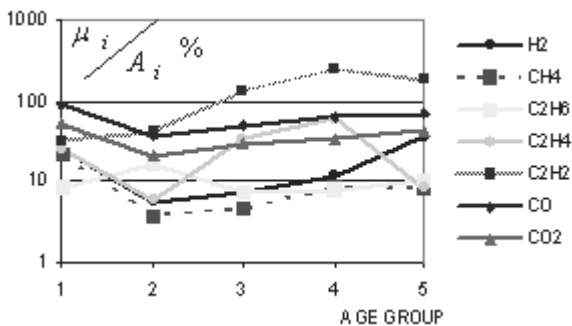


Fig. 2. Evaluation of key fault gases typical concentration levels within the framework of transformers' age groups.

## Conclusions

1. Study of scientific research papers shows that variety and dissimilarity of different DGA data interpretation methods can be applied in practice, unfortunately not a single one-interpretation method can be used for all-purpose application.
2. Due to relatively low loading of power transformers in Latvia there is higher probability of having the most undesirable condition, when key gas concentration limits based on standards or other diagnostic methods are not exceeded but at the same time there is a defect in the unit. This higher probability appoints the necessity to develop new diagnostic criterion for interpreting DGA results.
3. Calculation of average (typical) key gas concentration for varied transformer age groups and use of estimated values as comparative diagnostic indicator is proposed in this paper thus to open up opportunities for marking out transformers with possible defects more efficiently.

## References

[1] Annual report 2005, JSC „Latvenergo”, 2006. / Internet. <http://www.latvenergo.lv>

[2] “The main statements on development of energy sector in the time period from 2006.–2016 ”, Ministry of Economics of Republic of Latvia, 2005. / Internet. <http://www.em.gov.lv/> (in Latvian)

[3] Central Statistical Bureau of Latvia. / Internet. <http://www.csb.lv/>

[4] Cazes J. “Encyclopedia of Chromatography”, 2004 Update Supplement, Marcel Dekker Inc., NY, USA, 2004, p1672.

[5] Guide for the Interpretation of Gases Generated in Oil-Immersed Transformers, Institute of Electrical and Electronic Engineers. Standard IEEE C57-104™-1991, Institute of Electrical and Electronic Engineers, 1991. – 40 p.

[6] Pugh D.R. Advances in Fault Diagnosis by Combustible Gas Analysis // Minutes of Forty-First International Conference of Doble Clients, 1974, Section 10-1201.

[7] J.B.Digrigorio J.B. Dissolved gas analysis of mineral oil insulating fluids / Internet. <http://www.nttworldwide.com/tech2102.htm>

[8] Sayedsaad Co.: Gases analysis / Internet. <http://sayedsaad.com/transformer/index.html>

[9] Stebbins R.D., Kelly J.J., Myers S.D. // Power Transformer Fault Diagnosis, 1997 IEEE PES WM, Panel Session, New York, Feb 6, 1997. –pp. 463-468.

[10] Rogers R.R., U.K. Experience in the Interpretation of Incipient Faults in Power Transformers by Dissolved Gas-in-oil Chromatography Analysis (A Progress Report) // Minutes of Forty-Fourth International Conference of Doble Clients, 1977, Section 10-501.

[11] Duval M. et al., Update on Hydro-Quebec's Experience in the Interpretation of Dissolved Gas Analysis in HV Transformers, Paper 110-14, CIGRE Symposium, Berlin, 1993. –18 p.

[12] Dornenburg E., Strittmatter W. Monitoring Oil-Cooled Transformers by Gas Analysis // Brown-Boveri, Vol.61, No.5, 1970 – 238 p.

[13] Mineral Oil-Impregnated Electrical Equipment in Service-Interpretation of Dissolved and Free Gas Analysis. Standard IEC 60599:1999, International Electrotechnical Commission, 1999. –69 p.

[14] Huang Y.C., Huang C.M. Evolving Wavelet Networks for Power Transformer Condition Monitoring // IEEE Transactions on power delivery, Vol. 17, NO. 2, April 2002. –pp. 412-416

[15] Morais D.R., Rolim J.G. A Hybrid Tool for Detection of Incipient Faults in Transformers Based on the Dissolved Gas Analysis of Insulating Oil // IEEE Transactions on power delivery, Vol. 21, NO. 2, April 2006. –pp. 673-680.

[16] Dirba J., Vitolina S. The application of mathematical statistics in processing the DGA results for developing diagnostic criterion considering specific maintenance features of power transformers' in Latvia // ECT2007 Conference Proceeding on CD, Kaunas, Lithuania, 2007. – pp. 167 – 170

[17] Попов Г.В. Об оценке состояния трансформаторов по результатам хроматографического анализа // Электро. - 2003. - № 3. - с. 36-40.

[18] Technical maintenance of power stations, electrical networks and consumer's electrical installations, LEK 002, Latvian. – 73 p.



# Simulation of an electrical power system of compressor station of the main gas pipeline with electricity generating plant of own needs

Valery Goldshtein, Pavel Grachev, Youri Koubarkov

**Abstract:** The considered object represents an electrical power system consisting of a source of restricted power (gas-turbine electricity generating plant (GTEGS) of own needs of compressor station), connected to gas pumping over aggregates (GPA), consuming the basic power, and other less powerful customers of the electric power for service of compressor station.

**Keywords:** information, electrical system, substations, mathematical model, electric machines.

The approximate calculation has shown, that the start (straight line or with reactors) engines of 12500 kW is possible from GTEGS with turbogenerators TVF-100 or TVF-110. In this case from it can simultaneously work up to 6 GPA with engines of the indicated power [1].

The mathematical models for updated calculation of processes in an electrical power system with GPA are designed. The mathematical model of an electrical part of a system consists of model of a turbogenerator GTEGS, electric motors GPA and equivalent loads low-power.

The electromechanical converters were modelled with applying of the generalized theory of electric machines. At construction of computational model of transients in an electrical power system with GPA for simplification of model, at the registration of influencing on process of launch of an excitation winding and electrical asymmetry of starting windings of a rotary table, the transformation (conversion) of the generator and engine to equivalent twophase electric machines is conducted. The matrixes of transformations respond a condition of invariancy of power.

## Feed circuits electrodrive GPA GM from gas-turbine electricity generating plants of own needs.

The most widespread kinds of engines for the drive of centrifugal compressors now is electric motors and combustion turbines.

It is accepted to call centrifugal compressors with compression ratio superior 1,1, not furnished by devices for cooling of gas in compression process, centrifugal superchargers. On compressor station set 4 and more centrifugal superchargers electrically-driven. The working aggregates of compressor station partition on in bridge working groups. In each of these groups one supercharger or 2-3 sequentially of joint supercharger can work.

In a structure of a compressor unit electrically-actuated enters: a centrifugal supercharger boosting reduction gearbox, established between arbors of the elec-

tric motor and supercharger, electric motor with a control equipment, lubricating system, blower of the motor, instrumentations.

On compressor stations of gas mains (GM) electrically-driven of centrifugal superchargers the installed power of customers of the electric power can reach 100 MW and more.

Let's consider a feed circuit electrodrive GPA GM « of a dead-end type », that is counted basically on a feed given CS and exploited by staff CS. In a feed circuit of such type the shield unit is mated with a main instrument assembly CS. The distribution device DD 6 (10) kV contains here only cells indispensable for a feed of customers CS.

In a Fig. 1. the skeleton diagram of a feed of electric drives GPA with one turbogenerator of gas-turbine electricity generating plant of own needs (GTEGS) is figured.

The synchronous generator (GS) GTEGS is resulted in rotation by a combustion turbine (T) with an automatic regulator of speed (ARS). The synchronous generator has an automatic regulator of excitation (ARE), adjusting voltage on modular trunks. GS is hooked up to modular trunks through the disconnecter and double pole circuit-breaker defending from short circuits on modular trunks. The engines alternating-current GPA (M1, M2, M3, M4) paired to modular trunks through disconnectors and double pole circuit-breakers.

The transformer of own needs (TON) with voltage 6 (10) /4 kV in the same way paired to modular trunks. The management system CS should envision an individual drive of electric drives GPA to avoid invalid brownout on modular trunks.

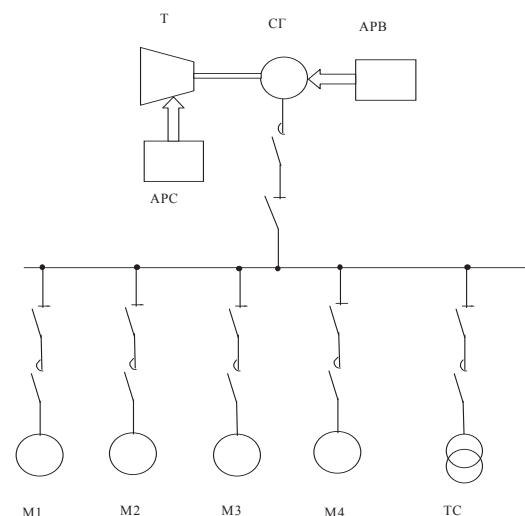


Fig 1.

The version of fulfilment GTS with two generators is possible.

### Mathematical model of processes in a system GPA at a feed of the electric drive from a source of restricted power

The turbogenerator GTEGS represents a non-salient pole synchronous machine with a solid rotor [2].

The mathematical model includes following group of equations: equations of electrical equilibrium; an equation of motion of a rotary table; equations for flux linkages of a winding; an equation for the electromagnetic moment [3].

The mathematical model allows for changes fissile and induced drags of electric motors GPA, arising at a frequency drift of a current in a winding the replacement, (expulsions,) conditioned by a phenomenon, of a current in sections of a winding at the expense of a skin effect in conductors submerged on ferromagnetic environment. The saturation of magnetic circuits of electric machines on the basic magnaflux is taken into account also.

The parameters of rotor contours, exitation winding and equivalent roll-damping winding, are resulted in a phase of a statoric winding. It allows to simplify both record, and procedure of the solution of a system of differential equations depicting process.

It will present equations for flux linkages of a circuit of a rotary table.

For an exitation winding

$$\Psi_f = L_{\sigma f} i_f + (M_{f1} (i_a \cos \gamma_a + i_b \cos \gamma_b + i_c \cos \gamma_c) + M_{ff} i_f + M_{fpd} i_{pd}).$$

For an equivalent winding of a rotary table on an axis d

$$\Psi_{pd} = L_{\sigma pd} i_{pd} + (M_{pd1} (i_a \cos \gamma_a + i_b \cos \gamma_b + i_c \cos \gamma_c) + M_{fpd} i_f + M_{pdpq} i_{pd}).$$

For an equivalent winding of a rotary table on an axis q

$$\Psi_{pq} = L_{\sigma pq} i_{pq} + (M_{pq1} (i_a \sin \gamma_a + i_b \sin \gamma_b + i_c \sin \gamma_c) + M_{pqpd} i_{pd}).$$

Identifications adopted in the formulas:

L - leakage inductance accordingly phases of a stator, exitation winding, equivalent winding of a rotary table on an axis d and q of a rotary table;

M - own (from a current in the winding) mutual inductances accordingly phases of a stator at orientation of its magnetic axis on an axis d and on an axis q of a rotary table, exitation winding, equivalent winding on axes d and q of a rotary table;

$M_{f1}$ ,  $M_{pd1}$ ,  $M_{pq1}$  - mutual inductances between a phase of a stator and, accordingly, exitation winding, equivalent winding on axes d and q of a rotary table;

$M_{fpd}$  - mutual inductance between an exitation winding and equivalent winding on an axis d of a rotary table; a, b, c - angles determining orientation in a considered instant of a centerline of a rotary table d concerning magnetic axes, accordingly, phases A, B and C of a stator.

Research of transient regimes in a system GPA at a feed of the electric drive from sources of restricted power.

The calculations were conducted on personal computers. The program envisions conversational operation. Setting pressure voltage GTEGS, the user selects calculation of this or that version.

For calculation the special package was used. The type of transient, operational mode and other data are set by the user in the file of input datas. The mode of repetition of several identical modes, for example of mode of launch or mode of retraction in a synchronism is possible. In the latter case initial values of variables are read out from files of zero conditions, in which one enters the name final values of variables obtained at the previous stage of calculation.

In a fig. 2 the computational oscillogramms of the moment and rotational speed, by the beginning of process of start STD is shown.

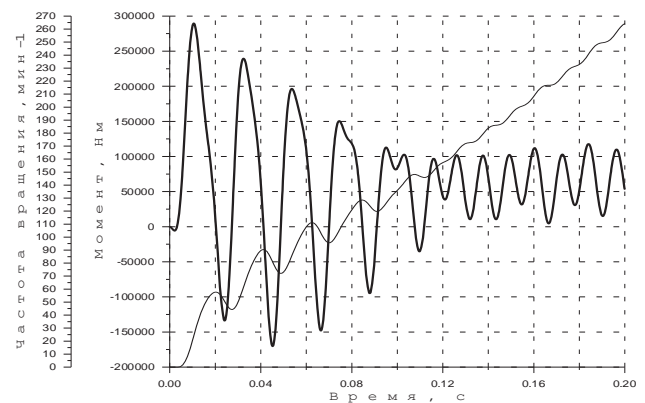


Fig. 2

### Variable parameters of the engine GPA

Let's put the charts of relations of parameters of the engine STD - 12500 from a current frequency in a rotary table. They are rotined in a fig. 1 and 2. In a fig. 1 the changes of coefficient of self-inductions and mutual inductances of the synchronous engine and in a fig. 2 - change of pure resistances of a winding of a rotary table of this engine are rotined.

These parameters are counted on a technique set up in [3] for several values of frequencies from 0 up to 50 Hz.

As follows from the charts of change of coefficient of self-inductions, at a current frequency of a rotary table less than 15 Hz is watched their sharp ascending. The curves of Fig. 2 change of coefficient of self-inductions and mutual inductances are entered into model of the synchronous engine STD. They are approximated by exponential functions.

At the introducing of functions depicting change of pure resistances of a rotary table, in model of the synchronous engine STD the capability of excess of rotational speed by synchronous was allowed, at retraction of the engine in a synchronism. The curves of changes of pure resistances are approximated by linear dependences.

## Activity of the electric drive GPA from the thiristor device of smoothly varying launch.

Usually at an engine start-up GPA for limitation of starting currents and impact moments will use reactors which are switched on sequentially with phase conclusions of the engine. The processes of launch GPA with STD - 12500 through standard reactors are illustrated by the computational oscillograms.

It is possible to reduce transient component of a current of a stator of the engine and by that to limit impact value of the moment at the expense of reduction rate of onset of the engine, applied on a stator, of voltage. However, thus the growth enforced component of a flow decreases also, that can result in reduction a mean accelerating torque of the engine (it takes place at reactor launch). Therefore limits of an alteration of speed of a supply voltage should be limited so that the reduction of the alternating transient moments did not reduce response of the electric drive.

It can be reached at control of speed of change of the applied voltage with the help of thiristor commutators with a controlled angle of actuation of thyristors. In such commutators will realise the exponential law of an angular variation of control of thiristor commutators. In [2] is rotined, that the control characteristics of the drive at an angular variation of control under the exponential law practically do not differ from the characteristics of amplitude, received at change, of the engine, applied on a stator, of voltage under the same law.

Therefore process of launch of the engine GPA with the thiristor commutator was modelled by change of a voltage excursion of a stator on a desired law.

The conducted researches have shown, that the optimal time constants of an angular variation of control of the thiristor device of launch lie within the limits of 0,01 - 0,02 seconds, depending on initial position of a rotary table STD.

Thus the considerable reduction asynchronous periodic component of the moment without essential reduction of average value of an accelerating torque is watched. However during an engine acceleration considerable is watched periodic component of the electromagnetic moment conditioned by an asymmetry of a rotary table STD.

## Conclusions

The researches have shown, that GPA with engines STD-6300 requires for normal start of electricity generating plant of own needs with a turbogenerator TVS-32. The start STD -12500 from stations by power 40 MVA with TVS-32 practically is impossible because of voltage falls at launch superior 25 %.

The start engines STD -12500 is possible from electricity generating plant, GTU by which one contains a turbogenerator TVF-100 or TVF-110. In this case from it

can simultaneously work up to 6 GPA with engines of the indicated power.

## References

- [1] The ACEC integrated gas expansion turbine and high frequency generator. ACEC-review No. 2 - 1986.
- [2] Slizskii E.P., Shkuta A.F., Bruev I.V. Self-start of electrodrive compressor stations of the main gas pipeline - M.: Nedra, 1991.- 187 ps.
- [3] Titov V.V., Hutoretskii G.M, Zagorodnaya G.A. Etc. Turbogenerators. Design and calculation.- L:Energiya, 1967.- 896 ps.

## Biographies



**Pavel Grachev** was born in Samara, Russia, on Octobre 30, 1947. He studied at the Technical University of Samara-Russia, and received degree of the candidate of engineering science from the same university in 1985.

His field of interest includes electrical machines, electrical networks and renewable energy sources (electrical aspects). He is today a Lecturer and Researcher in the Faculty of Electrical Engineering of the Technical University of Samara.

Pavel Grachev is with the Faculty of Electrical Engineering, Technical University of Samara, 224, Pervomaiskaya st., 443010 Samara, Russia.



**Valery Goldshtein** was born in Samara, Russia, on April 10, 1941. He studied at the Technical University of Samara-Russia, and received degree of the candidate of engineering science from Technical University of S-Peterburg in 1973 and the doctor of engineering science in 2006.

His field of interest includes areas of engineering of high tensions and electromagnetic compatibility. He is today a Professor and

Researcher in the Faculty of Electrical Engineering of the Technical University of Samara.

Valery Goldshtein is with the Faculty of Electrical Engineering, Technical University of Samara, 224, Pervomaiskaya st., 443010 Samara, Russia.



**Youri Koubarkov** was born in Samara, Russia, on August 20, 1944. He studied at the Technical University of Samara-Russia and has defended a thesis and has received a degree of the candidate of engineering science in 1976 in Technical University of S-Peterburg.

Since 1968 he worked in the Faculty of Electrical Engineering of the Technical University of Samara as a Lecturer and researcher in the field of software engineering for operational modes of electrical power systems.

Youri Koubarkov is with the Faculty of Electrical Engineering, Technical University of Samara, 224, Pervomaiskaya st., 443010 Samara, Russia (e-mail: tsara@sama.ru).

# Applying of an informational - analytical complex for the solution of technological and computational problems in electrical power systems of gas mains with high-voltage electric motors

Valery Goldshtein, Pavel Grachev, Youri Koubarkov

**Abstract:** Now there is a more and more actual implementation in a full volume of problems, bound with the solution of computational, reference, repair problems, with a tentative estimation of availability index of product of the equipment of substations (SS) of electrical power systems of firm, automatic formation of test schedules and repairs, budget documentation on their realization.

**Keywords:** information, electrical system, substations, mathematical model, electric machines.

Rational usage of the schemes of the substations, the calculations of operational modes, energy losses and selection of measures on their decrease, check of the equipment in a mode of a short circuit (SC) etc., provide at the end main role by selection of measures for economies of energy.

## Features and problems of simulation of electrical networks with usage of GIS-KNOW-HOWS

Usage a hybrid module in maintenance practices of electrical networks should implement in view of a number of features of their simulation as object of control (operational modes, economical optimization), with the solution of some problems, bound with a dynamic estimation of topological communications (commutation, affixture and deleting of objects) and accuracy of mapping of object on the topographic basis (positioning on terrain, improvement of exploitation), and also legal problems of usage of geo information know-hows (GIS-KNOW-HOWS).

The electrical networks are difficult on the configuration and are dynamical on time - their topology permanently changes pursuant to a current condition of switches.

The editing tools of the schemes of electrical networks should enable definition of set of special rules controlling permissible and invalid operations at definition of a switching sequence and change of their configuration.

## Problems of usage of GIS-KNOW-HOWS in electrical networks

Is amalgamated these problems it is possible to divide into three large groups, introduced by way of their installment development:

- Directory;
- Rated - analytical;

- Operative - administrative.

The directory group of problems to the present time has received the greatest development and already today can be successful enough be decided in domestic electrical networks in view of features, listed in the previous section.

Already now it is possible to tell, that the applying of GIS-KNOW-HOWS with their staticized graphic and theme databases about parameters of networks and their loads allows more confidently, objective and is justified:

To value admissibility and capability of fulfilment of the repair and emergency applications;

To give more particular and in-depth orders on fulfilment of repair, emergency and operational activities on power object;

In view of the theory of consulting models and available knowledge base to analyze distresses in electrical networks with the indicating of places of emergencies,

To reshape optimal policy of their liquidation with the control of a regularity of operating switchings.

To value a current situation in electrical networks, watching on an electronic card a substantial rule (situation, position) of operative - exit crews;

For the solution all indicated and number of other problems all should be considerably improved organizational technical activity in an electrical power system. Thus the developed information support on all data set about a production equipment of networks, lines of the communications, customers is indispensable, the retrospective information on different modes and events etc. Demands perfecting process of vocational education and retraining of staff of power services of firm. Its organization is impossible without creation of a developed system of a program - engineering simulator, is informational - teaching of the automated systems etc.

Outgoing from all said, there is an apparent necessity of mining of new breed of a management information system (MIS) of firm automation, oriented on complex problem solving, of electrical networks basing on modern information know-hows and means, adapted to problem solving arising before electrical power systems.

## Complex problem solving of automation of electrical networks

For the solution of computational and technological problems, problem of fulfilment of general repairs of the equipment on its technical condition in electrical power



systems of firm designed the Informational - technological complex (IAC) "«PEGAS»"

ITC "PEGAS" envisions federating with corporate economical, geoinformation and operative - dispatching systems both systems of the registration of the electric power and control of its quality. At partial or full absence of the called systems ITC will realise a minimumly indispensable set of their functions.

#### Assigning of a complex

- maintenance of leaving out of staff about a structure and characteristics of the established equipment of an electrical power system, its current condition, consumption and losses of the electric power, other generalized characteristics of primary activity. The information is caused directly from the scheme. Access to the schemes - from any workstation of a corporate network(grid).
- maintenance of engineering staff of manufacturing services by means of authentic and visual mapping and control of a condition of the particular equipment of substations (SS or MDS) and distributive networks (DN), secondary circuits and devices, means of the registration, telemechanics, communication. Maintenance by help information, means of the registration of defects, deviations, applications, duties, rights etc.
- the solution of rated - analytical problems of control of modes of an electrical power system by engineering staff of manufacturing services and, first of all, of problems of the analysis both minimization of technical and commercial losses of the electric power, as one of effective tools of increase of efficiency and improvement of economical outcomes of transmission systems, distribution and utilization of power.
- maintenance of activity of operative - dispatching staff by the information on a current condition of the equipment of an electrical power system.

The complex allows to organize on computers of firm, integrated local area network, number of workstations, for example: repair staff, staff of electrotechnical lab or service SI, chiefs of electrotechnical services, WTS, operating staff in a part of management of the log-books of defects and equipment failures etc. All workstations of one technologically directional division (for example, the electrosops) have the general database. To this a DB address with the inquiries and chiefs of firms arranging a system of the inquiries of a complex.

The graphic format, tested on much firms, of submission of the schemes "Modus" corporation (Moscow) allows to integrate the schemes, prepared in a nem, in different computational problems. Such schemes can be made accessible of any point of a corporate network through the Internet at unconditional

maintenance of safety requirements by means of protection of a corporate network from unauthorized access.

The following tools of the indirect producers are involved in a tendered system: operating system Windows NT-2000-XP, DBMS Oracle 8.1 or Access, graphic components of the corporation «Modus».

#### **Calculations of operational modes in an electrical power system of gas pipeline of aggregates**

One of primary goals of electrical power systems incorporating high-voltage electric motors, is the necessity of fulfilment of checks of the selected equipment of substation on thermal and dynamic stability, on a breaking capacity of disconnecting switches, and also selection steps of relay protection. Thus the problems on definition of values of currents SC, selection of design points SC, computational kind SC, computational duration of effect of currents SC should be resolved

The computational scheme understand the simplified single line scheme of an electric set with the indicating of all members and their parameters influential in a current of short circuit (SC).

Calculation of currents at three-phase SC run in the following order:

- For the given computational scheme of a system and designed substation make the electrical circuit of displacement and result resistance of members in basic conditions;
- For each unit of an equivalent circuit the equivalent impedance  $Z_{eq}$  concerning a point of a feed or power source is determined;
- Receiving voltage of the power source equal basic, determine parameters of currents SC in clusters of an equivalent circuit.

#### **Calculations of short-circuit currents in view of a replenishment from high-voltage engines**

At a short circuit in a system with a great many of powerful engines the essential influencing on nature of process and value of a current is rendered by groups of electric motors, live near to a damaged area. For asynchronous motors with a cage rotor at close SC the voltage on conclusions of the engine appears less their EMF and the engines pass in a mode of the generator dispatching a current in a place of short circuit(closing). Synchronous engines also supply a place SC.

Component of a current from engines it is necessary to allow at check of vehicles and conductors DD, and also at calculation steps of RPA for the equipment 6-10 kV. For these purposes it is enough to know initial value periodic component of a current SC, impact current and value periodic and aperiodic component of a current SC at the moment of disconnection of contacts of the disconnecting switch.

The initial value periodic component of a current SC from engines is determined by analogy with synchronous generators on expression

$$I_{n0\delta} = \frac{E_{\phi}''}{x_{\delta}''}$$

Where  $E_{\phi}''$  - supertransient EMF;

$x_{\delta}''$  - supertransient resistance induced drag of the engine.

As against generators the reserve electromagnetic both drop energy of engines is small also periodic component of a current SC, created by them, fast damps

$$I_{m\delta} = I_{n0\delta} \times e^{-t/T_{\delta}'}$$

Where  $T_{\delta}'$  - time constants of damping periodic component of a current SC from electric motors (average value for the equivalent engine can be accepted equal 0,07 seconds),

In time t the response time of the disconnecting switch can be accepted.

At absence of nameplate data of electric motors it is possible to use average values of supertransient EMF and supertransient resistance induced drags of engines under the table 1

**Table 1**

*Resistance induced drags of engines*

The type of a source of a replenishment of a place SC	$X_d''$	$E_f''$
Synchronous motors	0,2	1,07
Asynchronous motors	0,2	0,9

On operation conditions it is accepted, that the power 50-60 % from a general installed power of all electric motors, hooked up to a considered unit of a feed simultaneously participate in a replenishment electric motors.

### Calculations of short-circuit currents in view of regulation of voltage of transformers with RUP

In calculations of currents SC on the party of the lowest (mean) voltage of the transformer for definition of parameters relay the automatics are hardwired also it is necessary to estimate influencing of regulation of voltage under power (RUP) of transformers on value of currents SC.

The voltage  $U_k$  are adduced to nominal capacity of the transformer and voltage of the applicable derivation. The definition  $U_k$  is made for any derivation by a linear intrapropation between values at mean and applicable extreme derivations.

The maximum rating of a current SC, passing on the party HV at three-phase SC behind the transformer, is determined on expression

$$I_{к.макс}^{(3)} = \frac{U_{ном}}{\sqrt{3}(x_{с.макс} + x_{тр.мин})}$$

Where  $x_{с.макс}$  - least resistance of a feeding system in a maximum mode of its activity referred to voltage of the party SC;

$x_{тр.мин}$  - least resistance of the transformer (as a rule by activity of the transformer on a second to last branch line), referred to voltage of the party SC;

$U_{ном}$  - voltage rating of a network.

For the registration of imposing of a load current on a current SC and creations of some design margin the voltage of a feeding system can be accepted to equal voltage rating of a network.

The minimum value of a current SC, passing on the party HV at three-phase SC behind the transformer, is determined on expression

$$I_{к.мин}^{(3)} = \frac{U_{макс.с}}{\sqrt{3}(x_{с.мин} + x_{тр.макс})}$$

Where  $x_{с.мин}$  - greatest resistance of a feeding system in a minimum mode of its activity referred to voltage of the party SC;

$x_{тр.макс}$  - greatest resistance of the transformer referred to voltage of the party SC;

$U_{макс.с}$  - maximum main voltage applicable greatest "positive" to the derivation of a winding HV (on operation conditions of isolation under operating conditions this voltage limit is durable by a permissible greatest operation voltage, equal 126 kV, for networks 110 kV).

### Conclusions

The outcomes of calculations on separate power region and centers of a feed are resulted as the schemes of electrical power supply of separate clusters of a feed and data in digital tabulations, applicable to them.

The data on parameters of members (transformers, lines and engines) are received under the operating log-books or schemes or, at their absence, on reference data of the applicable type of the equipment.

The obtained outcomes of an intrusion allow to draw a conclusion, that the designed programmatic complex successfully decides problems, put before it, and can be advised for broad applying in electrical power systems of firms oil producing and oil gas refining of branch. The scalene in-service experience, obtained at it, allows to undertake the subsequent steps for its further perfecting and development.

## References

[1] Rule of the device of electric sets. 6 is.- M.: Energoatomizdat, 1985.

[2] Directives on calculation of short-circuit currents and selection of electric equipment / Under red. B.N.Neklepaev, - M.: ENAS, 2002. - 152 p.

[3] RD 34.20.501-95. Operating instructions of power plants and networks of Russian Federation, "RAO EES of Russia" 24.08.1995., 15 is. (with change №1, Minenergo of Russian Federation 17.07.2000 and "RAO EES of Russia" 23.06.2000).

## Biographies



**Valery Goldshtein** was born in Samara, Russia, on April 10, 1941. He studied at the Technical University of Samara-Russia, and received degree of the candidate of engineering science from Technical University of S-Peterburg in 1973 and the doctor of engineering science in 2006.

His field of interest includes areas of engineering of high tensions and electromagnetic compatibility. He is today a Professor and Researcher in the Faculty of

Electrical Engineering of the Technical University of Samara.

Valery Goldshtein is with the Faculty of Electrical Engineering, Technical University of Samara, 224, Pervomaiskaya st., 443010 Samara, Russia.



**Pavel Grachev** was born in Samara, Russia, on Octobre 30, 1947. He studied at the Technical University of Samara-Russia, and received degree of the candidate of engineering science from the same university in 1985.

His field of interest includes electrical machines, electrical networks and renewable energy sources (electrical aspects). He is today a Lecturer and Researcher in the Faculty of

Electrical Engineering of the Technical University of Samara.

Pavel Grachev is with the Faculty of Electrical Engineering, Technical University of Samara, 224, Pervomaiskaya st., 443010 Samara, Russia.



**Youri Koubarkov** was born in Samara, Russia, on August 20, 1944. He studied at the Technical University of Samara-Russia and has defended a thesis and has received a degree of the candidate of engineering science in 1976 in Technical University of S-Peterburg.

Since 1968 he worked in the Faculty of Electrical Engineering of the Technical University of Samara as a Lecturer and

researcher in the field of software engineering for operational modes of electrical power systems.

Youri Koubarkov is with the Faculty of Electrical Engineering, Technical University of Samara, 224, Pervomaiskaya st., 443010 Samara, Russia (e-mail: tsara@sama.ru).

# Probabilistic approach for thermal and electro-dynamics stresses distribution functions

Ciprian Nemes, Florin Munteanu

**Abstract:** Knowing the thermal and electro-dynamic stresses is crucial to a safe design of equipment and power system components, manufacturing and other key industries but the subject generally does not receive the proper attention in engineering probabilistic design. The magnitude of these stresses depends directly on the short-circuit currents and the fault time and indirectly on the structural system characteristic and state just prior to the fault, the type of fault, etc. These components may be assumed as random variables, so, in order to take in account these parameters in stress analysis, the probabilistic approach will be a new way to explore the engineering design. This paper is designed to provide systematic and relevant knowledge of the thermal and electro-dynamic stress probability distribution functions. It offers a balanced mix of concepts, analytical and applications, while avoiding lengthy analytical demonstrations.

**Keywords:** Thermal and electro-dynamic stresses, probability density function.

## Introduction

Thermal and electro-dynamic stresses can have a negative impact to the electrical equipment with immediate and/or long-term degradation effects. Electrical equipment failures can occur due to local degradation of the components as a consequence of the effect of the thermal or electro-dynamic stresses. Considering that the main cause which goes to the appearance of the thermal and electro-dynamic stresses in the electrical equipment is given by the short-circuit current in the electrical system, in the following, we will analyse the influence of the short-circuit current statistic character, on the thermal and electro-dynamic stresses.

The short-circuit currents and the thermal and electro-dynamic stresses represent important parameters that must be considered in the design of the system buses, breakers, the substation apparatus and, finally, in all aspects of the design of the electrical power sub-systems.

A fault may be appears anywhere in the system while the loads and the configuration of the network continuously changing, so the magnitude of the short-circuit currents has a statistic character, modelled as a random variable. Based on the analytic expressions of the thermal and electro-dynamic stress, depending on the amplitude and the distribution of the short-circuit current, the authors propose in this paper an original method to determine the analytic expressions of the thermal and electro-dynamic stress probability distribution functions.

## The Probabilistic analysis of the short-circuit currents

Based on the deterministic analysis of the three phase short-circuit currents and considering the fault's place as a random variable uniformly distributed, we presented in the other papers [1],[2] the way of changing of a random variable fault's place, in a random variable of the amplitude of the short-circuit current.

Generally, the probabilistic analysis of the short-circuit current, in the given point, is a function of the fault's place on the network line. This function is used together with the probability distribution function of the distance till the point of the fault on the line. Considering the impedance between the source and the fault location, as a function of the type of fault ( $TF$ ) and the condition of the network ( $C$ ), the probability distribution function of the current using the theory of the total probability is given by:

$$(1) \quad P(A) = \sum P(A_i)P(A|A_i),$$

applied to the probability distribution functions:

$$(2) \quad f_I(i) = \sum f_I |_{C,TF}(i|C,TF)P_C P_{TF},$$

where  $f_I |_{C,TF}(i|C,TF) = f_I(i)$  is the probability distribution function of the short-circuit current, conditioned by the type of particular fault and the system state.

For a network with a foregone configuration and with a certain type of fault, the size of the fault current is depending on the distance,  $x$ , from the source, this means  $I=J(x)$ . If the source – fault distance probability distribution function is  $f_X(x)$ , than the probability distribution function of the current may be calculated with the relation:

$$(3) \quad f_I(i) = \frac{dF_I(i)}{di} = \frac{d}{di} \left[ F_X(J^{-1}(i)) \right] = \frac{d}{di} \left[ \int_{-\infty}^{J^{-1}(x)} f_X(x) dx \right]$$

Derived from this change, in the mentioned papers, we developed the main expressions of the probability distribution functions of the short-circuit current, for different networks configurations.

The results of this analysis lead to the conclusion that, although the default place distribution is uniformly, the



default has the same probability to appear for the whole line and the probability is as smaller as its length is bigger. The probability of appearance of the short-circuit current are very different, the probability distribution function of the short-circuit current have a different shape, directly influenced by the network configurations. For most of the analysed configurations, we demonstrated that the small values of the short-circuit current have bigger probability than the current with big values. In other words, the frequency of the small current appearance is bigger than the frequency of big currents, the values of the frequencies depending on the configuration, dimension and system parameters. This reality can be explained by the fact that the growth of the line length on which the fault appears, lead to the decrease of the probability of the fault appearance in one point and the domain of definition of the variable short-circuit currents amplitude, increases.

From the study of the analysed network configurations, we can assume that the growth of the number of parallel lines or loops connected to the same bus system, lead to the acquiring of some probability distribution functions of short-circuit currents, centred to the small values.

Considering the currents limiting methods and the possibility of presence of the currents limiting equipment within the electrical power system, the authors obtained the mathematical expressions of the probability distribution function of the short-circuit currents. Depending on the probability of working with associated currents limiting equipment, the growth of the efficiency of the currents limiting equipment involves a study that brings into discussion the short-circuit currents distribution with or without currents limiting equipment.

### The probabilistic analysis of the thermal and electro-dynamic stresses

To evaluate the probability distribution function of the thermal and electro-dynamic stresses, we will consider the deterministic analysis of the stress induced by three-phase short-circuit currents.

The Figure 1 shows the history of the short-circuit current, with and without the automatic voltage regulator (AVR), whereby the relationship is shown between the thermal stress, peak short-circuit current,  $I_p$ , the subtransient short-circuit current,  $I_k''$  and the disconnecting short-circuit time,  $t_k$ .  $I_k''$  changes into the steady-state short-circuit current  $I_{k\infty}$ .

For faults located at a considerable distance from generators, it can be assumed that  $I_{k\infty}$  is equal to  $I_k''$ . With faults close to generators,  $I_{k\infty}$  is always less than  $I_k''$ .

The analytic expressions of the thermal and electro-dynamic stresses, depending on the short-circuit current are:

$$(4) \quad ST(t_k) = \int_0^{t_k} i_k^2(t) dt = \int_0^{t_k} i_{kp}^2 dt + \int_0^{t_k} i_{ka}^2 dt \approx I_{k\infty}^2 t_f,$$

and the peak short-circuit current  $I_p$  is determined from the subtransient short-circuit current  $I_k''$  in accordance with the following relation:

$$(5) \quad I_p = \sqrt{2} \cdot k_p \cdot I_k''$$

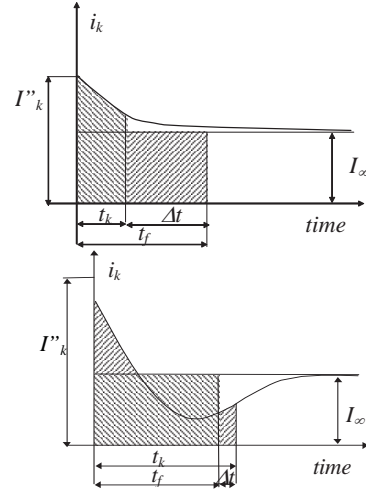


Fig.1. The history of the short-circuit current, without and with the AVR

Considering also the distributions of the short-circuit current, we propose, in what follows, an original method to determine the analytic expressions of the distribution functions of the thermal  $ST(t_k)$  and electro-dynamic  $I_p$  stresses [3].

$$(6) \quad f_{ST}(ST(t_k)) = f_I \left( \sqrt{\frac{ST(t_k)}{t_k}} \right) \cdot \left| \frac{1}{2\sqrt{ST(t_k)} \cdot t_k} \right|$$

and

$$(7) \quad f_{i_p}(i_p) = f_I \left( \frac{i_p}{\sqrt{2} \cdot k_p} \right) \cdot \left| \frac{1}{\sqrt{2} \cdot k_p} \right|$$

The main stress of electrical equipment means the thermal and electro-dynamic stress. Firstly, we consider the case of single line connected to a source, like in figure 2.

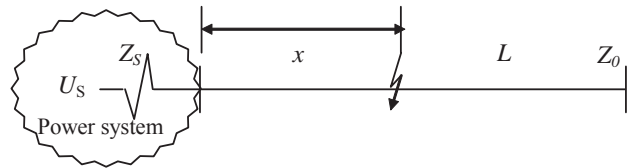


Fig. 2. The system with a single line to a source

In the case of a fault located at the distance  $x$  from the source, the probability distribution function of the short-circuit current is given by:

$$(9) \quad f_I(i) = \frac{U_S}{LZ_0 i^2} \quad \text{for} \quad \frac{U_S}{LZ_0 + Z_S} \leq i \leq \frac{U_S}{Z_S}$$

where:

- $U_S$  = is the phase-to-neutral system voltage;
- $Z_S$  = the impedance equivalent of the source;
- $Z_0$  = the specific impedance of the line.

The probability distribution function of the thermal stress is given by:

$$(10) \quad f_{ST}(ST(t_k)) = \frac{U_S \sqrt{t_k}}{2LZ_0 ST \sqrt{ST}} \quad \text{for} \quad \left( \frac{U_S}{LZ_0 + Z_S} \right)^2 t_k \leq ST(t_k) \leq \left( \frac{U_S}{Z_S} \right)^2 t_k$$

and the electro-dynamic stress distribution function is given by:

$$(11) \quad f_{i_p}(i_p) = \sqrt{2}k_p \cdot \frac{U_S}{LZ_0 i_p^2} \quad \text{for}$$

$$\sqrt{2}k_p \frac{U_S}{LZ_0 + Z_S} \leq i_p \leq \sqrt{2}k_p \frac{U_S}{Z_S}$$

For the studied configuration, beside the analytic expressions of the distribution functions, the way to obtain them by practice, using the transformations of variables or the Monte Carlo simulation is presented. All these practical applications have the role to validate the acquired analytic models.

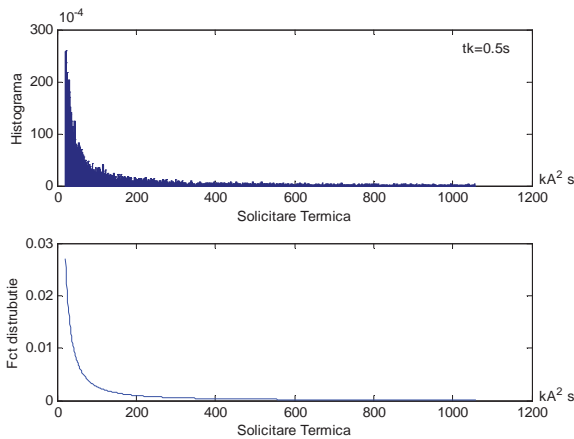


Fig. 3. The thermal stress pdf (simulation and analytical)

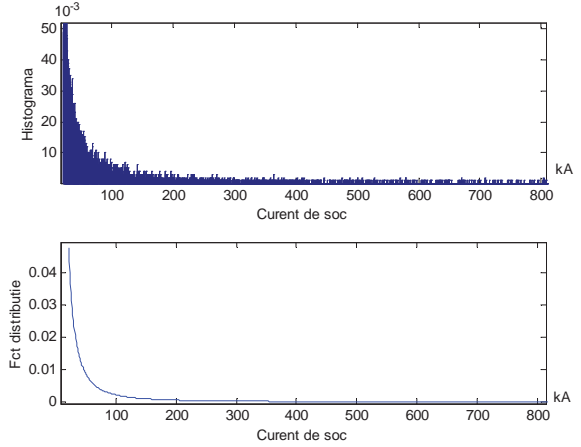


Fig. 4. The electro-dynamic stress pdf (simulation and analytical)

Taking into account the real networks configuration the result is the idea to model the probability distribution functions of thermal and electro-dynamic stresses, in case of complex configurations.

Therefore, in the following, the analysis of the distribution functions of thermal and electro-dynamic stresses was extended as well as for the case of a real complex system (a network of 110 kV), for which the authors established the distribution functions of short-circuit current using the analytic method and Monte Carlo simulation.

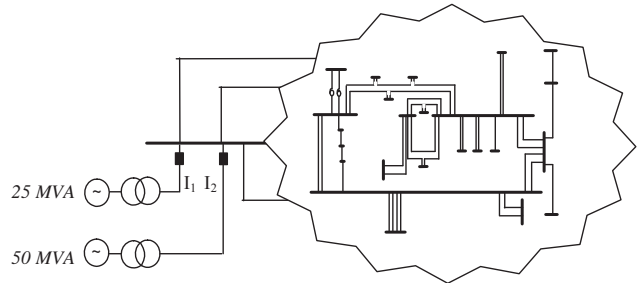


Fig.5. A real complex system network - 110 kV

To determine, in an analytic numerical way the distribution function, the analytic expressions obtained for the cases of the simple configurations were used and their combination, in common definitions intervals. To validate the obtained results, the function of the distribution in the case of the complex system was determined also by Monte Carlo simulation, both functions having a similar evolution. Both, the numerical calculations and the Monte Carlo simulation have been realised using Matlab software package with a view to determine and to combine the distribution functions, in common affiliation intervals.

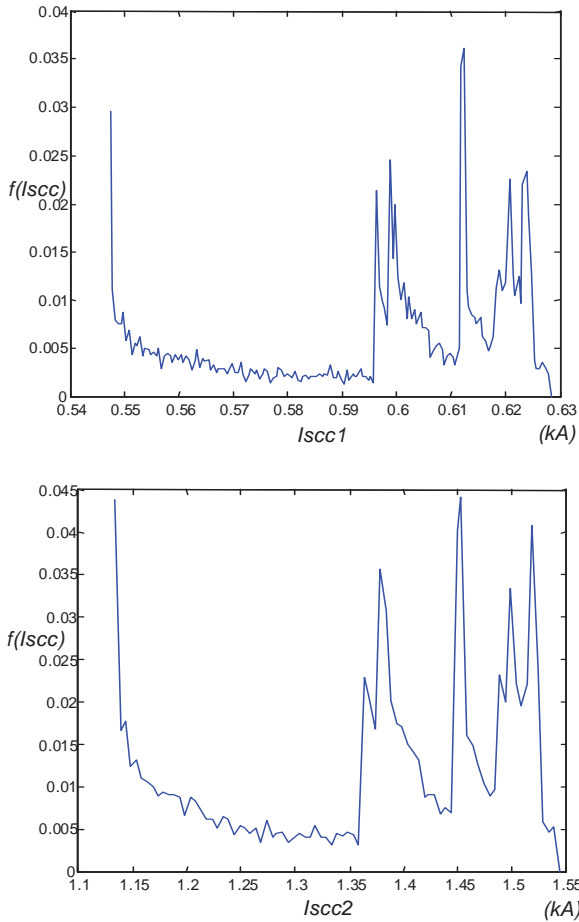


Fig. 6. Probability distribution functions for the short-circuit currents  $I_1$  and  $I_2$

The intention was to obtain the distribution functions of the thermal and electro dynamic stresses, in the case of the complex system 110 kV. The expressions of the thermal and electrodynamic stresses probability distribution functions from the case of simple configurations were obtained, using a mathematical analysis and also using Monte Carlo simulation. For the considered system it was settled the distribution functions of the two stresses, in the case of two switches.

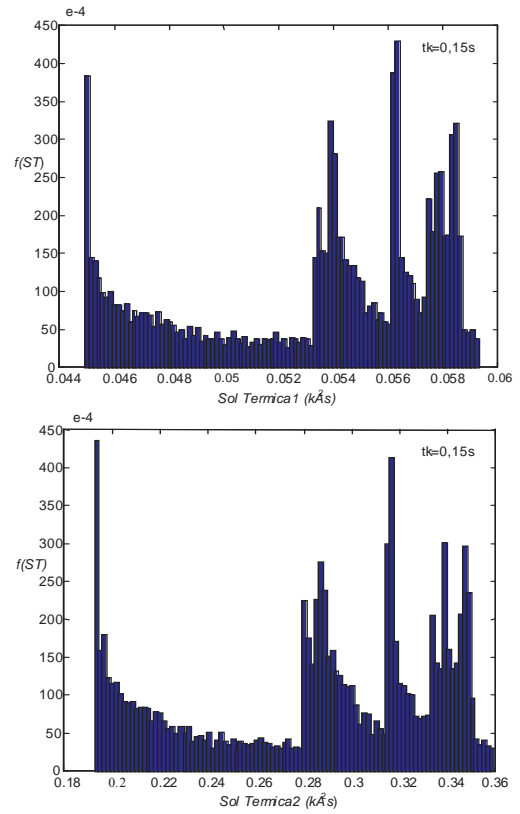


Fig. 7. Probability distribution functions for the thermal stress in the switches  $I_1$  and  $I_2$

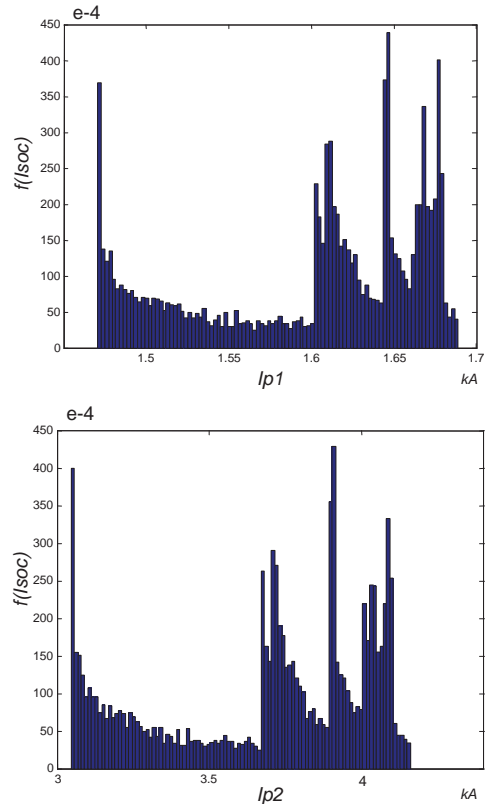


Fig. 8. Probability distribution functions for the electro dynamic stress in the switches  $I_1$  and  $I_2$

## Conclusion

When analysing the thermal and electro dynamic stresses, the conditions of the system are prior and these values are calculated depending on the short-circuit currents for the different combinations, on the local power involved, the systems configurations and on the time of fault. Usually we consider the most unfavourable situations, in order to limit the number of the case studies. The stresses caused by the three-phase faults located to the system buses are usually considered. The equipment is chosen from thermal and electro dynamic stresses restrictions, calculated in these points.

If the amplitude of these stresses is considered as random variables so, the probabilistic methods become very attractive solutions to analyse the stress magnitudes caused by short-circuit currents.

The probabilistic concepts concerning the values of the thermal and electro dynamic stresses can be used for the power system design, by calculating a security coefficient taking into account that the maximal values of the thermal or electro dynamic stress, that appear with a smaller probability that their minimal values.

## References

- [1] C. Nemeş, D. Ivas, 2004, "Probabilistic Approach for the Short-circuit Stress Used in the Reliability Indicators", "Buletinul Institutului Politehnic Iaşi", "tomul XLX(LIV)", pg. 129-138
- [2] C. Nemeş, D. Ivas, 2003, "Modelarea solicitării la scurtcircuit a echipamentelor din stațiile electrice în calculul indicatorilor de fiabilitatea a acestora", "Simpozion Național SIG", "SIG 2003 Oradea", Secțiunea 1, pag. 1.33
- [3] C. Nemeş, D. Ivas, Fl. Munteanu, 2004, "Modelarea distribuțiilor solicitărilor termice și electrodinamice la scurtcircuit în evaluarea fiabilității preliminate a echipamentelor din electroenergetică", "Rev. Energetica", "vol 52, nr. 6", pg 277-281.
- [4] C. Nemes Grant: CNCSIC-AT(29) 33GR/23.05.2007, Utilizarea modelelor analitice și a tehnicilor de inteligență artificială în optimizarea indicatorilor de fiabilitate a echipamentelor electroenergetice, prin monitorizarea solicitărilor.

## Biographies



**Ciprian Nemes** was born in Cluj, Romania, on May, 1975. He studied at the Technical University of Iasi and received Mster degree from the same university in 1999.

His field of interest includes the reliability of electrical equipment, renewable energy sources in the descentralizat network..

Ciprian Nemes is with the Faculty of Electrical Engineering, Technical University of Iasi, D. Mangeron 51-53 Blvd., Iasi, Romania (e-mail: cnemes@ee.tuiasi.ro).



**Florin Munteanu** was born in Iaai, Romania, on 1953. He graduated from the Technical University - Iasi, and received the PhD degree to same University.

In present, he is Professor in the Faculty of Electrical Engineering of the Technical University of Iasi.

Florin Munteanu is with the Faculty of Electrical Engineering, Technical University of Iasi, D. Mangeron 51-53 Blvd., Iasi, Romania .



# Optimal Operation Planning of Mosul Hydro Power Complex

## Part I: Mathematical Models

Dimo Stoilov, Maria Kaneva and Fawaz Syltan

**Abstract:** The Mosul Hydro Power Complex (MHPC) is the largest hydro power cascade in Iraq. The only one pump storage hydro power plant in the country operates here. The draw off mode is dominated by the water supply and irrigation needs, as well the temporary conditions of the destroyed power grid. This article presents the mathematical models for optimal operation planning of Mosul HPC during the currently existing and anticipated operation conditions in Iraq PS. A second article describes the results of the model analysis.

**Keywords:** hydro power complex optimal scheduling

### I. The Role of Mosul HPC in Iraq EPS

Mosul Hydro Power Complex is of major importance for the Electric Power System (EPS) of Iraq: this is the largest hydro cascade in the country and the only large pump storage HPP operates here. The main function of the MHPC is the electric energy production as well peak, control capacity, and quick mobilizing reserve provision. Apart from its electric power generation functions, the complex is used for the irrigation and supply of water for drinking and domestic purposes for the Northern region of the country. The maximum effective use of the complex contributes to increased benefits for the Iraq economy, which is of paramount importance during the current period of damages. The aim of this article is to show the identified possible modes of operation of the Mosul hydro cascade (currently and in the near future), the created models and the programs for their optimization. The results of the research carried out through them are described in another article.

The Mosul complex consists of four dams, two HPPs and one Pump Storage HPP [1]. Fig.1. illustrates the Main dam Mosul 1, the Regulating dam Mosul 2, the Upper reservoir of the Pump Storage HPP Mosul 3, and the Irrigation dam and the main hydro technical

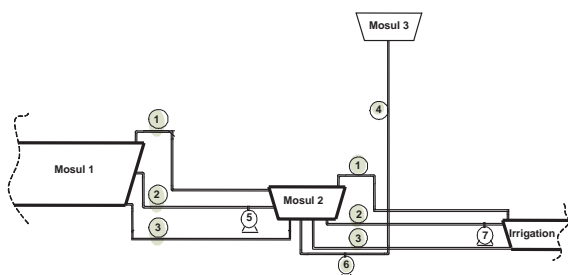


Fig.1. Diagram of Mosul Hydro Power Complex

constructions: 1. Spillways; 2. Pressure conduits; 3. Main water outlets, 4. Pressure head conduits of the Pump Storage HPP; 5. Turbines of the main HPP; 6. Turbines/Pumps of the Pump Storage HPP; 7. Turbines of the regulating HPP.

The table 1 presents the data regarding the dams, and the table 2 - regarding the turbines and pumps

Table 1

Main data regarding the Mosul HPC dams

Dam	Max volume, mil. m <sup>3</sup>	Max water level,m.	Min water level,m.
Mosul 1	11 200	330.30	300.00
Mosul 2	17.0	258.80	251.60
Mosul 3	1.6	597.80	576.60
Irrigation	1.5	247.70	242.00

Table 2

Main data regarding the hydro plants of Mosul HPC

HPP	Type of turbine	Number of units	Unit rated capacity, MW	Generator' voltage, kV
Mosul 1	Francis	4	178.5	15
Mosul 2	Kaplan	4	15	5.25
PSHPP	Francis	2	120/110	12

The remaining HPPs in Iraq are located mainly in the central part of the country. Their total installed capacity is about 1100 MW. However, because of different restrictions their operating power during the maximum load hours amounts about 700 MW. Their total annual electric power generation varies between 1800-2200 TWh, which represents about 80 % of the electric power generated by the Mosul HPC.

The conventional thermal power plants in the Iraq EPS use mainly black oil. Their total installed capacity is about 6300 MW, of which because of the war damages or poor maintenance currently operate about 2700 MW. The total installed capacity in gas electric power plants are about 3200 MW, of which currently operate about 1400 MW. In the Northern part of the country in the region of the Mosul city (the second biggest city after Baghdad in the country with population of the city and the region around it of almost 4 mil. people) two big thermal plants are located: Beji TPP with four units at black oil, each of which with operation capacity of up to 200 MW and the gas power plant (GPP) Kerkuk with 12 gas units with

operation capacity of 30 MW each. There are no combine heat and power plants in Iraq. The country is gasified.

The electric transmission network of Iraq is comparatively well developed. It consists of electric power lines and substations 400 and 132 kV. Because of the war in Iraq many power transmission elements are destroyed and the joint synchronous operation of entire system is impossible. The large power plants supply the consumers in their regions operating in island mode. This is valid also for the Mosul HPC, because the 400 kV lines connecting the Mosul region to the Southern part of the Iraq EPS have been cut off.

Before the start of the war the maximum loads for the Northern region of the country have been about 3200 MW during the afternoon and evening hours of the summer months June and July, and the minimum – about 1200 MW during the night hours of October and November. Now the level of loads is reduced but because of the restriction mode they may not be defined reliably. Their maximum satisfaction is the subject of the optimization problem for island mode operation of the Mosul HPC.

The maximum loads of the entire Iraq system have reached up to 10000 MW during the afternoon and evening hours of the summer months, and the minimum ones have been approximately 4200 MW during the night hours of October and November. It may be expected that the loads after restoring of the transmission grid and the power generation capacities will be approximately the same again.

## II. Main modes of operation of the MHPC

The war actions that took place until recently and the continuing terrorist actions, which happen almost every day, result in a total damage of the transmission grid of the Iraq EPS. The current and expected status require considering of three possible modes of operation of the Mosul hydropower complex, namely:

**First mode:** isolated island operation. Under this mode the Mosul hydropower complex operates isolated from the other power generation capacities in the EPS and supplies the consumers in the region of Mosul town. This is the prevailing mode during the recent years, which is expected to be applied for some time. Under this mode it is expedient to maximize the electric power generated in order to satisfy more consumers with greater duration and a greater degree of reliability. Obligatory supply of the priority consumers is assumed (hospitals, important public institutions and industrial sites) and interruptible mode for the remaining consumers. That is why under the first mode of operation we assume objective function “maximum electric power generation”. It should be noted that due to the isolated operation (lack of TPPs operating in parallel) under this mode, no operation of the Pump Storage HPP capacities is envisaged, because the eventual use of pumps would reduce the quantity of the electric power available to the consumers. The suggested linear optimization model in this case is presented below in III.1

**Second mode:** island operation of the Mosul HPC in parallel with two other plants: the nearly located TPP Beji comprising four thermal units of 200 MW each, at fuel oil, and the GPP Kerkuk, which comprises 12 gas turbines of 30 MW each. This mode is also applied long time during the year. Under this mode, like under the first one, it is not possible to fully satisfy the loads in the Northern region of the country during the peak hours. During the off peak hours it is possible the loads to be satisfied and even there is an option to reduce the load of the thermal plant units, but their longer switching off creates a deficit. Here it is expedient to apply criteria for minimum non supplied electric power, which in most cases is again reduced to objective function “maximum generation” from the Mosul HPC. The operation of the Pump Storage HPP under this mode may be expedient as a pump during the off-peak periods supplied by the local TPP and/or the gas power plant, also as a generator contributing to more complete satisfaction of the consumers during the peak hours. The suggested linear optimization model for this mode is presented in III.2

**Third mode:** parallel operation with the entire Iraq EPS. The beginning of such sustainable mode may not be forecasted. The expectations are for it to occur after three to five years. Its planning in advance, as well as testing of an adequate optimization model is topical because in Iraq there are enough built electric power generation capacities that could be brought into operating condition when restoring the coherence of the electric power system. The aim of the optimization in this case would be classic – minimum system operation costs, while covering the system load and provision of the required reserves. In this model the role of the Mosul HPC is a key and multifunctional one, as the greatest regulating capacity (HPPs in combination with the Pump Storage) in the country. Under such mode by using the Pump Storage HPP reducing of the costs for power regulation in the thermal plants should be expected, as well as reducing the costs for switching up and shutting down of TPP units and for hot reserve in the thermal plants. The suggested for this case mixed integer linear optimization model is provided in III.3.

## III. Description of the elaborated optimization models

For the described three main modes of operation of the Mosul HPC the authors have elaborated tailored models in the form of mixed linear objective function and constraints [2], [3]. This approach facilitates the elaboration of structuring and interface programs for use of standard program packages for mixed integer linear programming (CPLEX, LINGO, PCx etc.). The program realization of the models consists namely of the elaborated structuring programs. According to the preliminary established relatively constant data regarding the system (topology and characteristics of the water cascades, characteristics of the thermal plants, transmission capacities of the system) and accepted specifically for certain studied versions/scenarios of data

(water inflows, fuels availability, availability of the capacities, forecasted loads, desired reserves etc.) the structuring programs create a common matrix of the model (relevant number of variables and relevant number of constraints, define the values of the coefficients of the objective function and the constraints) and transmit it to be solved by the calculation kernel – programming package for mixed integer linear programming [4]. After completion of the calculations the programs extracts the solution from the calculation kernel and transforms it in a form convenient to the analyzing experts.

In the elaborated models the volumes of the reservoirs (dams) have been assumed as optimized variables, rather than their levels, due to certain advantages in the modeling. The automatic transformation volumes-levels are performed easily by using the storage-head curves of the reservoirs.

The models consider iteratively the dependence of the HPP power output on the head, which means that each following iteration for model calculation uses the coefficient values depending on the head, obtained for the relevant head from the previous iteration. Namely this approach allows the use of the more simple linear models.

The purpose of carrying out of variant planning and considering the stochastic nature of the water inflows require to perform calculations at least for three level of inflow availability (50%, 75% and 95%) under the three suggested models.

### III.1. Optimization model for isolated island mode of operation of Mosul HPC

#### Objective function:

$$(1) \text{ Max Electricity Generation} = \text{Max} \sum_{k \in K} \sum_{h \in H} p_h(k) \Delta t(k),$$

where:

$p_h(k)$  – power output from hydro unit h during the single interval k in MW;

$\Delta t(k)$  – duration of the single optimization interval k in hours;

K – the considered entire period of solving the problem (planning period);

H – the set of units in the HPPs for the Mosul complex;

#### Constraints:

##### Input-output/rate (I-O) curves of the HPP units.

They are defined through the following linear expressions:

$$(2) \quad p_h(k) = v_h(k) \underline{p}_h + \sum_{l=1}^L q_{hl} p_{hl}(k), \quad \forall h \in H, \forall k \in K;$$

$$(3) \quad q_{hl}(k) = v_h(k) \underline{q}_{hl} + \sum_{l=1}^L q_{hl} p_{hl}(k), \quad \forall h \in H, \forall k \in K;$$

$$(4) \quad 0 \leq p_{hl}(k) \leq \bar{p}_{hl}, \quad \forall h \in H, \forall l, \forall k \in K;$$

$$(5) \quad p_h(k) - v_h(k) \bar{p}_h \leq 0, \quad \forall h \in H, \forall k \in K,$$

where:

$v_h(k)$  – binary variable, which is equal to one only when unit h is in operation during the single optimization interval k;

$p_h(k)$  – power output for unit h during interval k;

$\underline{p}_h$  – minimal power output of unit h;

L – number of the sections l of the linear approximation for unit h;

$p_{hl}(k)$  – power output of section l of the approximation for unit h during interval k;

$\underline{q}_{hl}$  – water rate/discharge at the minimal power output of unit h;

$q_{hl}$  – slope for section l of the approximation of the I-O curve for unit h;

$q_h(k)$  – water discharge of unit h during interval k;

$\bar{p}_{hl}$  – maximal power output for section l of the approximation for unit h;

$\bar{p}_h$  – maximal power output for unit h.

The values of the above coefficients  $\underline{p}_h$ ,  $\underline{q}_{hl}$ ,  $q_{hl}$ ,  $\bar{p}_{hl}$  и  $\bar{p}_h$  for the different values of the water head (accounting the dependence of the I-O curves on the head) are specified iteratively during the process of model calculations. Due to this approach the linearity of the model is kept, at the same time the dependence of the power output on the water head is considered with sufficient accuracy. In the same way the effect of different elevation of the lower water level of the HPP under operation of a different number of units at certain power may be accounted for as well. The modeling through the suggested equations allows respecting the constraints for minimum and maximum power output of the water units (units operation scopes).

#### Obligatory/firm electricity supply to priority consumers:

$$(6) \quad \sum_{h \in H} p_h(k) \geq D_p(k) \quad \forall k \in K, \quad \text{where}$$

$D_p(k)$  – total load of the priority consumers for interval k, including the losses in the grid.

#### Maximum $V_s(k)$ and minimum $\underline{V}_s(k)$ water volumes stored in the reservoir s in the beginning of interval k:

$$(7) \quad \underline{V}_s(k) \leq V_s(k) \leq \bar{V}_s(k), \quad \forall s \in S, \forall k \in K, \text{ where:}$$

S – the set of the reservoirs (in this case the three dams considered)

#### Water balance equation for each period and for each reservoir:

$$(8) \quad V_s(k+1) = V_s(k) + i_s(k) - \sum_{h \in S_h} q_h(k) - q_s^s(k) - q_s^u(k) + \sum_{h \in \Omega_h} q_h(k) + q_h^s(k), \quad \forall s \in S, \forall k \in K,$$

where:

$i_s(k)$  – lateral inflow in the reservoir s,

$S_h$  – set of HPP units supplied from reservoir s,

$\Omega_h$  – set of HPP units supplying reservoir s,

$q_s^s(k)$  – spilling quantity from the reservoir s during the single interval k,

$q_h^s(k)$ - spilling quantity from the reservoir preceding  $s$ , and flowing into  $s$  during the single interval  $k$ ,  
 $q_s^u(k)$  – turbines bypass water discharge from reservoir  $s$  during the single interval  $k$ .

**Start and end (limited) volumes** of the reservoirs:

$$(9) \quad V_s(I) = V_{sI}, \quad \forall s \in S,$$

$$(10) \quad \underline{V}_s \bar{K} \leq V_s(\bar{K}+I) \leq \bar{V}_s \bar{K}, \quad \forall s \in S,$$

where:

$\bar{K}$  – index for last single interval  $k \in K$ ,

**Dependence of the spill quantities on the volume** of the reservoirs:

$$(11) \quad V_s^s(k) = V_{s0}^s + \sum_{l=1}^L V_{sl}^s(k), \quad \forall s \in H, \forall k \in K,$$

$$(12) \quad q_s^s(k) = \sum_{l=1}^L \beta_l V_{sl}^s(k), \quad \forall h \in H, \forall k \in K,$$

$$(13) \quad 0 \leq V_{sl}^s(k) \leq \bar{V}_{sl}^s, \quad \forall h \in H, \forall l, \forall k \in K$$

where:

$V_s^s(k)$  – spilling volume of reservoir  $s$ , i.e. the volume corresponding to the volume above the spill level for the spillway  $s$  during interval  $k$ ;

$V_{s0}^s$  – start spilling volume of reservoir  $s$ ;

$L$  – number of sections  $l$  of the linear approximation of the spill curve for the spillway of the reservoir  $s$ ;

$V_{sl}^s(k)$  – volume of section  $l$  of the approximation of the spill curve for the spillway of the reservoir  $s$  during interval  $k$ ;

$\beta_l$  – slope of section  $l$  of the approximation of the spill curve for the spillway of the reservoir  $s$ ;

$\bar{V}_{sl}^s$  – maximum volume of section  $l$  of the approximation of the spill curve for the spillway of the reservoir  $s$ ;

**Firm quantities for water supply** – for domestic drinking, industrial, and irrigation purposes:

This constraint is modeled by using the defined in equation (8) quantity  $q_s^u(k)$  – turbines bypass water discharge for the last (irrigation) reservoir of the cascade. Under it there are no HPP units and all the water is not treated by turbines. It should not be less than the required obligatory/firm quantity for water supply  $Q_s^w(k)$  from this reservoir. Therefore the following constraint is introduced for this reservoir:

$$(14) \quad q_s^u(k) \geq Q_s^w(k), \quad \forall s \in S, \forall k \in K.$$

The suggested first model may apply also to third mode (parallel operation of Mosul HPC with the remaining power plants in the EPS), when, due to some reason it is necessary to maximize the power generation output, for example in case of inflows greater than the expected quantities. In the general case this would minimize the required generation by the TPPs, but the influence on the total costs in the EPS may not be estimated without accounting for their specific characteristics.

### III.2. Optimization model for island operation of Mosul HPC in parallel with Beji TPP and Kerkuk GPP.

In this sub-section and further in presenting the model below the already introduced in III.1 symbols are used, complemented by the necessary new ones.

**Objective function:**

$$(15) \quad \text{Min Non-supplied energy} =$$

=Min

$$\sum_{k \in K} \Delta t(k) \left[ D(k) + \sum_{j \in J} v_j(k) p_j - \sum_{h \in H} p_h(k) - \sum_{t \in T} p_t(k) \right]$$

where:

$D(k)$  – total gross load of the unlimited consumers, including the losses in the grid during the interval  $k$ ;

$v_j(k)$  – binary variable, equal to one only when pump unit  $j \in J$  operates during the interval  $k$ ;

$J$  – the set of the pumping units,  $\forall j \in J$ ,

$p_j$  – power output of the pump unit  $j$ ,  $p_j = \rho_j Q_j$ . Here  $\rho_j$  is a conversion ratio in MWh/m<sup>3</sup> that depends on the head for pump unit  $j$ ;  $Q_j(k)$  – the pumped water quantity by unit  $j \in J$  during the interval  $k$ ;

$p_t(k)$  – operational/generation power output for thermal unit  $t$  during the interval  $k$ ;

$T$  – set of the units in TPPs (in this case the units of Beji TPP and Kerkuk GPP);

**Constraints:**

All constraints from the model shown in III.1 are valid here also. In order to consider the operation of TPPs and of the Pump Storage HPP, some constraints are transformed and others are added.

**The constraint from equation (6) for firm power supply of priority consumers** becomes the following:

$$(16) \quad \sum_{h \in H} p_h(k) + \sum_{t \in T} p_t(k) \geq D_p(k), \quad \forall k \in K.$$

**The balance constraint (8) for the volume of the reservoirs** shall also include the water quantities going through the pumps, therefore it becomes the following:

$$(17) \quad V_s(k+I) = V_s(k) + i_s(k) - \sum_{h \in S_h} q_h(k) - q_s^s(k) - q_s^u(k) + \sum_{h \in \Omega_h} q_h(k) + q_h^s(k) + \sum_{j \in \Omega_j} v_j(k) Q_j, \quad \forall s \in S, \forall k \in K,$$

where:

$\Omega_j$  – set of the pump units filling reservoir  $s$ ,

**The non-simultaneous operation of pumps and generation units** is represented through the following inequality

$$(18) \quad v_j(k) + v_h(k) \leq 1 \quad \forall k \in K, \forall j \equiv h \in H \cap J.$$

**The input-output (I-O) curves of the thermal units in Beji TPP and Kerkuk GPP** are given through the following linear expressions:



$$(20) \quad p_t(k) = v_t(k) \underline{p}_t + \sum_{l=1}^L p_{tl}(k), \quad \forall t \in T, \forall k \in K,$$

$$(21) \quad d_t(k) = v_t(k) \underline{d}_t \underline{p}_t + \sum_{l=1}^L d_{tl} p_{tl}(k), \quad \forall t \in T, \forall k \in K,$$

$$(22) \quad 0 \leq p_{tl}(k) \leq \bar{p}_{tl}, \quad \forall t \in T, \forall l, \forall k \in K,$$

$$(23) \quad p_t(k) - v_t(k) \bar{p}_t \leq 0, \quad \forall t \in T \cup H, \forall k \in K,$$

where:

$v_t$  – binary variable, equal to one only when unit  $t$  is in operation during the single interval  $k$ ;

$p_t(k)$  – operation/generation power output for unit  $t$  during interval  $k$ ;

$\underline{p}_t$  – minimum power output of unit  $t$ ;

$L$  – number of sections  $l$  of the linear approximation of the I-O curve for unit  $t$ ;

$p_{tl}(k)$  – power output of the section  $l$  of the I-O curve approximation for unit  $t$  during time interval  $k$ ;

$\underline{d}_t$  – costs (power price) at minimum power output of unit  $t$ ;

$d_{tl}$  – costs (power price) for section  $l$  of the I-O curve approximation for unit  $t$ ;

$d_t(k)$  – costs (power price) for unit  $t$  during time interval  $k$ ;

$\bar{p}_{tl}$  – maximum power output of section  $l$  of the I-O curve approximation for unit  $t$ ;

$\bar{p}_t$  – maximum power output of unit  $t$ .

Despite the constructed model is not cost-benefit oriented, the way of the I-O curves of the thermal units modeling enables estimation of the costs for each obtained solution. The modeling through the suggested equations enables accounting of thermal units' operation range as well.

The modeling of the possible remaining constraints for the thermal units (compliance between the states - operation, switching on and switching off; minimum up and down time for the TPP units; maximum number of units simultaneously switched up/shut down in given sub-intervals) are considered in [5]. They are essential for the short-term (daily and weekly) operation planning, but may be neglected for the longer-term planning (annual and multi-annual).

### III.3. Optimization model for parallel operation of the Mosul complex with the entire EPS of Iraq

#### Objective function:

$$(24) \quad \text{Min Costs} = \text{Min}[CSup + CSdown + Opex + CAS + CNP],$$

where:

$CSup$  – costs for units switching up during the entire planning period  $K$ ,

$CSdown$  – costs for units shutting down during the entire planning period  $K$ ,

$Opex$  – operational expenditures (costs) for electric power generation,

$CAS$  – costs for ancillary services (primary and secondary frequency regulation, reserves, etc.),

$CNP$  – costs for non-supplied electricity.

These costs and their inclusion in the objective function are considered in detail in [5]. The costs for units switching up and shutting down, for ancillary services and for non-supplied power are essential for the well developed operating in parallel and mutually supporting EPSs. In the near future for the Iraq system is expedient to consider only the operational costs for electric power generation that are the most significant and are derived as the total of the fuel costs and the other variable operational costs for all the operating thermal units for the entire planning period  $K$ . Therefore the objective function is simplified in the following way:

$$(24^*) \quad \text{Min Opex} = \sum_{k \in K} \sum_{t \in T} d_t(k)$$

These costs are included in the model through the I-O curves presented with the formulae 20-23.

#### Constraints:

The constraints from the models shown in III.1 and III.2 are valid. In addition:

A). Constraint (6) or respectively (16) for firm power supply to priority consumers is replaced by the following system constraints:

**Balance constraint** – the total power output of the TPP and HPP units and the non-supplied power to be equal to the load for the same single interval  $k$ :

$$(22) \quad \sum_{t \in T} p_t(k) + \sum_{h \in H} p_h(k) + \pi(k) - \sum_{j \in J} v_j(k) p_j = D(k),$$

$\forall k \in K$ , where:

$\pi(k)$  – non-supplied power during the interval  $k$ .

**Reliability constraints** – the power reserve to satisfy all types of reserve requirements in necessary quantity and quality, for example for the spinning reserve requirement:

$$(23) \quad \sum_{t \in T \cup H} (\bar{p}_t v_t(k) - p_t(k)) \geq R(k), \quad \forall k \in K, \text{ where:}$$

$R(k)$  – the minimum necessary spinning reserve during the single optimization interval  $k$ .

B). It is possible to become necessary to consider other constraints related to TPPs operation: minimum and maximum output (quota) for some power plants, maximum emissions quantity, and maximum number of simultaneously switched up units, etc. The modeling of these constraints is described in [5] and if necessary in the future they will be included in the model under consideration. An example of this is a constraint for maintained reserve for primary frequency control:

$$(24) \quad \sum_t x_t^l(k) R_t^l \geq R^l(k), \quad \forall k \in K, \text{ where:}$$

$t$  – index for the units providing primary regulation;

$R^l(k)$  – necessary reserve for primary frequency control for the single interval  $k$  for entire EPS;

$x_t^l(k)$  – binary variable, equal to one only when unit  $t$  takes part in the process of primary frequency control during the single interval  $k$ ;

$R_t^l$  – unit  $t$  reserve for primary control, settled for each unit that may take part in the primary control;

Similar constraints may be introduced for secondary and tertiary reserves as well. In such cases another constraint is introduced, considering that it is not possible to provide regulation from a unit that is out of operation.

$$(25) \quad x_t^l(k) - v_t(k) \leq 0, \quad \forall t, \forall k \in K$$

Operation range constraints for the units are also introduced, engendered by the participation in providing of primary control reserve:

$$(26) \quad p_t(k) + x_t^l(k) R_t^l - v_t(k) \bar{p}_t \leq 0, \quad \forall t, \forall k \in K,$$

$$(27) \quad p_t(k) - x_t^l(k) R_t^l - v_t(k) \underline{p}_t \geq 0, \quad \forall t, \forall k \in K.$$

Obviously the modeling of primary frequency control reserve requirement or other conditions engenders new state variables and new constraints for each unit. That is why an assessment should be done whether the model complication is justified for its respective use or research, since it leads to computing difficulties and it may turn out that solution obtaining is not possible [3].

## Conclusions

This article presents the possible modes of operation of the Mosul HPC and the created mathematical models for their optimization. The models have been tailored in the form of mixed integer linear objective function and constraints, which facilitates the elaboration of structuring and interface programs for their implementation with standard program packages for mixed integer linear programming. The results of the studies carried out through them have been analyzed and published in [6].

## References

- [1] Mosul Dam System, Technical documentation, GEMOOD Ltd, 1986.
- [2] Wood, A., Wollenberg. B. Power Generation, Operation, And Control, John Wiley & Sons, New York, 1996.
- [3] Williams H.P., Model Building In Mathematical Programming, Wiley, 1999.
- [4] Using the CPLEX Callable Library, Copyright © 1997, ILOG.
- [5] Stoilov, D., “Active Power Optimization in Power Systems”, Ph. D. Thesis, Technical University of Sofia, June 2002 (in Bulgarian)
- [6] Stoilov, D., F. Syltan. Optimal Operation Planning of Mosul Hydro Power Complex - Part II: Simulation Results and Analyses, Proceedings of Int. Conf. ELMA'2008, Sofia, Bulgaria, 2008.

## Biographies



**Dr. Dimo Stoilov** was born in Plovdiv, Bulgaria in 1969. In 1995 he graduated from the Electric Power Engineering Department of the Technical University (TU) – Sofia as M.Sc. in electrical engineering. He holds a M.Sc. in Applied Mathematics (TU-Sofia, 1998) and a Ph.D. (TU-Sofia, 2003) in Electric Power Grids and Systems. In the period 1997-2005 he worked as expert in the National Dispatch Center of the NEK-EAD. In 2005 he joined the Electrical Engineering Faculty of TU-Sofia, where in 2008 he was awarded the position of associate professor in Power Grids and Systems. His major interests are in the fields of power systems operation planning and control.

Dr. Dimo Stoilov is with the Faculty of Electrical Engineering, Technical University of Sofia, 8, Kl. Ohridski Blvd., 1000 Sofia, Bulgaria (e-mail: dstoilov@tu-sofia.bg).



**Dr. Maria Kaneva-Tsotcheva** graduated in the Electric Power Engineering Department of the Technical University (TU) – Sofia as M.Sc. in electrical engineering. She received her PhD degree in 1982 and joined the chair Electric Power Systems in Electrical Engineering Faculty of TU-Sofia in 1976. From 1993 she works as associate professor in Optimization in electric Power Systems in the same university. Here she teaches Optimization in EPS, Management of EPS (in Bulgarian and in English languages), Electric Power Systems (in French language), Power Plants (in French language), Power Systems Planning and Control (in French language) and others during her work with Technical University (TU) – Sofia. Her major interests are in the field of optimization, expert systems and management in contemporary EPS. Dr. Maria Kaneva-Tsotcheva is with the Faculty of Electrical Engineering, Technical University of Sofia, 8, Kl. Ohridski Blvd., 1000 Sofia, Bulgaria (e-mail: mkaneva@tu-sofia.bg)



**Fawaz Sultan Abdulaha** was born in Mosul, Iraq in 1960. In 1989 he graduated from the Technical University (TU) – Sofia as M.Sc. in electrical engineering. In 1990 he started his work as an engineer at Mosul Hydro Power Plant. Five years later he became director of the Mosul Hydro Power Cascade and remained on this position until 2003 when he joined the Technical University of Mosul academic staff. Currently he is assistant professor in electric power plants and systems. His research interests are in the fields of electric power plants construction and optimal power plants and systems operation. He is pursuing a Ph.D. degree at the Faculty of Electrical Engineering of TU-Sofia.

Fawaz Sultan is with Technical College – Mosul, Iraq (e-mail: fawazsultan@yahoo.com).

# Optimal Operation Planning of Mosul Hydro Power Complex

## Part II: Simulation Results and Analysis

Fawaz Syltan, Dimo Stoilov

**Abstract:** The Mosul Hydro Power Complex (MHPC) is the largest hydro power cascade in Iraq. The only pump storage hydro power plant in the country operates here. The draw off mode is dominated by the water supply and irrigation needs, as well the temporary conditions of the destroyed power grid. In [1] the mathematical models for optimal operation planning of Mosul HPC during the real current and anticipated operation conditions in Iraq PS are presented. This article describes the analyses performed by the elaborated models.

**Keywords:** hydro power complex optimal scheduling

### I. Introduction

The main characteristics of the Mosul Hydro Power Complex (MHPC) and its importance for the Iraq economy are described in [1]. In order to plan the effective functioning of the complex under the three possible operation modes in the current period of instability, the authors have elaborated optimization models and research programmes. The qualities of the models elaborated and the applicability of the programmes implementing them have been tested by a series of calculations. Economic estimations about the optimised annual production plan for MHPC are obtained. This article briefly describes the accepted initial assumptions and the results obtained during the studies performed with the models. They have been analysed in order to extract useful conclusions regarding MHPC scheduling, as well as the further application and development of the models in the Iraq EPS under the current wartime and the future peacetime operation conditions

### II. Assumptions

#### II.1 Modes and models

Three types of modes of the Mosul HPC are possible [1]: First mode – isolated island operation, Second mode – island operation in parallel with other two thermal power plants and third mode – parallel operation with the entire Iraq EPS. For each of these modes an optimization model for Mosul HPC operation has been elaborated. The first model applies objective function “maximum electricity generation”, the second – “minimum non-supplied electricity”, which in most cases is again brought to objective function “maximum generation” from the Mosul HPC, and the third one - the classical function “minimum Opex” (operational expenses). The

systems of constraints described in [1] have been applied for the relevant models.

#### II.2 Hydrological conditions

The optimal annual generation plans have been calculated under three levels of water inflow availability – 50%, 75%, 95%, defined on the basis of the statistical series for the inflows in the main dam of the complex (Mosul 1), presented in Table 1. For each of the elaborated three models three scenarios have been studied, corresponding to these water inflows.

**Table 1**

Monthly average inflows into dam Mosul 1 for three levels of availability, m<sup>3</sup>/sec.

	Jan-May	Jun-Sept	Oct-Dec
50%	2000	1100	600
75%	1200	800	550
95%	800	600	500

The initial levels/volumes of the dams are assumed to correspond to the average statistical levels for seven-year periods of normal, dry and very dry years.

Under all calculation scenarios it is assumed that the minimum average monthly flow underneath Mosul HPC, which provides the water supply and irrigation needs, as well the minimum flow for the ecosystem of the river valley, is 800 m<sup>3</sup>/s.

#### II.3 Operation conditions

Under all calculation scenarios a random allocation on the forced and planned outages have been assumed, based on a reasonable maintenance requirements of the TPP and HPP units.

##### II.3.1 Particularities of the model for isolated mode of operation

Due to the nature of the objective function (maximum electricity generation) no load schedule to be balanced is introduced.

The firm/obligatory power to be supplied to the priority consumers in the Mosul region is assumed for 100 MW.

The Mosul’s Main and Regulating HPPs are completely modeled, but the Pump Storage HPP (Mosul 3) is not included.

### II.3.2 Particularities of the model for island mode under parallel operation with TPP Beji and GPP Kerkuk

For modeling of the daily load cycles during the month an approximation of the load duration curve for the month with three-step curve is used, i.e. for each month three load blocks are formed. The first one is called maximum load block and corresponds to the maximum monthly load with assumed relative duration of 15 %. The second one is called interim load block and corresponds to the load between the minimum and the maximum. Its relative duration is of 50 %. The third one is called minimum load block and corresponds to the minimum monthly load with relative duration of 35 %. The power of these blocks multiplied to the corresponding duration in hours determines the forecasted monthly consumption at the three curve steps. The values of the forecasted loads regarding which the non supplied power and energy are reported, are presented in Table 2.

**Table 2**

*Loads in Northern Iraq, MW*

	Dec-Feb	March-April	May	Jun-Aug	Sept	Oct-Nov
block1	2500	2000	2700	3200	2700	2000
block 2	1800	1700	2100	2500	2100	1700
block 3	1500	1200	1700	2000	1700	1200

The firm/obligatory power to be supplied to the priority consumers in the Northern part of Iraq is assumed for 250 MW;

In addition to the Mosul's Main and Regulating HPP, the Pump Storage HPP, TPP Beji and GPP Kerkuk are completely modeled as well.

### II.3.3 Particularities of the model for parallel operation mode to the entire EPS of Iraq

Approximation of the load duration curve with three-step curve (three load blocks), similar to the one described for the previous mode, is used for modeling the daily load cycle during the month. The values of the forecasted loads, by which the calculations have been carried out, are presented in Table 3.

**Table 3**

*Loads in the entire Iraq EPS, MW*

	Dec-Feb	March-April	May	Jun-Aug	Sept	Oct-Nov
block1	8200	7000	9000	10000	9000	7000
block2	6400	5400	7000	7700	7000	5400
block3	5000	4200	5500	6000	5500	4200

In addition to the power plants of Northern Iraq, all thermal capacities in the Iraq EPS are completely modeled. This is necessary since the mode of operation of the Pump Storage HPP is exclusively determined by the

commitment and operation mode of the thermal power plants;

Due to lack of sufficient data for all remaining HPPs in the Iraq system (outside the Mosul HPC), their complete modeling was not possible. Since their average annual generation is about 80% of that of the Mosul HPC, and many of them operate in running river mode, therefore their importance as regulating capacity is of relatively small significance. Because of this it is admissible to accept general modeling with one equivalent HPP. The maximum power output of this equivalent HPP is equal to the sum of operating power output of all the remaining HPPs in the Iraq system, reaching 700 MW, and the monthly energy generation presented in Table 4 according to the water inflow availability accepted.

**Table 4**

*Energy production of the equivalent HPP (outside MHPC) in Iraq EPS, GWh*

	Jan	Feb	March	April	May	June
50%	8200	7000	9000	10000	9000	7000
75%	6400	5400	7000	7700	7000	5400
95%	5000	4200	5500	6000	5500	4200

	July	Aug	Sep	Oct	Nov	Dec
50%	8200	7000	9000	10000	9000	7000
75%	6400	5400	7000	7700	7000	5400
95%	5000	4200	5500	6000	5500	4200

## III. Results of the optimization models calculations

In order to determine the optimal values of the HPPs monthly generations, the monthly average capacity, dams volumes, accordingly levels and other variables under the described three models provisions, calculations have been performed applying a single planning interval of one month. Further on we explain the results of the calculations and the main findings.

### III.1 Optimal generation plan of Mosul HPC at isolated island mode of operation

Fig. 1 shows the plan for optimum generation of the Main HPP, and Fig. 2 – for the Regulating one.

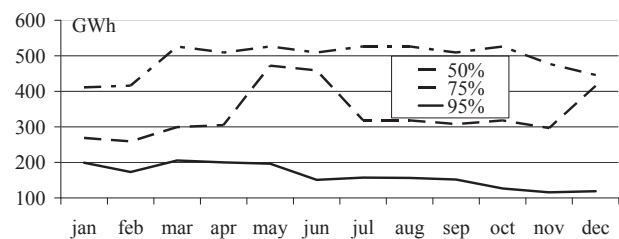


*Fig.1. Main HPP generation plan at isolated mode, GWh*



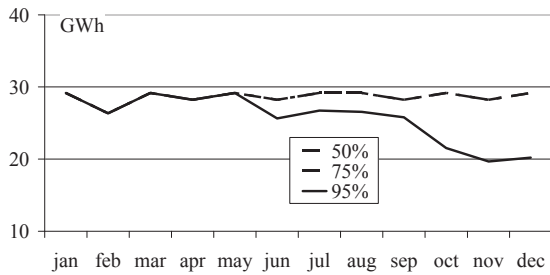


Fig.2.Regulating HPP generation plan at isolated mode, GWh

The shapes of average monthly capacities of the two HPPs are the same as the generation curves, since under this mode no load schedule for balancing is appointed.

It is observed the Main HPP operates at full capacity in normally wet year scenario, starting from March and ending in October, while during December and January the operation capacity is about 550 MW. Despite the operation at full capacity there is an inevitable spilling of the main dam Mosul 1 during the months of March, April and May in an average flow rate of 800, 900 and 860 m<sup>3</sup>/s accordingly.

In a dry year scenario the maximum power and the energy generation result during the months of May and June (about 637 MW and 472 GWh accordingly), and the minimal – during January and February (about 361MW and 259 GWh accordingly).

In a very dry year scenario the possible average power and the energy production follows the inflows.

In a normal wet and dry scenarios the energy production and the capacity of the Regulating HPP result in a practically equal level due to the small water processing capabilities of the turbines and the spilling of dam Mosul 2 throughout the whole year, but in a very dry year scenario the energy productions and the capacity from June to December are substantially reduced.

Fig. 3 shows the status of Mosul 1 dam volume for each month. It is clear that in case of normal wet year scenario the dam is full during the spring and summer months, while in dry year scenario it is impossible to be filled, and the optimal operation of the complex requires achievement of maximum water volume of about 9200 mil. m<sup>3</sup> during the month of May.

In case of very dry current year (after a long anterior dry period) the dam is constantly at minimum water volume and the turbines process the current inflow quantity only.

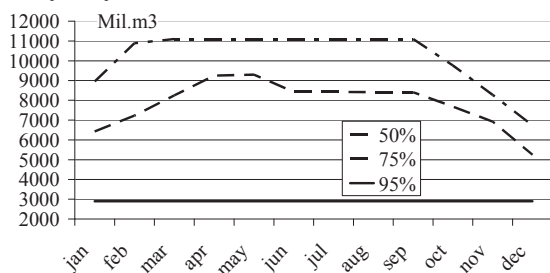


Fig.3. Volume diagram of the Mosul 1 dam at isolated mode of operation, Mil.m3

The water quantities released underneath the Mosul HPC to the irrigation dam and along the Tiger river valley are illustrated on Fig. 4. It can be seen, for the normal wet year scenario these quantities are about 1900 m<sup>3</sup>/s for the months during which the main dam spills – March, April and May, and for dry and very dry years they follow the generation schedule of the Main power plant. The compliance with the constraint for minimal released water quantity (800 m<sup>3</sup>/s) during dry year scenario, and the impossibility to obey it under the very dry year scenario, are quite obvious.

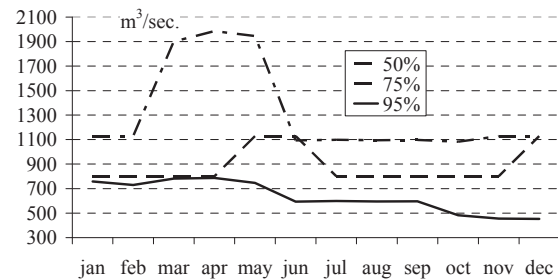


Fig.4.The water quantities released underneath the Mosul HPC at isolated mode, m<sup>3</sup>/sec

### III.2 Optimal generation plan of the Mosul HPC at island mode of operation in parallel with TPP Beji and GPP Kerkuk (Northern sub-system)

Fig.5 presents the plan for optimal generation of the Main HPP. In comparison to the plan at isolated island mode, there is a difference only for dry year scenario, because in normal wet year scenario the objective functions in both models strive to allow minimal spilling, while in case of very dry year the objective functions in both models require monthly processing of the entire inflow due to the irrigation and water supply necessities.

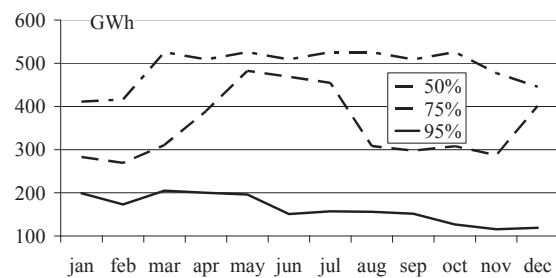


Fig.5. Main HPP production plan at island mode in parallel with northern TPPs, GWh

The production plan for the Regulating HPP is not shown individually, because it is identical to the one at the isolated island mode (Fig.2).

Figures 6, 7, and 8 show the average operation capacity of the Main HPP during the first, second and third load blocks accordingly. Their comparison shows the well expressed “peaking” of the Main HPP.

Figure 9 shows the allocation of the total non supplied electricity in each month (please remind that the objective function is minimum non supplied energy-n.s.e.), and figures 10, 11, and 12 – the non supplied power by the relevant load block.

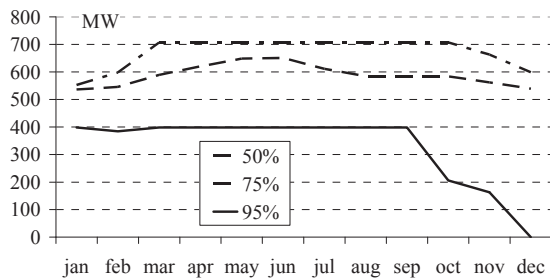


Fig.6. The average operation capacity of the Main HPP during the first load block at second mode

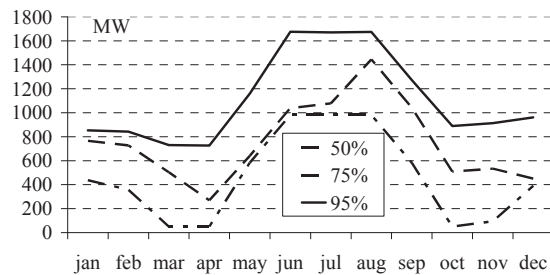


Fig.11. Average monthly non supplied power during the second load block in the northern part of Iraq, MW

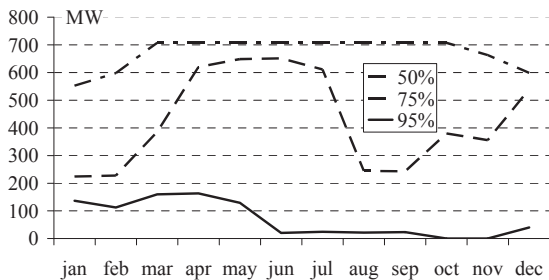


Fig.7. The average operation capacity of the Main HPP during the second load block at second mode

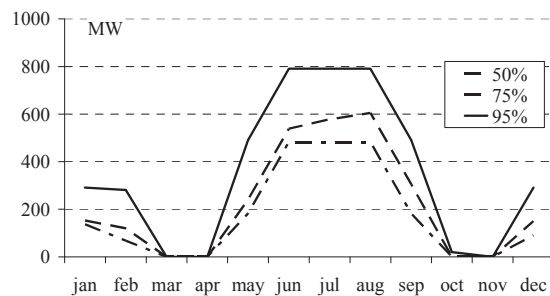


Fig.12. Average monthly non supplied power during the third load block in the northern part of Iraq, MW

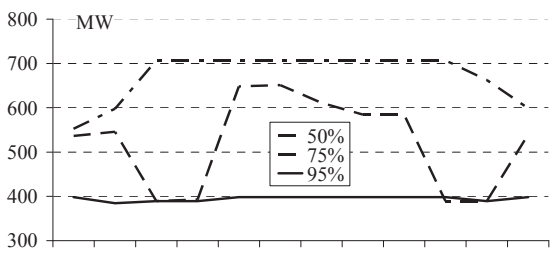


Fig.8. The average operation capacity of the Main HPP during the third load block at second mode

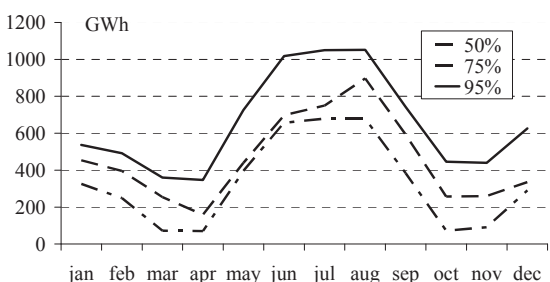


Fig.9. Monthly non supplied energy in the northern part of Iraq, GWh

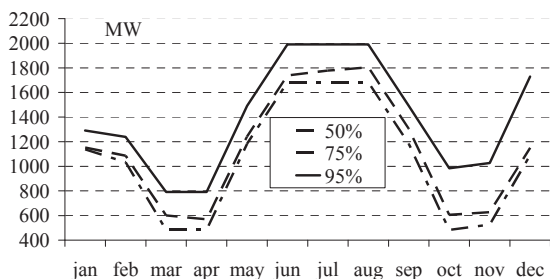


Fig.10. Average monthly non supplied power during the first load block in the northern part of Iraq, MW

It is seen that for all kind of scenarios (normal wet, dry and very dry) the non supplied electricity is zero only for the third load block during the months with the lowest demand (March, April, October and November). Strong dependence of the non supplied energy and inflow availability is noted: For the same months (March, April, October and November) the non supplied energy for very dry scenario is five times greater than the one at 50% inflow availability. The non supplied energy is about twice bigger in very dry year scenario than in normal wet year. In the first case the annual n.s.e. constitutes about 50% of the energy demanded annually in the Northern region, and in the second case - about 25% accordingly.

The results regarding the operation of the Pump Storage HPP are quite remarkable. The Pump Storage HPP operates only for March, April, October and November under the normal wet year scenario (during the high water and during the smallest demand). Under the dry and very dry year scenarios the pumps do not operate.

The released quantities for water supply and irrigation are similar to these under the isolated island mode except for the scenario of 75% hydro availability, when during the months of July and August greater quantities may be released because of the different optimal strategies of water process.

The volume status of Mosul 1 dam for each month at this mode is quite similar in comparison to the isolated operation mode. There is certain difference under the dry year scenario. The explanation is that the existence of the thermal power plants changes the strategy for water process, so as to enable the use of the greatest power of the HPP, when the loads are the greatest (the smaller loads may be supplied only by the thermal power plants) and thus reduction of the system non supplied power and energy is achieved.

Since the optimal generation of the Main power plant in normal wet year scenario is identical to the maximum energy production mode, the spilled water quantities from the main dam are the same as in the isolated island mode.

### III.3 Optimal generation plan for parallel operation mode of the Mosul HPC to the entire electric power system of Iraq

Fig.13 presents the plan for the optimal generation of the Main HPP. For very dry and normal wet year scenarios the plans are the same as in the previous two models. In case of normal dry year, when the possibility for spilling of the main dam is reduced and at the same time it is not necessary to release all the inflow quantity for irrigation, the strategy for water processing in the big system is quite different in comparison to the first two modes.

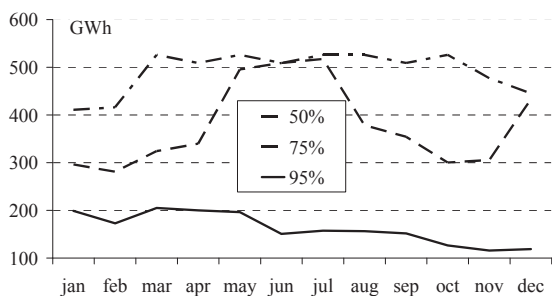


Fig.13. Main HPP production plan at parallel operation mode, GWh

The generation of the Regulating HPP does not differ substantially from the generation under the previous modes.

Figures 14, and 15, and 16 show the average generation capacity of the Main HPP during the first, second and third load blocks.

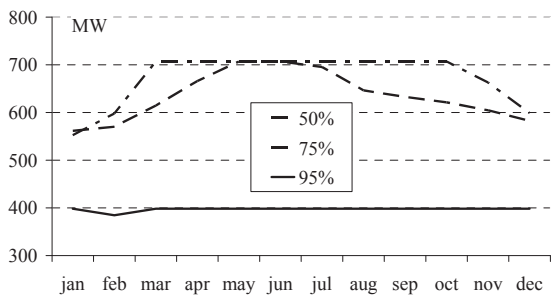


Fig.14. The average operation capacity of the Main HPP during the first load block at third mode, MW

For normal wet and very dry year scenarios the obtained average capacities differ substantially from these for island operation of the Northern part of the EPS mode, because the optimality conditions for entire EPS require maximum equalization of the system costs incremental rate for all single optimization intervals. The system costs incremental rate is in fact the marginal energy price in the EPS (load marginal cost). Therefore the determined production capacities strive at equalizing to the maximum degree the marginal energy prices by load blocks throughout the year.

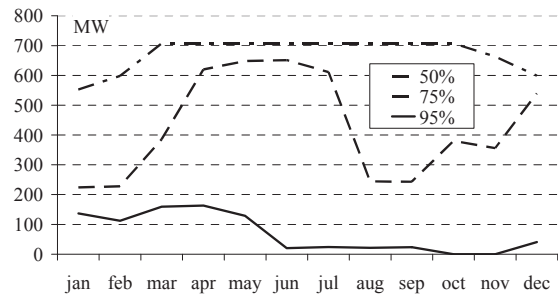


Fig.15. The average generation capacity of the Main HPP during the second load block, MW

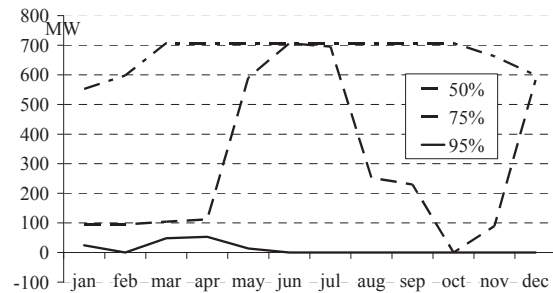


Fig.16. The average operation capacity of the Main HPP during the third load block at third mode, MW

Figure 17 shows the monthly operational costs of entire Iraq EPS, and figures 18, and 19, and 20 - the fluctuations of the marginal energy prices during the relevant load blocks.

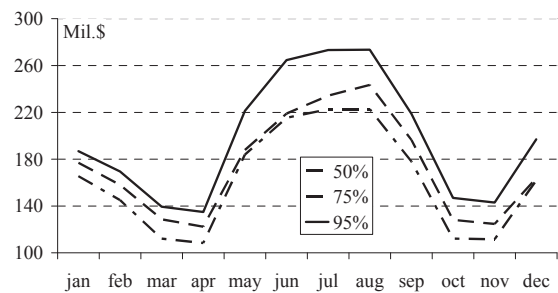


Fig.17. Monthly operational costs at entire EPS of Iraq, Mil.\$

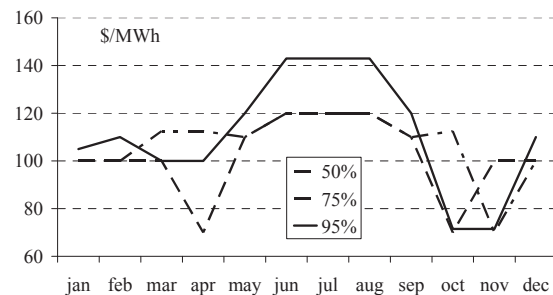


Fig.18. Monthly average marginal energy prices during the first load block at entire EPS of Iraq, \$/MWh

The strong dependence of the system costs and the marginal energy prices on the hydro availability scenario is quite clear. It is evident that under the three scenarios the differences in the marginal prices by months for the three load blocks are high – up to 100%. The differences in the marginal prices for the different load blocks of the single months are also quite high. The reason is that the

HPP capacities and their hydro availability are not sufficient to reach approximate equalizing of the marginal prices by months and by load blocks. This is natural – the TPP production in Iraq EPS is distinctly prevailing (average above 85%).

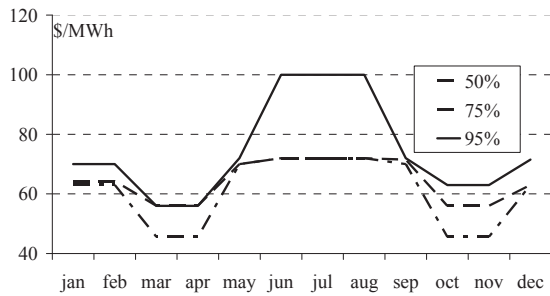


Fig.19. Monthly average marginal energy prices during the second load block at entire EPS of Iraq, \$/MWh

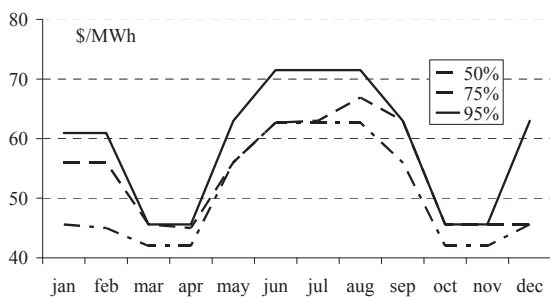


Fig.20. Monthly average marginal energy prices during the third load block at entire EPS of Iraq, \$/MWh

In this context it is easy to explain the intensive use of the Pump Storage HPP (figures 21, 22 and 23) – operating in pump mode during the third load block and generating during the first and second load blocks the PSHPP contributes to equalizing the marginal prices.

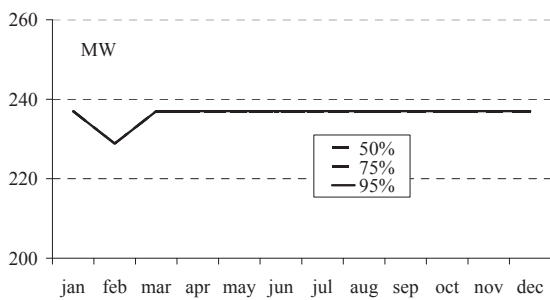


Fig.21. Monthly average generation of MHSPP during the first load block at entire EPS, MW

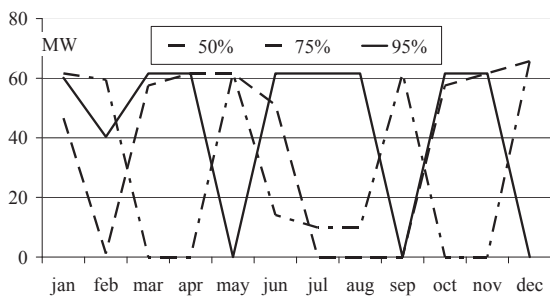


Fig.22. Monthly average generation of MHSPP during the second load block at entire EPS, MW

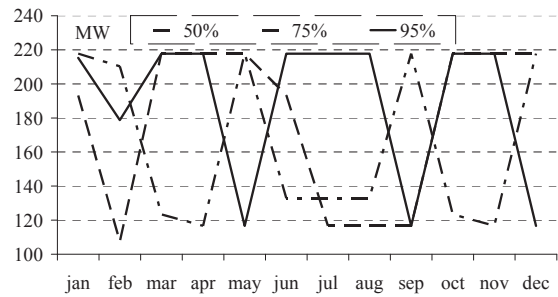


Fig.23. Monthly average pump load of MHSPP during the third load block at entire EPS, MW

Unfortunately the PSHPP capacities in the Iraq system are not sufficient in order to influence significantly. Because of the small volume of the upper reservoir the PSHPP is used only in the daily load regulation cycle and thus reduces the differences in the marginal prices between peak and off peak time during the day and night, but may not affect the differences between the main optimization intervals (in this case between the different months).

Fig. 24 shows the average monthly volume status of Mosul 1 dam. Compared to the modes of isolated operation and of parallel operation only to the Northern part of the EPS, there is certain difference in the dry year scenario. The explanation is that the existence of great number of thermal power plants and the operation in a large EPS change the strategy for water utilization. Because in the system there are enough capacities and there is no power deficit, the purpose now is the water produced energy to replace the most expensive thermal generation so as to reduce the marginal energy price in the system. That is why as whole greater stored water volumes are maintained under the dry year scenario - it is not necessary to use all the water to cover the deficit.

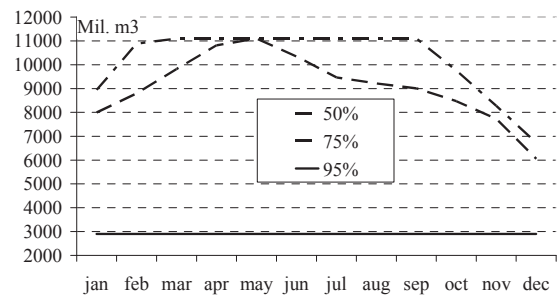


Fig.24. Volume diagram of the Mosul 1 at entire EPS mode of operation, Mil.m3

The water quantities released underneath the Mosul HPC to the irrigation dam and along the Tiger river valley differ from the previous two modes only in the case of 75% hydro availability because of the different optimal generation schedules for the Main HPP.

The spilled water quantities from the main dam are the same as for the previous two modes.

## Conclusions

1. Three main modes of operation of the Mosul HPC have been modelled, which cover the basic system configurations that could arise. The model studies carried



out for optimal plan of operation of the Mosul HPC lead to some conclusions common for the three modes in addition to the specific mode conclusions presented above:

- the optimization results strongly depend on the assumed inflow scenario for Mosul 1 dam. The energy production for a normal wet year scenario is about twice higher than the one during very dry years. The operational capacities and the monthly energy production of the HPPs are very different for each scenario. The non supplied energy (in island mode of Northern Iraq) and the marginal electricity prices (in mode of parallel operation to the entire EPS) are much higher during very dry year compared to the normal wet year scenario;

- In normal wet year scenario the spilling of the main dam during the months of March, April and May is not avoidable at all;

- In very dry year scenario the Main HPP processes the entire water inflow and the necessary for irrigation and water supply quantities are greater than the released quantities, except during the months of March and April;

2. The differences between the system costs and marginal energy prices for the entire system of Iraq amount to 100% under the different hydrological scenarios. The differences in the marginal prices for the particular load blocks of the different months are significant as well. This is due to the fact that HPP capacities in the Iraq system as a whole and their water resource availability are not sufficient to bring closer the marginal prices deviations.

3. Because of the small volume of the Mosul PSHP upper reservoir it is used only during the daily load regulation cycle, but may not affect the differences in the marginal prices between the main optimization intervals (in this case months).

Finally, it should be concluded that the optimization model studies, carried out for the three possible operation modes of Mosul HPC, may serve for the planning of HPPs operation, as well as for training of students and experts in the Republic of Iraq. The elaborated models and programmes may be adjusted to reflect specific possible future operation modes of the Mosul complex.

## References

[1] D. Stoilov, M. Kaneva, F. Syltan, Optimal Operation of Mosul Hydro Power Complex - Part I: Mathematical Models, Proceedings of Int. Conf. ELMA '2008, Sofia, Bulgaria, 2008.

## Biographies



**Fawaz Syltan Abdulaha** was born in Mosul, Iraq in 1960. In 1989 he graduated from the Technical University (TU) – Sofia as M.Sc. in electrical engineering. In 1990 he started his work as an engineer at Mosul Hydro Power Plant. Five years later he became director of the Mosul Hydro Power Cascade and remained on this position until 2003 when he joined the Technical University of Mosul academic staff. Currently he is assistant professor in electric power plants and systems. His research interests are in the fields of electric power plants construction and optimal power plants and systems operation. He is pursuing a Ph.D. degree at the Faculty of Electrical Engineering of TU-Sofia.

Fawaz Syltan is with Technical College – Mosul, Iraq (e-mail: fawazsyltan@yahoo.com).



**Dr. Dimo Stoilov** was born in Plovdiv, Bulgaria in 1969. In 1995 he graduated from the Electric Power Engineering Department of the Technical University (TU) – Sofia as M. Sc. in electrical engineering. He holds a M. Sc. in Applied Mathematics (TU-Sofia, 1998) and a Ph.D. (TU-Sofia, 2003) in Electric Power Grids and Systems. In the period 1997-2005 he worked as expert in the National Dispatch Center of the NEK-EAD. In 2005 he joined the Electrical Engineering Faculty of TU-Sofia, where in 2008 he was awarded the position of associate professor in Power Grids and Systems. His major interests are in the fields of power systems operation planning and control.

Dr. Dimo Stoilov is with the Faculty of Electrical Engineering, Technical University of Sofia, 8, Kl. Ohridski Blvd., 1000 Sofia, Bulgaria (e-mail: dstoilov@tu-sofia.bg).

# Electric Energy Quality in Low Voltage Electricity Supply System

Svetlana Tzvetkova, Vania Tzvetkova

**Abstract:** *The results from measurement of the indexes for electric energy quality in the electricity supply system of information centre are given in the paper. Analysis of the indexes for electric energy quality in done according to given in BSS EN 50160 norms.*

**Keywords:** *electric energy, index of quality, voltage, electricity supply system.*

## Introduction

The electric energy quality in the electricity supply system is formed in case of joint operation of different electrical installations and mechanisms that influence in different way on the indexes for electric energy quality.

The electric energy has to have the necessary quality and quantity indexes to be guarantee the normal operation of the electrical installations and mechanism. The physical process of electric energy generation and transfer is process in which is not possible all consumers to be supplied with electric energy with same parameters. The consumers have different sensibility to the electric energy quality too.

The standards and regulations give the requirements for the electrical energy in different points of the electricity supply system and for each consumer.

The standard BSS EN 50160 is basic standard for electric energy quality for low and medium voltage networks [1]. It includes the following basic indexes for electric energy quality: frequency deviation; voltage deviation; fast voltage fluctuations; flicker; unbalance; harmonics; interharmonics; voltage dips; transient processes; overvoltages; short-time interruptions; long-time interruptions.

Supporting of the indexes for electric energy quality in determinate limits ensure energy effective exploitation of the electrical installations and mechanisms [2]. The organizational and technical decisions have to be taken if these indexes are not supported in the established limits.

The results from measurement of the indexes for electric energy quality in the electricity supply system of information centre are given in the paper. Analysis of the indexes for electric energy quality in done according to given in BSS EN 50160 norms.

## Determination of the indexes for electric energy quality in low voltage electricity supply system

The experience shows that the determination of the indexes for electric energy quality by measurement with special instruments is the most accurate and the fastest method.

Investigation of the indexes for electric energy quality in the electricity supply system of information centre was done.

The measurements were done by special instrument for analysis of the indexes for electric energy quality Fluke 435 Power Quality Analyzer. This is a multifunctional instrument for detection and elimination of problems in three phase's networks. The instrument allows measuring of all electrical quantities and indexes for electric energy quality according to BSS EN 50160 [3]. They are the following:

- Phase values of voltage;
- Values of the line voltage;
- Phase values of current;
- Value of current in the neutral conductor;
- Frequency;
- Active power, reactive power and apparent power;
- Power factor;
- Active energy (consumption/generate);
- Reactive energy (inductive/capacitive);
- Voltage and current harmonics (up to 50<sup>th</sup> harmonic);
- Total Harmonic Distortion (THD);
- Interharmonics;
- Flicker;
- Voltage deviation;
- Overvoltages;
- Determination of the voltage dips and peaks;
- Determination of the voltage interruptions;
- Determination of transient processes;
- Level of pulsations;
- Unbalance.

Power Quality Analyzer Fluke 435 is used in 3-phase networks with or without neutral conductor. It has voltage and current inputs. The current clamps with different sensibility could be turn to the current inputs. The data are measured and recorded in SRAM memory. The measuring and recording data are accessible for reading by the communication port RS232 by software FLUKEVIEW working under WINDOWS.

The accuracy of measuring of Fluke 435 is:

- Voltage:  $\pm 0,5\%$  of nominal voltage;
- Current:  $\pm (1\%$  of the measured value + 5 digits + accuracy of current clamps/transformer);
- Power and energy:  $\pm (1,5\%$  of the measured value + 10 digits + accuracy of current clamps/transformer).

The main screen of the instrument, in case of monitoring of the electric energy quality, is shown on fig. 1. This screen shows whether the indexes for electric

energy quality respond to the requirements of BSS EN 50160.

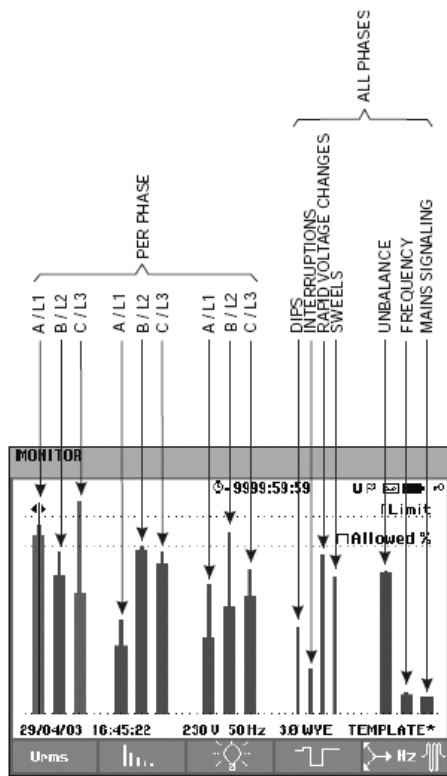


Fig. 1. Main screen of power quality analyzer Fluke 435

The length of the column is increased if corresponding index for electric energy quality is removed from its normal value. The column changes its color from green to red if the index for electric energy quality passes the given limit.

The indexes effective values of the voltage, harmonics and flicker have columns for each phase L1, L2 and L3.

The indexes voltage dips, voltage interruptions, fast voltage fluctuations, overvoltages, unbalance, frequency and transient processes have only one column. It presents the operation of the three phases.

The control point for measuring is the busbars of section 1 of main distribution board in case of normal operation regime. The time for measuring is 2 hours.

Section 1 of the main distribution board supplies consumers with voltage 0,4 and 0,23 kV. The consumers here are basically computer technique, UPS, air coolers and lighting.

The main screen of power quality analyzer Fluke 435 with the results from the measurement is shown on fig. 2.

The minimum, maximum and average value of the voltage for each phase for considered time period are given in Table 1.

The maximum voltage deviation of each phase is in the admissible norm from  $\pm 10\%U_n$  (rated voltage). The maximum frequency deviation is 0,009 Hz. Therefore, the voltage deviation and frequency deviation are in the admissible norms.

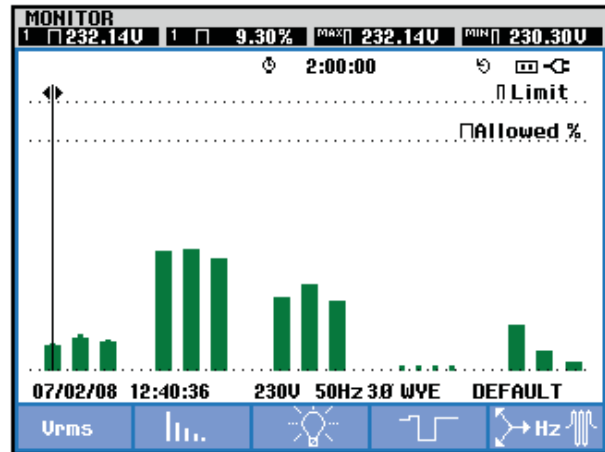


Fig. 2. Main screen with results from the measurement

Table 1

Effective values of the voltage

	Phase L1	Phase L2	Phase L3
$U_{\min}$ , V	228,9	227,69	229,2
$U_{\max}$ , V	229,06	228	229,43
$U_{\text{average}}$ , V	228,98	227,85	229,32

The voltage harmonics and total harmonic distortion for each phase L1, L2 and L3 are shown on fig. 3, fig. 4 and fig.5.

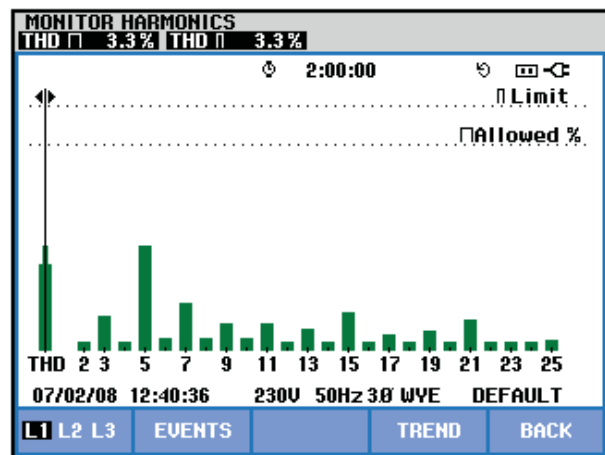


Fig. 3. Voltage harmonics and total harmonic distortion for phase L1

The odd voltage harmonics predominate. For the voltage this are 3, 5 and 11 harmonics. The maximum value have fifth voltage harmonic. Its values are 3,24% per phase L1, 3,39% per phase L2 and 3,36% per phase L3. These measured values are very lower than the admissible value 6% given in BSS EN 50160.

The voltage total harmonic distortion is 3,3% per phase L1 and L2 and 3,1% per phase L3. These values of the voltage total harmonic distortion are far under the admissible value from 8% for low voltage networks given

in BSS EN 50160.

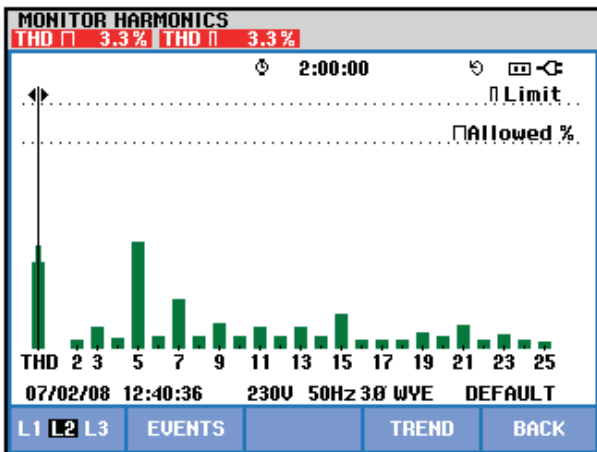


Fig. 4. Voltage harmonics and total harmonic distortion for phase L2

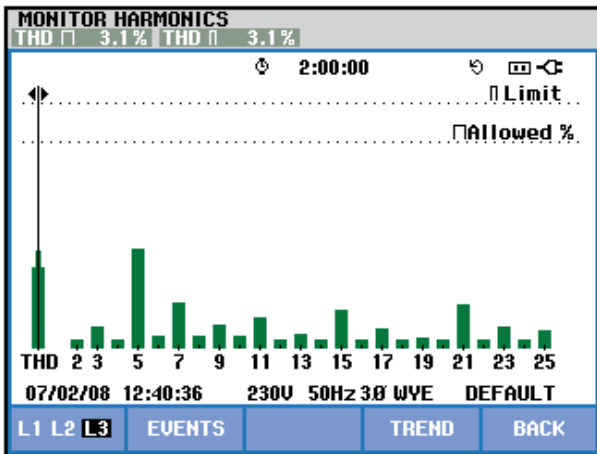


Fig. 5. Voltage harmonics and total harmonic distortion for phase L3

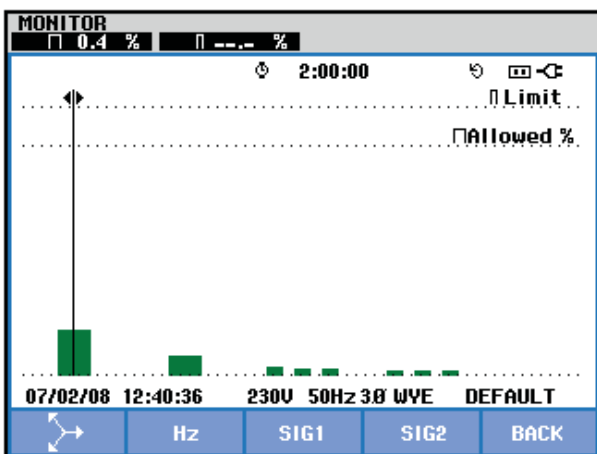


Fig. 6. Unbalance and frequency

The unbalance and frequency total for all phases are shown on fig. 6.

The voltage unbalance is insignificant – around 0,4%. This value is less than the norm from 2% given in BSS EN 50160.

The voltage dips, interruptions and overvoltages are not observed.

The fast voltage fluctuations are in the admissible from the standard norms. This is due to the fact that investigated main distribution board does not supply powerful consumers with fast changeable operating mode.

The results from the measurements in the busbars of section 1 of the main distribution board low voltage of information centre show that measured indexes of the electric energy quality are in the norms. The electric energy could not influence negative on the normal operation of the consumers.

### Conclusion

Using of the special instruments for determination of the electric energy quality according to BSS EN 50160 is recommended. The instruments have to respond to a number of conditions. The most important from them are the following:

- High accuracy of the measurements;
- High speed of record of the measuring quantities.

The results from the measurements in the busbars of section 1 of the main distribution board low voltage of information centre show that measured indexes of the electric energy quality are in the norms. The electric energy could not influence negative on the normal operation of the consumers.

The high quality electric energy that supply the consumer do not denote that there not other problems in the electricity supply system. The determination whether the electric energy is high quality is only one side of a problem. The energy of the consumer is possible to be high quality according to BSS EN 50160 but in the electricity supply system is possible to have very serious problems that are connected with reliability and safety.

The reasons may be the following:

- Unsuitable automatic equipment;
- Lack of selectivity between the circuit breakers;
- Unsuitable choice of conductors and cables;
- Insufficient environment protection of the electrical boards;
- Unsuitable scheme of operation and etc.

For this reason always together with the measurements we have to do analysis of the electric scheme and its elements. This will give full picture for the transitory state according to quality and for the future possible risks connected with reliability and safety.

### References

- [1] BSS EN 50160 “Voltage characteristics of electricity supplied by public distribution systems”, 2006.
- [2] Tzanev T., S. Tzvetkova, „Energy efficient exploitation of electricity supply systems”, Energy Forum’2008,



Varna, pp. 15-26, 2008.

[3] Tzanev T., S. Tzvetkova, V. Kolev, B. Tzaneva, V. Tzvetkova, "Analysys of the possibilities of instruments for electric energy quality measuring and assessment", Energy Forum'2006, Varna, pp. 224-231, 2006.

## Biographies



**Svetlana Tzvetkova** was born in Stevrek, Bulgaria, on November 9, 1969. She studied at the Technical University of Sofia-Bulgaria and received Dr. degree from the same university in 2004.

Since 1993 she worked in the Faculty of Electrical Engineering of the Technical University of Sofia as a Lecturer and researcher in the field of electrical equipment and technical exploitation of electrical installations.

Svetlana Tzvetkova is with the Faculty of Electrical Engineering, Technical University of Sofia, 8, Kl. Ohridski Blvd., 1000 Sofia, Bulgaria (e-mail: [stzvet@tu-sofia.bg](mailto:stzvet@tu-sofia.bg)).



**Vania Tzvetkova** was born in Stevrek, Bulgaria, on July 23, 1974. She studied at the Technical University of Sofia-Bulgaria.

Since 1998 she worked in Vocational Secondary School of Railway Transport as a teacher in the field of electrical equipment and electric supply.

Vania Tzvetkova is with the Vocational Secondary School of Railway Transport, 44, A. Strashimirov Str., 5100 Gorna Oriahovitza, Bulgaria (e-mail: [vaniatzvet@abv.bg](mailto:vaniatzvet@abv.bg)).

# LabVIEW Software Processing of the Power Quality Parameter Measuring Results

Milan M. Simić, Dragan S. Kovačević and Božidar R. Dimitrijević

**Abstract:** *Experimental results regarding to possibilities of using virtual instrumentation for statistical processing of measuring results obtained by digital instruments for power quality real-time monitoring, are presented in this paper. Measurements are performed at low-voltage side of 10kV/0.4kV transformer by using portable three-phase power quality analyzer CA 8334. LabVIEW programming application provides the power supply voltage waveform monitoring, with the software analysis and chronological recording of power quality parameter measuring results.*

**Keywords:** *power quality analyzers, virtual instruments, LabVIEW software processing.*

## Introduction

Quality degradation of electric power delivered to the individual customers, caused by influence of the different network problems and disturbances, directly contributes to decreasing of efficiency level in the power production, delivery and consumption. To prevent potential problems and customer equipment failures, the power distribution companies are obligated to provide the continuous control of power delivery and consumption processes, at different distribution network locations. Efficient and valid power quality monitoring procedure requires the development of distributed measurement system using for monitoring and analysis of measured power quality parameter values [1].

Reference nominal values and permissible intervals of these quality parameters are defined according to national and international power quality regulations and standards, such as European power quality standard EN 50160 [2,3]. This standard which defines the voltage characteristics of electricity supplied by public distribution systems, under normal working conditions, is adopted by the CENELEC European committee for electrotechnical standardization.

Possible solution for providing metrological assurance of an entire power distribution system considers using the number of measuring stations installed at remote network locations and controlled from the power supplier delivery center. In order to perform real-time monitoring of power quality parameter values, remote measuring stations must be supplied with digital instruments for measurement and chronological recording of standardized quality parameter values. Instruments developed for measurement of power quality parameters are commercially available in different constructive and functional solutions. Devices such as the transferable power quality analyzers LEM Memobox 808, LEM Q-Wave Power, Circutor AR5 or Chauvin Arnoux C.A. 8332/8334, are capable for performing the real-time monitoring of quality parameters [4,5]. These measuring instruments are programmed for functioning according to

the relevant power quality standards, including automatic generation of the final quality report, using corresponding PC software support for analyzing of recorded measuring results. Two-way data transfer between quality analyzers and standard PC computer is providing by using the serial communication interface RS-232. Majority of the present power quality measuring devices are capable of operating according to the following international quality standards: EN 50160, IEC 61000-4-7, IEC 61000-4-15, IEC 61000-4-30 and IEC 61010. Measurement, recording and the PC software analysis of following parameters is enabled [5]:

- power supply frequency variations;
- RMS values of voltages and currents per phases;
- voltage and current total harmonic distortion;
- voltage and current phase unbalance;
- active, reactive and apparent power values;
- consumed active, reactive and apparent energy;
- power factor values per phases;
- voltage and current harmonic components;

Procedure for software analyzing of quality parameter measuring results presented in this paper, is performed in LabVIEW virtual instrumentation software programming language [6]. Instrument using for measurement of power quality parameter values is the three-phase power quality parameter analyzer Chauvin Arnoux CA. 8334. Measured values are obtained from low-voltage side of 10kV/0.4kV distribution transformer, inside remote measuring station within a distributed measurement and information system using for power distribution network quality monitoring.

## Procedure for measurement of power quality parameter values

Relevant information for confirming the fulfilment of optimal power distribution network quality level, defined according to the power quality standards, can be provided only by measurement and processing of quality parameter values. A simplified hardware block configuration of the procedure for real-time measurement and software based processing of the voltage quality parameters, is presented in Fig.1. Measurement procedure is functionally based on a power quality analyzer C:A: 8334, supported by virtual instrumentation processing software LabVIEW, installed in a PC programming environment. These measurements are carried out according to the methodology prescribed by the European quality standard EN 50160, with a signal sampling frequency value of 12.8kHz per channel. Values obtained during measurement procedure are recorded into instrument memory at every 5 seconds. Through RS-232 two-way serial communication interface measured values

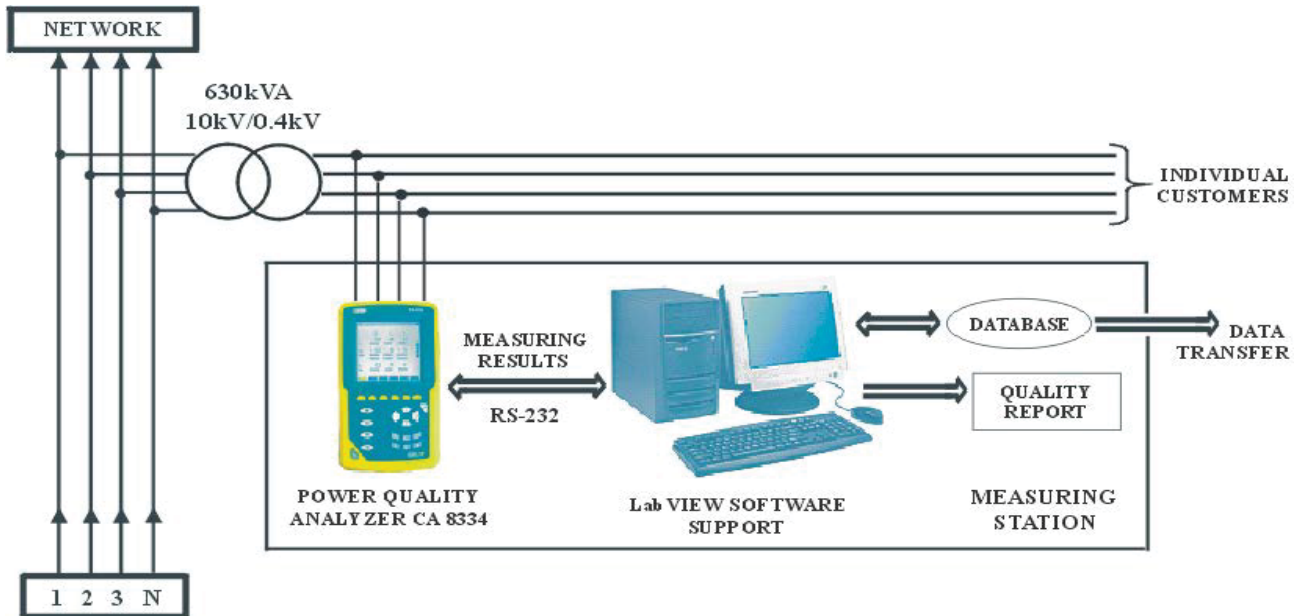


Fig.1. System for measurement and processing of the voltage quality parameter values

previously recorded into power quality analyzer memory, are sending directly to PC computer for further LabVIEW based software analyzing. Measuring instrument in Fig.1. connected at 0.4kV side of the distribution transformer, is enabled to perform the following functional activities [5]:

- measurement of the RMS three-phase voltage values with the specified nominal accuracy of  $\pm 0.5\%$ ;
- measurement of the RMS three-phase current values with the specified nominal accuracy of  $\pm 0.5\%$ ;
- measurement of the frequency with nominal accuracy of  $\pm 0.01\text{Hz}$  and power with accuracy level of  $\pm 1\%$ ;
- measurement of consumed energy with the specified nominal accuracy value of  $\pm 1\%$ ;
- measurement of the power factor with the specified nominal accuracy value of  $\pm 0.01$ ;
- measurement of the voltage and current high-order harmonic components of up to 50 order;
- measurement of total harmonic distortion THD with the specified nominal accuracy value of  $\pm 1\%$ ;

Valid measuring data related to real-time values of the controlled power quality parameters can be obtained only by measuring devices which are followed by appropriate metrological traceability chain. For providing measuring traceability of power quality analyzer, must be performed calibration procedure, which can be carried out in central calibration lab or directly inside measuring stations [7,8].

#### LabVIEW virtual instrumentation software support

Generally, virtual instrument consists of the standard PC computer or workstation equipped with corresponding application software support and cost-effective hardware components, such as plug-in data acquisition cards, which perform basic functions of the traditional instruments [9]. Graphical programming environment includes libraries of the predesigned components, which provide fast and easy implementation of the graphical user interface and control panels. Procedure for software based processing of power quality parameter measuring data described in this paper,

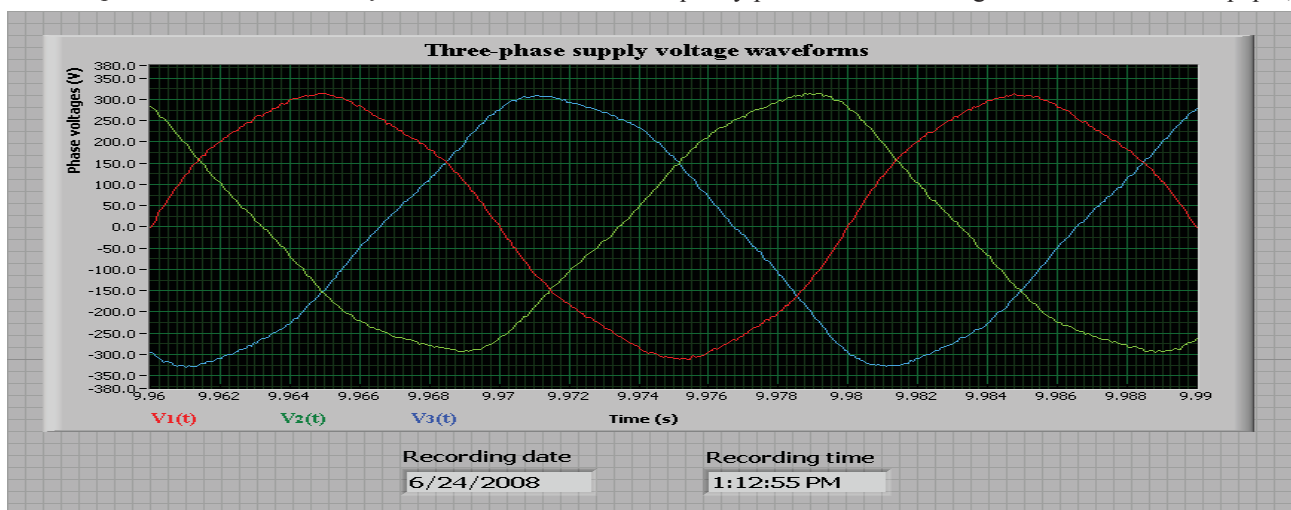


Fig.2. Front panel of the LabVIEW virtual instrument for monitoring of three-phase voltage waveforms

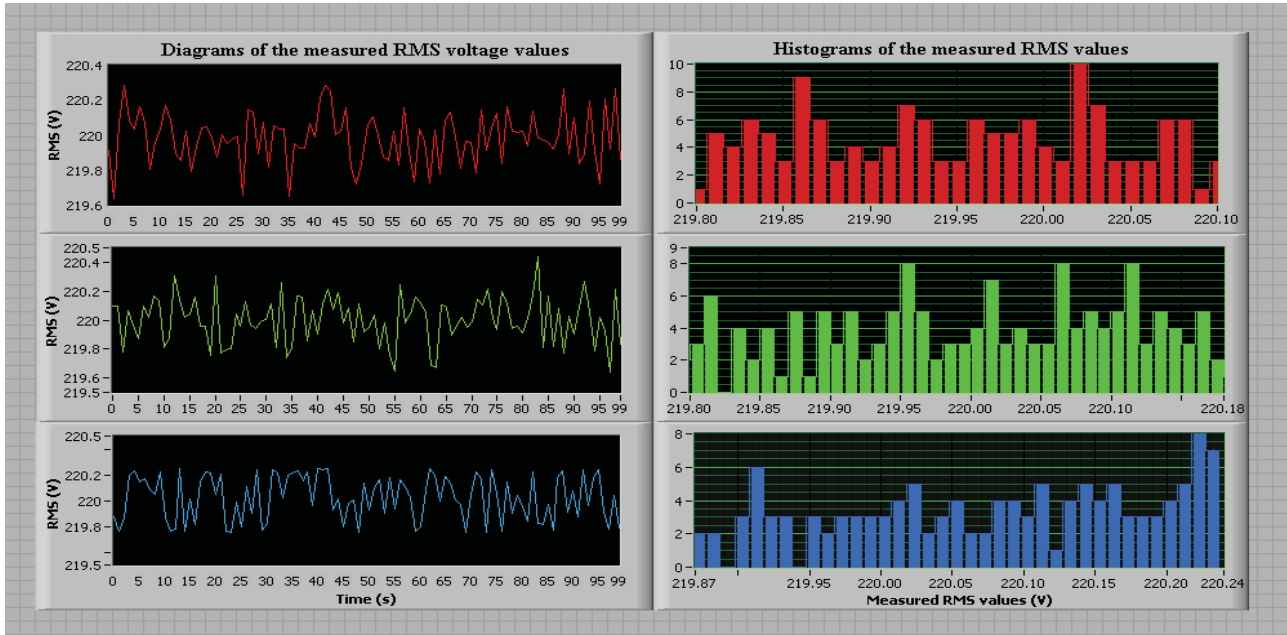


Fig.3. Diagrams and histograms of the measured RMS voltage values in LabVIEW software environment

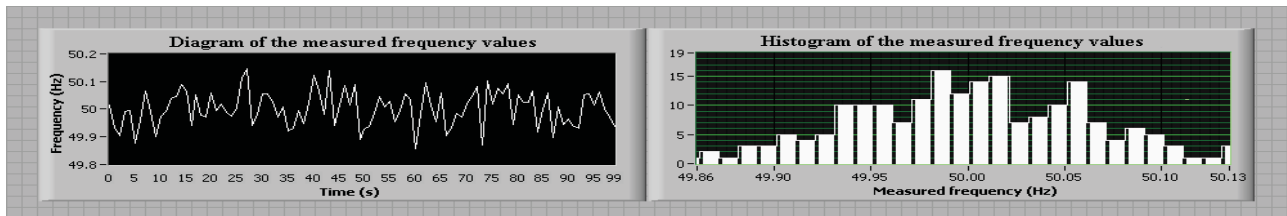


Fig.4. Diagram and histogram of the measured power supply frequency values

is performed by virtual instrumentation software support, LabVIEW. Designed programming application is realized for the purpose of presentation, statistical analysis and the recording of the measured supply frequency values, RMS values of three-phase power supply voltages, phases and measured voltage harmonic components. Front panel of a virtual instrument designed in the LabVIEW environment enabling graphical presentation of the three-phase supply voltage signal waveforms, including additional data about voltage recording date and time, is presented in the Fig.2.

Statistical processing of measuring data concerning the RMS values of the supply voltages per phases, performed by LabVIEW programming application, is given in Fig.3. This figure presents the time diagrams and corresponding frequency histograms for hundred successively measured RMS values of phase voltages. Diagram and histogram of the measured signal frequency values are shown in Fig.4. According to European power quality standard EN 50160 permissive range of delivery network frequency values is from the lower value of 49.5Hz to upper value of 50.5Hz. Minimum and maximum grid frequency values which are obtained during measuring process 49.84Hz and 50.15Hz are inside permissive range of  $\pm 0.5$ Hz in relation to 50Hz nominal frequency value, defined by EN 50160 standard.

The most interesting part related to analyzing of power quality parameter measuring data according to EN 50160 standard, considers estimation of the high-order harmonic components, which is described in next part of this paper.

### Harmonic analysis according to the EN 50160 power quality standard

European power quality standard EN 50160 regulates maximum acceptable values related to individual voltage harmonic components of up to the 25 harmonic order [3]. Harmonic values are defined in percentage relation to the reference power supply voltage value. Comparison of the measured high-order voltage harmonic component values with acceptable values prescribed by EN 50160 standard, from 3 to 19 order harmonics, is presented in the Table 1.

Table 1.

High order odd harmonic components of the supply voltage

Voltage harmonic order	Acceptable values per EN 50160 (%)	Max. measured values (%)
3	5	0.559
5	6	0.498
7	5	0.621
9	1.5	0.517
11	3.5	0.481
13	3	0.508
15	0.5	0.464
17	2	0.442
19	1.5	0.361

Conclusion that can be made from the measuring data presented in this table, is that all measuring harmonics are



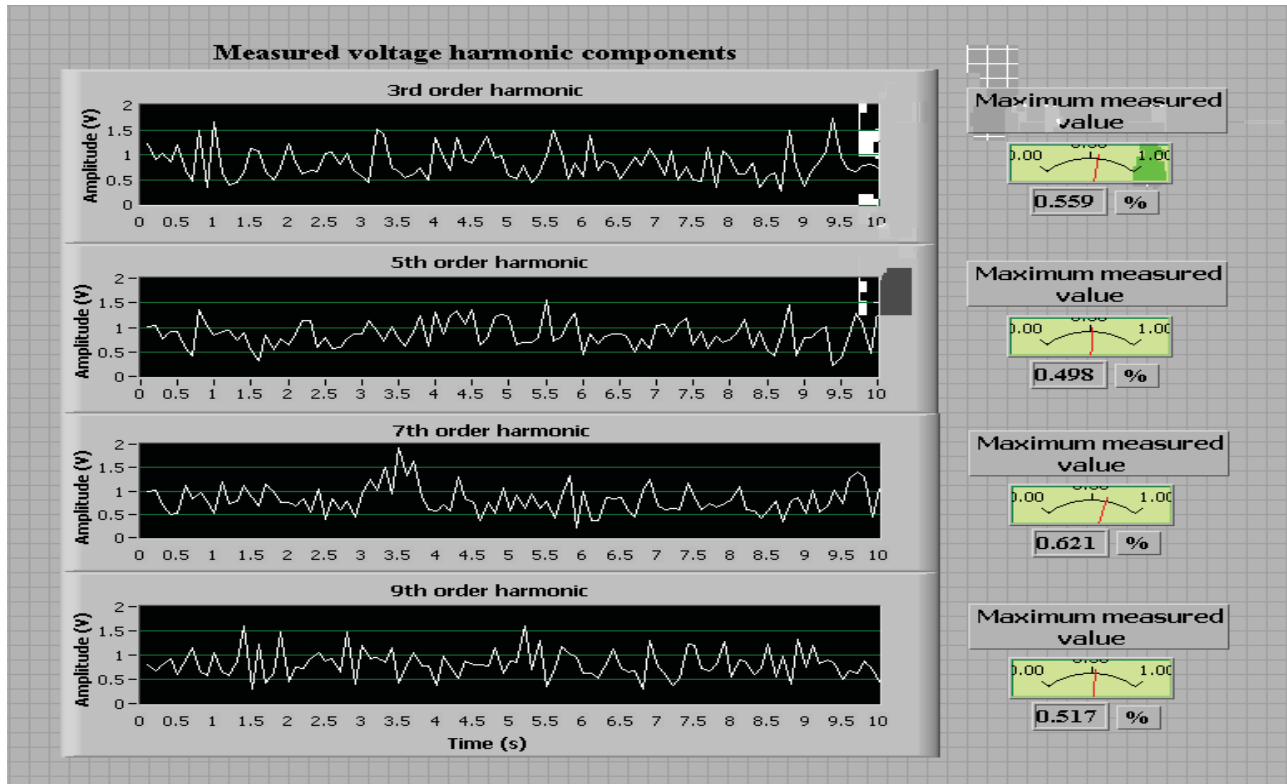


Fig.5. LabVIEW software analysis of the measured high-order voltage harmonic components

satisfied requirement of EN 50160, with maximum values which are lower than limit values defined by the standard.

Graphical presentation of measured voltage harmonic component values from the third to ninth order harmonic, including additional information related to the maximum measured values of analyzed individual voltage harmonic components is given on Fig.5. As in the cases of previous figures, presented time diagrams of obtained measuring results are recorded using LabVIEW processing software. Processed data of the measured power quality parameters, previously recorded in the measuring station database are finally transferring using communication network directly to distribution center of electricity supplier company. The final quality report contains information related to power quality level at specific delivery network point, including a detailed summary of detected unwanted network events.

### Conclusion

Procedure for software based processing of the power quality parameter values, developed by combining power quality analyzer Chauvin Arnoux C.A. 8334 and virtual instrumentation software support LabVIEW, is presented in this paper. Method is implemented into the distributed system for measurement and analyzing of power quality parameter values, consisting of the distribution center and number of remote measuring stations at different network locations. Software application designed in the LabVIEW programming environment enables graphical presentation and recording of the measuring results obtained by power quality analyzer. Statistical processing of measured RMS three-phase voltage values, grid frequency values and the voltage harmonics is performed, including presentation of

measuring data time diagrams and frequency histograms. Analysis of the measuring results regarding to high-order harmonics component values, carried out according to the power quality standard EN 50160, is confirmed complete fulfilment of standard requirements concerning maximum permissive values of the individual high-order harmonics.

### References

- [1] B. Dimitrijević, M. Simić. Metrological Support of the Distributed Power Quality Monitoring. Int. Conf ICEST 2007, Ohrid, Macedonia, 2007, Conference Proceedings, pp.97-100.
- [2] Standard EN 50160 Voltage Characteristics of Electricity Supplied by the Public Distribution Systems, Reo, UK.
- [3] EN 50160 Power Quality Standard, The Power Quality Access Meters and EN50160, Siemens, May, 2003.
- [4] LEM Q-WAVE Power Network Analyser - specifications, LEM NORMA GmbH, Austria, 2005 (www.lem.com).
- [5] Chauvin Arnoux C.A. 8334 Three-Phase Power Quality Analyzers - specifications, Chauvin Arnoux Group, 2004.
- [6] LabVIEW User Manual, National Instruments Corporat. USA, 2005 (www.ni.com).
- [7] B. Dimitrijević, M. Simić, D. Kovačević. Remote Providing Traceability of the Power Quality Meters. Int. Conf. Ee 2007, Novi Sad, Serbia, 2007, CD Conference Proceedings.
- [8] A. Ferrero, M. Lazzaroni, S. Salicone. A Calibration Procedure for a Digital Instrument for Electric Power Quality Measurement. IEEE Tran. on Instrumentation and Measurement Volume 51, Number 4, 2002, pp. 716-722.
- [9] G. Miljković, D. Denić, D. Živanović. Virtual Instruments as Educational Tool in Area of Measurements. Int. Conference SAUM 2007, Niš, Serbia, 2007, Conf. Proceedings, pp.106-109.

## Biographies



**Milan M. Simić** was born in Kragujevac, Serbia, on October 19, 1977. He graduated from University of Niš, Faculty of Electronic Engineering in 2002.

Since 2004 he worked in the Faculty of Electronic Engineering, as the assistant and researcher in the scientific field of metrology. His field of interest includes measurement of electrical quantities, especially measurement of the electrical power quality parameters.

Milan M. Simić is with the Faculty of Electronic Engineering, University of Niš, Aleksandra Medvedeva 14, 18000 Niš, Serbia (e-mail: milansm@elfak.ni.ac.yu).



**Dragan S. Kovačević** was born in Užice, Serbia, on November 22, 1957. He graduated from Belgrade University, Faculty of Electrical Engineering in 1982, and received PhD degree from University of Niš, Faculty of Electronic Engineering in 1999.

His field of interest includes electrical measurements, testing, monitoring and diagnostics of electrical energy equipment and systems.

Dragan S. Kovačević is with the Electrical Engineering Institute Nikola Tesla, Koste Glavinica 8a, 11000 Belgrade, Serbia (e-mail: dkovac@ieent.org).



**Božidar R. Dimitrijević** was born in Štrbovac, Serbia, on December 31, 1944. He graduated from University of Niš, Faculty of Electronic Engineering in 1970, and received PhD degree in 1980 from the same university.

Since 1991 he worked in the Faculty of Electronic Engineering, as a full-time university professor and researcher in the scientific field of the metrology. He participated in realization of many projects as assistant or project manager.

Božidar R. Dimitrijević is with the Faculty of Electronic Engineering, University of Niš, Aleksandra Medvedeva 14, 18000 Niš, Serbia (e-mail: bosko@elfak.ni.ac.yu).

# Energy Efficiency in Vector Controlled Variable Speed Drives VSD

Goran Rafajlovski and Krste Najdenkoski

**Abstract:** Today 40% of all energy consumption is in electrical energy and will grow to 60% by 2040. On the other side, the share of electrical energy which will be controlled by power electronics e.g. in variable speed drives will increase from 40% in 2000 to 80% in 2015. The ZVEI shows that a saving of 22.3TWh per year is possible by applying VSD in the German industry. The design challenge is to provide control in a simple way and to do it cost effectively. In most cases the smart use of power electronics and control techniques even can lead to significant cost savings with return on investment in a few months. The ongoing trend to replace analog with digital, standard U/f scalar control techniques with modern vector oriented control in VSD application is motivated not only by lower energy consumption but also better functionality and reliability of control, and reduced wear out of the complete e.g. drive system.

**Keywords:** variable-speed drive (VSDs), motor energy efficiency, vector control FOC, direct torque control

## Introduction

Insistent demand for energy-saving industrial and home appliances has recently escalated because of energy and environmental matter and the necessity to comply with new energy consumption regulations. These regulations force the development of energy-efficient motors for appliances such as washing machines, air conditioner compressor systems and fans [5]. Industrial motors and drives are estimated to consume 610 TWh or 64% of all electricity in industrial applications. Studies accomplished by the Electric Power Research Institute say that over 60% of industrial motors are operating under of their rated load capacity. By using VSDs a potential reduction of energy consumption of 20-30% is achievable [5]. The study concluded that 180 TWh is the potential to save energy using variable speed drives (VSDs), which accounts for 80 Mtons of CO<sub>2</sub> reduction .

The function of a variable-speed drive (VSDs) is to convert electrical energy to mechanical energy and vice versa. This is currently achieved almost exclusively via a magnetic field. Until today none new processes of energy conversion are known that may replace this in the next century. Until a few years ago, the induction machine was mainly used for constant-speed application. With recent improvements in semiconductor technology, power electronics and control techniques, the induction machine is seeing wider use in variable-speed application for increased efficiency. One of the key challenges to increased efficiency of electrical drive is to extend the

application areas of variable-speed drives using modern control techniques. This paper discuss how these challenges related to the induction machine are overcome to effect torque and speed control with that of the DC machine. The discussion focuses around various VSDs systems and their characteristics, as well as the domain of their application. The first section involves what is termed volts-per-hertz, or scalar control. The rest of the paper will present vector-controlled methods applied to the induction machine. These methods are aimed at bringing about independent control of the machine torque- and flux- producing stator currents. The goal of vector-controlled methods is to make the induction motor emulate the DC motor by transforming the stator currents to a specific coordinate system where one coordinate is related to the torque production and the other to the rotor flux. This so called field oriented control method (FOC) provides excellent dynamic response matching that of the DC machine [3], [4]. The main disadvantage is the computational overhead required in the coordinate transformation. With the advanced using the dynamic machine model, vector-controlled VSDs exhibit far better dynamic performance and better energy efficiency than VSDs with scalar control.

Direct Torque Control or DTC is the most advanced VSDs technology developed in the world [3]. With this control technology, field orientation is achieved without feedback using advanced motor theory to calculate the motor torque directly and without modulation. The controlling variables are motor magnetising flux and motor torque. DTC drives do not need a tachometer or encoder to monitor motor shaft speed or position in order to achieve the fastest torque response ever from an AC drive which saves initial cost. With a DTC controlled bridge harmonics can be significantly reduced [2], the low level current distortion is usually less than a conventional 6-pulse or 12-pulse configuration and power factor can be as high as 0.99.

## Scalar control

Scalar control method is derived from the steady state machine model and is satisfactory for many low-performance low - energy efficiency industrial and commercial application. The block diagram for the scalar-controlled induction drive is shown in Fig.1. The inverter DC-link voltage is obtained through rectification of the AC line voltage needed to drive the induction machine to implement frequency control. The drive uses a simple pulse-width-modulated (PWM) inverter whose

time-average output voltages follow a reference-balanced three-phase set, the frequency and amplitude of which are provided by the speed controller. The drive shown here uses an active speed controller based on a proportional integral derivative (PID), or other type of controller. The input to the speed controller is the error between a reference speed signal and the shaft speed of the machine. An encoder or other speed-sensing device is required to ascertain the shaft speed. The drive can be operated in the open-loop mode as well; however, the speed accuracy will be highly reduced.

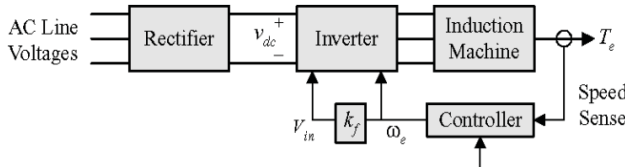


Fig.1 Scalar control of induction machine

Induction machine torque control is possible by varying the magnitude of the applied stator voltage. Speed control is accomplished by adjusting the input voltage until the machine torque for a given slip matches the load torque. However, the developed torque decreases as the square of the input voltage, but the rotor current decreases linearly with the input voltage [3]. This operation is inefficient and requires that the load torque decrease with decreasing machine speed to prevent overheating. In addition, the breakdown torque of the machine decreases as the square of the input voltage. Fans and pumps are appropriate loads for this type of speed control because the torque required to drive them varies linearly or quadratically with their speed.

One remaining complication is the fact that the magnetizing reactance changes linearly with excitation frequency. Therefore, with constant input voltage, the input current increases as the input frequency decreases. In addition, the stator leakage magnitude increases as well, possibly saturating the machine. To prevent this from happening, the input voltage must be varied in proportion to the excitation frequency. If the input voltage and frequency are proportional with proportionality constant  $K_f$ , the electrical torque developed by the machine is uniform throughout the full speed range and can be expressed as:

$$(1) T_e = \frac{3 \cdot |V_{in}|^2 \cdot s}{n_s \cdot R_2} = \frac{3 \cdot |V_{in}|^2 \cdot (n_s - n_r)}{n_s^2 \cdot R_2} = \frac{3 \cdot K_f^2}{R_2} \cdot (n_s - n_r)$$

where  $n_s$  and  $n_r$  are synchronous frequency and machine shaft speed both in electrical radians per second. In a practical drive, the relationship between the input voltage magnitude and frequency takes the form:

$$(2) |V_{in}| = K_f \cdot n_s + V_{offset}$$

where  $V_{offset}$  is a constant. The purpose of this offset voltage is to overcome the voltage drop created by the stator series resistance. The relationship (2) is usually a

piecewise linear function with several breakpoints in a standard scalar-controlled drive. This allows the user to tailor the drive response characteristic to a given application in order to achieve the better energy efficiency.

### Field oriented control FOC

The field oriented control FOC techniques bring overall improvements in drive performance over scalar control, with the advantages like higher efficiency, full torque control, decoupled control of flux and torque and improved dynamics. The basic idea of the FOC algorithm is to decompose a stator current into flux and torque producing components. Both components can be controlled separately after decomposition. The structure of the motor controller is then as simple as that for a separately excited DC motor. The microcomputer-based principled block structure of a field oriented vector control system is shown on fig 2. The control system is principally divided in three sections. One of them represents the object of control, i.e. the dynamic non-linear and multi-variable mathematical model of the induction motor. The second section is the inverter, i.e. its discrete mathematical model with a variable structure, and the third section represents the DSP (Digital Signal Processor) which is to perform the function of the entire control in the closed control system. It implements the controlling algorithms, the acquisition and estimation of valid data, transformation of the coordinates, as well as the synthesis algorithms of control circuit.

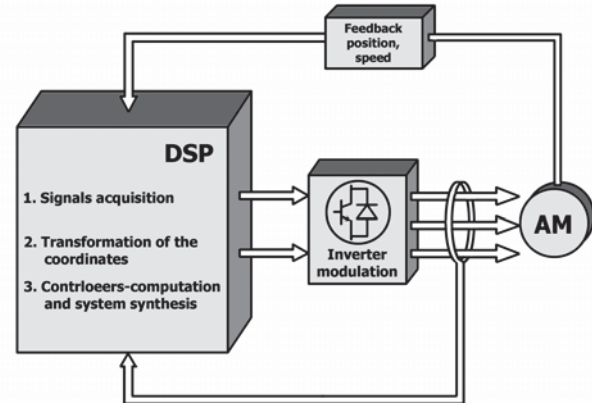


Figure 2. Principled block structure of vector control

Accordingly, vector control is a method for dynamic control of the speed and the torque of the induction motor through permanent control of the intensity and the angle of the space vectors of the electromagnetic variables. One of the most important benefits of this control is energy saving, because the vector control enables dynamic control of the factor of power. The vector oriented techniques can bring overall improvements in drive performance over scalar control. Main advantages of FOC are higher efficiency, full torque control, decoupled control of flux / torque and improved dynamics (fig. 3).



With all this in mind, it can be easy to explain the common tendency of the world's highly developed countries to accept vector control as a universal method for controlling VSDs drives.

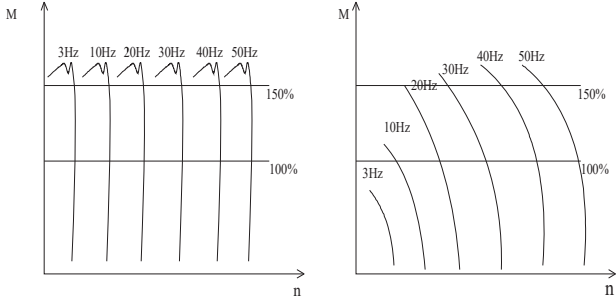


Fig.3 Torque-speed characteristic for U/f and FOC Control

A basic, common characteristic to all approaches toward the different types of vector control is the dynamic equivalent scheme of the induction machine (Fig.4) by the help of which the dynamic non-linear structure of the induction motor is transformed or approximated to the model of a DC engine with independent excitation. This results in the possibility of four-quadrant work-mode of the induction motor with full response and torque dynamics, as well as good performances of the drive down to zero-speeds.

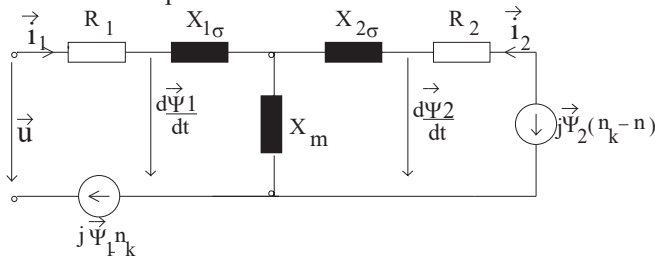


Figure 4. Dynamic equivalent scheme of the IM

According to [5], the state equations for the induction motor  $\vec{\Psi}_1 - \vec{\Psi}_2$  dynamic model in matrix form can be expressed as follows:

$$\begin{bmatrix} \dot{\Psi}_{1x} \\ \dot{\Psi}_{1y} \\ \dot{\Psi}_{2x} \\ \dot{\Psi}_{2y} \end{bmatrix} = \begin{bmatrix} -\frac{R_1}{\sigma \cdot X_1} & n_k & \frac{R_1 \cdot X_m}{\sigma \cdot X_1 \cdot X_2} & 0 \\ -n_k & -\frac{R_1}{\sigma \cdot X_1} & 0 & \frac{R_1 \cdot X_m}{\sigma \cdot X_1 \cdot X_2} \\ \frac{R_1 \cdot X_m}{\sigma \cdot X_1 \cdot X_2} & 0 & -\frac{R_2}{\sigma \cdot X_2} & n_k - n \\ 0 & \frac{R_1 \cdot X_m}{\sigma \cdot X_1 \cdot X_2} & -(n_k - n) & -\frac{R_2}{\sigma \cdot X_2} \end{bmatrix} \cdot \begin{bmatrix} \Psi_{1x} \\ \Psi_{1y} \\ \Psi_{2x} \\ \Psi_{2y} \end{bmatrix} + \begin{bmatrix} 1 & 0 \\ 0 & 1 \\ 0 & 0 \\ 0 & 0 \end{bmatrix} \cdot \begin{bmatrix} U_{1x} \\ U_{1y} \end{bmatrix}$$

Or in short matrix form:

$$(4) \dot{\underline{\Psi}}(t) = \underline{A} \cdot \underline{\Psi}(t) + \underline{B} \cdot \underline{U}(t)$$

(5)

$$\begin{bmatrix} \dot{i}_{1x} \\ \dot{i}_{1y} \end{bmatrix} = \begin{bmatrix} \frac{1}{\sigma \cdot X_1} & 0 & -\frac{X_m}{\sigma \cdot X_1 \cdot X_2} & 0 \\ 0 & \frac{1}{\sigma \cdot X_1} & 0 & -\frac{X_m}{\sigma \cdot X_1 \cdot X_2} \end{bmatrix} \cdot \begin{bmatrix} \Psi_{1x} \\ \Psi_{1y} \\ \Psi_{2x} \\ \Psi_{2y} \end{bmatrix}$$

in short form as:

$$(6) \underline{I}_1(t) = \underline{C} \cdot \underline{\Psi}(t),$$

where underline denotes matrix variable.

Similarly, the equation for the torque balance can be represented as:

$$(7) \dot{n} = \frac{1}{T_A} \left[ \frac{X_m}{\sigma \cdot X_1 \cdot X_2} \cdot (\Psi_{2x} \cdot \Psi_{1y} - \Psi_{2y} \cdot \Psi_{1x}) - M_t \right]$$

In (3), (5) and (7) indexes x, y denotes freely chosen frame of reference that rotate with angular speed  $n_k$ . The system matrix  $\underline{A}$ , regulation matrix  $\underline{B}$ , and resulting matrix  $\underline{C}$  contain the parameters of the control system, i.e. induction motor. Basically, there are two field oriented vector control techniques: indirect control- and direct control method (fig 5).

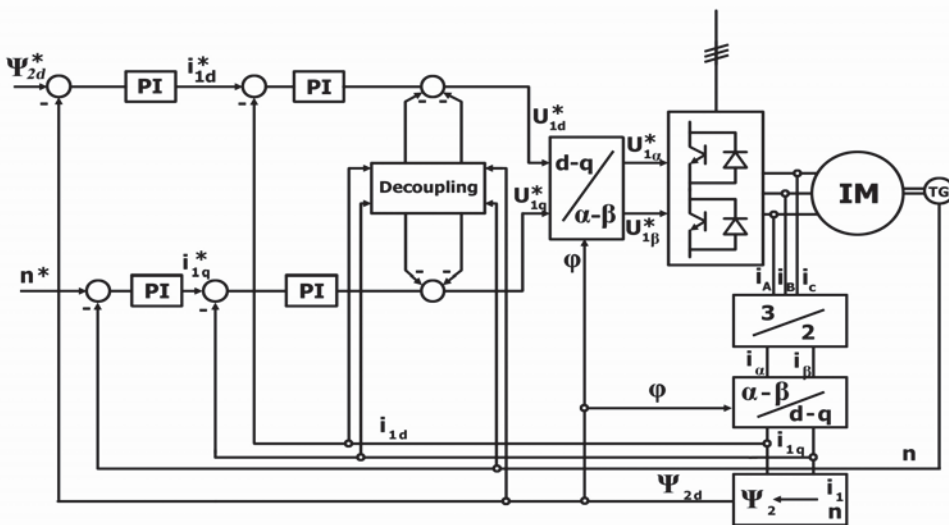


Fig.5 FOC of induction machine

**The indirect vector FOC control method** uses the mathematical model of the induction motor, i.e. for rotor flux-oriented control it uses the corresponding slipping relation and is very dependant on the change of the machine's parameters. This control method do not estimate or measure the space vector of the rotor flux, but use the slipping relation to calculate the output signals of the stator current's space vector (at vector control with a current inverter), or correspondingly the output signals of the stator's voltage space vector (at vector control with a voltage inverter). The basic idea of the FOC algorithm is to decompose a stator current into flux and torque producing components. Both components can be controlled separately after decomposition. The structure of the motor controller is then as simple as that for a separately excited DC motor. **Direct vector FOC control system** is based on measurement, acquisition and (or) estimation of the space angle of the rotor's flux. In order to avoid rotor flux acquisition problems, the recent general tendency is to leave the approach of measuring the flux through additionally embedded coils or Hall's probes, and to acquire the flux through appropriately adapted mathematical models for this purpose [4]. The measurement of the rotor flux mainly has disadvantages connected with the loss of machine's simplicity due to installing additional measurement elements in the course of constructing the machine and to extra expenses for additional signal processing equipment [3], [4], thus increasing the price and reducing the need to apply such control drives. The model-based acquisition of the rotor flux has a disadvantage related to the heating sensitivity of the parameters, which is closely related to the drive's state of the motor. In this sense, long-term researches have been implemented and many models in different coordinate systems for rotor flux acquisition have been developed, as well as qualitative-quantitative evaluation and compensation of the error which is due to the temperature and magnetic variability of the parameters.

### Direct torque control

According to the needs for an ever greater automation of the manufacturing processes, the servo systems most often operated by induction motors are becoming increasingly necessary for different applications, both in the field of robotics and the field of the numerically controlled machine tools. In recent years, especially in the highly developed industrial countries, a much intensified development of various concepts for VSDs field-oriented control can be noticed which, in a control sense, enables approximation of the induction torque to the DC motor. The latest development in VSDs control with high efficiency is the Direct Torque Control (DTC) method. Unlike the control system which is oriented to the space vector of the rotor's flux  $\vec{\psi}_2$ , on the  $\vec{i}_1 - \vec{\psi}_2$  dynamic model in a d-q coordinate system of IM and PWM of the voltage inverter, thereby using linear control technique and linear controllers, the direct torque

control systems have a different concept for vector control. These DTC systems are based on the space angle of the stator flux, on the model of the induction motor in a stationary frame of reference and on the space-vector modulation of the inverter. Thereby, this concept uses non-linear control techniques and non-linear controllers (Fig. 6).

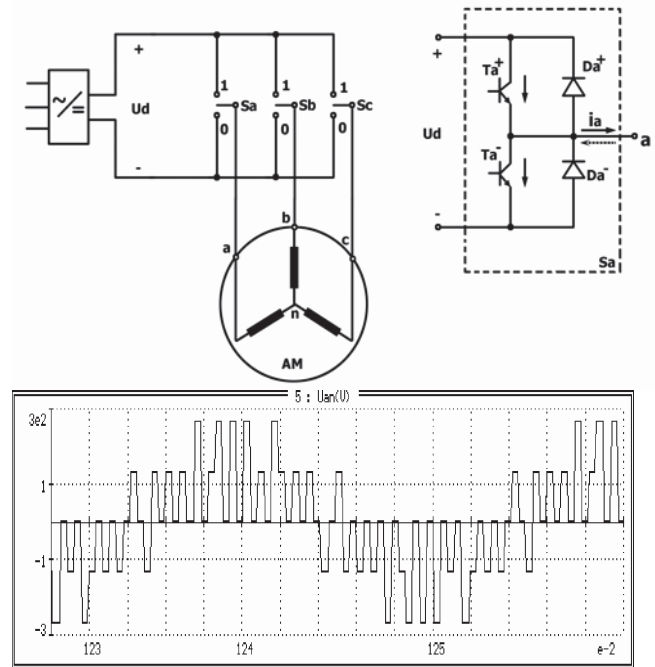


Fig.6 Power circuit of inverter fed IM and line voltage

The orientation of the control system to the space vector  $\vec{\psi}_1$ , greatly reduces the control structure's dependence on the temperature variations of the parameters of the equivalent induction motor scheme [6]. In contrast to FOC control systems in which the precision in the estimation of the space angle of the rotor's flux  $\vec{\psi}_2$  is directly dependent on the motor's parameters which determine the rotor's time-constant, in this vector control concept, there is no need to acquire the space angle of the rotor flux  $\vec{\psi}_2$ . The orientation of the control structure to the  $\vec{\psi}_1 - \vec{\psi}_2$  model of the induction motor in a stationary  $\alpha - \beta$  coordinate system avoids the need of coordinates transformation. Space-vector modulation enables optimum use of the inverter's dynamics, easy and simple optimization of the on-off switching frequency regarding the quality of the expected response of the controlled variables (flux, speed and torque.).

In fig.6 the power circuit of inverter fed IM and corresponding line voltage are presented. Ideally inverter can be considered as three 2-way switches connected between the two DC-busses. Thus the inverter could be characterised as a source of voltage pulses with constant amplitude  $2/3 U_d$  and controllable direction taking  $2^3 = 8$  different states. Six of these 1(001), 2(010), 3(011), 4(100), 5 (101) 6(110) correspondent to active

voltages with the same amplitude  $2/3 U_d$ , while the two others are null-voltage vectors 0(000), 7(111). Output voltage space vector of the inverter is:

$$(8) \vec{u}_1(t) = \frac{2}{3} U_d \cdot [\vec{1} \cdot S_a(t) + \vec{a} \cdot S_b(t) + \vec{a}^2 \cdot S_c(t)]$$

Where  $\vec{a} = e^{j\frac{2\pi}{3}}$  is a complex operator. Primary flux vector  $\vec{\psi}_1$  is calculated as integral of the inverter output voltage vector  $\vec{u}_1$  according to the relation:

$$(9) \vec{\psi}_1 = \int_0^t (\vec{u}_1 - R_1 \cdot \vec{i}_1) dt$$

$$(10) \vec{\psi}_1(t) = \frac{2}{3} \cdot U_d \cdot \left[ S_a(t) + S_b(t) \cdot e^{j\frac{2\pi}{3}} + S_c(t) \cdot e^{j\frac{4\pi}{3}} \right] \cdot t$$

Considering that the voltage drop in the winding is neglected the trajectory of stator flux moves in direction to the inverter output voltage vector. When output is one of the nonzero voltage vectors,  $\vec{\psi}_1$  moves with the constant velocity which is proportional to the output voltage. In the case of the zero voltage vector the velocity is very small and considered to be approximately zero because of the small value of the voltage drop ( $R_1 \cdot i_1$ ).

Therefore, by selecting these vectors appropriately, the trajectory of  $\vec{\psi}_1$  can follow up to the specified locus. By selecting adequate voltage vectors, module  $|\vec{\psi}_1|$  can be kept constant and the rotating speed of  $\vec{\psi}_1$  can be controlled by changing the output ratio between zero and non zero vectors.

Developed electrical torque can express as:

$$(11) M = \vec{\psi}_1 \times \vec{i}_1 = \text{Im}\{\vec{i}_1 \cdot \vec{\psi}_1\} = [\text{Re}\vec{\psi}_1 \cdot \text{Im}\vec{i}_1 - \text{Im}\vec{\psi}_1 \cdot \text{Re}\vec{i}_1]$$

Despite its control simplicity, the DTC method provides possibly the best dynamic response and energy efficiency of any of the methods (fig.7). The average switching frequency of the drive is lower as well, reducing switching loss, enhancing the energy efficiency, as compared with the FOC drive. Since the control basis is the stator flux linkage, the DTC drive is capable of advanced function such as performing “flying starts” and “flux braking”.

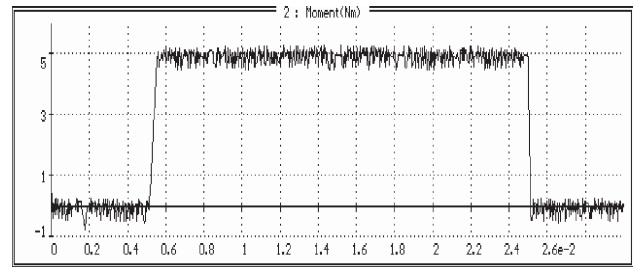


Fig.7 Torque response for DTC drive

With the feature called motor flux optimisation, the energy efficiency of the total drive (that is controller and motor) is greatly improved in fan and pump applications. For example, with 25% load there is up to 10% total energy efficiency improvement. At 50% load there can be 2% total efficiency improvement [2]. This directly impacts on operating costs. This feature also significantly reduces the motor noise compared to that generated by the switching frequency of a traditional FOC-PWM drive.

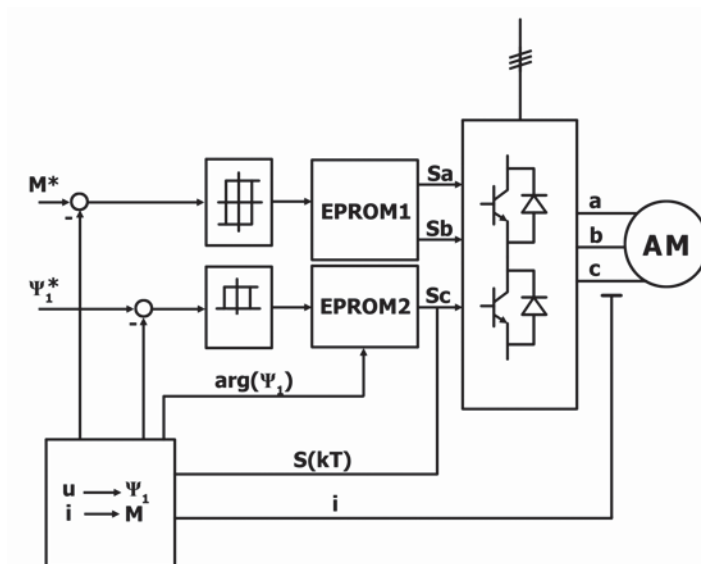
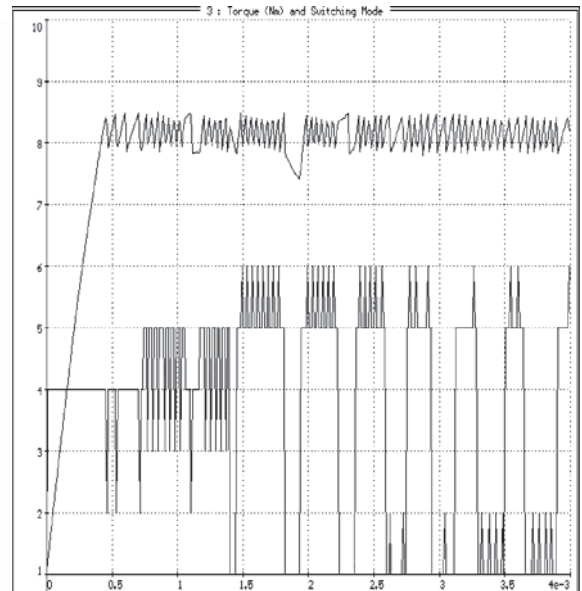


Fig.8 DTC of induction machine - Torque and appropriate space voltage vector



### Savings Potential

The largest potential for energy savings with variable speeds drive are generally in variable torque applications,

like centrifugal pumps and fans, where the power requirements changes as the cubes of speed. The estimated motor electricity consumption in the EU by 2015 is 721 TWh in industry and 224 TWh in the

tertiary/commercial sector [5]. For the assessment of electricity savings potential with the application of VSDs, two different scenarios [1] have been analyzed: the technical savings potential and economic savings potential assuming constant VSD prices. In general, VSDs are not cost effective in the lower power ranges. In data given in Table 1, only the power ranges with a cost of saved electricity (CSE) lower than the average price of kilowatt hours in the sector of application are considered. It is assumed there are no economic restrictions in the technical potential of VSDs. Furthermore Table I summarizes the technical and economic savings potential in the industrial and in the tertiary sector with the application of VSDs [1], [5].

Table 1  
EU Saving potential with application of VSDs by 2015

	Technical potential	Economical potential
Industry (TWh per year)	62	39
Tertiary (TWh per year)	22	8
Total (TWh per year)	84	47
Savings (Mton CO <sub>2</sub> /year)	33	19
Savings (Mil.€/ year)	5600	2050

The estimated economic electricity savings potential (assuming VSD constant prices) with the application of VSDs, by 2015, would translate into 19 Mton CO<sub>2</sub> savings, contributing to the goal of reducing the greenhouse gas emissions in the EU. Table I also shows the technical and economic potential CO<sub>2</sub> and Euro savings, considering average generated CO<sub>2</sub> emission of 0.4kg CO<sub>2</sub>/kWh and considering average price of 0.05 and 0.1 Euro/kWh in industry and tertiary sector, respectively, with the application of VSDs, by 2015.

### Conclusion

VSDs with choosing appropriate control (U/f control, vector control, DTC), with the fast development of the power semi-conducting components, and with the development of hybrid digital signal processing systems are a very relevant growing market, although only 25% of new motors are equipped with VSDs. They allow one to control with precision the speed and torque of induction motors, increasing its application spectrum having significant economical and technical advantages. Huge energy savings (it's been evaluated that around 10% of the generated energy can be saved), and the associated reduction in environmental emissions, are possible through the massive application of VSDs in a wide variety of loads in the different sectors of the industry. VSDs may introduce problems related to the motor efficiency and reliability, power quality, and EMI. Causes and cures for line interference, harmonics and motor damage must be considered in almost any VSDs application. They are discussed in detail in the IEEE 519 and NEMA MG1 Part 31 specifications, but the best defence is an experienced application engineer who is

familiar with operating plant and different control techniques.

In future, wider application of the DTC, (using fuzzy logic an artificial neural network based controllers) in application of VSDs is expected. However, there are several barriers, both technical and non-technical, which prevent a larger scale adoption of VSDs. Because of lack of knowledge of the VSDs economical and technical advantages in industrial and commercial sectors, actions to promote awareness of those advantages should be implemented.

### References

- [1] Anfbal T.de Almeida;Fernando J.T.E.Ferreira, and Dick Both: Technical and Economical Consideration in the Application of Variable-Speed Drives with Electric Motor Systems, IEEE Trans. on Industry Application Vol. 41, No1, Jan/Feb. 2005
- [2] ABB Industry Drives: Direct torque Control The world's most advanced AC drive technology
- [3] Bocker, Joachim; Mathapati, Shashidhar: State of the Art of Induction Motor Control, IEMDC-IEEE-Electrical Machines & Drives Conference, 2007, Volume 2 Issue, 3-5 May 2007 pp.1459-64
- [4] B. Bose, *Power Electronics and Variable Frequency Drives*. New York: IEEE Press, 1996.
- [5] ECPE Position Paper Energy Efficiency – the Role of Power Electronics, Nürnberg, March 2007
- [6] Goran Rafajlovski, Krste Najdenkoski: Modelling of Circuit Parameter Variation in Vector Controlled Induction Motor Drives, OPTIM'06, 10-th International Conference on Optimization of Electrical and electronic equipments, Romania Brasov, 2006, pp.1234-1241

### Biographies



**Goran Rafajlovski** was born in Skopje, Macedonia, on May 2, 1963. He graduated from the University - Skopje, received Master degree from University Zagreb Croatia in 1991 and Doctor degree from University of Skopje 1996. He is a Member of IEEE Power Engineering Society.

His field of interest includes electrical machines and drives, power electronics and energy efficiency control techniques. He is today a associate Professor in the Faculty of Electrical Engineering and Information Technologies of the Ss. Cyril and Methodius University, Karpos II b.b. 1000 Skopje, Macedonia (e-mail: [goran@feit.ukim.edu.mk](mailto:goran@feit.ukim.edu.mk))



**Krste Najdenkoski**, received his Ph.D. degree in Electrical Engineering from Faculty of Electrical Engineering -Skopje in 2003.

His area of interest are electrical machines, power transformers, power quality, energy efficiency systems and wind energy systems. He is a Member of IEEE Power Engineering Society and CIGRE Paris.

Currently he is a Assistant Professor at the Faculty of Electrical Engineering and Information Technologies, "Ss. Cyril and Methodius University" - Skopje, Republic of Macedonia (e-mail: [krste@feit.ukim.edu.mk](mailto:krste@feit.ukim.edu.mk))



# General Methods for Energy-Efficiency Investigation and Evaluation of Induction Motor Drives

Ognyan Dinolov

**Abstract:** A block diagram of complete general methods for energy-efficiency investigation and estimation is synthesized in this paper. The methods are applied and results are presented for a characteristic lathe. A new system of 28 indexes for energy efficiency estimation is submitted and computed. A comparison of energy efficiency levels between drives with induction motors with high and standard efficiency is accomplished.

**Keywords:** energy efficiency, induction-motor drives, methods of investigation

## Introduction

As a result of the advancing with high rates changes in the global climate, other ecological considerations and the depletion of primary energy sources reserves, energy efficiency (EE) improving has become a field – object of significant state funding and regulating in global aspect as well as in Bulgaria. In this connection, the efforts are directed at developing of a number of technical systems for monitoring and electric energy consumption analysis [3, 4, 6, 11] in which, in some cases, qualitative new criteria systems for investigation, estimation and comparison of EE are integrated [4]. Different approaches for EE increasing in the most frequently used induction-motor drives (IMD) are described in literature [9]. Irrespective of efforts on specified directions, the investigations conducted are various and not placed on a uniform methodical basics that should cover and generalize a wide range of production drives, as possible, and form the scientific ensuring of the EE investigations.

Being based on the problem presented, the following research purpose is set: To develop generalized and integral methods for investigation and evaluation of energy efficiency in asynchronous electric drives.

The following tasks have to be fulfilled in order to achieve the purpose:

- using the best background from the existing developments, to generalize and synthesize the methods block diagram;
- to determine the practical range of the methods application;
- based on the development, to conduct experimental research of a characteristic object so that the working capacity and the practical applicability of the submitted methods and means to be proved.

## Body

Due to the EE levels and indexes synthesized in [1, 4, 10], the examining of recent investigations in the

field [2, 4, 5] and further analysis a general methods for EE research, complete assessment and comparing in IMD can be composed and systematized.

The methods block diagram is shown in Fig. 1. The methodical research stages, connections and the sequence are shown in the figure. For clearness and coordination, all blocks show corresponding references.

In order to apply the methods it is beforehand necessary to determine and set the optimum level, the net losses level and the efficiency curve of powering induction motors (IM) (see group A).

The cycle, closed between the numbers 1, 2, 3, 4, 5 and 6 (Fig. 1) can be used for successful EE monitoring of all IMD available in production enterprises.

## Application Range of the Methods

The methods application is restricted by:

- The information availability for the IMD optimum load. When this information is not given by the drive producer the optimum level is accepted at a operation in which IM works with its higher efficiency. For that purpose, the rich data base for IM power characteristics in [8] is used for maximum efficiency determination. The information refers to IM that are manufactured by *Siemens, Balder UK, WEG, Leroy Somers* and other recent companies. The generalized curves, shown in [12], can be used for all manufacturers left.
- The possibility for electric loads measuring. In order to use selected electricity meters [4] it is necessary the IMD current circuit to be broken that necessitates drive stopping and switching the power supply off. In general case, this procedure is not impeded, except for these cases in that the consumers are crucial or technologically connected and the working condition stopping is undesirable because of high risk and other considerations.
- The possibility for net losses determination. The level should be determined by a theoretical approach in case of transport processes [2, 10]. Information for the mass, height and load (solids or fluids) transportation duration is necessary. The net losses can be also determined theoretically with all other IMD [10], but the no-load power might be used as well.

There are possibilities the developed methods to be referred and used for EE rate evaluation not only of electric drives but, also, of mechanisms and machines that are powered by combustion engines. For that purpose, the yield done by the mechanism has to be

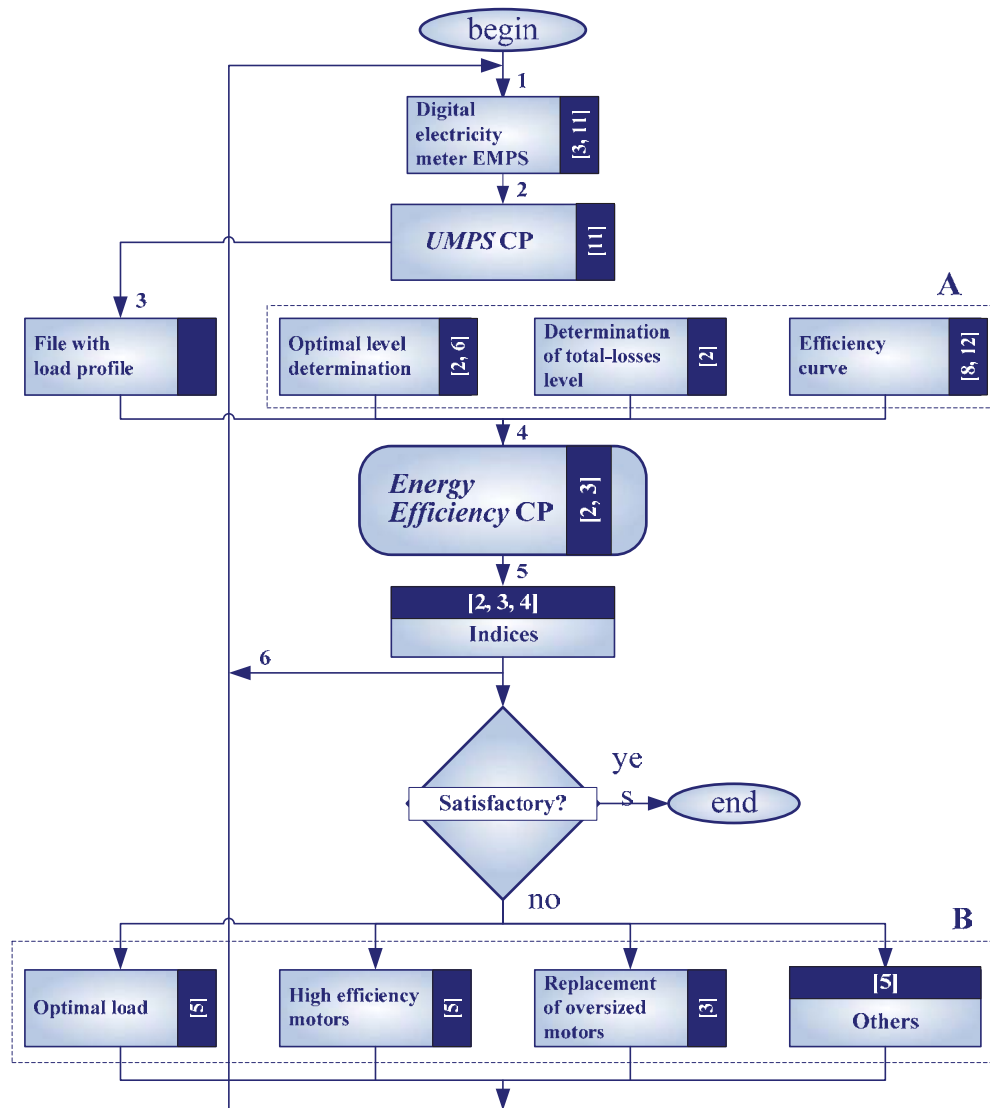


Fig.1. Generalized block diagram of methods for energy-efficiency investigation in asynchronous electrical drives: CP – computer program; A – preliminary obtaining of necessary information; B – approaches for energy-efficiency increasing

determined whereupon, with known fuel consumption and combustion heat, the thermal energy developed from fuel within the investigation period to be calculated. The optimum level will be again set by a priori information.

### High-Efficiency Motors

Excepting the absolute electric energy savings, replacing of IM with energy-efficient motors will also impact on the effective utilization rate. In order to ascertain this dependence, the criteria in *Indices* block (Fig.1) are computed under replacement of IM of a characteristic transport system [2] with higher efficiency motors. The rival motors have been selected from M11 catalogue of *Siemens*. The motors type data and the data for the computed values of indices for EE evaluation are listed in Table 1.

It is seen from the table that the higher IM efficiency increases effective IMD electric consumption rate in

actual as well as in optimum drive operation. The underlying criteria – actual and optimum relative consumption B7 and A6, decrease with average 2.58 % and 2.64 % respectively. Further improvement can be achieved with decreasing of IM drag torque (more perfect IMD) and with an approach of the actual drive load to the optimum. The methods for EE increasing shown in Fig.1 should be altogether applied.

The approach of replacement of standard with energy-efficient motors leads to better power effect in case of long IMD operation.

### Methods Application

Here, the methods created are applied up to the *Indices* block. The investigation object is a lathe C11B that is operated in the *Pretsz Inter Holding* plant, Ruse. The investigation data are obtained for two technological operations - opening drilling and taking of fixed width chips from a steel job. The results are showed in Table 1.

**Table 1**

Values of indices for energy-efficiency evaluation of five belt conveyors in case of replacing the existing induction motors with various types of high-efficiency motors

Indices	K <sub>1</sub>		K <sub>2</sub>		K <sub>3</sub>		S' <sub>1</sub>		S <sub>3</sub>	
	Actual state	ILG6 310-6AA	Actual state	ILG6 316-6AA	Actual state	ILG6 318-6AA	Actual state	ILG6 310-6AA	Actual state	ILG6 223-6AA
A1, kW	63.88	62.96	93.70	91.67	135.6	133.3	64.72	62.96	25.97	25.61
A2, kVAr	28.79	42.96	55.06	61.6	72.43	88.91	32.81	42.96	13.88	18.81
A3, min.	3.43	3.34	3.73	3.51	19.84	20.38	21.41	22.10	40.23	40.69
A4, kWh	1.86	1.72	4.44	3.98	21.91	22.38	7.32	7.43	14.25	14.21
A5, kWh	3.65	3.51	5.82	5.37	44.82	45.29	23.09	23.20	17.41	17.37
A6	2.03	1.96	4.21	3.87	1.96	1.98	1.47	1.47	5.51	5.50
B1, kW	33.83	32.15	72.58	69.11	84.60	84.21	32.50	32.15	23.66	23.35
B2, kVAr	26.45	40.69	56.74	54.9	68.88	81.17	24.38	40.69	13.60	17.26
B3, min.	78	78	73	73	75	75	79	79	79	79
B4, kWh	1.80	1.79	1.38	1.39	22.91	22.91	15.77	15.76	3.16	3.16
B5, kWh	42.18	40.00	86.92	82.70	82.84	82.35	27.03	26.57	27.99	27.58
B6, kWh	43.98	41.80	88.30	84.08	105.7	105.3	42.79	42.33	31.15	30.74
B7	24.46	23.30	63.87	60.62	4.62	4.59	2.72	2.69	9.86	9.73
C1, kW	–	–	–	–	–	–	–	–	–	–
C2, kW	32.45	30.77	71.44	67.97	66.27	65.88	20.53	20.18	21.26	21.00
D1	12.04	11.91	15.17	15.67	2.36	2.32	1.85	1.83	1.79	1.77
D2	22.73	23.33	19.59	20.79	3.78	3.68	3.69	3.57	1.96	1.94
D3, min	74.57	74.66	69.27	69.49	55.16	54.62	57.59	56.90	38.77	38.31
D4, kWh	40.32	38.27	82.48	78.72	60.93	59.97	19.71	19.14	13.74	13.38
E1, %	0	0	0	0.35	0	0	0	0	0	0
E2, %	2.60	2.00	0.55	0.5	1.49	1	2.94	2.00	0.18	0.13
E3, %	93.92	95.52	93.92	96.35	94.42	96.4	92.72	95.52	92.41	93.8
E4	0	0	0	0	0	0	0	0	0	0
E5	0.12	0.21	0.07	0.05	0.11	0.11	0.09	0.21	0.02	0.002
E6	0.91	0.83	0.86	0.83	0.88	0.83	0.89	0.83	0.88	0.81
F1, kW	2.275	–	2.462	–	3.460	–	2.342	–	1.040	–
F2	0.067	–	0.034	–	0.041	–	0.072	–	0.043	–
F3, kVAr	0.303	–	0.829	–	0.834	–	1.270	–	0.307	–
F4	0.011	–	0.015	–	0.012	–	0.052	–	0.022	–
G1, kWh/t	0.144	0.137	0.289	0.275	0.346	0.345	0.140	0.138	0.102	0.101
G2, kWh/t	0.121	0.115	0.243	0.231	0.291	0.290	0.118	0.116	0.086	0.085
G3, kWh/t	0.023	0.022	0.046	0.044	0.055	0.055	0.022	0.022	0.016	0.016
G4, kWh/MWh	18.05	17.15	36.24	34.51	43.38	43.22	17.56	17.37	12.78	12.62
G5	1.02	1.02	1.02	1.02	1.02	1.02	1.02	1.02	1.02	1.02

Within the period researched, the investigated lathe operates with approximately no-load regimes due to a systematic underloading that worsens its EE vastly. This is clearly obvious according to the levels of E4, E5, B1, B2 and B7 indices for the investigated operations.

**Table 2**  
Values of indices for energy-efficiency evaluation of a lathe for two technological operations

--	Opening drilling 31 mm	Chips taking 1 mm
<b>A1, kW</b>	6.60	6.60
<b>A2, kVAr</b>	3.35	3.35
<b>A3, min.</b>	0.27	0.19
<b>A4, kWh</b>	0.01	0.004
<b>A5, kWh</b>	0.03	0.02
<b>A6</b>	1.27	1.23
<b>B1, kW</b>	1.61	1.31
<b>B2, kVAr</b>	3.64	3.42
<b>B3, min.</b>	7	13
<b>B4, kWh</b>	0.02	0.02
<b>B5, kWh</b>	0.16	0.27
<b>B6, kWh</b>	0.19	0.29
<b>B7</b>	7.98	17.05
<b>C1, kW</b>	1.41	1.24
<b>C2, kW</b>	–	–
<b>D1</b>	6.28	13.86
<b>D2</b>	25.77	69.60
<b>D3, min</b>	6.73	12.81
<b>D4, kWh</b>	0.16	0.26
<b>E1, %</b>	0	0
<b>E2, %</b>	61.5	69.2
<b>E3, %</b>	90.92	90.92
<b>E4</b>	0	0
<b>E5</b>	0.49	0.53
<b>E6</b>	0.89	0.89
<b>F1, kW</b>	0.13	0.41
<b>F2</b>	0.08	0.31
<b>F3, kVAr</b>	0.08	0.09
<b>F4</b>	0.02	0.03

## Conclusions

1. Complete methods for investigation, total assessment and comparing of energy efficiency in asynchronous electrical drives are generalized and applied. By means of the methods, the methodical investigations order, stages, approaches for efficiency increasing, measuring units and computer programs are revealed and generalized. The methods application range is determined, as it is based on information available for the optimum load, possibilities for electric loads measuring and for determination of the net losses level. The cycle closed between the numbers 1, 2, 3, 4, 5 and 6 of the model block diagram (Fig.1) can be used for successful energy-efficiency monitoring of all existing electric drives in production plants.

2. Qualitative new data for the indices of estimation the rate of electric consumption effectiveness of a characteristic lathe are got. The high average value of the B7 index – specific electric power consumption in actual operation (12.52 units) shows very low levels of electric consumption effectiveness. The data reveal a high degree of lack of organization in production processes.

The results got show the importance and indispensability of energy-efficiency investigation of lathes and other metal working machines in operation.

3. The impact of induction motors energy class on investigated drives effectiveness and levels of variation of all submitted indices is determined. The replacement of existing conventional motors with high efficiency motors leads to decrease of the actual B7 and optimum A6 relative electrical energy consumption with 2.58 % and 2.64 % respectively.

## Acknowledgements

The author expresses sincere acknowledgements to his scientific supervisor Prof. Kondyu Andonov, Dr. Sc, as well as Assoc. Prof. Valentin Kirchev, PhD and Eng. Gyorgi Nedev for their valuable pieces of advice and responsive help and support.

## References

- [1] Andonov K., V. Kirchev, K. Enimanev, O. Dinolov. Levels for Electrical Consumption Monitoring in Industrial Enterprises. V<sup>th</sup> International Scientific Conference Management and Engineering '07, Sozopol, Bulgaria, June 18-22, 2007, pp. 384-389.
- [2] Andonov K., O. Dinolov, V. Kirchev, G. Nedev. Energy-Efficiency Investigation of a Coal-Feeding System. Energetica, №8, 2007, pp. 26 – 33.
- [3] Anonymous. Power Analyzer Software. Plant Engineering, March 2002, pp. 50 – 51.
- [4] Dinolov O. Generalized Model for Energy-Efficiency Estimation of Induction-Motor Drives. Energetica, 2007, № 5, pp. 37 – 43.
- [5] Dinolov O., G. Nedev, V. Kirchev, K. Andonov. Energy-Efficiency Investigation of a Dust Preparing System with Intermediate Bunker. Proceedings of Angel Kanchev University of Ruse, Vol. 46, Series 3.1, 2007, pp. 16 – 22.
- [6] Hammerstrom D., J. Gephart. Smart Technology Brings Power to The People. Power Engineering International, №10, 2006, pp. 45 – 46.
- [7] <http://www.mps.bg/>
- [8] Improve Motor System Efficiency for a Broader Range of Motors with MotorMaster+ International. U.S. Department of Energy – Energy Efficiency and Renewable Energy, Oct. 2005. Available at: [http://www1.eere.energy.gov/industry/best\\_practices/pdfs/mmplus\\_international.pdf](http://www1.eere.energy.gov/industry/best_practices/pdfs/mmplus_international.pdf).
- [9] Kirchev V., O. Dinolov. A Comparative Study of Possibilities for Energy-Efficiency Increasing in Induction-Motor Drives. Energetica, 2008, №1, pp. 35 – 43.
- [10] Mihailov L., K. Andonov, B. Botev, O. Dinolov, A. Krasteva. Levels for Energy-Efficiency Investigation of



Electrical Consumers. Proceedings of *Angel Kanchev* University of Ruse, Vol. 44, Series 3.1, 2005, pp. 177 – 185.

[11] *Power Logic* Monitoring System. *Merlin Gerin* Catalogue, Sofia, 2006, pp. 246 – 249.

[12] Stefanov I. *Power Engineering Manual*. Sofia, Technica, 1972, p. 1310.

### Biography



**Ognyan Dinolov** was born in Svishtov, Bulgaria, on May 15, 1981. He studied at the *Angel Kanchev* University of Ruse, Bulgaria and received Master degree from the same university in 2005.

His field of interest includes energy efficiency, renewable energy sources and high-efficiency motors. Today he is a PhD student in the Department of Electric Supply & Equipment at the *Angel Kanchev* University of Ruse, Bulgaria.

Ognyan Dinolov is with the Department of Electric Supply and Equipment, University of Ruse, 8 Studentska Str., 7017 Ruse, Bulgaria (e-mail: [dinolov@gmail.com](mailto:dinolov@gmail.com)).

# Technical and Economic Efficiency of Power Transformers On-line Diagnostic System Utilization

Lyubomir V. Dimitrov

**Abstract:** *The paper presented, discusses detailed technical-economic analysis of the cost effect and the benefits utilizing on-line diagnostics and monitoring of power transformers. Further to the results of this research, it is recommended to implement such systems for monitoring and diagnostics, in order to determine and discover early incipient faults and undertake the corresponding procedures to prevent utter failures and catastrophic consequences.*

**Keywords:** *Power Transformer; Cost Benefit; Analysis Monitoring ;On-line Diagnostic*

## Introduction

The Power transformers are essential components of the modern electrical systems. Very often, these are the considered to be the most expensive devices in an energy sub-station, as their utilization require great capital investment.

On the other hand, the transformers are key units, defining the load capacity that the corresponding energy sub-station generates as a part of the power network.

Greater part of the transformer family currently is out of date. The average age of such power transformers is about 25-30 years. This would lead to greater risks and more failures, that always bother the normal operation of

the systems, resulting in unexpected outages and severe problems regarding power distribution.

In order to decrease such risks of unexpected failures and frequent outages, new applications are widely implemented, lately. They are the transformer on-line condition monitoring systems.

## Monitoring Methods

The methods for monitoring and the spheres of their implementation are given below, in Table 1.

The application of such methods for on-line diagnostics theoretically should help to determine the anomaly – fault identification and serious failure condition. In fact, it is always a matter of consideration what method could be used. The experience shows that most of the transformers “live their life” of operation without any serious and extraordinary technical problems. It is not cost effective to utilize many devices for monitoring, that during the transformer lifetime would show no failure indications.

That’s one of the reasons to think about using a simple broadband method, initially to identify faults, that could realize protection and give early warnings about incipient defects. Further on, some of the other methods, given in Table 1, could be applied according to the nature and the place of the fault.

Table1

Monitoring Methods	Suitable for
Insulation Resistance (IR) & Polarization Index (PI)	Moisture & contamination
Insulation Capacitance	
Winding Ratio	Faulted turns
Winding Resistance	Conductor damage
Applied HV or Induced HV and PD	Poor dielectric
PD ( acoustic and electrical)	Detect and locate PD
Frequency Response Analysis (FRA) (Transfer function)	Winding displacement, possible loose winding, and core faults
Voltage Recovery	Moisture in paper And ageing of paper (Off-Line Test)
Vibration Analysis	Slack winding & Mechanical faults

Oil Tests	
Dissolved gas analysis (DGA)	Detecting incipient faults
Furan Analysis	Overheating and ageing of paper
Resistivity, Acidity	Ageing of oil
Dielectric loss angle (DLA) or Tan Delta	Moisture and contamination

One of the most famous methods for monitoring and diagnostics of the power transformers is discovery and analysis of the gases dissolved in the transformer oil. According to the experience, small amounts of oil are annually put to gas chromatography tests. Different gases, being generated in the oil, depend on the occurred fault type.

The presence of humidity in the transformers would trigger small electrical discharges, that generate mostly hydrogen (H<sub>2</sub>) and some methane (CH<sub>4</sub>).

The insulation defects of the magnetic circuit would generate circular currents and local over heating effect. As a result of this, in the oil appear most of all ethylene (C<sub>2</sub>H<sub>4</sub>) and methane (CH<sub>4</sub>). The amount of the hydrogen is also considerable. Hot areas of the winding terminals are causing also carbon oxide (CO), and then intermediate product gas (C<sub>2</sub>H<sub>4</sub>) and methane (CH<sub>4</sub>).

When during operation there are often moments of overload as well as cooling system outages, it is likely to have winding insulation overheating that cause thermal degradation of the isolating paper material. This type of fault is connected with emission of carbon oxide(CO). The process of degradation is unrecoverable. To evaluate the remaining operating hours of the transformer, having in mind the insulation damaged or old, there can be analyzed the carbon oxide (CO), carbon dioxide (CO<sub>2</sub>) as well as furan compounds in the oil. It is very hard to find all these, during the early stage of the monitoring. It is also seen, that in almost all cases CO and H<sub>2</sub> exist in considerable amounts. Thus, discovery of certain gas volumes means initial indication for a great number of problems. If higher concentration of these is observed, then it will be possible to use some of the methods described in Table 1. This is how the type and the validity of the fault are determined.

Based on these experiments, there exist already such electrochemical detection devices. Part of the oil [2] is flown through the detector and the unit gives signal when the level of the mentioned gases is high enough.

## Results

The monitoring of power transformers requires economic analysis, that would give answers about what will be the expenses and the benefits of its implementation.

The expenses are related directly with the purchase of equipment, installation and the corresponding tests and maintenance. The benefit of this monitoring implementation for a certain period (most often 1 year) could be evaluated by the risk:

$$(1) \quad R = P(x) \cdot C(x)$$

where P(x) is the probability the event x to happen; C(x) is the consequence of this event expressed in currency.

The effect after the implementation of such monitoring could be shown as follows:

$$E = R_M - R_0,$$

where R<sub>M</sub> is the risk to use monitoring and R<sub>0</sub> . the risk without monitoring.

It is possible to assume that the outages and the faults of the power transformers are independent events having discrete and permanent intensity. This happens fairly not so often and thus their distribution could be described easily by the Poisson expression [1]:

$$(2) \quad P(x) = \frac{\lambda^x}{x!} \cdot e^{-\lambda}$$

for a certain interval of time  $\lambda$  is the intensity of the failures.

It could be assumed that the power transformers could have  $\lambda \approx 0,015$  [1]; [3]

For a time period the expression (2) could be transformed as follows:

$$(3) \quad P(x, t) = \frac{\lambda \cdot t^x}{x!} \cdot e^{-\lambda t}$$

The period for testing is one year. Then the probability that for a year there will not be any defect could be:

$$P(x = 0) = 0,985.$$

The probability that for the same period there will be at least one fault is:

$$P_{(x \geq 1)} = 1 - P_{(x=0)}$$

In this case, the probability to appear only one fault is very important.

$$P(x = 1)$$

According to (2) this is  $P(x = 1) = 0,0148$

The occurrence of this fault could not be detected by the mentioned above relation???? regarding the dissolved in the oil gas volumes or by the chromatographic analysis. According to [2] the probability for this to happen is 70%

$$P_g = 0,7$$

On the other side, the effectiveness to discover such fault in these systems for on-line diagnostics is not 100%. The most pessimistic reading could be the value of 60%

$$P_d = 0,6.$$

In this case, the probability only one single fault to happen, for the period of one year and being not discovered with a system for on-line monitoring, will look like:

$$(4) P(x) = P(x=1) P_g P_d$$

$$P(x) = 0,7. P(x=1)$$

Apparently, when there's indication about fault for the same case should look as:

$$P(x) = 0,3. P(x=1)$$

When there's a system for on-line monitoring, the probability  $P_M(x)$  will be:

$$(5) P_M(x) = P(x=1) P_g P_d$$

where  $P_d = 0,4$  if the fault is not discovered and

$$P_d = 0,6 \text{ if the fault is discovered.}$$

When using formula equation (1), it is necessary to calculate the expenses  $C(x)$  when there is a fault, which will be different depending on the happening consequences. In general, the extent of the consequences – failures, could be split into **Major Failures** and **Catastrophic Failures**.



Fig.1.

Figure 1 shows the outlook of the main part of a transformer, which experienced catastrophic failures. In this case, it is necessary to replace the whole transformer, which results in huge expenses. Long term experience shows that 90% of the faults usually appear to be serious and 10% are considered catastrophic.

According to the international market prices, the expenses  $C_1$  to repair a serious major failure could come up to 15 000\$/ MVA [3]. When there's catastrophic failure leading to in replacement of the transformer, expenses are about  $C_2 = 50 000\$ /MVA$ .

The expenses for repairs when there's early fault discovery are considered quite small  $C_3 = 2000\$ /MVA$ .

The average outage period of the system (out of operation) is about 15 days. According to [3], the losses due to power replacement are  $C_4 = 50\$ /MWh$ . In such case, the cost of this risk for a transformer system without on-line monitoring system will be:

$$(6) R_{C1} = 0,9.C_1.P_{(x=1)}. P \text{ in case of serious faults}$$

$$(7) R_{C2} = 0,1.C_2.P_{(x=1)}. P_g \text{ in case of catastrophic fault}$$

In the first case  $R_{os} = 0,63.P_{(x=1)}$ .

$$R_{os} = 0,63.0,0148.C_1 = 0,00931 C_1$$

In the second case:  $R_{oc} = 0,00104.C_2$

The following expenses are separate  $R_{oe}$  because there's undistributed energy [3].

$$(8) R_{oe} = 24.S_H (0,00932 + 0,00104).T. C_4$$

where  $S_H$  is the nominal power of the transformer.  $T$  – number of the outage days The total cost of the risk without the system for on-line monitoring is:

$$(9) R_o = R_{oc} + R_{oc} + R_{oe}$$

When there is a system for on-line monitoring:

$$(10) R_{MS} = 0,9.C_1.P_{(x=1)}. P_g.P_d,$$

$$R_{MC} = 0,1 C_2.P_{(x=1)}.0,1P_g.P_d$$

or

$$(11) R_{MS} = 0,00372 C_1.$$

$$R_{MC} = 0,00042 C_2$$

The annual expenses for repairs, in case of early detection of incipient faults are:

$$(12) R_e = 0,4.C_3.P_{(x=1)} = 0,00592 C_3$$

The expenses, calculated by analogy with ( 8 ), if there is a system for on-line monitoring, will be:

$$R_{MS} = S_H (0,00372 + 0,00042).T.24. C_4$$

Finally, the total cost of the risk with a system for on-line monitoring is:

$$R_M = R_{MS} + R_{MC} + R_e$$

The annual benefit of the utilization of such system for on-line diagnostics is:

$$R_o - R_M = R$$

For example, if a transformer is taken having power rated of 100MVA, the profits will come up to 21 000\$. In



order to calculate the time for this return, it is necessary this benefit to be compared with the annual costs related to the price of the system and its corresponding maintenance.

Having in mind the calculations above, only the expenses about repairs and the lack of transformed energy are taken into account.

Besides the fact that these are the major part when calculating the expenses and the benefit, it is necessary to consider some other factors, such as:

- Reduction of maintenance cost
- Reduction of failure resolution cost
- Cost of loss generation (for GSU)
- Cost of power not delivered (for interconnection transformers) etc.

### Conclusion

On the ground of this research, it could be considered that utilization of systems for monitoring power transformer operation is necessary and should be by all means widened and encouraged. This will result in early detection of insipient faults as well as the ability to undertake the corresponding preventing steps to avoid the catastrophic consequences.

The devices for monitoring, if possible, should be simple, low cost and having good sensitivity.

As shown above, the implementation of such devices is justified both from the technical and economics point of view.

### References

- [1] Dimitrov,L.V.Berbatov,N.-“Evaluation on the effectiveness when introducing systems for on-line diagnostics of induction motors used in high reliability applications”- Proc.of Ninth International Conference of Electrical Machines drives and technologies ELMA 1999;p.110-116”.
- [2] Aubin. J., A.Bourgault,C.Rajotte;,P.Gervais, ”Profitability Assessment of Transformer On-Line Monitoring and Periodic Monitoring “EPRI Substation Equipment Diagnostic Conference X,San Antonio,Texas,February 2002.
- [3] Cigre Technical Brochure 248 “Guide on Economics of Transformer Management “, June 2004.



**Lyubomir Dimitrov** was born in Varna, Bulgaria, on Oktober 24,1944.He studied at the Technical University of Varna-Bulgaria and received Dr.degree from the Technical University of Sofia in 1978. Since 1971 he worked in the Faculty of Electrical Engineering of the Technical University of Varna as Ass.Professor in the design diagnostic and monitoring electrical mashines and electrical drives. Lyubomir Dimitrov is with the Faculty of of Electrical Engineering of the Technical University of Varna “Studentska Str.1”9010

(e-mail: lubo.dimitrov@mail.bg)

# Minimizing lighting flux of luminaries for street lighting systems designed by Small Target Visibility Criteria

Hristo Vasilev, Stanimir Stefanov and Krassimir Velinov

**Abstract:** In this report is presented the research for minimizing lighting flux of street luminaries. The purpose of this research is to define the minimal lighting flux of street luminaries necessary to reach lighting criteria. In this way, minimizing lighting flux, we have a possibility to decrease power consumption of lighting source, decrease the lighting pollution and increase energy efficiency of road lighting systems. The lighting criteria are according to the Small Target Visibility Criteria (STV) from ANSI/IESNA RP-800

**Keywords:** STV, street lighting, flux, minimizing, luminary

## Introduction

The increasing cost of energy is the main reason to look for the right solutions – how to reduce the energy consumption in the modern urban and production spheres. The street lightning is a necessary feature of the contemporary living and without this facility it would be difficult to travel and orientate ourselves in the cities, especially during the dark periods of the twenty – four – hours. But at the same time it is a significant consumer of electricity. One of the possible ways to reduce the energy consumption of street lighting system is to use sources of light which have a lower electricity power and appropriate distribution of lighting flux. These factors can assure the possibility for satisfactory levels of street lighting and at the same time they are energy effective. Although on the other hand, the lighting systems with lower power consumption are with lower lighting flux in comparison with these which have higher power consumption in case we compare lamps from the same type. If we aim to reduce the consumption of electricity, obviously we will have to find a way allowing us to find a distribution of the flux which provides the needed levels of lighting and using a minimum flux.

In this research we present our study on minimizing the flux and distributing the flux in the space in order to reach the standard levels, according to STV method and ANSI/IESNA RP-800 for the general type of streets [1].

## Explanation

STV method evaluates the visibility of a small object on the street lane from the position of the average moving observer, who is located 83 m away from the object observed, regarding the following factors:

- The luminance of the targets

- The luminance immediately background
- The adaptation level of the adjacent surroundings
- The disability glare.

The weighting average of the visibility level of these targets results in the STV. The veiling luminance ratio component is included in the STV calculation methodology.

To describe the photometric curves we have used the equation 1, based on polynomes of Legendre from 9<sup>th</sup> range[3].

$$(1) \quad I(\gamma, C) = \exp(d_0(\gamma_i) + d_1(\gamma_i)\widehat{C}_j + d_2(\gamma_i)\widehat{C}_j^2 + d_3(\gamma_i)\widehat{C}_j^3 + d_4(\gamma_i)\widehat{C}_j^4 + d_5(\gamma_i)\widehat{C}_j^5 + d_6(\gamma_i)\widehat{C}_j^6 + d_7(\gamma_i)\widehat{C}_j^7)$$

Where:

- $d_p(\gamma_i)$  ( $p=0,1,2,3,4,5,6,7$ ) are coefficients defined by orthogonal polynomes of Legendre as:

$$(2) \quad d_p(\gamma_i) = q_{p1}S_1(T_i) + q_{p2}S_2(T_i) + \dots + q_{pm}S_{m1}(T_i)$$

$S_k$  is polynome of Legendre from range  $k$ ,  $q_{pk}$  are unknown coefficients evaluated by the method of the smallest squares, and  $T_i$  is defined by:

$$(3) \quad T_i = \frac{2\gamma_i - \gamma_1 - \gamma_n}{\gamma_1 - \gamma_n}$$

$\gamma_1$  and  $\gamma_n$  are the first and last value of the angle  $\gamma$

$$(4) \quad \widehat{C}_j = \frac{C_j}{\max(C)} \text{ varies in the interval } [0,1]$$

-  $i$  is the index of the angle numbers  $\gamma$ , and  $j$  is the index for numbers of C-plains arranged regarding the tables of photometric curves.

According to [3] the present equation describes very precisely the photometric curves for street lighting systems and it is useful when we do mathematical optimization.

Minimizing the flux is done in MATLAB environment through the function and the created matlab files to calculate the street lighting in accordance with the methodology defined in ANSI/IESNA RP-800.

The main difficulty while minimizing the flux is to manage to achieve a distribution of flux which is possible to be implemented technically.

Therefore in case that the coefficient of enhancement for the intensity is lower than 7, the intensity for 1000 lm flux of the source for  $\gamma=0^\circ$ , should be 150 cd maximum and the biggest fluctuation between two adjoining intensities on  $\gamma$  for 1000 lm shouldn't exceed 200cd units.

The distribution of the flux and its minimal value in all the calculations made are significantly dependent on limited factors in the optimizing algorithm, as a result of this it's possible to achieve numerous combinations – satisfactory for the standard requirements with relatively similar values of flux.

The calculations show that we can not achieve the absolute minimum while minimizing, but after having made 10 000 – 14 000 calculation cycles for the function **fmincon** are achieved levels of flux which show minimizing below 1% for the following a few thousands of cycles.

What is more, in this case we have observed automatic interrupting of cycles because of the inability to satisfy two or more of the limited factors in the further minimization.

As a consequence of these results the number of cycles in the optimizing algorithm is limited up to the levels mentioned above depending on the variations of the flux.

The research concerns three of the most common types of streets according to [2] and described as the classes Local, Collector and Major according to[1].With dimensions and number of lanes as shown in the Table 1. and lighting standard defined in Table 2.

As per the standard each of the streets is divided into several sub – categories depending on the conflict-ability and the pedestrian areas. In the present research we present results concerning class “High” referring to pedestrian conflict areas. All the calculations are made about street pave class R3, one – sided lighting of streets with two lanes – classes Local and Collector and one-sided for unidirectional road - lane with three lines – class Major.

Classes roads

Road		
Road	Width one - way line, m	Number of one-way lines for
Major	3.5	2x2(3)
Collector	3.5	2x1
Local	3.5	2x1

Table 1

Table 2

Luminance and STV Criteria

Road and Pedestrian Conflict Area		STV Criteria	Luminance Criteria	
Road	Pedestrian Conflict Area	STV	$L_{avr}$ cd/m <sup>2</sup>	Uniformity Ratio $L_{max}/L_{min}$
Major	High	4.9	1.0	6.0
	Medium	4.0	0.8	6.0
	Low	3.2	0.6	6.0
Collector	High	3.8	0.6	6.0
	Medium	3.2	0.5	6.0
	Low	2.7	0.4	6.0
Local	High	2.7	0.5	10.0
	Medium	2.2	0.4	10.0
	Low	1.6	0.3	10.0

In the calculations above we have set up the following:

- the lighting sources are with spherical intensity of light, responding to the spherical intensities of sodium lamps high pressure from the range of power 50 -70- 100 – 150 W, type Long Life
- the luminaries are symmetrical towards the plain of length symmetry
- the maintenance factor is MF = 0.7
- the luminaries are located on even distance along the splitting line between the street and the pedestrian area, the are with height of hanging 6, 7 or 8m.
- the distances between poles are fixed between the most common ones - 30 and 35m, or in the other case we make variations around these distances for the above mentioned street classes.
- we have used 8 sources for forming lighting levels – 4 before the beginning of calculation field and 4 after the calculation field and all of them are one – pole distance away.
- while minimizing the flux the standard levels in Table 2. are taken under consideration

## Results

While carrying out our task to optimize the parameters we have achieved over 90 solutions, a significant part of them have been seen as inappropriate for technical implementation in spite of the fact they are satisfactory for limited factors.

On the figures from Fig.1. to Fig.6. are presented several of the most useful for the practice solutions. In these figures photometric curves are shown for relative flux 1000lm concerning the above mentioned powers of sodium lamps. Below each of the figures you can see:

- the class street,
- the minimizing values of flux luminaries -  $F_{lum}$ ,
- the illuminating flux falling over the street lane –  $F_{streets}$
- the illuminating flux of lighting source –  $F_{lamp}$ ,

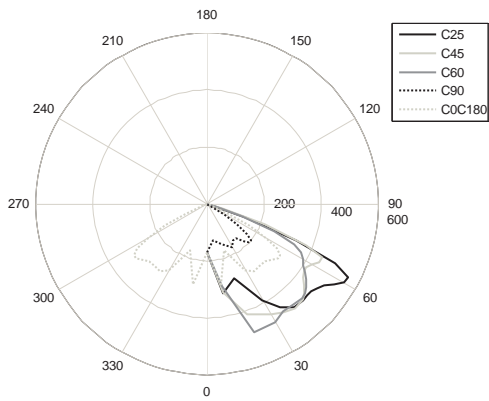


Fig.1. Photometric curves for class Major.  
 $H=8m, L=35m, F_{lamp}=17500lm, F_{lum}=1556lm, F_{street}= 8002lm,$   
 $\eta=0.89.$

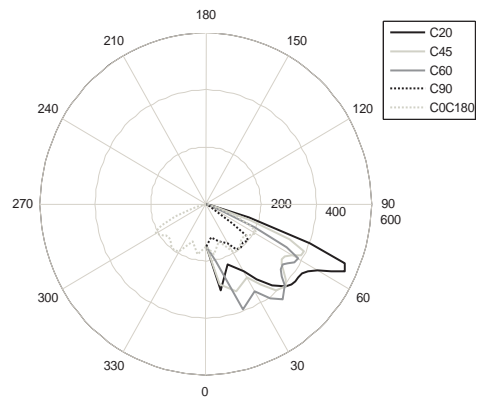


Fig.2. Photometric curves for class Major.  
 $H=7m, L=35m, F_{lamp}=17500lm, F_{lum}=12880lm, F_{street}= 7524lm,$   
 $\eta=0.74.$

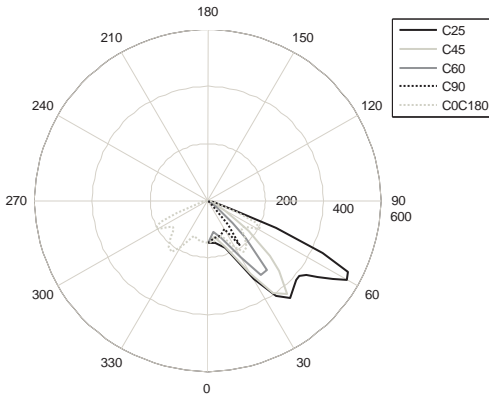


Fig.3. Photometric curves for class Collector .  
 $H=8m, L=35m, F_{lamp}=10700lm, F_{lum}=5155lm, F_{street}= 2856lm,$   
 $\eta=0.48.$

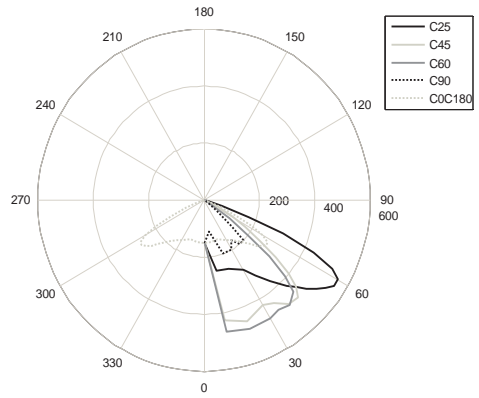


Fig.3. Photometric curves for class Collector .  
 $H=7m, L=30m, F_{lamp}=6600lm, F_{lum}=4508lm, F_{street}= 2480lm,$   
 $\eta=0.68.$

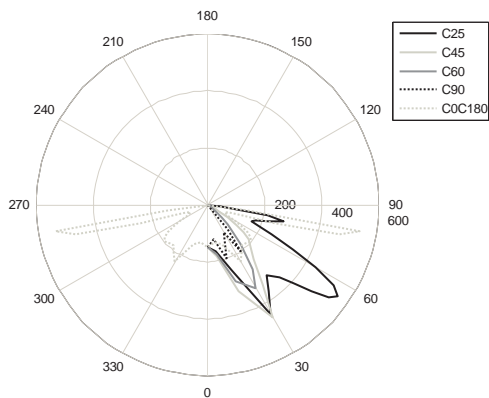


Fig.3. Photometric curves for class Local .  
 $H=7m, L=30m, F_{lamp}=4400lm, F_{lum}=2427lm, F_{street}= 1302lm,$   
 $\eta=0.55.$

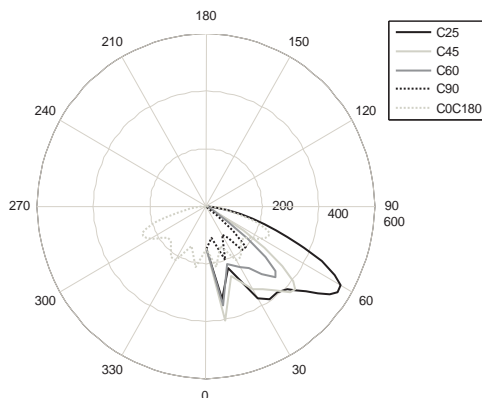


Fig.3. Photometric curves for class Local .  
 $H=7m, L=30m, F_{lamp}=4400lm, F_{lum}=2807lm, F_{street}= 1620lm,$   
 $\eta=0.64.$



- the height of hanging –  $H$ ,
- the distance between poles –  $L$ .
- the proportion  $\eta = \frac{F_{lum}}{F_{lamp}}$

In Table 3. is presented the calculated ratio

$$(5) \quad \kappa = \frac{F_{street}}{STV \cdot S_{cf}}$$

Where:

- $F_{street}$ , lm is the falling over the calculated field flux
- $S_{cf}$ , m<sup>2</sup> is the area of the calculated field

The relation above describes the characteristics of the flux which defines for the unity STV the parameter for 1 m<sup>2</sup> street area in the different street classes.

**Table 3**

*Lighting flux per meter square*

Road	mounting height /pole distance, m/m	STV Criteria	Luminance Criteria	
		STV	$F_{street}$ , lm	$\kappa$ , lm/m <sup>2</sup>
Major	8/35	4.9	8002	4.44
	7/35	4.9	7524	4.18
Collector	8/35	3.8	2856	3.07
	7/30	3.8	2480	3.10
Local	7/30	2.7	1302	2.30
	6/30	2.7	1620	2.86

As you can see in the figures and the presented standard requirements for the different classes of streets, for every single class of streets it is preferably to be used a luminary with a particular distribution of flux, appropriate for especially defined levels. For example the levels in Table.2 for “Local High” are accomplished with (DSLHP)(Discharge Sodium Lamp High Pressure) 50W and the levels “ Collector High” have special requirements for the source with intensity, which can ensure luminance similar to the one of the sodium lamp 70 W. As well as, because of the proximity of the standard levels of lighting of several of the sub – classes of the main types of streets, it is possible to be applied the same luminaries with the same intensity of the sources – for example “ Local High” and “ Collector Low”.

### Conclusion

In conclusion, when we analyze the results from our study, it is obvious that:

- The minimal fluxes which are necessary are 68 – 73% of the standard DSLHP 70 W for Collector streets and 74 – 88% of DSLHP 150 W for Major. Clearly, it is possible to create luminaries with the necessary distribution of lighting with efficiency 68 – 80% using this type of lamps.

- For Local streets we have concluded that the flux referring to the applied geometry is about 55 – 56% of this one which emits DSLHP 50 W. If the luminary has efficiency 70% and this kind of lamp, we have as a result a surplusage of flux about 600lm. The similar effect we observe while using 100W lamp for Collector streets.

- In all the variations of light distribution, the flux falling over the calculated field between poles, is within 56 - 60 % of the whole flux according to the photometric curves and there is a surplusage of 40 – 45% as well. These exceeding values, which we called “surplusages” could be limited in case we use the appropriate LED – source as sources of light or if the different fluxes can be distributed in an appropriate way of lighting pedestrian areas parallel to the streets. In case that in the pedestrian areas is used additional lighting we have surplusage of about 40-45%, which can be used for luminaries with repeated inner reflection which have lower power of light sources. In this way, by concentrating the out-going light flux only over the street lane, probably we can achieve satisfactory levels of lighting with reduced consumption of electricity.

- Maximum intensity  $I_{max}$  usually differs in the curves, it is not constant as location and varies in gama –  $\gamma=(55^{\circ}-62.6^{\circ})$  and  $C=(10^{\circ}-25^{\circ})$ , this fact in some cases would provoke difficulties in luminary production.

- As presented in Chart.5 it is obvious that the lighting flux over calculating field is minimal but the intensity for C plain  $0^{\circ}-180^{\circ}$  is close by value to  $I_{max}$  by gama above  $80^{\circ}$ . That distribution is difficult to be implemented technically which is a good example for the fact that in spite the minimal lighting flux we don’t have the possibility for practical application. We maybe have similar problem whit photometric curves present in Chart 4, because we have big increase of intensity from  $\gamma=0^{\circ}$  to  $\gamma=10^{\circ}$  for C plain from  $35^{\circ}$  to  $75^{\circ}$ .

- The results from the research and the data shown in Table 1.3 prove that there is not an equal dependence of the influence of the hanging height and pole – distance on the behavior of the minimum flux  $F_{street}$  needed to reach STV levels. But when we compare the hanging height and pole – distance about the technical implementation of luminaries with the above parameters we notice that it seems when the height is bigger we have more practical photometric curves. In this regard, to achieve the maximum effectiveness we have to find solutions consistent with both the minimum flux and the investments defined by hanging height and pole distance.

- A disadvantage in minimizing the flux is that the resulting photometric curves can satisfy the standard requirements only in case that the geometry of the lighting systems is the closest to the geometry by which the photometric curves are created.

The main problem with big differences of the geometry is that we register a significant inconformity of Uniformity Ratio -  $L_{max}/L_{min}$  regarding the standard values or recommended values.

## References

- [1] ANSI/IESNA RP-800 “Roadway lighting”, Reffirmed 2005.,pp.1-27.
- [2] МРРБ, Наредба №2 от 29 юни 2004 г. за планиране и проектиране на комуникационно-транспортните системи на урбанизираните територии, ДВ,бр.86 и бр.94,2004г.,
- [3] Велинов, К. Хр. Василев, Влияние на геометричните параметри и нормативните ограничения върху оптималното светлоразпределение на уличните осветители. Осветление’2007 - XIII Национална конференция Варна,2007 г., Сборник доклади.стр.94-104.

## Biographies



**Hristo Vasilev** was born in, village Debnevo, county Lovech , Bulgaria, on October 10, 1945. Graduated Higher Mechanical and Electrical Institute in Sofia in 1972.

Since 1973 he has worked in the Faculty of Electrical Engineering of the Technical University of Sofia. Hi is Professor by “Lighting technique and sours of light”

Hristo Vasilev is with the Faculty of Electrical Engineering, Technical University of Sofia, 8, Kl. Ohridski Blvd., 1000 Sofia, Bulgaria (e-mail: denimaltd@denima2001.com)



**Stanimir Stefanov** was born in Kazanlak, Bulgaria, on November 30, 1970. He graduated from the Technical University – Sofia ,branch Sliven as Magister by Electrical Engineering,.

He is today a PhD student in the Faculty of Electrical Engineering of the Technical University – Sofia. Since 2001 he has worked as assistant professor in branch Plovdiv of

Technical University – Sofia

Stanimir Stefanov is with the Faculty of Electrical and Automation Engineering, Technical University of Sofia, branch Plovdiv, 25, Tz.Dustabanov str., 4000 Plovdiv, Bulgaria(e-mail: denimaltd@denima2001.com)



**KrassimirVelinov** was born in, Sofia, Bulgaria, on April 24, 1952. Graduated Higher Mechanical and Electrical Institute in Sofia in 1977.

Since 2004 he has worked in the Faculty of Mining Electromechanics of the University of mining and geology "ST. IVAN RILSKI"

Hi is associate professor in Faculty of Mining Electromechanics. Field of interest includes lighting systems, electrical networks and renewable energy sources.

Krassimir Velinov is with the Faculty of Mining Electromechanics, University of Mining and Geology “St. Ivan Rilski” ”Studentski grad”, ul. “Stoyan Edrev”, Sofia – 1700, Bulgaria (e-mail: candela@mail.bg ; WEB <http://lighting-bg.eu> )

# Optimization of LED's Lighting Distribution in Road Lighting Luminaire

Valchan Gueorgiev, Hristo Vasilev

**Abstract:** An approach for optimal design of light distribution of LED road lighting luminaire with LEDs as a light source is introduced. The luminaire is comprised of a set of 24 light emitting diodes with power of 1 W each. The highest possible average illuminance is obtained with a given set of LEDs by varying the orientation of each elementary light source. The way of overcoming the large scale problem is detailed as well as some practical considerations for building such kind of luminaire.

**Keywords:** Large Scale optimization, LED, Road Lighting.

## Introduction

The optimal light distribution is one of the main problems that stand before the designers of street luminaires with LED. This type of luminaires became popular, because of recently introduced powerful white LED with good characteristics. At the same time the first samples of such LED luminaires showed poor light distribution. The reason for that is that they were designed according to the principles and experience in the design of road luminaires with conventional discharge lamps.

In some cases it is preferable the use of super powerful LED (50 W and more), but in this case problems with the cooling occur and it is hard to deal with the problem of their improper for road lighting applications light distribution.

Most of the producers, at the second generation of LED road luminaires, prefer to use number of less powerful (1 – 3 W) LED. The efforts are concentrated on the change of the light distribution curve of every LED in a way that it nears the most the optimal light distribution curve of the conventional luminaires with high pressure sodium lamps or the metal – halide lamps. The most popular method used for achieving that is addition of the same reflector to every LED. This method, although common to the principles used up to now limits the flexibility, which can be achieved by using many different light sources.

## Luminaire with individually oriented LEDs

LEDs are referred to as light sources with concentrated light distribution. In fact a lot of the

powerful LEDs are produced with light distribution near to the cosine. On Fig. 1 are shown the light distribution curves of two - 1W LED of leading companies (Luxeon K2 and Cree Xlamp XR-E).

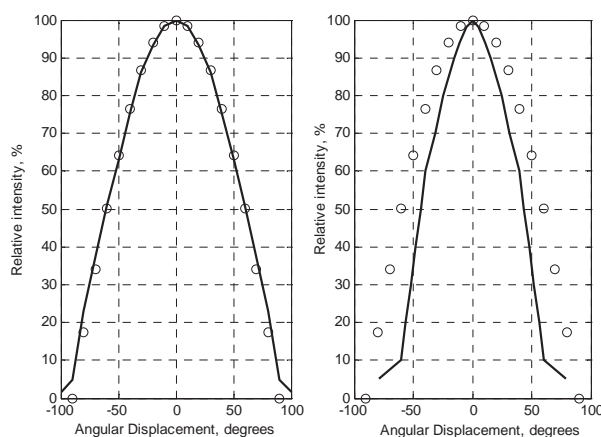


Fig. 1 Example of light distribution curves (relative intensity in % vs. angular displacement) for two different 1W LEDs. The theoretical cosine distribution is given with circle marks.

The typical for the LEDs concentration of the luminous flux in comparatively small solid angle can be an advantage in the construction of road luminaires if every LED is individually directed to a sudden angle in relation to the normal of the luminaire. Using this principle the light distribution curve of the whole luminaire can be flexibly modulated.

The attempts for nearing the light distribution curve of the LEDs luminaire to that of accepted for optimal conventional luminaire with discharge lamp are not necessary. Instead the problem of optimization using integral criterion, such as the average illumination of the roadway may be introduced.

In the current paper the problem for finding the optimal average illumination of the roadway with respect to the general uniformity that is set, by varying the individual direction of every LED in the luminaire.

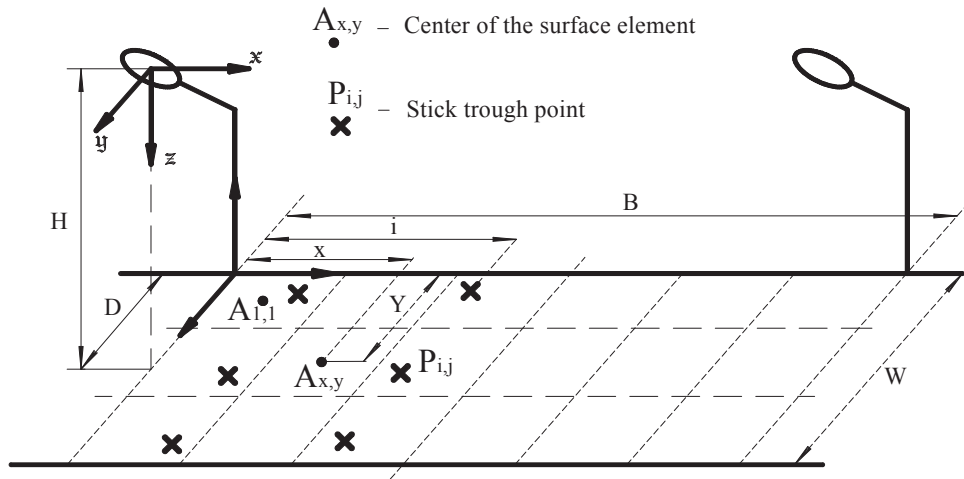


Fig. 2 Street geometry.

For the decision of this problem, it is accepted, that the luminaire consists of 24 LEDs Luxeon K2 with individual luminous flux of 46 lm each. It is also accepted, that the luminaire is symmetrical regarding its longitudinal axis, which means that as parameters of the optimization remain only the directions of 12 LEDs from half of the luminaire. The geometry of the roadway that is considered is shown on Fig. 2. The width of the street, the distance between fixtures and the height of the luminaire are accepted to be constant and their values are:

- B= 20 m,
- H=6 m,
- W=5 m.

Fixing these parameters is not too restrictive for the applicability of this decision, because the values accepted are very common, wide used and described in the literature.

Placing the luminaire 6m above the surface of the roadway allows that it can be regarded to as spot light source. That makes the calculation of the illumination easier and also lets the optimization problem be decided without respect to the geometry of the luminaire.

### Direction of the LEDs

It is accepted, that every LED has a degree of freedom that lets it be directed arbitrarily in the lower semi sphere. With respect to the fact that the luminaire is considered a spot light source, the direction of every LED can be described by two angles -  $\gamma$  and  $\delta$ . A draft of the geometrical considerations, defining the direction of a LED is shown on Fig.3. The frame of reference, shown on the figure is placed in the centre of the luminaire, and the axis z is directed towards the roadway.

### Average illumination and general uniformity of the roadway

The classical approach for defining the average illumination on the roadway is used. The surface of the

road is separated to surface elements. By means of the Lambert's law the illumination  $E_{x,y}$  in the center of each element is calculated

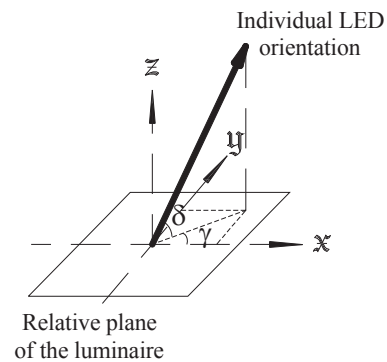


Fig. 3 Determination of LED direction.

The average illumination is calculated with the expression:

$$(1) \quad E_{av} = \frac{1}{N} \sum_{x=1}^X \sum_{y=1}^Y E_{x,y} \quad N = X + Y$$

Here X and Y are the numbers of units respectively in the direction of  $\mathbf{x}$  and  $\mathbf{y}$  axis.

The general uniformity is defined by the expression:

$$(2) \quad g_0 = \frac{E_{min}}{E_{av}}$$

Where  $E_{min}$  is the illumination of the darkest surface element.

Other qualitative indices of the lighting system, like glare, surrounding illumination are not considered, because such luminaries so far are used mainly for lighting lanes, parks and not busy streets.



### Optimization problem

The goal is achieving the highest possible average illumination on the roadway, with restriction of the general uniformity below and variation of the directions of the separate LEDs. This way the average illumination becomes objective function in the optimization problem for finding a maximum, the angles  $\gamma_i$  и  $\delta_i$  that set the orientation of every LED are parameters of the optimization and the average illumination is regional limitation.

The expression 3 is mathematical interpretation of the problem.

$$(3) \quad \begin{cases} \max \{E_{av}(\gamma_1 \dots \gamma_n, \delta_1 \dots \delta_n)\} \\ g_0 \geq G \end{cases},$$

Where  $n = 12$  is the number of the LEDs in the luminaire and  $G = 0,6$  is the minimal possible value of the general unevenness.

The average illumination is found as point decision in the space of the optimization parameters and practically cannot define the functional dependence, that gives connection between  $E_{av}$  and the direction angles  $\gamma_1 \dots \gamma_n, \delta_1 \dots \delta_n$ . That makes impossible the use of highly effective methods of protuberant programming. It is even hard to be defined a starting point, which meets the restrictive conditions.

Deciding the problem by means of the scanning method is also impossible. If it is accepted that every of the angles  $\gamma_1 \dots \gamma_n, \delta_1 \dots \delta_n$  changes between 0 and 70 degrees through 5 degrees, there will be  $75^{24}$  iterations, which is a number with forty five zeroes.

For the purpose of limiting the size of the problem and the time for the decision of iteration, the fact that the condition of maximum of the average illumination practically means concentrating of the possibly biggest part of the luminous flux on the roadway, is used. In that case, the roadway can be broken to a network of stick trough points, as the axis of every LED can be directed to each of these points, but not in any other direction. The network of stick trough points covers the roadway from the projection of the luminaire to the middle of the distance between the fixtures, because of the symmetry of the luminaire and the operation of the adjacent one. The network of stick trough points is shown with crosses on Fig.2., where it doesn't match with the centers of the surface elements, where the illumination is calculated.

First only one LED is considered and it is directed to every of the stick trough points. Simultaneously the illumination, that is been created in every of the surface elements is calculated and the results are kept in an array with dimensions  $X*Y$ . For all the stick trough points  $I*J$  such arrays will be obtained, where  $I$  and  $J$  are the numbers of the stick trough points in the direction of  $x$  and  $y$  axis.

After that using the principle of the superposition, the average illumination of sudden composition of stick trough points of the LEDs is obtained by the means of gathering of 12 arrays and taking the average value. For calculating the general unevenness it is necessary to define the element with minimal value in the sum of the arrays. These procedures cut the time needed on iteration, but nevertheless the problem remains with great size.

If it is accepted that  $I = 13, J = 7$ , or there are 45 stick trough points altogether, the full scanning will make  $91^{12}$  iterations. A draft of the roadway, the projections of two adjacent luminaries and the stick trough points in this case is shown on Fig.4.

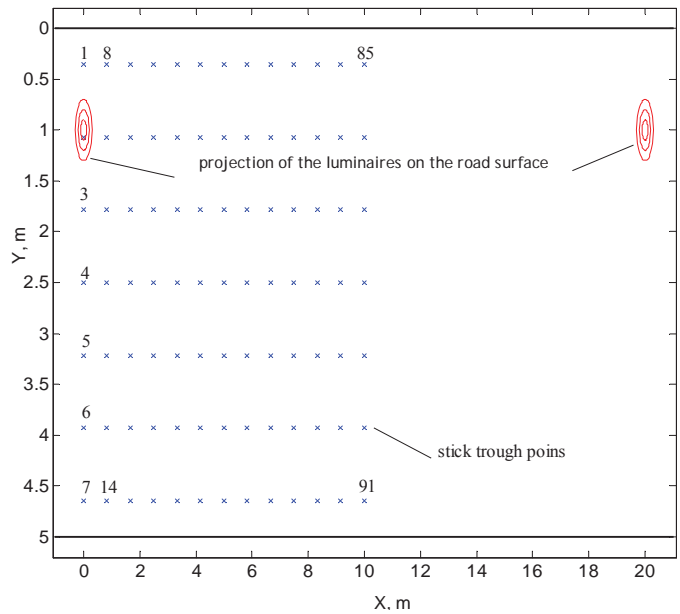


Fig. 4 Road surface with stick trough points in which the LEDs are directed.

In the calculations the influence of the adjacent luminaire is taken in consideration, as well as the illumination produced by the symmetrical part of the luminaire, which is not included in the optimization problem.

The problem of finding the starting point that complies with the limitations remains. The chosen value of  $G = 0.6$  is relatively hard condition and on the base of the engineering experience it is hard to find decisions complying with it.

That is why as a first step in finding a solution of the problem stays the problem of finding such an allocation of the individual directions of the LEDs that provides for maximal uniformity. For this purpose, a method that can be described as heuristic algorithm is used. It is described in the following points:

1. An unspecified initial distribution of the directions of the LEDs is chosen, in other words an unspecified multitude  $M$  of  $n = 12$  stick trough points is defined.
2. Knowing the illumination, created on every surface element from the LED directed to the

stick trough point, and with the use of principal of the superposition the illumination of each surface element, caused by the joint action of all n LEDs is defined.

3. The surface elements with maximal and minimal illumination are defined.
4. It is defined which of the LEDs from the M multitude creates the greatest illumination in the surface element with maximal illumination.
5. This LED (this stick trough point), is taken out of the multitude M and is replaced with another stick trough point, that creates maximal illumination on the surface element with minimal illumination. The multitude M now is filled with a new composition of points.
6. The procedure is repeated from point 2. The condition for a successful cycle is continuous taking out and putting into M of same elements, without improvement of the uniformity.

The experience shows that the method is very agreeable and leads to a decision after 5 – 10 iterations.

The decision found, which has maximal uniformity is used as a starting point for a procedure of optimization of the illumination. The standard method of seeking is used for that goal, but with less number of parameters. The directions of most LEDs are fixed to stick trough points defined by the heuristic algorithm and the rest of the LEDs are directed. The problem is decided with variation of the parameters of 4 LEDs. The analysis of the results shows that it is not necessary to change the parameters of more LEDs than that. This is obvious from the boundary values of the general uniformity, found at maximal general illumination (table 1).

The direct use of LEDs with cosine light distribution means that the idea of individual direction of the separate light sources in the luminaire cannot be completely used, because the wide light distribution curve will lead to great diffraction of the luminous flux out of the surface of the road. With using proper lens, the luminous flux may be concentrated in a narrower solid angle, which helps achieving more concentrated light distribution curve of the separate LED. For modeling such a concentration the following expression is used:

$$(4) \quad I = I_m \cdot \cos^n(\gamma),$$

Where:

- I is the luminous intensity on  $\gamma$  angle (the light distribution is considered absolutely symmetrical in relation to the axis of the LED),
- $I_m$  is the maximal luminous intensity, ( $\gamma = 0$ ), calculated by the condition for keeping a constant value of the full luminous flux (in this case 46 lm),
- n is exponent.

The highest the value of n, the more concentrated the light distribution curve is. This is shown on Fig.5.

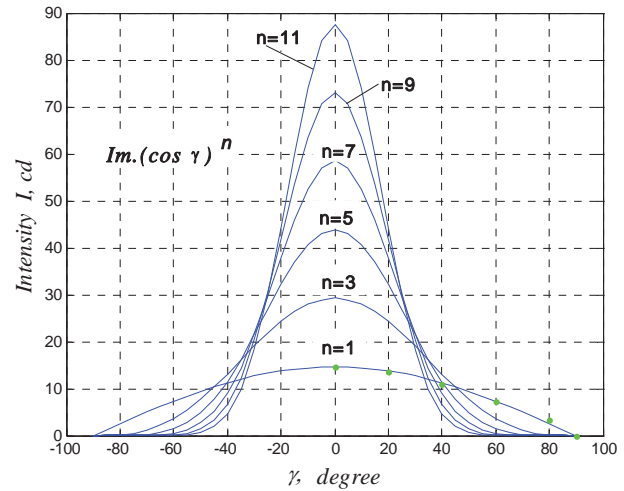


Fig. 5 Light distribution curves with different values of the exponent n.

**Table 1**  
Maximal general illumination at different degree of concentration of the light distribution curve of a single LED

		Eav	$g_0$	$k_1$	$k_2$	$k_1$	$k_2$
$\cos^1\gamma$	max illumination	No decision c $g_0 > 0,6$					
$\cos^{1.5}\gamma$	max illumination	<b>2,98</b>	<b>0.60</b>	<b>53</b>	<b>82</b>	<b>88</b>	<b>88</b>
	max uniformity	2,9	0.63	85	85	88	88
$\cos^2\gamma$	max illumination	<b>3,22</b>	<b>0.60</b>	<b>19</b>	<b>75</b>	<b>88</b>	<b>88</b>
	max uniformity	3,02	0.66	85	85	88	88
$\cos^3\gamma$	max illumination	<b>3,68</b>	<b>0.60</b>	<b>11</b>	<b>32</b>	<b>88</b>	<b>88</b>
	max uniformity	3,38	0.71	56	84	88	88
$\cos^4\gamma$	max illumination	<b>4,06</b>	<b>0.60</b>	<b>4</b>	<b>4</b>	<b>88</b>	<b>88</b>
	max uniformity	3,76	0.71	13	77	88	88
$\cos^5\gamma$	max illumination	<b>4,44</b>	<b>0.60</b>	<b>5</b>	<b>5</b>	<b>20</b>	<b>90</b>
	max uniformity	4.13	0.63	1	1	14	91
$\cos^6\gamma$	max illumination	<b>4,95</b>	<b>0.60</b>	<b>4</b>	<b>4</b>	<b>18</b>	<b>68</b>
	max uniformity	4.33	0.70	1	1	14	91
$\cos^7\gamma$	max illumination	<b>5,36</b>	<b>0.60</b>	<b>4</b>	<b>4</b>	<b>18</b>	<b>54</b>
	max uniformity	4.53	0.72	1	1	7	77
$\cos^8\gamma$	max illumination	<b>5,70</b>	<b>0.60</b>	<b>4</b>	<b>4</b>	<b>18</b>	<b>46</b>
	max uniformity	4.84	0.76	1	5	14	91
$\cos^9\gamma$	max illumination	<b>6,00</b>	<b>0.60</b>	<b>4</b>	<b>4</b>	<b>4</b>	<b>46</b>
	max uniformity	5.08	0.78	1	5	14	77
$\cos^{10}\gamma$	max illumination	<b>6,26</b>	<b>0.60</b>	<b>4</b>	<b>4</b>	<b>4</b>	<b>39</b>
	max uniformity	5.37	0.78	1	5	20	63
$\cos^{11}\gamma$	Only decision	5,66	0.60	11	19	88	88

The decisions obtained for the maximal average illumination at different degree of concentration of the light distribution curve, are shown in table 1. From all the 12 LEDs, 8 are directed according to the basic decision (stick trough point 88) and 4 are varied at full

combination of the possible stick trough points. For comparison at the same table is shown the point with maximal uniformity. With  $k_1, k_2, k_3,$  and  $k_4$  are marked the numbers of the stick trough points, according to Fig.4, to which the separate LEDs are directed to get an optimal decision.

The distribution of the illumination on the surface of the road, at the biggest received average illumination, namely 6,26 lx, is shown on Fig. 5.

At exponent out of the limits of  $n \in (1.5 - 11)$ , the problem has no decision, because of the limitation of the general uniformity.

The following conclusions can be made:

1. With increasing of the concentration of the light distribution curve of separate LED, the average illumination raises. This is due to the less light losses, result of its diffusion out of the roadway.
2. If the concentration of the light distribution curve of the separate LEDs is too big, the condition for uniformity cannot be fulfilled. It is probable whenever using more elementary light sources, to be possible to fulfill the above mentioned condition if the elementary luminous fluxes are more concentrated.
3. Optimal values are received when the LEDs are directed to the axis of the roadway.
4. For a particular light distribution curve of the separate LEDs, the values of  $E_{av}$  in the point with minimal average illumination and the point with maximal general uniformity do not differ a lot (max 30% at  $\gamma = 9$  and 11, where the concentration of the light distribution curve of the separate LED is maximal).

The theoretical maximal average illumination can be received from the expression:

$$(5) \quad E_{av} = \frac{\Phi}{S}$$

where  $\Phi$  is the general luminous flux,  $S$  is the area of the roadway. In the current case we have 24 LEDs with 46lm each and size of the roadway 5x20m.

Therefore:

$$(6) \quad E_{av} = \frac{24 \times 46}{20 \times 5} = 11.04 \text{ lx}$$

Even in the best case around 50% of the luminous flux is lost.

### Considerations about the practical realization of the idea.

It is a fact, that the experience in directing of separate LEDs in different directions is already used by some constructors for making street luminaires. The means for achieving that are mainly through mechanical positioning of part of the LEDs to sudden angle in regard to the normal of the luminaire.

The draft of the idea that stays at the base of the optimization problem decided is shown on fig. 6. All the

LEDs (3) lay at the same plane and are equipped with lens (2), that concentrate their luminous flux. At the ideal case it can be assumed, that after the lens, the whole luminous flux of the LEDs is concentrated in a cylindrical shaft of light. There are Frennel lens (1), built in the refractor that refract the falling light shaft and direct it in the desired direction (5).

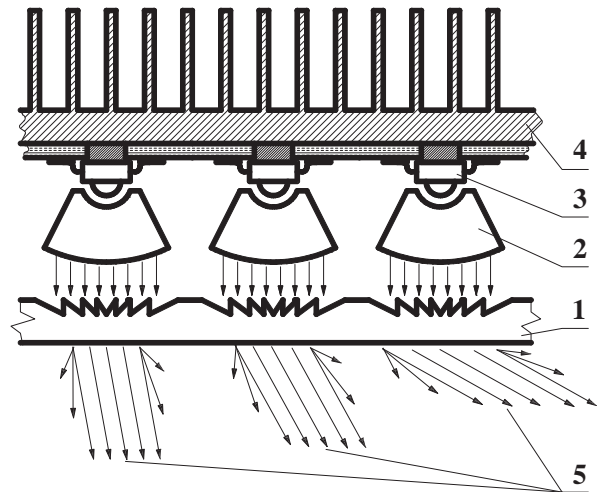


Fig. 6. Practical realization of LED luminaire with individually directed LEDs. Symbols on the figure 1 – refractors with built in frennel lens for distraction of the luminous flux, 2 – protuberant lens for lamination of the flux, 3 – LED, 4 – radiator, 5 – out coming luminous flux from the luminaire, oriented in different individual directions

No matter if a special body is used – cooler or standard radiator (4), the mounting and cooling of the LEDs is easier, because of their plane position.

The angle of direction of the out coming from the luminaire light depends only on the construction of the frennel lens. That provides the luminaire with additional flexibility, because only by changing the refractor, a different integral light distribution curve can be achieved.

### Conclusion

The possibilities of increasing the efficiency of streetlighting luminaires with LEDs have been studied. The efficiency is improved by concentrating the maximal portion of light flux on the road surface and minimizing parasitic surrounding illuminance. The minimal required uniformity is taken into account. This is achieved by determined the individual orientation of each LED in the luminaire.

### References

- [1] Василев Хр., В. Георгиев, Нажежаеми лампи, компактни луминисцентни лампи или светодиодни лампи ??, Енергиен форум2007, Варна, България том 2, 2007, стр. 208-214.
- [2] „LED luminaires fall short in initial round of testing by DOE” LEDs magazine, issue11, Feb. 2007

[3] Simpson Robert S,” Lighting Control-Technology and Application”, Focal Press, Oxford, 2003, ISBN0240515668

[4] CIE technical report “Measurement of LEDs”, , CIE 127-1997, ISBN 3900734844

[5] On the verge: LEDs are ready to challenge incumbent light sources in the streetlighting market, LEDs magazine, October, Feb. 2007



**Valchan Georgiev** was born in Pazardzik, Bulgaria, on March 2, 1974. He studied at the Technical University of Sofia-Bulgaria and received PHD degree from the same university in 2004.

He has been working in the Faculty of Electrical Engineering of the Technical University of Sofia as an assistant professor since 1998. His field of interest includes electrical apparatus and electrical networks.

Vulchan Georgiev is with the Faculty of Electrical Engineering, Technical University of Sofia, 8, Kl. Ohridski Blvd., 1000 Sofia, Bulgaria (e-mail: [vulchy@tu-sofia.bg](mailto:vulchy@tu-sofia.bg)).



**Hristo Vasilev** was born in Lovech, Bulgaria. He graduated from the Technical University - Sofia.

His field of interest includes electrical lighting systems, electrical networks and renewable energy sources. Currently he is a professor in the Faculty of Electrical Engineering of the Technical University – Sofia.

Hristo Vasilev is with the Faculty of Electrical Engineering, Technical University of Sofia, 8, Kl. Ohridski Blvd., 1000 Sofia, Bulgaria (e-mail: [denimaltd@denima2001.com](mailto:denimaltd@denima2001.com), [www.denima2001.com](http://www.denima2001.com))



# Improving the Efficiency of Lighting in Public Alleys by Accounting for Diffuse-Reflected Luminous Flux

Angel Pachamanov, Konstantin Hristov, Vessela Daskalova

**Abstract:** The main purpose of the lighting in public alleys and local roads of categories P1, P2, P3 is to provide a specified level of vertical illuminance on the faces of pedestrians. When designing luminaries for these types of streets, most attention is paid to the direct flux that provides the specified level of illuminance. By accounting for the proportion of reflected flux from the roadway and pedestrian sidewalks, the design of such luminaries can be improved to decrease the direct component of the flux to faces, which leads to a reduction in the energy costs for lighting.

**Keywords:** street lighting, local roads, public alleys

## Introduction

To help reduce crime in low-traffic areas, lighting installations must provide vertical illuminance on the faces of pedestrians of 3, 1 or 0,6 lx depending on the category of public alleys and local roads they service (P1, P2 or P3, see Table 1). Typically, the design of luminaries for public alleys ensures that the latter requirement is satisfied by the component of the flux from the luminary that is directed at faces (Fig. 1). In reality, the faces of pedestrians in public alleys are illuminated also by the reflected component of the flux from the roadway and the sidewalks. Taking these components into account when designing luminaries for public alleys will reduce the necessary amount of direct flux towards the sidewalk, and will consequently decrease the required power capacity of the lighting installation.



Fig.1. Public alley with luminaries creating vertical illuminance on faces of pedestrians [1]

Table 1

Values of light technical parameters (LTPs) for local roads [1,2]

Lighting category	Minimum average illuminance, $E_{AV}$ [lx] initial/maint	Minimum initial illuminance, $E_{MIN}$ [lx]	Maximum illuminance uniformity, $E_{MIN} / E_{AV}$	Minimum initial vertical illuminance, $E_V$ [lx]
P1	10/7	3	10	3
P2	5/3,5	1	10	1
P3	3/2	0,6	10	0,6

This report suggests a methodology for taking into consideration the reflected component of the flux that contributes to the vertical and semi-cylindrical illuminance on the faces of pedestrians given the luminance or the flux distribution of the sidewalk and the road [2]. The research can be useful for constructing more effective optical systems for luminaries for public alleys and local roads, which are the dominant type of luminaries in towns and villages [3,4].

## Determining the component of the flux reflected from the sidewalk and the roadway

As a first approximation in the computation of the reflected flux from the sidewalks and the roadway, only the part of the diffuse-reflected flux is determined in order to calculate the vertical illuminance on the face of a pedestrian walking on the right-hand-side sidewalk.

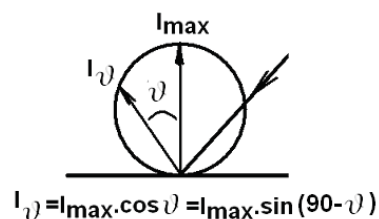


Fig.2 Lambert's Law for diffusion-reflected horizontal surface

Lambert's Law states that when a surface is diffusion-reflecting, the vector-points of the luminous intensities of the reflected light form the surface of a sphere (Fig. 2), irrespectively of the direction of the rays falling on the surface. From the definition for luminous intensity  $I = d\Phi / d\Omega$  (quantity of luminous flux  $d\Phi$ , irradiated in elementary space angle  $d\Omega$ ) and Lambert's Law  $I_{\nu} = I_{\max} \cdot \cos \nu$ , it can be deduced that  $I_{\max} = \Phi_{A-refl} / \pi$ , where

$\Phi_{refl}$  is the flux reflected by a unit surface  $A$  of a sufficiently small size.

The reflected flux can be determined if the luminance of every unit area as well as the integral diffusion road surface coefficient  $\rho_{road}$  and sidewalk coefficient  $\rho_{sw}$  for the used light source are known:

$$(1) \quad \Phi_{A\_refl\_road} = \rho_{road} \cdot \Phi_A = \rho_{road} \cdot E_A \cdot A,$$

$$(2) \quad \Phi_{A\_refl\_sw} = \rho_{sw} \cdot \Phi_A = \rho_{sw} \cdot E_A \cdot A.$$

The derivation of the relationships for calculating the vertical illuminance can be understood by studying Fig. 3. There are  $NM$  unit areas under consideration, each of which has length  $S$  (spacing). The sidewalk and the roadway are divided laterally into  $NX$  sections, each of which is in turn divided into  $NY$  parts between two sequential luminaries. Hence, every unit area has three indices  $A[m,j,i]$ , where  $m=1 \dots NM$ ,  $j=1 \dots NY$ ,  $i=1 \dots NX$ .

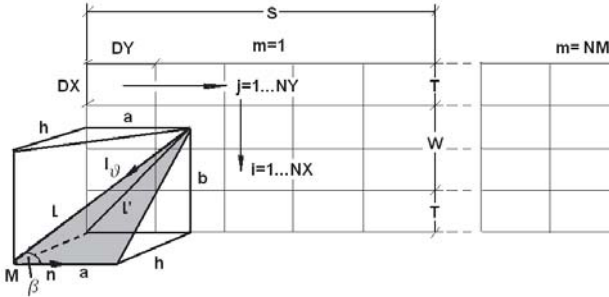


Fig. 3. Problem set-up

The contribution of unit area  $A[m,j,i]$  (in the case from Fig. 3,  $A[1,2,2]$ ) in forming the vertical illuminance at point  $M$  is calculated from the formula:

$$(3) \quad E_{vert}[m, j, i] = \frac{I_{\theta}[m, j, i] \cdot \cos \beta[m, j, i]}{l^2[m, j, i]},$$

where  $I_{\theta}[m,j,i]$  is the luminance intensity,  $l[m,j,i]$  is the distance from unit area  $A[m,j,i]$  to point  $M$ , and  $\beta[m,j,i]$  is the angle between the falling ray and the normal to the plane in which point  $M$  lies (Photometric Distance Law).

It is evident from Fig. 3 that  $l^2 = a^2 + b^2 + h^2$ , where for every  $m, j$  and  $i$

$$(4) \quad l[m, j, i] = \sqrt{a^2[m, j] + b^2[i] + h^2},$$

respectively

$$(5) \quad a[m, j] = m \cdot S + DY(j - 0,5) \quad \text{and}$$

$$(6) \quad b[i] = W + 2 \cdot T - DX(i - 0,5),$$

In formulas (4)-(6),  $h$  is the height of point  $M$  relative to the level of the roadway,  $W$  is the width of the roadway,  $S$  is the spacing,  $DY = S/NY$ , and  $DX = (W + 2 \cdot T)/NX$ .

The luminous intensity is calculated from Lambert's Law:

$$(7) \quad I_{\theta}[m, j, i] = I_{max} \cdot [m, j, i] \cdot \cos \theta,$$

where:

$$(8) \quad I_{max}[m, j, i] = \frac{\Phi_{A\_refl}}{\pi} = \rho \frac{E[m, j, i] \cdot DX \cdot DY}{\pi}$$

and

$$(9) \quad \cos \theta = \sin(90 - \theta) = \frac{h}{l[m, j, i]}.$$

The remaining term in formula (3),  $\cos \beta[m,j,i]$ , is calculated using  $a[m,j]$  and  $l[m,j,i]$  from formulas (5) and (4) provided earlier:

$$(10) \quad \cos \beta[m, j, i] = \frac{a[m, j]}{l[m, j, i]}.$$

The total vertical illuminance on the face at point  $M$  at a height  $h$  from the level of the roadway is calculated by summing up the contribution of every unit area. Hence,

$$(11) \quad E_{vert} = \sum_{m=1}^{NM} \sum_{j=1}^{NY} \sum_{i=1}^{NX} E_{vert}[m, j, i].$$

The connection between vertical and semi-cylindrical illuminance is the constant  $2/\pi$ , so

$$(12) \quad E_{SC} = \frac{2}{\pi} E_{vert}.$$

The methodology presented in this section is implemented in a software program in a high-level algorithmic language. The program enables multiple runs of the calculations for different input conditions.

### Calculations

Two cases of illuminating a roadway of 6 m width and two sidewalks of 3 m width are presented in order to illustrate the methodology and the software.

In the first case, a classical installation with left single-row allocation of luminaries is considered. The light distribution of the luminaries is obtained by solving an optimization problem [3,4]. The following input data are selected according to the format of the program for light calculations [5]:

Single digit indicating the mode of operation	2
Any 72 character name desired by the user	up to 72
Symmetrical/Asymmetrical light distribution	1/0 1
Calculation of illuminance?	1/0 1
Luminaire light distribution (file):	DL92
Road surface reflection (file):	rr03
Identification number of luminaire:	92

Luminous flux of lamp: 2,00 klm  
 Flashed area of the luminaire: 0,1 m<sup>2</sup>  
 Upcast angle of the luminaire, as installed: 0  
 Reflection properties of the road surface (R-table) 3  
 Average luminance coefficient of the R-table: 0,07 cd/m<sup>2</sup>/lx  
 Arrangement of the luminaries  
 (1- Single-side (left), 4- Opposite) 1  
 Mounting height of the luminaries (H): 7,5 m  
 Luminaire spacing (S): 40 m  
 Width of the carriageway (WK): 6 m  
 Width of the median (WM): 0 m  
 Overhang – left luminaries (OH1): 1.75 m  
 Overhang – right luminaries (OH2): 0 m

2.50 \* 1.2 2.3 2.1 2.1 1.8 1.5 1.8 2.1 2.1 2.3  
 \*\*\*\*\*

Given the light distribution on the roadway and the sidewalks (Table 2), the vertical and the semi-cylindrical illuminance on the face of a pedestrian is calculated with the above-mentioned algorithm. The software product developed for this purpose is used to perform the calculations for two types of road surfaces: R3 (C2) with  $\rho_{road}=0,1$  and R1 (C1) with  $\rho_{road}=0,2$ . In both cases the reflection coefficient of the sidewalks is  $\rho_{sw}=0,3$ .

The input data for the calculation are:

2 10 12 12 40 2  
 2.8 4.2 5.2 5.5 9.1 10.5 9.2 6.9 4.9 3.8 2.6 1.2  
 2.1 2.3 5.4 6.1 6.1 9.2 7.1 5.5 3.7 3.3 2.8 2.3  
 2.0 2.7 3.6 4.4 6.2 6.2 5.9 4.7 3.5 3.1 2.5 2.1  
 1.5 2.1 2.4 2.7 3.5 3.6 3.6 3.4 3.0 2.6 2.3 2.1  
 0.8 0.8 0.9 1.1 2.1 2.2 2.2 2.1 2.0 1.9 1.8 1.8  
 0.4 0.5 0.3 0.8 1.8 2.1 1.8 1.7 1.7 1.6 1.5 1.5  
 0.8 0.8 0.9 1.1 2.1 2.2 2.2 2.1 2.0 1.9 1.8 1.8  
 1.5 2.1 2.4 2.7 3.5 3.6 3.6 3.4 3.0 2.6 2.3 2.1  
 2.0 2.7 3.6 4.4 6.2 6.2 5.9 4.7 3.5 3.1 2.5 2.1  
 2.1 2.3 5.4 6.1 6.1 9.2 7.1 5.5 3.7 3.3 2.8 2.3

The selected data are input into the software program for light calculation in a text file in the following form:

2  
 Public alley 0.25\*1.3=0,33/0.4/0.3/20  
 1 1 dl92r03  
 92 02.00 0.10 00.00 3.00 0.070  
 1. 07.50 40.00 06.00 0.00 1.75 0.00

**Explanation:** E<sub>HOR</sub>(M,J,I), lx при 2 10 12 12 40 2, where  
 NM=2 NY=10 NX=12 W+2T=12m S=40m ”2”E<sub>xop</sub>-data  
 LTP: L<sub>AV</sub>=0,33; U<sub>L</sub>=0.4; U<sub>O</sub>=0.3; TI=20  
 Fi<sub>sum</sub>=2000 lm for 12\*40=480 m<sup>2</sup>  
 (4,17 lm/m<sup>2</sup> for Lav=0.38 cd/m<sup>2</sup>)=10,97 (lm/m<sup>2</sup>)/(cd/m<sup>2</sup>)

Results from the calculations are shown in table 2.

**Table 2**

Results from the calculation of a public alley lighting installation with LTP: L<sub>AV</sub>=0,33; U<sub>L</sub>=0.4; U<sub>O</sub>=0.3; TI=20

Luminance distribution in one luminaire spacing (cd/m<sup>2</sup>):

Observer position: R = 5.00; S = 0.00  
 R / S 60.0 64.0 68.0 72.0 76.0 80.0 84.0 88.0 92.0 96.0  
 \*\*\*\*\*  
 0.50 \* .20 .22 .20 .18 .16 .20 .30 .53 .47 .34  
 1.50 \* .35 .27 .34 .36 .43 .63 .73 .81 .75 .38  
 2.50 \* .42 .39 .38 .42 .50 .73 .78 .83 .76 .56  
 3.50 \* .33 .28 .29 .30 .34 .47 .58 .67 .60 .41  
 4.50 \* .24 .20 .21 .23 .24 .31 .41 .49 .40 .28  
 5.50 \* .16 .13 .15 .17 .17 .22 .30 .33 .26 .17  
 \*\*\*\*\*

The results from calculating the vertical illuminance of road surface class R3 (directed diffusion reflection) are presented in Table 3, and the results for road surface class R1 (almost diffusion reflection) are presented in Table 4.

**Table 3**

Results from the calculation of E<sub>vert</sub> and E<sub>sc</sub> for public alley with road surface class R3 and LTP: L<sub>AV</sub>=0,33; U<sub>L</sub>=0.4; U<sub>O</sub>=0.3; TI=20; type of installation “Single row - left”

**Total light technical parameters of the installation:**

Average luminance Lav= 0.38 cd/m<sup>2</sup>  
 Overall Uniformity Uo= 0.35  
 Longitudinal uniformity Ul= 0.42  
 Veiling luminance Lv= 0.11 cd/m<sup>2</sup>  
 Threshold Increment (Glare) TI= 15.31 %  
 Discomfort glare control mark D= 5.94  
 Surround Illuminance  
 Left 48.61 %  
 Right 57.69 %  
 Average illuminance 3+3 m left  
 sidewalk 2.21 lx  
 roadway 4.55 lx  
 Average illuminance 3+3 m right  
 sidewalk 2.31 lx  
 roadway 4.00 lx

**OUT-R3-15.txt**

Point M height for calculated Evert 1.50 m  
 Reflection of the road surface  $\rho_{road}$  0.10  
 Reflection of the sidewalk  $\rho_{sw}$  0.3  
 Width of the roadway+2\*s sidewalk 12.0 m  
 Luminaries spacing (S) 40.0 m  
 Value of the Evert-face 0.16 lx  
 Value of the Esc-face=(2/pi).Evert-face 0.10 lx  
 Evert-face/ Ehor-av=100\*0,16/2,31 6,93%

Illuminance distribution in one luminaire spacing (lx):

R / S 60.0 64.0 68.0 72.0 76.0 80.0 84.0 88.0 92.0 96.0  
 \*\*\*\*\*  
 2.50 \* 2.8 2.1 2.0 1.5 .8 .4 .8 1.5 2.0 2.1  
 1.50 \* 4.2 2.3 2.7 2.1 .8 .5 .8 2.1 2.7 2.3  
 0.50 \* 5.2 5.4 3.6 2.4 .9 .3 .9 2.4 3.6 5.4  
 \*\*\*\*\*  
 0.50 \* 5.5 6.1 4.4 2.7 1.1 .8 1.1 2.7 4.4 6.1  
 1.50 \* 9.1 6.1 6.2 3.5 2.1 1.8 2.1 3.5 6.2 6.1  
 2.50 \* 10.5 9.2 6.2 3.6 2.2 2.1 2.2 3.6 6.2 9.2  
 3.50 \* 9.2 7.1 5.9 3.6 2.2 1.8 2.2 3.6 5.9 7.1  
 4.50 \* 6.9 5.5 4.7 3.4 2.1 1.7 2.1 3.4 4.7 5.5  
 5.50 \* 4.9 3.7 3.5 3.0 2.0 1.7 2.0 3.0 3.5 3.7  
 \*\*\*\*\*  
 0.50 \* 3.8 3.3 3.1 2.6 1.9 1.6 1.9 2.6 3.1 3.3  
 1.50 \* 2.6 2.8 2.5 2.3 1.8 1.5 1.8 2.3 2.5 2.8

E<sub>VERT-FACE</sub>(M,J,I), mlx  
 0.17 0.35 0.64 0.34 0.89 1.71 2.64 3.75 5.47 27.87 41.24 32.55  
 0.25 0.36 1.12 0.57 0.78 1.63 1.73 1.84 1.66 5.73 5.87 5.33  
 0.21 0.34 0.56 0.28 0.47 0.57 0.64 0.60 0.51 1.51 1.31 1.15  
 0.11 0.18 0.23 0.10 0.14 0.17 0.18 0.19 0.18 0.50 0.46 0.43  
 0.04 0.04 0.05 0.02 0.05 0.06 0.06 0.06 0.06 0.18 0.17 0.17  
 0.01 0.02 0.01 0.01 0.03 0.03 0.03 0.03 0.03 0.08 0.08 0.08  
 0.02 0.02 0.02 0.01 0.02 0.02 0.02 0.02 0.02 0.06 0.06 0.06  
 0.02 0.04 0.04 0.02 0.02 0.02 0.02 0.02 0.02 0.05 0.05 0.04  
 0.02 0.03 0.04 0.02 0.03 0.03 0.03 0.02 0.02 0.04 0.04 0.03  
 0.02 0.02 0.05 0.02 0.02 0.03 0.02 0.02 0.01 0.03 0.03 0.02  
 0.02 0.03 0.04 0.01 0.02 0.03 0.02 0.02 0.01 0.03 0.02 0.01  
 0.01 0.01 0.03 0.01 0.01 0.02 0.01 0.01 0.01 0.02 0.02 0.01  
 0.01 0.01 0.02 0.01 0.01 0.01 0.01 0.01 0.01 0.01 0.01 0.01  
 0.00 0.01 0.01 0.00 0.00 0.00 0.00 0.00 0.00 0.01 0.01 0.01  
 0.00 0.00 0.00 0.00 0.00 0.00 0.00 0.00 0.00 0.01 0.01 0.01  
 0.00 0.00 0.00 0.00 0.00 0.00 0.00 0.00 0.00 0.00 0.00 0.00  
 0.00 0.00 0.00 0.00 0.00 0.00 0.00 0.00 0.00 0.00 0.00 0.00  
 0.00 0.00 0.00 0.00 0.00 0.00 0.00 0.00 0.00 0.00 0.00 0.00

0.00 0.00 0.00 0.00 0.00 0.00 0.00 0.00 0.00 0.00 0.00 0.00 0.00 0.00  
 0.00 0.00 0.01 0.00 0.00 0.00 0.00 0.00 0.00 0.00 0.00 0.00 0.00 0.00

**Table 4**

Results from the calculation of  $E_{vert}$  and  $E_{SC}$  for public alley with road surface class R1 and LTP:  $L_{AV}=0,33$ ;  $U_L=0,4$ ;  $U_0=0,3$ ;  $TI=20$ ; type of installation "Single row - left"

OUT-R1-15.txt	
Point M height for calculated Evert	1.50 m
Reflection of the road surface $\rho_{road}$	0.20
Reflection of the sidewalk $\rho_{sw}$	0.30
Width of the roadway+2*sidewalk	12.0 m
Luminaries spacing (S)	40.0 m
Value of the Evert-face	0.19 lx
Value of the Esc-face=(2/pi).Evert-face	0.12 lx
Evert-face/Ehor-av=100*0,19/2,31	8,23%

$E_{VERT-FACE}(M,J,I)$ , mlx

0.17	0.35	0.64	0.68	1.78	3.41	5.28	7.51	10.94	27.87	41.24	32.55
0.25	0.36	1.12	1.14	1.57	3.25	3.47	3.68	3.33	5.73	5.87	5.33
0.21	0.34	0.56	0.55	0.94	1.13	1.28	1.20	1.02	1.51	1.31	1.15
0.11	0.18	0.23	0.20	0.29	0.33	0.37	0.38	0.36	0.50	0.46	0.43
0.04	0.04	0.05	0.05	0.10	0.11	0.12	0.12	0.12	0.18	0.17	0.17
0.01	0.02	0.01	0.02	0.05	0.06	0.06	0.06	0.06	0.08	0.08	0.08
0.02	0.02	0.02	0.02	0.04	0.04	0.04	0.04	0.04	0.06	0.06	0.06
0.02	0.04	0.04	0.03	0.04	0.05	0.05	0.05	0.04	0.05	0.05	0.04
0.02	0.03	0.04	0.04	0.05	0.06	0.05	0.04	0.03	0.04	0.04	0.03
0.02	0.02	0.05	0.04	0.04	0.06	0.05	0.04	0.03	0.03	0.03	0.02
0.02	0.03	0.04	0.03	0.04	0.05	0.05	0.03	0.02	0.03	0.02	0.01
0.01	0.01	0.03	0.02	0.02	0.03	0.03	0.02	0.01	0.02	0.02	0.01
0.01	0.01	0.02	0.01	0.02	0.02	0.02	0.01	0.01	0.01	0.01	0.01
0.00	0.01	0.01	0.01	0.01	0.01	0.01	0.01	0.01	0.01	0.01	0.01
0.00	0.00	0.00	0.00	0.00	0.00	0.00	0.00	0.00	0.01	0.01	0.01
0.00	0.00	0.00	0.00	0.00	0.00	0.00	0.00	0.00	0.00	0.00	0.00
0.00	0.00	0.00	0.00	0.00	0.00	0.00	0.00	0.00	0.00	0.00	0.00
0.00	0.00	0.00	0.00	0.00	0.00	0.00	0.00	0.00	0.00	0.00	0.00
0.00	0.00	0.00	0.00	0.01	0.01	0.01	0.00	0.00	0.00	0.00	0.00
0.00	0.00	0.01	0.00	0.00	0.01	0.01	0.00	0.00	0.00	0.00	0.00

In the second case used to illustrate the application of the methodology, the distribution of the direct component of the luminous flux (in lx) is given by unit areas of the roadway (road surface type R3 with average luminance factor 0,07 cd/m<sup>2</sup>/lx). The luminaries are of the "flat beam" type, arranged in two rows, and simultaneously illuminate the sidewalks and the roadway (each with luminous flux of the light source of 312,5 lm). These fluxes are obtained by solving an optimization problem [3] for height of hanging of the luminaries of 1.2m and the following light technical parameters: average luminance of the roadway  $L_{AV} \geq 0,66$  cd/m<sup>2</sup>, longitudinal luminance uniformity  $U_L = L_{min}/L_{max} \geq 0,4$ , total uniformity  $U_0 = L_{min}/L_{AV} \geq 0,3$ , and glare  $TI \leq 20$ . The roadway is divided into  $NX=6$  strips of 1m, each with  $NY=8$  parts of 1.0m. The distance between two luminaries is  $S=8m$ , and the number of considered unit areas in the calculation of the vertical illuminance of the face (point M from Fig. 3) is  $NM=3$ . The following are the input data used in the calculations:

3	8	12	12	8	1						
0.6	1.2	1.1	1.1	1.2	0.6	0.6	1.2	1.1	1.1	1.2	0.6
0.9	1.8	1.4	1.4	1.8	0.9	0.9	1.8	1.4	1.4	1.8	0.9
1.5	2.6	1.8	1.8	2.6	1.5	1.5	2.6	1.8	1.8	2.6	1.5
2.6	3.6	2.2	2.2	3.6	2.6	2.6	3.6	2.2	2.2	3.6	2.6
4.6	4.6	2.7	2.7	4.6	4.6	4.6	4.6	2.7	2.7	4.6	4.6

7.9 4.3 4.6 4.6 4.3 7.9 7.9 4.3 4.6 4.6 4.3 7.9  
 16.5 6.6 10.9 10.9 6.6 16.5 16.5 6.6 10.9 10.9 6.6 16.5  
 41.7 25.3 4.9 4.9 25.3 41.7 41.7 25.3 4.9 4.9 25.3 41.7  
**Explanations:** Fi(M,J,I), lx for 3 8 12 12 8 1, where  
 NM=3 NY=8 NX=12 W+2T=12m S=8m "1"Fi-data  
 LTP:  $L_{AV}=0,66$ ;  $U_L=0,4$ ;  $U_0=0,3$ ;  $TI=20$   
 $Fi\_sum=625$  lm for  $12*8=96$  m<sup>2</sup>  
 (6,51 lm/m<sup>2</sup> for  $L_{AV}=0.66$  cd/m<sup>2</sup>)= $9,86$  (lm/m<sup>2</sup>)/(cd/m<sup>2</sup>);

Results from the calculations are shown in Table 5.

**Table 5**

Results from the calculation of  $E_{vert}$  and  $E_{SC}$  for public alley with road surface class R3 and LTP:  $L_{AV}=0,66$ ;  $U_L=0,4$ ;  $U_0=0,3$ ;  $TI=20$ ; type of installation "flat beam"

Out-r3-15.txt	
Point M height for calculated Evert	1.50 m
Reflection of the road surface $\rho_{road}$	0.10
Reflection of the sidewalk $\rho_{sw}$	0.30
Width of the roadway+2*sidewalk	12.0 m
Luminaries spacing (S)	8.0 m
Value of the Evert-face	0.17 lx
Value of the Esc-face=(2/pi).Evert-face	0.11 lx
Evert-face/ Ehor-av=100*0,17/6,51	2,6%

$E_{VERT-FACE}(M,J,I)$ , mlx

0.00	0.01	0.01	0.00	0.01	0.01	0.01	0.06	0.12	1.04	3.90	5.58
0.01	0.03	0.03	0.02	0.03	0.03	0.06	0.21	0.37	2.67	8.34	8.90
0.03	0.07	0.07	0.03	0.07	0.07	0.12	0.37	0.50	2.99	7.94	7.21
0.06	0.12	0.10	0.05	0.12	0.14	0.22	0.50	0.52	2.58	6.48	6.09
0.12	0.17	0.14	0.07	0.16	0.24	0.36	0.54	0.49	2.14	4.87	5.75
0.23	0.17	0.24	0.11	0.14	0.37	0.53	0.41	0.61	2.43	2.82	5.82
0.49	0.26	0.56	0.25	0.20	0.68	0.92	0.49	1.05	3.95	2.80	7.69
1.23	0.96	0.24	0.10	0.69	1.47	1.90	1.46	0.35	1.26	7.37	12.99
0.02	0.04	0.05	0.02	0.03	0.02	0.02	0.06	0.06	0.21	0.25	0.13
0.03	0.06	0.06	0.02	0.04	0.02	0.03	0.06	0.06	0.20	0.27	0.15
0.04	0.08	0.07	0.03	0.05	0.03	0.04	0.07	0.06	0.19	0.29	0.18
0.06	0.10	0.07	0.03	0.05	0.05	0.05	0.08	0.06	0.18	0.32	0.24
0.10	0.11	0.08	0.03	0.06	0.07	0.08	0.09	0.06	0.18	0.32	0.33
0.15	0.10	0.12	0.05	0.05	0.10	0.11	0.07	0.08	0.25	0.24	0.45
0.29	0.13	0.25	0.09	0.06	0.18	0.19	0.08	0.15	0.47	0.30	0.76
0.66	0.45	0.10	0.04	0.21	0.38	0.42	0.27	0.06	0.18	0.94	1.57
0.01	0.02	0.02	0.01	0.01	0.00	0.00	0.01	0.01	0.03	0.04	0.02
0.01	0.03	0.02	0.01	0.01	0.01	0.01	0.01	0.01	0.04	0.05	0.02
0.02	0.03	0.03	0.01	0.01	0.01	0.01	0.02	0.01	0.04	0.06	0.03
0.03	0.04	0.03	0.01	0.02	0.01	0.01	0.02	0.01	0.04	0.07	0.05
0.04	0.05	0.03	0.01	0.02	0.02	0.02	0.02	0.01	0.04	0.08	0.08
0.07	0.04	0.05	0.02	0.02	0.03	0.03	0.02	0.02	0.06	0.06	0.11
0.13	0.06	0.10	0.03	0.02	0.06	0.06	0.03	0.04	0.13	0.08	0.21
0.30	0.19	0.04	0.01	0.08	0.13	0.14	0.09	0.02	0.05	0.27	0.46

**Conclusion**

1. The performed calculations show that the largest contribution in forming the vertical illuminance on the face of a pedestrian is from the luminance of the sidewalk, on which the pedestrian is walking. As is evident from Table 1, the normative value for the minimum vertical illuminance on the face is equal to the minimum normative horizontal luminance of the roadway, which is about five times smaller than the average normative horizontal luminance. For the two cases studied in this report, the percentage of the vertical illuminance that can be attributed to the diffusion component of the roadway flux and the sidewalk flux represents 6,93% and 2,6%, respectively, from the average required vertical illuminance on faces. Road



surface of type R1 increases the first value to 8,23% of the average horizontal illuminance, and, correspondingly, to 41,15% of the minimum required vertical illuminance on faces;

2. If the street is in a pedestrian zone and the pedestrian is walking in the middle of the street, the values of the vertical illuminance on the face of the pedestrian will be two times higher. The diffusion component of the luminous flux can provide about 60-70% of the required value for the vertical illuminance in a lighting installation of the classical kind, and about 25-30% in installation of the “flat beam” type. The remaining 30-40% (respectively, 70-75%) must be provided by the direct luminous flux of the luminaries;

3. With regard to the luminance of the roadway, a lighting installation of the “flat beam” type is  $10,97/9,86=1,11$  times more efficient than the classical installation. However, with regard to ensuring vertical illuminance on the faces of pedestrians, the classical type lighting is  $2*0.16/0.17=1,88$  times better. This is logical, because in lighting of the “flat beam” type, the optimization of the luminaries’ light distribution is done under constraints on luminance uniformity, rather than constraints on horizontal illuminance.

### Acknowledgements

This research was supported by funding from the Ministry of Education and Science, National Science Fund, contract № MU-FS-07 “Energy Conservation through Lighting Systems Optimization for Streets and Road Tunnels.”

### References

- [1] Genesis Automation and Lightlab International, Report on Energy Savings Opportunities in Street lighting, June 1999
- [2] CIE Publication No.92 (1992). “Guide to the Lighting of Urban Areas”
- [3] Pachamanov A., D. Pachamanova. Optimization of the Light Distribution of Luminaries for Tunnel and Street Lighting, Engineering Optimization, 40 (1), January 2008, pp. 47-65 (Taylor & Francis, United Kingdom, <http://www.tandf.co.uk/>)
- [4] Пачаманов А. Енергоспестяване и осветителна техника (енергоефективно осветление). Издателство “Авангард-Прима”. София, 2007
- [5] Пачаманов А. Фотометрия и осветителни уредби (лабораторни упражнения). Издателство “Авангард-Прима”, София 2006

### Biographies



**Angel Pachamanov** was born in Kardjali, Bulgaria, on February 15, 1950.

*Education:* 1969-1974 Technical University of Sofia, Electrotechnical Department, Mag.Eng.; 1978-1980 Technological University of Sofia, Postgraduate education in automatic systems, M.Sc.; 1986-1988 Technical University of Sofia, Dr.Eng. in Lighting Technics and Sources of Lighting

*Job Experience:* 1974-1976 Power engineer; 1976-1982 Deputy head of the Power Department; 1982-1985 Head of the Power Department at the Plant for Flat Glass and China in Razgrad, Bulgaria; 1985-1995 Scientific researcher at the Laboratory of Lighting in the Technical University of Sofia; since 1995 Senior scientific researcher; Associate Professor, teaching Lighting and Special lighting installation systems, Irradiating systems, Energy Saving and Automation – at the Department of Electric power supply and lighting technics, Faculty of Electrical Engineering, Technical University of Sofia.

Angel Pachamanov is with the Faculty of Electrical Engineering, Technical University of Sofia, 8, Kl. Ohridski Blvd., 1000 Sofia, Bulgaria. E-mail: [pach@tu-sofia.bg](mailto:pach@tu-sofia.bg)

**Konstantin Hristov** graduated from the Technical University 4-year Bachelor’s program in Electrical Power Generation and Electrical Equipment at the Department of Electrical Power Supply, Electrical Equipment and Electrical Transport on May 2002. In 2004 he defends a master’s degree in the same program, specializing Lighting Techniques. Currently he is a free-lance designer and works on his doctor’s thesis according to contract № MU-FS-07 “Energy Conservation through Lighting Systems Optimization for Streets and Road Tunnels” of the Ministry of Education and Science, The National Science Fund E-mail: [ko.hristiv@mail.bg](mailto:ko.hristiv@mail.bg)



**Vesela Daskalova** was born in Dobrich, Bulgaria, on July 22, 1985. She graduated from the Technical University 4-year program in Electrical Power Generation and Electrical Equipment at the Department of Electrical Power Supply, Electrical Equipment and Electrical Transport in May 2008. Currently, she is completing her thesis requirement for obtaining a Bachelor of Science degree in engineering.

E-mail: [vesela.daskalova@gmail.com](mailto:vesela.daskalova@gmail.com)

# European Trends in Interdisciplinary Postgraduate Education

Maria G. Ioannides, Rossie Betcheva and Fotini Ioannidou

**Abstract:** *The higher education is crossing international and social borders, expands the pool of those entering universities and prepares the graduates to become successful in the global economy while working together with people of diverse specializations. Successfully addressing these issues requires innovative solutions, and approaches, involves curricular transformations that will improve student involvement, learning and professional careers.*

*In this paper, we present the European trends in interdisciplinary postgraduate education, as resulted from a research carried out in the framework of the ESTIA-Net Thematic Network.*

**Keywords:** *Interdisciplinary Studies,*

## 1. Interdisciplinarity Issues

In academia, physical sciences, human sciences and social sciences, an *interdisciplinary field* is a term in the teaching professions. The terms *Multidisciplinary field* and *Interdisciplinary fields* have been introduced in many modern technical professions which need cross traditional academic boundaries, as new professions have emerged. The term was applied within education and training in reference to the needs of definition and qualities of studies that cut across several established disciplines or traditional fields of study as stimulated by the advance of knowledge. Subsequently, the term has also come to be applied to new professions and old fields where the professional must have advanced credentials in several fields of study, [1].

Historically, the concept comes from Greek Philosophy where the roots of the concepts lie in a number of ideas of an unified science, general knowledge, synthesis and integration of knowledge, and from Greek Historians who took elements from other fields of knowledge, such as medicine or philosophy, to explain their ideas.

*Interdisciplinarity factors* involves researchers, students, and teachers in the goals of connecting and integrating several academic disciplines, professions, or technologies, along with their specific perspectives, in the pursuit of a common task. Interdisciplinary approaches focus on problems too complex to be dealt with the knowledge and tools of a single discipline. Interdisciplinarity is a remedy to the excessive specialization, dependent to those who specialize in one field of study. Without specialists, interdisciplinarians would have no information and no leading experts. The focus of interdisciplinarity is on the need to transcend

disciplines, viewing excessive specialization as problematic both scientifically and politically. When interdisciplinary collaboration or research results in new solutions to problems, much information is given back to the various disciplines involved. Therefore, both disciplinarians and interdisciplinarians are in complementary relation to one another.

The adjective *interdisciplinary* is used when researchers from two or more disciplines pool their approaches and modify them so that they are better suited to the problem, including the case of the team-taught course where students are required to understand a given subject in terms of multiple traditional disciplines.

*Interdisciplinary is interchanged with multidisciplinary.*

*Interdisciplinarity* in an evolving field with definitions not yet established for some related fields. An interdisciplinary project is made up of people from multiple disciplines and professions who are engaged in creating and applying new knowledge as they work together as equal stakeholders in addressing a common challenge. The key question is what new knowledge of an academic discipline nature, which is outside the existing disciplines, is required to address the challenge. The nature of the challenge, either its scale or complexity, requires that many people have interactional expertise to improve their efficiency working across multiple disciplines as well as within the new interdisciplinary area. An interdisciplinary person is a person with degrees from one or more academic disciplines with additional interactional expertise in one or more additional academic disciplines, and new knowledge that is claimed by more than one discipline. Over time, interdisciplinary work can lead to an increase or a decrease in the number of academic disciplines.

*Multidisciplinarity* is joining together two or more disciplines *without integration*. Each discipline yields discipline specific results while any integration would be left to a third party. A multidisciplinary project is made up of people from different disciplines and professions who are engaged in working together as equal stakeholders in addressing a common challenge. The key question is how well can the challenge be decomposed into nearly separable subparts, and then addressed via the distributed knowledge in the community or project team. The lack of shared vocabulary between people and communication overhead is an additional challenge in these communities and projects. However, if similar challenges of a particular type need to be repeatedly addressed, and each challenge can be properly

decomposed, a multidisciplinary community can be exceptionally efficient and effective. A multidisciplinary person is a person with degrees from two or more academic disciplines, so one person can take the place of two or more people in a multidisciplinary community or project team. Over time, multidisciplinary work does not typically lead to an increase nor a decrease in the number of academic disciplines.

From the disciplinary perspective, much interdisciplinary work may be seen as "soft," lacking in rigor, or ideologically motivated; these beliefs place barriers in the career paths of those who choose interdisciplinary work. For example, interdisciplinary grant applications are often refereed by peer reviewers drawn from established disciplines; not surprisingly, interdisciplinary researchers may experience difficulty getting funding for their research. In addition, untenured researchers know that, when they seek promotion and tenure, it is likely that some of the evaluators will lack commitment to interdisciplinarity. They feel that making a commitment to interdisciplinary research will increase the risk of being denied tenure.

Because most participants in interdisciplinary ventures were trained in traditional disciplines, they must learn to appreciate differing perspectives and methods. An interdisciplinary program may not succeed if its members remain stuck in their disciplines and attitudes.

Interdisciplinary Study Programs may fail if they are not given sufficient autonomy. For example, interdisciplinary faculty are usually recruited to a joint appointment, with responsibilities in both an interdisciplinary program and a traditional discipline. If the traditional discipline makes the tenure decisions, new interdisciplinary faculty will be not fully committed to interdisciplinary work.

Due to these barriers, interdisciplinary research areas are strongly motivated to become disciplines themselves. If they succeed, they can establish their own research funding programs and make their own tenure and promotion decisions. In so doing, they lower the risk of entry. Examples of former interdisciplinary research areas that have become disciplines include *neuroscience*, *cybernetics*, *biochemistry* and *biomedical engineering*. These new fields are not referred to as *interdisciplines*.

*Interdisciplinary Study Programs* arise when the traditional disciplines are unable to address an important problem, such as Bioinformatics, Molecular Biology, etc. *Interdisciplinary Studies* is an academic program seeking to synthesize broad perspectives, knowledge, skills, interconnections, and science. Interdisciplinary programs may be founded in order to facilitate the study of subjects which have some coherence, but which cannot be adequately understood from a single disciplinary perspective.

## 2. Motivations, Obstacles and Approach

The higher education faces significant challenges in crossing international, and social borders in order to expand the pool of those entering universities and prepare

the graduates to become successful in the global economy while working together with people of diverse specializations. Successfully addressing these issues requires innovative solutions, and approaches, involving curricular transformations that will improve student involvement, learning and professional careers.

The people decide for postgraduate education for various reasons: advancing their professional career, new job options requiring new fields of competencies, social needs for new knowledge, changes in structure of society, family and personal needs.

Most of the time, difficulties in following new postgraduate curricula arise from: weakness of background in the field of new studies, difficulty in identifying appropriate curricula, minimal availability of free time to spend in study, often, lack of financial resources and lack of appropriate university courses.

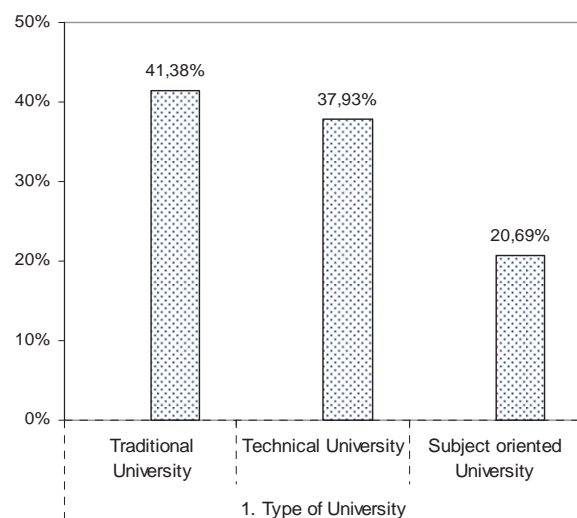
To address the above issues, we decided to study the trends in interdisciplinary education and to identify interdisciplinary degree courses in European countries, involving engineering, computers, applied sciences as well as life, social, economic and management disciplines, [2]-[5].

## 3. Methodology and Results

A questionnaire has been designed by the authors and was sent to many European universities. The questionnaire is given in reference [6]. Many scientists, partners of ESTIA-Net, [3] were asked to fill in the answers. Mostly, they responded by filling the answers to the questionnaire and adding opinions, suggestions, and comments. In the following, we present the results from questionnaires and their evaluation.

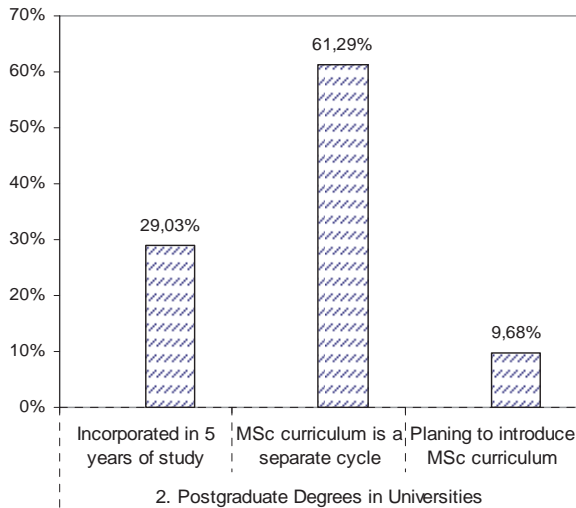
### 1. Type of University

The postgraduate interdisciplinary course can be implemented in a Traditional University 41,38% and/ or Technical University, 37,93% and/or in a Subject-Oriented University 20,69%, Figure 1.



2. Structure of Master Degrees in University

The majority of recommendations, 61,29%, indicate that the MSc degree must be a separate cycle of studies, a smaller percent, 29,03% recommend to incorporate it in 5 years of study, others, 9,68% are still planning to introduce MSc degree, Figure 2.



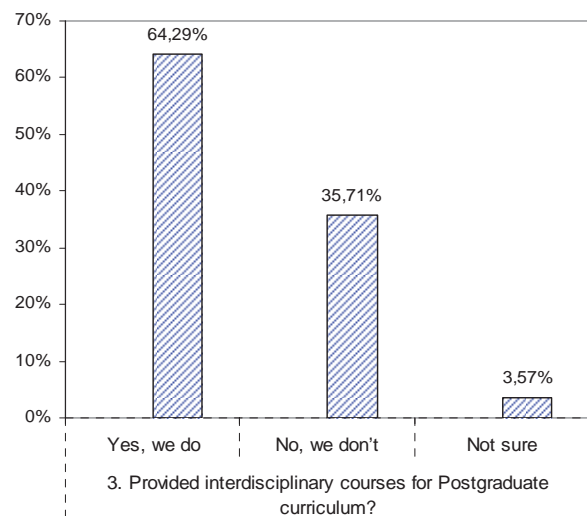
3. Provide interdisciplinary courses for MSc curriculum

The existing postgraduate curricula provide interdisciplinary courses, 64,29%, other do not, 35,71% or are not sure, 3,57%. Results show that interdisciplinary courses are widely accepted, Figure 3.

The participation of women in postgraduate education, both as professors and as students is less than 50%, Figures 4 and 5. In 88,89% of cases, the women as professors and in 74,07% of cases, the women as students, participate less than men. These percents show that the existent system of postgraduate education is not friendly to women.

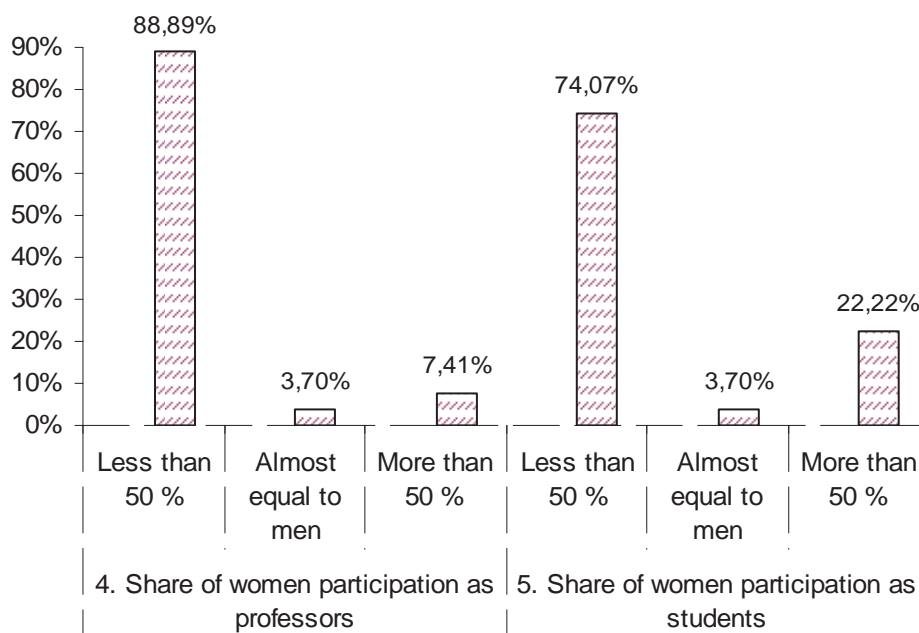
6. Planing to develop interdisciplinary courses for MSc curriculum

The majority of universities 73,08% are planning to develop interdisciplinary courses for MSc curriculum, Figure 6.

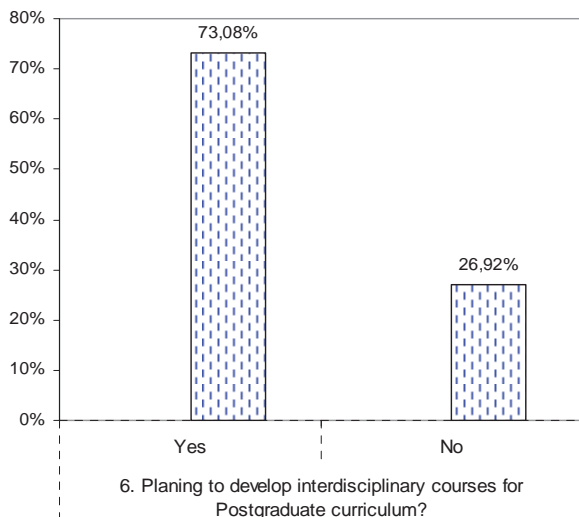


4. Women participation in postgraduate education as professors

5. Women participation in postgraduate education as students





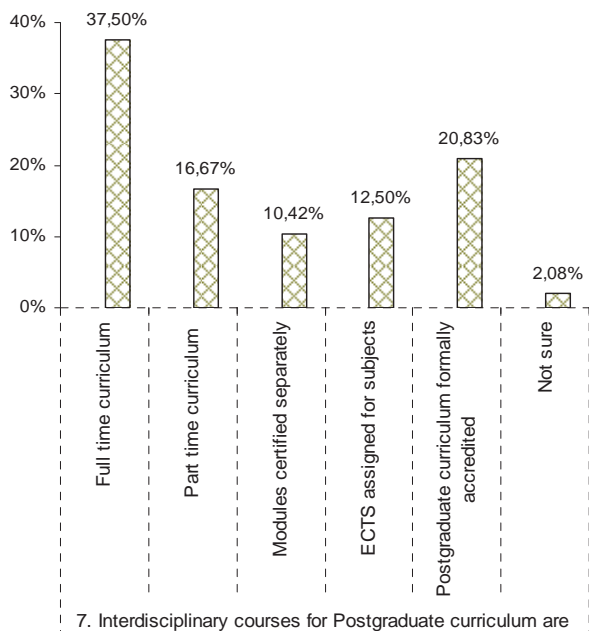


7. System for interdisciplinary courses for MSc curriculum

The interdisciplinary courses are offered as:

- Full time curriculum, 37,50%
- Formally recognized and accredited, 20,83%
- ECTS are accepted to be assigned, 12,50%

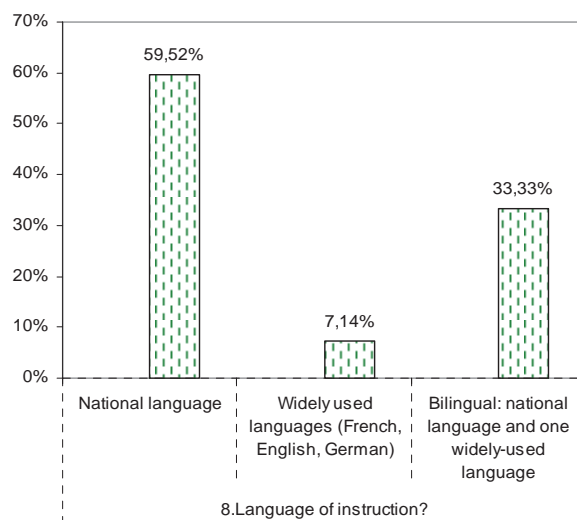
However, as an increased flexibility, some subjects as part-time participation are present, 16,67%. Also, there are some modules with separate certification, 10,42%, Figure 7.



7. Interdisciplinary courses for Postgraduate curriculum are

8. Languages of instruction

In the present, the national language for teaching is predominant in most universities, 59,52%, Figure 8. Then, the bilingual instruction involving both the national and a foreign language comes as a second preference, 33,33%. Last preference is the entire teaching in a foreign widely used language, 7,14%.



8. Language of instruction?

9. Subjects in interdisciplinary postgraduate curriculum

The following analysis and classification was made according to the obtained percents, Figure 9.

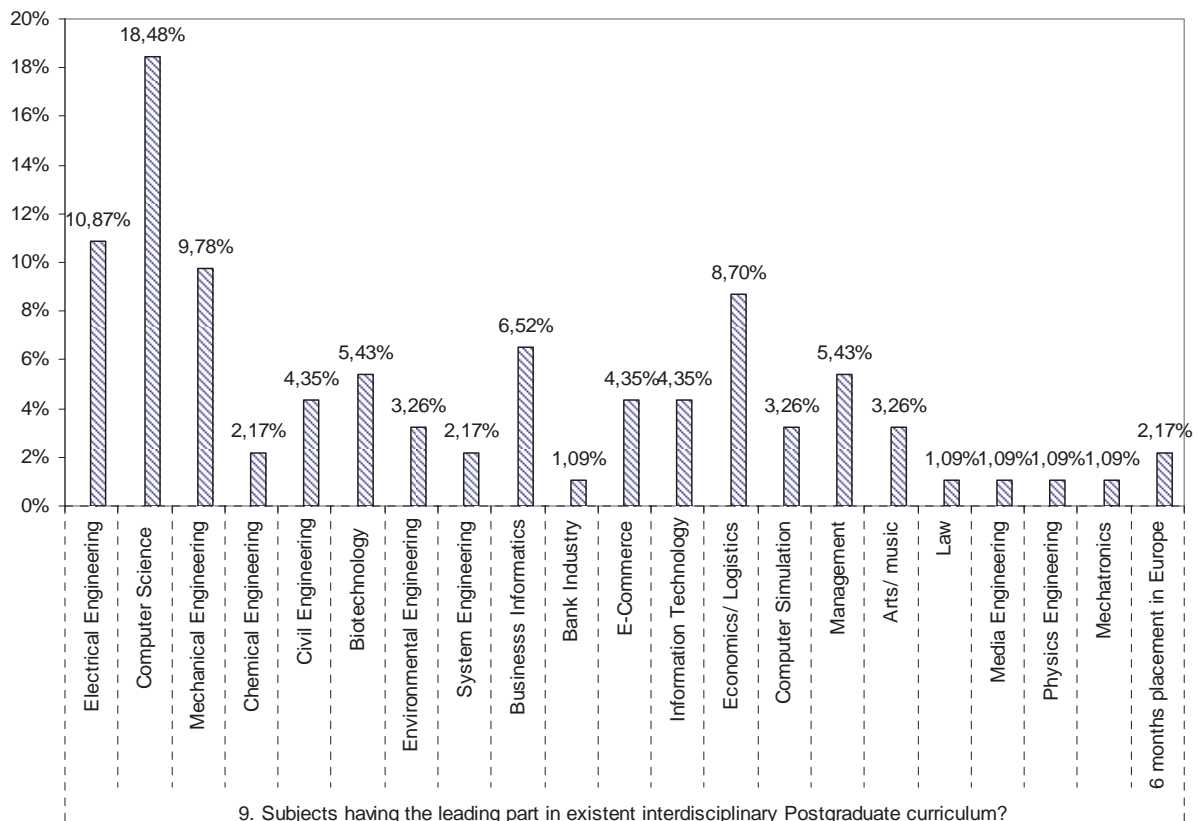
In the existent interdisciplinary curricula there are present the following four Groups of Specialties A1-A4, see Tables 1 to 4:

- Group A1: Engineering subjects
- Group A2: Business – Economics - Life
- Group A3: Applied Science-Arts
- Group A4: Selected Specializations

GROUP A1: ENGINEERING SUBJECTS	TABLE 1
Computer Science	18,48%
Electrical Engineering	10,87%
Mechanical Engineering	9,78%
<i>Total</i>	<i>39,45%</i>

<i>GROUP A2: BUSINESS - ECONOMICS - LIFE</i>	<b>TABLE 2</b>
Economics/ Logistics	8,70%
Business Informatics	6,52%
Management	5,43%
Biotechnology	5,43%
<i>Total</i>	<i>26.09%</i>

<i>GROUP A3: APPLIED SCIENCE-ARTS</i>	<b>TABLE 3</b>
Civil Engineering	4,35%
E-Commerce	4,35%
Information Technology	4,35%
Environmental Engineering	3,26%
Computer Simulation	3,26%
Arts/ Music	3,26%
<i>Total</i>	<i>22,83%</i>



GROUP A4: SELECTED SPECIALIZATIONS	TABLE 4
Chemical Engineering	2,17%
System Engineering	2,17%
Media Engineering	1,09%
Physics Engineering	1,09%
Mechatronics	1,09%
Bank Industry	1,09%
Law	1,09%
6-months job placement in Europe	2,17%
Total	11,96%

## 5. Conclusions

Our research has been carried out in many European universities to identify the trends and the needs for interdisciplinary courses at postgraduate level.

The results show that the existent courses can be organized in four major categories: Engineering subjects (39, 45%), Business-Economics subjects (26,09%), Applied Sciences-Arts (22,83%) and Selected Specializations (11,96%).

Thus, the trends can be used for the design of future Interdisciplinary Studies at postgraduate level.

## 6. Acknowledgement

This work has been partially funded from the contract 110068-CP-2-2004-1-GR-Erasmus-TN Socrates Estia-Net. The authors express their gratitude to the DG Education & Culture and the Education, Audiovisual and Culture Executive Agency for their kind support.

## 7. References

- [1] <http://en.wikipedia.org/wiki/Interdisciplinary>
- [2] M. G. Ioannides, ESTIA-Net-Opening up electrical engineering, computer technology and applied sciences to successful women careers. In *Compendium 2003 Thematic Networks*, and *Compendium 2004 Thematic Networks*, Ed. European Commission, DG Education and Culture, Socrates, pp. 11-12, 2003 and pp. 13-14, 2004.
- [3] ESTIA-Net Project website: <http://www.estiatn.net>
- [4] R. Betcheva and M. G. Ioannides, Interdisciplinarity of Education in Engineering and Applied Science Life Long Learning to Increase the Participation of Women, Hellenic National and International Life Long Learning Conference Jointly with EULLearn Thematic Network Workshop, Oral communication, October 14-15, 2005, Larissa, Greece, slides 1-23.
- [5] M. G. Ioannides and F. Ioannidou, Increasing the competitiveness of women in the technologic and scientific labour market. The ESTIA Net project, Hellenic National and International Life Long Learning Conference Jointly with EULLearn Thematic Network Workshop, Oral communication, October 14-15, 2005, Larissa, Greece, slides 1-27.
- [6] F. Ioannidou, R. Betcheva and M. G. Ioannides, Interdisciplinary Postgraduate Education: Actual Trends in Europe, *Proceedings of The 2nd Int. Conf. on Interdisciplinarity*

in Education ICIE'06, ISBN 978-960-89028-2-7, ISSN 1790-661X, pp. 33-43.

[7] M. G. Ioannides and F. Ioannidou, *Designing Innovative Interdisciplinary Postgraduate Curricula in Engineering, Computers and Health Sciences*, Book of Abstracts of the 2<sup>nd</sup> Int. Conf. in Interdisciplinarity in Education, May 17-19, 2006, Athens, Greece, ISBN 960-89028-3-5, ISSN 1790-661X, pp. 23-25.

[8] F. Ioannidou, Z. Puklus and S. Zanakis, An Approach for Tuning Postgraduate Curricula in European Universities, Proceedings of The 3<sup>rd</sup> Int. Conf. on Interdisciplinarity in Education as International Forum for Multi-Culturality, Multi-Ethnicity and Multi-Disciplinarity In European Higher Education and Research MULTI-FORUM'07, March 15-17, 2007, Athens, Greece, pp. 191-201

## Biographies



**Maria G. Ioannides** is Professor in the School of Electrical & Computer Engineering of the National Technical University of Athens, Greece. Her research area covers control of electric drives, small and special electric motors, renewable energy sources, biocomputing, education methods curriculum development, women in sciences. Participated as scientific responsible or principal investigator in more than 30 research projects of the Greek government, European

Community and U.S.A. Dr. Ioannides is the author of more than 200 journal papers, conference proceedings papers, technical books and technical reports. Is member and reviewer in many Scientific Committees of International Conferences and International Journals and participated to more than 70 international conferences and workshops.

Dr. Ioannides is Senior Member of IEEE, Member of Electric Machinery Committee of IEEE, IASTED, Technical Chamber of Greece, Electromechanical Energy Conversion Committee of TCG.

Address for correspondence: National Technical University of Athens, Faculty of Electrical and Computer Engineering, Heroon Polytechniou 9, 15773 Athens, Greece, mioannid@ece.ntua.gr; www.ntua.gr



**Rositza (Rossie) Betcheva** is Professor in the University of Chemical Technology and Metallurgy, Sofia, Bulgaria and Dean of the Office for Foreign Students and Education in Foreign Languages. Professor Betcheva participated in many European, international and national research programmes and has published many papers in scientific journals and conference proceedings.

Address for correspondence: University of Chemical Technology and Metallurgy, 8 Kl. Ohridski, 1756 Sofia, Bulgaria, E-mail: [betcheva@uctm.edu](mailto:betcheva@uctm.edu)



**Fotini G. Ioannidou**, received her PhD from the Medical School of the National and Kapodistrian University in Athens and specialization in Maxillo-facial Surgery from the Evangelismos Hospital and Medical School of the National and Kapodistrian University in Athens, Greece. Currently she is Doctor of A' Rank to the Thrasio General Hospital in Elefsina, Attiki and Researcher to the National Technical University of Athens.

Participated in many European, international and national research programmes and has published many papers in scientific journals and conference proceedings.

Address for correspondence: National Technical University of Athens, School of Electrical and Computer Engineering, Heroon Polytechniou 9, 15773, Athens, Greece, fioann@otenet.gr

# Magnetic field calculus for block permanent magnet system

Ana Mladenović and Slavoljub Aleksić

**Abstract:** The paper presents the magnetic field calculation of permanent magnet system, which component parts are block magnets homogeneously magnetized in known direction. Method used in the paper is based on a system of equivalent magnetic dipoles. The results that are obtained using this analytical method are compared with results obtained using COMSOL Multiphysics software. Magnetic field and magnetic flux density distributions of permanent magnet are also shown in the paper.

**Keywords:** Magnetic field, Permanent magnet, Magnetic dipole

## Introduction

Permanent magnetism is one of the oldest continuously studied branches of the science. There are many properties of permanent magnets that are taken in to consideration when designing a magnetic for a certain device. Most often the demagnetization curve is the one that has the greatest impact on its usability. Curve shape contains information on how the magnet will behave under static and dynamic operating conditions, and in this sense the material characteristic will constrain what can be achieved in the device's design. The  $\mathbf{B}$  versus  $\mathbf{H}$  loop of any permanent magnet has some portions which are almost linear, and others that are highly non-linear. Permanent magnets have been employed in a variety of electrical devices for a long time now. This work is motivated by the need for different shaped permanent magnets in great number of electromagnetic devices.

Determination of the magnetic field components in vicinity of permanent magnets, starts with presumption that magnetization,  $\mathbf{M}$ , of permanent magnet is known. The following methods can be used in practical calculation:

- Method based on determining distribution of microscopic Ampere's current;
- Method based on Poisson and Laplace equations, determining magnetic scalar potential; and
- Method based on a system of equivalent magnetic dipoles [1].

The third method that is mentioned in the paper for magnetic field calculation is based on superposition of elementary results obtained for elementary magnetic dipoles.

Elementary magnetic dipole (Fig.1) has magnetic moment

$$(1) \quad d\mathbf{m} = \mathbf{M} dV'$$

This magnetic moment produces, at field point  $P$ , elementary magnetic scalar potential

$$(2) \quad d\varphi_m = \frac{1}{4\pi} \frac{\mathbf{R} d\mathbf{m}}{R^3} = \frac{1}{4\pi} \frac{\mathbf{R}\mathbf{M}}{R^3} dV',$$

where  $R = |\mathbf{r} - \mathbf{r}'|$  is distance from the point where the magnetic field is being calculated to elementary source, and  $\mathbf{R} = \mathbf{r} - \mathbf{r}'$ .

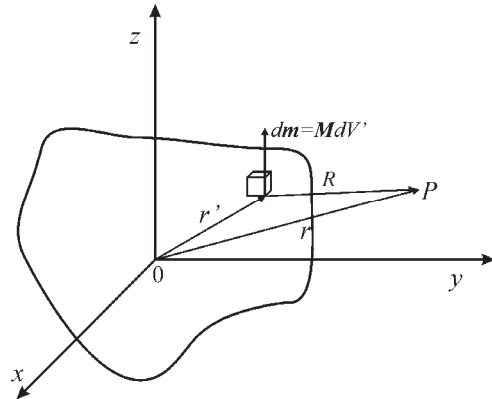


Fig.1. Elementary magnetic dipole.

After integration magnetic scalar potential is obtained as

$$(3) \quad \varphi_m = \frac{1}{4\pi} \int_V \frac{\mathbf{R} d\mathbf{m}}{R^3} = \frac{1}{4\pi} \int_V \frac{\mathbf{R}\mathbf{M}}{R^3} dV'.$$

Magnetic field vector can be expressed as

$$(4) \quad \mathbf{H} = -\text{grad } \varphi_m.$$

## Problem definition

The method that is described above is used for determining the magnetic field components of the block permanent magnet system presented in the Fig.2. The certain modification of this system might find its application in modern hard drives. Each of these block permanent magnets is homogeneously magnetised in longitudinal direction,

$$(5) \quad \mathbf{M} = M(\pm \hat{x}).$$

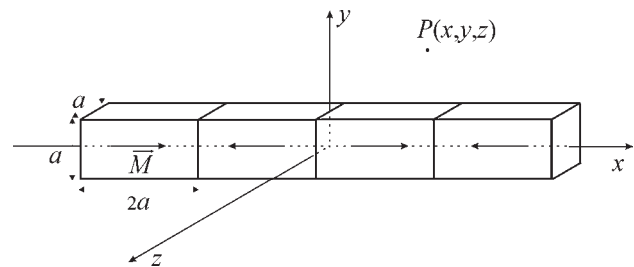


Fig.2. Block permanent magnet system.



Outside the permanent magnet, magnetic scalar potential, at the field point  $P(x, y, z)$ , could be presented using the expression (3).

As magnetization has only  $x$  component, scalar product  $\mathbf{R} \cdot \mathbf{M}$  is formed as

$$(6) \quad \mathbf{R} \cdot \mathbf{M} = [(x-x')\hat{x} + (y-y')\hat{y} + (z-z')\hat{z}]M\hat{x},$$

therefore,

$$(7) \quad \mathbf{R} \cdot \mathbf{M} = (x-x')M.$$

Distance from the point where the magnetic field is being calculated to elementary source is

$$(8) \quad R = \sqrt{(x-x')^2 + (y-y')^2 + (z-z')^2}.$$

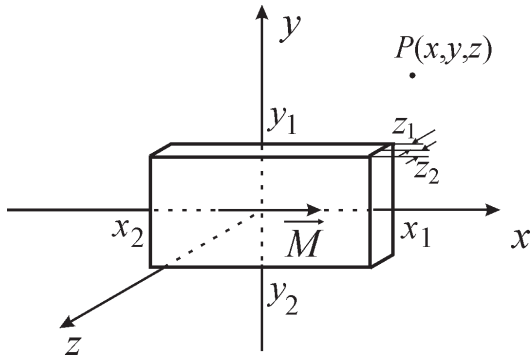


Fig.3. Block permanent magnet

Finally, substituting the expressions (7) and (8) in (3), magnetic scalar potential produced by a block magnet that is homogeneously magnetized in positive direction of  $x$  axis (Fig.3) is formed as

$$(9) \quad \varphi_m = \frac{M}{4\pi} \int_{x_1}^{x_2} \int_{y_1}^{y_2} \int_{z_1}^{z_2} \frac{(x-x')dx'dy'dz'}{[(x-x')^2 + (y-y')^2 + (z-z')^2]^{3/2}}.$$

The solution of this integral is

$$(10) \quad \varphi_m(x, y, z) = \frac{M}{4\pi} (V[x-x_2, y-y_1, y-y_2, z-z_1, z-z_2] - V[x-x_1, y-y_1, y-y_2, z-z_1, z-z_2]),$$

where function  $V$  has the following form:

$$(11) \quad V(a, x_1, x_2, z_1, z_2) = x_2 \ln \frac{C_2}{C_3} + x_1 \ln \frac{C_1}{C_4} + z_1 \ln \frac{C_5}{C_8} + z_2 \ln \frac{C_6}{C_7} - 2|a| \text{Arctg} \frac{C_5 \cdot C_8 + a^2 + z_1^2 + z_1(C_5 + C_8)}{|a|(C_8 - C_5)} + 2|a| \text{Arctg} \frac{C_7 \cdot C_6 + a^2 + z_2^2 + z_2(C_6 + C_7)}{|a|(C_6 - C_7)}$$

and

$$C_1 = z_1 + \sqrt{a^2 + x_1^2 + z_1^2}; \quad C_2 = z_2 + \sqrt{a^2 + x_2^2 + z_2^2};$$

$$C_3 = z_1 + \sqrt{a^2 + x_2^2 + z_1^2}; \quad C_4 = z_2 + \sqrt{a^2 + x_1^2 + z_2^2};$$

$$C_5 = x_1 + \sqrt{a^2 + x_1^2 + z_1^2}; \quad C_6 = x_2 + \sqrt{a^2 + x_2^2 + z_2^2};$$

$$C_7 = x_1 + \sqrt{a^2 + x_1^2 + z_2^2}; \quad C_8 = x_2 + \sqrt{a^2 + x_2^2 + z_1^2}.$$

Magnetic scalar potential of the whole system is the sum of magnetic scalar potentials obtained for each magnetized block.

For the system presented in the Fig.2 magnetic scalar potentials of the block magnets may be presented using the function  $V$  as

$$(12) \quad \varphi_{m1} = \frac{M}{4\pi} \left( V[x+4a, y+\frac{a}{2}, y-\frac{a}{2}, z+\frac{a}{2}, z-\frac{a}{2}] - V[x+2a, y+\frac{a}{2}, y-\frac{a}{2}, z+\frac{a}{2}, z-\frac{a}{2}] \right),$$

$$(13) \quad \varphi_{m2} = \frac{M}{4\pi} \left( V[x, y+\frac{a}{2}, y-\frac{a}{2}, z+\frac{a}{2}, z-\frac{a}{2}] - V[x+2a, y+\frac{a}{2}, y-\frac{a}{2}, z+\frac{a}{2}, z-\frac{a}{2}] \right),$$

$$(14) \quad \varphi_{m3} = \frac{M}{4\pi} \left( V[x+2a, y+\frac{a}{2}, y-\frac{a}{2}, z+\frac{a}{2}, z-\frac{a}{2}] - V[x, y+\frac{a}{2}, y-\frac{a}{2}, z+\frac{a}{2}, z-\frac{a}{2}] \right),$$

$$(15) \quad \varphi_{m4} = \frac{M}{4\pi} \left( V[x-2a, y+\frac{a}{2}, y-\frac{a}{2}, z+\frac{a}{2}, z-\frac{a}{2}] - V[x-4a, y+\frac{a}{2}, y-\frac{a}{2}, z+\frac{a}{2}, z-\frac{a}{2}] \right).$$

Magnetic scalar potential of the whole system which consists of four block permanent magnets is

$$(16) \quad \varphi_m = \varphi_{m1} + \varphi_{m2} + \varphi_{m3} + \varphi_{m4}.$$

After determining magnetic scalar potential magnetic field component can be easily calculated using the expression (4).

## Numerical results

Distribution of magnetic field, in  $x_0y$  plane, outside the permanent magnet is illustrated in the Fig.4. It is obtained using the analytical method for magnetic field determination.

Magnetic field distribution for the same system, obtained using the COMSOL Multiphysics software are presented in the Fig.5. Distribution of magnetic flux density is shown in the same figure with arrows and its intensity is presented with gradient of gray. Magnetization of each block in the system is 750kA/m.

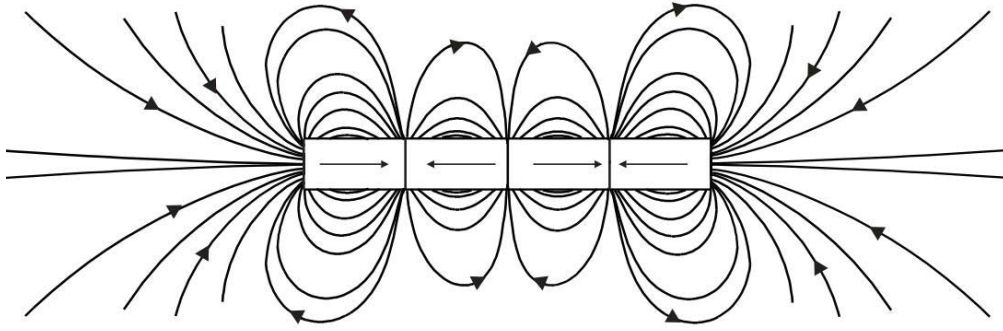


Fig.4. Distribution of magnetic field obtained using the analytical method.

Comparing these two figures it can be concluded that results of the analytical method are confirmed in satisfactory manner using COMSOL Multiphysics software.

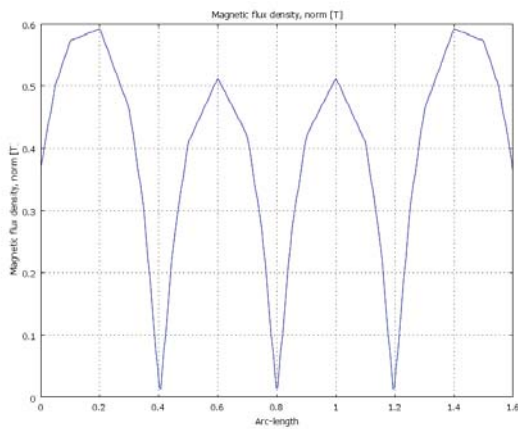


Fig.6. Magnetic flux density inside the blocks of the system along the direction  $y = 0$ .

Fig.6 presents magnetic flux density inside the system along the direction  $y = 0$ . It is obvious that magnetic flux density has the highest values inside of blocks and the lowest values in the border area between neighbouring blocks.

### Conclusion

The permanent magnet system which consists of block permanent magnets, homogeneously magnetized in known direction, is observed in the paper. Method that is used for magnetic field determination is based on superposition of results that are obtained for elementary magnetic dipoles. Magnetic field and magnetic flux density distribution of permanent magnet is also presented in the paper. Magnetic field lines have the same form and the same direction as magnetic flux density lines, outside the magnet. Results obtained by analytical method are satisfactory confirmed using COMSOL Multiphysics software. This system may be applicable for approximation of the system of permanent magnets which can be found in hard drives.

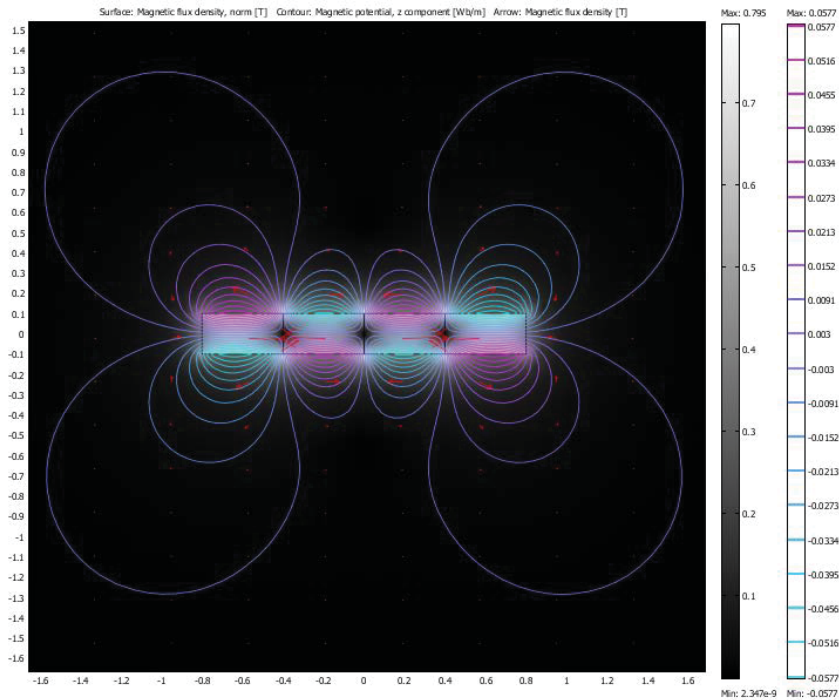


Fig.5. Distribution of magnetic field obtained using COMSOL Multiphysics software.

## References

- [1] Fundamentals of Modern Electromagnetics for Engineering, Part I: Static and Stationary Electrical and Magnetic Field, Edited by Hermann Uhlmann, Technische Universitaet Ilmenau, Germany 2005.
- [2] Permanent magnet materials and their application, Peter Cambel, Cambridge University Press 1994.
- [3] Ana N. Mladenović, Slavoljub R. Aleksić: "Toroidal shaped permanent magnet with air gap", International Conference on Applied Electromagnetics PES2005, Niš 23<sup>rd</sup>-25<sup>th</sup> May 2005, Proceedings of Extended Abstracts, pp. 23-24.
- [4] Ana N. Mladenović, Slavoljub R. Aleksić: "Methods for magnetic field calculation", 11<sup>th</sup> International Conference on Electrical Machines, Drives and Power Systems ELMA 2005, Sofia, Bulgaria, 15-16 September 2005, Vol.2, pp. 350-354.
- [5] Ana N. Mladenović, Slavoljub R. Aleksić: "Determination for different shaped permanent magnets", VII International Symposium on Electromagnetic Compatibility and Electromagnetic Ecology, St.Petersburg, Russia, 26<sup>th</sup> -29<sup>th</sup> June 2007, Proceedings, pp. 84-87.
- [6] Ana N. Mladenović: "Permanent magnet homogeneously magnetized along its axes", International PhD-Seminar "Computational Electromagnetics and Technical Application", Proceedings of Full Papers, Banja Luka, Bosna and Herzegovina, 28 August-01 September 2006, pp.171-174.
- [7] Ana N. Mladenović, Slavoljub R. Aleksić: "Magnetic field calculation of permanent magnet", International Scientific Colloquium, Ilmenau, Germany, 11<sup>th</sup>-15<sup>th</sup> September 2006, Proceedings, pp.185-186.
- [8] A. Canova, G. Gruossu, M. Repetto: "Response surface method for Finite element based optimization of tubular linear permanent magnet motor", International Conference on Applied Electromagnetics PES2003, Niš 2003, Proceedings of Full Papers, pp.29-32.
- [9] Slavoljub Aleksić and Ana Mladenović, "Magnetic field determination of different shaped permanent magnets", Discrete and Computational Mathematics, Nova Science Publisher, Inc, New York 2008.

## Biographies



**Ana N. Mladenović** was born in Niš, Serbia on July 29, 1977. In 1996 she enrolled in the Faculty of Electronic Engineering, University of Niš, Serbia, with computer science as a major. Graduated in 2003 with graduation comprehension thesis "Sphere screens calculation". Started postgraduate studies at the department of Theoretical Electrical Engineering of the same Faculty, in 2004.

Since 2003 she's been involved in various research projects as a teaching and research assistant at the department of Theoretical Electrical Engineering. Her main field of interest is magnetism and permanent magnets. She is author or co-author of more than fifteen papers presented at National and International conferences.

Ana Mladenović is with the Faculty of Electronic Engineering, University of Niš, Aleksandra Medvedeva 14, 18000 Niš, Serbia (e-mail: ana@elfak.ni.ac.yu).



**Slavoljub Aleksić** was born in Berčinac, Serbia, in 1951. He enrolled in the Faculty of Electronic Engineering (FEE), University of Niš in 1970. He received Dipl. Ing., M. Sc. and Ph. D. degree at the FEE in 1975, 1979 and 1997, respectively.

He was elected for an assistant, associate and full professor at the same Department in 1980, 1997 and 2008, respectively.

Received his tenure in 2008.

Slavoljub Aleksić is with the Faculty of Electronic Engineering, University of Niš, Aleksandra Medvedeva 14, 18000 Niš, Serbia (e-mail: slavoljub.aleksic@elfak.ni.ac.yu).

# Nonlinear Grounding Design: Sphere Grounding Electrode

Bojana Petković, Zlata Cvetković and Slavoljub Aleksić

**Abstract:** *This paper elaborates one elementary, but generally applicable method which can be applied in the case when high currents are driven to grounding electrodes and non-linear effect cannot be neglected. This method enables potential and electric field distribution determination as well as corona region dimension and grounding conductance calculation, [1], [2]. Potential deviation and boundary condition satisfaction for electric field are checked and compared using point matching method and least squares method.*

**Keywords:** *sphere grounding electrode, corona, point matching method, least squares method.*

## Introduction

Since grounding is a common feature of virtually every electrical network, there is a strong need for defining grounding parameters and electrode behavior research when the electrode is driven by small current as well as the electrode is driven by high current. When grounding electrodes are driven by relatively small currents, the standard procedure gives linear relations between electrical values of interest. The experience shows that the strength of the electric field cannot be larger than so-called critical value, when sparking begins. Therefore, linear relations are only applicable as long as the electric field strength is smaller or equal to the critical value.

If grounding electrode has spikes and/or sharp edges, linear approaches cannot be applied. In general, when driving currents are so large, that the electric field strength would be greater than critical, a corona charge is formed around the electrode and the limit effect begins. The corona charge decreases the electric field strength and limits resulting field to the critical value. As a consequence of this limiting effect, a nonlinear and nonhomogeneous region is being created around the grounding electrode. This eliminates linear analysis and the problem becomes very complex, implying solving of nonlinear partial differential equations.

Using boundary condition that the electrode is equipotential, the non-linear algebraic equations can be established, whose solution gives electric field strength distribution along privileged lines as well as the shape and dimensions of corona region. This approach also enables calculation of an existing non-linear dependence between current intensity and potential of grounding and, upon this, calculation of the non-linear grounding conductance.

In order to find a simple practical solution of this problem, this paper elaborates one elementary, but generally applicable method, which is independent on the electrode shape and dimension.

## Method description

Let us consider grounding electrode which is deeply buried in the ground of conductivity  $\sigma$  and critical electric field strength  $E_k$ . If current driven to the electrode is larger than critical, the region around the electrode becomes a corona region.

The method which is, in this case, able to determine potential distribution and electric field strength dependence on the distance from the electrode is based on two presumptions. The first presumption is that the corona charge does not distort the shape of field lines compared to the linear regime. Electric field lines are still normal on the electrode surface and field lines have radial direction at large distances from the grounding electrode. The second presumption is that the electric field has uniform intensity along the force line in the corona region. The field intensities are different from line to line and on the field line that passes through the spike of the electrode the electric field strength is the largest and equal to the critical value. Using boundary condition that the electrode is equipotential, nonlinear algebraic equations can be established, whose solution gives electric field strength and shape and dimensions of the corona region. This approach enables determination of potential distribution, electric field strength dependence and corona region dimension and it also enables calculation of nonlinear conductance  $G$ . The theoretical investigation is applied to a sphere grounding electrode.

## Method application

The method proposed above will be applied on an isolated sphere grounding electrode, using three types of approaches: analytical approach, point matching method and least squares method. These three ways were used for determining potential distribution, electric field strength and grounding conductance. Obtained results will be compared.

### *Analytical Approach (AA)*

Let us consider sphere grounding electrode radius  $a$ . The electrode is driven by current  $I$  and deeply buried in the ground of conductivity  $\sigma$  and critical electric field  $E_k$ . Sparking begins when driven current is larger than



critical  $I_k$  and a corona charge is formed around the electrode. The ratio of grounding conductances in linear and nonlinear regime is

$$(1) \quad \frac{G_0}{G} = 2\sqrt{\frac{I_k}{I}} - \frac{I_k}{I}.$$

### Point Matching Method (PMM)

In order to find potential distribution and electric field strength in the electrode surroundings, point fictitious sources will be used. The total number of fictitious sources is  $2N$ . They will be placed symmetrically regarding to the centre of the sphere at places

$$(2) \quad z_n = \frac{2n-1}{2N+1}a, \quad n=1,2,\dots,N, \quad z = \pm z_n.$$

Boundary condition that the potential on the electrode surface is equal to  $U$  should be satisfied in  $N$  points chosen on the upper half of the sphere:

$$(3) \quad R_m = a, \quad \theta_m = \frac{m-1}{N-1} \frac{\pi}{2}, \quad N > 1, \quad m=1,2,\dots,N.$$

In this way, a system of linear equations is formed and after determining the unknown currents of fictitious sources, the grounding conductance in linear regime can be calculated.

After equalizing the electric field strength on the electrode surface and at the point on the boundary of the corona region, but on the same field line, dimension of corona region can be calculated.

Ratio of grounding conductances in linear and nonlinear regime can be obtained as

$$(4) \quad \frac{G_0}{G} = \frac{\sum_{n=1}^N \frac{I_n}{2\pi\sigma} \left[ \frac{b(b-a)}{(b^2+z_n^2)^{3/2}} + \frac{1}{(b^2+z_n^2)^{1/2}} \right]}{\sum_{n=1}^N \frac{I_n}{2\pi\sigma} \frac{1}{(a^2+z_n^2)^{1/2}}},$$

where  $b$  is radius of the corona region formed around the electrode.

### Least Squares Method (LSM)

The arrangement of fictitious sources will be the same as in PMM usage. In this case boundary condition matching is being done in points on the grounding sphere electrode surface:

$$(5) \quad z_m = a \cos \theta_m, \quad r_m = a \sin \theta_m, \quad \theta_m = \frac{m-1}{M-1} \frac{\pi}{2},$$

$m=1,2,\dots,M > N$ .

After minimizing the functional

$$(6) \quad F = \sum_{m=1}^M \left\{ \sum_{n=1}^N \frac{I_n}{4\pi\sigma} \left[ \frac{1}{\sqrt{a^2+z_n^2-2az_n \cos \theta_m}} + \frac{1}{\sqrt{a^2+z_n^2+2az_n \cos \theta_m}} \right] - U \right\}^2,$$

the following system is obtained:

$$(7) \quad \sum_{n=1}^N \frac{I_n}{4\pi\sigma} \sum_{m=1}^M \left[ \left( \frac{1}{k_{n1}} + \frac{1}{k_{n2}} \right) \times \left( \frac{1}{k_{v1}} + \frac{1}{k_{v2}} \right) \right] =$$

$$= U \sum_{m=1}^M \left( \frac{1}{k_{v1}} + \frac{1}{k_{v2}} \right), \quad v=1,2,\dots,N$$

$$k_{n1} = \sqrt{a^2+z_n^2-2az_n \cos \theta_m};$$

$$k_{n2} = \sqrt{a^2+z_n^2+2az_n \cos \theta_m};$$

$$k_{v1} = \sqrt{a^2+z_v^2-2az_v \cos \theta_m};$$

$$k_{v2} = \sqrt{a^2+z_v^2+2az_v \cos \theta_m}.$$

After solving this system, the unknown currents of fictitious sources are determined and the procedure and formulae are the previous subsection.

### Numerical Results

The ratio of grounding conductances in linear and nonlinear regime,  $G_0/G$ , using the analytical approach and point matching method with different number of fictitious sources is presented in Table 1. The same ratio but using the analytical approach and least squares method for  $N=3$  and different number of matching points is given in Table 2.

**Table 1**

Ratio of grounding conductances,  $G_0/G$ , using AA and PMM.

$I/I_k$	AA	PMM $N=2$	PMM $N=3$	PMM $N=5$
1	1.00000	1.00000	1.00000	1.00000
1.5	0.96632	0.96586	0.96623	0.96632
2	0.91421	0.91324	0.91404	0.91421
5	0.69442	0.69242	0.69412	0.69442
10	0.53245	0.53039	0.53217	0.53245
20	0.39721	0.39540	0.39698	0.39721
100	0.19000	0.18896	0.18988	0.19000

**Table 2**

Ratio of grounding conductances,  $G_0/G$ , using AA and LSM.

$I/I_k$	AA	LSM $M = 5$	LSM $M = 20$	LSM $M = 50$
1	1.00000	1.00000	1.00000	1.00000
1.5	0.96632	0.96621	0.96621	0.96621
2	0.91421	0.91397	0.91398	0.91398
5	0.69442	0.69397	0.69399	0.69399
10	0.53245	0.53201	0.53202	0.53202
20	0.39721	0.39683	0.39684	0.39684
100	0.19000	0.18979	0.18979	0.18979

Results given in Table 1 show that the ratio decreases when current driven to the ground electrode increases. A good convergence is obtained using PMM. There is also a very good agreement of the results obtained by the Analytical approach and PMM with a proper number of fictitious sources. Very big number of fictitious sources is not recommended. Table 2 shows that increment of matching points number in LSM contributes to better agreement with values obtained analytically.

Influence of fictitious sources number on potential deviation at the electrode surface and on the electric field vector boundary condition satisfaction, when point matching method is used, is shown in Fig. 1- Fig. 4.

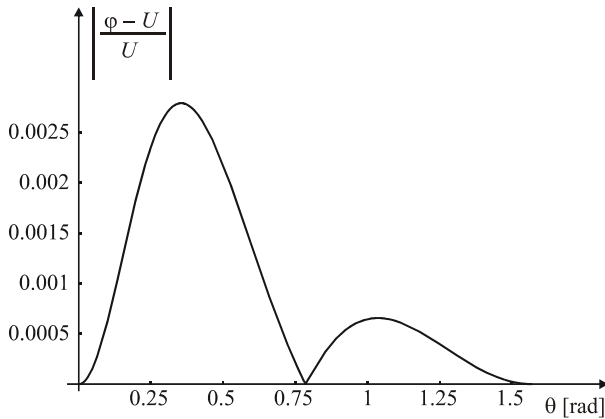


Fig.1. Potential deviation at the electrode surface using PMM for  $N = 3$ .

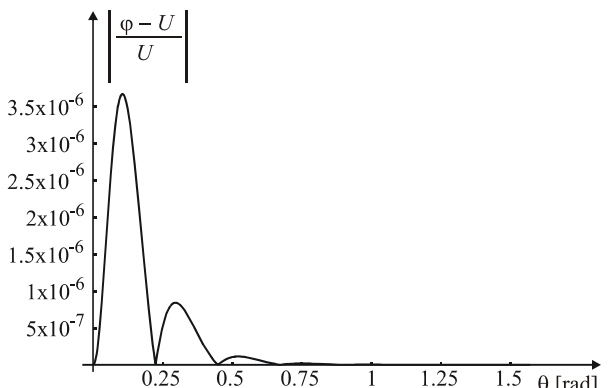


Fig.2. Potential deviation at the electrode surface using PMM for  $N = 8$ .

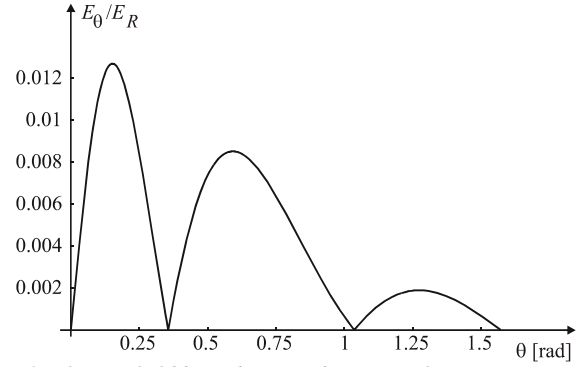


Fig.3. Electric field boundary condition satisfaction using PMM for  $N = 3$ .

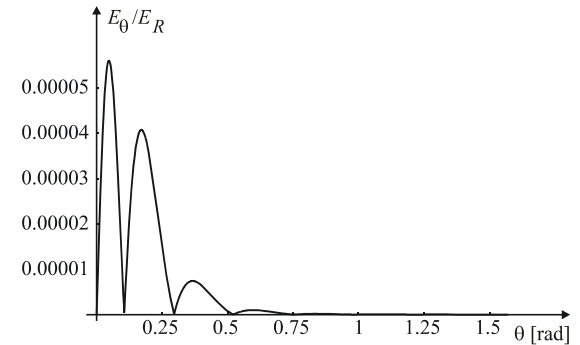


Fig.4. Electric field boundary condition satisfaction using PMM for  $N = 8$ .

From the previous figures the following can be concluded:

- Potential boundary condition is only satisfied in matching points;
- With greater number of fictitious sources potential deviation at the electrode surface becomes smaller; too large number of fictitious sources leads to bad conditioned system;
- The greater number of fictitious sources, the smaller ratio of tangential and normal component of the electric field vector at the electrode surface, i.e. better tangential component electric field vector boundary condition satisfaction.
- Electric field vector tangential component becomes zero somewhere around the middle of neighboring matching points.

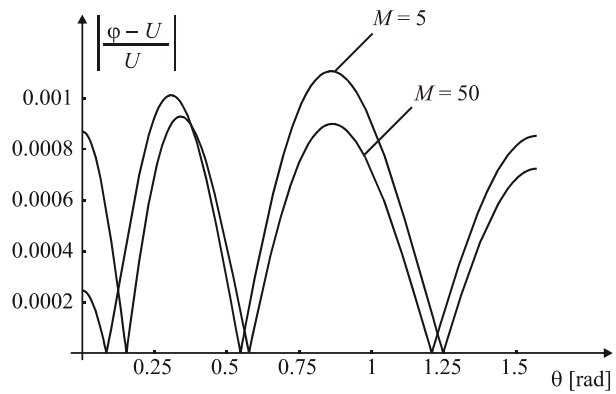


Fig.5. Potential deviation at the electrode surface using LSM for  $N = 3$ ,  $M = 5$  and  $M = 50$ .

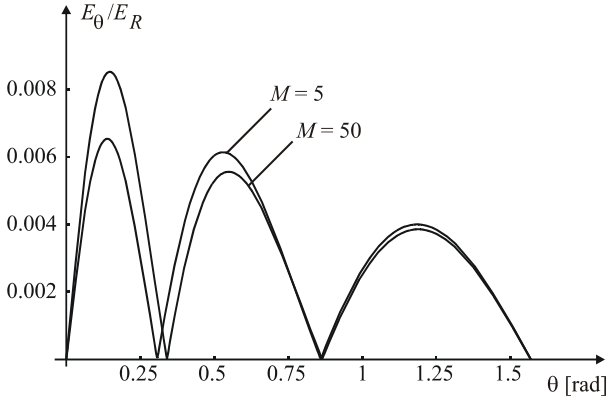


Fig. 6. Electric field boundary condition satisfaction using LSM for  $N = 3$ ,  $M = 5$  and  $M = 50$ .

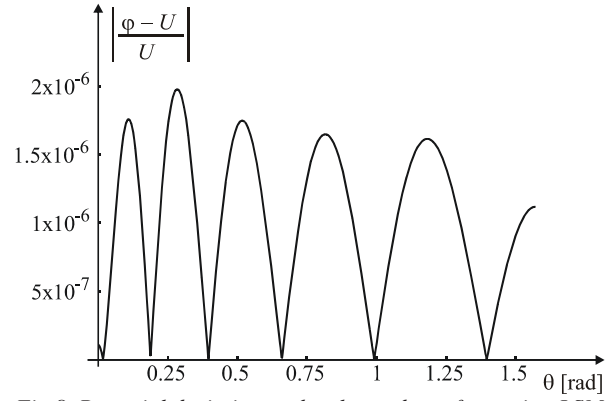


Fig. 8. Potential deviation at the electrode surface using LSM for  $M = 10$  and  $N = 6$ .

Influence of matching points number on potential deviation at the electrode surface and on the electric field vector boundary condition satisfaction, when least squares method is applied, is shown in Fig. 5 and Fig. 6, respectively.

Fig. 5 and Fig. 6 show the following:

- Matching points number insignificantly influences on potential deviation as well as on boundary condition satisfaction of electric field vector tangential component;
- The ratio of tangential and normal component of electric field vector has local maximum at the point where the difference  $\phi - U$  is equal to zero;
- The ratio of tangential and normal component of electric field vector has local minimum in points where potential deviation is the largest; those points of maximal satisfaction of tangential component electric field vector boundary condition satisfaction are around the middle of distance between points where that satisfaction is the smallest.

Fig. 7 and Fig. 8 present the influence of fictitious sources number increase on potential deviation at the electrode surface using LSM. Fig. 9 and Fig. 10 show the influence of fictitious sources number on electric field vector boundary condition satisfaction when LSM is applied.

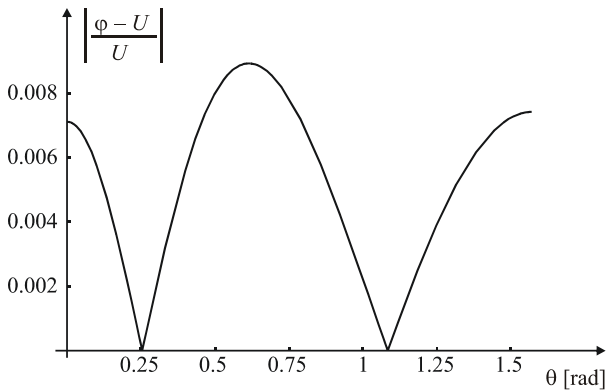


Fig. 7. Potential deviation at the electrode surface using LSM for  $M = 10$  and  $N = 2$ .

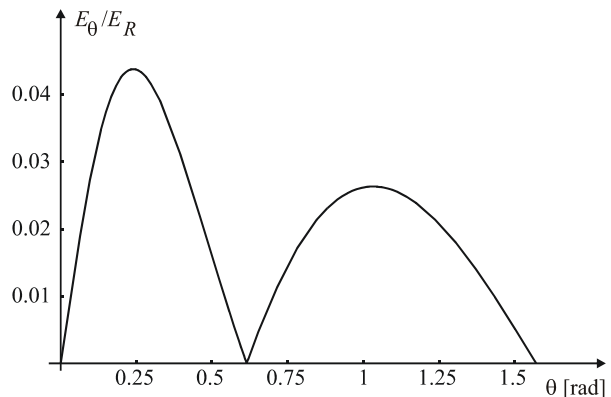


Fig. 9. Electric field boundary condition satisfaction using LSM for  $M = 10$  and  $N = 2$ .

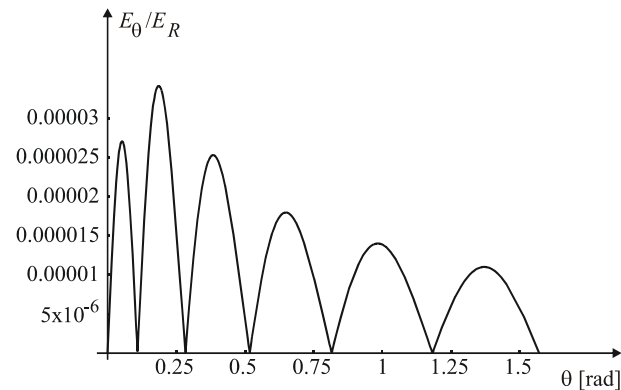


Fig. 10. Electric field boundary condition satisfaction using LSM for  $M = 10$  and  $N = 6$ .

Figs. 7 – 10 show that:

- Fictitious sources number significantly influences on potential deviation as well as on boundary condition satisfaction of electric field vector tangential component;
- The ratio of tangential and normal component of electric field vector has local maximum at the point where the difference  $\phi - U$  is equal to zero;
- Electric field vector tangential component becomes zero somewhere around the middle of neighboring matching points.

## Conclusion

One very simple, but exact method has been developed for determining electric field and potential in the case when high currents are driven to grounding electrodes and non-linear effect cannot be neglected. It enables calculation of corona region dimension as well as grounding conductance by using an Analytical approach, Point matching method and Least squares method.

A good convergence is obtained using PMM and LSM. Increment of fictitious sources number in PMM and matching points number in LSM contributes to better agreement with values obtained analytically. Fictitious sources number significantly influences on potential deviation as well as on boundary condition satisfaction of electric field vector tangential component in both methods application.

## References

- [1] D. M. Veličković, B. R. Nikolić, "Non-linear grounding design", 48. International Kolloquium, Information Technology and Electrical Engineering, Ilmenau, Germany, pp. 393-394, September, 22-25, 2003.
- [2] D. M. Veličković, B. R. Nikolić, " Calculation of electric field and potential in the case of nonlinear grounding", Summer School-Modern Aspects of Theoretical Electrical Engineering, Sozopol, Bulgaria, pp. 121-124, September 29-October 3, 2002.
- [3] T. Sugimoto, Y. Yumita, Y. Higashiyama, "Multiple-spark discharge occurring between a charged conductive plate and a grounded sphere electrode", IEEE Transactions on Industry Application, vol. 40, No. 3, pp. 911-916, May/June, 2004.
- [4] M. J. Nahman, Grounding neutral point in a distribution network, Scientific book, ISBN 06-783/1, Belgrade, 1980.
- [5] E. Garbagnati, A. Geri, G. Sartorio, G. M. Veca: "Non-linear behavior of ground electrodes under lightning surge currents: Computer modeling and comparison with experimental results", IEEE Trans. Magnetics, March, 1992, vol. 28, no. 2, pp. 1442-1445.
- [6] S. Boggs: "Overview of dielectrics", Electrical Insulation Research Center, University of Connecticut, USA, [www.Electrical-Insulation.org](http://www.Electrical-Insulation.org).
- [7] D. M. Veličković, F. H. Uhlmann, K. Brandisky, R. D.

Stantcheva, H. Brauer: "Fundamentals of Modern Electromagnetics for Engineering", Textbook for Graduate Students, TU Ilmenau, Germany, June 2005.

## Biographies



**Bojana Petković** was born in Niš, Serbia, on August 27, 1977. She graduated from the Faculty of Electronic Engineering in Niš in 2002 and she got a second Master degree from the same faculty in 2008.

Since 2002 she has been working at the Faculty of Electronic Engineering as researching teaching assistant at the Department of Theoretical Electrical Engineering.

Her researching areas are: nonlinear effects in grounding, numerical methods, optimization, genetic algorithm application.

Bojana Petković is with the Faculty of Electronic Engineering, University of Niš, 14, Aleksandra Medvedeva Street, 18000 Niš, Serbia (e-mail: [bojana.petkovic@elfak.ni.ac.yu](mailto:bojana.petkovic@elfak.ni.ac.yu)).



**Zlata Cvetković** was born in Blace, Serbia, on February 10, 1956. She received the M.Sc. degree in 1991 and Ph.D. degree in 2002 from the Faculty of Electronic Engineering, University of Niš. From May 1990 she has been working at the Department of Theoretical Electrical Engineering at the Faculty of Electronic Engineering. Since 2007 she has been working as an Associate Professor. Her scientific research is focused on the analysis of the nonuniform transmission lines, numerical methods in electromagnetics, analysis and design of electrostatic systems for uniform fields generation.

Zlata Cvetković is with the Faculty of Electronic Engineering, University of Niš, 14, Aleksandra Medvedeva Street, 18000 Niš, Serbia (e-mail: [zlata.cvetkovic@elfak.ni.ac.yu](mailto:zlata.cvetkovic@elfak.ni.ac.yu)).



**Slavoljub Aleksić** was born Berčinac, Serbia, on January 20, 1951. He studied at the He studied at the Faculty of Electronic Engineering in Niš, Serbia, and got M.Sc. and Ph. D. degree 1979 and 1997, respectively. At the same faculty at the Department of Theoretical Electrical Engineering he works as a full professor. The main topics of his researching are: skin effect in electroenergetic conductors, cable terminations, lightning and grounding, antennas, bioeffects and permanent magnets.

Slavoljub Aleksić is with the Faculty of Electronic Engineering, University of Niš, 14, Aleksandra Medvedeva Street, 18000 Niš, Serbia (e-mail: [slavoljub.aleksic@elfak.ni.ac.yu](mailto:slavoljub.aleksic@elfak.ni.ac.yu)).



# Linear Elecrtic Circuit Analysis based on the Graph Theory obtaining all Possible Paths in the Graph Model

Simona Filipova-Petrakieva, Valeri Mladenov

**Abstract:** A new method for AC analysis of the linear electrical circuits is suggested. It consists of solving the linear equation system, based on the graph theory. Firstly, the linear system presents as a signal graph model with initial vertexes, respecting to the energy sources (voltage and currents) and immediate vertexes, associated to the unknown variables (currents, voltages and etc.). Second, it determines all possible paths reached to the unknown variables from the initial vertexes of the graph studied. Third, these paths aggregates, taking in mind the respective coefficient of the graph arcs and it gets the expressions about the studied currents and voltages with respect to the power sources in the circuit considered. The new method proposed is simpler than traditional methods solving the linear equation systems and it requires smaller number of calculations than using the Mason's gain formula. The applicability of the method proposed is illustrated to the numerical example for solving the linear equation system of 3-rd order.

**Keywords:** linear electrical circuit analysis, mesh analysis, nodal analysis, graph theory, Mason's gain formula

## Introduction

It is well known that the behaviour of an arbitrary linear electrical circuit can be obtained by the following linear system:

$$(1) \begin{cases} a_{11}x_1(t) + a_{12}x_2(t) + \dots + a_{1n}x_n(t) = f_1(t) \\ a_{21}x_1(t) + a_{22}x_2(t) + \dots + a_{2n}x_n(t) = f_2(t) \\ \dots \\ a_{n1}x_1(t) + a_{n2}x_2(t) + \dots + a_{nn}x_n(t) = f_n(t) \end{cases}$$

where:

$x(t) = [x_1(t), x_2(t), \dots, x_n(t)]^T$  - vector of unknown variables (currents, voltages);

$f(t) = [f_1(t), f_2(t), \dots, f_n(t)]^T$  - vector of input power sources (voltage and current sources);

$a_{ij}$ ,  $i, j = \overline{1, n}$  - coefficients, taking in mind the circuit parameters ( $R, L, C$ ) variation over its behaviour.

The standard linear system (1) can be solved using the some traditional numerical methods, based on Gause's method, Gause-Jordan's method, Kramer's formulas [1, 2]

To simplify the graph presentation of system (1) it can be rewritten as follows:

$$(2) \begin{cases} x_1(t) = +b_{12}x_2(t) + \dots + b_{1(n-1)}x_{(n-1)}(t) + b_{1n}x_n(t) + b_{11}f_1(t) \\ x_2(t) = b_{21}x_1(t) + \dots + b_{2(n-1)}x_{(n-1)}(t) + b_{2n}x_n(t) + b_{22}f_2(t) \\ \dots \\ x_n(t) = b_{n1}x_1(t) + b_{n2}x_2(t) + \dots + b_{n(n-1)}x_{(n-1)}(t) + b_{nn}f_n(t) \end{cases}$$

where:

$$\left. \begin{aligned} b_{ss} &= 0, \quad b_s = \frac{1}{a_{ss}} \\ b_{ks} &= -\frac{a_{ks}}{a_{kk}}, \quad k = \overline{1, n} \end{aligned} \right\} s = \overline{1, n}.$$

Then the system (2) can be modelled by the following directed graph model:  $G = \langle V, L \rangle$  (Fig. 1)

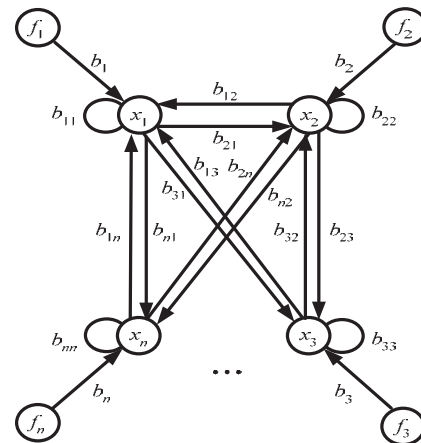


Fig. 1

where:

$V = \{x_1(t), x_2(t), \dots, x_n(t)\}$  - the set of vertexes, associated to the unknown variables in the circuit studied;

$L = \{L_{ij}, L_i\}$  - the set of arcs, taking in mind the direction of the interaction between the elements  $x_i$  and  $x_j$  of the set  $V$ , i.e.  $L_{ij} = (x_i \rightarrow x_j)$ .

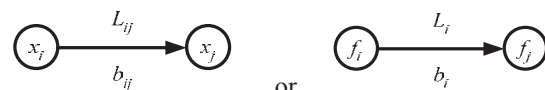


Fig. 1a

## Problem statement

The main aim of the linear electrical circuit analysis problem is obtaining the analytical expressions of the unknown variables  $x_i(t)$ ,  $i = \overline{1, n}$  as functions of the

input power sources  $f_i(t)$ ,  $i = \overline{1, n}$  using the parameters of the circuit studied.

The basic linear equation system can be written in form (1) as a result of applying the basic methods for circuit analysis – mesh or nodal analysis ((3a) and (4a), respectively). We get the transformed system (2) using the same above methods, in forms ((3b) and (4b), respectively). The associated directed graphs are shown on the Fig. 2 and 3 [3].

### 1. Mesh analysis

$$(3a) \begin{cases} Z_{11}\dot{I}'_1 + Z_{12}\dot{I}'_2 + \dots + Z_{1k}\dot{I}'_k = \pm \dot{E}'_1 \\ Z_{21}\dot{I}'_1 + Z_{22}\dot{I}'_2 + \dots + Z_{2k}\dot{I}'_k = \pm \dot{E}'_2 \\ \dots \\ Z_{k1}\dot{I}'_1 + Z_{k2}\dot{I}'_2 + \dots + Z_{kk}\dot{I}'_k = \pm \dot{E}'_k \end{cases}$$

where:

$\dot{I}' = [\dot{I}'_1, \dot{I}'_2, \dots, \dot{I}'_k]^T$  - vector of loop's currents;

$Z_{ss}$ ,  $s = \overline{1, k}$  - own impedances in loop  $s$ , i.e. the sum of impedances in loop  $s$ ;

$Z_{ps}$  - joint impedances between the loops  $p$  and  $s$ , i.e. the sum of the impedances, both included in  $p$  and  $s$  loops;

$\dot{E}'_s$ ,  $s = \overline{1, k}$  - the algebraic sum of voltage sources, included in loop  $s$ .

$$(3b) \begin{cases} \dot{I}'_1 = -\frac{Z_{12}}{Z_{11}}\dot{I}'_2 - \dots - \frac{Z_{1k}}{Z_{11}}\dot{I}'_k \pm \frac{1}{Z_{11}}\dot{E}'_1 \\ \dot{I}'_2 = -\frac{Z_{21}}{Z_{22}}\dot{I}'_1 - \dots - \frac{Z_{2k}}{Z_{22}}\dot{I}'_k \pm \frac{1}{Z_{22}}\dot{E}'_2 \\ \dots \\ \dot{I}'_k = -\frac{Z_{k1}}{Z_{kk}}\dot{I}'_1 - \frac{Z_{k2}}{Z_{kk}}\dot{I}'_2 - \dots - \frac{Z_{k(k-1)}}{Z_{kk}}\dot{I}'_{(k-1)} \pm \frac{1}{Z_{kk}}\dot{E}'_k \end{cases}$$

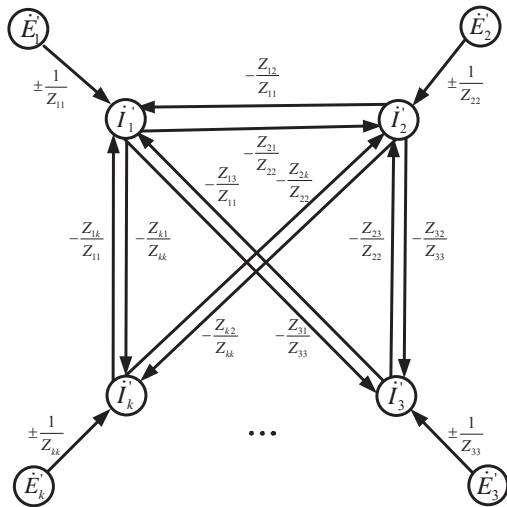


Fig. 2 The signal graph associated to the linear system

### 2. Nodal analysis

$$(4a) \begin{cases} Y_{11}\dot{V}_1 - Y_{12}\dot{V}_2 - \dots - Y_{1n}\dot{V}_n = \pm \dot{J}e'_1 \pm \sum_{\substack{j=1 \\ j \neq 1}}^n Y_{1j}\dot{E}_j = \pm \dot{J}e''_1 \\ -Y_{21}\dot{V}_1 + Y_{22}\dot{V}_2 - \dots - Y_{2n}\dot{V}_n = \pm \dot{J}e'_2 \pm \sum_{\substack{j=1 \\ j \neq 2}}^n Y_{2j}\dot{E}_j = \pm \dot{J}e''_2 \\ \dots \\ -Y_{(n-1)1}\dot{V}_1 - Y_{(n-1)2}\dot{V}_2 - \dots - Y_{(n-2)(n-1)}\dot{V}_{(n-2)} + Y_{(n-1)n}\dot{V}_{(n-1)} = \\ = \pm \dot{J}e'_{(n-1)} \pm \sum_{\substack{j=1 \\ j \neq (n-1)}}^n Y_{(n-1)j}\dot{E}_j = \pm \dot{J}e''_{n-1} \end{cases}$$

where:

$\dot{V} = [\dot{V}_1, \dot{V}_2, \dots, \dot{V}_{n-1}, \dot{V}_n = 0]^T$  - vector of potentials in the circuit's nodes;

$Y_{ss}$ ,  $s = \overline{1, (n-1)}$  - own admittances concerning the  $s$ -th node, i.e. the sum of admittances of the branches, connected to the node  $s$ ;

$Y_{ps}$  - the admittance of the branches lied between the nodes  $p$  and  $s$ ;

$\dot{J}e'_s$ ,  $s = \overline{1, (n-1)}$  - the algebraic sum of current sources in the branches, connected to node  $s$ ;

$\dot{E}_j$  - the algebraic sum of voltage sources, lied between the nodes  $j$  and  $s$ .

$$(4b) \begin{cases} \dot{V}_1 = +\frac{Y_{12}}{Y_{11}}\dot{V}_2 + \dots + \frac{Y_{1(n-1)}}{Y_{11}}\dot{V}_{n-1} \pm \frac{1}{Y_{11}}\dot{J}e''_1 \\ \dot{V}_2 = +\frac{Y_{21}}{Y_{22}}\dot{V}_1 + \dots + \frac{Y_{2(n-1)}}{Y_{22}}\dot{V}_{n-1} \pm \frac{1}{Y_{22}}\dot{J}e''_2 \\ \dots \\ \dot{V}_{n-1} = +\frac{Y_{(n-1)1}}{Y_{(n-1)(n-1)}}\dot{V}_1 + \frac{Y_{(n-1)2}}{Y_{(n-1)(n-1)}}\dot{V}_2 + \dots + \frac{Y_{(n-1)(n-2)}}{Y_{(n-1)(n-1)}}\dot{V}_{n-2} \pm \\ \pm \frac{1}{Y_{(n-1)(n-1)}}\dot{J}e''_{n-1} \\ \dot{V}_n = 0 \end{cases}$$

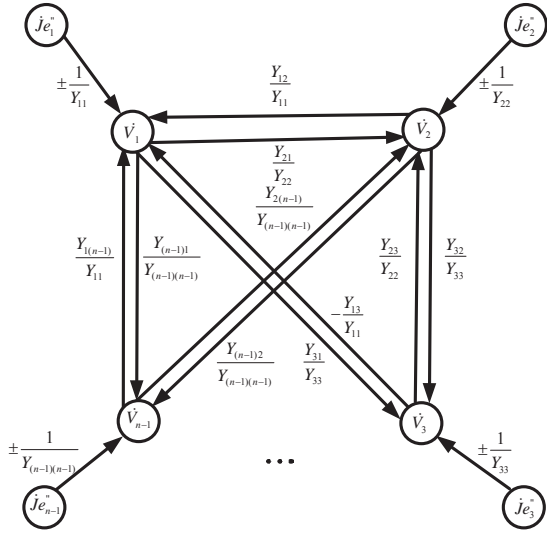


Fig. 3 The signal graph associated to the linear system

*Remark:* It is introduced the following notes about the variables  $n, m, k$  in the circuit studied:

$n$  – the number of the nodes;

$m$  – the number of branches;

$k = m - (n - 1)$  – the number of independent closed loops.

### Algorithm solving the linear equation system based on graph theory

The new algorithm, solving the system (2), requires the following input data:

$n$  – the numbers of graph vertexes, where  $n'$  – the number of initial graph vertexes,  $n''$  – the number of intermediate graph vertexes and  $n = n' + n''$ ;

*Remark:* In particular (fig. 2 and 3),  $n'$  and  $n''$  are the numbers of the power voltages' and currents' sources and loops' currents' and nodes' potentials in the circuit considered, respectively.

$V^{start} = \{V_i, i = \overline{1, r_{start}}, r_{start} < n\}$  – the set of all initial graph vertexes;

$V^{end} = \{V_i, i = \overline{1, r_{end}}, r_{end} < n\}$  – the set of all end graph vertexes.

It can be described with following procedure.

#### Step 1

It determines two squared ( $n \times n$ ) matrix associated to each vertex  $V_k, k = \overline{1, n}$

$$(5a) \quad H_{in}(k) = [h_{ij}^{in}]_{i,j=\overline{1,n}}$$

$$h_{ij}^{in} = \begin{cases} 1, & \exists \text{arc from } V_i \text{ to } V_j; \\ 0, & \text{otherwise.} \end{cases} \quad k = \overline{1, n}$$

$$(5b) \quad H_{out}(k) = [h_{ij}^{out}]_{i,j=\overline{1,n}}$$

$$h_{ij}^{out} = \begin{cases} 1, & \exists \text{arc from } V_j \text{ to } V_i; \\ 0, & \text{otherwise.} \end{cases} \quad k = \overline{1, n}$$

The matrices  $H_{in}(k)$  and  $H_{out}(k)$  take in mind the arcs inputting in and outputting from the vertex considered  $V_k$ , respectively.

#### Step 2

For each intermediate graph vertex  $V_k, k = \overline{1, n''}$  it determines:

##### 2.1. 1-st iteration - 1-step reachability

2.1.1. The reachability matrix:

$$(6) \quad H_{in}^{k(1)} = H_{in}(k), \quad k = \overline{1, n''}$$

2.1.2. All possible paths from the initial graph vertexes  $V_k, k = \overline{1, n'}$ , take in mind the 1 in matrix  $H_{in}(k)$ .

2.1.3. The expressions about the considered variables  $x_k(t), k = \overline{1, n''}$  as functions of the input power sources  $f_k(t), k = \overline{1, n'}$  using the information from 2.1.2.

##### 2.2. 2-nd iteration - 2-step reachability

2.2.1. The reachability matrix:

$$(7) \quad H_{in}^{k(2)} = H_{out}(1).H_{in}^{k(1)} + H_{out}(2).H_{in}^{k(1)} + \dots + H_{out}(n).H_{in}^{k(1)}$$

2.2.2. All possible paths from the initial graph vertexes  $V_k, k = \overline{1, n'}$ , take in mind the 1 the multiplications in resulting matrix, calculating by (7).

2.2.3. The expressions about the considered variables  $x_k(t), k = \overline{1, n''}$  as functions of the input power sources  $f_k(t), k = \overline{1, n'}$  using the information from 2.2.2.

##### 2.n. s-th iteration - s-step reachability

2.s.1. The reachability matrix:

$$(8) \quad H_{in}^{k(s)} = H_{out}(1).H_{in}^{k(s-1)} + H_{out}(2).H_{in}^{k(s-1)} + \dots + H_{out}(s).H_{in}^{k(s-1)}$$

2.s.2. All possible paths from the initial graph vertexes  $V_k, k = \overline{1, n'}$ , take in mind the 1 the multiplications in resulting matrix, calculating by (8).

2.s.3. The expressions about the considered variables  $x_k(t), k = \overline{1, n''}$  as functions of the input

power sources  $f_k(t)$ ,  $k = \overline{1, n}$  using the information from 2.s.2.

The stop criteria of calculating process on step  $s$  is arising the multiplications  $b_{ij}b_{ji}$  above the line of some of the fractions of the resulting expressions from 2.s.3.

The final expressions are obtained after dividing the expressions from 2.s.3 to the determinat of the matrix of coefficient from the right side of the system (2).

### Illustrative example

The applicability of the method suggested is illustrated to the numerical example for solving the linear equation system of 3-rd order (Fig. 4).

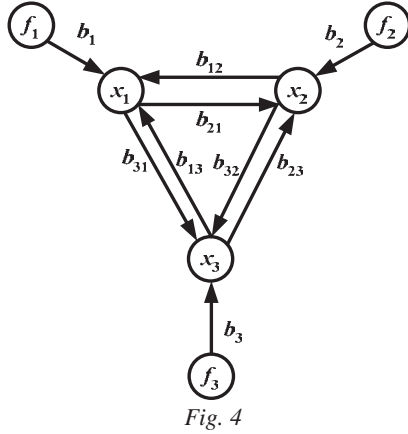


Fig. 4

In this case, the initial system (2) is written in the following form:

$$(9) \quad \begin{cases} x_1(t) = & + b_{12}x_2(t) + b_{13}x_3(t) + b_1f_1(t) \\ x_2(t) = b_{21}x_1(t) + & + b_{23}x_3(t) + b_2f_2(t), \\ x_3(t) = b_{31}x_1(t) + b_{32}x_2(t) + & + b_3f_3(t) \end{cases}$$

resp.

$$(9a) \quad \begin{cases} x_1(t) - b_{12}x_2(t) - b_{13}x_3(t) = b_1f_1(t) \\ -b_{21}x_1(t) + x_2(t) - b_{23}x_3(t) = b_2f_2(t) \\ -b_{31}x_1(t) - b_{32}x_2(t) + x_3(t) = b_3f_3(t) \end{cases} \Leftrightarrow Bx = g$$

Using the traditional methods, the solution of linear equation system (9) is following:

$$(10) \quad \begin{aligned} x(t) &= [x_1(t), x_2(t), x_3(t)]^T = \\ &= \begin{bmatrix} \frac{(-1+b_{23}*b_{32})*b_1*f_1-(b_{12}+b_{13}*b_{32})*b_2*f_2-(b_{12}*b_{23}+b_{13})*b_3*f_3}{\det(B)} \\ \frac{-(b_{21}+b_{31}*b_{23})*b_1*f_1+(-1+b_{13}*b_{31})*b_2*f_2-(b_{23}+b_{13}*b_{21})*b_3*f_3}{\det(B)} \\ \frac{-(b_{21}*b_{32}+b_{31})*b_1*f_1-(b_{32}+b_{12}*b_{31})*b_2*f_2+(-1+b_{12}*b_{21})*b_3*f_3}{\det(B)} \end{bmatrix} \\ \det(B) &= -1+b_{23}*b_{32}+b_{12}*b_{21}+b_{13}*b_{31}+b_{21}*b_{13}*b_{32}+b_{31}*b_{12}*b_{23} \end{aligned}$$

Applying the new method, based on graph theory, the final solution gets by following way:

### 1-st iteration

$$(11) \quad x^{(1)}(t) = \begin{bmatrix} x_1^{(1)}(t) \\ x_2^{(1)}(t) \\ x_3^{(1)}(t) \end{bmatrix} = \begin{bmatrix} \frac{-b_1*f_1}{\det(B)} \\ \frac{-b_2*f_2}{\det(B)} \\ \frac{-b_3*f_3}{\det(B)} \end{bmatrix}$$

### 2-nd iteration

$$(12) \quad x^{(2)}(t) = \begin{bmatrix} x_1^{(2)}(t) \\ x_2^{(2)}(t) \\ x_3^{(2)}(t) \end{bmatrix} = \begin{bmatrix} x_1^{(1)}(t) + \frac{b_{23}*b_{32}*b_1*f_1-b_{12}*b_2*f_2-b_{13}*b_3*f_3}{\det(B)} \\ x_2^{(1)}(t) + \frac{-b_{21}*b_1*f_1+b_{13}*b_{31}*b_2*f_2-b_{23}*b_3*f_3}{\det(B)} \\ x_3^{(1)}(t) + \frac{-b_{31}*b_1*f_1-b_{32}*b_2*f_2+b_{12}*b_{21}*b_3*f_3}{\det(B)} \end{bmatrix}$$

### 3-rd iteration

$$(13) \quad \begin{aligned} x^{(3)}(t) &= \begin{bmatrix} x_1^{(3)}(t) \\ x_2^{(3)}(t) \\ x_3^{(3)}(t) \end{bmatrix} = \begin{bmatrix} x_1^{(2)}(t) - \frac{b_{13}*b_{32}*b_2*f_2+b_{12}*b_{23}*b_3*f_3}{\det(B)} \\ x_2^{(2)}(t) - \frac{b_{31}*b_{23}*b_1*f_1+b_{13}*b_{21}*b_3*f_3}{\det(B)} \\ x_3^{(2)}(t) - \frac{b_{21}*b_{32}*b_1*f_1+b_{12}*b_{21})*b_3*f_3}{\det(B)} \end{bmatrix} = \\ &= \begin{bmatrix} \frac{(-1+b_{23}*b_{32})*b_1*f_1-(b_{12}+b_{13}*b_{32})*b_2*f_2-(b_{12}*b_{23}+b_{13})*b_3*f_3}{\det(B)} \\ \frac{-(b_{21}+b_{31}*b_{23})*b_1*f_1+(-1+b_{13}*b_{31})*b_2*f_2-(b_{23}+b_{13}*b_{21})*b_3*f_3}{\det(B)} \\ \frac{-(b_{21}*b_{32}+b_{31})*b_1*f_1-(b_{32}+b_{12}*b_{31})*b_2*f_2+(-1+b_{12}*b_{21})*b_3*f_3}{\det(B)} \end{bmatrix} \end{aligned}$$

### 4-th iteration

$$(14) \quad x^{(4)}(t) = \begin{bmatrix} x_1^{(4)}(t) \\ x_2^{(4)}(t) \\ x_3^{(4)}(t) \end{bmatrix} = \begin{bmatrix} x_1^{(3)}(t) + \frac{(b_{21}*b_{13}*b_{32}+b_{31}*b_{12}*b_{23})*(b_1*f_1+b_2*f_2+b_3*f_3)}{\det(B)} \\ x_2^{(3)}(t) + \frac{(b_{21}*b_{13}*b_{32}+b_{31}*b_{12}*b_{23})*(b_1*f_1+b_2*f_2+b_3*f_3)}{\det(B)} \\ x_3^{(3)}(t) + \frac{(b_{21}*b_{13}*b_{32}+b_{31}*b_{12}*b_{23})*(b_1*f_1+b_2*f_2+b_3*f_3)}{\det(B)} \end{bmatrix}$$

$$\det(B) = -1+b_{23}*b_{32}+b_{12}*b_{21}+b_{13}*b_{31}+b_{21}*b_{13}*b_{32}+b_{31}*b_{12}*b_{23}+b_{13}*b_{31}$$

It is obvious, that that the final solution of system (9) obtains on the 3-rd iteration of the proposed procedure because the fact that the multiplications on type  $(b_{21} * b_{13} * b_{32} + b_{31} * b_{12} * b_{23})$  arised on the 4-th iteration of the algorithm suggested. It shows that we go between the vertexes  $x_1(t) - x_2(t) - x_3(t)$ , formed the closed loop in graph model considered (Fig.4).

### Conclusion

The new graph method suggested is better than traditional math's methods, solving the linear system of circuit equations, because it consists of  $n$  multiplications of squared  $(nxn)$  matrices on the  $i$ -th iteration and the most of elements of these matrices are 0, compared with



the Gauss method which has a  $(i+1)$  multiplications on the  $i$ -th iteration. The number of necessary iterations in both methods is  $n$ .

The new graph method proposed is simpler than well known method based on Mason's gain formulae because of the fact that it is necessary to determine only all possible paths in graph considered from initial to intermediate graph vertexes and to take in mind the respective weight coefficients of these arcs, while Mason's gain formula require obtaining of the all possible paths between the arbitrary graph vertexes; all pairs loops, which have no joint arcs; all three loops, which have no joint arcs; all four loops, which have no joint arcs and etc. and to take in mind the associated coefficients on these paths.

### References

- [1] W. Press, B. Flannery, S. Teukolsky, W. Vetterling, Numerical Recipes, Cambridge University Press
- [2] Форсайт, Дж., М. Малкълм, К. Молър, Компютърни методи за математични пресмятания, Наука и изкуство, София 1986
- [3] Фархи, С., С. Папазов. Теоретична електротехника, ч. I, Издателство Техника, София, 1992, 664 стр.



**Simona Petrakieva** was born in Sofia, Bulgaria, on May 25, 1971. She has studied at the Technical University of Sofia-Bulgaria and received Phd degree there in 2005.

She has worked in the Faculty of Automatics in the Technical University of Sofia since 2000 as an assistant professor.

She works in: analysis and synthesis of the linear and nonlinear electrical circuits, graph theory, systems' stability analysis, neural networks.

Simona Petrakieva is with the Faculty of Automatics, Technical University of Sofia, 8, Kl. Ohridski Blvd., 1000 Sofia, Bulgaria (e-mail: petrakievas-te@tu-sofia.bg)



**Valeri Mladenov** was born in Vratza, Bulgaria, on December 3, 1960. He has studied at the Technical University of Sofia-Bulgaria and received Phd degree there in 1993.

He has worked in the Faculty of Automatics in the Technical University of Sofia since 1986 (an assistant professor), 1999 (associate professor) and since 2004 Dr. Mladenov is head of department Theory of Electrical Engineering.

He interested in: analysis and synthesis of the linear and nonlinear electrical circuits, neural networks, signal processing, graph theory.

Valeri Mladenov is with the Faculty of Automatics, Technical University of Sofia, 8, Kl. Ohridski Blvd., 1000 Sofia, Bulgaria (e-mail: valerim@tu-sofia.bg)

# Reconstruction of Current Density Vectors by Locally Measured Magnetic Field Data

Iliana Marinova and Valentin Mateev

**Abstract:** In this paper we apply an inverse approach for 3D current sources reconstruction using measured magnetic field data. The reconstruction approach is based on the 3D Green's function. The developed approach was effectively applied for current source distribution reconstruction of coil in linear non-magnetic media.

**Keywords:** inverse source problem, Green's function, magnetic field, current distribution.

## Introduction

The current density vector distributions are of paramount importance solving various problems during nondestructive testing (NDT), electromagnetic compatibility, identifications, medical diagnosis and etc [1-14].

In eddy current NDT, current source reconstruction algorithms and methods are widely used to realise precise testing, control and inspection. The locally measured data of the electromagnetic field during NDT are processed for defects and cracks identification and visualisation by reconstruction algorithm. The current distribution changes according to relative space locations, shapes, numbers and dimensions of the existed defects or cracks in inaccessible for direct measurements region.

Current source distributions in biological structures are extremely important for medical diagnosis and therapy treatments in various biomagnetic applications.

Magneto CardioGraphy (MCG) and Magneto EncephaloGraphy (MEG) process measured biomagnetic field data outside the human body, near the chest or head, for inside current imaging used for medical diagnoses.

In magnetic stimulation therapy applications, current pulses are supplied to the coil to produce a strong magnetic field to stimulate nerve fibres. Magnetic stimulation occurs as result of the current flow and the accompanying electric field induced in the tissue by an externally applied magnetic field. Determination of magnetic field and current distributions in the tissue in order to generate prescribed stimulation effect is an inverse source problem [10].

The current density distribution is basic part in coil design optimisation and electromagnetic systems syntheses.

In this paper we apply an inverse approach for 3D current sources reconstruction using measured magnetic field data. The reconstruction approach uses 3D Green's function. The magnetic fields are measured in a surface mesh over the tested object region. These data are used

for field source reconstruction in inaccessible for direct measurements region.

The developed reconstruction approach is effectively applied for current source distribution reconstruction of a circular coil in linear non-magnetic media.

## Problem description

The investigated magnetic fields exist in domains shown in Fig.1.

Let consider the domains  $\Omega$ ,  $\Omega_1$  and  $\Omega_2$ , to be the whole domain, current source domain and the surrounding domain respectively, ( $\Omega = \Omega_1 \cup \Omega_2$ ). The domain  $\Omega_2$  is separate in two sub domains  $\Omega_2^I$  and  $\Omega_2^{II}$ , ( $\Omega_2 = \Omega_2^I \cup \Omega_2^{II}$ ). The magnetic field distribution could be directly measured only in a region  $\Omega_2^I$ . The  $\Omega_2^{II}$  is treated as an inaccessible for direct magnetic field measurements region.

The measured magnetic field distribution is used for field source determination in  $\Omega_1$  region.

After the field source determination in  $\Omega_1$  region the magnetic field distribution in all  $\Omega$  domains can be achieved and visualized.

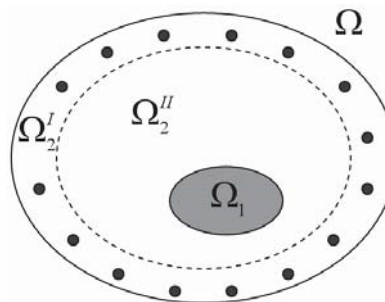


Fig.1. Schematic diagram of magnetic field domains.

## Magnetic field distribution

Distribution of static magnetic field in 3D free space created by circular coil in domains from Fig.1 will be analyzed.

As mention above  $\Omega$ ,  $\Omega_1$  and  $\Omega_2$  are the whole domain, coil and the air domain respectively, shown in Fig.2.

The magnetic field distribution in  $\Omega$  is analyzed by magnetic vector potential  $\mathbf{A}$  introduced by, where  $\mathbf{B}$  is the magnetic flux density vector,  $\mathbf{B} = \mu\mathbf{H}$ ;  $\mathbf{H}$  is the

magnetic field intensity vector;  $\mu = \mu_0$  is magnetic permeability of vacuum.

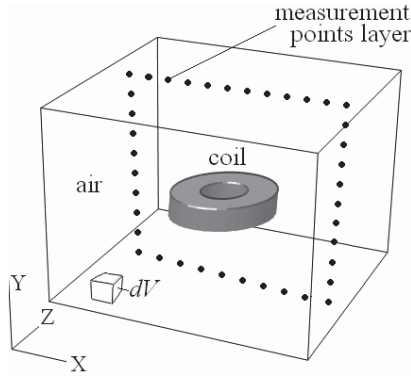


Fig.2. Model geometry structure.

The governing equation with magnetic vector potential in  $\Omega$  domain is as following

$$(1) \quad \frac{1}{\mu} \nabla^2 \mathbf{A} = -\mathbf{J},$$

where  $\mathbf{J}$  is the source current density vector.

Equation (1) is solved for domain structure in Fig.2 with Coulomb gauge  $\nabla \cdot \mathbf{A} = 0$  in  $\Omega$  volume and Dirichlet boundary condition.

Magnetic field is measured in points of the region  $\Omega_2^I$ . Single layer of measurement mesh is shown in Fig.2. Full measurement mesh completely surrounds the  $\Omega_2^{II}$  region.

### Reconstruction approach

The developed approach is suitable for current source distribution reconstruction of coil in homogenous, linear non-magnetic media ( $\mu = \mu_0$ ). Solution of (1) for magnetic vector potential  $\mathbf{A}$  is expressed by (2)

$$(2) \quad \mathbf{A} = \mu \int_{\Omega} G \mathbf{J} d\Omega.$$

where  $G$  is 3D Green's function given by equation (3)

$$(3) \quad G = \frac{1}{4\pi r},$$

where  $r$  is the distance radius-vector between coordinates of each measurement mesh nodes and current source nodes,

$$(4) \quad r_{ij} = \sqrt{(x_j - x_i)^2 + (y_j - y_i)^2 + (z_j - z_i)^2}$$

where  $(x_i, y_i, z_i)$  are coordinates of each measurement mesh node;

$(x_j, y_j, z_j)$  are coordinates of current source nodes.

In order to realize the reconstruction approach the whole domain  $\Omega$  is divided in elementary volumes  $dV_j (j = 1, \dots, m)$ . The magnetic field distribution is measured in  $n$  points in  $\Omega_2^I$  as shown in Fig. 2.

For determination of field sources distribution (2) is transformed in system of linear equations (5).

$$(5) \quad \mathbf{Y} = \int_{\Omega} \mathbf{C} \mathbf{X} d\Omega,$$

where  $\mathbf{Y}$  is the vector with measured values  $\mathbf{Y}_i$  presented by (6) and (7)

$$(6) \quad \mathbf{Y} = [Y_1, Y_2, \dots, Y_n]^T.$$

$$(7) \quad \mathbf{Y} = \sum_{j=1}^m c_j x_{ij} = c_1 x_{s1} + c_2 x_{s2} + \dots + c_m x_{sm}.$$

where  $x_j$  is given by equation (8)

$$(8) \quad \mathbf{x}_{sj} = \mathbf{X}_{sj} dV_j.$$

In elementary domain  $dV$  a constant current density value is used  $\mathbf{X}_{sj} = \text{const}$ .

$\mathbf{c}_i$  is determine with equation (9) by Green's function  $G_{ij}$  for  $i = 1, \dots, n$  and  $j = 1, \dots, m$ .

$$(9) \quad \mathbf{c}_j = [G_{1j}, G_{2j}, \dots, G_{nj}]^T.$$

Finally  $\mathbf{c}_i$  is given by equation (10).

$$(10) \quad \mathbf{c}_j = \frac{\mu_0}{4\pi} \left[ \frac{n_j e_{1j}}{r_{1j}}, \frac{n_j e_{2j}}{r_{2j}}, \dots, \frac{n_j e_{nj}}{r_{nj}} \right].$$

where:

$\mathbf{n}_j$  is the normal direction vector with direction of  $\mathbf{x}_{sj}$ ;

$\mathbf{e}_{ij}$  - direction vector between current source  $j$  - point to field measurements  $i$  - point;

$r_{ij}$  - radius vector between current source  $j$  - point to field measurements  $i$  - point. [9]

### Implementation

Proposed reconstruction approach is applied with modeled magnetic field distribution.

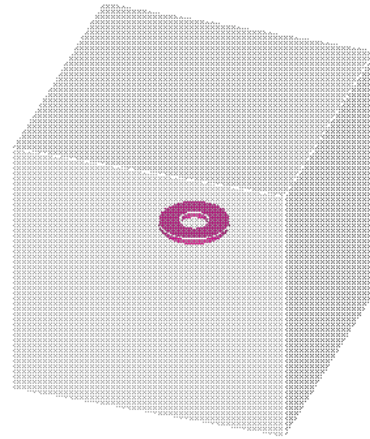


Fig.3. FEM model geometry.

For modeling of magnetic field distribution in 3D free space produced by circular coil a Finite Element Method (FEM) model is developed. The model geometry is shown in Fig.3.

The coil dimensions are: outer diameter - 60mm, inner diameter - 30mm and depth - 15mm. The  $\Omega$  region

is a cube with sides equal to 200mm. Measurement mesh around the  $\Omega_2^I$  region is with equal step of 5mm in X, Y and Z directions.

Coil current density is  $5A/mm^2$  on its cross-section.

Magnetic field intensity vectors  $\mathbf{H}$  distribution around the coil is visualized and shown in Fig.4.

The magnetic field intensity vectors  $\mathbf{H}$  distribution around the coil in measurement mesh nodes was captured and stored.

Magnetic field intensity vectors  $\mathbf{H}$  in measurement mesh nodes are shown in Fig.5.

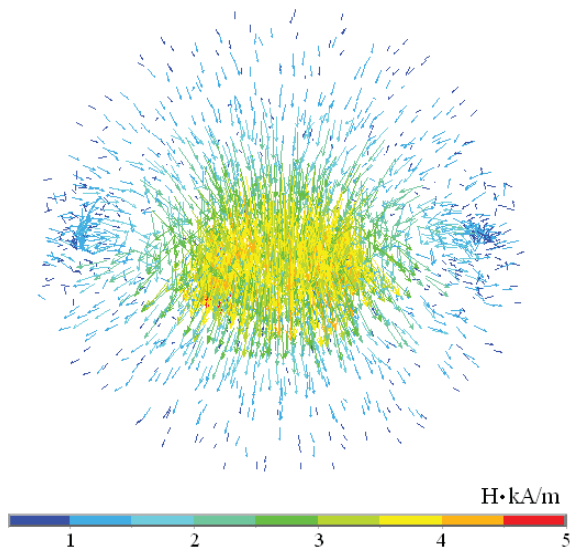


Fig.4. Magnetic field intensity vectors around the coil.

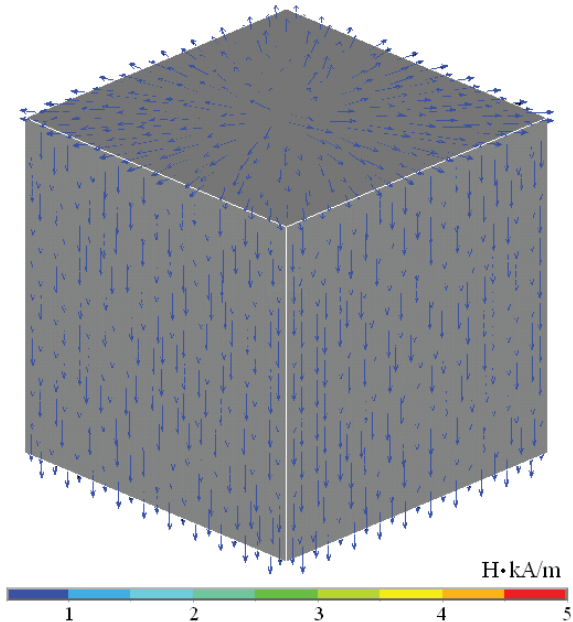


Fig.5. Magnetic field intensity vectors in  $\Omega$  surface.

Stored field data was processed with proposed reconstruction approach.

Reconstruction approach is realized as Matlab program. All mathematical operations as matrix storage, solvers and visualization functions. are handled by Matlab environment.

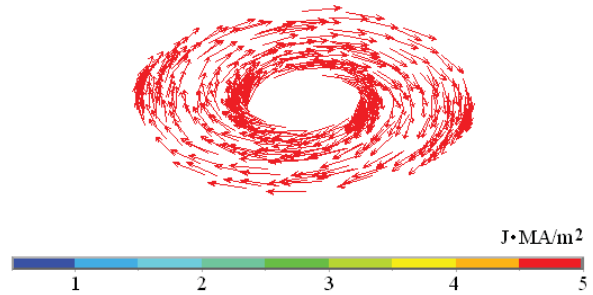


Fig.6. Current density vectors.

The 3D reconstruction of the source current vectors distribution are realized and visualized in Fig.7. The inverse problem for current source distribution reconstruction in the region of interest  $\Omega$  is solved.

In order to compare the results obtained by 3D reconstruction approach we use the known excitation source current vectors used in FEM model shown in Fig.6.

It was found good coincidence of the results obtained using the 3D reconstruction approach in Fig.7. and those from FEM model in Fig.6.

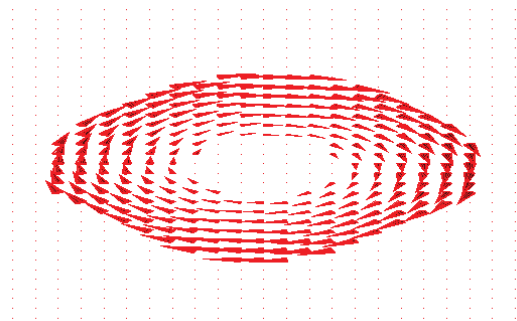


Fig.7. Reconstructed current density vectors.

## Conclusion

In this paper we apply an inverse approach for 3D current sources reconstruction using magnetic field locally measured data. The reconstruction approach uses the 3D Green's function.

The developed reconstruction approach is effectively applied for current source distribution reconstruction of a circular coil in linear non-magnetic media.

Finite element numerical experiment was made for determination of magnetic field distribution around circular coil. The magnetic field values in measurement mesh was stored and visualized. Stored data was processed with proposed reconstruction approach. The magnetic field distribution is determined in a surface mesh over the tested object region. This data is used for



field source reconstruction in the inaccessible for direct measurements region.

The proposed approach can be used in many practical activities for electrical current determination and visualisation in inaccessible region only by measured external magnetic field. Also activities in NDT, biomagnetic applications, magnetic field experimental studies, coil optimisation or education studies could be realized by this approach.

The proposed approach could be further developed for current source distribution reconstruction of conductor in non-linear magnetic media.

Researches over the proposed approach sensitivity and accuracy could be further conduct. Also a practical application of the approach must be made.

### Acknowledgements

Parts of this research are supported by project 8059NI-1 of the R&DS at TU-Sofia.

### References

- [1] Kojima, F., K. Ito. Reconstruction of Magnetic Charge Densities Using Regularization of Bounded Variations under Noisy Observations. *International Journal of Applied Electromagnetics and Mechanics*, Vol. 19, 2004, pp. 309-313.
- [2] Rubinacci, G., A. Tamburrino, S. Ventre, F. Villone. Shape Identification in Conductive Materials by Electrical Resistance Tomography in E'NDE. *Electromagnetic Non-destructive Evaluation*, Vol. VI, IOS Press, 2002, pp. 13-20.
- [3] Huang, H., T. Takagi and H. Fukutomi. Fast Signal Predictions of Noised Signals in Eddy Current Testing. *IEEE Trans. Magn.* Vol. 36, No. 4, July 2000, pp. 1719-1723.
- [4] Marinova, I., S. Hayano, Y. Saito. Inverse Approach For Shape Design Of Magnetic Core. *IEEE Trans on Magnetics*, Vol. 31, No. 3, May, 1995, pp. 1992-1995.
- [5] Marinova, I., H. Endo, S. Hayano, Y. Saito. Image Reconstruction for Electromagnetic Field Visualization by an Inverse Problem Solution. *Int. Journal of Applied Electromagnetics and Mechanics*, Vol. 15, 2001/2002, IOS Press, pp. 403-408.
- [6] Marinova, I., H. Endo, S. Hayano, Y. Saito. Inverse Electromagnetic Problems by Field Visualization. *IEEE Trans. Magn.* Vol. 40, No. 2, 2004, pp.1088-1093.
- [7] Doi, T., S. Hayano, I. Marinova, Y. Saito. Defect Recognition in Conductive Materials by Local Magnetic Field Measurement. *Journal of Applied Physics*, Vol. 75, No. 10, 1994, pp. 5907-5909.
- [8] Endo, H., Y. Saito. Smart Visualization and Computer Vision in Electromagnetism. *Int. Journal of Applied Electromagnetics and Mechanics*. Vol. 15, 2001/2002, IOS Press, pp. 337-342.
- [9] Ячев, И., И. Маринова. Числени методи за моделиране на вериги и полета - I. Издателство на ТУ-София, 2007.
- [10] Marinova, I., L. Kovachev. Inverse Approach for Determination of the Coils Location During Magnetic Stimulation. 3-rd Japanese-Bulgarian-Macedonian joint seminar on applied electromagnetics. Ohrid, 2000, pp. 140-145.

[11] Tamburrino, A., G. Rubinacci. A new non-iterative inversion method for Electrical Resistance Tomography. *Inverse Problems*, Vol. 18, 2002, pp. 1809-1829.

[12] Tamburrino, A., G. Rubinacci, M. Soleimani, W. Lionheart. A Noniterative Inversion Method For Electrical Resistance, Capacitance And Inductance Tomography For Two Phase Materials. *proceedings of 3rd World congress on Industrial Process Tomography*, The Rockies, Alberta, Canada, 2003.

[13] Rubinacci, G., A. Tamburrino. A non-iterative ECT data inversion algorithm. *Proc. of the 8-th International Workshop on Electromagnetic Nondestructive Evaluation*, Saarbruecken, Germany, 2002.

[14] F. Ferraioli, A. Formisano, R. Martone "An Electrical Resistive Tomography Based on Direct Information E'NDE 2003 Saclay, Paris, France.



**Iliana Marinova** was born in Pleven, Bulgaria, on June 10, 1959. She studied at the Technical University of Sofia and received PhD. degree from the same university in 1989.

Since 1988 she worked in the Faculty of Electrical Engineering of the Technical University of Sofia as a associate professor and researcher.

Her field of interest includes inverse problems in electromagnetics and biomagnetics, electromagnetic fields, numerical methods, finite element method, boundary integral equation method, computer-aided design, optimization, image processing and visualization.

Iliana Marinova is with the Faculty of Electrical Engineering, Technical University of Sofia, 8, Kl. Ohridski Blvd., 1000 Sofia, Bulgaria (e-mail: iliana@tu-sofia.bg).



**Valentin Mateev** was born in Sofia, Bulgaria, on March 1, 1979. He graduated from the Technical University of Sofia with Master degree in electrical engineering.

Since 2006 he worked in the Faculty of Electrical Engineering of the Technical University of Sofia as a assistant and PhD student.

His field of interest includes inverse problems in electromagnetics, electromagnetic fields, finite element method, image processing, computer-aided design.

Valentin Mateev is with the Faculty of Electrical Engineering, Technical University of Sofia, 8, Kl. Ohridski Blvd., 1000 Sofia, Bulgaria (e-mail: vmateev@tu-sofia.bg).

# Magnetic Field Visualization by Array Sensor Systems

Valentin Mateev and Iliana Marinova

**Abstract:** In this paper, Anisotropic Magneto-Resistive (AMR) sensors are applied for magnetic field measurements. AMR sensors are combined in array probes in order to increase productivity of measurement process and improving the performance of probes. Proposed sensor could be used for measurements of magnetic field applied to biomagnetic structures, non-destructive testing as well as for field distribution investigations and calibrations. Software tool for measured field data visualization is developed.

**Keywords:** magnetoresistive sensors, sensor array, magnetic field distribution, biomagnetic structures.

## Introduction

Magnetic fields measurements are widely used in medicine for magnetic therapy and diagnosis. The main advantages are noninvasive, noncontact and painless nature of the magnetic field interactions.

Magnetic field measurements are applied in magnetic and eddy current non-destructive testing (NDT) and inspections. [10-18, 21-25]

Magnetic fields measurements are also needed for field distribution investigations and calibrations.

Precise determination of magnetic field distribution in order to assure high measurement accuracy is important experimental problem [1].

In this paper the Anisotropic Magneto-Resistive (AMR) sensors are applied for magnetic field measurements. AMR sensors are based on Anisotropic magnetoresistance effect: the resistivity of ferromagnetic alloys measured in a direction parallel to the magnetization of permalloy film is slightly higher than the resistivity measured perpendicular to the magnetization. The main advantages of AMR sensors compared to Hall effect sensors are:

- high sensitivity;
- higher accuracy;
- no piezo effect;
- higher operational temperatures.

AMR sensors are combined in array probes in order to increase productivity of measurement process and to improve the performance of probes applied for magnetic field measurements in space around coils.

The AMR magnetic sensors and sensor arrays offer improvements in speed and resolution in eddy-current testing and bio-magnetic imaging.

Arrays of AMR magnetic sensors allow rapid scanning of an area of interest in a single pass. The small size and low power consumption of these solid-state magnetic sensors enable the fabrication of compact arrays

of sensors on circuit boards and even on-chip sensor arrays.

The use of magneto-resistive sensors and gradient sensors is demonstrated in detection and magnetic imaging in eddy current non-destructive testing [2-5]. These solid-state magnetic sensors can be used in arrays of multiple sensors on a single chip facilitating rapid scanning of an area in a single pass rather than by single-point, raster scanning.

Arrays of very small magnetic sensors can be used to detect very small magnetic fields with very high spatial resolution.

The applications of magneto-resistive sensor array devices include magnetic biosensors, bio-magnetic sensors, non-destructive evaluation, and magnetic imaging.

## AMR Sensors

AMR sensors Philips KMZ10B are used. The KMZ10B is a sensitive magnetic field sensor, employing the magnetoresistive effect of thin-film permalloy. Its properties enable this sensor to be used in a wide range of applications for current and field measurement, revolution counters, angular or linear position measurement, proximity detectors, etc.

KMZ10B field resolution is about 1nT in frequency range from DC to 1MHZ). [5, 6]

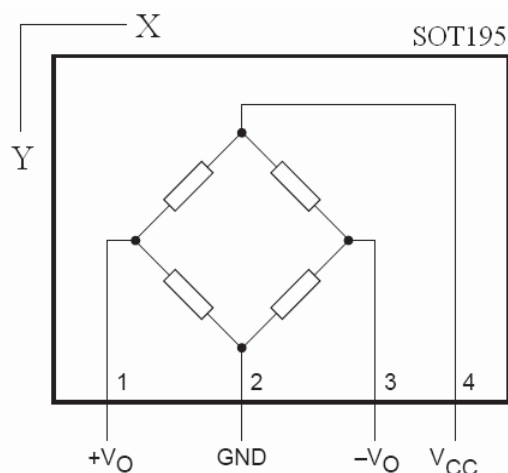


Fig.1. KMZ10B circuit diagram.

KMZ10B1 operational voltages are:

$\pm V_O$  is output voltage;

$V_{CC}$  - supply voltage;

GND - ground potential.

KMZ10B1 magnetic field sensitive direction is Y – axes according to Fig. 1-4.

KMZ10B1 sensor inner circuit and SOT – 195 package is shown in Fig.1. [5-6]

A detailed description of physical principles of sensor function of AMR sensors can be found in [5].

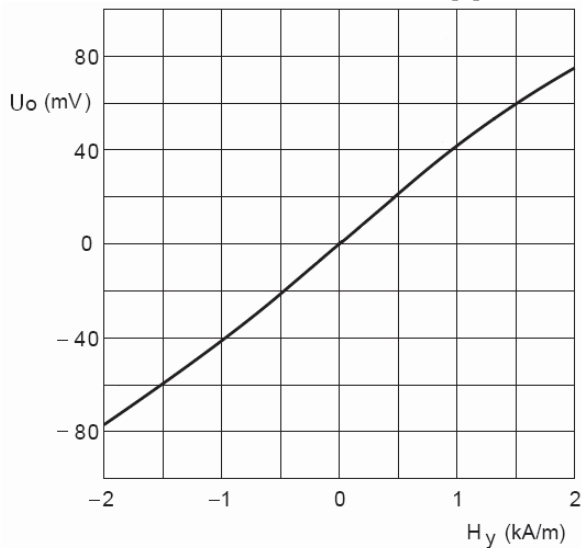


Fig.2. Sensor output characteristic.

Measured voltage is related to magnetic field intensity by sensor output characteristic. Sensor output characteristic at 10V supply voltage is shown in Fig. 2. Magnetic flux density  $B_y$  is calculated by equation(1).

$$(1) \quad B_y = \mu_0 H_y .$$

where  $\mu_0$  is magnetic permeability of vacuum,  $\mu_0 = 1,25 \cdot 10^{-6} \text{ H / m}$ .

Maximal magnetic field straight  $H_y$  value that can be measured accurately by the sensor is 2kA/m or in air the flux density  $B_y$  will be 2,5mT.

### Sensor Arrays

Sensor array design depends largely upon the specific application. Arrays can include two- and three-axis sensors to measure vector fields. They can be configured as extended one-dimensional arrays to survey a wide area in a single pass. Two-dimensional arrays of sensors can be left in place to survey an area without moving the array.

The design of a two-dimensional array with 9 sensors is shown in Fig.3. Each sensor is a Wheatstone bridge shown in Fig.1. The bridges are connected in parallel with a common supply and ground. An example of a two-dimensional array of seven sensors is shown in Fig.4.

This array can assure direct magnetic field image as well as field gradient in XZ plane.

The total width of both arrays is 16 mm and the length is 22 mm. They are detecting the vertical component (Y) of the magnetic field.

Design of a two-dimensional array with 8 sensors is shown in Fig.5. This type of sensor can assure simultaneously information of two components of magnetic field flux density components (X-Y).

### Measurements setup

Several types for sensor signal pick up circuit systems are considered. Fig. 6-8.

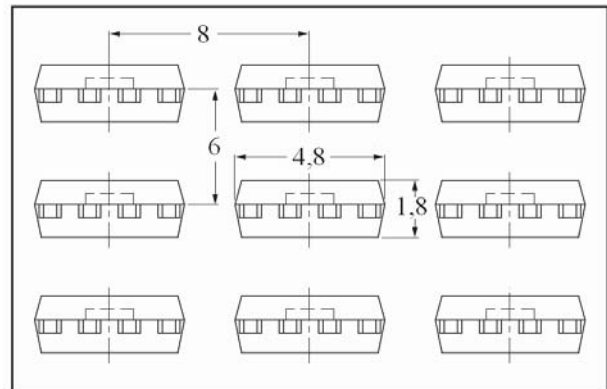


Fig.3. 3x3-element square array.

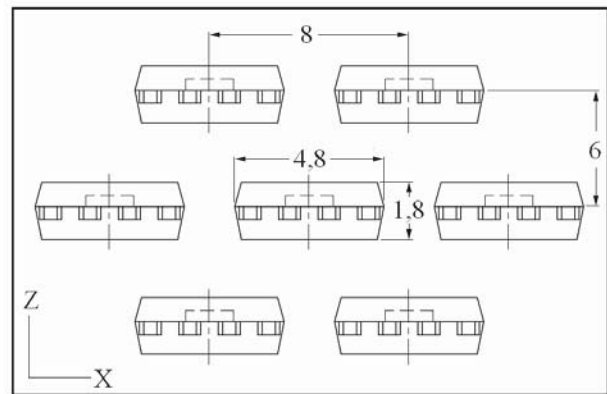


Fig.4. 7-element hexagonal array.

First array circuit shown in Fig.5 is based on National Instruments USB-6008 data acquisition device. Voltage range of USB-6008 is 10V at resolution 14,7mV with accuracy  $\pm(1,7\%)$  [7]. Limitation of this circuit is the number of analog input channels of data acquisition device.

Second array circuit shown in Fig.6 uses multiplexing IC controlled by a signal generator. Pick-up voltage signal is measured with Protek-506 Digital multimeter with voltage range 400mV at resolution 0,1mV with accuracy  $\pm(1,5\%)$ . [9]

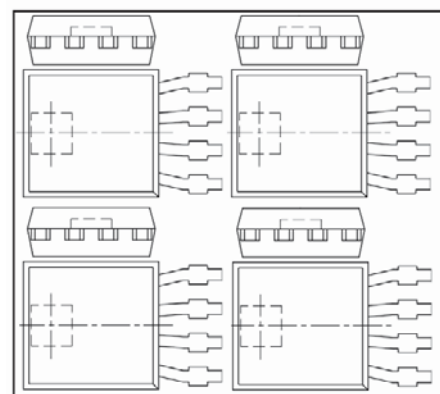


Fig.5. X-Y magnetic field flux density components array.

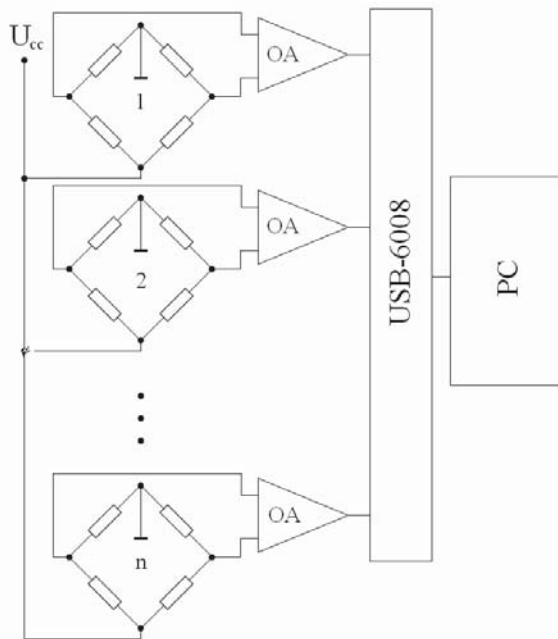


Fig.6. Signal pick-up circuit with USB-6008.

USB-6008 is directly connected to the PC and LabVIEW. Virtual instrument is created for signal processing and storage.

Protek-506 uses RS-232 interface for data collection [9].

Third array circuit shown in Fig.8 is a combination of both previously considered systems. It uses multiplexing IC controlled by a signal generator and USB-6008 DAQ device. Multiplexor IC unit controls the portions of data to USB-6008 DAQ device. Maximal capacity of this circuit with 8ch. (multiplexor IC)  $\times$  8ch.(DAQ)=64ch. or 64 sensor elements.

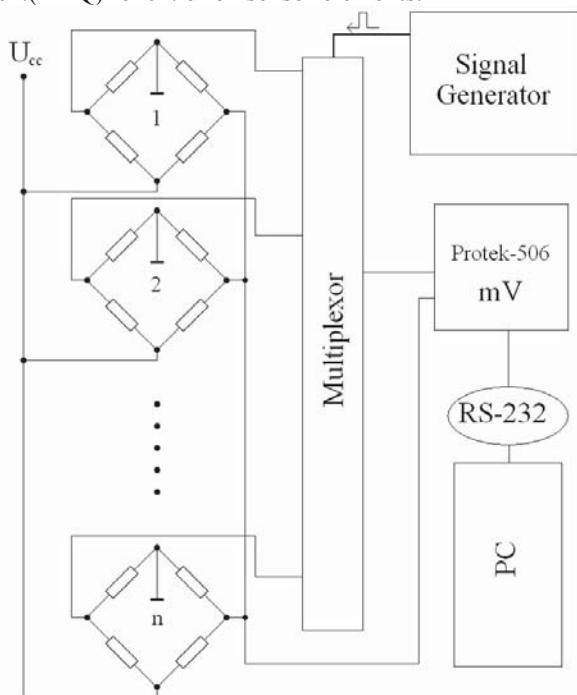


Fig.7. Signal pick-up circuit with Protek506.

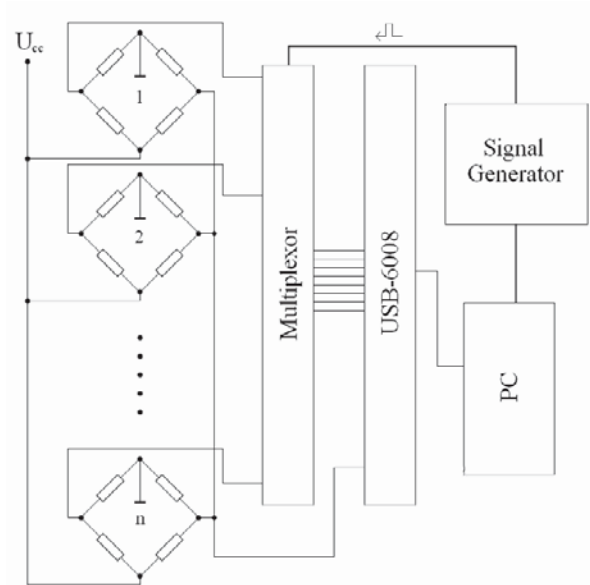


Fig.8. Signal pick-up circuit.

### Signal multiplexing

Multiplexer, shown in Fig.8, activates eight pick-up AMR sensors at the time. The receiving configuration may be composed up to 64 sensor elements. Eight channels are activated in eight acquisition time intervals (or time slots of DAQ) to activate the complete probe in a very short period of time.

This multiplexing technique provides a large coverage in a single inspection pass while maintaining high scanning resolution.

Also, it reduces the need for complex robotics to move the probe so the simple manual scan is often enough when using width array probe.

### Field source

Magnetic field distribution around coil is measured. Coil has 5500 turns and it is fed with 50mA current. Coil spool dimensions are shown in Fig.9.

### Field distributions

Magnetic field distribution is measured in XZ plane around the coil. Measurement grid with 10mm step by X and Z axis is used. Measured distribution is shown in Fig.8.

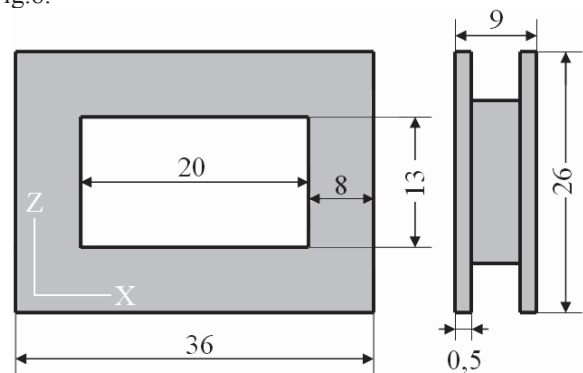


Fig.9. Coil spool.



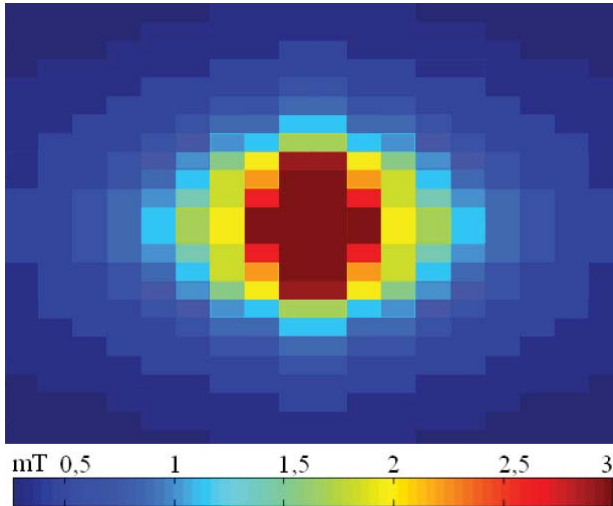


Fig.10. Measured flux density  $B_y$  around the coil with single AMR sensor.

For measured results comparison a magnetic field distribution model is developed.

Magnetic flux density caused by coil is calculated by Biot-Savart law (2).

$$(2) \quad B_y(x, y, z) = \frac{\mu_0}{4\pi} \int_{\Omega} \frac{J}{r^2} d\Omega .$$

where

$B_y(x, y, z)$  is the magnetic flux density y-component

in  $(x, y, z)$  position around the coil;

$r$  - radius vector between measurement sensor position and coil given by (3);

$J$  - current density in coil;

$\Omega$  - area of interest around the coil.

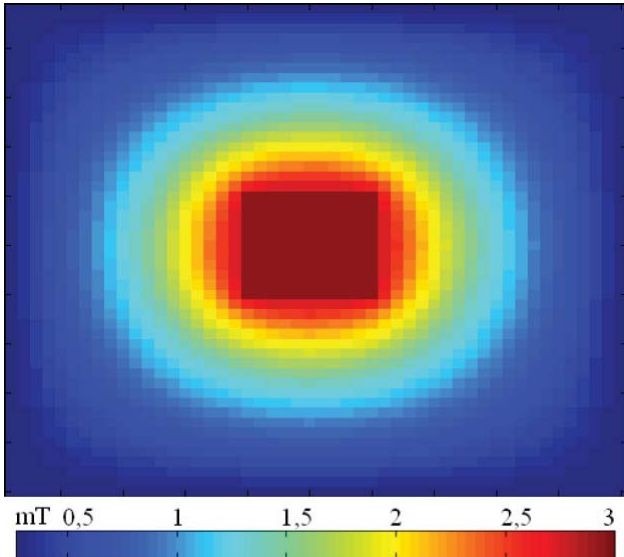


Fig.11. Modeled  $B_y$  distribution.

$$(3) \quad r = \sqrt{(x - x_0)^2 + (y - y_0)^2 + (z - z_0)^2} .$$

Calculated results for component  $B_y$  of coil from Fig.8 is shown in Fig.9.

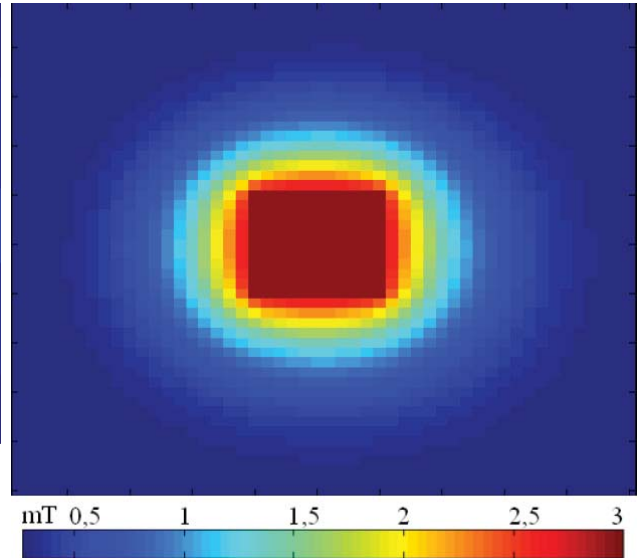


Fig.12. Measured flux density  $B_y$  around the coil with 3x3 array sensor.

### Software module

A computer software for magnetic field modelling, simulation and visualisation of data measured by different types of array sensors is developed.

The program is built as a MatLab toolbox with its own Graphical User Interface (GUI).

The program uses as an input measured data. Data can be read from ASCII file or real time measuring process through Analogue to Digital Converter (ADC) hardware interfacing directly with MatLab or LabVIEW.

Software module can also handle sensor performance simulations using the Biot-Savart law for magnetic field distribution determination.

The program uses MatLab environment functions as:

- filtering and statistical capabilities for processing the noised measured data;
- mathematical functions for signal and data processing and storage;
- visualisation functions for presenting end exporting the results.

Developed software module is suitable for education and demonstrations purposes.

### Conclusion

This paper describes the AMR magnetic sensor arrays. Proposed sensors can be applied for magnetic field measurements in biological structures during magnetic therapy and diagnosis as well as for field distribution investigations.

Two schemes for signal pick-up are considered.

Developed experimental set-up can be applied for further sensor and coil explorations.

Developed software module can be applied for magnetic field explorations and visualisations.

The software module is suitable for education purposes.

## Acknowledgements

Parts of this research are supported by project 8059NI-1 of the R&DS at TU-Sofia.

## References

- [1] Marinova, I., L. Kovachev. Inverse Approach For Determination Of The Coils Location During Magnetic Stimulation. 3-rd Japanese-Bulgarian-Macedonian joint seminar on applied electromagnetics. Ohrid, 2000, pp. 140-145.
- [2] Smith, C., B. Schneider, A. Pohm. High-Resolution, Chip-Size Magnetic Sensor Arrays. *Sensors Magazine*, 2003, Vol. 20(3), pp. 44-49.
- [3] Marchand, B., F. Vacher, C. Gilles-Pascaud, JM. Decitre, C. Fermon. High Resolution Eddy Current Probes For Non Destructive Testing. 34th Annual Review of Progress in Quantitative Nondestructive Evaluation. AIP Conference Proceedings, 2008, Vol. 9(75), pp. 313-320.
- [4] Vacher, F., C. Gilles-Pascaud, J.M. Decitre, C. Fermon, M. Pannetier. Non Destructive Testing with GMR Magnetic Sensor Arrays. ECNDT, 2006, Vol. 4, pp. 13-18.
- [5] Philips Semiconductors. KMZ10B Magnetic Field Sensor - Product Specification. 1998.
- [6] Philips Semiconductors. Magnetic Field Sensors - General. 1998.
- [7] National Instruments Corporation. USB-6008/6009 User Guide And Specifications. 2005.
- [8] Костов, И., Й. Шопов. Определяне на направлението на вектора на слаби магнитни полета за целите на безразрушителния контрол чрез кординатни магниточувствителни сензори. Сборник с доклади от XIV-ти Национален Научен Симпозиум с Международно Участие "Метрология и Метрологично Осигуряване 2004", ТУ – София, България 2004, стр.163-166.
- [9] <http://www.protekttest.com>
- [10] Rubinacci, G., A. Tamburrino, S. Ventre, F. Villone. Shape Identification In Conductive Materials By Electrical Resistance Tomography In E<sup>2</sup>NDE. *Electromagnetic Non-destructive Evaluation*, Vol. VI, 2002, pp. 13-20.
- [11] Huang, H., T. Takagi, H. Fukutomi. Fast Signal Predictions Of Noised Signals In Eddy Current Testing. *IEEE Transactions on Magnetics*, Vol. 36(4), July 2000, pp. 1719-1723.
- [12] Marinova, I., S. Hayano, Y. Saito. Inverse Approach for Shape Design of Magnetic Core. *IEEE Transactions on Magnetics*, Vol. 31(3), 1995, pp. 1992-1995.
- [13] Doi, T., S. Hayano, I. Marinova, Y. Saito. Defect Recognition in Conductive Materials by Local Magnetic Field Measurement. *Journal of Applied Physics*, Vol. 75(10), 1994, pp. 5907-5909.
- [14] Michael, C., T. Bratland, C. Smith and R. Schneider. A New Perspective on Magnetic Field Sensing. *Sensors Magazine*, Vol. 15, no. 12, 1998, pp. 34-46.
- [15] Smith, C. and R. Schneider. Low-Field Magnetic Sensing with GMR Sensors: The Theory of Solid-State Sensing. *Sensors Magazine*, Vol. 16, no. 9, 1999, pp. 76-83.
- [16] Wolf, S., D. Awschalom, R. Buhrman, J. Daughton, S. Molnar, M. Roukes, A. Chtchelkanova and D. Treger. Spintronics: A Spin Based Electronics Vision for the Future. *Science*, vol. 294, 16 November 2001, pp. 1488-1495.
- [17] Schneider, R., J. Anderson, M. Tondra, C. Nordman, A. Jander, Z. Qian and Jim Daughton. First Results From Packaged Low-Power Spin Dependent Tunneling Sensors. *Military Sensing Symposia*, Adelphi, MD, September 24, 2002.
- [18] Smith, C., B. Schneider and A. Pohm. High- Resolution, Chip-Size Magnetic Sensor Arrays. *Sensors Magazine*, Vol. 20, no. 3, March 2003, pp. 44-49.
- [19] Smith, C., R. Schneider and M. Tondra, Biosensors: a New Use for Solid-State Magnetic Sensors. *Sensors Magazine*, Vol. 16, no. 12, December 1999, pp. 14-20.
- [20] Pappas, D. Imaged Audio Tapes Using Scanning Magneto-Resistive Microscopy. *Journal of Research of the National Institute of Standards and Technology*, Vol. 105, No.2, 2000 pp. 334.
- [21] Wincheski, B. and M. Namkung. Review of Progress in QNDE. Vol. 18, Plenum, New York, 1999, p. 1177.
- [22] Dogaru, T. and S. Smith. Detection of cracks near sharp edges by using giant magnetoresistance-based eddy current probe. *SPIE Proceedings*, 2000, p. 211.
- [23] Dogaru, T. and S. Smith. A GMR based eddy current sensor. *IEEE Trans. Magn*, MAG-37, 2001, p. 3831.
- [24] Dogaru, T., C. Smith, R. Schneider, and S. Smith. New Directions In Eddy-Current Sensing Technology. *Sensors Magazine*, Vol. 18, no. 6, June 2001, p. 56.
- [25] Smith, C., R. Schneider and M. Tondra. Biosensors: a New Use for Solid-State Magnetic Sensors. *Sensors Magazine*, Vol. 16, no. 12, December 1999, pp. 14-20.
- [26] Baselt, D., G. Lee, M. Natesan, S. Metzger, P. Sheehan and R. Colton. A biosensor based on magneotoresistance technology. *Biosensors & Bioelectronics*, Vol 13, 1998, pp. 731-739.



**Iliana Marinova** was born in Pleven, Bulgaria, on June 10, 1959. She studied at the Technical University of Sofia and received PhD. degree from the same university in 1989.

Since 1988 she worked in the Faculty of Electrical Engineering of the Technical University of Sofia as a associate professor and researcher.

Her field of interest includes inverse problems in electromagnetics and biomagnetics, electromagnetic fields, numerical methods, finite element method, boundary integral equation method, computer-aided design, optimization, image processing and visualization.

Iliana Marinova is with the Faculty of Electrical Engineering, Technical University of Sofia, 8, Kl. Ohridski Blvd., 1000 Sofia, Bulgaria (e-mail: [iliana@tu-sofia.bg](mailto:iliana@tu-sofia.bg)).



**Valentin Mateev** was born in Sofia, Bulgaria, on March 1, 1979. He graduated from the Technical University of Sofia with Master degree in electrical engineering.

Since 2006 he worked in the Faculty of Electrical Engineering of the Technical University of Sofia as a assistant and PhD student.

His field of interest includes inverse problems in electromagnetics, electromagnetic fields, finite element method, image processing, computer-aided design.

Valentin Mateev is with the Faculty of Electrical Engineering, Technical University of Sofia, 8, Kl. Ohridski Blvd., 1000 Sofia, Bulgaria (e-mail: [vmateev@tu-sofia.bg](mailto:vmateev@tu-sofia.bg)).

# The Switching Analysis of the Three-Phase Bridge Rectifier

Mitică Iustinian Neacă

**Abstract:** The paper presents a series of results obtained in the working frame of the switching phenomenon approach for a particular case of a three-phase bridge rectifier. The analysis underlines the aspects to be considered for the rectifier study in the working frame of the real theory approach and of the conventional theory approach.

**Keywords:** bridge circuits, rectifier, switching angle

## 1. The real theory approach

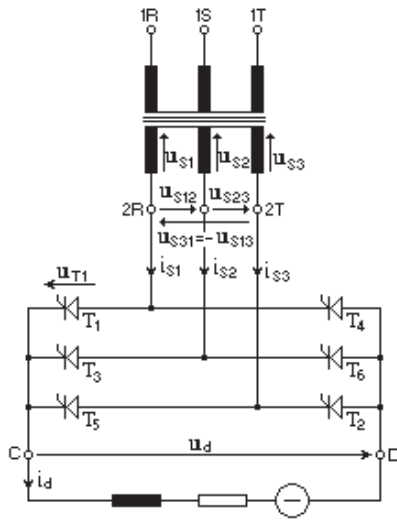


Fig.1. Three-phase bridge rectifier

For a three-phase bridge rectifier represented by Fig.1 we represented the switching circuit schematic in Fig.2, considering the switching of current from the thyristor T<sub>1</sub> on the thyristor T<sub>3</sub>. One considers the rectifier supplying by a direct symmetrical three-phase voltage system.

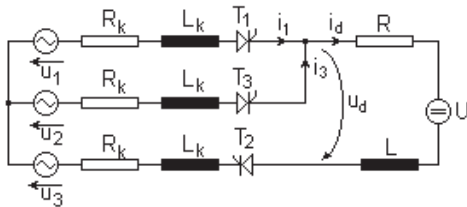


Fig.2. Switching circuit schematic

The equation describing the circuit before the switching ( $t < t_0$ ) is:

$$(1) \quad \begin{aligned} i_d(R + 2R_k) + \frac{di_d}{dt}(L + 2L_k) + U &= u_1 - u_3 = \\ &= \sqrt{6} \cdot U_f \sin\left(\omega t - \frac{\pi}{6}\right) \end{aligned}$$

It admits the following solution for the load current:

$$\begin{aligned} i_d(t)_{t < t_0} &= \frac{1}{(R + 2R_k)e^{\frac{R+2R_k}{L+2L_k}t}} \left( -U \cdot e^{\left(\frac{R+2R_k}{L+2L_k}t\right)} + C_{11}(R + 2R_k) + \right. \\ &+ (R + 2R_k) \int \left( \sqrt[3]{-1} \sqrt{1,5} \frac{U_f}{L + 2L_k} \left( -1 + (-1)^{\frac{1}{3}} \right) e^{\frac{R+2R_k}{L+2L_k}t} \cos \omega t + \right. \\ &\left. \left. + (-1)^{\frac{11}{6}} \sqrt{1,5} \frac{U_f}{L + 2L_k} \left( 1 + (-1)^{\frac{1}{3}} \right) e^{\frac{R+2R_k}{L+2L_k}t} \sin \omega t \right) \cdot dt \right) \end{aligned}$$

At the moment  $t_0 = \frac{1}{\omega} \left( \frac{5\pi}{6} + \alpha \right)$  (where  $\alpha$  represents the control angle), the T<sub>3</sub> firing is commanded and the current will switch until the moment  $t_1 = \frac{1}{\omega} \left( \frac{5\pi}{6} + \alpha + \gamma \right)$  when T<sub>1</sub> should be blocked.

During this period:

$$(2) \quad \begin{cases} i_1 + i_3 = i_d \\ L_k \frac{di_1}{dt} + R_k i_1 - L_k \frac{di_3}{dt} - R_k i_3 = u_1 - u_2 = \\ = \sqrt{6} \cdot U_f \sin\left(\omega t + \frac{\pi}{6}\right) \\ L_k \frac{di_1}{dt} + R_k i_1 + (L + L_k) \frac{di_d}{dt} + (R + R_k) i_d + U = \\ = u_1 - u_3 = \sqrt{6} \cdot U_f \sin\left(\omega t - \frac{\pi}{6}\right) \end{cases}$$

The system solving yields the solutions for  $i_1, i_3$  and

$i_d$ :

$$\begin{aligned} i_1(t)_{t_0 < t < t_1} &= -\frac{U}{2R + 3R_k} + C_{21} e^{\frac{-2R-3R_k}{2L+3L_k}t} - \frac{C_{22}}{e^{\frac{R_k}{L_k}t}} + \\ &+ \frac{(-1)^{\frac{4}{3}} \sqrt[3]{\frac{3}{8}} \cdot U_f}{L_k e^{\frac{R_k}{L_k}t}} \int \left( -1 + (-1)^{\frac{1}{3}} \right) e^{\frac{R_k}{L_k}t} \cos \omega t \cdot dt + \end{aligned}$$

$$\begin{aligned}
& + \frac{(-1)^{\frac{4}{3}} \sqrt{\frac{3}{8}} U_f}{L_k e^{\frac{R_k t}{L_k}}} \int \left( j + (-1)^{\frac{5}{6}} \right) e^{\frac{R_k t}{L_k}} \sin \omega t \cdot dt + \\
& + \frac{\sqrt[3]{-1} \sqrt{\frac{3}{8}} \cdot U_f}{2L + 3L_k} \cdot e^{\frac{-2R-3R_k}{2L+3L_k} t} \int \left( 3 \left( -1 + (-1)^{\frac{1}{3}} \right) e^{\frac{2R+3R_k}{2L+3L_k} t} \cos \omega t - \right. \\
& \left. - \left( j + (-1)^{\frac{5}{6}} \right) \cdot e^{\frac{2R+3R_k}{2L+3L_k} t} \sin \omega t \right) \cdot dt \\
i_3(t)_{t_0 < t < t_1} & = -\frac{U}{2R + 3R_k} + C_{21} e^{\frac{-2R-3R_k}{2L+3L_k} t} + \frac{C_{22}}{e^{\frac{R_k t}{L_k}}} + \\
& + \frac{(-1)^{\frac{1}{3}} \sqrt{\frac{3}{8}} \cdot U_f}{L_k e^{\frac{R_k t}{L_k}}} \int \left( -1 + (-1)^{\frac{1}{3}} \right) e^{\frac{R_k t}{L_k}} \cos \omega t \cdot dt + \\
& + \frac{(-1)^{\frac{1}{3}} \sqrt{\frac{3}{8}} \cdot U_f}{L_k e^{\frac{R_k t}{L_k}}} \int \left( j + (-1)^{\frac{5}{6}} \right) e^{\frac{R_k t}{L_k}} \sin \omega t \cdot dt + \\
& + \sqrt[3]{-1} \sqrt{\frac{3}{8}} \cdot \frac{U_f}{2L + 3L_k} \cdot e^{\frac{-2R-3R_k}{2L+3L_k} t} \int \left( 3 \left( -1 + (-1)^{\frac{1}{3}} \right) e^{\frac{2R+3R_k}{2L+3L_k} t} \cdot \right. \\
& \cdot \cos \omega t - \left. \left( j + (-1)^{\frac{5}{6}} \right) \cdot e^{\frac{2R+3R_k}{2L+3L_k} t} \sin \omega t \right) \cdot dt \\
i_d(t)_{t_0 < t < t_1} & = -\frac{2U}{2R + 3R_k} + 2C_{21} e^{\frac{-2R-3R_k}{2L+3L_k} t} + \\
& + \frac{\left( (-1)^{\frac{1}{3}} + (-1)^{\frac{4}{3}} \right) \sqrt{\frac{3}{8}} \cdot U_f}{L_k e^{\frac{R_k t}{L_k}}} \int \left( -1 + (-1)^{\frac{1}{3}} \right) e^{\frac{R_k t}{L_k}} \cos \omega t \cdot dt + \\
& + \frac{\left( (-1)^{\frac{1}{3}} + (-1)^{\frac{4}{3}} \right) \sqrt{\frac{3}{8}} \cdot U_f}{L_k e^{\frac{R_k t}{L_k}}} \int \left( j + (-1)^{\frac{5}{6}} \right) e^{\frac{R_k t}{L_k}} \sin \omega t \cdot dt + \\
& + \sqrt[3]{-1} \sqrt{\frac{3}{2}} \cdot \frac{U_f}{2L + 2L_k} \cdot e^{\frac{-2R-3R_k}{2L+3L_k} t} \int \left( 3 \left( -1 + (-1)^{\frac{1}{3}} \right) e^{\frac{2R+3R_k}{2L+3L_k} t} \cdot \right. \\
& \cdot \cos \omega t - \left. \left( j + (-1)^{\frac{5}{6}} \right) \cdot e^{\frac{2R+3R_k}{2L+3L_k} t} \sin \omega t \right) \cdot dt
\end{aligned}$$

After switching ( $t > t_1$ ) the equation, which describes the circuit, is:

$$\begin{aligned}
(3) \quad & i_d(R + 2R_k) + \frac{di_d}{dt}(L + 2L_k) + U = u_2 - u_3 = \\
& = \sqrt{6} \cdot U_f \sin\left(\omega t - \frac{\pi}{2}\right)
\end{aligned}$$

Having the result:

$$\begin{aligned}
i_d(t)_{t > t_1} & = C_{31} e^{\frac{R+2R_k}{L+2L_k} t} - \frac{1}{M} \left( L^2 \omega^2 U + 4LL_k \omega^2 U + \right. \\
& \left. + 4L_k^2 \omega^2 U + R^2 U + 4RR_k U + 4R_k^2 U + \sqrt{6} U_f R^2 \cos \omega t + \right.
\end{aligned}$$

$$\begin{aligned}
& + \sqrt{96} U_f R R_k \cos \omega t + \sqrt{96} U_f R_k^2 \cos \omega t + \\
& + \sqrt{6} U_f L R \omega \sin \omega t + \sqrt{24} U_f L_k R \omega \sin \omega t + \\
& + \sqrt{24} U_f L R_k \omega \sin \omega t + \sqrt{96} U_f L_k R_k \omega \sin \omega t
\end{aligned}$$

where

$$M = (R + 2R_k)(L^2 \omega^2 + 4LL_k \omega^2 + 4L_k^2 \omega^2 + R^2 + 4RR_k + 4R_k^2)$$

The four constants from the above currents expressions can be determined considering the switching process at the initial and final conditions:

$$(4) \quad \begin{cases} i_d(t_0)_{t_0 \leq t_0} = i_1(t_0)_{t_0 \leq t \leq t_1} \\ i_3(t_0)_{t_0 \leq t \leq t_1} = 0 \\ i_3(t_1)_{t_0 \leq t \leq t_1} = i_d(t_1)_{t_1 \geq t_1} \\ i_1(t_1)_{t_0 \leq t \leq t_1} = 0 \end{cases}$$

The determination of the switching angle  $\gamma = f(R, R_k, L, L_k, U, \alpha)$  for the real case can be performed considering identical waveforms of the currents through the three supplying phases and imposing the periodicity condition for current through load:

$$(5) \quad i_d \left( \frac{1}{\omega} \left( \frac{5\pi}{6} + \alpha \right) \right) \Big|_{t \leq t_0} = i_d \left( \frac{1}{\omega} \left( \frac{7\pi}{6} + \alpha \right) \right) \Big|_{t \geq t_1}$$

## 2. The conventional theory approach

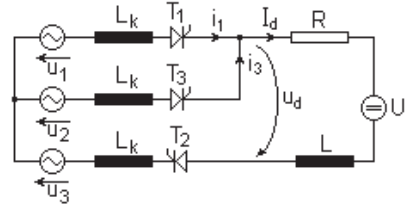


Fig.3. Simplified schematic of the switching circuit

Although the preliminary determination is rigorous, the great amount of parameters required to be known and the expressions complexity requires that in practice the  $\gamma$  angle's calculation should be performed under some conventional simplifying hypothesis:

- the load current  $i_d = I_d = ct$ ;
- the currents through the supplying phases have trapezoidal shapes ( $\tau_z = \frac{L}{R} \rightarrow \infty$ );
- the resistance on the supplying phase  $R_k \rightarrow 0$ .

In these conditions the switching circuit schematic is presented in Fig.3 and it is described by the system of equations:



$$(6) \begin{cases} i_1 + i_3 = I_d \\ L_k \frac{di_1}{dt} - L_k \frac{di_3}{dt} = u_1 - u_2 = \sqrt{6} \cdot U_f \sin\left(\omega t + \frac{\pi}{6}\right) \\ L_k \frac{di_1}{dt} R \cdot I_d + U = u_1 - u_3 = \sqrt{6} \cdot U_f \sin\left(\omega t - \frac{\pi}{6}\right) \end{cases}$$

Its solving and the consideration of an initial condition  $i_3(t_0) = 0$  allows us to obtain the switching current expression:

$$(7) \quad i_3(t) = \frac{\sqrt{6}}{2} \cdot \frac{U_f}{\omega L_k} \left( \cos \alpha + \cos\left(\omega t + \frac{\pi}{6}\right) \right)$$

We denote  $I_{k \max} = \frac{\sqrt{6} \cdot U_f}{2\omega L_k}$  and we assume that the switching process ends at the moment  $t_1 = \frac{1}{\omega} \left( \frac{5\pi}{6} + \alpha + \gamma \right)$ . Then we get:

$$(8) \quad \gamma = \arccos\left(\cos \alpha - \frac{I_d}{I_{k \max}}\right) - \alpha$$

The last equation defines the switching angle's variation in the space  $\left\{ \gamma, \alpha, I_{rap} = \frac{I_d}{I_{k \max}} \right\}$ . The generated surface is depicted by Fig.4 and Fig.5.

We denote by  $\gamma_0 = \arccos\left(1 - \frac{I_d}{I_{k \max}}\right)$  the switching angle for  $\alpha = 0^\circ$  and we get the equation:

$$(9) \quad \gamma = \arccos(\cos \alpha + \cos \gamma_0 - 1) - \alpha$$

Its transcendental derivative:

$$(10) \quad \frac{d\gamma}{d\alpha} = \frac{\sin \alpha}{\sqrt{1 - (\cos^2 \gamma_0 + \cos \alpha - 1)}} - 1$$

is represented in Fig.6 and indicates the fact that, through the increase of  $\gamma_0$  the function  $\gamma = f(\alpha)$  displaces from  $\alpha = 90^\circ$  ( at  $I_d = 0$  ) toward  $\alpha = 60^\circ$ .

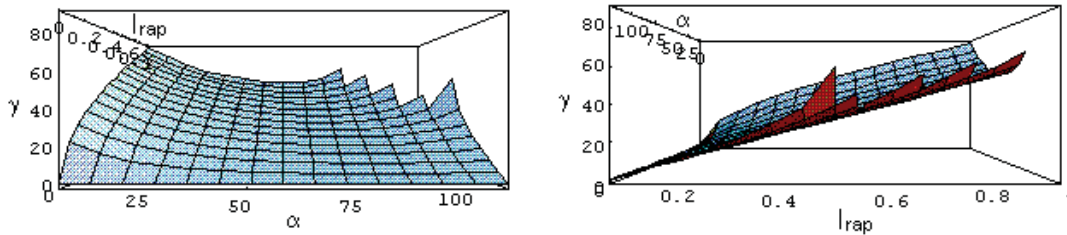


Fig.4. Variation of the switching angle with respect to  $I_{rap}$  and control angle

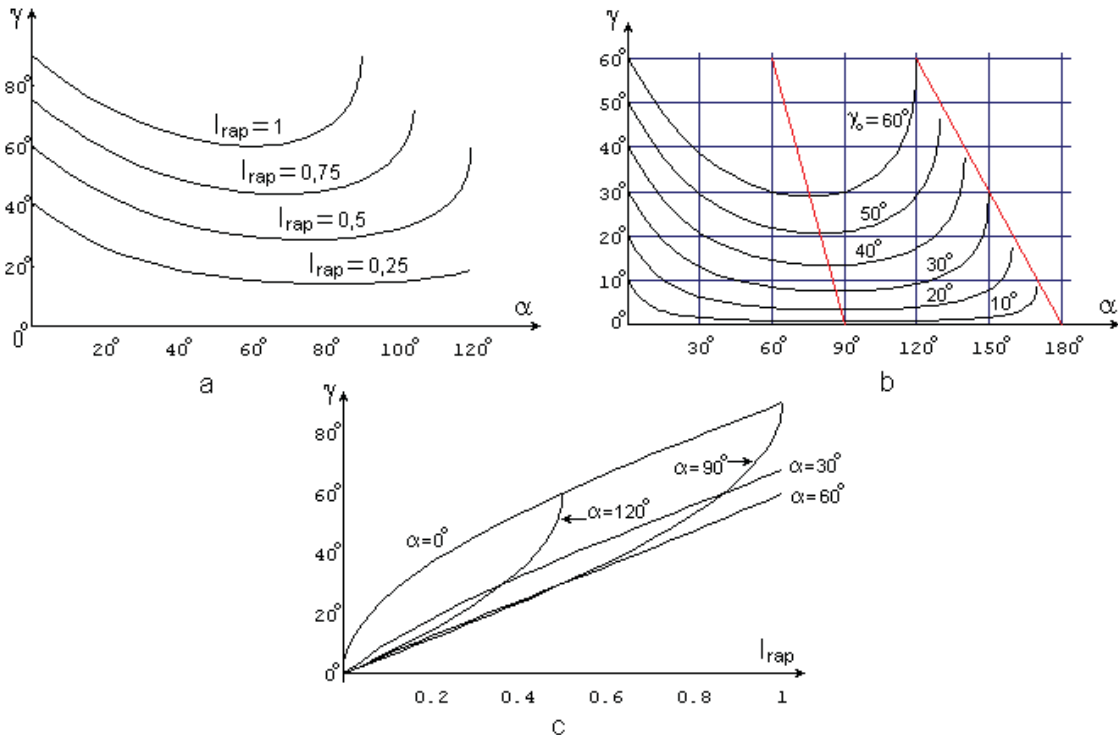


Fig.5. Influences over the switching angle

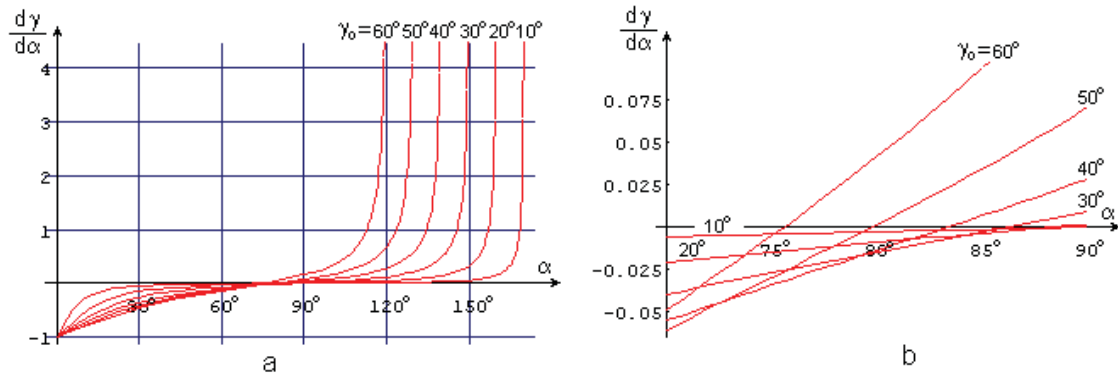


Fig.6. The position of the switching angle's minimum proportional to the command angle

The derivation of the  $i_3(t)$  current expression allows the emphasizing of two aspects:

- the maximum value of the increasing slope of the current is  $\omega I_{k\max} = \frac{\sqrt{6} \cdot U_f}{2L_k}$  ;
- the variation slope of the current through the thyristor, which starts a conduction process, is positive only for  $\omega t \in \left[ \frac{5\pi}{6}, \frac{11\pi}{6} \right]$  .

Then the maximum admitted control angle has the expression [5] :

$$(11) \quad \alpha_{\max} = \arccos\left(\frac{I_d}{I_{k\max}} - 1\right)$$

### 3. Consideration of a non-zero resistance at the primary circuit

Considering a non-zero resistance  $R_k \neq 0$  one obtains a switching current with the expression:

$$i_3 = I_{kR\max} \left[ \sin\left(\omega t - \frac{5\pi}{6} - \varphi\right) - \sin(\alpha - \varphi) \cdot e^{-\frac{\omega t - \frac{5\pi}{6} - \alpha}{\omega\tau}} \right] + 0,5I_d \left( 1 - e^{-\frac{\omega t - \frac{5\pi}{6} - \alpha}{\omega\tau}} \right)$$

Where:

$$I_{kR\max} = \frac{\sqrt{6} \cdot U_f}{\sqrt{(2R_k)^2 + (2\omega L_k)^2}} \quad \text{and} \\ \varphi = \arctan \frac{\omega L_k}{R_k}$$

### Conclusion

The consideration of the switching phenomenon requires the consideration of a series of correspondences:

- the mean rectified voltage presents a diminished value ;
- the control angle must not overcome a maximum admitted value ;
- during the rectifier study in the working frame of the real theory [2], [3] one must have in view the reciprocal influence between the rectified current and the switching angle. As a consequence in the expression (8), instead of  $I_d$  one must use the value  $I_{da}$ , corresponding to the control angle  $\alpha$  .

### References

- [1] M. H. Rashid, "Power Electronics Handbook"; ACADEMIC PRESS, 2001.
- [2] A. Kloss, "Oberschwingungen"; VDE-Verlag GmbH, Berlin und Offenbach, 1989.
- [3] A. Kloss, "Leistungselektronik ohne Ballast"; Franzis-Verlag GmbH, München, 1980.
- [4] N. Mohan, T. M. Undeland, W. P. Robbins, "Power Electronics – Converters, Applications and Design"; John Wiley & Sons, 2003.
- [5] A. Bitoleanu, S. Ivanov, M. Popescu, "Convertoare statice"; Ed. Infomed Craiova, 1997.

### Biographie



**Mitică Iustinian Neacă** was born in Tunarii Vechi, Dolj, Romania, on June 01, 1958. He studied at the Faculty of Electrical Engineering from the University of Craiova - Romania, and received Dr. degree from the same university in 2000.

Since 1991 he is working at the Faculty of Electrical Engineering of the University of Craiova. His field of interest includes electric heating, quality of the electric power in power electronics circuits and renewable energy

sources (electrical aspects).

Mitică Iustinian Neacă is with the Faculty of Electrical Engineering, University of Craiova, Bdul Decebal, nr. 107, 200440, Craiova – Romania, (e-mail: ineaca@elth.ucv.ro).

# The Influence of the Output's Deforming Regime of a Commanded Rectifier over its Input Functioning Regime

Mitică Iustinian Neacă, Andreea Maria Neacă

**Abstract:** The present article is proposing to show the way how the deforming regime, which affects the current at the output of a three-phased bridge rectifier, influences the current, absorbed by the rectifier from the supply, inducing in the point of the supply an non-sinusoidal regime.

**Keywords:** bridge rectifier, deforming regime, harmonics influence

## 1. Introduction

We consider the three-phased bridge rectifier from Fig.1. The modification of the form of the rectified current distributed on the charge having the constant of time  $\tau = \frac{L}{R}$  having a finite value (which places the analysis on the context of the real theory [1]) is made in fact on the transfer of this current through the rectifier from the supply phases. The numerous mathematical simulations made in the context of the conventional theory and the real theory have sent to the idea that the harmonic spectrum of the current through the phases of the rectifier is modifying very little, only at the amplitude of the harmonics, not in their order.

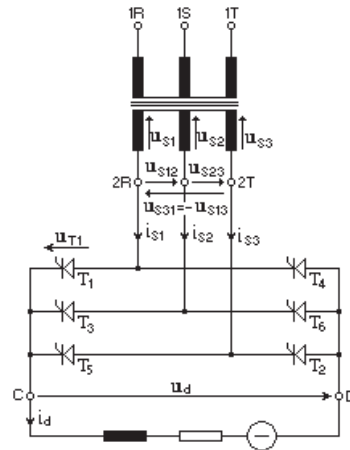


Fig.1. The three-phase bridge rectifier

In Fig.2 is shown the waveform and the harmonic spectrum in the conditions of the two theories for an command angle  $\alpha = 30^\circ$ ,  $\tau = 0,002$  s and

$$I_{rap} = \frac{2\omega L_K I_d}{\sqrt{6} \cdot U_f} = 0,355098.$$

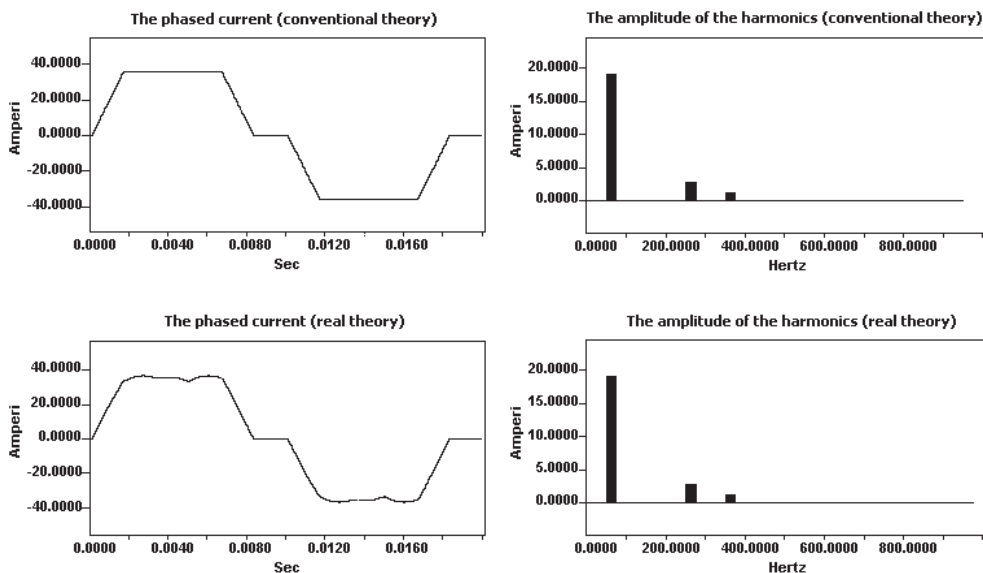


Fig.2. The phased current (the conventional theory/real theory)  
The amplitude of the harmonics (the conventional theory/real theory)

We can see that the two spectrums are alike, and the values of the harmonics are (in Amps):

Table 1

	Conventionally theory	Really theory
harm.1	19.2955	19.3156
harm.5	2.9368	3.0476
harm.7	1.5187	1.4250
harm.11	0.2080	0.0292
harm.13	0.0786	0.1269
harm.17	0.2498	0.2291
harm.19	0.2078	0.1692

## 2. Mathematical Foundation

The explanation of the way how the deformation of the current through the charge influences the current taken by the rectifier from the supply is based on the next mathematical idea:

We consider two periodical functions, with the same period, which satisfy the conditions of Diriclet and can be developed in Fourier complex series:

$$(1) \quad g_1(t) = g_1(t + kT) = \sum_{-\infty}^{+\infty} \underline{C}_{1n} \cdot e^{jn\omega t}, \quad \text{where}$$

$$\underline{C}_{1n} = \frac{1}{T} \int_0^T g_1(t) \cdot e^{-jn\omega t} \cdot dt, \quad \text{and}$$

$$(2) \quad g_2(t) = g_2(t + kT) = \sum_{-\infty}^{+\infty} \underline{C}_{2n} \cdot e^{jn\omega t}, \quad \text{where}$$

$$\underline{C}_{2n} = \frac{1}{T} \int_0^T g_2(t) \cdot e^{-jn\omega t} \cdot dt$$

The function  $f(t) = g_1(t) + g_2(t) = f(t + kT)$  can be developed like  $f(t) = \sum_{-\infty}^{+\infty} \underline{C}_{fn} \cdot e^{jn\omega t}$ , where:

$$(3) \quad \underline{C}_{fn} = \frac{1}{T} \int_0^T f(t) \cdot e^{-jn\omega t} \cdot dt = \frac{1}{T} \int_0^T [g_1(t) + g_2(t)] \cdot e^{-jn\omega t} \cdot dt = \frac{1}{T} \int_0^T g_1(t) \cdot e^{-jn\omega t} \cdot dt + \frac{1}{T} \int_0^T g_2(t) \cdot e^{-jn\omega t} \cdot dt = \underline{C}_{1n} + \underline{C}_{2n}$$

From the above we can say that it can be replaced the calculus of the developing in Fourier series of the composed function  $f(t)$ , with the operation of summing the harmonics of the two functions and the algebraically summing of the coefficients on each common harmonic. In case of the rectifier considered (in supply phases), over the harmonic spectrum of the trapezoidal wave we superpose the harmonic spectrum due to the rectified current.

## 3. The influence of a harmonic of the rectified current over the supply phases current

We take the harmonics in order  $k = 6v$ ,  $v = 1, 2, 3, 4, \dots$  is:  $i_k = \sqrt{2} \cdot I_k \cos(k\omega t)$ .

Although the periods of variation of the current in phase are function of the command angle  $\alpha$  and of the switching angle  $\gamma$ , we can consider with a good approximation that the wave is symmetrical compared with the point  $\alpha + \frac{\gamma}{2} - \frac{\pi}{6}$ , the symmetry being an even type, this means  $f(t) = f(T - t)$ . In consequence, the wave will discompose only in harmonics in cosine that will complete the wave of phase current from the idealized theory. At the translation with  $\frac{T}{4} = \frac{\pi}{2}$  the function becomes odd, and the developing in Fourier series will contain only the harmonics in odd order in cosine:

$$(4) \quad f(t) = \sum_{p=0}^{\infty} M_{2p+1} \cdot \cos(2p+1)\omega t, \quad \text{where}$$

$$(5) \quad M_{2p+1} = \frac{8}{T} \int_0^{\frac{T}{4}} f(t) \cdot \cos(2p+1)\omega t \cdot d\omega t = \frac{4}{\pi} \int_{\alpha+\gamma}^{\alpha+\frac{\gamma}{2}+\frac{\pi}{3}} \sqrt{2} \cdot I_k \cdot \cos k\omega t \cdot \cos(2p+1)\omega t \cdot d\omega t$$

Results

$$(6) \quad M_{2p+1} = \frac{2\sqrt{2}I_k}{\pi} \left[ \frac{1}{k+2p+1} \left[ \sin(k+2p+1) \left( \alpha + \frac{\gamma}{2} + \frac{\pi}{3} \right) - \sin(k+2p+1)(\alpha+\gamma) \right] + \frac{1}{k-2p-1} \left[ \sin(k-2p-1) \left( \alpha + \frac{\gamma}{2} + \frac{\pi}{3} \right) - \sin(k-2p-1)(\alpha+\gamma) \right] \right]$$

This mathematical idea is available for  $v = 1, 2, 3, \dots$ , in Fig.3 are presented, reported at unit, the influences that the 6-th order harmonics of the rectified current have on the harmonics of the current from first phase of the rectifier power supply. To obtain the absolute value of the harmonics influence, the value from the graphic must to be multiplied with the amplitude of the 6-th order harmonics of the output current for the command angle and  $I_{rap}$  respectively.

The five graphics show a wavy variation for the harmonics components, when  $\alpha$  and  $I_{rap}$  are changing. Considering the fact that the variation of the parameter  $I_{rap} = \frac{I_d}{I_{k \max}}$  for a certain command angle is possible only if we consider the charge variable, the graphics presented in Fig.3 are quite difficult to use by the user of the rectifier.



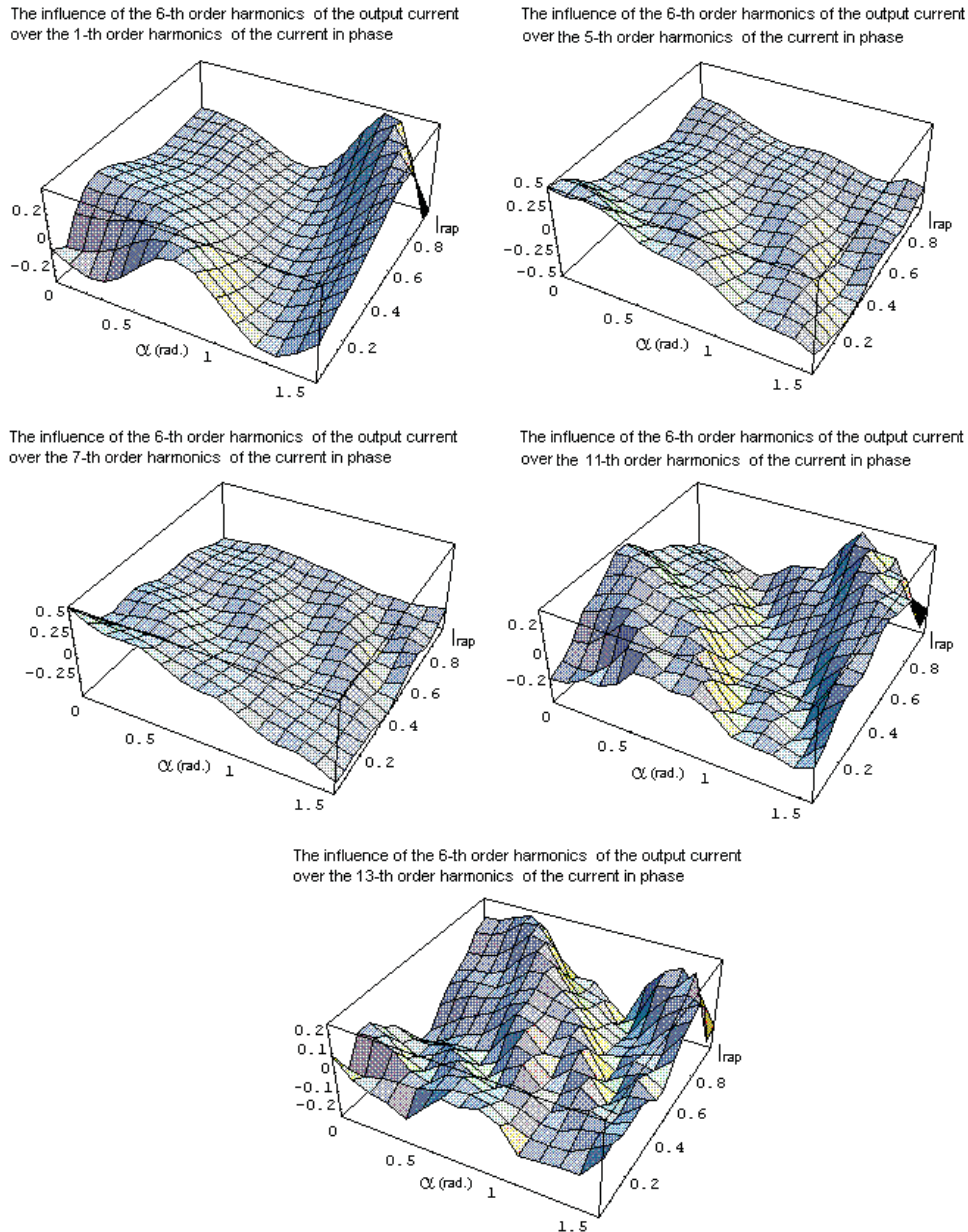


Fig.3. The influence of the harmonics 6 of the current rectified over the current from charging phases

At constant load ( $\tau = const.$ ) and at a certain command angle, corresponds a certain pair  $(I_{da}, \gamma)$  and at  $L_k = const.$ , results a certain value for  $I_{rap}$ . We have created through mathematical simulation a punctual database, where for each command angle  $\alpha = 0^\circ, 15^\circ, 30^\circ, 45^\circ, 60^\circ, 75^\circ, 89^\circ$ , we have calculated  $I_{da}, \gamma$  and  $I_{rap}$ . Based on the corresponding values of the harmonics of the rectified current we have calculated at the end the values of the coefficients of the harmonics transferred in the wave of the current of the 1-th phase power supply of the rectifier. The database has been calculated for two time constants of the charge  $\tau = 0,0005s$  and  $\tau = 0,0025s$ . Then are calculated the algebraically sums of the harmonic's coefficients, and the total influence of the harmonics 6,12,18 of the rectified

current over the harmonics of the current from phase of power supply.

Even if the harmonics in order  $3(2p+1)$  have coefficients different from zero, their last value can be negligible, because the principal wave does not contain these harmonics.

In Fig.4 is presented in a compared way the influence of the 6-th order harmonics and the influence of the sum of the harmonics 6, 12 and 18 of the rectified current over the harmonics of the phases supply current, for the two values of  $\tau$ . The similar way of variation indicates the fact that the influence of the harmonics in order 6 is much more powerful.

Because the graphics had been made after some linear approximations, it shows a few electrical degrees zone for the values of the command angle, where the curves pass

through zero. If we draw directly the variation of the harmonic coefficients for a certain value of the  $I_{rap}$  parameter, we obtain a common point of intersection of

the curves with the Ox axe. (For example, for  $I_{rap} = 0,355098$  all the harmonic influences become zero at  $\alpha = 57,2958$  electrical degrees).

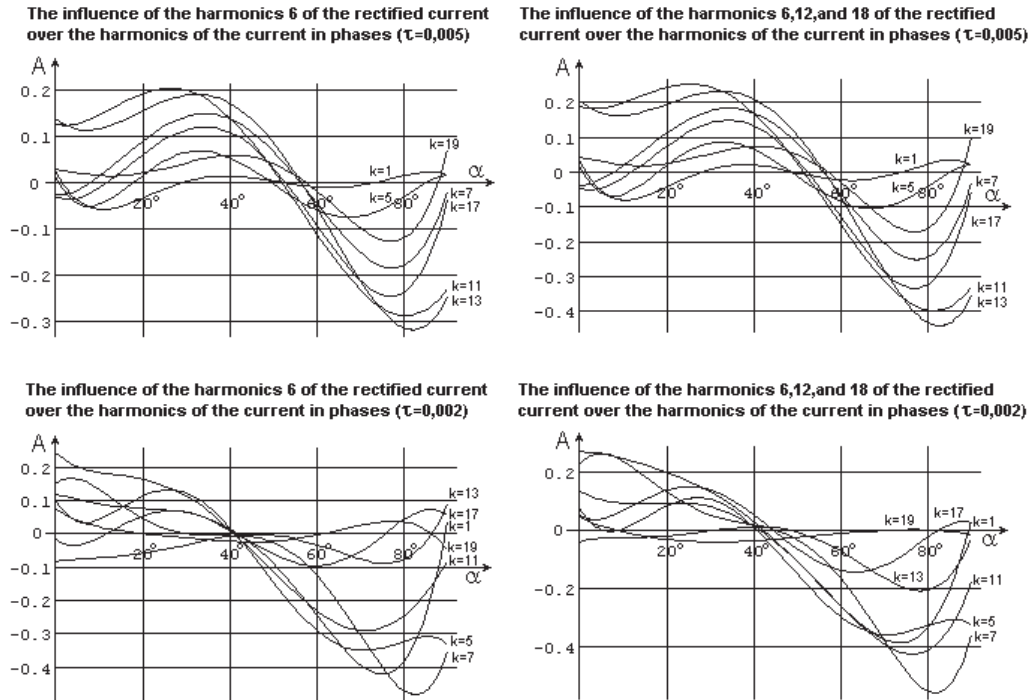


Fig.4. The influence of the harmonics of the rectified current over the harmonics of the current in charging phase

If consider the idealized theory ( $\gamma = 0$ ), for a command angle  $\alpha = 0^\circ$  we obtain:

$$\begin{aligned}
 M_{2p+1} &= \frac{2\sqrt{2}I_k}{\pi} \left[ \frac{1}{k+2p+1} \left[ \sin\left(k+2p+1\right)\left(\frac{\pi}{3}\right) \right] + \right. \\
 (7) \quad & \left. + \frac{1}{k-2p-1} \left[ \sin\left(k-2p-1\right)\left(\frac{\pi}{3}\right) \right] \right] = \\
 &= \frac{2\sqrt{2}I_k}{\pi} \left[ \frac{1}{k+2p+1} \left[ \sin\left(2v\pi + (2p+1)\frac{\pi}{3}\right) \right] + \right. \\
 & \left. + \frac{1}{k-2p-1} \left[ \sin\left(2v\pi - (2p+1)\frac{\pi}{3}\right) \right] \right]
 \end{aligned}$$

and in the end:

$$(8) \quad M_{2p+1} = -\frac{2\sqrt{2}I_k}{\pi} \cdot \frac{2(2p+1)}{k^2 - (2p+1)^2} \cdot \sin(2p+1) \frac{\pi}{3}$$

At  $2p+1 = 3(2r+1)$  (multiple of 3) are annulling the harmonic coefficients, because:

$$(9) \quad 2p+1 = 3(2r+1) \Rightarrow \sin(2p+1) \frac{\pi}{3} = \sin(2r+1)\pi = 0$$

For the others coefficients:

$$(10) \quad 2p+1 = 3(2r+1) \pm 2 \Rightarrow \sin(2p+1) \frac{\pi}{3} = \mp \frac{\sqrt{3}}{2}$$

And:

$$(11) \quad M_{3(2r+1) \pm 2} = \pm \frac{2\sqrt{3} \cdot [3(2r+1) \pm 2]}{\pi [k^2 - [3(2r+1) \pm 2]^2]} \cdot (\sqrt{2} \cdot I_k)$$

The use of the formula from upstairs permits the calculus of the dependence of the harmonics 1, 5, 7, 11, 13, 17, 19, 23, 25 of the current in phase compared with the harmonics 6, 12, 18, 24 of the rectified current :

Table 2

	harm.6	harm.12	harm.18	harm.24
$M_1$	-0,031	-0,008	-0,003	-0,002
$M_5$	0,501	0,046	0,018	0,01
$M_7$	0,594	-0,081	-0,028	-0,015
$M_{11}$	-0,143	0,527	0,059	0,027
$M_{13}$	0,108	0,573	-0,092	-0,035
$M_{17}$	-0,074	-0,129	0,536	0,065
$M_{19}$	0,064	0,097	0,566	-0,097
$M_{23}$	-0,051	-0,066	-0,124	0,540
$M_{25}$	0,047	0,057	0,092	0,563

Even if the presented case is very restrictive ( $\alpha = \gamma = 0^\circ$ ) it is useful for a first approximation of the harmonic influence from the output through the input of the rectifier. For this need it can be used also the nomogram made probably like an experiment at the Technique Wuppertal Academy [1] from Fig.5.

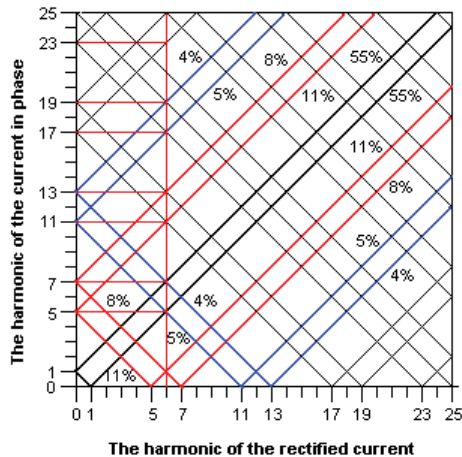


Fig.5. Calculus nomogram of the harmonics influence

The ripple of the rectified current (continuous theoretically) and the appearance of the harmonics sent to the influence of the harmonic content into a part of the alternating current of the rectifier. The spectrum himself doesn't change in a big way with the appearance or the removal of some harmonics, because he contains harmonics in order  $k = 5, 7, 11, 13, 17, 19, \dots$  if we still take in count the ripple rectified current phenomena the amplitude of these harmonics is modifying in a big way, like in Fig.6.

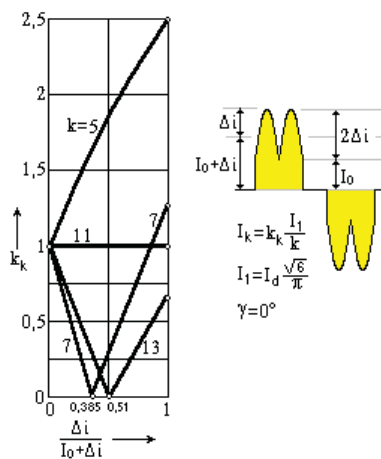


Fig. 6: The modify of the harmonics in function with the rectified current ripple

It has to be mentioned that this graphic is made in conditions when the switching angle had been considered zero [1]. From the graphic we can see the grow of the 5-th order harmonic, the oscillation of the harmonics 7 and 13 and the constancy of the 11-th order harmonic. The

17-th order harmonic and the 23-th order harmonic remain practically uninfluenced just like the harmonics 11, harmonics 19 is becoming zero for a 0,62 ripple of rectified current and the harmonics 25 becoming zero for a 0,67 ripple of rectified current. The grow of the curve of the rectified current is obtained when we modify the constant of time of the load.

### Conclusion

The article is proposing to show the way how the deforming regime, influences the current, absorbed by the rectifier from the supply, inducting in the point of the supply a non-sinusoidal regime. The ripple of the rectified current (continuous theoretically) and the appearance of the harmonics on this side sent to the influence of the harmonic content into a part of the alternating current of the rectifier. The spectrum himself doesn't change in a big way with the appearance or the removal of some harmonics, because he contains harmonics in order  $k = 5, 7, 11, 13, 17, 19, \dots$ . The ripple rectified current phenomena take modifying in big way the harmonic's amplitude of supplying current.

### References

- [1] A. Kloss, "Oberschwingungen", VDE-Verlag GMBh, Berlin und Offenbach, 1989 .
- [2] M. Grötzbach, "Berechnung der Oberschwingungen im Netzstrom von Drehstrombrücken-schaltungen bei unvollkommener Glättung des Gleichstroms", ETZ-Archiv 7 (1985) H.2.
- [3] J. Schwarz, "Analyse des Stromes durch eine von Stromrichtern gespeiste ohmsch-induktive Last", Z.elekt.Inform.-u.Energietechnik, Leipzig 8 (1978) 2.

### Biographies



**Mitică Iustinian Neacă** was born in Tunarii Vechi, Dolj, Romania, on June 01, 1958. He studied at the Faculty of Electrical Engineering from the University of Craiova - Romania, and received Dr. degree from the same university in 2000.

Since 1991 he is working at the Faculty of Electrical Engineering of the University of Craiova. His field of interest includes electric heating, quality of the electric power in power electronics circuits and renewable energy sources (electrical aspects). Mitică Iustinian Neacă is with the Faculty of Electrical Engineering, University of Craiova, Bdul Decebal, nr. 107, 200440, Craiova – Romania, (e-mail: [ineaca@elth.ucv.ro](mailto:ineaca@elth.ucv.ro)).



**Andreea Maria Neacă** was born in Craiova, Dolj, Romania, on February 22, 1985. Since 2004, she studies at the Faculty of Automatics, Computers and Electronics from the University of Craiova – Romania. Her field of interest includes computers engineering and software engineering. Andreea Maria Neacă is student at the Faculty of Automatics, Computers and Electronics, University of Craiova, Bdul Decebal, nr. 107, 200440, Craiova – Romania, (e-mail: [neaca\\_andreea@yahoo.com](mailto:neaca_andreea@yahoo.com)).

# SPICE Investigation of Transients in the Multiphase Bridge Transistor DC-DC Converters with Charge Mode Control

Georgi Kunov, Elissaveta Gadjeva and Marian Popov

**Abstract:** Multiphase full bridge transistor DC-DC converter with PPhM (pulse-phase modulation) and charge mode control system is developed and simulated in the present paper. The work of the control system with four-phase shifted bridge transistor DC-DC converters is simulated using the OrCAD PSpice program. The transients in the power circuit at the start are investigated.

**Keywords:** Full bridge transistor DC-DC converter, Pulse-phase modulation, Control system, PSpice simulation, Transient analysis

## Introduction

The idea of multiphase work of DC-DC converters arises in the period of the mass application of thyristors in the practice, compensating their low frequency parameters. The theoretical analysis of these circuits in the steady state is given in the literature [1]. Their main advantages are proved: decreasing the pulsations of the input and output currents and, as a result, decreasing the level of the emitted radio disturbances; decreasing the weight and the size of the DC-DC converter at a whole. Recently, this idea is revived by manufacturers of specialized chips for the needs of power supply in computer industry. A typical example is the integrated circuit TPS40090 of Texas Instruments [2]. A characteristic feature of all IC's of this type is that they are designed for parallel operation of multiphase BUCK converters.

Recently, the regulation of PWM in DC-DC converters is based on voltage mode or current mode control [4]. Charge mode control is proposed for the first time in [5] for BOOST DC-DC converters. The same principle of control is used in [6] and [7], applied to BUCK converters. The approach is applied to Phase Shifted PWM bridge converter in [8].

In the present paper, the charge mode control is applied to Phase Shifted PWM bridge converter current-double rectifier. A control system is synthesised and the work together with the power circuit is simulated. The transients in the power circuit at the start and the current sharing are investigated.

## Charge current mode controlled phase shifted full bridge inverter with current-double rectifier

The principle of operation of the single-phase Phase Shifted bridge inverter is illustrated using time diagrams shown in Fig. 1, which power circuit is shown in Fig. 2. The pulses V(CL1) generated by the independent clock

generator are applied to the clock input (CLK) of T-trigger (Fig. 3). Its outputs GA1 and GA2 commute transistors MA1 and MA4. The same pulses are used for synchronizing the work of an externally clocked R-S flip flop (Fig. 4). The R-S flip flop is clocked by the output pulses ChC\_A, generated by the charge current mode controller (Fig. 5). The clock pulses V(CL1) of the clock generator and V(ChC\_A) of the charge current comparator are phase shifted. This phase shifting depends on the time interval for the output current increasing from its minimal value  $I(RAc_s)_{min}$  to its maximum value  $I(RAc_s)_{max}$ . The increasing current determines for this time interval trapezoid, which area is integrated by the capacitor CACH in the charge current mode controller – the signal V(CAch:2). The trapezoid area is determined by  $V(CAch:2)_{max}$ , which depends on the defined  $V_{chref}$ . The phase shifting defines the time duration of two-polar pulses in the diagonal of the transistor converter.

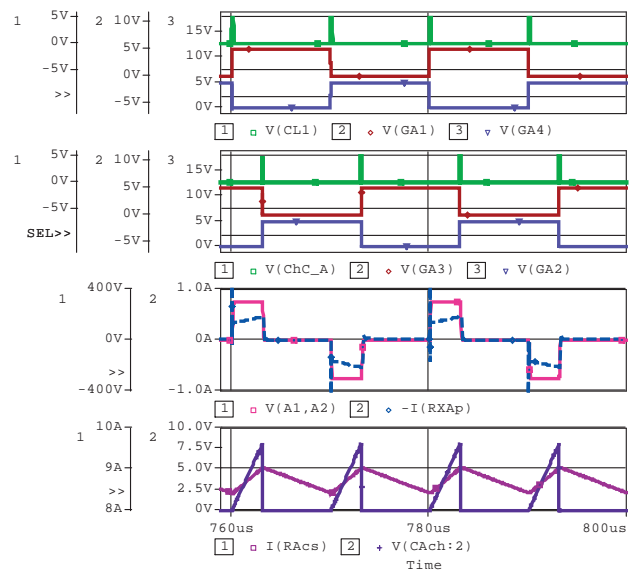


Fig. 1. Principle of operation of charge current mode Phase Shifted PWM bridge transistor converter.

## Multi-phase full bridge converter gate drive topology

The timing diagrams, illustrating the principle of operation of the four-phase full bridge transistor converter with charge current mode Phase Shifted PWM are shown in Fig. 6. The power circuit of the four-phase converter consists of four equal stages. One of them is shown in Fig. 2. The stages are denoted by corresponding



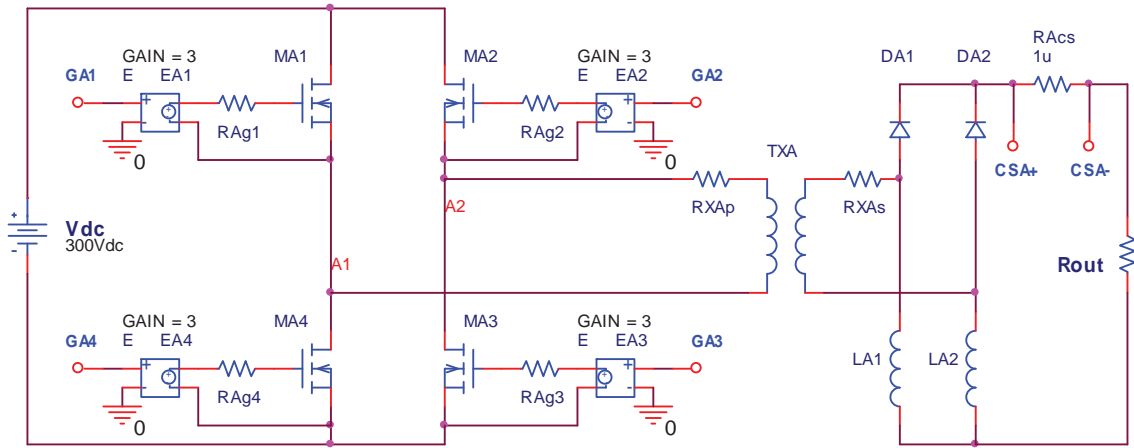


Fig. 2. Current mode Phase Shifted PWM full bridge transistor converter.

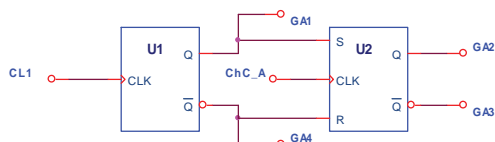


Fig. 3. Full bridge gate drive generation.

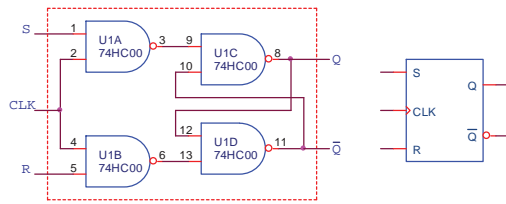


Fig. 4. R-S flip flop internal diagram with external clocking.

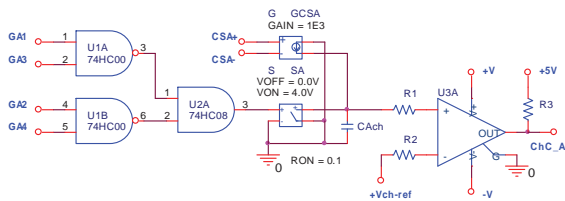


Fig. 5. Charge current mode controller.

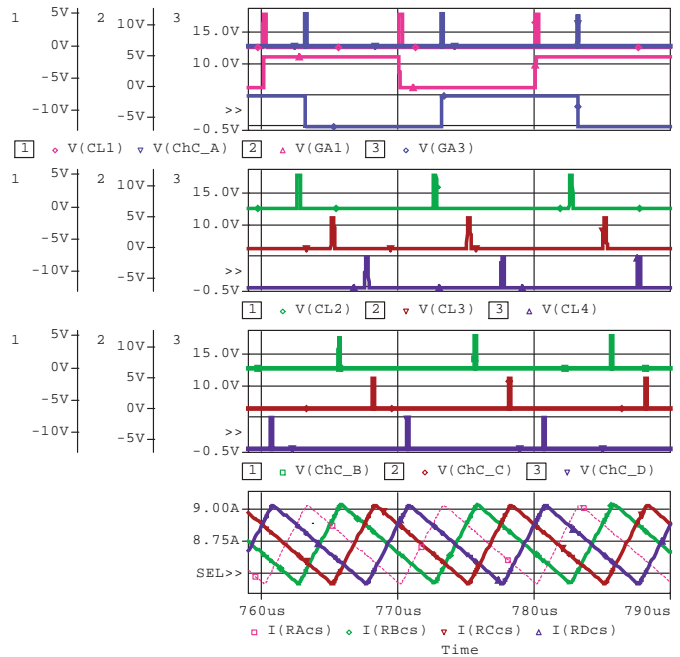


Fig. 6. Timing diagram of four phase full bridge transistor converter with charge current mode Phase Shifted PWM.

indexes A, B, C and D. Their gate drive topology is represented in Fig. 7. The triggers, which form the control impulses GB1, GB4; GC1, GC4; GD1, GD4, are synchronized with the signals GA1, GA4 and are switched by the clock impulses CL2, CL3 and CL4. The control pulses GB2, GB3; GC2, GC3 and GD2, GD3 are formed similarly to the pulses shown in Fig. 1. The clock pulses CL1\_m, CL2\_m, CL3\_m and CL4\_m have auxiliary function. They commute the right vertical legs of the transistor converters for the critical situations when the voltage across the capacitor  $C_{ch}$  is less than the defined parameter  $V_{chref}$ . This situation occurs when the load resistance  $R_{out}$  has a very large value, or, at the

beginning of the transient process, when the load current increases very slowly due to the big time constant of the load, defined by small values of the resistance  $R_{out}$ .

### Determination limiting values of the load resistance $R_{out}$

In order to realize the charge current mode control (ChCMC) approach, the following condition has to be fulfilled: the integral of the arising current in the separate stages for the corresponding time interval  $V_{ch}(t)$  has to be not greater than the maximal value of the voltage  $V_{chrefmax}$ .

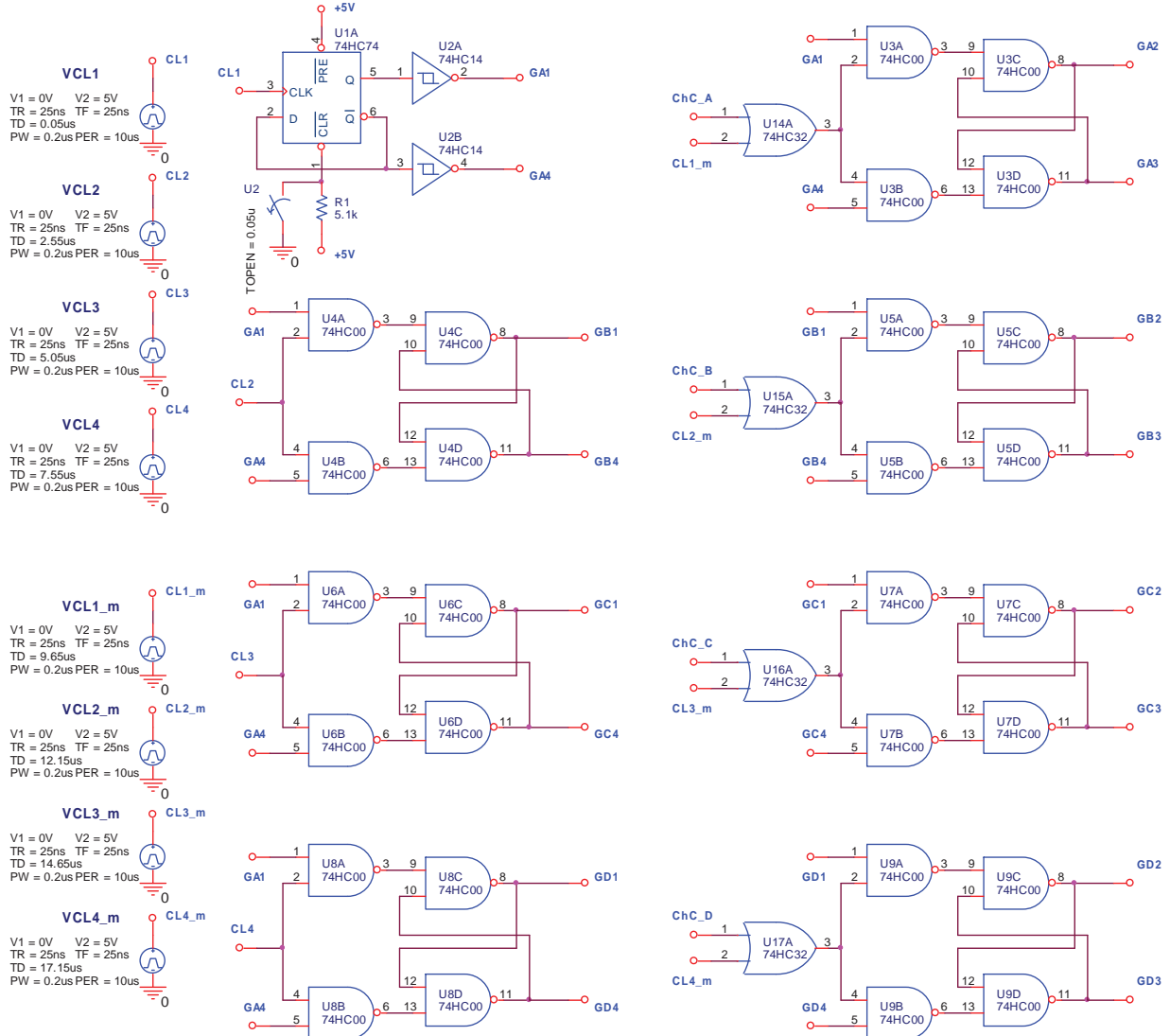


Fig. 7. Multiphase full bridge converter gate drive topology

$V_{Ch}(t)$  corresponds to the area of the trapezoid, obtained by the initial (minimal) current value  $I_{Rcsmin}$  and the end (maximal) value  $I_{Rcsmax}$  during the time interval for current increase. This area can be approached by the maximal output voltage  $V_{outmax}$ , minimal output current  $I_{outmin}$  and maximal integration time  $t_{chmax}$ , corresponding to a maximal duty cycle  $D_{max}=t_{chmax}/T_{CL}$ . This case corresponds to a maximal load resistance  $R_{outmax}$ . The other boundary-mode of operation corresponds to a minimal output voltage  $V_{outmin}$ , maximal output current  $I_{outmax}$  and minimal integration time  $t_{chmin}$ , corresponding to a minimal duty cycle  $D_{min}=t_{chmin}/T_{CL}$ . This case corresponds to a minimal load resistance  $R_{outmin}$ .

The output resistance for the described modes of operation is in the form:

$$(1) \quad R_{outmax} = \frac{V_{outmax}}{I_{outmin}} = \frac{V_{out} D_{max}}{4I_{Rcsmin}}$$

$$(2) \quad R_{outmin} = \frac{V_{outmin}}{I_{outmax}} = \frac{V_{out} D_{min}}{4I_{Rcsmax}}$$

The voltage  $V_{out}$  is the maximal (theoretically) voltage, applied to the input of the rectifier by duty cycle  $D=1$ .

The following dependence is valid for the voltage  $V_{Ch}$ :

$$(3) \quad V_{Ch} = \frac{I_{ch} t_{ch}}{C_{ch}}$$

The current  $I_{ch}$  is a function of the arising current through the corresponding stage:

$$(4) \quad I_{ch} = V_{Res} G = I_{Res} G = kI_{Res}$$

Replacing (4) in (3), the following dependence for  $I_{Rcs}$  is obtained:

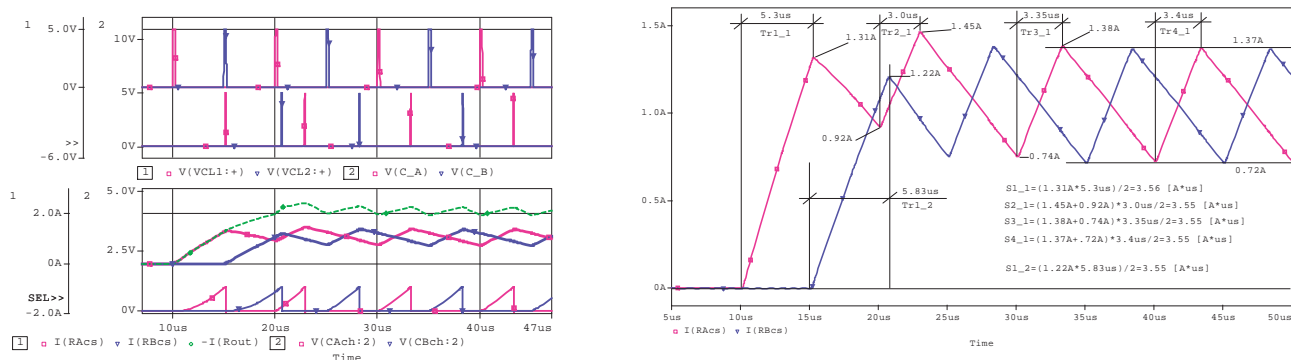


Fig. 8. Transients by the work of two phase shifted charge current mode controlled converters.

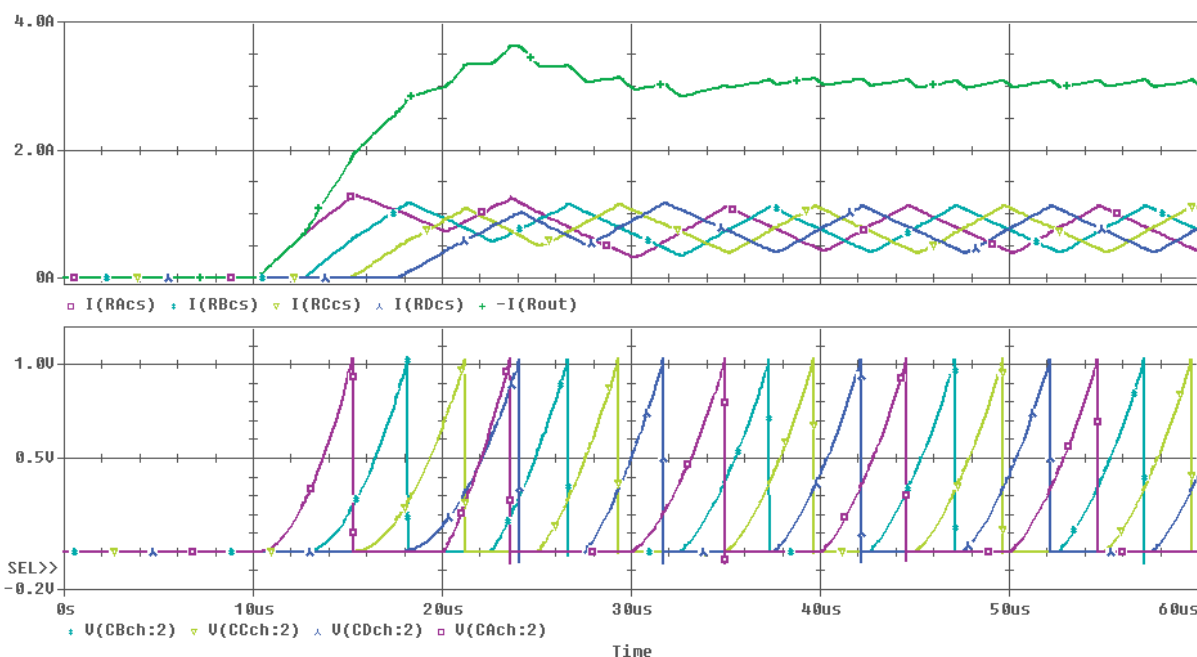


Fig.9 Transients at the start of four working in parallel phase shifted converters.

$$(5) \quad I_{Rcs} = \frac{V_{Cch} C_{ch}}{kDT_{CL}}$$

where

$T_{CL}$  is the period of the clock generator

$$t_{ch} = D \cdot T_{CL}$$

$C_{ch}$  – the integrating capacitor

Replacing (5) in (1) and (2), the following expression for the acceptable range of variation of the load resistance is obtained:

$$(6) \quad \frac{R_{out\ max}}{R_{out\ min}} = \left( \frac{D_{max}}{D_{min}} \right)^2$$

$D_{max}$  and  $D_{min}$  are limited by the selected period of the clock generator  $T_{CL}$  and by the frequency characteristics of the semiconductor elements (transistors and diodes).

For example, for  $T_{CL}=10\mu s$  and minimal commutation time of the devices  $1\mu s$ , the corresponding values are  $t_{chmin}=1\mu s$  and  $t_{chmax}=9\mu s$ . In this case  $R_{outmax}/R_{outmin} = 81$ . For the case of  $T_{CL}=25\mu s$  and the same minimal commutation time of the devices, the ratio  $R_{outmax}/R_{outmin} = 576$  is obtained.

The boundary values of the load resistance depend on circuit parameters and can be obtained from (1), (2) and (5) in the form:

$$(7) \quad R_{out\ max} = \frac{kV_{dc} D_{max}^2 T_{CL}}{8V_{chref\ max} C_{ch} N_{Tr}}$$

$$(8) \quad R_{out\ min} = \frac{kV_{dc} D_{min}^2 T_{CL}}{8V_{chref\ min} C_{ch} N_{Tr}}$$

where

$V_{dc}$  is the power supply voltage

$N_{Tr}$  – transformer ratio.

## Results of the PSpice simulation of the transients

The transients by the work of two-phase shifted charge current mode controlled converters, obtained using the PSpice simulator [9], are given in Fig. 8. It is seen that as a result of the applied principle of equal areas for the intervals of output current arising for both converters, current sharing is obtained.

The transients at the start of four working in parallel phase shifted converters are presented in Fig. 9.

## Regulation characteristics

Regulation characteristics of four phase shifted bridge transistor DC-DC converter  $I_{out} = f(V_{chref})$  are given in Fig. 10 for four values of the load resistance  $R_{out}$ .

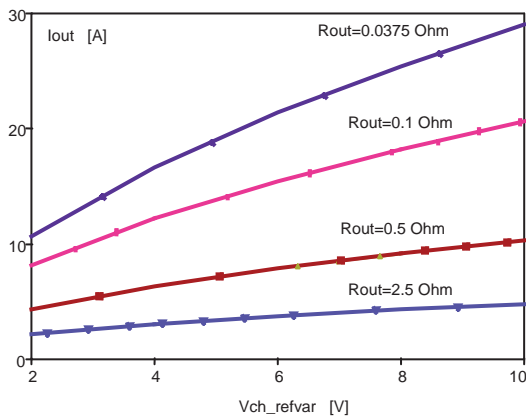


Fig.10. Regulation characteristics of four phase shifted bridge transistor DC-DC converter  $I_{out} = f(V_{chref})$ .

## Conclusion

A charge mode control has been applied to Phase Shifted PWM bridge converter current-double rectifier. The control system is synthesised and the work together with the power circuit is simulated. The boundary values of the load resistance are determined which ensure a proper work corresponding to the charge current mode principle of operation. The transients in the power circuit at the start and the current sharing are simulated using the PSpice program. Based on simulation results, the regulation characteristic is obtained in the graphical analyzer Probe.

## Acknowledgements

This research is in the framework of the BY-TH-115/2005 project.

## References

- [1] Rudenko, V., V. Sanko, I. Chijenko. Converter technique. Kiev, Vischa shkola, 1978.
- [2] High-Frequency, Multiphase Controller TPS40090, Texas Instruments, 2006, <http://www.ti.com>

- [3] UNITRODE – Product & Application Handbook, 1995-1996.

- [4] Ericson, R., D. Maksimović. Fundamentals of Power Electronics. University of Colorado Boulder, Colorado, 1999.

- [5] Capel, A. Charge Controlled Conversion Principle in DC/DC Regulators Combines Dynamic Performance and High Output Power. IEEE Power Electronic Specialists Conference Record, pp. 264-276. 1979.

- [6] Tang, W., F.C. Lee, R.B. Ridley, I. Cohen. Charge Control: Modeling, Analysis and Design. IEEE Power Electronics Specialists Conference, 1992 Record, pp. 503-511.

- [7] Smedley, K., S. Čuk. One-Cycle Control of Switching Converters. IEEE PESC, 1991, pp.888-896.

- [8] Kunov, G., E. Gadjeva, M. Popov, N. Todorov. Development and Spice Simulation of Current Mode Control System for Multiphase Full Bridge Transistor DC-DC Converter. XLIII International Scientific Conference ICEST'2008, Serbia, Nish, June 25-27, 2008.

- [9] PSpice User's Guide, Cadence Design Systems, 2003.

## Biographies



**Georgi Kunov** was born in Mizia, Bulgaria, on June 28, 1951. He graduated from the Technical University of Sofia.

Since 1978 he worked in the Department of Power Electronics, Faculty of Electronic Engineering and Technologies, Technical University of Sofia.

His field of interest includes semiconductor converters for power supply and electro technological applications, control

systems for power electronics converters.

Georgi Kunov is with the Faculty of Electronic Engineering and Technologies, Technical University of Sofia, "Kliment Ohridski" Blvd. No.8, bl. 1, 1000 Sofia, Bulgaria, e-mail: [gkunov@tu-sofia.bg](mailto:gkunov@tu-sofia.bg).



**Elissaveta Gadjeva** was born in Sofia, Bulgaria, on July 14, 1948. She graduated from the Technical University of Sofia, and received PhD degree from the same university. She is today an Associated Professor at the Department of Electronics, Faculty of Electronic Engineering and Technologies, Technical University of Sofia.

Hers field of interest includes CAD in electronics, computer modeling and simulation of electronic circuits.

Elissaveta Gadjeva is with the Faculty of Electronic Engineering and Technologies, Technical University of Sofia, "Kliment Ohridski" Blvd. No.8, bl. 1, 1000 Sofia, Bulgaria, e-mail: [egadjeva@tu-sofia.bg](mailto:egadjeva@tu-sofia.bg).



**Marian Popov** was born in Sofia, Bulgaria, on Sep, 15 1971. He graduated from Department of Power Electronics, Faculty of Electronic Engineering and Technologies, Technical University of Sofia in 1996.

His field of interest includes semiconductor converters for power supply and electro technological applications, control systems for power electronic converters, application of LabVIEW in power electronic

circuit diagnosis.

Marian Popov is currently with Ultraflex Int. 154-1 Remington Blvd, Ronkonkoma NT11779 USA, e-mail: [mariannp@abv.bg](mailto:mariannp@abv.bg).



# Equipment for Infrared Cleaning of Oil Contaminations

Peter Dineff, Nikola Shojlev, Tamara Pencheva, Petko Mashkov and Berkant Gyoch

**Abstract:** Equipment for dry cleaning of aluminum caps from oil and grease contaminations using infrared radiation evaporation is developed. The caps are moved on automatically by hopper along wire way with flow rate 60 – 100 caps/min. Oil contaminations after deep drawing of aluminum caps for food and pharmacy industries are cleaned effectively by application of the equipment.

**Keywords:** heat infrared cleaning, deep drawn aluminium caps.

## Introduction

Infrared heating is preferable technology for different purposes mainly due to a lot of advantages. They are important for design of equipment for radiation oil contaminations cleaning technologies. Most important ones are [1]:

- Non contact heating ensures very good quality at technological operations.

- High energy efficiency of heating.

- High-speed heating which allows high velocity of surface thermal processing of treated materials, heating and cooling.

- Low thermal inertia of the process and short time for heating and cooling.

- Good possibility for precise control of the processes.

- Pure process and pure heat source – there is no contacts with other objects (thermal conductivity) or gases and vapors (convection).

- Module design of heaters, which ensure flexibility and adaptability of technological equipment – it becomes easy to realize different temperature treatment profiles along the caps' way.

Upper mentioned infrared heating advantages are related strong to *IR* metal large square emitters [1] which combine good properties of metal heaters (low inertia, good possibilities of operation control, good mechanical properties) with good emissivity (over 0.9), proper to ceramic *IR* emitters.

In practice all organic materials (plastics, wood, cloths and others) absorb very well *IR* radiation from the middle *IR* spectral region ( $\lambda = 3 \div 8 \mu\text{m}$ ). Thermal conductivity of organic materials is low which determines heat processes as surface ones.

The aim of this paper is to represent equipment developed for *IR* radiation cleaning of polymeric surfaces from oil and grease contaminations by evaporation. The equipment and technology are tested successfully at industrial conditions and are supported with patent, [2].

## Experimental investigations

In Fig. 1 general view of the equipment is shown.

The equipment for *IR* radiation cleaning is developed for application to technological oil and grease contamination upon polymeric coated aluminum caps, deep drawn for pharmacy and food industry.

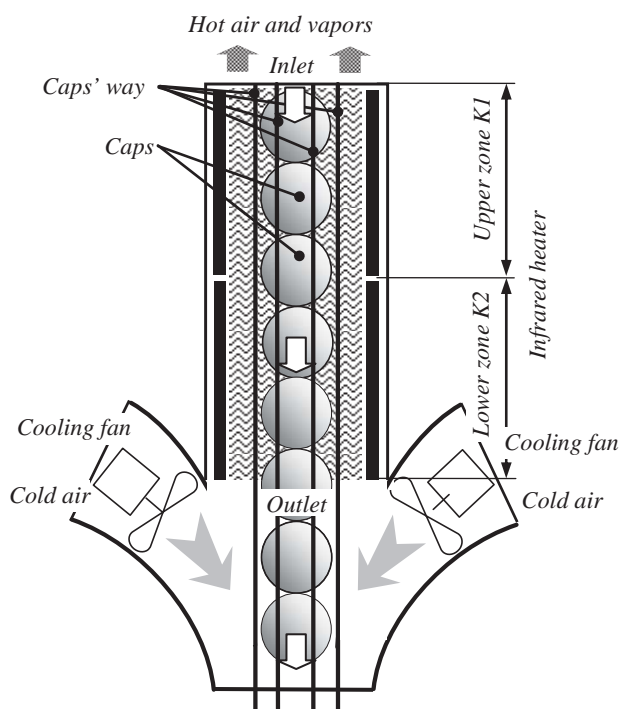


Fig. 1. Equipment for *IR* radiation oil contaminations cleaning.

Technological oil contaminations on the outside polymer cap's surface (epoxy or epoxy phenolic, polyester, or melamine resin protective lacquer) is mainly of medical white oil (*paraffinum liquidum*, mineral oil, cas. № 8042-47-5) with density  $825 \div 840 \text{ kg/m}^3$ , molecule mass about 280 (carbon number  $C_{15 \div 26}$ ), ignition temperature about  $200^\circ\text{C}$ .

Experimental investigations with two types of "white" oil „Marcol 52” (ESSO, USA) and „Ondina Shell 909” (Shell, Austria) are carried out. Behavior of both of them at thermal evaporation is similar and they are statistically undistinguished for this technology. The situation is the same when white oil on the caps contains small amounts of hydraulic oil ( $5 \div 10 \text{ vol. } \%$ ).

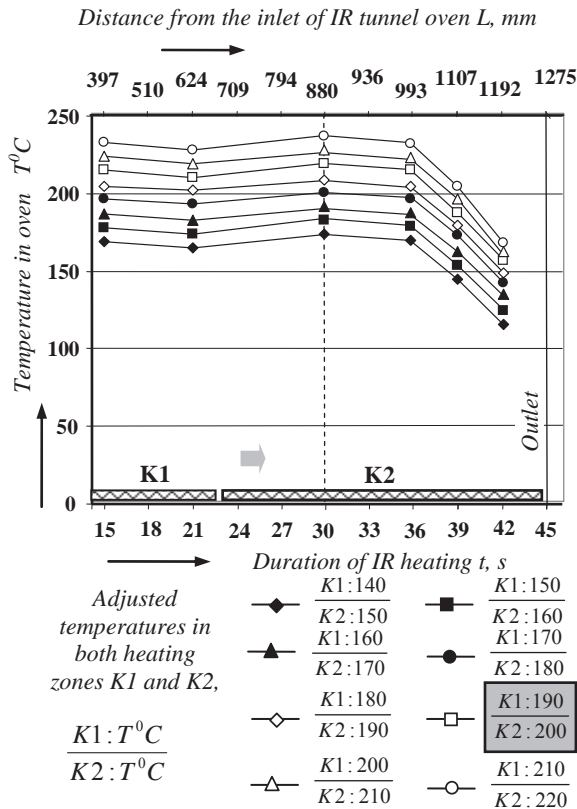


Fig. 2. Temperature distribution  $T(L)$  along the length  $L$  of IR tunnel oven (temperature profile) in connection with time  $t$  from the entrance of caps to the tunnel at rate 60 caps/min at different adjusted temperatures for both temperature controllers: K1 for upper zone and K2 for lower zone.

The equipment for IR radiation oil contamination cleaning has the following constructive features, Fig. 1:

- Vertical "II"-shaped IR heater around the caps' wire way.
- The hole of the "II"-shaped IR heater makes possible easy mounting and dismounting of the wire way.
- The "II"-shaped IR heater consists of two parts which determine two heating zones – upper (K1) and lower (K2), Fig. 1. The temperature in both zones is independently controlled.
- The caps axes are horizontally oriented during their movement through the IR tunnel oven. Caps' movement is forced by gravity. Feeding of the conveyor is automatically by hopper.
- At every tact of conveyor the caps move to the next position. This movement is controlled by gate which lets pass one cap at every cycle open - close (at rate 60 times/min). In this manner of movement's control there are always 45 caps in the hot tunnel of the IR oven.

- The temperature profile along the hot tunnel of the IR oven is set by influence of two air flows from two fans, Fig. 1. Fans flows, as it is known from the Bernoulli's principle, lead to drawing down hot air and vapors opposite to the convection in the tunnel. By this design of equipment it is possible to control hot air and vapors flow direction and its velocity.

Experimental investigations are performed using aluminum caps' 28x38 mm after deep drawing (HDDC - Herti Deep Drawn Pilfer Proof Closure) with standard dimensions (for bottle throat 28x38 mm, DIN 6094-7):  $D = 28 \pm 0.4$  mm;  $H = 38 \pm 0.2$  mm and average cap's weight  $2.3 \div 2.4$  g.

## Results and discussions

Temperature profile along the hot tunnel of IR oven is set by influence of two air flows from two symmetrically located fans, Fig. 2, according to the Bernoulli's principle. This design of equipment leads to drawing down hot air and vapors from the outlet of the oven's tunnel.

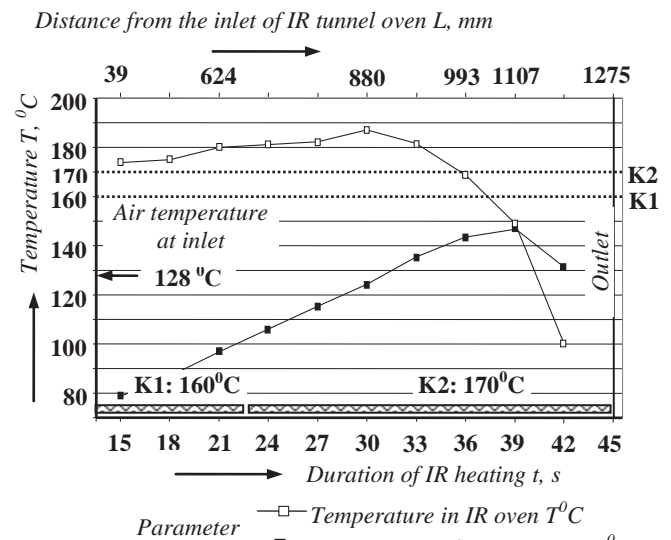


Fig. 3. Temperature profile in hot tunnel of IR oven and caps' temperature profile during passing through the tunnel; adjusted controllers' temperatures for upper (K1) and lower (K2) zones are 160/170°C. Temperature of leaving mixture of air and oil vapors at inlet of the oven is 128°C.

As can be seen from Fig. 3, temperature profile is with relatively flat maximum in zone K2 (880 mm) and relatively uniform distribution of temperatures along 1000 mm distance from inlet of the oven. Temperatures are higher than adjusted temperature for upper zone K2, Fig. 3.

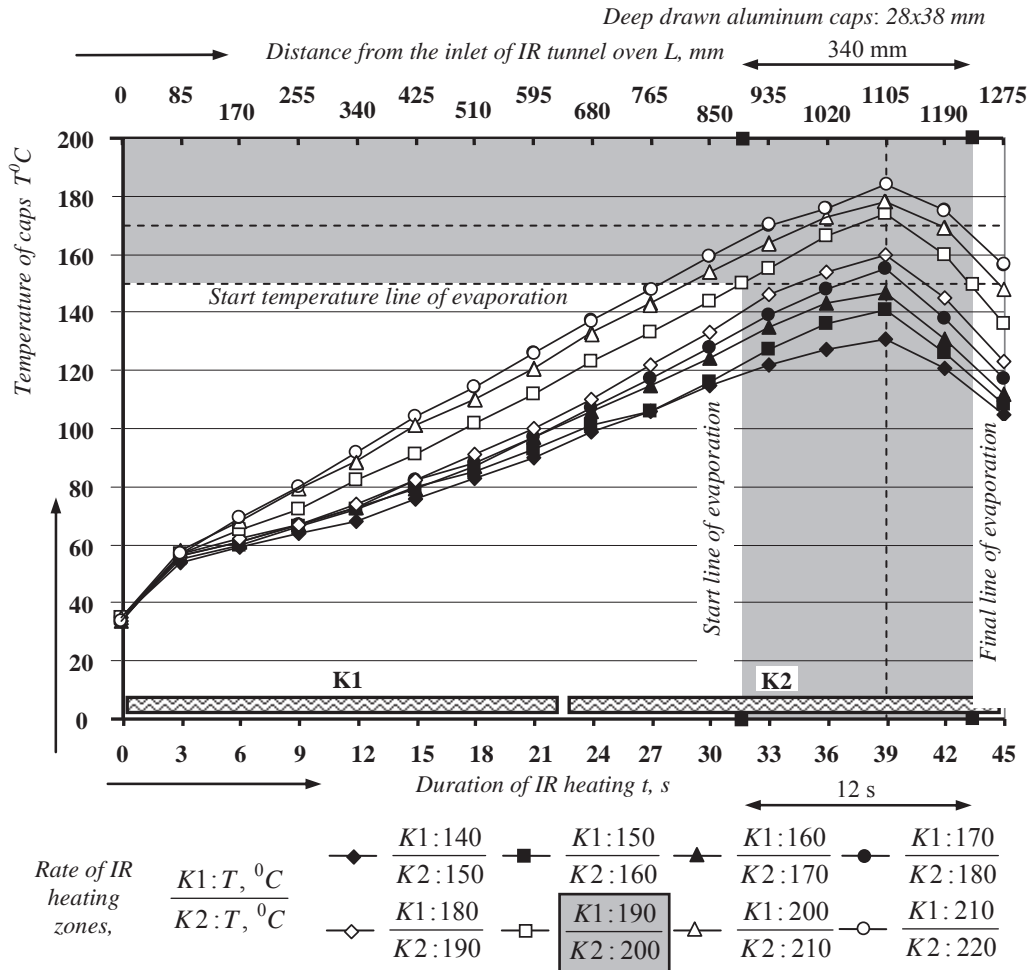


Fig. 4. Caps' temperature profile at different temperature operation regimes of IR oven. In grey color the area of intensive oil evaporation is shown. The most effective operating regime for oil cleaning: adjusted temperatures for K1 and K2 zones are 190/200°C.

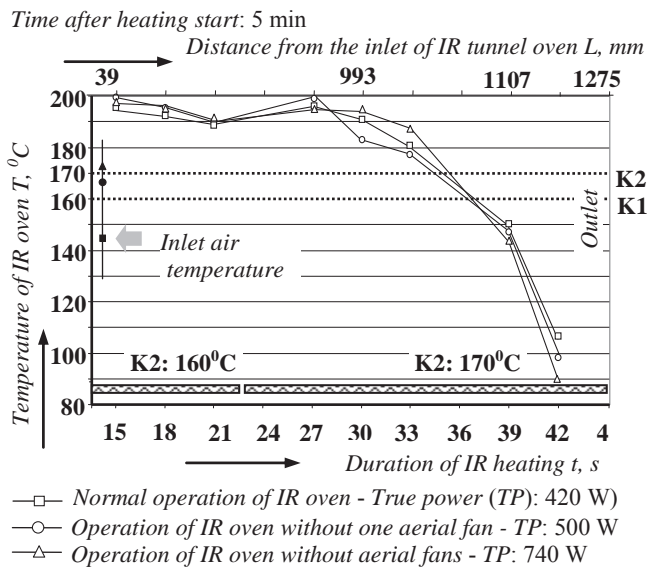


Fig. 5. Influence of fans (Bernoulli's effect) on temperature profile of the IR oven - 5 minutes after start.

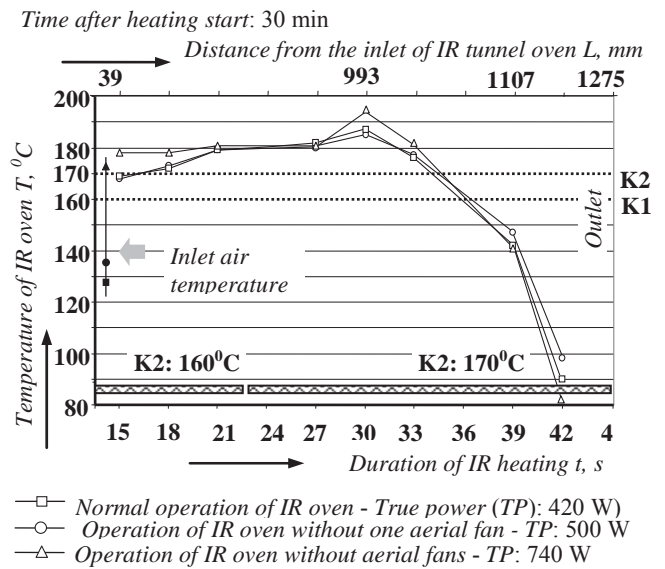


Fig. 6. Influence of fans (Venturi's effect) on temperature profile of the IR oven - 30 minutes after start.

From the static experiments (without caps' movement) of IR oil cleaning technology it is known that oil intensive evaporation begins at temperature in the oven's tunnel over 170°C. Investigations show that at operating regime with adjusted temperatures for zones K1 and K2 160°C/170°C temperature is over 170°C along the tunnel at distance 993 mm from the inlet of the oven, but cleaning effect is not satisfactory. Surface caps' temperature (measured by thermocouples) remains under 150°C, Fig. 3.

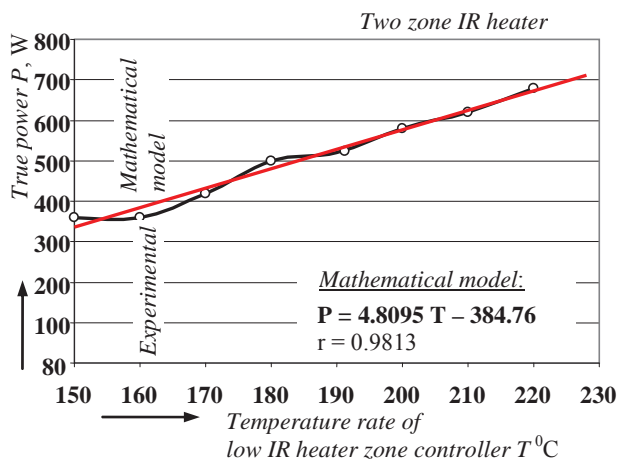


Fig. 7. True power variations of the IR furnace in dependence of temperature at normal operation – with two operating fans (Venturi's effect).

For all operation regimes of the IR oven temperature profile of the thermal treating of caps is investigated. The amount of the evaporated oil is measured gravimetrically.

Technological process becomes effective when adjusted temperatures for both controllers reach up to 190°C/200°C. Intensive oil evaporation is carried out between 900 mm and 1125 mm along the tunnel of the oven (which corresponds to time 32 ÷ 43 s from the inlet of caps in the tunnel), Fig. 4.

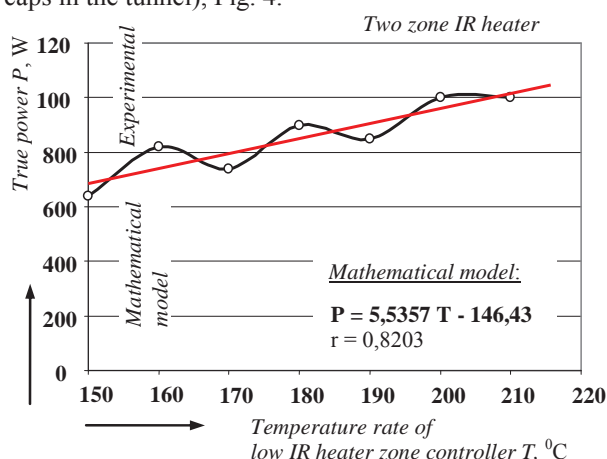


Fig. 8. True power variations of the IR furnace in dependence on temperature at failure operation – with two non operating fans (without Venturi's effect).

- Fans' operation (or Venturi's effect) is very important because of its influence on temperature

distribution along the oven as at start of IR oven operation, Fig. 5, and at stationary operation regime of the oven, Fig. 6. It is impressive that when both fans don't operate, temperature profile in the oven changes significantly, Fig. 5 and Fig. 6, and true power consumed from the oven increases almost two times, Figs. 7 and 8.

- It is necessary to protect IR oven from breakdown stopping of one or both fans because it'll disturb normal oven's operation.
- Additional investigations on the polymer coating quality at prolonged stay in the tunnel at normal operation of the heaters are carried out. This is breakdown regime of the conveyor operation when the caps' transport is stopped due to any reason. It is found that there are some polymers' coatings for which those operating regime doesn't cause reject. There are some others (with light colors) which appearance becomes worse.
- The investigations on the polymer coating quality at breakdown regime of the conveyor operation, when the caps' transport is stopped and then the IR heaters' power supply is turned off, are carried out too. The obtained results show that the caps cool together with the oven, and surface coating quality rests well enough. This fact shows that it is necessary to use protection so that when caps' transport is stopped IR heaters power supply to be switched off.

Experiments demonstrate that the IR oven should be switched on when oven's tunnel is full of caps. The caps' movement starts when the temperature distribution along the tunnel becomes stationary according to adjusted temperatures' values of the controllers.

## Conclusions

As a result of the experimental investigations on operation of developed and produced equipment for IR radiation oil contaminations cleaning, possibility for application of this kind of technology in industry is proven. It is realised at relatively high productivity of conveyor – 60 ÷ 100 caps/min, or 3 600 ÷ 6 000 caps/h.

## Acknowledgements

The National Science Fund, Ministry of Education and Science of Bulgaria, is gratefully acknowledged for the financial support of research project VU-EES-301/2007.

Herty, Ltd., (Shumen, Bulgaria) is gratefully acknowledged for the support of research project VU-EES-301/2007.

## References

- [1] Mashkov P., T. Pencheva, D. Popov, V. Mateev. Electronic Pulse Control for Low Inert Infrared Heaters. Proceedings of the 12<sup>th</sup> International Conference ELECTRONICS ET'2003, Sozopol, Bulgaria, 2004, 369 – 375.
- [2] Dineff, P., N. Shojlev, T. Pencheva, and P. Mashkov. Method and Device for Oil Contamination Cleaning of Caps and Closures. BG Patent Application No 109 981 20080204.



## Biographies



**Peter Dineff** was born in Sofia, Bulgaria, on July 02, 1947. He graduated the Technical University of Sofia – Mr.S in Electrical Engineering, Ph.D. in Electrical technology, Lecturer and Assoc. Professor in the field of Electrical processing and apparatus. Since 1991 he is Assoc. Professor at the Faculty of Electrical Engineering of Technical University of Sofia. Main field of interest: electrical processing and apparatus, material (polymer) science, surface engineering, electrochemistry. He has large activities in the field of innovation and invention. Peter Dineff is in the Faculty of Electrical Engineering of Technical University of Sofia, 8 St. Kliment Ohridski Blvd, 1000 Sofia, Bulgaria, (e-mail: dineff\_pd@abv.bg).



**Nikola Shoylev** was born in Vratza, Bulgaria, on February 19, 1949. Died on April 20, 2008. He graduated the Technical University of Sofia – Mr. S. in Electrical Engineering, Ph. D. in Electrical processing and apparatus, Doctor of Technical Science (1999). He was Engineer in the Atom Power Plant of Kozloduy (1972-1974). He was Research associate on electrical technology in Institute of Electrical Industry (1974–1986). Since 1991 he was Associate Professor, and since 2001 - Professor in the Electrical engineering at the University of Chemical Technology and Metallurgy - Sofia. Main field of interest: electrical engineering, power engineering, electrical technology, robotics, transfer of technology, and expertise in the field of innovations.



**Tamara Pencheva** was born on January, 1948. She graduated from the Faculty of Radio-electronics in Saint-Petersburg Politechnical University “Kalinin” – Mr.S. in Physics of semiconductors; Ph.D. at Physical-Technical Institute “Ioffe”, Russian Academy of Sciences – in Physics of waves processes. Since 1974 she worked in the Faculty of Electrical Engineering of University of Rousse “Angel Kanchev” as a lecturer and Assoc. Professor in the field of physics, infrared heating and optoelectronics. Tamara Pencheva is a Head of Physics Department in University of Rousse. Her address is: 8 Studentska Str., 7017 Rousse, Bulgaria (e-mail: tgp@ru.acad.bg).



**Petko Mashkov** was born in Rousse, Bulgaria, on August 30, 1955. He graduated from the Sofia University “Kliment Ohridski” – Mr.S. in Physics of semiconductors; University of Rousse “Angel Kanchev” – Mr.S. in Internal combustion engines. Since 1980 he worked in the Faculty of Electrical Engineering of the University of Rousse “Angel Kanchev” as a researcher and lecturer in the field of infrared heating, physics and electronics. His address is: 8, Studentska Str., 7017 Rousse, Bulgaria (e-mail: pmashkov@ru.acad.bg).



**Berkant Gyoch** was born in Razgrad, Bulgaria, on May 24, 1977. He graduated from University of Rousse “Angel Kanchev” – Mr.S. in Telecommunications. His field of interest includes optoelectronics; thin layers; microelectronic technologies. Today he is a Ph.D. student in the Faculty of Electrical Engineering of University of Rousse. His address is: 8, Studentska Str., 7017 Rousse, Bulgaria (e-mail: b\_gyoch@ru.acad.bg).

# Infrared Oil Contamination Cleaning Technology for Polymer Surfaces

Peter Dineff, **Nikola Shojlev**, Tamara Pencheva, Petko Mashkov and Berkant Gyoeh

**Abstract:** The investigation deals with development of dry method for polymer surfaces cleaning from oil and lubricant contaminations by infrared evaporation. Parts to be cleaned are transported in vertically oriented wire way passing through tunnel IR oven forced by their own weight. Oil vapors and hot air move to the upper side of the oven, opposite to the parts' movement direction.

**Keywords:** infrared evaporation; infrared cleaning technology for polymer surfaces.

## Introduction

In practice it is often impossible to avoid oil contaminations during wide-used pressing operations, especially at deep drawing of metal screw caps for food and pharmacy industry.

Oil contaminations upon polymer protecting coating of caps are non-desirable. They reduce adhesion of next layers during side printing and lacquering and raise dust contamination on aluminum caps during next technological processings.

Different application of "wet" cleaning processes, like swift-flowing washing [1] or ultrasonic cleaning bath for pharmaceutical ampoules and bottles, wafer, contact lenses, and connectors [2, 3, 4 and 5] are well known. Wet cleaning methods possess an essential disadvantage – need of drying after degreasing processes. This technological process lasts long and consumes large amount of electrical energy. Although the quality achieved by ultrasonic cleaning process is excellent, as a whole wet cleaning's energy efficiency is very low.

At proper temperature in order to evaporate oil contaminations resistance furnaces for surface "dry" cleaning are often used. Additionally for relatively thin oil layers (200 ÷ 500 nm) flame, plasma surface cleaning and other processes are applied.

Infrared heating is preferable technology for different purposes mainly due to some advantages which it offers:

- No contact heating ensures very good quality at technological operations.
- One stage heating with high energy efficiency.
- Possibility of high-speed heating which allows high velocity of surface thermal processing of treated materials, heating and cooling.
- Low thermal inertia of the process and short time for heating and cooling.
- Good possibility for precise control of the processes.
- Pure process and pure heat source – there is no fuels and fuel burning.
- Flexibility and adaptability of technological equipment and possibility for module design of heaters.

The main task of the investigation is to present a new "dry" technology for cleaning of polymer surfaces from oil and grease contaminations by infrared heating.

The investigation deals with cleaning of outer polymer layer upon aluminum cylindrical caps after two-stage deep drawing from oil contaminations (lubricating and hydraulic) and liquid lubricants ("white" oil or liquid paraffin). Infrared cleaning by evaporation is realized by low inert infrared heaters with large area and emissivity of 0.90 ÷ 0.95 in the spectral region 3 ÷ 10  $\mu\text{m}$ .

## Experimental investigations

In connection with development of technology some main experimental investigations are carried out:

- Static technological investigation for one or three caps in line which are pushed in and pulled out the opened tunnel of infrared oven.
- Dynamic technological investigation for moving caps. Its movement is realized by influence of gravity at 60 caps/min movement rate through the tunnel of vertical infrared furnace.
- Dynamic technological investigation for moving caps with automatic loading of furnace tunnel by hopper and air transport in wire way at 60 caps/min movement rate.

Technological contamination on outer polymer surface (of epoxy or epoxy phenol, polyester, or melamine resin protective lacquer) of caps and closures is mainly from medical white oil (*paraffinum liquidum*, *mineral oil*, cas. № 8042-47-5) with density 825 ÷ 840  $\text{kg/m}^3$ , molecular mass about 280 (carbon number  $\text{C}_{15-26}$ ), ignition temperature about 200°C.

Surface contamination is imitated in two ways:

- Oiling of two parallel bands on the caps' surface (bands 2 in Fig. 1) using cotton-wool impregnated with corresponding lubricant. Dry band 1 in Fig. 1 between two oiled ones allows determining visually the degree of oil evaporation. When the oil is fully evaporated, the borders between bands 1 and 2 disappear.

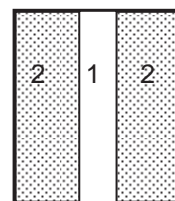


Fig. 1. Special oil treatment of caps' surface: 1 – control zone without oil; 2 – oiled zones.

- Oiling of the surfaces of 1200 caps by aerosol oil cloud from 2 m height. After that the caps are shackled up in polyethylene sack during 5 min. The oil quantity (3.0 mg/cap) and its distribution onto the caps' surfaces imitate the worst case of contamination, which is with middle probability in real production.

Oil contamination can be seen as an oil layer onto caps' head and outer cylindrical caps' surface combined with small amount of droplet fraction.

Experimental investigations are carried out using aluminum cylindrical caps (after deep drawing) *HDDC* (*Herti Deep Drawn Pilfer Proof Closure*) 28 x 38 mm with standard dimensions:  $D - 28 \pm 0.4$  mm (for bottle mouth 28 x 38 mm according to DIN 6094-7),  $H - 38 \pm 0.2$  mm and an average weight of one cap  $2.3 \div 2.4$  g.

Middle infrared spectral region is preferable for industrial applications because most of materials absorb very well infrared radiation (over than 90 %) between 3 and 10  $\mu\text{m}$ . Infrared large square metal emitters in use like ceramic emitters belong to so called dark emitters. Their work temperatures are below 650  $^{\circ}\text{C}$ , (1000 K) and over 80 % of emitted energy is with wavelengths over 3  $\mu\text{m}$ . The maximum of the spectral distribution of emitted energy is in infrared spectral region (with wavelengths  $2 \div 4$   $\mu\text{m}$ ) and more than 70 % of energy is with wavelengths  $4 \div 10$   $\mu\text{m}$ .

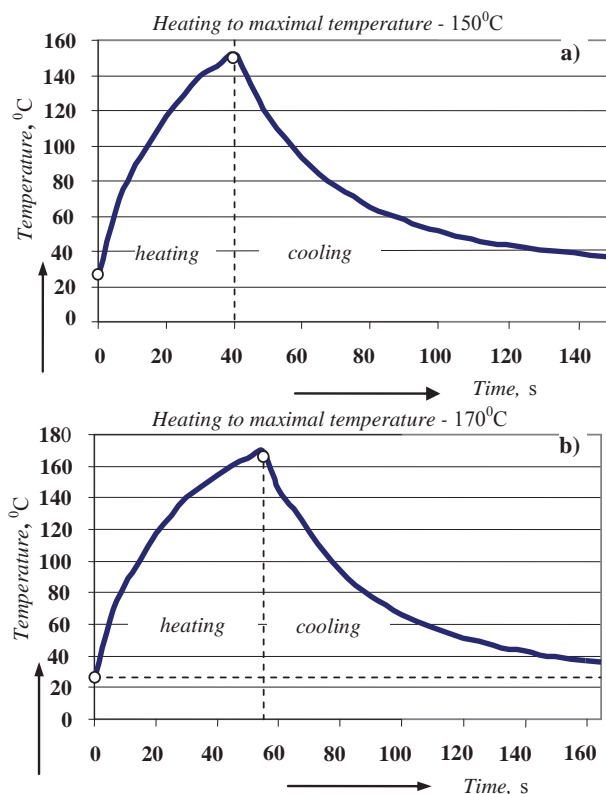


**Fig. 2.** Dynamics of heating to limited maximal temperature  $T_{\text{max}}$  and cooling at room temperature out of IR oven of caps *HDDC* 28x38 mm: a)  $T_{\text{max}} = 150^{\circ}\text{C}$ ; b)  $T_{\text{max}} = 170^{\circ}\text{C}$ .  $150^{\circ}\text{C}$  – beginning of intensive evaporation;  $170^{\circ}\text{C}$  – full oil evaporation.

Infrared large square metal heaters (stainless steel with surface enriched with chromium oxide) have emissivity over 0.9, like the best ceramic heaters for this applications.

Surface temperature of caps is measured in the line of touch between two caps, auxiliary of the *IR* oven channel, because this place is in shadow at *IR* radiation treatment. Temperature is measured by thermocouple type K.

Rest oil contaminations on the caps' surface is measured by gravimetric method after cleaning in ultrasonic bath with proper washing solution during 40 s and thermal drying in oven at 105  $^{\circ}\text{C}$  until reaching constant weight.

## Results and discussions

Dynamics of temperature changes on the caps' surface at oil evaporation are investigated. After reaching determined maximal temperature  $T_{\text{max}}$  (from 130 $^{\circ}\text{C}$  to 170 $^{\circ}\text{C}$ ) caps are pulled out from the hot zone and are cooled at room temperature staying in the wire way.

From the analysis of the experimental study and obtained results (see Fig. 2) the following conclusions can be done:

- Two kinds of "white" oil in use „*Marcol 52*” (*ESSO*, USA) and „*Ondina Shell 909*” (*Shell*, Austria) are statistically indistinguishable in respect to thermal evaporation. The same may be said about white oil contamination by hydraulic oil (up to 5  $\div$  10 vol. %).
- Surface temperature of *IR* heaters reaches maximal values about 240 $^{\circ}\text{C}$ .
- At maximal temperatures on the caps' surfaces up to 130 $^{\circ}\text{C}$  there is no significant oil evaporation.
- At maximal temperature 150 $^{\circ}\text{C}$  significant oil evaporation occurs, but at thick oil layers oil contaminations rest on the caps' surfaces.
- At maximal temperature of 170 $^{\circ}\text{C}$  complete evaporation of oil layer occurs independently of oil layer thickness, i.e. at this temperature full surface cleaning of caps is guaranteed.
- If caps' surface temperature rises over 210 $^{\circ}\text{C}$   $\div$  220 $^{\circ}\text{C}$  undesirable changes in lacquer coating may be observed – color changes and surface layer cracking.
- Time for free cooling of the caps after their heating to  $T_{\text{max}}$  doesn't change significantly with increasing of  $T_{\text{max}}$ : for instance, at heating caps to 130 $^{\circ}\text{C}$  cooling time to 37 $^{\circ}\text{C}$  is 110 s, and at 170 $^{\circ}\text{C}$  this time is the same, 110 s.
- Time for caps' heating to  $T_{\text{max}}$  changes significantly at  $T_{\text{max}}$  increasing: for instance, heating time to 130 $^{\circ}\text{C}$  is about 25 s, while the heating time to 170 $^{\circ}\text{C}$  is about 55 s, i.e. about two times longer.

• Long duration of the caps' heating process requires long tunnel of the *IR* oven. So at velocity of 60 caps/min the tunnel length should be 2.70 m.

• This result sets the requirements for the next stage of experimental investigation (dynamic experiment): to short the oven's length and to enhance heaters'

temperature. This will reduce the time for reaching of required temperature, in this way the IR heating efficiency will raise at significantly shorter oven's tunnel length.

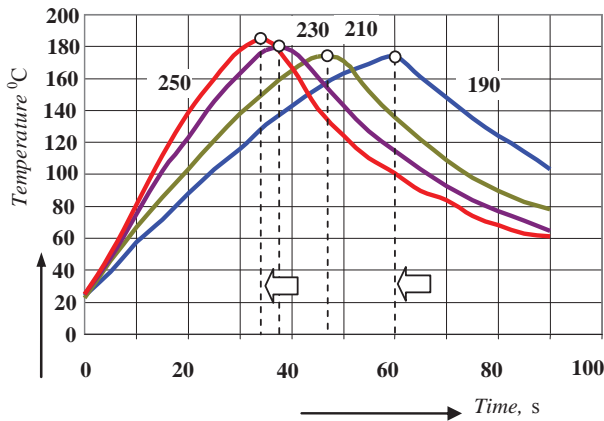


Fig. 3. Heating process control in accordance with air maximal temperature (250°C, 230°C, 210°C and 190°C) at the entrance of heated infrared oven.

Caps move through the horizontal tunnel of linear IR oven in wire way made from stainless steel. The wire way is heated almost uniformly in a zone definite by IR heaters along the oven's length. End effects may be seen at distance 60 mm inside from the end of the oven, Fig. 4. Temperature decrease very quickly to safe temperatures for operators' – 37°C, at distance about 90 mm out of the oven, Fig. 4.

An additional investigation is carried out at enhanced temperatures of IR emitters, see Fig. 3. Temperature control is realized in accordance to outlet gases' and vapors' maximal temperature in the entrance of vertical IR oven, Fig. 5,  $\alpha = 90^\circ$ .

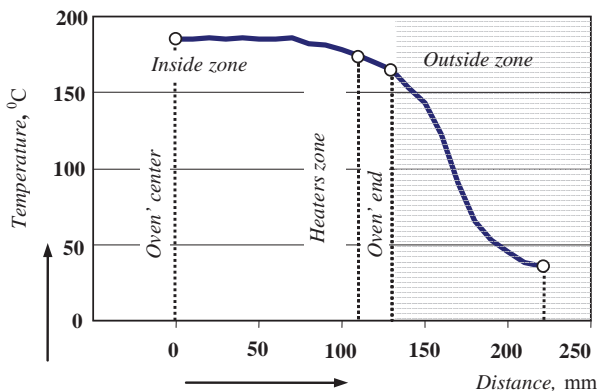


Fig. 4. Temperature distribution in stationary regime on the hottest wire from the wire way through the tunnel IR oven (along the oven's length). The wire's temperature decreases to 37°C at distance about 90 mm out of the oven. The oven in this experiment is disposed horizontally

It may be accepted that contacts between the caps and wire way is not a problem for quality of caps coating because wire's temperatures are close to surface caps temperatures. Out of the oven the wire way temperature

decreases very quickly from 160°C to human's body temperature at distance about 90 mm.

According to the results concerning IR oil cleaning of caps in stationary regime, some main conclusions may be done:

- Caps' heating in stationary regime is realized at limited air temperatures in the tunnel of the oven - about 250°C and IR emitters' temperature – about 280°C.
- Influence of shadowing between caps in the row as and shadowing from the wire way upon the time of reaching of required temperature for full oil cleaning is not significant.

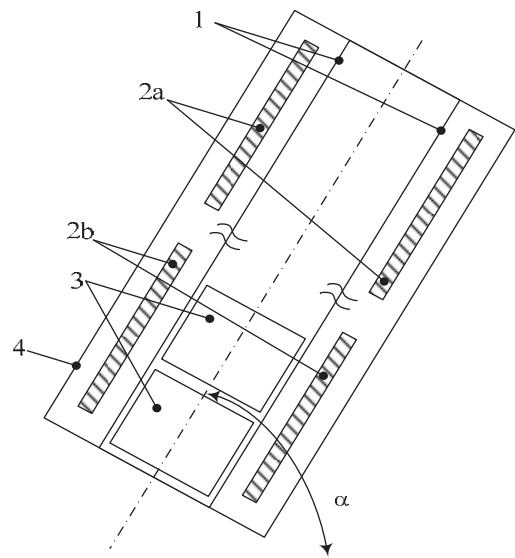


Fig. 5. Experiments at different values of angle between ovens' axis: 1- wire way; 2a and 2b – upper and lower parts of the heaters; 3- caps; 4 – oven' body.

Experiments at different values of angle between ovens' axis and horizontal plane are carried out, see Fig. 5. The obtained results show that the optimal disposition is vertical. At these conditions convection in the oven's tunnel may be essential for the caps preheating. This effect may be used in a way that hot air and oil vapors should move in direction opposite to the movement of caps to be cleaned.

Equipment with two sections of the heaters is developed. Temperature control is carried out by two thermo-controllers tuned up for the temperature of down heating section to be with 10°C higher than for the upper heating section.

Oven heating begins from room temperature. The wire way is filled with caps. When the temperature reaches value set by controller the movement of caps begins. The rate of the caps movement is determined by control of the gate at the end of the tunnel oven. Forced by gravity the caps move step by step at every cycle: open – close the gate. The cycle is 1 s, i.e. the productivity of the equipment is 60 caps per minute.



At every of investigated operating regimes of the equipment for the caps passed through the oven next tests are made:

- i) the level of the whole contamination determination, greasing and dust dispersion contaminations;
- ii) ultrasonic test of coating strength and adhesion;
- iii) technological test – the operation side printing – printing and lacquer.

The cleaning efficiency after thermal treating is determined by the rest quantity of white oil on the caps' surface by weight method.

The caps may be considered as clean at rest oil contamination less than 0.3 mg/cap.

Investigations of different operating regimes of the equipment are carried out: adjusted temperatures of both temperature controllers are 190<sup>0</sup>C/20<sup>0</sup>C, 200<sup>0</sup>C/210<sup>0</sup>C and 210<sup>0</sup>C/220<sup>0</sup>C. The results obtained show that the cleaning is effective for high initial caps' greasing of about 3 mg/cap and rate of conveyor feeding of 60 caps/min. Average *IR* oven's temperature (temperature of the air and oil vapors in the entrance of the oven) is 200<sup>0</sup>C ± 15<sup>0</sup>C.

For lower initial caps' greasing (of 0.5, ..., 1.0, ..., 2.0 mg/cap) at the same rate of feeding (of 60 caps/min) it is reasonable to consider that good enough cleaning quality of caps' surface (to satisfy standards' requirements) may be reached using regimes 170<sup>0</sup>C/180<sup>0</sup>C, 180<sup>0</sup>C/190<sup>0</sup>C and 180<sup>0</sup>C ± 10<sup>0</sup>C.

Investigations for regimes in wider temperature regions 170<sup>0</sup>C/200<sup>0</sup>C and 180<sup>0</sup>C/200<sup>0</sup>C show that relatively high cap oil contaminations (about 1.0 mg/cap) rest after treatment. Probably it is due to lack of correspondence between rate of feeding and temperature profile along the tunnel of *IR* oven at adjusted temperatures of both temperature controllers. The reason for upper mentioned result is also connected with the manner of caps' oiling for these experiments. The caps are oiled by spraying, that is why there are oil droplets and drops on the surface. At normal operating conditions those type of oil contamination is very rear. In this way chosen manner of caps' oiling imitates the worst possible oil contamination. During normal technological operation regimes oil is usually used as lubricator at deep drawing and oil is in form of thin layer on the caps' surface without drops and droplets. It is known that it is more difficult to evaporate drops and droplets comparing with a film. By this way in experiments additional trials for the method efficiency determination are foreseen. Experiments show that at proper regimes of operation of developed equipment even at this situation problems with caps' cleaning may be solved successfully. It guarantees applicability of developed technology in industry.

Experimental investigations for application of *IR* cleaning technology at conditions very close to real operation of conveyor are carried out. Optimal results for oil contaminations cleaning by *IR* evaporation are obtained at regime 190<sup>0</sup>C/200<sup>0</sup>C.

Calculation of energy efficiency of *IR* cleaning technology is based on the fact that average power of the

heaters during operation is 550 W and specific energy consumption is about 1.53 10<sup>-4</sup> kWh/cap (0.15 Wh/cap).

## Conclusions

As a result of theoretical and experimental investigations a new dry technology for cleaning of aluminium caps with polymer coating for food and pharmacy industries from technological oil and grease contaminations by infrared evaporation is developed. Its applicability in industry is proven at productivity of 60 caps per minute.

## Acknowledgements

The National Science Fund, Ministry of Education and Science of Bulgaria, is gratefully acknowledged for the financial support of research project VU-EES-301/2007.

Herty, Ltd., (Shumen, Bulgaria) is gratefully acknowledged for the support of research project VU-EES-301/2007.

## References

- [1] Carpmaels & Ransford. Can treating apparatus. UK Patent B67 C1/00 1429450 19740607;
- [2] Park Jeong Hun, Pyun Do Seon. Wafer cleaning unit using ultrasonic cleaner. KR Patent H01 L21 20040029578 20021001;
- [3] Rudenko, B. Method of ultrasonic cleaning of contact lenses. UA Patent B08 B3/12 20050012016U 20051214;
- [4] Hesch, L., A. Leichliter. Ultrasonic device for cleaning connectors. US Patent B08 B3/12 20050203781 20050815;
- [5] Gilbert, N., K. Williams. Ultrasonic cleaning method and apparatus. WO Patent A6 L2/025 2006US29982 20060810;.

## Biographies



**Peter Dineff** was born in Sofia, Bulgaria, on July 02, 1947. He graduated the Technical University of Sofia – Mr.S in Electrical Engineering, Ph.D. in Electrical technology, Lecturer and Assoc. Professor in the field of Electrical processing and apparatus. Since 1991 he is Assoc. Professor at the Faculty of Electrical Engineering of Technical University of Sofia. Main field of interest: electrical processing and apparatus, material (polymer) science, surface engineering, electrochemistry. He has large activities in the field of innovation and invention. Peter Dineff is in the Faculty of Electrical Engineering of Technical University of Sofia, 8 St. Kliment Ohridski Blvd, 1000 Sofia, Bulgaria, (e-mail: dineff\_pd@abv.bg).



**Nikola Shoylev** was born in Vratza, Bulgaria, on February 19, 1949. Died on April 20, 2008. He graduated the Technical University of Sofia – Mr. S. in Electrical Engineering, Ph.D. in Electrical processing and apparatus, Doctor of Technical Science (1999). He was Engineer in the Atom Power Plant of Kozloduy (1972-1974). He was Research associate on electrical technology in Institute of Electrical Industry (1974–1986). Since 1991 he was Associate Professor, and since 2001 - Professor in the electrical engineering at the University of Chemical Technology and Metallurgy - Sofia. Main field of interest: electrical engineering, power engineering, electrical technology, robotics, transfer of technology, and expertise in the field of innovations.



**Tamara Pencheva** was born on January, 1948. She graduated from the Faculty of Radio-electronics in Sant-Petersburg Politechnical University “Kalinin” – Mr.S. in Physics of semiconductors; Ph.D. at Physical-Technical Institute “Ioffe”, Russian Academy of Sciences – in Physics of waves processes. Since 1974 she worked in the Faculty of Electrical Engineering of

University of Rouse “Angel Kanchev” as a lecturer and Assoc. Professor in the field of physics, infrared heating and optoelectronics. Tamara Pencheva is a Head of Physics Department in University of Rouse. Her address is: 8 Studentska Str., 7017 Rouse, Bulgaria (e-mail: [tgp@ru.acad.bg](mailto:tgp@ru.acad.bg)).



**Petko Mashkov** was born in Rouse, Bulgaria, on August 30, 1955. He studied at the Sofia University “Kliment Ohridski” – Mr.S. in Physics of semiconductors; Rouse University – Mr.S. in Internal combustion engines. Since 1980 he worked in the Faculty of Electrical Engineering of the Rouse University as a Lecturer and researcher in the field of infrared heating and electronics. Petko Mashkov is in the Faculty of Electrical Engineering, Rouse

University, 8, Studentska Str., 7017 Rouse, Bulgaria (e-mail: [pmashkov@ru.acad.bg](mailto:pmashkov@ru.acad.bg)).



**Berkant Gyoch** was born in Razgrad, Bulgaria, on May 24, 1977. He studied at the Rouse University “Angel kanchev”–Mr.S. in Telecommunications. His field of interest includes optoelectronics; thin layers; microelectronic technologies. He is today a PhD student in the Faculty of Electrical Engineering of the Rouse University. Berkant Gyoch is in the Faculty of Electrical

Engineering, Rouse University, 8, Studentska Str., 7017 Rouse, Bulgaria (e-mail: [b\\_gyoch@ru.acad.bg](mailto:b_gyoch@ru.acad.bg)).

# Modeling of processes at polyamide parts' IR welding

Angel Valentinov Valchev, Petko Hristov Mashkov, Tamara Grigorievna Pencheva,  
Berkant Seydali Gyoch

**Abstract:** *The modeling of processes at polyamide parts' IR welding. In that paper the General Heat Transfer modelling method is used. It is a part of the program product Comsol Multiphysics version 3.3. Using built-in program for time dependent analysis choice of optimal temperature regime for IR plastic's welding is performed. This method allows reducing the losses of time and materials and makes easier the choice of optimal parameters of this technological operation. This modelling method permits to foresee temperature distribution in the sample's depth in dependence on time and radiation power (heaters' temperature), which is practically impossible to be measured. It is very important for the welding joints quality because it is necessary plastics to be melted to the definite depth on the whole area during heating process. At the same time surface temperature should not reach definite temperature (in dependence of the type of the plastics). Beyond that temperature the sample's adhesion worsens. A verification of the modeling results is made by investigations of surface temperature changes during welding using a special non-contact measuring system. The agreement between modeling and experimental results is very good and they are applied into industrial production.*

**Keywords:** IR welding, plastics, polyamide, simulation, modelling, heat transfer.

## Introduction

Using of infrared heating has many advantages compared to the other methods for plastic welding. It is a non-contact method; it is faster; more economical, easier for automation [4]. Therefore the method has a large application in industry [1, 7]. The industry necessities require the improvement and optimizing of the production process which leads to saving of power, time and materials. The modeling of processes at plastic details' infrared welding quickly achieves the rational solution in order to provide a higher work quality. The infrared welding of plastic details is performed using oven with infrared heaters for the middle infrared spectral region. The investigations are performed when the, material for welding is polyamide for three temperature regimes. The investigations are connected with temperature distribution in the depth of details during the heating process. The tasks of heat

treatment are: plastic should be melted to the depth of 1mm on the whole treated area; the surface temperature of the detail should not exceed definite temperature; the duration of the treatment should be as short as it is possible. This definite temperature depends on the type of the plastic (for polyamide 6 it is about 280°C [7]). If the temperature of the plastic exceeds this temperature destruction occurs which strongly worsens the adhesion between welding details.

Experimental investigations of temperature distribution in the detail's depth during heat treatment are practically impossible. That's why modeling results are very important for choice of optimal temperature regimes for plastics' welding. Verification of modeling results is made by investigations of surface temperature changes during welding using a special non-contact measuring system [13].

## Modeling Approach

The problem mentioned above is resolved with the help of the program product Comsol Multiphysics version 3.3 with using the modeling method for General Heat Transfer. The scheme of oven is given in

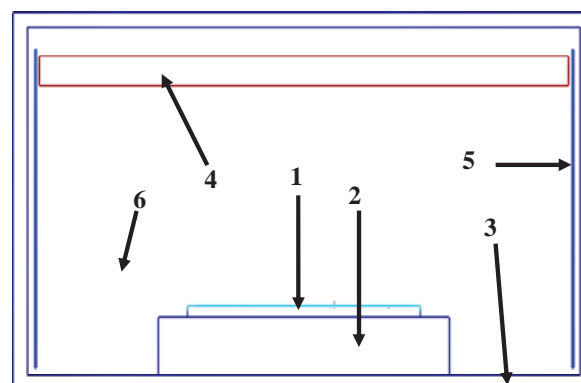


Fig. 1. Scheme welding oven with infrared heaters: 1 – experimental sample; 2 – fixture accessory for the detail; 3 – corps; 4 – infrared heaters; 5 – aluminum foil; 6 – air

Figure 1. The corps (3) is parallelepiped with walls made by stainless steel. They are covered by aluminum foil (5) on the inner side. It is used as heat reflector. The welding detail (1) is made by polyamide with thickness  $D=4$  mm. It is put on fixture accessory (2), used for the positioning and substitution of the experimental samples. The fixture accessory (2) is preheated at temperature 80°C. For welding detail's (1) replacement it is necessary the corps (3) to be with

vertical movement ability and the fixture accessory (2) to be with horizontal movement ability. This sample replacement is performed outside the oven. The heater's (4) temperature is constant and the distance between its surface and the welding detail's (1) surface is 80 mm. This distance is filled by air (6). During a thermal treatment it is possible to investigate temperature-time dependencies for any sample's at equal time step. In that paper temperature-time dependencies are performed for points from experimental sample: on the upper surface (depth  $d_0=0$  mm),  $T_{\text{Surf}}$ , in depth  $d=1$  mm (the position of  $d$  is defined towards the sample's upper surface)  $T_{\text{Depth}}$ . The end of the temperature regime is considered to be in the case when the material's melting point in depth  $d$  is achieved (for polyamide, melting point is  $T_{\text{Depth}} = 220^\circ\text{C}$  [9]). For any element's material properties, boundary conditions and subdomain settings are defined by using the main equations describing the interior heat transfer [3].

Modeling of processes at polyamide parts' IR welding, the main equations, material properties and boundary conditions are specified.

*The conductive heat transfer equation:*

$$(1) \quad \delta_{ts} \rho C_p \frac{\partial T}{\partial t} + \nabla \cdot (-k \nabla T) = Q,$$

where  $T$  is the temperature,  $\rho$  is the density,  $\delta_{ts}$  is a time-scaling coefficient,  $C_p$  is the heat capacity at a constant pressure,  $k$  is the thermal conductivity,  $t$  is the time,  $Q$  is a heat source or heat sink [8].

For steady state analysis the first term on left side is not used. To realize the soldering regime cycle (Figure 1) it is necessary to use the time-dependent transient analysis. The time-scaling coefficient  $\delta_{ts}$  is normally set to one.

*Adding Convective Heat Transfer*

The convective Heat transfer is used for description of temperature distribution with air flow cooling in IR camera. This section describes the equation, boundary conditions, and other properties in the General Heat Transfer application mode for modeling problems that involve convective heat transfer.

*Conservative convective and conductive Heat transfer equation:*

$$(2) \quad \delta_{ts} \rho C_p \frac{\partial T}{\partial t} + \nabla \cdot (-k \nabla T + \rho C_p u T) = Q,$$

where  $T$  is the temperature,  $\rho$  is the density,  $\delta_{ts}$  is a time-scaling coefficient,  $C_p$  is the heat capacity at a constant pressure,  $k$  is the thermal conductivity,  $t$  is the time,  $Q$  is a heat source or heat sink,  $u$  is the velocity field [6].

In the paper the heat transfer is chosen conservative formulation for the conduction and convection equation:

### Boundary Conditions

Here COMSOL Multiphysics uses two types of boundary conditions, the Dirichlet type and the

Neumann type. The Dirichlet type is used to set a temperature on a boundary

$$(3) \quad T = T_0.$$

The Neumann type is used to set the heat flux on a boundary:

$$(4) \quad -n \cdot q = q_0.$$

Where:  $T_0$  is prescribed temperature,  $q$  is the heat flux vector,  $h$  is the heat transfer coefficient,  $n$  is the normal vector of the boundary,  $q_0$  is inward heat flux, normal to the boundary [8].

The Heat Transfer Module uses the following more general formulation of (5)  $-n \cdot q = q_0 + h(T_{\text{inf}} - T)$ .

Where:  $T_{\text{inf}}$  is the external bulk temperature. This specifies the heat flux in terms of an explicit heat flux,  $q_0$ , and a heat transfer coefficient,  $h$ , relative to a reference temperature,  $T_{\text{inf}}$ .

The thermal insulation condition is obtained by setting  $q_0 = 0$ .

The expression within the parentheses in (2) defines the heat flux vector. For transport through conduction and convection this equation yields:

$$(6) \quad q = -k \nabla T + \rho C_p T u,$$

where  $q$  is the heat flux vector. If the heat transfer is by conduction only,  $q$  is determined by

$$(7) \quad q = -k \nabla T \quad [8].$$

The Heat transfer Module's standard boundary conditions used for this paper model implementation are represented in accordance with equations (3), (6) and (7).

*Temperature* boundary condition used for all heaters' boundary surfaces (Figure 1.). It is expressed as equation (3). This boundary condition is chosen because of the IR heater's thermal distribution character investigated in previous work [8]. The heaters' temperature is constant during the whole soldering cycle.

The *heat source/sink* boundary condition is chosen for all geometry boundary surfaces exposed directly to the heat influence. This boundary condition is expressed as:

$$(8) \quad \begin{aligned} & -n_u \cdot (-k_u \nabla T_u + \rho_u C_{pu} T_u u_u) - \\ & n_d \cdot (-k_d \nabla T_d + \rho_d C_{pd} T_d u_d) = q_0 + h(T_{\text{inf}} - T) \end{aligned}$$

The subscript indices  $u$  and  $d$ , respectively represent geometry objects' upper and down side. The meaning of the others equation symbols is mentioned above.

The *continuity* boundary condition is chosen for all geometry boundary surfaces which are not exposed directly to the heat influence. This boundary condition is expressed as:

$$(9) \quad \begin{aligned} & -n_u \cdot (-k_u \nabla T_u + \rho_u C_{pu} T_u u_u) - \\ & n_d \cdot (-k_d \nabla T_d + \rho_d C_{pd} T_d u_d) = 0 \end{aligned}$$

The subscript indices  $u$  and  $d$ , respectively represent geometry objects' upper and down side [8].



The *thermal insulation* boundary condition is chosen for all heating chamber walls' surfaces expressed as:

$$(10) \quad -n \cdot (-k \nabla T + \rho C_p T u) = 0$$

*Material properties and initial conditions.*

The ambient temperature's value is set to 300K. This temperature is the sample's initial temperature. For setting the model geometry materials' properties (Figure 1.) it is used a special program application materials' coefficients library. The material properties are determined and shown in Table 1.

The air parameters in use are temperature dependent [8]:

$$(11) \quad \rho = \frac{(p_0 M_w)}{(RT)},$$

where  $p_0=101.3\text{kPa}$ ,  $M_w=0.0288$  (kg/mol) is molecular mass,  $R = 8.314$  (J/molK) is gas constant,  $C_p=1100$  (J/kgK) is heat capacity[11]:

$$(12) \quad \log k = (-3.723 + 0.865 \log(T)).$$

Table 1: Material properties

Material property	Heating Steel	PA6[9]
Density $\rho$ (kg/m <sup>3</sup> )	7850	1140
Thermal conductivity $k$ (W/mK)	44.5	0.24
Heat capacity $C_p$ (J/kgK)	475	1670

## Modelling Results

The dependence of  $T_{\text{Surf}}$  and  $T_{\text{Depth}}$  variation versus time for three different values of  $T_{\text{Heater}}$  is represented at Figure 2 a,b,c. The heaters' temperatures are chosen in accordance to the infrared welding criteria of polyamide details [5]. The aim of the comparison is the choosing of the most suitable temperature regime in

accordance to the production requirement for temperature regime duration admissible limits (7 – 45 s) and the processing temperature [2].

The temperature regime at Figure 2a is performed at  $T_{\text{Heater}} 570^\circ\text{C}$  and time 42 s. The main disadvantage is the duration is close to the upper admissible limit mentioned above. It means that this regime is not efficient and it could not provide high rates of productivity. The temperature regime shown in Figure 2c is performed at  $T_{\text{Heater}} 652^\circ\text{C}$  and time 28 s. The main disadvantage is that feature for  $T_{\text{Surf}}$  is too steep. It increases too fast and reaches the polyamide definite temperature ( $280^\circ\text{C}$ ) [2].

The temperature regime shown in Figure 2b is performed at  $T_{\text{Heater}} 603^\circ\text{C}$ , time 32 s. the maximal obtained value of  $T_{\text{Surf}}$  is  $266^\circ\text{C}$ , so it is safe for the polymer.

The polyamide detail's temperature distribution in detail's depth  $D$ , obtained at the end of the considered temperature regimes is represented at Figure 3a, b. The charts depict a group of features achieved at different values of  $T_{\text{Heater}}$  °C and times for performing the temperature regimes 28 s, 32 s and 42 s. For all considered regimes in the depth  $d=1\text{mm}$  the obtained temperature is about  $220^\circ\text{C}$ , the polyamide melting point. Therefore the features from Figure 3 have a common intersection point. The steepness of the features decreases for depths  $>d=1$  mm. This result is in good agreement with the requirement for melting detail's thickness (about 1 mm).

The temperature distribution in depth  $D$  is shown at Figure 4. It is achieved with the help of the program product Comsol Multiphysics version 3.3. The character of the temperature distribution is defined from horizontal isotherms. They have a linear character in the detail's middle area (dashed area Figure 4). It is a distinguishing feature for the uniformity of polyamide properties. The curves around polyamide

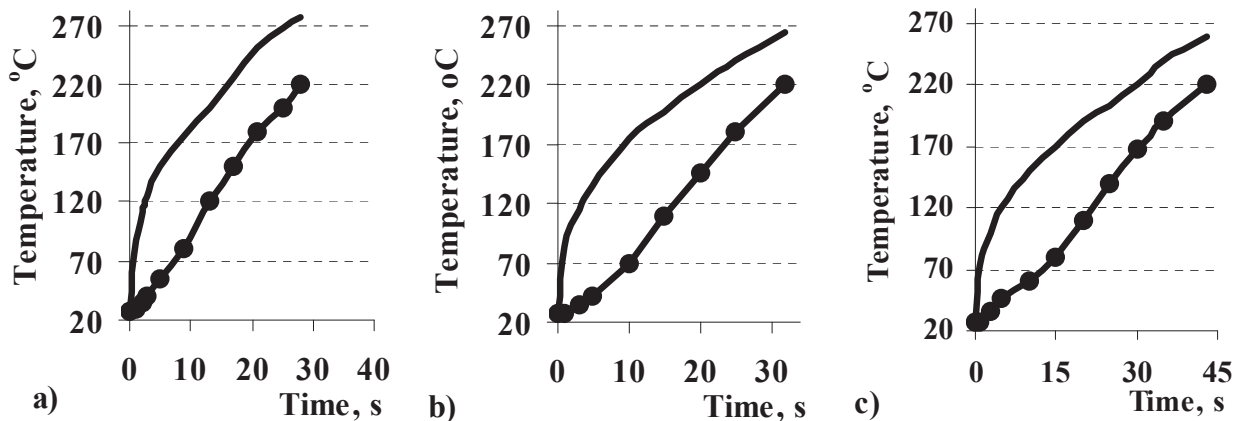


Fig. 2. Temperature – time dependencies for detail's surface  $T_{\text{Surf}}$ (——) at  $d_0$  and in depth of  $d=1\text{mm}$ ,  $T_{\text{Depth}}$

(●——●) at constant heaters' temperature  $T_{\text{Heater}}$ :

- a)  $T_{\text{Heater}} 570^\circ\text{C}$ , duration of thermal treatment 42 s;
- b)  $T_{\text{Heater}} 603^\circ\text{C}$ , duration of thermal treatment 32 s;
- c)  $T_{\text{Heater}} 652^\circ\text{C}$ , duration of thermal treatment 28 s.

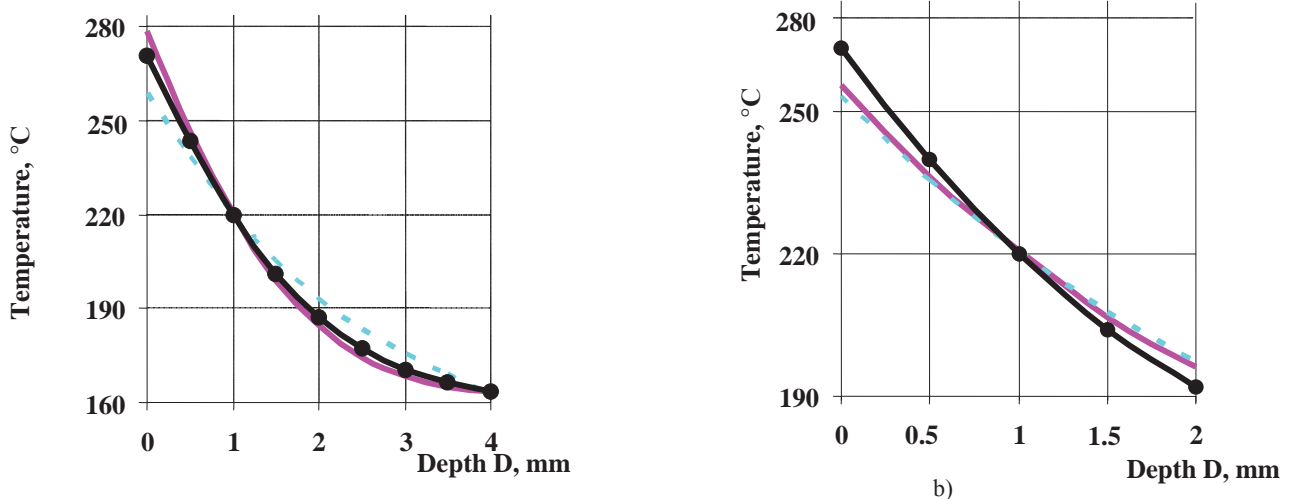


Fig. 3. Temperature distribution in the polyamide 6 detail depth: a) for the whole detail thickness, 4 mm; b) in depth 2 mm

$T_{\text{Heater}} 652^{\circ}\text{C}$  duration of thermal treatment 28 s ( — );  
 $T_{\text{Heater}} 603^{\circ}\text{C}$  duration of thermal treatment 32 s ( - - - ● - - - );  
 $T_{\text{Heater}} 570^{\circ}\text{C}$  duration of thermal treatment 42 s ( ···· ).



Figure 4. . Temperature distribution in detail's depth obtained for  $T_{\text{Heater}} 652^{\circ}\text{C}$  and time 28 s.

D, mm	Temperature Range (°C)	D, mm	Temperature Range (°C)	D, mm	Temperature Range (°C)
0 mm	249.37-255 °C	0 mm	236-262 °C	0 mm	272.18 °C
	227.4-249.37 °C		237.7-236 °C		237.36-269.5 °C
1 mm	217.55-227.4 °C	1 mm	221.7-237.77 °C	1 mm	222-237.36 °C
	196.88-217.55 °C		210.6-221.7 °C		209-222 °C
2 mm	186.2-196.88 °C	2 mm	191.65-210.6 °C	2 mm	190.4-209 °C
			178.97-191.65 °C		172.5-190.4 °C
3 mm	175.8-186.2 °C	3 mm	162.5-178.97 °C	3 mm	162.3-172.5 °C
	162.28-175.8 °C				
4 mm		4 mm		4 mm	

Fig. 5. Temperature distribution in detail's depth, D mm at: a -  $T_{\text{Heater}} 570^{\circ}\text{C}$ , and time 42 s; b -  $T_{\text{Heater}} 603^{\circ}\text{C}$ , and time 32 s; c -  $T_{\text{Heater}} 652^{\circ}\text{C}$ , and time 28 s

left and right ends are defined by the detail's geometry and the one-direction heat transfer. The bigger density of the isotherms at the (upper detail's area Figure 4) is in agreement with the features' steeper area from Figure 3. The dashed area from Figure 4 is used to perform comparison the temperature distribution in detail's depth D for different temperature regimes Figure 5a,b,c.

It is practically impossible modeling results for temperature distribution in detail's depth to be checked by experimental investigations.

The obtained modeling results verification is done with the help of special infrared camera equipment for detail's surface scanning and measurement.

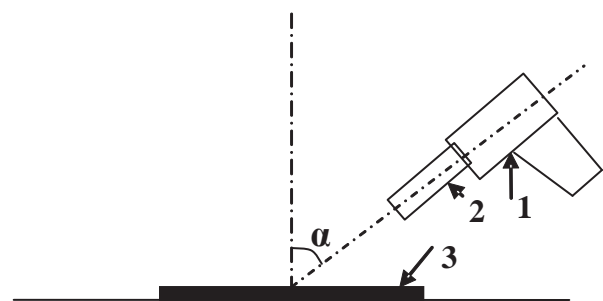


Fig. 6. Measurement's principle scheme: 1 – IR Thermometer; 2 – Collimator; 3 – experimental sample;  $\alpha$  – Angle between the normal to sample's surface and IR thermometer's optical axis.

The correlation between experimental and modeling results is good. The differences between them do not exceed 7-8°C (Figure 7).

Therefore it is possible to consider that the model

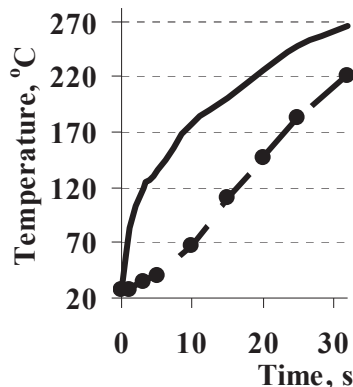


Fig. 7. Temperature – time dependencies for detail's surface  $T_{Surf}$  (—) at  $d_0$  and in depth of  $d=1mm$ ,  $T_{Depth}$  (●----●), measured by IR thermometer at a constant temperature  $T_{Heate}$  603°C, duration of thermal treatment 32 s.

results are reliable and can be applied for real plastic infrared welding equipment adjusting.

The comparison criterion of three temperature regimes, Figure 5 a,b,c is the vicat softening point A temperature  $T_{VSTA}$ . This is the temperature over which the plastic details' deformation is irreversible. For polyamide it is 198° C [12]. The depth  $D_1$  which this  $T_{VSTA}$  is obtained is a criterion for plastic welding quality [6]. This depth should be as small as possible. The comparison between three regimes with comparison to  $D_1$  is represented in Table 2:

Table 2: The obtained  $T_{VSTA}$  in depth  $D_1$

Temperature regime	$D_1$ , mm
$T_{Heater}$ 570°C and time 42 s	1.26
$T_{Heater}$ 603°C and time 32 s	1.2
$T_{Heater}$ 652°C and time 28 s	1.14

The smallest value of the depth  $D_1$  is obtained for the temperature regime with the smallest duration  $T_{Heater}$  652°C and time 28 s. But the disadvantages mentioned above for that regime prompt us to prefer the temperature regime  $T_{Heater}$  603°C and duration 32 s as optimal.

## Conclusion

The modeling with the help of the program product Comsol Multiphysics version 3.3 could be used for the description and investigation of polyamide details welding by infrared heating. This method allows the estimation of temperature - time dependences in any point of the treated detail during thermal treatment.

The comparison between three temperature regimes is performed. The most proper temperature regime in accordance to industry claims is chosen. It is

performed at  $T_{Heater}$  603°C and duration 32 s. During this temperature regime the maximal value of surface temperature is smaller than the polyamide definite temperature. The duration of that temperature regime is in the admissible limits for temperature regime performing in production process, 7 – 45 s. The (vicat softening point A)  $T_{VSTA}$  is obtained in admissible small depth  $D_1$ .

The modeling results are verified by experimental investigations and are applied for optimizing production processes in industry.

## Acknowledgements

The investigation in that paper performed in pursuance of the project BY – EEC – 301/2007.

## References

- [1] Mashkov P., Pencheva T., Popov D., "Application of Low Inert Infrared Heaters for Soldering Processes", Proc. of IEEE, 27<sup>th</sup> International Spring Seminar on Electronics Technology – ISSE 2004, Sofia, Bulgaria, 2004, pp. 366–370.
- [2] 2.3.1. INTRODUCTION. 2.3.2. GENERAL FEATURES. 2.3.3. GUIDELINES FOR SELECTION OF POLYMERS AND PROPERTIES. 2.3.4. THERMOPLASTIC GROUPS. 2.3.4.1.1 ...[www.me.gatech.edu/jonathan.colton/me4210/thermoplast\\_chap.pdf](http://www.me.gatech.edu/jonathan.colton/me4210/thermoplast_chap.pdf)
- [3] Incropera Frank P., DeWitt David P., Bergman Theodore L., Lavine Adrienne S., "Fundamentals of Heat and Mass Transfer", Published 2006 John Wiley, ISBN: 0471457280, pp 57-97.
- [4] PDL, "Handbook of Plastics Joining A Practical Guide", Plastics Design Library of William Andrew, Inc. Copyright 1997. ISBN: 1-884207-17-0, p99.
- [5] PDL, "Handbook of Plastics Joining A Practical Guide", Plastics Design Library of William Andrew, Inc. Copyright 1997. ISBN: 1-884207-17-0, p96.
- [6] SCHNEIDER H., "Process for welding two plastic parts", EP1344630A2, claim [0014], 2003, <http://v3.espacenet.com/textdoc?DB=EPODOC&IDX=EP1344630&F=0&QPN=EP1344630&RPN=EP1344630&DOC=c3a34af198500ac5803df7ae7630d7a74e>
- [7] <http://www.ptonline.com/articles/200410fa2.html>
- [8] [http://srb.stanford.edu/GP200/files\\_2005/COMSOL\\_D\\_C\\_heat.pdf](http://srb.stanford.edu/GP200/files_2005/COMSOL_D_C_heat.pdf)
- [9] [http://www.matweb.com/search/datasheet\\_PDF.aspx?MatGUID=5f673a2dc2da416bab9bfca7b2d8dcd9](http://www.matweb.com/search/datasheet_PDF.aspx?MatGUID=5f673a2dc2da416bab9bfca7b2d8dcd9)
- [10] [http://www.gcip.co.uk/pdf/safetydata/Ertalon%206PL\\_A.pdf](http://www.gcip.co.uk/pdf/safetydata/Ertalon%206PL_A.pdf)
- [11] C. Bailey, "Modeling the Effect of Temperature on Product Reliability," Proc. 19<sup>th</sup> IEEE SEMITHERM Symposium, 2003.
- [12] <http://www.heller-handel.de/english/Pa6rv38.pdf>
- [13] In situ non contact temperature measurements on PCB during soldering process Petko Mashkov, Tamara Pencheva, Angel Valchev and Berkant Gyoch, Proc. of IEEE, 31<sup>th</sup> International Spring Seminar on Electronics Technology – ISSE 2008, Budapest, Hungary, 2008, pp. 264–268.

## Biographies



**Angel Valchev** was born in Stara Zagora, Bulgaria, on December 07, 1981. He studied at the Rouse University “Angel kanchev” – Mr.S. in Telecommunications. His field of interest includes infrared heating and electronics. He is today a Ph.D student in the Faculty of Electrical Engineering of the Rouse University.

Angel Valchev is in the Faculty of Electrical Engineering, Rouse University, 8, Studentska Str., 7017 Rouse, Bulgaria

(e-mail: [avalchev@ru.acad.bg](mailto:avalchev@ru.acad.bg)).



**Tamara Pencheva** was born on January, 1948. She studied at the Faculty of Radio-electronics in Sant-Petersburg Politechnical University “Kalinin” – Mr.S. in Physics of semiconductors; Ph.D. in Physical-Technical Institute “Ioffe”, RAN – in Physics of waves processes.

Since 1974 she worked in the Faculty of Electrical Engineering of the Rouse University as a Lecturer and Assoc. Professor in the field of infrared heating and electronics.

Tamara Pencheva is in the Faculty of Electrical Engineering, Rouse University, 8 Studentska Str., 7017 Rouse, Bulgaria (e-mail: [tgp@ru.acad.bg](mailto:tgp@ru.acad.bg)).



**Petko Mashkov** was born in Rouse, Bulgaria, on August 30, 1955. He studied at the Sofia University “Kliment Ohridski” – Mr.S. in Physics of semiconductors; Rouse University – Mr.S. in Internal combustion engines.

Since 1980 he worked in the Faculty of Electrical Engineering of the Rouse University as a Lecturer and researcher in the field of infrared heating and electronics.



**Berkant Gyoch** was born in Razgrad, Bulgaria, on May 24, 1977. He studied at the Rouse University “Angel kanchev” – Mr.S. in Telecommunications.

His field of interest includes optoelectronics; thin layers; microelectronic technologies. He is today a PhD student in the Faculty of Electrical Engineering of the Rouse University.

Berkant Gyoch is in the Faculty of Electrical Engineering, Rouse University, 8, Studentska Str., 7017 Rouse, Bulgaria (e-mail: [b\\_gyoch@ru.acad.bg](mailto:b_gyoch@ru.acad.bg)).



# Modeling of heat transfer during soldering process by control of operation of heaters

Sava Ivanov Kontrov, Maria Ivanova Marinova, Angel Valentinov Valchev,  
Tamara Grigorievna Pencheva, Borislav Hristov Dimitrov

**Abstract:** *Abstract: The investigation deals with modeling of soldering processes in new equipment for surface mounting technologies (SMT) with new type of low inert heaters for the middle infrared spectral region. The results obtained may be used for optimization of soldering equipment control during soldering processes. It is very important, especially for high integration packages. The main parameters for heat transfer processes are analyzed. The heat transfer modeling method for the soldering processes of SMDs to printed circuit boards using low inert infrared heaters is presented. It is realized with Comsol Multiphysics 3.3. Influence of main parameters of heaters' operation and hot gas circulation on temperature distribution on PCB is investigated.*

**Keywords:** *Modeling of soldering processes, SMD's soldering*

## Introduction

Nowadays in electronic industry enhancement of electronic elements' density upon Printed Circuit Board (PCB), utilization of PCB with large area and implementation of lead free solder pastes introduces new demands to soldering equipment [1 - 5]. High integration component packages demand precise control of the parameters of the soldering regime. At the same time these highly integrated circuits are relatively expensive and failures are absolutely undesirable. Up to this investigation it was considered that for soldering of high integration component packages convection type soldering ovens are preferred to the infrared (IR) type radiation ovens because of possibility to control precisely temperature regimes during soldering process. It is considered that infrared ovens are unsuitable for these types of high integrated chips [3].

The results of experimental investigations of applicability of new kind soldering equipment for soldering of Surface-Mounted Devices (SMDs) to PCB using IR radiation are presented in [5]. The equipment is based on low inert infrared heaters for the middle infrared spectral region. Infrared heating in the heating camera is combined with forced air convection [2, 3 and 5]. Due to the low inertia of the heaters desirable soldering cycles may be realized precisely. By electronic control of the

operation of the heaters fast changes in their surface temperature may be achieved. The whole soldering cycle may be realized at the same place – without conveyor. The equipment allows in situ control of the spectral characteristics of radiation emitted by the heaters and the part of energy transported by the hot gas circulating in the heating camera. Previous investigations [5] show that this type of equipment is very suitable for realization of individual temperature cycles for every PCB in dependence of its size, electronic component's density and others.

In this paper the main results of thermal processes modeling for new type IR soldering equipment for large area high integration circuits are presented. To estimate influence of different parameters of soldering camera operation modeling of thermal processes in dependence of heater's operation mode, air flow velocity, etc. during soldering is performed. The modeling of soldering process is realized using the program product COMSOL Multiphysics version 3.3. The best obtained results for soldering camera's operation parameters are chosen in accordance with requirements given in [3, 5, 9, 10].

## Description of the object for modelling

Previous investigations [10], connected with thermal process modeling during soldering of SMD to PCB show that best results may be achieved when heater's surface temperature and air temperature variations are used as inlet parameters. The soldering processes are realized by control of operation of the heaters in dependence of temperature in one point on the PCB (in a solder joint). In Figure 1 a typical soldering cycle for SMDs chips is shown [3, 9]. Experiments are carried out using soldering equipment, designed and produced in our

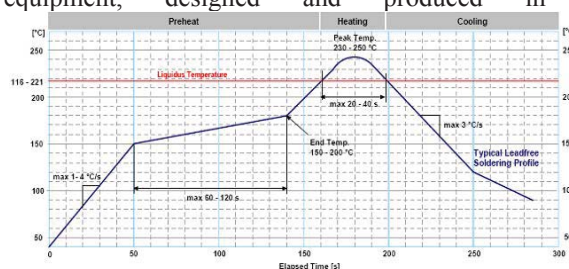


Fig. 1: Typical soldering cycle for SMD chip (lead free soldering).

laboratory [5]. Soldering camera is without conveyer (Figure 2) - PCB doesn't move and the whole soldering cycle is realized at the same place. Temperature variations in different points of the PCB may be measured and controlled in situ during the soldering.

The heaters are made from thin metal sheets. Special coating upon the surface of the heaters ensures emissivity about 0.9. They are warmed up directly by electric current and their temperature can be increased with the rate more than 15°C/s. Radiation power density emitted

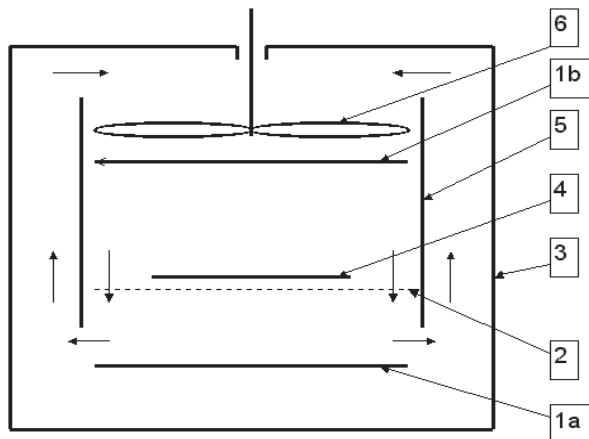


Fig. 2. Cross-section view of an experimental soldering machine: 1a and 1b – heaters; 2 – grid; 3 – heating chamber; 4 – PCB; 5 – reflecting screens; 6 – fan.

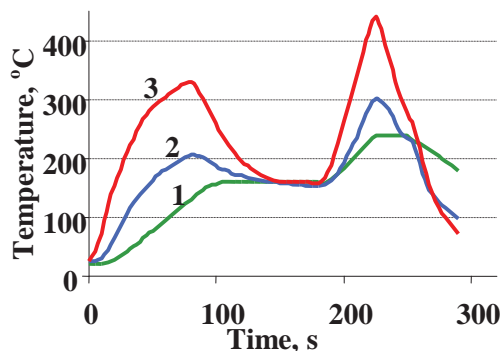


Fig. 3. Temperature-time dependencies during soldering processes: 1 – of the solder joint on PCB; 2 – of circulating gas; 3 – on the heater's surface (maximal temperature of the solder joint is about 240°C).

from these heaters is uniform upon the whole processing area. In combination with hot air flow these heaters ensure minimal temperature differences on PCB's surface. The hot air (or inert gas) circulating in the heat camera passes through the heaters and is warmed up. In this way there is no need of additional gas heating.

Temperature-time dependencies during typical soldering cycle (see Figure 1), realized in upper described equipment is obtained in [5]. Temperature variations during soldering cycle for heaters' surface temperature and air temperature are used for modeling thermal processes on surface and solder joints of the chip. Experiments are carried out with the chips with size (13/7

mm), because in this case maximal thermal differences between these points (Points 1, 2, 3 - Figures 4,5) during soldering cycles can be expected.

### Modelling Approach

For realization of the thermal processes modeling during soldering of SMDs to PCB the main equations, material properties and boundary conditions are specified.

The conductive heat transfer equation:

$$(1) \quad \delta_{ts} \rho C_p \frac{\partial T}{\partial t} + \nabla \cdot (-k \nabla T) = Q,$$

where  $T$  is the temperature,  $\rho$  is the density,  $\delta_{ts}$  is a time-scaling coefficient,  $C_p$  is the heat capacity at a constant pressure,  $k$  is the thermal conductivity,  $t$  is the time,  $Q$  is a heat source or heat sink [6].

For steady state analysis the first term on left side is not used. To realize the soldering regime cycle (Figure 1) it is necessary to use the time-dependent transient analysis. The time-scaling coefficient  $\delta_{ts}$  is normally set to one.

#### Adding Convective Heat Transfer

The convective Heat transfer is used for description of temperature distribution with air flow cooling in IR camera. This section describes the equation, boundary conditions, and other properties in the General Heat Transfer application mode for modeling problems that involve convective heat transfer.

Conservative convective and conductive Heat transfer equation:

$$(2) \quad \delta_{ts} \rho C_p \frac{\partial T}{\partial t} + \nabla \cdot (-k \nabla T + \rho C_p \mathbf{u} T) = Q,$$

where  $T$  is the temperature,  $\rho$  is the density,  $\delta_{ts}$  is a time-scaling coefficient,  $C_p$  is the heat capacity at a constant pressure,  $k$  is the thermal conductivity,  $t$  is the time,  $Q$  is a heat source or heat sink,  $\mathbf{u}$  is the velocity field [6].

In the paper the heat transfer is chosen conservative formulation for the conduction and convection equation:

#### Boundary Conditions

Here COMSOL Multiphysics uses two types of boundary conditions, the Dirichlet type and the Neumann type. Use the Dirichlet type to set a temperature on a boundary

$$(3) \quad T = T_0,$$

and use the Neumann type to set the heat flux on a boundary

(4)  $-n \cdot \mathbf{q} = q_0$  where:  $T_0$  is prescribed temperature,  $\mathbf{q}$  is the heat flux vector,  $h$  is the heat transfer coefficient,  $\mathbf{n}$  is the normal vector of the boundary,  $q_0$  is inward heat flux, normal to the boundary [6].

The Heat Transfer Module uses the following more general formulation of

(5)  $-n \cdot \mathbf{q} = q_0 + h(T_{inf} - T)$ . Where:  $T_{inf}$  is the external bulk temperature. This specifies the heat flux in terms of an explicit heat flux,  $q_0$ , and a heat transfer coefficient,  $h$ , relative to a reference temperature,  $T_{inf}$ .

The thermal insulation condition is obtained by setting  $q_0 = 0$ .

The expression within the parentheses in (2) defines the heat flux vector. For transport through conduction and convection this equation yields:

$$(6) \quad q = -k\nabla T + \rho C_p T u,$$

where  $q$  is the heat flux vector. If the heat transfer is by conduction only,  $q$  is determined by

$$(7) \quad q = -k\nabla T \quad [6].$$

The Heat transfer Module's standard boundary conditions used for this paper model implementation are represented in accordance with equations (3), (6) and (7).

The *Temperature* boundary condition used for all heaters' boundary surfaces (Figure 2.). It is expressed as equation (3). This boundary condition is chosen because of the IR heater's thermal distribution character investigated in previous work [10]. The heaters' temperature is constant during the whole soldering cycle.

The *heat source/sink* boundary condition is chosen for all geometry boundary surfaces exposed directly to the heat influence. This boundary condition is expressed as:

$$(8) \quad \begin{aligned} -n_u \cdot (-k_u \nabla T_u + \rho_u C_{pu} T_u u_u) - \\ n_d \cdot (-k_d \nabla T_d + \rho_d C_{pd} T_d u_d) = q_0 + h(T_{inf} - T) \end{aligned}$$

The subscript indices **u** and **d**, respectively represent geometry objects' upper and down side. The meaning of the others equation symbols is mentioned above.

The *continuity* boundary condition is chosen for all geometry boundary surfaces which are not exposed directly to the heat influence. This boundary condition is expressed as:

$$(9) \quad \begin{aligned} -n_u \cdot (-k_u \nabla T_u + \rho_u C_{pu} T_u u_u) - \\ n_d \cdot (-k_d \nabla T_d + \rho_d C_{pd} T_d u_d) = 0 \end{aligned}$$

The subscript indices **u** and **d**, respectively represent

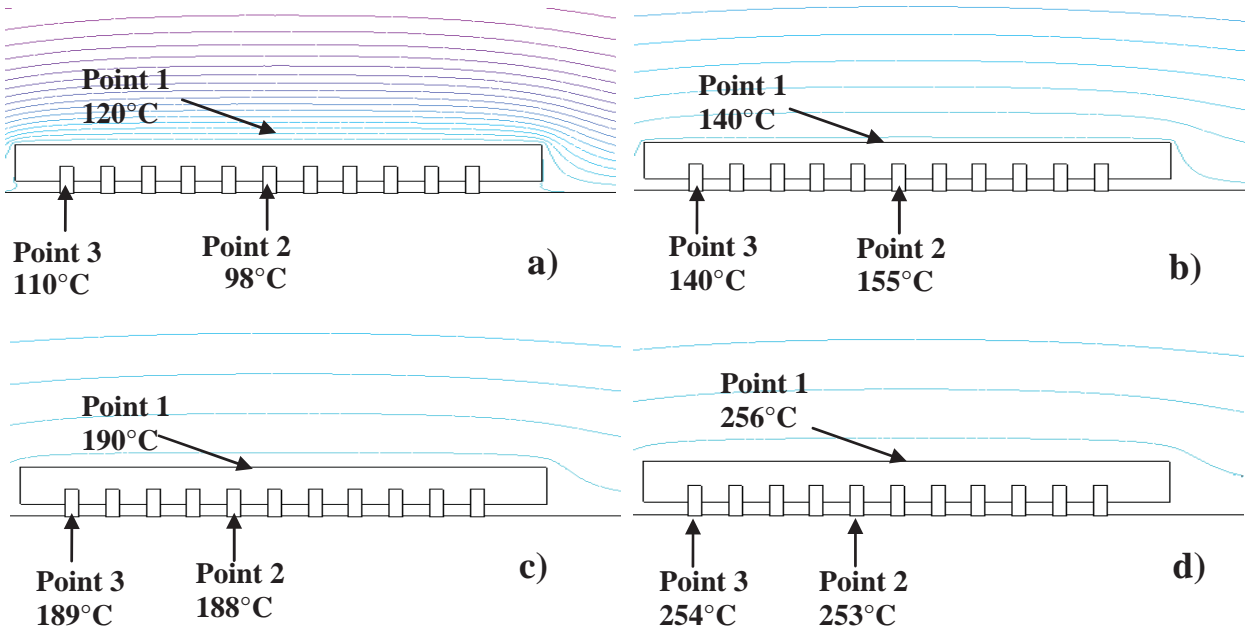


Fig. 4. First mode of operation of the soldering camera – without forced air convection: temperature distribution at: a) 40 seconds; b) 60 seconds, c) 150 seconds d) 250 seconds, from the beginning of the soldering cycle. Where: 1- temperature on the surface of the chip, 2 – temperature in a solder joint in the center of the chip; 3 – temperature in a solder joint at the end of the chip.

geometry objects' upper and down side.

The *thermal insulation* boundary condition is chosen for all heating camber walls' surfaces expressed as:

$$(10) \quad -n \cdot (-k\nabla T + \rho C_p T u) = 0$$

*Material properties and initial conditions.*

The ambient temperature's value is set to 300K. This temperature is the SMD chip's initial temperature. For setting the model geometry materials' properties (Figure 2 ) it is used a special program application materials' coefficients library. The material properties are determined and shown in Table 1:

Table 1: Material properties

Material property	Heating Steel	PCB [7]
Density $\rho$ (kg/m <sup>3</sup> )	7850	1900
Thermal conductivity $k$ (W/mK)	44.5	0.3
Heat capacity $C_p$ (J/kgK)	475	1369

The air parameters in use are temperature dependent [8]:

$$(11) \quad \rho = \frac{(p_0 M_w)}{(RT)},$$

where  $p_0=101.3\text{kPa}$ ,  $M_w=0.0288$  (kg/mol) is molecular mass,  $R = 8.314$  (J/molK) is gas constant,  $C_p=1100$  (J/kgK) is heat capacity[8]:

$$(12) \quad \log k = (-3.723 + 0.865 \log(T)),$$

$$(13) \quad \eta = 6.0 \times 10^{-6} + 4.0 \times 10^{-8} T.$$

The direction of the air flow is normal to the chip surface. Its velocity is 0.2 m/s and it is defined at

previous work [10].

### Modelling Results

As it is known [2, 3, 5] convection type ovens are recommended for reflow soldering of high integrated circuits. To estimate the influence of forced air flow in this new soldering equipment thermal processes for two modes of operation of the heating camera are modeled.

- First mode of operation – without forced air convection. Heating is realized only by infrared radiation from the heaters.

convection the calculated temperature differences between Point 1, Point 2 and Point 3 decrease significantly. As it can be seen it is between 1 and 2 degrees in Figures 5c, d.

It means that the second mode of operation of soldering equipment is more proper and the solder joints should be with better quality than the first mode. Therefore the mode of operation when infra red heating is supplemented with forced air convection is more suitable than the case without air flow especially for soldering of high integrated chips to PCB.

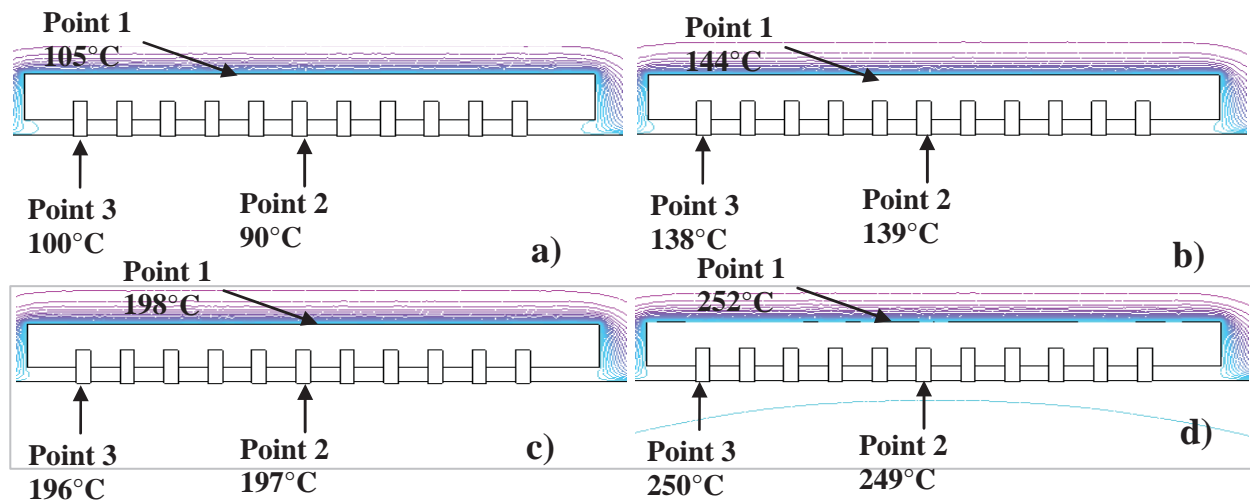


Fig. 5. Second mode of operation of the soldering camera – without forced air convection: temperature distribution at: a) 40 seconds; b) 60 seconds, c) 150 seconds, d) 250 seconds, from the beginning of the soldering cycle. Where: 1- temperature on the surface of the chip, 2 – temperature in a solder joint in the center of the chip; 3 – temperature in a solder joint at the end of the chip.

- Second mode of operation – with forced air convection in the heating camera. Air flow passes through the heaters and there is no need of additional gas heating.

First mode of operation modeling results connected with time-temperature dependences in a few points of the chip during soldering cycle are shown in Figure 4.

As it can be seen from the Figures 4a,b,c,d when the heating process is performed by infrared radiation only and it is not supplemented with forced air convection, differences between temperatures on the surface in the center and at the end of the chip are too big (up to 30 degrees).

Temperatures become almost equal at the end of the preheating, but during reflow process temperature differences increase again, Figure 4d. These big temperatures' gradients may cause thermal deformations and warp of the chip and PCB [3, 5] which causes failure of the solder joints. As it was mentioned above this is inadmissible.

Modeling results for second mode of operation of the heating camera (with forced air convection) are presented in Figure 5.

The best results are obtained at air flow velocity of 2 m/s for camera's narrow areas. In the case of forced

### Conclusions

Thermal processes modeling during soldering of SMDs to PCB with the program product Comsol Multiphysics version 3.3 is suitable to determine the temperature variations in IR camera and on the PCB during soldering cycle. It is a big advantage because the temperature distribution in different points on PCB (especially in solder joints) is very hard to be measured. The best results are obtained for the air flow velocities about 0.2 m/s (for the narrow part of the camera 2 m/s). There is small temperature difference between PCB and chip's pins, obtained by modeling. It may be considered that the obtained from the model results are in good accordance with experimental results. It may be concluded that the proposed method for modeling of heat transfer during soldering processes can be successfully used for choosing of proper soldering camera's operation parameters.

### References

- [1] J. Howell, R. Buckius, "Fundamentals of engineering thermodynamics", McGraw-Hill, Inc. New York, etc. 1992, pp. 1033.
- [2] J. Morton, "An industrial oven", GB Pat. 2368629, 2002.



- [3] K. Takahashi, "Apparatus and method for soldering electronic components to printed circuit boards", USPat. 6,575,352, 2003.
- [4] R. Siegel, J. Howell, "Thermal radiation heat transfer", Mc Graw-Hill Book Inc. New York, 1972. pp. 905.
- [5] P. Mashkov, T. Pencheva, D. Popov, B. Gyoch, "Apparatus and method for soldering electronic components to printed circuit boards", Proc. of IEEE, 28<sup>th</sup> ISSE'05, Austria, pp. 406-411
- [6] [http://srb.stanford.edu/GP200/files\\_2005/COMSOL\\_DC\\_heat.pdf](http://srb.stanford.edu/GP200/files_2005/COMSOL_DC_heat.pdf)
- [7] C. Bailey, "Modeling the Effect of Temperature on Product Reliability," Proc. 19th IEEE SEMITHERM Symposium, 2003.
- [8] J.M. Coulson and J.F. Richardsson, *Chemical Engineering*, Vol 1, Pergamon Press, 1990, appendix.
- [9] [http://www.skyworksinc.com/products\\_display\\_item.asp?did=4002](http://www.skyworksinc.com/products_display_item.asp?did=4002)
- [10] I. Evstatiev, T. Pencheva, P. Mashkov "Heat transfer modeling for soldering processes of SMD's to printed circuit boards using low inert infrared heaters", IEEE, 28<sup>th</sup> ISSE'05, Austria, pp 128-133.

## Biographies



**Sava Kontrov** was born on June, 1942. He studied at TU Varna- Mr.S. in Electrical Machines.

Since 1970 he worked in Faculty of EMA as a Lecturer, Assoc. Prof. and Professor in the field of Electrotechnologies and Electrothemy. He has supervised over 60 scientific elaborations.

His fields of research are: Electrical Technologies, Electrothermal processes and devices, New Heating Elements, Electrotechnologies for Ecology purposes,

Electrical household apparatus

Sava Kontrov is in the Faculty of Electrical Engineering, TU-Varna, 1 Studentska str., 9010 Varna, Bulgaria (email: [etet\\_tu@abv.bg](mailto:etet_tu@abv.bg))



**Maria Marinova** was born in Popovo, Bulgaria, on February, 1963. She studied at the Faculty of EMA.

Since 1989 she worked in Faculty of EMA as a Lecturer and Assoc. Prof in the field of the modeling, control and reliability of eltrical engineering devices and processes. She received Dr. Degree from the same university in 1994 and Assoc. Prof. Degree in 2003. Maria Marinova is author of over 45 scientific articles and 3 author's

certificates.

Maria Marinova is in the Faculty of Electrical Engineering, TU-Varna, 1 Studentska str., 9010 Varna, Bulgaria (email: [m\\_i\\_m@abv.bg](mailto:m_i_m@abv.bg)).



**Tamara Pencheva** was born on January, 1948. She studied at the Faculty of Radio-electronics in Sant-Petersburg Politechnical University "Kalinin" – Mr.S. in Physics of semiconductors; Ph.D. in Physical-Technical Institute "Ioffe", RAN – in Physics of waves processes.

Since 1974 she worked in the Faculty of Electrical Engineering of the Rousse University as a Lecturer and Assoc. Professor in the field of infrared heating and electronics.

Tamara Pencheva is in the Faculty of Electrical Engineering, Rousse University, 8 Studentska Str., 7017 Rousse, Bulgaria (e-mail: [tgp@ru.acad.bg](mailto:tgp@ru.acad.bg)).



**Angel Valchev** was born in Stara Zagora, Bulgaria, on December 07, 1981. He studied at the Rousse University "Angel Kanchev" – Mr.S. in Telecommunications. His field of interest includes infrared heating and electronics. He is Ph.D student in the Faculty of Electrical Engineering of the University of Rousse.

Angel Valchev is in the Faculty of Electrical Engineering, Rousse University, 8, Studentska Str., 7017 Rousse, Bulgaria (e-mail: [avalchev@ru.acad.bg](mailto:avalchev@ru.acad.bg)).



**Borislav Dimitrov** studied at the Faculty of Electrical Engineerig .

Since 2004 he is a PhD student at department of Electrical engineering and Electrotechnologies . He has worked as a lecturer in the same department since 2006. His field of interest is concerned with: Electrothermal devices – electrical resistance furnaces with periodical action (chamber and shaft); Modeling methods of processes and devices: Finite Elements Methods, Differential Equation Systems

Borislav Dimitrov is in the Faculty of Electrical Engineering, TU-Varna, 1 Studentska str., 9010 Varna, Bulgaria (e-mail : [b\\_dim@mail.bg](mailto:b_dim@mail.bg)).

# Spontaneous Filamentary Pattern Formation in One-Dimensional Dielectric-Barrier Discharge at Atmospheric Pressure in Air

Peter Dineff, Dilyana Gospodinova

**Abstract:** In a linear dielectric-barrier air discharge between diametrically opposite sides of a narrow tube with wire CuZn37 electrodes inside, discharge filaments stabilize at regular intervals along the tube's length forming a spontaneous linear pattern. A preliminary new model of the pattern-formation dynamics is described, motivating further investigation on space-resolved imaging and investigations of surface and volume remnant charge distributions.

**Keywords:** memory effect, one-dimensional barrier air discharge, pattern formation dynamics, remnant repulsion, surface and volume remnant charge distribution

## Introduction

Dielectric-barrier electrical discharges (silent discharges, atmospheric glow discharge, barrier discharge - DBD) at atmosphere-pressure and room-temperature are used on a large industrial scale. They combine the advantages of non-equilibrium plasma properties with the ease of atmospheric-pressure operation. A prominent feature is the simple scalability from small laboratory reactors to large industrial installations with megawatt input powers. Efficient and cost-effective all-solid-state power supplies are available. The preferred frequency range lies between 1 kHz and 10 MHz, the preferred pressure range between 10 kPa and 500 kPa. Industrial applications include ozone generation, pollution control, surface treatment, high power CO<sub>2</sub> lasers, ultraviolet excimer lamps, excimer based mercury-free fluorescent lamps, and flat large-area plasma displays. Depending on the application and the operating conditions the discharge can have pronounced filamentary structure or fairly diffuse appearance [1, 2].

In general case, DBDs are not uniform and consist of numerous filaments distributed in the discharge gap. The physics of microdischarges as part of a filament is based on an understanding of the formation and propagation of electron avalanches; the avalanche to streamers transaction; the formation of cathode directed streamer; the surface path charge on dielectric barriers surface and volume microdischarge remnant, consequent plasma channel degradation. The electrons in the conducting plasma channel established by the streamers dissipate from the gap in about 40 ns, while the heavy and slowly drifting positive ions remain in the discharge gap for several microseconds, Table 1. Deposition of electrons from the conducting channel onto the anode dielectric barrier results in charge accumulation and prevents new avalanches and streamers nearby until the cathode and anode are reversed. The usual operation frequency used

in the DBDs is around 20 kHz; therefore, the voltage polarity reversal occurs from 20 nsec to 25 μsec. After the voltage polarity reverses, the deposited negative charge facilitates the formation of new avalanches and streamers in the same spot. As a result, a many-generation family of streamers is formed, which is macroscopically observed as a bright filament that appears to be spatially localized. Thus, a filamentary pattern in DBD is a lot of group of microdischarges or filament that form on the same spot each time the polarity is changed [3, 4].

J. Guikema and all. (2000) are presented observations of periodic linear filament patterns and apparent spatiotemporal chaos in an effectively one-dimensional (1D-) DBD configuration — that is, a DBD in which filaments are constrained to a line perpendicular to the applied electric field, [5, 6].

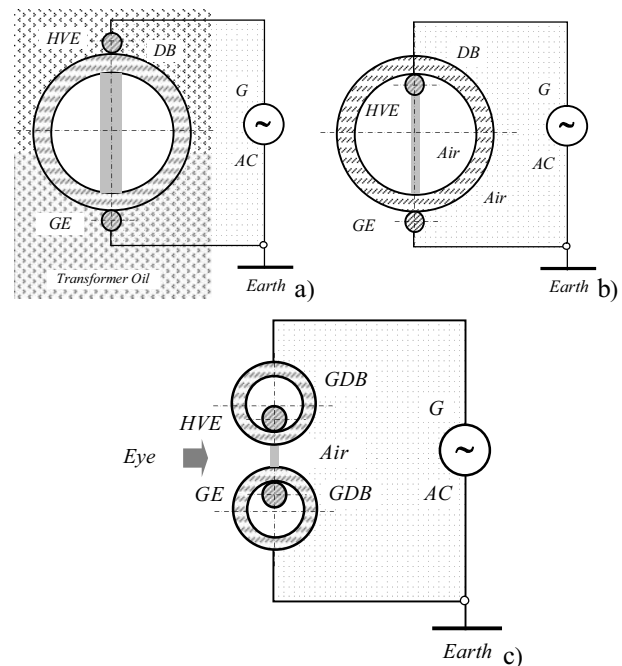


Fig. 1. One-Dimensional (1D-) Dielectric-Barrier Discharge cells used to capture close-up images of the discharge gap, where filaments form spontaneously periodic linear patterns along the tube length: **a** – Guikema's symmetrical discharge cell with two barriers; **b** – asymmetrical discharge cell with one barrier; **c** – symmetrical discharge cell with two glass tube-barriers.

HVE – high-voltage electrode; GE – grounded electrode; GDB (DB) – glass dielectric-barrier; G – AC generator.

Their discharge cell is a 30-cm-long, cylindrical glass tube with a 2.0-mm inner diameter and a 7.5-mm outer diameter. Stripes of silver paint, 3 mm wide, are applied

on diametrically opposite portions of the outer surface. Sparking around the outside of the cell is avoided by means of a jacket of insulating transformer oil, which is contained within a second glass tube, Fig. 1a.

**Spontaneous pattern formation - phenomena of microdischarge interaction**

*Electron avalanche.* An initial electron starting from some point in the discharge gap, or from the dielectric barrier that covers the cathode in the case of well-developed DBD, produces secondary electrons by direct ionization and develops an electron avalanche. In air at atmospheric pressure the *Grouping factor* is  $G = 5$ , i.e., only one of out 5 electrons results in electron avalanche, Fig. 2.

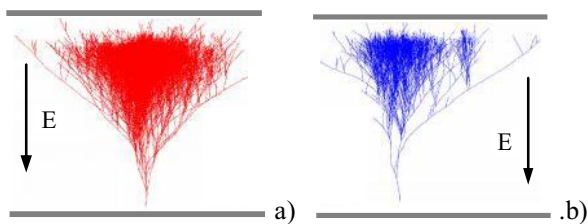


Fig. 2. Fluctuation of electron density in an electron avalanche: a - minor in non-electronegative gases; b - important in electronegative gases.

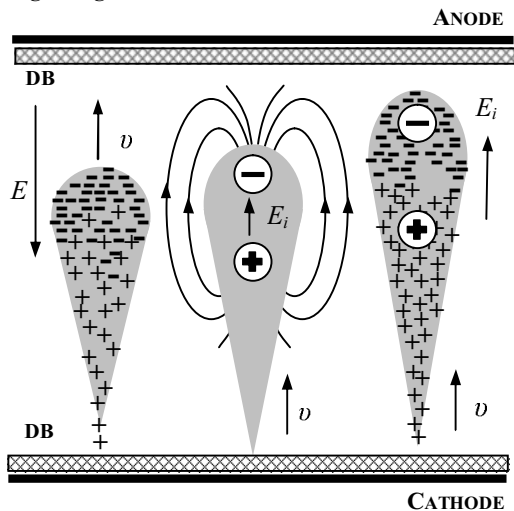


Fig. 3. Development of electron avalanche forward in discharge gap, split of free negative (electrons) and positive (ions) charges in avalanche and increase of local electric field  $E_i$ .

*Electron avalanche to streamer transition.* If the avalanche is large enough (*Meek's condition*:  $E \sim E_i$ ), a cathode-directed streamer is initiated - usually from the anode region, Fig. 3.

The streamer bridges the gap in a few ( $1 \div 10$ ) nanoseconds and forms a conducting channel of weakly ionized plasma. Intense electron current will flow through this plasma channel until the local electric field  $E_i$  collapses, Fig. 4

Collapse of the local electric field  $E_i$  is caused by both the charges accumulated (path) on the dielectric surface and ionic space charge. Ions are too slow to leave the gap for the duration of this new electron current peak.

*Microdischarge.* This group of local processes which takes place in the discharge gap initiated by the electron avalanche and developed until local electric field collapse (electron current termination) is called a microdischarge.

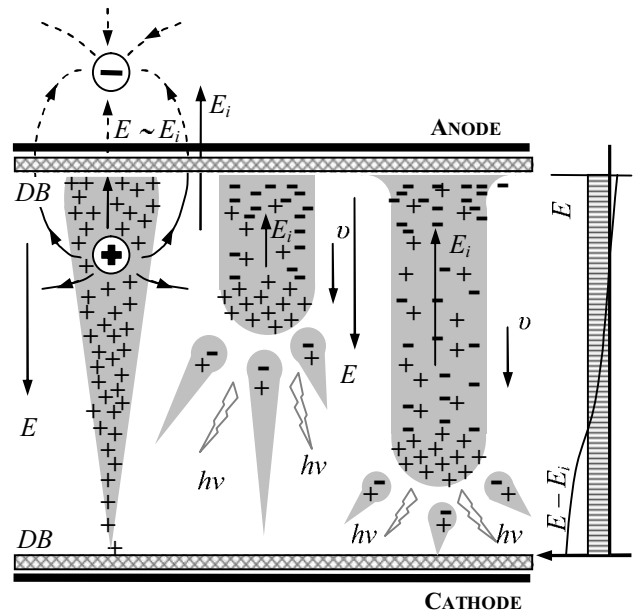


Fig. 4. Development of electron avalanche forward in discharge gap split of free negative (electrons) and positive (ions) charges in avalanche and increase of local electric field  $E_i$ .

*Microdischarge remnant.* After electron current termination there is no more electron-ion plasma in the main part of the microdischarge channel, but the high level of vibrational and electronic excitation in the channel volume along with charges deposited on the surface and ionic charges in the volume allow us to separate this region from the rest of the discharge gap, and we call it the microdischarge remnant. Positive ions of the remnant, or positive and negative ions in the case of an electronegative gas, slowly move to the electrodes resulting in low and very long ( $\sim 10 \mu\text{sec}$  for 1 mm of gap) falling ion current, Figs. 5 and 6.

**Table 1**

Calculated microdischarge characteristics for DBD, [3].

DBD – 1 mm gap, air, 100 mPa	Duration	Charge
Microdischarge (200 $\mu\text{m}$ radius)	40 nsec	$10^{-9}$ C
■ Electron avalanche	10 nsec	$10^{-11}$ C
■ Cathode-directed streamer	1 nsec	$10^{-10}$ C
■ Plasma channel	30 ns	$10^{-9}$ C
Microdischarge remnant	1 msec	$\geq 10^{-9}$ C

*Filamentary pattern formation.* The microdischarge remnant will facilitate the formation of new microdischarges in the same spot as the polarity of the applied voltage changes. This filament is actually microdischarges that repeatedly strike at the same place as the polarity of the applied voltage changes, thus appearing as bright filaments to the observer's eye. That is

why it is possible to see single filaments in *DBD*. If microdischarges formed at a new spot each time the polarity changed, the discharge would appear uniform. The residual positive charge, together with the deposited negative charge in the case of the dielectric surface, influences the formation of nearby families of avalanches and streamers and, therefore, the formation of neighbouring microdischarges.

*Microdischarges interaction.* The mechanism of influence is the following: positive charge (or dipole field in the case of deposited negative charge, Fig. 4) intensifies the electric field in the cathode area of the neighbouring microdischarge and decreases the electric field in the anode area. The avalanche-to-streamer transition depends mostly on the near-anode electric field (from which new streamers originate), the formation of neighbouring microdischarges is actually prevented, and microdischarges effectively repel each other.

*Short-range order between discharges.* This quasi-repulsion between microdischarges leads to the formation of short-range order that is related to a characteristic repulsion distance between microdischarges. Observation of this cooperative phenomenon depends on several factors, including the number of microdischarges occurring and the operating frequency, Fig. 5.

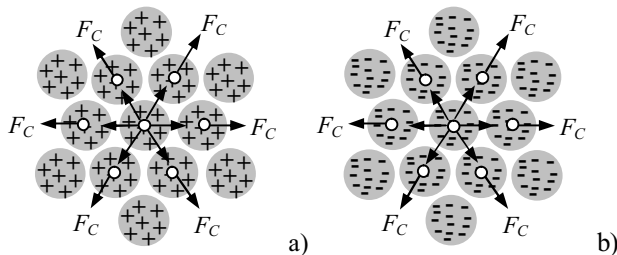


Fig. 5. Short-range (first radius of repulsion) order between ionic charges in the volume – positive space discharge remnant (a) and charges deposited (path) on the surface – negative surface discharge remnant (path).

For example, when the number of microdischarges is not large enough (when the average distance between microdischarges is larger than the characteristic interaction radius), no significant microdischarge interaction is observed. When the AC frequency is too low to keep the microdischarge remnants from dissipation, microdischarge repulsion effects are not observed. Low frequency means that the period is longer than the typical life time of the microdischarge remnant or ‘memory effect’ life time. In addition, *DBD* cells operated at very high frequencies (in the megahertz range) will not exhibit microdischarge repulsion because the very high frequency switching of the voltage interferes with ions still moving to electrodes (for a detailed explanation of the ion trapping effect and an estimation of the frequency at which it becomes significant see). The formation of microdischarge patterns in *DBDs* has been investigated both from theoretical and experimental perspectives, [3, 4, 5 and 6].

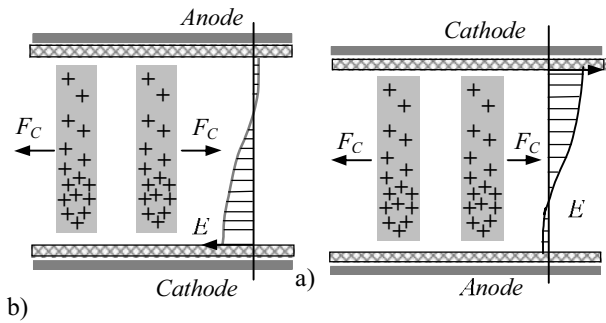


Fig. 6. Repulsion between ionic space charges of discharge remnant and the near-cathode electric field intensity  $E$  at the fin of the microdischarge and at the beginning the next one.

*Mechanism of spontaneously filament formation.* It is implied by microdischarge patterns observed that the microdischarge interaction should have two main features:

- repetition of microdischarges at the same place during each voltage cycle due to the existence of a pre-ionized positive channel (and surface negative charge) left by the previous microdischarge – microdischarge *remnant* – this effect of repetition of microdischarges at the same place usually is called *memory effect*. This effect results in the spontaneously filament formation and dynamic;
- “repulsion” of nearby microdischarge within the same voltage half-cycle by the microdischarge *remnant* – path or charge deposited on the dielectric barrier surface and positive space charge, because of local electric field distortion. This “repulsion” results in the self-organization of microdischarges into a regular short-range structure;
- local decrease (distortion) of electrical field near each microdischarge space that prohibit the appearance of new microdischarge at the same place at higher voltage – the permitted space with higher electrical strength is between two local distortion prohibited spaces.

*Self-organization of microdischarges.* It appears to be a strong effect and dominant feature of the dielectric barrier discharge. The underlying memory, repulsion and prohibition effects thus create quasi-Coulomb crystal filaments patterns in *DBDs*, [3, 4, 5 and 6]

### One-Dimensional Dielectric-Barrier Discharge at Atmospheric Pressure in Air

Owing to the curvature of the outer surface of the two CuZn37 wire electrodes ( $\varnothing$  0.15 mm; Aggie, Ltd., Switzerland), our one-dimensional *DBD* in air at atmospheric pressure and room temperature is tightly constrained in one lateral dimension and supports purely 1D - filament patterns between the glass tubes (distance between the electrodes  $d = 1,5$  mm) along the tube’s length. With larger distance between electrodes (to  $d = 6$  mm), we have not seen some wandering of filaments in the dimension perpendicular to the cylindrical axis. However, having chosen electrodes with a small diameter smaller than the characteristic size of a discharge footprint, i.e., patch of deposited negative surface charge, we observe a



suppression of filaments not localized to the plane containing the electrode axes.

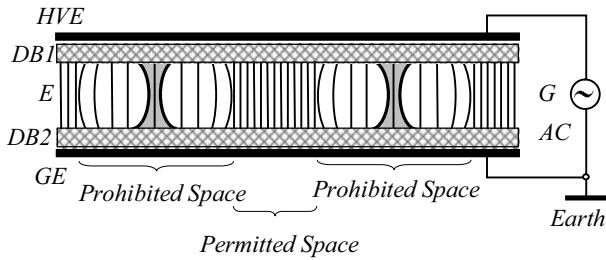


Fig. 7. Local discharge distortions of electrical field form spaces permitted for the appearance of new discharges at higher voltage.

Thus, we call this an effectively containing the electrode axes 1D-system and expect to model it using 1D- discharge remnant surface and space charge and current distributions integrated over the radial dimension of the be-cylindrical discharge gap, Fig. 1c.

A digital cameras (in visible and infrared light range) allow us to record pictures of the discharge and to analyze the digitized frames. The spacing measurements presented below were obtained with a resolution of about 120 pixels per 10 mm along the tubes axis. The average spacing is calculated for each image as the distance between the centers of widely separated (nonadjacent) filaments, divided by the number intervening filament spaces.

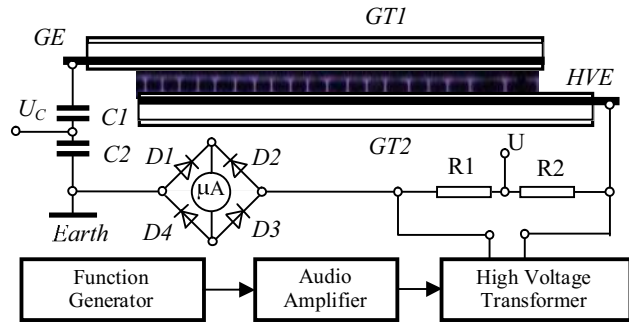


Fig. 8. Schematic of experimental setup for electrical diagnostics of one-dimensional dielectric barrier discharge by the static and dynamic volt-ampere characteristics.

Another diagnostic involves the circuit shown in Fig. 8. We monitor the voltage (RMS) across the wire electrodes and the current (AVG) through the discharge gap. We will have occasion examine with a discharge running the jumps in current corresponding to a specific filamentary space distribution along the electrode's axis, [7]. IR-image, show-image patterns, volt-ampere characteristic, electrical parameters, and the specific real power of DBD, are submitted on Figs. 9÷12.

### Conclusion

As a last point, we note that space-resolved imaging and appointed operational zone has given us a way of identifying and distinguishing between complex patterns that are otherwise difficult to recognize.

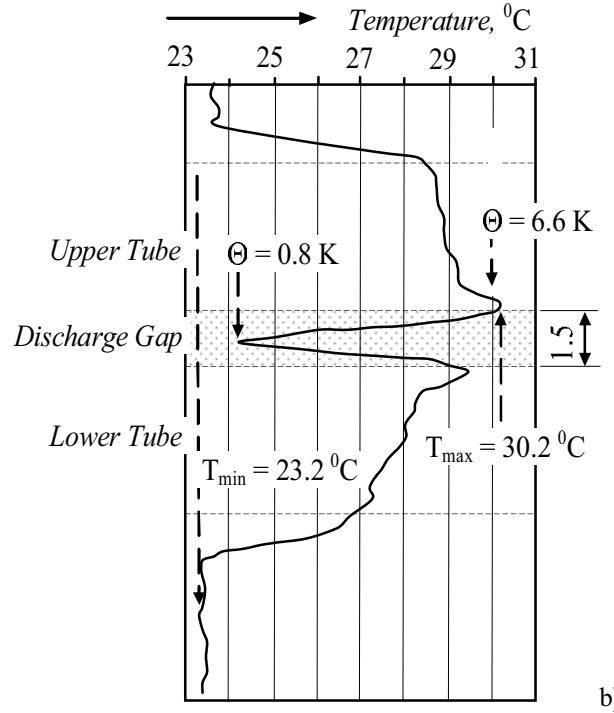
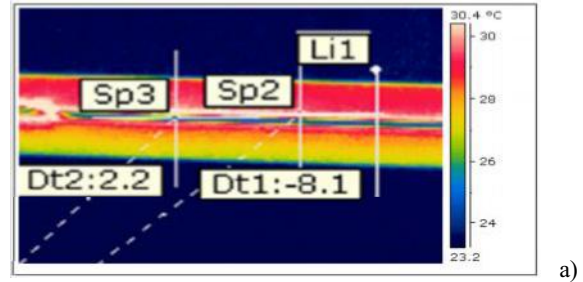
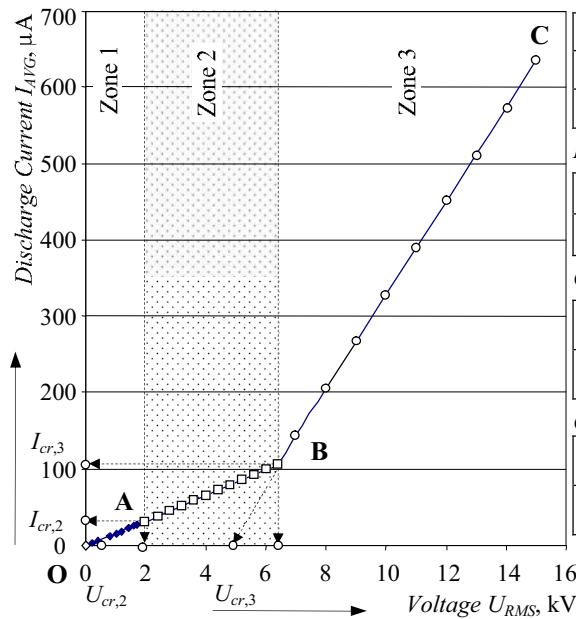


Fig. 9. IR-image (a) of discharge gap with two glass tube – Li1 is the cross-section in that the distribution of IR-radiation ( $\lambda = 7.5 \div 13.0 \mu\text{m}$ ) temperature in discharge gap and on the surface of dielectric glass tube barriers was measured. IR-radiation was emitted as from homogenous source - no filamentary pattern was observed. The temperature of overheated media was from 0.8 to 6.6 K (ThermaCAM P640, Flir Systems, Ltd., Sweden: 640x480 pixels; 0.060 K at 30 °C; 24 x 18 °/0.3 m; 0.65 mRad).

The dark space of “oxygen” operating zone without bright filamentary pattern surprises us, but it is well known that the ozone impact synthesis and active products of ozone destruction take place in the coldest plasma space and the highest electrical field.

The small diameter of electrodes determines very intensive electric field at low voltage amplitude (up to 6.6 kV) and small specific real power (up to 8 mW/m), i.e., the right condition for “oxygen” containing cold plasma existence. But there was any light, any birthing filament. The fact that such stable filamentary structures typically arise under very specific conditions, usually after a transition to a stable states of the system, suggests that they may provide important clues to the underlying pattern-formation dynamics.

**A. Volt-ampere Characteristic of one-dimensional DBD**



**B. Parameters of one-dimensional DBD**

Zone 1	$I_{AVG} = 15.9518 U_{RMS} - 0.4096; r_1 = 0.9988$
Zone 2	$I_{AVG} = 17.0000 U_{RMS} - 2.4667; r_2 = 0.9999$
Zone 3	$I_{AVG} = 61.3510 U_{RMS} - 285.8520; r_3 = 0.9988$

*Burning Voltages (RMS Value)*

Zone 2	$U_{b,2} = 0.145 \text{ kV}$
Zone 3	$U_{b,3} = 4.659 \text{ kV}$

*Critical Voltages (RMS Value)*

Zone 2	$U_{cr,2} = 1.962 \text{ kV}$
Zone 3	$U_{cr,3} = 4.659 \text{ kV}$

*Critical Discharge Currents (Average Value)*

Zone 2	$I_{cr,2} = 30.896 \mu\text{A}$
Zone 3	$I_{cr,3} = 106.157 \mu\text{A}$

**C. Images and show patterns of one-dimensional DBD at various driving voltage (RMS)**

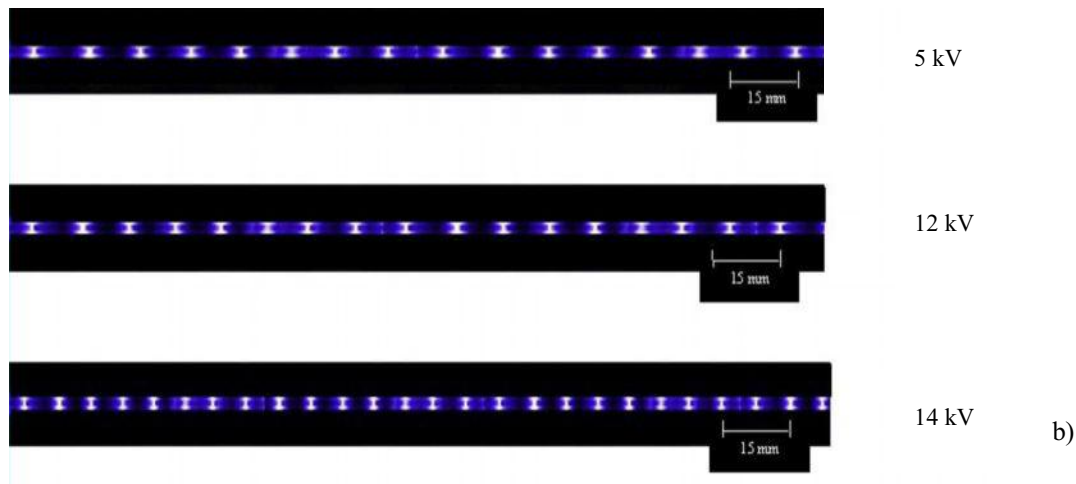


Fig. 10. Static volt-ampere characteristic (A) of one-dimension DBD in air at atmospheric pressure and room temperature for 50 Hz (industrial frequency) was taken down – discharge gap or distance between the two glass barriers  $d = 1.5 \text{ mm}$ , thickness of glass dielectric barrier  $b = 1.0 \text{ mm}$ : zone 1 – non-operational zone without discharge (OA); zone 2 – first or “oxygen” operational zone (AB); and zone 3 – second or “nitrogen” operational zone (BC). Parameters (B) of one-dimensional DBD in air at atmospheric pressure were estimated. Three images and show patterns (CB) of the DBD at various driving voltage amplitudes ( $U_{RMS}$  is indicated for each image – the maximal value is defined -  $U_{max} = \sqrt{2} U_{RMS}$ ) were recorded: up to 4.659 kV – dark space without filamentary patterns (not shown); 5, 12 and 14 kV – spontaneous filamentary patterns displayed in “nitrogen” operational zone – the image revealing a stable pattern front that can occasionally be seen – filaments strike at random times and places.

The technique and results reported here mark a significant step in the process of analyzing and understanding spontaneous pattern formation in DBD’s at atmospheric pressure. We hope our work will prompt theoretical effort directed toward establishing a link between the power supply conditions of DBD and

the macroscopic patterns in which the filaments are organized.

**Acknowledgements**

The financial support of the Technical University of Sofia, and the Ministry of Education and Science of Bulgaria, for the Research Project Grant No. 08027-ni-1/2008 is gratefully acknowledged.

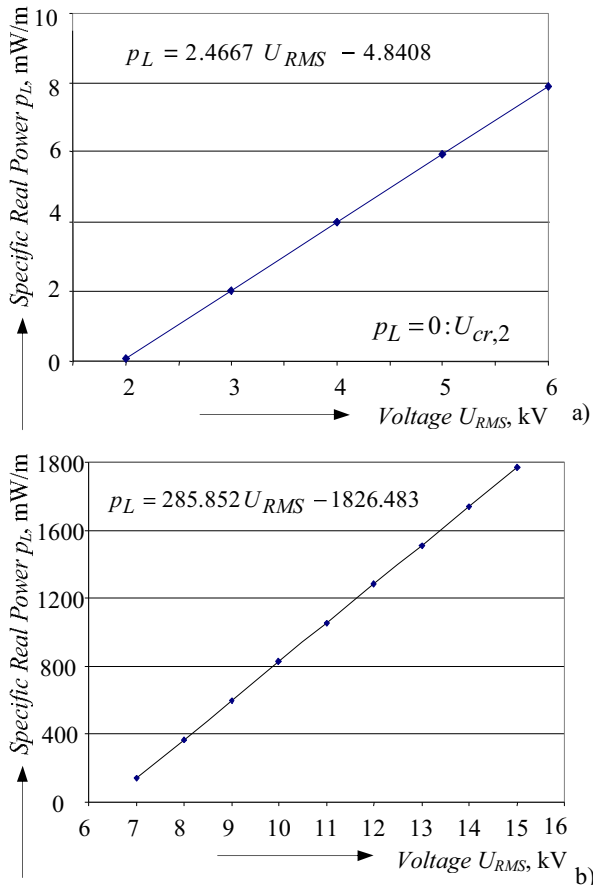


Fig. 11. Change of (for 1 m of linear discharge length) specific real power  $p_L$  at various driving voltage amplitude ( $U_{max} = \sqrt{2} U_{RMS}$  for the "oxygen" (a) and "nitrogen" (b) operational zone of one-dimensional DBD in air at atmospheric pressure and room temperature for 50 Hz (industrial frequency)).

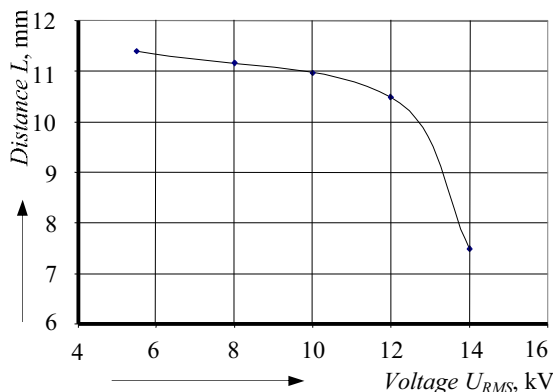


Fig. 12. Change of average distance between neighbour filaments  $L$  at various driving voltage.

## References

[1] Kogelschatz, U., Dielectric-barrier Discharges: Their History, Discharge Physics, and Industrial Applications. – Invited Overview. Plenum Publishing Corporation, Plasma

Chemistry and Plasma Processing, 2002, Vol. 23, No. 1, pp. 1÷46.

[2] Schütze, A., J. Jeong, S. Babayan, J. Park, G. Selwyn, and R. Hicks. The Atmospheric-Pressure Plasma Jet: A Review and Comparison to Other Plasma Sources. – Invited Paper. IEEE Transactions on Plasma Science, 1998, Vol. 26, No. 6, pp. 1685÷1694.

[3] Fridman, A., A. Chirokov and A. Gutsol. Non-thermal atmospheric pressure discharges. - Topic Review. Institute of Physics Publishing, Journal of Physics D: Applied Physics, 2005, Vol. 38, No. 2, pp. 3727÷3751.

[4] Chirokov, A., A. Gutsol, A. Fridman, K. Sieber, J. Grace, and K. Robinson. Self-Organization of Microdischarges in Dielectric Barrier Discharge Plasma. IEEE Transactions on Plasma Science, 2005, Vol. 33, No.2, pp. 300÷3001.

[5] Guikema, J., N. Miller, J. Niehof, M. Klein, and M. Walhout. Spontaneous Pattern Formation in an Effectively One-Dimensional Dielectric-Barrier Discharge System. Physical Revue Letters, 2000, Vol. 85, No. 18, pp. 3817÷3820.

[6] Klein, M., N. Miller, and M. Walhout. Time-resolved imaging of spatiotemporal patterns in a one-dimensional dielectric-barrier discharge system. American Physical Society, Physical Review E, 2001, Vol. 64, 026402, pp. 1÷5.

[7] Dineff, P., D. Gospodinova. Electric Characteristics of Barrier Discharge. XXXVI. International Scientific Conference on Information, Communication and Energy Systems and Technologies "ICEST 2003". Sofia, Bulgaria, October 16÷18, 2003. Proceedings, Heron Press, Ltd., 2003, pp. 442 ÷ 445.

## Biographies



**Peter Dineff** was born in Sofia, Bulgaria, on July 02, 1947. He studied at the Technical University of Sofia, Bulgaria, and received Ph.D. degree in Electrical Processing and Apparatus. Since 1991 he is a lecturer and assoc. professor in Electrical technology and processing at the Faculty of Electrical Engineering of Technical University of Sofia, Bulgaria. Main field of interest: electrical processing and apparatus, material (polymer) science, surface engineering, electrochemistry.

Peter Dineff is with the Faculty of Electrical Engineering of Technical University of Sofia, 8, St. Kliment Ohridski Blvd., 1000 Sofia, Bulgaria (e-mail: dineff\_pd@abv.bg).



**Dilyana Gospodinova** was born in Sofia, Bulgaria, on December 12, 1976. He studied at the Technical University of Sofia, Bulgaria, and received Ph.D. degree in Electrical Processing and Apparatus.

Since 2006 she is an Assistant professor on Plasma technology in the Faculty of Electrical Engineering of Technical University of Sofia in the field of electrical processing and apparatus.

Dilyana Gospodinova is with the Faculty of Electrical Engineering, Technical University of Sofia, 8, Kl. Ohridski Blvd., 1000 Sofia, Bulgaria (e-mail: dilianang@abv.bg).

# Methods for Test and Analysis of Electrical Machines and Transformers Insulation

Lyubomir V. Dimitrov and Stefka G. Kanturska

**Abstract:** The present paper discusses some possibilities of applications of modern methods to test and analyze the electrical machines and high voltage transformers insulation. The analysis is done by a special application tool in MATLAB software, that has been designed to perform Fuzzy Logic algorithm. The evaluation is carried out using Fuzzy Logic in order to increase the accuracy of the results and to have the correct conclusions about this condition.

**Keywords:** Insulation, Insulation Testing, Fuzzy Logic

## Introduction

Winding Insulation Resistance between machine body and between machine windings is measured during almost all motor and transformers tests. This is done for every independent circuit consecutively, as all the rest of the circuits remain connected to the grounded machine body.

In the cases with the alternative current machines, measurements are concerning the insulations of each phase, as well as each transformer winding. The classic method to measure the windings insulation is using the Meg-Ohm check (Insulation Tester), having direct current generator with outputs 500V; 1000V and 2500V. Most of these devices have manual driven mechanism. This limits the testing period and usually the generated voltage is not stable. The range of such devices does not exceed 1000 MΩ. Besides this, the readings are analogue, which means that the sensitivity is poor, especially when the values are changing fast.

The appearance of electronics and the development of battery technology revolutionized the design of insulation testers. Modern instruments are line or battery-powered and produce very stable test voltages under a wide variety of conditions. They are also able to measure very small currents so that their insulation resistance measuring range is extended several thousandfold into the teraohm (TΩ) range. Some can even replace the pencil and paper, which were formerly used to manually collect results, by recording data in memory for later download and analysis.

The results from the measurements are recorded in the device memory and could be recalled later on for analysis. The application of such modern devices to measure the insulation resistance offers more efficient ways to evaluate the windings condition. The absolute

value of the insulation resistance ( $R_{i3}$ ) does not always dispose well the winding technical condition. Its relative alteration for a period of time for a single object, allows to catch the alteration of this condition and to read and consider the impact of factors such as moisture and dirt etc.

## Testing Methods

As a technical condition criteria of the insulation could be used several indicators:

### 1. Spot Reading Test

The test voltage is applied for a short, specific period of time (typically 60 seconds as usually any capacitive charging current will have decayed by this time) and a reading is then taken. The reading can then be compared to the minimum installation specifications. Unless the result is catastrophically low, it is best used when trended against previously obtained values.

Table 1 provides minimum applied DC voltage MΩ testing. Higher voltages may be applied based on site-specific requirements and procedures.

The values of the applied voltage depend on the nominal windings rated voltage and are given in Table 1. [3]

**Table 1**

Single measurement of  $R_{i3}$  after applying testing DC voltage for 60s.

Winding rated voltage, ( V )	Insulation resistance test direct voltage, ( V )
< 1000	500
1000 – 2500	500 - 1000
2501 – 5000	1000 - 2500
5001 – 12000	2500 - 5000
> 12 000	5000 – 10 000

The minimum values recommended according to the same standard are given in Table 2. It is always necessary to remember the fact that the  $R_{i3}$  strongly depends on temperature. The increase of 10°C leads to two times decrease in the value of  $R_{i3}$ . In this respect the measurements should be carried out in one and the same environmental conditions.



**Table 2**

*Recommended minimum Insulation Resistance Values at 40°C*

Minimum insulation Resistance	Test specimen
$R_{ins.1 min} = kV + 1, M\Omega$	For most windings made before about 1970, all field windings, and others not described below
$R_{ins. 1 min} = 100 M\Omega$	For most DC armature and AC windings built after about 1970 (form-wound coils)
$R_{ins. 1 min} = 5 M\Omega$	For most machines with random-wound stator coils and form wound coils rated below 1 kV.

**2. Recording the value of  $R_{ins.}$  on each 10 s using modern devices.**

This is the possibility to determine the absorption coefficient (**Dielectric Absorption**) DA, which is the relation of  $R_{ins.(60s)} / R_{ins.(30s)}$ .

$$(1) \quad DA = \frac{R_{ins.(60s)}}{R_{ins.(30s)}}$$

where  $R_{ins.(60s)}$  and  $R_{ins.(10s)}$  are the values of the insulation resistance when applying testing voltage for periods of 60s and 10s respectively.

Due to absorption, the capacity of the winding is charged by the direct current but for different times depending on the certain moisture extent in the insulation. This allows easy determination of values not permitted for  $DA \leq 1,25$  as well as acceptable for  $DA \geq 1,5$ .

**3. Index of polarization –PI.**

The index of polarization – PI, is the relation between  $R_{ins.}$ , measured 10 min after and the reading measured 1 min after.

$$(2) \quad PI = \frac{R_{ins.(10 min)}}{R_{ins.(1 min)}}$$

Regarding insulation classes B, F and H, the minimal values of PI should be greater than 2 ( $PI > 2$ ). In general, lower values of PI show changes in the quality of the insulation (bad insulation). The higher values ( $PI > 4$ ) show very good insulation condition. While reporting this index, the modern testing equipment automatically reads the DA, because the measurement of  $R_{ins.}$  is carried out each 10 seconds.

**4. Testing using step voltage alteration (Step voltage Test)**

When the insulation is good, the increase of the testing voltage induces current rise, while the insulation resistance remains permanent. Every deviation of the current value is a signal for a defect in the insulation. A

very common procedure is the method using standard voltage step increase by 500V, five times to reach 2500V. The time to increase the voltage for each step is 1 min, as by the end of this period the  $R_{ins.}$  value is being recorded. Every noticed and unusual decrease of  $R_{ins.}$  indicates incipient insulation defect.

Figure 1 shows the changing of the insulation resistance [1] for a motor, when the testing voltage increases step by step as discussed above. The curve (1) on the figure is concerning the alteration of  $R_{ins.}$ , when there's moisture and dirt; curve (2) shows good condition of the insulation.

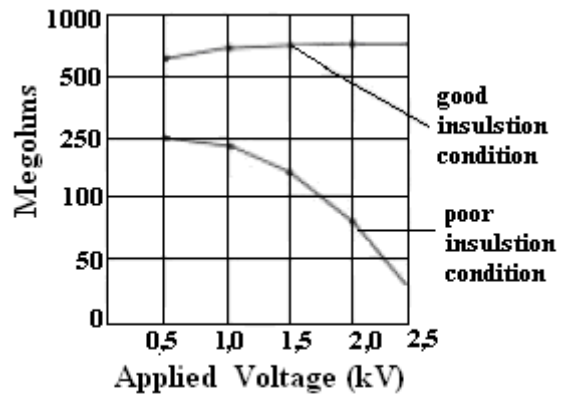


*Fig.1. Step Voltage Step Graph.*

In common the deviation of the values of  $R_{ins.}$  (about 25% and more) on each step of the test voltage speak about moisture and dirt in the insulation. The PI test is not applicable for oil transformers.

**5. Testing using dielectric discharge**

**( Discharge DD Test )**

This is comparatively new method to test the insulation condition. Since the other methods are based on current measurement in the process of charging the dielectric capacity, the dielectric discharge test measures the discharging current via a resistor (Fig.2) The magnitude of the discharging current depends only on the resistor value and the extent the insulation is charged to.

The test starts with charging up to 2,5 kV for 10 to 30 min periods.

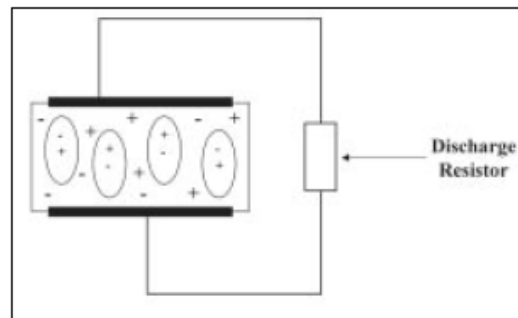


*Fig.2. Discharge of Test Item's Stored Charge.*

For this period runs a full charge and the dielectric absorption is in fact, complete. After that, the voltage is switched off and the insulation capacity is discharged via a discharge resistor. After 60 s of discharge, the value of the remaining current is being measured.

The results of the measurement are considered using the dielectric discharge coefficient:

$$(3) DD = \frac{\text{Current...flowing..after..1 min(nA)}}{\text{Test...Voltage(V)..x..Capacitance(\mu F)}}$$

The typical values, gained after the tests on synchro high voltage generators, show that when  $DD(\frac{mA}{V.F}) > 7$

the insulation condition is **bad**, when  $3 > DD(\frac{mA}{V.F}) > 7$  - **questionable**; and when  $DD(\frac{mA}{V.F}) < 2$  - **good**.

These values could be used when testing any multilayer insulation.

The criteria mentioned so far, regarding the insulation condition change in wide limits and are all result of expert evaluation.

## Experimental Results

When evaluating the insulation the method of ... could be used. "Fuzzy Logic". Words (terms) are entered as so called **linguistic variables** and not figures. In this case, the **Polarization index- PI**, as well as the **Absorption coefficient – DA** are chosen as linguistic variables. The meaning of these could be considered with the terms **BAD, QUESTIONABLE and GOOD**.

To make one linguistic variable real, it is necessary to determine the exact physical meaning of the terms, concerning this variable. For example, the PI index could have values between 0 and 4. According to the theory of diluted fuzzy rules, each of these values could be any number between 0 and 1, that determines the extent of belonging or attachment of a variable to a certain rate, for example – **BAD, QUESTIONABLE or GOOD**.

The extent of attachment to these rates is defined as so called Membership function  $\mu(x)$ . It could have different graphical expression, depending on optimistic or pessimistic determination or reading of the variable values. As an output function is considered the condition of the insulation. On Fig.3 and Fig.4 are shown the Membership functions of the two parameter indicators – the **Polarization index - PI** and the **Absorption coefficient –DA**, according to the above defined limits.

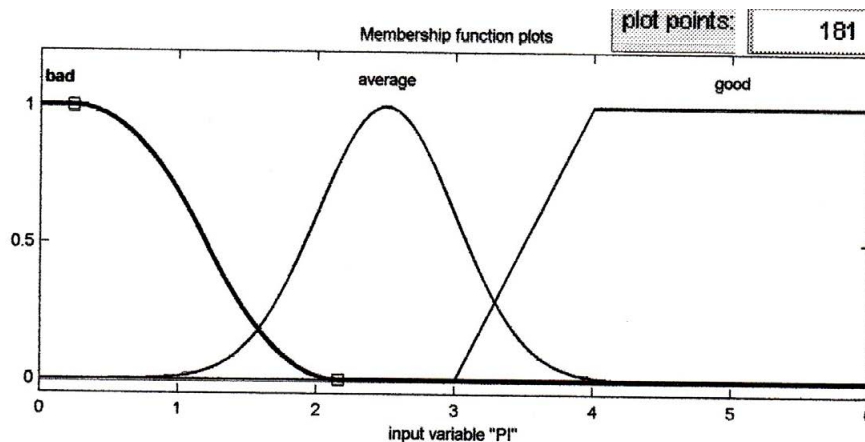


Fig.3. Membership function PI

The connection between the input and the output parameters is given in the so called Table of the Fuzzy Rules. The realization of the necessary operations when applying these rules is carried out using the software application "MATLAB 7" (Fuzzy logic Toolbox). The output function. Insulation consists in evaluation of the

insulation peculiarity and is shown on Fig.5. This condition is considered as bad, questionable and good. The range to carry this evaluation is between 0 and 100 units.

Fig.6 and Fig.7 show two cases of determination the good and the bad insulation condition.

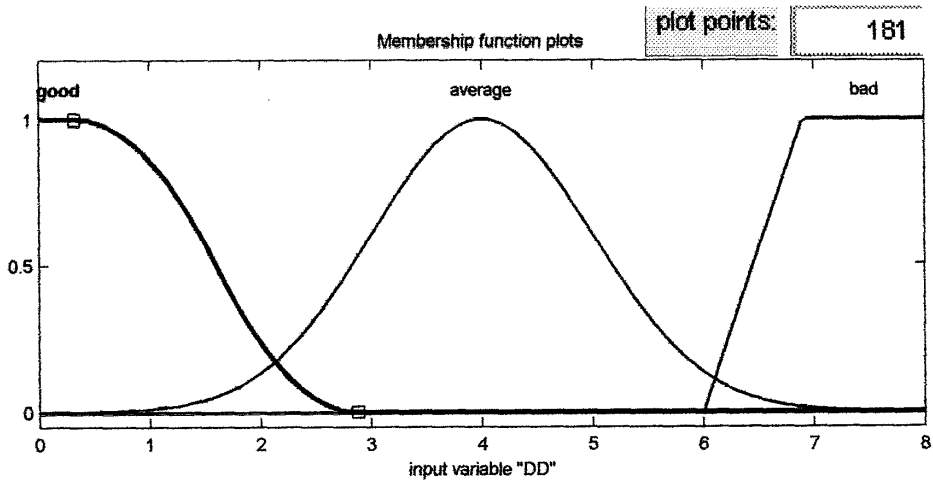


Fig.4. Membership function DD

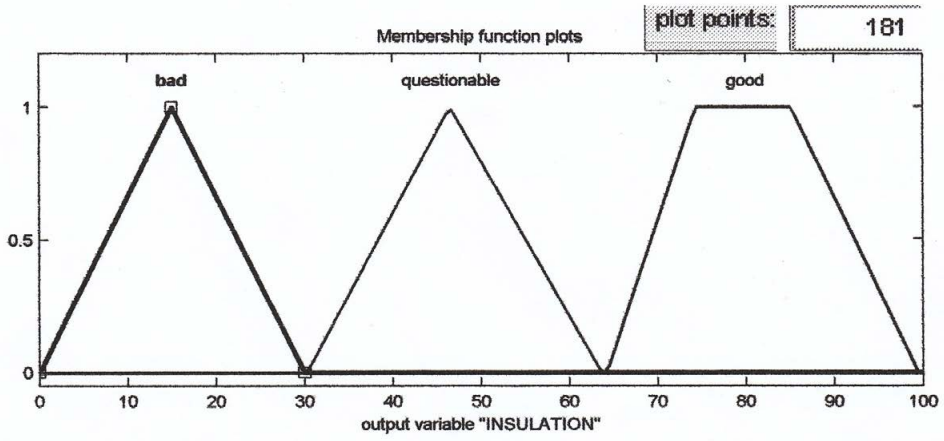


Fig.5. Output variable "Insulation"

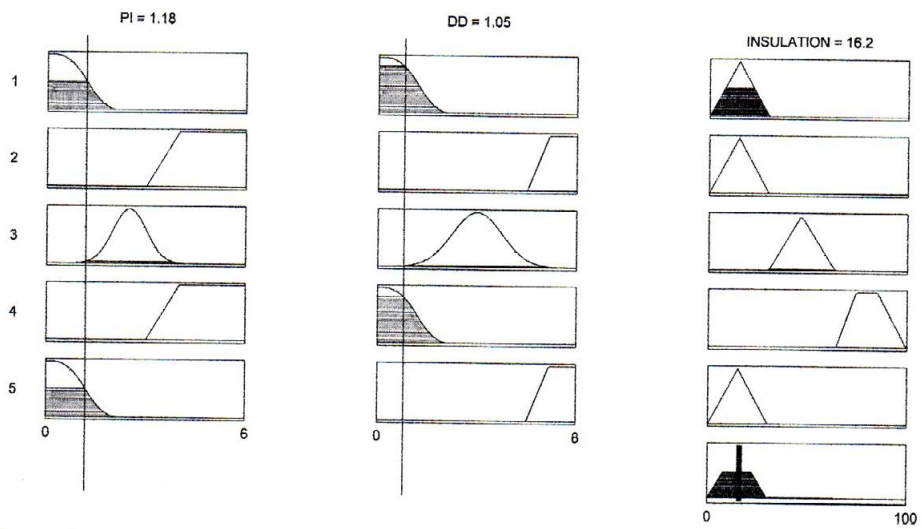


Fig.6. Rule Viewer for "Bad Insulation"

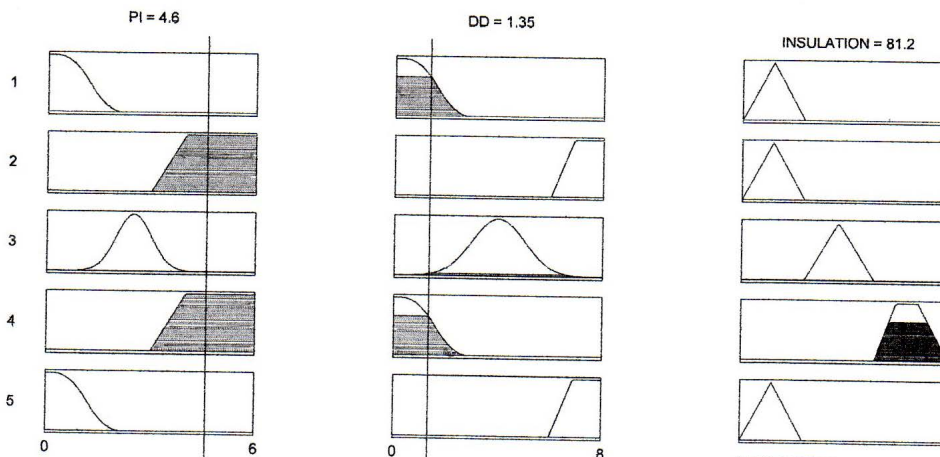


Fig.7.Rule Viewer for "Good Insulation"

Table 3 shows some of the rules used in the different phased variants.

Table 3

<p>1. If (PI is bad) and (DD is good) then (INSULATION is bad) (1)          2. If (PI is good) and (DD is bad) then (INSULATION is bad) (1)          3. If (PI is average) and (DD is average) then (INSULATION is questionable) (1)          4. If (PI is good) and (DD is good) then (INSULATION is good) (1)          5. If (PI is bad) and (DD is bad) then (INSULATION is bad) (1)</p>
---

### Conclusion

The application of Fuzzy Logic Rules to evaluate the windings insulation resistance of the electrical machines and high voltage transformers, allows carrying the corresponding preventive action, if necessary, having also in mind the values of the PI and DD accordingly. The leading role, with regards to the quality aspect of these figures of the insulation resistance, is taken by the experts, who determine the amount of the input and output parameters, the number of each variable term, as well as the type of the function assignment.

### References

- [1] Jones D.O.; Joweft J.R. ;Thomson E.;Danner D.S – "A Guide to Diagnostic Insulation Testing above 1 kV;AVO International June 2002.
- [2] Matlab,Fuzzy Logic Toolbox-Users Guide.
- [3] IEEE Std 43-2000 –Recommended Practice for Testing Insulation Resistance of Rotating Machinery, March 2000.

### Biographies



**Lyubomir Dimitrov** was born in Varna, Bulgaria, on Oktober 24,1944.He studied at the Technical University of Varna-Bulgaria and received Dr.degree from the Technical University of Sofia in 1978.

Since 1971 he worked in the Faculty of Electrical Engineering of the Technical University of Varna as Ass.Professor in the design diagnostic and monitoring electrical machines and electrical drives. Lyubomir Dimitrov is with the Faculty of of Electrical

Engineering of the Technical University of Varna "Studentska Str.1"9010

lubo.dimitrov@mail.bg



**Stefka Kanturska** was born in Svishtov,Bulgaria, on January 8,1946. Shi studied at the Technical University of Varna-Bulgaria and received Dr.degree from the Shipping University of Sankt Peterburg in 1980.

Stefka Kanturska is with the Faculty of Architecture of the Free University of Varna "Chajka." 9000

sgkanturska@abv.bg



# Equipment for infrared welding of large area plastic details

Petko Mashkov, Tamara Pencheva, Berkant Gyoch, Angel Valchev

**Abstract:** *New equipment for infrared welding of large area plastic details is designed and produced. New welding equipment is based on application of new type infrared heaters for the middle infrared spectral region. They are made from thin metal sheets, covered by a special coating with emissivity over 0.9 and are warmed up directly by electric current. Variations of heater's design, combined with electronic control of their operation give possibility to choice optimal variant in dependence on the type of treated material, size of details, necessary time for welding process, etc.*

**Keywords:** *infrared welding, welding of plastic materials*

## Introduction

Plastics' welding is widespread technological operation in industry and may be realized by different manners – by hot air heating; by contact heating, by infrared heating; high frequency and microwave heating, ultrasonic welding, etc. Production of eco – filters for automotive industry brings new demands to quality of welded details. Preferred methods of welding for this type of plastic details are by hot air and by infrared heating [1 - 5]. Welding by hot air may be successful for details, made from polypropylene. When they are from polyamide, this type of welding is applicable for small details only. When material is polyamide filled with glass particles welding with hot air doesn't give good results. More over, at hot air welding energy consumption is too big. It is combined with big compressed air consumption. Both of them are too expensive.

Welding by infrared (IR) heating is widely used for this type of details for automotive industry and may be classified according to spectral characteristics of used radiation. When the radiation is from the near IR spectral region ( $\lambda \leq 2.5\mu\text{m}$ ) usually the heaters are halogen lamps. They allow achieving of big intensity of the radiation over the treated area, but they have some disadvantages. The effectiveness of application of radiation from the near infrared spectral region depends on the details' colors. It's a problem to achieve uniform radiation's intensity onto large areas; control of the parameters of lamps' operation isn't simple; the life of the halogen lamps in real production conditions isn't long enough [4, 5].

According to upper mentioned reasons welding of plastics details by radiation from the middle infrared spectral region ( $2.5\mu\text{m} \leq \lambda \leq 10\mu\text{m}$ ) is preferred. Almost all plastic details, used in industry, absorb radiation from this spectral region very well independently of their colors. Many kind of infrared emitters for the middle IR region are used in industry [1-5]. Some of them possess

good effectiveness to transfer electric energy (or energy from gas burning) to radiation's energy. But almost all of known infrared emitters have a big disadvantage – they are too inert. That is why it is difficult to control thermal processes, especially when they are short, like welding with duration about 10 – 40 seconds.

By application of low inert IR heaters for the middle IR spectral region we successfully solved problems, connected with welding of large area plastic details for automotive industry. At the same time productivity was enhanced some times, supplemented with significant decreasing of energy consumption.

## Problem statement

Generally, the problems during welding of plastic details for automotive industry are connected with:

- Large area of heated details which must be melted (diameter up to 180 mm).
- Necessity of uniform temperature distribution on the whole area of details.
- Plastics should be melted to the depth of 1 mm upon the whole area.
- The thickness of the details is between 3 mm and 4 mm; during melting of upper 1 mm layer the detail should not change the shape.
- The surface of melted plastic materials should not be overheated. If its surface temperature is raised over determined temperature for material in use the sample surface layer destructs, which worsen strongly adhesion and properties of welded joints.
- Complicated form of some of details makes uniform melting of plastics on the whole area very difficult.
- Necessity of application of shields in order to protect some parts of heated detail.
- The duration of the process must be short for good productivity. On the other hand the time of the heating must be long enough to melt the detail to the desirable depth without preheating the surface.
- To achieve good and uniform quality of the products it is necessary to have possibility for precise control of IR radiation intensity with high rate, because during this technological process conditions change fast: the heaters and details move; atmosphere in the heating volume is changed at every welding cycle; fixture accessories are with different temperatures, etc.

## Experimental equipment

### A. Heaters

To solve upper mentioned problems a new type of low inert heaters for the middle IR spectral region are

used. They are made from thin metal sheets (0.5mm) from Ni – Cr – Fe alloy. Most of the heaters with metal surface can't transfer effectively electric energy to energy of radiation, because of low emissivity of the surface. This is significant disadvantage and prevents successful application of metal Ni – Cr heaters as infrared emitters. This problem is successfully solved by covering the surface of the heaters with a special coating, containing mainly Cr<sub>2</sub>O<sub>3</sub>. This compound has appropriate spectral radiation characteristics. Emissivity of Cr<sub>2</sub>O<sub>3</sub> is over 0.9 for the whole spectral region from the visible to the far infrared spectral region. More over, this high emissivity is almost independent from the temperature, which is very important. This kind of coating on the surface of the heaters makes them effective infrared emitters. The heaters are warmed up directly from the electric current through the heater's bands. This ensures very low inertia of the heaters – their surface temperature may be varied with rate more than 10K/s. These properties of the heaters make them suitable for applications at various thermal processes. Additionally, by electronic control of the operation of the heaters realization of desirable thermal processes with high precision may be achieved – for example, soldering cycles, welding, etc. [1, 2].

The heaters may be produced with different design – with equal belts' width (Fig. 1), or with different belts' width (Fig. 2).

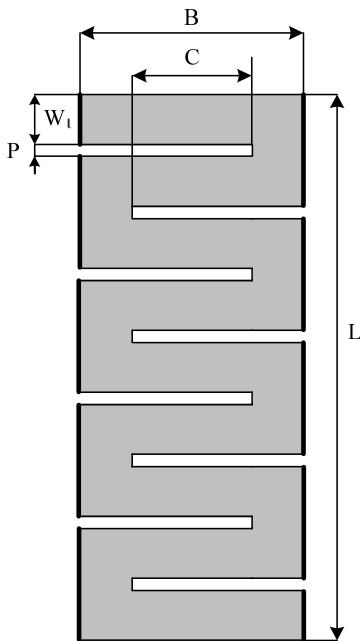


Fig. 1. Flat heater. All heaters' belts are with equal width ( $W_1 = 4 \text{ mm}$ ).

The size  $c$  of the heaters usually is between 140 mm and 200 mm; the size  $L$  – up to 500 mm or longer, in dependence of the parameters of the heating camera. The flat shape of the heating elements allows achieving uniform intensity of the radiation during thermal treatment on large areas.

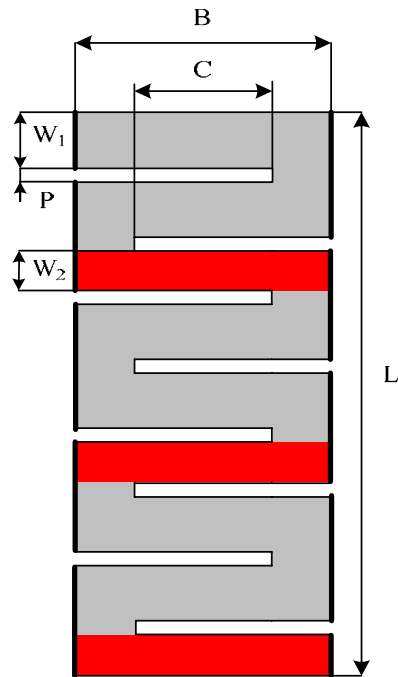


Fig. 2. Heater with different belts' width:  $W_1 = 4 \text{ mm}$ ,  $W_2 = 3 \text{ mm}$ .

Usually working temperatures of the heaters are between 370K and 900K and emitted radiation from the heaters' surface, in accordance to Plank's law, belongs to the middle infrared spectral region. When the design of the heater is like that, shown in Fig. 1, the surface temperatures of all heaters' belts are practically equal. Spectral distribution of the emitted radiation may be calculated by Plank's law (1):

$$(1) \quad E(\lambda, T) = \frac{C_1}{\lambda^5} \frac{1}{e^{\frac{c_2}{\lambda T}} - 1}$$

Here  $\lambda$  is the wave length,  $T$  is the heater's surface temperature, and  $C_1 = 3,74 \cdot 10^{-16} \text{ W.m}^2$ ,  $C_2 = 1,4388 \cdot 10^{-2} \text{ m.K}$  are first and second Plank's constants.

The desirable intensity of radiation may be adjusted by variation of the heaters' temperature (which changes spectral distribution of energy too) and by proper choice of the belts' density (parameter  $p$  in Fig. 1).

Infrared radiation from the middle IR spectral region is very suitable for thermal treatment for a lot of materials. Most of materials (for example, plastics) have spectral characteristics, close to the black body for this spectral region. That is why radiation from the middle IR region is very effective for heating, melting, welding for almost all plastics materials, independently of their color. Sometimes, to make the equipment more universal, it is desirable to use radiation with extended spectral distribution. Then it is proper to use design of the heater, shown in Fig. 2. Since the heaters' belts are connected in series, the current through them is the same and the electronic controller for the operation is one for the whole heater. Surface temperatures of the belts with different width are different too. The temperature differences at belts' dimensions, shown in Fig. 2, are about 50 – 80K.

At this design every third belt is narrower. Because of small belts' width (3mm – 4mm) at distance about 50mm from the heaters' plane radiation intensity distribution may be considered as equal.

The disadvantage of this solution for heater's design is complicated production of the heaters.

Heaters with another design, shown in Fig. 3, are produced. Experimental equipment for welding of large area plastic details is realized using this kind of heaters.

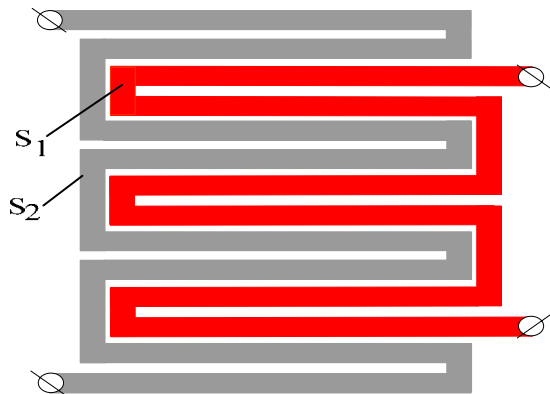


Fig. 3. Flat heater with two sections S1 and S2

This design of flat heaters is proposed in [2] and gives a lot of advantages. Operation of both sections of the heater is controlled independently. Their surface temperatures can be quite different and may be varied by different manners. It gives possibility to realize various temperature profiles of thermal treatments, proper for materials with very different properties. By electronic control of the sections' operation proper intensity of the radiation for the treated material and desirable spectral distribution of the emitted energy may be adjusted.

Experiments showed that the welding equipment realized with "two section heaters", Fig. 3, is more universal and gives better results compared to equipments realized by flat heaters, shown in Fig. 1 and Fig. 2. But this solution has a significant disadvantage. When the heated zone is for one detail only, it is a square with size 190/190 mm. In this case electric resistances of both heaters' sections are too small, which is a problem for ensuring power supply and electronic control of operation of the heater. On the other hand, two controllers for one work place isn't a cheap decision.

Another variant of welding equipment's construction turned out to be very successful. The heater sections are two and their bands are with equal width (like the design, shown in Fig. 1). The disposition of the sections in the heating camera is at two levels. Below view of the heater is similar to the view in Fig. 3, but section 1 is disposed about 15 mm upper than section 2 (Fig. 4 – 4a and 4b). The heater is surrounded by shields with high reflection (about 0.85). The both sections of the heater are connected in series and their operation is controlled by one controller. Because of the disposition in the camera the surface temperature of the upper section is

significantly higher – about 70 degrees than the temperature of the lower section.

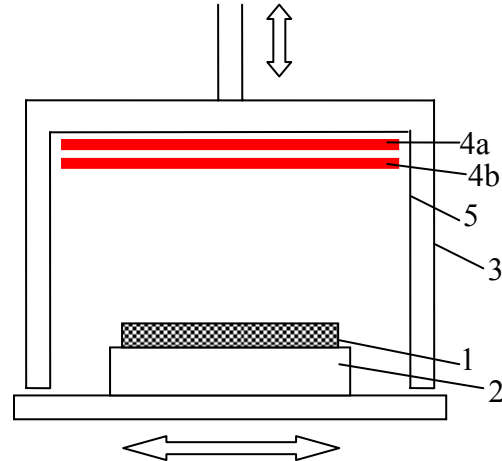


Fig. 4. Camera for infrared welding of large area plastic details: 1 – plastic detail; 2 – fixture accessory for the detail; 3 – corps; 4 – heater (4a – upper section, 4b – lower section); 5 – reflectors.

This kind of solution shows a lot of advantages, compared to other variants of heating camera design. The electric resistance of the heater isn't too small and there are no problems with power supply and control of the operation of the heaters. Only one controller is used for one work place. The spectral distribution of emitted energy of the heater is expanded compared to this at variant with one section heater, where all heaters' belts are with equal surface temperature. By application of Plank's law (1) spectral distributions of emitted energy for two variants are calculated and compared (Fig. 5).

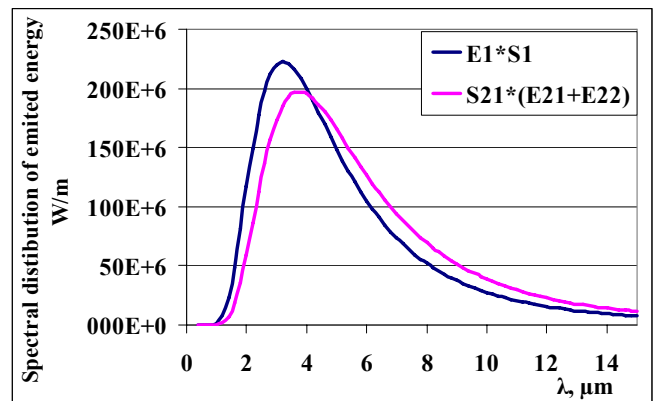


Fig. 5. Spectral distribution of emitted energy for two variants of heater's design:  $E1 \cdot S1$  – for one section flat heater;  $S21 \cdot (E21 + E22)$  – for two heater's sections, disposed at two levels.

These variants of welding equipment are realized and compared at real production conditions.

At the first variant – the heater is made from 24 belts 4/180 mm; emitting area is  $S_1 = 34,56 \cdot 10^{-3} \text{ m}^2$ . Operating temperature is about  $T_1 = 872 \text{ K}$ .

At the second variant – the heater consists of two sections, each of them with 20 belts, 4/180 mm. Emitting area of each section is  $S_{21} = S_{22} = 28,8 \cdot 10^{-3} \text{ m}^2$ . Operating temperature of the first section is  $T_{21}=800\text{K}$ ; operating temperature of the second section is  $T_{22}= 730\text{K}$ .

At these conditions intensities of the radiation emitted from the heaters are equal for both variants of construction. It can be checked up by application of Boltzmann's law (or by integration, using Plank's law):

$$(2) \quad \varepsilon\sigma S_1 T_1^4 = \varepsilon\sigma S_{21} T_{21}^4 + \varepsilon\sigma S_{22} T_{22}^4$$

Thermal losses are ignored for both cases. Intensity of the radiation for both variants is very close (about  $3,2 \text{ W/cm}^2$ ), but as it can be seen from Fig. 5, spectral distribution of the radiation is different. For "two levels" heater the spectrum of emitted radiation is extended and the maximum of the spectral distribution is moved to the longer wavelengths. Experiments show that this is very important for welding of plastics and for obtaining good quality of welding joints. Infrared radiation with longer wavelengths penetrates more deeply in the plastic. Surface preheating is smaller, so, destruction of the surface layer is much smaller and the adhesion between welded details is significantly better.

Very important for good work of welding equipment is the manner of control of heaters' operation. Experiments with different kind of voltage regulators are made. Voltage regulators with pulse – phase modulation or pulse – width modulation don't give good results. Instability of voltage supply doesn't permit to achieve uniformity of production conditions and high quality of welded details. Much better results are obtained by application of constant value control of the voltage supply. In this case the problems may be classified in two groups: first – the power of the heaters in some cases is over 10 KW and it's a problem to use such voltage regulators, they are too expensive. Second type of the problems is connected with the manner of operation of the welding machine (Fig. 4). One operating cycle includes next steps:

- the heating camera is empty and closed for about 15 – 50 seconds;
- then the corps 3 is lifted up, the detail on the fixture accessory comes in;
- the corps is moved down;
- the melting of the surface layer of the plastic detail passes (about 15 – 50 seconds);
- the corps 3 is lifted;
- the detail on the fixing accessory is moved out;
- the corps is moved down.

The conditions during these operations may be very different – the temperature of the ambient air, the temperature of the details and fixing accessory may vary significantly. That's why to keep the voltage supply constant is not enough. The best results are obtained by measuring the surface temperature of the heater's belts and control it to be constant. This ensures constant irradiation intensity and allows achieving repeatability of

the production conditions. By small changes of the time for melting of the detail the conditions' variations may be compensated. For realization of this temperature control two problems have to be solved. First, the temperature is measured by thermocouple (type K) which is mounted on the surface of one of the heaters belts. But they are connected directly to the voltage supply (220 V or 380 V, 50 Hz). This makes necessary using of insulating amplifier between thermocouple and the controller.

The other problem is connected with the velocity of thermal processes during welding. They are relatively fast – the duration of the welding cycle is about 9 – 50 seconds. At these conditions the big advantage of this type of heaters (ability to change their surface temperature with the rate more than 10 K per second) becomes very important. But experiments show that it's not easily to control the heaters' surface temperature with desirable precision. With standard controller (Moeller) variations of  $\pm 10\text{K}$  around desirable temperature value are achieved, which is not so good.

The best results at real industrial conditions are obtained by application of analog measuring system [3] which outlet signal is used for pulse – width modulation of heaters' operation (with the period 1 s). By changing the mark to space ratio of heaters' operation the desirable surface temperature of the heaters is hold up with variations not more than  $\pm 3\text{K}$ .

In Fig. 6 an experimental results for surface temperature changes during welding cycle for plastic detail (polypropylene) are presented. The temperature was measured by thermocouple type K.

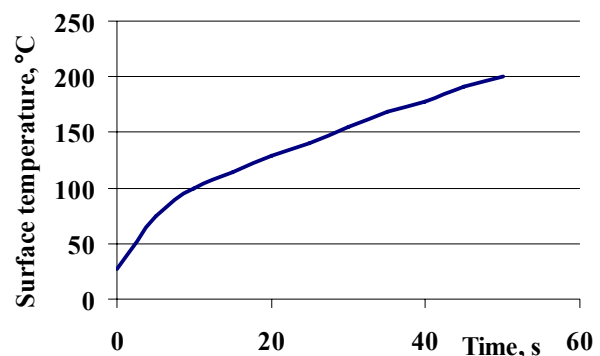


Fig. 6. Dependence of surface temperature from time during welding cycle for polypropylene detail.

Welding equipment is introduced in a plant where details for automotive industry are produced. This type of equipment, based on low inert infrared heaters, shows a lot of advantages. High quality of welding joints for polyamide details filled with glass particles is achieved, which was impossible earlier. Expenses for electric power consumption decreased over than three times. The consumption of compressed air decreased significantly. Welding of details with larger size on the existing machines became possible. The productiveness and the quality of the production were raised.



## Conclusions

A new type of welding equipment based on low inert infrared heaters is developed and tested at real production conditions. In comparison with other welding methods (by hot air, contact methods, welding by radiation from visible and near infrared spectral regions and others) this type of welding shows a lot of advantages:

- best quality of welding joints comparing with other methods of welding;
- uniformity of the welding joints onto large areas;
- possibility to weld details with complicated shapes;
- minimal deformation of these details in comparison with other methods;
- applicability of the equipment for all plastic materials used in the plants;
- high accuracy of the control;
- reproducibility of the welding process' parameters, etc.

## Acknowledgements

The National Science Fund, Ministry of Education and Science of Bulgaria is gratefully acknowledged for the financial support of research project VU-EES-301/2007.

## References

- [1] Mashkov, P., T. Pencheva, B. Gyoch, D. Popov. Infrared radiation spectrum control during soldering processes applying low inert heaters, Proceedings of IEEE, 29<sup>th</sup> International Spring Seminar on Electronics Technology - ISSE 2006, St. Marienthal, Germany, 2006, pp. 429 – 434.
- [2] Mashkov, P., T. Pencheva, D. Popov, Application of low inert infrared heaters for soldering processes, Proc. of IEEE, 27<sup>th</sup> International Spring Seminar on Electronics Technology – ISSE 2004, Sofia, Bulgaria, 2004, pp. 366–370.
- [3] Mashkov, P., T. Pencheva, D. Popov, V. Mateev. Electronic pulse control for low inert infrared heaters. - Proceedings of the 12th International Conference in ELECTRONICS ET'2003, Sozopol, Bulgaria, 2003, 369 – 375.
- [4] PDL, "Handbook of Plastics Joining A Practical Guide", Plastics Design Library of William Andrew, Inc. Copyright 1997. ISBN: 1-884207-17-0, p99.
- [5] PDL, "Handbook of Plastics Joining A Practical Guide", Plastics Design Library of William Andrew, Inc. Copyright 1997. ISBN: 1-884207-17-0, p96.

## Biographies



Petko Mashkov is in the Faculty of Electrical Engineering, Rouse University, 8, Studentska Str., 7017 Rouse, Bulgaria (e-mail: [pmashkov@ru.acad.bg](mailto:pmashkov@ru.acad.bg)).



Professor in the field of infrared heating and electronics.

Tamara Pencheva is in the Faculty of Electrical Engineering, Rouse University, 8 Studentska Str., 7017 Rouse, Bulgaria (e-mail: [tep@ru.acad.bg](mailto:tep@ru.acad.bg)).



Berkant Gyoch is in the Faculty of Electrical Engineering, Rouse University, 8, Studentska Str., 7017 Rouse, Bulgaria (e-mail: [b\\_gyoch@ru.acad.bg](mailto:b_gyoch@ru.acad.bg)).



Engineering of the Rouse University.

Angel Valchev is in the Faculty of Electrical Engineering, Rouse University, 8, Studentska Str., 7017 Rouse, Bulgaria (e-mail: [avalchev@ru.acad.bg](mailto:avalchev@ru.acad.bg)).

**Petko Mashkov** was born in Rouse, Bulgaria, on August 30, 1955. He studied at the Sofia University "Kliment Ohridski" – Mr.S. in Physics of semiconductors; Rouse University – Mr.S. in Internal combustion engines.

Since 1980 he worked in the Faculty of Electrical Engineering of the Rouse University as a Lecturer and researcher in the field of infrared heating and electronics.

**Tamara Pencheva** was born on January, 1948. She studied at the Faculty of Radio-electronics in Sant-Petersburg Politechnical University "Kalinin" – Mr.S. in Physics of semiconductors; Ph.D. in Physical-Technical Institute "Ioffe", RAN – in Physics of waves processes.

Since 1974 she worked in the Faculty of Electrical Engineering of the Rouse University as a Lecturer and Assoc.

Professor in the field of infrared heating and electronics.

Tamara Pencheva is in the Faculty of Electrical Engineering, Rouse University, 8 Studentska Str., 7017 Rouse, Bulgaria (e-mail: [tep@ru.acad.bg](mailto:tep@ru.acad.bg)).

**Berkant Gyoch** was born in Razgrad, Bulgaria, on May 24, 1977. He studied at the Rouse University "Angel kanchev" – Mr.S. in Telecommunications.

His field of interest includes optoelectronics; thin layers; microelectronic technologies. He is today a PhD student in the Faculty of Electrical Engineering of the Rouse University.

Berkant Gyoch is in the Faculty of Electrical Engineering, Rouse University, 8, Studentska Str., 7017 Rouse, Bulgaria (e-mail: [b\\_gyoch@ru.acad.bg](mailto:b_gyoch@ru.acad.bg)).

**Angel Valchev** was born in Stara Zagora, Bulgaria, on December 07, 1981. He studied at the Rouse University "Angel kanchev" – Mr.S. in Telecommunications. Since 1980 he worked in the Faculty of Electrical Engineering of the Rouse University as a Lecturer and researcher in the field of infrared heating and electronics.

His field of interest includes infrared heating and electronics. He is today a Ph.D student in the Faculty of Electrical

Engineering of the Rouse University.

Angel Valchev is in the Faculty of Electrical Engineering, Rouse University, 8, Studentska Str., 7017 Rouse, Bulgaria (e-mail: [avalchev@ru.acad.bg](mailto:avalchev@ru.acad.bg)).

# Analysis of Thermal Field of LED Heat Sinks for Road Luminaires

Valchan Gueorgiev, Ivan Yatchev, Krastio Hinov

**Abstract:** The thermal analysis of LED cooled by heat sink is discussed in the paper. The conventional approach uses circuit theory and manufacturer supplied data for thermal resistance of the heat sink. The custom-made luminaire body is used as a heat sink in road luminaires with LEDs according to the latest tendentious. Therefore the conventional approach cannot be used because the thermal resistance is unknown. It is known that more than 50% of the failures in power electronic circuits are due to thermal breakdown of the active device. Thermal breakdown occurs when the junction temperature reaches close to 155°C. Thermal analysis is of immense use, not only for finding the optimum power handling capacity of the given heat sink but can also be used for designing the heat sink for the required power dissipation. The steady state temperature of the custom luminaire, which is the most important thermal feature, can be determined by the use of the field approach. The description of the geometry of the heat sink can be obtained by the design documentation.

**Keywords:** LED luminaire, thermal analysis

## Introduction

The advantages that light emitting diodes offer make many specialists to consider them to be the lighting source of the future. The attempts in design of road lighting luminaires with that light source started immediately after introduction of high power white LEDs. At the beginning the conventional light source like sodium or metal halide lamps in the road luminaires have been directly replaced by low number of LEDs. There were serious considerations against such approach and the first design attempts supported them completely. Aside from lighting distribution another problem that was also easy to guess turned to be very important – the thermal design of the LED luminaires. When the high power LEDs have been introduced it was clear that they will need a serious heat sink in other to operate with power level close to the nominal value. The producers include a thermal resistance of the LED for each package and type of mounting. That would solve the problem with thermal analysis if a standard heat sink was in use. The thermal resistance as well as the surface of the standard heat sinks is relatively precisely determined and printed in the datasheets. It makes the calculation of the steady state temperature of the LED easy for computing. The procedure is formalized and well known. It is very convenient in spotlight design where single modules of very high power LEDs (50 W or more) are used. The body of the luminaire, which is used as a heat sink, is often with regular shape.

The problem arises when a standard heat sink cannot be used in the application. Even the minor practical experience in the area of street lighting with LEDs shows that a good lighting performance can be achieved by using relatively big number of high power (but not extremely high power) LEDs are used and they are individually oriented in such a manner so entire light flux or almost entire light flux falls on the surface of the street but not dispersed in the ambient space. The need of individual LED orientation entails the need of custom luminaire body that not only supports LEDs but also acts as a heat sink and cools them.

Moreover the heat sinking body also forms the appearance of entire luminaire and has to satisfy the designer's style requirements that actually determine the shape of the luminaire. Thereof it is very important for the designer to have an adequate technique to check the thermal behavior of its new product.

That technique has to be precise because of some specific features of the semiconductor LEDs that are in use currently but namely:

- The temperature of the junction can not exceed about 180 °C, that means that the temperature of the package surface should stay below about 90 °C;
- The life of a LED depends of its thermal exhaustion. The light flux decreases during the exploitation of the LED and that decrease is faster when a LED is thermally overloaded.
- It is normal in the summer evenings, just at the time when streetlights should be turned on, the temperature of the luminaire to reach 70 °C even in the temperate climate.

## Thermal Analysis

The thermal approach uses the circuit theory to analyze thermal processes. The circuit model can be represented with the schematic of Fig.1.

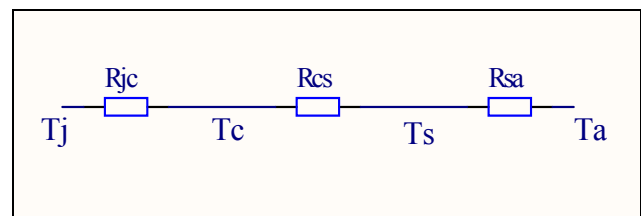


Fig.1. Classical Circuit Thermal Model.

Here:

Tj - Maximum semiconductor junction temperature;

Rjc - Thermal resistance, junction to case;

Tc - Case temperature;

$R_{cs}$  = Thermal resistance, case to heat sink;  
 $T_s$  = Heat sink temperature;  
 $R_{sa}$  = Thermal resistance, heat sink to ambient.  
 $T_a$  = Ambient temperature

The total power dissipation in a LED is given by:

$$(1) P_{tot} = I \cdot U_f,$$

Where  $I$  is the current through the diode and  $U_f$  is the forward voltage drop across it.

The heat dissipated in the anode-cathode junction flows through the thermal resistance between the junction and the mounting base, then through the heat sink and dissipates in the ambient.  $P_{tot}$  can be regarded as the thermal current and the temperature between the junction and the ambient  $\Delta T = T_j - T_a$  as the thermal voltage. Then by Ohm's law analogy:

$$(2) P_{tot} = \frac{T_j - T_a}{R_{jc} + R_{cs} + R_{sa}}.$$

All semiconductor failure mechanisms are temperature dependent and so the lower the junction temperature, the higher is the reliability of the circuit. The junction temperature depends on both the power dissipated in the device and the thermal resistance associated with the device.

$R_{jc}$  is a function of the semiconductor design and is a fixed number given in the manufacturer's datasheet. It cannot be influenced by the addition of a heat sink or any external agent.

$R_{cs}$  can be minimised by the application of silicon grease on the semiconductor mounting surface area. There are different empirical rules that can help in its calculation.

$R_{sa}$  is the most important and most controllable parameter. Exactly this parameter is missing when custom heat sinking body is used. It is a function of the convection coefficient ( $h_c$ ) and the heat sink surface area ( $A$ ), and can be expressed by the formula:

$$(3) R_{sa} = \frac{1}{h_c \cdot A}, \quad \text{°C/W}.$$

Convection coefficient is very difficultly determined because of the custom shape and different air conditions.

Instead of using the conventional circuit approach thermal problem can be solved by thermal field analysis. With this approach no additional specific information about the heat sink is necessary. The analyses is done base on the geometry of the heat sink that is already available.

### Modeling of LED

A Luxeon K2 cool white Led is considered in the analysis. A precise picture of the construction of the LED is given in Fig. 2 for two different points of view. It consists of active silicon chip, inactive silicon chip used as a padding, copper hexahedral heat sink, plastic body and transparent resin lens. Leads are used for electrical connection but not for heat sinking.

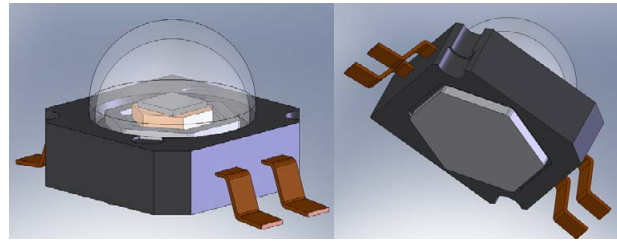


Fig.2. Lumiled K2 in 2 different projections.

The elements of the model with their approximate dimensions are given in Table1.

Table 1

Dimensions of the LED

Material	Length, mm	Breadth, mm	Thickness, mm
Active chip	1.65	1.65	0,2
Inactive chip	1.4	hex	0.5
Copper heat sink	2.3-3	hex	2.3
Body	7.3	7.3	2.5
Lens	ø 5,5	-	-

The LED structure as per Table 1 is first modelled. Actual dimensions specified in the datasheet are used. The luminaire body, used for heat sinking, is shown in Fig.3. It is made by extruded aluminum. The overall structure used for the simulation is shown in Fig. 4. Twelve LEDs are placed in the luminaire in 30 mm by each other. The thermal analyses can be made for a short piece containing just one of those 12 LEDs without loss of generality. That fact as well as the symmetry of the luminaire let only one fourth of a single LED assembly to be considered (Fig 4.). A slight simplification of the LED model itself is also necessary [3,5,6]. The extremely small dimensions are removed. Leads are also removed from the model because they do not take significant part in thermal process. Those measures must be taken to decrease the number of elements as well as for reducing the stress of the mesh generator. Tests with two different software packages (ANSYS and COSMOS) showed that mesh generators can be used without problems even for the most complex model of the LED when it is analyzed separately. But when the entire assembly has to be meshed the complex model requires too many resources. With the simplification already described the decision is achieved with 232844 elements and 328949 nodes. The thermal resistance of the LED and the other thermal connections is taken into account. Its value is concentrated in the gap formed between the contacting surfaces of the copper part of the LED and aluminum heat sink. The LED is considered soldered on an aluminum printed circuit board, which is excluded from the model for simplicity.

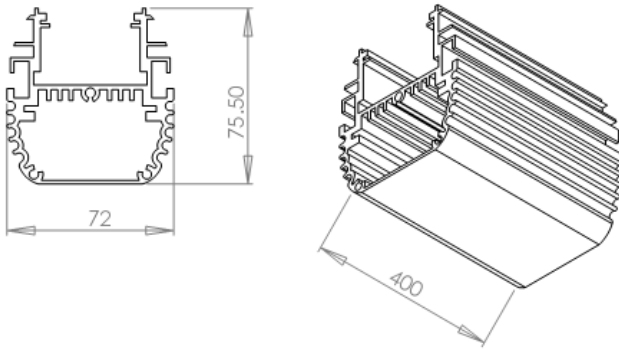


Fig.3. Dimensions of the heat sink.

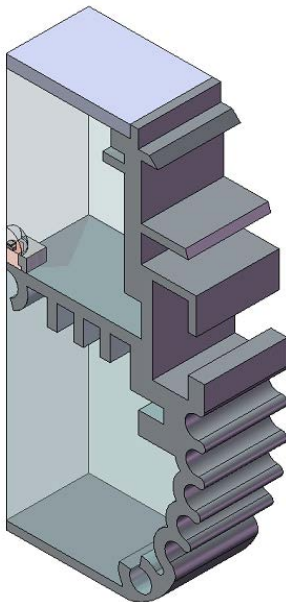


Fig.4. Isometric view of the module used for modeling.

The physical properties of different materials [2,4] are to be keyed in by the user, as given in Table 2. The entire power is assumed to dissipate in the full volume of active silicon chip, as heat generation rate in W. Initial heat sink temperature is defined as room temperature (310 K). Film coefficient, nothing but the heat transfer coefficient of the convection is 50 throughout, assuming natural convection. The structure of the LED and the heat sink is drawn in SOLIDWORKS. The task is solved with the help of COSMOS software, which is used as a plug in to the SOLIDWORKS. This is very convenient when a new luminaire is being developed because the design documentation (if created in SOLIDWORKS) is used directly in the thermal analyses without additional geometry modeling.

The finite element model uses tetrahedral elements. The material properties according to Table 2 are applied to different volumes. No heat flux boundary conditions

are applied to the symmetry surfaces as well as to both surfaces normal to longitudinal axis.

The convection is applied to all the exterior areas and the analysis is repeated for different wattages. The reference temperature (initial heat sink temperature) is taken as the room temperature. The steady state nodal solution with the temperature variation as the contour plot is shown in Fig 5, Fig 6, for 1 W and 3 W applied power respectively. Fig. 7 is a magnified image of the zone around LED from Fig. 6.

Table 2

Properties of the materials of the model

Material	Mass density, Kg/m <sup>3</sup>	Thermal conductivity, W/m.K	Specific heat, J/Kg.K
Al alloy	2700	200	900
Si	2330	149	710
Air	1.1	0.027	1000
glass	2457.6	0.75	834
Cu	8900	390	390
PPS	1000	0.25	-

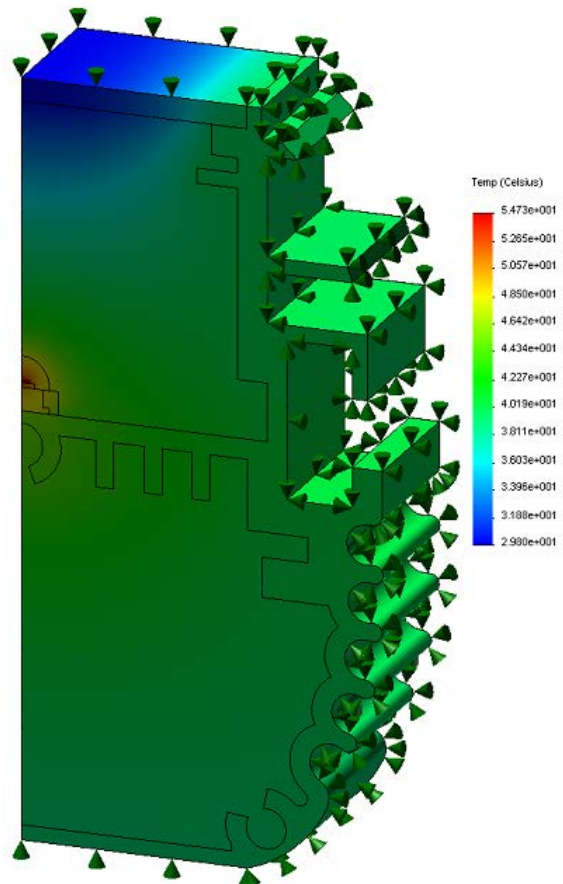


Fig.5. Temperature distribution with power of 1 W.



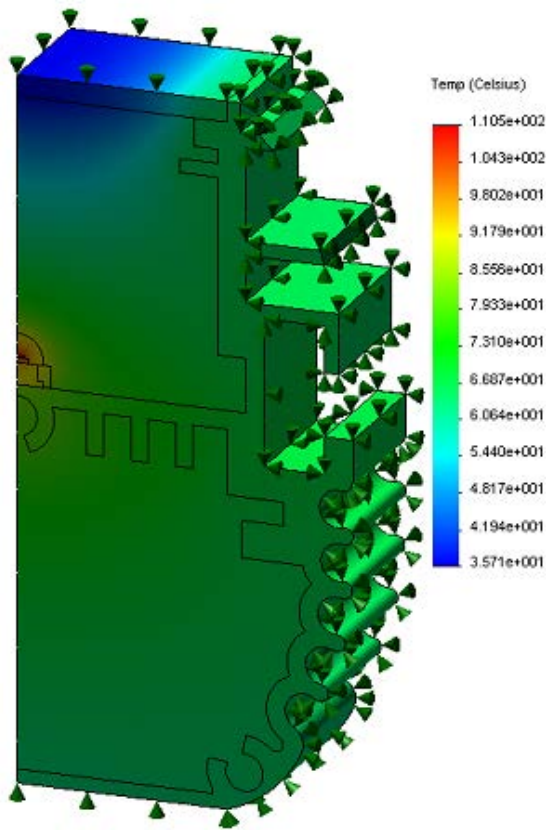


Fig.6. Temperature distribution with power of 3 W.

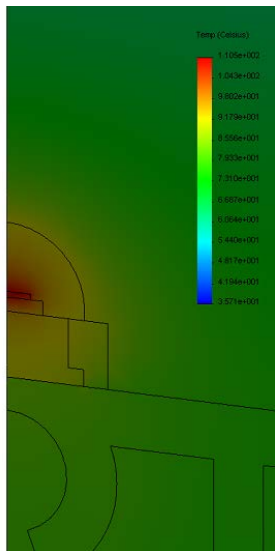


Fig.7. Temperature distribution in the zone of LED with power of 3 W.

### Experimental setup and comparison of the results

The experimental results are obtained using the circuit shown in Fig. 8. The same power as used in the simulation is applied to the circuit. Care should be taken to maintain  $U_f$  and  $I$  at constant values as the temperature

rises. Experimental results are obtained with the entire heat sink and 12 working LEDs. The temperature is measured with IR thermometer with precision of 1°C in the range -50°C to 250 °C.

$$(4) \quad T_j = P_{tot} (R_{jc} + R_{cs} + R_{sa}) + T_a .$$

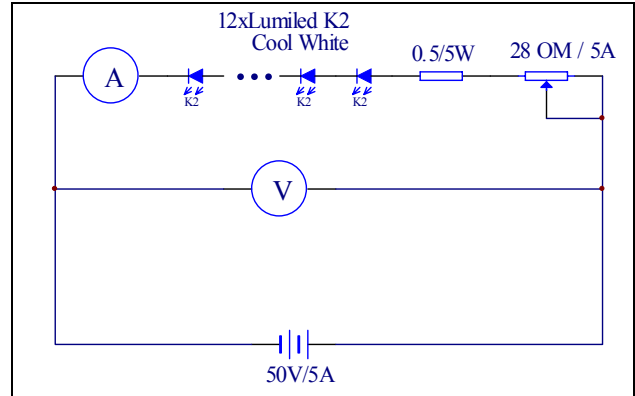


Fig.8. Circuit diagram

Table 3

Comparison of results with heat sink

All LEDs voltage, $U_f$ , V	All LEDs current, $I$ , A	Single LED power, W	Case temperature, Model, °C	Case temperature, Experiment, °C
40.2	0.15	0.5	34.5	33
41.6	0.29	1	43	42.5
42.0	0.57	2	60	58
42.6	0.85	3	73	70

The comparison of the results is given in the Table 3. The results show good correlation between the simulation and experimental results. From the results, the junction temperature can be predicted using the equation (4). The main uncertainty in FE approach of solving the problem remains the value of film coefficient that determines the heat transferred through the surrounding surface by convection. Just tentative figures of its diapason of variation according to different cooling conditions are published [6,7]. The good match between experimental and computed results for different power rates shows that its value is well chosen in that particular case. In practice the convection conditions can change depending on type of mounting, dust contamination, ambient temperature.

### Conclusion

The analysis of thermal processes in a LED cooled by heatsink with natural convection is performed by means of finite element method. That makes possible the steady state temperature of the LED to be determined even with custom shape of the heat sink that is the common case for road luminaires.

## References

- [1] Rangarajan R, A Kandaswamy, R Haripriya, Ms R Nithya, Finite Element Thermal Modelling of Power Transistor, IE(I) Journal-ET, Vol 87, January 2007.
- [2] Anderson D., T. Truslove, J Kubie, Thermal modelling and optimization of heat transfer in a high-temperature theatre luminaire, Proceedings of the Institution of Mechanical Engineers, Part C: Journal of Mechanical Engineering Science, Volume 217, Number 9 / 2003, Professional Engineering Publishing, ISSN 0954-4062.
- [3] Tiller, D.; R. Jaekel, K. Chan, Performance of selected fluorescent lighting products, Industry Applications Society Annual Meeting, 1992., Conference Record of the 1992 IEEE Volume , Issue , 4-9 Oct 1992 Page(s):1900 - 1907 vol.2
- [4] Buck G., W. Li, T Tong, Numerical modeling and passive thermal control of external lighting systems for Space Station Freedom, AIAA journal, AIAA-1993-2842.
- [5] Clarke J., M Janak, Simulating the Thermal Effects of Daylight-controlled Lighting, Energy Systems Research Unit, University of Strathclyde, Glasgow G1 1XJ, <http://www.strath.ac.uk/Departments/ESRU>
- [6] N Y A Shamma, M P Rodriguez, A T Plumpton and D Newcanbe. Finite Element Modelling of Thermal Fatigue Effect in IGBT Modules, Proceedings of IEE Circuits, Devices, and Systems, vol 148. no 2, April 2001.
- [7] A D Karus and A B Cohen. Thermal Analysis and Control of Electronic Equipment, Mc Graw-Hill, 1983.

## Boigraphies



**Valchan Georgiev** was born in Pazardzik, Bulgaria, on March 2, 1974. He studied at the Technical University of Sofia-Bulgaria and received PHD degree from the same university in 2004.

He has been working in the Faculty of Electrical Engineering of the Technical University of Sofia as an assistant professor since 1999. His field of interest includes electrical apparatus and electrical networks.

Vulchan Georgiev is with the Faculty of Electrical Engineering, Technical University of Sofia, 8, Kl. Ohridski Blvd., 1000 Sofia, Bulgaria (e-mail: [vulchy@tu-sofia.bg](mailto:vulchy@tu-sofia.bg)).



**Ivan Yatchev** was born in Sofia, Bulgaria, in 1958. He studied at the Technical University of Sofia - Bulgaria and received PhD and DSc degrees from the same university in 1988 and 2006.

Since 1988 he worked in the Faculty of Electrical Engineering of the Technical University of Sofia as Research Associate, Assistant Professor, Associate Professor and Professor in the field of Electrical Apparatus.

Ivan Yatchev is with the Faculty of Electrical Engineering, Technical University of Sofia, 8, Kl. Ohridski Blvd., 1000 Sofia, Bulgaria (e-mail: [yatchev@tu-sofia.bg](mailto:yatchev@tu-sofia.bg)).



**Krastio Hinov** was born in Bulgaria, on October 8, 1953. He graduated from the Technical University – Sofia.

He started his career as a researcher in the Institute for Instrument Design. Since 1998 hi has been working in the Technical University of Sofia as an assistant professor and associate professor in the field of electrical apparatus.

Krastio Hinov is with the Faculty of Electrical Engineering, Technical University of Sofia, 8, Kl. Ohridski Blvd., 1000 Sofia, Bulgaria (e-mail: [k\\_hinov@yahoo.co.uk](mailto:k_hinov@yahoo.co.uk)).

# Modelling of Electric Field Treatment of Granular Materials

Gantcho Bojilov, Ilona Seikova and Ivan Yatchev

**Abstract:** In the present paper, the electric field in the granular material is modelled using the finite element method. The field is considered to be governed by Laplace's equation and plane-parallel approximation is employed. The results are obtained using BELA finite element method program. The studied material consists of seeds. Six variants of the seed parameters are considered. The parameters varied are the dielectric constants of the core of the seed, its outer shell, and of the surrounding medium.

**Keywords:** granular materials, electric field treatment, finite element method.

## Introduction

High or moderate voltage low-frequency electric field treatment [1-5] is considered as an effective non-thermal processing method especially for thermosensible materials due to the limited increase in temperature during processing.

The essence of these methods is based on the interactions of the electric field with the material undergoing mechanical, physical, chemical or biochemical transformations. Many of these interactions depend on the local electric field and are highly correlated to the dielectric properties of the material (complex relative permittivity). In most real systems, and particularly in multicellular systems in the divided state, such as particulates, powders or similar, there is an extremely high spatial heterogeneity with respect to their dielectric properties. This heterogeneity is probably the most crucial phase in the implementation of a method, since it reflects the feasibility of the technique and the accuracy and repeatability of the processing.

The electric field treatment is also very important for the nanotechnology. Some results and discussion of the surface-geometrical parameters of various particle polarizabilities that are of importance in the modeling of material effects in the nanoscale are given in [6].

The objective of this work is to identify some processing basis of inhomogeneity in granular materials exposed to an external electric field. Electric field distributions for all structural elements are predicted, by solving constant property Laplace's equations, using finite element method. Comparative modelling study is performed involving different potential dielectric permittivity of the participating media. The effect of inhomogeneities in electrical field processing is illustrated with application involving treatment of natural granular materials, such as seeds and grains.

## Finite Element Modelling

The model considers multicellular system of dielectric media exposed to external electric field. Inside the system multilayered particles (cells) create multiple inhomogeneities on a length scale of their size. These kinds of systems can be found on a microscopic scale. Also, similar multiple interfaces problems appear on a macroscopic scale for granular structure with inner and outer coverings with size over the millimeter scale.

Each dielectric is assumed to be uncharged and has zero conductivity and constant dielectric permittivity. Neglecting any effects due to heat and mass transfer, and the interaction between granulates; the system reduces to the Laplace's equation.

The model for analysis is shown in Fig. 1. It consists of seeds (each of them composed of core and shell) and surrounding medium.

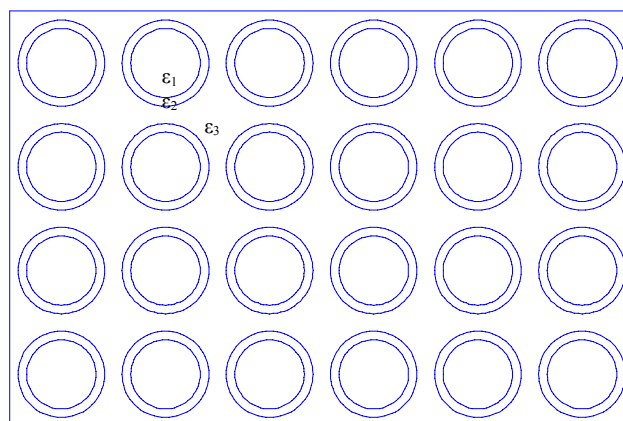


Fig.1. The studied model.

Two-dimensional (plane-parallel) approximation of the field is considered. There are three dielectric constants of the three materials included in the model –  $\epsilon_1$  of the core,  $\epsilon_2$  of the shell and  $\epsilon_3$  of the surrounding medium.

The dimensions are as follows:

- core diameter: 0.4 mm;
- shell outer diameter: 0.5 mm;
- distance between the centers of two adjacent seeds: 1.1 mm.

The boundary conditions employed for the Laplace's equations are of two kinds:

- Dirichlet boundary condition on the upper and lower boundary of the studied domain with the respective potential on each of them;
- Homogeneous Neumann boundary condition on the left and right boundary.

The applied voltage is 200 V, i.e. on the upper boundary the potential is set to 200 V, on the lower one homogeneous Dirichlet boundary condition is imposed. Thus the homogeneous electric field intensity would be 833 V/cm.

The finite element method is employed for the above described problem for analysis of electric field. The program BELA [7] has been employed for the analysis. It works with first order triangular finite elements.

The finite element mesh consists of about 32500 elements. A fragment of the mesh is shown in Fig. 2.

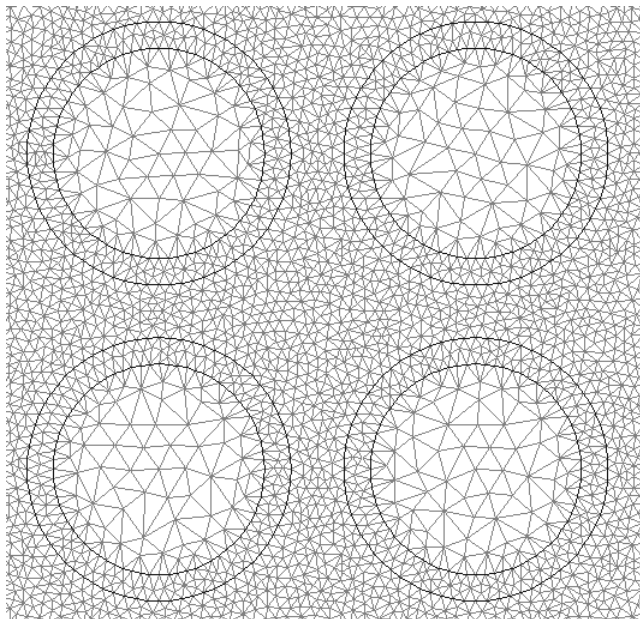


Fig.2. Finite element mesh (fragment).

## Results

Results are obtained for different combinations of the three dielectric constants. The electric field intensity and distributions for 6 different cases are shown in Figs. 3-8. Electric scalar potential distribution for three cases is shown in Figs. 9-11.

The values of the maximal  $(E_i)_{max}$  and minimal intensities  $(E_i)_{min}$  inside the seeds at two cross-sections parallel to the poles and the equator are also computed and presented in Table 1.

It is demonstrated that through simple system of monosized bi-layer seeds with different dielectric permittivity than its surrounding can lead to substantially different electric field distributions. The model results show that some parts of the solid dielectrics may experience electroporation effect associated to the localised high intensity zones.

For the case of low-permittivity suspending medium ( $\epsilon_3 = 1$ ) the high intensity zones are nearly excluded from the seeds (cases 1 and 2), whereas for the cases of high-permittivity medium ( $\epsilon_3 \geq 10$ ) the intraparticle field is larger than the extraparticle field over most of the seeds (cases 3-6). Two main features are observed as relative permittivity  $\epsilon_1/\epsilon_2$  changed from 0.428 to 2.333.

When  $\epsilon_1 < \epsilon_2$  high intensity zones are peaked within the inner core (medium<sub>(1)</sub>) even for weak-permittivity surrounding medium (case 3.). High intensities  $(E_1)_{max}$  and  $(E_2)_{max}$  occur at seed's equator while minimum intensity zone tended to develop right at both poles such as significant intensities differences within the shell will occur. Further increase in the relative permittivity of  $\epsilon_3/\epsilon_1 > 6.666$  accentuates the differences leading to high intensity zone appearing also in the shell (medium<sub>(2)</sub>) (case 5). This will probably result in selectivity loss for the rest of the material, giving low repeatability and accuracy of the electric treatment.

When  $\epsilon_2 < \epsilon_1$  the induced intensities are largest within the outer shell (medium<sub>(2)</sub>). The response field gains at the seed's poles such as maximum intensities  $(E_2)_{max}$  on the low-permittivity side and minimum intensities  $(E_1)_{min}$  on the higher-permittivity side occur (case 4). For a sufficiently large relative permittivity of  $\epsilon_3/\epsilon_2 > 6.666$  the intensity  $(E_2)_{max}$  is almost uniform throughout shell, making electroporation to be favored here (case 6).

Table 1

Computed values of the electric field intensity for different configurations

Case study	Relative permittivity medium and seed			Intensities in the seed core Vcm <sup>-1</sup>		Intensities in the seed shell Vcm <sup>-1</sup>		Entire system Vcm <sup>-1</sup>
	$\epsilon_3$	$\epsilon_3/\epsilon_1$	$\epsilon_3/\epsilon_2$	$(E_1)_{max}$	$(E_1)_{min}$	$(E_2)_{max}$	$(E_2)_{min}$	$(E_i)_{max}$
1	1	0.666	0.285	792	712	697	381	1536
2.	1	0.285	0.666	539	464	1229	470	1727
3.	10	6.666	2.857	1283	1013	1285	445	1285
4	10	2.857	6.666	893	750	1646	943	1646
5	80	53.333	22.857	1451	1011	1466	428	1451
6	80	22.857	53.333	1002	770	1673	1070	1673



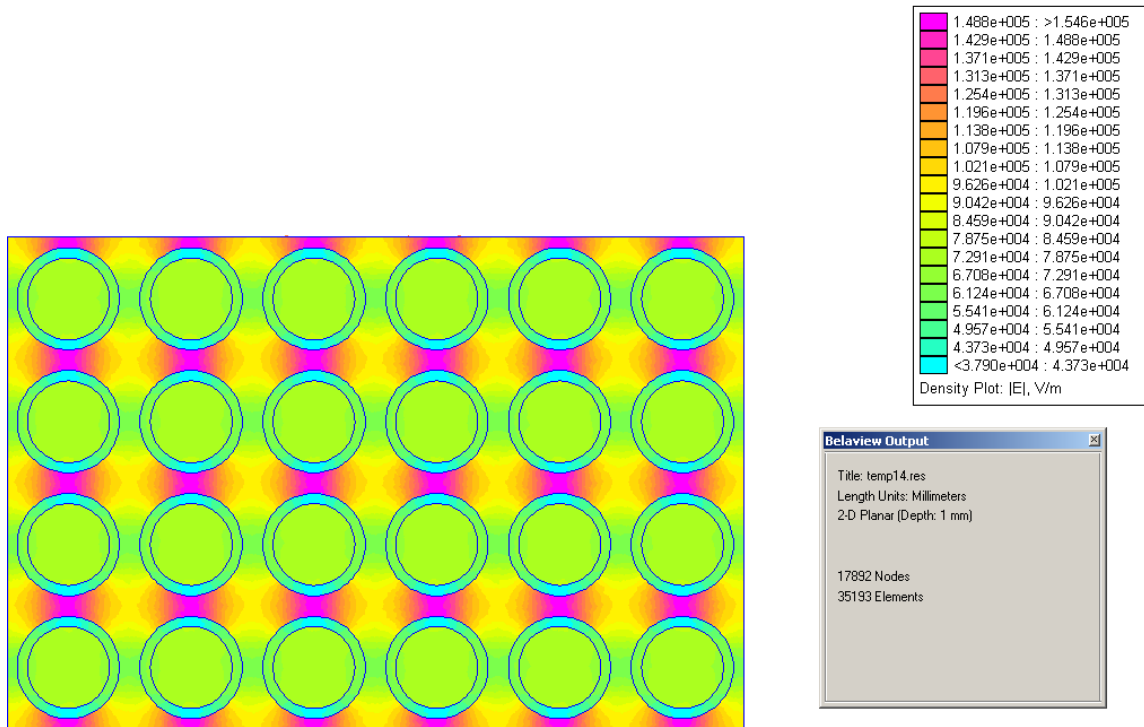


Fig.3. Electric field intensity distribution for  $\epsilon_{1,\text{core}}=1.5$ ,  $\epsilon_{2,\text{shell}}=3.5$ ,  $\epsilon_{3,\text{medium}}=1$ .

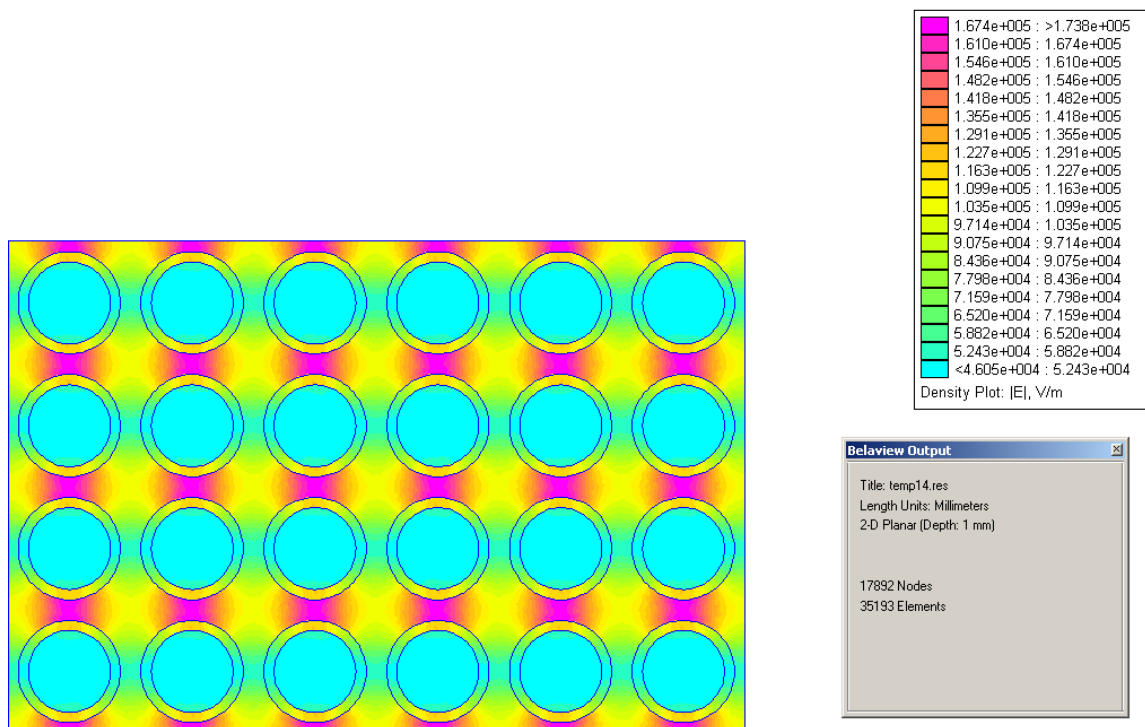


Fig.4. Electric field intensity distribution for  $\epsilon_{1,\text{core}}=3.5$ ,  $\epsilon_{2,\text{shell}}=1.5$ ,  $\epsilon_{3,\text{medium}}=1$ .

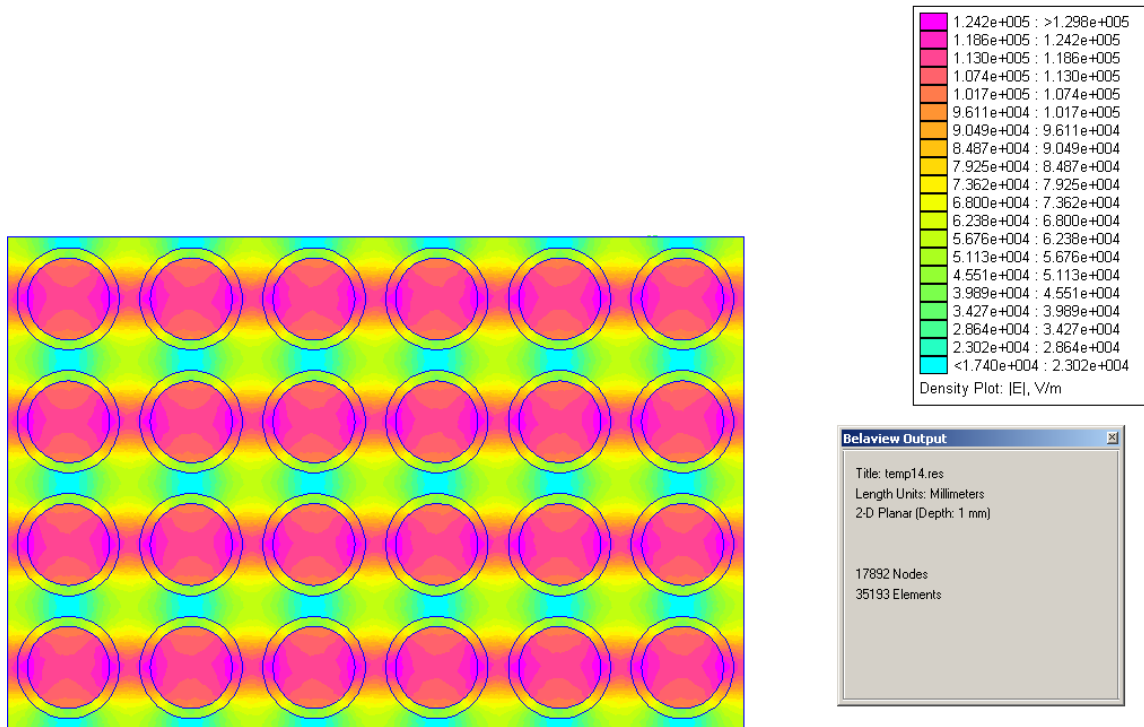


Fig.5. Electric field intensity distribution for  $\epsilon_{1}=1.5$ ,  $\epsilon_{2}=3.5$ ,  $\epsilon_{3}=10$ .

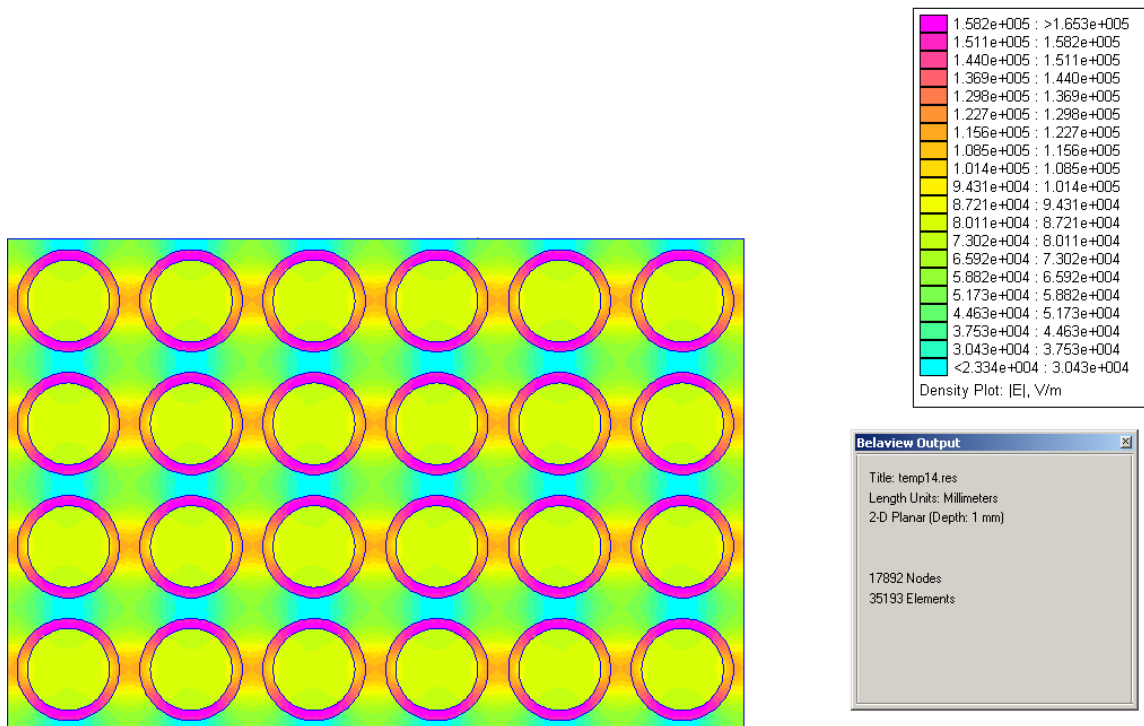


Fig.6. Electric field intensity distribution for  $\epsilon_{1}=3.5$ ,  $\epsilon_{2}=1.5$ ,  $\epsilon_{3}=10$ .

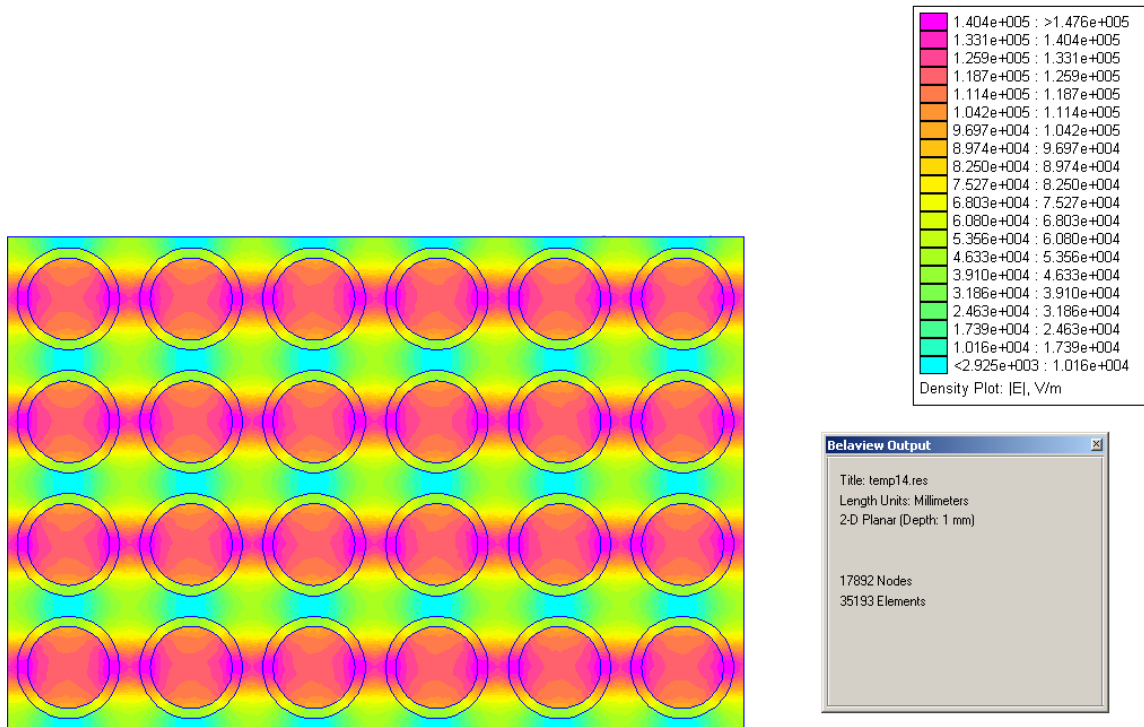


Fig.7. Electric field intensity distribution for  $eps\_core \epsilon_1=1.5$ ,  $eps\_shell \epsilon_2=3.5$ ,  $eps\_medium \epsilon_3=80$ .

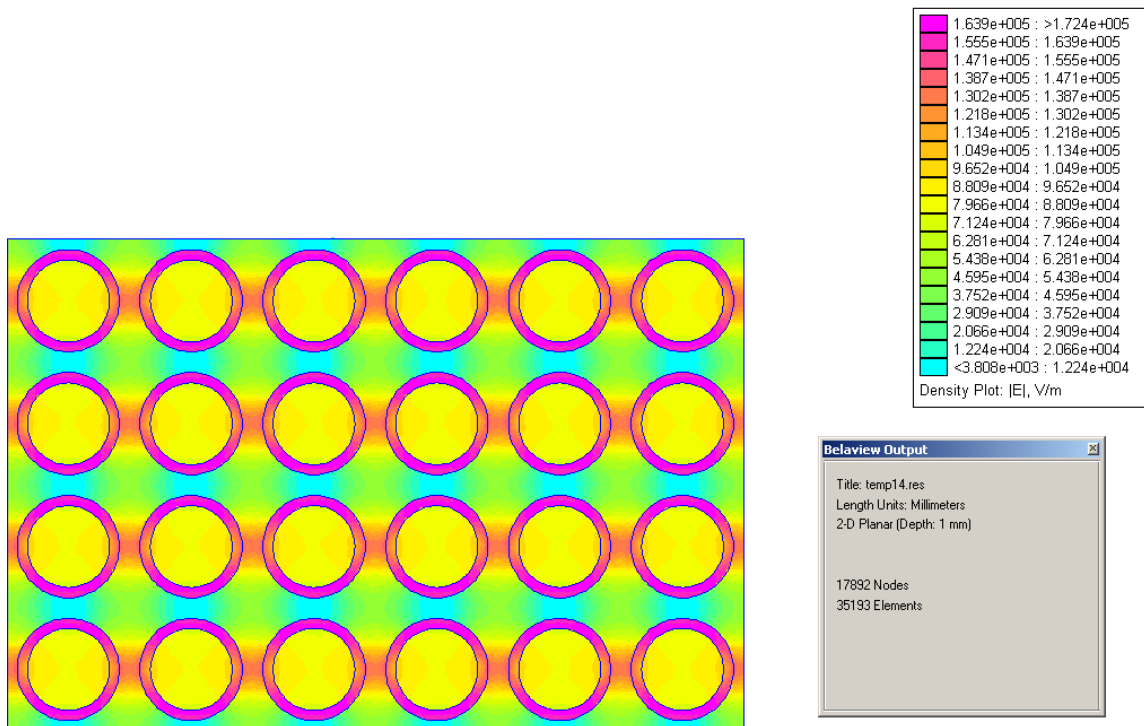


Fig.8. Electric field intensity distribution for  $eps\_core \epsilon_1=3.5$ ,  $eps\_shell \epsilon_2=1.5$ ,  $eps\_medium \epsilon_3=80$ .

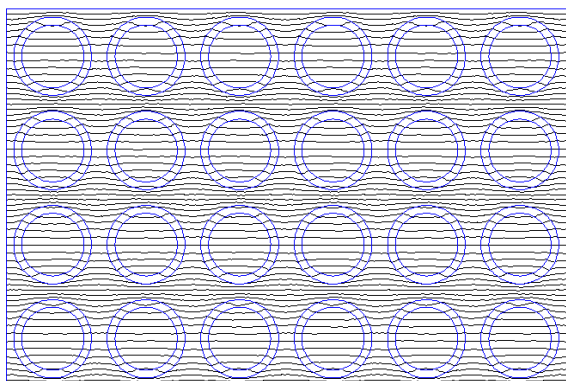


Fig.9. Equipotential lines for  $\epsilon_1=1.5$ ,  $\epsilon_2=3.5$ ,  $\epsilon_3=1$ .

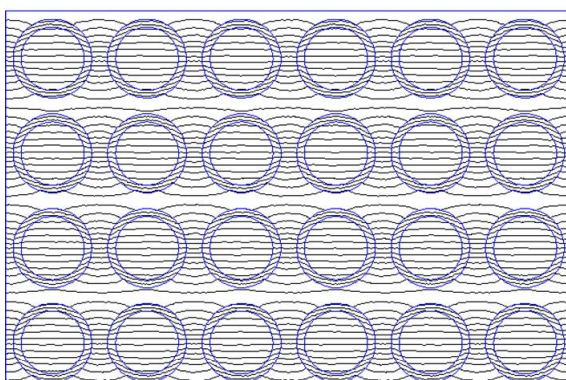


Fig.10. Equipotential lines for  $\epsilon_1=3.5$ ,  $\epsilon_2=1.5$ ,  $\epsilon_3=10$ .

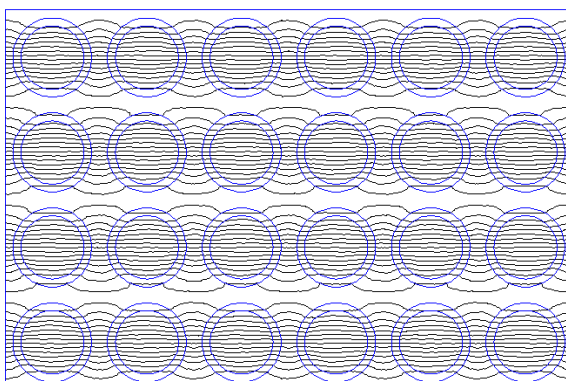


Fig.11 Equipotential lines for  $\epsilon_1=3.5$ ,  $\epsilon_2=1.5$ ,  $\epsilon_3=80$ .

## Conclusion

The modeling study illustrates the importance of considering multicellular models for the response of complex granular system to electric fields. The model provides an estimate of actual local electric field distribution and can be useful for comparative analysis. The results can be used to determine the needed intensity, which has to be applied to achieve effective treatment, almost eliminating significant field amplification. Further development of the work could include three-dimensional and time-dependent modelling.

## Acknowledgements

The authors acknowledge gratefully the support for this work from the project AUF - Pole d'excellence regional CIFR SciTech/2008.

## References

- [1] Savova, M., H.J. Bart, I. Seikova, Enhancement of mass transfer in solid-liquid extraction by pulsed electric field, Journal of the University of Chemical Technology and Metallurgy, 40, 4, 2005, pp. 251-255.
- [2] Angersbach, A., V. Heinz, D. Knorr. Electrophysiological model of intact and processed plant tissues: cell disintegration criteria. Biotechnology Progress, 15, 1999, pp.753-762
- [3] Krassowska, W., P.D. Filev. Modeling Electroporation in a Single Cell, Biophysical Journal, V. 92, 2007, pp. 404-417
- [4] Savova, M., I. Seikova. Kinetics of extraction from solid plant tissues by pulsed electric field treatment. International Conference of the Chemical Societies of the South - East European Countries ICOSECS 5, 10-14.09.2006, Ohrid.
- [5] Prangrle, B.J. et al. Microwave Thawing of Cylinders. AIChE Journal, vol. 37, No. 12, 1999, pp. 1789-1800.
- [6] Sihvola, A. Dielectric Polarization and Particle Shape Effects. Journal of Nanomaterials, Volume 2007, Article ID 45090, 9 pages, doi:10.1155/2007/45090.
- [7] Meeker, D. BELA Finite Element Electrostatics Solver Version 1.0. User's Manual, 2003.

## Biographies



**Gantcho Bojilov** was born in Burgas, Bulgaria, on June 6, 1938. He studied at the Technical University of Sofia and received PhD and DSc degrees from the same university in 1971 and 1992.

Since 1963 he worked in the Faculty of Electrical Engineering of the Technical University of Sofia as Assistant Professor, Associate Professor and Professor in the field of Electrical Machines.

Gantcho Bojilov is with the Faculty of Electrical Engineering, Technical University of Sofia, 8, Kl. Ohridski Blvd., 1000 Sofia, Bulgaria (e-mail: gboj@tu-sofia.bg).



**Ilona Seikova** was born in Blagoevgrad, Bulgaria, on August 17, 1957. She studied at the Technical University of Budapest-Hungary and received PhD degrees from the National Polytechnic Institute of Toulouse-France in 1982. Since 1982 she worked in the Faculty of Chemical Engineering of the University of Chemical Technology and Metallurgy of Sofia as Assistant Professor and Associate Professor in the field of heat and mass transfer processes.

Ilona Seikova is with the Faculty of Chemical Engineering, University of Chemical Technology and Metallurgy of Sofia, 8, Kl. Ohridski Blvd., 1000 Sofia, Bulgaria (e-mail: i.seikova@uctm.edu).



**Ivan Yatchev** was born in Sofia, Bulgaria, in 1958. He studied at the Technical University of Sofia and received PhD and DSc degrees from the same university in 1988 and 2006.

Since 1988 he worked in the Faculty of Electrical Engineering of the Technical University of Sofia as Research Associate, Assistant Professor, Associate Professor and Professor in the field of Electrical Apparatus.

Ivan Yatchev is with the Faculty of Electrical Engineering, Technical University of Sofia, 8, Kl. Ohridski Blvd., 1000 Sofia, Bulgaria (e-mail: yatchev@tu-sofia.bg).



# Determination of Induction Machine Parameters in Case of Dynamic and Steady-State Operating Modes

Dimitar Spirov, Pencho Vladimirov

**Abstract:** A methodology, algorithms and mathematical models for determination of induction machine parameters by means of voltages and current measurements in case of idle running regarding dynamic and steady-state operating modes have been developed. In order to determining of induction machine parameters dynamic and steady-state induction machine models have been developed on the basis of electrical machines generalized theory. The built-in functions of software package MATLAB have been used for solving a system of non-linear equations. The reliability and efficiency of the methodology, algorithms and mathematical models developed have been corroborated by experimental investigations results for quantities in case of idle running.

**Keywords:** induction machine, starting, idle no-load running, voltages and currents

## Introduction

The recognition of the concrete motor parameters exact values is necessary for induction machine operating and energy characteristics determination in case of dynamic and steady-state modes.

It is necessary in up-to-date vector control systems a set of variables such as linkage fluxes, motor torque and angular speed of the rotor to be real-time computed by micro-processor system (observer) on the basis of preliminarily known and given values of the induction machine windings resistances and inductances and voltages and currents digital measurement [1].

The difficulties in accordance with induction machine electro-magnetic parameters experimental determination are consisted in the fact that the proper phase inductances, mutual inductances between phases or equivalent circuit parameters excepting the phase windings resistances resist an immediately measurement. The determination of their values by means of another quantities analytically connected with is difficult because of unknown parameters greater number than variables measured one. Therefore possibilities for additional variables measurement are looking for [2].

Paper deals with development of methodology, algorithms and mathematical models for determination of induction machine parameters by means of voltages and current measurements in case of idle running regarding dynamic and steady-state operating modes. It is necessary to obtain dependences of windings resistances and inductances depending on currents in induction machine T-shape equivalent circuit.

## Mathematical model

The resistance  $R_s$  of stator winding phases could be immediately measured by ways known and reduced to the operating temperature [3].

It is convenient to obtain induction machine stator winding voltages in co-ordinate system  $\alpha, \beta$  by means of linkage flux represent vectors and result is:

$$(1) \quad \begin{aligned} u_{s\alpha} &= R_s i_{s\alpha} + \frac{d\psi_{s\alpha}}{dt}; \\ u_{s\beta} &= R_s i_{s\beta} + \frac{d\psi_{s\beta}}{dt}. \end{aligned}$$

When starting the induction machine in mode of ideal idle running  $i_r=0$ , for stator linkage flux components it can be written:

$$(2) \quad \begin{aligned} \psi_{s\alpha} &= L_s i_{s\alpha} + L_m i_{r\beta} = L_s i_{s\alpha}; \\ \psi_{s\beta} &= L_s i_{s\beta} + L_m i_{r\alpha} = L_s i_{s\beta}, \end{aligned}$$

where

$$(3) \quad L_s = \frac{\psi_s}{i_s}$$

is stator winding phase static inductance.

It is known that in case of non-linear change of the linkage flux [4]

$$(4) \quad \frac{d\psi}{dt} = \frac{d\psi}{di} \frac{di}{dt} = L_d \frac{di}{dt},$$

where  $L_d = d\psi/di$  is dynamic inductance.

The relation between static inductance  $L_{st} = \psi/i$  and dynamic one  $L_d$  is [4]:

$$(5) \quad L_d = L_{st} + \frac{dL_{st}}{di} i.$$

Since during starting process until reaching to steady-state mode the stator current  $i_s$  changes from  $I_{smin}$  to  $I_{smax}$ , by means of (3) can be obtain  $L_s = f(i_s)$  for stator current whole operating range.

The particular components and stator linkage flux can be expressed, as follows:

$$(6) \quad \begin{aligned} \psi_{s\alpha} &= \int_t^{t+\Delta t} (u_{s\alpha} - R_s i_{s\alpha}) dt; \\ \psi_{s\beta} &= \int_t^{t+\Delta t} (u_{s\beta} - R_s i_{s\beta}) dt; \end{aligned}$$

$$(7) \quad \psi_s = \sqrt{\psi_{s\alpha}^2 + \psi_{s\beta}^2}.$$

In order to determine  $R_r$  and  $L_m$  the static model of the machine can be used:

$$(8) \quad \begin{aligned} u_{s\alpha} &= R_s i_{s\alpha} - \omega_s \psi_{s\beta}; \\ u_{s\beta} &= R_s i_{s\beta} + \omega_s \psi_{s\alpha}; \\ 0 &= R_r \frac{\psi_{s\alpha} - L_s i_{s\alpha}}{L_m} - \omega_{sl} \frac{L_m i_{s\beta} + L_r \psi_{s\beta} - L_r L_s i_{s\beta}}{L_m}; \\ 0 &= R_r \frac{\psi_{s\beta} - L_s i_{s\beta}}{L_m} + \omega_{sl} \frac{L_m i_{s\alpha} + L_r \psi_{s\alpha} - L_r L_s i_{s\alpha}}{L_m}; \end{aligned}$$

where  $\omega_{sl} = \omega_s - \omega_r$ .

The determination of  $R_r$  and  $L_m$  can be carry out by means of *MATLAB* built-in function for dynamic system parametric model evaluation through an optimization method [5]. For that purpose the function *leastsq* from *Optimization Toolbox* is used, which minimizes square error criteria and package for dynamic systems modeling *Simulink*. The diagram for continuous model parameters evaluation through optimizing approach is given on Fig. 1. The optimizing procedure includes determining a sequence of dynamic system adjustable model parameters which transforms into sequence of transient characteristics inclining to reference standard (experimental) characteristic with defined accuracy. The measured and transformed component of stator current  $i_{s\alpha}$  is assumed for reference standard characteristic. For model adjustable from (9) the following has been obtained:

$$(9) \quad i_{s\alpha} = \frac{\omega_{sl} L_r u_{s\alpha} + R_r u_{s\beta} + [\omega_s \omega_{sl} (L_s L_r - L_m^2) - R_s R_r] i_{s\beta}}{R_r L_s \omega_s + \omega_{sl} R_s L_r}$$

The optimizing procedure processes error difference between the two quantities and corrects adjustable model parameters. This procedure reiterates until  $i_{s\alpha}$  from the model adjustable comes up to the reference (experimentally taking down)  $i_{s\alpha}$  with accuracy defined.

The adjustable model input data are stator voltages and currents measured in case of steady-state mode and transformed in co-ordinate system  $\alpha, \beta$  and parameters  $R_s, L_s$  and  $L_r$ . The parameters  $R_s$  and  $L_s$  are determined higher-up, regarding  $L_r$  with sufficient accuracy is accepted that  $L_r = L_s$ .

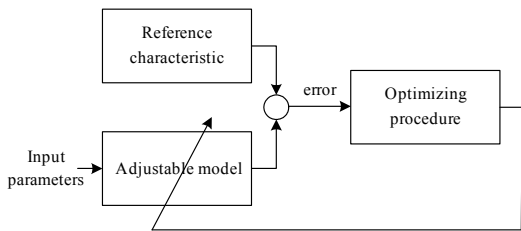


Fig. 1. Diagram of model parameters optimal adjustment

Since the stray leakage fluxes are closed through the air it can be assumed that stray leakage inductances of the stator and rotor are saturation independent [6]. Then the dependence  $L_m = f(i_m)$  can be obtained from

$$(10) \quad L_{\sigma s} = L_s - L_m;$$

$$(11) \quad L_m(i_m) = L_s(i_s) - L_{\sigma s},$$

because in case of ideal idle running  $i_s = i_m$ .

## Results Obtained

In order to check methodology, algorithms and mathematical models for determination of induction machine parameters developed an induction motor type T100LB-4 (manufacturer *ELMA*, JSC–Trojan, Bulgaria) has been investigated experimentally. The technical data of the induction motor are given in ANNEX 1.

The stator windings resistances have been measured by means of multipurpose precise measuring bridge ‘Wheatstone–Tomson’. The result obtained for the stator phase resistance mean value  $R_s$ , reduced to operating temperature is  $R_{s75} = 2,258 \Omega$ .

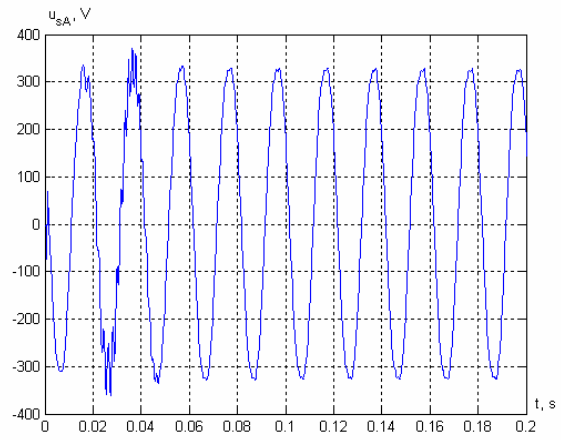


Fig. 2. Dependence  $u_{sA} = f(t)$

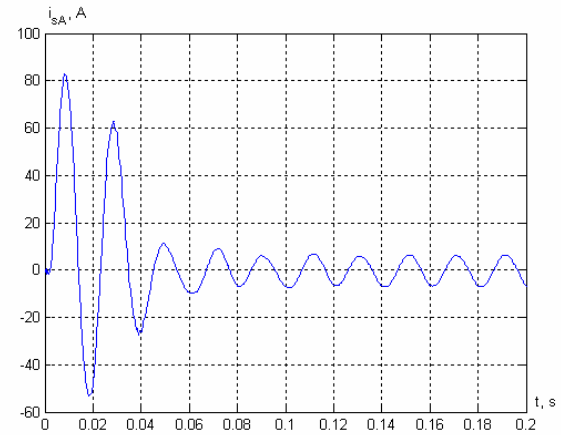


Fig. 3. Dependence  $i_{sA} = f(t)$

The experimental investigations of the induction motor have been carried out by means of computer based system including data acquisition card (DAQ) and graphically programming software *LabVIEW*<sup>®</sup> (*National Instruments Corporation*) [7]. Through computer system variables  $u_{sA}, u_{sB}, u_{sC}, i_{sA}, i_{sB}$  and  $i_{sC}$  have been recorded in case of induction machine starting from idle running until reaching to steady-state mode. As it is stated in [8] the

parameters determination can be done in case of real idle running test which is easier to carry out compared to ideal idle running test since the error is relatively small.

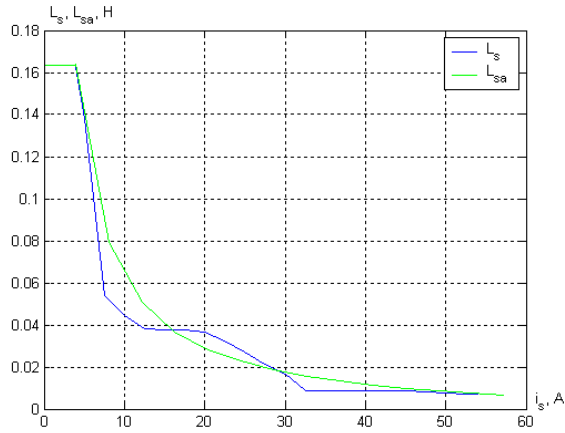


Fig. 4. Dependence  $L_s, L_{sa}=f(i_s)$

The dependences of  $u_{sA}$  and  $i_{sA}$  towards the time in case of induction machine starting from idle running until reaching to steady-state mode are represented on fig. 2 and fig. 3.

Through (6), (7) and (3) the dependence  $L_s=f(i_s)$  for starting mode has been obtained, besides the results are systematically shown in Table 1 and displayed in Fig. 4.

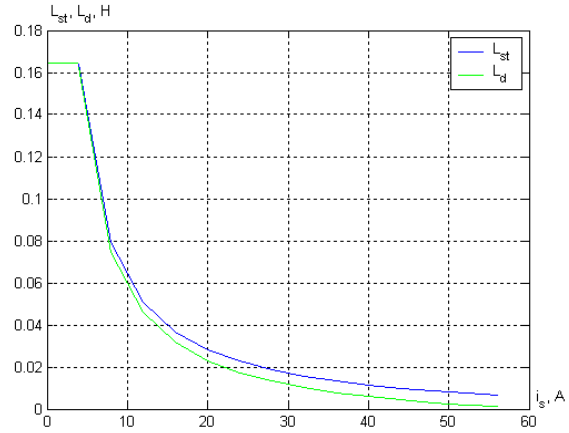


Fig. 5. Dependence  $L_{st}, L_d=f(i_s)$

Table 1

Dependence  $L_s=f(i_s)$

$i_s, A$	4,0	5,0	7,5	10,0	12,5	15,0	17,5	20,0	22,5	25,0	27,5
$L_s, mH$	167,1	138,02	53,79	44,62	38,42	37,82	37,82	36,76	32,24	26,87	21,26

Prolongation

$i_s, A$	30,0	32,5	35,0	37,5	40,0	42,5	45,0	47,5	50,0	52,5	54,15
$L_s, mH$	16,55	8,91	8,91	8,91	8,91	8,69	8,53	8,35	7,58	7,34	7,19

For the aim of the investigations it is necessary to approximate the dependence of non-linear parameter  $L_s$ , towards the current  $i_s$ , by means of some analytical dependences, such as polynomial, spline, exponent, logarithmic or hyperbolic function [4]. The mathematical models very often used for representation of induction machine magnetization curve – arctangent, tangent hyperbolic, exponential и rational модели – are explained and investigated in [4]. After calculating verifications it is found to be most convenient to split the dependence of the inductance towards the current in two intervals. In the first interval for non-saturated magnetic circuit it is with invariable size of magnitude and can be represented by a straight line. By means of the software package *Sigma Plot* [9] for the second interval the following approximation dependence as most suitable has been determined:

$$(12) \quad L_{st} = \frac{a}{b+i} + c.$$

The dynamic inductance  $L_d$  for the second interval according to (4) has been determinate:

$$(13) \quad L_d = \frac{ab}{(a+i)^2} + c.$$

The approximation dependences  $L_{sta}$  and  $L_{da}$  are displayed in Fig. 5.

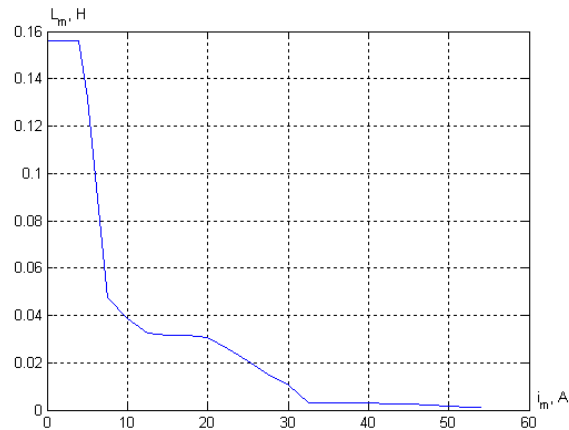


Fig. 6. Dependence  $L_m=f(i_m)$

From Fig. 4 can be obtained  $L_s$  for  $I_{s0}$ , besides the value obtained is given in Table 2.

The values of  $R_r$  and  $L_m$  (given in Table 2) for idle running have been obtained by means of the optimization procedure.

Through (10) and (11) the dependence  $L_m=f(i_m)$  has been graphically plotted and displayed in Fig. 6.

**Table 2**  
Results obtained from the experimental investigations and computations

Parameter	From experimental investigations	By calculation methodology	$\varepsilon$ , %
$R_s, \Omega$	2,258	2,31	-2,30
$L_s, H$	0,167	0,162	2,99
$L_r, H$	0,167	0,163	2,4
$R_r, \Omega$	2,2553	2,329	-3,27
$L_m, H$	0,1572	0,154	2,04

The parameters of induction machine T-shape equivalent circuit determined through a manufacturer calculation methodology in ideal idle running are given in Table 2.

The relative errors of the quantities values determinate by the calculation methodology compared to measured and determinate in case of ideal idle running these ones have been obtained. The relative very good similarity of the results obtained corroborates the reliability and efficiency of the calculation methodology used.

### Conclusion

The methodology, algorithms and mathematical models developed provide a possibility for determination of induction machine resistances  $R_s$  and  $R_r$ , inductances  $L_s$ ,  $L_r$  and  $L_m$ , by means of voltages and currents measurements in case of idle running mode regarding dynamic and steady-state operating modes. The experimental investigations results obtained for the quantities in case of induction machine starting and breaking in idle running mode corroborate the reliability and efficiency of the methodology algorithms and mathematical models developed.

### ANNEX 1

#### Technical data of induction motor type T100 LB-4

$P_N=3,00kW$ ;  $U_N=380V$ ;  $I_N=6,8A$ ;  $f=50Hz$ ;  $p_p=2$ ;  $n_N=1410min^{-1}$ ;  $M_N=20,434Nm$ ;  $\eta=0,81$ ;  $\cos\varphi=0,82$ ;  $J_m=0,01099kgm^2$ .

### ANNEX 2

#### Parameters of induction motor type T100 LB-4

Parameters	$R_s, \Omega$	$X_{os}, \Omega$	$R_r, \Omega$	$X_{or}, \Omega$	$X_m, \Omega$
$s=0,0$	2,258	2,488	2,329	2,949	48,4

$$L_s(i_s) = \begin{cases} 0,167, & \text{if } 0 < i_s \leq 4 \\ 0,694 \\ 0,1 + i_s - 0,0055, & \text{if } i_s > 4 \end{cases}$$

### References

[1] Bojilov, G. Regarding induction motors electromagnetic parameters determination. Annals of Technical University - Sofia, Vol. 51, 2001, pp. 9-15. (in Bulgarian)

[2] Spirov D. Energy-economical control of an induction machines by means of magnetic field orientation. PhD Dissertation, Technical University - Gabrovo, 2006. (in Bulgarian)

[3] Dimitrov, D. A., I. J. Vaklev, D. K. Sotirov, M. P. Stojanov. Electric machines test handbook. Sofia, Tehnika, 1991. (in Bulgarian)

[4] Vladimirov, P. An induction machine non-linear mathematical model in case of dynamic and steady-state regimes. Annals of University of Craiova, Electrical Engineering Series 2007.

[5] Tzonev, P., P. Daskalov. Theoretical investigations methods (systems identification). Rouse, 2002. (in Bulgarian)

[6] Kopylov, I. P. Mathematical modeling of electric machines. Moskva, Vyssha shkola, 2001, p. 327. (in Russian)

[7] Vladimirov, P., S. Rachev. Lifting mechanisms induction machines transient processes and dynamic loads, Journal of the Technical University - Gabrovo, Vol. 30, 2004, pp. 135-150. (in Bulgarian)

[8] Vladimirov, P. Induction machine parameters determination by means of voltages and currents measurements in case of stopping. „Electrotechnics and Electronics”, 2007. (in Bulgarian)

[9] Sigma Plot 8.02 Demo, User's Guide, SPSS Inc, 2003.

### Biographies



**Dimitar Spirov** was born in Hisarya, Bulgaria, on May 2, 1978. He studied at the Technical University of Gabrovo-Bulgaria and received Dr. degree from the same university in 2007.

Since 2007 he worked in the University of Food Technology - Plovdiv as a lecturer. His research interests include dynamic modes and loads and energy efficiency of the induction machines and electric drives.

Dimitar Spirov: Department of Electrical Engineering, University of Food Technologies, 26, Maritza Blvd., 4002 Plovdiv, Bulgaria (e-mail: [dimitar\\_spirov@abv.bg](mailto:dimitar_spirov@abv.bg))



**Pencho Vladimirov** was born in village Gorna Lipnitsa, province V.Tarnovo, Bulgaria, on December 2, 1942. He studied at the Technical University of Sofia - Bulgaria and graduated in 1968. He received the PhD degree and DSc degree, in 1978 and 2008, respectively.

Since 1970 he worked in the Technical University - Gabrovo as a lecturer. In 1982, he was elected Assoc. Prof. in Electrical Machines. His research interests include dynamic modes and loads and energy efficiency of the induction machines and electric drives.

Pencho Vladimirov: Department of Electrical Engineering, Technical University - Sofia, 4, H. Dimitar str., 5300 Gabrovo, Bulgaria (e-mail: [pvlad@iname.com](mailto:pvlad@iname.com))



# Computer System for Analysis of the Size of Vibrations at Frequency Control of Induction Motors

Totylo Iliev, Plamen Danailov

**Abstract:** The paper presents a system aimed at recording simultaneously, in a suitable format, the change of frequency at an induction motor deployment and the vibrations at a preliminarily determined point. The system works jointly with an optoelectronic vibration sensor designed by the authors as well as with other vibration sensors.

**Keywords:** measurement, vibrations, induction motor, synchronization.

## Introduction

When the frequency control method is used for induction motors, their angular speed changes within a great range and it is possible to maintain any speed with a big torque. Usually in technology lines the most appropriate speed is chosen by its automatic control. The vibrations excited at some very specific for this line frequencies can lead to unacceptably high amplitudes and the respective consequences. It is possible that the system for automatic control of angular speed “chooses” the most inappropriate one following other criteria. In order to find these resonance frequencies, a vibration sensor is suitable as well as an apparatus for measurement of the frequency supplied. The size of the vibrations is measured by means of piezoelectric, vortex-current, optoelectronic [1] and other accelerometers and the obtained electric signal is recorded for storage and further processing. At stationary mode of operation, usually the main frequency  $n$  is also main frequency of the electric signal from the vibration sensor. However, when frequency changes, inconformity is noted between them both and as a consequence, it is difficult to obtain synchronization when an oscillograph is used.

In Fig. 1 a part of the system aimed at forming short pulses when passing through zero of each of the phases is shown. The element OR unites the pulses of the three phases and pulses with frequency equal to  $6n$  are obtained at its output. When other experiments were done with sensors for vibration measuring, one of the major problems was the lack of synchronization. The internal synchronization of the oscilloscope works well only at a constant input frequency (e. g. at  $n = 50\text{Hz}$ ).

When the supply voltage of the induction motor is higher than 380V, it is necessary to use voltage or current transformers. The symmetry of the three phases does not allow finding subsequently which pulse from which phase comes. When frequency control is used, phases are not changed – for example for reversing of the motor.

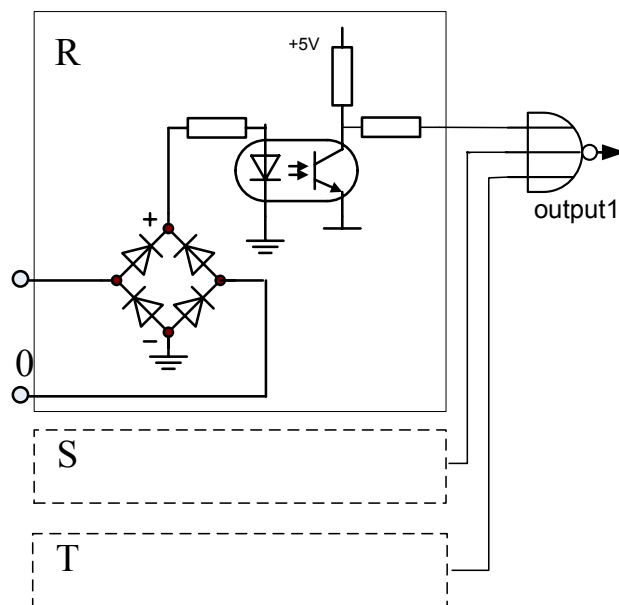


Fig. 1

In order to find out from which phase is the respective synchronizing pulse, a scheme solution is proposed (Fig. 2) with one-shot multivibrators with different time constants. An advantage of the method is the preservation of the leading edges of the pulses, which is significant when defining subsequently the frequency at a specific moment. The constant amplitude of the pulses in TTL allows processing of information by microcontrollers of the series pic, avr, etc. The time diagram in Fig. 3 illustrates the operation of the schemes shown in Fig. 1 and Fig. 2.

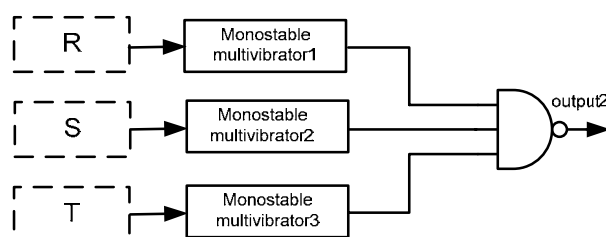


Fig. 2

At the input of the scheme in Fig. 1, the three phases for frequency control of induction motors are supplied. When passing through zero the light-emitting diode connected through a bridge rectifier is not on and this turns off the respective phototransistor creating a short positive pulse. After the scheme OR the pulses are

unified and an output frequency 6 times higher is obtained at output 1. If one-shot multivibrators with different time constants are engaged (Fig. 2), it is easy to recognize the different phases of the scheme output – output 2.

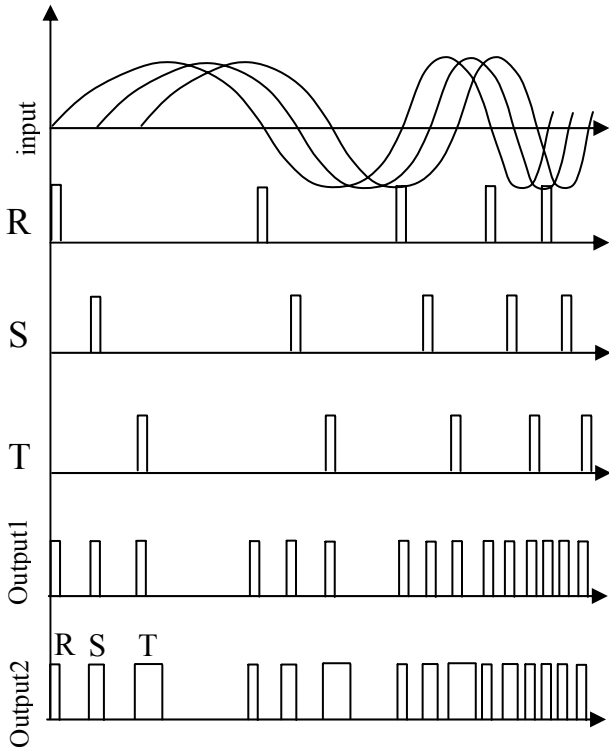


Fig. 3

Another scheme solution is shown in Fig. 4. The signals of the three phases are supplied to an adder realized with an operational amplifier. In this case the output voltage depends on the relation between the input resistor and the resistor defining the feedback respectively:

$$(1) \quad U_R = \frac{R_1}{R_0}, U_S = \frac{R_2}{R_0}, U_T = \frac{R_3}{R_0}$$

When the choice of  $R_1$ ,  $R_2$  and  $R_3$  is appropriate, the amplitude of the pulses of the respective phases will be different. This method is suitable for recording the vibration signal in format \*.wav. At the one of the channels of the computer sound card (e.g. the right one) the signal from the vibration sensor is supplied and at the other channel – the synchronizing signal from output 3 (Fig. 4).

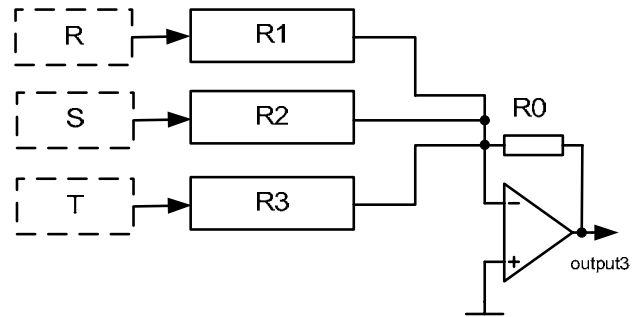


Fig. 4

Fig. 5 shows the time diagrams at this amplitude coding of the phases.

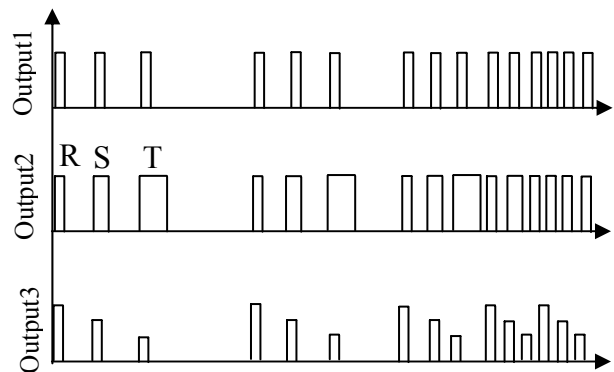


Fig. 5

The whole block scheme of the system before its connection with PC is shown in Fig. 6. Taking into account the frequency band of the investigated vibrations and the pilot synchronizing signal, it is possible to use a classic computer audio card as analogue-digital converter (ADC). In order to directly observe the process, it is possible to engage in parallel a common two-beam oscilloscope. When investigating shorter transition periods, a computer oscilloscope is used with the purpose of obtaining higher frequency of the signals analogue-to-digitization.

In order to more precisely evaluate the level of vibrations, their spectral composition, their root-mean-square value, etc., the digitized signal is processed by the program MATHCAD [1]. The additional availability of the moments of passing through zero of the alternating and by frequency supply voltage facilitates analyzing the level of vibrations in the preceding process.

In Fig. 7 the graphic representation of the vibrations from the optoelectronic sensor when changing the supply frequency from 10Hz to 50Hz is shown. It can be seen that in the beginning of the graph the amplitude of the vibrations is small and it increases gradually with the increase of the frequency. The maximum follows at about 20Hz and a decrease of their level at 50 Hz can be noted.

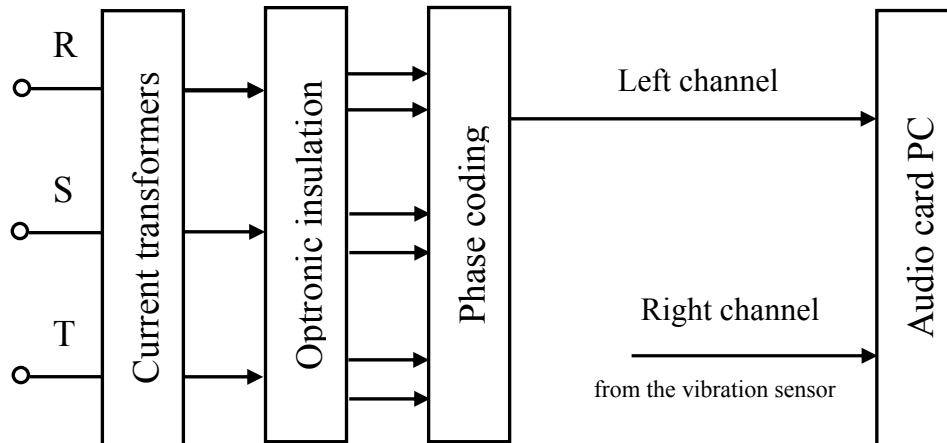


Fig. 6.

Vibration

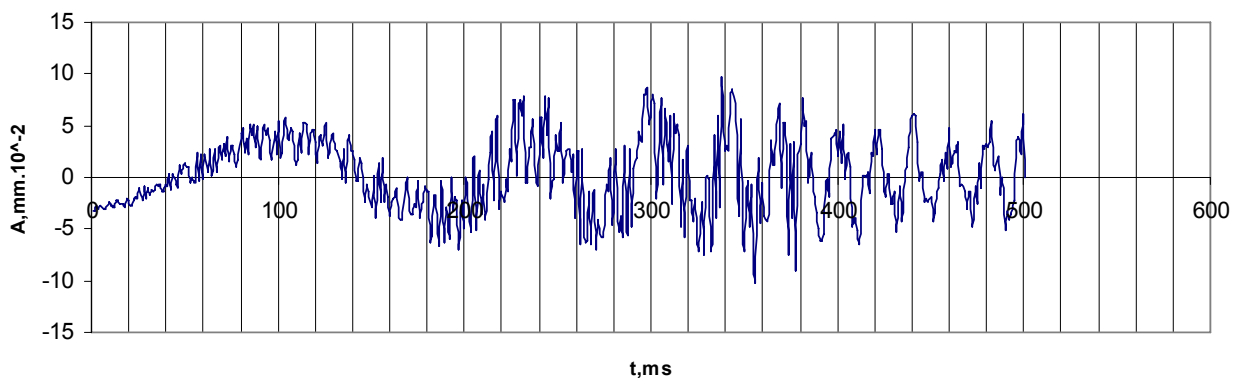


Fig.7

## Conclusion

The simultaneous record of the two signals – the one from the vibration sensor [2] and the pilot signal showing the current supply frequency – makes it possible to analyze in a deeper way the reasons causing the vibrations of the electrical machine. For example, the main frequency of the vibrations coincides with the moment rotation frequency of the motor and comparing it with the supply frequency provides approximate information about the slip coefficient.

The system also allows recording only the pilot signal with the purpose to precisely measure the supply frequency subsequently and especially when this frequency is a subject of control realized by feedback of a technological process.

## References

- [1] Iliev T., Plamen Danailov, A method of recording and analyzing the spectral structure of electrical signals obtained by optical sensors for vibration measurement of electrical machines, XV-th International Symposium on Electrical Apparatus and Technologies, 31May – 1 June 2007, Plovdiv,
- [2] Илиев Т., П. Данаилов, Компютърно моделиране на оптоелектронен датчик за изследване на електрически машини, XVII-ти Научен Симпозиум с международно

участие “Метрология и Метрологично Осигуряване 2007”, септември 2007 г., Созопол



Gabrovo, 4 H. Dimitar Street, 5300 Gabrovo, Bulgaria (e-mail: totyo\_iliev@abv.bg).

**Totyo Iliev** was born in Gabrovo, Bulgaria, on 3 November 1955. He studied at the Technical University of Gabrovo - Bulgaria and obtained a doctor's degree from the same university in 1991.

Since 1993 he has worked in the Faculty of Electrical Engineering at the Technical University of Gabrovo as a Lecturer. Since 1997 he has worked as an Associate Professor.

Totyo Iliev is with the Faculty of Electrical Engineering at the Technical University of



Electrical Engineering at the Technical University of Gabrovo, 4 H. Dimitar Street, 5300 Gabrovo, Bulgaria (e-mail: pbdan@abv.bg).

**Plamen Danailov** was born in Gabrovo, Bulgaria, on 3 October 1956. He graduated from the Higher Pedagogical Institute of Shumen in Physics and Mathematics. He worked as a constructor of electronic appliances at TU-Gabrovo. At present he is a Senior Assistant Professor in the Department of Physics at the Technical University of Gabrovo. His scientific interests are in the field of optoelectronics and optical measurements of vibrations of electrical machines.

Plamen Danailov is with the Faculty of

# Electromagnetic Parameters of a Non-Salient-Pole Vortex Machine Taking into Account the Influence of the Working Chamber

Konstantin Kostov

**Abstract:** In the present work, the electromagnetic parameters of a non-salient-pole vortex machine are determined for the basic field harmonic. The analysis is carried out on the basis of relationships for the field and the shielding coefficient, which have been derived earlier.

**Keywords:** vortex machine, magnetic shield, electromagnetic parameters.

The vortex machine [1], [2] is a device that creates a rotating magnetic field by means of an inductor similar to the stator in a.c. electric machines. The rotating magnetic field drives multiple ferromagnetic working particles exerting a technological effect upon the treated material. The technological process of the vortex machine is performed in a chamber that shields the field to a certain extent. Useful working flux is solely that part of the magnetic flux which enters the chamber. The rest of the magnetic flux is considered as a leakage. We shall determine the working flux and the leakage flux defined by the chamber and then we shall calculate their respective inductive resistances. We shall operate only with the field created by the basic harmonic of the mmf.

The field in the chamber is a circular rotating field and it may be assumed that field has been formed from two pulsating initial fields (fields in the absence of a chamber). The induction module and that of its flux in the chamber per one pole pitch for rotating field are equal to their respective amplitudes for each of the fields pulsating inside it.

In [3], it is found that the amplitude of the pulsating field intensity in the chamber is

$$H_1 = \sqrt{2}k_{w1}A|K|,$$

where  $K$  is a complex number, a field-shielding coefficient.

The amplitude of the flux in the chamber per one pole pitch is obtained by integrating the radial component of the magnetic induction amplitude along its internal surface of radius  $r_1$ , Fig. 1. Let the pulsating field is oriented along the Y axis. In such a case

$$(1) \quad \begin{aligned} \Phi_{\eta} &= \mu_o \sqrt{2}k_{w1}Al_{\delta}|K| \int_{-\frac{\pi}{2}}^{\frac{\pi}{2}} r_1 \cos \alpha \cdot d\alpha = \\ &= \mu_o \sqrt{2}k_{w1}Al_{\delta}d_1|K|, \end{aligned}$$

where

$\Phi_{\eta}$  is the flux amplitude in the chamber per one pole pitch; and

$d_1 = 2r_1$  is the internal chamber diameter.

The flux of the rotating field is a result of the mmf of all the phase windings and has a module equal to the amplitude  $\Phi_{\eta}$  of the flux of the pulsating field. When rotating, it induces an emf of self-induction, which is calculated so:

$$(2) \quad \begin{aligned} E_1 &= \pi\sqrt{2}fwk_{w1}\Phi_{\eta} = 2\pi\mu_o fwk_{w1}^2Al_{\delta}d_1|K| = \\ &= 4\mu_o mfw^2k_{w1}^2l_{\delta}\frac{d_1}{D}|K|I, \end{aligned}$$

where  $D = 2R$  is the diameter of the inductor. The main inductive resistance is determined from this expression, taking into account the impact of the other phases, when there is a chamber:

$$(3) \quad x_1 = 4\mu_o mfw^2k_{w1}^2l_{\delta}\frac{d_1}{D}|K|.$$

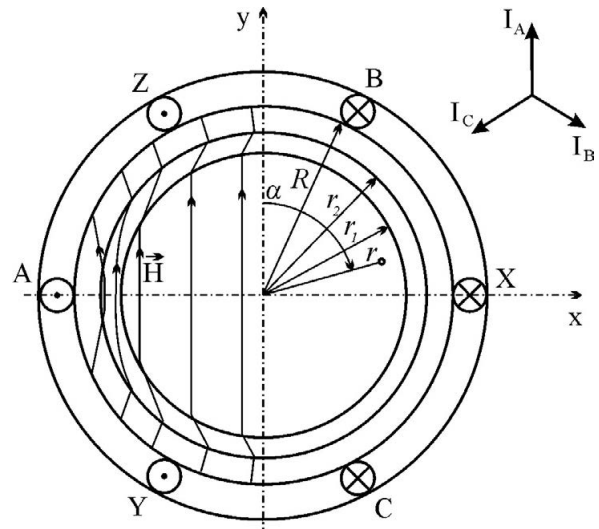


Fig. 1

It is possible to calculate the flux passing through the inductor's rim. The rotating field with module  $H_o$  is considered as created from two initial (in the absence of a chamber) pulsating fields along the X and Y axes, which are phase-shifted at  $\pi/2$ :

$$\dot{H}_{ox} = H_o e^{j(\psi - \pi/2)}, \quad \dot{H}_{oy} = H_o e^{j\psi},$$

where  $\psi$  is the initial phase of the field along Y.  $\dot{H}_{oy}$  is ahead of  $\dot{H}_{ox}$  for we assume that the rotation direction is



from the Y axis towards the X axis (clockwise). When a chamber is present, each of them creates respective radial components at a point of the inductor's rim with angular coordinate  $\alpha$ . In accordance with the formula derived in [3] these are:

$$(4) \quad \begin{aligned} \dot{H}_{3R(x)} &= H_o e^{j(\psi-\pi/2)} (1+2s) \sin \alpha, \\ \dot{H}_{3R(y)} &= H_o e^{j\psi} (1+2s) \cos \alpha, \end{aligned}$$

where  $s$  is a dimensionless complex coefficient. It is calculated by using a formula derived in [3].

In the last equations the index in brackets indicates from which field the radial component has been created.  $\dot{H}_{3R(x)}$  and  $\dot{H}_{3R(y)}$  are in quadrature on the complex plane, so that in the presence of a chamber the resultant field  $\dot{H}_{3R}$  has a module and phase, respectively

$$(5) \quad \begin{aligned} H_{3R} &= H_o |1+2s|, \\ \arg \dot{H}_{3R} &= \arg(1+2s) + \psi - \pi/2 + \arccotg \frac{|\dot{H}_{3R(y)}|}{|\dot{H}_{3R(x)}|} = \\ &= \arg(1+2s) + \psi - \alpha. \end{aligned}$$

Here,  $\dot{H}_{3R}$  is the complex amplitude of the radial component of the intensity along the inductor's rim,  $\psi$  being the initial phase of the current of that phase, the axis of which is oriented along the ordinate.

We integrate the radial induction over the inductor's surface per one pole pitch:

$$\dot{\Phi}_{3R} = \mu_o H_o (1+2s) e^{j\psi} l_\delta R \int_{-\pi/2}^{\pi/2} e^{-j\alpha} d\alpha = \mu_o H_o (1+2s) e^{j\psi} l_\delta D$$

Here,  $H_o$  is determined in accordance with the formula derived in [3]:

$$H_o = \sqrt{2} k_{w1} A$$

Let us consider the mutual location of the fluxes and the current of phase A, the axis of which is oriented along the ordinate, at the time when that current is maximum, i. e.  $H_{oy}$  is also maximum, so the initial phase  $\psi = \pi/2$ . It is obtained

$$\dot{\Phi}_{3R} = \mu_o \sqrt{2} k_{w1} A l_\delta D e^{j\pi/2} (1+2s).$$

The module of  $\dot{\Phi}_{3R}$  is

$$(6) \quad \Phi_{3R} = \mu_o \sqrt{2} k_{w1} A l_\delta D \left| e^{j\pi/2} (1+2s) \right| = \mu_o \sqrt{2} k_{w1} A l_\delta D |1+2s|,$$

so that  $\dot{\Phi}_{3R} = \Phi_{3R} e^{j\varphi}$ .

In the last formula  $\varphi$  is an argument of the complex number  $G = e^{j\pi/2} (1+2s)$ . We represent  $\Phi_{3R}$  in the form

$$(7) \quad \Phi_{3R} = \mu_o \sqrt{2} k_{w1} A l_\delta D |G|.$$

Fig. 2 shows a vector diagram with the mutual location of the current of phase A,  $\dot{\Phi}_{3R}$  and  $\dot{\Phi}_\eta$  in the complex plane. At any time, fluxes  $\dot{\Phi}_{3R}$  and  $\dot{\Phi}_\eta$  are related to the same pole pitch, for which  $-\pi/2 \leq \alpha \leq \pi/2$ .  $\dot{\Phi}_\eta$  lags at angle  $\gamma$  from the current of phase A.  $\dot{\Phi}_{3R}$  is at angle  $\varphi$  from the real axis. At the same moment, the current is at its positive maximum. The difference  $\dot{\Phi}_{\kappa AM} = \dot{\Phi}_{3R} - \dot{\Phi}_\eta$  is a flux of leakage that does not enter the chamber. Its module can be found according to the cosine theorem. Having in mind that the angle  $\beta$  between  $\dot{\Phi}_{3R}$  and  $\dot{\Phi}_\eta$  is defined from the equality expression  $\beta = \varphi - \gamma - \pi/2$ , it is obtained:

$$\begin{aligned} \Phi_{\kappa AM} &= \sqrt{\Phi_{3R}^2 + \Phi_\eta^2 - 2\Phi_{3R}\Phi_\eta \cos \beta} = \sqrt{\Phi_{3R}^2 + \Phi_\eta^2 - 2\Phi_{3R}\Phi_\eta \sin(\varphi-\gamma)}. \\ \Phi_\eta \text{ and } \Phi_{3R} \text{ from (1) and (7), respectively, are replaced} \\ \text{and the expression is rationalized:} \end{aligned}$$

$$\begin{aligned} \Phi_{\kappa AM} &= \mu_o \sqrt{2} k_{w1} A l_\delta \sqrt{D^2 G^2 + d_1^2 |K|^2 - 2DGd_1 |K| \sin(\varphi-\gamma)} = \\ &= \mu_o \sqrt{2} k_{w1} A l_\delta D G_1, \end{aligned}$$

$$\text{where } G_1 = \sqrt{G^2 + \frac{d_1^2}{D^2} |K|^2 - 2G \frac{d_1}{D} |K| \sin(\varphi-\gamma)}.$$

The flux  $\Phi_{\kappa AM}$  is a part of  $\Phi_{R3}$  and creates an emf in the winding:

$$E_{\kappa AM} = \pi \sqrt{2} f w k_{w1} \Phi_{\kappa AM} = \pi \sqrt{2} f w k_{w1} \mu_o \sqrt{2} k_{w1} A l_\delta D G_1 = 4 \mu_o m f w^2 k_{w1}^2 l_\delta G_1 I.$$

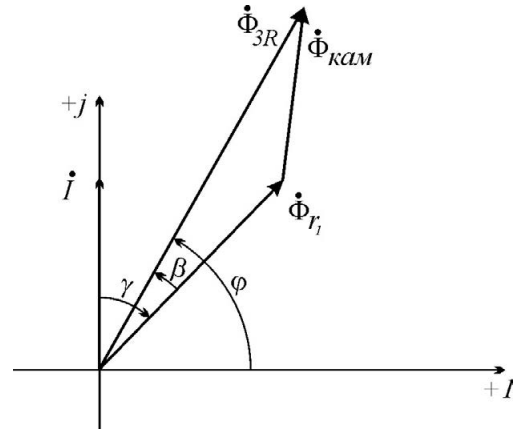


Fig. 2 1

The inductive resistance of the leakage due to the shielding effect of the chamber is

$$(8) \quad x_{\kappa AM} = 4 \mu_o m f w^2 k_{w1}^2 l_\delta G_1.$$

In the same manner as in electric machinery theory, we determine the relative permeance:

$$(9) \quad \lambda_{\kappa AM} = \frac{x_{\kappa AM}}{4 \mu_o \pi f \frac{w^2}{pq} l'_\delta} = \frac{4 \mu_o m f w^2 k_{w1}^2 l_\delta G_1}{4 \mu_o \pi f \frac{w^2}{pq} l'_\delta} = \frac{mpq k_{w1}^2 G_1 l_\delta}{\pi l'_\delta}.$$

The total inductive resistance of leakage can be obtained by summing up the individual components:

$$(10) \quad x_{\sigma} = 4\mu_0 \pi f \frac{W^2}{pq} l'(\lambda_{\kappa} + \lambda_{\kappa op} + \lambda_{\iota} + \lambda_{\Delta} + \lambda_{\kappa AM}),$$

where  $\lambda_{\kappa}$ ,  $\lambda_{\kappa op}$  and  $\lambda_{\iota}$  are the relative permeances for the slot leakage, for that of the tooth crown, and for the front leakage, respectively. For these it is possible to refer to formulae in the specialized literature on a.c. electric machines. In (10), it is supposed that the permeance of the differential leakage does not change in the presence of the chamber. As its fraction for the vortex machine is too small, this will introduce a negligible error.

The formulae obtained for the basic harmonics of the magnetic flux and of the emf, for the main inductive resistance and the inductive resistance of the differential leakage are necessary for the analysis of processes in the vortex machine and for its calculation.

## References

- [1] Ta-Hsin, Ch., W. Lee, L. Chen. Method and device for grinding particulates. USA Patent № 6719610, 2004.
- [2] Jones, T. B. Electromechanics of particles. Cambridge Univ. Press, 2006.
- [3] Kostov, K. Magnetic field, parameters and electromagnetic calculation of vortex machine (in Bulgarian). MGU “St. I. Rilski”, Sofia, 2007.

## Biography



**Konstantin Kostov** was born in Byala Slatina, Bulgaria, on March 22, 1947. He graduated from the Technical University of Sofia-Bulgaria and received Dr. degree from the same university in 2007.

Since 1975 he has worked at the Faculty of Mining and Electromechanics of the University of Mining and Geology “St. I. Rilski” as a lecturer and a senior expert. He is concerned with the magnetic field and its

effect of forces acting upon ferromagnetic particles.

Konstantin Kostov is with the Faculty of Mining and Electromechanics, University of Mining and Geology “St. I. Rilski”, 1700 Sofia, Bulgaria (e-mail: ccostow@yahoo.com).

# Simplified Method of Defining the Torque, the Shaft Load Moment and the Moment of Inertia for Power Tools

Milko Dochev – TK-Lovech

**Abstract:** A method of defining the torque, the shaft load moment and the moment of inertia of power tools shaft has been described. The method can be used without the application of any special transducers of the torque, such as the "torductor" types, as well as loading devices, such as inductions brakes. For that purpose an observing method and the functional connection between the moment of inertia and the acceleration are used.

**Keywords:** power tools (PT), torque, shaft load moment, moment of inertia.

## Introduction

For measuring and defining the shaft load moment mechanic and electrical transducers and loading devices are mainly used. They are expensive and not always available. That is why for practical aims an experimental-computing method for defining the torque, the shaft load moment and the moment of inertia, described in the abstract, can be used.

In the known literature on the theory of automatic electric drive when exploring the dynamics it is common to work with the so called Movement Equation:

$$(1) \quad M - M_s = J \cdot \varepsilon,$$

Where:

$M$  and  $M_s$  are torque and shaft load moment,  $J$  stands for moment of inertia,  $\varepsilon$  is the angle acceleration of the shaft. Equation (1) refers mainly to regimes of acceleration of inertia masses.

In number of cases using special sensors of the mechanical moment of the shaft (for example some from the system "torductor") is needed, which despite their high price are not quite exact [2]. On the other hand, there are no such sensors applicable to the moment of inertia.

Source [4] gives the developed  $\varepsilon$ -method for identification of  $M_c$  and  $J$ , by which the measurement of the acceleration, as well as the torque is needed.

When speed sensor and corresponding computing device are available, acceleration defining is not a problem. Provided that the pace of time difference is small, even the simplest two-points-computing system for acceleration defining will bring exact results. The acceleration will be defined by two subsequently measured speed values  $\omega_2$  and  $\omega_1$ :

$$(1a) \quad \varepsilon \approx \frac{\omega_2 - \omega_1}{\Delta t}$$

Unfortunately, in number of cases the fitting of the electric drive with torque sensor can be difficult because of mechanical, constructive or meteorological reasons. Finding a solution that is not connected with assembling such device to the PT shaft, is the advantage of the work and allows of applying the method in exploitation conditions, as well.

## Essence of the method

An opportunity to exclude the need of sensor for the torque is to work with torque equal to null. Such is the so called self-stop regime, when the instrument, for example grinder, has been spinned to some speed and the motor is switched off. In that case (1) is transferred into:

$$(2) \quad -M_s = J \cdot \varepsilon_s, \text{ which means negative acceleration.}$$

Two subsequent experiments can be made. The instrument is turned on, spinned in idle running and then turned down. The two experiments are different in adding a new inertia mass (additional flywheel) to the spindle, whose additional inertia moment is known. This could for example be the abrasive disk of a machine. By one and the same speed only the accelerations in the two cases are calculated. The first one, when there is no additional mass, is defined by (2). For the second we have the following:

$$(3) \quad -M_s = (J + J_{add}) \cdot \varepsilon_{s1}$$

The equation of the right sides of (2) and (3) (where if the speed is equal, so is the shaft load moment) leads to:

$$(4) \quad J \cdot \varepsilon_s = (J + J_{add}) \cdot \varepsilon_{s1}$$

An equation of the instrument's  $J$  inertia moment, that is searched for, can be then derived:

$$(5) \quad J = J_{add} \frac{\varepsilon_s}{\varepsilon_s - \varepsilon_{s1}}$$

After substitution in (2) the shaft load moment  $M_s$  is as follows:

$$(6) \quad M_s = J_{add} \cdot \frac{\varepsilon_s \cdot \varepsilon_{s1}}{\varepsilon_s - \varepsilon_{s1}}$$

The described procedure can be carried out for plenty of different speeds. Corresponding to that, from the multitude of relevant accelerations by self-stop in (3) and (6) the loading mechanical characteristic of the tool  $\omega = f(M_c)$  can be deduced.

The developed approach allows trough control on the acceleration the values of torque  $M$  to be also defined for the same diapason of speeds, that means the mechanical characteristic of the tool  $\omega = f(M)$ .

Indeed, taking into account (6) and (5), it can be derived from (1) that:

$$(7) \quad M = J_{add} \cdot \frac{\varepsilon_{s1} \cdot (\varepsilon_s + \varepsilon)}{\varepsilon_s - \varepsilon_{s1}}$$

Where  $\varepsilon$  stands for the acceleration by electric turning on of the motor, with the starting key constantly pressed and acceleration according to (1).

Defining in advance the inertia moment values of the additional flywheel  $J_{add}$  should not be a problem at all. If the flywheel is a empty cylinder with outside diameter  $D$  and inside diameter  $d$ , thickness  $l$  and is made of material with density  $\rho$ , then according to (2) follows that:

$$(8) \quad J_{add} = \frac{\pi \cdot \rho \cdot l}{32} \cdot (D^4 - d^4)$$

The arguments exposed till here are related to a case when the researched object is completely unknown, that means by maximal "insufficiency" of preliminary information. For the most common situation the inertia will not only be a constant, but will also be previously known from catalogues or other information sources. Then unknown and object of research are only the two moments- torque and shaft load moments.

In that situation the need of experiments with additional inertia mass is no longer valid, and the machine spins and stops by its own in accordance with equations (1) and (2). Consequently, (2) directly gives the function  $\omega = f(M_c)$  on he process of self-stop, and

after substituting (2) in (1) we received about the acceleration process as following:

$$(9) \quad M = J \cdot (\varepsilon - \varepsilon_s)$$

By which to receiving of the machine mechanical characteristic  $\omega = f(M)$  is possible.

Knowing in advance the correlation of the reduction gear  $i$ , the relation between the torque of the motor  $M_m$  and the torque of the instrument  $M$  is:

$$(10) \quad M = M_m \cdot i$$

(11) Corresponding to that the relation of speeds is:  $\omega = \omega_m / i$ .

That allows the receiving of a mechanical characteristic of the motor:  $M_m = f(\omega_m)$ .

### Conclusion:

The method proposed here was tested with the help of a computer simulation, where it showed high exactness: the mistake about a wide diapason of parameter variations did not exceed 0,5%.

The suggested method gives the opportunity to observe the torque, the shaft load moment and the inertia moment of a PT shaft trough controlling only the speed and the time for spinning and self-stop. The analysis of the received mechanical characteristics allows diagnosis of the condition of both machine's mechanical part and its electric drive motor, as well, without the need of disarticulating the power tools.

### References

- [1] Чиликин М. Г., В. И. Ключев – Теория автоматизированного электропривода, М., Энергия, 1979
- [2] Билдирев, Ж – Основы на електрозадвигването – Сборник задачи – С., Техника 1972
- [3] Билдирев, Ж., Л. Попов – Наблюдател на момента на вала при един клас електрозадвигвания, "МЕТРОЛОГИЯ" 2002
- [4] Zheko S. Bildirev, Milko G. Dochev, Stefan V. Stojchev Monitoring of the torque, the shaft load moment, the braking moment and the moment of inertia for sewing machines drives-Smolq, 2006

### Biography

**Milko Dochev** was born in Lovech, Bulgaria, on November 17, 1958. He has graduated at the Technical University- Sofia in 1984 in the subject Electric Machines and Apparatuses, and in 1985 in his second subject Electronic Technique and Technologies. During 1985-1995 he worked as an Research Worker at the Electroindustry Institute- Sofia. He has been an Assistant Professor at Technical College- Lovech since 1992.

His scientific interests and works are in the field of methods and instruments for control, diagnosis, exploitation and repair of electric machines and apparatuses, and particularly professional power tools.

Milko G. Dochev – TK-Lovech, 5500 Lovech- 31 S. Saev Street, [e-mail: dochev@mail.bg](mailto:dochev@mail.bg), GSM 0887284990

# Electro drive system with single-tree phase quasyresonance cycloconverter

Tsvetozar Petkov, Lubomir Genchev

**Abstract:** The development of the asynchronous electro driving systems requires researches about scheme solutions that control the motor effectively with high energy parameters. The paper shows a method for obtaining low regulated velocities of induction motor by non-complicate scheme and using the resonance phenomena for improve the characteristics of the driving systems. This is a method, which use direct conversion of frequency, created on the basis of a single-tree phase quasyresonance cycloconverter.

**Keywords:** cycloconverter, induction motor, quasyresonance

## Introduction

Depending of requirements of the driving mechanism is necessary to use most suitable method for control of the induction motor. Some applications require low regulated velocities also like gradual starting and stopping process and opportunity to work in recuperation regime. Most of the frequency converters have AC/DC block and the realization of the recuperation regime requires complicate scheme with big number of elements. One of possible idea is to use a cycloconverter, the advantages of these converters is in the direct changing the frequency and well provide the regime with recuperation.

The application of resonance phenomena on electro driving systems with induction motor is not investigated in detail yet, therefore interesting task is to research and develop this idea [3,5].

## Presentation

The suggested scheme of the single-tree phase quasyresonance cycloconverter is shown on fig.1 it contains six triacs, a capacitor connected in series and a three-phase induction motor. In cases of achievement of some special regimes is necessary to connect an extra induction like is swown:

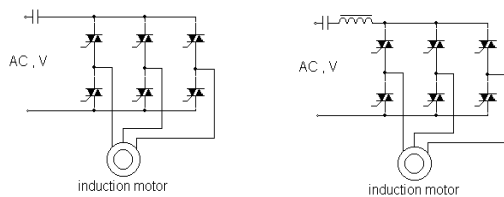


Fig. 1. The suggested schemes of the quasyresonance cycloconverters.

The control system passes impulses in straight sequence which is synchronized to the supplying voltage. As a result of this controlling method, in the stator coils of the induction motor flows a symmetrical tree-phase system of currents [3,4,5]. The form of the current curve for one phase of the motor, for several frequencies, when the basis frequency is 50 Hz, is shown on fig.2. The result of changing the number of the semi waves in one period is a change in the frequency and the synchronic speed respectively.

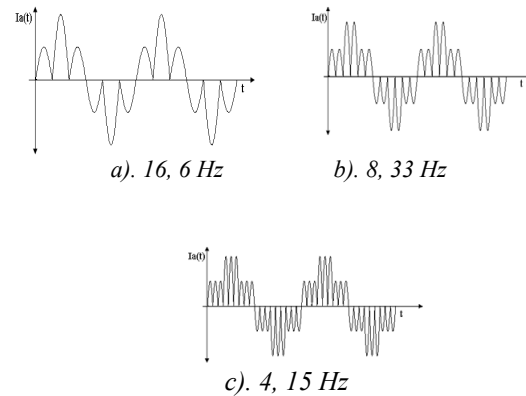


Fig. 2. The Current curves for one phase of the motor for different frequencies.

The sequence of conection of the phases of the motor for one frequency is shown on the next figures

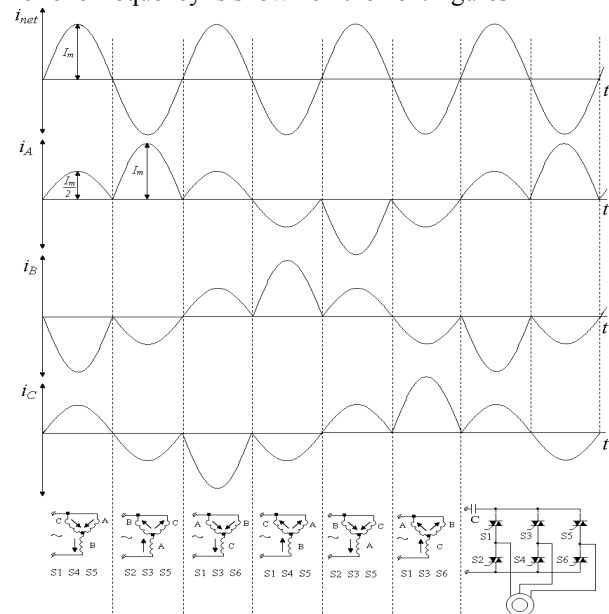


Fig. 3. Connection of the phases for each semi period



The value of the motor speed is changed gradually divisible to three. The current that is used by the electrical net has a sinusoidal form, because control impulses are passed when the current crosses zero, this means that the device does not import in the supplying net higher harmonics which is a big advantage of the method. Other advantage is the ability to work in recuperation without any change in sequence of control impulses or switching of power elements.

The analysis of the characteristics and energy parameters of the induction motor for steady-state regimes could be made about "T"- equivalent scheme [1]. Any moment in the time the converter connect the phases of the motor two in parallel and one in series as a shown on fig.3. This allows investigating some of the characteristics of the suggesting system by using this connection.

First of all is necessary to find equivalent impedance for one phase of the motor from "T" equivalent scheme:

$$(1) \quad Z_{ph} = R_1 + j \left[ \frac{\left( \frac{R'_2}{s} + jx'_{2\sigma} \right) \cdot x_\mu}{\frac{R'_2}{s} + j(x'_{2\sigma} + x_\mu)} + x_{1\sigma} \right]$$

were:

$Z_{ph}$  - equivalent impedance for one phase;

$R_1$  - resistance of the stator coil;

$x_{1\sigma} = 2\pi \frac{f}{n} L_{1\sigma}$  - reactance of disperse of the privet loop;

$R'_2$  - resistance of the rotor loop;

$x'_{2\sigma} = 2\pi \frac{f}{n} L_{2\sigma}$  - reactance of disperse of the secondary loop;

$x_\mu = 2\pi \frac{f}{n} L_\mu$  - reactance of the magnetic loop;

$L_{1\sigma}$  - inductance of disperse of the stator;

$L_{2\sigma}$  - inductance of disperse of the rotor loop;

$L_\mu$  - inductance of the magnetic loop;

$n = 3, 6, 9, 12, \dots$  - dividing coefficient of the cycloconverter;

$f$  - frequency of the supplying net.

To finding the impedance of the all system have use a following formulas were the complex reactance of the capacitor is included.

$$(2) \quad Z_{eqv} = Z_{ph} + \frac{Z_{ph}^2}{2 \cdot Z_{ph}} - j \frac{1}{2\pi \cdot f \cdot C}$$

were:

$Z_{eqv}$  - equivalent impedance of the system;

$C$  - capacitance of the capacitor;

After that is possibly to find the current from supplying net:

$$(3) \quad \dot{I}_{net} = \frac{U_{net}}{Z_{eqv}}$$

The phase current could be described by using Fourier transform then the effective value of the current for one phase of the motor is determined by following expression:

$$(4) \quad I_1 = \sqrt{I_{(1)}^2 + I_{(2)}^2 + \dots + I_{(k-1)}^2 + I_k^2}$$

were:

$I_1$  - effective value of the current for one phase of the motor;

$I_{(1)} \dots \dots \dots I_{(k)}$  - effective value of the first and the hider harmonics;

$k$  - number of the harmonic.

In order to make easier the finding of the effective value of the current for one phase of the motor may suppose:

$$(5) \quad I_1 = \frac{2}{3} |\dot{I}_{net}|$$

After determine the phase current in order to achieve mechanical characteristic is necessary to determine the rotor current by following expression:

$$(6) \quad \dot{I}'_2 = I_1 \cdot \frac{jx_\mu}{\frac{R'_2}{s} + j(x'_{2\sigma} + x_\mu)}$$

The electromagnetic power delivered from the stator to the rotor is define by following expression:

$$(7) \quad P_{em} = m \cdot |\dot{I}'_2|^2 \cdot \frac{R'_2}{s}$$

were:

$P_{em}$  - the electromagnetic power;

$m$  - the number of the phases.

After that the electromagnetic torque is finding:

$$(8) \quad M_{em} = \frac{P_{em}}{\omega_0}$$

were:

$M_{em}$  - electromagnetic torque;

$\omega_0 = \frac{2\pi f}{n \cdot p}$  - speed of the magnetic field;

$p$  - The number of the poles.

The changing of the power factor could be found when determine the equivalent impedance (2) of the equivalent scheme in complex value including the

complex reactance of the capacitor. The function  $\cos(\varphi)=f(s)$  is given with the following expression:

$$(9) \quad \cos(\varphi) = \frac{\operatorname{Re}(Z_{eqv})}{|Z_{eqv}|}$$

With suggested method could be found the coefficient of efficient:

$$(10) \quad \eta = \frac{P_{em}}{U_{net} |I_{net}| \cdot \cos(\varphi)}$$

From these expressions could be made important conclusions about steady-state regimes of work.

Depending on the capacitance of the capacitor the work regime is change. When the equivalent impedance of the system cycloconverter-induction motor is much smaller then the reactance of the capacitor, it would be supposed that the induction motor is feed from three phase constant current's source. In this condition the power factor is not very high, because the load have straight capacitive character. The mechanical characteristics have small maximum slip, small overload capability and small start torque fig 4. This is due to the decrease of the magnetic field. This condition is a result of increasing of the rotor current and its unmagnetizing action [2].

The researches are made for induction motor type 90 S 2.B5 - 545 HB, made in Trojan, Bulgaria with the following parameters:

$$P_n = 1.5 \text{ [kW]}, \cos(\varphi) = 0.8, \omega_n = 301 \text{ [rad/s]},$$

$$I_n = 6.0 \text{ [A]}, \lambda = M_{max}/M_n = 2$$

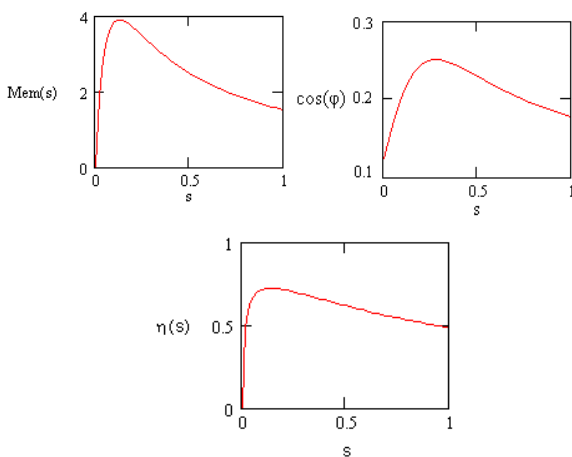


Fig. 4. Characteristics for constant current regime

To achieve overload capability commensurably with feeding from voltage source and high energy parameters is necessary to increase the value of the capacitance.

When the value of the capacitance is bigger it's possible to determine the ratio of the current on the stator coils. The stator current is higher than the nominal value, because the capacitor and the equivalent system

cycloconverter-induction motor form a RLC circuit connected in series. In result of deep saturation of the magnetic circuit, could be assumed that the magnetic flux is not changed when the slip increase. The overload capability is high, the power factor is smaller than the nominal value, the character of the load is still capacitive.

When the equivalent inductance of the system cycloconverter – induction motor is approximately equal to reactance of the capacitor, the work regime is very close to the resonance e.g. quasyresonance. The investigations show that the overload capability is highest and the power factor reaches a maximum value, the start torque is highest too fig 5. In order to achieve the resonance is possible to connect an extra induction as is shown on fig 1.

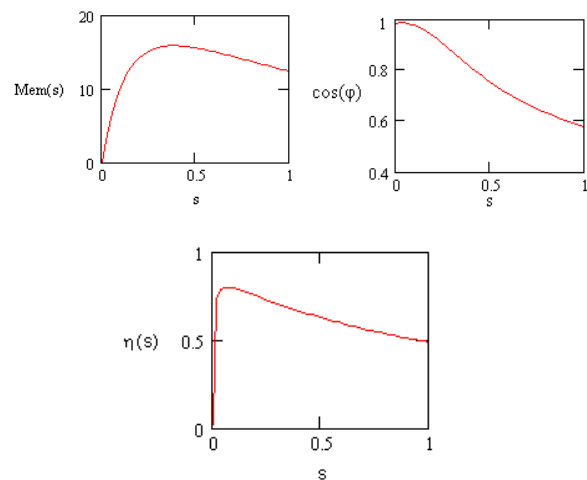


Fig. 5. Characteristic for quasyresonance regime.

Because the resonance is in series, the stator's current is much higher than the nominal and depends on the value of equivalent resistant, this allows a short time work regime. The cooling system is independent because when the velocities are low, the self ventilation is inefficacious.

## Applications

In mechanisms that require restriction of the dynamic efforts, the main task of the electro motion system is achieving high speed of motion with gradual starting and stopping process of the driving load [3], for example cranes, elevators and others.

One of possible applications of this electro drive could be found in horizontal and vertical driving mechanisms of cranes. For this propose start-stopping device for horizontal driving mechanism of a crane has been create. The suggesting scheme of the device is shown on the next figure. The device contains the suggested system with induction motor with electromagnetic brake, an extra contactors for each ways of movement and control station for the operator of the crane.

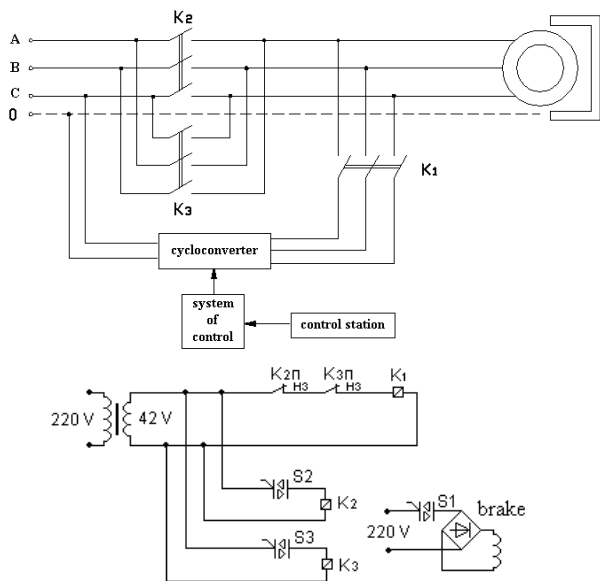


Fig. 6. Start-stopping device

When the cranes operator take a signal for movement of the load, the system of control based on microcontroller, give impulse for take off the electromagnetic brake. After that the system of control passes impulses which determine low speed of movement of the driving load.

Gradual, system of control increase the frequency given to the induction motor. In result of this, the driving load achieve soft starting process. After achieve the biggest frequency from the cycloconverter, the system connect the induction motor to the supplying net on the basic frequency(50 Hz). When the signal from cranes operator is for stop, the system of control gradually decrease the frequency in result of this the induction motor work in recuperation and the load achieve soft stopping process.

Other application is possible to find in domestic devises as washing machines and others.

## References

- [1] Ангелов, А Електрически машини част 1 , София „Техника” 1976 г.
- [2] Ключев, В Теория на електрозадвигването София техника 1989 г.
- [3] Petkov Ts Start-stop device for elevating mechanisms. UNITEX 2006, Gabrovo, Bulgaria pp. 74-77
- [4] Genchev, Ts. Petkov. Frequency method for obtaining low velocities. ELMA 2005, Sofia pp. 160-162
- [5] Грико В. “Статические преобразователей на несущей частоте” Электротехника” 1969 г. Рр 66-68

## Biographies



**Tsvetozar Petkov** was born in Pleven, Bulgaria, on March 15, 1977. He studied at the Technical University of Gabrovo-Bulgaria and received Master degree from the same university in 2002. He is today a PhD student in the Faculty of Electrical Engineering of the Technical University – Gabrovo.

His field of interest includes electrical machines, electrical drives and renewable energy sources.

Tsvetozar Petkov is with the Faculty of Electrical Engineering, Technical University of Gabrovo, 4, H. Dimitar str., 5300 Gabrovo, Bulgaria (e-mail: tsvetozar\_petkov@mail.bg)



**Lubomir Genchev** was born in Gabrovo, Bulgaria, on October 29, 1937. He graduated from the Technical University - Sofia, Since 1972 he worked in the Faculty of Electrical Engineering of the Technical University of Gabrovo as a Lecturer and researcher in the field of theory of control and electrical drives.

His field of interest includes electrical machines, electrical drives, theory of control

Lubomir Genchev is with the Faculty of Electrical Engineering, Technical University of Gabrovo, 4, H. Dimitar str., 5300 Gabrovo, Bulgaria. (e-mail:lubomir\_genchev@mail.bg)

# Global Irradiance throughout the Day in Gabrovo

Milka Konsulova

**Abstract:** *The purpose of the presented paper is to give particular information about solar irradiance. Designer and worker on the field of renewable energy need such information. Atmospheric science and meteorology are very important and close related to renewable energy practice. Sun irradiance in this work is measured with pyranometer CM3 and results are given*

**Keywords:** *renewable energy, solar irradiance, pyranometer CM3*

## Introduction

Solar radiation has been called the fuel of photovoltaics, and its characteristics form the basis of system design, from array construction to the reliability of electricity supply by stand-alone photovoltaic systems. The understanding of solar radiation forms arguably the most ancient part of physical science but it is only recently that the statistical nature of solar energy has been understood in some detail. A number of sophisticated computer models are now available.

Climate and solar radiation impact both on system supply side issues and on system demand side issues. Designers need both solar data and temperature data. Temperature affects the performance of photovoltaic devices per se. It also has a strong bearing on the demands of the energy required for heating and cooling.

Relating supply and demand within any renewable energy structure requires study of the inter-relationships between supply and demand. One has to establish the resources that need to be devoted to energy storage to achieve an acceptably reliable energy supply from an intermittent supply resource. Ideally one needs long-term time series of solar radiation data and temperature data for each specific site at the hourly level. Such data are relatively rare, so in recent years statistical approaches have been developed to help fill the gap. Long series of daily data are needed for sizing and modelling of stand-alone systems. Effective statistical approaches have to recognise the links between solar radiation data and temperature data.

The world is a big place. No one can be familiar with more than a small part of it. There are great dangers in photovoltaics design, if designers attempt to guess in the assessment of design risks the properties of the radiation climate at unfamiliar places. As globally based climatological tools are becoming more widely available, designers should make themselves aware of the powers of the new tools for design assessment in renewable energy design. Such tools should not be looked on as luxuries. They deliver quality controlled programmed results very

efficiently to users. Photovoltaics design depends on the successful harnessing the available climatological information to the detailed task of design. The gap between what data national meteorological services can provide and what systems designers actually need is currently often quite wide.

In discussing the various terms in the radiation fluxes, it has tacitly been assumed that averages over the year or over longitudes or latitudes have a well-defined meaning. However, as is well known, the climate is not completely periodic with a one-year cycle, even if the solar energy input is so to a very large degree. The short-term fluctuations in climate seem to be very important, and the development over a time scale of a year depends to a large extent on the detailed initial conditions. Since, owing to the irregular short-term fluctuations, the initial conditions at the beginning of subsequent years are not exactly the same, the development of the general circulation and of the climate as a whole does not repeat itself with a one-year period.

Although the gross seasonal characteristics are preserved as a result of the outside forcing of the system (the solar radiation), the year-average values of such quantities as mean temperature or mean cloudiness for a given region or for the Earth as a whole are not the same from one year to the next.

This implies that the components of the net radiation flux do not have the same annual average values from year to year. In particular, the disposition of incoming radiation as rejected, scattered, direct and absorbed radiation is very sensitive to variations in cloud cover, and therefore exhibits substantial changes from year to year.

## Purpose of the Paper

The purpose of the presented paper is to give particular information about solar irradiance in Gabrovo, Bulgaria.

## Design of the Measuring System

Design of the measuring system is shown on Fig.1

There are:

- 1 – pyranometer CM3 (Kipp&Zonen)
- 2 – cable
- 3 – amplifier CT24 (Kipp&Zonen)
- 4 – DC supply
- 5 – voltmeter
- 6 - PC



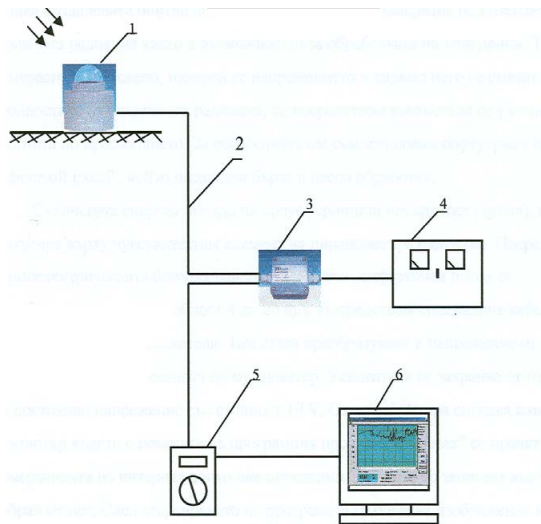


Fig.1 Design of measuring system

### Results

All measurements are made on the roof of Technical University- Gabrovo. On the figure 2, fig.3, fig.4 and fig.5 are shown typical data for two years: 2002 and 2007.

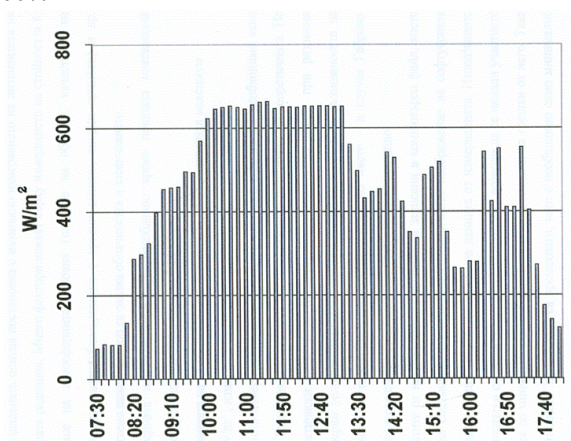


Fig.2 Solar irradiance for 11.07.02

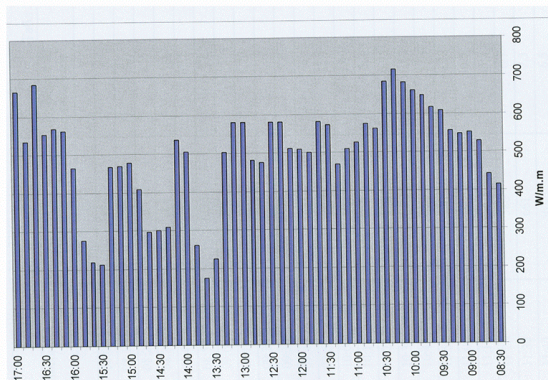


Fig.3 Solar irradiance for 02.07.07

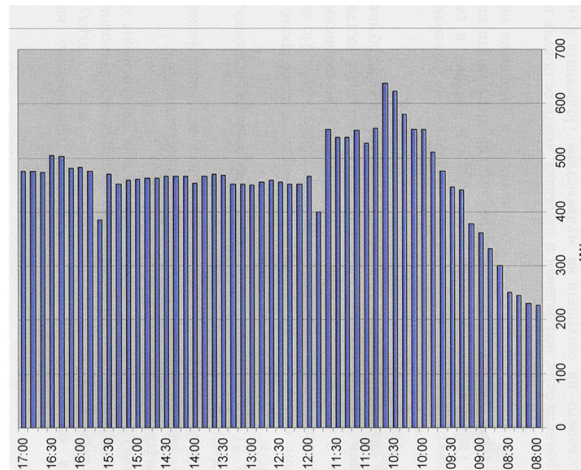


Fig.4 Solar irradiance for 01.07.07

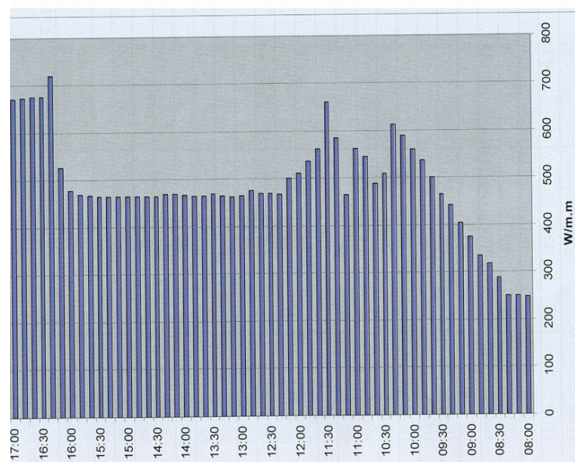


Fig.5 Solar irradiance for 04.07.07

All characteristics show the dependence between solar irradiance and hour at the day.

On the figure 2 is shown characteristic for July 2002. The day was sunny, hot (32 Grad C), light clouded.

On the figure 3, 4 and 5 are shown characteristic for July 2007. Conditions are:

For fig.3: light clouded; hot (33 deg C)

For fig.4: without clouds, 34 deg C

For fig.5: without clouds, 34 deg C

There are differences for characteristic for 2002 and 2007. The temperature is equal, the season is the same (July), and this can be explained with climate changes.

Discussion of the results is the follows:

- All characteristics for July 2002 have a sinus form or form near to sinus form
- For year 2007 there aren't such sinus form
- For year 2007 pick of the solar irradiation is at 10,30 a clock
- Solar irradiance is constant after 10,30 a clock and at 16 a clock is another pick.



## Conclusion

For designer of solar system (PV or water system) is very important to know the exactly solar irradiance for the place where the plant or system will be used. Designer needs meteorological data. This is the cause to put meteorological station near the PV system. In this paper are shown a real data for solar irradiation for Gabrovo, Bulgaria.

## References

- [1] Quaschnig V. Regenerative Energiesysteme, Carl Hanser Verlag, Muenchen, 1999
- [2] Консулова М. Възобновяеми енергийни източници, Университетско издателство “В. Априлов”, Габрово, 2006
- [3] Консулова М. Спънчеви лентови диаграми, Научна конференция Унитех 05, Габрово, 2005
- [4] Konsulova M., Sonnen Banddiagrammen, IWK Satera 07, Mittweida, BRD, 2007

## Biographies



**Milka Konsulova** was born in Kazanlak, Bulgaria, on July 31, 1944. She graduated at the Technical University - Sofia, and received PhD degree from the same university.

Her field of interest includes electrical devices, electrical supply and renewable energy sources. She is today an Assoc. Professor at Technical University – Gabrovo, Department Electrical Supply and Equipment in the Faculty of Electrical Engineering.

Milka Konsulova is with the Faculty of Electrical Engineering, Department Electrical Supply and Equipment, Technical University of Gabrovo, 4, H. Dimitar Str., 5300 Gabrovo, Bulgaria (e-mail: milkakonsulova@yahoo.com)

# Analysis of the Daily and Monthly Solar Radiation for the Region of Ruse

Ivaylo Stoyanov and Nicolay Mihailov

**Abstract:** In this study are presented generalized results of a long study of the daily and monthly solar radiation on the territory of the University of Ruse in the period January 2005 – December 2007. The direct solar radiation has been measured with pyranometer CM11. A repeatedness of direct solar radiation has been defined and is shown the maximum duration of usage of the solar radiation by months.

**Keywords:** solar radiation, statistical analysis.

## Introduction

The direct solar radiation is the major part of the the solar energy, reaching the earth. It's values differ for the different months of the year, because it depends on a number of factors (the angle, under which the solar rays fall on the earth, the position of the sun, the cloudiness, transparency of the atmosphere etc.) [1]. For example with a cloudless sky (0 balls [3]) the main factors, determining the direct solar radiation are astronomical, i.e. the direct solar radiation depends mainly on the Sun position, the geographic position and declination of the Sun. That's why after the sunrise, the solar radiation increases until noon, when it has its maximum, after which it decreases until the sundown. In reality the variation of the direct solar radiation is quite uneven, and significant differences are being observed [2, 4]. For example on a typical solar, cloudy and mixed day, the maximal values of the solar radiation are in the time interval 10:00-16:00, but the difference in the levels is 5 to 6 times. Such difference is also observed between the different months of the year. On the other hand the design and the reliable exploitation of PV systems require up-to-date statistical information for the available resource of the solar radiation of a specific region. That's why it is interesting to know the maximum levels and their duration for the different months of the year.

The aim of the present article is analysis of daily and monthly level of direct solar radiation for the region of Ruse and determined the maximum duration of usage during the different months.

## Scheme of the study

The analysis of the solar radiation for the city of Ruse has been made on the basis of measurements of the direct and integrated values of the solar radiation in the area of the University of Ruse, situated at 43°49'22" northern latitude and 26°1'19" eastern longitude. The measured values of the solar radiation in the period 2005 – 2008, have been compared with similar results for the same period.

The investigation of the solar radiation has been carried out with a specialized measuring system, which consists of a pyranometer CM 11 [5], an integrator (SOLRAD Integrator) and a personal computer (PC) (see Fig.1).

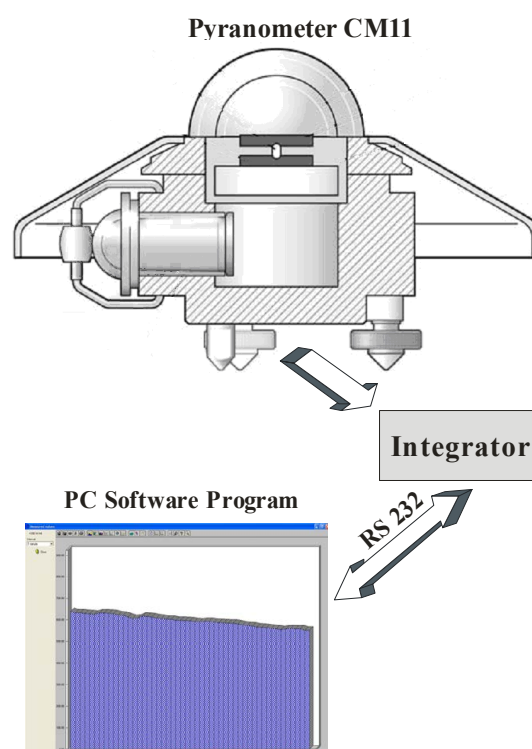


Fig.1. Pyranometer CM 11 and connection of readout Integrator SOLRAD with PC.

The pyranometer transforms the current level of solar radiation into analogue voltage signal, which is passed on to the integrator. The received information for the solar radiation is stored and processed and after that is passed on in a suitable form to the personal computer through a standard interface RS 232. With the help of a specialized software application, the values of the solar radiation are stored in a database and can be visualized in real time as well as for a past period.

## Materials and methods

Preliminary investigations show that the temporary sequence of direct solar radiation (H) values obtained should be viewed as a stochastic process, which does not contain a development trend [4]. The maximal value of the mean solar radiation for the month of June is 711,5 MJ.m<sup>-2</sup> which is 72 MJ.day<sup>-1</sup> as shown in Table 1.

**Table 1**  
Integrated values of the solar radiation  $H(t)$ , in  $MJ.m^{-2}$ , for the observed period.

Month	Year			
	2005	2006	2007	Average
January	139,5	138,9	137,5	<b>138,6</b>
February	196,2	202,1	186,5	<b>194,9</b>
March	373,4	366,9	350,2	<b>363,5</b>
April	496,2	495,6	479,1	<b>490,3</b>
May	620,8	683,4	645,4	<b>649,9</b>
June	679,1	726,3	729,0	<b>711,5</b>
July	703,4	495,0	775,1	<b>657,8</b>
August	600,9	687,1	571,5	<b>619,8</b>
September	380,9	473,8	506,4	<b>453,7</b>
October	306,1	345,4	232,8	<b>294,8</b>
November	109,8	233,1	125,3	<b>156,1</b>
December	113,4	147,5	85,7	<b>115,5</b>
<b>Average</b>	<b>393,3</b>	<b>416,3</b>	<b>402,0</b>	

The big difference in the integrated monthly values of the solar radiation is confirmed by estimating the sample range of the monthly value of  $H(t)$  in the one year extract by

$$(1) \quad R = \bar{H}_{\max} - \bar{H}_{\min} = 596 \text{ MJ.m}^{-2},$$

where  $R$  is the sample range of the monthly value of the  $H(t)$ ;

$\bar{H}_{\max}$  - the maximal value of the solar radiation from column 4 of Table 1;

$\bar{H}_{\min}$  - the minimal value of the solar radiation.

This confirms the fact for the uneven distribution of the direct solar radiation for the region of Ruse through the different months. It can be seen that the deviation of the measured values for the different months is relatively steady around the determined mean monthly values for the investigated period, i.e. no essential differences in the

solar radiation levels are being observed. On the other hand are observed proportional values for the summer months (from may to august) and for the winter months (from November to February) and the ratio of the solar radiation levels is about 5-6 times. That's why it is important to know the maximal duration and repeatedness of the measured values.

That's why it is important to determine a suitable statistical indexes, which will help to make a suitable analysis. For this purpose the coefficients of the shape  $K_S$  and the load  $K_L$ , can be used:

$$(2) \quad K_S = \frac{H_{MS}}{\bar{H}}; \quad K_L = \frac{\bar{H}}{H_{\max}},$$

$$\text{where } H_{MS} = \sqrt{\frac{H_1^2 \Delta T_1 + H_2^2 \Delta T_2 + \dots + H_{12}^2 \Delta T_{12}}{\sum_{i=1}^{i=12} \Delta T_i}}$$

is the mean square of the solar radiation;

$\sum_{i=1}^{i=12} \Delta T_i$  - the duration of the time interval;

$$\bar{H} = \frac{\sum_{i=1}^{i=12} H_i}{12} \text{ - the mean value;}$$

$H_{\max}$  - the maximum observed value.

The annual coefficient of the shape  $K_S$  is 1 if the solar radiation is constant through the period observed, i.e. it characterizes the irregularity of the process. For its better physical research corresponding monthly coefficients are suggested.

## Results and discussion

The determination of the values of the coefficients  $K_S$  and  $K_L$  has been accomplished on the basis of mean values by months for the observed period (see Table 2).

When  $K_S$  is closer to 1, the deviation of the solar radiation levels is smaller than the mean yearly values (see Fig.2). The analysis of figure 2 shows that even the smallest deviations are observed during the summer months and the biggest – during the winter months. This is explained by the fact that the summer months have the biggest impact on the mean yearly values of the solar radiation (see the last row of Table 1).

**Table 2**

Values of the coefficients of the shape  $K_S$  and the load  $K_L$  for the different months

	Jan	Feb	Mar	Apr	May	Jun	Jul	Aug	Sep	Oct	Nov	Dec
$K_S$	1,04	1,02	1,02	1,03	1,01	1,00	1,00	1,02	1,05	1,07	1,08	1,05
$K_L$	0,65	0,74	0,74	0,74	0,80	0,82	0,86	0,78	0,69	0,57	0,61	0,64

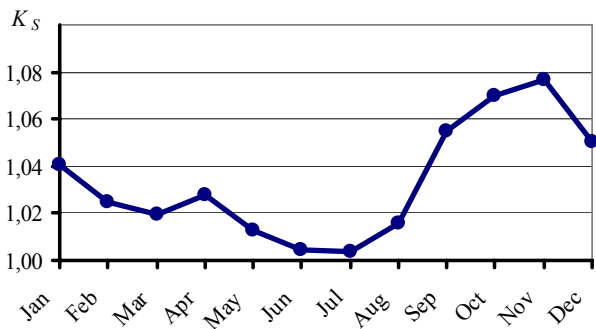


Fig.2. Variation of  $K_S$  through the different months of the year.

This trend is confirmed by certain month daily values of the direct solar radiation (see Fig. 3). Through the months April, May, June, July and August,  $K_v = (1,0 - 1,02)$ , i.e. the unevenness of the solar radiation is very limited ( $\bar{H} = 16,3 - 24,1 \text{ MJ.m}^{-2}$ ). These values, combined with the rest factors, as duration of the Sun shining, transparency of the atmosphere and others, allows to effectively use the PV systems.

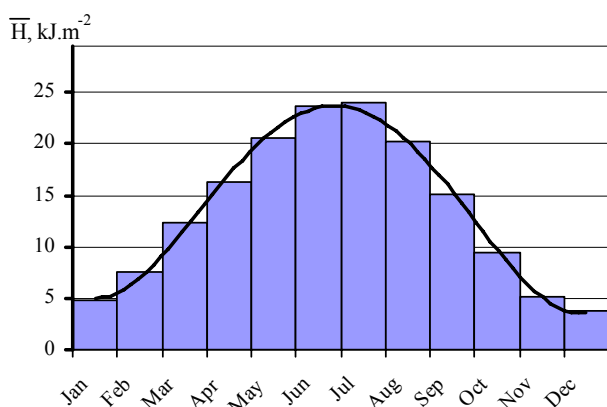


Fig.3. Mean monthly values of direct solar radiation.

The maximal values of the solar radiation, reaching a perpendicular surface, for the observed period, have been registered between 22 of May and 10 of June. Usually during a cloudless sunny day, they vary in the interval  $(1,02 - 1,1) \text{ kW.m}^{-2}$  from 12:00 to 14:00. The fact that the maximal ray of solar radiation is a little earlier than the summer, can be explained with the fact that the transparency of the atmosphere in May and June is better.

The coefficient of load  $K_L$  allows to perform different technical and economical analyses when designing a PV system. It is defined by equation (2) and presumes knowledge about the maximal monthly of  $H(t)$ . By

calculating this coefficient, is obtained information about the expected value of a given random variable ( $H$ ) getting closer to the maximal value. The  $K_L$  values vary from 0 to 1. The bigger  $K_L$  is, the better the chance to work with maximal solar radiation level.

On Fig.4 is shown the variation of  $K_L$  for the observed period. It can be seen that from May to August (inclusive)  $K_L \geq 0,8$ , which means that for this period there is a very good evenness of the solar radiation levels.

With the help of the coefficient of load  $K_L$  can be determined the maximal duration of usage  $T_m$ , in days, of the solar radiation for a given period of time, using the following formula:

$$(3) \quad T_m = K_L \cdot N,$$

where  $N$  is the duration of the period, days.

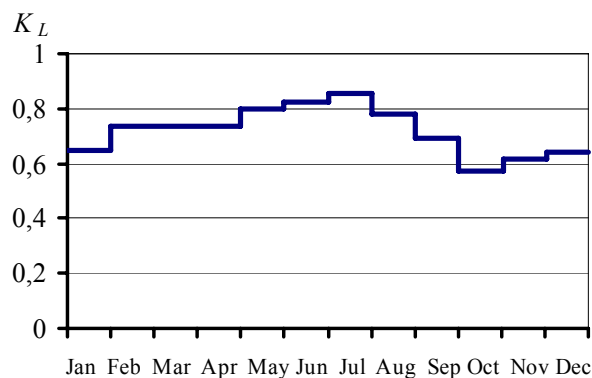


Fig.4. Variation of  $K_L$  for the observed period.

In Table 3 are given the calculated values of  $T_m$  for the different months of the year.

It can be seen that longest duration of usage of the PV installations can be made for the months May, June, July and August. For example for July  $T_m = 26,6$  days. The maximal value of the daily integrated solar radiation is  $H_{\max} = 28,1 \text{ MJ.m}^{-2}$ , i.e. the PV installation will be loaded on maximum for 26, 6 days.

Table 3

Values of the coefficients of the shape  $K_S$  and the load  $K_L$  for the different months

	Jan	Feb	Mar	Apr	May	Jun	Jul	Aug	Sep	Oct	Nov	Dec
$K_L$	0,65	0,74	0,74	0,74	0,80	0,82	0,86	0,78	0,69	0,57	0,61	0,64
$N$ , days	31	28	31	30	31	30	31	31	30	31	30	31
$T_m$ , days	20,1	20,6	22,8	22,2	24,7	24,6	26,6	24,2	20,7	17,8	18,4	19,9

It is a matter of interest to determine the maximal yearly usage of the PV installations (see Fig. 5).

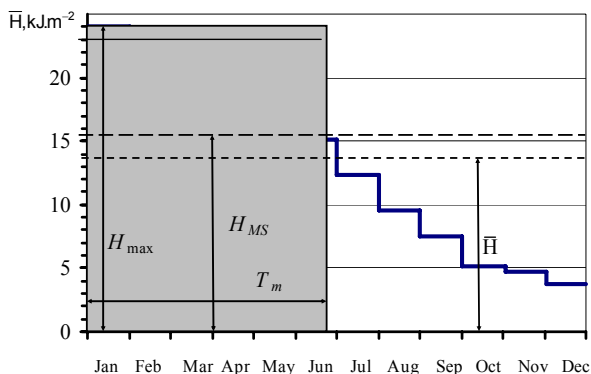


Fig. 5. Arranged diagram of the process  $H(t)$  for the observed period.

The yearly coefficient of load  $K_L$  for the observed period is 0,56. For a year with 365 days and  $\bar{H}_{\max} = 24,1$  MJ.m<sup>-2</sup> (for July – see figure 3), the maximal yearly expected usage of the PV installation is  $T_m = 205,9$  days, which corresponds to 6,8 months.

### Conclusion

It has been determined that there is a essential difference in the levels of solar radiation (about 5-6 times) for the different months for the region of Ruse. It is suggested to us the coefficients of load and form for analysis of the solar radiation levels.

The maximal duration of usage of the solar radiation by months has been estimated. The longest usage is for July – 26,6 days, and for a year it is 205,9 days.

These values can be used when designing installations, using solar energy.

### References

- [1] Лингова, Ст. Слънчева радиация. Българо-английско дружество Пъблиш-Сай-Сет-Агри ООД, София, 1995, 213 с.
- [2] Стоянов, И., Н. Михайлов. Изследване динамиката на годишната слънчева радиация в град Русе. Научни трудове РУ'2005, том 44, серия 3.1, секция "Електротехника, електроника и автоматика", Русе, 2005, стр. 172-177.
- [3] <http://bg.wikipedia.org/wiki/Облак>.
- [4] Mihailov N., I. Stoyanov. Evaluation of the Sunny Energy Potential for the Area of Rousse, The International Conference on Electrical Machines and Power Systems (ELMA 2005), 15-16 September, Sofia, Bulgaria, 2005., pp. 411-414.
- [5] Pyranometer CM 11, Manual, Kipp & Zonen.

### Biographies



**Ivaylo Stoyanov** was born in Ruse, Bulgaria, on August 23, 1969. He studied at the University of Ruse - Bulgaria and received Dr. degree from the same university in 2005.

Since 1996 he worked in the Faculty of Electrical and Electronic Engineering of the University of Ruse as a Lecturer and researcher in the field of renewable energy sources and LV electrical installations.

Ivaylo Stoyanov is with the Faculty of Electrical and Electronic Engineering, Department, Electrical Power Engineering, University of Ruse, 8, Studentska Street, 7017 Ruse, Bulgaria (e-mail: [stoyanov@ru.acad.bg](mailto:stoyanov@ru.acad.bg)).



**Nicolay Mihailov** was born in Ruse, Bulgaria, on November 27, 1947. He graduated from the University of Ruse, and received Dr. degree from the same university in 1983.

His field of interest includes renewable energy sources (electrical aspects), electrical materials and engineering technologies in the agriculture. He is today an associated professor in the Faculty of Electrical and Electronic Engineering of the University of Ruse.

Nicolay Mihailov is with the Faculty of Electrical and Electronic Engineering, Department Electrical Power Engineering, University of Ruse, 8, Studentska Street, 7017 Ruse, Bulgaria (e-mail: [mihailov@ru.acad.bg](mailto:mihailov@ru.acad.bg)).



# Determination of the Electrical Energy, Obtained From Direct Transformation of Solar Energy from a PV Generator

Ivaylo Stoyanov

**Abstract:** The amount of generated energy from one PV module depends on a number of factors like the type of the electrical load, the meteorological conditions, the time frame of usage etc. In this study is proposed a way to determine the optimal regime of a PV module by its P-A characteristic. The obtained results can be used for optimization of the characteristics and the parameters of autonomous PV systems.

**Keywords:** Photovoltaic Panels, Optimal Tilt Angle, .

## Introduction

The home solar system (HSS) is the most used conception for electrification of remote regions. Through them the consumer receives about (150 ... 250) Wh, depending on its location [3, 9, 10]. In the systems for home electrification of remote regions, their power doesn't surpass the HSS ones, but their energy is generated centrally and is being spread through the local electrical grid [7,6]. This way is being ensured more power for the individual consumers, which allows to use more consumers. The optimal sizing and the choice of the power system depends mostly on the power of the load, the meteorological conditions, the time frame for its usage etc. The size of the PV generator should be conformed with the energy consumption and the solar radiation in the most unfavorable month of the year – January. The PV generator in a HSS usually consists of 1-2 PV modules, 32 to 40 cells each (usually 36). Such standard modules are used for charging of an accumulator battery with the help of a charging controller. Depending on the size and the technology, each PV modules generates 40-120 W in optimal conditions: direct solar radiation  $H = 1000 \text{ W.m}^{-2}$  and temperature of the modules - 25 °C.

On the other hand most of the home electrical devices are intended for  $U_n = 230 \text{ V}$ ,  $f = 50 \text{ Hz}$ , and the PV generators are DC sources, which means the stored DC energy in the accumulator should be transformed to AC with the use of an inverter. One typical HSS for basic electrification consists of the following elements (fig. 1): PV generator, accumulator battery, charge generator and directly connected DC consumers [4].

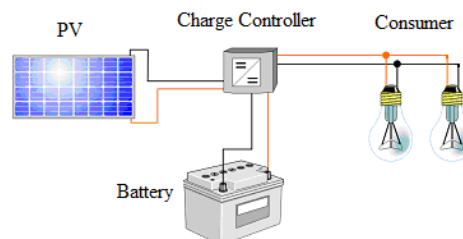


Fig.1. Typical configuration of a HSS.

The maximal effectiveness is about 15% for modules from single-crystal silicon PV cells, and about 12% - for modules from polycrystalline silicon PV cells. The obtained electrical energy depends mainly on the level of solar radiation, the temperature of the PV cell and the angle of the module towards the sun.

The goal of this study is to determine the electrical energy, obtained from an autonomous solar system in optimal work conditions of the PV modules.

## Materials and methods

In order to achieve the goals of the study, has been carried out measurements in the area of the University of Ruse, situated at 43°49'22" northern latitude and 26°1'19" eastern longitude. They have been carried out with the help of a specialized measuring system, which consists of two single-crystal silicon PV modules (SunSet AS110) (see Table 1) [8], installed on the roof of corpus 10 of the University, a specialized charge controller, accumulator battery and consummator – 2 Incandescent lamps (see Fig.2). The values of the current and voltage of the PV generator have been gathered with the help of a USB-6008 modules from National Instruments [5], and of the panel temperature with a DT838 temperature sensor.

Table 1

Parameters of solar generators type AS 110

Описание	Стойност
Максималната мощност, $P_{max}$ , W	110
Номинален ток $I_n$ , A	6,6
Номинално напрежение $U_n$ , V	16,7
Ток на късо съединение $I_{sc}$ , A	7,5
Напрежение на празен ход $U_{oc}$ , V	20,7

One of the PV modules is with a fixed angle 43°, and the second one is equipped with a following system.

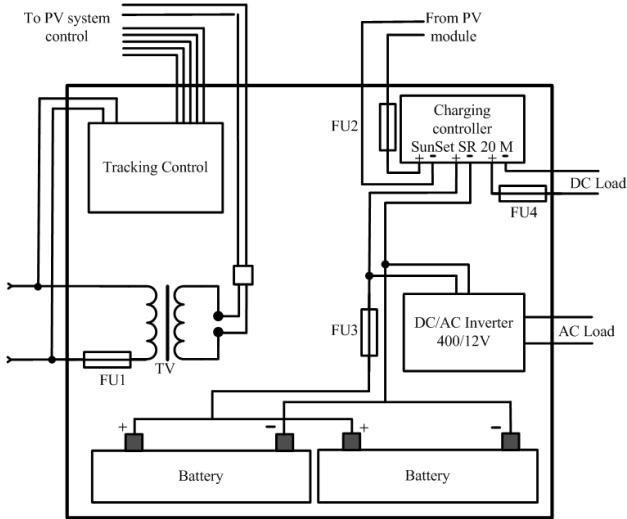


Fig. 2. Block-scheme of the experimental equipment

Simultaneously have been carried out measurements of the direct radiation level  $H$ , in  $W \cdot m^{-2}$ .

The electrical energy obtained from a PV module can be calculated according to [1]:

$$(1) \quad E_{PV} = H(\beta)S\eta_{PV}(1-\rho)k,$$

where  $E_{PV}$  is the electrical energy, obtained from a PV modules, Wh;

- $H$  - the direct solar radiation,  $W \cdot m^{-2}$ ;
- $\beta$  - the angle of the PV module, towards the horizon,  $^\circ$ ;
- $S$  - the surface of the PV generator,  $m^2$ ;
- $\eta_{PV}$  - the efficiency of the PV modules;
- $\rho$  - the coefficient of the loses caused by the conductors;
- $k$  - the coefficient of the difference between the optimal and actual work point of the PV modules.

The coefficient  $k$  is being determined from the (A-V) characteristic of the used PC module (see Fig.3).

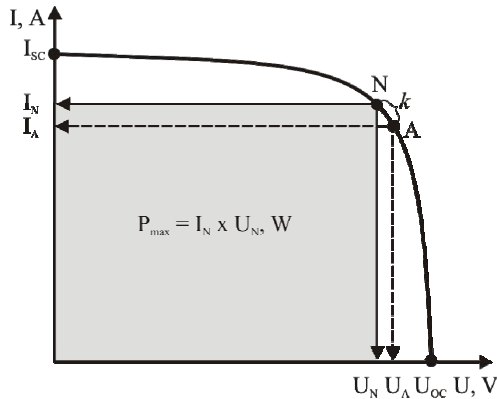


Fig.3. Block-scheme of the experimental installation

Reduction of the coefficient  $k$  can be achieved by mathematical interpolation of the I-V characteristic, for obtaining the optimal work point and alteration of the parameters of the PV system (the angle) with the help of the following system.

It is known that the generator current  $I$  of a PV cell can be determined with good accuracy from [2]

$$(2) \quad I = I_{SC} - I_{SI} \left( e^{\lambda U_i} - 1 \right) - I_L,$$

where  $I_{SC}$  is the short circuit current of the cell, A;

$I_{SI}$  - the diode reverse saturation current, A;

$I_L$  - the current from nonequilibrium carrier, A;

$\lambda$  - a coefficient, which depends on the value of the elemental charge  $q$  and the radiated

thermal energy  $kT$  ( $\lambda = \frac{q}{kT}$ );

$k$  - the Boltzmann constant;

$T$  - the thermodynamic temperature, K.

In order to determine the optimal work point  $N$ , showed on figure 3, for every module (i) is determined the coordinates  $I_{Ni}, U_{Ni}$ , for which the obtained output power is maximal.

$$(3) \quad I_{Ni} = I_{Li} \left( 1 - \frac{1}{\lambda U_{Ni}} \right);$$

$$(4) \quad U_{Ni} = U_{OCi} - \frac{1}{\lambda} \ln(1 + \lambda U_i),$$

where  $U_{OCi}$  is the open circuit voltage of the [i] PV cell, V.

The extreme value of the voltage  $U_{Ni}$  is given in a hidden way. The evaluation of this parameter can be made after breaking down equation (4) in formal power series:

$$(5) \quad U_{Ni} \approx \frac{2}{3} U_{OCi},$$

which leads to

$$(6) \quad U_{Ni} = U_{OCi} - \frac{1}{\lambda} \ln \left( 1 + \lambda \frac{2}{3} U_{OCi} \right).$$

A PV generator consists of  $n$  elements, which are connected together. When consecutively connected the output voltage of the PV generator can be calculated as an algebraic sum of the voltages  $U_i$  of the different elements:

$$(7) \quad U_{PV} = \sum_{i=1}^{i=n} U_i.$$

Analogous the open circuit voltage is:

$$(8) \quad U_{PVoc} = \sum_{i=1}^{i=n} U_{OCi}.$$

If the characteristic of the different elements are harmonized, then:

$$(9) \quad U_{PV} = nU_i;$$

$$(10) \quad U_{PVoc} = nU_{OCi}.$$

Then the optimal work point of the PV generator is:

$$(11) \quad I_N = I_L \left( 1 - \frac{3}{2\lambda U_{PVoc}} \right);$$

$$(12) \quad U_N = U_{PVoc} - \frac{1}{\lambda} \ln \left( 1 + \frac{2}{3} \lambda U_{PVoc} \right).$$

The determined optimal values of the current and voltage from equations (11) and (12) are based on the I-V characteristic of the PV generator, obtained from a certain level of solar radiation.

## Results

The mathematical models and their equivalent schemes, used for simulation of different work regimes don't give precise description of the processes in a PV generator. This is explained with a number of assumptions and limitation of their usage. For example on figure 4 is shown a dependency between the voltage and the output power of the pV generator for level of the solar radiation  $H = 920 \text{ W.m}^{-2}$ . These values are from a cloudless sunny day (23.06.2006). It can be seen that depending on the size of the load, connected to the PV generator, the values of the current, voltage and the generated power vary. The normal work range can be easily determined from the graphic (the marked area) for the specific occasion. The optimal work point N corresponds to the maximum of the generated power in the marked area.

The accounted values for the most effective regime of the PV generator differ a little from those on table 1, because the last describe the process for solar radiation level  $H = 1000 \text{ W.m}^{-2}$ . It is also seen that the smallest deviation from the optimal work regime leads to significant reduction of the generated power and the PV system as a whole.

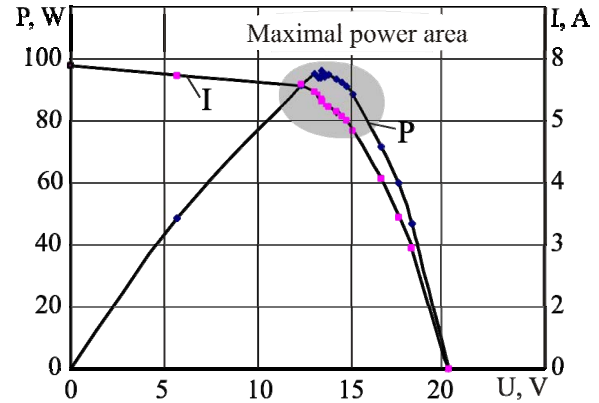


Fig.4. Power characteristics of a PV generator for a cloudless sunny day and solar radiation level  $H = 920 \text{ W.m}^{-2}$

The shown information is describing a small interval of time.

More interesting is the dynamics of the process in time (see Fig.5).

For a cloudless sunny day the variation of the direct solar radiation in time is in a parabolic dependency, corresponding to the Sun azimuth (see Fig.5, a). The maximal values are observed between 12,30 and 14,40 h. The registered deviations of the solar radiation are caused by the small cloudiness for small intervals of time.

On Figure 5,b is shown the variation of the temperature of the PV generator. It increases constantly and about 9:00 reaches a steady value – the working temperature (about  $45 \text{ }^\circ\text{C}$ ), which remains unchanged in time for the most of the day with accuracy  $\pm 5 \text{ }^\circ\text{C}$ . The decrease in the temperature of the PV modules can be explained with the decreased level of solar radiation and the wind.

On Fig.5,c is presented the variation of the DC power  $P$ , in W, at the outputs of the PV generator, which is passed on to the charge controller. It is calculated according to:

$$(13) \quad P = UI.$$

The moment values of the power are with a discretion of  $\Delta t = 10 \text{ min}$ . The dependency has similar alteration to the one of the solar radiation level. The maximal power at the outputs of the PV panel is from 9,30 to 18,30 h. Its value varies in the (80 ... 98,32) W interval and remains relatively steady in time.

This is caused by the fact that the generated power depends on the solar radiation level (when the radiation increases so does the power), as well as the temperature of the panel (when the temperature decreases the power increases).

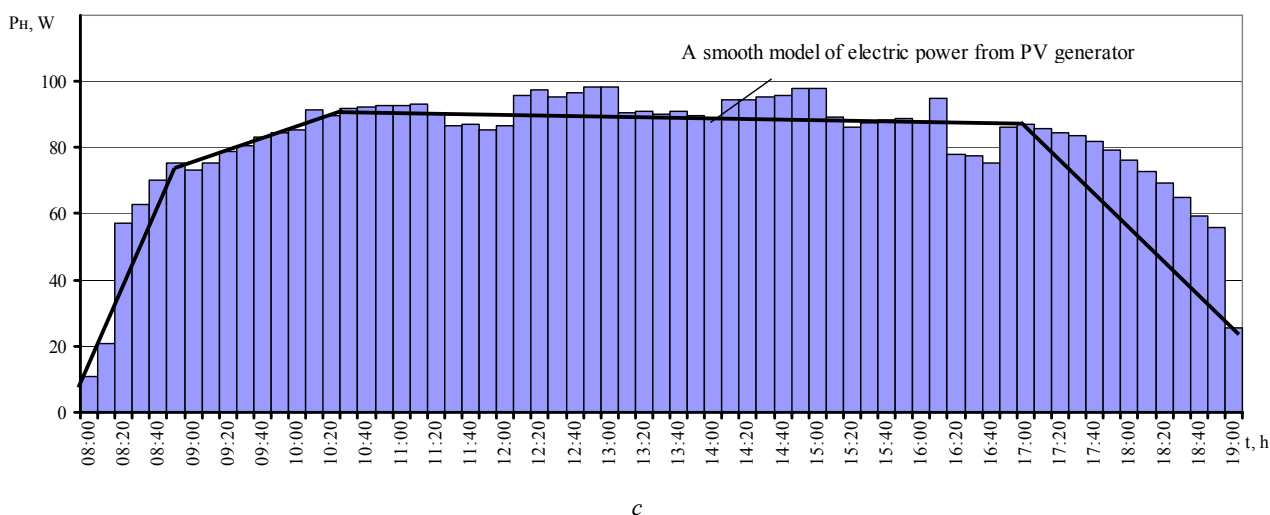
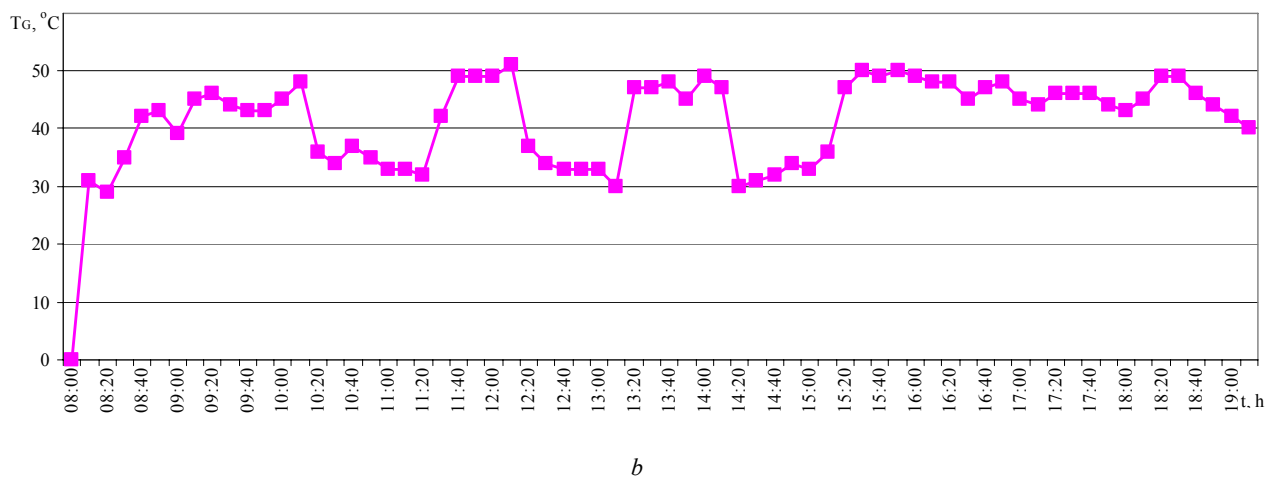
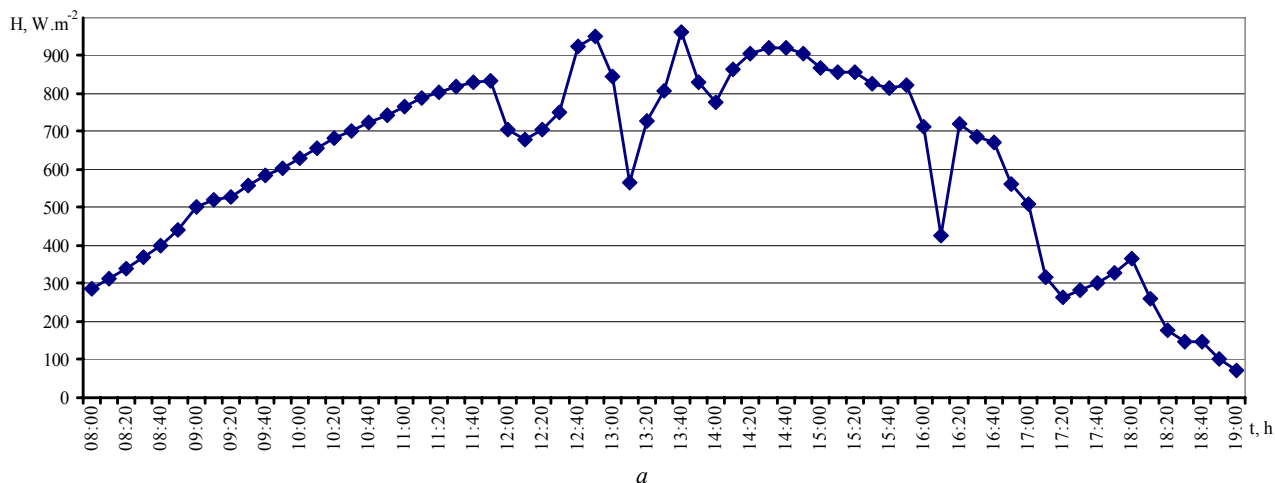


Fig.5. Dynamics of the direct solar radiation (a), the temperature of the PV module (b) and the generated power with optimal angle (c) from a AS 110 PV generator on 07.06.2008 z.

The power characteristic can be described as a trapezium (figure 5,c). This helps to easily determine the generated energy from a PV generator (it corresponds to the surface of the trapezium).

It can be also determined by equation (1) or by:

$$(14) \quad E_{pV} = P.t = \sum p_i \Delta t ,$$

where P is the integrated power from the PVS, W;

$p_i$  - the mean power for the i interval of discretion, W.

When comparing the obtained power from PVS with and without a following system, is seen that the presence of such system increases the power significantly for a long period of the day (see Fig.6).

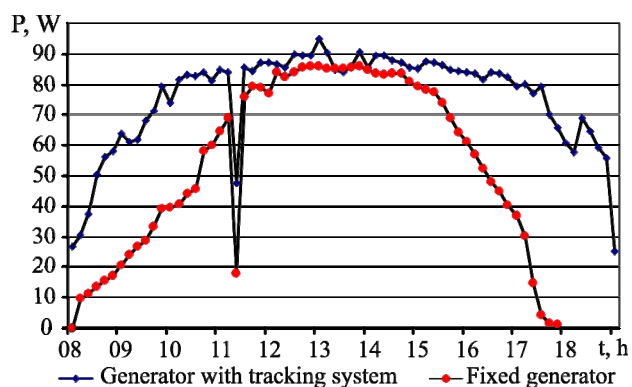


Fig.6. Comparison between the PV generator power with and without a following system.

The power variation is similar but when a following system is available the generated power is significantly more, especially before and after noon. This is explained by the fact that the fixed systems are installed with angle suitable for the noon Sun, and through the rest of the day the solar rays fall under smaller angle. This leads to reduction in the power and the duration of work of the PV generator. It has been determined that the difference in the energy for different typical days reaches 20-30 % more for the system with a following system.

### Conclusion

It has been proven that the amount of generated energy from a PV generator depends on a number of factors like the type of the electrical load, the time frame of usage etc. A following system is proposed to increase the effectiveness of the PV generator. They can lead to a 20-30% incensement in the generated power from a PVS.

The obtained results can be used for optimization of the working characteristics and parameters of autonomous PV systems.

### References

- [1] Карабанов, С., В. Симкин. Преобразование энергии солнечных модулей. Международная конференция Возобновляемая Энергетика 2003, 4-6 ноября, Санкт-Петербург, 2003, pp. 225 – 230.
- [2] Карабанов, С., Ю. Кухмистов, Ю. Россия. Расчет наземных фотоэлектрических систем с использованием метеорологических данных. Международная конференция Возобновляемая Энергетика 2003, 4-6 ноября, Санкт-Петербург, 2003, pp. 219 – 224.
- [3] Agüera, A. López , I. Fernández Otero, R. Martínez Farreres and I. Rodríguez Cabo. Quality check protocol for control the losses of power on large associations of photovoltaic generators. International Conference on Renewable Energies and Power Quality (ICREPQ'07), Sevilla, Spain, 28 – 30 March, 2007, [www.icrepq.com/icrepq07/293\\_fernandez.pdf](http://www.icrepq.com/icrepq07/293_fernandez.pdf).
- [4] Fraunhofer Institute for Solar Energy Systems ISE, Freiburg, Germany.
- [5] <http://sine.ni.com/nips/cds/view/p/lang/en/nid/14604>.
- [6] <http://solar.sharppusa.com/solar/home/0,2462,,00.html>.
- [7] <http://www.sungevity.com>.
- [8] <http://www.sunset-solar.de>.
- [9] Messenger, R. A. and J. Ventre. Photovoltaic Systems Engineering – Second Edition. Taylor & Francis e-Library, 2005.
- [10] Zадde, B. Nikitin, S. Strebkov. PV System for domestic appliance in Russia. 7<sup>th</sup> International conference on Solar energy at high latitudes, NorthSun'97, June 9-11, Espoo-Otaniemi, Finland, 1997, pp. 250 – 254.

### Biographies



**Ivaylo Stoyanov** was born in Ruse, Bulgaria, on August 23, 1969. He studied at the University of Ruse - Bulgaria and received Dr. degree from the same university in 2005.

Since 1996 he worked in the Faculty of Electrical and Electronic Engineering of the University of Ruse as a Lecturer and researcher in the field of renewable energy sources and LV electrical installations.

Ivaylo Stoyanov is with the Faculty of Electrical and Electronic Engineering, Department, Electrical Power Engineering, University of Ruse, 8, Studentska Street, 7017 Ruse, Bulgaria (e-mail: [stoyanov@ru.acad.bg](mailto:stoyanov@ru.acad.bg)).



# Current Hour Consumption Forecast

Rositsa Angelova, Todor Gichev and Galina Cherneva

**Abstract:** This paper examines the task of forecasting the electricity consumption for the next hour at the end of every hour for twenty-four hours. Using the algorithm presented, a forecast has been prepared for the current hour consumption during a week.

**Keywords:** forecasting, power consumption, calculation

## Introduction

With forecasting the electric power consumption in the Republic of Bulgaria, it is possible to formulate different problems. One of them is to look for the forecast month consumption during next month at the end of every month. The second problem is to forecast the average hour consumption for the days of the forthcoming month at the end of every month. The third problem that can be assigned is to determine the consumption for the next hour at the end of every hour during a 24-hour period. The present paper is dedicated to a solution of that problem. First, the real hour consumption on the days of a week is analysed. On that basis, a corresponding previous day is determined for each day of the week. The formalized algorithm to find out the current consumption for a given day uses the information about the hour consumption for the corresponding previous day. The real and forecast consumptions for the days of one week calculated by the algorithm suggested are given at the end of the paper. The data of the real hour consumptions have been taken from the website of the Electric Power System Operator EAD.

## 1. Analysis of hour consumption for 24 hours.

Some peculiarities of the hour consumption can be seen from the diagram of the consumptions for the days of a week. The diagrams of the consumptions during the week from 7 to 13 July 2008 are built in Fig. 1. From it, one can see that the hour consumptions for Tuesday, Wednesday, Thursday and Friday are of a similar nature. The consumptions during the rest of the week, on Monday, Saturday and Friday, are more specific. For that reason, for the needs of the algorithm further formulated, we have determined the corresponding previous day for each day of the week under examination in Table 1. It is convenient to begin counting the hours in a 24-hour period at 21:00 of the previous evening. In this way, the examined hours 0:00, 1:00, 2:00, 3:00 at night are understood as real hours of the previous day: for Monday those are the hours of last Sunday, for Tuesday they are the hours of last Monday, etc. The two ways of counting the real hours, beginning from 21:0, and the substituted ones, beginning from 0:00, are marked along the abscise axis in Fig.1.

To restore the continuity of the hour consumption during a 24-hour period that is interrupted by the change of time in autumn and spring, it is necessary to accomplish displacement of hours with one ahead from the day of the change in October to the day of the second change in March when we return back to normal numbering.

**Table 1**

*Previous day*

Day of the current week	Previous day
Monday	Monday of the previous week
Tuesday	Friday of the previous week
Wednesday	Tuesday of the current week
Thursday	Wednesday of the current week
Friday	Thursday of the current week
Saturday	Saturday of the previous week
Sunday	Sunday of the previous week

Once again, due to convenience in the further considerations, the set of hours during a 24-hour period will be divided into two parts. The set  $\Delta_1$  includes the hours from 0:00 to 14:00 (according to the newly introduced counting) and the set  $\Delta_2$  includes the rest of hours, from 14:00 to 24:00. For each of those sets  $\Delta_i$ ,  $i=1,2$ , the consumptions  $W(t)$  can be approximated according to the method of the smallest squares with a polynomial of the fourth power:

$$(1) \quad W_{0i}(t) = a_i + b_i t + c_i t^2 + d_i t^3 + e_i t^4, \quad t \in \Delta_i.$$

The coefficients of polynomials  $W_{01}(t)$ ,  $W_{02}(t)$  for  $\Delta_1$  and  $\Delta_2$  for Wednesday (09.07. 2008) are given in Table 2.

The diagrams of the real consumptions  $W(t)$  and the values of polynomials  $W_{01}(t)$ ,  $W_{02}(t)$  for  $t \in \Delta_1$  and  $t \in \Delta_2$  are built in Fig.2.

**Table 2**

*The coefficients to the polynomials  $W_{01}(t)$ ,  $W_{02}(t)$  for 09.07.2008*

	$\Delta_1$	$\Delta_2$
$a_i$	4518,1348	-34637.2726
$b_i$	127,728	8066.2377
$c_i$	-94,8118	-610.1037
$d_i$	11,054021	21.029137
$e_i$	-0,358651	-0,265734
$\varepsilon_i$	32,51	6.769

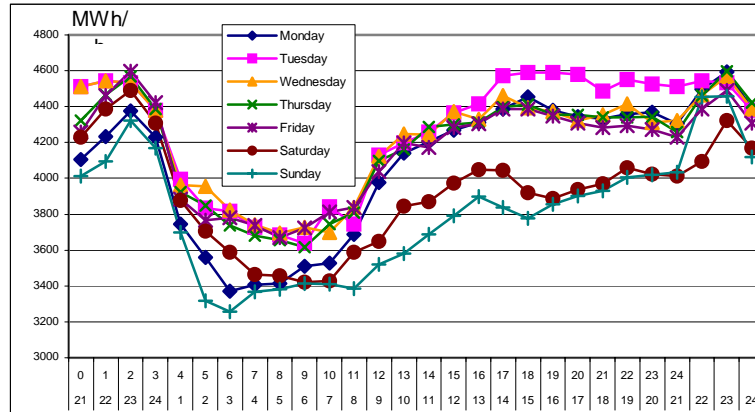


Fig.1. The consumptions during the week from 7 to 13 July 2008.

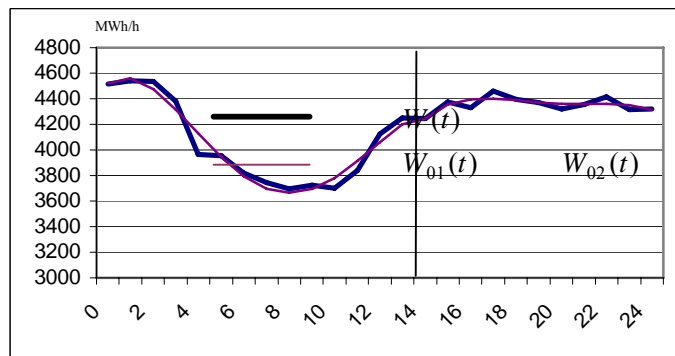


Fig.2. The real consumptions  $W(t)$  and the values of polynomials  $W_{01}(t)$ ,  $W_{02}(t)$  for  $t \in \Delta_1$  and  $t \in \Delta_2$

Table 3

Results of numerical experiments

t	14.07 Monday		15.07 Tuesday		16.07 Wednesday		17.07 Thursday		18.07 Friday		19.07 Saturday		20.07 Sunday	
	W(t)	$W_0(t)$	W(t)	$W_0(t)$	W(t)	$W_0(t)$	W(t)	$W_0(t)$	W(t)	$W_0(t)$	W(t)	$W_0(t)$	W(t)	$W_0(t)$
0	4034	4092	4364	4277	4307	4378	4287	4368	4250	4293	4294	4229	4168	3984
1	4456	4301	4598	4527	4473	4613	4446	4415	4501	4461	4545	4455	4299	4281
2	4457	4356	4661	4513	4444	4547	4459	4316	4573	4416	4446	4453	4304	4262
3	4120	4180	4469	4345	4165	4283	4247	4149	4351	4235	4342	4245	4114	4026
4	3703	3872	3958	4113	3770	3970	3786	3969	3910	3971	3895	4004	3837	3739
5	3451	3597	3652	3897	3663	3718	3677	3785	3619	3717	3767	3760	3678	3526
6	3406	3373	3625	3693	3706	3571	3504	3652	3555	3489	3621	3574	3569	3438
7	3475	3295	3579	3572	3675	3519	3440	3533	3492	3396	3597	3451	3498	3411
8	3504	3336	3557	3564	3632	3548	3424	3506	3450	3416	3609	3427	3576	3387
9	3452	3476	3596	3661	3723	3641	3525	3571	3475	3527	3672	3472	3472	3425
10	3554	3631	3715	3791	3702	3807	3679	3677	3560	3678	3774	3600	3471	3464
11	3817	3809	3878	3914	3764	3941	3798	3850	3750	3815	3747	3736	3433	3501
12	4008	3918	4102	3995	4028	4013	3977	3994	4041	3935	3756	3624	3496	3468
13	4159	4233	4229	4174	4185	4196	4111	4182	4165	4107	3920	3805	3627	3554
14	4253	4215	4247	4226	4229	4298	4179	4215	4214	4202	3903	3961	3724	3739
15	4313	4294	4375	4292	4252	4385	4250	4238	4340	4258	4012	4000	3866	3814
16	4444	4354	4464	4355	4226	4402	4304	4245	4429	4316	4059	4003	3947	3854
17	4506	4409	4509	4401	4273	4389	4292	4249	4528	4349	4034	3977	3892	3853
18	4492	4435	4452	4413	4165	4368	4330	4223	4506	4388	3997	3949	3873	3854
19	4547	4424	4432	4396	4209	4312	4306	4238	4429	4398	3917	3959	3786	3883
20	4468	4434	4354	4368	4201	4288	4285	4227	4427	4367	3945	3968	3885	3884
21	4397	4404	4347	4320	4112	4304	4290	4210	4267	4322	3975	3983	4034	3923
22	4450	4366	4343	4284	4218	4285	4239	4244	4336	4242	4083	4006	4114	4009
23	4410	4356	4384	4263	4252	4288	4269	4253	4332	4245	4074	4032	4144	4081
24	4364	4338	4307	4271	4287	4315	4250	4289	4294	4286	4168	4036	4168	4052
$\delta$	0.019		0.017		0.026		0.015		0.018		0.019		0.017	

## 2. Algorithm of current hour consumption forecasting

The problem is to work out the consumption forecast for the hours of a certain day of the week. The algorithm suggested supposes that the consumption data for the previous day according to Table 1 are known. The composition of the forecast begins with the hours of set  $\Delta_1$ . Let  $t_0$  is an hour of that set  $\Delta_1$  and  $t_0 \leq 13$ . The consumptions

$$(2) \quad W(0), W(1), \dots, W(t_0), W(t_0+1), \dots, W(14),$$

are examined where  $W(0), W(1), \dots, W(t_0)$  are the consumptions for the hours of the day examined and  $W(t_0+1), \dots, W(14)$  are the consumptions for the respective hours of the previous day. The consumptions (2) are approximated using the method of the smallest squares with polynomial  $W_{01}(t)$  (1) of the fourth power. The forecast value for the consumption at  $(t_0+1)$  is  $W_{01}(t_0+1)$ . These calculations are accomplished for  $t_0$  from 1 to 13. Further, let  $t_0$  is an hour of set  $\Delta_2$  of the day examined and  $t_0 \leq 13$ .

The conceptions

$$(3) \quad W(14), W(15), \dots, W(t_0), W(t_0+1), \dots, W(24),$$

are examined where  $W(14), W(15), \dots, W(t_0)$  are for the hours of the day under examination and  $W(t_0+1), \dots, W(24)$  are for the respective hours of the previous day. The consumptions (3) are approximated using the method of the smallest squares with polynomial  $W_{02}(t)$  (2) of the fourth power. The forecast value at  $(t_0+1)$  is  $W_{02}(t_0+1)$ . The calculations are accomplished for  $t_0$  from 14:00 to 23:00.

In this way, beginning from Monday, the forecast for the consumptions for all hours of a 24-hour period during a week can be made up. The algorithm described above has used the idea of successive analysis of time lines set in the method of SSA [1].

## 3. Results of numerical experiments.

To check the accuracy of the forecast according to the algorithm described, the consumptions for 24 hours during two weeks, from 7 to 20 July 2008, have been examined. Using the consumptions for 24 hours during the first week, the consumptions for the previous 24-hour periods of the second week, which the forecast is composed for, are determined. The forecasts obtained  $W_0(t)$  and the real consumptions  $W(t)$  in MWh/h are successively given in Table 3 from Monday to Sunday. The average relative errors  $\delta$  written in the last line of the table have been calculated by the formula

$$(4) \quad \delta = \left( \sum_{t=0}^{24} \frac{|W(t) - W_0(t)|}{W(t)} \right) (25)^{-1}$$

## References

- [1] Golyandina, N.E. Method "Гусеница"-SSA: Analysis of Time Lines, Sanct Petersburg, 2004.



**Rositsa Kotseva Angelova** works as associate professor of electrical engineering in the Higher School of Transport "T. Kableshkov", Sofia, from 1999. She is Ph Doctor from 1976 and works in the field of circuits and systems.

Rositsa Angelova is with the Department of Electrical Engineering, Higher School of Transport, 158, Geo Milev Blvd., 1574 Sofia, Bulgaria.

(e-mail: rositsa\_angelova@yahoo.com).



**Todor Rachev Gichev** is professor of mathematics in the University of Architecture, Civil Engineering and Geodesy, Sofia, from 1990. He is Ph Doctor (1973, Moscow University) and Doctor of Mathematical Sciences (1987). He works in the field of mathematical modeling in the economy and the electrical engineering.



**Galina Cherneva** was born in Sofia, Bulgaria, on May 20, 1962. She studied at the Technical University of Sofia-Bulgaria and received PhD degree in 2007.

Since 1986 she worked in the Higher School of Transport "Todor Kableshkov" – Sofia as a Lecturer. Her field of interest includes electric circuits and systems.

Galina Cherneva is with the Department of Electrical Engineering, Higher School of Transport, 158, Geo Milev Blvd., 1574 Sofia, Bulgaria (e-mail: cherneva@vtu.bg).

# Voltage phase angles determination by distributed intelligence

Lazar Petkanchin

**Abstract:** In the article a possibility is investigated for crucial voltage phase angles determination on the basis of available information in the node, i.e. by means of "distributed intelligence".

**Keywords:** Distributed intelligence, Electric Power Systems, Phase angles determination

## Introduction

One of the basic tasks in the area of electric power systems /EPS/ underlying in the European Union seventh framework program is reliability and intelligence improvement, especially by introducing devices and systems with distributed intelligence. These devices and systems are installed in EPS objects. They utilize in real time, local variables /U, I, P, Q/ and special algorithms for observation, signalization and control of the object. Also they can offer the staff decisions for actions. That means they use in real time EPS variables and regimes. These devices and executed algorithms are on the basis of EPS theory. They are based on the contemporary information technology basis. The devices and systems with distributed intelligence have the following advantages: possibility to execute computation and logical operations, only local variables are used, fast actions, higher reliability.

## Voltage Phase Angles as Control Variables

Within each from EPS possible regimes - normal, troubled (before blackout), during blackout and restoring (after blackout), the devices with distributed intelligence could be useful. In the control process of all EPS regimes, voltage phase angles in main nodes are very important variables. Different methods and devices for voltage phase angles determination are used. For some EPS, with high complexity (the contemporary EPS), the question could be raised, which from many voltage phase angles of selected line towards all other EPS nodes is crucial for steady state stability in the time moment considered. Or which from all the EPS nodes is the crucial steady state stability node for voltage phase angle for the line. For example, in transmission system 400 kV, what is the crucial node for the line 400 kV "Otechestvo" in Bulgaria - Portugal substation "Recorei" or some other node? In the general case, the crucial point cannot coincide with a real bus, which requires a new vision on steady state stability. In one big and complex EPS it is possible, during normal regimes, to have some voltage phase angles between different nodes greater than 90 degrees. This also requires local variables to be utilized. The experience of the EPS shows that the most dangerous black outs occurred in case of gradual violation of active

or reactive power balances /steady state stability/. However, during permanent changing of EPS regimes, one can pose the question if the crucial node does not change with the regime changes, i. e. crucial node for the selected line changes in time. Each EPS line will have its own crucial node for a particular regime. Therefore, in EPS there are  $n(n-1)$  crucial points, (assuming that the crucial nodes for two line ends are different and that the crucial point coincides with EPS nodes), where "n" is the number of nodes. Among these many voltage phase angles, we have to determine the maximum voltage phase angle, which is the crucial voltage phase angle for steady state stability. Of course, for different EPS regimes, the crucial angle can be between different nodes. For EPS with hundred nodes,  $n(n-1)$  is equal to 9900 angles, therefore we have to monitor only the important lines for crucial angles.

When in EPS there is considerable percentage of decentralized generation (wind and photovoltaic), that in a short time period could considerably change generation, the preliminary computation of voltage angles and settings of the control automation and emergency controls is difficult and could be incorrect. In such cases, the application of devices with distributed intelligence is the best option. That means we shall use algorithms in real time with local variables for determination of crucial voltage angles.

The article investigates the possibility for estimation of crucial voltage phase angles by devices that use local variables, i.e. the distributed intelligence application is proposed as a proper solution.

According to well known equations the transmitted power through a transmission line is:

$$(1) \quad P = (U_1 U_2 / Z_{12}) \sin \delta_{12};$$

$$(2) \quad I = \Delta U / Z_{12};$$

$$\Delta U = U_1 - U_2$$
$$(3) \quad \Delta U = U_1^2 + U_2^2 - 2U_1 U_2 \cos \delta_{12}$$

where:  $U_1$  and  $U_2$  are the voltage vectors of the both nodes (line sides),  $Z_{12}$  is the impedance between nodes,  $\delta_{12}$  is the phase-angle between  $U_1$  and  $U_2$ .

If we let  $U_1 U_2 / Z_{12} = \text{const} = P_{\text{max}}$ , then  $P = P_{\text{max}} \sin \delta_{12}$ . Obviously, P can be measured through measuring  $\delta_{12}$  and necessary control could be performed, so as to move  $\delta_{12}$  away from the dangerous zone – the vicinity of  $\pi/2$  /rad/, that is often done in practice. The distance between both sides could be considerable. To overcome this difficulty several methods are used – voltage signal transmission from one end to the other end by telemetering, creation of a model and using the measured current through line, to estimate the voltage vector at the opposite end of the line. There are successful experiences for angles measurements by transmission of starting

signal /GPS/ to the nodes of EPS and in relation to this signal the angles between the voltages at the ends of the lines are calculated. Based on these, one could decide about necessary control /place, type and intensity/ to be performed for liquidation of the dangerous state of EPS.

If we assume  $U_1 \approx U_2 = U$ ,

$$(4) \quad \text{then } \Delta U = 2U \sin(\delta_{12}/2) \quad ;$$

$$(5) \quad P = (U^2 \sin \delta_{12}) / Z_{12} \quad ;$$

$$(6) \quad I = \Delta U / Z_{12} = [2U \sin(\delta_{12}/2)] / Z_{12}$$

The voltage errors  $\Delta U_E$  % calculated according to the expression  $\Delta U_E \% = \{(\Delta U [4] - \Delta U [3]) / U_n\} 100$ ; by  $U = 1$  p.u., are less than 3% for voltages from 0,95 to 1,05 and angles  $\delta_{12}$  from  $0^\circ$  to  $70^\circ$ . Angle  $\delta_{12}$  changes much more (hundreds of percent - for example  $10^0 \div 40^0$ ) than the voltage between (5%÷10%), i.e. the dependence is much more sensitive to the angle changes.

$$(7) \quad \text{According to (5) } dP/d\delta_{12} = (U^2 \cos \delta_{12}) / Z_{12} \quad ;$$

$$(8) \quad \text{According to (6) } dI/d\delta_{12} = [U \cos(\delta_{12}/2)] / Z_{12} \quad .$$

By dividing we obtain:

$$(9) \quad dP/dI = (U \cos \delta_{12}) / \cos(\delta_{12}/2) \quad .$$

From (9) for different  $\delta_{12}$  values we can compute  $dP/dI$ . by  $U = 1$  p. u., for selected angles they are given in table 1.

**Table 1**

$\delta_{12}$ /degrees/	1	10	30	50	70	90
dP/dI	0,999	0,9875	0,8965	0,709	0,417	0

The derivatives  $dP/d\delta_{12}$  and  $dI/d\delta_{12}$  can not be estimated on the spot, because  $\delta_{12}$  can not be measured on the spot.

For  $dP/dI$  determination, we can use the derivatives  $dP/dt$  and  $dI/dt$ . They can be measured on the spot. Then it is possible to determine the quotient  $(dP/dt):(dI/dt) = dP/dI$ . To avoid division by zero when  $dI/dt = 0$  we have to take appropriate measures.

This quotient between values determined on the spot, will be denoted by "R" -  $R = dP/dI$ . Then (9) becomes:

$$(10) \quad R = (U \cos \delta_{12}) / \cos(\delta_{12}/2) \quad .$$

To determine  $\delta_{12}$  we have to solve transcendental equation:

$$(11) \quad R \cos(\delta_{12}/2) - U \cos \delta_{12} = 0 \quad .$$

The angle  $\delta_{12}$  defined above will be referred to as "local crucial phase angle /LCPA/".

## Results

During normal regimes, when the current and power do not change, nevertheless the derivatives  $dP/dt$  and  $dI/dt$  can be obtained. Always there are small random swings into  $\delta_{12}$ , P and I, therefore the derivatives for the respective regime can be measured.

In fig. 1 is shown, obtained by model,  $d(P+n)/d(I+n)$  - (2), P - (1), I - (3), for constant P and I, and with available noises "n"- (4).

In fig. 2 are shown graphics of equations [5] and [6], power - (1) and current - (2). Steady state stability is violated behind  $dP/d\delta < 0$  behind  $\delta > 0$ . Dangerous zone

is around  $90^\circ$  then  $dP/d\delta = \xi$  at  $dI/d\delta \neq 0$  - therefore  $dP/dI \approx 0$ , what is used for signaling crucial regimes,  $\xi$  is a small number which is chosen preliminary.

In fig. 3 a graphical example is shown of equation (11) for  $R = 0,709$  at  $U = 1$  p. u. (2) -  $R \cos(\delta_{12}/2)$  and (1) -  $U \cos \delta_{12}$ . The cross point is the solution  $\delta_{12} \approx 50$  degrees.

In table 2, results of model investigations at constant current, power and voltage phase angle plus Gaussian or white noises are shown. Results by model investigations for  $dP/dI$  measurement, according to table 2, compared to computed at  $U = 1$  p. u. of  $dP/dI$  in table 1, show errors below 1 %.

**Table 2**

$\delta_{12}(^\circ)$	1	10	30	50	70	90	
dP/dI	0,999	0,988	0,896	0,709	0,417	-0,001	(I)
dP/dI	0,999	0,988	0,897	0,709	0,418	0,002	(II)

by Gaussian noise- (I); by white noise - (II).

## Conclusion

The investigations prove that systems for LCPA determination could be designed as local, using local variables, i.e. this is an example of distributed intelligence application, which gives possibility for fast local actions when crucial voltage phase angle is near  $90^\circ$ . After the development of such devices, the theoretical results should be proven in EPS practice. If the results of field tests are positive, then we can implement them in EPS. Their implementation will have positive effect on increasing EPS reliability.

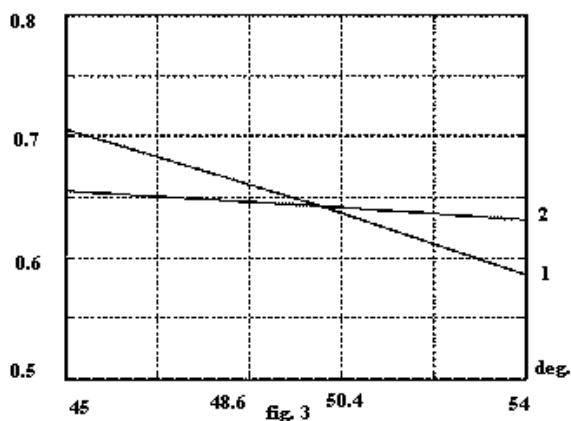
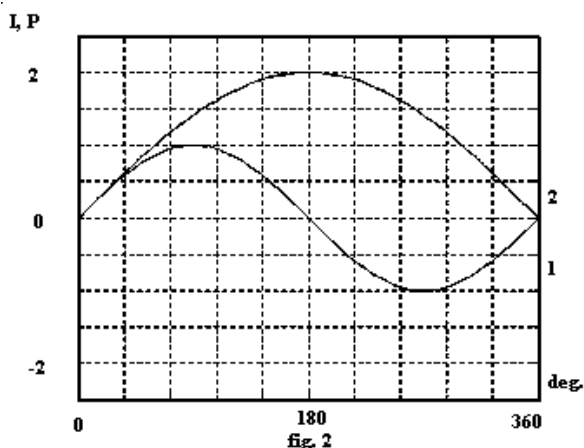
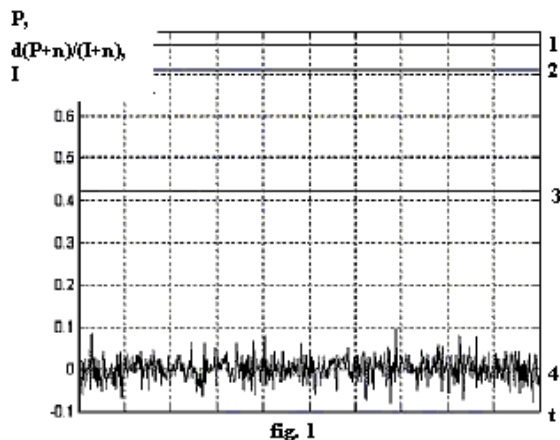
The necessity of centralized information systems for EPS control centers and their successful performance are beyond any doubt. In a large EPS there are hundreds of variables: relays protections, automations, variable values and others. During a cascade blackout, when fast changes of variables are usual, powerful computers, sophisticated algorithms and time is necessary to process the information and to elaborate the decisions. As a result the response time of the whole system increases and the reliability decreases.

During the last years in connection to the increase of the transmission of large power flows in the already very complicated power systems we see the appearance of accidents with very heavy consequences in the EPS of Europe and USA. They are due to the steady state stability conditions violation. An example is the accident in USA and Canada on August 14, 2003. During this accident were disconnected about 63 000 MW of consumer load, 400 transmission lines and 531 generation units in 261 power plants. About 50 million of people experienced disturbances in power supply for several days. The Electric Power Research Institute (EPRI) issued plan for "Intelligrid" with an implementation cost of US \$ 160 billion over 20 years.

Through implementation of distributed intelligence devices in EPS, we achieve decrease of the time period for response actions for real situation in EPS, and



improve the reliability, using only local variables, simple algorithms, small and cheap devices. In this way the capabilities are improved for limitation of the large power system accidents caused by steady state stability disturbances.



## References

- [1] Pourbeik P., P. S. Kundur, C. Taylor. Power Grid Blackout, IEEE Power & Energy September/October 2006, pp. 22-29.
- [2] Dale J., Postmortem Analysis of power Grid Blackouts, IEEE Power & Energy September/October 2006, pp. 30-35.
- [3] Cedric Carnal, Petra Reinhardt. PSGuard contributes to UCTE grid reconnection, ABB Review, 1/2005, pp.22 - 25.
- [4] Petkantschin L., u. a., Pendelsperreinrichtung fur Distanzschutz, Elektrische, 1981, Nr. 9, pp. 481-483.
- [5] Petkantschin L., G. Zvetanov. Delestage automatique reagissant aux oszilation de la tension, Bulletin de l'Union les centrales Suisse d'Electricite; de l'association L'Electriciens, 1983, Nr 4, pp. 202-204.



**Lazar T. Petkanchin** graduated with an MSc in Electrical Engineering in Technical University Sofia - 1954, obtained his PhD in 1967 and his Doctor of Technical Sciences in 1987. He has worked as a Researcher and Senior Researcher at «TECHENERGO». Professor at the faculty of Electrical Engineering, President of the supervisory board of National Electric Company, Vice President of the Committee of Energy. He is author of more than 140 publications. He has been President of Scientific and Technical Union of Power Engineers in Bulgaria and Chairman of the Bulgarian Energy Agency. He is a member of the IEEE, member of the National Committee of World Energy Council. His scientific interests are in the field of power systems control, hydro stations automation and relays protection.

Lazar Petkanchin is with Faculty of Electrical Engineering, Technical University of Sofia, 8, Kl. Ohridski blvd. 1000 Sofia, Bulgaria (e-mail: lpetkanc@tu-sofia.bg).

# Asset Optimization in EPS

Maria Kaneva

**Abstract:** *Modern electric power industry is radically different from the one we knew dozen of years ago. The difference in the way it functions today imposes the differences in the way it is managed and planned. The physical process, indeed, is the same in its conversions between different types of energies. What is new is the way the different players in EPS operate on the market for electric energy. The asset optimization (AO) is one of the elements of this new practice. Designed for the finance purposes attainment asset management (AM) was successfully adopted of power systems and was developed further into asset optimization. To stress on importance of AO for utility companies in deregulated EPS, to show some of its applications in different parts of the system illustrated with some examples are the tasks of this paper.*

**Keywords:** *Electric Power Systems, Asset optimization*

## Introduction

Electric Power System (EPS) is composed of many and varied parts: power plants and sub-stations, transmission and distribution grids, protection and control equipment. Almost each of them is autonomously managed; they are irregularly distributed upon the territory and most have expensive asset: boilers, turbines, generators, transformers, power lines, relay protection systems, others. What is especially valid for EPS is that assets require huge investments to be acquired and considerable amount of money to function. These capital-intensive assets need to be used in the most effective way – this is the aim of every owner (ranging from a society to a state). In the same moment the functioning of every such element influences the functioning of almost every other one. The failure of critical equipment can impact the entire system behavior. In EPS it happens that one failure provokes the series of others because the technological process is tremendously fast and complex. Over the recent 15 years in big parts of the world (such as North America and in lesser extend – in West Europe) the investments in new assets declined significantly. As a result the serious blackouts took place [1]. In the less developed parts of the world one can take preventive measures to avoid such undesirable events. In both cases AO gives opportunities to overcome the drawbacks of the past decisions, to ensure reliable operation avoiding catastrophic failures and to improve return /profitability (bottom line results). New participants in the market for electric energy, new forms of ownership, new goals, new practices of decision making, and much more – all this requires big changes in human thinking, in overall view point.

AM is term that came from financial industry and means search of best trade-off between risk and return [2]. Investor set acceptable risk and AM is used to achieve this level of risk with a highest return. In EPS AM means the process of maximizing return on investment of In other words the AM is a utility strategy to balance performance, cost and risk. When the result to be obtained is to maximize shareholder value while meeting all constraints (performance, cost and risk ones) the problem becomes optimizational – this is AO.

## AO in different parts of the EPS and time scales

Very different from all other contemporary systems, EPS needs special consideration. First: decisions taken for one key asset functioning (and/or development) influence the functioning (and/or development) of the others and of the system as a whole. Second: the systems works in the situation of uncertainty – load, equipment, undesirable accidental events. Third: almost every part of the system faces limitations of resources of different kinds. And last but not least: multiple objectives are pursuit during the EPS operation – minimize cost, minimize financial risk, maximize profit, maximize reliability.

These particularities existed from the very beginning of EPS functioning. In our days, however, faults are more costly and impacts have wider ranges, mistakes are severely punished often with bankruptcy. Even though it is still not the case for Bulgaria it is important to take advantage of the experiences in the world's leading EPS.

What is an asset? This can be any part of plant equipment, as well as the plant as a whole, transmission lines, process automation systems, load contracts, cash flow, wholesale traders, and employees. Any combination of these assets represents a portfolio.

AO in one utility or system is a term that covers the whole process of maximizing performance and minimizing cost in life-long period of equipment. This term embraces operation, maintenance, utilization, strategic planning of all physical: technical, mechanical, human, as well as informational and all other resources over their entire life cycle. From chronological point of view there are different tasks and problems in different time horizons [3]. This division of tasks is familiar to power engineers and managers [4] and is not treated herein. The specific asset management decision problems include (a) Operation; (b) Short-term maintenance selection and scheduling, (c) Long-term maintenance planning, and (d) Facility planning. This

devison is some what artificial, based on time chorizon differences, and are unified by common goal to meet the load requirements [4] during every possible period of time in the most economic way.

AO is not a single activity; it is a set of different functions conducted with a goal to find and follow optimal trade-off between certain objectives, most of them controversial such as – cost and reliability, revenue and investment. Using AO every utility that has specific aims because of respective context can assure desired operation of its assets, attain desired cost reduction, develop its asset structure via asset planning that maximizes expected pay-off and reduces risks. In power industry today managers are trying to maximize shareholder value of their company – be it generating, transmission or distribution one. This is performed within constraints of various characters: safety, technical, environmental, regulatory, others.

AO is a complete integral tool for overall management in most effective way of one utility. In this way managers assure shot-term earnings and better competitive positions. AO provides non financial rewards – it helps to avoid “silo effect” in organization, it fasters management process via real-time information and it changes the way of decision-taking and employee thinking. Thus it has impact on every area within the utility.

On the other hand the objectives of the participants in electricity market are competitive. Their manners of operation and their strategies will be rather different. The specificity of EPS namely its parallel work in common of all its elements in operation at every given moment requires that the operation of the whole set of elements is economic and reliable. Obviously the objectives of the individual participants and of the entire system differ considerably. Nevertheless they meet on the market and every one of them influences the functioning of the whole EPS, hence – of the whole country or even much bigger regions. This dependency is more obvious when considering the planning process in EPS.

**Operation.** In EPS utilities are mainly divided into three groups: generation, transmission and distribution.

One *generating* company commits its generating units to a certain capacity, chooses between various types of fuel to use and services to offer, decides about emissions and their trade on the market, prepares bids to offer, calculates risks and revenue. What is necessary is real-time information in the specific context to operations, maintenance, engineering, and management.

Real time performance measurement and analysis software solution improves plant productivity by identifying ways to increase overall equipment effectiveness, a key performance indicator. Some companies pvide user-friendly software automates data collection and analysis, and provides reports tailored to plant management’s needs [9]. In such a way the asset reliability and productivity increase while

the return on maintenance investments reach its maximum. Asset performance base lines are set, while real-time assessment of key performance indicators and asset optimization solutions identify performance gaps and improvement opportunities.

*Transmission* utilities and *distribution* utilities have a lot of common. They are asset intensive and hence can be favorably influenced by AO. The objective is to take asset-related decisions resulting in greater shareholder value. In [2] are explain objectives that are not AO objective. What AO is, like it was stated above, is balance between performance, cost and risk that allows all spending decisions to be aligned with corporate objectives.

Every power transmission company has its own control center used for centralized maintaining of different types of equipment. The failure in one key element can impact the entire grid including the supplied distribution grids and can even provoke additional failures.

With slow load grow, aging equipment, regulatory uncertainty these utilities are looking for ways to increase their profit. These companies utilize AM and AO to reduce spending, manage risk, taking appropriately decisions.

AO for operation like real time activity is centered in reliability. It encompasses online monitoring of the system asset conditions and continuous analysis of huge quantities of data.

In the midterm horizon AO is economy-centered. It has the following goals to attain [2]. On one hand it seeks optimizing competitive cost and corporation financial and physical risk dependent on planned and forced outages of assets. On the other hand is pursuit of extending life span of asset and optimizing recourse allocation for utilizing company asset.

**Development.** AO in long-term has its specific features. In vertically integrated EPS the planning of development was a centralized function under state and regulatory oversights. This function was (in Bulgaria still *is*) least-cost centered generation and transmission investment. The problems are solved with regard to system operation and non-supplied energy constraints. In today’s competitive electricity markets all players can participate not only in operation, but in planning of EPS too. Since the objectives and the constraints of electricity market participants are rather conflicting their planning strategies could be very different. In developed countries practice has shown that major investments are in generation asset planning and only small part is in network development. The overall operation of the EPS is responsibility of Independent System Operator (ISO). The latter assure secure operation of competitive participants through their cooperation. In the process of planning must be incorporate load growth, fuel prices and availability, market prices forecast, transportation possibility and congestions, cost and payoff based on predicted market prices and risk level. Reliability is the most important measure of transmission and distribution

performance. The utilities are required by ISO to meet reliability level. Reliability is actually a major cost source. If performance and risk goals can not be met asset owners must manage the risk of not meeting them. For optimal scheduling of future and existing generating assets is important to plan in: deployment, types of units and their capacities, geographical sites, strategies for their development in time and the return of asset investment. This planning has salient stochastic character and uses stochastic optimization methods where the solutions are trade-off between economic and security goals.

AO is proactive – instead of reacting posteriori this approach provides with tools for preventive measures and alternative actions in advance as well as with estimation of related costs, risks and benefits

### **AO models for EPS**

AO is a business approach. Its models have structure like every other optimization model: objective function (OF) and constraints. In every particular problem the OF can be different. It is not recommended to use as a goal minimum of investments in assets or cost of their utilization. For a utility in competitive environment such as the electricity market it is better to maximize profit/return on these investments or costs. It is possible to minimize risk – physical or financial. Another OF to minimize is security or the quantity of non distributed energy because of interruptions of supply.

Obviously the optimization problems of AO are very varied. It is the result of the attempt to cover the whole complexity of the physical system, financial conditions, environmental limitations, legal requirements and more. This holistic approach is essential because every one utility has many diverse assets. These assets are interdependent – the work of one set in a given power plant influences the work of every other one, and of the whole system. The possibility to have a relevant picture is of primordial importance in competitive environment. It requires identifying assets to be taken into consideration, available assets in given time, trading and marketing positions. Only via this complexity recognition the management can attain the best results in form of revenue or profit, overcome the “silo effect”, utilize the full range of possibilities of IT, relate functioning to corporate goals, improve problem solving process, and increase yields.

In complex system to optimize there are a lot of goals to be achieved. Often it is not easy to choose one goal for OF and the others – for constraints. If the choice is to reduce financial risk, for example, the constraints to be subjected to are credit and risk limits. Technical constraints are not easy to include, but one convenient form is assets’ operation financial results, here reflected the changeable price of electricity on the market and customers behavior.

If the OF is to increase revenue the most important constraints are the ones relayed to the physical markets for resources and the competitors’ behavior. Constraints can be to achieve a given percentage of growth, a given amount of dividend or earnings.

Generally speaking the optimization can be simple or very complex. The approaches to be used can be traditional or more sophisticated (like probabilistic, fuzzy, etc.). The choice is of the utility management.

In all cases it is advisable to incorporate in the process the top level management, responsible for corporate strategy.

The attainment of the most favorable condition of a defined goal relative to given resources and constraints is the process of optimization. It is not a single solution achievement. This is a continuous activity that needs to be divided into steps, related to people, time and resources [6]–[13].

In practice some companies offer flexible and extensible approach using Service-Oriented Architecture (SOA) and Web Services integrating multiple data sources and analytical procedures [11], [12], [13].

### **Steps of the AO process**

Goals, constraints and resources, are interrelated. No matter how they are determined. The AO as a process consists of numerous steps. In literature [5] is stressed on the importance for plant operators “to focus investments to maximize competitive viability” and “position their companies for superior economic return over the longer term”. The quotation gives illustration of common goal for utilities today. The purpose of this paper is not to repeat the profound and useful enumeration of activities’ steps representing AO process in an enterprise. It is of interest to stress on two important (jet not only interesting) issues there.

The first is the importance and complexity of activity portfolio identifying all known current and future items at the plant or network. Having the forecasted output and predicted price that form the expected revenue minus the expected costs formed by the activity portfolio gives the expected value created by the plant over time. In the presented model risk and contingences are included by their expected cost as a product of the probability and the financial impact. For the process map thus created is important that it must be understand and support of the people responsible for its everyday application. Other information is used relevant to strategy and resources (financial budget constraints, plant corporate goals, others).

The second issue to be mentioned is that once the long-range work plan is produced it needs to be evaluated and adjusted in given periods or because of some events.

Obviously the activities of creation and adjustment of this plan are numerous and time- and work-consuming. This is the reason to implement optimization process. Every item of assets has its NPV

(net present value) calculated on the basis of its cost, benefit and risk. But it is not the final step – more useful if to compare the ratio of every item in the plant or one portfolio of its benefit and its cost [5]. In real world cases there are different constraints: physical (resource constraints) and financial (budgets) ones. The OF to be maximized is cumulative (of all portfolio items) benefit and cost. The optimization technique to be applied is linear programming [5]. It is worth to use optimization procedure because of the necessity to review and recalculate a considerable volume of calculations periodically.

### Conclusion

Specific feature of AO is that it requires the adequate corporate culture, business approach and effective information systems. Managers in different levels of organizational structure of one utility are responsible for decisions like: how to use the organizational funds, where to invest, whether to shut down or to keep an asset working and with how much power, what kind of data are necessary and how to acquire them and so forth. This is a mix of technical, organizational, financial decisions that are to decide:

- how to optimize capital resources to acquire new assets or prolong the life of existing ones to attain best positions on the market;
- in what manner to utilize the asset so that to maximize profit
- what contract for product and/or service to offer to customers.

Why is AO so useful? It makes the equipment like boilers, turbines, pumps, exchangers, valves, furnaces, mills, instruments, transformers, and other process equipment to work in as consistent, effective and reliable way as possible. It is not only real-time operation that AO changes, but also the process of midterm scheduling, and long-term planning. AO in one company helps understand their key value drivers and achieve consistent growth, attain bigger earnings and lower costs, identify profitable opportunities, save resources and time, function in the best way in competitive environment. It gives “soft” benefits to the company too in enriching skills and moral of the employees, destroy “silo” walls, and much more.

### References

- [1] Pourbeik, P., Taylor, C.: The anatomy of a Power Grid Blackout – Root Causes and Dynamics of Recent Major Blackouts. IEEE Power and Energy Magazine 4(5), 2006, 22-29
- [2] Brown R., B.Humphrey, Asset Management for Transmission and Distribution, IEEE power & energy magazine, may/june, 2005, 39-45;
- [3] Shahidepour M., R.Ferrero, Time management for assets, IEEE power & energy magazine, may/june, 2005, 33-38;
- [4] Кънева М., Оптимизация в електроенергийната система, Авангард, София, 2006г.;
- [5] Colombo P., Eight Steps to Optimize Your Strategic Assets, IEEE power & energy magazine, may/june, 2005, 46-54;
- [6] <http://www.ic.gc.ca/epic/site/mse-epe.nsf/en/ep00092e.html>
- [7] <http://www.emersonprocess.com/Optimize/amssinde.htm>
- [8] [http://www.nexant.com/docs/service/Nexant\\_EMART\\_2004\\_Asset\\_Optimization.pdf](http://www.nexant.com/docs/service/Nexant_EMART_2004_Asset_Optimization.pdf)
- [9] <http://www.abbaustralia.com.au/product/seitp334/bb06198da13c99eb8525719a004f4187.aspx?tabKey=7>
- [10] [http://findarticles.com/p/articles/mi\\_m0EIN/is\\_ai\\_75814351](http://findarticles.com/p/articles/mi_m0EIN/is_ai_75814351)
- [11] Alonso, G., Casati, F., Kuna, H., Machiraju, V.: Web Services: Concepts, Architecture and Applications. Springer-Verlag, 2004
- [12] Lalanda, P.: An E-Service Infrastructure for Power Distribution. IEEE Internet Computing 9(3), 2005, 52-59
- [13] Wuttig, H.: Asset Optimization: Challenging the next millennium, ABB Review, 1, 2000

### Biographies



**Dr. Maria Kaneva-Tsocheva** graduated in the Electric Power Engineering Department of the Technical University (TU) – Sofia as M.Sc. in electrical engineering. She received her PhD degree in 1982 and joined the chair Electric Power Systems in Electrical Engineering Faculty of TU-Sofia in 1976. From 1993 she works as associate professor in Optimization in electric Power Systems in the same university. Here she teaches Optimization in EPS, Management of EPS,

Electric Power Systems, Power Plants (in French language, Power Systems Planning and Control and others during her work with Technical University (TU) – Sofia. Her major interests are in the field of optimization, expert systems and management in contemporary EPS. Dr. Maria Kaneva-Tsocheva is with the Faculty of Electrical Engineering, Technical University of Sofia, 8, Kl. Ohridski Blvd., 1000 Sofia, Bulgaria (e-mail: mkaneva@tu-sofia.bg)



# Sensor Button 2 / The next generation Sensor Button /

Dimitar Iliev Nurkov

**Abstract.** In now days many sensor systems exist in the world, you can find them everywhere around us. The sensors are the connection between the real and the virtual world. These systems can exist in different forms and dimensions. But the sensor systems made to be integrated in the cloths have to be designed by the criteria of wearability. Those wearable sensor nodes have to observe and recognize the activities and the environment of the object. For this reason miniaturized low-power signal processing algorithms have to be implemented to run in real-time at low power levels. Wearable computing is the missing part between the human world and the existing mobile devices.

**Keywords:** Wearable Computing, Context Recognition, Electronic Packaging, Sensor Integration, Miniaturization

## Introduction

This project is a continuation of the main idea, developed by a team of the Technical University of Zurich to create one complete sensor node, integrated in a button [1]. Following this idea in 2005 they made the first prototype of Sensor Button. This first version, with total volume of 7065 mm<sup>3</sup>, is the base for our project.

The development of the wearable computing and the microelectronic technology require a new design of the Sensor Button, including future miniaturization, new components and more sensor integration, with complete covering of the criteria of wearability. To achieve a new complete context recognition system, new motion sensors have to be added. In this direction, Sensor Button 2 is able to integrate more motion sensors and the possibility to have physiology sensing. This Sensor Button 2 allows making one big step toward to the future of the wearable computers, a step to one complete, fully integrated, MCM based /Multi Chip Module/ system.

In this new version of Sensor Button, we focus the attention in the sensor integration (sensors per metric unit). With this criterion of measure we can evaluate and show the future development of the wearable sensor systems. The sensor integration in the wearable systems depends mostly of the development of the sensors and the complexity of the recognition tasks. The simple dependency, more sensors – more possible activities to be recognized, pushes a lot of organization to focus of development of these systems.

The small, low power, on-body networks allow a real time observation of the object. For this reason these on-

body networks have to be always on, to provide useful information for the behavior, the activities and the environment in different subjects. In this way one system combination of accelerometer, magnetic field sensor, gyroscope and microphone could be used for complete 3D recognition of the activities (hand moving, going upstairs, going downstairs, running etc.).

## Basic system architecture

The whole system consists of a number of different modules, assembled in one package. The elements of this module are: Sensors /including analog output and digital output sensors/, Analog to Digital Converter /ADC/, Microcontroller /uC/, Radio Frequency Unit /RF Unit/ and Power Supply /represented on Figure 1/. The future sensor button design will enlarge the number of activities to be recognized (identified) and will be miniaturized in 3D.

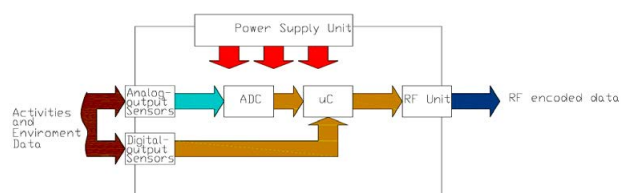


Fig. 1. Basic system architecture

For this reason, the new design will be based on the design of the existing Sensor Button Design and the progress of the wearable systems and the microelectronics technologies. The criteria of “Wearability” and Functionality will be completed with the possibility of integration in a MCM /Multi Chip Module/.

In Figure1 we can also see the division of two ways of sensing – sensors with analog outputs and sensors with digital outputs. This division based on the sensor progress has the tendency of miniaturization of the analog part. The miniaturization of the analog part will minimize the power consumption and in the same time will simply the required amplifiers and Analog to Digital Converters.

Also the new concept of wireless microcontrollers will combine the Radio Frequency /RF/ Unit and the microcontroller core. This will provide possibilities for integration of more functions in one package.

## Sensors

### *Motion sensor AMI601*

The AMI601 is a motion sensor that integrates a 3-axis magnetic sensor and a 3-axis accelerometer with their controller IC in a single small package [5]. The 3-axis magnetic sensor consists of 3 magneto-impedance sensor elements set in mutually orthogonal position. The 3-axis accelerometer consists of three sets of a magneto-impedance sensor and a micro magnet on a cantilever to detect acceleration, with the three sets in mutually orthogonal position.

The controller IC of the AMI601 consists of a circuit for detecting the magnetic signals from the 6 MI-sensor elements, an amplifier capable of compensating each sensors offset and setting appropriate sensitivity values, a temperature sensor for measuring the ambient temperature, a 12bitAD converter, an I2C serial output circuit, a constant voltage circuit for power control and a 8032 micro-processor controlling each circuit.

### *Integrated Dual-Axis Gyro IDG-300*

The IDG-300 is an integrated dual-axis angular rate sensor (gyroscope) [4]. It uses InvenSense's proprietary and patented MEMS technology with vertically driven, vibrating masses to make a functionally complete, low-cost, dual-axis angular rate sensor. All required electronics are integrated onto a single chip with the sensor.

The IDG-300 gyro uses two sensor elements with novel vibrating dual-mass bulk silicon configurations that sense the rate of rotation about the X - and Y-axis (in-plane sensing). This results in a unique, integrated dual-axis gyro with guaranteed-by-design vibration rejection and high cross-axis isolation. It is specifically designed for demanding consumer applications requiring low cost, small size and high performance.

### *Microphone AKU2004*

The AKU2004 is a surface-mountable CMOS MEMS Digital-Output Microphone which is ideal for use in microphone array applications where a high degree of noise immunity is required [6]. The AKU2004 integrates an acoustic transducer, analogue output amplifier, and a 4th\_order sigma-delta modulator on a single chip. The output of the microphone is pulse density modulated (PDM); a single-bit digital output stream that can be decimated by a digital filter in downstream electronics such as an audio CODEC, DSP, or baseband processor for a high degree of design flexibility and freedom. The digital output is more robust than the low-level analogue output signals of the standard ECM and therefore saves significant time and expense in system design and eliminates the dependence on shielded cables for signal routing. Additionally, the small form factor of the AKU2004 allows placement of the microphone in the acoustically optimal position in portable electronic devices. The AKU2004 therefore enables simple, robust design and a reduction of external components.

## Wireless microcontroller

CC2430 Wireless microcontroller combines in one system on a chip the three existing units on the diagram of fig. 1— Analog-to-Digital Converter /ADC/, Microcontroller /uC/ and Radio Frequency Unit /RF Unit/ [3].

### *Microcontroller core*

The CC2430 enables ZigBee® nodes to be built with very low total bill-of material costs. The CC2430 combines the excellent performance of the leading CC2420 RF transceiver with an industry-standard enhanced 8051 MCU, 128 KB flash memory, 8 KB RAM and many other powerful features.

The CC2430 is highly suited for systems where ultra low power consumption is required. This is ensured by various operating modes. Short transition times between operating modes further ensure low power consumption.

- High performance and low power 8051 microcontroller core
- 128 KB in-system programmable flash
- 8 KB RAM, 4 KB with data retention in all power modes
- Powerful DMA functionality
- Watchdog timer
- One IEEE 802.15.4 MAC timer, one general 16-bit timer and two 8-bit timers
- Hardware debug support
- Peripherals
- CSMA/CA hardware support.
- Digital RSSI / LQI support
- Battery monitor and temperature sensor
- 12-bit ADC with up to eight inputs and configurable resolution
- AES security coprocessor
- Two powerful USARTs with support for several serial protocols
- 21 general I/O pins, two with 20mA sink/source capability

### *Radio Frequency Unit*

- 2.4 GHz IEEE 802.15.4 compliant RF transceiver (industry leading CC2420 radio core)
- Excellent receiver sensitivity and robustness to interferers
- Very few external components
- Only a single crystal needed for mesh network systems
- RoHS compliant 7x7mm QLP48 package
- Low current consumption (RX: 27 mA, TX: 27 mA, microcontroller running at 32 MHz)
- Only 0.5  $\mu$ A current consumption in power down mode, where external interrupts or the RTC can wake up the system
- 0.3  $\mu$ A current consumption in stand-by mode, where external interrupts can wake up the system

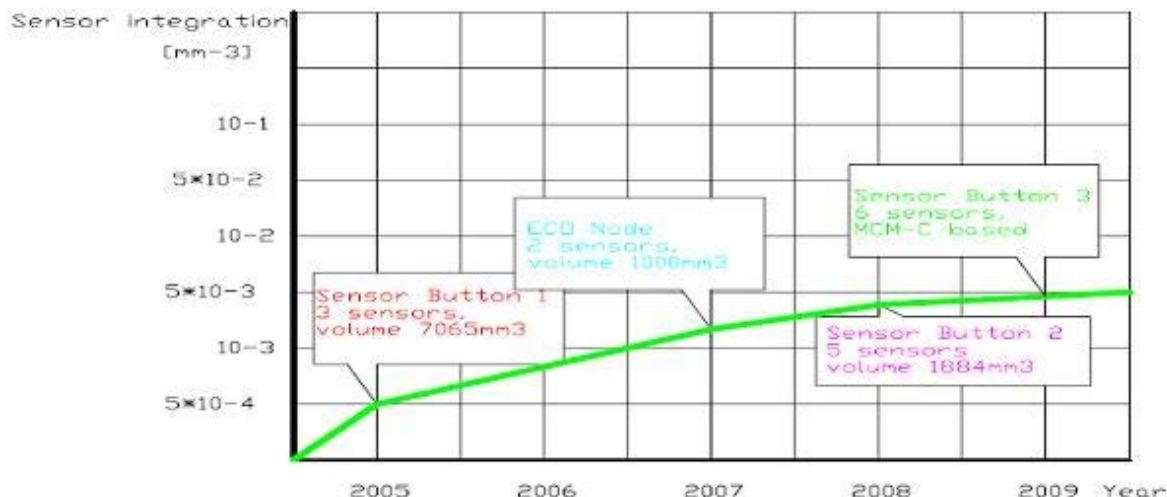


Fig. 2. Sensor integration

- Very fast transition times from low-power modes to active mode enables ultra low average power consumption in low duty cycle systems
- Wide supply voltage range (2.0V - 3.6V)

### Power Supply Unit

The power unit will combine battery and low voltage boost converter. The total power consumption is calculated in the base of absolute maximum ratings of the components. The expected maximum peak current consumption is 50 mA.

The power consumption can be reduced in the process of design and optimization of the appropriate working algorithm. The use of digital output sensors allows for obtaining a direct feedback from the microcontroller which would help to avoid the continuous working time of the sensors.

### Sensor Integration

One of the most important criteria to evaluate the existing sensor platforms is the *sensor integration*. In term of wearable computing we use the sensor integration in meaning of sensors per  $mm^3$ . To show the future development of the wireless sensor platforms and to situate the Sensor Button 2, we made this graphic in base of some existing platforms [2].

From Figure 2 we can see the expected development in the wireless sensor systems. The next step for our research will be a MCM based Sensor Button.

### Conclusion and Future Work

The new Sensor Button represents one complete, wearable system with power recognition possibilities. This new version gives the possibilities to study a huge number of activities. This version gives the bases of the new era in wearable sensor platforms – the MCM Sensor Button.

In the next years we will focus our attention in the development, improvement and implementation of the Sensor Button. Finally we expect to develop MCM based Sensor Button 3, with the real *wearable system on chip*.

### References

- [1] Bharatula N. B., Lukowicz P., Troster G.: Functionality-Power-Packaging Considerations in Context Aware Wearable Systems
- [2] Tummala R.: Fundamentals of Microsystems Packaging, McGraw-Hill, 2004, Second Edition.
- [3] Homepage of Texas Instruments. <http://www.ti.com> (2008)
- [4] Homepage of IvenSense. <http://www.ti.com/> (2008)
- [5] Homepage of Aichi Micro Intelligent Corporation. <http://www.aichi-mi.com/> (2008)
- [6] Homepage of Akustica digital microphones. <http://www.akustica.com/> (2008)

### Biographies



**Dimitar Nurkov** was born in Gotse Delchev, Bulgaria, on June 01, 1984. He graduated from the Technical University - Sofia, and received Master degree from the same university.

His field of interest includes wearable computers, system and package integration, power line communication. He is today a PhD student in the French Faculty of Electrical Engineering in the Technical University – Sofia.

Dimitar Nurkov is with the French Faculty of Electrical Engineering, Technical University of Sofia, 8, Kl. Ohridski Blvd., 1000 Sofia, Bulgaria (e-mail: nurkoff@gmail.com)

Table 1

Power consumption

Components	Maximum current @	Maximum power
CC2430	26.9mA@3.0V	~80.7mW
IDG300	9.5mA@3.3V	~31.3mW
AKU2004	0.75mA@3.0V	~2.3mW
AMI601	11.0mA@3.0V	~33.0mW

# Investigation of High Power Bolted Busbar Connectors with Longitudinal Slots

Raina Tzeneva

**Abstract:** In this paper high power bolted busbar connectors which pads and busbars are sectioned by cutting one or two longitudinal slots in order to increase the real contact area and to improve the reliability of their performance are investigated. Applying the method of finite elements models of contact pressure, contact penetration, electric current density and Joule heat are obtained. It has been estimated that the new cases lead to a raise in contact pressure  $P$  and contact penetration  $\mu$  in the interface between the busbar and the pad.

**Keywords:** bolted busbar connectors, contact penetration, contact pressure, current density distribution longitudinal slots

## Introduction

Reliable joints in copper and aluminium busbar conductors can be made very simply by bolting. Bolted joints are compact and efficient but have a somewhat more uneven contact pressure compared to clamped plates joints.

A review of factors that affect the connector performance and detailed analysis of the degradation mechanisms of power connections are given in [1] [2].

There are two major factors that affect the reliability of a power joint. The first one is the design of the connection and the material from which it is fabricated. The second one is the environmental influence to the joint.

## Theoretical Background

It is well known that real contact surfaces are not flat and when contact is made between two metals localized metallic contacts appear. As the contact force increases the number and the area of these small metal-to-metal contact spots will increase. These spots, termed  $\alpha$ -spots, are small cold welds insuring the only conducting paths for the transfer of the electrical current.

The real contact area also named conducting area is a fraction of the apparent contact area, determined by the dimensions of the contact parts. Generally it is smaller than 1%.

From these simple considerations it is clear that one of the most important requirements for good connector performance is for the real area of the contact to be sufficient large.

In order to increase the real contact area Boychenko and Dzektsler [3] have shown that changing the connection design can equally be effective in increasing the contact area. In other words, cutting slots in the

busbar in a manner as shown in Fig.1, the actual surface area of a joint can be increased by 1.5 to 1.7 times of that without slots. The contact resistance of joint configuration with slots (b) is 30-40% lower than that of (a) and is mechanically and electrically more stable when subjected to current cycling test [4], [5]. The beneficial effect of sectioning the busbar is attributed to a uniform contact pressure distribution under the bolt, which in turn, creates a larger contact area.

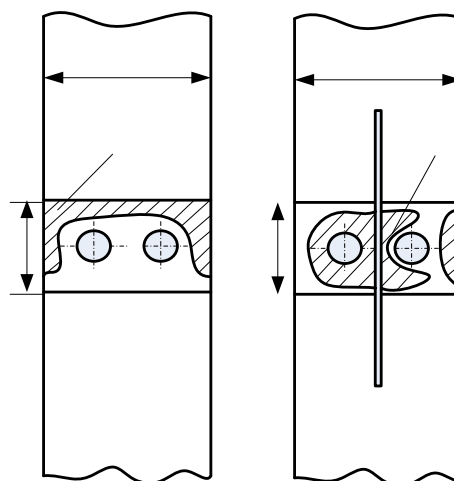
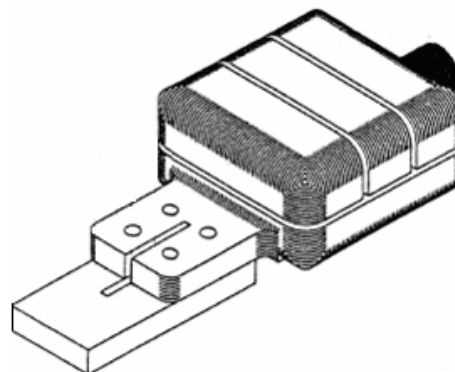
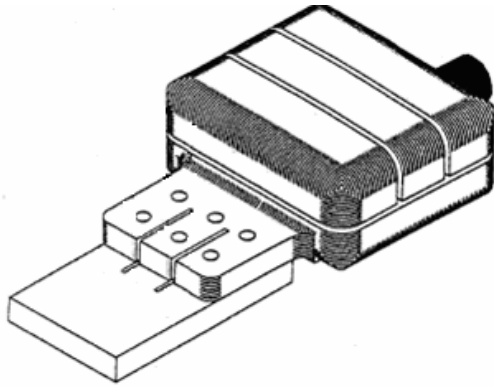


Fig.1. Effect of making a slot in the overlapping busbar joint

This idea is developed by M. Braunovic [4]. Fig. 2 depicts typical high voltage 700 kV power connectors used for connections of stranded conductors and for connecting a variety of power equipment at the substation site. These connectors are made of two parts: keeper and current-carrying member comprised of a grooved section and flat end (pad, tongue). The conductor is secured in the grooves by either high-strength aluminum (7075 grade) or steel bolts. Keeper and current-carrying part are made of cast or wrought aluminum.



a)



b)

Fig. 2. New connector design; a) the keeper is sectioned into two or b) three segments by longitudinal slots

In the case of an old connector design, the keeper is made of a solid block of cast aluminium while in the new connector design; the keeper is sectioned into two - Fig. 2a or three - Fig. 2b segments. Numerous report from the field showed that in the old connector design, contact resistance between the current-carrying part and conductor was unstable that often lead to unacceptable overheating of the joint as a whole. This was associated with the inability of a relatively large and rigid keeper to maintain a good contact between the conductor and current-carrying part of a connector. Sectioning the keeper mitigated the problem and significantly improved both mechanical and electrical stabilities of a joint. Beneficial effect of sectioning was associated with a more uniform stress distribution between the keeper and conductor that assured a larger contact area at the conductor-connector current carrying interface.

The results of contact resistance measurements show clearly that the electrical and mechanical integrities of bolted high-power connectors can be significantly improved by sectioning, that is cutting longitudinal slots into the current carrying parts (pads). The observed improvement was associated with a more uniform stress distribution under the bolts in the sectioned joint segments and significantly lower tendency to misalignment.

### Modelling Bolted Busbar Connection with Longitudinal Slots

In this paper an attempt to discuss how introducing longitudinal slots in high power bolted busbar connectors changes the contact pressure and contact penetration in the interface between the pad and their influence on the true contact area and therefore on the contact resistance. Additionally current conduction analysis is used to analyze the electric field distribution changes.

The investigated connectors in this work are of new design, that is with sectioned keeper part, whose current-carrying pads have four and six -bolt holes. The pads are modified by cutting slots 4 mm wide and 72mm long as seen in Fig.3. Bolt hole diameter is 13.2mm for the 12.7mm bolt diameters. All dimensions in the figure are in mm. The thickness of the connector's pads is 25mm

and is made of aluminium. The busbars were made of the same grade aluminium. The behavior of these connectors is compared with the same connectors, having no slots in their pads.

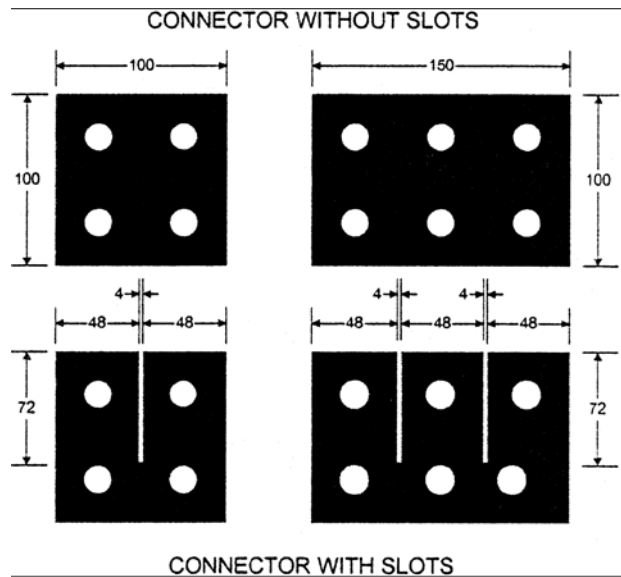


Fig. 3. Schematic of contact surfaces of the connector current-carrying pads without and with slots

The mechanical changes, associated with the contact penetration depth and the contact pressure, in the contact area between two busbars in a bolted busbar connection are studied by the help of the finite elements simulation tool ANSYS Workbench. If a higher contact penetration increases  $\alpha$ -spots both in numbers and dimensions, which in turn expand the true contact area and decreases contact resistance, then a new design could be introduced for this connection. Typical bolted busbar connectors with longitudinal slots are shown in Fig. 4.

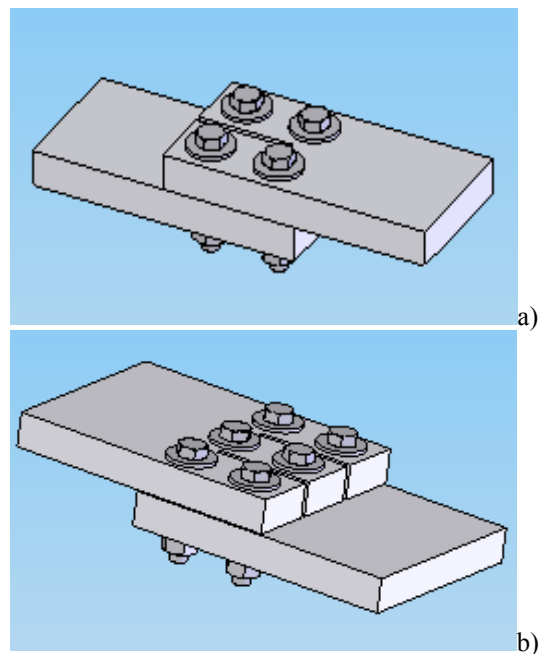


Fig. 4. Slotted assemblies with 2 -a) and 3 -b) slots.



The investigated assembly consists of:

- Alluminium busbars (Young's modulus  $E = 0.7 \cdot 10^{11} \text{Pa}$ , Poisson's ratio  $\mu = 0.35$ , width 100mm and 150mm, height 25mm, length 160mm, busbars' overlap 100mm with 4 holes of  $\text{Ø}13.2\text{mm}$  and 150mm with 6 holes of 13.2mm;

- Fasteners: bolts – Hex Finished Bolt\_AI-HFBOLT 0.5-20-3-1.25-N, steel  $E = 2.10^{11} \text{Pa}$ ,  $\mu = 0.3$ ; nuts – Heavy Hex Nut\_AI-HHNUT 0.5000-13-D-N, steel  $E = 2.10^{11} \text{Pa}$ ,  $\mu = 0.3$ ; washers – Flat Washer Type A Wide\_AI-FW 0.5, steel  $E = 2.10^{11} \text{Pa}$ ,  $\mu = 0.3$ . Tension in each bolt  $F = 12559 \text{N}$ .

Models are studied for contact pressure  $P[\text{Pa}]$  and penetration  $\mu[\text{m}]$  within the busbars electrical interface.

The aspect of model meshing is distinguished as a key phase for proper analysis of the problem. This is because on the one hand it is an established certainty that the reason for the good quality of physical space triangulation is closely related to the consistent mapping between parametric and physical space.

On the other hand a properly meshed model will present a fairly close-to-reality detailed picture of stress distributions which is a hard task for analytical solution and is usually an averaged value. It is evident from Fig.5 and Fig.6, for the uneven allocation of penetration, that the 2 investigated designs bring even more complexities.

In the solving process the meshed models incorporate the following elements: 10-Node Quadratic Tetrahedron, 20-Node Quadratic Hexahedron and 20-Node Quadratic Wedge. Contacts are meshed with Quadratic Quadrilateral (or Triangular) Contact and Target elements.

Contact penetration for connector with 1slot (2 sectors) is shown in Fig.5. Fig.6 presents the same characteristic for connector with 2 slots (3 sectors).

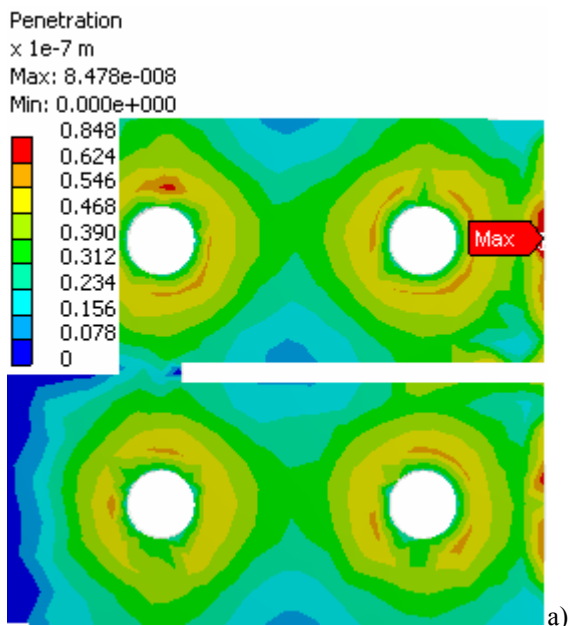


Fig.5. Contact penetration for connector with 1 slot (2 sectors)

### Penetration

Type: Penetration

Unit: m

Time: 1

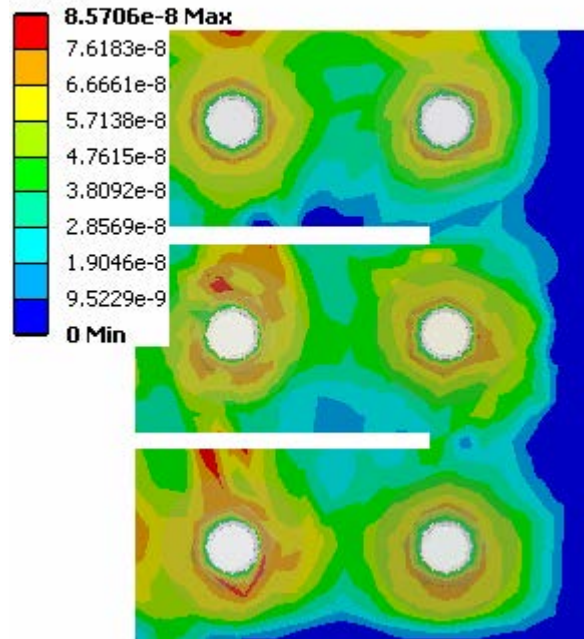


Fig.6. Contact penetration for connector with 2 slot (3 sectors)

Table 1 shows the comparison between the max values of the contact pressure  $P_{\max}$  and contact penetration  $\mu_{\max}$  for the connectors with and without slots.

Table 1

Comparison of  $P_{\max}$  and  $\mu_{\max}$  for connectors with and without slots

	no slots	1 slot	no slots	2 slots
$P_{\max}, \text{Pa}$	1.046e7	1.266e7	9.511e6	1.061e7
%	100	121.03	100	111.57
$\mu_{\max}, \text{m}$	7.025e-8	8.478e-8	7.405e-8	8.571e-8
%	100	120.68	100	115.75

### Electric Field Distribution

Current conduction analysis is used to analyze a variety of conductive systems. Generally, the quantities of interest in a current conduction analysis are voltages, current densities, electric power losses (Joule heat).

Several computer models smooth the research progress of the current density and Joule heat distribution changes that take place within the bolted busbar connection, due to the introduced longitudinal slots (sectors). The FEA package ANSYS 11 is employed in the analysis of the electric field and the Joule heat distributions. The model is meshed with the SOLID 232 element - a 3-D, 10-node, tetrahedral current-based electric element. The element has one degree of freedom, voltage, at each node and is based on the electric scalar potential formulation. It is applicable to the low frequency time-harmonic quasistatic electric field analyses.

The current density distribution in the bolted busbar assembly without –a) and with 1 slot –b) is shown in Fig 7.

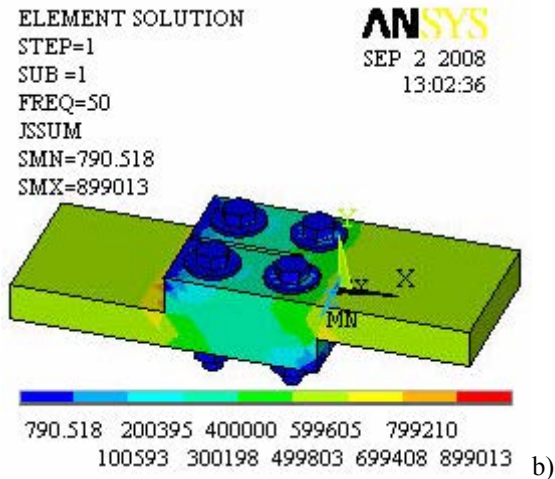
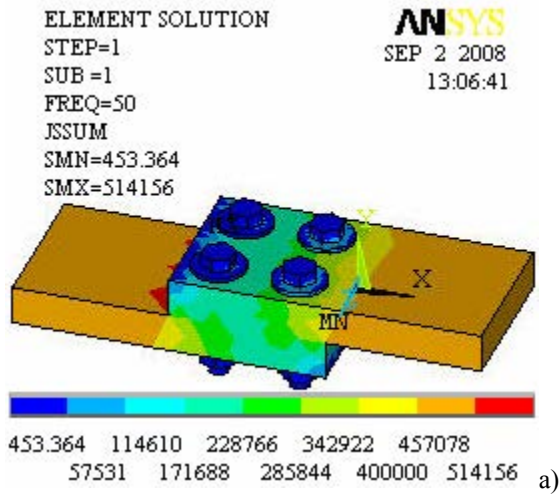


Fig.7. Current density distribution in the bolted busbar assembly without –a) and with 1 slot –b)

Another very important characteristic is the heat generated by the current flow. Joule heat distribution in the connector without –a) and with 1 slot –b) is illustrated in Fig.8.

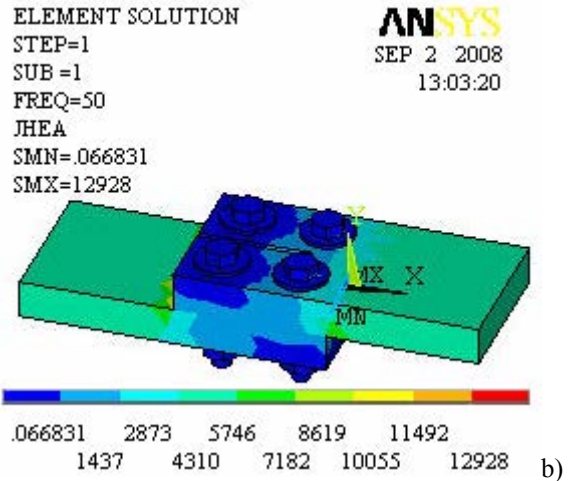
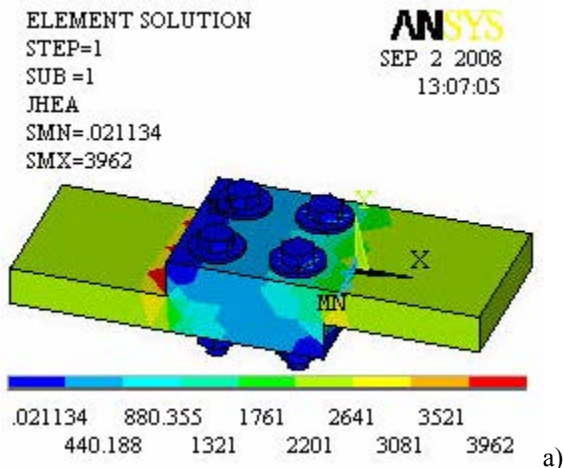


Fig.8. Joule heat distribution in the connector without –a) and with 1 slot –b)

Fig. 9 shows the current density distribution in the bolted busbar assembly with 2 slots. The distribution of the Joule heat, generated by the current flow in the connector with 2 slots is illustrated in Fig.10.

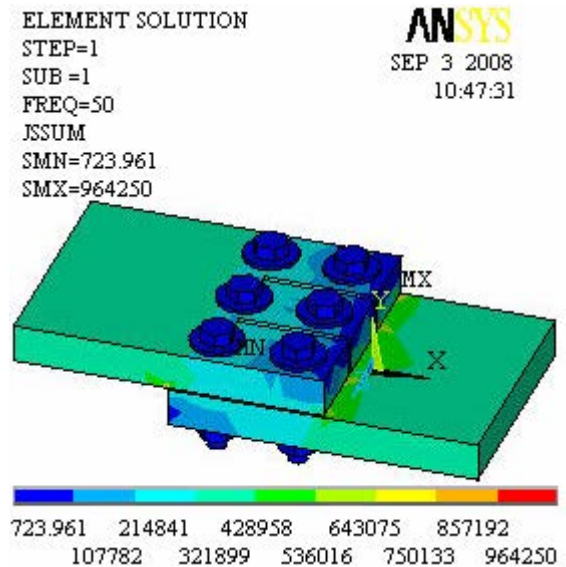


Fig.9. Current density distribution in the bolted busbar assembly with 1 slot

An assessment of the max values of the current density  $j_{max}$  and Joule heat  $J_{max}$  for the connectors with and without slots is given in Table 2.

**Table 2**  
Comparison of  $j_{max}$  and  $J_{max}$  for connectors with and without slots

	no slots	1 slot	no slots	2 slots
$j_{max}$ , A/m <sup>2</sup>	514156	899013	959010	964250
%	100	174.85	100	100.5
$J_{max}$ , J	3962	12928	14339	14637
%	100	326.3	100	102.08

ELEMENT SOLUTION  
 STEP=1  
 SUB= 1  
 FREQ=50  
 JHEA  
 SMN=.08794  
 SMX=14637

ANSYS  
 SEP 3 2008  
 10:49:08

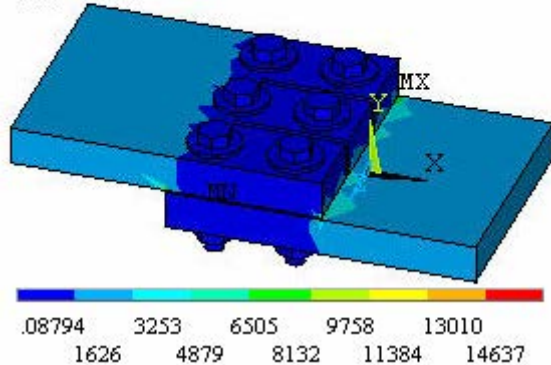


Fig.10. Joule heat distribution in the connector with 2 slots

### Discussion and Conclusion

As summarized in Table 1 the new design of high power bolted busbar connectors, introducing one or two longitudinal slots 4 mm wide and 72mm long leads to rise in max contact pressure of 21% for the connector with one slot and 11.6% for the two slotted connector. The max contact penetration increases with 20.7% for the connector with two sectors and 15.7% for this one with three sectors. Therefore, the true area of metal to metal contact is maximized within the electrical interface and that leads to reduced contact resistance and more efficient performance of the connectors of new design.

The generalized data in Table 2 show that the new connection design with one slot exhibits a significant increase in the max current density (74.8%) and Goule heat (more than three times), but it is concentrated in very small zones around the slots and edges. The max current density and the max Goule heat generated dos not change with introducing longitudinal slots for the connector with three sectors therefore its thermal behaviour is perfect.

The idea of introducing slots in high power bolted busbar connections is additionally developed in 3 new designs, where the slots are a part of the bolt holes: slotted bolt holes - design S, slotted bolt holes, ending with small holes – design SH and groups of small holes around the bolt holes – design G. In all of these cases the rise of contact pressure and contact penetration is about 50% and the experimentally proved reduction of contact resistance is significant [6], [7], [8], [9], [10], [11].

### References

[1] Slade P., M. Dekker. Electrical Contacts. Boston, MA:IIT, 1999, p.155  
 [2] Timsit R. S. The Technology of High Power Connections: A Review”, 20-th International Conference on Electrical Contacts, Zurich, Switzerland, p. 526, 2002.

[3] Boychenko V. I., N. N. Dzekter. Busbar Connections (in Russian), Energia, 1978.  
 [4] Braunovic M. Effect of Connection Design on the Contact Resistance of High Power Overlapping Bolted Joints, IEEE Transactions on Components, Packaging and Manufacturing Technology, vol. 25, Issue 4, pp. 642-650, Dec. 2002.  
 [5] Braunovich M. Effect of Connection Design on the Performance of Service Entrance Power Connectors, IEEE Transactions on Components, Packaging and Manufacturing Technology, vol. 27, Issue 1, pp.72-78, March 2004.  
 [6] Tzeneva R., P. Dineff, Y. Slavtchev. Bolted Busbar connections, XIV-th International Symposium on Electrical Apparatus and Technologies SIELA’2005, 2-4 June2005, Proceedings of papers, vol. I, pp. 207-211, Plovdiv, Bulgaria, 2005.  
 [7] Tzeneva R., Y. Slavtchev, N. Mastorakis, V. Mladenov. Bolted Busbar connections with Slotted Bolt Holes, WSEAS Transactions on Circuits and Systems, Issue 7, vol. 5, pp. 1021-1027, July 2006.  
 [8] Tzeneva R., Y. Slavtchev, V. Mladenov. Bolted Busbar Connections with Slotted Bolt Holes, Proceedings of the 10-th WSEAS Conference on Circuits, Vouligmani Beach, Athens, pp. 91-95, Greece, July 2006.  
 [9] Tzeneva R., P. Dineff. Bolted Busbar Connections with Particularly Slotted Bolt Holes, Proceedings of the XLI International Conference on Information, Communication and Energy Systems and Technologies ICEST’06, pp. 371-374, 29-th June-01-st July, Sofia, Bulgaria, 2006.  
 [10] Tzeneva R. Electric Field Distribution in Perforated Bolted Busbar Connections. XV-th International Symposium on electrical Apparatus and Technologies SIELA2007, vol. I, pp. 91-96, 31 May-1June 2007, Plovdiv, Bulgaria, 2007  
 [11] Tzeneva R., P. Dineff. Effect of Perforation in High Power Bolted Busbar Connections, Proceedings of the XLII International Scientific Conference on Information, Communication and Energy Systems and Technologies ICEST’07, Proceedings of Papers, Volume 2, 24-27-th June, Ohrid, Macedonia, pp. 667-670

### Biography



Raina Tzeneva was born in Pernik, Bulgaria, on September 16, 1948. He studied at the Technical University of Sofia-Bulgaria and received Dr. degree from the same university in 1983.

Since 1979 he worked in the Faculty of Electrical Engineering of the Technical University of Sofia as a researcher and Lecturer in the field of low-voltage switchgear and control gear.

Raina Tzeneva is with the Faculty of Electrical Engineering, Technical University of Sofia, 8, Kl. Ohridski Blvd., 1000 Sofia, Bulgaria (e-mail: tzeneva@tu-sofia.bg).



# Theoretical Analysis on Implementing Electric Filters in a Poultry Farm

Dimcho Kiriakov

**Abstract:** Based on experimental data, a mathematical model describing the degree of cleaning the air around a sample electric filter has been built. Following a number of calculations and using the suggested algorithm for implementing electric filters in poultry farms, the optimal number and layout of sample electric filters for the poultry farm under investigation have been determined while keeping to the required veterinary-hygienic norms..

**Keywords:** electric filter, dust, mathematical model, optimization.

## Introduction

The dust content in poultry farms for cell breeding of birds is lowered most frequently by the existing ventilation systems. During the winter months, for the purpose of saving heat, the use of those systems is limited and the dust content in the rooms where the birds are raised increases up to 20 mg/m<sup>3</sup> [1]. Preliminary experimental research shows that this specific dust (down, fodder particles, etc.) can be caught by electric filters [6]. The optimization of this equipment is an indelible part of its implementation. Different types of electric filters utilized mainly in industry have been discussed in works on the subject[7]. Some optimizations have been realized [4], but there are no known results from their use in poultry farms.

The purpose of the research completed is to apply new methods for implementing electric filters in poultry farms. Those new methods will make it possible to achieve the required veterinary-hygienic norms in a given farm for cell breeding of birds with a minimum number of filters.

## Description

Through the suggested algorithm for determining the layout of sample electric filters implemented in a poultry farm both the distance between the filters and their number can be specified for the farm under investigation. For this purpose the following stages must be covered [3]:

- the area in the farm where the birds reside has a length of 74 m, and a width of 14 m, i.e.  $S_{fm}=1036 \text{ m}^2$ ;
- the dust content around a sample electric filter has been investigated. The experimental data received for the degree to which the air has been cleaned around the

electric filter  $\eta$  depending on the distance  $x$  from it are given in Table 1. To establish the graphic equation  $\eta=f(x)$ , as well as to obtain the respective mathematical model, the mean values of  $\eta$  are used [5].

x,m	0	1	2	3	4	5	6
$\eta_1, \%$	80,47	70,22	54,22	30,06	16,81	9,33	4,18
$\eta_2, \%$	79,92	71,34	53,46	31,92	15,8	9,28	4,92
$\eta_3, \%$	78,74	71,98	52,49	31,11	15	8,48	3,8
$\bar{\eta}, \%$	79,71	71,18	53,39	31,03	15,87	9,03	4,3

**Table 1**

Results from the experimental investigations of the degree of cleaning the air  $\eta$  around a sample electric filter depending on the distance  $x$  from the filter

The graphic equation  $\eta=f(x)$  for the interval  $x=(0\div6)$  m with optimum values of mode parameters of a sample electric filter taken from the experimental data in Table 1 is shown on Fig. 1. It can be clearly seen that with the distance from the filter increasing, the degree of cleaning the air  $\eta$  decreases. This can be explained by the mixing of the air cleaned by the filter with the polluted air in the room. The graph's characteristic shows that it can be described as a third degree parabola.

The results from the statistical processing of the experimental data from Table 1 are given in Table 2. For this purpose the software STATISTICA 8 has been used.

The coefficient determining a third degree parabola is  $R^2=0,996$ , which shows that this model provides a precise description of the equation  $\eta=f(x)$ . This fact has been confirmed also by Fischer's criterion  $F_{(3;3)}=254,43$  and the level of significance  $p=0,00042 \ll 0,05$ . All regression coefficients are meaningful for a level of significance  $\alpha=0,2$ . Thus the model we have been looking for will appear as

$$(1) \quad \eta = 80,57 - 6,68x - 5,02x^2 + 0,67x^3,$$

$$F_{(0,05;3;3)}=9,28;$$

- Following some experiments, it has been determined that the dust concentration in a room of calm birds is usually within the limits of (7...11)mg/m<sup>3</sup> [2]. Further it is assumed that

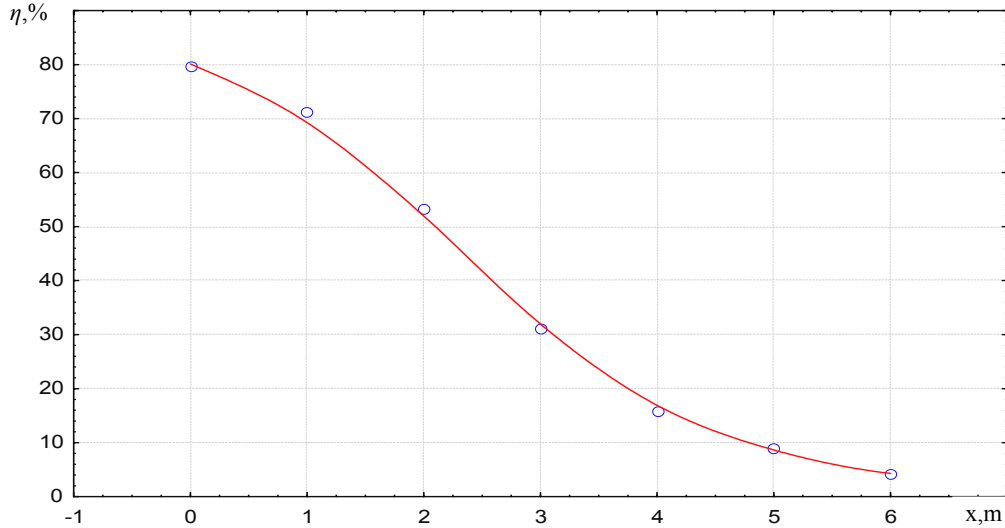


Fig.1 Dependence of the degree of cleaning the air  $\eta$  around a sample electric filter on the distance  $x$  from it

**Table 2**  
Coefficient of exactness  $R^2$ , Fischer criterion  $F$  and regression coefficients  $B$

Regression Summary for Dependent Variable: y (Spreadsheet1)						
R= ,99804058 R <sup>2</sup> = ,99608499 Adjusted R_ = ,99216999						
F(3,3)=254,43 p<,00042 Std.Error of estimate: 2,7010						
N=7	Beta	Std.Err. of Beta	B	Std.Err. of B	t(3)	p-level
Intercept			80,56762	2,602773	30,95453	0,000074
x	-0,47258	0,290915	-6,67758	4,110653	-1,62446	0,202744
x2	-2,21672	0,742539	-5,01560	1,680083	-2,98533	0,058348
x3	1,78874	0,487821	0,67389	0,183781	3,66679	0,035078

$$g=10\text{mg}/\text{m}^3;$$

- the area of the mathematical model (1) is found after integrating the investigated limits (0...6)m [8]

$$(2) \quad S_1=S_2= \int_0^6 (80,57 - 6,68x - 5,02x^2 + 0,67x^3) dx =$$

$$= 80,57 \int_0^6 dx - 6,68 \int_0^6 x dx - 5,02 \int_0^6 x^2 dx + 0,67 \int_0^6 x^3 dx =$$

$$= 80,57(6-0) - 6,68 \frac{1}{2} (6^2-0) - 5,02 \frac{1}{3} (6^3-0) + 0,67 \frac{1}{4} (6^4-0) =$$

$$220,38 \text{ m}^2,$$

And then the total area is found

$$(3) \quad S=S_1+S_2=440,76 \text{ m}^2.$$

Dividing the area  $S$  to the degree of cleaning the air  $\eta_{\text{зад}}=60\%$ , which determines the dust concentration corresponding to the veterinary-hygienic norms  $g=4 \text{ mg}/\text{m}^3$ , we find the distance between two electric filters  $L$ , that coincides with those norms

$$(4) \quad L = \frac{S}{\eta_{\text{зад}}} = 440,76/60=7,34 \text{ m}.$$

By analogy, we find the distance  $x_{s1}$  from the end electric filter to the periphery of the bird zone, where the mean value of the area  $S_1$  corresponds to the required veterinary-hygienic norms.

$$(5) \quad x_{s1} = \frac{S_1}{\eta_{\text{зад}}} = 220,38/60=3,67\text{m}.$$

The area covered by one operating electric filter will have the shape of a circle with a radius  $\frac{L}{2}$  and an area of

$$(6) \quad S''_{\text{ef}} = \pi \left(\frac{L}{2}\right)^2 = 3,14 (3,67)^2 = 42,29 \text{ m}^2.$$



Then the number of electric filters needed for work in the bird room will be

$$(7) \quad n = \frac{S_{nm}}{S_{ef}} = \frac{1036}{42,29} = 24,5.$$

It is convenient to round it to 24. Then they will be arranged in two rows, twelve filters in each row. Along the width of the bird zone they will cover a distance of  $2L=14,68$  m, which is larger than 14 m and there will be

an overlapping of  $\frac{14,68 - 14}{2} = 0,34$  m. The distance

covered by the electric filters along the length of the bird zone will be  $12L=88,1$  m, which is larger than 74 m and

there will be an overlapping of  $\frac{88,1 - 74}{12} = 1,17$  m.

## Conclusion

The results achieved allow the observance of the desired veterinary-hygienic norms when a minimum number of sample electric filters is laid out correctly in the poultry farm under investigation.

## Acknowledgements

The author is grateful to the management of the Poultry Farm in Lomtsi, Targovishte Region, for their cooperation for the duration of the experiments.

## References

- [1] Каминский, А., Е. Живописцев. Итоги науки и техники. Серия Электрификация и автоматизация сельского хозяйства, том Электронно – йонная технология в сельскохозяйственном производстве. ВИНТИ, М., 1985.
- [2] Киряков, Д. В. Запращеност във ферма за клетъчно отглеждане на птици с конвенционална вентилационна система. Научни трудове на Р.У. „А. Кънчев”, т. 44, серия 3.1, стр. 96-98, Русе, 2005.
- [3] Киряков, Д., Н. Михайлов. Алгоритъм за определяне разположението на електрофилтри при внедряване в птицевъдни ферми. Международна научна конференция ЕЛМА-2008, Т.У. София, Приета за печат, София, 2008.
- [4] Кузманов, Е., В. Стефанов. Оптимизиране работата на електрофилтър, предназначен за малки помещения. Сп. Селскостопанска техника, бр. 1, 2000, стр.47-49
- [5] Митков, Ат., Д. Минков. Статистически методи за изследване и оптимизиране на селскостопанска техника – II ч. Земиздат, С., 1993.
- [6] Михайлов, Н., В. Стефанов, Д. Киряков. Възможност за използване на електрофилтри във ферми за клетъчно отглеждане на птици. IX международен научен конгрес “Механизация и енергия в СС”, гр. Измир, стр.200-202, Турция, 2005.
- [7] Русанов, А. Справочник по пыле и золоулавливаю. Энергоатомиздат, М., 1983.
- [8] Kreyszing, E. Advanced engineering mathematics, seventh edition. John Wiley and Sons, Inc. 1993.

## Biographies



**Dimcho Kiriakov** was born in the village of Shtraklevo, Ruse, Bulgaria, on March 17, 1959. He graduated from the Technical University - Ruse, and received Dr. degree from the same university.

He has worked in the Faculty of Electrical and Electronic Engineering as a lecturer since 1987 and his field of interest includes automation of the microclimate in poultry farms.

Dimcho Kiriakov is with the Faculty of Electrical and Electronic Engineering, University of Ruse, 8, Studentska str., 7000 Ruse, Bulgaria (e-mail: kiriakov@ru.acad.bg)

# Algorithm for Determining the Layout of Electric Filters while Implementing them in Poultry Farms

Dimcho Kiriakov and Nikolay Mihailov

**Abstract:** An algorithm has been offered that allows us to estimate the minimum number and the layout of electric filters for which the required veterinary-hygienic norms are met when the dust content in the poultry room is known.

**Keywords:** electric filter, mathematical model, optimization.

## Introduction

Electric filters have a number of advantages to other dust catchers such as universality, high productivity, a high degree of dust catching, low energy consumption, ability to work with hot gases, etc., which gives them priority when we choose equipment for cleaning air and gas emissions from solid and liquid particles. The optimization of their operation is an indelible part of their utilization. It leads to maximum efficiency implementation of this hi tech equipment. Different types of electric filters utilized mainly in industry have been discussed in works on the subject [5]. Some optimizations have been realized, but there are no known results from their use in poultry farms, which necessitates further research in this sphere [1].

The purpose of this research is to suggest new methods, which allow the proper selection of the number and layout of electric filters while implementing them in poultry farms.

## Description

The norms apply to the cases of using more than one electric filter for each poultry room, which leads to more even cleaning of the air in their living ambience. With a proper layout, the desired veterinary-hygienic norms are achieved by using a minimum number of electric filters [2,3].

The main stages in determining the layout of the electric filters to be implemented in poultry farms are:

- calculating the area of the poultry room  $S_{mm}$ . Only the air in their living ambience needs to be cleaned;
- determining the impact of one filter on the surrounding ambience, i.e. the degree of air cleaning  $\eta$  depending on the distance  $x$  from it -  $\eta=f(x)$  (fig.1);
- measuring the dust concentration in the poultry room;
- calculating the distance between two working electric filters.

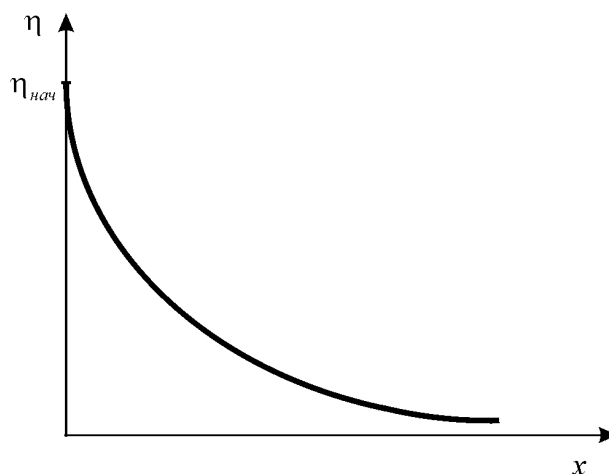


Fig.1 Degree of air cleaning  $\eta$  depending on the distance  $x$  from the electric filter

When two adjacent filters are in operation, there is some interrelation between them, which can be perceived from their characteristics on fig. 2, i.e. there is some overlapping. This can be accounted for by determining the areas of their interrelation

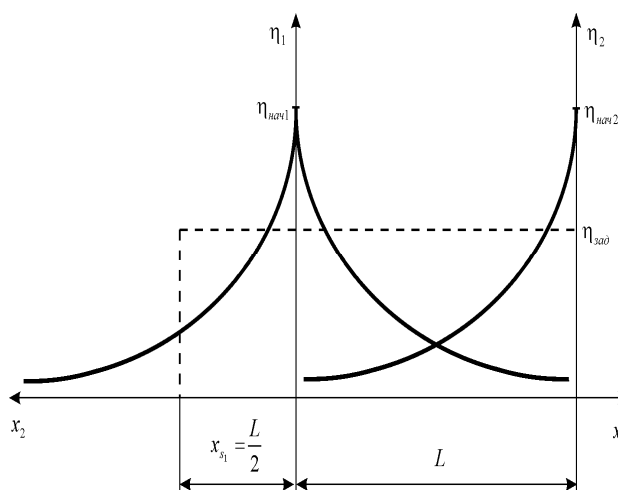


Fig.2 Interrelation between two adjacent electric filters during their operation

$\eta=f(x)$  after integration [4]

$$(1) \quad S_1=S_2=\int_0^{x_1} f(x)dx,$$

And then calculating the total area

$$(2) \quad S=S_1+S_2.$$

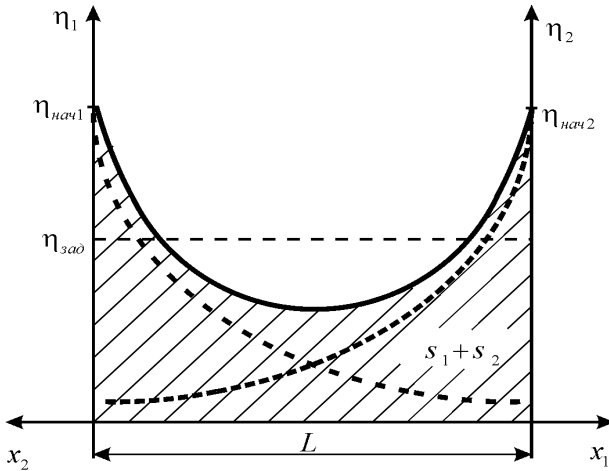


Fig.3 Calculating the distance  $L$  between two operating electric filters taking into account their interrelation

When the area  $S$  is divided by the mean value of the degree of air cleaned, which coincides with the required veterinary-hygienic norms  $\eta_{3a\delta}$ , we find the distance between the two electric filters  $L$ , for which these norms can be achieved (fig.3)

$$(3) \quad L = \frac{S}{\eta_{3a\delta}}.$$

Analogously, we calculate the distance  $x_{s1}$  from an end electric filter to the periphery of the poultry zone, for which the mean value of the area  $S_1$  corresponds to the required veterinary-hygienic norms

$$(4) \quad x_{s1} = \frac{S_1}{\eta_{3a\delta}} = \frac{L}{2};$$

- determining the total number of electric filters. The area covered by one electric filter, which is part of the total poultry area, will have a square shape with side length  $L$  (fig.4) and area

$$(5) \quad S'_{\text{ef}} = L^2,$$

And the area covered by one working electric filter will have the shape of a circle with a radius  $\frac{L}{2}$  and area (fig.4)

$$(6) \quad S''_{\text{ef}} = \pi \left(\frac{L}{2}\right)^2.$$

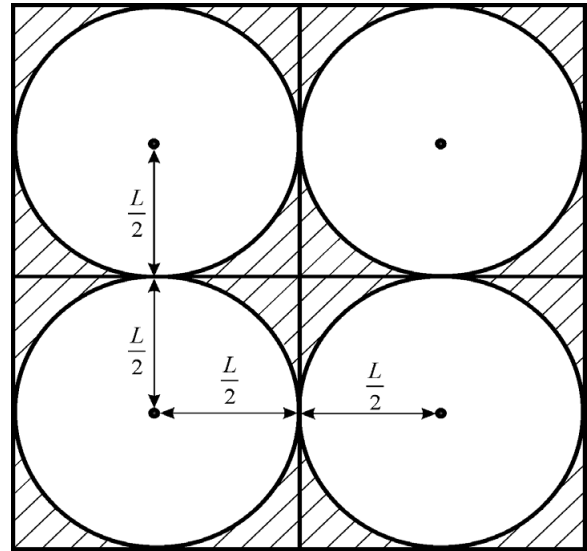


Fig.4 Electric filters layout without overlapping of working zones

It can be established that if we take into account  $S'_{\text{ef}}$  when determining the total number of electric filters, the angles of each square will not be covered by the operation of the respective electric filter, i.e. the quality of air cleaning there will be lower. This necessitates the use of  $S''_{\text{ef}}$ . Then

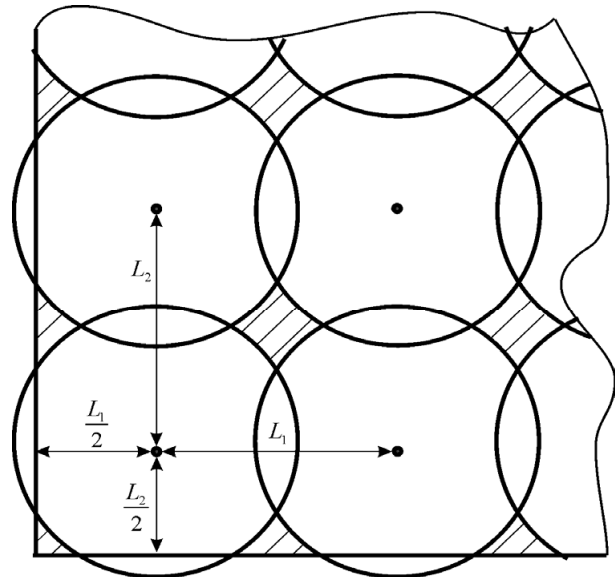


Fig.5 A layout of electric filters with their operating areas overlapping

the estimated number of electric filters needed for work in the poultry room will be

$$(7) \quad n = \frac{S_{nm}}{S''_{\text{ef}}}.$$

When  $S''_{\text{эф}}$  is used the area of the uncovered zones will decrease, and there will be zones of overlapping (fig.5), while the mean value of the degree of cleaning for all those spots will be close to the required one.

The number of electric filters needed for operation in the poultry room calculated in this way is tentative because:

- the dust concentration in the air is not a constant;
- practically, only in a specific case can we place a whole number of electric filters in the poultry area. Usually,  $n$  is a fraction which has to be rounded, and this means that the zones of overlapping will be different along the length and width of the room;
- the mathematical models describe the experimental data with a certain error, etc.

### Conclusion

The algorithm suggested allows the exact specifying of the minimum number of electric filters and their layout when implementing them in poultry farms in such a way that the required veterinary-hygienic norms are met.

### References

- [1] Кузманов, Е., В. Стефанов. Оптимизиране работата на електрофилтър, предназначен за малки помещения. Сп. Селскостопанска техника, бр. 1, 2000, стр.47-49.
- [2] Наредба №13 за защита на работещите от рискове, свързани с експозицията на химични агенти при работа. Д. В., бр. 8, стр. 51, 30.01.2004.
- [3] Наредба №44 за ветеринарномедицинските изисквания към животновъдните обекти. Д.В., бр. 41, стр. 44, 19.05.2006.
- [4] Никольский, С. М. Курс математического анализа. ФИЗМАТЛИТ, М., 2000.
- [5] Русанов, А. А. Справочник по пыли и золоулавливанию. Энергоатомиздат, М., 1983.

### Biographies



**Dimcho Kiriakov** was born in the village of Shtraklevo, Ruse, Bulgaria, on March 17, 1959. He graduated from the Technical University - Ruse, and received Dr. degree from the same university.

He has worked in the Faculty of Electrical and Electronic Engineering as a lecturer since 1987 and his field of interest includes automation of the microclimate in poultry farms.

Dimcho Kiriakov is with the Faculty of Electrical and Electronic Engineering, University of Ruse, 8, Studentska str., 7000 Ruse, Bulgaria (e-mail: [kiriakov@ru.acad.bg](mailto:kiriakov@ru.acad.bg))



**Nikolay Mihailov** was born in Ruse, Bulgaria, on November 27, 1947. He graduated from the university of Ruse and received his Doctoral degree from the same university in 1983.

His field of interest includes renewable energy sources (electrical aspects), electrical materials and engineering technologies in agriculture. He is associate professor in the Faculty of Electrical and Electronic Engineering

with the University of Ruse.

Nicolay Mihailov is with the Faculty of Electrical and Electronic Engineering with the University of Ruse, 8 Studentska str., 7017 Ruse, Bulgaria (e-mail: [mihailov@ru.acad.bg](mailto:mihailov@ru.acad.bg))

# A method of synthesis of proton exchange membrane fuel cell

Ruslan Ivanov

**Abstract:** A method of synthesis of electrode-catalyst with multilayered catalyst structure for membrane-electrode assembly (MEA), which provides for enhanced reaction surface, has been developed through magnetron sputtering. Fuel cells MEA has been prepared through the method that has been developed. The volt-ampere characteristics of the fuel cells that have been prepared are studied. The results analysis shows that the catalyst reaction surface has increased and as result of this, the current density is five times higher compared to one-layered two-dimensional catalyst structure.

**Keywords:** fuel cell, magnetron sputtering, multi-layered catalyst structure

## Introduction

Proton exchange membrane (PEM) fuel cells have a great application potential as mobile and stationary power supply to electric consumers. For such applications it is necessary that they work at high power densities and at the same time they have small quantities of catalyst that has been used, volume, weight, price, [1-7]. Nowadays the price of PEM fuel cells is high for their commercialization. In order that their price may decrease, the membrane-electrode-assembly characteristics (MEA) should be improved. In this aspect, methods for their production that provide for increased usage of catalyst material have been increasingly developed, [8, 9]. Methods for preparing MEA electrode-catalyst layer through “spay” method, [9], method of screen-printing, [10], deposition of catalyst layer in the form of coating in vacuum, [11, 12] are described in literature. Amongst the variety of methods, the method of catalyst coating deposition in vacuum is being outlined as the most perspective one because:

- It allows deposition of catalyst material with nano-sizes;
- It provides for uniform distribution over electrode surface;
- It allows a precise control over the quantity of catalyst material that is deposited;
- The process of deposition of catalyst is a simple one and is widely used in production of integrated circuits.

The objective of the current work is to prepare and study MEA for PEM fuel cell depositing multi-layered catalyst nano-coating over electrodes using the method of magnetron sputtering and thermal evaporation in vacuum.

## Experiment

A woven fabric cloth is graphitized in vacuum furnace under specifically defined time-temperature law.

The graphitized cloth is activated aiming at increasing its high specific surface area.

Ion conducting polymer as Nafion-115 has been processed in advance. A standard procedure is used for the purpose, described in [13], according to which a proton conductive membrane is consecutively processed with hydrogen peroxide solution and sulphuric acid at temperature of 80 - 100°C for 1 hour. The membrane is additionally cleaned and activated using glowing discharge. Thus the membrane is placed in gas discharge area of highly energetic argon ions for 1 hour.

## Preparing electrodes with one catalyst layer through thermal evaporation in vacuum

An existing vacuum installation is adapted for the purpose of the current study.

A working space is formed around tungsten evaporator, presented in figure 1, aiming at decreasing losses in process of evaporating catalyst material.



Fig.1. Tungsten evaporator with chromium-nickel sheet iron screen.

A graphitized cloth is placed in the space that has been formed. Preliminary experiments are undertaken to define the technological parameters of the process of thermal evaporation of catalyst material. The current fluctuation frontiers of thermal cleaning are defined -  $I_e$ , current of electricresistant heating for thermal evaporation -  $I_e$ , pressure of residual atmosphere in vacuum chamber -  $p$ , catalyst material losses in the process of coating deposition. The results are presented in table 1.



**Table 1**  
Technological parameters of the process of catalyst coating deposition through vacuum thermal evaporation

MEA №	Technological parameters				$m_{Pt}$ , mg/cm <sup>2</sup>
	$I_c$ , A	$T_{cleaning}$ , min	$p$ , mbar	$I_{evap}$ , A	
MEA1	10	60	$2 \cdot 10^{-6}$	150	0,2
MEA2	10	60	$2 \cdot 10^{-6}$	150	0,3
MEA3	10	60	$2 \cdot 10^{-6}$	150	0,1

**Preparing electrodes with one catalyst layer through magnetron sputtering in vacuum.**

Graphitized cloth is connected to specifically constructed holder and is placed in vacuum chamber for magnetron sputtering, figure 2, in order that catalyst coating may be deposited.



Fig.2. Magnetrons for catalyst sputtering in vacuum

The chamber pressure is pumped to reach  $1 \cdot 10^{-6}$  mbar. Argon gas is fed and in the condition of dynamic vacuum the pressure reaches  $3 \cdot 10^{-3}$  -  $3 \cdot 10^{-2}$  mbar. In the presence of ionization pressure, the gas is ionized and argon ions bombard the catalyst target. The catalyst particles being sputtered are deposited over the graphitized cloth and an active catalyst layer is formed. The catalyst material that is used in the experiments is platinum but it can be alloys based on it. The resultant quantity of platinum and the respective technological parameters-magnetron current,  $I_m$ , magnetron pressure,  $U_m$ ; operating pressure,  $P_{Ar}$  are presented in table 2.

**Table 2**  
Technological parameters of the process of catalyst coating deposition through magnetron sputtering in vacuum

MEA №	Technological parameters			$v_s$ , mg/cm <sup>2</sup> /min	Num ber of layers	$m_{Pt}$ , mg/ cm <sup>2</sup>
	$I_m$ , A	$U_m$ , V	$P_{Ar}$ , mbar			
MEA 14	1	900	$3 \cdot 10^{-2}$	0,056	5	0.3
MEA 15	1	900	$3 \cdot 10^{-3}$	0,028	5	1.6
MEA 16	1	900	$3 \cdot 10^{-3}$	0,028	3	0.3
MEA 17	1	900	$3 \cdot 10^{-3}$	0,028	1	0.3
MEA 18	1	900	$3 \cdot 10^{-3}$	0,028	5	0.28

After the catalyst layer has been formed, a thin layer of Nafion polymer and alcohol solution is deposited over graphitized cloth. Then the electrode that has been prepared is dried at temperature of 100 - 300°C for 1 - 2 hours.

**Preparing electrodes with multi catalyst layers through magnetron sputtering in vacuum.**

The multilayered catalyst electrodes are prepared depositing catalyst coating over graphitized cloth at pressure of the gas atmosphere of  $3 \cdot 10^{-3}$  -  $3 \cdot 10^{-2}$  mbar. After the necessary quantity of Pt has been deposited, Nafion solution is deposited over graphitized cloth. The procedure is repeated until the necessary layers (PTFE-Pt) and quantity of platinum are formed, figure 3.



Fig.3. Block diagram of electrode-catalyst structure of MEA

**Preparing MEA**

The processed polymer membrane is dried and a layer of polytetrafluoroethylene (PTFE) solution is deposited over the electrode area. Electrodes with sizes 5x5 cm are formed from the graphitized cloth over which a Pt coating has been deposited through vacuum thermal

evaporation and electrodes with sizes 2x2 cm are formed from the graphitized cloth over which a Pt coating is deposited through vacuum magnetron sputtering. Minimization of the contact electrical resistance between the electrodes and ion conducting membrane, and increasing the number of phase boundaries of catalyst-electrolyte as well are carried out using hot pressing methods.

MEA that have been prepared by different quantity of catalyst material and methods of forming electrode-catalyst layer are used in fuel cell production.

#### Defining MEA volt-ampere characteristics

The MEA that has been prepared, presented in figure 4, is placed between two silicon gaskets.



Fig.4. MEA prepared in accordance with the current study

MEA and the gaskets are positioned between two plates with gas channels. The pressure necessary to make the fuel cell tight is carried out by bolts. The fuel cell prepared in accordance with the current study is presented in figure 5.

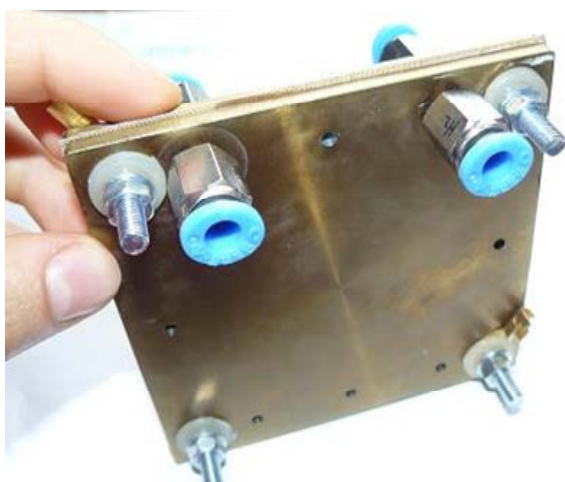


Fig.5. PEM fuel cell prepared in accordance with the current study.

Before defining the polarization curves of the MEA that have been prepared, they are activated in accordance with procedures described in [14].

Volt-ampere characteristics are defined after the PEM fuel cell has been working for 1 hour and pressure defined at temperature of 50°C, and maintaining optimal operating parameters of reacting gases.

#### Results analysis

Volt-ampere characteristics of the fuel cells that have been prepared through vacuum thermal evaporation and magnetron sputtering are presented respectively in figure 6 and 7.

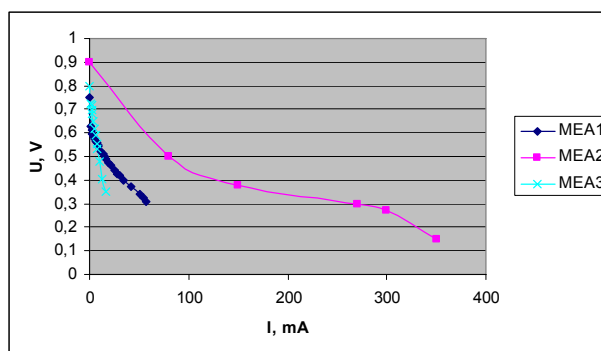


Fig.6. Volt-ampere characteristics of MEA that are being studied, prepared through vacuum thermal evaporation.

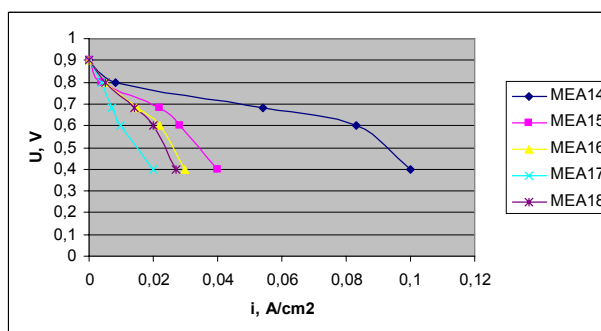


Fig.7. Volt-ampere characteristics of MEA that are being studied, prepared through vacuum thermal evaporation.

According to figure 6 the maximum current density of MEA that has been prepared through thermal evaporation of catalyst material is 15mA/cm<sup>2</sup> and the deposited quantity of platinum is 0,3 mg/cm<sup>2</sup>. The graphic dependence shows that the open circuit voltage of samples MEA1 and MEA3 is under 0,8 V, which is due to great activation losses. Activation losses in fuel cells are due to the processes of adsorption of reagent particles, electron transfer, desorption of product particles and electrodes' characteristics. The current densities in these cases are respectively 3 and 1 mA/cm<sup>2</sup>. This is due to low catalyst activation surface i.e. reduced numbers of reaction fields-electrolyte-catalyst-gas. As a result of increasing the number of reaction points through higher quantity of catalyst material for MEA2, figure 6, the current density increases up to 15 mA/cm<sup>2</sup>.

Nevertheless, the number of catalyst points is relatively small and the utilization efficiency of catalyst is insufficient.

This disadvantage is eliminated through increasing the active catalyst surface. The catalyst material that has been deposited over gas diffusion layer through magnetron sputtering in vacuum provides for current density increase and utilization efficiency of catalyst material respectively, figures 6 and 7, respectively graphics MEA2 and MEA17.

### Conclusion

Proton exchange membrane fuel cells have been prepared which catalyst layers are prepared through magnetron sputtering in vacuum and vacuum thermal evaporation. The fuel cells that have been prepared are activated and tested. Their volt-ampere characteristics are defined. The results analysis shows that the MEA electrode-catalyst layers that have been prepared by magnetron sputtering have better characteristics compared to those that have been prepared by thermal evaporation in vacuum. It is observed that the catalyst performance increases in the case of preparing electrode-catalyst layer through PTFE catalyst sublayers. In this occasion the PEM fuel cell current density is 5 times higher than that of fuel cells with one-layer catalyst structure.

### References

- [1] Fuel Cell Handbook, 6<sup>th</sup> edition, U. S. Department of Energy, November 2002, p.1.
- [2] S. Hirano, J. Kim, S. Sriaivasan, *Electrochim. Acta* 42 (1997) 1587.
- [3] S. Gamburgzev, A. J. Appleby, *J. Power Sources* 107 (2002) 5.
- [4] R. Richards, R. Mertel, H. Bannemann, *Fuel cells Bull.* 37 (2001) 7.
- [5] R. Mosdale, S. Srinivasan, *Electrochim. Acta* 40 (1995) 413.
- [6] T. Susai, M. Kaneko, K. Nakato, T. Isono, A. Hamada, Y. Miyake, *Int. J. Hydrogen Energy* 26(2001) 631.
- [7] M.J. Escudero, E. Hontanon, S. Sewartz, M. Bautonner, L. Daza, *J. Power Sources* 106 (2002) 206.
- [8] C. H. Hsu, C. C. Wan, *J. Power Sources* 115 (2003) 268.
- [9] G. Sassikumar, J.W. Ihm, H Ryu, *J. Power Sources* 132 (2004) 11.
- [10] C. S. Kim, Y. G. Chun, D. H. Peck, D. R. Shin, *Int. J. Hydrogen energy* 23 (1998) 1045.
- [11] S. Y. Cha, W. M. Lee, *J. Electrochem. Soc.* 146 (1999) 4055.
- [12] A.T. Haug, R. E. White, J. W. Weidner, W. Huang, S. Shi, T. Stoner, N. Rana, *J. Electrochem. Soc.* 149 (2002) A280.
- [13] J. Larminre, A. Dicks, *Fuel cell systems explained*, 2003.
- [14] P. Иванов, М. Минчев, *Определяне характеристики на горивна клетка с протонообменна мембрана, Е+Е*, 2006.

**Ruslan Ivanov** was born in Rouse, Bulgaria, on September 26, 1979. He graduated from the Technical University – Sofia.

His field of interest includes renewable energy sources, hydrogen energy system, fuel cell, materials with hydrogen absorption properties, electrolysers and etc. He is today a PhD student in the Faculty of Electrical Engineering of the Technical University – Sofia.

Ruslan Ivanov is with the Faculty of Electrical Engineering, Technical University of Sofia, 8, Kl. Ohridski Blvd., 1000 Sofia, Bulgaria (e-mail: [rus\\_ivanov@tu-sofia.bg](mailto:rus_ivanov@tu-sofia.bg))

# Measuring Electrical and Thermal Characteristic Using a Digital Multimeter and LabVIEW

Stoill Stannev

**Abstract:** Modern digital multimeters can be connected to personal computers in order to transfer data. This could be an easy and comfortable way to monitor and log different processes. One of the main problems is that usually software bundled with these multimeters is unsatisfactory for some particular needs. This article describes an easy way for creating advanced applications for monitoring and logging data using LabVIEW.

**Keywords:** DMM, data logging, LabVIEW, multimeter, temperature monitoring

## Introduction

Most modern digital multimeters (DMM) can be connected to a computer using the RS232 interface (usually known as *com port*). This makes them proper for data logging. Indeed, many users complain that software, supplied by the DMM manufacturers has very limited abilities and is often not proper for their needs. Creating advanced applications for communication between the computer and the DMM and for processing the acquired data is not a hard task even for those, who are not much experienced in programming. This article describes how to create such a software tool, using LabView.

## Concepts

Communication between a computer and a DMM through the RS232 interface usually works the following way: the computer sends a request to the DMM and it returns the required data. The data returned shall be parsed and converted to a user friendly format.

## Acquiring the request string

One of the problems is that usually DMM request strings are not published in the user manuals. One of the methods to find the request string is to make a computer programme that tries all possible requests, until receiving an answer from the DMM. This could be a solution for some of the cases, when the request is not longer than one or two bytes. When the request is sent, the answer is not received immediately, but with some delay. If this delay is 1 second, then for a one byte long request the maximum time for finding the correct string is  $2^8=256$  seconds. For a five byte request finding the exact string may take up to  $2^{8.5}=1099511627776\text{sec}\approx 35\,746$  years. Such a long time is unacceptable but another solution is available.

The com port can be *sniffed*, or in other words all the data send and received through the port can be observed by the user. A programme, called *sniffer* shall be used.

An application named *Free Serial Port Monitor* was found appropriate. Finding the request string with it is quite easy.

First, the application shall be installed and run. From its menu *File/New Session* shall be selected. Then *Next* shall be pressed, *Serial Port Monitor* shall be selected. When it comes to entering *Serial Device Name*, the name of the COM port, to which the DMM is attached, shall be selected. On the next step all the visualizers shall be selected. Upon pressing *Finish* the port monitor is ready. After that the software, supplied with the DMM shall be started, adjusted and run. In fact, connecting the multimeter itself may not be necessary, but the COM port number shall be entered manually, if this is available for the application.

After running the DMM bundled application, the request sent can be seen in the *Request View* panel (Fig. 1). On the figure it can be seen that the request has ASCII code H44 (decimal 68, the *H* character in front of the numbers stands for *hexadecimal*), which corresponds to the capital letter D. The letter D can be seen on the right side of the panel. Because the multimeter software made four requests, before giving up with an error message, the request string is displayed four times. These characters were displayed with 1 second delays between each of them, because such were the settings of the DMM application.

## Parsing data

Data sent from the DMM (*Acquired data array* on Fig. 5) needs to be parsed. This task can take a lot of time and shall be done very carefully, in order to evade mistakes. Different multimeters use different data formats. Usually it consists of several bytes. Some of the bytes contain the measurement quantity, other indicate the measurement unit (volts, ampere, ac, dc, etc).

There are two main methods for representing the data-using hexadecimal values or binary-coded decimal (BCD).

In the first case the value is represented as a hexadecimal number and it has to be converted to a decimal. Usually the value cannot be represented by one byte only, so it takes two or more bytes. To acquire the value the higher byte shall be multiplied by  $2^8=256$  (or  $2^7=128$  if 7 bit transfer mode is used) and added to the lower byte.

(1) Value= HB.256+LB

After that a decimal delimiter shall be placed at the right place. Usually its location is determined from some of the other bytes in the string.



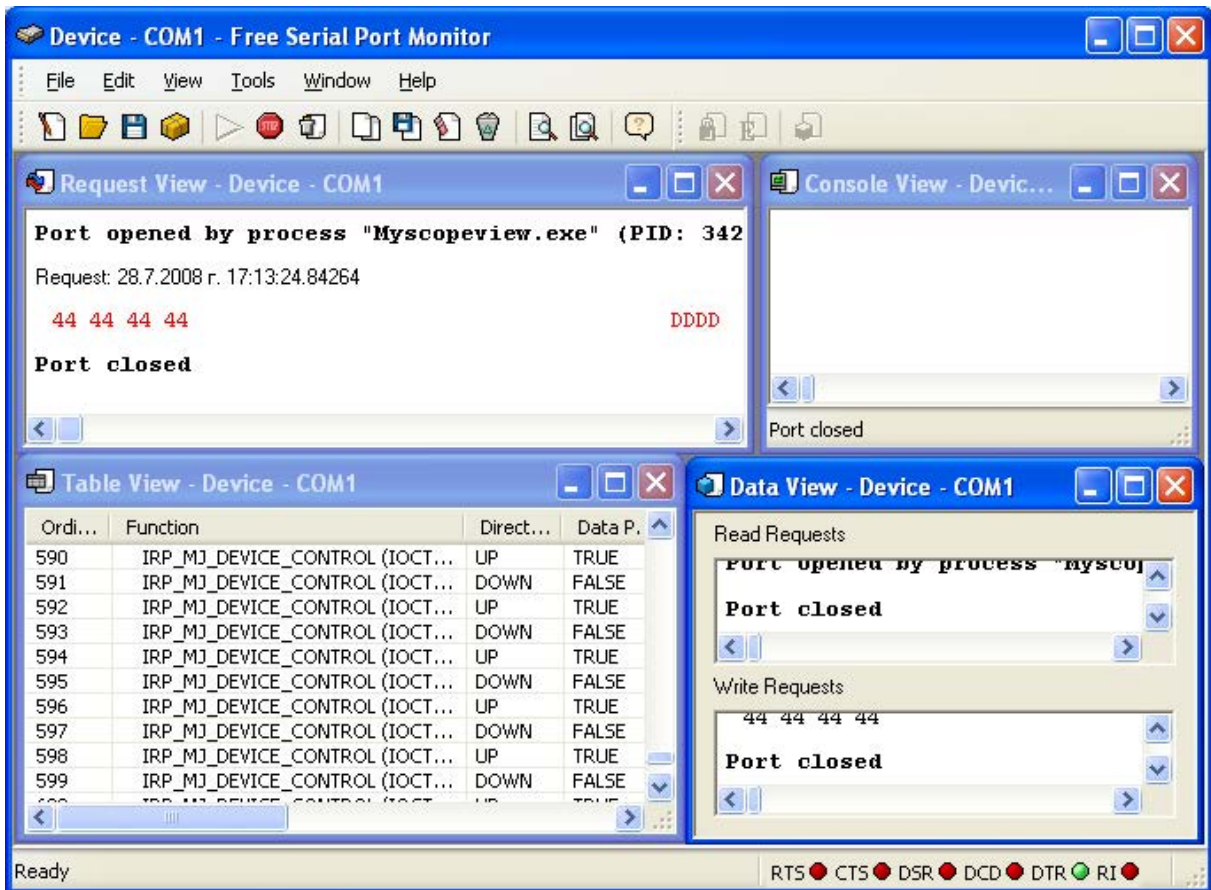


Fig. 1

When the number is written as BCD, it shall be converted to decimal the following way:

(2)  $FHB.1000 + SHB.100 + FLB.10 + SLB$  where:

HB= higher byte

LB= lower byte

FHB= firsts semibyte of the higher byte

SHB= firsts semibyte of the higher byte

FLB= firsts semibyte of the higher byte

SLB= firsts semibyte of the higher byte

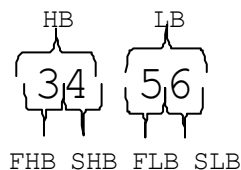


Fig 2

For example if the higher byte is H34 and the lower is H56 the number is  $3.1000+ 4.100+ 5.10+6= 3 456$ . A visual representation of a BCD byte is displayed on figure 2.

In order to find how data shall be parsed, a stabilised signal source shall be used.

Here is how acquiring temperature reading with a multimeter MS1280 can be achieved. It is determined that the request for this DMM is the character D (ASCII

H44, D68). Comparing data, displayed on the meter display and the received bytes leads to the conclusion that in bytes №3 and №4 (counting starts from byte №0) temperature is sent as centigrade, and in bytes №6 and №7 temperature is given as Fahrenheit degrees. If the first semibyte of byte №2 is 0 the measured value is positive, and if it is 1, measured value is negative (i.e. 0 stands for + and 1 for -).

### Example

This method was originally developed for logging temperature during mechanical endurance tests of on-load tap changers, but an example for measuring temperature rise of a transformer will be shown. A DMM MS1280 is used. It is equipped with a thermocouple type K. The thermocouple is attached with thermoconductive glue to the external part of the coil of a transformer. The resistance of the load of the transformer is decreased in two steps, thus increasing the current and respectively the temperature rise.

The request is found to be the capital character D. The multimeter uses BCD data representation. Temperature is represented in whole centigrade (i.e. no fraction part) in bytes №3 (higher) and №4 (lower). The sign of the temperature (+ or -) is represented in the first four bits of byte- 0 stands for -, and 1 stands for +.



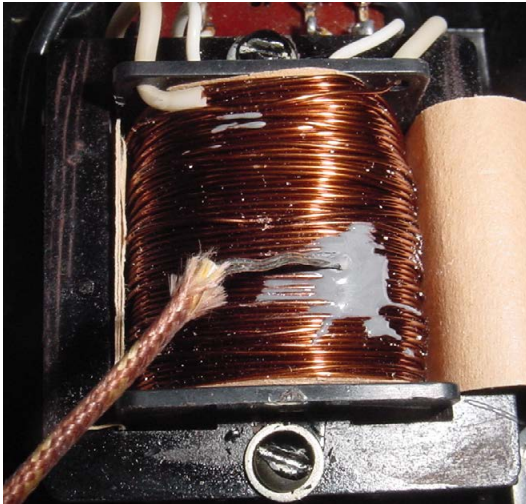


Fig. 3

In order to determine the ASCII code of a character, the *TypeCast* function of LabVIEW shall be used (located in *Functions menu/Advanced/Data Manipulation*). The input character shall be connected to the input terminal of the function and a constant with representation U8 (unsigned 8-bit integer) shall be connected to the *Type* terminal). The received number is split into semibits and sent to a *XY graph*, together with the time. The readings and the time are stored into a file after each value is acquired. This ensures that data will not be lost in case of a problem with the computer. The virtual instrument is done in such a way that data from new measurement sessions is added to those from previous one, unless a new file name is selected. The back panel of the virtual instrument is displayed on Fig. 4 (subinstruments used are shown at the upper part of the figure). The *Serial*

*Read* subinstrument is located in the virtual instrument library *smplser.llb* under the name *Serial Read with Timeout.vi*.

On the front panel (Fig. 5) a temperature rise curve of the transformer at two different loads (respectively currents) is displayed.

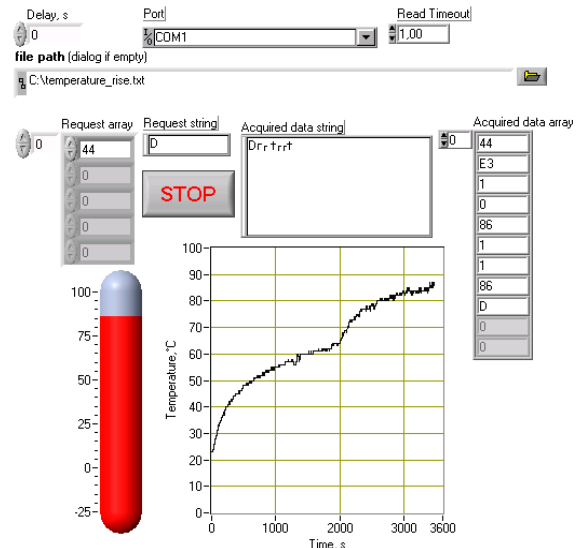


Fig 5

### Conclusion

The presented method may be an affordable solution for monitoring and data logging. The given examples are realised with LabVIEW, which is already taught in some of the technical universities, but they can be rewritten in another programming language. Measurement precision depends on the DMM used, but later data processing is

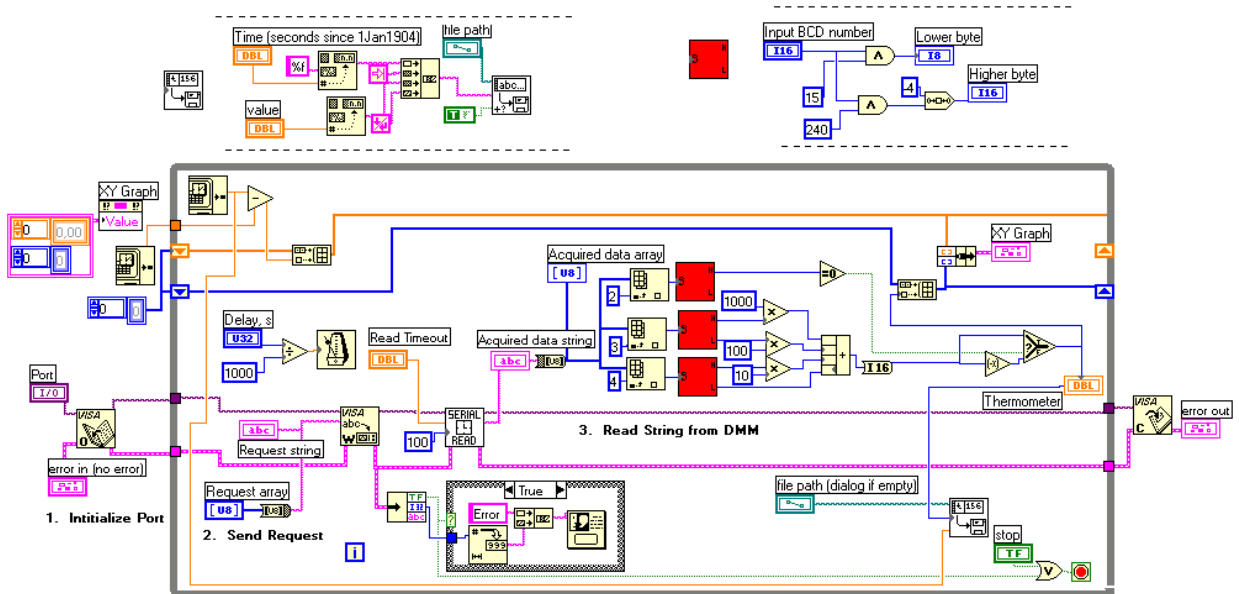


Fig. 4

available. Stored data can be manipulated and visualised with other programs (MS Excel, OpenOffice.org Spreadsheet, etc). One of the main negatives of the method is that it allows only a small number of simultaneously monitored values, because the common multimeters are single channel and computers rarely have more than two RS232 ports. Because parsing method is found by empirical means, it may cause errors.

## References

- [1] R. Bitter, T. Mohiuddin, M. Nawrocki *LabView: Advanced Programming techniques*, CRC Press, 1991
- [2] J. Kring, *LabVIEW for Everyone: Graphical Programming made Easy and Fun*, Prentice Hall, 2006



**Stoill Stannev** was born in Plovdiv, Bulgaria on December 28, 1978. He studied at the Technical University of Sofia-Bulgaria and received a master degree from the same university in 2002.

Since 2002 he works in Hyundai Heavy Industries Co. Bulgaria as a test engineer.

His field of interest includes on- load tap changers, data acquisition, test optimization and automation. Today he is a PhD student in

the Faculty of Electrical Engineering of the Technical University – Sofia.

Stoill Stannev is with the Hyundai Heavy Industries Co. Bulgaria, 41, Rouzhen Blvd., 1271 Sofia, Bulgaria (e-mail: sstanev@mail.ru)

# Impact of Wall Luminance on Surface Luminance in Road Tunnels

Angel Pachamanov, Dessislava Pachamanova, Kirilka Ivanova

**Abstract:** In order to ensure safe entry into a road tunnel, the average luminance of the walls must be commensurate with the average luminance of the road surface. The calculation of the luminance of the road surface usually excludes the component of the flux reflected by the walls and the ceiling of the tunnel, which leads to an increase in the required power for installations. This report analyzes the effect of the reflected component of the flux on the luminance of the road surface given relationships between the luminance of the walls, the ceiling and the road surface.

**Keywords:** tunnel lighting, light distribution, road surface reflection

## Introduction

Normative documents for design of lighting installations require that the wall's luminance be greater than or equal to the luminance of the road surface (Fig.1).

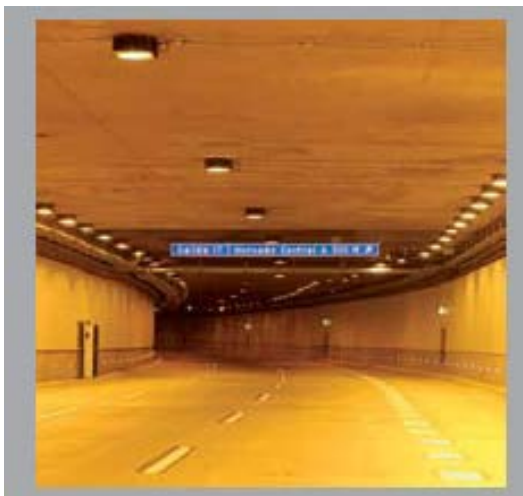


Fig.1. Typical luminance distribution in a road tunnel [1]

The design of tunnel lighting installations is usually done with computer programs for street lighting, which calculate the luminance of the road surface by using only the direct component of the flux from the luminaries. In order to satisfy the requirement that the luminance of the walls be equal to the luminance of the road surface, the luminaries for tunnel lighting are designed so that a fraction of the flux from the lighting sources falls directly on the walls. Therefore, the luminance of the road surface is increased by the flux reflected from the walls. Some flux is reflected off the ceiling as well. If one could

estimate the percentage of the luminance of the road surface that can be attributed to the flux reflected from the walls and the ceiling, it would be possible to reduce the amount of the direct flux from the light source to the road surface. This would lead to a reduced power requirement for the installation and, consequently, to savings in terms of investments and realized power consumption.

This report discusses a method for estimating the influence of the component of the luminous flux that is reflected from the walls and the ceiling on the luminance of the road surface. For that purpose, the surfaces of the walls and the ceiling are treated as luminaries with light distributions typical for vertical and horizontal diffusion-reflecting flat surfaces.

## Light distribution of horizontal and vertical flat element

### (A) Horizontal diffusion-reflecting surface

According to Lambert's Law, when a surface is diffusion-reflecting, the vector-points of the luminous intensities of the reflected light form the surface of a sphere, irrespectively of the direction of the rays falling on the surface (Fig. 2).

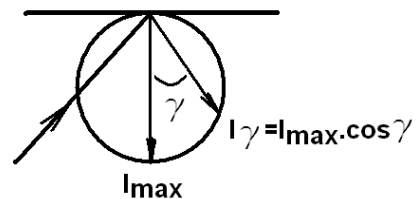


Fig.2. Lambert's Law for diffusion-reflecting horizontal flat surface

From the definition for luminous intensity  $I = d\Phi/d\Omega$  (quantity of luminous flux  $d\Phi$ , irradiated in elementary space angle  $d\Omega$ ) and Lambert's Law  $I_\gamma = I_{\max} \cdot \cos \gamma$  for reflected light from diffusion-reflecting surface, it can be deduced that  $I_{\max} = \Phi_{\text{refl}}/\pi$ , where  $\Phi_{\text{refl}}$  is the flux reflected by a surface of a sufficiently small unit area  $S$ .

If the horizontal light-reflecting element (light-reflecting surface) is treated as a luminary with efficiency 100 % and conditional luminous flux 1000 lm, the values of the luminous intensities can be expressed according to the required format (Fig.3) for calculating the distribution of the luminance of the road surface. Each value of luminous intensity in the table required by the computer program for light technical calculations can be obtained from the following formula:

$$(1) \quad I(C, \gamma) = \frac{1000}{\pi} \cos \gamma.$$

$$(2) \quad I(C_x, \gamma) = \frac{1000}{\pi} \sin C_x \cdot \sin \gamma.$$

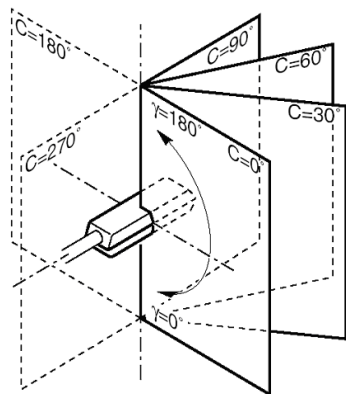


Fig.3. Standard format for luminaire light distribution (I-table) in candelas per 1000 lamp lumens for street and tunnel luminaires

#### B. Vertical diffusion-reflecting surface

When the surface is vertical diffusion-reflecting, according to Lambert's Law the photometric body of the reflected light is also a sphere, but its centre is not located on the photometric axis, in relation to which the reported angle  $\gamma$  is calculated. Hence, the light distribution curve for every C-plane is different, because it is a result of the intersection between the sphere that is shifted by  $I_{\max}/2$  relative to the axis of the assigned C-planes.

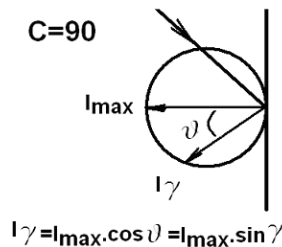


Fig.4. Lambert's Law for diffusion-reflecting vertical flat-surface

Fig. 4 shows the intersection of the plane C90 with the photometric body of the reflected light (a sphere with radius  $I_{\max}/2$ ), and it can be seen that  $\gamma=90-\psi$ . It's known [3] that every intersection of a plane with a sphere creates a circumference with a different diameter  $I(C_x, \gamma=90)=I_{\max} \cdot \cos(90-C_x)=I_{\max} \cdot \sin C_x$ . In this case, if the vertical lighting element is treated as a luminaire with efficiency 100 % and conditional luminous flux 1000 lm, the light distribution curves can be expressed according to the CIE format requirements for calculating the luminance of the road surface. Each value of  $I(C, \gamma)$  is obtained from the formula:

The calculated values of the luminous intensities from formulas 1 and 2 for:

$C=270, 285, 300, 310, 315, 320, 325, 330, 335, 340, 345, 350, 355, 0, 5, 10, 15, 20, 25, 30, 35, 40, 45, 50, 60, 75, 90, 105, 120, 130, 135, 140, 145, 150, 155, 160, 165, 170, 175, 180$

and

$\gamma=0, 10, 20, 30, 35, 40, 45, 47.5, 50, 52.5, 55, 57.5, 60, 62.5, 65, 67.5, 70, 72.5, 75, 77.5, 80, 82.5, 85, 87.5, 90, 92.5, 95, 97.5, 100.0, 102.5, 105.0, 120, 135, 150, 165, 180$

are shown in Tables 1 and 2.

Table 1

Luminous intensities for diffusion-reflecting horizontal flat-surface  $I(C_x, \gamma)$ , cd/klm (file DL61)

$\gamma$	0,0	10,0	20,0	30,0	35,0	40,0	45,0	47,5	50,0	52,5	55,0
$I(\gamma)$	318	313	299	276	261	244	225	215	205	194	183
$\gamma$	57,5	60,0	62,5	65,0	67,5	70,0	72,5	75,0	77,5	80,0	82,5
$I(\gamma)$	171	159	147	135	122	109	96	82	69	55	42
$\gamma$	85,0	87,5	90,0								
$I(\gamma)$	28	14	0								

Table 2

Luminous intensities for diffusion-reflecting vertical flat-surface  $I(C_x, \gamma)$ , cd/klm (file DL62)

$\gamma \setminus C$	0	5	10	15	20	25	30	35	40	45	50	60	75	90
	180	175	170	165	160	155	150	145	140	135	130	120	105	
0,0	0	0	0	0	0	0	0	0	0	0	0	0	0	0
10,0	0	5	10	14	19	23	28	32	36	39	42	48	53	55
20,0	0	9	19	28	37	46	54	62	70	77	83	94	105	109
30,0	0	14	28	41	54	67	80	91	102	113	122	138	154	159
35,0	0	16	32	47	62	77	91	105	117	129	140	158	176	183
40,0	0	18	36	53	70	86	102	117	132	145	157	177	198	205
45,0	0	20	39	58	77	95	113	129	145	159	172	195	217	225
47,5	0	20	41	61	80	99	117	135	151	166	180	203	227	235
50,0	0	21	42	63	83	103	122	140	157	172	187	211	236	244
52,5	0	22	44	65	86	107	126	145	162	179	193	219	244	253
55,0	0	23	45	67	89	110	130	150	168	184	200	226	252	261
57,5	0	23	47	69	92	113	134	154	173	190	206	232	259	268
60,0	0	24	48	71	94	117	138	158	177	195	211	239	266	276
62,5	0	25	49	73	97	119	141	162	181	200	216	245	273	282
65,0	0	25	50	75	99	122	144	165	185	204	221	250	279	288
67,5	0	26	51	76	101	124	147	169	189	208	225	255	284	294
70,0	0	26	52	77	102	126	150	172	192	212	229	259	289	299
72,5	0	26	53	79	104	128	152	174	195	215	233	263	293	304
75,0	0	27	53	80	105	130	154	176	198	217	236	266	297	307
77,5	0	27	54	80	106	131	155	178	200	220	238	269	300	311
80,0	0	27	54	81	107	132	157	180	201	222	240	271	303	313
82,5	0	28	55	82	108	133	158	181	203	223	242	273	305	316
85,0	0	28	55	82	108	134	159	182	204	224	243	275	306	317
87,5	0	28	55	82	109	134	159	182	204	225	244	275	307	318
90,0	0	28	55	82	109	135	159	183	205	225	244	276	307	318
92,5	0	28	55	82	109	134	159	182	204	225	244	275	307	318
95,0	0	28	55	82	108	134	159	182	204	224	243	275	306	317
97,5	0	28	55	82	108	133	158	181	203	223	242	273	305	316
100,0	0	27	54	81	107	132	157	180	201	222	240	271	303	313
102,5	0	27	54	80	106	131	155	178	200	220	238	269	300	311
105,0	0	27	53	80	105	130	154	176	198	217	236	266	297	307
120,0	0	24	48	71	94	117	138	158	177	195	211	239	266	276
135,0	0	20	39	58	77	95	113	129	145	159	172	195	217	225
150,0	0	14	28	41	54	67	80	91	102	113	122	138	154	159
165,0	0	7	14	21	28	35	41	47	53	58	63	71	80	82
180,0	0	0	0	0	0	0	0	0	0	0	0	0	0	0

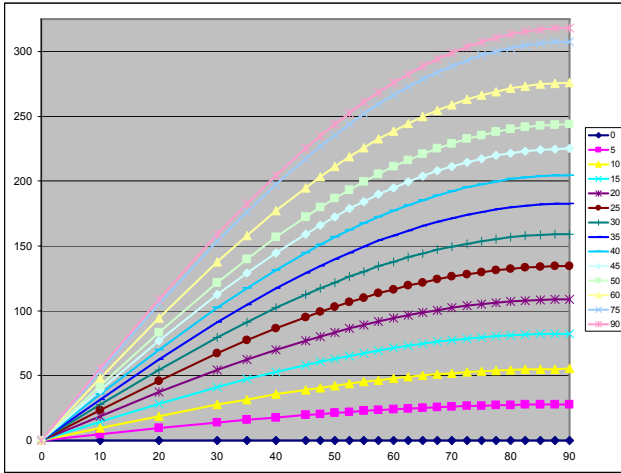


Fig.5. Luminous intensities for diffusion-reflecting vertical flat-surface  $I(C_x, \gamma)$ , cd/klm ( $\gamma=0 \dots 90$  and parameter  $C_x=0, 5, \dots 90$ )

**Calculations**

As illustrated in Fig. 1, the walls and the ceiling can be divided into light-reflecting unit surfaces of specific dimensions, and every surface can be treated as a luminaire with luminous flux  $\Phi_{\text{orp}}=I_{\text{max}} \cdot \pi=L.S.\pi$ , where S is the area of the unit surfaces. (For example, the unit area can be 1x2 m for the walls and 2,5x2 m for the ceiling).

If the luminance of the walls is assumed to equal the luminance of the road surface, e.g., 100 cd/m<sup>2</sup>, then the influence of these “luminaries” can be determined with the help of a computer program for calculating street lighting installations, in which every luminaire emits flux  $\Phi_{\text{refl}}=L.S.\pi=100.1.2.3,14=628$  lm. In this case, four “street lighting installations” should be considered, with mounting height of the luminaries (H) 3,5 m, 2,5 m, 1,5 m, and 0,5 m, respectively, and with the following input data [4]:

```

Single digit indicating the mode of operation      2
Any 72 character name desired by the user        up to 72
Symmetrical/Asymmetrical light distribution      1/01
Calculation of illuminance? 1/0
Luminaire light distribution (file):              DL62
Road surface reflection (file):                  rr03
Identification number of luminaire:              62
Luminous flux of lamp:                           0,63 klm
Flashed area of the luminaire:                   0,1 m2
Upcast angle of the luminaire, as installed:    0
Reflection properties of the road surface (R-table) 3
Average luminance coefficient of the R-table:    0,07 cd/m2/lx
Arrangement of the luminaries
(1- Single-side (left), 4- Opposite)            4
Mounting height of the luminaries (H):          3,5 m
Luminaire spacing (S):                           2 m
Width of the carriageway (WK):                   10 m
Width of the median (WM):                        0 m
Overhang – left luminaries (OH1):               0 m
Overhang – right luminaries (OH2):              0 m

```

The so determined data are entered into an input file for the computer program for street lighting [4], and only

the mounting height of the luminaries (H=3,5 2,5 1,5 0,5 m) is different in the four cases. The first input file for calculating and installation with H=3,50 m has the following format:

```

2
Wall 1x2m, Phi=L.S.pi=100.2.3,14=628 lm
1 dl62rr03
62 00.63 0.10 00.00 3.00 0.070
4. 03.50 02.00 10.00 0.00 0.00 0.00

```

**Results from the four cases:**

*I. Mounting height of the luminaries: 3,5 m*

Observer position: R = 5.00; S = 0.00

Luminance distribution in one luminaire spacing

R/S	60.0	60.2	60.4	60.6	60.8	61.0	61.2	61.4	61.6	61.8
0.50	*	0.63	0.63	0.63	0.63	0.63	0.63	0.63	0.63	0.63
1.50	*	1.18	1.18	1.18	1.18	1.18	1.18	1.18	1.18	1.18
2.50	*	1.19	1.20	1.20	1.20	1.21	1.21	1.21	1.20	1.19
3.50	*	1.11	1.11	1.11	1.11	1.11	1.11	1.11	1.11	1.11
4.50	*	1.09	1.09	1.10	1.10	1.10	1.09	1.10	1.10	1.10
5.50	*	1.09	1.09	1.10	1.10	1.10	1.09	1.10	1.10	1.10
6.50	*	1.11	1.11	1.11	1.11	1.11	1.11	1.11	1.11	1.11
7.50	*	1.19	1.20	1.20	1.20	1.21	1.21	1.21	1.20	1.19
8.50	*	1.18	1.18	1.18	1.18	1.18	1.18	1.18	1.18	1.18
9.50	*	0.63	0.63	0.63	0.63	0.63	0.63	0.63	0.63	0.63

Average luminance: Lav = 1.04 cd/m<sup>2</sup>

*II. Mounting height of the luminaries: 2,5 m*

Observer position: R = 5.00; S = 0.00

Luminance distribution in one luminaire spacing

R/S	60.0	60.2	60.4	60.6	60.8	61.0	61.2	61.4	61.6	61.8
0.50	*	0.81	0.81	0.79	0.79	0.79	0.80	0.80	0.80	0.79
1.50	*	1.62	1.64	1.65	1.64	1.66	1.66	1.65	1.62	1.62
2.50	*	1.46	1.46	1.45	1.45	1.45	1.45	1.44	1.45	1.45
3.50	*	1.33	1.33	1.33	1.33	1.32	1.32	1.32	1.32	1.32
4.50	*	1.23	1.23	1.23	1.24	1.24	1.24	1.25	1.23	1.22
5.50	*	1.23	1.23	1.23	1.24	1.24	1.24	1.25	1.23	1.22
6.50	*	1.33	1.33	1.33	1.33	1.32	1.32	1.32	1.32	1.32
7.50	*	1.46	1.46	1.45	1.45	1.45	1.45	1.44	1.45	1.45
8.50	*	1.62	1.64	1.65	1.64	1.66	1.66	1.65	1.62	1.62
9.50	*	0.81	0.81	0.79	0.79	0.79	0.80	0.80	0.80	0.79

Average luminance: Lav = 1.29 cd/m<sup>2</sup>

*III. Mounting height of the luminaries: 1,5 m*

Observer position: R = 5.00; S = 0.00

Luminance distribution in one luminaire spacing

R/S	60.0	60.2	60.4	60.6	60.8	61.0	61.2	61.4	61.6	61.8
0.50	*	1.70	1.71	1.70	1.67	1.64	1.65	1.66	1.67	1.69
1.50	*	1.96	1.99	1.98	1.96	1.94	1.94	1.93	1.93	1.94
2.50	*	1.32	1.33	1.35	1.35	1.38	1.39	1.37	1.33	1.31
3.50	*	1.04	1.08	1.08	1.08	1.05	1.05	1.05	1.06	1.07
4.50	*	0.98	0.96	0.98	0.96	1.00	1.00	1.00	0.97	0.98
5.50	*	0.98	0.96	0.98	0.96	1.00	1.00	1.00	0.97	0.98
6.50	*	1.04	1.08	1.08	1.08	1.05	1.05	1.05	1.06	1.07
7.50	*	1.32	1.33	1.35	1.35	1.38	1.39	1.37	1.33	1.31
8.50	*	1.96	1.99	1.98	1.96	1.94	1.94	1.93	1.93	1.94
9.50	*	1.70	1.71	1.70	1.67	1.64	1.65	1.66	1.67	1.69

Average luminance: Lav = 1.40 cd/m<sup>2</sup>



IV. Mounting height of the luminaries: 0,5 m

Observer position: R = 5.00; S = 0.00

Luminance distribution in one luminaire spacing

R / S	60.0	60.2	60.4	60.6	60.8	61.0	61.2	61.4	61.6	61.8	
0.50	*	9.23	8.27	6.39	5.21	4.72	4.91	5.45	6.60	7.66	8.82
1.50	*	2.22	2.00	1.97	1.88	1.85	1.84	1.87	2.04	2.14	2.18
2.50	*	0.32	0.32	0.32	0.32	0.00	0.02	0.01	0.27	0.30	0.32
3.50	*	0.00	0.00	0.00	0.00	0.00	0.00	0.00	0.00	0.00	0.00
4.50	*	0.00	0.00	0.00	0.00	0.00	0.00	0.00	0.00	0.00	0.00
5.50	*	0.00	0.00	0.00	0.00	0.00	0.00	0.00	0.00	0.00	0.00
6.50	*	0.00	0.00	0.00	0.00	0.00	0.00	0.00	0.00	0.00	0.00
7.50	*	0.32	0.32	0.32	0.32	0.00	0.02	0.01	0.27	0.30	0.32
8.50	*	2.22	2.00	1.97	1.88	1.85	1.84	1.87	2.04	2.14	2.18
9.50	*	9.23	8.27	6.39	5.21	4.72	4.91	5.45	6.60	7.66	8.82

Average luminance: Lav = 1.79 cd/m<sup>2</sup>

If the luminance of the ceiling is assumed to be 20% of the luminance of the road surface, i.e., 20 cd/m<sup>2</sup>, the proportion of the luminance of the road surface contributed by the “fictitious” luminaries on the ceiling can be determined with the help of the computer program for calculating street installations, in which every luminaire has flux  $\Phi_{\text{opp}}=L.S.\pi=20.2.5.2.3,14=314$  lm. In this case, two “configurations of street installations” must be examined, differing only in the position of the luminaries. The inputs files for calculating the installations have the following format:

```

2
Ceiling 2,5x2m, Phi=I.pi=L.S.pi=20.2.5.2.3,14=314 lm
1 1dl61rr03
61 00.31 0.10 00.00 3.00 0.070
4. 05.50 02.00 10.00 0.00 1.25 1.25
    
```

```

2
Ceiling 2,5x2m, Phi=I.pi=L.S.pi=20.2.5.2.3,14=314 lm
1 1dl61rr03
61 00.31 0.10 00.00 3.00 0.070
4. 05.50 02.00 10.00 0.00 3.75 3.75
    
```

**Results obtained for the impact of a diffuse luminous flux from the ceiling on the luminance of the road surface:**

I. Overhang of the luminaries OH1=OH2=1,25 m

Mounting height of the luminaries (H): 5,5 m

Observer position: R = 5.00; S = 0.00

Luminance distribution in one luminaire spacing

R / S	60.0	60.2	60.4	60.6	60.8	61.0	61.2	61.4	61.6	61.8
0.50	*	.79	.80	.80	.80	.79	.79	.79	.79	.80
1.50	*	.97	.97	.97	.97	.97	.97	.97	.97	.97
2.50	*	.98	.98	.98	.98	.98	.97	.98	.98	.98
3.50	*	.82	.82	.82	.82	.82	.82	.81	.81	.81
4.50	*	.71	.72	.72	.72	.72	.72	.72	.71	.71
5.50	*	.71	.72	.72	.72	.72	.72	.72	.71	.71
6.50	*	.82	.82	.82	.82	.82	.82	.81	.81	.81
7.50	*	.98	.98	.98	.98	.98	.97	.98	.98	.98
8.50	*	.97	.97	.97	.97	.97	.97	.97	.97	.97
9.50	*	.79	.80	.80	.80	.79	.79	.79	.79	.80

Average luminance: Lav = 0.85 cd/m<sup>2</sup>

II. Overhang of the luminaries OH1=OH2=3,75 m

Mounting height of the luminaries (H): 5,5 m

Observer position: R = 5.00; S = 0.00

Luminance distribution in one luminaire spacing

R / S	60.0	60.2	60.4	60.6	60.8	61.0	61.2	61.4	61.6	61.8
0.50	*	0.55	0.55	0.55	0.55	0.55	0.55	0.55	0.55	0.55
1.50	*	0.73	0.73	0.73	0.73	0.73	0.73	0.73	0.73	0.73
2.50	*	0.99	0.99	0.99	0.99	0.99	0.99	0.99	0.99	0.99
3.50	*	1.30	1.30	1.30	1.30	1.30	1.30	1.30	1.30	1.30
4.50	*	1.47	1.48	1.48	1.48	1.48	1.47	1.47	1.47	1.47
5.50	*	1.47	1.48	1.48	1.48	1.48	1.47	1.47	1.47	1.47
6.50	*	1.30	1.30	1.30	1.30	1.30	1.30	1.30	1.30	1.30
7.50	*	0.99	0.99	0.99	0.99	0.99	0.99	0.99	0.99	0.99
8.50	*	0.73	0.73	0.73	0.73	0.73	0.73	0.73	0.73	0.73
9.50	*	0.55	0.55	0.55	0.55	0.55	0.55	0.55	0.55	0.55

Average luminance: Lav = 1,01 cd/m<sup>2</sup>

**Conclusion**

1. The presented calculations suggest that when the luminance of the walls is equal to the luminance of the road surface (100 cd/m<sup>2</sup>), the luminance of the road surface increases by 1,04+1,29+ 1,4+1,79=5,52 cd/m<sup>2</sup>, which is due to the luminous flux diffused by the walls. A ceiling with luminance equal to 20 % of the luminance of the road surface (20 cd/m<sup>2</sup>) adds another 0,85+1,01=1,86 cd/m<sup>2</sup>. The total luminance of the road surface will be 107,38 cd/m<sup>2</sup> instead of 100 cd/m<sup>2</sup>, i.e., the lighting installation overcompensates by about 7 %. The installment of 7 % more luminaries not only increases the amount of capital investment, but also leads to higher energy costs during the operation of the installation.

2. An important conclusion is that allocating a substantial amount of luminous flux for direct illumination of the walls from the luminaries on the ceiling (as Fig.1 shows, about 30-40% of the flux of the lighting sources falls directly on the walls) is not justified, because the flux reflected by the walls provides only 5% of the luminance of the road surface. This is logical, as a small part of the flux reflected from the walls is directed against traffic – a fundamental principle, which explains why counterbeam lighting is more energy-efficient than symmetrical lighting. Moreover, with counterbeam lighting, bright walls reduce the contrast quotient  $q=L_{AV}/E_V$ , because they create high vertical luminance  $E_V$  in the control plane opposite to the direction of traffic at average luminance of the road surface  $L_{av}$ .

3. The illumination of the walls improves the conditions for orientation when entering the tunnel, but using ceiling lightings is a costly solution. The requirement for illuminating the walls refers to heights up to 2 m above the road surface, which suggests that using new methods such as laterally located luminaries of the type “flat beam” that are installed at low height will decrease considerably the energy used for lighting [5].

4. In terms of energy consumption, it is more efficient for the luminous flux of the main luminaries to point directly towards the road surface [6]. Drivers can be made aware of the location of the walls by installing

lighting strips with high luminance, such as contours formed by lighting diodes. The combination of luminaries of the type “flat beam” with contours formed by lighting diodes can decrease twofold the energy costs for the lighting of the tunnel.

### Acknowledgements

This research was supported by funds from the Ministry of Education and Science, The National Science Fund, contract № MU-FS-07 “Energy Conservation through Lighting Systems Optimization for Streets and Road Tunnels.”

### References

- [1] [http://www.schreder.ca/documents/en/Schreder\\_Tunnel.pdf](http://www.schreder.ca/documents/en/Schreder_Tunnel.pdf)  
Costeranera Norte tunnel, Santiago, Chile
- [2] CIE Publication 30.2, Calculation and Measurement of Luminance and Illuminance in Road Lighting, International Commission on Illumination (CIE), 1982
- [3] [http://en.wikipedia.org/wiki/Sphere#cite\\_note-2](http://en.wikipedia.org/wiki/Sphere#cite_note-2) Eleven properties of the sphere
- [4] Пачаманов А. Фотометрия и осветителни уредби (лабораторни упражнения). Издателство “Авангард-Прима”, София 2006
- [5] Трифонов Н., А. Пачаманов, Д. Пачаманова. Уредба за насречно адаптивно осветление на пътни тунели. Заявка за патент на полезен модел № 1365/24.09.2007 г.
- [6] Пачаманов А. Енергоспестяване и осветителна техника (енергоефективно осветление). Издателство “Авангард-Прима”. София, 2007

### Biographies



**Angel Pachamanov** was born in Kardjali, Bulgaria, on February 15, 1950.

*Education:* 1969-1974 Technical University of Sofia, Electrotechnical Department, Mag.Eng.; 1978-1980 Technological University of Sofia, Postgraduate education in automatic systems, M.Sc.; 1986-1988 Technical University of Sofia, Dr.Eng. in Lighting Technics and Sources of Lighting

*Job Experience:* 1974-1976 Power engineer; 1976-1982 Deputy head of the Power Department; 1982-1985 Head of the Power Department at the Plant for Flat Glass and China in Razgrad, Bulgaria; 1985-1995 Scientific researcher at the Laboratory of Lighting in the Technical University of Sofia; since 1995 Senior scientific researcher; Associate Professor, teaching Lighting and Special lighting installation systems, Irradiating systems, Energy Saving and Automation – at the Department of Electric power supply and lighting technics, Faculty of Electrical Engineering, Technical University of Sofia.

Angel Pachamanov is with the Faculty of Electrical Engineering, Technical University of Sofia, 8, Kl. Ohridski Blvd., 1000 Sofia, Bulgaria (e-mail: pach@tu-sofia.bg).



**Dessislava Pachamanova** is an associate professor in the Mathematics and Sciences Division of Babson College. She holds an A.B. in Mathematics (*magna cum laude*) from Princeton University and a Ph.D. in Operations Research from the Sloan School of Management at the Massachusetts Institute of Technology.

Dr. Pachamanova's research interests are in the areas of optimization, simulation, and statistics, and their applications in finance, management, computing, and engineering. Her primary research area can be defined as the theory and practice of robust optimization. Her secondary research areas include education, engineering and telecommunications, open source software (computer science and management), and simulation.

E-mail Address [dpachamanova@babson.edu](mailto:dpachamanova@babson.edu)

Homepage <http://faculty.babson.edu/dpachamanova/>

**Kirilka Ivanova** graduated from the Technical University 4-year program in Electrical Power Generation and Electrical Equipment at the Department of Electrical Power Supply, Electrical Equipment and Electrical Transport in May 2008. Currently, she is completing her thesis requirement for obtaining a Bachelor of Science degree in engineering.

# Impact of Diffuse-Reflected Luminous Flux on Wall Luminance in Road Tunnels

Angel Pachamanov, Stoyan Petrov, Vesselina Rahneva

**Abstract:** According to the requirements for tunnel road lighting, the luminance of the walls must be equal to the luminance of the road surface. This requirement is satisfied by directing part of the luminous flux of the luminaries to the tunnel walls. In reality, a component of the luminous flux reflected by the road surface falls on the walls as well. Accounting for it results in more precise sizing of the lighting installation, and consequently leads to lower cost of capital and energy consumption.

**Keywords:** tunnel lighting, light distribution, road surface reflection

## Introduction

To establish conditions for safe travel through road tunnels, tunnel lighting installations provide luminance of the walls equals to the luminance of the road surface [1,2] by directing a portion of the luminaries' flux to the walls (Fig. 1).

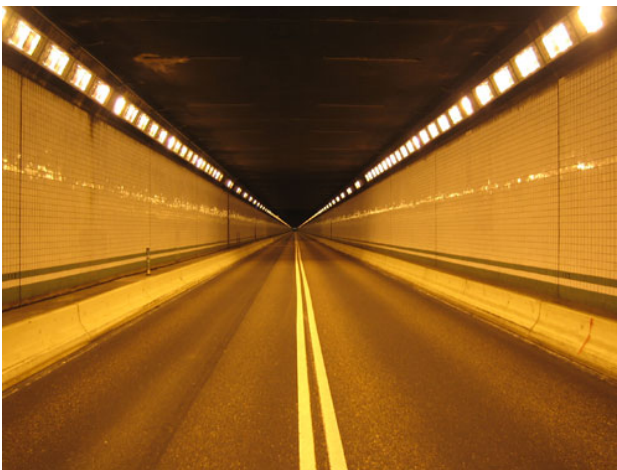


Fig.1 Providing the necessary luminance of the walls by direct luminous flux

In reality, a reflected component of the luminous flux by the road surface reaches the walls. When designing tunnel luminaries, it is important to know how big the latter component is. Accounting for the component ensures that the luminaries' optical systems are constructed in such a way as to send only the minimum necessary amount of their flux to the walls. In this way, the efficiency of use of the luminous flux will increase,

which will consequently lead to reduced power consumption for the lighting installation.

This report estimates the magnitude of the component of the luminous flux reflected by the road surface that falls on the walls, using a developed software product for optimizing the distribution of the tunnel luminaries [3] and given distributions of the direct flux of the light sources to the road surface [4,5]. The suggested method and software product are used in the design of energy-efficient optical systems for tunnel luminaries.

## Algorithm for estimating the reflected component of the flux by the road surface

It is well-known that road pavements reflect light falling on them in a directed-diffuse manner. For road pavements of type C1 (R1), the diffuse component is dominant, while for road pavements of type C2 (R3), it is significantly smaller [4]. Nevertheless, in order to simplify the problem, the report will assess only the diffuse component of the reflected flux by the road pavement and its contribution to the formation of the luminance on the walls.

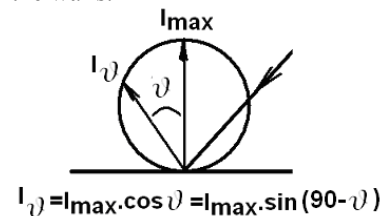


Fig.2. Lambert's Law for a diffuse-reflecting horizontal surface

For diffuse-reflecting flat surface, the indicatrix of road pavement reflection is a sphere, regardless of the direction of the falling rays (Fig. 2 – Lambert's Law). From the definition of luminous intensity  $I = d\Phi/d\Omega$  (spatial density of the reflected flux in the upper hemisphere) and Lambert's Law  $I_\theta = I_{max} \cdot \cos\theta$ , it can be derived that  $I_{max} = \Phi_{A-refl}/\pi$ , where  $\Phi_{A-refl}$  is the flux reflected by a surface with unit area  $A$  of a sufficiently small size. The reflected flux can easily be estimated if the fallen  $\Phi_A$  flux on each unit area of the road surface (or the illuminance  $E_A$ ) and the integral coefficient of road pavement reflection  $\rho_{road}$  for the considered luminaire are known:

$$(1) \quad \Phi_{A-refl} = \rho_{road} \cdot \Phi_A = \rho_{road} \cdot E_A \cdot A.$$

The derivation of the algorithm can be traced in Fig. 3.  $NM$  number of sections are considered, each with length  $S$  (spacing in street lighting). The road surface is divided into  $NX$  strips across, and each bar is divided into  $NY$  pieces between two neighboring luminaries. Hence, each unit area  $A$  has 3 indexes  $[m,j,i]$ , where  $m=1\dots NM$ ,  $j=1\dots NY$ , and  $i=1\dots NX$ .

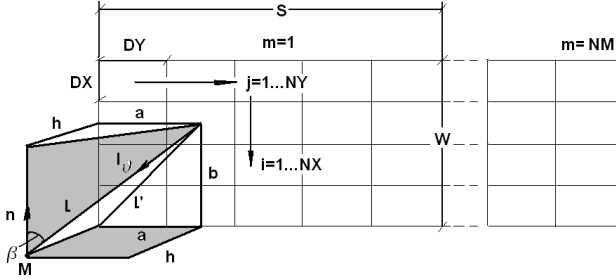


Fig.3. Problem set-up

The contribution of unit area  $A[m, j, i]$  of the road surface (in the case presented in Fig. 3,  $A[1,2,2]$ ) to the luminance of the wall in the unit area in which the point  $M$  lies is calculated from the formula:

$$(2) \quad L[m, j, i] = \rho_{wall} \frac{E_{vert}[m, j, i]}{\pi}$$

To calculate the vertical illuminance  $E_{vert}[m,j,i]$  for each unit area of the road surface  $A[m,j,i]$ , one must know the luminous intensity  $I_b[m,j,i]$ , the distance  $l[m,j,i]$ , and the angle  $\beta[m,j,i]$  between the falling beam and the normal to the unit area in which point  $M$  lies:

$$(3) \quad E_{vert}[m, j, i] = \frac{I_b[m, j, i] \cdot \cos \beta[m, j, i]}{l^2[m, j, i]}$$

As Fig. 3 shows,  $l^2 = a^2 + b^2 + h^2$ , where for each  $m, j$  and  $i$ :

$$(4) \quad l[m, j, i] = \sqrt{a^2[m, j] + b^2[i] + h^2},$$

where

$$(5) \quad a[m, j] = m \cdot S + DY(j - 0,5) \quad \text{and}$$

$$(6) \quad b[i] = W - DX(i - 0,5),$$

In formulas (4)-(6),  $h$  is the height of point  $M$  relative to the level of the road,  $W$  is the width of the road,  $S$  is the "spacing",  $DX = W/NX$ , and  $DY = S/NY$ .

The luminous intensity  $I_b[m,j,i]$  is calculated Lambert's Law:

$$(7) \quad I_b[m, j, i] = I_{max} \cdot [m, j, i] \cdot \cos \vartheta,$$

where

$$(8) \quad I_{max}[m, j, i] = \rho_{настлика} \frac{\Phi[m, j, i]}{\pi} \quad \text{and}$$

$$(9) \quad \cos \vartheta = \sin(90 - \vartheta) = \frac{h}{l[m, j, i]}.$$

The only unknown quantity in formula (3) is  $\cos \beta[m,j,i]$ , which can be expressed through  $b[i]$  and  $l[m,j,i]$  defined earlier in formulas (6) и (4):

$$(10) \quad \cos \beta[m, j, i] = \frac{b[i]}{l[m, j, i]}.$$

The total luminance of the wall at a height  $h$  from the road surface is obtained as the sum of the contributions of the luminances of all unit sections, i.e.:

$$(11) \quad L_{wall} = \sum_{m=1}^{NM} \sum_{j=1}^{NY} \sum_{i=1}^{NX} L[m, j, i].$$

Since to the left of point  $M$ , the road surface creates the same luminance on the wall, the value obtained from formula (11) should be doubled.

The methodology presented in this section is implemented in a software program in a high-level algorithmic language. It is part of a software package developed to optimize the light distribution of luminaries for tunnel lighting [5]. The software program enables multiple runs of the calculations for different starting conditions.

### Calculations

The application of the software program will be discussed for the road surface of a tunnel illuminated in two different ways: upper ceiling counterbeam lighting [4] and side counterbeam 'flat-beam' lighting [5]. In both cases, the optimal light distribution of the luminaries' flux is obtained by solving an optimizing formulation, so that the required luminance of the road surface is achieved with minimal lighting flux [4,5].

Table 1 shows the distribution of the direct component of the flux of luminaries (in lm) by unit area of the road surface (pavement type R3 with average luminance factor 0,07 cd/m<sup>2</sup>/lx) in two-rowed ceiling system of luminaries of the "asymmetrical-counterbeam" type [5]. The values for the luminous flux were obtained for a suspension height for luminaries of 5 m and the following light technical parameters (LTP): average luminance of road surface  $L_{AV} \geq 100$  cd/m<sup>2</sup>, longitudinal luminance uniformity  $U_L = L_{min}/L_{max} \geq 0,6$ , overall luminance uniformity  $U_0 = L_{min}/L_{AV} \geq 0,4$ , glare (threshold increment)  $TI \leq 15$ . The road surface is divided into  $NX=10$  strips of 1 m, each with  $NY=8$  sections of 0,5 m. The distance between two luminaries is  $S=4$  m and the number of the considered unit areas that contribute to the vertical illuminance of the wall (point  $M$  in Fig.3) is  $NM=5$ .

**Table 1**

Input data for direct luminous flux (lm) by unit area of the road surface in installation of type 'counterbeam-ceiling'

5 8 10 10 4 (NM=5 NY=8 NX=10 W=10m S=4m)										
573	846	1118	1426	1573	1573	1426	1118	846	573	
594	849	1208	1668	1810	1810	1668	1208	849	594	
630	853	1291	1882	2064	2064	1882	1291	853	630	
663	836	1314	1955	2324	2324	1955	1314	836	663	
681	783	1249	1805	2335	2335	1805	1249	783	681	
685	711	1137	1601	1854	1854	1601	1137	711	685	
695	664	1070	1731	2008	2008	1731	1070	664	695	
753	686	1122	1835	2160	2160	1835	1122	686	753	

Table 2 shows the distribution of the direct component of the luminous flux (in lm) by unit area of the road surface in two-rowed side luminaries of the 'flat beam' type with mounting height 1,2 m [5]. The values of the flux are obtained under the condition that the same light technical parameters as in the installation of the "counterbeam-ceiling" type are achieved. Because of the specific way of distribution of the flux, the total luminous flux with which the required average luminance of the road surface is achieved ( $L_{AV} \geq 100$  cd/m<sup>2</sup>) is in this case about 2 times smaller (26014 lm as opposed to 51041 lm in "counterbeam-ceiling").

**Table 2**

Input data for direct luminous flux (lm) by unit area of the road surface in installation of type "flat-beam"

5 8 10 10 4 (NM=5 NY=8 NX=10 W=10m S=4m)										
497	270	262	325	341	341	325	262	270	497	
638	334	312	383	389	389	383	312	334	638	
826	402	360	445	437	437	445	360	402	826	
1090	451	399	503	480	480	503	399	451	1090	
1441	449	426	547	513	513	547	426	449	1441	
1537	447	459	564	524	524	564	459	447	1537	
2312	533	525	535	501	501	535	525	533	2312	
3511	670	500	452	426	426	452	500	670	3511	

### Output files in the two cases for h=1,75 m:

#### outcl 17.txt – ceiling lighting

Point M height for calculated Evert	1.75 m
Reflection of the pavement $\rho_{road}$	0.10
Reflection of the wall $\rho_{wall}$	0.50
Width of the roadway (W)	10.0 m
Luminaries spacing (S)	4.0 m
Doubled value of the Evert	98.72 lx
Luminance of wall ( $L_{wall}$ )	15.71 cd/m <sup>2</sup>
Average luminance if $L_{AV} = \rho_{road} \cdot E_{AV,ROAD} / \pi$	81.24 cd/m <sup>2</sup>
Doubled value of the E <sub>VERT</sub>	116.93 lx
Luminance of wall ( $L_{wall}$ ) from -5*S to +5*S	18.61 cd/m <sup>2</sup>

#### E<sub>VERT</sub>(M,J,I), lx

0.03478 0.07051 0.13249 0.25078 0.43265 0.72165 1.17610 1.77144 2.44677 1.40109  
0.03567 0.06983 0.14077 0.28698 0.48325 0.79596 1.29040 1.72513 2.05528 1.10180  
0.03704 0.06834 0.14555 0.31013 0.51991 0.83615 1.28851 1.52018 1.50794 0.73833  
0.03777 0.06444 0.14110 0.30249 0.53812 0.83744 1.12888 1.19490 0.99590 0.45437  
0.03724 0.05739 0.12591 0.25754 0.48578 0.72697 0.84769 0.84173 0.60781 0.27042  
0.03562 0.04902 0.10621 0.20734 0.33997 0.48752 0.59652 0.55603 0.35839 0.16132  
0.03409 0.04263 0.09156 0.20075 0.31958 0.43864 0.50407 0.37722 0.22015 0.10055  
0.03456 0.04066 0.08707 0.18846 0.29485 0.38761 0.41461 0.28597 0.15269 0.06947  
0.02445 0.04594 0.07802 0.12855 0.18259 0.23033 0.24959 0.20776 0.12937 0.03493  
0.02341 0.04196 0.07529 0.13109 0.17762 0.21559 0.22670 0.16557 0.09130 0.02471  
0.02282 0.03816 0.07146 0.12831 0.17064 0.19989 0.19960 0.13222 0.06595 0.01841  
0.02197 0.03370 0.06433 0.11524 0.16161 0.18330 0.16288 0.10191 0.04743 0.01396

0.02057 0.02834 0.05392 0.09180 0.13657 0.15044 0.11902 0.07433 0.03322 0.01056  
0.01880 0.02304 0.04319 0.07019 0.09130 0.09797 0.08423 0.05258 0.02295 0.00799  
0.01728 0.01923 0.03572 0.06543 0.08342 0.08743 0.07325 0.03892 0.01656 0.00620  
0.01694 0.01772 0.03289 0.05984 0.07590 0.07789 0.06297 0.03246 0.01341 0.00522  
0.01164 0.01949 0.02879 0.04017 0.04689 0.04723 0.03999 0.02601 0.01313 0.00313  
0.01089 0.01743 0.02734 0.04066 0.04593 0.04548 0.03853 0.02281 0.01058 0.00259  
0.01042 0.01561 0.02570 0.03978 0.04475 0.04365 0.03606 0.01997 0.00863 0.00222  
0.00989 0.01364 0.02304 0.03592 0.04320 0.04157 0.03129 0.01680 0.00693 0.00191  
0.00916 0.01140 0.01931 0.02890 0.03736 0.03552 0.02429 0.01330 0.00537 0.00161  
0.00831 0.00924 0.01553 0.02240 0.02563 0.02410 0.01822 0.01015 0.00407 0.00135  
0.00761 0.00771 0.01294 0.02122 0.02407 0.02241 0.01677 0.00807 0.00319 0.00115  
0.00744 0.00713 0.01203 0.01976 0.02253 0.02079 0.01521 0.00719 0.00279 0.00105  
0.00512 0.00789 0.01065 0.01353 0.01433 0.01312 0.01017 0.00613 0.00293 0.00068  
0.00480 0.00710 0.01025 0.01398 0.01445 0.01313 0.01028 0.00569 0.00252 0.00060  
0.00461 0.00642 0.00978 0.01397 0.01449 0.01308 0.01007 0.00526 0.00218 0.00055  
0.00440 0.00566 0.00890 0.01289 0.01440 0.01292 0.00913 0.00465 0.00185 0.00050  
0.00410 0.00478 0.00758 0.01059 0.01280 0.01142 0.00738 0.00386 0.00151 0.00045  
0.00375 0.00392 0.00620 0.00839 0.00902 0.00801 0.00576 0.00308 0.00120 0.00039  
0.00346 0.00332 0.00525 0.00812 0.00870 0.00769 0.00549 0.00255 0.00098 0.00035  
0.00342 0.00311 0.00496 0.00772 0.00836 0.00735 0.00516 0.00236 0.00089 0.00033  
0.00237 0.00348 0.00447 0.00539 0.00545 0.00477 0.00356 0.00208 0.00097 0.00022  
0.00225 0.00317 0.00437 0.00569 0.00563 0.00491 0.00371 0.00200 0.00087 0.00021  
0.00218 0.00290 0.00423 0.00580 0.00578 0.00503 0.00375 0.00191 0.00078 0.00019  
0.00210 0.00260 0.00392 0.00545 0.00587 0.00509 0.00349 0.00174 0.00068 0.00018  
0.00198 0.00222 0.00339 0.00456 0.00533 0.00461 0.00320 0.00148 0.00057 0.00017  
0.00183 0.00185 0.00281 0.00368 0.00383 0.00331 0.00232 0.00122 0.00047 0.00015  
0.00171 0.00158 0.00242 0.00362 0.00377 0.00324 0.00227 0.00103 0.00039 0.00014  
0.00171 0.00150 0.00232 0.00351 0.00369 0.00317 0.00218 0.00098 0.00037 0.00014

#### outfb 17.txt – technology 'flat beam'

Point M height for calculated Evert	1.75 m
Reflection of the pavement $\rho_{road}$	0.10
Reflection of the wall $\rho_{wall}$	0.50
Width of the roadway (W)	10.0 m
Luminaries spacing (S)	4.0 m
Doubled value of the Evert	41.21 lx
Luminance of wall ( $L_{wall}$ ) from -5*S to +5*S	6.558 cd/m <sup>2</sup>
Average luminance if $L_{AV} = \rho_{road} \cdot E_{AV,ROAD} / \pi$	41.41 cd/m <sup>2</sup>
Doubled value of the E <sub>VERT</sub>	59.6 lx
Luminance of wall ( $L_{wall}$ ) from -5*S to +5*S	9.49 cd/m <sup>2</sup>

#### E<sub>VERT</sub>(M,J,I), lx

0.03017 0.02250 0.03105 0.05715 0.09379 0.15644 0.26805 0.41513 0.78088 1.21525  
0.03831 0.02747 0.03636 0.06589 0.10386 0.17107 0.29630 0.44556 0.80856 1.18341  
0.04856 0.03221 0.04059 0.07333 0.11008 0.17703 0.30467 0.42391 0.71066 0.96803  
0.06210 0.03476 0.04285 0.07783 0.11114 0.17296 0.29045 0.36284 0.53726 0.74701  
0.07880 0.03291 0.04295 0.07805 0.10673 0.15972 0.25689 0.28709 0.34854 0.57221  
0.07993 0.03082 0.04288 0.07304 0.09609 0.13779 0.21014 0.22447 0.22532 0.36197  
0.11339 0.03422 0.04492 0.06205 0.07974 0.10944 0.15579 0.18509 0.17672 0.33449  
0.16115 0.03971 0.03880 0.04642 0.05815 0.07644 0.10213 0.12744 0.14913 0.32392  
0.02120 0.01466 0.01828 0.02930 0.03958 0.04993 0.05688 0.04869 0.04129 0.03030  
0.02515 0.01651 0.01944 0.03010 0.03817 0.04633 0.05205 0.04276 0.03592 0.02654  
0.02992 0.01799 0.01993 0.03034 0.03613 0.04232 0.04720 0.03687 0.03108 0.02413  
0.03612 0.01818 0.01953 0.02965 0.03338 0.03786 0.04191 0.03094 0.02559 0.02294  
0.04352 0.01625 0.01839 0.02782 0.03000 0.03305 0.03607 0.02535 0.01905 0.02235  
0.04217 0.01449 0.01743 0.02473 0.02580 0.02769 0.02967 0.02123 0.01443 0.01792  
0.05750 0.01543 0.01752 0.02022 0.02081 0.02181 0.02264 0.01910 0.01330 0.02063  
0.07898 0.01731 0.01466 0.01474 0.01497 0.01536 0.01551 0.01447 0.01310 0.02435  
0.01010 0.00622 0.00675 0.00915 0.01017 0.01024 0.00912 0.00609 0.00419 0.00272  
0.01170 0.00686 0.00706 0.00934 0.00987 0.00978 0.00885 0.00589 0.00416 0.00279  
0.01366 0.00735 0.00717 0.00941 0.00947 0.00924 0.00853 0.00557 0.00407 0.00291  
0.01626 0.00736 0.00699 0.00924 0.00892 0.00859 0.00805 0.00510 0.00374 0.00314  
0.01938 0.00653 0.00659 0.00876 0.00821 0.00780 0.00736 0.00453 0.00308 0.00342  
0.01864 0.00581 0.00627 0.00789 0.00724 0.00681 0.00642 0.00410 0.00256 0.00303  
0.02531 0.00619 0.00635 0.00656 0.00601 0.00559 0.00518 0.00396 0.00256 0.00382  
0.03471 0.00697 0.00536 0.00487 0.00444 0.00410 0.00375 0.00321 0.00272 0.00489  
0.00444 0.00252 0.00250 0.00308 0.00311 0.00284 0.00232 0.00144 0.00093 0.00059  
0.00516 0.00279 0.00265 0.00321 0.00311 0.00282 0.00236 0.00147 0.00099 0.00065  
0.00605 0.00302 0.00273 0.00330 0.00307 0.00277 0.00238 0.00147 0.00103 0.00072  
0.00723 0.00306 0.00270 0.00332 0.00297 0.00267 0.00235 0.00141 0.00100 0.00082  
0.00868 0.00274 0.00259 0.00321 0.00281 0.00251 0.00224 0.00132 0.00086 0.00094  
0.00842 0.00247 0.00250 0.00296 0.00255 0.00226 0.00203 0.00124 0.00075 0.00088  
0.01152 0.00266 0.00257 0.00251 0.00217 0.00192 0.00170 0.00125 0.00079 0.00116  
0.01594 0.00303 0.00221 0.00190 0.00165 0.00145 0.00127 0.00105 0.00087 0.00155  
0.00206 0.00111 0.00105 0.00123 0.00118 0.00104 0.00081 0.00049 0.00031 0.00019  
0.00242 0.00125 0.00113 0.00131 0.00121 0.00106 0.00085 0.00052 0.00034 0.00022  
0.00286 0.00137 0.00118 0.00137 0.00122 0.00106 0.00089 0.00053 0.00037 0.00025  
0.00346 0.00140 0.00119 0.00140 0.00121 0.00105 0.00090 0.00053 0.00037 0.00030  
0.00419 0.00127 0.00116 0.00138 0.00117 0.00101 0.00088 0.00051 0.00033 0.00035  
0.00411 0.00116 0.00114 0.00130 0.00108 0.00093 0.00082 0.00049 0.00029 0.00034  
0.00569 0.00127 0.00119 0.00112 0.00094 0.00081 0.00070 0.00051 0.00032 0.00046  
0.00795 0.00146 0.00103 0.00086 0.00073 0.00062 0.00054 0.00044 0.00036 0.00063

The results from the calculations of the vertical illuminance and luminance of the wall for different values of h (height of point M relative to the level of the



road) are given in Tables 3 and 4. Fig. 4 and Fig. 5 present the results graphically.

The programming product provides a version of the calculation of the vertical illuminance and the luminance of the wall that applies in the case when the pavement is evenly illuminated, i.e., each unit area has the same illuminance, equal to the average illuminance of "the spacing". The luminance of each unit area of the pavement in this case is calculated from the formula:

$$(12) \quad L[m, j, i] = \rho_{road} \frac{E_{AV.SURFACE}}{\pi}$$

The resulting values for the vertical illuminance and the luminance of the wall for this version are shown in the output file in smaller font, and in Tables 3 and 4 the values are marked with «'» (apostrophe). The ratio  $L_{AV}/L'_{AV}$  in Tables 3 and 4 provides information on the extent to which the uneven illumination of the road surface is more effective than the even one. Exactly because uneven illumination of the road surface is more efficient than even illumination, installations of the "flat-beam" type are more effective in satisfying the quality indicators than installations of the "counterbeam-ceiling" type.

**Table 3**

*Luminance of the wall by the luminous flux reflected by the road surface in installation of type 'counterbeam-ceiling'*

h, m	$E_{av-vert}$ , lx	$L_{wall}$ , cd/m <sup>2</sup>	$L_{AV}/L'_{AV}$ , cd/m <sup>2</sup>	$E'_{av-vert}$ , lx	$L'_{wall}$ , cd/m <sup>2</sup>
0,25	64	10,2	100/81,2	127	20,1
0,75	90	14,3	100/81,2	124	19,7
1,25	96	15,3	100/81,2	121	19,2
1,75	99	15,7	100/81,2	117	18,6
2,25	99	15,7	100/81,2	113	18,0
2,75	97	15,4	100/81,2	108	17,2

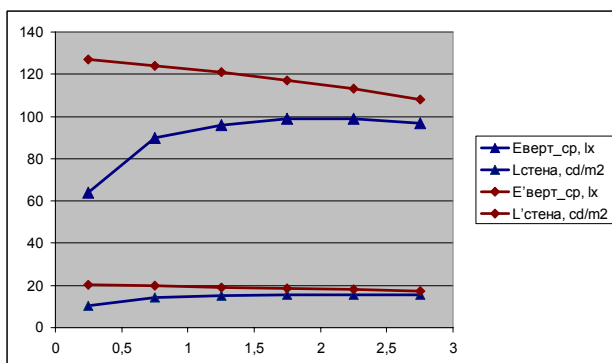


*Fig.4. Vertical illuminance and luminance of the wall by the reflected luminous flux for type 'counterbeam-ceiling'*

**Table 4**

*Luminance of the wall by the luminous flux reflected by the road surface in installation of type 'flat-beam'*

h, m	$E_{av-vert}$ , lx	$L_{wall}$ , cd/m <sup>2</sup>	$L_{AV}/L'_{AV}$ , cd/m <sup>2</sup>	$E'_{av-vert}$ , lx	$L'_{wall}$ , cd/m <sup>2</sup>
0,25	46,1	7,3	100/41,4	64,5	10,3
0,75	51,2	8,2	100/41,4	63,1	10
1,25	44,7	7,1	100/41,4	61,5	9,8
1,75	41,2	6,6	100/41,4	59,6	9,5
2,25	37,7	6,2	100/41,4	57,5	9,2
2,75	36,5	5,8	100/41,4	55,2	8,8

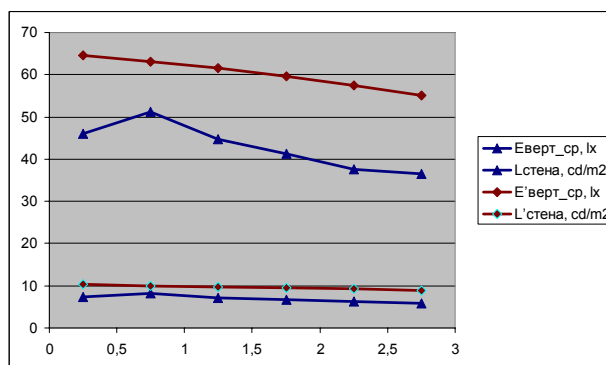


*Fig.5. Vertical illuminance and luminance of the wall by the reflected luminous flux for type 'flat-beam'*

## Conclusion

The results from the calculations show that for luminance of the road surface of 100 cd/m<sup>2</sup>, the flux reflected by the road surface to the walls for installations of the "counterbeam-ceiling" type contributed about 15 cd/m<sup>2</sup>, which is 15% of the required value. In installations of the 'flat-beam' type, the contribution is about two times smaller, but this is due to the twice smaller luminous flux which is needed for attaining the required average luminance of the road surface. If the directed component of the flux is taken into consideration, it is possible that an installation of the 'flat-beam' type will contribute about 15% of the required illuminance of the walls too. Nevertheless, it is evident that the flux reflected by the pavement can 'relieve' the main luminaries by only about 15% of the required direct flux to the walls. Bright walls improve the conditions for orientation in entering a tunnel, but more efficient methods for their illumination could be considered:

1. It is rational to use the specifics of the "flat-beam" technology in tunnel lighting. The luminaries are mounted on the side, on the walls, at a height of 1.2 m. In this case, it is logical to provide illumination of the walls from the luminaries themselves, through a special opening on the top or a refractor. Hence, in addition to the road surface, up to 2m of the height of the walls will be illuminated.

2. The orientation of drivers in the tunnel (which is the main purpose of bright walls) in an installation of the “flat-beam” type is ensured by the luminaries themselves, as they are mounted on the walls. It is probably unnecessary to ensure luminance of the walls that is equal to the luminance of the road surface. Perhaps for the “flat-beam” technology, the required value of luminance from the old recommendations of the International Commission on Lighting is sufficient - the walls should be with luminance equal to 50% of the luminance of the road surface.

3. In terms of energy conservation, it is more effective for the orientation of the driver to the location of the walls to be ensured by mounting luminous strips with high luminance, such as contours of LEDs. The combination of luminaries of the “flat-beam” type with the contours of LEDs may turn out to be a very good solution for energy-efficient tunnel lighting.

### Acknowledgements

This research was supported by funding from the Ministry of Education and Science, National Science Fund, contract № MU-FS-07 “Energy Conservation Through Lighting Systems Optimization For Streets And Road Tunnels”

### References

- [1] CIE Publication 88 (1990). *Guide for the Lighting of Tunnels and Underpasses, International Commission on Illumination (CIE)*
- [2] CEN/TC 169/WG6. *Lighting Applications: Tunnel Lighting, Technical Report No. 458/2002-09-08*
- [3] Pachamanov A., D. Pachamanova. *Optimization of the Light Distribution of Luminaries for Tunnel and Street Lighting, Engineering Optimization, 40 (1), January 2008, pp. 47-65 (Taylor & Francis, United Kingdom, <http://www.tandf.co.uk/>)*
- [4] Пачаманов А. *Енергоспестяване и осветителна техника (енергоефективно осветление). Издателство “Авангард-Прима”. София, 2007*
- [5] Трифонов Н., А. Пачаманов, Д. Пачаманова. *Уредба за насрецино адаптационно осветление на пътни тунели. Заявка за патент № 1365/24.09.2007 г.*

### Biographies



**Angel Pachamanov** was born in Kardjali, Bulgaria, on February 15, 1950.

*Education:* 1969-1974 Technical University of Sofia, Electrotechnical Department, Mag.Eng.; 1978-1980 Technological University of Sofia, Postgraduate education in automatic systems, M.Sc.; 1986-1988 Technical University of Sofia, Dr.Eng. in Lighting Technics and Sources of Lighting

*Job Experience:* 1974-1976 Power engineer;

1976-1982 Deputy head of the Power Department; 1982-1985 Head of the Power Department at the Plant for Flat Glass and China in Razgrad, Bulgaria; 1985-1995 Scientific researcher at the Laboratory of Lighting in the Technical University of Sofia; since 1995 Senior scientific researcher; Associate Professor, teaching Lighting and Special lighting installation systems, Irradiating systems, Energy Saving and Automation – at the Department of Electric power supply and lighting technics, Faculty of Electrical Engineering, Technical University of Sofia. Angel Pachamanov is with the Faculty of Electrical Engineering,

Technical University of Sofia, 8, Kl. Ohridski Blvd., 1000 Sofia, Bulgaria. E-mail: pach@tu-sofia.bg

**Stoyan Perov** graduated a 5-year master’s program in Electrical Power Generation and Electrical Equipment at the Department of Electrical Power Supply, Electrical Equipment and Electrical Transport in 2002. Currently he is a designer in “Filcab”-Plovdiv and works on his doctor’s thesis according to contract № MU-FS-07 “Energy Conservation through Lighting Systems Optimization for Streets and Road Tunnels” of the Ministry of Education and Science, The National Science Fund, E-mail: sto\_pet@abv.bg



**Vesselina Rahneva** was born in Kazanlak, Bulgaria, on July 4, 1984. She graduated from the Technical University 4-year program in Electrical Power Generation and Electrical Equipment at the Department of Electrical Power Supply, Electrical Equipment and Electrical Transport in May 2008. Currently, she is completing her thesis requirement for obtaining a Bachelor of Science degree in engineering. Vesselina Rahneva is with the

Faculty of Electrical Engineering, Technical University of Sofia, 8, Kl. Ohridski Blvd., 1000 Sofia, Bulgaria. E-mail: vrahneva@mail.bg

# Start-up process of high-pressure sodium lamps

Galia Veskova Georgieva-Taskova

**Abstract:** This paper presents the results of a research done on the start-up process of discharge lamp ignition up to the transition into a steady-state mode of operation. The paper studies the change in the basic electrical characteristics: current, voltage, power, frequency. Conclusions have been drawn about this initial period in the ignition of discharge lamps and their application and possibilities of use in street lighting.

**Keywords:** high-pressure sodium lamps electrical characteristics, street lighting.

## Introduction

The ever-increasing costs of generating electricity have prompted utilities to look into conservation and peak demand reduction programs. Some of these programs include encouraging consumers to use energy efficient lighting systems. Manufacturers are also introducing new lighting technologies and numerous products designed to reduce energy consumption. Most of the new technologies are based on high frequency switching techniques that may influence the electrical supply. In general, the new lamps operate at lower power factor and may produce additional wave distortions.

In this paper the gas discharge lamps used in street lighting were studied. These lamps are high quality sodium high-pressure lamps with PIA technology, a discharge tube with an integrated antenna and a transparent outer tube. A high-pressure sodium lamp SON-T PIA PLUS 100W, manufactured by Philips Company, is presented in Fig. 1 [1, 2, 3].



Fig.1. High-pressure sodium lamp SON-T PIA PLUS 100W

While all high intensity discharge (HID) lamps offer outstanding efficiency and long life, there are distinct differences in performance among the five basic types of

HID lamps. The Fig. 2 should help to understand these differences so that can select the right lamp for certain application [4].

	Colour Temperature Options (K)	Colour Rendering (Ra)	Life (Hours)	Efficiency (LPW)
Metal Halide	3000 (WDL) 3500 (BDL) 4000 (NDL) 6000 (DL)	65-93	3,500-20,000	68-105
High Pressure Sodium	2 000	25-60	28,500-55,000	66-150
Mercury	3 500 4 000	42-52	12,000-24,000	19-63
Low Pressure Sodium	1 800		16 000	100-198

Best option      Good option

Fig.2. Key performance criteria

The major applications of HID lamps could be summarized in the following figure (Fig. 3) [4].

Major applications	Retail	Display	Commercial Interior	Sports Lighting	Stadium	High Bay	Industrial	Warehouses	Amenity	Pedestrian Areas	Floodlighting	Security	Street Lighting	Highways	Horticulture
Metal Halide	•	•	•	•	•	•	•	•	•	•	•	•	•	•	•
High Pressure Sodium															
Mercury															
Low Pressure Sodium															

Fig.3. Major applications of HID lamps

The high-pressure sodium lamp using for street lighting shall meet some criteria. For example, minimum standards for public lighting infrastructure in the Queenstown Lakes District Council shall meet the following criteria [5]:

1. Be capable of accommodating all of the following lamp sources within a “family” of housings:
  - High pressure sodium;
  - Metal halide.
2. Accommodate wattages ranging from 50 watt up to 250 watt.
3. Have a minimum laboratory tested and approved ingress protection rating of IP54 for lamp housing and IP44 for gear housing that will last throughout the rated service life of the equipment. All gaskets should be solid (not foam) and silicon or proven equivalent with permanent shape memory (restored to original shape after accessing the equipment throughout the service life.
4. Where accessible to the public it shall not be possible to access components without the use of special

tools. For street lanterns, access for lamp replacement shall be achievable without the use of any special tools.

5. Sealed optical assembly / chamber.
6. Control gear mounted on an easily removable plate.
7. Hinge or similar to retain the cover during maintenance.
8. Be provided with internal fuse protection.
9. Be capable of side entry, top entry or post top entry.
10. Control gear and lamp isolation when opened.
11. Have minimum power factor of 0.9 lag.
12. Have adjustable lamp position.
13. Have maximum energy loss of 10% and comply with NZ Minimum Energy Performance Standards (MEPS).
14. Have a minimum total light output ratio of 65%.
15. Comply with the requirements of applicable New Zealand and/or international standards. The complying standard shall be documented in the application.

16. Have a zero upward wasted light output ratio (UWLOR). Consideration will be given to special circumstances where the use of luminaries with a UWLOR above 0% is considered necessary. This should be discussed with QLDC prior to lodging an application.

17. Be capable of the following configurations where appropriate:

- Flat glass (aeroscreen) lens;
- Drop glass lens;
- Tear Drop lens;
- Other (please state type and reason).

This paper deals with the performance parameter measurements under varying voltage levels. The main purpose of the presented research is to measure the electrical quantities during high-pressure sodium lamp ignition in the process of resonance as well as the period of establishing a steady-state operating mode. These measurements are necessary due to importance of basic electric characteristics of the lamp for its appropriate application.

### Basic electrical characteristics measurements

Tests were conducted to determine the electrical characteristics of a high-pressure sodium lamp as a function of input frequency. A commercially available lamp (SON-T PIA PLUS 100W) was tested to determine the variations of electrical characteristics with varying input frequency.

In these tests the frequency was varied and the current, voltage and active power of the lamp were recorded. The all measurements were recorded during lamp ignition in the process of resonance as well as the period of establishing a steady-state operating mode.

Digital and analog meters were used to record the electrical quantities (current and voltage waveforms and the frequency spectrum) after being calibrated and certified for accuracy. In the experiments a

programmable digital oscilloscope OWON PDS 6062T was used.

The testing cycle consisted of varying the frequency from the level at which the lamp start (33 kHz) up to 82 kHz in discrete steps. Readings of all electrical parameters were recorded at each incremental step during the variation of the frequency.

It is to be noted that the lamp was new and was only used for the purpose of this experiment. All the measurements were performed at DENIMA Co [6].

Electrical circuit arrangement for lamp operation was realized in which suitable throttle and ignition devices were selected for the respective luminary. Realized electrical circuit arrangement is presented in Fig. 4.

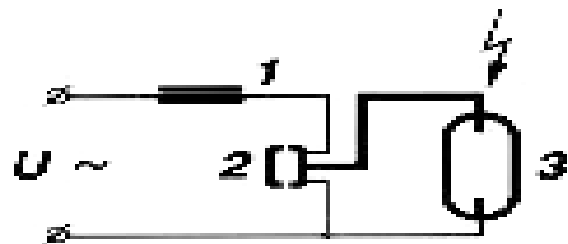


Fig.4. Electrical circuit arrangement for lamp operation: 1 – Ballast; 2 – Ignition device; 3 – Lamp.

Typical arc attachment of an emitter covered high pressure mercury lamp electrode is shown in Fig. 5.

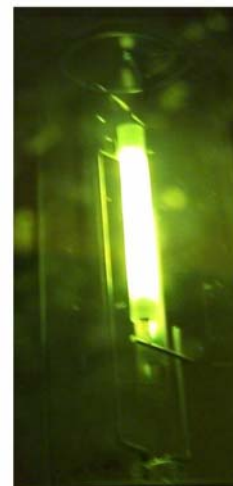


Fig.5. Typical arc attachment

Table 1 presents the results of measurements for determining experimentally all parameters of a luminous lamp operating with high-frequency electronic ballast (HFEB) of adjustable frequency.

For the measurements made the range of frequency is  $F = 33 \text{ kHz} \div 82 \text{ kHz}$ . The frequency is changed in such a way that first resonance occurs and then the lamp operates in a normal mode. The lamp ignites at 200V (amplitude value).

The results of the tests carried out with the considered high-pressure sodium lamp are represented graphically in Fig. 6 – Fig. 8. The measurement data were processed by using the software package Matlab 7.0.

**Table 1**

*Results of electrical parameters measurements*

Type of lamp	$P_{mp}$ [W]	Value measured					
		$F$ , [kHz]	$U$ , [V]	$U_{jl}$ , [V]	$I_H = I_L$ , [A]	$I_{jl}$ , [A]	$P_{cx}$ , [W]
100W	60	33	200	150	1,8	1,8	126
		35		147	1,8	1,7	120
		42		140	1,8	1,66	100
		52		136	1,8	1,28	70
		62		128	1,8	1,11	50
		82		120	1,8	0,89	38

where  $P_{mp}$ , [W] is power (lamp wattage);  
 $F$ , [kHz] – frequency;  
 $U_{jl}$ , [V] – lamp voltage;  
 $I_L$ , [A] – ballast current;  
 $I_{jl}$ , [A] – lamp current;  
 $P_{cx}$ , [W] – circuitry power.

In the Fig. 6 the characteristic of  $P = f(I)$  is presented. The characteristic of  $U = f(I)$  and  $F = f(I)$  are presented, respectively in Fig. 7 and Fig. 8.

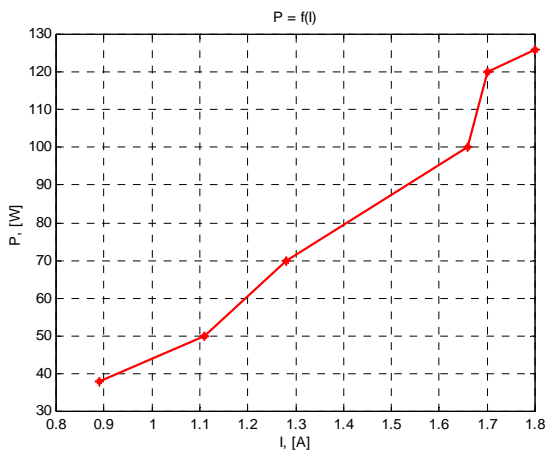


*Fig. 6. Plot of  $P = f(I)$*

The results showed an acceptable correlation between the various electrical parameters measured and the changes in the applied frequency.

As it could be seen the sodium lamps in the process of heating are ignited at 33 kHz,  $P_{mp} = 60$  W and reaches 120 W. Fig. 7 showed that the resonance occurs at two frequencies:

- at 33 kHz basic harmonic;
- at 66 kHz second harmonic.

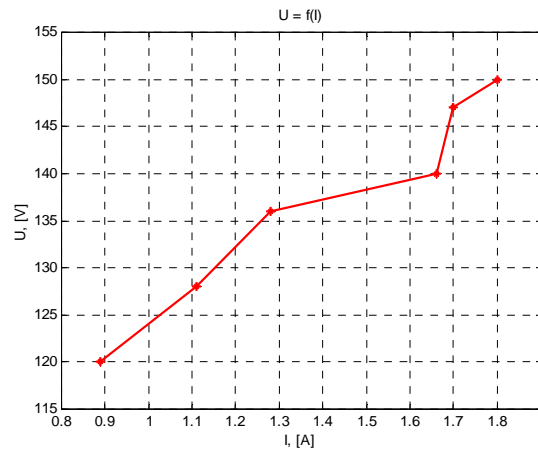


*Fig. 7. Plot of  $U = f(I)$*

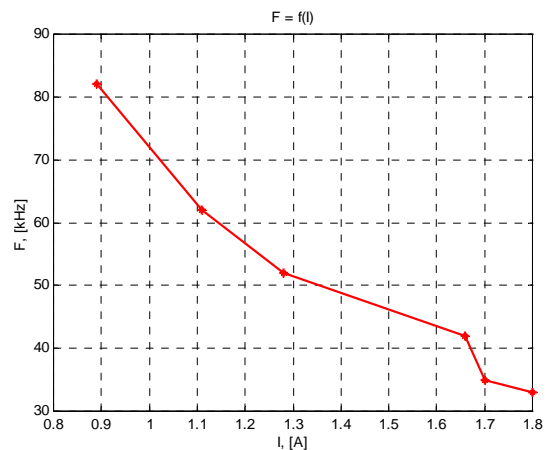


*Fig. 8. Plot of  $F = f(I)$*

At 35 kHz the resonance disappears and the lamp starts to operate in a normal mode. The phenomenon also occurs at  $P_{mp}$ , the resonance being intensified under power overload.

Recorded resonance between the adjacent inductive and capacitive elements of the power system could be explained as a result of the increase in the harmonic contents. For confirmation of this assumption the harmonic contents of the input current should be investigated when the lamp was operated at different frequencies.

### Conclusion

It has been found that sodium lamps in the process of heating are ignited at 33 kHz,  $P_{mp} = 60$  W and reaches 120 W. Resonance occurs at a 33 kHz basic harmonic as well as at a second harmonic of 66 kHz. At 35 kHz the resonance disappears and the lamp starts to operate in a normal mode. The phenomenon also occurs at  $P_{mp}$ , the resonance being intensified under power overload.

However, further tests may be needed for the confirmation of the assumption that recorded resonance is a result of the increase in the harmonic contents.



Measured harmonic contents will indicate whether available energy saving lamp is adequate and does not contribute to an increase in harmonics.

### Acknowledgement

The author would like to acknowledge the support of prof. Hristo Vasilev and DENIMA Co.

### References

- [1] Ignition systems for HID lamps, Philips
- [2] [www.mastersonpia.com](http://www.mastersonpia.com)
- [3] [www.eur.lighting.philips.com/bgr\\_bg/](http://www.eur.lighting.philips.com/bgr_bg/)
- [4] The General Electric Lighting Lamp Catalogue, available at internet [http://www.ge.com/ru/ru/docs/514140\\_HID.pdf](http://www.ge.com/ru/ru/docs/514140_HID.pdf)
- [5] <http://www.qldc.govt.nz/Documents/ContentDocuments/Final%20Minimum%20Standards%20for%20Public%20Lighting%20Infrastructure%20to%20be%20vested%20in%20QLDC%20AUG%202006.pdf>
- [6] [www.denima\\_2001.bg](http://www.denima_2001.bg)

### Biographies



**Galia Georgieva-Taskova** was born in Lom, Bulgaria, on December 17, 1975. He studied at the Technical University of Sofia-Bulgaria.

Since 2006 he worked in the Faculty of Electrical Engineering of the Technical University of Sofia. He is today a PhD student in the Faculty of Electrical Engineering of the Technical University – Sofia.

Galia Georgieva-Taskova is with the Faculty of Electrical Engineering, Technical University of Sofia, 8, Kl. Ohridski Blvd., 1000 Sofia, Bulgaria (e-mail: [gvgt@tu-sofia.bg](mailto:gvgt@tu-sofia.bg)).